TAPPI JOURNAL

2017 TAPPI Journal Yearbook

Copyright© 2018 by
TAPPI PRESS
15 Technology Parkway South, Suite 115
Peachtree Corners, GA. 30092 USA
www.tappi.org
All rights reserved

Copyright© 2018 by



TAPPI PRESS
15 Technology Parkway South, Suite 115
Peachtree Corners, GA. 30092 U.S.A. www.tappi.org
All rights reserved

The Association assumes no liability or responsibility in connection with the use of this information or data, including, but not limited to, any liability or responsibility under patent, copyright, or trade secret laws. The user is responsible for determining that this document is the most recent edition published.

To obtain copyright permission to photocopy pages from this publication for internal or personal use, contact Copyright Clearance Center, Inc. (CCC) via their website at www.copyright.com. If you have questions about the copyright permission request process, please contact CCC by phone at +1-978-750-8400.

To obtain copyright permission to use excerpts from this publication in another published work, send your specific request in writing to TAPPI PRESS, 15 Technology Parkway South, Suite 115, Peachtree Corners, GA 30092 U.S.A. or by fax to +1-770-446-6947.

ISBN: 978-1-59510-280-5
TAPPI PRESS Order Number: 0101R351EL
Printed in the United States of America

Please note: The following TAPPI Journal pages are sequenced chronologically according to publication order. Therefore, you can expect breaks in page numbering, as time sensitive, full-page advertisements have been removed for your convenience.

Welcome to the 2017 *TAPPI Journal* YEARBOOK



For TAPPI, 2017 proved again that knowledge-sharing fuels our industry's progress.

This philosophy has driven our association's growth for more than a century. It is why we publish *TAPPI Journal (TJ)*, a leading research publication. In eleven issues a year, *TJ* reflects the research many scientists and students are doing to advance our industry. Last year, *TJ* included peer-reviewed papers on nanotechnology, tissue, biorefining, and lignin valorization—all areas of exciting innovation.

As an association, TAPPI's efforts also support these vital research areas. For example, in 2017:

- More than 300 industry professionals gathered in Montreal for the largest International Conference on **Nanotechnology for Renewable Materials** ever. As part of the expanded program, TAPPI's Nanotechnology Division hosted its first end-user panel which brought together cellulose nanomaterial (CNM) producers and end users. TAPPI Nano 2018 also features an end-user panel, plus a keynote address from a Ford Motor Company research scientist discussing new market opportunities for CNMs.
- We launched our first-ever standalone tissue event, in conjunction with RISI, a leading provider of industry information. The event was so successful that **Tissue 2018** has already been scheduled for October 2 - 5.
- Our **PEERS Conference** in November featured more than 100 presentations in 10 technical conference tracks, addressing topics in pulping, engineering, environmental, recycling, and sustainability. It was once again co-located with TAPPI's International Bioenergy and Bioproducts Conference (**IBBC**), bringing together experts from around the world interested in leveraging our industry's knowledge and assets to produce fuel, energy, and chemicals from biomass.

In 2017, TAPPI expanded its other learning opportunities in several key areas. **TAPPI Academy** includes new courses in every format—eLearning (where we've added the Tissue 201: Operations and Runnability courses); Face-to-Face; and Company Classroom. At **TAPPI PRESS**, look for brand-new publications: *Brownstock Washing Fundamentals and Practices*, *Advances in Papermaking Wet End Chemistry Application Technologies*, *Nanocellulose: Producers, Products and Applications Guide for End Users*.

But TAPPI is about more than providing resources for our members. The truth is, TAPPI members—their knowledge, experience, talent, and drive—provide a tremendous resource for our industry. Our ***TJ* Peer Reviewers** also represent an important resource, and I'd like to thank them for sharing their expertise.

While being a peer reviewer takes time, it offers outstanding benefits: it can help build your reputation as an expert in your chosen field and increases your professional exposure by establishing relationships with reputable colleagues. In addition, *TJ* submissions often provide a first-look into the latest research on processes and products in the pulp and paper industry, as well as related fields such as nanocellulose, biorefinery, and nonwovens.

This past year, TAPPI expanded its **global presence** to 85 countries and added **2,885 new members**—the highest FY new member count in almost 20 years. If you're one of those new members, welcome. I firmly believe you've made a career-building decision to join us, and I hope you'll take full advantage of all that our association offers. If you're a returning member, welcome back! I hope 2018 will bring you even more opportunities to grow your professional knowledge and contacts through TAPPI.

In that spirit, I hope you find this *2017 TAPPI Journal Yearbook* a useful resource. Thank you for all you do to keep our industry, and our association, innovative and dynamic.

Sincerely,



Larry N. Montague
TAPPI President & CEO

TAPPI *Journal* Abstracts 2017- By CATEGORY

BLEACHING

Generalized steady-state model for chlorine dioxide brightening of hardwood kraft pulps

By: BRIAN N. BROGDON

May, pp. 263-272 A generalized, steady-state model for the first chlorine dioxide brightening (D_1) stage is proposed for North American hardwood kraft pulps. The model predicts the post-D_1 brightness obtained for a given chlorine dioxide (ClO_2) charge based on three equation parameters. Data from laboratory D_1 studies were examined with the model to determine the relationships of the parameters to extracted pulp properties. The asymptotic D_1 brightness limit at extremely high bleach charges was ~93% ISO for most hardwood pulps. This parameter can be calculated from the limiting light absorption coefficient of D_1 kinetic studies (≈ 0.10 m^2/kg) and the unbeaten light scattering coefficient of the pulp. A second parameter was linearly correlated to the extracted kappa number of the hardwood pulp. This relationship seems to be affected by the chosen kraft pulping process (e.g., liquor or dissolved solids profiling). The final parameter is the extracted pulp brightness. The hardwood D_1 model forecasted the brightness values of laboratory pulps that differ from measured values of ±0.5 to ±0.6 points. Daily averages of bleach plant data for a southeastern U.S. hardwood fiber line were examined with the model. Predictions were generally 0.5 points higher than the measured mill brightness values. This observation implied that the D_0 (EOP) pulp contained a small amount of extraction washer carryover (~0.4 kappa units on pulp) that was consuming ~1.2 kg ClO_2/ton pulp, which was not accounted for in the hardwood D_1 model.

Application: These models are simple and can be easily programmed into computer spreadsheets, which can be used to calculate optimum bleach set points and to minimize manufacturing costs.

Brogdon is president, Future Bridge Consulting Services LLC, Marietta, GA, USA. Email Brogdon at Brian.Brogdon@gmail.com .

Improving the efficiency of hydrogen peroxide bleaching of chemimechanical pulp by continuous replenishment of bleaching chemicals

By: XIANQI SUN, QINGXI HOU, BINGXU ZHANG, AND GUANTING ZHAO

June, pp. 331-339 Hydrogen peroxide (H_2O_2) commonly used to bleach chemimechanical pulp. A decrease in the concentrations of the bleaching reagents throughout the bleaching process results in low bleaching efficiencies. In this study, chemical solutions were continuously added into the pulp slurry during the bleaching process to maintain constant concentrations of H_2O_2 and total alkali in the bleaching system to improve bleaching efficiency. The results showed that when the H_2O_2 and total alkali concentrations were maintained at 4.5 g/L and 0.79 g/L, respectively, for 50 min, the bleaching efficiency reached 16.79 (Δ% ISO brightness/Δ% H_2O_2 consumed [on ovendry pulp]), which was significantly higher than 7.38 obtained by using the high-consistency bleaching method. The results confirmed that continuous replenishment of chemical solutions into the bleaching system to maintain the constant chemical concentrations improved the efficiency of H_2O_2 bleaching of the chemimechanical pulp.

Application: Continuous replenishment of H_2O_2 during chemimechanical pulp bleaching improves bleaching efficiency and reduces production costs.

Sun, Zhang, and Zhao are students, and Hou is professor, Tianjin Key Laboratory of Pulp & Paper, Tianjin University of Science & Technology, Tianjin, China. Email Hou at qingxihou@tust.edu.cn .

Techno-economic analysis of ECF bleaching and TCF bleaching for a bleached eucalyptus kraft pulp mill

By: TIAGO DE ASSIS, JORDAN PERRIN, HASAN JAMEEL, RICHARD PHILLIPS, DOMINIQUE LACHENAL, ADRIANNA KIRKMAN, and RONALDS GONZALEZ

October, pp. 583-594 An early stage techno-economic analysis was performed to compare a traditional elemental chlorine free (ECF) sequence (O O D_0 [EOP] D_1 P) with the proposed totally chlorine free (TCF) sequence (O O A $[ZEO]_1$ $[ZEO]_2$ P)] for a bleached eucalyptus kraft pulp mill. Similar operating costs (ECF = US$465/a.d. metric ton; TCF = US$468/a.d. metric ton) and similar internal rate of return (ECF = 16.5%; TCF = 16.4%) were obtained. Although the TCF case has lower revenue with surplus steam, savings with chemicals (e.g., sodium chlorate and methanol) pays for the higher consumption of electricity. Probabilistic analyses were also performed to evaluate the financial risks associated with the variability of chemical costs and electricity price. Probabilistic analyses have shown that the price volatility of sodium hydroxide and sodium chlorate have a significant impact on the probability distribution of internal rate of return (IRR). Despite its promising potential, the new TCF sequence has only been tested in laboratory scale and further scale up has to be performed to validate the technology. However, the techno-economic economic analysis shows that the proposed TCF technology has promising potential for future industrial application.

Application: Mills might consider the proposed TCF sequence as an alternative for bleached pulp manufacturing.

de Assis is a doctoral student, Jameel and Gonzalez are professors, Phillips is professor emeritus, and Kirkman is academic dean in the College of Natural Resources, Department of Forest Biomaterials, North Carolina State University, Raleigh, NC, USA. Perrin is a postdoctoral student at Aalto University Department of Forest Products Technology, Aalto, Finland. Lachenal is a professor at Grenoble INP-Pagora, Laboratory of Pulp and Paper Science and Graphic Arts, Saint-Martin d'Hères, France. Email Jameel at jameel@ncsu.edu .

BIOENERGY

Addition of corn stover arabinoxylan into hardwood during pulping for improved physical properties

By: ANURAG MANDALIKA and TROY M. RUNGE

September, pp. 495-504 Agricultural residues, such as corn stover, are being considered for biofuels and bioproducts. They represent inexpensive, pentosan-rich feedstock that are available in abundance. These materials are typically pretreated to make them more amenable to biological processes such as fermentation. One such treatment involves extraction using alkali to remove the hemicellulose, leaving the cellulose more accessible for chemical or enzymatic hydrolysis. Extracted xylan hemicellulose may be considered for use in pulp and paper, or for providing a potential value stream from cellulosic ethanol biorefineries. To be useful, the extracted xylan should be concentrated and adsorbed into the pulp using existing equipment or a minimal number of new unit operations. In this work, we explored the concept of size-exclusion membrane-filtration to concentrate xylan that was extracted from corn stover in mild alkaline

conditions. We examined hollow-fiber and tangential-flow filtration types and achieved a nearly two-fold increase in the xylan concentration using the former with a 50 kDa molecular weight cut-off (MWCO) membrane. Cassette-type tangential-flow filtration resulted in slightly greater xylan concentration with the use of a 10 kDa MWCO membrane. Hemicellulose extracts were then used as an additive during kraft pulping of hybrid poplar to show that the xylan could be adsorbed onto pulp fibers and retained even after washing. Pulp tensile strength improved after xylan addition following refining. An average of 33% of the xylan added in this method was retained, with xylan loading between 5 wt% and 20 wt%, compared with the control pulp sample that did not have added xylan. These results suggest potential for further exploration of biorefinery extracts use as additive feedstock for pulping. The study, being an evaluation of the proof-of-concept, aims to push research and optimization in this area that will lend well to scale-up and commercialization.

Application: This work benefits mills in demonstrating that adjunct hemicelluloses may be incorporated into their pulp products, and if obtained from a low-cost source, could provide an increase in sellable pulp mass. This work also underlines the importance of hemicellulose content on pulp properties.

Mandalika is graduate student and Runge is associate professor, Department of Biological System Engineering, University of Wisconsin-Madison, Madison, WI, USA. Email Runge at trunge@wisc.edu .

Cellulosic ethanol byproducts as a bulking agent

By: J.M. CONSIDINE, D. COFFIN, J.Y. ZHU, D.H. MANN, and X. TANG

January, pp.37-44 Financial enhancement of biomass value prior to pulping requires subsequent use of remaining materials; e.g., high value use of remaining stock material after cellulosic ethanol production would improve the economics for cellulosic ethanol. In this work, use of enzymatic hydrolysis residual solids (EHRS), a cellulosic ethanol byproduct, were investigated as a bulking agent. The study examined the effect across several grammages, 20 g/m^2 –200 g/m^2, and EHRS substitution levels, 10%, 15%, and 20%. EHRS retention was examined with light scattering. EHRS loading increased bulk while reducing tensile strength, compression strength, and stiffness.

Application: Byproducts of cellulosic ethanol production can be used as a bulking agent.

Considine is material research engineer at the USDA Forest Service, Forest Products Laboratory, Madison, WI, USA. Coffin is professor, Miami University, Oxford, OH, USA. Zhu is research general engineer, Mann is physical science technician, and Tang is engineering technician at the USDA Forest Service, Forest Products Laboratory, Madison, WI, USA. Email Considine at jconsidine@fs.fed.us.

Drying characteristics of biosludge from pulp and paper mills

By: GEANNA HOVEY, D. GRANT ALLEN, and HONGHI TRAN

August, pp. 465-473 Handling and disposal of biosludge has been a persistent problem for many pulp and paper mills primarily because of the material's high moisture content and poor dewatering and drying characteristics. Most biosludge is landfilled or incinerated, and some is used as a soil amendment. To incinerate biosludge, the mills mix it with primary sludge, mechanically dewater the mixture to 15%–30% solids, and burn it with hog fuel in biomass boilers. For biosludge to burn effectively, however, it must be dewatered or dried to at least 30%–35% solids. A systematic study was conducted to examine the drying characteristics of

biosludge collected from pulp and paper mills at various temperatures using a thermogravimetric dryer. The drying behavior of the tested biosludges was similar, adding fillers such as wood fines and biomass boiler fly ash to biosludge up to 30 wt% did not significantly affect the drying rate, higher organic content might make biosludge more difficult to dry, and increasing drying temperature significantly increases the drying rate as expected.
Application: Mills can optimize their biosludge handling and disposal practices by understanding the material's drying characteristics.

Hovey is a graduate student; Allen is professor and chair; and Tran is Frank Dottori Professor of Pulp and Paper and director of the Pulp and Paper Centre, Department of Chemical Engineering and Applied Chemistry, at the University of Toronto, Toronto, ON, Canada. Email Tran at honghi.tran@utoronto.ca .

Operating parameters affecting the thermal performance of biomass boilers
By: NAZ ORANG, HONGHI TRAN, ANDY JONES, and F. DONALD MCCABE
August, pp. 453-461 Operating data of a bubbling fluidized bed (BFB) boiler and three stoker grate (SG) biomass boilers from different pulp mills were analyzed over a 2-year period. The results show that in all cases, the thermal performance decreases markedly from 5.5 to 4 lb steam/lb dry biomass as the feedstock moisture content increases from 40% to 60%. The BFB boiler had better thermal performance, although it operated in a higher moisture content range compared with the SG boilers. Multivariate analysis was also performed on one of the SG boilers to determine operating parameters that affect thermal performance. The results show that furnace temperature, oil flow rate, and induced draft fan current positively correlate with thermal performance, while the feedstock moisture content, total air flow, and excess oxygen (O_2) negatively correlate with thermal performance. This implies that when making modifications to improve thermal performance, it is important to take into account correlations among various parameters. In some cases, one positively correlated parameter might cause an increase in a negatively correlated parameter. The net effect might be a decrease in thermal performance.
Application: Mills can find the most suitable way to optimize boiler operation with minimal process upsets.

Orang is a Ph.D. candidate; Jones is an adjunct associate professor; and Tran is Frank Dottori Professor of Pulp and Paper and director of the Pulp and Paper Centre, Department of Engineering and Applied Chemistry, University of Toronto, Toronto, ON, Canada. McCabe is senior process engineer, Irving Pulp and Paper Ltd., Saint John, NB, Canada. Email Tran at honghi.tran@utoronto .

Process for producing acetic acid in hardwood kraft pulp mills
By: RAVIKANT PATIL, JOSEPH GENCO, HEMANT PENDSE, and ADRIAAN VAN HEININGEN
May, pp. 287-300 To determine the economic feasibility of producing acetic acid from commercial hardwood chips in kraft pulp mills, laboratory experiments were conducted to obtain sufficient data to perform a preliminary economic analysis for a proposed acetic acid recovery process. The acetyl groups in northeast hardwood were hydrolyzed from the xylan polymers in the wood to obtain sodium acetate. The extraction experiments were performed by using 4%–6% sodium hydroxide at low temperature (50°C–80°C). Sodium acetate from the extract was concentrated and then converted into acetic acid and sodium hydroxide by salt splitting using bipolar membrane electrodialysis (BPMED). Flow diagrams were prepared and cost estimates

made for the capital and operating costs for the proposed acetic acid recovery process. The discounted cash flow rate of return on investment was estimated for pulp mills in the range of 1000–2000 tons/day. A preliminary economic analysis showed that the discounted cash flow rate of return on investment is primarily a function of (1) the plant size, (2) the selling price of acetic acid, and (3) the content of acetyl groups present in wood species. The income for the process and thus the rate of return on investment increases with increasing acetyl content in the wood and selling price of the acetic acid. When food grade acetic acid is produced, for example, the rate of return varies between 9% and 16% depending upon the size of the pulp mill, assuming the wood contains 3.5% acetyl groups on a dry basis and the selling price of acetic acid is US$900/ton.
Application: A process to recover acetic acid or acetate salt as a byproduct of kraft pulp mills will be useful to scientists and engineers who are developing the biorefinery concept.

Patil is a postdoctoral student, Genco is a professor emeritus, Pendse is chair of the Chemical and Biological Engineering Department, and van Heiningen is a professor of Chemical Engineering at the University of Maine, Orono, ME, USA. Email Genco at JGenco@umche.maine.edu .

LIGNIN

Accelerated aging of bio-oil from lignin conversion in subcritical water

By: HUYEN NGUYEN LYCKESKOG, CECILIA MATTSSON, LARS OLAUSSON, SVEN-INGVAR ANDERSSON, LENNART VAMLING, and HANS THELIANDER

March, pp. 123-141 Accelerated aging of bio-oil derived from lignin was investigated at different aging temperatures (50°C and 80°C) and times (1 hour, 1 day, 1 week, and 1 month). The bio-oil used was produced by the hydrothermal liquefaction of kraft lignin, using phenol as the capping agent, and base (potassium carbonate and potassium hydroxide) and zirconium dioxide as the catalytic system in subcritical water. Elemental composition, molecular weight (by using gel permeation chromatography), and chemical composition (by using gas chromatography–mass spectrometry and 2D nuclear magnetic resonance [18.8 T, DMSO-d_6]) of the bio-oil were measured to gain better understanding of the changes that occurred after being subjected to an accelerated aging process. The ligninderived hydrothermal liquefaction bio-oil was quite stable compared with biomass-pyrolysis bio-oil. The yield of the low molecular weight fraction (light oil) decreased from 64.1% to 58.1% and that of tetrahydrofuran insoluble fraction increased from 16.5% to 22.2% after aging at 80°C for 1 month. Phenol and phenolic dimers (Ar–CH_2–Ar) had high reactivity compared with other aromatic substituents (i.e., methoxyl and aldehyde groups); these may participate in the polymerization/condensation reactions in the hydrothermal liquefaction bio-oil during accelerated aging. Moreover, the 2D heteronuclear single quantum coherence nuclear magnetic resonance spectra of the high molecular weight fraction (heavy oil) in the aged raw oil in the aromatic region showed that the structure of this fraction was a combination of phenol-alkyl patterns, and the guaiacol cross-peaks of Ar_2, Ar_5, and Ar_6 after aging indicate that a new polymer was formed during the aging process.
Application: Pulp mill personnel can use this information when considering technology to extract lignin from black liquor and process it further into bio-oil.

Nguyen Lyckeskog is a doctoral candidate, Mattsson is a post-doctoral student, and Andersson, Vamling, and Theliander are professors at Chalmers University of Technology, Department of Chemistry and Chemical Engineering, Gothenberg, Sweden. Olausson is with Valmet Power AB, Gothenberg, Sweden. Email Theliander at hanst@chalmers.se .

An easy and reliable method for syringyl: guaiacyl ratio measurement

By: RAQUEL PRADO, LISA WEIGAND, SHIKH M.S.N.S. ZAHARI, XABIER ERDOCIA, JASON P. HALLETT, JALEL LABIDI, and TOM WELTON

March, pp. 145-152 Lignin structure elucidation is one of the main targets for biorefinery related research. Because ofits complexity, obtaining reproducible results in a straight-forward way is very important. One of the values that is used to compare different lignins is the syringyl: guaiacyl (S/G) ratio, which has been measured in different ways. The most reliable result is obtained for nitrobenzene oxidation, but this involves a complex process. In this work, the S/G ratios measured by pyrolysis-gas chromatography mass spectrometry (py-GCMS) and heteronuclear single quantum coherence-nuclear magnetic resonance (HSQC-NMR) spectroscopy were compared with attenuated total reflection infrared (ATR-IR) spectroscopy results to establish a reliable, quick, and simple method for the measurement. To achieve this, two mathematical models were applied with multivariate data analysis software. A partial least squares regression model for py-GCMS gave the best result.

Application: This study describes an easy way to characterize lignin.

Prado is researcher, Zahari is professor, and Welton is dean, Department of Chemistry; Hallett is senior lecturer, Department of Chemical Engineering; and Weigand is Ph.D. student, Department of Chemistry and Department of Chemical Engineering, Imperial College London, London, UK. Erdocia is doctor and Labidi is professor, Chemical and Environmental Engineering Department, University of the Basque Country, San Sebastian, Spain. Email Welton at t.welton@imperial.ac.uk .

Analysis of economically viable lignin-based biorefinery strategies implemented within a kraft pulp mill

By: CÉDRIC DIFFO TÉGUIA, ROD ALBERS, and PAUL R. STUART

March 157-169 Many pulp and paper companies are considering implementing a lignin-based biorefinery to diversify their core business to new products and improve their longer-term competitiveness. The best strategy to achieve might not be obvious, considering the lignin extraction process and derivatives to be implemented over the longer term that meet market and business objectives, and provide competitive advantage. In this article, various lignin biorefinery strategies were considered in a case study involving lignin precipitation processes integrated within an existing kraft mill, and solvent pulping processes that would be implemented in parallel to the existing mill processes using additional hardwood. The analysis aimed to identify the conditions under which various strategies would represent suitable investments. Operating constraints in the case study mill limited lignin extraction to 85 metric tons/day from 15% of the mill's black liquor, whereas 260 metric tons/day lignin could be extracted by solvent pulping 1500 metric tons/day of hardwood. The preferred strategies identified by the study were lignin precipitation to phenolic resins production, and solvent pulping to carbon fiber production. The first product-process strategy requires lower investment, provides high returns (internal rate of return [IRR] of 39% to 43%), and is more easily implemented in the near term. Solvent pulping resulted in reasonable profitability (IRR of 18% to 25%), with higher production volumes and a diversified product portfolio, and was considered more suitable as a longer-term strategy. Business model robustness and long-term competitiveness can be better assured by combining both strategies. It was shown that 1) government support to offset capital cost, and 2) high derivatives market prices positively influence lignin valorization strategies, which are sensitive to technology and market maturity.

Application: This study illustrates how a technical and economic analysis could be used to identify lignin-based biorefinery strategies that represent an attractive investment.

Diffo is post-doctoral fellow and Stuart is professor, Natural Sciences and Engineering Research Council of Canada (NSERC) Chair in Design Engineering, Department of Chemical Engineering, École Polytechnique de Montréal, Montréal, QC, Canada. Albers is manager, energy and bioproduct development, West Fraser Timber Company, Quesnel, BC, Canada. Email Stuart at paul.stuart@polymtl.ca .

Decision-making process for the identification of preferred lignin-based biorefinery strategies

By: CÉDRIC DIFFO TÉGUIA, SOPHIE D'AMOURS, ROD ALBERS, and PAUL STUART

April, pp. 229-240 The lignin biorefinery is emerging; there has been significant progress in recent years regarding lignin extraction and conversion processes, their implementation at the commercial scale, and the validation of lignin substitution potential in various applications. In this paper, seven strategies for implementing the lignin-based biorefinery into a kraft pulp mill were considered, and different performance metrics for these strategies were calculated in order to identify the "most preferred". The different options addressed two distinctly different objectives that companies can consider regarding their biorefinery strategy, either (1) a near-term mill-level profitability improvement vision, or (2) a longer-term revenue growth-oriented vision. A phased-implementation approach was systematically defined for each option in order to mitigate technology and market risks. Lignin product applications that were considered included phenol replacement in phenol-formaldehyde (PF) resins, polyols replacement in polyurethane (PU) foams, and polyacrylonitrile (PAN) replacement in carbon fiber. A Multi-Criteria Decision-Making (MCDM) panel was executed for evaluating the seven lignin-based biorefinery strategies, using a set of economic, market risk, and competitiveness criteria. Although the panel selected Internal Rate of Return (IRR) as the most important criterion, Competitiveness on Production Costs (CPC) appeared to be the most important factor for distinguishing between lignin strategy options. CPC reflects the robustness of the biorefinery strategy relative to an aggressive price-cutting strategy from the competition. Overall, strategies involving lignin precipitation were more attractive economically, while those involving larger-scale solvent pulping processes and the associated larger revenue streams were considered better long-term strategies. The most preferred strategy considered by the panel was for precipitated lignin sold for both PF resin and PU foam applications. The next preferred strategy considered lignin sales to the same market segments, but at larger volumes. The next closely-ranked strategy considered the production of a lignin-based PF resin at the host mill. These three strategies were identified as "preferred," for further, more detailed assessment.

Application: This paper provides an evaluation of lignin-based biorefinery strategies in the context of retrofit implementation within a market kraft pulp mill. The evaluation is made though a Multi-Criteria Decision-Making panel, whose members considered a set of profitability, market, and risk-based criteria.

Diffo Téguia is post-doctoral student and Stuart is professor at Polytechnique Montréal, Montréal, QC, Canada. D'Amours is professor, Université Laval, Quebec City, QC, Canada. Albers is manager, Energy and Bioproduct Development, West Fraser Timber Co. Ltd., Quesnel, BC, Canada. Email Stuart at paul.stuart@polymtl.ca.

Evaluation of the particle size of organosolv lignin in the synthesis of resol resins for plywood and their performance on fire spreading

By: ELECTRA PAPADOPOULOU, SOTIRIS KOUNTOURAS, KONSTANTINOS CHRISSAFIS, MIKELIS KIRPLUKS, UGIS CABULIS, PAVLA ŠVÍGLEROVÁ, and BOUCHRA BENJELLOUN-MLAYAH

July, pp. 409-416 Scientists today are intensively seeking alternatives to petrochemical materials. Among others, lignin is a promising candidate because it is available in large quantities while its chemical structure makes its use possible in a variety of chemical reactions. Lignin, received by numerous methods from various feedstocks, is a promising material for the synthesis of many products like active carbon, thermosetting and thermoplastic polymers, surfactants, phenolic chemicals, etc. In this paper, the potential of using Biolignin – a trademarked organosolv lignin from straw prepared by Compagnie Industrielle de la Matière Végétale (CIMV; Neuilly-sur-Seine, France) – in the synthesis of phenol-formaldehyde (PF) resins was studied by CHIMAR HELLAS S.A. (Kalamaria, Greece). Before its use, Biolignin was further purified and subjected to mechanical treatment for the reduction of its particle size in order to increase its reactivity. The effectiveness of the treatment was verified by atomic force microscopy (AFM) measurements that were carried out by SYNPO Company (Pardubice, Czech Republic). Resol phenolic resins were prepared with various substitution levels of phenol up to 80%. However, their synthesis process was smooth only up to the substitution level of 50%. The properties of the resins were determined with typical lab analysis. Their thermal behavior was studied with differential scanning calorimetry (DSC) and thermogravimetric analysis (TGA) measurements that were conducted by the Aristotle University of Thessaloniki in Greece. Their bonding ability was evaluated by CHIMAR HELLAS via their application in the production of plywood panels of three layers that were prepared following a simulation of the industrial process. The panels were tested for their properties according to the relevant European standards, while their performance relative to fire was studied with cone calorimetry measurements that were performed by the Latvian State Institute of Wood Chemistry (LIWC; Riga, Latvia). All results were compared with that of a typical PF resin. It was found that the particle size of lignin affects the performance of the resins, while lignin-based PF resins are suitable for the production of plywood panels and have somewhat better performance relative to fire than typical PF resins. This study has been performed within the framework of the European project BIOCORE (biocommodity refinery for biofuels, chemical intermediates, polymers and materials).

Application: This study informs readers that the performance of organosolv lignin in the synthesis of PF resins may be improved with adjustments to its particle size. Lignin-based PF resins render to plywood panels better performance to fire.

School of Physics, Solid State Department, at the University of Thessaloniki in Thessaloniki, Greece. Kirpluks is researcher and Cabulis is director at the Latvian State Institute of Wood Chemistry, Polymer Laboratory, in Riga, Latvia. Švíglerová is researcher at SYNPO A.S., Pardubice, Czech Republic. Benjelloun- Mlayah is R&D director at Compagnie Industrielle de la Matière Végétale (CIMV) in Labège, France. Basque Country, San Sebastian, Spain. Email Welton at t.welton@imperial.ac.uk .

Melt-blown compostable polyester films with lignin

By: WOLFGANG G. GLASSER, ROBERT LOOS, BLAIR COX, and NHIEM CAO

March, pp. 111-121 Compostable films for such uses as packaging and agricultural soil covering materials were first produced on commercial scale from blends of biodegradable polyesters and a modified kraft lignin. The lignin consisted of an industrial product isolated according to the LignoBoost process. The lignin modification involved homogeneous phase reaction with propylene oxide, and the films were melt-blown from a pelletized compound consisting of up to a 30% blend of lignin derivative with commercial biodegradable polyester. The 12–93 μm thick films combined the characteristics of lignin as modulus-building and environmentally degradable polymer with those of the strength-building thermoplastic polyester. Although the modified lignin paralleled the behavior of native lignin in wood by resisting rapid and full conversion to carbon dioxide in a simulated composting environment, two thirds of the film mass biodegraded within 12 weeks of composting, with the remainder turning into (humus-like) water-soluble solids and particles <2 mm in size. The lignin derivatives suffered from the release of trace amounts of malodorous volatiles containing reduced sulfur when subjected to melt-blowing. The objectionable odor was virtually unnoticeable in injection-molded solid parts.

Application: The use of kraft lignin as a contributing thermoplastic polymer component of melt-blown film and injection-molded products from sustainable resources with environmental compatibility helps the kraft pulping process advance toward a multi-purpose biorefining technology with increased income potential.

Glasser is professor emeritus, Department of Sustainable Biomaterials, Virginia Polytechnic Institute and State University, Blacksburg, VA, USA. Loos is senior scientist, Biopolymers, at BASF SE, Ludwigshafen, Germany. Cox is rocket scientist, Orbital ATK, Dulles, VA, USA. Cao is CEO, CycleWood Solutions, Fayetteville, AK, USA. Email Glasser at wglasser@vt.edu .

Recent advances in lignin-based polyurethanes

By: YUN-YAN WANG, CHARLES M. CAI, and ARTHUR J. RAGAUSKAS

April, pp. 203-207 Given the rise in demand for sustainable renewable biofuels and promising developments in cellulosic ethanol, the valorization of lignin has become essential for biorefining operations, especially with today's low-cost energy production state of affairs. In the past 40 years, numerous efforts have been devoted to incorporate lignin and lignin derivatives into commercial polymeric materials. One of the promising strategies is to utilize multifunctional lignin macromolecules or oligomers as the replacement of polyols during polyurethane synthesis. In this review, recent advances in fabricating polyurethane foams, films, and adhesives with modified or unmodified lignins are examined. The mechanical and thermal properties of these lignin-based polyurethanes were correlated to their formulations, lignin molecular weight, and polydispersity, as well as the structural features of different lignin preparations. Recalcitrance and strong intermolecular interactions of lignin macromolecules are known to prevent them from effective incorporation into other polymeric materials, covalently or noncovalently. Therefore, this review intends to summarize the methods that improve the reactivity of lignin through chemical modification such as depolymerization, demethylation, and chain extension. Future developments and applications will be examined with a special emphasis on tailoring lignin structure to specific applications.

Application: Lignin can be used as polyols to produce polyurethane foams, films, and adhesives.

Center for Renewable Carbon, University of Tennessee Institute of Agriculture, Knoxville, TN, USA. Cai is an assistant research engineer and adjunct professor, Department of Chemical and Environmental Engineering, University of California – Riverside, Riverside, CA, USA. Ragauskas is professor/Governor's Chair in Biorefining, Oak Ridge National Laboratory; Department of Chemical and Biomolecular Engineering; Department of Forestry, Wildlife, and Fisheries; and Center for Renewable Carbon; University of Tennessee, Knoxville, TN, USA. Email Ragauskas at aragausk@utk.edu .

Toward valorization of lignin: characterization and fast pyrolysis of lignin recovered from hot-water extracts of electron-beam irradiated sugar maple

By: DEREK CORBETT, OFEI MANTE, and BILJANA BUJANOVIC

April, pp. 213-226 This paper provides an analysis of lignin-rich (>80%) solids recovered as a byproduct of hot-water extraction (HWE) pretreatment performed on sugar maple (*Acer saccharum*) (autohydrolysis at 160ºC for 2 h). The effects of electron beam irradiation (EBI) pretreatment before HWE were assessed with regard to lignin removal during HWE and selected features of the recovered lignin. The results of catalytic fast pyrolysis – gas chromatography-mass spectrometry (Py-GCMS) are also discussed. EBI of sugar maple increased lignin removal (delignification) during subsequent HWE; however, recovery of dissolved lignin and lignin degradation products from the hot water extract was hindered. Variation of EBI energy dosages before HWE had little effect on lignin recovered from extracts, except for a slightly reduced molecular weight, as evidenced by size exclusion chromatography. The recovered lignin was hypothesized to have advantages for Py-GCMS compared with common technical lignins, such as kraft or dilute acid hydrolysis lignin, because of lower ash and sulfur content and fewer condensed structures (i.e., increased reactivity). The Py-GCMS results showed that the hot water-extracted ligninrich samples produced less residual char than kraft and commercial dilute acid hydrolysis lignin samples; however, yields to simple phenols were reduced compared with kraft lignin results, mostly because of the high syringyl-unit content of the hardwood-derived lignin.

Application: This research could benefit a mill's research and development efforts toward developing products other than paper from lignocellulosic material.

Corbett (who completed this work as a graduate student at State University of New York [SUNY] College of Environmental Science and Forestry) is research analyst/Ph.D. student, North Carolina State University, College of Natural Resources, Department of Forest Biomaterials, Raleigh, NC, USA. Mante is research chemical engineer, RTI International, Energy Technologies Division, Durham, NC, USA. Bujanovic is associate professor, SUNY College of Environmental Science and Forestry, Department of Paper and Bioprocess Engineering, Syracuse, NC, USA. Email Corbett at dbcorbet@ncsu.edu .

NANOTECHNOLOGY

Novel thin functional coatings for paper by foam coating

By: KARITA KINNUNEN-RAUDASKOSKI, TUOMO HJELT, ULLA FORSSTROM, PATRIZIA SADOCCO, and JOUNI PALTAKARI

April, pp. 179-186 Conventional coating methods are currently being challenged by newly developed technologies that can result in products with interesting properties and competitive prices. Versatile foam coating is one such promising technology. Foam coating is carried out

using different foam application methods, and the viscoelastic nature of the foam allows the use of a large variety of materials. Paper was coated with nanomaterials on a pilot scale using a method based on slot die application combined with foam destruction by absorption and infrared drying. A thin layer of titanium dioxide/zinc oxide (TiO_2/ZnO) functionalized cellulose nanofibrils (CNF) creates antimicrobial properties in the paper, and a thin layer of CNF-TiO_2 alone has substantial ability to oxidize nitric oxide (NO) and nitrogen oxides (NOx). These results illustrate methods that can be used to create novel functional properties for different end-use applications. Thin functional layers could bring added value to current products and also create opportunities to introduce novel products for several industrial areas using web-type manufacturing processes.

Application: The versatile foam coating method, using foam as a transferring media, allows manufacturers to modify web surfaces with a large variety of materials, from nanoparticles to highly viscous material such as cellulose nanofibers.

Kinnunen-Raudaskoski is co-founder and research director, Paptic Ltd., Espoo, Finland. Hjelt is senior scientist and Forsström is principal scientist, VTT Technical Research Centre of Finland, Espoo, Finland. Sadocco is director with Innovhub SSI Paper Division, Milan, Italy. Paltakari is a professor, School of Chemical Technology, Aalto University, Aalto, Finland. Email Kinnunen-Raudaskoski at karita.kinnunen@paptic.fi .

Paper coated with sonochemically synthesized zinc oxide nanoparticles: Enhancement of properties for preservation of documents

By: SUCHISMITA MAJUMDAR, ANIRBAN ROY, ISITA NANDI, PRANTIK BANERJEE, SWAPNA BANERJEE, MAHUA GHOSH, and SAMPA CHAKRABARTI

January, pp. 25-33 Sonochemically synthesized zinc oxide (ZnO) nanoparticles were coated on paper for enhancing its properties in view of the preservation of documents. The paper used for accession register was used as substrate. Physical, chemical, optical, hydrophobic, and antifungal properties of the coated and uncoated papers were compared. Nanoparticles were synthesized with ultrasound from organic precursors and were characterized by X-ray diffraction (XRD) and field emission scanning electron microscopy (FESEM), whereas coated and uncoated papers were examined following standard procedures as described by the Bureau of Indian Standards (BIS). It was observed that coating with nanoparticles imparted mechanical strength, water repellence, and antifungal properties to the paper without compromising its printability. Hence, coated paper is comparatively more suitable for preservation of written or printed documents than uncoated paper.

Application: In this work, we coated paper with sonochemically synthesized zinc oxide nanoparticles and explored various properties of the coated paper, including the antifungal property. It was observed that coating with nanoparticles imparts mechanical strength, water repellence, and antifungal properties without compromising printability. This enhanced the durability of accession register paper; hence, documents can be preserved for longer.

Majumdar is research scholar in Document Preservation, Department of Library and Information Science, University of Calcutta, Kolkata, India. Roy is research scholar in Nanoparticle Synthesis and Coating, Department of Chemical Engineering, University of Calcutta, Kolkata, India. Nandi is research scholar in Antifungal Properties, Department of Chemical Technology, University of Calcutta, Kolkata, India. P. Banerjee is a former research scholar in Nanoparticle Synthesis and Coating, Department of Environmental Science, University of Calcutta, Kolkata, India. S. Banerjee is professor and supervisor

of Document Preservation studies, Department of Library and Information Science, University of Calcutta, Kolkata, India. Ghosh is assistant professor and supervisor of Antifungal Property studies, Department of Chemical Technology, University of Calcutta, Kolkata, India. Chakrabarti is professor in the Department of Chemical Engineering and research coordinator for Nanoparticle Synthesis and Coating studies at the Center for Research in Nanoscience & Nanotechnology, University of Calcutta, Kolkata, India. Email Chakrabarti at sampac.2008@gmail.com .

Physical handsheet properties of pulp furnishes containing attritor-treated fibers
By: DAVID E. KNOX, PETER W. HART, HUMPHREY J. MOYNIHAN, and NICHOLE M. KILGORE
January, pp. 9-15 Several articles have been published during the past 30 years on different methods to produce micro- to nanosize cellulose particles from pulp. Unfortunately, a general lack of information exists on the impact of differing manufacturing process methods upon the product properties obtained from these differing methods. Literature data show that wet processing of small-sized cellulosic fibers generates handsheets with approximately equal or higher density and modulus of elasticity than controls for a given amount of added microcellulose. The current work evaluated small particle generation from pulp fibers via dry processing methods and compared the physical properties of dry versus wet processed particles. Dry processing to obtain microcellulose gave considerably lower sheet density and modulus as compared with wet processed microcellulose. The lower modulus can be compensated for by refining base fibers more aggressively to obtain higher density and higher modulus sheets. Dry processing methods for making microcellulose and their impact on final board properties, including modulus and smoothness, will be discussed.
Application: The impact of attritor-processed fiber on handsheet physical properties might have potential for commercial applications.
Knox is retired, Hart is director of Fiber Technology and Innovation, Moynihan is a senior research engineer, and Kilgore is a researcher, WestRock, Richmond, VA, USA. Email Hart at peter.hart@westrock.com .

NONWOOD PULPING
Kinetics of sulfur dioxide-alcohol-water (SAW) pulping of sugarcane straw (SCS)
Low-temperature precausticizing — a hopeful approach for green liquor desilication
By: ASIF MASIH SHARAZI and ADRIAAN VAN HEININGEN
June, pp. 313-328 Pulping kinetics of sugarcane straw (SCS) using the sulfur dioxide (SO_2)-alcohol-water (SAW) system were investigated with different solvents (methanol, ethanol, and isopropanol) in order to evaluate the effect of the solvents. The methanol, ethanol, and isopropanol SAW pulps are identified as SMW, SEW, and SPW, respectively. The pulping experiments were carried out at 135°C, 145°C, and 155°C with cooking liquor (L/F = 4 L/kg feedstock) composition; SO_2/alcohol/water of 12/44/44 w%. The pulps were characterized in terms of yield, kappa number, viscosity, cellulose, and hemicellulose and lignin content. After a fast initial dissolution phase, two regimes of delignification were identified in all solvent systems: a bulk and a residual phase. Bulk delignification and xylan removal followed first order kinetics in residual lignin and xylan, respectively, while the cellulose hydrolysis rate was zeroth order in cellulose. Linear relationships between Klason lignin content and kappa number were developed for each solvent system after correcting the acid insoluble lignin for ash and non-

oxidizable matter. The corrected lignin content on original SCS was used to develop the bulk delignification kinetics. Rate constants and activation energies for bulk delignification, xylan removal, and cellulose hydrolysis were evaluated for each pulping system. In terms of degree of delignification, the pulping systems followed the sequence of: SMW <SEW <SPW. Bleachable grade pulps with acceptable intrinsic viscosity (>800 ml/g) were produced in SEW and SPW systems, while the lower rate of delignification and higher rate of cellulose hydrolysis in SMW yielded much lower viscosity pulps of higher kappa number at the same pulping temperature and time. The results are explained in terms of the effective acidity and lignin/carbohydrate dissolution properties of the pulping liquors.
Application: Based on the knowledge developed in this study, isopropanol can be considered in SAW pulping processes. The use of isopropanol will reduce the capital cost and safety regulations. However, recovery potential of isopropanol still needs to be evaluated.

Sharazi is a doctorate student and van Heiningen is professor in the Department of Chemical and Biological Engineering at the University of Maine, Orono, ME, USA. Email Sharazi at asif.sharazi@maine.edu .

Low-temperature precausticizing — a hopeful approach for green liquor desilication
By: XINXING XIA, FANG WANG, XIAOJING QIN, TINGTING TANG, and TIANWEN ZHOU
February, pp. 57-61 We investigated silica removal by low-temperature precausticizing and the properties of second causticizing calcium carbonate (CCC). The results showed that about 89.3% of silica removal was achieved when 20% (the stoichiometric ratio) of causticizing quicklime was added for precausticizing at 20ºC for 60 min. After that, silica removal became slow. When no precausticizing quicklime was used to remove silica, the CCC particles had a rhombohedral crystal structure covered with amorphous material. As precausticizing quicklime was increased to 30%, the amorphous material and the crack disappeared, and the specific surface area decreased significantly. When CCC was used as filler, the Cobb value decreased significantly, and the sizing effect improved as precausticizing quicklime increased.
Application: Understanding the properties of CCC with different quicklime contents for low-temperature precausticizing, and its effect on paper quality, can mitigate the issues caused by "silica influence" and enable papermakers to reuse CCC produced from the chemical recovery process of wheat straw soda pulping.

Xia is professor, and Wang, Qin, Tang, and Zhou are graduate students, Zhejiang Sci-Tech University, Hangzhou, Zhejiang, China. Email Xia at xingxingxia2000@hotmail.com .

Pulping and bleaching of Malaysian oil palm empty fruit bunches
By: ROBERT W. HURTER and MEDWICK V. BYRD
June, pp. 361-370 Oil palm empty fruit bunch (EFB) was evaluated as a raw material for papermaking pulp production. The EFB was chopped, screened, and washed before cooking. Preliminary bench-scale trials were carried out using soda and soda-anthraquinone cooking followed by bleaching using elemental chlorine free and totally chlorine free sequences. Pilot-scale soda cooking was carried out in a 2300 L spherical digester using the soda process followed by a three-stage elemental chlorine free bleaching sequence. Unbleached and bleached EFB pulps were tested for physical and optical properties. Comparisons were made between the properties of the EFB pulps and bleached kraft eucalyptus pulp. The EFB unbleached and bleached pulps were acceptable for papermaking.

Application: For mills located near oil palm plantations, EFB could be a low-cost fiber resource for pulping.

Hurter is president, Hurter Consult Inc., Ottawa, ON, Canada. Byrd is associate teaching professor, North Carolina State University, Raleigh, NC, USA. Email Hurter at bob@hurterconsult.com .

Removal of silicon from green liquor with low-temperature precausticizing

By: XINXING XIA, FANG WANG, SHAN SUN, and QIAN HU

January, pp. 17-21 Nonwood materials contain a high percentage of silicon, which causes numerous problems in the chemical recovery section. Researchers previously proposed the method of silicon removal by two-stage causticizing at temperatures of 90ºC to 95ºC, finding that the desilication rate was about 72.9% and the causticizing efficiency was 22.7% when 30% of the causticizing quicklime (calcium oxide; CaO) was added. The present paper deals with the desilication of green liquor recovered from wheat straw black liquor by a low-temperature precausticization method. The results showed that about 89.3% silicon removal and 10.3% causticizing efficiency were achieved under the following precausticizing conditions: added lime amount of 20%, temperature of 20ºC, and reaction time of 60 min. While precausticizing at 90ºC with the same lime amount, only about 63.5% silicon removal and 13.0% causticizing efficiency were gained. Therefore, precausticizing with low temperature was beneficial for silicon removal and retention of carbonate (CO_3^{2-}).

Application: Removal of silicon from green liquor with precausticizing at low temperature can effectively increase the desilication rate, which could mitigate the issues caused by "silicon influence" and improve the recycling of lime mud.

Xia is professor at the Pulp and Papermaking Center, Zhejiang Sci-Tech University, Hangzhou, China, and State Key Laboratory of Pulp and Paper Engineering, South China University of Technology, Guangzhou, China. Wang, Sun, and Hu are graduate students of Zhejiang Sci-Tech University, Hangzhou, China. Contact Xia at xinxingxia2000@hotmail.com .

NONWOVENS

Oil absorption and desorption by polypropylene fibers

By: PRAVEEN KUMAR YEGYA RAMAN, AKSHAY JAIN, and SESHADRI RAMKUMAR

September, pp. 507-513 Oil spill is a threat to the ecosystem, and there is a need for the development of highly efficient oil sorbents for environmental remediation. In this study, four different types of polypropylene fibers were evaluated for their oil absorbency and desorption characteristics. These fibers varied in their fineness and structural characteristics, i.e., hollow or solid. A modified ASTM methodology was used in the study to better represent the oil sorption capacity of a sorbent. To the best of our knowledge, this is the first study to present the effect of fiber fineness and structure on the oil desorption behavior of polypropylene fibers. Results showed that finer fibers had higher oil sorption capacity (g/g) than the coarser fibers. There was no statistical difference in the rate of desorption among the solid fibers; however, the hollow fiber had a statistically higher rate of desorption than the solid fibers.

Application: This study will help with the development of efficient sorbents, which will have high oil sorption capacity and ease of transportation.

Yegya Raman was research assistant, Jain was graduate research assistant, and Ramkumar is professor at the Nonwovens and Advanced Materials Laboratory, Texas Tech University, Lubbock, TX, USA. Email Ramkumar at s.ramkmuar@ttu.edu .

PAPER PROPERTIES

Innovative technology for making improved paper from the poorest fibers

By: MARION STERNER and MIKAEL MAGNUSSON

November, pp. 633-637 The trademarked Papermorphosis technology, consisting of two novel units for separately increasing cross direction (CD) and machine direction (MD) elongation over purely mechanical processes, has been successfully tested on recycling fiber, reaching high elongation values in each direction of over 15% in CD or 20% in MD. Increase of elongation has also had a positive influence on the relative tensile energy absorption (TEA) values in CD and MD. It is well known that mechanical properties in paper basically depend on fiber choice, headbox properties, and refining. With the novel system, elongations in cross direction (CD) and machine direction (MD) can be individually customized, even in paper grades with lower strength deriving from recycled fiber. Customizing elongations also has the effect of improving or better balancing TEA values in both directions. The aim is to improve existing recycling papers and to broaden the use of recycling fiber with respect to the past.

Application: For mills, using this technology on recycled papers or recycled fibers as blends might lower costs for raw materials and refining.

Sterner is head of Research & Development for Gruppo X di X Gruppo srl, Venice, Italy. Magnusson is senior research associate, RISE Bioeconomy (Invenntia AB), Stockholm, Sweden. Email Sterner at marion.sterner@gruppox.it .

PAPERMAKING

Effect of conductivity on paper and board machine performance— a review and new experiences

By: LEBO XU, PRZEMYSLAW E. PRUSZYNSKI, and PETER W. HART

October, pp. 567-579 The current trend to further reuse water within paper mills has resulted in more accumulated salts, as reflected by increased conductivity values. Although conductivity measurement is widely used in paper mills, its fundamental principles and interpretation are not often fully understood. This keeps papermakers from reaching the full benefits of using conductivity measurements to help manage the wet end chemistry of paper or board machines. High and variable conductivity affects the intrinsic properties of pulps, the performance of chemical additives, and the interaction between them. This paper reviews principles of conductivity; its measurement; its effect on important aspects of papermaking operations, such as retention, drainage, sizing, strength development and deposit control; and the fundamentals behind the effects of conductivity on the papermaking process. Specific mill examples are also provided. Potential solutions for operating a mill under high and variable conductivity conditions are discussed.

Application: Understanding the principles of conductivity measurement and its limitations can help mills interpret the effect of high ion concentration on the papermaking processes. It will also help papermakers gain insight into issues associated with increased and changing conductivity for troubleshooting.

Xu is senior R&D scientist/engineer, WestRock, Richmond, VA, USA. Pruszynski is global technical specialist, Nalco Water, Naperville, IL, USA. Hart is director, Fiber Technology and Innovation, WestRock, Richmond, VA, USA. Email Hart at peter.hart@westrock.com.

Estimating limits of wet pressing on paper machines

By: J. DAVID MCDONALD AND RICHARD J. KEREKES

February, pp. 81-87 Water removal by wet pressing on paper machines depends on many factors such as press impulse, pressure, basis weight, equilibrium moisture, rewet, furnish, and fabric properties. These factors must be considered together to estimate wet pressing limits, such as the possibility of attaining 65% solids content on commercial paper machines. We have made such estimates employing the Decreasing Permeability Model (DPM) of wet pressing. This paper describes the utility of this approach and discusses some findings, such as the large dependence of low basis weight grades on equilibrium moisture content, maximum nip pressure, and rewet. The model also estimates the impact of basis weight, web temperature, double-felting, and incoming web solids on water removed.

Application: This study applied the DPM to quantify the factors that determine water removal in wet pressing, and in particular, factors to achieve high solids content. More generally, the DPM can be used to optimize existing presses and guide research and development towards the most cost effective ways to improve water removal.

McDonald is president, JDMcD Consulting Inc., Vaudreuil- Dorion, QC, Canada. Kerekes is professor emeritus, University of British Columbia, Vancouver, BC, Canada. Email McDonald at mcdonald.jdavid@gmail.com .

Finite element analysis of the thermal bending of a chilled cast thermo roll

By: THOMAS WIDMAIER, JUKKA PIRTTINIEMI, ESA PORKKA, PANU KIVILUOMA, and PETRI KUOSMANEN

June, pp. 345-357 A previously-created roll model based on the ultrasound measurements of a chilled cast iron thermo roll of a soft calender was used to create a finite element (FE) model of the same roll. The FE analysis was used to simulate the behavior of the roll when heated and in changing operating conditions. The main interest was to study the thermal bending of the roll model. The simulated behavior was consistent with known behavior of the thermo rolls in general, and when compared to actual measurements carried out in the calender, the results of the simulation showed similar behavior between the roll model and the actual roll. The main difference was in the absolute value of the bending, but the bending directions were practically the same. These results are promising for future research to develop methods to avoid or minimize the negative effects of the thermal deformations in thermo rolls.

Application: This paper discusses some of the phenomena caused by temperature changes in paper machine thermo rolls. The studied phenomena include mainly thermal deformations, i.e., bending. This study is relevant to finding the cause for some calender-related problems, including thermo rolls.

Widmaier is a post-doctoral research scientist, Kiviluoma is senior university lecturer, and Kuosmanen is professor in the Department of Mechanical Engineering, Aalto University School of Engineering, Aalto, Finland. Pirttiniemi is CEO and Porkka is chief engineer, Dynator Oy, Helsinki, Finland. Email Widmaier at Thomas.Widmaier@aalto.fi.

Modeling the influence of forming fabric structure on vacuum box dewatering
By: BJÖRN SJÖSTRAND, CHRISTOPHE BARBIER, and LARS NILSSON
August, pp. 477-483 This investigation used numerical models to describe forming section sheet dewatering at the high vacuum suction boxes. Three different fabric structures were examined with numerical models for single-phase flow of air and for two-phase flow of air and water. This was done to evaluate how forming fabric structure influences sheet dewatering. The numerical models were compared with an experimental study of the same fabrics investigated on a laboratory suction box. The small differences in dewatering rate in the experimental study could be simulated with the models, which confirmed the validity of the models. This implies that these numerical models can be used to describe new fabrics and how they will respond in the papermaking process.
Application: This article explains how numerical models can be used by manufacturers of paper machine clothing to obtain insights into how forming fabrics influence dewatering processes without investments in laboratory equipment and time-consuming experimental work.

Sjöstrand is a Ph.D. student and Nilsson is professor, Department of Engineering and Chemical Sciences, Karlstad University, Karlstad, Sweden. Barbier is paper physics specialist, R&D Gruvön, BillerudKorsnäs AB, Sweden. Email Sjöstrand at bjorn.sjostrand@kau.se .

Three-dimensional pore structure visualization and characterization of paper using X-ray computed tomography
By: YVES DEFRENNE, VASILI ZHDANKIN, SAHANA RAMANNA, SHRI RAMASWAMY, and BANDARU V. RAMARAO
September, pp. 519-530 Porous biomaterials such as paper and board have a complex structure that influences their mechanical, optical, and transport properties and thereby their performance during manufacturing and end uses. Reconstruction of the three-dimensional (3D) pore spaces in paper was obtained by X-ray computed tomography and used to study the structure and its impact on properties. A set of laboratory-made paper samples of varying freeness was prepared, and the 3D structures of the samples were visualized and characterized. Tomographic reconstruction images were processed using techniques such as anisotropic diffusion, minimum error thresholding, and isolated voxel removal to enhance image quality. The pore structures were analyzed to determine porosity, fiber-pore interfacial surface area, geometric tortuosity, and pore size distributions (using a sphere growing algorithm). These properties were compared with experimental data and were found to be in good agreement. The results from 3D visualization and characterization were then compared with experimental data of various samples using conventional pore structure characterization techniques, such as mercury intrusion porosimetry.
Application: Image processing techniques can help mills better understand the complex structure of porous biomaterials that influences properties and performance of manufactured products.

Defrenne is process engineer at Appvion Inc., Appleton, WI, USA. Zhdankin is staff engineer at Segate Technology, Shakopee, MN, USA. Ramanna is a doctoral candidate and Ramaswamy is a professor and head of the Department of Bioproducts and Biosystems Engineering, at the University of Minnesota, St. Paul, MN, USA. Ramarao is professor and director, Empire State Paper Research Institute, at the State University of New York College of Environmental Science and Forestry (SUNY-ESF), Syracuse, NY, USA. Email Ramaswamy at shri@umn.edu .

PROCESS CONTROL

Reduction of alkali loss in an ash leaching system

By: CARLA CÉLIA ROSA MEDEIROS, FLÁVIA AZEVEDO SILVA, SAULO GODOY PIGNATON, ESTANISLAU VICTOR ZUTAUTAS, and KLEVERSON FIGUEIREDO

July, pp. 383-391 There are many points in a kraft mill where the alkaline compounds are purged from the process. Several effluents, solid waste, and air emissions contain alkali, which leads to the necessity of chemical makeups to maintain the liquor balance. The main loss of alkali at the Veracel mill is present in the wastewater from the recovery boiler; more precisely, it is from the ash leaching system, which represents 80% of the total losses. To minimize the alkaline losses while keeping the chloride level in the recovery cycle under control, a project was developed at Veracel. Key actions were taken by adjusting the control loops of the ash leaching system, mainly on the slurry density and purge control. These adjustments led to a decrease in alkali losses and to an increase of treated ash, and kept the chloride level of the recovery boiler dust at 2.6%.

Application: This research demonstrates how alkaline losses can be reduced by automation solutions in the ash leaching system.

Medeiros is Recovery & Utilities (R&U) specialist; Silva is technical control manager; Pignaton is R&U technical assistant; and Zutautas is R&U technical coordinator, at Veracel Celulose S.A., Eunápolis, Brazil. Figueiredo is process optimization specialist, Andritz, Eunápolis, Brazil. Email Medeiros at carla.medeiros@veracel.com.br .

Understanding conductivity and soda loss

By: MICHAEL T. BROWN and PETER W. HART

February, pp. 65- 75 For more than 40 years, conductivity has been the inline measurement of choice for inferring black liquor/soda losses from brownstock washing. If properly applied, conductivity can provide a benefit in tracking changes in black liquor filtrate concentration. The implied concentration changes in turn can be used to provide feedback for dilution factor or shower flow control on the last stage of a brownstock washing system. A further extrapolation of this application is the correlation (or lack of correlation) of conductivity to soda loss. For each type of conductivity-based application, there are fundamental principles and assumptions that must be understood and managed to achieve the expected outcomes. The fundamentals of conductivity, the application of conductivity to measure black liquor losses during brownstock washing, and laboratory considerations when attempting to correlate inline process conductivity to absolute sodium content are reviewed and investigated. Finally, the operational objectives and measurement alternatives for employing conductivity measurements are discussed.

Application: Mills can gain knowledge about the theory, practice, and limitations associated with conductivity measurements, which can be used as a reliable feedback control mechanism for controlling brownstock washers.

Brown is chemical pulping specialist at WestRock, Norcross, GA, USA. Hart is director, fiber technology and innovation, WestRock, Atlanta, GA, USA. Email Hart at peter.hart@westrock.com .

PULPING

Determining wash loss levels in the brownstock pulp washing line using different methods

By: RIKU KOPRA AND OLLI DAHL

May, pp. 253-259 The purpose of brownstock pulp washing is to recover the maximum amount of dissolved inorganic and organic material using a minimal amount of water. Brownstock washing is a notable subprocess in chemical pulping because it has effects on the subsequent treatments of the pulp and is also the first step in the chemical recovery cycle. Without effective washing, the economic viability of chemical pulp production is affected. The performance of washing can be described in two main ways: using wash loss, which describes the amount of washable compounds in the pulp suspension that could have been removed in washing; or the dilution factor, which represents the net amount of water that is added during washing. The amount of sodium in the pulp suspension after washing has typically been used as an indicator of wash loss, usually expressed as kg sodium sulfate/ovendry ton of washed pulp. Other common measurement methods are conductivity, chemical oxygen demand (COD), total organic carbon (TOC), dissolved dry solids (DDS), and lignin concentration. Scandinavian pulp mill softwood and hardwood fiber lines were investigated using various measurement methods in the pulp phases to gain better understanding of wash loss. The concentration of DDS in the streams was measured using a refractometer and laboratory scale. The pH, conductivity, lignin content, TOC, and COD were measured to look for any correlations. Using different methods, the level differences remain constant, but it is difficult to control the washing process with sufficient precision using individual measurements. The measurement methods must also be continuous and reliable to be used to monitor and control washing.

Application: Proper measurement techniques can help mills detect a wash line's problem areas; predict wash efficiency in real-time; and control washers' operation, water usage, and chemical consumption, which have a direct impact on the economics of other processes.

Kopra is RDI scientist at the Fiber Laboratory, South-Eastern Finland University of Applied Sciences, Savonlinna, Finland. Dahl is a professor at Aalto University School of Chemical Engineering, Department of Bioproducts and Biosystems, Clean Technologies Research Group, Espoo, Finland. Email Kopra at Riku.kopra@xamk.fi .

Impact of dissolved matter in the oxygen delignification stage

By: CAROLINE WILKE, NICLAS ANDERSSON, AND ULF GERMGÅRD

May, pp. 275-284 The presence of dissolved matter in the pulp suspension in an oxygen (O_2) delignification stage, consisting mainly of dissolved lignin, is normally considered to negatively affect the delignification rate due to the competing reactions between the fiber bound lignin and the lignin dissolved in the filtrate. Recirculated oxidized filtrate from the post-O_2 washing is usually considered to be less harmful to the delignification efficiency than unoxidized dissolved matter originating from the cooking stage. To develop a better understanding of the mechanisms of the dissolved matter's reactions and impact on the O_2 stage performance, laboratory oxygen delignification experiments with varying levels of unoxidized and oxidized dissolved matter were conducted. The results showed that unoxidized dissolved matter had a negative impact on the delignification in the O_2 stage, whereas oxidized dissolved matter actually had a positive effect. The delignification efficiency of the laboratory experiments thus depends on both the amount of dissolved matter and its origin. The pulp viscosity decreased with increasing dissolved matter content irrespective of its origin but at higher COD levels; however, the viscosity drop was larger for the unoxidized dissolved matter. In terms of selectivity, the oxidized filtrate had a

similar impact as additional NaOH charge. Both types of filtrates consumed hydroxide and the final pH decreased with increasing dissolved matter content. The final pH was significantly lower in the unoxidized filtrate experiments at higher COD levels, indicating a high reactivity between the unoxidized dissolved matter and the oxygen in the reactor. Based on the results, further understanding is achieved about the relation between pre-O_2 washing performance and process configuration in an actual mill case, as well as the impact of dissolved matter on delignification. The importance of efficient removal of harmful unoxidized dissolved matter is verified, but the results also suggest that the oxidized dissolved matter that is recirculated from post-O_2 washing actually has a significant positive impact on the delignification and is not just a potential problem in case of carryover to the bleach plant. Subsequently, pulp washing efficiency is critical both pre- and post-O_2.

Application: The results from the study reinforce the importance of well-performing brownstock washing to minimize the carryover of unoxidized dissolved matter from the cooking stage. However, because the oxidized post- O_2 filtrate actually has a significant positive impact when recirculated, this can be exploited to improve delignification and reduce alkali consumption in the O_2 stage. Subsequently, optimum operation of pre- and post-O_2 washers will depend on the mill's washer configuration.

Wilke is development engineer at BTG Instruments AB, Säffle, Sweden, and post-graduate student at Karlstad University in Karlstad, Sweden. Andersson is head of R&D and Business Development at BTG Instruments AB, Säffle, Sweden. Germgård is professor of Pulp Technology at Karlstad University, Karlstad, Sweden. Email Wilke at caroline.wilke@btg.com .

In-process detection of fiber cutting in low consistency refining based on measurement of forces on refiner bars

By: R. HARIRFOROUSH, J. OLSON, and P. WILD

April, pp. 189-199 A major drawback of low consistency refining is the degradation of mechanical properties due to fiber cutting at high refining energies. Conventional strategies to avoid fiber cutting are based on post-refining measurement of pulp properties and, typically, this does not enable rapid adjustment of refiner operation in response to the onset of fiber cutting. The objective of this study is to detect the onset of fiber cutting by using custom-designed piezoelectric force sensors that measure shear and normal forces applied to pulp fibers by the refiner bars. Trials are performed in an AIKAWA/Advanced Fiber Technologies Inc. 16-in. single-disc low consistency refiner. The trials are run using mechanical softwood SPF (spruce, pine, and fir) pulp with 378 ml CSF at 2.5% and 3.5% consistency at rotational speeds of 800 rpm, 1000 rpm, and 1200 rpm. Distributions of the peak normal and shear forces and peak coefficient of friction are determined for each operating condition, and a two-parameter Weibull function is fit to each of these distributions. The scale parameter, which is one of the key parameters of the Weibull function, is calculated, and length-weighted fiber length is plotted as a function of this parameter. The results show that the onset of fiber cutting consistently corresponds to a distinct transition in the plot of length-weighted fiber length versus scale parameter. This transition is believed to be caused by a fundamental transition in the fiber-bar interaction. Moreover, frequency analysis of the sensor data shows that the magnitude of the dominant frequency remains relatively constant while the plate gap is reduced, up to a threshold value, which corresponds to the onset of fiber cutting. These results suggest that these sensors have potential to be used for in-process detection of the onset of fiber cutting.

Application: The application of this study is in-process detection of fiber cutting in low-consistency mechanical refining.

Harirforoush is a Ph.D. candidate in the Department of Mechanical Engineering and the Institute for Integrated Energy Systems (IESVic), and Wild is professor of Mechanical Engineering and director of IESVic, at the University of Victoria, Victoria, BC, Canada. Olson is associate dean of Research and Industrial Partnership, Faculty of Applied Science; professor of Mechanical Engineering; and FPInnovations professor at the University of British Columbia – Point Grey Campus, Vancouver, BC, Canada. Email Harirforoush at rharirfo@uvic.ca .

Low consistency refining of mechanical pulp — system design

By: CHRISTER SANDBERG, JAN-ERIK BERG, and PER ENGSTRAND

July, pp. 419-429 Many mechanical pulping mills use low consistency (LC) refining for energy efficient fiber development. In this study, energy efficiency and pulp quality were evaluated for six processes, of which four included LC refining. We studied two different types of chip refiners – single disc (SD) and double disc (DD) – with LC refining in the main and reject lines. All process combinations have been used in the Holmen Paper Braviken mill, Sweden, to make thermomechanical pulp for printing papers. LC refining was more energy efficient than high consistency (HC) refining at certain tensile index increases in all evaluated combinations. LC refining in the main line had somewhat higher energy efficiency than did LC refining in the reject line. The type of chip refiner (DD or SD) did not affect the efficiency or pulp property development in LC refining. The process with a combination of DD chip refining and LC refining had the highest energy efficiency (tensile index at certain specific energy consumption). All processes with LC refining produced pulp with somewhat lower light scattering and fiber length than did the corresponding system with only HC refining. Thus, for printing papers, the best combination was LC refining with DD chip refining. LC refiners seem to have a narrow range in specific energy for maximum energy efficiency and a good balance between tensile index increase and fiber length reduction. Much higher specific energy was applied on reject pulp. However, the reject share was only around 30%. The LC refining specific energy, based on main line production, was around 80 kWh/air-dried metric ton (a.d. metric ton), whereas up to 180 kWh/a.d. metric ton was applied in main line.

Application: LC refining can improve the process efficiency for mechanical pulping, but it is important to optimize HC and LC refining together to achieve the best combination of pulp quality and energy efficiency.

Sandberg is R&D specialist (part-time), Holmen Paper, Norrkoping, Sweden, and project manager (part-time), Mid Sweden University, Sundsvall, Sweden. Berg is project secretary and researcher, Fiber Science and Communication Network (FSCN), Mid Sweden University, Sundsvall, Sweden. Engstrand is professor, FSCN, Mid Sweden University, Sundsvall, Sweden. Email Sandberg at christer.sandberg@holmenpaper.com.

RECOVERY CYCLE

Formation mechanisms of "jellyroll" smelt in kraft recovery boilers

By: HONGHI TRAN and ANDREW K. JONES

October, pp. 597-606 Molten smelt normally flows smoothly down the smelt spout of a recovery boiler like water, but at times it suddenly becomes sluggish and forms a viscous blob on

the spout trough that partially or completely blocks the smelt flow. This form of smelt is commonly referred to as "*jellyroll*" smelt. How such smelt forms has been a puzzle to boiler operators and mill personnel for years. Numerous mill observations and the results of a recent study performed on both smoothly flowing smelt and jellyroll smelt collected from a recovery boiler suggest that that jellyroll smelt can form through three main mechanisms: i) the freezing of the molten smelt, ii) the melting of fallen deposits, and iii) the inclusion of a large amount of unburned char in the molten smelt. These mechanisms are consistent with mill experience that jellyroll smelt tends to form in older recovery boilers burning liquor with low solids and low sulfidity.

Application: This paper discusses three mechanisms through which jellyroll smelt forms and provides operating strategies for minimizing jellyroll smelt formation.

Tran is Frank Dottori Professor of Pulp & Paper Engineering, Department of Chemical Engineering & Applied Chemistry, at the University of Toronto, Toronto, ON, Canada. Jones is senior engineering fellow at International Paper, Loveland, OH, USA. Email Tran at honghi.tran@utoronto.ca .

RECYCLING

Deinking process water flotation: An innovative solution to improve deinking and papermaking processes efficiency

By: THIERRY DELAGOUTTE, BRUNO CARRÉ, and ELISA ZENO

November, pp. 645-652 High and uncontrolled surface active substances (SAS) concentrations in deinking line process waters strongly disturb flotation deinking. Indeed, their adsorption at air/water and ink/water interfaces stabilizes air bubbles and ink particles, reducing ink collection during flotation. In addition, foam stabilization promoted by SAS reduces froth drainage and consequently enhances suspended solids losses. All in all, selectivity of flotation is negatively affected by excessive SAS concentrations. Floating process water with adapted technology, a patented solution, is an efficient way to decrease SAS concentration and thereby recover flotation deinking selectivity. This concept was tested at industrial scale with success. First loop clear filtrates of a deinked pulp line (for newsprint production) were floated. At steady state, this treatment allows a 20% reduction of the SAS concentration in first loop process water. Evaluation of ink removal selectivity at pre-flotation and post-flotation showed a significant improvement in comparison with reference values. During the trial, the mill could either produce pulp with lower ink content and consequently higher brightness (50 ppm effective residual ink concentration [ERIC] less, corresponding to a 1 brightness point increase) for similar losses, or similar pulp quality with 1% to 2% yield improvement, representing a huge cost reduction. In addition, beneficial side effects were reported, such as reduced deinking chemicals consumption (soda, silicate, and bleaching agents) and better paper machine runnability, especially in terms of stickies breaks.

Application: Mills might be able to increase brightness or yield in their deinking line using the process described here.

Delagoutte and Zeno are research engineers and Carré is team manager at the Centre Technique du Papier (CTP), Grenoble, France. Email Delagoutte at Thierry.Delagoutte@webctp.com .

Effect of surface treatment with biodegradable materials on properties of linerboard made from old corrugated containers (OCC)

By: SOMAYEH HEYDARI, AHMAD REZA SARAEYAN, and ALIREZA SHAKERI

September, pp. 535-541 Linerboard produced from old corrugated containers (OCC) shows lower strength properties in comparison with linerboard produced from virgin fibers. This study determined the influence of surface treatment with polyvinyl alcohol (PVOH), ethylene vinyl alcohol (EVOH) (as synthesized biodegradable polymers), chitosan, and anionic starch (as biobased and biodegradable polymers) on properties of sheets produced from OCC. The polymers were applied from aqueous biodegradable dispersion, by using a laboratory-scale coater. This research investigated the burst index, tensile index, stiffness, water resistance, air resistance, and water absorption. The results showed that paper surfaces treated with water-soluble polymers increased the mechanical properties. In addition, PVOH increased the burst index value 136% and EVOH increased the tensile index, tear index, and stiffness values by 84.3%, 108.6%, and 22.43%, respectively. The anionic starch increased air resistance to 34.7% and chitosan decreased water absorption to 12.3%.

Application: Surface treatments with biopolymers can increase the strength properties of linerboard produced from old corrugated containers.

Wood and Paper Engineering, Gorgan University of Agricultural Sciences and Natural Resources, Gorgan, Iran. Shakeri is an associate professor of polymer engineering in the School of Chemistry, University of Tehran, Tehran, Iran. Email Heydari at somayeh_heydari88@yahoo.com .

Fractional pulping of packaging board in high consistency drum pulping

By: HEIKKI UPOLA, ARI ÄMMÄLÄ, and MIRJA ILLIKAINEN

February, pp. 89-95 A wide variety of packaging materials with different wetting rates and wet strength properties are used in old corrugated container (OCC) processing. The disintegration rates of the different grades also vary and enable the use of the fractional pulping concept where easily disintegrated material is removed at the early stages. In the present study, fractional drum pulping was studied by pulping (Pilot drum pulping) and fractionating (Tampella oscillating screen) a mixture of strong-grade kraftliner and weak-grade fluting at high consistency to determine if energy consumption could be reduced. The results showed that a 25% energy saving could be realized through fractional pulping and an even higher potential might be possible if pulping conditions are optimized. Average fiber length, fines content, and ash content in the separated fractions were analyzed. The separated short fiber fractions and long fiber fractions could be individually processed, thus decreasing the volumes in the unit processes on the OCC line.

Application: Mills can increase capacity and improve energy savings in OCC recycling processes.

Upola is a doctoral student, Ämmälä is an adjunct professor, and Illikainen is a professor at the University of Oulu, Oulu, Finland. Email Upola at heikki.upola@oulu.fi.

How old are fibers in paper for recycling and what is their life expectancy? A contribution to the life cycle assessment of wood fiber-based products

By: GERT MEINL, LYDIA TEMPEL, MIKE SCHIEFER, and CONSTANZE SEIDEMANN

July, pp. 397-405 Mean fiber age (i.e., the mean number of production cycles that fibers in a given paper material have undergone so far) can be calculated theoretically on the basis of mass flows in a given paper recycling loop. Mean fiber age distributions can be calculated in multiple, connected recycling loop systems, which are typical of countries and regions with high recovered paper utilization and recycling rates. The calculation uses a graph theory approach. The same approach shows there is a second important value that highlights another aspect of the circular economy – the number of future material uses. This value quantifies how often the fibers in a given paper product will be used on average till their end of life. Put simply, the fiber age describes the past and the number of future material uses describes the future of the fibers in a paper or board product. Calculated results for the European region are presented and compared for fiber age and number of future material uses. Both values add up to a total number of material uses and should be used together.

Application: Mills will have information for comparing resource efficiency of their wood fiber-based paper products with those of other mills and other sectors. This will help solve allocation problems in life cycle assessment.

Meinl, Tempel, Schiefer, and Seidemann are scientists at Papiertechnische Stiftung, Munich, Germany. Email Meinl at gert.meinl@ptspaper.de .

Improved deinking and stickies removal

By: CESAR BASILIO

November, pp. 639-642 Previous work had shown that a novel flotation deinking reagent using modified kaolin was able to more efficiently separate and remove ink and dirt particles from recovered paper. The mechanism for this reagent is based on the ability of the modified kaolin to act as a collector for the fine ink, dirt, and contaminant particles. Deinking mills using this reagent experienced deinked pulp with an increase in brightness and lower dirt count values. Further work has been carried out to determine whether this mechanism can be used to improve the removal of stickies in recovered pulp. Test results showed that use of this modified kaolin together with a reagent capable of effectively separating the sticky contaminants from the fiber improved the removal of stickies. The synergy of this reagent with the modified kaolin further improved ink and dirt removal.

Application: Mills can take advantage of this technology to help handle their stickies issues.

Basilio is group leader at Thiele Kaolin Company, Sandersville, GA, USA. Email Basilio at cesar.basilio@thielekaolin.com .

New automated method for macrocontaminant analysis: Industrial applications

By: SYLVIE OSSARD, PATRICK HUBER, PASCAL BOREL, DAVY SOYSOUVANH, and THIERRY DELAGOUTTE

November, pp. 623-631 In recycled paper processes, stickies are the origin of many production disturbances. In this paper, we present how the recently developed method for macrocontaminant analysis was used with industrial samples for process analysis. The new automated stickies measurement method allows (i) determination of the threedimensional (3D) morphology of screened particles (without any deformation) and (ii) classification of the particles as stickies among contaminants. This is achieved by a combination of laser triangulation and local near-

infrared spectroscopy (NIR). Measurement of macrocontaminants in pulp samples and their classification allow meaningful evaluation of their specific removal. Chemical nature and amount of the macrocontaminants coming from different raw materials were studied and were shown to be very different in two different mills. In an Asian mill, a low removal of pressuresensitive adhesives (PSAs) in the process (46%) was found in comparison with high removal of other stickies (99%). Applications of this device are shown, while the new on-line sensor for macrocontaminant analysis is being developed.

Application: This study demonstrates how mills can analyze stickies removal throughout the recycling process. As a consequence, they could control the process depending on the chemical nature of incoming stickies contamination.

Ossard, Huber, Borel, and Delagoutte are project engineers and Soysouvanh is team leader at the Centre Technique du Papier (CTP), Grenoble, France. Email Huber at Patrick.Huber@webCTP.com .

TISSUE

Visual discrimination of hygiene tissue softness in the absence of haptic feedback

By: JESSICA CARETTE, PIERRE-MAJORIQUE LEGER, and SYLVAIN SENECAL

August, pp. 439-449 Our perception of the softness of materials is dominated by the subjective interpretation of haptic stimuli — touch. Although softness is defined by the way a material deforms when force is applied, other sensorial inputs, such as vision and hearing, can be used to complement haptic feedback or when the material cannot be touched. Surface and bulk softness elements of hygiene tissue, such as surface roughness, embossing pattern, and bulk can be assessed visually. Softness is reported as the number one desired quality of hygiene tissue. So, it is of paramount importance to understand the criteria a consumer uses to judge softness visually. Consumers must rely on these other non-tactile senses at point-of-purchase or in e-commerce because they cannot interact with a product to judge the softness. This study proposes that a consumer can accurately gauge softness by sight alone, and that factors such as color tone, embossing, and image quality all affect the perception of softness. Stiffness and mechanical properties of the sheet cannot be observed by eye and can contribute to errors in visual judgement. We conducted an experiment using a complete pair ratio (round-robin) type comparison to evaluate the perceived softness of altered images of hygiene tissue with unaltered images. Images of hygiene tissue were altered to represent different lighting conditions or product color and digital image degradation. Our results suggest that yellow hygiene tissue is perceived as less soft than blue, and un-embossed tissue as less soft that embossed tissue. Reducing the image resolution to 10% of the original did not negatively affect the perception of softness.

Application: In product development, color and embossing pattern can be manipulated to influence the consumer's perception of product softness. Images displayed digitally can be optimized in a similar manner.

Carette is innovation manager, Cascades Tissue Group, Candiac, QC, Canada, and a former MBA student at HEC Montréal, Montréal, QC, Canada. Léger is professor, Department of Information Technologies, and Sénécal is professor, Department of Marketing, at HEC Montréal, Montréal, QC, Canada. Email Carette at jessica_carette@cascades.com .

WASTEWATER TREATMENT

Degradation of 2,4-dichlorophenol by melamine amine celluloseimmobilized lacasses

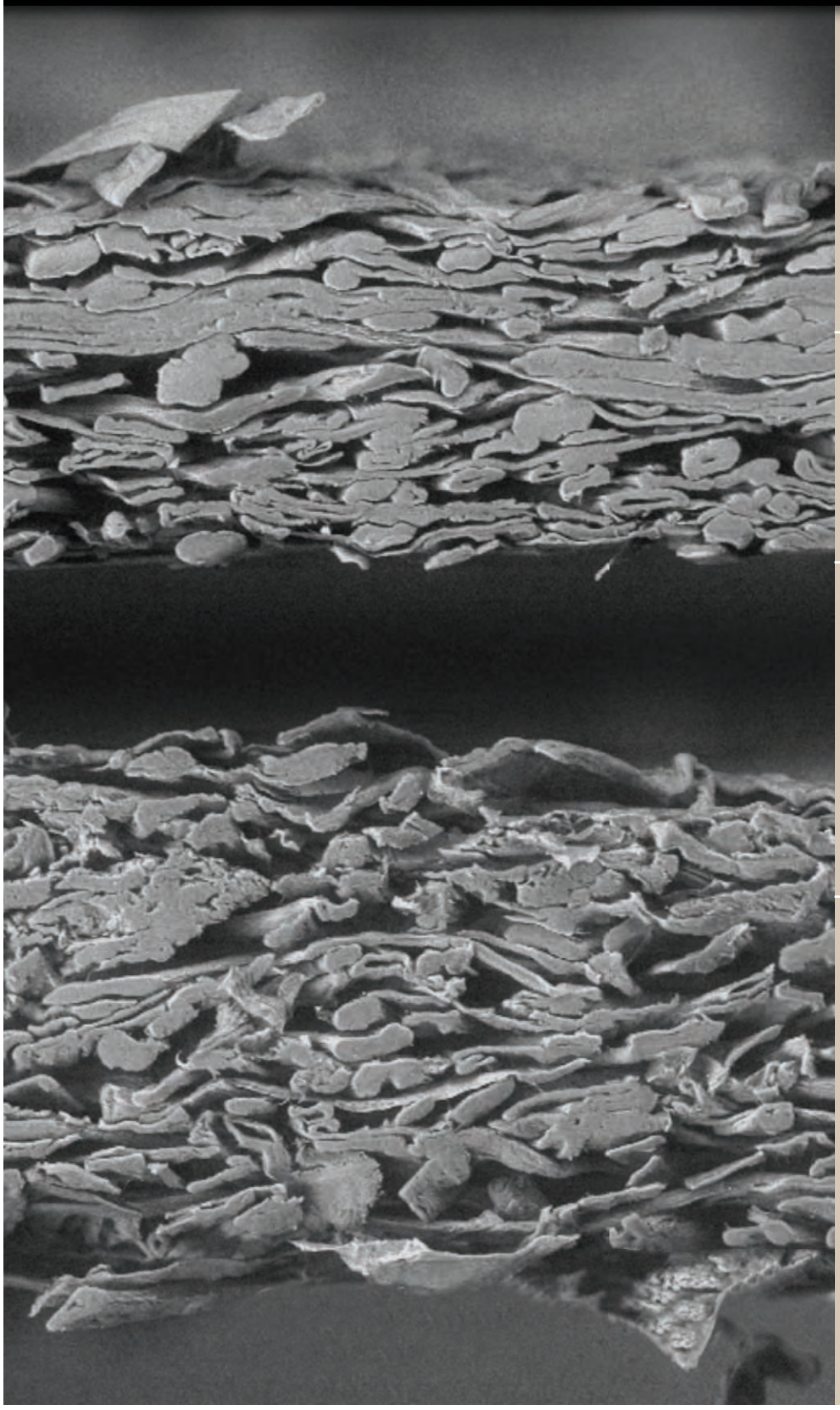
By: ZHEN WANG, PINGPING BIN, YING LIU, YU LIU, GUIHUA YANG, and LUCIAN LUCIA

October, pp.559-564 Epoxidized dialdehyde cellulose (EDC) was prepared and grafted with melamine to obtain melamine grafted epoxidized dialdehyde cellulose (EDC-melamine); the products were characterized by various methods and were used as carriers to immobilize laccase. Results show EDC-melamine can immobilize laccase effectively and have higher enzymatic activity compared with EDC. Furthermore, the enzymatic activity of EDC-melamine was found to be as high as 865 U•mg-1, compared with 140U•mg^{-1} for EDC. The removal efficiency of 2,4 dichlorophenol (2,4-DCP) for EDC-melamine immobilized laccase was about 71.5% at 40°C for 4 h at 10.0 mg•L^{-1} and dosage of laccase = 0.2 g/L. The removal efficiency can remain greater than 63%, even after six cycles.

Application: This topic provides a new method to immobilize laccases. The product can be used to treat wastewater polluted by phenol and shows excellent performance.

Wang is professor and director of Environmental Science, School of Environmental Science and Technology; Bin and Ying Liu are M.S. students; and Yu Liu and Yang are professors at the Key Laboratory of Pulp & Paper Science and Technology, Ministry of Education, Qilu University of Technology, in Jinan, Shandong, China. Lucia is associate professor, Department of Forest Biomaterials, North Carolina State University, Raleigh, NC, USA, and is also distinguished professor of Green Chemistry for Qilu University of Technology. Email Wang at wangzhenyft@126.com .

TAPPI JOURNAL
WWW.TAPPI.ORG
THE PAPER AND PACKAGING INDUSTRIES' TECHNICAL RESOURCE
JANUARY 2017 | VOL. 16 NO.1



NANOTECHNOLOGY 9
Physical handsheet properties of pulp furnishes containing attritor-treated fibers
David E. Knox, Peter W. Hart, Humphrey J. Moynihan, and Nichole M. Kilgore

NONWOOD PULPING 17
Removal of silicon from green liquor with low-temperature precausticizing
Xinxing Xia, Fang Wang, Shan Sun, and Qian Hu

NANOTECHNOLOGY 25
Paper coated with sonochemically synthesized zinc oxide nanoparticles: Enhancement of properties for preservation of documents
Suchismita Majumdar, Anirban Roy, Isita Nandi, Prantik Banerjee, Swapna Banerjee, Mahua Ghosh, and Sampa Chakrabarti

BIOREFINERY 37
Cellulosic ethanol byproducts as a bulking agent
J.M. Considine, D. Coffin, J.Y. Zhu, D.H. Mann, and X. Tang

January 2017

TABLE OF CONTENTS VOL. 16 NO. 1

5 **EDITORIAL**
Planning for 2017 PEERS Conference: Maximizing success through innovation
Brian N. Brogdon and Mark Lebel

9 **NANOTECHNOLOGY**
Physical handsheet properties of pulp furnishes containing attritor-treated fibers
David E. Knox, Peter W. Hart, Humphrey J. Moynihan, and Nichole M. Kilgore

17 **NONWOOD PULPING**
Removal of silicon from green liquor with low-temperature precausticizing
Xinxing Xia, Fang Wang, Shan Sun, and Qian Hu

25 **NANOTECHNOLOGY**
Paper coated with sonochemically synthesized zinc oxide nanoparticles: Enhancement of properties for preservation of documents
Suchismita Majumdar, Anirban Roy, Isita Nandi, Prantik Banerjee, Swapna Banerjee, Mahua Ghosh, and Sampa Chakrabarti

37 **BIOREFINERY**
Cellulosic ethanol byproducts as a bulking agent
J.M. Considine, D. Coffin, J.Y. Zhu, D.H. Mann, and X. Tang

»COVER CREDIT: SEM images of softwood pulp-based handsheets made with 20% attritor-treated fibers (bottom) appeared noticeably thicker (less dense) than the untreated control handsheets (top) in research by Knox et al. (p. 9).

TAPPI JOURNAL
WWW.TAPPI.ORG

Editor-in-Chief
Scott Rosencrance scott.rosencrance@kemira.com
+1 770 429-2753

Associate Editor
Brian N. Brogdon brian.brogdon@gmail.com
+1 678 581-9114

Editorial Director
Monica Shaw mshaw@tappi.org
+1 770 367-9534

Vice President, Operations
Eric Fletty efletty@tappi.org

PRESS Manager
Jana Jensen jjenson@tappi.org
+1 770 209-7242

Webmaster
Trina Heath theath@tappi.org
+1 770 209-7416

***TJ* EDITORIAL BOARD**

Brian N. Brogdon, FutureBridge Consulting & Training LLC
brian.brogdon@gmail.com, +1 678 581-9114

David A. Carlson, Carlson Consulting
dacarlson39@aol.com, +1 847 323-2685

Jere W. Crouse, JWC Consulting
cj522@inwave.com, +1 608 362-4485

Mahendra Doshi, Doshi and Associates
mahen@aol.com, +1 920 832-9101

Marc Foulger, GL&V USA Inc.
Marc.foulger@glv.com +1 315 767-2920

Peter W. Hart, MeadWestvaco Corporation
pwh3@meadwestvaco.com, +1 409 276-3465

Carl J. Houtman, USDA Forest Products Laboratory
choutman@fs.fed.us, + 1 608 231-9445

John A. Neun, Albany International
John.Neun@albint.com, +1 518 275-8139

Jim Niemiec, Verso Corporation
jim.niemiec@versoco.com, +1 715 422-7404

Steven P. Ottone, Omya
steven.ottone@omya.com, +1 919 641-7854

Gaurav Pranami, Imbed Biosciences
gpranami@imbedbio.com, +1 515 230-7005

Arthur Ragauskas, Oak Ridge National Laboratory
aragausk@utk.edu

Gerard J.F. Ring, University of Wisconsin—Stevens Point
gerrryring@wi-net.com, +1 715 592-3732

Scott Rosencrance, Kemira Chemicals
scott.rosencrance@kemira.com, +1 770 429-2753

Ricardo B. Santos, MeadWestvaco Corporation
ricardo.santos@mwv.com, +1 540 969-2426

Paul Wiegand, NCASI
pwiegand@ncasi.org, +1 919 941-6417

Junyong Zhu, USDA Forest Products Laboratory
jzhu@fs.fed.us, +1 608 231-9520

Join TAPPI *today!*

TAPPI JOURNAL is a free benefit of TAPPI membership, and is only available to members. To join TAPPI, to renew your TAPPI Membership, or to learn about other valuable benefits, visit www.tappi.org.

TAPPI, 15 Technology Parkway S., Suite 115, Peachtree Corners, GA 30092, publishes *TAPPI JOURNAL* monthly.

ATTENTION PROSPECTIVE AUTHORS: All papers published are subject to *TAPPI JOURNAL's* peer-review process. Not all papers accepted for review will be published. Before submitting, check complete author guidelines at http://www.tappi.org/s_tappi/doc.asp?CID=100&DID=552877.

Statements of fact and opinions expressed are those of individual authors. TAPPI assumes no responsibility for such statements and opinions. TAPPI does not intend such statements and opinions or construe them as a solicitation of or suggestion for any agreed-upon course of conduct or concerted action of any sort.

Copyright 2017 by TAPPI, all rights reserved. For copyright permission to photocopy pages from this publication for internal or personal use, contact Copyright Clearance Center, Inc. (CCC) via their website: www.copyright.com. If you have questions about the copyright permission request process, please contact CCC by phone at +1 978 750-8400. To obtain copyright permission to use excerpts from this publication in another published work, send your specific request in writing to Editor, TAPPI JOURNAL, 15 Technology Parkway S., Suite 115, Peachtree Corners, GA 30092, USA; or by fax to +1 770 446-6947. Send address changes to TAPPI, 15 Technology Parkway S., Suite 115, Peachtree Corners, GA 30092, USA; Telephone +1 770 446-1400, or FAX +1 770 446-6947. www.tappi.org

Physical handsheet properties of pulp furnishes containing attritor-treated fibers

DAVID E. KNOX, PETER W. HART, HUMPHREY J. MOYNIHAN, AND NICHOLE M. KILGORE

ABSTRACT: Several articles have been published during the past 30 years on different methods to produce micro- to nanosize cellulose particles from pulp. Unfortunately, a general lack of information exists on the impact of differing manufacturing process methods upon the product properties obtained from these differing methods. Literature data show that wet processing of small-sized cellulosic fibers generates handsheets with approximately equal or higher density and modulus of elasticity than controls for a given amount of added microcellulose. The current work evaluated small particle generation from pulp fibers via dry processing methods and compared the physical properties of dry versus wet processed particles. Dry processing to obtain microcellulose gave considerably lower sheet density and modulus as compared with wet processed microcellulose. The lower modulus can be compensated for by refining base fibers more aggressively to obtain higher density and higher modulus sheets. Dry processing methods for making microcellulose and their impact on final board properties, including modulus and smoothness, will be discussed.

Application: The impact of attritor-processed fiber on handsheet physical properties might have potential for commercial applications.

Ball milling of cellulosic fibers has historically been performed as a method to change the crystalline structure of cellulose [1]. Later work determined that changes in the cellulose crystal structure could be accomplished with or without enzymatic or chemical pre- or cotreatments [2]. These treatments were designed to accelerate the desired changes in crystalline structure and to deconstruct cellulose-based fiber and wood to analyze their chemical constituents. More recently, research has focused upon enzymatic-assisted ball milling deconstruction of fibers to make the cellulose more reactive toward fermentation for biorefinery applications [2–7]. Milling of cellulose has also been claimed to be a scalable method of obtaining nanocellulose from aqueous solutions [8,9]. Ball milling imparts significant amounts of energy into the fibers or wood being studied, resulting in an alteration of the cell wall components. Because the cell wall components are modified during processing, direct ball milling is not necessarily a suitable method for obtaining pure lignocellulosic components of the cell wall. However, ball milling can be a useful analytical method when combined with other analytical methods. The amount of chemical degradation or other physical transformations that occurs during ball milling is often cited as part of experimental studies. For the current work, ball milled fibers resulting in effects on board properties will be reported, not specific fiber modifications resulting from the ball milling process.

Previous research has been done on ball milling of fibers to elucidate chemical and structural issues related to different wood species. These types of data may provide future collaborative information, which supports how these materials behave in product applications related to paperboard [10,11]. In this light, it is essential to understand that while fundamental aspects of cellulose fiber milling are known, board based applications of the cellulose from this process have not been fully explored. Wood flour applications in paperboard have been examined [11]; however, to the extent that the wood flour is generally provided as an unbleached residual material at a relatively large particle size, wood flour is not directly of interest with respect to bleached board where high brightness materials would be needed. Wood flour has been semi-bleached to reasonable brightness levels, but the incorporation of a secondary wood flour bleaching process into a mill would not likely be economical.

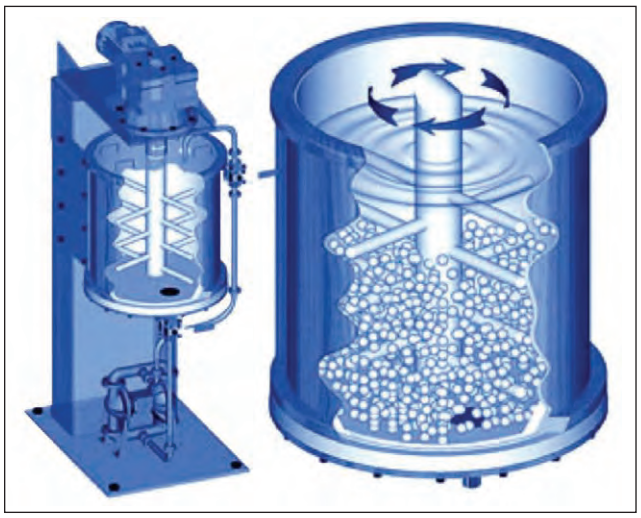
The current study examines the role of dry pulverized pulp fibers in the production of lower density bleached board. Our focus on dry grinding was driven by previous work in wet grinding of cellulosic fibers to micro- and nanosize materials, which imparted well-known effects such as drainage reduction, board densification, and material handling problems. Our purpose is not to discuss many of the relevant factors of pre- and primary mechanical treatments on fibers. Recent work has attempted to categorize several factors of importance [12,13].

Preparation of attritor-treated fibers

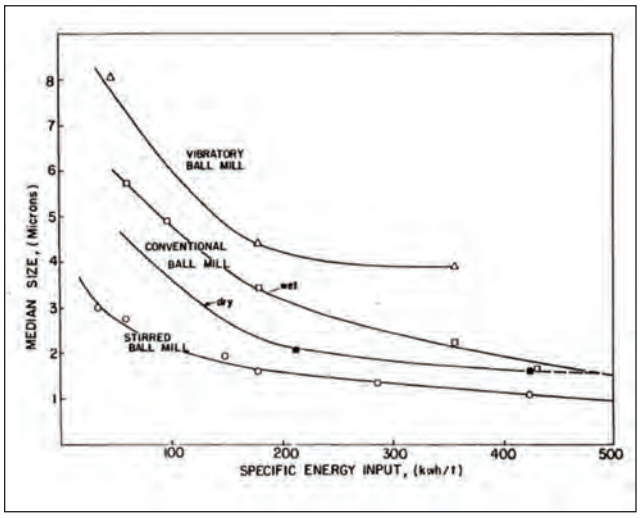
The current work used attritor-based technology for dry grinding of cellulose fibers. Attritor-treated pulp fibers were prepared using stirred ball mill devices from Union Process Inc., Akron, OH, USA. A diagram of the basic attritor unit used in this study is shown in **Fig. 1**.

Several key variables for use of attritors include shaft rotation speed; rod size, angle and geometry; grinding ball size; grinding temperature; and input power. Many attritors are equipped with temperature control, but for the attrition of cellulose in this study, we allowed the mechanical energy of the attritor to raise the temperature of the system and did not attempt to thermostatically control the system temperature.

The efficiency of particle size reduction for a given specific energy input for an attritor as compared with other types of ball mills is shown **Fig. 2** for the ultrafine girding of copper ore concentrates (chalcopyrite) [14]. While Fig. 2 illustrates that attritors are designed to handle and pulverize materials in the smaller size ranges (i.e., 1–2 μm or less), they are available for milling of cellulosic materials if the appropriate sized material is introduced into the devices.



1. Schematic of attritor used for micronizing cellulose.



2. Comparative particle size reduction for attritor (stirred ball) versus ball milling.

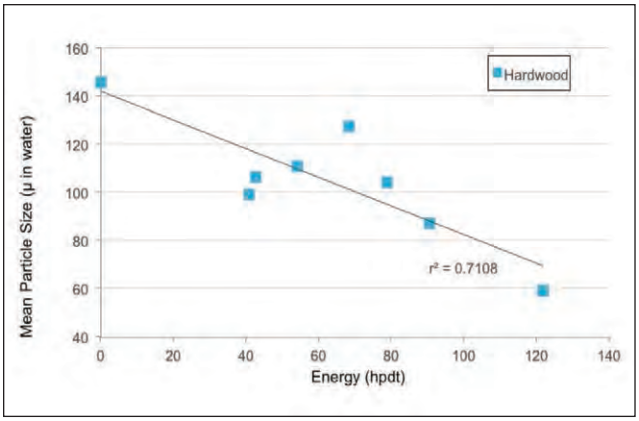
Attritors are used for the production of ultrafine pigments for paints, pyrotechnics, and fine-powder metal applications, including catalysts. Additional information regarding attritor operation variables, as well as how attritors differ from other grinding devices (e.g., vibrator ball mills), is available [15].

Attritors may be run in batch, semibatch, or continuous modes, depending on the applications. For the current work, cellulosic pulp fibers were prepared in semicontinuous mode with a pulp flake of 3/4 in. x 3/4 in. being added to the attritor for a given period (usually 15 min), allowing the resultant powder to be sieved through the bottom opening. The pulp powder was then weighed and a corresponding amount of additional pulp flake was added to the unit.

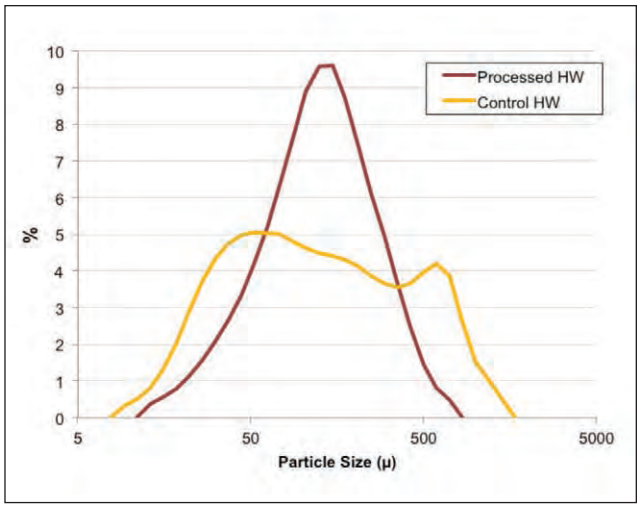
All work was conducted at nearly 100% (nominal) solids. Because of the energy imparted to the pulp during the attrition process, the unit would generally heat to >115°C, so it was anticipated that except for tenaciously bound water, all the residual moisture would be evaporated.

Figure 3 shows the correlation between energy input in the attritor and the particle size reduction of a commercial once-dried hardwood market pulp. No dispersants were added during measurement of the particle size distribution, so agglomeration tendencies may be greater than what is sometimes seen in protocols where dispersants are added before measurement. A relatively good correlation was obtained for the particle size range shown with higher energy input resulting in smaller materials. Some deviation was noted in these semicontinuous experiments. These deviations could be related to agglomeration during particle size analysis or to minor variations in the semicontinuous experimental protocol. In general, these results suggest that one can very likely tailor the energy inputs to a desired particle size and then use that particle for building a board product, depending on paper machine dynamics and product requirements.

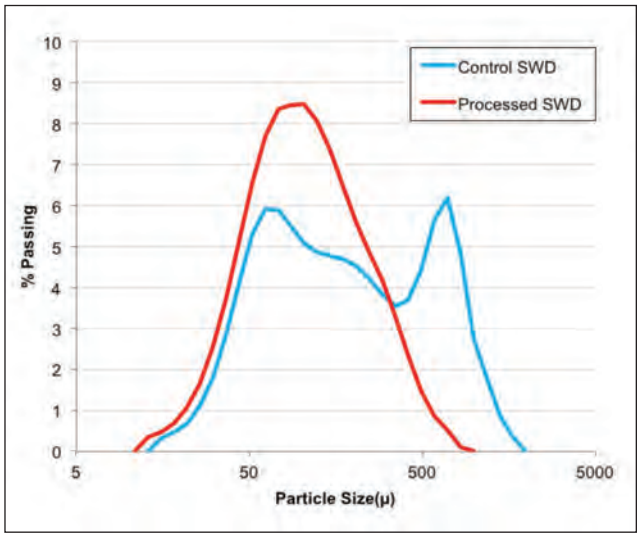
Figure 4 shows the mean particle size for standard hardwood and semicontinuous attritor treatment of hardwood fi-



3. Particle size reduction for hardwood pulps (hpdt = horsepower-days/short ton).



4. Particle size distribution for control hardwood and processed hardwood at 70 hpdt.



5. Particle size distribution for control softwood and processed softwood at 100 hpdt.

bers processed at approximately 70 hp-days/short ton (hpdt). Particle size distributions (PSD) were measured using a Microtrac S3500 (Microtrac, Montgomeryville, PA, USA) particle size analyzer (PSA). For the analysis conditions used, we saw a significant diminution of the higher end (long fiber) peak. The large spike in material around 100 μm is likely explained by particle agglomeration phenomena occurring in the aqueous solution that was used as a carrier during the measurement process. All samples were diluted to an approximate 1% solution and then tested in the PSA instrument. Each sample was sonicated for 1 min before being introduced into the measurement cell and no dispersant was added. Even with the potential for particle agglomeration during the measurement and analysis, a significant reduction in the hardwood fiber particle size resulting from the attritor process was noted.

For softwood, a typical PSD reduction curve is shown in **Fig. 5**. The results show a large decrease in the high-end particle size of pine fiber and a shift toward the lower end (about 100 μm) range. These data are for energy inputs of about 100 hpdt.

Sample	Catalyst	Energy, hpdt	Mean Particle Diameter, μm
1	0	0	443
2	0	57	375
3	0	85	268
4	A	78	84
5	B	79	114
6	A+B	82	69
7	A+B	120+	Aerosol

I. Mean particle size of softwood samples after attritor treatment with and without catalysts at given grinding energy inputs.

The application of catalysts during attritor processing also appears to have a positive impact on size reduction of the pine fibers. Two different catalysts were employed individually and concomitantly. As expected, the experimental data for samples 1–3 (**Table I**) show that increasing energy inputs results in a reduction in the measured mean particle size diameter. Comparing sample 3 with samples 4–6 demonstrates that the use of one or two catalysts is quite effective in terms of particle size reduction at essentially equivalent energy inputs. Combining the two catalysts resulted in more effective particle size reduction for a given energy input.

It was possible to make exceptionally finely ground softwood fibers (sample 7). If the milling time with the attritor is extended for the conditions of sample 6 (i.e., higher energy input), then the material became small enough to become electrically charged and to form an aerosol. This was an interesting outcome; however, it is a condition to avoid as it could result in a dust explosion. We report this observation as a precautionary warning to have proper grounding and collection devices for this type of material when applying these processing conditions.

METHODS

Bleached hardwood and bleached softwood pulp samples were refined with a Valley beater to freeness targets; 120 g/m² and 240 g/m² handsheets were made of each pulp type as received and at each level of refining for physical testing. The paper property tests performed on the handsheets included caliper, tensile, and elastic modulus. The test samples were allowed to condition in a controlled humidity environment and were tested in that same environment. Testing was performed according to TAPPI Standard Test Methods (**Table II**).

Impact of attritor-treated fibers on handsheet properties

Because of the high cost of hardwoods in selected mill locations, the handsheet investigation was conducted with handsheets made of a combination of attritor-treated and untreated

Test Method	Title
T 402	Standard conditioning and testing atmospheres for paper, board, pulp handsheets, and related products
T 200	Laboratory beating of pulp (Valley beater method)
T 205	Forming handsheets for physical tests of pulp
T 220	Physical testing of pulp handsheets
T 410	Grammage of paper and paperboard
T 494	Tensile properties of paper and paperboard (using constant rate of elongation apparatus)

II. TAPPI Standard Test Methods used for testing.

Condition, 120 g/m²	CSF, mL	Density, lb/mL/3000 ft²	Modulus of Elasticity, ksi	Sheffield Smoothness
RL 0	745	8.51	439	370
RL 0 + 10% AP	755	7.98	351	388
RL 0 + 20% AP	750	7.54	325	396
RL 1	670	9.56	677	315
RL 1 + 10% AP	675	8.62	603	379
RL 1 + 20% AP	700	8.37	489	395
RL 2	625	9.94	767	280
RL 2 + 10% AP	650	7.61	614	386
RL 2 + 20% AP	650	8.01	499	399
RL 3	570	10.29	834	271
RL 3 + 10% AP	590	8.58	721	365
RL 3 + 20% AP	620	8.21	600	390

III. Data for softwood furnishes and handsheet properties that contain various levels of attritor-treated pulp fibers (RL = refining level on the untreated softwood pulp; AP = attritor-treated softwood pulp fibers).

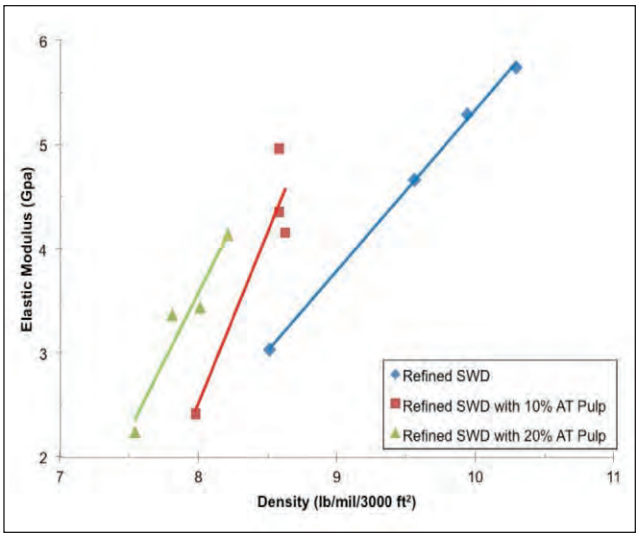
softwood pulp fibers. These handsheets were prepared and tested according to TAPPI Standard Test Methods (Table II).

Initial efforts were made to enhance the properties of attritor-based fibers using refining. These efforts were not successful because the attritor-treated fibers had no propensity to hydrate. It is speculated that attritor-treated fibers, having been once dried and ground, have become fully hornified. Additional work would be needed to fully understand these effects. In lieu of developing methods for refining the attritor-treated fibers, we opted to refine the untreated softwood pulp and then added the attritor-treated fibers (as is) to the refined softwood pulp. The CSF values for the different softwood pulps employed in this study are shown in **Table III**, as are freeness values for the combined pulps and the sheet densities and moduli values. In Table III, RL stands for refining level on the untreated softwood pulp and AP stands for attritor-treated softwood pulp fibers.

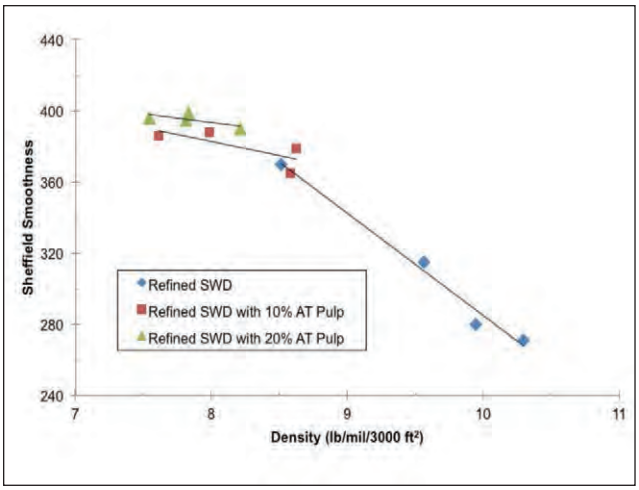
Table III shows the various conditions that were used to demonstrate the impact of attritor-treated fiber addition on the densities and moduli of softwood pulp furnishes refined to different levels. For these examples, we used a pine pulp that was processed in an attritor at approximately 85 hpdt. No attempt was made to examine the effects of catalysts on the resulting attritor treatment of pine fibers when it was added to untreated pine pulp furnishes in the handsheet studies.

For the laboratory handsheets, we refined the base softwood pulp to a given CSF value and then added either 10% or 20% of the attritor-treated fibers; tests were conducted on handsheets for sheet density, modulus, and smoothness (Sheffield units). Obviously, the CSF can be related to the modulus and other sheet properties, but because the industry tends to sell paperboard on caliper and resultant stiffness, which is related to the modulus, we focused on the density and the modulus for these handsheets.

Figure 6 shows the relationship between density and modulus for the handsheets in this study. Each curve represents a series of refined softwood pulp sheets with a certain percentage of attritor-treated fibers. The data for each linear series that is the nearest to the graph's origin correspond to refined softwood pulp at RL 0 (lowest level), whereas the data for each series that is the most distant correspond to refined softwood pulp at RL 3 (highest level).



6. Density versus elastic modulus for refined softwood and refined softwood with attritor treatment.

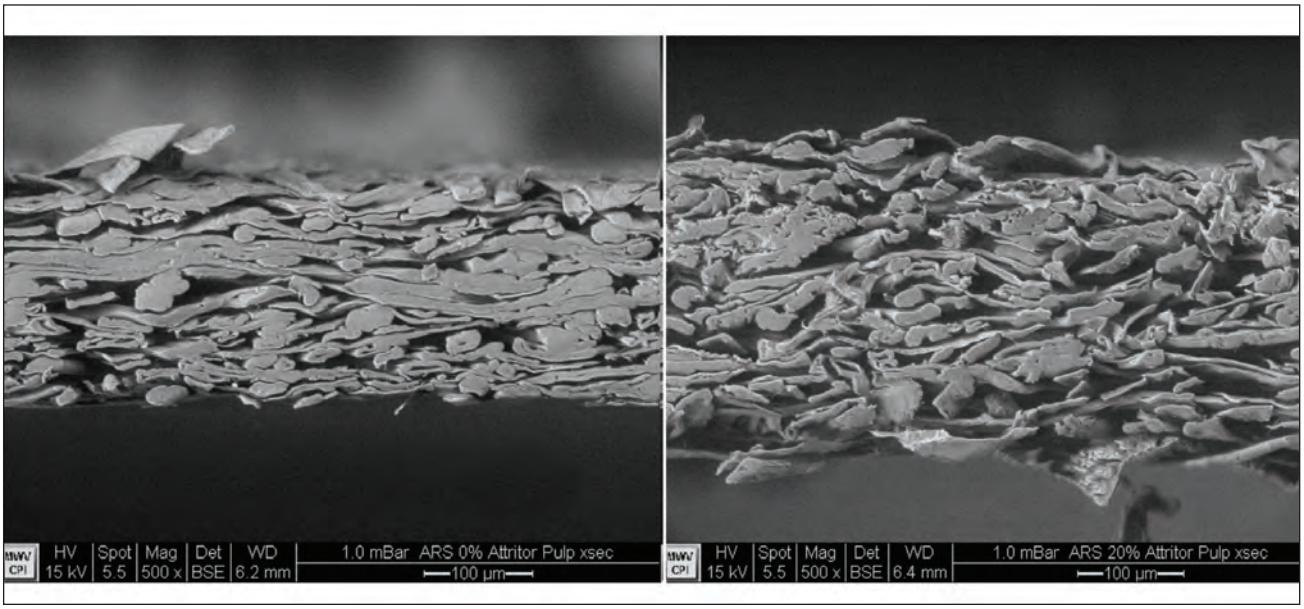


7. Sheffield smoothness versus density for refined softwood and refined softwood with attritor treatment.

Figure 6 shows that the addition of the attritor-treated fibers to the softwood pulp causes a decrease in sheet modulus and density. However, it is important to note that the sheet modulus can be increased by refining the untreated softwood pulp that contains attritor-treated fibers. While this was done for laboratory handsheets, the fact that the CSF goes up for attritor-containing pulp furnishes offers the intriguing option of putting small particle size pulps into the sheets without affecting drainage.

The current work only considers the in-plane modulus; while out-of-plane modulus would likely change, we are continuing to examine this variable. Nonetheless, over the range of 0% to 20% addition to the untreated softwood pulp, the use of attritor-treated fibers can lower sheet density at a given modulus. Also, if a product paperboard can withstand a decrease in modulus of 20%, then a 10% attritor-treated fiber addition could be tolerated with little additional refining of the untreated softwood pulp. A potential 10% reduction in fiber usage and lower bulk could be realized with a 10% addition and some additional refining. Thus, it may be possible to substitute shorter fiber pulps (e.g., hardwood pulps) with attritor-treated softwood fibers in certain circumstances for paperboard pulp furnishes.

As more attritor-treated fibers are added to the softwood furnish, the handsheet density decreases and the surface of the handsheets becomes rougher. **Figure 7** shows the results of Sheffield smoothness for the various handsheets. These data are for raw handsheets, which were not coated or calendered, and only represent the potential impact of this type of additive on sheet properties in a laboratory setting. Surface properties are a prime qualifier for many paperboard



8. Side scanning electron microscopy view of pulps containing 0% attritor and 20% attritor.

products, so the option to re-engineer a top ply or coating to regain smoothness needs to be carefully examined. The fact that the addition of attritor-treated fibers to the pulp furnish caused an appreciable increase in surface roughness is a strong indicator that additional investigation would be required before it could be feasible in commercial applications.

Visually, the results of our study are evident from the side-on scanning electron microscopy photos (**Fig. 8**). The micrograph of softwood furnish without attritor-treated fibers is shown on the left, whereas the furnish containing 20% attritor-treated fibers is shown on the right; the scale bar represents 100 μm. The handsheets with 20% attritor-treated fibers are noticeably thicker (less dense) than the control sheets with only untreated softwood pulp.

CONCLUSIONS

We have shown that blending dry grinding of softwood fibers (once dried) to a softwood pulp furnish can yield handsheets with lower density as compared with a control softwood pulp furnish without attritor-treated fibers. While this lowers the sheet modulus, it is possible to refine the base softwood pulp furnish to regain sheet modulus. Balancing these effects offers an option to use less fiber in paperboard construction, depending upon product specifications.

Handsheets containing attritor-treated fibers, which have lower sheet densities, have appreciably rougher surfaces, as quantified by Sheffield smoothness values, than control without attritor-treated fibers. This was observed regardless of the level of refining of the base softwood pulp furnish.

Additional research is needed to understand the energy inputs and particle sizes obtained with attritor processing of pulp fibers, as well as how attritor-treated fibers when blended with pulp furnishes affect paper machine drainage. Control of sheet surface roughness to allow for graphic printing requirements would also have to be investigated before this technology could be implemented on the industrial scale. **TJ**

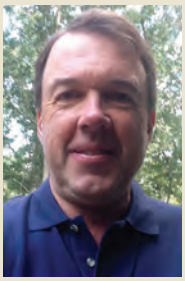
LITERATURE CITED

1. Howsmon, J.A. and Marchessault, R.H., *J. Appl. Polym. Sci.* 1(9): 313(1959).
2. Fan, L.T., Lee, Y-H, and Beardmore, D.H., *Biotechnol. Bioeng.* 22(1): 177(1980).
3. Mais, U., Esteghlalian, A.R., Saddler, J.N., et al., *Appl. Biochem. Biotechnol.* 98(1): 815(2002).
4. Millett, M.A., Effland, M.J., and Caulfield, D.F., in *Hydrolysis of Cellulose: Mechanisms of Enzymatic and Acid Catalysis* (R.D. Brown Jr. and L. Jurasek, Eds.), American Chemical Society, Washington, D.C., 1979, pp. 71-89.
5. Zhu, L., O'Dwyer, J.P., Chang, V.S., et al., *Bioresour. Technol.* 99(9): 3817(2008).
6. Van de Vyver, S., Geboers, J., Jacobs, P.A., et al., *ChemCatChem* 3(1): 82(2011).
7. Tassinari, T.H., Macy, C.E., and Spano, L.A., *Biotechnol. Bioeng.* 24(7): 1495(1982).
8. Moon, R.J., Martini, A., Nairn, J., et al., *Chem. Soc. Rev.* 40(7): 3941(2011).
9. Amin, K.N.M., Annamalai, P.K., Morrow, I.C., et al., *RSC Adv.* 70(5): 57133(2015).

ABOUT THE AUTHORS


Knox


Hart


Moynihan


Kilgore

Several different wet techniques have been employed in the manufacture of nanofibrilated cellulose (NFC). In our work, we attempted to determine how dry processed NFC would affect the physical properties of paper.

A substantial body of work exists that examines NFC from wet processing methods. The current work used an attritor (dry) processing method. Rehydrating the attritor-processed NFC was difficult. Eventually, we resorted to some pulp refining on the attritor pulp included in the blend to get the material into the sheet.

The attritor-processed material had a significant impact on bulk at similar stiffness. The impact on sheet smoothness was unexpected and unfortunate. Attritor-processed pulps might have the ability to alter the bulk-stiffness relationship of some board grades. In addition, attritor processing requires less energy than several other methods of processing.

Our next step is to examine the impact of attritor processing on different fiber sources and how these pulps affect handsheet physical properties. Another objective is to perform a full financial cost-benefit analysis for the resulting products.

Knox is retired, Hart is director of Fiber Technology and Innovation, Moynihan is a senior research engineer, and Kilgore is a researcher, WestRock, Richmond, VA, USA. Email Hart at peter.hart@westrock.com.

10. Pettersen, R.C., in *The Chemistry of Solid Wood* (R.M. Rowell, Ed.) American Chemical Society, Washington, D.C., 1984, pp. 57-126.
11. Beasley Jr., B.F., Cross, A.L., Michael, R., et al., U.S. pat. app. 2005/0051290 (Mar. 10, 2005).
12. Nechyporchuk, O., Belgacem, M.N., and Bras, J. *Ind. Crops Prod.* 93: 2(2016).
13. Zhang, L., Tsuzuki, T., and Wang, X., *Cellulose* 22(3): 1729(2015).
14. Herbst, J.A. and Sepulveda, J.L., *Proc. Tech. Program: Int. Powder Bulk Solids Handl. Process. International Powder and Bulk Solids Handling and Processing Conference*, Industrial and Scientific Conference Management, Chicago, 1978, pp. 452-470.
15. Union Processes Inc., "Technical papers." Available [Online] www.unionprocess.com/tech.html <21June2016>.

Removal of silicon from green liquor with low-temperature precausticizing

XINXING XIA, FANG WANG, SHAN SUN, AND QIAN HU

ABSTRACT: Nonwood materials contain a high percentage of silicon, which causes numerous problems in the chemical recovery section. Researchers previously proposed the method of silicon removal by two-stage causticizing at temperatures of 90°C to 95°C, finding that the desilication rate was about 72.9% and the causticizing efficiency was 22.7% when 30% of the causticizing quicklime (calcium oxide; CaO) was added. The present paper deals with the desilication of green liquor recovered from wheat straw black liquor by a low-temperature precausticization method. The results showed that about 89.3% silicon removal and 10.3% causticizing efficiency were achieved under the following precausticizing conditions: added lime amount of 20%, temperature of 20°C, and reaction time of 60 min. While precausticizing at 90°C with the same lime amount, only about 63.5% silicon removal and 13.0% causticizing efficiency were gained. Therefore, precausticizing with low temperature was beneficial for silicon removal and retention of carbonate (CO_3^{2-}).

Application: Removal of silicon from green liquor with precausticizing at low temperature can effectively increase the desilication rate, which could mitigate the issues caused by "silicon influence" and improve the recycling of lime mud.

Unlike wood, nonwood materials such as wheat straw, reed, and bamboo contain a high percentage of silicon, which causes serious problems in the chemical recovery process [1,2]. Therefore, many researchers have investigated desilication methods. Silicates can be removed from the system by introducing carbon dioxide into the black liquor, converting soluble sodium silicate (Na_2SiO_3) into silica particles that can be separated from the black liquor by sedimentation [3,4]. Approximately 90% of the constituent silicates can be removed from black liquor. However, this separation process is slow because of the small particle size of silica. Runge et al. [5] described the method of removing silicon by a combination of dermal mechanical treatment and caustic chip extraction. However, only about 80% of the silicon was removed. Bohmer [6] proposed the addition of sodium aluminate or bauxite to precipitate the silica as zeolite. High silica removal efficiency was claimed, but the process does not seem to have been developed. Silicon can also be removed by adding carbon dioxide (CO_2) into the green liquor to convert Na_2SiO_3 into calcium silicate [7]. The lime mud can be used as filler after removing silicon. But sodium hydroxide (NaOH) should be added to the green liquor to return to its original pH. Rao et al. [8] proposed two-stage causiticizing whereby silica was selectively precipitated in the first stage and the mud discarded so that relatively clean mud was generated in the second stage. When adding 30% of the causticizing calcium oxide (CaO), commonly referred to as quicklime, to react with green liquor for 30 min at 90°C to 95°C in the first step, only 72.9% of the silicon was removed and the causticizing efficiency was 22.7%. The present paper deals with the desilication of green liquor by a low-temperature precausticization method, since the reaction rate between sodium carbonate (Na_2CO_3) and calcium hydroxide ($Ca(OH)_2$) decreases with temperature [9], which is beneficial for silicon removal.

EXPERIMENTAL

Materials

For these experiments, the green liquor from wheat straw soda pulping was collected from Xingbao Paper Industry Co. Ltd. in Xianyang, Shaanxi Province, China. Calcium oxide was provided by Sinopharm Chemical Reagent Co. Ltd., Shanghai, China.

Silicon removal process with precausticizing

A certain amount of quicklime and distilled water were added to a flask to slake for 30 min at 80°C. Then, the green liquor was reacted with calcium hydroxide to precipitate silicon. The effect of reaction time, quicklime content, and precausticizing temperature on desilication rate and causticizing efficiency were investigated.

Determination of mixed alkali in green liquor

The concentrations of NaOH and Na_2CO_3 in the green liquor were measured by HCl titration [10].

Determination of silicon content

The silicon content in green liquor was measured with spectrophotometry [11]. The silicon reacts with molybdic acid

Composition	Total Alkali (as NaOH)	Active Alkali (as NaOH)	Sodium Carbonate	Silicon Dioxide
Content, g/L	104.3	11.1	123.5	4.2

I. Analysis of green liquor.

(H_2MoO_4) to form $H_8[Si(Mo_2O_7)_6]$ in weak acidic solutions, and then the silicon-molybdate ligand is converted to $H_8[SiMo_2O_5(Mo_2O_7)_5]$ after reacting with ferrous sulfate ($FeSO_4$). The absorbance of $H_8[SiMo_2O_5(Mo_2O_7)_5]$ was determined with the spectrophotometer at 680 nm. The silicon content was obtained by standard colorimetric analysis.

RESULTS AND DISCUSSION

Analysis of green liquor

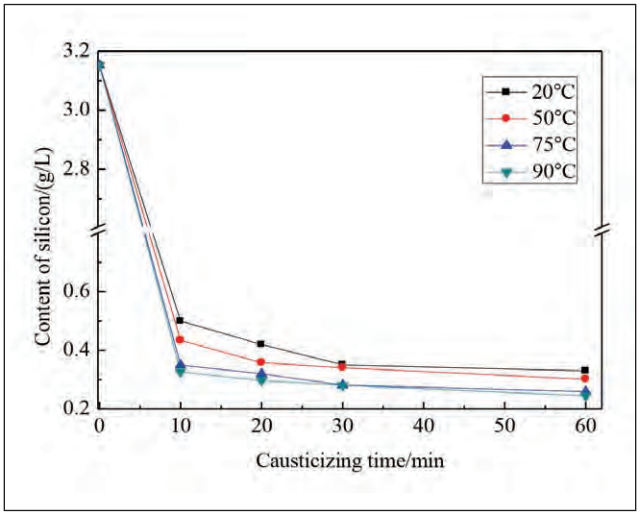
The composition of the green liquor is shown in **Table I**. Sodium carbonate and active alkali were the main ingredients of green liquor. The content of silicon dioxide was 4.2 g/L, which will cause serious problems for the chemical recovery process and the recycling of lime mud.

Effect of temperature on causticizing performance

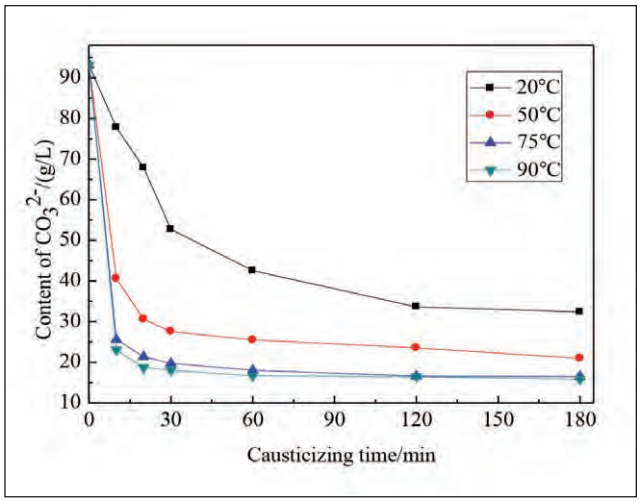
Figure 1 shows the effect of causticizing temperature on silicon content in green liquor with the molar ratio of $Ca(OH)_2$ to Na_2CO_3 of 1:1. No matter how high the reaction temperature, the silicon content in green liquor decreased quickly within the first 10 min, which indicated a fast reaction rate between Na_2SiO_3 and $Ca(OH)_2$. At the same causticizing time, the silicon contents were almost the same when the temperature changed from 20°C to 90°C, which demonstrated that the causticizing temperature had little effect on the reaction rate between Na_2SiO_3 and $Ca(OH)_2$.

Figure 2 shows the effect of causticizing temperature on the content of CO_3^{2-} in green liquor with the molar ratio of $Ca(OH)_2$ to Na_2CO_3 of 1:1. The content of CO_3^{2-} decreased quickly when the reaction temperature increased from 20°C to 90°C at the same reaction time, which indicated that the reaction rate between Na_2CO_3 and $Ca(OH)_2$ was influenced by temperature. When the causticizing time was 10 min, 30 min, and 60 min with the reaction temperature of 20°C, the content of CO_3^{2-} was 77.8 g/L, 52.7 g/L, and 42.5 g/L, respectively. When the reaction temperature raised to 90°C with the causticizing time of 10 min, 30 min, and 60 min, the content of CO_3^{2-} was 23.0 g/L, 18.0 g/L, and 16.7 g/L. Therefore, low-temperature causticization decreased the causticizing reaction rate.

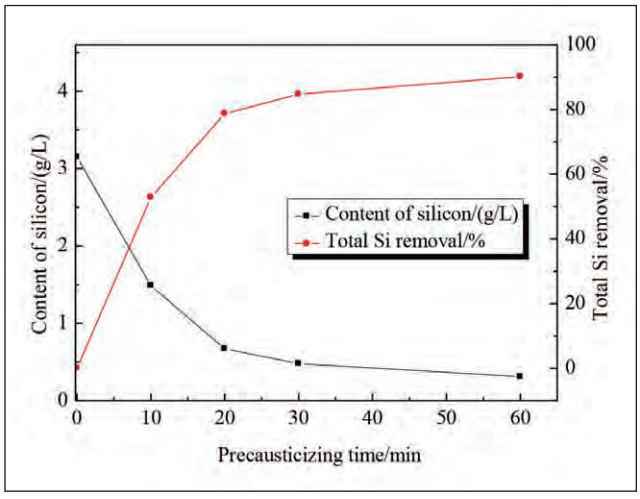
These results demonstrated that the reaction rate between Na_2CO_3 and $Ca(OH)_2$ at high temperature was faster than that



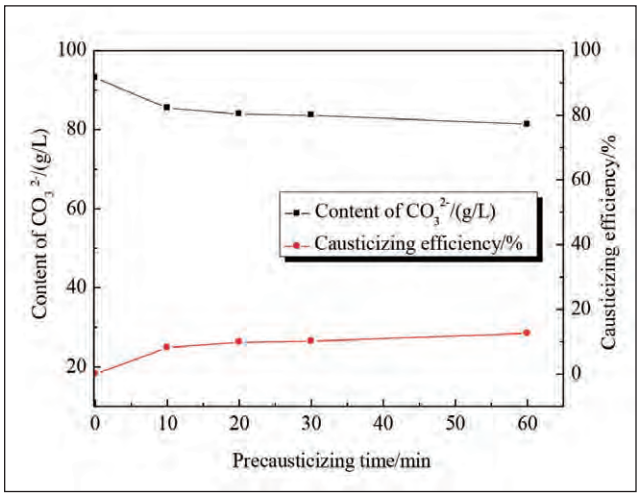
1. Effect of causticizing temperature on silicon content in green liquor.



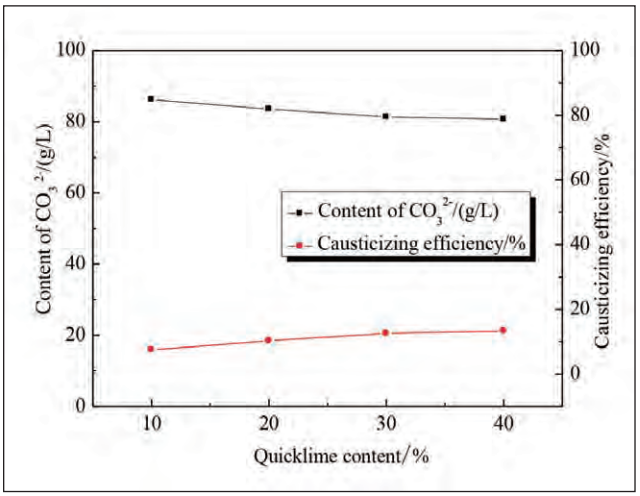
2. Effect of causticizing temperature on the content of carbonate (CO_3^{2-}) in green liquor.



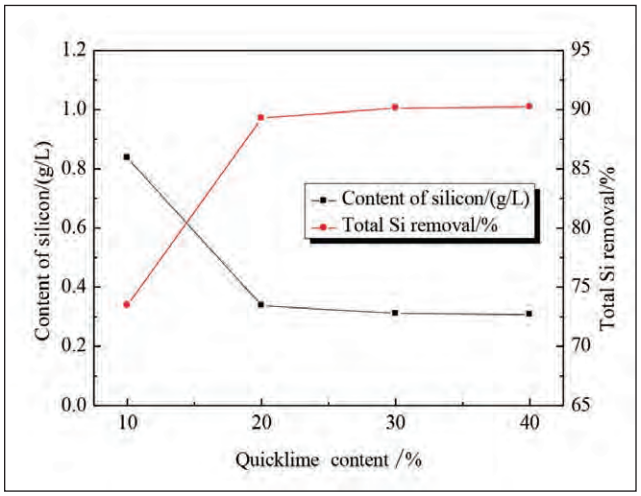
3. Effect of precausticizing time on silicon removal.



4. Effect of precausticizing time on causticizing reaction.



6. Effect of quicklime content on causticizing reaction.



5. Effect of quicklime content on silicon removal.

at low temperature. However, reaction temperature had no significant effect on the reaction rate between Na_2SiO_3 and $Ca(OH)_2$. Thus, precausticizing at low temperature could simultaneously remove silicon and retain CO_3^{2-}.

Silicon removal with low-temperature precausticizing

Effect of precausticizing time on silicon removal and causticizing reaction

The silicon was removed by adding 30% of causticizing quicklime to green liquor to selectively precipitate silicon at 20°C. **Figure 3** shows that by increasing precausticizing time, the silicon content in green liquor decreased quickly. The content of silicon reduced to 0.7 g/L, and about 79.0% of silicon was removed when the precausticizing time reached 20 min. The desilication rate slowly increased after about 30 min. About 90.1% of silicon was removed when the reaction time reached 60 min.

Figure 4 shows that the content of CO_3^{2-} in green liquor decreased with increased precausticizing time. The causticizing efficiency increased by 10.2% within the first 30 min. When the reaction time increased from 30 min to 60 min, the causticizing efficiency increased from 10.2% to 12.6%. Causticizing efficiency increased slowly with reaction time. This is because the reaction rate of causticizing decreased at 20°C, which was beneficial to saving CO_3^{2-}. Considering the desilication rate and causticizing efficiency, silicon removal was studied with the reaction time for 60 min.

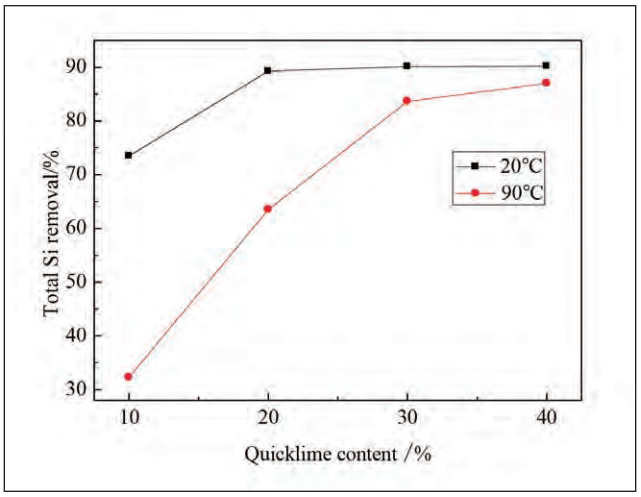
Effect of quicklime content on silicon removal and causticizing reaction

A part of the total quicklime (10% to 40% of stoichiometric ratio) was added to green liquor for precausticizing for 60 min at 20°C. **Figure 5** shows that the desilication rate increased from 73.5% to 89.3% when the content of quicklime increased from 10% to 20%. The removal of silicon increased slowly as quicklime was continuously added. The content of silicon reduced to 0.3 g/L and about 90.2% of the silicon was removed when the quicklime was 40% of the stoichiometric ratio.

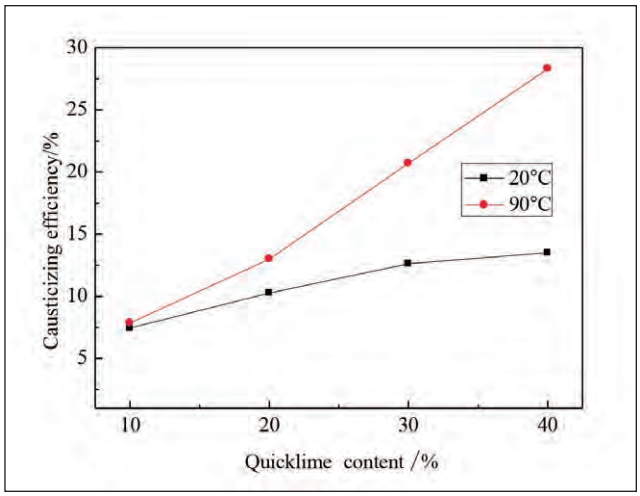
Figure 6 shows that the content of CO_3^{2-} decreased as the quicklime content increased. The causticizing efficiency increased from 7.4% to 12.7% when the quicklime content was increased from 10% to 30%. The causticizing efficiency slowly increased as the quicklime increased to 40% of the stoichiometric ratio. This is because the low temperature decreased the rate of causticizing reaction.

Effect of precausticizing temperature on desilication rate and causticizing efficiency

Figure 7 and **Figure 8** show the effect of precausticizing temperature on desilication rate and causticizing efficiency. As shown in Fig. 7, compared with 20°C, the desilication rate with precausticizing at 90°C was lower under the same reaction conditions. With the increasing of quicklime, this trend was relatively decreased. This is because the reaction rate between $Ca(OH)_2$ and Na_2CO_3 decreased under low temperature conditions, which was beneficial to the reaction be-



7. Effect of precausticizing temperature on desilication rate.



8. Effect of precausticizing temperature on causticizing efficiency.

tween Na_2SiO_3 and $Ca(OH)_2$. Figure 8 shows that the causticizing efficiency increased with increased quicklime content at 20°C and 90°C. The increasing trend of causticizing efficiency at 90°C was obviously higher than that at 20°C. When the quicklime content increased from 20% to 40%, the causticizing efficiency increased by 2.5% and 15.3% at 20°C and 90°C, respectively.

Overall, when 20% of causticizing quicklime was added to removal and 10.3% of causticizing efficiency were achieved. While precausticizing at 90°C with the same added lime amount, only about 63.5% of silicon removal and 13.0% of causticizing efficiency were gained. Therefore, precausticizing at low temperature was beneficial for silicon removal and retention of CO_3^{2-}.

Mills could use the method described here to mitigate the problems of "silicon influence" in the chemical recovery process and improve the recycling of lime mud. Our next step is to identify an industry partner to work with on removing silicon using low temperature precausticizing.

ABOUT THE AUTHORS



Xia



Wang



Sun



Hu

We choose this topic to research because many mills with straw pulping face problems caused by high silicon content of green liquor in the chemical recovery system. While there are many methods of silicon removal, they hardly offer an effective way to achieve high desilication rate.

Previous research studied the method of silicon removal with precausticizing at high temperature, where low desilication rate and high causticizing efficiency were achieved. In this study, silicon was removed with low-temperature precausticizing. Compared with high-temperature precausticizing, the desilication rate increased and causticizing efficiency decreased under the low temperature.

The most difficult aspect of this research was to find out how the causticizing temperature affected the reaction between $Ca(OH)_2$ and Na_2CO_3 and $Ca(OH)_2$ and Na_2SiO_3. We dealt with this by studying the concentrations of SiO_3^{2-} and CO_3^{2-} in green liquor at different causticizing temperatures. We discovered that the causticizing temperature had no significant effect on the reaction rate between Na_2SiO_3 and $Ca(OH)_2$, but it obviously affected the reaction rate between Na_2CO_3 and $Ca(OH)_2$.

Interestingly, we found that when adding 20% of causticizing quicklime to remove silicon with precausticizing for 60 min at 20°C, 89.3% of silicon

Xia is professor at the Pulp and Papermaking Center, Zhejiang Sci-Tech University, Hangzhou, China, and State Key Laboratory of Pulp and Paper Engineering, South China University of Technology, Guangzhou, China. Wang, Sun, and Hu are graduate students of Zhejiang Sci-Tech University, Hangzhou, China. Contact Xia at xinxingxia2000@hotmail.com.

remove silicon with precausticizing for 60 min at 20ºC, 89.3% of the silicon was removed and the causticizing efficiency was only 10.3%. The desilication rate and causticizing efficiency were 63.5% and 13.0% with the same conditions at 90ºC. Thus, precausticizing under low temperature achieved high desilication rate and low causticizing efficiency.

CONCLUSIONS

The causticizing temperature had no significant effect on the reaction rate between Na_2SiO_3 and $Ca(OH)_2$, but it obviously affected the reaction rate between Na_2CO_3 and $Ca(OH)_2$. When adding 20% of causticizing quicklime to remove silicon with precausticizing for 60 min at 20ºC, 89.3% silicon removal and 10.3% causticizing efficiency were achieved. While precausticizing at 90ºC with the same lime amount, only about 63.5% silicon removal and 13.0% causticizing efficiency were gained. Therefore, precausticizing with low temperature was beneficial for silicon removal and retention of CO_3^{2-}. **TJ**

ACKNOWLEDGEMENTS

This work was supported by State Key Laboratory of Pulp and Paper Engineering, South China University of Technology (201509) and Science Foundation of Zhejiang Sci-Tech University (14012081-Y). The authors would like to acknowledge all the assistants in the project group and concerned industrial partners for providing the materials.

LITERATURE CITED

1. Wu, F.Q., *North Pulp Pap.* 18(4): 21(1997).
2. Lin, T., Li, X., Xu, Y., et al., *BioResources* 9(3): 4690(2014).
3. Myreen, B., *Int. Chem. Recovery Conf.*, TAPPI PRESS, Atlanta, GA, USA, 1998, p. 823.
4. Myreen, B., U.S. pat. 6,183,598 (Feb. 6, 2001).
5. Runge, T.M. and Paul, S., *TAPPI J.* 14(11): 743(2015).
6. Bohmer, V.J., *Tappi J.* 67(11): 116(1984).
7. Xia, X.X., Wang, X., Du, M.Z., et al., *TAPPI J.* 13(7): 41(2014).
8. Rao, G.V., Murthy, N.V.S.R., Annamraju, P.V., et al., *Appita* 41(1): 33(1988).
9. Zhan, H.Y., *Pulp and Paper – Chemistry and Chemical Technology*, China Light Industry Press, Beijing, 2006, p. 317.
10. Shi, S.L. and He, F.W., *Analysis and Test of Pulping and Papermaking*, China Light Industry Press, Beijing, 2009.
11. Xia, X.X., Du, M.Z., and Geng, X.J., *TAPPI J.* 12(3): 35(2013).

Paper coated with sonochemically synthesized zinc oxide nanoparticles: Enhancement of properties for preservation of documents

SUCHISMITA MAJUMDAR, ANIRBAN ROY, ISITA NANDI, PRANTIK BANERJEE, SWAPNA BANERJEE, MAHUA GHOSH, AND SAMPA CHAKRABARTI

ABSTRACT: Sonochemically synthesized zinc oxide (ZnO) nanoparticles were coated on paper for enhancing its properties in view of the preservation of documents. The paper used for accession register was used as substrate. Physical, chemical, optical, hydrophobic, and antifungal properties of the coated and uncoated papers were compared. Nanoparticles were synthesized with ultrasound from organic precursors and were characterized by X-ray diffraction (XRD) and field emission scanning electron microscopy (FESEM), whereas coated and uncoated papers were examined following standard procedures as described by the Bureau of Indian Standards (BIS). It was observed that coating with nanoparticles imparted mechanical strength, water repellence, and antifungal properties to the paper without compromising its printability. Hence, coated paper is comparatively more suitable for preservation of written or printed documents than uncoated paper.

Application: In this work, we coated paper with sonochemically synthesized zinc oxide nanoparticles and explored various properties of the coated paper, including the antifungal property. It was observed that coating with nanoparticles imparts mechanical strength, water repellence, and antifungal properties without compromising printability. This enhanced the durability of accession register paper; hence, documents can be preserved for longer.

Papers are mainly used for printing and writing, and thereby, for storage and preservation of data and information. Other applications of paper include packaging, cleaning, decoration, filtration, and chromatography. Environmental effects, like attack by moisture, and microbial effects, like attack by bacteria and fungi, sometimes prevent storage of documents for long periods. Accidental spillage of water or coloring material may also lead to spoilage of the documents. Hence, development of water and stain-repellent paper, as well as antimicrobial paper, is in demand today. Semiconductors, such as zinc oxide (ZnO) and titanium dioxide (TiO_2), have photocatalytic characteristics, whereas their nanoparticles also have some water repellency and antimicrobial properties.

In the present work, we have treated paper with ZnO nanoparticles to improve its surface functionality so that it does not get wet or stained easily and can resist microbial and fungal attack. The objective of the research was to enhance the quality of paper used in the accession register of a library so that important documents are not easily destroyed or mutilated. The accession register is the record of books and other resources in a library. This register should have some specific fields, including accession number, date of arrival, author, call number, supplier name, supplier address, publisher name, place of publisher, and price of the book; this information may vary from library to library. It is therefore a very important document and should be preserved for long periods. To accomplish this objective, we have coated paper with sonochemically synthesized ZnO nanoparticles and explored various properties of the coated paper, including its antifungal property, as climatic conditions are especially favorable for fungal growth in tropical countries like India. The nanoparticles were synthesized from two different organic precursors, and the influence of the precursors was also compared.

There are not many available references on smart paper with nanoparticle coating. Functionalization of paper surfaces was reviewed by Ngo et al. in 2011 [1]. Various techniques of impregnation of nanoparticles onto the heterogeneous lignocelluosic matrix of paper have been reported. Different aspects of enhancement of properties such as self-cleaning and antimicrobial effects are also described. Imparting water repellency to paperboard using silica and TiO_2 nanoparticles has been reported by Stepien et al. [2]. Silver nanoparticle coating on a paper surface imparted antimicrobial property. Gottesman et al. [3] reported sonochemical coating of silver nanoparticles on the surface of paper. Zinc oxide nanoparticles have been used for preservation of old manuscripts by Afsharpour et al. [4]. Antimicrobial [5,6] and antifungal [6,7]

properties of ZnO nanoparticles have been reported by many researchers. Photocatalytic paper has been prepared using ZnO nanorods into the softwood pulp by Barua et al. [8]. They used this photocatalytic paper for photocatalytic degradation of methyl orange dye in wastewater under visible light irradiation. Antibacterial property of the paper was also explored. Purification of indoor air by using wallpaper coated with TiO_2 was studied by Yu and Brouwers [9] under visible light irradiation. Ngo et al. [1] also reported destruction of volatile organics from contaminated soil by using photocatalytic coating. Starch-ZnO nanocomposite was coated on a sheet of paper, and its improvement in terms of mechanical and antimicrobial properties was studied by Prasad et al. [10].

MATERIALS AND METHODS

Materials

Materials included zinc acetate (dihydrate), $Zn(CH_3COO)_2$, (molecular weight 219.49; purchased from Merck Ltd. India, Mumbai, India); zinc acetyl acetonate, $Zn(acac)_2$, (molecular weight 263.6082; purchased from MP Biomedicals SARL, Illkirch-Graffenstaden, France); ethanol; and triple distilled water of pH 6.8 and conductivity 4-7 micro mhos as solvent. All the reagents used in the present investigation were of analytical grade.

Sonochemical synthesis and coating of paper with ZnO nanoparticles — procedure

A 230 ml of 0.02(M) solution of zinc acetate in aqueous alcohol (210 ml water and 20 ml of ethanol) was taken in a conical flask in a bath-type sonicator (Model Microclean 101 with 20 kHz frequency and 40 W power, Oscar Ultrasonics; Mumbai, India). The clear solution with starting pH 5.8–6.1 was then sonicated at 65°C for 2 h. For the synthesis of zinc oxide nanoparticles from acetyl acetonate (acac) precursor in a probe type sonicator, 1 mmol of $Zn(acac)_2$ was taken with 20 ml of ethanol, and it was shaken thoroughly until the solutes were completely dissolved. After that, 210 ml of water was added to make the total volume of the solution 230 ml and exposed to ultrasound using a 30 ±3 kHz frequency ultrasonic probe (Model D-120/P, Trans-O-Sonic; Mumbai, India) at 120 W for a period of 40 s. The pulse mode used was "1 s on and 1 s off" for optimum use of ultrasonic power. Therefore, the actual time of sonication was 20 s. In both cases, after sonication, the contents became slightly turbid. In this synthesis process, no alkali has been added for hydrolysis, making this an eco-friendly process. Since probe-type sonication is a direct one, the time required is less compared to the indirect bath-type sonicator.

This turbid solution is mainly the post synthesis phase of nanoparticles containing solution. After synthesis, the nanosized ZnO containing turbid solution was poured onto a petri dish of 6 in. diameter, and 10 cm × 10 cm pieces of paper were kept immersed in it. Then, they were dried in open air, and after drying, pressed in a compression mold press at a pressure of 3.25 Kg cm^{-2}. After curing, the samples were preserved in a dessicator.

Characterization of synthesized nanoparticles before coating — procedure

The sol was separately centrifuged, washed, and dried to isolate the nanoparticles for characterization. Nanoparticles have been characterized by X-ray diffraction (XRD) and field emission scanning electron microscopy (FESEM). Structural characterization was performed with an X'Pert-PRO instrument diffractometer (PANanalytical; Almelo, The Netherlands) using Cu Kα (λ=1.5406) at a scanning rate of 1°/min, generator voltage of 40 kV, and current of 30 mA in the range from 10° to 90°. The XRD patterns of the nanoparticles were verified by comparison with the Joint Committee on Powder Diffraction Standards (JCPDS) data (Nos. 36-1451). Sizes of the nanoparticles have been calculated using the well-known Scherrer equation [11]:

$$t = 0.9\lambda/BCos\theta$$

where, t is the grain thickness, λ is the wavelength of the X-ray, B is the full-width at half-maximum (FWHM) value of the XRD peaks, and θ is the diffraction angle. Cell volume and lattice parameters (a and c) were calculated by UnitCellWin freeware using the non-linear least squares cell refinement program with regression diagnostics. It refines cell parameters from powder diffraction data. Size and surface morphology of ZnO was analyzed using FESEM (Supra 35VP, Carl Zeiss; Oberkochen, Germany). The samples for FESEM were prepared on glass slides. The pH was measured using a Testr24 digital pH meter (Blk 55, Eutech Instruments; Ayer Rajah Crescent, Singapore). Thicknesses of the treated and untreated samples were measured using a digital micrometer (IP65, Mitutoyo; Tokyo, Japan). Photographs were taken using an MI Redmi Note mobile phone (Xiaomi; Beijing, China).

Characterization of nanoparticle-coated paper — procedure

Images of coated and uncoated fabric were taken by a Zeiss EVO18 SEM instrument (Carl Zeiss; Oberkochen, Germany) with Oxford INCA penta FET X3 attachment that can handle wet biological samples, often called BioSEM. Mechanical, optical, and chemical characterizations of the nanoparticle-coated and uncoated samples of accession register paper have been examined in accordance with the respective standards from the Bureau of Indian Standards (BIS) mentioned here.

Grams per square scales (GSM) was measured by weighing balance (APX200, Denver Instruments; Göttingen, Germany). The test method used for measuring the GSM is as per BIS Standard IS:1060 Part-I, 1966 (2004), "Methods of sampling and test for paper and allied products." Thickness, loading, load at maximum load, tensile strength, percentage total elongation at maximum force, percentage total elongation at fracture, strain at maximum load, strain at maximum extension, strain at break, stiffness, and Young's modulus were tested by universal testing machine (Nexygen Plus, Lloyd Instruments, Ametek Company; Sussex, England) as per ASTM D 2370 "Standard test

Variety of ZnO	a=b, Å	C, Å	Cell Volume, Å^3	Average Size, nm
Standard wurtzite	3.249	5.206	47.12	
From zinc acetate	3.27780	5.228	48.64	27.7
From zinc acetyl acetonate	3.23857	5.188	47.12	32.82

I. Crystal characteristics of zinc oxide nanoparticles (ZnO-NP).

method for tensile properties of organic coatings." For these measurements, samples of size 90 mm × 40 mm were used. Folding endurance was tested by a folding endurance tester (Kohler-Molin type, Fibretec Instruments; Roorkee, India) using BIS IS:1060 Part-I, 1966 (2004). Determination of wax pick number was performed using Dennison standard paper testing waxes and BIS IS:1060 Part-III, 1969 (2004). A digital pH meter from Testing Instrument Manufacturing Co. (Kolkata, India) was used for measuring the pH using BIS IS:1060 Part-I, 1966 (2004).

Optical property tests were performed with a digital opacity tester from S.C. Dey and Co. (Kolkata, India). BIS IS:1060 Part-I, 1966 (2004), was referred to for assessing the opacity percent.

A few chemical tests in relation to chloride, sulfate, and fatty acids were performed in accordance with BIS IS:1060 Part-II, 1960 (1997) and cellulose content was also tested in accordance with BIS IS:1060 Part-II, 1960 (1997). The reagents primarily used are silver nitrate ($AgNO_3$), barium chloride ($BaCl_2$), sodium hydroxide (NaOH), solvent ether, and potassium chromate (K_2CrO_4) (E-Marck; Darmstadt, Germany). Filter paper No. 42 (Whatman; Maidstone, UK) was used.

Water repellence or hydrophobicity was studied by pouring a drop of water onto the nanoparticle coated paper with a micropipette. Cobb test was performed for ascertaining similar properties according to BIS IS:1060 Part-I, 1966 (2004) by Cobb tester (S.C. Dey and Co.).

Antifungal capability test by disk diffusion method

The antifungal activity testing was done with one microorganism *Aspergillus niger*. A density of 10^8 CFU ml^{-1} of the test organism in the inoculum suspension was used to obtain semi-confluent growth on the potato dextrose agar (PDA) medium. The inoculum was prepared by suspending enough well-isolated colonies from a 24-h PDA plate in saline water. The dried surface of the PDA plate was inoculated by spreading the entire surface with 0.1 ml of inoculum of the test organisms. Circular pieces of ZnO nanoparticle coated papers, 5 mm in diameter, were placed uniformly on the surface of the inoculated plates and incubated at 25±1°C for 24 h. After incubation, assessment was based on the absence or presence of fungal growth on the tested samples and in the inhibition zone that was formed. At least three sets were tested and the average diameter (less than 5% deviation) of the inhibition zone has been reported in all cases.

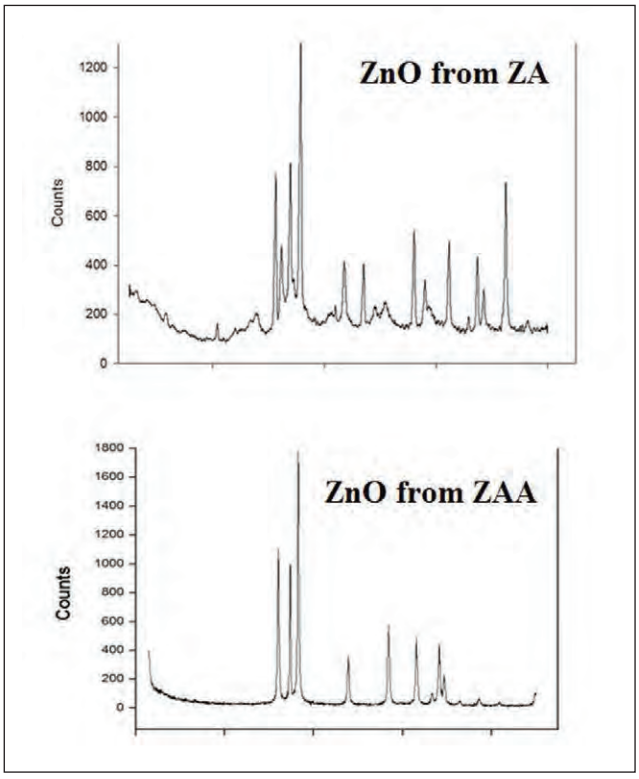
RESULTS AND DISCUSSION

Characterization of ZnO nanoparticles

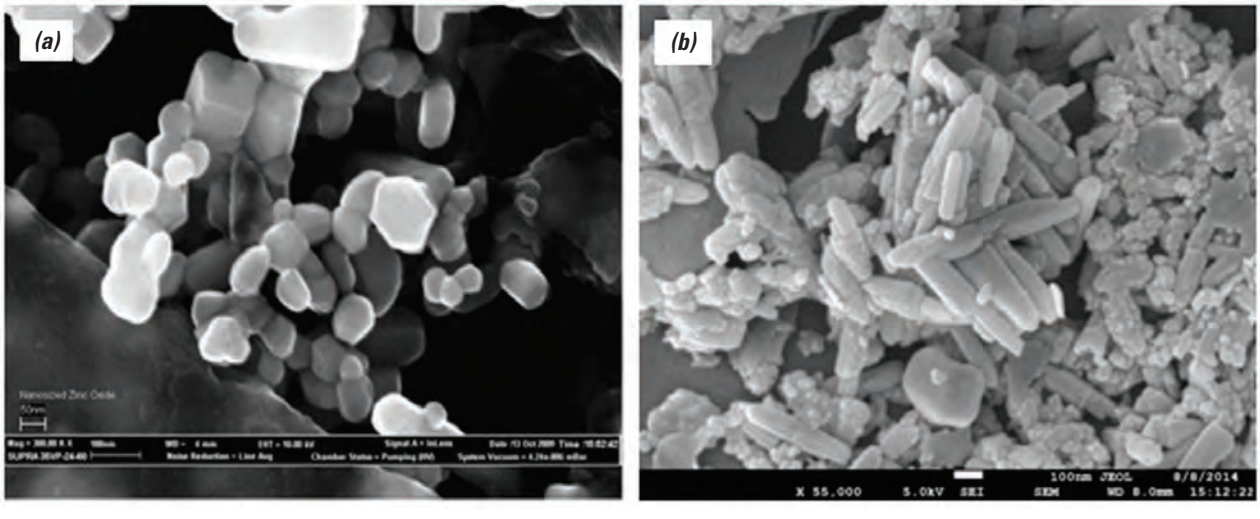
Sonochemically synthesized ZnO nanoparticles have been characterized by the previously mentioned analytical techniques and instruments.

Powder XRD analysis

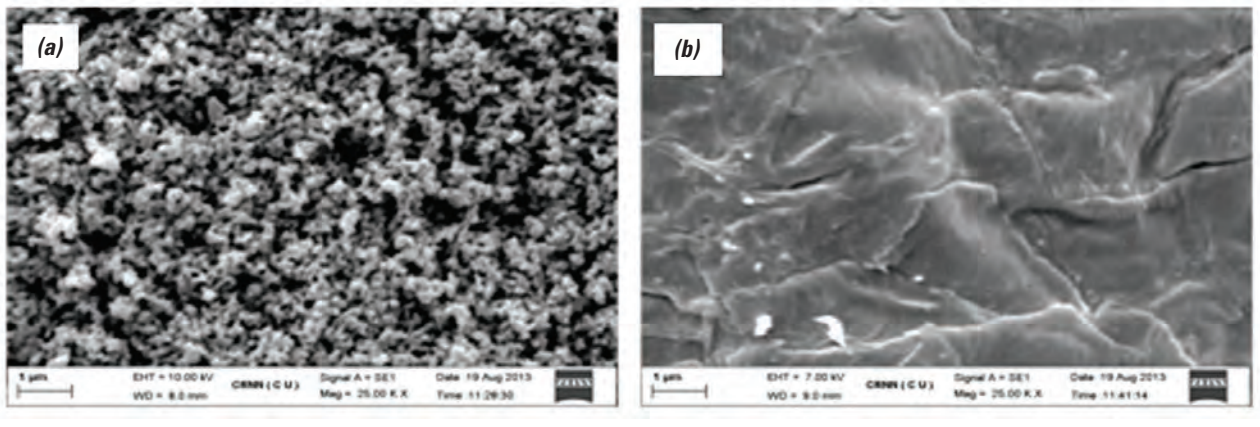
The XRD data of ZnO synthesized using zinc acetate in ethanolic medium were compared with that of standard wurtzitic ZnO crystal structure (**Table I**). It is observed from the XRD data that ZnO synthesized from both zinc acetate and zinc acetyl acetonate precursors in the ethanol medium had a strong diffraction peak for the [1 0 1] plane (**Fig. 1**), characteristic of the wurtzitic structure [12], and it may be noted that ZnO synthesized using both the precursors possessed perfect wurtzitic structure. Grain sizes are 27.7 nm (from zinc acetate) and 32.82 nm (from zinc acetyl acetonate), as shown in Table I. However, ZnO from zinc acetyl acetonate was more crystalline.



1. X-ray diffraction (XRD) patterns of zinc oxide nanoparticles (ZnO-NP) prepared from different precursors (ZnO = zinc oxide; ZA = zinc acetate; ZAA = zinc acetyl acetonate).



2. Scanning electron microscopy (SEM) micrographs of ZnO-NP prepared from (a) zinc acetate and (b) zinc acetyl acetonate.



3. (a) Coated, and (b) uncoated paper samples.

FESEM analysis

The morphology of ZnO nanoparticles is shown in **Figs. 2a-b**. FESEM figures show that the ZnO crystals from zinc acetate crystalline were disc-like appearance with a hexagonal cross section. The nanoparticles synthesized from the zinc acetyl acetonate precursor were rod-like with a hexagonal cross section. The latter appeared to be more crystalline compared to the former, which supported the observations from the XRD.

Characterization of the nanoparticle-coated paper

BioSEM images

From the SEM images in **Fig. 3a** (coated paper sample) and **Fig. 3b** (uncoated sample), the uniform coating on the paper surface was confirmed.

Mechanical properties

Mechanical properties of paper after coating with nanoparticles are very important for the end use of the paper. **Table II** shows comparative data on the mechanical properties of the coated and uncoated samples.

Grammage and thickness

The grammage (g/m^2) of the available market papers as tested for ascertaining the quality of the paper used for printing the accession register shows that the paper has an approximate grammage of 66.92 g/m^2 and thickness of 0.09 mm. Grammage for paper coated with ZnO from acetate precursor and from acetylacetonate precursors were 76.79 and 74.77 g/m^2, respectively. Corresponding thicknesses were 0.11 and 0.10 mm, respectively. The results indicated that the samples gained mechanical strength after coating, since increases in grammage and thickness generally indicate an increase in strength related properties, as per BIS IS:1848 (2007) "Writing and printing papers – Specification."

Tensile strength, fold endurance, and tear index

According to BIS IS:1763-1961 (2002), "Specification for sub-

Properties	Uncoated Base Paper	Coated with ZnO-NP from Acetate	Coated with ZnO-NP from Acetyl Acetonate
Grammage (g/m²)/ coat weight	66.92	76.79	74.77
Thickness, mm	0.09	0.11	0.10
Nanoparticle loading, mg/cm²	-	0.987	0.785
Load at maximum load, kN	0.014	0.022	0.027
Tensile strength	10.346	18.944	21.221
Percentage total elongation at maximum force, %	8.939	4.945	4.993
Percentage total elongation at fracture, %	9.109	5.37	4.993
Strain at maximum load, N/m²	0.089	0.049	0.050
Strain at maximum extension, N/m²	0.098	0.06	0.057
Strain at break, N/m²	0.091	0.054	0.050
Young's modulus	449.52	669.211	1046.652
Stiffness, N/m	20977.609	26099.243	43959.399

II. Mechanical properties of paper with and without ZnO-NP coating.

Properties with Average Value	Uncoated Base Paper	Treated with ZnO-NP from Acetate	Coated with ZnO-NP from Acetyl Acetonate
pH	7.5	6.11	6.22
Water soluble chlorides as NaCl%	0.14 as Cl%	0.17	0.19
Water soluble sulfates as Na_2SO_4%	0.22 as SO_4%	0	0

III. Chemical properties of paper with and without ZnO-NP coating (NaCl = sodium chloride; Na_2SO_4 = sodium sulfate).

stances of paper and pulp board": "The determination of strength may relate to a) tensile strength and stretch (or elongation), b) breaking length, c) bursting strength, d) folding endurance, and e) tearing resistance." From Table II, it is observed that the tensile strength, Young's modulus, and stiffness increase, showing an enhancement in mechanical strength of the paper by coating. Young's modulus and tensile strengths are maximum for the sample coated with ZnO synthesized from the acetyl acetate precursor. Tear indices after coating were nearly doubled, though the fold endurance remained nearly unchanged.

Wax pick number

This number indicates the surface strength of the paper that can endure pressing by the printing press. With this accession register paper, tests of wax pick number resulted in "no pick on 7A" for both uncoated and coated paper. Hence, it can be concluded that there was no change in the printability of the paper after coating. Wax grades range within 3A to 8A. For offset printing, a range between 5A to 10A is admissible.

Optical properties of the coated and uncoated paper

The optical properties of paper are mainly brightness, whiteness, and color. However, opacity is considered essential as far as printing and book papers are concerned. The opacity of fiber is influenced by thickness, amount and kind of filler, degree of bleaching, and coating, etc. This test is performed to ascertain the quality of the available accession register papers before nanoparticle coating. Opacity is expressed in percentage. Opacity is measured by the percentage of light absorbed by a sheet of paper.

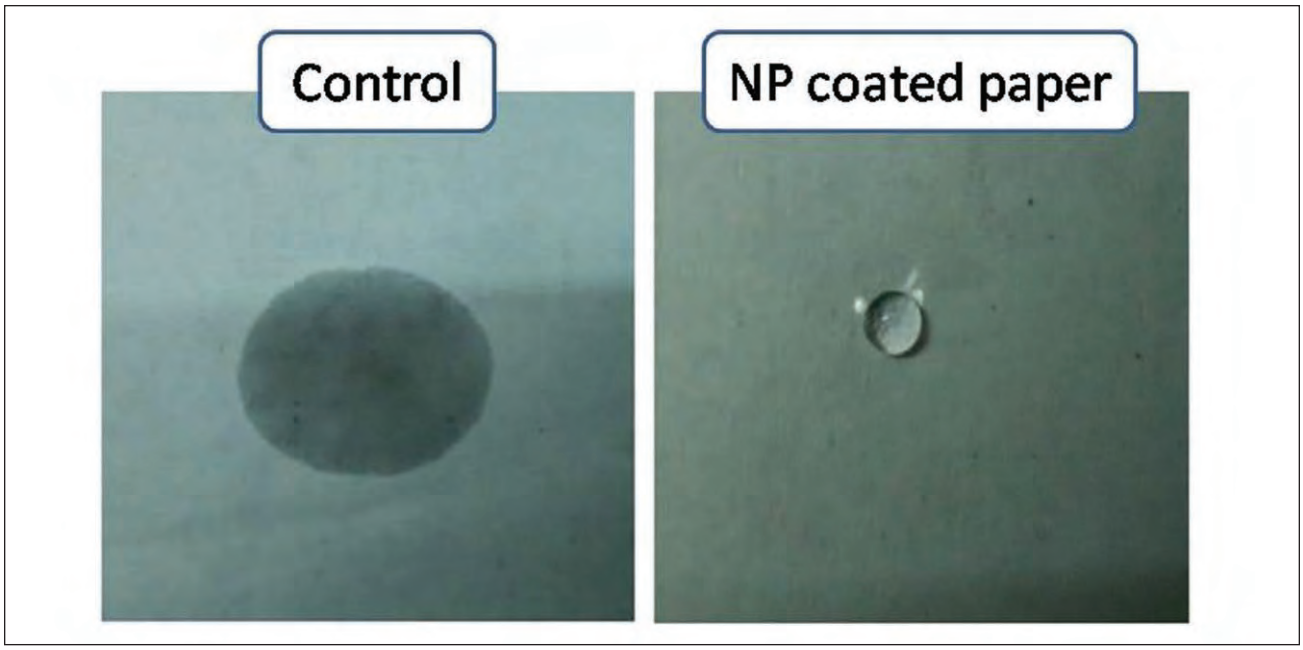
For "account book paper," the standard percent opacity required is 80, as per BIS IS:1060 Part-I, 1966 (2004), whereas by coating it is slightly decreased to 74. This is due to the action of organic compounds on the surface during coating, because the nanoparticles are synthesized from organic precursors in the presence of alcohol.

Chemical properties

Table III shows chemical properties of paper with and without ZnO-nanoparticle (NP) coating

pH, cellulose, and fatty-acid contents

The pH is one measure of paper's stability, as it indicates the degradation of α-cellulose. There is a standard requirement of neutral pH (7.0) for writing and printing papers, as per BIS IS:1848 (2007). However, the pH here decreased a little after



4. Water repellency image.

coating, but this may be considered as near neutral pH (6.1–6.2) that hardly affects stability. Moreover, the cellulose content and fatty acid content did not vary much after coating (less than 1%).

Chloride, chlorine, and sulfates

An important step in papermaking is bleaching, and chlorine and chlorine compounds are used at this stage. The kraft and sulfite processes of pulping can impart sulfates in paper. From a safety and environmental point of view, it is necessary to analyze the chlorine and sulfate content of paper. Chlorine free paper is categorized as either totally chlorine free (TCF) or elementally chlorine free (ECF). TCF papers are produced with pulp that has been bleached without any type of chlorine or that has not been bleached at all. ECF papers are produced via bleaching with chlorine derivatives like chlorine dioxide (ClO_2), but without elemental chorine (Cl). Recycled papers are processed chlorine free (PCF), i.e., no chlorine or chlorine derivatives were used in the process of recycling. Tests for chlorine are significant to ascertain the traces of chlorine, if any. No significant amount of chlorine or sulfate was detected in either the coated or uncoated paper here.

Accelerated aging test

To ascertain the life of the paper samples, an accelerated aging test was performed at 100 ±5°C for 3 h as per BIS IS:5086, 1993(2004), "Stencil paper specification." The result showed that neither the uncoated or the coated sample was sticky or brittle. Therefore, the paper can be suitably used for storage and handling.

Water repellency

For both types of coating, a 5 µl drop of water was discharged from a syringe onto the paper, and the time up to which it had not soaked into the surface was measured. For the coated paper, the drop of water remained for 1.5 h showing the lotus-leaf effect of the nanoparticles, whereas on the uncoated sample of paper (control), it soaked in immediately. **Figure 4** shows that the coated paper became water repellent.

In addition, water repellence of the coated sample was measured in terms of contact angle using a goniometer (Model 290, Ramé-Hart Instrument Co.; Succasunna, NJ, USA). In this case, angles were measured in three locations of a particular sample, and the results are shown in **Fig. 5**. The images were taken at 0, 10, and 30 min intervals, respectively.

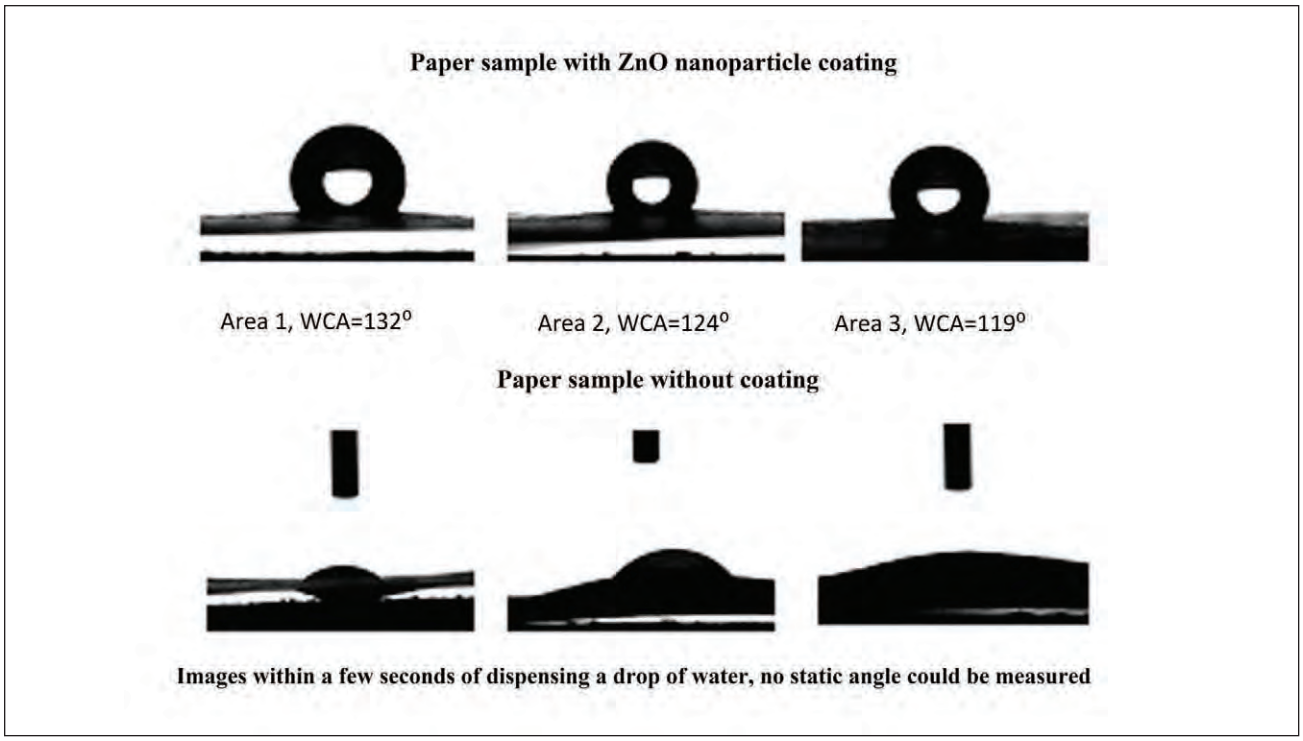
The average angle of contact is 125°, which indicates hydrophobicity of the coated fabric compared to practically 0° angle of the uncoated fabric. An angle of contact more than 90° indicates hydrophobicity.

Cobb test

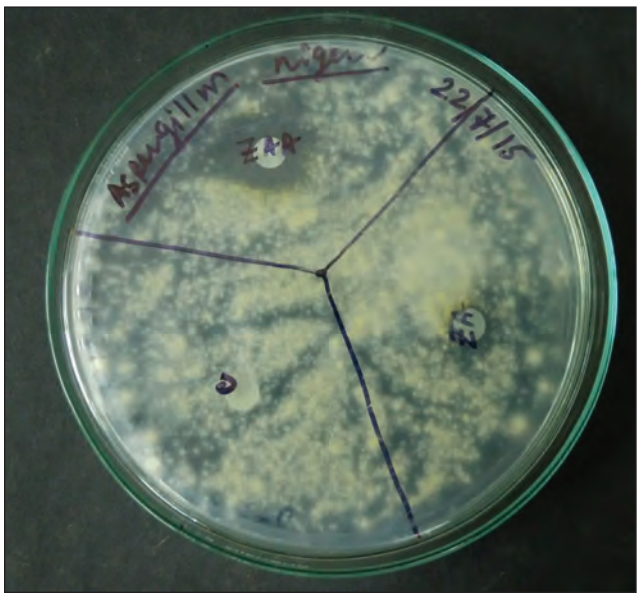
Cobb test was also performed to examine water absorption of the coated and uncoated samples [13]. It was observed that the Cobb value (60 s) decreased drastically from about 300 mg in uncoated paper to 12.7 mg and 54.6 mg, respectively, after coating with the ZnO nanoparticles obtained from acetate and acetyl acetonate precursors. This indicates hydrophobicity and agrees with the observations of water repellency tests described previously. However, there may be some adsorption of water on the nanoparticles with high surface area.

Antifungal property

In the context of preservation of documents, fungal deterioration of paper materials is of great significance in tropical countries like India where temperature and humidity are favorable for fungus growth. A few fungi responsible for biodeterioration of old books are *Aspergillus niger*, *Cephalosporiumcore-*



5. Contact angle and water repellency of ZnO-NP coated paper.



6. Antifungal activity of ZnO-NP treated papers showing zone of inhibition against fungi tested using a disc diffusion method.

moides, *Paecilomycesvariotii*, and *Starchiomyceskurchellomyces*. Of these, *Aspergillus niger* or black mold is the most prevalent. The antifungal activity of ZnO-NP coated paper samples were assessed in parallel with a control sample (a film-forming material without ZnO nanoparticles), and the results are shown in **Fig. 6**. Circular paper pieces (5 mm) coated with ZnO nanoparticles synthesized from acetate and acetyl acetonate were marked as ZA and ZAA, respectively, and the control sample was marked as C. Figure 6 shows a clear zone of inhibition around ZnO treated paper discs (inhibition zone diameter was 10.75 mm for ZA and 13.3 mm for ZAA), whereas the control paper disc shows no sign of inhibition. This suggests that the nanoparticle coating makes the paper antifungal and better for preservation of documents.

Many researchers have reported antibacterial [5,6] and antifungal [6,7] activities of ZnO-NP. However, the mechanism of the inhibitory effect of ZnO-NP on the microbes is not yet completely understood [7]. There may be two possible mechanisms: one is by the production of reactive oxygen species (ROS) even under room lighting, and the other is by deposition of very tiny nanoparticles on the membrane surface or at the cytoplasm/periplasm, thereby disrupting the cell membrane. In the case of fungi, He et al. [7] suggested that ZnO-NP may affect cell functions and increase the nucleic acid content of the cell due to the stress response of fungal hyphae. An increase in carbohydrates owing to the self-protecting mechanism in the fungal cell has also been reported by many researchers [14,15]. All these mechanisms ultimately lead to the malfunction or death of microbial cells, and hence, the antimicrobial activity of ZnO-NP can be explained.

CONCLUSIONS

The accession register is a unique and irreplaceable administrative document that establishes the legal right of ownership. It contains key information about the resources of the library, archive, or museum's objects and serves as the basis for setting up its entire documentation system. The preservation of such documents is very important. Though

digital preservation has been introduced at various levels, the importance of classical hard document has not yet been outdated.

The properties of paper are the significant determinants for preservation. On the other hand microbial deterioration, especially mold infestation, is an alarming issue that conservators have to deal with. Moisture absorption and a damp environment accelerate the deterioration. Maintaining an accession register in legible condition is still a concern for the librarians, conservators, and the archivists.

In this study, paper used in the accession register was coated with zinc oxide nanoparticles sonochemically synthesized from acetate and acetyl acetonate precursors. Compared with the uncoated paper sample, it was observed that most of the mechanical, optical and chemical properties were enhanced by nanoparticle coating, whereas the printability was not compromised. A resistance to fungal attack was also developed by coating.

The results here provide significant input for advanced papermaking technology, and nanoparticle coating may be employed in papers used for important documents that require preservation for future generations. **TJ**

ACKNOWLEDGEMENTS

Author Majumdar acknowledges the UGC Minor Research Project No. F.PHW-085/11-12 dated 08.08.11 and author Roy acknowledges TEQIP, phase-II, University of Calcutta, for financial support. The authors wish to thank Sujoy Debnath in the Department of Polymer Science and Technology, University of Calcutta; Dr. R.K. Mondol, director of Aglow Quality Control Laboratory, for tests on paper samples; Dr. Rabibrata Mukherjee, IIT-KGP, for water repellence tests, and CRNN for

ABOUT THE AUTHORS



Majumdar



Roy



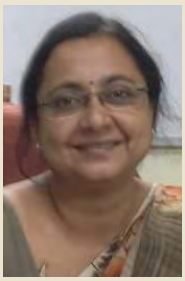
Nandi



P. Banerjee



S. Banerjee



Ghosh



Chakrabarti

As a chemical engineer, I (Chakrabarti) work on the synthesis and application of nanoparticles and wanted to explore the use of my synthesized nanoparticles for document preservation. While a few authors have reported the antimicrobial effects of nanoparticle coating on textile or paper, none of them explored all the physical, antifungal, mechanical, and water repellence effects of such nanoparticle coating. Also, none of them examined such coating from the angle of document preservation.

The most challenging aspect of this research was uniform coating of the paper. We addressed this using procedures described in the Methodology section of this paper.

Ultimately, we discovered that coating with nanoparticles enhances the property of printable paper. It was most interesting to see that the water repellent paper demonstrates the "lotus-leaf" effect of the nanoparticle film.

For mills, an improved paper quality is achievable if the proper nanoparticle coating process can be introduced. Our next step is scaling up the process with a paper industry initiative.

Majumdar is research scholar in Document Preservation, Department of Library and Information Science, University of Calcutta, Kolkata, India. Roy is research scholar in Nanoparticle Synthesis and Coating, Department of Chemical Engineering, University of Calcutta, Kolkata, India. Nandi is research scholar in Antifungal Properties, Department of Chemical Technology, University of Calcutta, Kolkata, India. P. Banerjee is a former research scholar in Nanoparticle Synthesis and Coating, Department of Environmental Science, University of Calcutta, Kolkata, India. S. Banerjee is professor and supervisor of Document Preservation studies, Department of Library and Information Science, University of Calcutta, Kolkata, India. Ghosh is assistant professor and supervisor of Antifungal Property studies, Department of Chemical Technology, University of Calcutta, Kolkata, India. Chakrabarti is professor in the Department of Chemical Engineering and research coordinator for Nanoparticle Synthesis and Coating studies at the Center for Research in Nanoscience & Nanotechnology, University of Calcutta, Kolkata, India. Email Chakrabarti at sampac.2008@gmail.com.

FESEM and BioSEM; Professor Dipankar Chattopadhyay, Department of Polymer Science and Technology, University of Calcutta, for XRD; and Dr. Bidhan Das, Indian Institute of Packaging(IIP), Kolkata, for various tests of paper samples.

LITERATURE CITED

1. Ngo, Y.H., Li, D., Simon, G.P., et al., *Adv. Colloid Interface Sci.* 163(1): 23(2011).
2. Stepien, M., Saarinen, J.J., Teisala, H., et al., *Appl. Surf. Sci.* 258(7): 3119(2012).
3. Gottesman, R., Shukla, S., Perkas, N., et al., *Langmuir* 27(2): 720(2011).
4. Afsharpour, M., Imani, S., and Abdolmohammadi, S., *World Acad. Sci. Eng. Technol.* 5(4): 409(2011).
5. Raghupathi, K.R., Koodali, R.T., and Manna, A.C., *Langmuir* 27(7): 4020(2011).
6. Singh, P. and Nanda, A., *J. Chem. Pharm. Res.* 5(11): 457(2013).
7. He, L., Liu, Y., Mustapha, A., et al., *Microbiol. Res.* 166(3): 207(2011).
8. Baruah, S., Jaisai, M., Imani, R., et al., *Sci. Technol. Adv. Mater.* 11: 055002(2010).
9. Yu, Q.L. and Brouwers, H.J.H., *Appl. Catal.* B92(3-4): 454(2009).
10. Prasad, V., Shaikh, A.J., Kathe, A.A., et al., *J. Mater. Process. Technol.* 210(14): 1962(2010).
11. Patterson, A.L., *Phys. Rev. Lett.* 56(10): 978(1939).
12. Duncan, B., Mera, R., Leatherdale, D., et al., National Physical Laboratory (NPL) Report, DEPC-MPR-020, Middlesex, UK, p. 29.
13. Kim, K.J., Sung, W.S., Moon, S.K., et al., *J. Microbiol. Biotechnol.* 18(8): 1482-4(2008).
14. Kim, K.J., Sung, W.S., Suh, B.K., et al., *BioMetals* 22(2): 235(2008).

Cellulosic ethanol byproducts as a bulking agent

J.M. CONSIDINE, D. COFFIN, J.Y. ZHU, D.H. MANN, AND X. TANG

ABSTRACT: Financial enhancement of biomass value prior to pulping requires subsequent use of remaining materials; e.g., high value use of remaining stock material after cellulosic ethanol production would improve the economics for cellulosic ethanol. In this work, use of enzymatic hydrolysis residual solids (EHRS), a cellulosic ethanol byproduct, were investigated as a bulking agent. The study examined the effect across several grammages, 20 g/m^2 –200 g/m^2, and EHRS substitution levels, 10%, 15%, and 20%. EHRS retention was examined with light scattering. EHRS loading increased bulk while reducing tensile strength, compression strength, and stiffness.

Application: Byproducts of cellulosic ethanol production can be used as a bulking agent.

The pulp and paper industry has the necessary infrastructure to process large amounts of woody biomass, whose increased use is one component of an effort to reduce the prevalence and severity of U.S. forest fires. Additional revenue streams that utilize existing capability, perhaps with minor modifications, are attractive to the industry. One potential revenue stream is cellulosic biofuel such as bioethanol, a renewable fuel, from underutilized woody materials not suitable for pulp production.

A substantial amount of research has been conducted using woody biomass for biofuel production in the past two decades [1], which included the utilization of underutilized woody biomass like pine beetle killed lodgepole pine [2] and forest harvest residue [3]. In cellulosic biofuel production, woody materials undergo a chemical pretreatment step, similar to pulping and carried out in a pulp digester, and then are enzymatically hydrolyzed to sugars. The sugars are then fermented to biofuel such as bioethanol. Significant amounts of woody materials, or enzymatic hydrolysis residue solids (EHRS), remain after enzymatic hydrolysis. EHRS consist of lignin and some unhydrolyzed polysaccharides such as cellulose and hemicelluloses. The amount of polysaccharides in EHRS depends on the degree of enzymatic hydrolysis. Because biofuel is a commodity product with low economic value, an economically viable production of biofuel requires the utilization and valorization of EHRS. Combustion of EHRS is one option, as it contains a substantial amount of lignin (higher heating value than carbohydrates). However, using EHRS as a bulking material may be a better choice in terms of valorization and environmental impact.

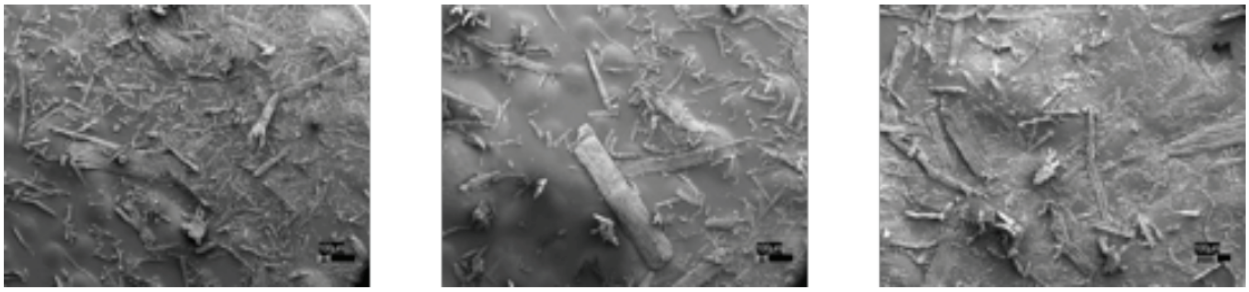
Rising pulp cost is a constant concern within the paper industry, and researchers are investigating methods of increasing material bulk while maintaining properties. Here, we investigate the use of EHRS to increase paper bulk and examine changes in the resulting mechanical and optical properties.

Papermakers understand that an inverse relationship exists between tensile strength and bulk. Some cellulosic material, such as microfibrillated cellulose, has been used to increase tensile strength [4-8] and reduce permeability but at the expense of increased drying energy. Special additives can be used to improve retention and drainage [5,7]. Sometimes, a significant amount of additive material (e.g., 5% by weight or greater) was needed before the effect was noticed [6].

However, processes that improve strength typically reduce bulk. Creative selection and processing of fines may alter the severity of the strength-bulk relationship [9]. Milled dry kraft fibers are effective debonders and bulking agents [10]. Lee et al. [11] used wood powder as a bulking agent. In a mill trial making duplex board, the wood powder addition was used as an alternative to old corrugated containers (OCC) and because it provided similar bulk with reduced drying costs. High-yield pulps have been used to increase bulk and opacity in kraft pulps but can also improve formation [12]. Lee et al. [13] found that another organic filler, brewer's grain, also increased bulk and reduced drying energy, and its particle size was an important controlling feature.

Cannell and Cockram [14] provide a good review of the many variables that the mill manager must control to achieve good printability, high opacity and good strength. Long fibers improve tear but have low printability and poor formation. Conversely, short fibers have good surface smoothness and opacity but low tear. Small fiber diameters improve printability, opacity, and softness; large fiber diameters increase bulk and reduce smoothness and printability. Thick fiber walls reduce tensile strength, cause greater linting, and reduce smoothness.

In this work, we present a framework for investigating the effect of incorporating processed biomass in a paper network. This framework can help choose potential users of the specified processed biomass by examining its effect on a range of paper grammages and biomass loading levels. EHRS served as a model processed biomass for this proposed framework. We



1. Scanning electron microscope (SEM) images of hydrolyzed material. Background features are artifacts of imaging.

believe that EHRS can contribute physical properties to improve opacity and increase bulk. Specifically, this work examines the use of EHRS as a bulking agent in a kraft pulp. Because bulk increases were the objective of this work, a high yield pulp was used; if this study showed EHRS increased bulk, it can be inferred that the same would be true for less bulky base pulps. Beneficial use of EHRS can provide additional revenue to the papermaker, improve the economics of cellulosic ethanol production, and increase the use of forest biomass, a renewable resource.

MATERIALS

Handsheets examined in this work were composed of a mixture of kraft pulp fibers and hydrolyzed cellulosic solids. The kraft pulp was made from lodgepole pine with a 60 min ramp from 80°C–170°C followed by a 25 min cook at 15.7% active alkalinity and 30% sulfidity. The resulting pulp had 67% yield, 106 kappa no., 19.8% solids as chips, and 16.7% solids once shredded.

EHRS was the residue of enzymatic hydrolysis of a lodgepole pine pulp produced from a bisulfite pretreatment [15] at sodium bisulfite loading of 6 wt% on wood (oven dry basis) at 180°C for 30 min in a laboratory pulping digester. The pretreated lodgepole pine wood chips were refined in a 12 in. laboratory disk refiner (Sprout-Waldron Operation, Koppers Company; Muncy, PA, USA) with a disk plate pattern D2-B505 having a plate gap of 1 mm. Added water served to facilitate refining and wash pulp and resulted in pulp discharging consistency of 10%. Pretreatment removed approximately 25% of lignin, over 50% of xylan, and 75% of mannan, which created a pulp enriched with glucan (approximately 50%). As a first trial, the pretreatment condition was mild and at a slightly acidic condition that was not optimized for sugar production but rather to result in a solids similar to chemithermomechanical pulp (CTMP). Low dosages of cellulase (Celluclast 1.5 L, Novozymes, Sigma-Aldrich; St. Louis, MO, USA) of 7 filter paper unit (FPU)/g glucan and beta-glucosidase (Novozyme 188, Sigma-Aldrich) of 10 CBU/g glucan were used. Enzymatic hydrolysis was conducted at 50°C at a solids loading of 12%. Coupled with low severity pretreatment, the low enzyme dosage produced a glucan saccharification of approximately 27%, or approximately 30% monomeric sugar yield from carbohydrates when hemicelluloses were taken into account. Enzymatic saccharification of xylan and mannan was minimum. Resulting EHRS was enriched with lignin, although a substantial amount of cellulose and small amount of hemicellulose remained.

Figure 1 shows three example scanning electron microscope (SEM) images of hydrolyzed material. The material had many different sizes and aspect ratios. No additional refining was used before incorporating in the kraft pulp used for the handsheets. Because of the high yield of the EHRS we expected it would act as a debonder.

HANDSHEET PRODUCTION

Handsheets of a range of grammages, 20 g/m²–200 g/m², loaded with different amounts of EHRS, 10%, 15%, and 20%, were produced. The range of grammages and EHRS loading levels were used to identify potential paper products that would benefit from increased bulk. Solids contents of the pulp and EHRS were determined after their respective production. Appropriate amounts of pulp and EHRS were mixed prior to disintegration according to the amount of EHRS loading, either 0% (control), 10%, 15%, or 20% EHRS on a dry weight basis. After weighing for correct amounts of pulp and EHRS, the mixture was disintegrated for 5000 revolutions. The handsheets were made according to TAPPI Standard Test Method T 205 sp-12 "Forming handsheets for physical tests of pulp," with the exception that water at 27°C was used in pulp disintegration instead of at 20°C. Precise grammage control was not used during production because individual handsheet grammage was determined and used to present results on a specific weight basis. For each nominal handsheet weight, two handsheets were made and weighed, and if necessary, small measured additions of water or pulp mixture were added to the doler tank. Handsheets were ring-dried overnight at 23°C and 50% relative humidity (RH). Before testing, the handsheets were preconditioned for 12 h at 27°C and 30% humidity and reconditioned at 23°C and 50% RH for 12 h.

It is not possible to determine with any precision the

amount of EHRS in the handsheets. We expected that during initial drainage of the handsheet, a portion of the EHRS and pulp fines would pass through the screen. Eventually the filter cake effect would prevent additional losses. The net effect would be a lower amount of EHRS and fines in the final material than was introduced in the handsheet mold.

Handsheet caliper was measured using TAPPI Standard Test Method T 411 om-10 "Thickness (caliper) of paper, paperboard, and combined board." Because of the pulp coarseness here, this method tended to overestimate caliper, especially in the higher grammage handsheets.

MATERIAL TESTS

Increased bulk generally reduces stiffness and strength and increases opacity. Tensile, ultrasonic, and compression testing were used to examine the effect of EHRS loading, to demonstrate the disruption in the fiber network caused by EHRS, and to probe the level of EHRS loading that would create a non-commercially viable product. Opacity evaluation was used as a non-mechanical evaluation technique to probe EHRS retention.

Tensile tests

Tensile tests were performed according to TAPPI Standard Test Method T 494 om-88 "Tensile properties of paper and paper board (using constant rate of elongation apparatus)," with a few exceptions, on an Instron (Norwood, MA, USA) Model 5865 test machine equipped with pneumatic grips. All specimens were 15 mm wide and were cut with a Thwing-Albert (West Berlin, NJ, USA) Precision Cutter. Specimens at nominally 20 g/m² were supported by an envelope paper during cutting. Specimens from handsheets at 80 g/m² and higher were tested with line clamps, 100 mm gauge length, at a rate of 20 mm/min. Because line clamps caused failure at the clamps for handsheets below 80 g/m², those specimens were tested with textured, flat platen grips. The flat platen grips covered a larger portion of the specimen and made it necessary to reduce the gauge length to 75 mm. To keep the recommended test period within TAPPI Standard Test Method T 494 om-88 guidelines, the rate of elongation was reduced to 10 mm/min for the specimens tested with the flat platen grips. Grip elongation and applied force were collected at 10 Hz.

Only data from specimens whose failure occurred away from the grips were analyzed. Grip elongation was converted to strain using the appropriate gauge length, and tensile applied force was converted to force/width using specimen width. Converted data were analyzed by fitting to the empirical equation suggested by Andersson and Berkyto [16] and given by:

$$\sigma = C_1 \tanh[C_2(\epsilon - \delta)] + C_3(\epsilon - \delta) \quad (1)$$

where:
σ = stress, kN/m
ε = strain, grip displacement/gauge length, m/m
C_1,C_2,C_3 = empirical constants
δ = strain offset, empirical constant

Fitting to Eq. (1) was performed in Matlab via the built-in *nlinfit* function. The initial portion of each tensile test, where grip slippage was evident, was not used in the fitting. For handsheets at nominal 20 g/m², data below 2 N were not used; for nominal 40 g/m² and 60 g/m², data below 3 N were not used; for all other grammages, data below 4 N were not used. The upper data cutoff was at maximum tensile force, i.e., tensile strength. Failure strain, ϵ_{max}, was the strain at the tensile strength. Because initial stiffness is quite sensitive to grip slippage and different low force cutoffs were used for different grammages, initial tensile stiffness was not a reliable comparison in this work. Tensile energy absorption, TEA, was determined by integrating Eq. (1) and evaluating at $\epsilon = \epsilon_{max}$, giving TEA = $C_1/C_2 \ln(\cosh(C_2 * \epsilon_{max})) + C_3\epsilon_{max}^2/2$.

Ultrasonic testing

Ultrasonic testing measures the time-of-flight of a longitudinal sound wave (supersonic pulse) to travel through the sheet between two probes of fixed distance. For each handsheet, ultrasonic tests were performed with a Nomura Shoji (Tokyo, Japan) SST-250 paper tester in which the transmission probe oscillated at 25 kHz. A central circular region, with 15-cm diameter, was examined for each specimen. Ultrasonic velocity was measured from 0 to 175° in 5° increments, giving 36 measurements for each handsheet. Specific stiffness was the mean ultrasonic velocity squared, $Q_{specific}$ = (mean(velocity))². Ultrasonic velocities of nominal 20 g/m² handsheets are not reported because they were a web of discrete fibers and violated the continuum requirement for ultrasonic stiffness identification.

Compression strength

For handsheets above 100 g/m², compression strength was measured with a Büchel Stripcompression Tester BK-155 (Veenendaal, Netherlands).

Optical testing

For control and 20% EHRS loaded handsheets above 40 g/m² nomimal, absorption and scattering coefficients were identified using the procedure given in [17,18] because the material was unbleached, nearly opaque, and contained lignin. Most opacity measurements are intended for bleached material and would be unable to differentiate between materials here due to the significant light scattering. The procedure [17] is able to identify the Kubelka–Munk coefficients, *k* (specific absorption coefficient), and *s* (specific scattering coefficient) by examining transmission and reflectance in the infrared spectrum. The *k* values were similar for both control and 20% EHRS loaded materials

	Kraft Pulp	EHRS
Fines [1, 2], %	3.5	29.11
Mean length[2], mm	2.04	0.35
Mean curl index[2]	0.43	0.30
Mean kink index, 1/mm	0.40	1.20
Mean fiber width, µm	36.7	40.3
Coarseness, mg/m	N/A	0.29

[1] Length weighted.
[2] Fibers < 0.20 mm.

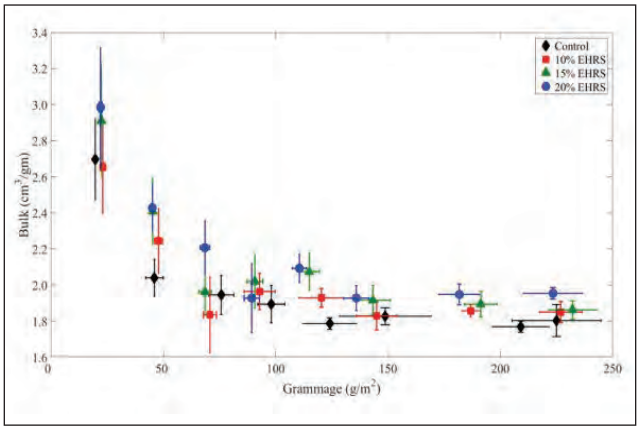
I. Fiber and fines analysis.

because they were of similar color and contained similar amounts of lignin. Results for the Kubelka-Munk specific scattering coefficient, *s*, are in the Discussion section.

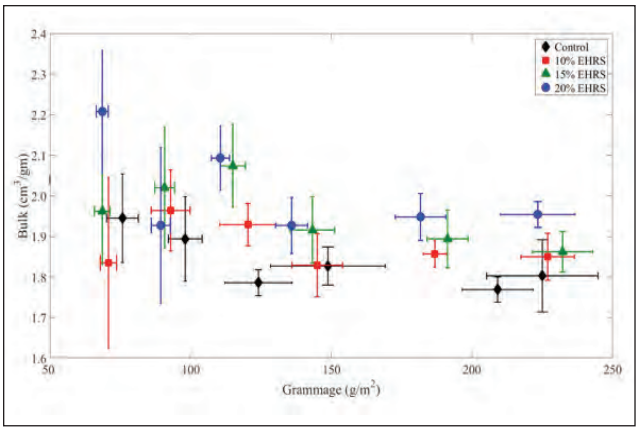
RESULTS

The physical characteristics of the kraft pulp and EHRS material were examined with a Fiber Quality Analyzer (OpTest Equipment; Hawkesbury, ON, Canada) and are listed in **Table I**. Pulp preparation was designed to produce few fines and maintain fiber length. EHRS material had a large amount of fines and short fibers. Pulp curl and kink indices indicate the pulp fibers were straight with few abrupt angles. EHRS curl index indicates the material was composed of generally straight fibers, whereas the kink index indicates that some folding of fibers was present. As expected, fiber widths were similar for each material. The EHRS material was quite coarse but was likely influenced by the large amount of short fibers.

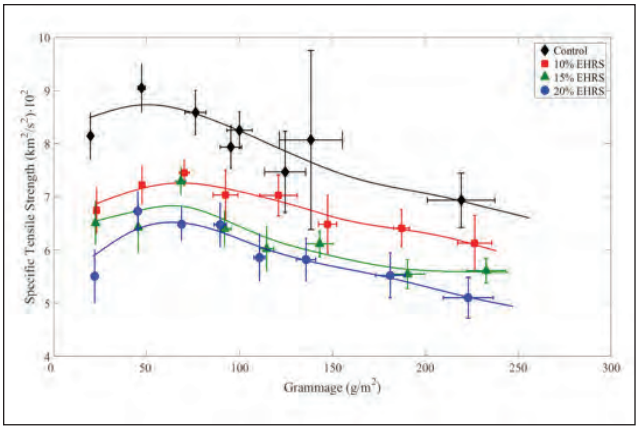
Figure 2 and **Figure 3** show that the addition of EHRS did add bulk; Fig. 3 uses the same data, but includes only those materials greater than 40 g/m². Each data marker is located at the mean grammage and mean bulk for each handsheet set; errors bars denote standard deviation. Significant bulk increases were not evident until grammages were above 100 g/m², at which point each additional amount of EHRS increased bulk. It is not possible to use microscopy to verify amount of EHRS retention. A combination of a coarse furnish and the lack of filter caking yielded inconsistent bulk improvements at low grammages. At high grammages, the increased amount of fibers reduced the number of pores and improved fines retention.



2. Enzymatic hydrolysis residual solids (EHRS) material increased handsheet bulk. Horizontal and vertical error bars span a standard deviation from the mean value in all four directions.

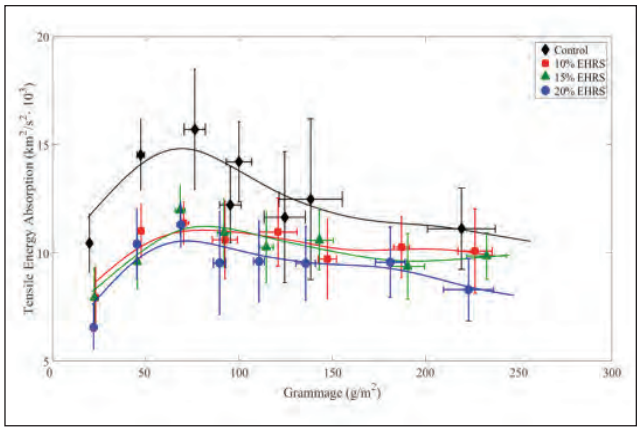


3. EHRS material increased handsheet bulk on reduced x-axis scale. Horizontal and vertical error bars span a standard deviation from the mean value in all four directions.

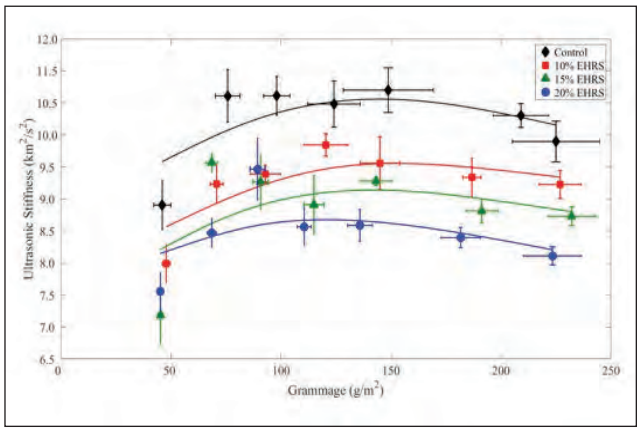


4. Specific tensile strength for each handsheet. Lines are smoothed cubic splines intended to guide the reader's eye. Horizontal and vertical error bars span a standard deviation from the mean value in all four directions.

Figure 4 shows the specific tensile strength results for the materials in this study. The general trend for each material in Fig. 4 agrees with data of I'Anson and Sampson [19], which they related to Wiebull's failure theory. At low grammages, the material is nearly discrete and stress transfer between fibers is inefficient, e.g., creating bending moments between two perpendicular bonded fibers. Additional fibers improve stress transfer efficiency. Finally, inefficiency occurs with more fibers as probability of weak zones increases. For the control material, weak zones occurred in regions of poor bonding. Tensile failure strain, not shown, had a large amount of scatter and no general trends were observed. So, although specific tensile



5. Tensile energy absorption (TEA). Lines are smoothed cubic splines intended to guide the reader's eye. Horizontal and vertical error bars span a standard deviation from the mean value in all four directions.



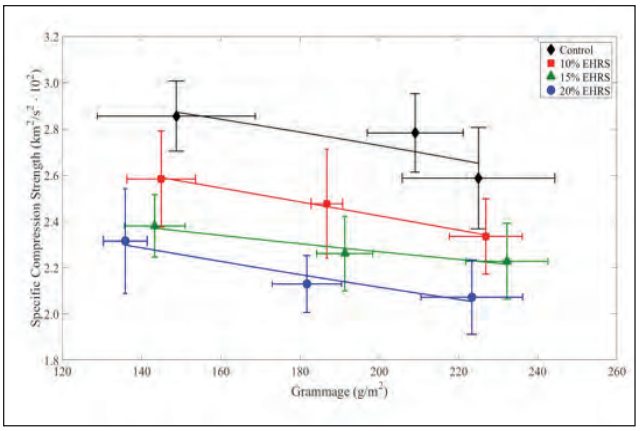
6. Ultrasonic stiffness. Lines are smoothed cubic splines intended to guide the reader's eye.

strength was reduced, stretch was largely unaffected.

TEA results are shown in **Fig. 5**; even the smallest addition level of EHRS (10%) produced large TEA reduction. Higher levels of EHRS addition did not create more reduction. As in specific strength, TEA peaked near 60 g/m² and decreased with grammage.

Ultrasonic stiffness measurement requires a continuum [20], which was violated by the 20 g/m² handsheets, and those results are not included. The results for the 40 g/m² handsheets could also be reasonably questioned. In **Fig. 6**, the ultrasonic stiffness increased with grammage up to about 120 g/m². Removal of the data below 50 g/m² would indicate a gradual reduction of ultrasonic stiffness with increased grammage. This reduction likely occurs because the weak/soft zones of the handsheets increased with grammage, reducing the velocity and increasing the attenuation of the bulk ultrasonic wave.

For handsheets above 100 g/m², compression strength is shown in **Fig. 7**. The bond disruption caused by EHRS reduced compression strength and was generally in proportion



7. Compression strength. Lines are smoothed cubic splines intended to guide the reader's eye.

to the addition of EHRS. The gradual decrease of compression strength with increased grammage is similar to the loss in tensile strength and reflects the greater likelihood for defects at higher grammages.

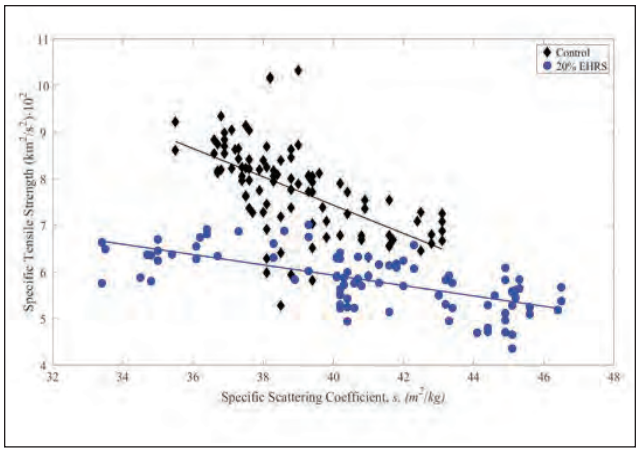
DISCUSSION

This study demonstrates some of the challenges to the papermaker. Although several variables were examined, namely grammage and EHRS loading level, many other variables, namely processing and refining of control pulp and EHRS, were not examined. A more detailed examination of processing and refining may be helpful when addressing the requirements of a particular product. Prescribed refining of fines [9] has been used to maintain tensile index.

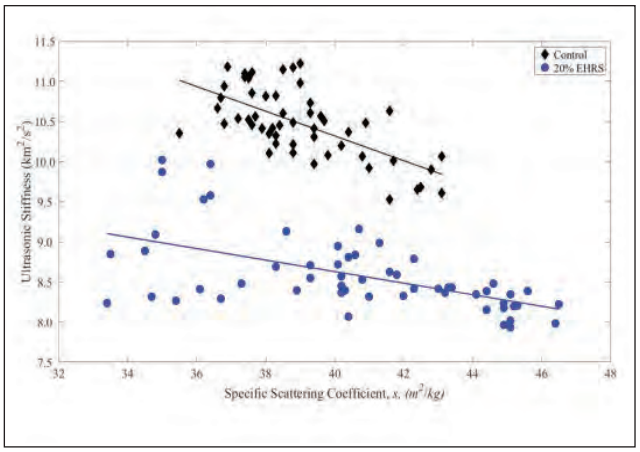
Economically beneficial use of EHRS is important to the success of biofuels. Unlike other bulking agents, such as thermomechanical pulp (TMP) fibers, wood powder, etc., EHRS is a low-value byproduct. Creation of bulk demonstrated here, while controlling physical and mechanical properties, adds value to EHRS and creates an additional revenue stream for cellulosic ethanol production.

It was not possible to directly determine the amount of EHRS in each handsheet. Loss of specific tensile strength shown in Fig. 4 provides good evidence that EHRS was retained in the sheet and that higher dosages of EHRS resulted in additional EHRS retention. Loss of specific tensile strength between control and 10% EHRS was similar to the loss between 10% EHRS and 20% EHRS materials. Given this behavior, it seems reasonable to expect that if 5% EHRS loaded handsheets had been produced, their specific tensile strength would tend to lie midway between the control and 10% loaded material and would likely be an appropriate loading level for commercial products.

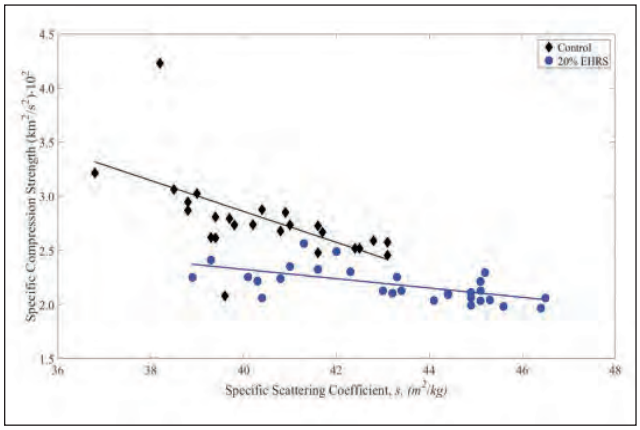
Strength is controlled by weak regions [19], which increase in number with added material and was similar in both tension, Fig. 4, and compression, Fig. 7. Bulking increased the probability density of weak regions. In some instances, fines act as small fibers, which assist inter-fiber bond formation



8. Light scattering and tensile index. Lines are smoothed cubic splines intended to guide the reader's eye.



10. Light scattering and ultrasonic stiffness. Lines are smoothed cubic splines intended to guide the reader's eye.



9. Light scattering and compression index. Lines are smoothed cubic splines intended to guide the reader's eye.

[21]. However, EHRS behaved more like inorganic fillers, which interfere with fiber bonds and reduce tensile index and Scott Bond [22].

The mechanisms that influence stiffness and strength are not the same [23]. Stiffness is relatively insensitive to material heterogeneities, whereas strength is greatly influenced. Fiber bonding has a significant influence on both. Loss of ultrasonic stiffness, as seen in Fig. 6, was almost independent of EHRS loading up to 100 g/m². Above that grammage, the ultrasonic stiffness was not independent of EHRS loading, likely caused by increased bond disruption, which affects the ability of the bulk wave to travel through the material.

Specific tensile stiffness, which is not shown, is not a relevant property to compare EHRS addition among the various grammages. Because ultrasonic stiffness is a bulk material property, the differences between EHRS loading amounts better represent network behavior. Coffin et al. [24] attributes the differences between these measurements to time dependent behavior, experimental errors, and difficulty in slope determination for the tensile stiffness. Machine compliance of the tensile tester also increases with greater material stiffness, i.e., the tensile stiffness will be reduced more at higher grammages than lower grammages as the machine compliance effects become more dominant.

At 20% EHRS loading, the EHRS decreased scattering, **Fig. 8**, at the similar tensile indices. This would occur if EHRS filled void spaces and reduced surface roughness [25]. Here, EHRS material was not refined, but purposeful fines refining can improve scattering and tensile index [26].

Figure 8 also indicates the significant effect of EHRS addition; this effect is similar in compression strength, as shown in **Fig. 9**. Changes in relationship between scattering and strength are less sensitive with addition of EHRS than that of the control material. These data indicate that for these materials, strength can be predicted by amount of kraft fibers and a bonding factor, where the bonding factor is given by s. Knowledge of the relationship between strong fibers, scattering (i.e., bonding), and strength is important in process control systems.

EHRS addition creates extensive bond disruption and reduces ultrasonic stiffness. **Figure 10** suggests that the bond disruption is so prevalent that increased scattering (more bond disruption) causes less network disturbance because the additional EHRS has less probability of disrupting critical bonding regions. Increased scattering for the control material proportionally decreased ultrasonic stiffness more; the increased scattering was directly disrupting critical bonding regions.

CONCLUSION

This study suggested a framework for the investigation of incorporation of processed biomass in a paper sheet in order to provide important information regarding mechanical, physical, and optical property changes. Potential users will be able to make decisions on this biomass as an additive for their products. Furthermore, this framework provides a basis for investigation of the use of other processed biomass in cellulose-fiber materials.

Addition of EHRS increased bulk and reduced tensile strength, ultrasonic stiffness, and specific compression strength in proportion to the amount of EHRS addition.

Stretch was unaffected by EHRS addition. Specific tensile energy absorption had significant reduction across all grammages, regardless of the amount of EHRS added.

The effect of EHRS was similar to that of other bulking materials where bulk is increased at the expense of strength properties. When increased bulk is desired in paper materials, use of EHRS would improve the economic viability of cellulosic ethanol production and provide an additional revenue stream for papermakers.

Light scattering was related to specific tensile strength, specific compression strength, and ultrasonic stiffness, but the relationship was different with EHRS addition. EHRS decreased the sensitivity of these properties to scattering differences.

Optimizing ethanol production and paperboard properties by feedstock source, byproduct refining, and end product requirements is a difficult task but also promises significant economic reward. **TJ**

ACKNOWLEDGEMENTS

The authors thank Mrs. Vance Setterholm for her financial support of this work in honor and memory of Mr. Vance Setterholm's lifelong paper physics accomplishments. A large portion of the experimental work was completed by Gina C. Snavely during her internship at USDA Forest Products Laboratory.

LITERATURE CITED

1. Zhu, J.Y. and Pan, X.J., *Bioresour. Technol.* 101(13): 4992(2010).
2. Zhou, H., Zhu, J.Y., Luo, X., et al., *Ind. Eng. Chem. Res.* 52(45): 16057(2013).
3. Zhu, J.Y., Chandra, M.S., Gu, F., et al., *Bioresour. Technol.* 179: 390(2015).
4. Eriksen, Ø., Syverud, K., and Gregersen, Ø., *Nord. Pulp Pap. Res. J.* 23(3): 299(2008).
5. Taipale, T., Osterberg, M., Nykänen, A., et al., *Cellulose* 17(5): 1005(2010).
6. Missoum, K., Martoïa, F., Belgacem, M.N., et al., *Ind. Crops Prod.* 48: 98(2013).
7. Petroudy, S.R.D., Syverud, K., Chinga-Carrasco, G., et al., *Carbohydr. Polym.* 99: 311(2014).
8. Su, J., Mosse, W.K.J., Sharman, S., et al., *Cellulose* 20(4): 1925(2013).
9. Chen, J., Zhang, M., Yuan, Z., et al., *BioResources* 8(4): 6309(2013).
10. Su, J., Zhang, L., Batchelor, W., et al., *Cellulose* 21(4): 2901(2014).
11. Lee, J.Y., Kim, C.H., Seo, D.J., et al., *TAPPI J.* 13(11): 17(2014).
12. Gao, Y., Rajbhandari, V., Li, K., et al., *TAPPI J.* 7(4): 4(2008).
13. Lee, J.-Y., Kim, C.-H., Lim, G.-B., et al., *Appita J.* 67(2): 122(2014).
14. Cannell, E. and Cockram, R., *Pulp Pap. Can.* 74(5): 61(2000).
15. Zhu, J.Y., Pan, X.J., Wang, G.S., et al., *Bioresour. Technol.* 100(8): 2411(2009).

ABOUT THE AUTHORS

Bulking agents can reduce fiber costs. We decided to examine the byproducts of cellulosic ethanol production as bulking agents to improve cellulosic ethanol economics. This work supports earlier work where identification of material properties was critical.

We did encounter difficulty in directly determining the amount of EHRS in the handsheets, but use of light scattering provided a good surrogate for direct determination. We also discovered that much work remains to be done. EHRS, and other bulking agents, may be viable,
but require optimization for particular applications. Our most interesting finding was that the mechanical properties varied directly with EHRS addition.

Bulking agents are in great demand. Production of bulking agents from low value wood may add a revenue stream for mills. Our next step is to examine processing the bulking agent to reduce mechanical property loss.

Considine is material research engineer at the USDA Forest Service, Forest Products Laboratory, Madison, WI, USA. Coffin is professor, Miami University, Oxford, OH, USA. Zhu is research general engineer, Mann is physical science technician, and Tang is engineering technician at the USDA Forest Service, Forest Products Laboratory, Madison, WI, USA. Email Considine at jconsidine@fs.fed.us.


Considine


Coffin

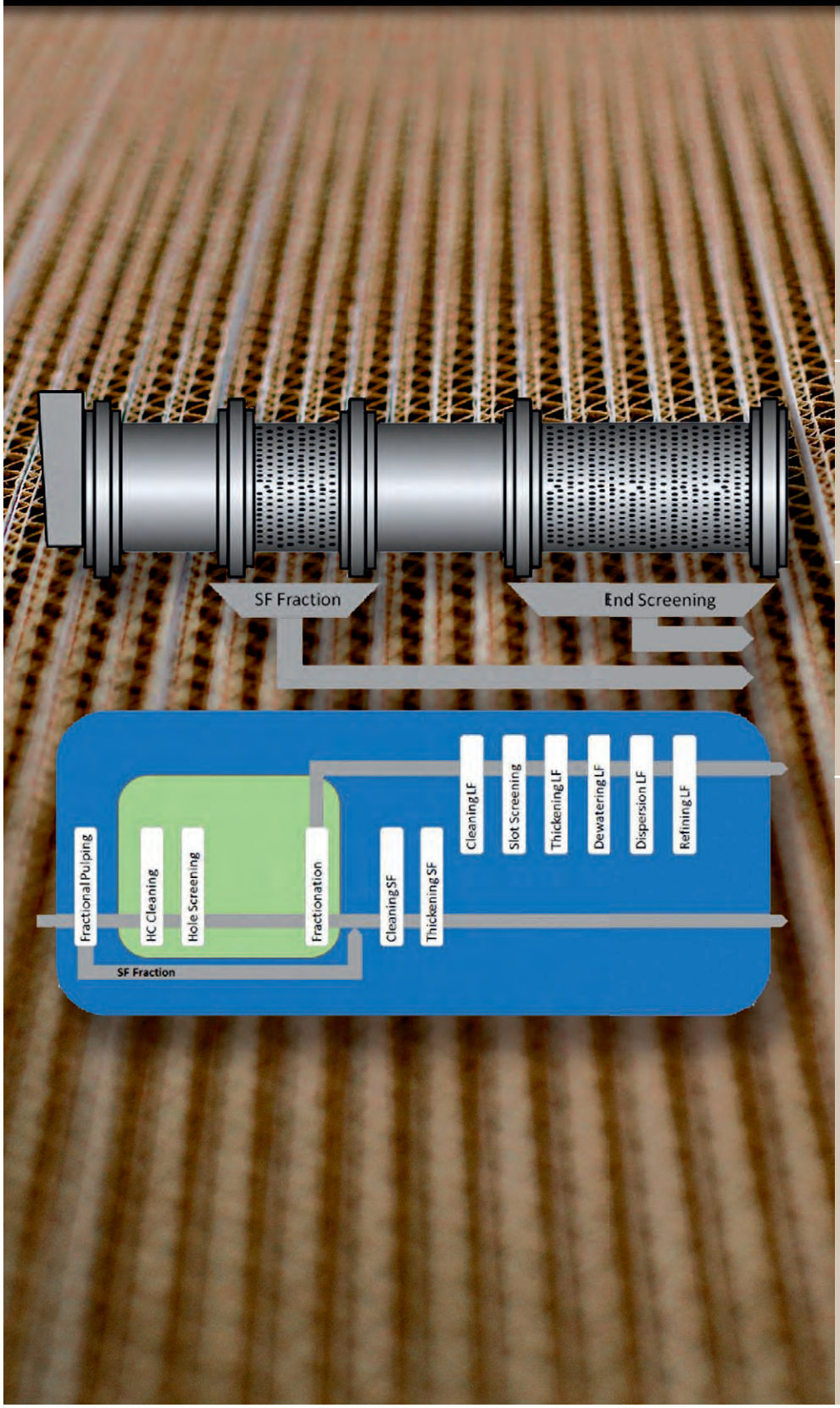

Zhu


Mann


Tang

16. Andersson, O. and Berkyto, E., *Sven. Papperstidn.* 54(13): 437(1951).
17. Vahey, D.W., Zhu, J.Y., and Houtman, C.J., *Prog. Pap. Recycl.* 16(1): 3(2006).
18. Vahey, D.W., Zhu, J.Y., and Houtman, C.J., U.S. Patent 7,495,221 (Feb. 24, 2009).
19. I'Anson, S.J. and Sampson, W.W., *Compos. Sci. Technol.* 67(7): 1650(2007).
20. Habeger, C.C., Mann, R.W., and Baum, G.A., *Ultrasonics* 17(2): 57(1979).
21. De Silveira, G., Zhang, X., Berry, R., et al., *J. Pulp Pap. Sci.* 22(9): J315(1996).
22. Gerli, A., Eigenbrood, L.C., and Nurmi, S., *TAPPI J.* 10(2): 17(2011).
23. Niskanen, K. and Kärenlampi, P., in *Paper Physics*, Fapet Oy, Helsinki, 1998, Chap. 5.
24. Coffin, D., Lif, J., and Fellers, C., *Nord. Pulp Pap. Res. J.* 19(2): 257(2004).
25. Retulainen, E., Nieminen, K., and Nurminen, I., *Appita J.* 46(1): 33(1993).
26. Gorski, D., Mörseburg, K., and Johansson, L., *Nord. Pulp Pap. Res. J.* 26(3): 232(2011).

TAPPI JOURNAL
WWW.TAPPI.ORG
THE PAPER AND PACKAGING INDUSTRIES' TECHNICAL RESOURCE
FEBRUARY 2017 | VOL. 16 NO.2



NONWOOD PULPING 57
Low-temperature precausticizing — a hopeful approach for green liquor desilication
Xinxing Xia, Fang Wang, Xiaojing Qin, Tingting Tang, and Tianwen Zhou

PROCESS CONTROL 65
Understanding conductivity and soda loss
Michael T. Brown and Peter W. Hart

PAPERMAKING 81
Estimating limits of wet pressing on paper machines
J. David McDonald and Richard J. Kerekes

RECYCLING 89
Fractional pulping of packaging board in high consistency drum pulping
Heikki Upola, Ari Ämmälä, and Mirja Illikainen

February 2017

TABLE OF CONTENTS VOL. 16 NO. 2

53 **EDITORIAL**
From rocket science to innovation in bioenergy & bioproducts
Danny Haynes

57 **NONWOOD PULPING**
Low-temperature precausticizing — a hopeful approach for green liquor desilication
Xinxing Xia, Fang Wang, Xiaojing Qin, Tingting Tang, and Tianwen Zhou

65 **PROCESS CONTROL**
Understanding conductivity and soda loss
Michael T. Brown and Peter W. Hart

81 **PAPERMAKING**
Estimating limits of wet pressing on paper machines
J. David McDonald and Richard J. Kerekes

89 **RECYCLING**
Fractional pulping of packaging board in high consistency drum pulping
Heikki Upola, Ari Ämmälä, and Mirja Illikainen

»COVER CREDIT: Researchers Upola et al. (p. 89) describe how fractional pulping might provide an opportunity for more efficient drum pulper designs used in the old corrugated container (OCC) recycling process. The short fiber (SF) fraction could bypass the coarse cleaning and screening, along with pressure screen fractionation, needed by long fiber (LF) fractions, resulting in energy savings.

TAPPI JOURNAL
WWW.TAPPI.ORG

Editor-in-Chief
Scott Rosencrance scott.rosencrance@kemira.com
+1 770 429-2753

Associate Editor
Brian N. Brogdon brian.brogdon@gmail.com
+1 678 581-9114

Editorial Director
Monica Shaw mshaw@tappi.org
+1 770 367-9534

Vice President, Operations
Eric Fletty efletty@tappi.org

PRESS Manager
Jana Jensen jjenson@tappi.org
+1 770 209-7242

Webmaster
Trina Heath theath@tappi.org
+1 770 209-7416

***TJ* EDITORIAL BOARD**

Brian N. Brogdon, FutureBridge Consulting & Training LLC
brian.brogdon@gmail.com, +1 678 581-9114

David A. Carlson, Carlson Consulting
dacarlson39@aol.com, +1 847 323-2685

Jere W. Crouse, JWC Consulting
cj522@inwave.com, +1 608 362-4485

Mahendra Doshi, Doshi and Associates
mahen@aol.com, +1 920 832-9101

Marc Foulger, GL&V USA Inc.
Marc.foulger@glv.com +1 315 767-2920

Peter W. Hart, MeadWestvaco Corporation
pwh3@meadwestvaco.com, +1 409 276-3465

Carl J. Houtman, USDA Forest Products Laboratory
choutman@fs.fed.us, + 1 608 231-9445

John A. Neun, John A. Neun LLC
john.neun@gmail.com, +1 518 275-8139

Jim Niemiec, Verso Corporation
jim.niemiec@versoco.com, +1 715 422-7404

Steven P. Ottone, Omya
steven.ottone@omya.com, +1 919 641-7854

Gaurav Pranami, Imbed Biosciences
gpranami@imbedbio.com, +1 515 230-7005

Arthur Ragauskas, Oak Ridge National Laboratory
aragausk@utk.edu

Gerard J.F. Ring, University of Wisconsin—Stevens Point
gerrryring@wi-net.com, +1 715 592-3732

Scott Rosencrance, Kemira Chemicals
scott.rosencrance@kemira.com, +1 770 429-2753

Ricardo B. Santos, MeadWestvaco Corporation
ricardo.santos@mwv.com, +1 540 969-2426

Paul Wiegand, NCASI
pwiegand@ncasi.org, +1 919 941-6417

Junyong Zhu, USDA Forest Products Laboratory
jzhu@fs.fed.us, +1 608 231-9520

Join TAPPI *today!*

TAPPI JOURNAL is a free benefit of TAPPI membership, and is only available to members. To join TAPPI, to renew your TAPPI Membership, or to learn about other valuable benefits, visit www.tappi.org.

TAPPI, 15 Technology Parkway S., Suite 115, Peachtree Corners, GA 30092, publishes *TAPPI JOURNAL* monthly.

ATTENTION PROSPECTIVE AUTHORS: All papers published are subject to *TAPPI JOURNAL's* peer-review process. Not all papers accepted for review will be published. Before submitting, check complete author guidelines at http://www.tappi.org/s_tappi/doc.asp?CID=100&DID=552877.

Statements of fact and opinions expressed are those of individual authors. TAPPI assumes no responsibility for such statements and opinions. TAPPI does not intend such statements and opinions or construe them as a solicitation of or suggestion for any agreed-upon course of conduct or concerted action of any sort.

Copyright 2017 by TAPPI, all rights reserved. For copyright permission to photocopy pages from this publication for internal or personal use, contact Copyright Clearance Center, Inc. (CCC) via their website: www.copyright.com. If you have questions about the copyright permission request process, please contact CCC by phone at +1 978 750-8400. To obtain copyright permission to use excerpts from this publication in another published work, send your specific request in writing to Editor, TAPPI JOURNAL, 15 Technology Parkway S., Suite 115, Peachtree Corners, GA 30092, USA; or by fax to +1 770 446-6947. Send address changes to TAPPI, 15 Technology Parkway S., Suite 115, Peachtree Corners, GA 30092, USA; Telephone +1 770 446-1400, or FAX +1 770 446-6947. www.tappi.org

Guest Editorial



DANNY HAYNES
2017 IBBC Technical Program Chair

From rocket science to innovation in bioenergy & bioproducts

I came to the pulp and paper industry from the aerospace industry (predicting thermal environments of launch vehicles) by answering an advertisement from AkzoNobel for a deinking specialist. Back in 1994, the recycling industry was working to recover valuable fiber that was being wasted in landfills. There were many technical hurdles to recycling paper — among them, removing the ink and not enough trained people for the challenge. My boss looked outside the industry to give me an opportunity to use rocket science in my more than 20 years of developing and innovating in our industry, with the latest effort being in bioproducts.

Today, our industry is making good use of our naturally renewable resource for bioenergy and seeking innovative ways to convert biomass into a wide range of bioproducts. AkzoNobel still looks outside the box for sustainable pathways by asking for innovators and startup companies to "Imagine Chemistry" and provide sustainable chemicals for the world (https://imaginechemistry.akzonobel.com/), with this year's platform open until March 16.

International Bioenergy & Bioproducts Conference

The International Bioenergy & Bioproducts Conference (IBBC) focuses on new technologies using renewable materials from biomass to produce chemicals and fuels to support the growing bioeconomy. When IBBC started, it offered a frontier of possibilities, with no certain path to success in the field. Today, we have production of lignin and several possible routes to a range of bioproducts.



You have an opportunity to put on your innovation cap and participate in the 2017 International Bioenergy & Bioproducts Conference (IBBC) that will be held at the new Hilton Norfolk the Main in Norfolk, VA, USA.

You have an opportunity to put on your innovation cap and participate in the 2017 International Bioenergy & Bioproducts Conference (IBBC) that will be held at the new Hilton Norfolk the Main in Norfolk, VA, USA. IBBC is co-located with the 2017 Pulping, Engineering, Environmental, Recycling and Sustainability (PEERS) Conference. Mark your calendars for the dates of November 5-9, 2017, for these two valuable TAPPI events with just one registration. The TAPPI IBBC website is now live at http://tappi-ibbc.org/ with travel and hotel information. Information regarding registration, workshops, technical program, committee meetings, and other events will follow in the coming weeks and months.

How you can present at 2017 IBBC

The IBBC technical programming committee is currently soliciting abstracts for presentations, panel discussions, and student posters. Students are also able to learn the art of quick communication of ideas in our special Rapid

Fire Showcase before the poster exhibit. We are seeking presentations in a broad range of topics, including innovative bioproducts, pathways for conversion of biomass, and developments of a bioeconomy. This year, you can hear both the biorefinery-based papers from PEERS along with the power point presentations of IBBC so that you have full access to some of the latest developments and research in the field.

You can download the Call for Abstracts from the web page http://tappi-ibbc.org/program/invitation-to-present/. IBBC is also open to other ideas that are of interest to the bio-based community. Please feel free to contact us with suggestions for session and panel discussions.

Abstracts for both IBBC and PEERS can be submitted through TAPPI's new Speaker Management System http://speakermanagement.tappi.org/. You may need to recreate a new login account. Instructions for creating an account and submitting an abstract can be found at the previously mentioned web link. If you have any trouble, please do not hesitate to contact Jessica Reaves or Pat Stiede at TAPPI for help.

The deadline for abstract submissions is March 24, 2017. The PEERS committee will meet on April 13, 2017, to review submissions and to organize the technical program.

So, prepare to network and learn about lignin recovery, applications for lignin, development of sugar based products, production of wood pellets, torrification, transformation of biomass, leveraging mill assets, biomass utilization — and more — at the 2017 IBBC in Norfolk. **TJ**

Danny Haynes is the Technical Program Chair for the 2017 IBBC and works for AkzoNobel Specialty Chemicals Business Area as a Common Application Team Leader. Email Danny at danny.haynes@akzonobel.com.

Low-temperature precausticizing — a hopeful approach for green liquor desilication

XINXING XIA, FANG WANG, XIAOJING QIN, TINGTING TANG, AND TIANWEN ZHOU

ABSTRACT: We investigated silica removal by low-temperature precausticizing and the properties of second causticizing calcium carbonate (CCC). The results showed that about 89.3% of silica removal was achieved when 20% (the stoichiometric ratio) of causticizing quicklime was added for precausticizing at 20°C for 60 min. After that, silica removal became slow. When no precausticizing quicklime was used to remove silica, the CCC particles had a rhombohedral crystal structure covered with amorphous material. As precausticizing quicklime was increased to 30%, the amorphous material and the crack disappeared, and the specific surface area decreased significantly. When CCC was used as filler, the Cobb value decreased significantly, and the sizing effect improved as precausticizing quicklime increased.

Application: Understanding the properties of CCC with different quicklime contents for low-temperature precausticizing, and its effect on paper quality, can mitigate the issues caused by "silica influence" and enable papermakers to reuse CCC produced from the chemical recovery process of wheat straw soda pulping.

Nonwood raw materials, such as wheat straw, bamboo, and reed, contain a moderate amount of silica, which causes serious problems in the chemical recovery process [1,2]. As we described before [3], many researchers [4-8] have tried to find effective ways to remove silica in the pulping process. The most successful approach to silica removal so far seems to be by precipitation from green liquor by partial acidification with carbon dioxide, or by addition of quicklime.

Myreen [9,10] suggested precipitating the silica by introducing carbon dioxide into the black liquor to convert sodium silicate into silica. In this process, about 90% of silica was removed, but foaming, precipitation, and adequate control of pH remained issues. Xia et al. [11] suggested precipitating silica by introducing carbon dioxide into green liquor. About 99% of silica removal was achieved with this method, and precipitation and foaming were no longer a problem, but adequate control of pH remained an issue.

Rao et al. [12] proposed two-stage causticizing to remove silica from green liquor in bamboo pulping. The silica was selectively precipitated in the first step by adding 30% of the causticizing quicklime at about 90°C to 95°C, and the lime mud generated was discarded. In the second step, the rest of the causticizing lime was added and the lime mud generated was calcined for reuse in the causticizing section. About 56% of the silica was removed by the first stage. However, about 44% of silica was left in the lime mud generated in the second stage. The selectivity of the process was not particularly good, and it does not seem to have been developed further. A rather different approach is to precipitate the silica onto the pulp [13]. This gives effective fixing of the silica, but reduces pulp strength, and silica also fixes onto equipment. Consequently, there has been no effective process to remove the silica from the green liquor yet. We investigated low-temperature precausticizing for silica removal, with good results.

EXPERIMENTAL

Materials

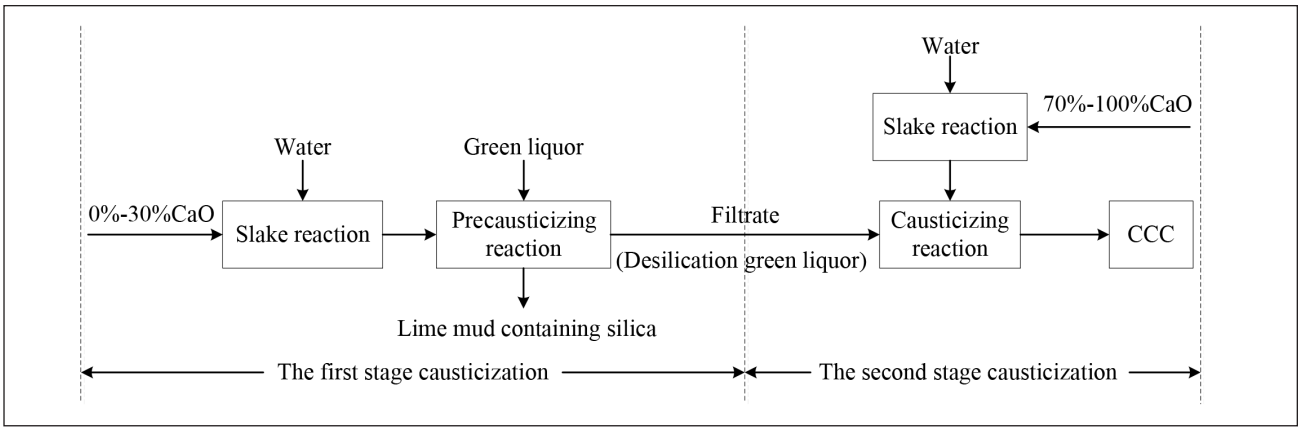
Green liquor from wheat straw soda pulping was collected from Xingbao Paper Industry Co. Ltd. in Xianyang, Shanxi Province, China. Calcium oxide was provided by Sinopharm Chemical Reagent Co. Ltd., Shanghai, China.

Determination of silica content in green liquor

The content of silica in green liquor was measured with spectrophotometry [14]. In weak acidic solutions, silica reacts with complex agent of ammonium molybdate to form silicon-molybdate ligand. The ligand is then reduced by ferrous sulfate to form $H_8[SiMo_2O_5(Mo_2O_7)_5]$. The absorbance of $H_8[SiMo_2O_5(Mo_2O_7)_5]$ was measured at 680 nm using a 722S spectrophotometer (Shanghai Arris Light Technology Co. Ltd.; Shanghai, China). The silica content was obtained by colorimetric analysis.

Two-stage causticization

Figure 1 shows a diagram of two-stage causticization. In the first stage (precausticization), a part of the total quicklime requirement (0% to 30% of the stoichiometric ratio) was



1. Diagram of two-stage causticization.

mixed with distilled water at a quicklime concentration of 20% by weight to prepare milk of lime using a slaking temperature of 80ºC and reaction time of 30 min. Then green liquor was reacted with calcium hydroxide to remove silica. The precausticizing was done at 20ºC with constant stirring for 60 min. At the end of the reaction time, the causticized slurry was filtered, and the filtrate was used for the second stage causticization. In the second stage, the filtrate obtained from the first stage was causticized with the slaked lime. The second stage used a filtrate loading rate of 0.094 mL/s, loading period of 90 min, temperature of 80ºC, and stirring speed of 300 rpm. After the reaction, the CCC was washed with water until neutral, then subjected to quality analysis.

Characterization of the CCC

The crystal forms of the CCC were examined with a D/MAX-1200 X-ray diffraction (XRD) analyzer (Rigaku Corporation; Tokyo, Japan), and the morphology of CCC was visualized with a Quanta 200 scanning electron microscope (FEI; Eindhoven, The Netherlands). The specific surface area was measured with a Micromeritics Instrument Corporation (Norcross, GA, USA) Gemini VII surface area analyzer. Fourier transform infrared spectroscopy (FTIR) spectra were obtained with a Nicolet 5700 FTIR spectrometer (Thermo Fisher Scientific; Waltham, MA, USA) using potassium bromide pellets.

Handsheet preparation

To a bleached hardwood kraft pulp, 0.15% of alkyl ketene dimmer as sizing agent, 20% of CCC as filler, 0.05% of cationic polyacrylamide, and 0.2% of bentonite as retention agents were added in sequence under mixing. Then, laboratory paper sheets (handsheets) were formed with a sheet former. Cobb value was determined according to TAPPI Standard Test Method T 441 om-09 "Water absorptiveness of sized (non-bibulous) paper, paperboard, and corrugated fiberboard (Cobb test)."

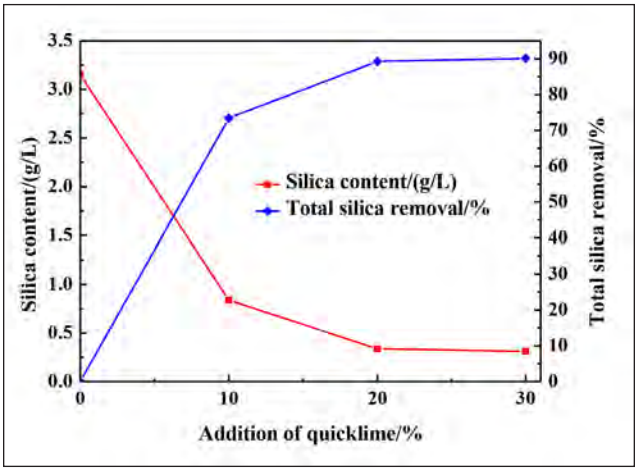
RESULTS AND DISCUSSION

Analysis of green liquor

Table I shows the composition of the green liquor. Sodium carbonate and active alkali were the main components of the green liquor. The content of silica was 4.2 g/L, which will cause serious problems in the recycling of lime mud.

Effect of low-temperature precausticizing on silica removal

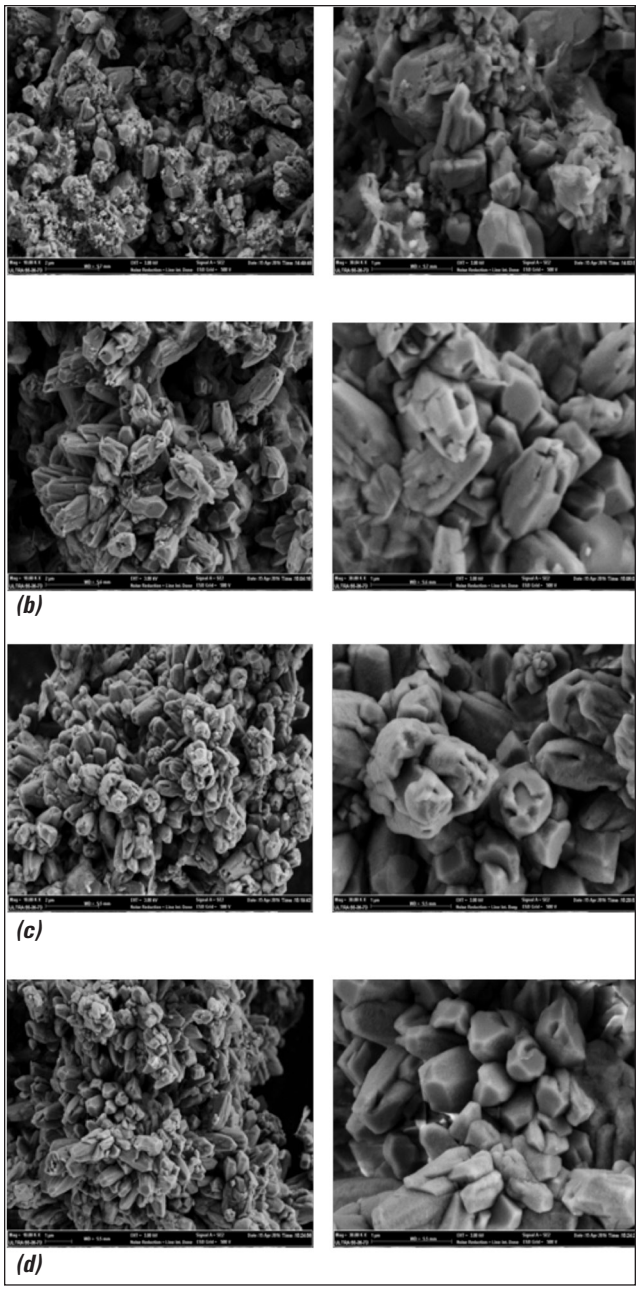
As Rao et al. [12] described, during two-stage causticization, silica is preferentially precipitated, followed by causticization when quicklime is added. This can be attributed to the faster rate of reaction between sodium silicate and calcium hydroxide compared with that between sodium carbonate and cal-



2. Effect of addition of precausticizing quicklime on silica removal.

Composition	Total Alkali (as NaOH)	Active Alkali (as NaOH)	Sodium Carbonate	Silicon Dioxide
Content, g/L	104.3	11.1	123.5	4.2

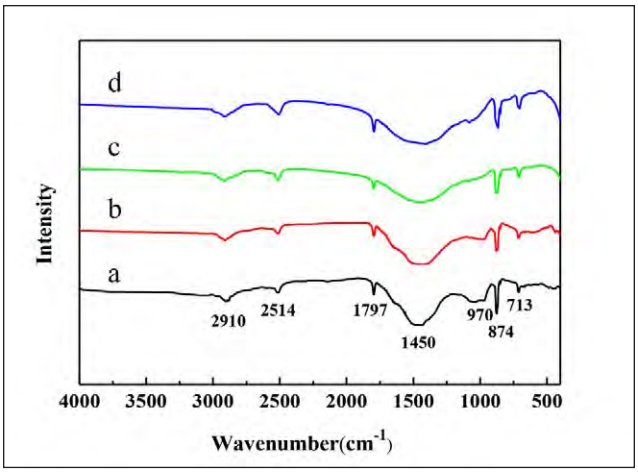
I. Analysis of green liquor.



3. Scanning electron microscope (SEM) images of causticizing calcium carbonate (CCC) with different added amounts of precausticizing quicklime: a = 0% of causticizing quicklime, b = 10% of causticizing quicklime, c = 20% of causticizing quicklime, d = 30% of causticizing quicklime.

cium hydroxide. Low temperature reduces the causticizing reaction rate between sodium carbonate and calcium hydroxide, which is beneficial to the reaction between sodium silicate and calcium hydroxide [15].

A part of the causticizing quicklime (0% to 30% stoichiometric ratio) was added to the green liquor at 20°C for precausticization. **Figure 2** shows that about 73.5% of silica was removed when 10% of quicklime was added. The desilication rate increased to 89.3% when the quicklime



4. Fourier transform infrared (FTIR) spectroscopy spectra of CCC with different added amounts of precausticizing quicklime: a = 0%, b = 10%, c = 20%, d = 30%.

dosage increased to 20%; after that, silica removal became slow. About 90.1% of silica removal was achieved when 30% of quicklime was used.

Morphology of CCC with low-temperature precausticizing

The chemical reactions during causticizing are as follows:

$$Ca(OH)_2+Na_2CO \rightarrow OaOH_3+2NaOH \quad (1)$$

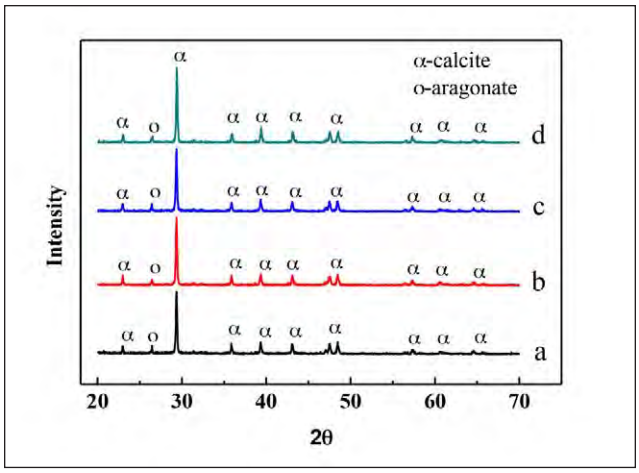
$$Ca(OH)_2+Na_2SiO_3+H_2OHOOH \rightarrow SiO_2 \rightarrow H_2O+2NaOH \quad (2)$$

The first and second reactions take place simultaneously, so the calcium silicate is generated with the calcium carbonate in the causticizing process. The morphology of CCC is not only affected by the causticizing reaction, but also by the calcium silicate generation.

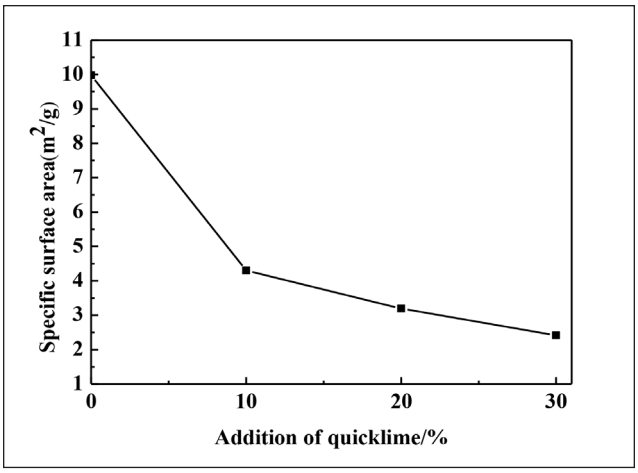
Figure 3 shows the morphology of the CCC formed in the second causticizing process after low-temperature precausticization. When no precausticizing quicklime was used to remove silica, the CCC particles had a rhombohedral crystal structure covered with amorphous material (Fig. 3a). As 10% of precausticizing quicklime was used (Fig. 3b), the amorphous material almost disappeared and the CCC particles had a rhombohedral crystal structure with cracks on the surface. The same was true with 20% of precausticizing quicklime (Fig. 3c). As the precausticizing quicklime was increased further, to 30% (Fig. 3d), the amorphous material disappeared completely, and the CCC particles had a clear rhombohedral crystal structure with no crack.

FTIR spectrum

FTIR is an effective method to evaluate the presence and the extent of silica in CCC. As shown in **Fig. 4**, the bands at 1450 cm^{-1} ($V_3(CO_3)$), 874 cm^{-1} ($V_2(CO_3)$), and 713 cm^{-1} ($V_4(CO_3)$) belong to the characteristic calcium carbonate absorption



5. X-ray diffraction (XRD) analyzer spectra of CCC with different added amounts of precausticizing quicklime: a = 0%, b = 10%, c = 20%, d = 30%.



6. Specific surface area of CCC with different added amounts of precausticizing quicklime.

bands [16]. The band at 970 cm^{-1} is the result of symmetric stretching of the Si–O-Si bonds [17]. When the precausticizing quicklime was 0% and 10% of the stoichiometric ratio, the band at 970 cm^{-1} was clearly observed. As the precausticizing quicklime increased to 30%, the band at 970 cm^{-1} disappeared, proving that the silica was almost totally removed.

Crystal forms of CCC

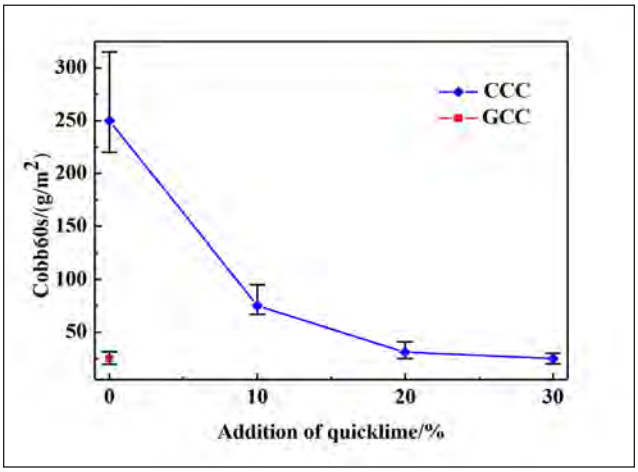
The crystal forms of the CCC were measured by powder XRD. As shown in **Fig. 5**, no matter how much of the precausticizing quicklime was added, the crystals of CCC were both calcite and aragonite [18-19]. The characteristic absorption peak of calcium silicate was not observed. This suggested that the calcium silicate itself did not polymerize to form crystal. However, as shown in Fig. 2 (especially Fig. 2a), some amorphous material was in the CCC. Amorphous basically means non-crystalline. As such, it cannot be detected by XRD analysis. It is likely that the amorphous material was calcium silicate hydrate gel, a well-known compound present in hydrated cement (concrete).

Specific surface area of CCC

The specific surface area of the CCC was tested with the low-temperature nitrogen adsorption method. As the added amount of quicklime for precausticization was increased, the specific surface area of the CCC decreased rapidly (**Fig. 6**). The specific surface area of un-precausticizing CCC was 9.98 m^2/g. As the precausticizing quicklime increased to 30% of the stoichiometric ratio, the specific surface area decreased by nearly 76%, to 2.41 m^2/g. This was the result of the change in morphology of the CCC caused by the removal of silica in the precausticizing process.

Effect on paper sizing of CCC with low-temperature precausticizing

As shown in **Fig. 7**, as precausticizing quicklime increased, the Cobb value decreased rapidly and the sizing effect improved. When the precausticizing quicklime increased from 0% to 20%,



7. Effect of precausticizing quicklime addition on paper sizing degree (CCC = causticizing calcium carbonate; GCC = ground calcium carbonate).

the Cobb value decreased from 250.3 g/m^2 to 31.2 g/m^2, which met the sizing requirement for fine paper. This resulted from the presence of hydroxyl in calcium silicate hydrate, which increased the hydrophilicity of the CCC. In addition, the high surface area and porosity of CCC with high silica content increased the absorption of alkyl ketene dimers, thus leading to the difficulty of sizing [20]. When the added amount of precausticizing quicklime increased to 30%, the Cobb value was 25.1 g/m^2. Therefore, low-temperature precausticizing is an effective method to remove silica from green liquor.

CONCLUSIONS

When 20% (the stoichiometric ratio) of quicklime was added for precausticizing at 20°C for 60 min, about 89.3% of silica removal was achieved; after that, silica removal became slow. When no precausticizing quicklime was used to remove silica, the CCC particles had a rhombohedral crystal structure covered with amorphous material. When the precausticizing quicklime was increased to 30%, the amorphous material and

the crack disappeared, and the specific surface area decreased significantly. When the CCC was used as filler, with the increasing of precausticizing quicklime, the Cobb value decreased significantly and the sizing effect improved. **TJ**

ACKNOWLEDGEMENTS

This work was supported by the State Key Laboratory of Pulp and Paper Engineering, South China University of Technology (201509), and Science Foundation of Zhejiang Sci-Tech University (14012081-Y). The authors would like to acknowledge all the assistants in the project group and the industrial partners who provided the materials.

LITERATURE CITED

1. Lin, T., Li, X., Xu, Y.J., et al., *BioResources* 9(3): 4690(2014).
2. Runge, T.M. and Paul, S., *TAPPI J.* 14(11): 743(2015).
3. Xia, X.X., Wang, X., Tong, S.H., et al., *BioResources* 10(2): 3694(2015).
4. Bohmer, V.J., *Tappi J.* 67(11): 116(1984).
5. Folke, J. and Guerra, M., *Chemosphere* 24(4): 371(1992).
6. Xu, Y.J., Sun, H., Li, X., et al., *BioResources* 10(2): 1988(2015).
7. Wang, P., Pan, D., Chen, Y., et al., *China Pulp Pap.* 22(11): 14(2003).
8. Mandavgane, S.A., Paradkar, G.D., Varu, J., et al., *Indian J. Chem. Technol.* 14(6): 606(2007).
9. Myreen, B., *Int. Chem. Recovery Conf.*, TAPPI PRESS, Atlanta, GA, USA, 1998, p. 823.
10. Myreen, B., U.S. pat. 6,183,598 (Feb. 6, 2001).
11. Xia, X.X., Du, M.Z., and Geng, X.J., *TAPPI J.* 12(3): 35(2013).
12. Rao, G.V., Murthy, N.V.S.R., Annamraju, P.V., et al., *Appita* 41(1): 33(1988).
13. Tutus, A. and Eroglu, H., *Appita* 56(2): 111(2003).
14. Shi, Y.Q., Ding, L.B., Li, P., et al., *J. Chem. Ind. For. Prod.* 38(1): 25(2004).
15. Zhan, H.Y., *Pulp Science & Technology*, China Light Industry Press, Beijing, 2009.
16. Nyquist, R.A., Putzig, C.L., and Leugers, M.A., *Infrared and Raman Spectral Atlas of Inorganic Compounds and Organic Salts*, Academic Press, San Diego, CA, USA, 1997.
17. Gamelas, J., Lourenco, A.F., Ferreira, P.J., *J. Sol-Gel Sci. Technol.* 59(1): 25(2011).
18. Zhu, G.Y., Li, H.Q., Li, S.P., et al., *J. Cryst. Growth* 428: 16(2015).
19. Haruo, K., Yasunori, N., and Mitsutaka, K., *Powder Technol.* 129: 15(2003).
20. Bartz, W.J., Darroch, M.E., and Kurrle, F.L, *TAPPI J.* 77(12): 139(1994).

ABOUT THE AUTHORS

We chose this topic to research because many mills with nonwood materials face problems caused by high silica content in green liquor during chemical recovery. We tried to remove silica with low-temperature precausticizing and had amazing results.

Previous research studied the method of silica removal with precausticizing at high temperature, which had lower desilication rate than that at low temperature.

The most difficult aspect of this research was to find out how precausticizing quicklime affects the properties of causticizing calcium carbonate (CCC) and paper quality when used as filler. We accomplished this with characterization methods that included scanning electron microscopy, Fourier transform infrared spectroscopy, X-ray diffraction, surface area, and Cobb value of paper.

We discovered that when 20% quicklime (the stoichiometric ratio) was added for precausticizing for 60 min at 20°C, about 89.3% of silica removal was achieved; after that, silica removal became slow.

We found that CCC particles all formed with calcite and aragonite. As the precausticizing quicklime increased, the amorphous material and the crack disappeared, and the specific surface area decreased significantly. When the CCC was used as filler, with the increasing of precausticizing quicklime, the Cobb value decreased significantly and the sizing effect obviously improved.

Mills could use this method to mitigate the problems of "silica influence" in the chemical recovery process and improve the recycling of lime mud.

Our next step is to find an industry partner to work with on removing silica with low-temperature precausticizing.

Xia is professor, and Wang, Qin, Tang, and Zhou are graduate students, Zhejiang Sci-Tech University, Hangzhou, Zhejiang, China. Email Xia at xingxingxia2000@hotmail.com.


Xia


Wang


Qin


Tang


Zhou

Understanding conductivity and soda loss

MICHAEL T. BROWN AND PETER W. HART

ABSTRACT: For more than 40 years, conductivity has been the inline measurement of choice for inferring black liquor/soda losses from brownstock washing. If properly applied, conductivity can provide a benefit in tracking changes in black liquor filtrate concentration. The implied concentration changes in turn can be used to provide feedback for dilution factor or shower flow control on the last stage of a brownstock washing system. A further extrapolation of this application is the correlation (or lack of correlation) of conductivity to soda loss. For each type of conductivity-based application, there are fundamental principles and assumptions that must be understood and managed to achieve the expected outcomes. The fundamentals of conductivity, the application of conductivity to measure black liquor losses during brownstock washing, and laboratory considerations when attempting to correlate inline process conductivity to absolute sodium content are reviewed and investigated. Finally, the operational objectives and measurement alternatives for employing conductivity measurements are discussed.

Application: Mills can gain knowledge about the theory, practice, and limitations associated with conductivity measurements, which can be used as a reliable feedback control mechanism for controlling brownstock washers.

Electrical conductivity (or specific conductance) of an electrolyte solution is a measure of its ability to conduct electricity. Much work has been done over the past 30–40 years to use electrical conductivity (EC) to measure black liquor losses during brownstock washing. There are some advantages to using this electrochemical measurement but there are also many disadvantages and misconceptions. First, EC probes are relatively inexpensive, easy to install, and provide a continuous signal with a quick response to changes in ionic concentration. The probe installation does not require any specialized sampling system. The probe can be placed directly into process lines and, except for periodic cleaning, it is low maintenance.

Unfortunately, EC measurements are not ion specific. Changes in any species within the solution exhibiting ion activity (both anodic and cathodic) will result in changes in the EC measurement. Such measurements are quite sensitive to temperature changes, and, even with temperature compensation, are only functional over a relatively narrow temperature range. In addition, some EC probes are subject to drift, as well as probe saturation; this results in either erroneous or flat-line responses. Finally, EC correlation to absolute concentration changes (e.g., sodium sulfate [Na_2SO_4], sodium hydroxide, sodium carbonate) has significant limitations when applied to black liquor.

FUNDAMENTALS OF CONDUCTIVITY

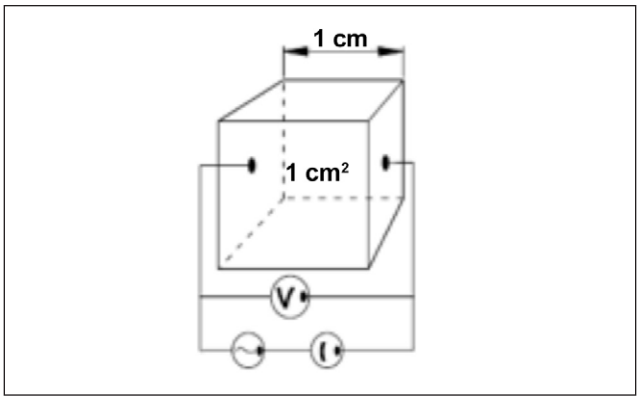
In the context of aqueous solutions, EC is a measure of the ability of the solution to conduct an electric current. Electrical conductivity measurements are affected by the concentration of the ions in solution (i.e., the higher the ion concentrations, the higher the EC values), the temperature of the solution (i.e., the higher the temperature, the higher the EC value), and the specific nature of the ions present (i.e., the higher specific ability and higher valence of the ions, the higher the EC value).

Electrical conductivity is measured as the inverse of resistance (R). From Ohm's Law (V = I * R), EC can be determined by applying a voltage (V) across two electrodes in a solution and measuring the induced current (I). Electrical conductivity is then calculated by dividing the current by the voltage. Using 1/R as the reciprocal of EC, EC= I/V.

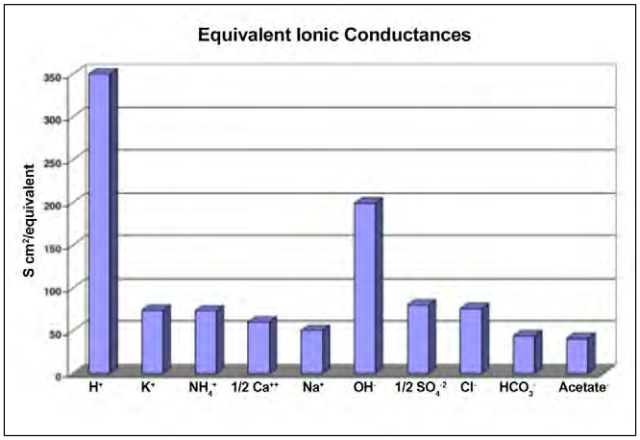
Historically, EC was measured in mhos or mmhos. Currently, the accepted SI unit for EC is Siemens/cm (S/cm) where a Siemen is equivalent to 1/ohms. Thus, the conductance in Siemens is the reciprocal of the resistance in ohms.

The unit conductivity cell

The strict definition of electrical conductivity is the amount of current passing between two standard plates (electrodes) of opposite charge (cathode [+] and anode [-]) of known area and separation distance. To accommodate a range of conductivities and to establish a benchmark standard, a cell constant (a result of the distance between electrodes divided by the cross-sectional area of the electrodes) is provided for each probe, with units of cm^{-1}. A cell constant of 1 is defined for electrodes each with a surface area 1 cm x 1 cm and separated at a distance of 1 cm. In terms of dealing with solutions, consider measuring the ionic activity of 1 cm^3 of solution between the standard plates. **Figure 1** [1] is a representation of the standard EC cell with a cell constant of 1.



1. Cell constant derivation [1].



2. Conductance of selected common ions at 25°C and 1 equivalent [3].

Ion type and pH impact

A large disparity in ion strength exists between different ion species. A conductivity reading of 9.2 S/cm, for instance, indicates a solution of either 18% potassium chloride or 6% potassium hydroxide [2]. **Figure 2** [3] shows the conductance of several ions common to the pulp and paper industry. It also shows that the presence of either the hydroxide ion (OH^-) or hydrogen ion (H^+) will contribute far more than other ions to the overall EC of a solution and even mask the presence of some salts (2). Therefore, the solution pH will have a major impact on the solution conductivity as the pH moves farther from 7.0 in either direction.

The term equivalent ionic conductance is used when referring to the conductance of a single ion species in its single valence state. Thus, divalent ions such as Ca^{+2} and SO_4^{-2} are expressed as ½ Ca^{+2} and ½ SO_4^{-2}, respectively.

Black liquor contains, as a minimum, OH^-, Na^+, CO_3^{-2}, Ca^{+2}, and SO_4^{-2} ions. Four of these ions are listed in Fig. 2. Therefore, it can be inferred that a change in the amount of any one of these species, particularly OH^-, can affect the measured EC of a black liquor solution.

Conductivity-concentration relationship

Frequently, EC measurements have been used as a surrogate measurement of black liquor or saltcake losses in pulp washing systems. As such, it is necessary to convert EC measurements of S/cm to concentration-based units of mass per unit volume such as g/L or lb/gal. As stated previously, EC is affected by a change in the ion species whether they be positively (cation) or negatively (anion) charged. The EC of a solution in theory is a function of the sum of the individual active ion equivalent conductivities multiplied by their individual concentrations. A mathematical model of this is represented in Eq. (1):

$$k = \sum_{i=1}^{n} \alpha_i l_i C_i \qquad (1)$$

where:

k = conductivity of the solution

α_i = fraction of the i^{th} constituent (of n ions) present as a free ion

λ_i = equivalent conductivity of the i^{th} ion

C_i = concentration of the i^{th} ion specie.

The equivalent conductivity, λ, of several ion species can be found in publically available tables; examples of these are shown in **Table I** [4]. There are also published conductivity factors of λ_i/C_i or EC per some standard concentration expressed as µS/cm per mg/L [4]. **Table II** [4] lists conductiv-

Cation	Equivalent Conductivity, $cm^2\ equiv^{-1}\ ohm^{-1}$	Anion	Equivalent Conductivity, $cm^2\ equiv^{-1}\ ohm^{-1}$
H^+	349.7	OH^-	198.0
Li^+	38.7	Cl^-	76.3
Na^+	50.1	HSO_3^-	50.0
K^+	73.5	HCO_3^-	44.5
NH_4^+	73.7	CO_3^{-2}	72.0
Mg^{+2}	53.1	SO_4^{-2}	79.8
Ca^{+2}	59.5	$HCOO^-$	56.0
Ba^{+2}	63.7	CH_3COO^-	40.9

I. Equivalent conductivities of aqueous ions at 25°C [4]. Note that 1 equivalent equals 1 mol for monovalent ions and ½ mol for divalent ions.

Ion	Conductivity Factor, mS/cm per mg/L
Cations	
Ca^{+2}	2.60
Mg^{+2}	3.82
K^{+}	1.84
Na^{+}	2.13
Anions	
HCO_3^{-}	0.715
Cl^{-}	2.14
SO_4^{-2}	1.54
NO_3^{-}	1.15

II. Examples of conductivity factors [4].

ity factors for several ion species of interest in brownstock washing. While both anions and cations carry current, they do so to different degrees. In general, divalent cations have higher specific conductivity than monovalent ones. This is not true of anions. **Table III** shows a simple example of how to use Eq. (1) to determine the theoretical conductivity of a sodium sulfate solution of a known concentration.

One simply multiplies the known concentration of each ion by its conductivity factor to determine the conductivity contribution of the ion. Then, one sums the conductivity contribution of each ion, in this case just two, to obtain the conductivity of the solution, in this case 880 µS/cm. From this information, it is possible to determine the dissolved inorganic solids to be 427.5 mg/L. In black liquor, organic dissolved solids also contribute to total dissolved solids (TDS); therefore, the amount of dissolved organics must also be known to determine the TDS of any black liquor sample. It has been shown that the inorganic components contribute significantly more to the total conductivity of black liquor than do the organic components [5].

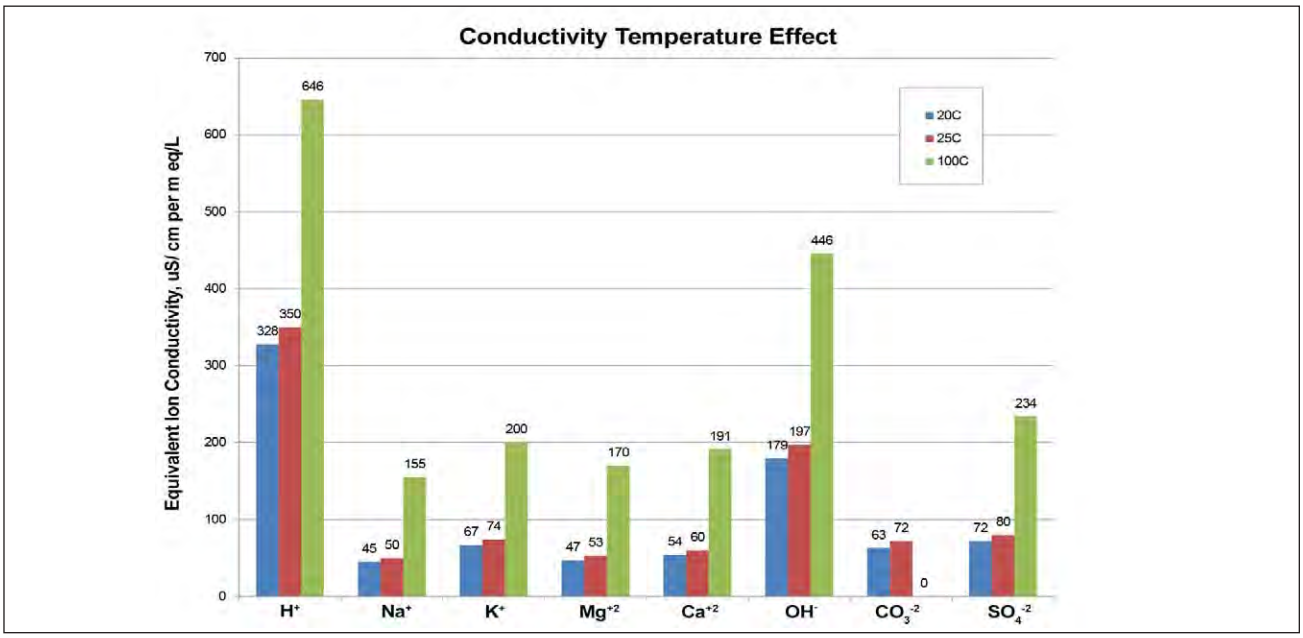
In general, for washer control, the inverse of this process is employed. The practical implication is that if the conductivity, the conductivity factor, and the species molar distribution are all known, then the concentration can be calculated. This approach could work if it can be assumed that the relative ratios among the species were constant and those ratios were known. For the example case shown in Table III, the $Na+:SO_4^{-2}$ ratio is 346.2:51.9 or 7.237:1. Unfortunately, in practice, these ratios do not stay constant.

Temperature impact

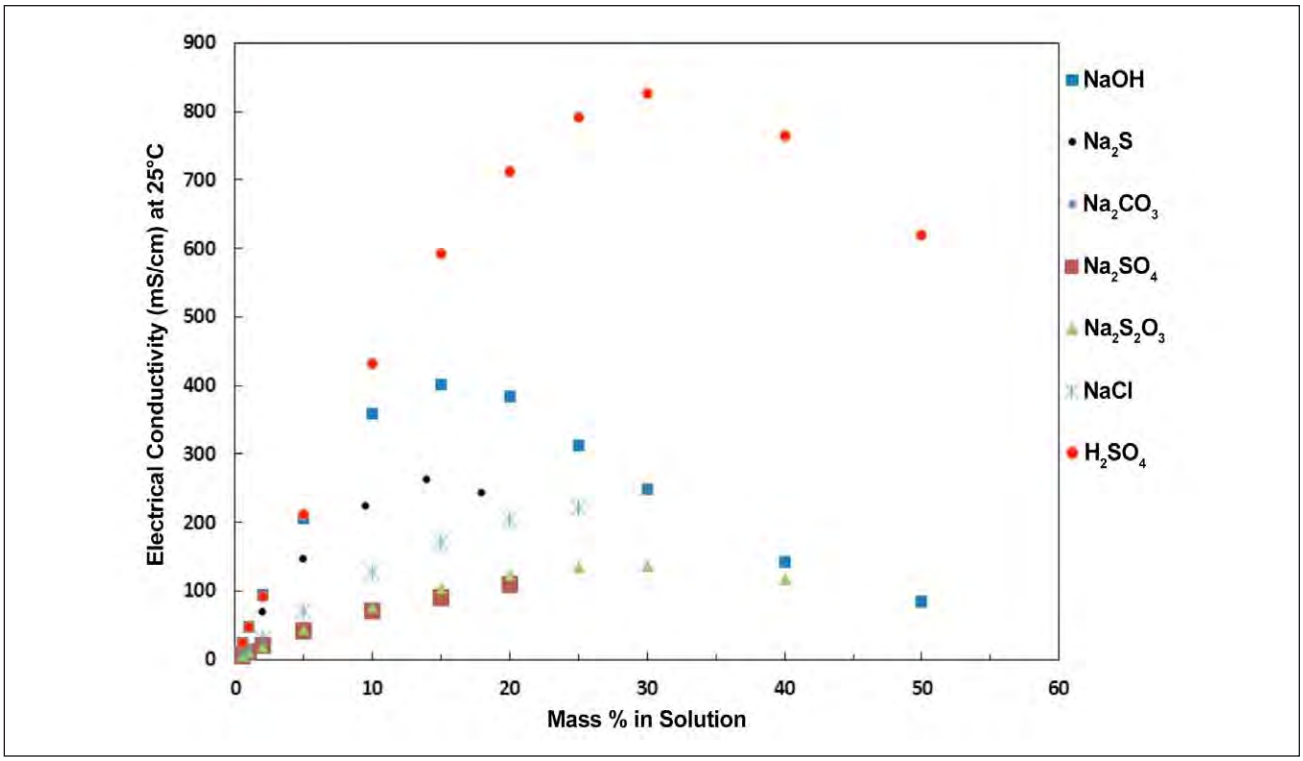
The activity of each ionic species behaves differently to changes in temperature. **Figure 3** [6] is a graph of a select

Ion	From Table II Conductivity Factor, µS/cm per mg/L	Example Concentration, mg/L	Calculate Conductivity, µS/cm
Na^{+}	2.13	375.6	800
SO_4^{-2}	1.54	51.9	80
	Total	427.5	880

III. Conductivity calculated from concentration.



3. Temperature effect on conductivity for select ions [6]. Note that 1 equivalent = 1 mol for monovalent ions and ½ mol for divalent ions.



4. Change of the conductivity with increasing concentration [7–9].

group of ions. The y-axis is the equivalent ion conductivity and the blue, red, and green bars display the equivalent ion conductivity for each of these ions at 20°C, 25°C, and 100°C, respectively. With the exception of the H^+ ion, all of the other inorganic ions are expected to be present to some degree in black liquor. From these results, it might be concluded that the presence of OH^- in any appreciable amount will skew the reading. In addition, the carbonate ion behaves differently than the other ions, reversing its EC value once a certain temperature is reached. As sodium carbonate can account for as much as 20% of the sodium present in a black liquor solution because of inherent inefficiencies in the causticizing process, its inverse behavior with temperature makes it difficult to develop universal temperature compensation. Finally, as typical operating temperatures for the last-stage shower water of brownstock washers are about 65°C–75°C, the temperature compensation is important for high-quality EC measurements to predict black liquor concentrations.

Common ion effect, nonlinearity, and dissociation of ions

A theoretical EC limit is reached as the compounds of interest dissociate into ions and move about the diluted solution. As the general ion concentration increases, more ions dissociate into the solution, increasing the EC. This continues until the space between the free-moving ions decreases and their potential to reunite with oppositely charged ions increases to the point that they begin to reform back into salts. Thus, it is not practical to correlate conductivity to black liquor solids above a certain concentration. That concentration limit is beyond the scope of this paper.

Figure 4 shows the data taken from three literature sources [7–9] for the most prevalent inorganic sodium compounds found in black liquor, plus sulfuric acid for comparison. Each of the species shown, except for sodium chloride, reaches a maximum electrical conductance. As the concentration of the species increases beyond its maximum conductance point, the specie's conductance will steadily decrease as its concentration further increases. The problem is that for any given EC for each ion species, only two different concentrations are possible. It is further compounded by the fact that many ion species are present and concentrations of these species change as process conditions change (e.g., causticizing efficiency, residual effective alkali). On the positive side, the concentrations of washed pulp filtrate should be low enough (<1%) to avoid this effect. However, weak electrolytes, such as the organic salts formed from the lignin, increase in conductivity as the solution becomes more dilute.

BROWNSTOCK WASHING APPLICATION

It is prudent to discuss the larger objectives and key process indicators (KPIs) of brownstock washing before covering field measurement applications, probe locations, and laboratory methods used to correlate EC values to soda losses and washer efficiencies.

Parameters of interest in brownstock washing

Brownstock washing is uniquely positioned at the crossroads of

the fiber line and the recovery processes, and its performance affects both areas. Both areas have parameters of interest, and brownstock washing also has environmental implications. When establishing a washing control program, it is important to define the operational parameters of interest, to be able to measure those parameters, and to be able to control the process to maintain those parameters within acceptable limits.

There are a myriad of ways to expresses washer losses, such as soda losses, inorganic solids, organic solids, total black liquor solids, chemical oxygen demand (COD), bound soda, and total soda in either metric or English units of mass. The denominator fiber mass can be equally diverse, employing such units as o.d. tons, a.d. tons, machine dried (m.d.) tons, brown tons, bleach tons, metric tons, and short tons. The issues to be addressed before any work is done are to define what will be measured and why, how it will be measured (often the only issue defined in practice), how the information will be used, what measurement frequency is required, and what degree of accuracy and precision/repeatability is demanded. A few of these will be explored.

Soda loss

Historically, brownstock washer soda loss has been defined as the pounds of equivalent saltcake (Na_2SO_4) lost per ton of air-dried pulp washed. The reality is, of course, that a minimal amount of sodium sulfate is present in the washer filtrate; rather, all of the sodium-based compounds are converted to their stoichiometric equivalent Na_2SO_4. Much like sodium oxide has been the standard expression of equivalent sodium compounds present in white, green, and black liquors (to a lesser degree), saltcake has been used for decades as the equivalent sodium compound of choice for washer losses. Historically, it has been the predominant makeup chemical in the recovery furnace before the environmental push to low-odor recovery boilers in the 1970s. Despite few mills still using saltcake as a makeup chemical, old habits are hard to break and it remains the reference expression for many unbleached mills today.

COD

During the Cluster Rule years of the early 1990s, organic loading on the bleach plant became a priority. For mills with bleach plants, the logical new washer loss parameter of choice has become the COD test. COD more closely correlates to first-stage bleaching chemical usage and the organic chemistry involved. As an environmental parameter, COD also became more popular because results can be achieved in an hour or so, whereas BOD_5 by design is a 5-day test. Unfortunately, COD does not reliably correlate well with biological oxygen demand (BOD) for reasons beyond the scope of this paper.

Total dissolved solids

Strictly in terms of the washing operation, total dissolved solids (TDS) is the parameter of interest for several reasons. First, displacement ratio (reduction of dissolved solids/maximum reduction of dissolved solids possible), wash yield (dissolved solids removed/dissolved solids entering), Norden's modified efficiency factor, and equivalent displacement ratio number all use dissolved solids in their determination. Second, all washer material balance calculations must use dissolved solids mass. Third, it is a relatively easy test to run and new laboratory devices can complete the task in less than 15 min. This would apply to not only the last-stage filtrate squeezing, but to all shower streams, vat liquors, and previous-stage mat squeezings. Fourth, knowing dissolved solids losses at the washers can help account for changes in daily solids burned in the recovery boiler and even the steam used to evaporate the water associated with those solids. Neither conductivity nor COD can contribute toward the understanding of any of these parameters.

Balancing pulp cleanliness and first-stage black liquor solids

The most basic parameter of interest is pulp cleanliness. Black liquor-laden pulp can cause a number of downstream issues, including increased first-stage bleaching chemical usage and wet-end chemistry problems on the paper machine. Both the machine and bleach plants run at a significantly lower pH than the brownstock washers, so downstream acid usage is directly affected by the amount of high-pH black liquor carried over with the pulp.

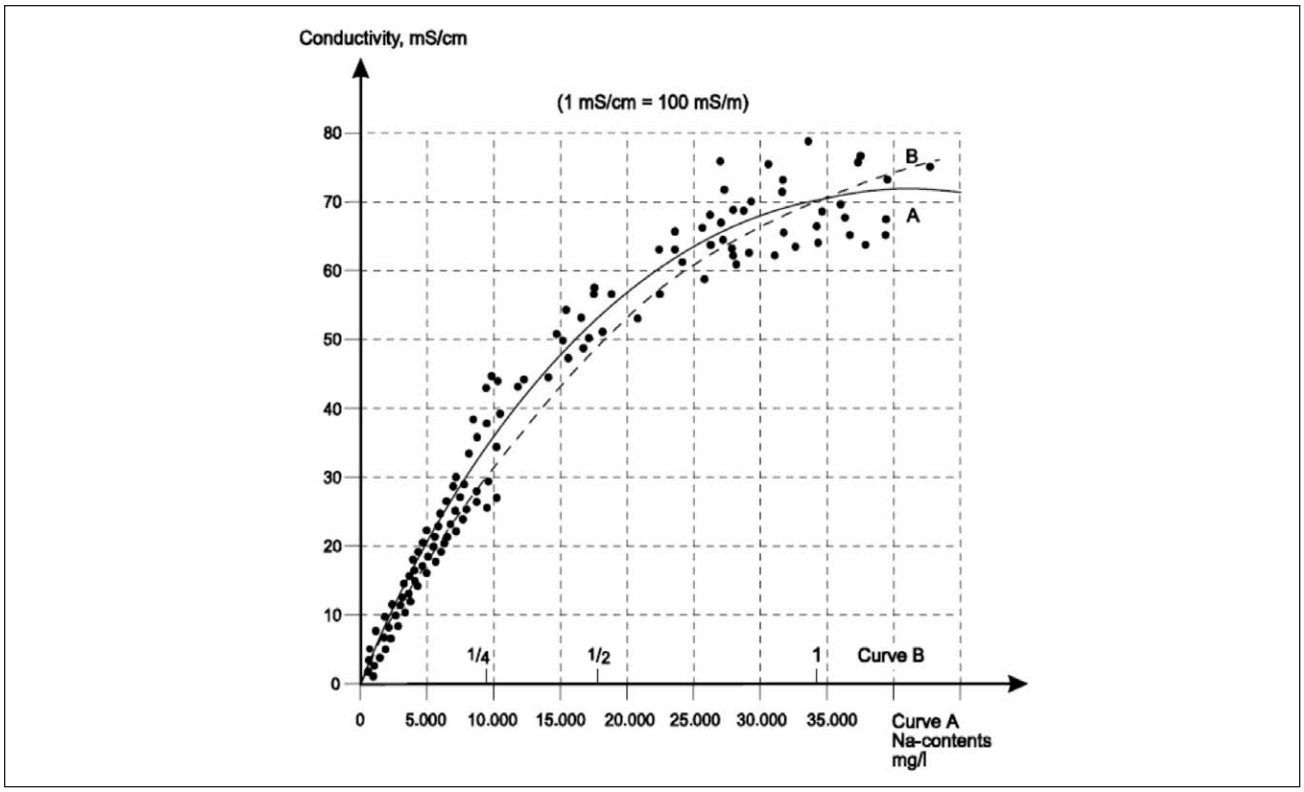
The amount of sodium in the black liquor leaving with the pulp has obvious direct cost implications. In most washing systems, it is the only parameter tested or measured. There is no direct online/inline measurement of sodium losses. Several inferential measurement technologies are available, each with their advantages and disadvantages. Conductivity is one of these methods.

Of note, EC measurements respond almost exclusively to changes in inorganic chemistry; therefore, EC is not a direct predictor of organic black liquor solids losses during washing. Rather, EC measurements infer that changes in the inorganic losses during brownstock washing correlate with changes in organic solids losses as well.

As brownstock washing is a balancing act between obtaining well-washed pulp with a minimal amount of shower water and obtaining a high TDS concentration in the black liquor being sent to recovery, it is important to establish good and reasonable control boundaries for each end. A maximum soda loss limit on the washed pulp leaving the last washer is typically specified to control the negative impact on bleaching chemical demand, cost of sodium makeup chemicals, or wet-end chemistry on the paper machine. A minimum TDS concentration on the liquor being sent to recovery from the first-stage washer is typically defined by the mill evaporator capacities. These two operating parameters are typical process boundaries employed in industrial brownstock washing.

Relating field measurements to laboratory tests and operational KPIs

For at least 40 years, inline conductivity probes have been used



5. Change of the conductivity with increasing concentration [1].

in brownstock filtrate lines to infer soda losses (i.e., pounds Na_2SO_4 per ton of pulp.) Some mills report excellent correlation while others are unsuccessful. Mills that are successful tend to have more stable process conditions. Successful conductivity measurement must start with relatively stable brownstock washer operating temperatures with consistent wash water cleanliness and well-performing temperature compensation algorithms. When the washer filtrate or wash water temperature varies, the conductivity measurements can become unpredictable. Stable cooking conditions and consistent wash water quality also improve conductivity reliability for control purposes.

Sampling and testing

Sampling and testing, whether applied to a measurement calibration-correlation or to routine laboratory testing (e.g., of liquor, effluent, or water), should all be conducted with thoroughly defined, followed, and understood procedures using laboratory-grade diligence. For the soda loss discussion alone, these will be covered in more depth to appreciate where erroneous results might occur.

Accuracy, repeatability, and reproducibility

Numerous statistical terms and applications are applied to liquor and pulp laboratory testing and correlation. The two most often mentioned are accuracy and repeatability. Joint ANSI/TAPPI Test Method T 1200 sp-14 "Interlaboratory evaluation of test methods to determine TAPPI repeatability and reproducibility" defines repeatability as an estimated limit below which the difference between two test results is expected to fall 95% of the time, when the results are obtained at a single laboratory. Repeatability reflects the variability inherent in the experimental system used to determine its value. Unlike repeatability, the term accuracy compares test results against a stable standard with sheet grammage (Mylar plastic sheet) and brightness (MgO disk) being examples. Although used frequently, the term accuracy has no relevance to parameters such as kappa number, for which there is no stable standard to calibrate.

The accuracy of a conductivity probe may be measured against a standard solution of known concentration in the laboratory, but when EC values are used to infer black liquor losses, accuracy is no longer relevant. There is no black liquor calibration standard; therefore, the best that can be done is to rely on repeatability and the correlation coefficient between the filtrate and the conductivity readings. Certainly the operating temperature in the field is higher than the laboratory-tested temperature. So, with lab conductivity, we cannot totally rely on a sample collected in the field, even when carefully sealed and tested in the lab, because the two probes will likely have different cell constants and temperature compensation algorithms.

Analytical determination of soda loss

How samples are taken and tested are important considerations in accurately determining the mass-ratio of saltcake pounds per pulp tons. First, the last-stage pulp mat filtrate

must be properly sampled. Variations in procedures exist. The sample may be an individual hand-squeezed sample or a composite taken over several hours. Samples are often taken at a single location across the width of the washer. It is well known that mat filtrates vary in soda content and mat consistency both across the mat and over time at a single location on the drum. As a result of this variation, an often underappreciated element of any sampling procedure is how well the sample represents the larger process. If a sample is taken, for instance, at a point across the washer where the mat is noticeably thinner and dryer, that filtrate will likely be cleaner than the rest of the pulp and render a nonrepresentative result.

The next consideration is how sodium content of the sample is determined. While a few mills might still go no further than to use an in-house table developed decades earlier relating laboratory conductivity to saltcake loss, most mills likely have advanced to the point where a central laboratory mass spectrometer or atomic absorption laboratory unit is employed to measure soda losses. Here, it is important to understand whether the sodium concentration is expressed in units of mass/unit filtrate volume (e.g., g/L) or in sodium mass/mass of filtrate (e.g., ppm.) If sample dilution (using deionized water) is part of the procedure, then that must be taken into account as well. It will be assumed that the sampling and testing procedures were properly prepared and carefully followed to obtain an accurate concentration. The result must still be expressed on the same mass basis as the pulp.

Determination of the reference pulp mass

The sodium concentration in the pulp mat sample must be proportioned to the o.d. pulp mass. The most direct approach is to take a large stock sample (>100 g) off the washer just before it enters the repulper while being careful not to lose any filtrate in the sampling process. The collected sample is bagged and taken to the laboratory, where it is weighed as received, dried, and then weighed again for o.d. mass. The sample's consistency is determined from these two mass measurements. The squeezed sample should ideally be taken from the same sample. By knowing the consistency and the soda content of the squeezed sample, it is now possible to calculate the soda loss.

Successful correlation between conductivity and soda loss

The fact is that some mills have (or claim to have) successfully correlated field conductivity to soda loss. While this seemingly contradicts the previous arguments, there is at least one explanation. Most correlations between conductivity and soda loss are done in a short-term period. In this context, the production rate, operating conditions, and white liquor chemistry are relatively stable and result in a reasonable short-term correlation. Causticizing efficiency, which defines the carbonate content in the black liquor even if highly variable, would likely not affect the residual liquor chemistry within a period of 8–12 h when considering the residence time and mixing within a typical white liquor storage system. Thus, stable conditions might render favorable correlation, assuming laboratory procedures are also carefully followed.

Figure 5 [1] illustrates a characteristic correlation between black liquor sodium content and conductivity from an equipment supplier using EC probes to monitor and control brownstock washing. This figure includes two different curves. Curve A shows conductivity versus sodium content from an entire continuous diffuser washing plant, while curve B represents the black liquor obtained from the digester at the blow line diluted to various dilution levels (i.e., ¼, ½, and undiluted) [1]. Figure 5 confirms that at low sodium concentrations (<10 mg Na^+/L) a near linear correlation to conductivity can be achieved; however, above 10 mg Na^+/L concentration, more statistical scatter is evident.

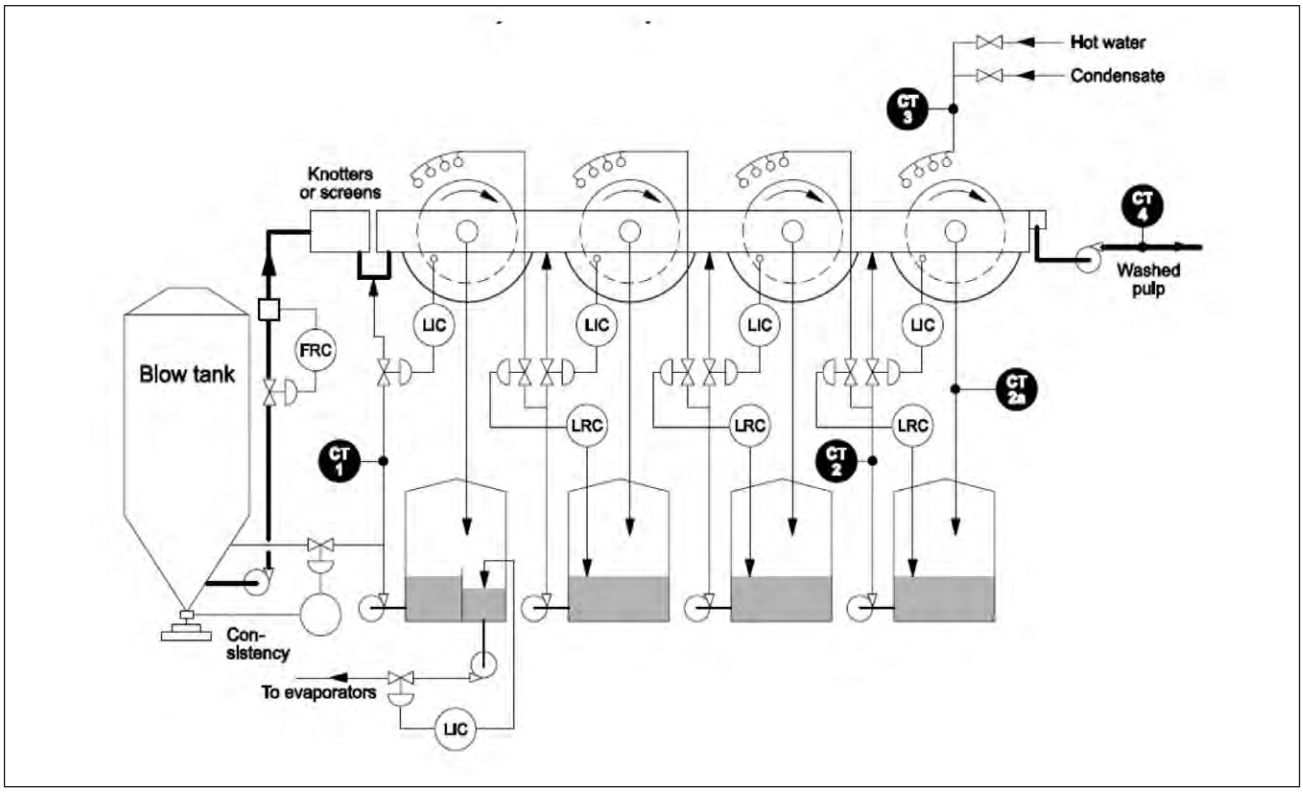
Investigators at a university [10] reported a linear correlation between the measured EC values and inorganic levels found in black liquor filtrates of a brownstock washing system. Sodium, the most prevalent inorganic component of black liquor, usually represents all the inorganics. This implies that conductivity can be correlated to sodium content.

Measurement location

For EC measurements to work as a pulp washing control method, the locations of probes and an understanding of the actual measurement being employed are essential. The probe needs to be located in a weak liquor stream with a reasonably stable operating temperature. Relative changes in the EC measurement can be used as a surrogate to monitor changes that arise during the brownstock washing process with technical success. Employing the EC probe as a method of closing the last-stage shower water flow control loop with direct EC feedback has proven valuable in several of our mills. **Figure 6** [1] represents a recommendation from an equipment supplier on the location of conductivity probes for a vacuum washer. These recommendations are not necessarily endorsed by us.

Measuring the pulp as it leaves the washer before further dilution results in an ideal location to represent washer effectiveness; however, this location is an extremely difficult application for a conductivity probe. If the EC is measured in the pulp stream after repulper dilution, what is being measured is the combination of soda loss in the pulp along with the dilution water EC. When the combined measurement is used for control, changes in repulper dilution water will be interpreted by the EC measurement as changes in brownstock washing efficiency. Electrical conductivity measurements from the combined streams cannot be used for displacement ratio calculations. However, if the mill is only interested in the relative changes in the amount of black liquor leaving the system and reasonably maintains constant repulper dilution flows, then this application is appropriate.

Another common probe location is in the last-stage filtrate line. If the EC measurement is located in the last-stage filtrate line, it should track final filtrate concentration changes; how-



6. Suggested conductivity probe (CT) locations [1].

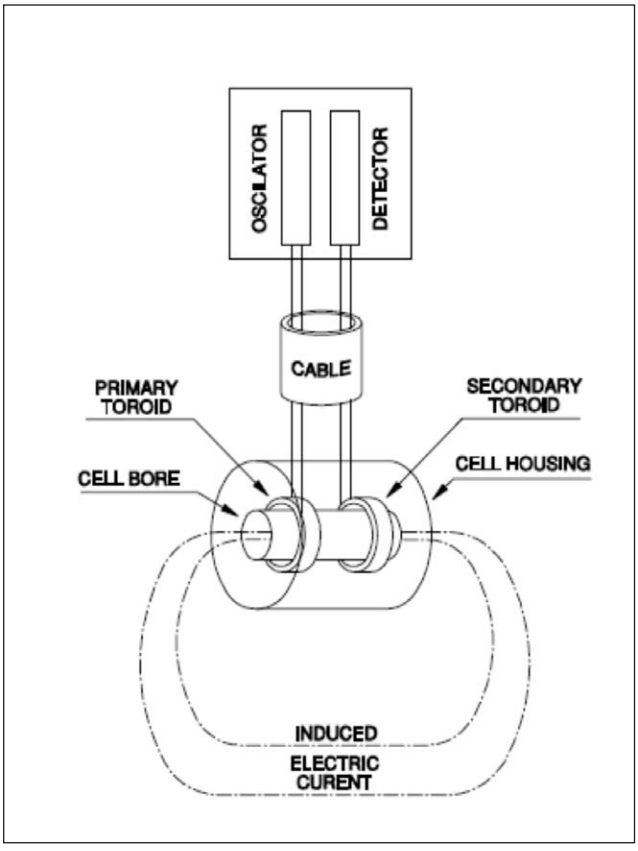
ever, it will not be representative of the liquor that leaves with the pulp [11]. Locating the probe on the outlet of the filtrate dilution pump of the last washing stage is of limited value because of the large capacity turnover time in the filtrate tank and the mixing effects that preclude the system ever reaching equilibrium. The resulting time constant of the filtrate tank system is too large when compared with the changes occurring on the washer for adequate control. Locating an EC probe in the first stage of brownstock washing will result in probe saturation. A saturated probe does not respond to changes in the black liquor concentration, which results in poor process control.

Conductivity probe selection

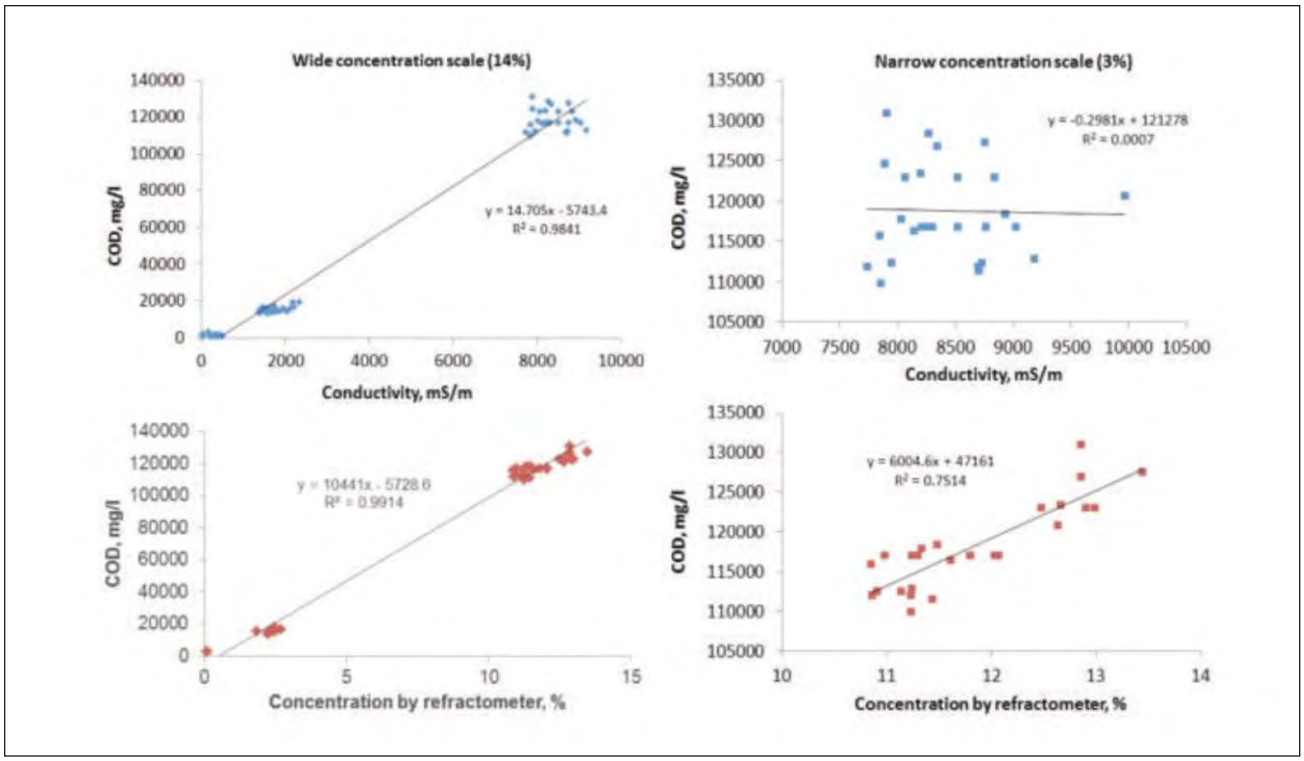
There are many conductivity probe configurations representing differing probe types, metallurgy, and cell constants. If conductivity is going to be employed, then the equipment manufacturer should be directly involved in the probe selection process.

Toroidal conductivity probe

For harsh inline applications or applications under pressure (e.g., pulp washing) and for applications in solutions (e.g., white liquor) that tend to form hard scales, traditional conductivity probes are not reliable. Instead of using two electrodes, a toroidal-shaped electrode may be employed for fiber-free, filtrate applications. The kinetic energy of the ionic solution flowing through the hole in the toroidal electrode induces a



7. An inductive toroidal sensor [1].



8. Correlation of chemical oxygen demand (COD) and black liquor solids measured by refractometer and conductivity probes [12].

current in the inductive coil magnet housed in the probe. The current may then be measured to determine the EC of the solution. In addition to withstanding pressurized, higher temperature conditions, all of the wetted parts of the probe are typically constructed of inert PEEK polymer (polyetheretherketone). **Figure 7** [1] illustrates an inductive toroidal sensor.

Alternative measurements

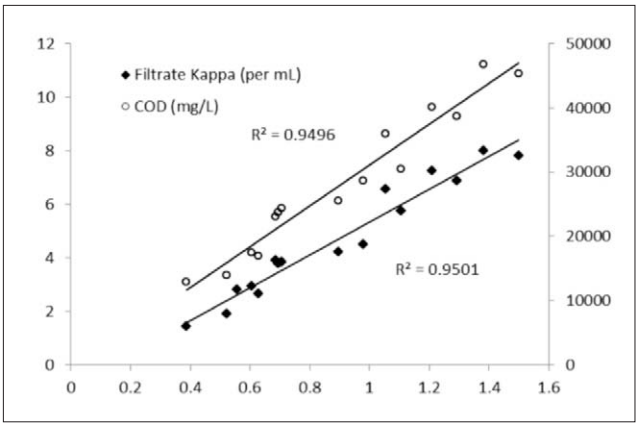
Several new technologies have been introduced in the past few years that offer promise to more accurately measure washer losses.

Refractive index

One equipment supplier [12] has developed a refractometer probe that has had success in correlating to brownstock washer losses in general. It has the advantage of being inserted into either a filtrate or stock stream and can be removed without shutting down the process. In addition, on a drum displacement washer system, refractive index measurements have been shown to correlate well to COD [12]. Recent work has shown that while conductivity may have success over a wide measurement span, it displays significant scattering relative to the refractometer when applied over a narrow range as shown in **Fig. 8** [12].

Dissolved lignin transmitter

A new technology using an advanced optical measurement probe has successfully measured dissolved lignin in a brownstock washer pulp slurry. The equipment supplier of this technology [13] has shown linear correlations obtained from the probe's sensor signal values to laboratory measurements of the filtrates' kappa numbers and COD values (**Fig. 9**).



9. Filtrate kappa (per mL filtrate; left y-axis) and COD (mg/L filtrate; right y-axis) versus sensor signal (x-axis) [13].

CONCLUSIONS

Electrical conductivity has been successfully employed in feedback control of brownstock washer systems for several decades. Some mills have reported good success with conductivity-based control systems while others have experienced extreme difficulties.

It is important to understand that EC measurements only measure ion species within an aqueous solution. Electrical conductivity measurements have been correlated to black li-

quor concentrations, but those correlations change when the temperature of the solution changes and when the relative concentrations of the different ionic species changes. For example, small increases in the residual alkali (OH^- concentration) result in significant increases in the reported EC measurement. Process temperatures >25°C can result in decreases in the EC measurement, particularly with the CO_3^{-2} ion contribution as seen in Fig. 3.

Placement of EC probes is also important to successful control loop operation. Conductivity probes should only be employed in relatively low concentration solutions. Placing an EC probe toward the front end of the washing system will result in probe saturation and poor process control. Placing an EC probe in the discharged pulp stream after the last repulper will result in a combined measurement of the true pulp cleanliness (from an inorganic viewpoint) and the EC measurement of the repulper dilution water. Therefore, changes in repulper dilution flow (or concentration) will erroneously infer changes in washer performance. The ideal location for an EC probe is in the pulp being discharged from the last stage of washing before the addition of dilution water. In practice, this location is extremely difficult to locate and maintain a working EC probe that will reliably provide measurements. Placing a probe in the intermediate shower water lines fed from any of the liquor filtrate tanks will result in significantly long process time constants for the washer controls because of the long residence times in the filtrate tanks. In addition, the filtrate in these tanks rarely comes to process equilibrium with the washed pulp so the EC measurements obtained from these locations are not truly representative of the washer performance. **TJ**

LITERATURE CITED

1. Kemotron A/S, "In-line measurements as the basis of process control systems in pulp mills," brochure no. 990.68/2, Kemotron A/S, Kongens Lyngby, Denmark.
2. Josephson, W.E., "Brownstock washer optimization and control," Ph.D. dissertation, Auburn University, Auburn, Alabama, 1995.
3. Gray, D. M., "A comprehensive look at conductivity measurement in steam and power generation waters," *Off. Proc.–Int. Water Conf.*, Engineers' Society of Western Pennsylvania, Pittsburgh, PA, USA, 2006. Available [Online] www.mt.com/dam/mt_ext_files/Editorial/Generic/7/Paper-THOR-Gray-CONDUCTIVITY_Editorial-Generic_1201100849793_files/iwc_06-29_gray_conductivity.pdf <21June2016>.
4. Adamson, A.W., in *A Textbook of Physical Chemistry*, 2nd edn., Academic Press, New York, 1979, Chap. 12.
5. Trinh, D.T., Collins, R.L., and McDonald, J.D., *J. Pulp Pap. Sci.* 15(2): J47(1991).
6. Landolt-Börnstein, *Zahlenwerte und Funktionen aus Naturwis Senschaften und Technik (Numerical Data and Functional Relationships in Science and Technology)*, 6th edn., vol. II, part 7, Springer-Verlag, Berlin, 1960.
7. Mettler-Toledo, "Reducing common errors in conductivity measurements," Mettler-Toledo white paper brochure, Mettler-Toledo, Columbus, OH, USA, 2012. Available [Online] www.mt.com/dam/MT-NA/pHCareCenter/Conductivity_Reduce_Common_Errors_WP.pdf <21June2016>.

ABOUT THE AUTHORS

We chose this topic because the application of conductivity measurements seems to be a misunderstood and sparsely researched subject. Conductivity measurements apply to virtually every brownstock washer mill, so it is something that is important to understand.

Our research complements previous work that has discussed conductivity in general and washer losses in particular. What is different here is that we cover the application of this measurement to the brownstock soda losses. The difficulty was in finding papers that would bridge the gap between theory and application as it relates to using conductivity as a surrogate measurement of soda loss. This paper finally does that. Publicly available papers, some mill washer testing work, as well as personal experience covering more than 40 years were required to complete this work.

This work expanded our understanding of the importance of temperature on conductivity measurements, the reformation of salts in an electrolytic solution at higher concentrations, and the resulting erroneous conductivity readings associated with them. The inverse conductivity of the CO_3^{-2} ion at elevated temperatures and the process implications associated with the causticizing efficiency upstream from the washers and digesters were all interesting and important realizations.



Brown



Hart

This paper offers insights into the measurement of soda losses for every brownstock washer operation at every kraft mill, as well as the benefits and limitations of using conductivity measurements generally and applied to washer losses specifically. The next step is to apply these learnings to our fleet of more than 40 brownstock washer lines.

Brown is chemical pulping specialist at WestRock, Norcross, GA, USA. Hart is director, fiber technology and innovation, WestRock, Atlanta, GA, USA. Email Hart at peter.hart@westrock.com.

8. Haynes, W.M., Ed., *Handbook of Chemistry and Physics*, 91st edn., CRC Press, Boca Raton, FL, USA, 2010, pp. 5–71.

9. Emerson Process Management, "Conductance data for commonly used chemicals," brochure no. 44-6039/rev. B., Emerson Process Management, Irvine, CA, USA, 2010. Available [Online] http://www2.emersonprocess.com/siteadmincenter/PM%20Rosemount%20Analytical%20Documents/LIQ_MAN_6039_Conductance_Data_Commonly_Used_Chemicals.pdf <17Sept2016>.

10. Josephson, W.E., Krishnagopalan, G.A., and Cullinan, H.T., *Tappi J.* 76(9): 197(1993).

11. Turner, P.A. and Livingstone, L., *Pulp Pap. Can.* 96(6): 72(1995).

12. Kopra, R., Koivula, K., and Dahl, O., *TAPPI J.* 14(2): 83(2015).

13. Andersson, N., Wilke, C., Biazzo, T., et al., *TAPPI J.* 13(10): 39(2014).

Estimating limits of wet pressing on paper machines

J. DAVID MCDONALD AND RICHARD J. KEREKES

ABSTRACT: Water removal by wet pressing on paper machines depends on many factors such as press impulse, pressure, basis weight, equilibrium moisture, rewet, furnish, and fabric properties. These factors must be considered together to estimate wet pressing limits, such as the possibility of attaining 65% solids content on commercial paper machines. We have made such estimates employing the Decreasing Permeability Model (DPM) of wet pressing. This paper describes the utility of this approach and discusses some findings, such as the large dependence of low basis weight grades on equilibrium moisture content, maximum nip pressure, and rewet. The model also estimates the impact of basis weight, web temperature, double-felting, and incoming web solids on water removed.

Application: This study applied the DPM to quantify the factors that determine water removal in wet pressing, and in particular, factors to achieve high solids content. More generally, the DPM can be used to optimize existing presses and guide research and development towards the most cost effective ways to improve water removal.

State-of-the-art press sections using shoe presses and high web temperatures are able to achieve web solids in excess of 50%. In contrast, wet pressing laboratory experiments at high pressures and long times have shown that it is possible to obtain solids contents over 60% [1-5] and, in one case, as high as 71% [2]. These results have encouraged the papermaking community to optimize the wet pressing process and develop new technologies in order to approach these values.

In the United States alone, 400 million GJ/year of energy is required to dry paper at a cost of $1.5 billion [6]. Agenda 2020 has identified drier webs leaving the press section as a high priority area and has set the ambitious goal of reaching 65% solids entering the dryer section. They have formed a group of suppliers, papermakers, and researchers to understand the potential for much drier webs and devise possible solutions.

In the laboratory, a wet web can be pressed for seconds, minutes, and even days. However, in a modern, high-speed paper machine, even with a shoe press, the web is only pressed for several milliseconds. During this time, a significant amount of water must flow not only between fibers, but also through lumens and pores of individual fibers. Given the differences between laboratory conditions to reach equilibrium and commercial conditions, what are the practical limits to water removal?

More than 30 years ago, Busker and Cronin [1] made a comprehensive review of the importance of wet pressing variables. They identified eight primary wet press variables which they defined as those that could affect sheet dryness by four percentage points or more: post-nip rewet, ingoing web moisture, grammage, furnish, double-felting, web temperature, press impulse, and felt pressure uniformity.

To estimate the limits of wet pressing on paper machines, all of the previously mentioned factors must be considered together. To accomplish this, we recently extended the Decreasing Permeability Model (DPM) of wet pressing to limiting conditions by including an equilibrium term to represent the maximum dryness [5,7]. In this paper, we employ this model to quantify the effect of pressing parameters and conditions affecting the limits to water removal in commercial operations.

THE DECREASING PERMEABILITY MODEL

The DPM was derived from equations for fluid flow through porous media [5,7] on the premise that the rate of water removal diminishes as pressing proceeds because of decreasing permeability faced by the remaining water as it is progressively expelled from between fibers and from the lumens and pores of fibers. The DPM assumes the following: unidirectional flow; negligible flow resistance from the felt in comparison to the web; a vented press; and rewet affected primarily by felt design.

$$m = (m_0 - m_e)\left(1 + \frac{An(m_0 - m_e)^n I}{\nu W^2}\right)^{\frac{-1}{n}} + m_e + \frac{R}{W} \qquad (1)$$

where:

m_0 = moisture ratio before pressing

m_e = equilibrium moisture ratio

I = press impulse (nip load divided by speed), kPa.s

W = basis weight, kg/m²

υ = kinematic viscosity of water, m²/s

A = specific permeability, g/m
n = compressibility factor
R = rewet, kg/m^2

The first of the 3 terms on the right hand side of Eq. (1) represents the "dewatering term." This gives the moisture left in the web after water has been expelled by pressure exerted over time to overcome resistance to flow. The second term is the equilibrium moisture content at the maximum pressing pressure. This moisture can be lowered by increasing this pressure. The third term, rewet, is described in the following paragraph.

Rewet is a poorly defined concept in the pressing literature. We have defined it in a rigorous manner in conformity with our model as water expelled by hydrodynamic force overcoming flow resistance in the web but which remains with the web upon separation from the felt. We do not specifically speculate on the mechanism as to whether it is due to some back-flow from the felt or simply surface water held by surface tension during film splitting from the felt. Whatever the mechanism, rewet is water remaining with the web that must be removed in subsequent drying.

For extremely long pressing times as in a laboratory press, $I \rightarrow \infty$, and therefore:

$$m_\infty = m_e + \frac{R_\infty}{W} \tag{2}$$

where m_∞ is the moisture content after a very long time of pressing. In the absence of rewet, this moisture equals the equilibrium moisture:

$$m_\infty = m_e \tag{3}$$

The rewet term depends on furnish and fabric properties as well as factors such as speed and the available water, $m_O - m_e$, shown in Eq. (4) [5], but is independent of the total water content of the felt [8].

$$R = k(m_O - m_e)^q \tag{4}$$

Clearly, there is no rewet when the ingoing moisture content equals the equilibrium moisture content.

Press nips are efficient in removing water when the initial moisture (m_O) is large, but this may be offset by more water available for rewetting. However, there is a practical upper limit to m_O because, if excessive, the nip will be saturated and crushing will result.

The equilibrium moisture ratios of wet webs have been measured in many laboratory studies [1-4] and are summarized in [5]. These studies have shown equilibrium moisture to depend on applied pressure, p, in the form of Eq. (5), where c and a are furnish-dependent constants:

$$m_e = cp^{-a} \tag{5}$$

Equation (5) is an empirical equation fitted in [5] to experimental data from the literature [1-4] for long pressing times. Constants c and a are for specific furnishes and the equation is valid up to the maximum pressure tested. These pressures were 6.3 MPa for TMP giving a web solids of 71% [2] and 53.4 MPa for kraft giving a web solids of 63% [4]. The highest peak pressures exerted in commercial wet presses are on the order of 10 MPa, and the simulated pressures in this paper are less than those measured in the laboratory experiments.

For practical convenience, this equation may be approximated by an analogous expression in line loading, P (kN/m):

$$m_e = gP^{-h} \tag{6}$$

It should be noted, however, that this equation is only valid for a specific nip geometry determined by felt design, press roll diameters, and cover or belt compressibility. Accordingly, it can only be used with caution as a first order approximation in modeling different pressing conditions.

In summary, press impulse overcoming flow resistance determines the amount of water expelled from the web between the limits of initial moisture and equilibrium moisture, while maximum pressure determines the level of the equilibrium moisture.

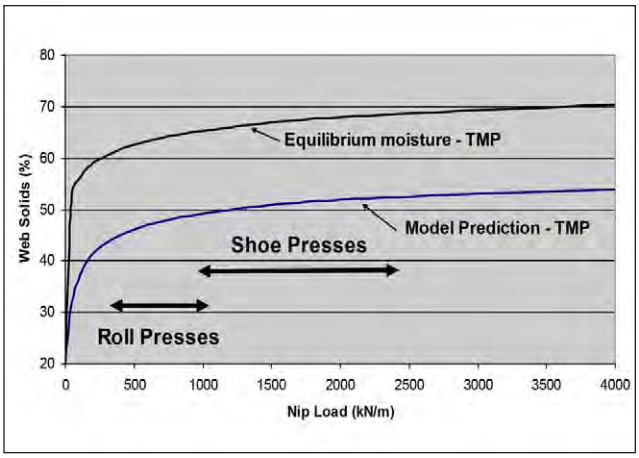
ESTIMATES FROM THE DPM

Furnish-dependent coefficients (A and n) have been measured by fitting the DPM equation to commercial paper machine measurements [5,7,9-11] and data from pilot pressing trials [5,7,9-12] (**Table I**). In this paper, we employ the DPM to examine the relative importance of the press operating condi-

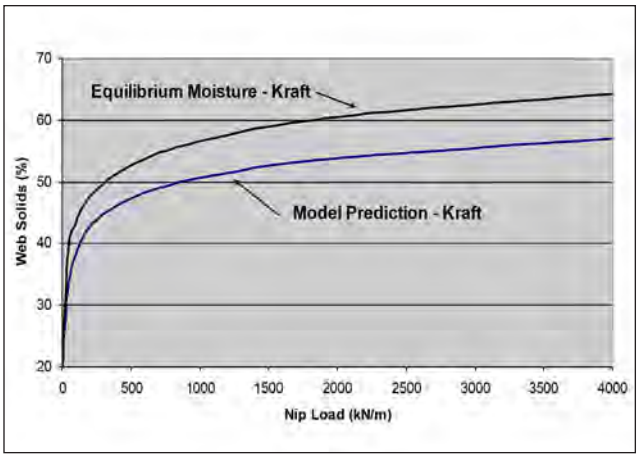
Furnish	A*, g/m	n	g	h	c	a	References
Thermomechanical pulp	5.24×10^{-10}	1.290	1.72	0.17	0.682	0.20	[5,7]
Kraft	1.61×10^{-9}	0.738	1.94	0.27	1.30	0.23	[5,7]

* at 20°C.

I. Furnish coefficients for the decreasing permeability model.



1. Press dewatering of thermomechanical pulp (TMP) furnish assuming machine speed of 1500 m/min, web temperature of 50°C, basis weight of 50 g/m², incoming web solids of 20%, and rewet of 20 g/m². The equilibrium web solids content was calculated using Eq. (6) with the coefficients in Table I.



2. Press dewatering of kraft furnish assuming machine speed of 1500 m/min, web temperature of 50°C, basis weight of 60 g/m², incoming web solids of 20%, and rewet of 10 g/m². The equilibrium web solids content was calculated using Eq. (5) and the coefficients in Table I.

tions (press impulse, maximum pressure, basis weight, and temperature), furnish (specific permeability and compressibility), and felt design (rewet) to estimate the highest attainable web solids contents in paper machine press sections.

Line load and press impulse

A primary variable for expelling water from a web in pressing is the press impulse, defined as the product of pressure and time of pressing. It can also be expressed as the line loading divided by the machine speed. Generally, given the decreasing permeability faced by water in interstices of compacted webs, and within lumens and cell wall pores, as well as the short residence time in nips and rewet, the resulting dryness after pressing is often far from its equilibrium moisture content (m_e).

In earlier work, we simulated pressing for infinite time in a pilot press having roll diameters of 0.75 m by placing the wet handsheets on the felt and passing them through the nip between the two rolls. The sheets stuck to the roll surface and were captured after passage through the nip. Multiple passes were made until sheet moisture content no longer changed [7].

The data for a TMP furnish were fitted to Eq. (6) and extrapolated to line loads (P) beyond the levels of current pressing technology to show the limit for water removal (**Fig. 1**). For example, at a line loading of 1000 kN/m and an infinite time of pressing, it would be possible to reach 65% solids. This finding is supported by a comparison to laboratory pressing results of Maloney et al. [2] for TMP by fitting Eq. (5) to their data, which gave c=0.682 and a=0.2. For Maloney's maximum pressure of 6.3 MPa, Eq. (5) gives a solids content of 68%. This level was also measured experimentally. In short, our result is reasonable.

From these findings and Eq. (1), for a press load of 1000 kN/m and speed of 1500 m/min, the water remaining in the web is comprised of 54% equilibrium moisture and 40 % rewet (R). Thus, only 6% of the remaining water could be removed by a longer pressing time. On the other hand, a larger pressure would increase both the press impulse and decrease the equilibrium moisture. If pressure were increased by a factor of 1.6 to 10 MPa in Eq. (5), the result would be a 70% solids content. In comparison, increasing line loading in Eq. (6) by the same factor would give P=1600 kN/m, which from Eq. (6) gives about 68% solids content.

In summary, these results show that pressing under these conditions reaches a plateau solids content near 1000 kN/m. Further increases in loading produces little additional dewatering. The limiting factor is equilibrium moisture content. In actual paper machine presses, the solids contents are much lower, as shown in Fig. 1. The likely cause is rewet.

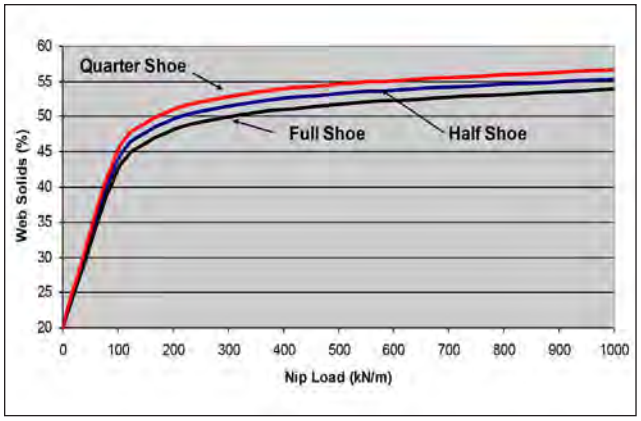
Similar results to those previously mentioned were found for a kraft softwood furnish shown in **Fig. 2**. Here, an equilibrium solids content of 65% was attained around 4000 kN/m. This same equilibrium solids content was experimentally measured by Maloney et al. [2] at about 6.3 MPa. Laivins and Scallan [4] measured this level of solids content in their experiments at about at about 20 MPa. Interestingly, in this latter case, doubling the pressure to 53 MPa only raised the solids content to 66%.

Pressure

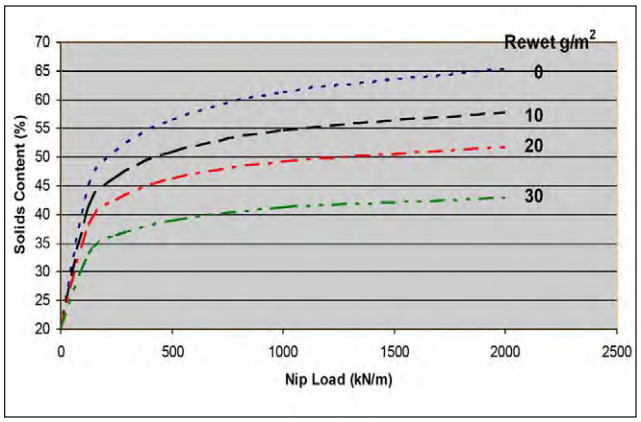
Shortening the length of the shoe-press nip at the same nip load increases maximum applied pressure. Although the press impulse is constant, the higher pressure lowers the equilibrium moisture (m_e) as shown in **Fig. 3**.

Furnish

In a previous study [13], a "pressability index" was developed to evaluate press dewatering of several furnishes refined to different levels. This work confirmed that: previously-dried



3. Applying greater pressure at the same press impulse gives higher press solids for a TMP furnish. The operating conditions are: machine speed of 1500 m/min, web temperature of 50°C, basis weight of 50 g/m², incoming web solids of 20%, and rewet of 20 g/m².



4. Effect of rewet for a TMP furnish assuming machine speed of 1500 m/min, web temperature of 50°C, basis weight of 50 g/m², and incoming web solids of 20%. The equilibrium web solids content was calculated using Eq. (6) with the coefficients in Table I.

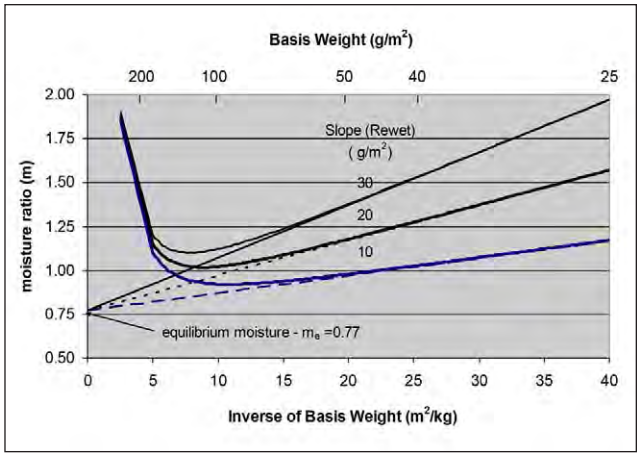
pulps were easier to dewater than never-dried pulps; higher pressed solids can be obtained by adding fillers that do not swell in water; and refining makes the furnish more difficult to dewater.

In more recent work, the furnish-dependent coefficients A and n were determined for a number of different furnishes using a pilot roll press [11,12]. These coefficients were used with the DPM in proprietary applications to evaluate existing press operating conditions, recommend changes to optimize dewatering, and evaluate investments in press rebuilds [12].

As shown in Figs. 1 and 2, the kraft furnish reported in [5,7] dewatered more easily than the TMP furnish and the equilibrium solids content reached 65% at extreme nip loads.

Rewet

As described earlier, we define rewet as water that has been expelled from the web by hydrodynamic force overcoming flow resistance in the web but which remains with the web



5. Pressed moisture ratios of a kraft furnish assuming machine speed of 1500 m/min, nip load of 1000 kN/m, incoming web solids of 20%, a web temperature of 50°C, and three levels of rewet. The equilibrium web solids content was calculated using Eq. (5) with the coefficients in Table I.

upon separation from the felt. It is noteworthy that such "separation" rewet also takes place in the absence of a pressurized nip when a paper web separates from a forming fabric on a paper machine [14]. Rewet levels as high as 1000 g/m² have been reported for coarse fabrics used in two roll pulp dewatering presses [15]. Such high levels may be "post-nip rewet" that occurs if the felt remains in contact with the web after the nip and increases with contact time [16]. For lightweight paper grades, rewet is probably between 5 and 35 g/m², which is still significant [10,11]. The effect of various levels of rewet are shown in **Fig. 4**.

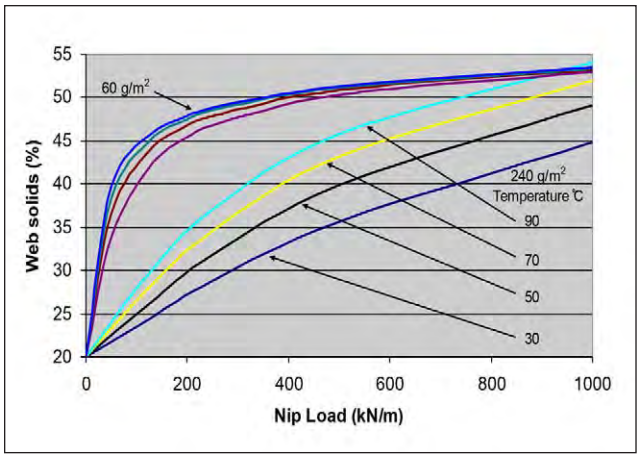
Basis weight

The nonlinear nature of press dewatering is most apparent when considering the effect of basis weight. With decreasing basis weight, pressed solids content may increase or decrease depending on the amount of rewet and the shape of the dewatering curve (**Fig. 5**). Low basis weight reduces the moisture ratio of the pressed sheet as a result of decreased flow path length. However, this is countered by rewet, which becomes a larger fraction of the web mass. This is illustrated for the kraft furnish at three different rewet levels plotted as the inverse of basis weight in Fig. 5. The straight lines are Eq. (2) with intercept m_e = 0.77. As basis weight is reduced (i.e., as 1/W is increased), the dewatering curve asymptotically approaches a straight line with R as the slope.

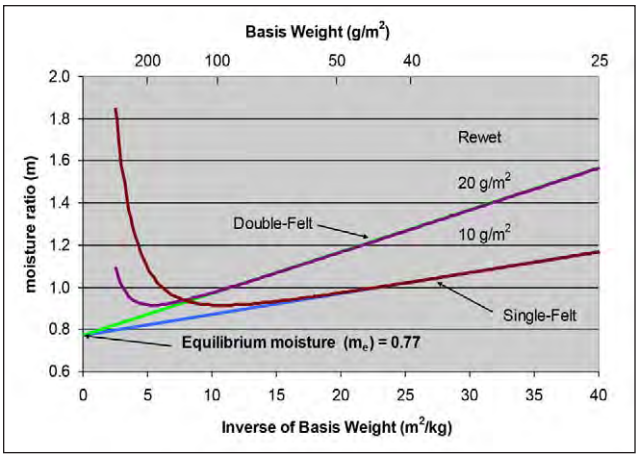
Comparisons of the straight lines with the curves in Fig. 5 reveal an important finding. For basis weights below 50 g/m² (1/W> 20 m²/kg), solids content after pressing is entirely determined by equilibrium moisture (y-axis intercept) and rewet (slope of the line).

Temperature

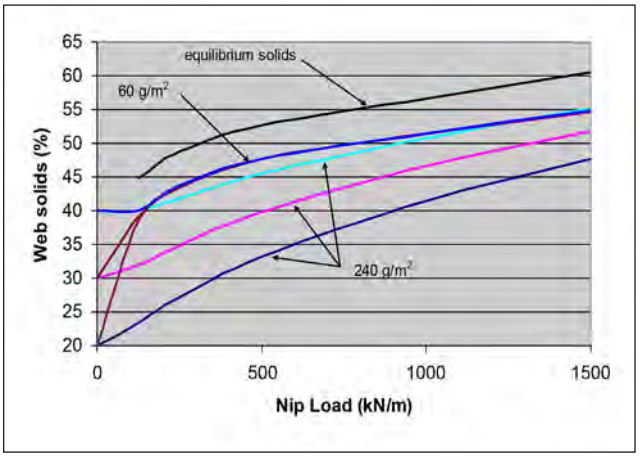
Increased temperature is known to reduce web moisture content after pressing [1]. Although they did not describe their



6. Effect of temperature on dewatering of kraft furnish assuming machine speed of 1500 m/min, incoming web solids of 20%, and rewet of 10 g/m² for basis weights of 60 g/m² and 240 g/m². The equilibrium web solids content was calculated using Eq. (5) with the coefficients in Table I.



7. Kraft furnish 1500 m/min, 1000 kN/m nip load, 50°C, m_0 = 4, assuming rewet of 10 g/m² for a single-felted nip and 20 g/m² for a double-felted nip.



8. The pressed solids content of a kraft furnish after a simulated second shoe-press at differing levels of incoming solids content (20%, 30%, and 40%) and basis weights (60 g/m² and 240 g/m²). The other conditions are: machine speed of 1500 m/min, web temperature of 50°C, and rewet of 10 g/m². The equilibrium web solids content was calculated using Eq. (5) with the coefficients in Table I.

method, Busker and Cronin reported that web solids increased from 0.5% to 1.3% per 10°C increase in web temperature [1]. A value of 1%/10°C was found for press simulator experiments with 120 g/m² pads [17], as well as pilot machine trials with 127 g/m² linerboard [18] and 40-55 g/m² newsprint [19]. These values were obtained under controlled conditions with extensive instrumentation, so they are probably the most reliable. Measurements on commercial paper machines gave values of 2.5%/10°C for 127 g/m² linerboard [20], 1.5%/10°C for 67 g/m² fine paper [20], 1.5%/10°C for 48 g/m² newsprint [21], and 0.7%/10°C for 120 g/m² fluting grade [21].

In our earlier application of the DPM [9], we showed that the effect of temperature on viscosity in the dewatering term of Eq. (1) accounted for an increase in solids in the range from 0.5% to 2.5 % per 10°C increase in temperature.

The effect of temperature also depends upon pressing conditions and basis weight. For a heavy web of 240 g/m² where the first term in Eq. (1) dominates, the solids content is increased by 1% for every 10°C increase in temperature (**Fig. 6**). In contrast, for a light web (60 g/m²) where the equilibrium and rewet terms dominate, the effect of temperature is of the order of 0.5%/10°C at press nip loadings representative of typical roll presses (Fig. 6).

Another potential effect of temperature may be its influence on equilibrium moisture content under pressing conditions. Here, the effect of temperature is no longer on the rate of dewatering caused by viscosity change, but rather on web permeability through changed pore structure. For example, increased pliability may lead to more pore closure under pressure, or the opposite, easier pressure-forced opening of new pathways. This subject clearly requires further study.

Single versus double felting

Double felting of the first press reduces the flow path by allowing water to flow from both surfaces of the web. Water flows outward from a neutral plane in the middle of the web, so in effect it behaves as if it is half the basis weight. Double felting is beneficial for heavier grades > 100 g/m² (<10 m²/kg). For example, at 200 g/m², double felting gives 5% higher solids content than single felting. However, because of rewetting on both the top and bottom sides of the web, it is less effective for lighter grades (<100 g/m²) as shown in **Fig. 7**.

Effect of incoming moisture

The effect of the amount of water entering the second of two shoe presses is shown in **Fig. 8**. For a heavy grade (240 g/m ²), the solids content after pressing depends on the web solids content entering that nip, even up to a nip load of 1500 kN/m. However, for a lighter grade (60 g/m²), the pressed solids are independent of the incoming solids for all but the lightest nip

loads, which is in accord with measurements after the first press nip on a pilot paper machine [22]. This occurs because the web is already near equilibrium and therefore the outgoing nip moisture is simply the sum of the equilibrium solids content and rewet.

Fabric design

Felts with batt fibers having small diameters have been shown to reduce the amount of rewetting [5], but the exact mechanism is unknown. Some researchers hold that non-uniform distribution of pressure exerted by the felt creates uncompressed zones in the web that become pockets of higher moisture and that this "unpressed" water is interpreted as rewet [23]. However, measurements by Beck [24] in an instrumented pilot press nip indicated that a rough felt (with larger diameter batt fibers) gave a higher mid-nip web solids content but more rewet than the smooth felt. The net result at the nip exit was a lower web solids content from the rough felt than from the smooth felt because of rewetting. This observation has been corroborated by pilot pressing experiments on market pulp where rough felts gave better water removal than smooth felts [25]. The non-uniform pressure gave lateral channels of high permeability that enhanced water removal. This is a subject worthy of further study.

CONCLUSIONS

Our calculations using the Decreasing Permeability Model (DPM) have quantified the factors that affect press section water removal. Because the equations are nonlinear, it is not possible to draw general conclusions for all grades. For heavyweight grades (> 100 g/m^2) with a state-of-the-art press section (two shoe presses), optimizing press impulse, basis weight, web temperature, and felt configuration will have a significant impact on the web solids.

For lightweight grades (< 100 g/m^2) with a modern press section, the final solids content after pressing depends only on the equilibrium moisture (m_e) and the amount of rewet (R). Our findings suggest that higher solids contents can only be achieved by lowering the equilibrium moisture and minimizing rewet. Equilibrium moisture depends on furnish and peak pressure. Temperature may be a factor, but this requires further study.

Although rewet is poorly understood, indirect evidence suggests that incoming moisture, machine speed, and felt/web structure are important. We believe that understanding the behavior of water at the felt/paper interface as the surfaces separate would suggest ways to minimize rewetting. This is another topic deserving further study.

In conclusion, equilibrium moisture and rewet need to be reduced in order to obtain a pressed web solids of 65%. **TJ**

ABOUT THE AUTHORS

This research was motivated by the goal of 65% pressed solids set by Agenda 2020 in its dryer web project. As we participated in this project, we understood that the many factors affecting pressing are not independent and had to be considered together to reach this target. We realized that our Decreasing Permeability Model (DPM) could be used to evaluate these factors in a comprehensive manner.

This research is an application of the DPM, which was initially published in *TAPPI Journal* using data from surveys of Canadian paper machine press sections (*Tappi J.* 74(12): 142,150(1991)). Later, we accounted for rewet in *Tappi J.* 78(11): 107(1995). Numerous other publications in *TAPPI Journal* and other journals applied the model to different paper grades and further developed the model to include a term to represent the equilibrium moisture — the limiting moisture that can be achieved in a specific press nip.

The DPM is based on the concept that the nip pressure is exerted on water between and within in the fibers. This differs from the conventional pressing models that are based on parallel pressures acting on water and fibers. Acceptance of the DPM has been surprisingly slow, likely due to the intuitive appeal and long history of the conventional model, despite its flaws and lack of predictive capability. We have addressed this over the years by publishing numerous successful applications of the DPM on paper machines.

What was most interesting in this research was that the three terms in the equation correspond precisely to the qualitative descriptions that have been applied for more than 50 years: the flow-controlled regime, the pressure controlled (rewet) regime, and limiting consistency. Achieving 65% solids by pressing in a commercial machine is probably not possible, but improvements to existing operations can be made.

For mills, the DPM can be used to identify the most cost effective ways to increase press section water removal. Our findings suggest two areas that need further study to open possibilities for higher solids content in wet pressing: rewet and equilibrium moisture.



McDonald



Kerekes

McDonald is president, JDMcD Consulting Inc., Vaudreuil-Dorion, QC, Canada. Kerekes is professor emeritus, University of British Columbia, Vancouver, BC, Canada. Email McDonald at mcdonald.jdavid@gmail.com.

LITERATURE CITED

1. Busker, L.H. and Cronin, D.C., *Pulp Pap. Can.* 85(6): T138(1984).
2. Maloney, T., Todororiv, A., and Paulapuro, H., *Nord. Pulp Pap. Res. J.* 13(4): 285(1998).
3. Holstege, G., *TAPPI J.* 81(6): 115(1998).
4. Laivins, G.V. and Scallan, A.M., *Tappi J.* 77(3): 125(1994).
5. McDonald, J.D., McDonald, E.M., and Kerekes, R.J., *J-FOR* 3(2): 52(2013).
6. Brown, Ron, Hansen, Fred, Mallory James, et al., "Forest Products Industry Technology Roadmap," www.agenda2020.org, 2010. Available [Online] http://www.agenda2020.org/uploads/1/1/4/1/11419121/fpi_roadmap_2010.pdf <27Feb2017>.
7. Kerekes, R.J., McDonald, E.M., and McDonald, J.D., *J-FOR* 3(2): 46(2013).
8. McDonald, J.D. and Pikulik, I.I., *Tappi J.* 70(2): 77(1987).
9. McDonald, J.D. and Kerekes, R.J., *Tappi J.* 74(12): 142(1991).
10. McDonald, J.D. and Kerekes, R.J., *Tappi J.* 78(11): 107(1995).
11. McDonald, J.D., Hamel, J., and Kerekes, R.J., *J. Pulp Pap. Sci.* 26(11): 401(2000).
12. McDonald, J.D. and Amini, J., *TAPPI J.* 83(2): 79(2000).
13. McDonald, J.D. and Pikulik, I.I., *Tappi J.* 72(10): 95(1989).
14. McDonald, D., "Web rewetting by forming fabrics," *Process Prod. Qual. Conf. Trade Fair,* TAPPI PRESS, Atlanta, GA, USA, 1999.
15. Luotonen, A., and Sämpi, J., "Dewatering in double wire pulp machine -- press theory and test results," *TAPPI Eng. Conf.*, TAPPI PRESS, Atlanta, 1995.
16. McDonald, J.D. and Pikulik, I.I., *Nord. Pulp Pap. Res. J.* 3(3): 115(1988).
17. Anderson, L. and Back, E., "The effect of temperature up to 90ºC on dewatering of wet paper webs, evaluated in a press simulator," *TAPPI Eng. Conf.*, TAPPI PRESS, Atlanta, 1981.
18. Royo, M. and Thorp, B., *PIMA* 63(9): 38(1981).
19. Batty, R.C., Daunais, R., and Pye, I.T., *J. Pulp Pap. Sci.* 9(4): TR106(1983).
20. Hodges, C.R., *Tappi* 60(7): 94(1977).
21. Lehtinen, A., *Pap. Age* 15(11): 32(1979).
22. Pikulik, I.I., Garner, R.G., Daunais, R., et al., *Pulp Pap. Can.* 93(1): 30(1992).
23. Vomhoff, H. and Gullbrand, O., *Papier* T104(11): 40(2004).
24. Beck, David A., "Re-examining wet pressing fundamentals: A look inside the nip using dynamic measurement," *TAPPI Engineering Conf.*, TAPPI PRESS, Atlanta, 1986.
25. McDonald, J.D., Pikulik, I.I., Ko, P.L., et al., *J. Pulp Pap. Sci.* 28(1): 17(2002).

Fractional pulping of packaging board in high consistency drum pulping

HEIKKI UPOLA, ARI ÄMMÄLÄ, AND MIRJA ILLIKAINEN

ABSTRACT: A wide variety of packaging materials with different wetting rates and wet strength properties are used in old corrugated container (OCC) processing. The disintegration rates of the different grades also vary and enable the use of the fractional pulping concept where easily disintegrated material is removed at the early stages. In the present study, fractional drum pulping was studied by pulping (Pilot drum pulping) and fractionating (Tampella oscillating screen) a mixture of strong-grade kraftliner and weak-grade fluting at high consistency to determine if energy consumption could be reduced. The results showed that a 25% energy saving could be realized through fractional pulping and an even higher potential might be possible if pulping conditions are optimized. Average fiber length, fines content, and ash content in the separated fractions were analyzed. The separated short fiber fractions and long fiber fractions could be individually processed, thus decreasing the volumes in the unit processes on the OCC line.

Application: Mills can increase capacity and improve energy savings in OCC recycling processes.

Packaging board is one of the most recycled raw materials in the world. The recycling rate of packaging board is 74% on average in Europe but can be as high as 80% in some countries, such as Belgium [1,2]. The recycling process for packaging board is the simplest method in the field of fiber recycling. The different types of packaging grades vary due to their various uses, and strength properties of packaging materials vary greatly. Corrugated board is a multilayered product, and each layer has its own purpose. Depending on its intended use, corrugated board can be produced partially from recycled packaging material instead of virgin materials.

The first unit process in old corrugated container (OCC) recycling is pulping, where recovered board bales are disintegrated into a pumpable suspension and coarse contaminants are removed. Two processes are used to pulp packaging board. One is continuous low consistency vat pulping (LC, consistency <6%) using a rotor that produces high shear forces, which disintegrate board into a fiber suspension [3,4]. In continuous LC pulpers, the disintegrated material is continuously removed during pulping. The other pulping option is a rotating drum, where the board is disintegrated at high consistency (HC, consistency <19%) by impact due to the repeated lifting and falling of the material [5]. After the pulping process, contaminants are separated from the pulp suspension in different unit operations and the pulp suspension can be divided into a short fiber fraction and a long fiber fraction.

A drum pulper typically consists of two sections. The first section of the drum is used to disintegrate the packaging board, and the second section is used as a screen to separate the disintegrated pulp suspension from coarse contaminants and flakes. Consistency in the disintegration section is 14%–20%, and is lowered to 3%–5% in the separation section to achieve efficient screening.

The target of pulping is to achieve high material efficiency by avoiding fiber losses due to the rejection of nondisintegrated fiber material (i.e., flakes). The disintegration forces in the pulper must overcome the wet strength of the material during pulping. Because of the wide variety of packaging materials used, weaker wet strength materials disintegrate faster than stronger materials during pulping. This leads to a situation where the pulper lifts and uses energy in material that has already been disintegrated. Thus, it could be beneficial to remove disintegrated material from the pulper at the early stage of pulping so that unnecessary material movement is avoided [6]. This approach has been studied in LC pulping where two batch pulpers are used in series with a screening stage between the pulpers [7,8]. First, 2 min of pulping was carried out for the whole OCC batch. Then, the disintegrated pulp was screened out and the pulping of the undisintegrated material was continued in another pulper unit. Even though the results were promising, fractional pulping has not yet become a commercially common concept. The fractional pulping concept in HC pulping has been studied from the perspective of the deinking process [9], but the fractional pulping of OCC at HC has not yet been studied.

The present work is a study of the fractionation of packaging material pulp in an HC pulper. The aim was to study how effectively disintegrated materials can be separated in a drum pulper. Pulp properties (ash content, fiber length, and fines content) were studied after fractionation at different pulping

Material	Grammage, g/m²	Ash Content 525°C, %	Tensile Index, kNm/kg	Wet Tensile Index, kNm/kg	Average Fiber Length, mm
Kraftliner (virgin fibers)	120	2.8	131.7	13.0 (9.8% wet/dry)	1.2
Fluting (secondary fibers)	90	11.8	80.1	2.1 (2.7% wet/dry)	0.8

I. Properties of kraftliner and fluting materials.

times to evaluate how easily disintegrating fluting could be separated from kraftliner, which has a higher wet strength, and how this affects the total energy demand of pulping with a chosen fractionation point.

MATERIALS AND METHODS

The materials used in this study were virgin-pulp containing linerboard and recycled pulp containing fluting; both materials were obtained from a Nordic board factory. **Table I** summarizes the specifications for the materials used. Ash content was analyzed with a PrepASH129 (Precisa Gravimetrics; Dietikon, Switzerland) according to TAPPI T 211 om-02 "Ash in wood, pulp, paper, and paperboard: combustion at 525°C." The tensile strengths of the materials were tested with an Instron 5544 (Instron; Norwood, MA, USA) equipped with a 100 N load cell using the TAPPI T 456 om-03 "Tensile breaking strength of water-saturated paper and paperboard."

The material was cut into 200 mm x 400 mm specimens. The specimens were stored at 50% relative humidity and 24°C temperature. Materials were mixed with each other before being loaded into the drum pulper. **Figure 1** is an image of the pilot scale drum pulper used in this study. The diameter of the drum is 1.5 m, the width is 0.26 m, and the lifters are 0.1 m. The circumferential velocity of the drum during pulping was adjusted to 1.3 m/s. The drum pulper was rotated by two 2.2 kW motors.

In this study, two pulping trial series were conducted. In both trials, the consistency was adjusted to 15%. The temperature at the beginning of pulping was adjusted to 24°C. In industrial processes, a temperature of 50°C is typically used. A lower temperature was chosen for this study to eliminate the effect of temperature changes during pulping and fractionation with used setup. A Tampella oscillating screen (Ø 4 mm) was used to fractionate pulp gently without excess disintegration of flakes. **Figure 2** is a schematic of the experimental setup.

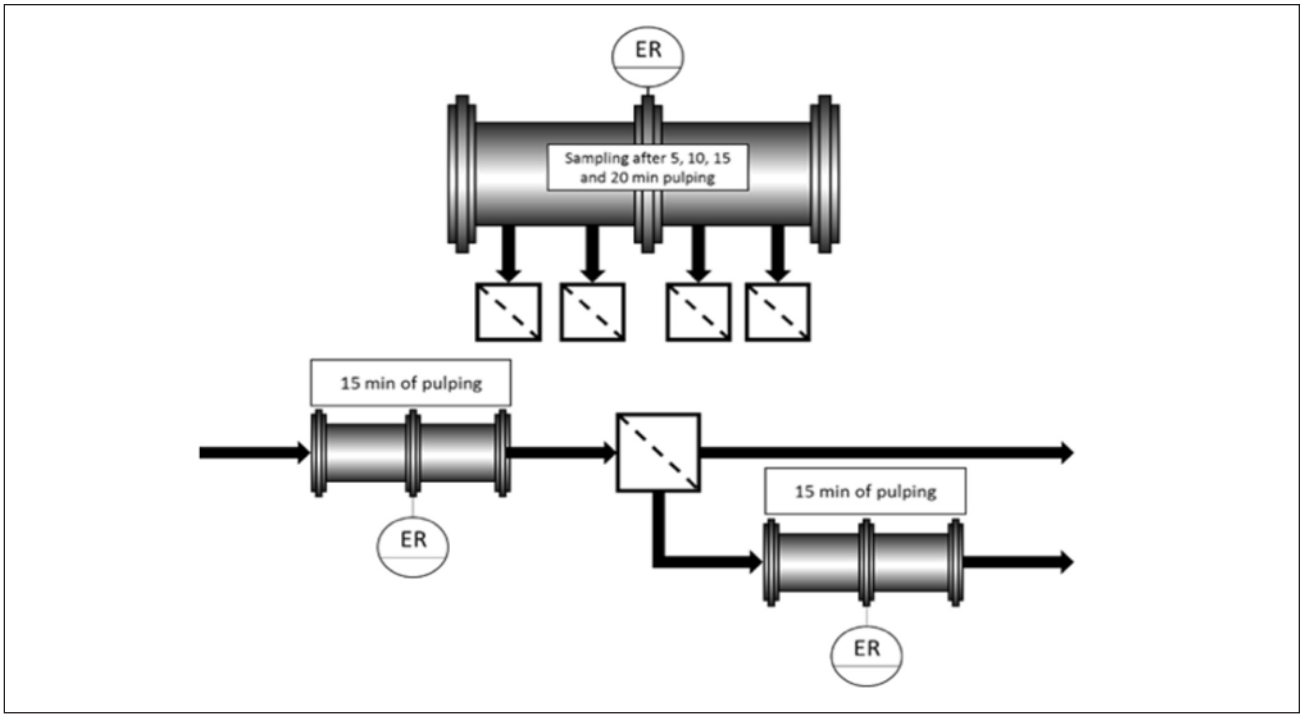
In the first trial (reference), the pulping batch size was 100 kg consisting of 7.5 kg kraftliner and 7.5 kg fluting (50:50). Pulping kinetics were performed and after 5, 10, 15, and 20 min, the pulper was stopped and 300 g of pulp were sampled for laboratory analysis. Samples were fractionated with a Tampella vibration screen with a hole diameter of 4 mm (**Fig. 3**).The sample size in the screen fractionation was 200 g (of dry matter content). The consistency was adjusted to 0.5% before each fractionation. Both reject and accept samples were collected for further analysis.



1. Drum pulper with 1.5 diameter, 8 lifters, and 10 cm lifter size.

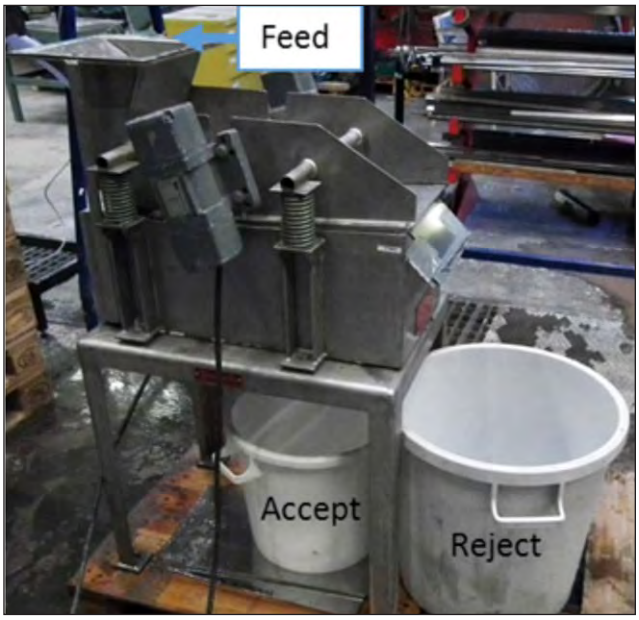
Various characteristics from the fractions (fine content, average fiber length, and ash content) were analyzed. Fines content was measured using Somerville equipment (Techlab Systems; Itasca, IL, USA) with 200 mesh wire; 80 L of water was used to wash the fines. Average fiber length (length weighted) was analyzed with a Fracon (Metso; Helsinki, Finland) tube flow fractionation device equipped with a charge-coupled device camera that allowed the analysis of fiber length through an image analysis procedure [10]. Ash content in the reject and accept samples was analyzed with a PrepASH (Precisa PrepASH129) by incinerating samples at 525°C.

A second series of trials was performed to compare the disintegration of the board mixture and the energy consumption in fractional pulping to conventional drum pulping (first trial acted as reference). In this trial, the whole batch was diluted and fractionated after 15 min of pulping in screening consistency of 0.5%. A batch size of 166 kg was used with the same consistency and mixture as in the reference pulping process. The reason for the larger batch size was an attempt to obtain the same batch size after fractionation as in the reference sample. After fractionation, the consistency of the reject material was measured from the reject and adjusted back to 15% and pulping was allowed to continue for another 15



2. Schematic of experimental setup used in fractional drum pulping study. Top: first trial pulping (reference), bottom: second pulping (fractional pulping where whole batch was fractionated). Consistency in each pulping was adjusted to 15% with starting mixture of 50:50 kraftliner and fluting.

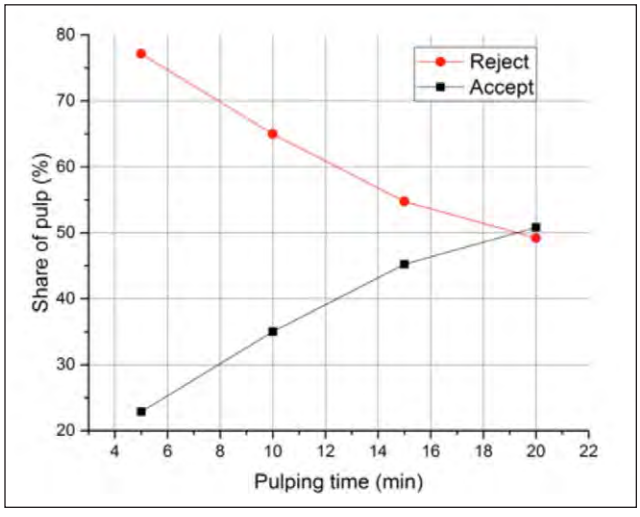
min. During fractionation, 46.5% of pulp went to accept. Somerville flake content was used to evaluate the efficiency of the pulping process along with energy consumption data. The analysis was conducted according to TAPPI T 275 sp-02 "Screening of pulp (Somerville-type equipment)." For screening, a 40-g sample of dry matter content was taken, and the flake content was calculated as the mass of the retained pulp on the screen compared with the mass of the feed sample.



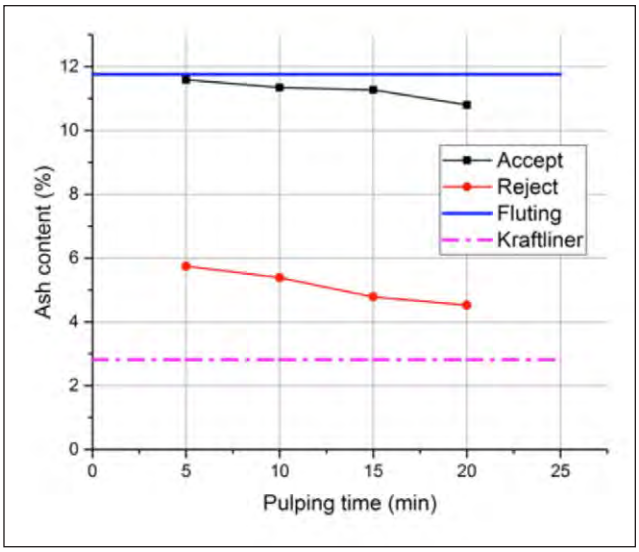
3. Tampella oscillating screen (Ø 4 mm). The feed sample was divided into reject (flakes) and accept (disintegrated pulp) samples. For all fractionations, feed consistency was adjusted to 0.5%.

RESULTS

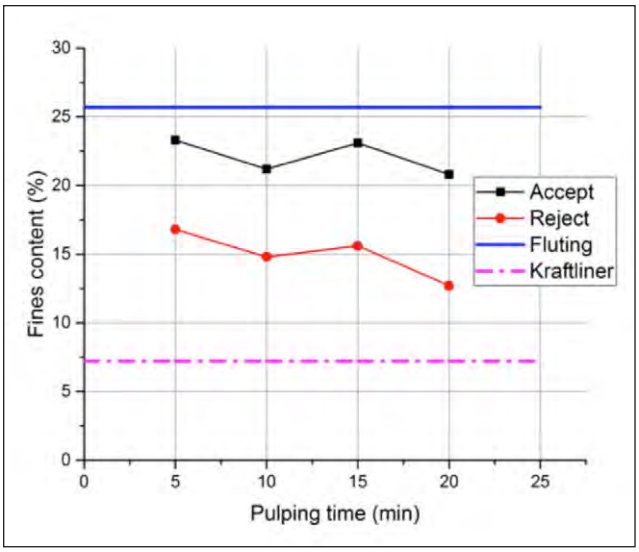
For the reference pulping, the mass reject rate experimentally calculated at various sampling times by vibration screen is shown in **Fig. 4**. As the pulping progressed, the share of the accepted material increased due to the defibering actions of the pulper.



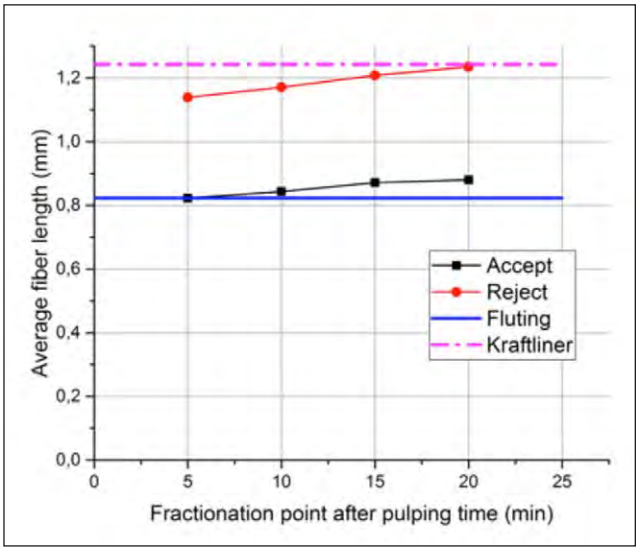
4. Shares of accept and reject in fractionation as a function of pulping time.



5. Ash content of fractionation accept and reject as a function of pulping time.



7. Fines content of accept and reject as a function of pulping time.



6. Length-weighted fiber length of fractionation accept and reject as a function of pulping time.

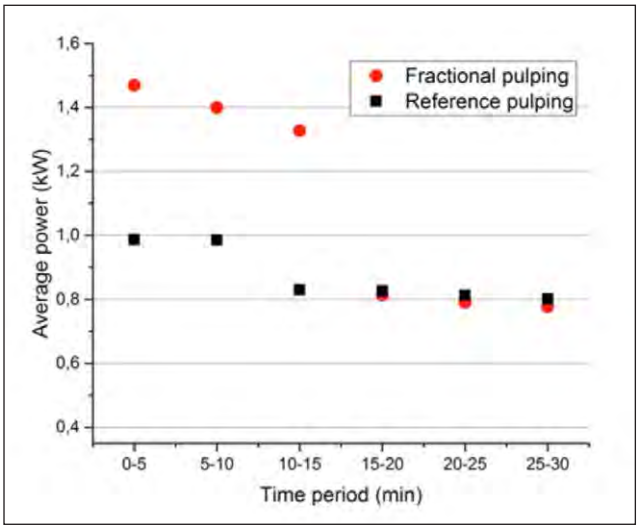
The average fiber length, fines, and ash contents were analyzed from each fractionation sample. The results from this analysis are illustrated in **Figs. 5**, **6**, and **7**, respectively.

As expected, a greater number of longer fibers were found in the fractionation reject than in the fractionation accept. Average fiber length increased in the fractionation accept and fractionation reject as the pulping proceeded. The length difference remained virtually unchanged. After 5 min of pulping, the fractionation accept had the same average fiber length as fluting, indicating that fluting disintegration mainly occurs in the early stage of pulping. After 20 min of pulping, fiber length in the fractionation reject reached the same level as that in the kraftliner, indicating that all fluting basically disintegrated in this phase.

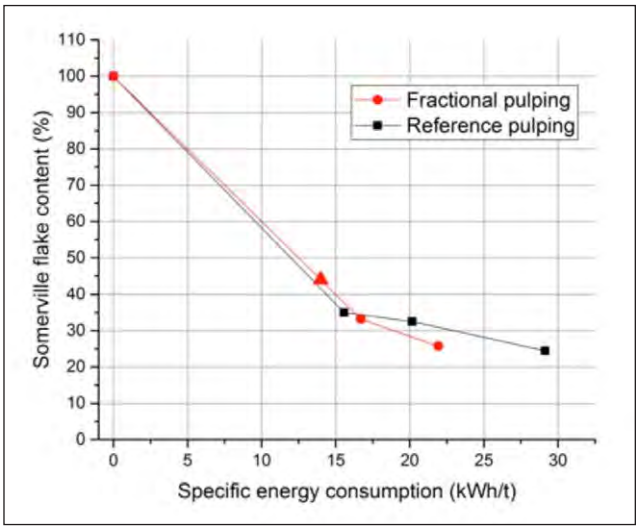
Fines and ash contents were higher in the accept than in the reject. Decreasing trends in their contents were seen both in the fractionation accept and reject. Unlike fiber length, the ash and fines contents of the reject did not reach the contents of the kraftliner, indicating lower separation in fractionation.

In the second series of trials, we studied how fractionation affects pulping efficiency. The average power consumption for the fractional pulping and the reference pulping is shown in **Fig. 8**. Initially, the pulping power consumption was at a higher level because of the greater batch size (i.e., the degree of filling in the pulping). Later, the fractionation power consumption remained at the same level because the degree of filling remained the same.

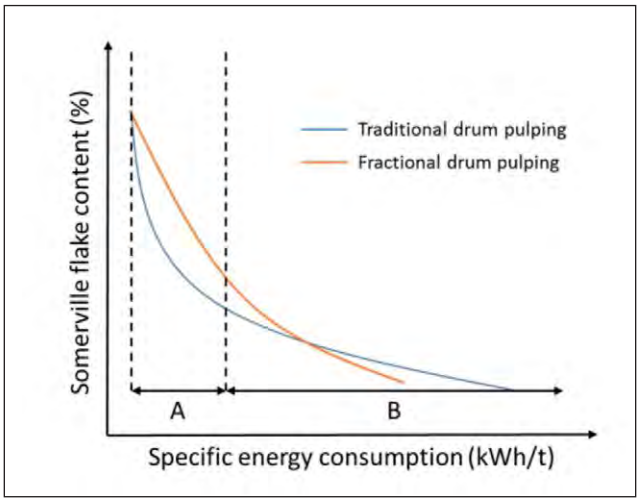
Pulping efficiency (i.e., the degree of disintegration level



8. Average power consumption between periods. Fractionation point occurred 15 min after pulping. Starting batch sizes in the fractional and reference pulping were 166 kg and 100 kg, respectively.



9. Somerville flake content after 15, 20, and 30 min of reference and fractional pulping. Triangle symbol indicates the fractionation point. Fractional pulping total Somerville flake content is calculated from final pulp Somerville flake content recombined with the screening accepts according to the mass split; 47% of the dry mass was removed from the pulper in the fractionation.



10. Illustration of disintegration efficiency in drum pulping. Phase A is disintegration at the beginning of pulping and phase B is pulping after fractionation in the case of fractional pulping.

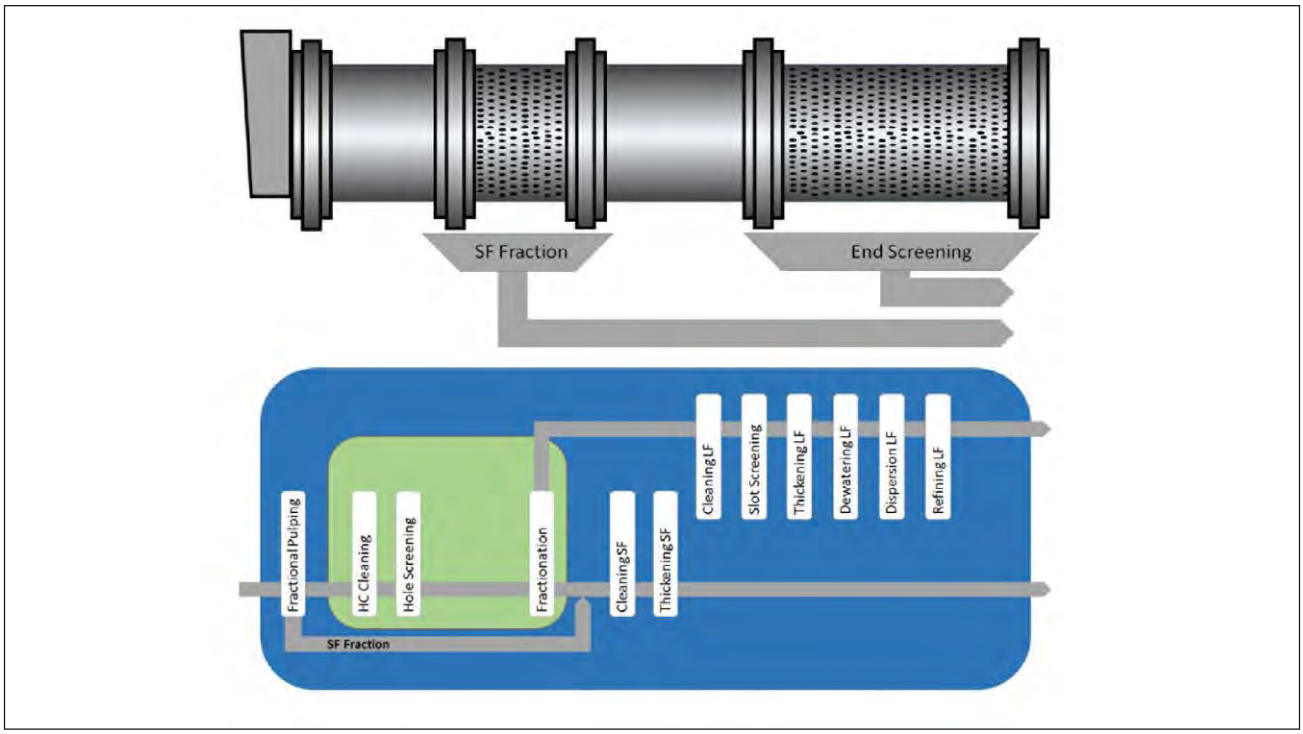
measured by the Somerville flake content as a function of specific energy consumption) is presented in **Fig. 9**. With fractional pulping, specific energy consumption was about 25% lower at the 25% flake content level than in the reference pulping. Initially, the reference pulping seemed to have more efficient disintegration; the lower filler degree probably offered more favorable wetting and disintegration conditions. Fractional pulping, however, gave better disintegration efficiency at the later stages of pulping than did the reference pulping.

DISCUSSION

In OCC processes, a wide variety of different packaging materials all have different properties, such as wet tensile strength. Disintegration of different materials is known to occur with different kinetics depending on the materials' wet strength properties [3]. The idea of fractional pulping is to easily remove disintegrating material (i.e., material having a low wet strength) from the pulper at the early stage of pulping to decrease the pulper's load and thus increase pulping efficiency. Fractionation is done to separate long and short fibers into different layers of product or different products or to remove ash and fines from the stock [11].

In our previous study [12], the amount of mass was found to have a positive effect on the disintegration of stronger materials. Fractional pulping would have decreased disintegration kinetics after fractionation if operated at the traditional fill level. In addition, the material after fractionation can be considered to have good quality properties (Figs. 4, 5, and 6) of the product produced from it. On the basis of these determinations, it could be beneficial to have an optimal fill level after fractionation to maximize energy efficiency at the end of pulping. Therefore, the starting fill level should be higher than usually used in traditional drum pulpers. With an increased fill level, fractional pulping would have decreased disintegration kinetics and efficiency (**Fig. 10**, phase A) and increased total energy consumption at the beginning stages of pulping. However, the specific energy demand would be lower after the decreased load in fractionation (Fig. 10, phase B). Energy savings with the setup used in the present study was approximately 20%, not taking into account the energy consumption for separation. The fractional pulping here was probably not optimal; however, a considerable energy saving was still achieved.

In addition to the energy savings in fractional pulping, two fractions having different fiber and papermaking potentials are obtained. The analysis indicates good results in the selective separation of different types of materials because of the different wet strength properties and wetting kinetics of the raw materials. It has been shown in different studies that previous recycling cycles increase the fibers' internal and external fibrillation, which increases tensile strength; however, simultaneously, fiber shortening and cutting also occur, which increases the fines content in recycled pulp and decreases the strength properties of the resulting product [13,14]. Recycling increases the nonpaper component content in recycled fiber products, which also has a negative effect on strength properties [15]. Because of this, fluting disintegrates rapidly in the early stages of pulping. In the present study, the rapid disintegration of fluting could be seen in the fiber length; the fractionation accept after 5 min of pulping had practically the same fiber length as the fluting. As pulping proceeded, the kraftliner began to disintegrate, causing the fractionation accept fiber length and the fractionation reject fiber length to increase because the amount of fluting decreased. Similar, but inverse, trends were also seen for ash and fines contents.



11. Possible concept advantages of fractional pulping. The green area represents opportunities for possible energy savings in cleaning processes. LF = long fiber fraction and SF = short fiber fraction. SF fraction might need additional cleaning processes.

In this study, the dropping height of the pilot drum was relatively low compared with industrial drum pulpers, which resulted in low disintegration kinetics of stronger material as well as high residual flake content after 20 min of pulping. In our previous study [12], the dropping height was found to be important in the disintegration of stronger raw materials.

Fractional pulping might provide an opportunity for the design of OCC processes with smaller units and decreased energy consumption or increased capacity of the process line. Easily disintegrated grades usually are also short-fibered grades and the short fiber fraction could bypass coarse cleaning and screening as well as pressure screen fractionation. This concept, presented in **Fig. 11**, could lead to energy savings in cleaning, coarse screening, and pressure screen fractionation because of lower volumes being processed. Energy savings depend on the fractionation split as well as the selectivity of fractional pulping. On the other hand, there is also an option to increase the capacity of the pulping process.

Table II summarizes the rough estimation of energy saving potential in the fractional pulping concept on the basis of the raw material and fractionation selectivity in this study. Results from various shares of the short fiber fraction together with the pulp properties for the short fiber and long fiber fractions are presented. Energy savings potential can be cal-

Share of Short Fiber Accept in Pulping	0	25%	40%	50%
Coarse screening, kW·h/t	12	9.0	7.2	6.0
Fractionation, kW·h/t	5	3.8	3.0	2.5
Total energy consumption, kW·h/t	17	12.8	10.2	8.5
Energy saving potential, kW·h/t	0	4.3	6.8	8.5
Ash content in reject, %	-	5.7	5.0	4.5
Ash content in accept, %	-	11.5	11.3	10.9
Average fiber length in accept, mm	-	0.82	0.85	0.87
Average fiber length in reject, mm	-	1.14	1.18	1.23

II. Estimated energy savings from cleaning processes and qualities of fractions.

culated from the total energy consumption with the share of short fiber accept in pulping. For example, with 60% short fiber accept, the energy savings would be 10.2 kW·h/t.

It is difficult to estimate the optimal fractionation point in the pulper. Variables such as ash contents, average fiber length, and fines content change depending on the fractionation point, which affects the quality aspects of the fractions. On the other hand, energy consumption aspects change depending on the fractionation point. This raises the question of determining the significance of the quality aspects and efficient pulping (minimum fiber loss) versus energy consumption savings. According to previous studies and patents, both fractions might need separate cleaning devices [8,16].

CONCLUSIONS

Fractional pulping is a method that can be used to potentially decrease energy consumption in OCC pulping. Pulp can be fractionated according to the disintegration rates of different grades; that is, between weaker, shorter-fiber products (e.g., fluting) and stronger, longer-fiber products (e.g., kraftliner). Fractional pulping could make it possible to reduce the size of unit processes in OCC lines or increase pulping capacities. **TJ**

LITERATURE CITED

1. CEPI, "Key statistics: European pulp and paper industry 2013," Confederation of European Paper Industries, Brussels, 2013. Available [Online] http://digibook.digi-work.com/Digibooks.aspx/Get/cepi/1191/Final_Key_statistics_2013pdf <16Dec2015>.
2. Eurostat, "Packaging waste statistics," European Commission -- Publications Office, Luxembourg City, 2015. Available [Online] http://ec.europa.eu/eurostat/statistics-explained/index.php?title=Packaging_waste_statistics&direction=prev&oldid=272015 <1Feb2017>.
3. Holik, H., "Towards a better understanding of the defibering process," *TAPPI Eng. Conf., [Proc.]*, TAPPI PRESS, Atlanta, GA, USA, 1988.
4. Savolainen, A., Jussila, T., and Nikula, S. *Tappi J.* 74(11): 147(1991).
5. Fabry, B., *Prog. Pap. Recycl.* 19(3): 17(2010).
6. Scott, G.M. and Abubakr, S., *Prog. Pap. Recycl.* 3(3): 50(1994).
7. Seifert, P. and Long, K.J., *Tappi* 57(10): 69(1974).
8. Chung, S.H., *Prog. Pap. Recycl.* 12(3): 21(2002).
9. Kemppainen, K., Körkkö, M., and Niinimäki, J., *BioResources* 6(3): 2977(2011)
10. Laitinen, O., Kemppainen, K., Stoor, T., et al., *BioResources* 6(1): 672(2011)
11. Doshi, M.R., *Prog. Pap. Recycl.* 12(3): 4(2002).
12. Upola, H., Ämmälä, A., Kankaanpää, V., et al., *Prog. Pap. Recycl.* 15(1): 33(2016).
13. Kačík, F., Čabalová, I., and Kačíková, D., "Changes of macromolecular properties of recycled pulp fibres," *SGEM 2011 Conf. Proc.*, SEGM World Science, Vienna, 2011.
14. Kang, T., and Paulapuro, H., *Pulp Pap. Can.* 107(7–8): 51(2006).
15. Kuys, K. and Zhu, T.Q.Y., "Surface chemistry of total chlorine free bleached eucalypt kraft pulp," *48th Appita Conf.*, Appita, Bundoora, Australia, 1994.
16. Chung, S.H., U.S. pat. 6,340,407 (Jan. 22, 2002).
17. Holik, H. and Schabel, S., in *Recycled Fibre and Deinking* (U. Höke and S. Schabel, eds.), 2nd edn., Paper Engineers Association, Helsinki, 2009, p. 141.

ABOUT THE AUTHORS

We chose this topic because pulping is one of the most energy consuming unit operations in the OCC recycling process. Only a few publications exist about OCC pulping, especially drum pulping. In packaging material recycling, there is huge material diversity, all of which have different strength properties. Previous fractional pulping studies show there is potential in this kind of system.

Even though the experiment setup looks simple, the workload during the pulping and fractionation stage, including the preparation, was huge. We were surprised about the analysis results regarding differences in fiber length and ash content.

Our hope is that these results can give some basic knowledge about drum pulping and some new ideas for new, next-generation drum pulpers that work more efficiently. Surely, there is potential.



Upola



Ämmälä



Illikainen

Upola is a doctoral student, Ämmälä is an adjunct professor, and Illikainen is a professor at the University of Oulu, Oulu, Finland. Email Upola at heikki.upola@oulu.fi.

TAPPI JOURNAL
WWW.TAPPI.ORG
THE PAPER AND PACKAGING INDUSTRIES' TECHNICAL RESOURCE
MARCH 2017 | VOL. 16 NO.3



SPECIAL LIGNIN VALORIZATION CONTENT

SPECIAL FEATURE 107
Lignin carbon fiber: The path for quality
Qiang Li, Arthur J. Ragauskas, and Joshua S. Yuan

LIGNIN PRODUCTS 111
Melt-blown compostable polyester films with lignin
Wolfgang G. Glasser, Robert Loos, Blair Cox, and Nhiem Cao

LIGNIN CONVERSION 123
Accelerated aging of bio-oil from lignin conversion in subcritical water
Huyen Nguyen Lyckeskog, Cecilia Mattsson, Lars Olausson, Sven-Ingvar Andersson, Lennart Vamling, and Hans Theliander

LIGNIN CHARACTERIZATION 145
An easy and reliable method for syringyl:guaiacyl ratio measurement
Raquel Prado, Lisa Weigand, Shikh M.S.N.S. Zahari, Xabier Erdocia, Jason P. Hallett, Jalel Labidi, and Tom Welton

ECONOMIC ANALYSIS 157
Analysis of economically viable lignin-based biorefinery strategies implemented within a kraft pulp mill
Cédric Diffo Téguia, Rod Albers, and Paul R. Stuart

March 2017

TABLE OF CONTENTS VOL. 16 NO. 3

103 EDITORIAL
Lignin: Today and tomorrow
Art J. Ragauskas

107 SPECIAL FEATURE
Lignin carbon fiber: The path for quality
Qiang Li, Arthur J. Ragauskas, and Joshua S. Yuan

111 LIGNIN PRODUCTS
Melt-blown compostable polyester films with lignin
Wolfgang G. Glasser, Robert Loos, Blair Cox, and Nhiem Cao

123 LIGNIN CONVERSION
Accelerated aging of bio-oil from lignin conversion in subcritical water
Huyen Nguyen Lyckeskog, Cecilia Mattsson, Lars Olausson, Sven-Ingvar Andersson, Lennart Vamling, and Hans Theliander

145 LIGNIN CHARACTERIZATION
An easy and reliable method for syringyl:guaiacyl ratio measurement
Raquel Prado, Lisa Weigand, Shikh M.s.n.s. Zahari, Xabier Erdocia, Jason P. Hallett, Jalel Labidi, and Tom Welton

157 ECONOMIC ANALYSIS
Analysis of economically viable lignin-based biorefinery strategies implemented within a kraft pulp mill
Cédric Diffo Téguia, Rod Albers, and Paul R. Stuart

»COVER CREDIT: Arthur J. Ragauskas, *TJ* Editorial Board Member and organizer of this special Lignin Valorization issue, wishes to thank R. Davies of the Renewable Biomaterials Institute at Georgia Institute of Technology, Atlanta, GA, for graphic design assistance and L. Petridis of Oak Ridge National Laboratory, Oak Ridge, TN, for the lignin image, which was generated based on small-angle neutron scattering (SANS) data.

TAPPI JOURNAL
WWW.TAPPI.ORG

Editor-in-Chief
Scott Rosencrance scott.rosencrance@kemira.com
+1 770 429-2753

Associate Editor
Brian N. Brogdon brian.brogdon@gmail.com
+1 678 581-9114

Editorial Director
Monica Shaw mshaw@tappi.org
+1 770 367-9534

Vice President, Operations
Eric Fletty efletty@tappi.org

PRESS Manager
Jana Jensen jjenson@tappi.org
+1 770 209-7242

Webmaster
Trina Heath theath@tappi.org
+1 770 209-7416

***TJ* EDITORIAL BOARD**

Brian N. Brogdon, FutureBridge Consulting & Training LLC
brian.brogdon@gmail.com, +1 678 581-9114

David A. Carlson, Carlson Consulting
dacarlson39@aol.com, +1 847 323-2685

Jere W. Crouse, JWC Consulting
cj522@inwave.com, +1 608 362-4485

Mahendra Doshi, Doshi and Associates
mahen@aol.com, +1 920 832-9101

Marc Foulger, GL&V USA Inc.
Marc.foulger@glv.com +1 315 767-2920

Peter W. Hart, WestRock
peter.hart@westrock.com, +1 409 276-3465

Carl J. Houtman, USDA Forest Products Laboratory
choutman@fs.fed.us, + 1 608 231-9445

John A. Neun, John A. Neun LLC
john.neun@gmail.com, +1 518 275-8139

Jim Niemiec, Verso Corporation
jim.niemiec@versoco.com, +1 715 422-7404

Steven P. Ottone, Omya
steven.ottone@omya.com, +1 919 641-7854

Gaurav Pranami, Imbed Biosciences
gpranami@imbedbio.com, +1 515 230-7005

Arthur Ragauskas, Oak Ridge National Laboratory
aragausk@utk.edu

Gerard J.F. Ring, University of Wisconsin—Stevens Point
gerrryring@wi-net.com, +1 715 592-3732

Scott Rosencrance, Kemira Chemicals
scott.rosencrance@kemira.com, +1 770 429-2753

Ricardo B. Santos, WestRock
ricardo.santos@westrock.com, +1 540 969-2426

Paul Wiegand, NCASI
pwiegand@ncasi.org, +1 919 941-6417

Junyong Zhu, USDA Forest Products Laboratory
jzhu@fs.fed.us, +1 608 231-9520

Join TAPPI *today!*

TAPPI JOURNAL is a free benefit of TAPPI membership, and is only available to members. To join TAPPI, to renew your TAPPI Membership, or to learn about other valuable benefits, visit www.tappi.org.

TAPPI, 15 Technology Parkway S., Suite 115, Peachtree Corners, GA 30092, publishes *TAPPI JOURNAL* monthly.

ATTENTION PROSPECTIVE AUTHORS: All papers published are subject to *TAPPI JOURNAL's* peer-review process. Not all papers accepted for review will be published. Before submitting, check complete author guidelines at http://www.tappi.org/s_tappi/doc.asp?CID=100&DID=552877.

Statements of fact and opinions expressed are those of individual authors. TAPPI assumes no responsibility for such statements and opinions. TAPPI does not intend such statements and opinions or construe them as a solicitation of or suggestion for any agreed-upon course of conduct or concerted action of any sort.

Copyright 2017 by TAPPI, all rights reserved. For copyright permission to photocopy pages from this publication for internal or personal use, contact Copyright Clearance Center, Inc. (CCC) via their website: www.copyright.com. If you have questions about the copyright permission request process, please contact CCC by phone at +1 978 750-8400. To obtain copyright permission to use excerpts from this publication in another published work, send your specific request in writing to Editor, TAPPI JOURNAL, 15 Technology Parkway S., Suite 115, Peachtree Corners, GA 30092, USA; or by fax to +1 770 446-6947. Send address changes to TAPPI, 15 Technology Parkway S., Suite 115, Peachtree Corners, GA 30092, USA; Telephone +1 770 446-1400, or FAX +1 770 446-6947. www.tappi.org

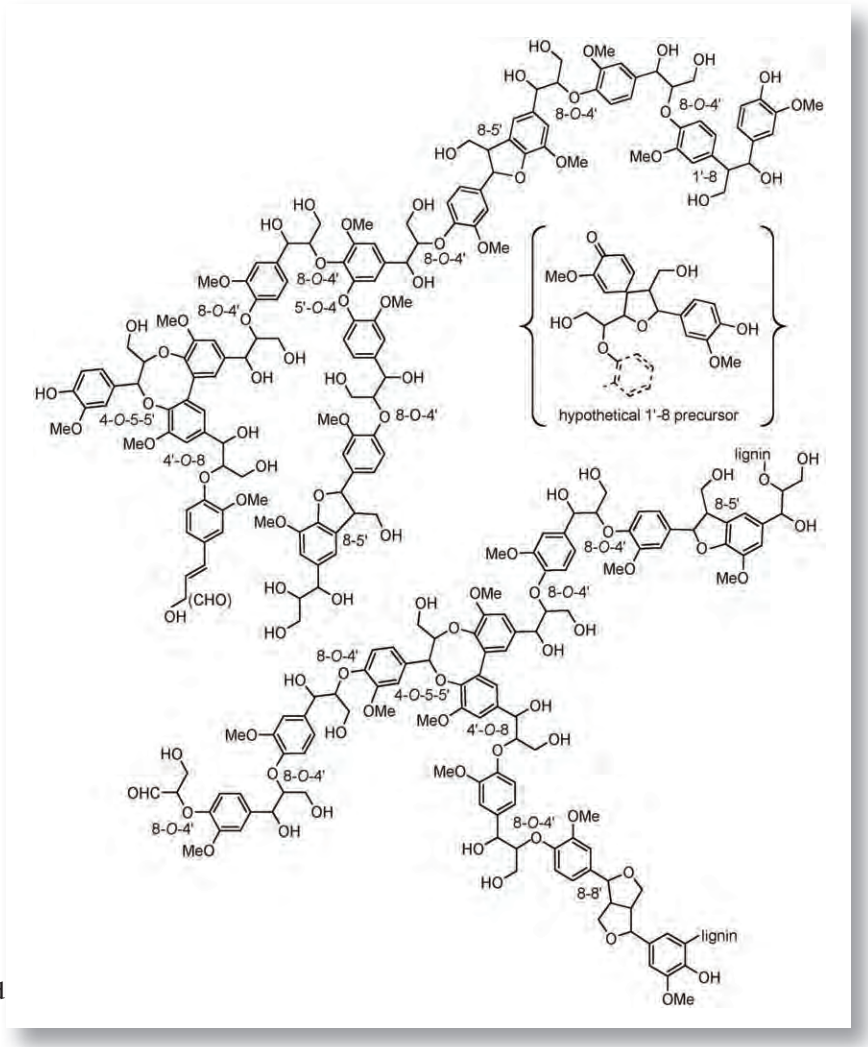
Editorial



ARTHUR J. RAGAUSKAS
TAPPI Journal Editorial Board Member

Lignin: Today and tomorrow

At its foundation, the chemical pulping industry was and is still centered around removal of lignin (**Fig. 1**) to produce high-quality cellulosic fibers. For sulfite pulping, the industry has well-established lignin isolation and conversion techniques to utilize lignin in several applications, including vanillin synthesis, binders, dispersion agents, emulsifiers, anti-corrosion agents, UV-absorbers, battery components, and anti-flammability agents in the future [2,3].



1. Illustrative softwood native lignin structure [1].

Challenging the status quo

Although the kraft industry has historically focused largely on pulp production and lignin for energy production, several developments have begun to challenge this convention from (a) enhanced energy efficiencies for pulp/papermaking [4], (b) lignin isolation technologies that can be incorporated into the kraft pulping platform [5,6], (c) an enhanced understanding of the structure of lignin during and after kraft pulping [7,8], and (d) new valorization conversion chemistries to convert kraft lignin to bio-derived chemicals, materials, and fuels [9,10,11]. In parallel, significant efforts are being directed to convert lignin from cellulosic ethanol plants to bio-derived products. In both cases, these efforts are being championed to garner greater value from lignin, enhance mill operations, and improve capital effectiveness.

Promising developments in lignin applications

Although the manufacturing platforms for kraft pulping and cellulosic ethanol are different, they will undoubtedly both benefit from lignin valorization studies. Even a brief review of lignin utilization efforts highlights several promising translational research outcomes, including:

- Shinano, T. and Matsumura, Y., "Lubricant composition containing lignin compound," *Jpn. Kokai Tokkyo Kobo*, 2017, JP 2017008218 A 20170112.
- Wang, X.M., et al., "High residual content (HRC) kraft/soda lignin as an ingredient in wood adhesives," *PCT Int. Appl.*, 2016, WO 2016165023 A1.

- Mukerjee, S., et al., "High recycle content polyols from thermoplastic polyesters and lignin or tannin for manufacturing polyurethanes," *U.S. Pat. Appl. Publ.*, 2016, US 20160208044 A1 20160721.
- Stevens, Eugene S., "Extruded starch-lignin foams," *U.S. Pat. Appl. Publ.*, 2016, US 20160368186 A1 20161222.
- Garoff, N. and Walter, S., "Electrically dissipative foamable polymer composition comprising conductive carbon powder produced from lignin," *PCT Int. Appl.*, 2015, WO 2015173724 A1 20151119
- Zhang, Li., et al., "Production of carbonaceous nanofibrous materials with ultra-high specific surface area from alkali (kraft) lignin," U.S. pat. (2015), US 9190222 B1 20151117

Special *TAPPI Journal* issue: Lignin valorization

Although the cost of lignin as a bioresource remains important, additional factors are developing, including its natural anti-oxidant properties, sustainability, biodegradability, UV-absorbance, and as a unique resource for aromatic compounds. Equally important is the next generation of students and entrepreneurs dedicated to understanding the properties of lignin and, in turn, valorizing this unique polymer.

This special issue of *TAPPI Journal* is dedicated to the valorization of lignin and provides a sampling of lignin research studies going on globally. Please stay tuned for additional lignin research to appear in the April 2017 issue of *TAPPI Journal*. **TJ**

Arthur J. Ragauskas is a member of the TAPPI Journal *Editorial Board and is professor/Governor's Chair in Biorefining, Oak Ridge National Laboratory; Department of Chemical and Biomolecular Engineering; Department of Forestry, Wildlife, and Fisheries; and Center for Renewable Carbon; University of Tennessee, Knoxville, TN, USA.*

LITERATURE CITED

1. U.S. Department of Energy Genomic Science, Biological and Environmental Research Information System (BERIS), "Contemporary view of lignin substructures." Available [Online] https://public.ornl.gov/site/gallery/detail.cfm?id=131&topic=&citation=8&general=&restsection <23March2017>.
2. Rueda, Cristina, Calvo, Pedro A., Moncalian, Gabriel, et al., "Biorefinery options to valorize the spent liquor from sulfite pulping," *J. Chem. Technol. Biotechnol.* 90(12): 2218(2015).
3. Matsushita, Yasuyuki, "Conversion of technical lignins to functional materials with retained polymeric properties," *J. Wood Sci.* 61(3): 230(2015).
4. Bajpai, Pratima, *Pulp and Paper Industry Energy Conservation*, Elsevier, Amsterdam, The Netherlands, 2016.
5. Joensson, Ann-Sofi and Wallberg, Ola, "Cost estimates of kraft lignin recovery by ultrafiltration," *Desalination* 237(1-3): 254(2009).
6. Ziesig, Rufus, Tomani, Per, Schweinebarth, Hannah, et al., "Production of a pure lignin product, part 1: distribution and removal of inorganics in *Eucalyptus globulus* kraft lignin," *TAPPI J.* 13(3): 65(2014).
7. Gellerstedt, Goran, "Pulping chemistry," in *Wood and Cellulosic Chemistry* (David N.-S. Hon and Nobuo Shiraishi, Eds.) 2nd edn., 2001, pp. 859-905.
8. Froass, Peter M., Ragauskas, Arthur J., and Jiang, Jian E., "NMR studies. Part 3. Analysis of lignins from modern kraft pulping technologies," *Holzforschung* 52(4): 385(1998).
9. Ragauskas, A.J., Beckham, G.T., Biddy, M.J., et al., "Lignin valorization: Improving lignin processing in the biorefinery," *Science* 344(6185): 1246843-1(2014).
10. Behling, R., Valange, S., and Chatel, G., "Heterogeneous catalytic oxidation for lignin valorization into valuable chemicals: what results? What limitations? What trends?" *Green Chem.* 18(7): 1839(2016).
11. Gellerstedt, G., "Softwood kraft lignin: Raw material for the future," *Ind. Crops Prod.* 77: 845(2015).

Lignin carbon fiber: The path for quality

QIANG LI, ARTHUR J. RAGAUSKAS, AND JOSHUA S. YUAN

Lignin represents an abundant biopolymer and a major waste from lignocellulosic processing plants, yet the utilization of lignin for fungible products remains one of the most challenging technical barriers for pulp mills and the modern biorefinery industry [1]. In recent decades, lignin has been sought after as a precursor polymer for carbon fiber due to the high carbon content (up to 60%). Lignin carbon fiber is expected to be compatible with the market size of the pulp and paper industry and may have transformative impact on petroleum-based carbon fiber [1].

CHALLENGES IN FABRICATING LIGNIN

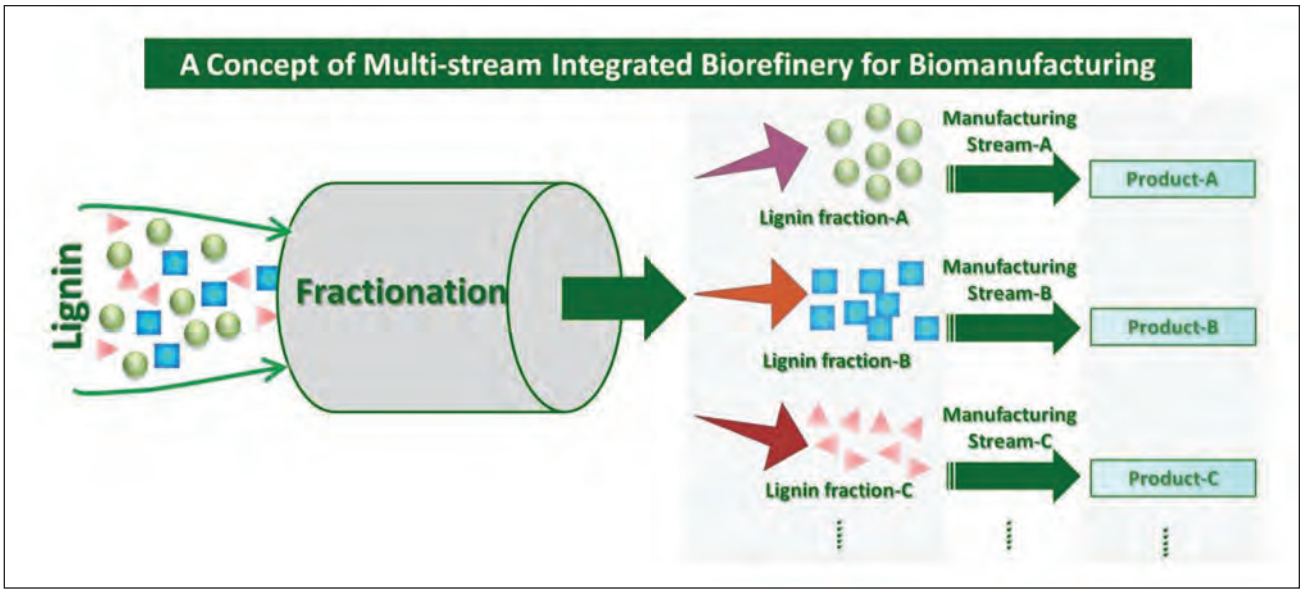
Current strategies for fabricating lignin carbon fiber include blending lignin with other polymers served as plasticizers [2], reinforcing lignin carbon fiber using functional materials like carbon nanotube [3] and cellulose nanofiber [4], and modifying lignin phenolic hydroxyl groups (Ar-OH) through esterification [5,6]. Nevertheless, the quality and mechanical performance of current lignin carbon fiber are still too low to compete with commercialized petroleum-based carbon fiber, making lignin carbon fiber impractical for industrial application.

The real challenge of the poor quality lies in the heterogeneity of the lignin structure, which is caused by broad molecule weights, various interunitary linkages, and diverse functional groups. These inherent molecular characteristics could hinder the crystallite turbostratic carbon structure formation during the carbonization and graphitization of lignin carbon fiber. Thereby, the modification of lignin molecules toward more uniform structure could be the path for producing quality lignin carbon fiber.

TOWARDS HIGHER QUALITY LIGNIN CARBON FIBER

Two recent works have shed light onto the path for quality lignin carbon fiber. In the first work, Sun et al. (2016) [7] have shown the potential of organosolv lignin as the precursor of quality lignin fiber. Organosolv lignin is derived from organic solvent-based extraction of biomass and is purer than most other types of lignin due to less polysaccharide content and modified condensed structures [7,8]. In fact, the most abundant industrial lignin is currently generated from the widely-used kraft pulping process, namely kraft lignin. Most types of lignin, including kraft lignin, need to be purified and further fractionated to improve their uniformity before manufacturing carbon fiber toward high quality.

Recently, Li et al. (2017) [9] have shown that biochemical fractionation using an enzyme-mediator system can derive lignin fractions to produce carbon fiber with certain mechan-



1. Lignin fractionation to enable multiple product streams for biomanufacturing.

ical performance similar to some commercial carbon fibers. The carbon fiber derived from fractionated lignin improved spinnability, fiber morphology, and crystallite structure, all of which might have led to the improved mechanical performance and quality. The underlying molecular mechanisms for improved spinnability and crystallite structure could be due to the more uniform molecular weights, interunitary linkages, and functional groups. The detailed mechanisms are yet to be revealed.

POTENTIAL OF A MULTI-STREAM INTEGRATED BIOREFINERY

Despite the need for further studies, the recent work unveiled the potential of a multi-stream integrated biorefinery for biomanufacturing enabled by lignin fractionation and utilization. As shown in **Fig. 1**, lignin fractionation could produce multiple lignin streams with different uniformity and chemical characteristics. The fractionated lignin streams could be used as starting materials for multiple biomanufacturing streams to make different final value-added products.

Basically, previous studies have demonstrated that low molecular weight lignin fraction is more suitable for bioconversion for lipid [10,11], bioplastics [12,13], and asphalt binder modifier [14], and high molecular weight lignin fraction could be better feedstock for carbon fiber, as demonstrated in the recent work [7,9]. The multiple lignin streams will inevitably enhance cost-effectiveness and sustainability for both the pulp and paper industry and lignocellulosic biorefineries. **TJ**

LITERATURE CITED

1. Ragauskas, A.J., Beckham, G.T., Biddy, M.J., et al., *Science* 344(6185): 709(2014).
2. Kadla, J.F. and Kubo, S., *Composites, Part A* 35(3): 395(2004).
3. Liu, H.C., Chien, A., and Newcomb, B.A., *ACS Sustainable Chem. Eng.* 3(9): 1943(2015).
4. Ago, M., Okajima, K., Jakes J.E., et al., *Biomacromolecules* 13(3): 918(2012).
5. Thunga, M., Chen, K., Grewell, D., et al., *Carbon* 68: 159(2014).
6. Ding, R., Wu, H., Thunga, M., et al., *Carbon* 100: 126(2016).
7. Sun, Q., Khunsupat, R., Akato, K., et al. *Green Chem.* 18(18): 5015(2016).
8. Sadeghifar, H., Wells, T., Khuu Le, R., et al., *ACS Sustainable Chem. Eng.* 5(1): 580(2017).
9. Li, Q., Xie, S., Serem, W.K., et al., *Green Chem.*, 2017, DOI: 10.1039/c6gc03555h.
10. Zhao, C., Xie, S., Pu, Y., et al., *Green Chem.* 18(5): 1306(2016).
11. Xie, S., Sun, Q., Pu, Y., et al., *ACS Sustainable Chem. Eng.* 5(3): 2215(2017).
12. Lin, L., Cheng, Y., Pu, Y., et al., *Green Chem.* 18(20): 5536(2016).
13. Shi, Y., Li, Q., Wang, X., et al., *Process Biochem.* 52: 238(2017).
14. Xie, S., Li, Q., Karki, P., et al. *ACS Sustainable Chem. Eng.*, 2017, DOI: 10.1021/acssuschemeng.6b03064.

ABOUT THE AUTHORS

Li is a postdoctoral researcher and Yuan is associate professor and director with the Synthetic and Systems Biology Innovation Hub, Department of Plant Pathology and Microbiology, and Institute for Plant Genomics and Biotechnology, Texas A&M University, College Station, TX, USA. Ragauskas is professor/Governor's Chair in Biorefining, Oak Ridge National Laboratory; Department of Chemical and Biomolecular Engineering; Department of Forestry, Wildlife, and Fisheries; and Center for Renewable Carbon; University of Tennessee, Knoxville, TN, USA.



Li



Yuan



Ragauskas

Melt-blown compostable polyester films with lignin

WOLFGANG G. GLASSER, ROBERT LOOS, BLAIR COX, AND NHIEM CAO

ABSTRACT: Compostable films for such uses as packaging and agricultural soil covering materials were first produced on commercial scale from blends of biodegradable polyesters and a modified kraft lignin. The lignin consisted of an industrial product isolated according to the LignoBoost process. The lignin modification involved homogeneous phase reaction with propylene oxide, and the films were melt-blown from a pelletized compound consisting of up to a 30% blend of lignin derivative with commercial biodegradable polyester. The 12–93 μm thick films combined the characteristics of lignin as modulus-building and environmentally degradable polymer with those of the strength-building thermoplastic polyester. Although the modified lignin paralleled the behavior of native lignin in wood by resisting rapid and full conversion to carbon dioxide in a simulated composting environment, two thirds of the film mass biodegraded within 12 weeks of composting, with the remainder turning into (humus-like) water-soluble solids and particles <2 mm in size. The lignin derivatives suffered from the release of trace amounts of malodorous volatiles containing reduced sulfur when subjected to melt-blowing. The objectionable odor was virtually unnoticeable in injection-molded solid parts.

Application: The use of kraft lignin as a contributing thermoplastic polymer component of melt-blown film and injection-molded products from sustainable resources with environmental compatibility helps the kraft pulping process advance toward a multi-purpose biorefining technology with increased income potential.

This report describes the first commercial application of industrially generated, chemically modified kraft lignin in melt-blown, environmentally degradable (compostable) polyester film products following hydroxypropylation.

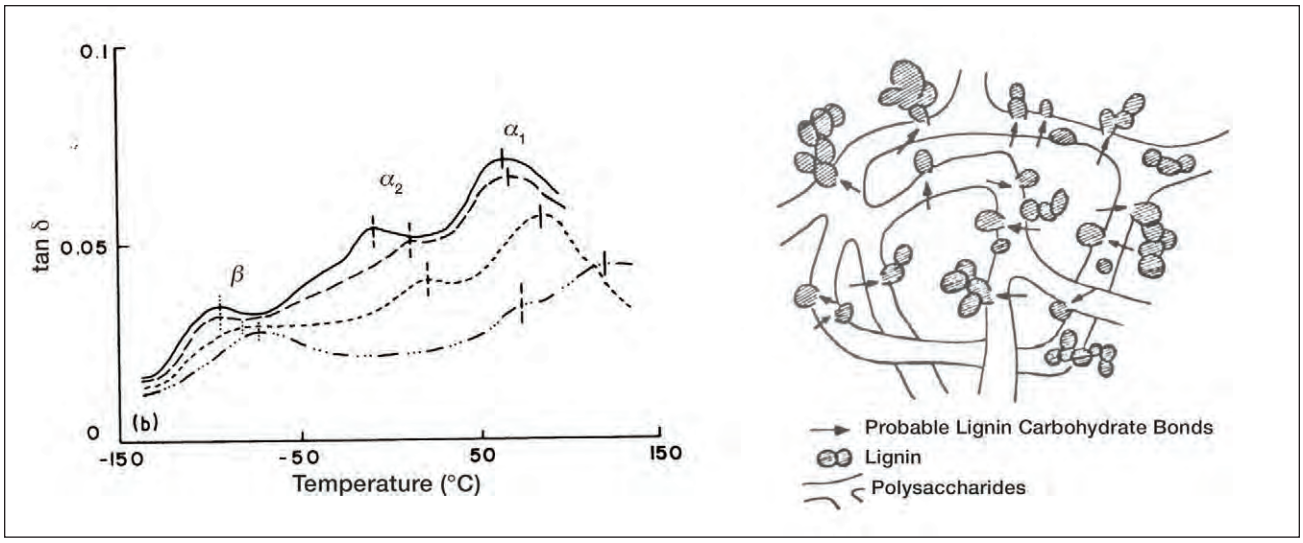
Lignin is the second most abundant natural (sustainable) polymer on earth. It is also the most abundant aromatic polymer in nature that serves land plants as matrix component in cellulose fiber-based composites; as modulus-raising copolymer with non-crystalline polysaccharides; and as natural defense against biological and atmospheric degradation [1,2]. Lignin is separated from the plant-biocomposite (mostly wood) in large quantities during papermaking. This resource, which is generated in amounts of approximately 0.5 ton per ton of pulp, is used primarily as in-house process fuel or as polymeric, water-soluble dispersant/surfactant (about 1,000,000 tons per year worldwide) [3]. Recent advances have improved the option of recovering lignin from the kraft pulping process, and this isolation method is beginning to be adopted on industrial scale [4]. Isolated kraft lignin is therefore considered a new resource for the development of sustainable and environmentally degradable polymeric materials on the scale of as much as 78 million tons per year worldwide [5]. In addition to kraft pulping, the emerging cellulosic biofuels industry is projected to potentially generate about 62 million tons of lignin by 2022 [5-8].

Lignin nature and sources

In its native state, lignin is insoluble (with the exception of minor fractions that are solvent-soluble, such as *Brauns* native lignin [1]), exhibiting typical network character. It is also thermally undeformable. Its insolubility has long been considered to be the result of its crosslinked network structure [1,2]. This has, however, been demonstrated to be mostly incorrect. In moist wood or other plant biocomposites, lignin does show a surprisingly low glass-to-rubber transition temperature (T_g), which signifies a loss in modulus in response to heating [9-11]. This T_g of lignin is in the same range as linear polystyrene.

Under dynamic mechanical thermal analysis (DMTA), an analytical method typically used in polymer science to identify phase structure and compatibility of multi-phase materials in composites and blends, the mechanical response of moisturized wood to heating revealed two distinct molecular phases [9]. This indicates that the amorphous matrix of the biocomposite consists of two molecular entities, each of sufficient independent size (sub-micron) to raise its own T_g, representing non-crystalline heteropolysaccharides (also called hemicelluloses) and lignin (**Fig. 1**, left) [9]. The T_g of wood, which is generally significantly below the T_g of isolated lignin, is somewhat species-dependent [10,11].

The absence of network character necessitates an alternate explanation for the insolubility and thermal non-deformability of the non-crystalline matrix of the biocomposite. In the last 40+ years, this behavior has been attributed to block (or graft) copolymer instead of network architecture [12,13]. Figure 1 (right) shows a simplified view of its structure [13]. As a result of the copolymer structure, the two-phase amorphous matrix displays network-like properties, insolubility and thermal non-deformability, which necessitate hydrolysis of ether



1. Dynamic mechanical thermogram of solid wood (left) illustrating the glass-to-rubber transitions of the biphasic amorphous matrix component of biocomposite wood at different moisture contents. α_1 and α_2 represent the thermal transitions of lignin and non-crystalline carbohydrates, respectively. (After Kelley et al. [9]). Model of block copolymer (right) illustrating the lignin-carbohydrate complex according to Košiková et al. [12].

bonds connecting lignin with carbohydrates for such matrix removal as needed for fiber liberation by pulping.

The lignin-carbohydrate complex has long been recognized as fragile (i.e., susceptible to hydrolytic cleavage) and renewable in the presence of moisture [14-19]. This behavior is considered the basis of the understanding of wood as an "intelligent composite material" [20-23]. The molecular basis of this reversibility (i.e., of hydrolytic depolymerization and repolymerization) revolves around the ease of forming reactive intermediates, quinone methides, that may recombine with carbohydrates and restore insolubility and non-deformability. This dynamic regeneration process of copolymer architecture is responsible for the need to apply lignin-degrading chemistry for obtaining bleached (lignin-free) pulp fibers, which has been corroborated by numerous studies over many years [14-19].

The isolation of the highly crystalline polysaccharide component (cellulose) from wood in fiber form, which requires the dissolution of the matrix (i.e., the delignification or pulping process) can be accomplished using aqueous solutions with pH levels ranging from very low (acid sulfite process) to very high (kraft process), or with organic solvents having solubility parameters resembling those of lignin (organosolv process). By these treatments, lignin becomes soluble (a) in aqueous medium in salt-form, sulfonate or phenolate (lignin sulfonate or kraft lignin), or (b) as organic solvent-soluble molecules with reduced (by hydrolysis) molecular weight (organosolv lignin). In addition to hydrolysis of the lignin-carbohydrate bonds, efficient delignification requires chemical action aimed at (a) raising the degree of modification with sulfonate groups through the use of aqueous solutions of sulfur dioxide or bisulfite salts (sulfite process), (b) effective hydrolytic cleavage (assisted by the addition of semi-catalytic sulfide salts) of alkyl-aryl ether bonds within lignin, causing a rise in phenolic hydroxyl group content (kraft process), or (c) mild hydrolytic separation of solvent-soluble lignin fragments with reduced molecular weight from the lignin-carbohydrate complex (organosolv process) [1,2]. Each process carries the risk for side reactions that typically result in an increase in the T_g of lignin [24,25].

The resulting solubilized lignins are distinct from each other while retaining their elevated molecular weight, their varied functional character, and their branched nature [11,24,25]. As sulfonated entities (i.e., lignin sulfonates), they remain water-soluble at any pH-level. As kraft lignins, they gradually lose their water solubility at pH levels below about 8-9. As organosolv lignins, they become insoluble when exposed to environments with adjusted solubility parameter (so-called non-solvents) and/or temperature. The separation of lignin from the native lignin-carbohydrate complex (i.e., the block copolymer) requires chemical action resulting in structural modifications of different types and degrees [24,25]. Unwanted side reactions involving necessary reactive intermediates, such as benzylic cations and quinone methides, may give rise to condensed structures with reduced solubility and reduced thermal deformability (i.e., raised T_g) while preserving their major varied functionality [24]. This change in structural character is more pronounced in sulfite and kraft lignins than in organosolv lignins. The latter, therefore, retain a high degree of solubility (in organic solvents) and a more moderate T_g.

Lignin sulfonates remain water-soluble polymers with high molecular weight. When isolated from associated inorganic salts and sugars by such processes as ultrafiltration, ion exchange, or spray drying, they are powerful surfactants and dispersants. These products have captured commercial markets in excess of 1 million tons per year worldwide [3].

Kraft lignins are rarely isolated in separated form and instead used mostly for fuel purposes after concentration by water evaporation. This process is designed to recover inorganic pulping chemicals (sodium hydroxide and sodium sulfide), plus steam for electric power. Much research effort has focused on the use of kraft lignins in polymeric materials, with or without chemical modification, such as water-soluble surfactants, adhesive additives (phenolic resins and other thermosets), and in components of thermoplastics, mostly after some type of chemical modification aimed at overcoming the recognized molecular intractability based on the absence of solubility and thermal deformability.

Organosolv lignins have been much sought-after polymers for materials applications [8,26]. Their potential contribution to desirable properties paralleling those of lignin in the native biocomposite has been widely demonstrated in the laboratory and on a semi-industrial scale. However, this type of lignin is constrained by cost and availability factors. There are presently no known commercial suppliers.

This introduction is to emphasize that, while all isolated lignins preserve most of the inherent polymer properties, such as modulus, multi-functionality, sustainability, and biological degradability, significant differences exist between isolated lignins that invite strategies for developing materials applications in which the native properties are used for the benefit of the final product [27-29].

Lignin modifications

For lignins to make an effective entry into commercial materials markets, specialized isolation methodologies or chemical modification approaches must become practical. Numerous studies have demonstrated that lignin can be readily converted into a soluble, reactive, and thermally deformable polymer by chemical modification. This topic has been the subject of several recent reviews [8,29-31]. Among the many modification methods explored, one of the simplest, most property-altering, and most cost-effective techniques involves a reaction with alkylene oxides, especially propylene oxide [27-50]. As a component of thermoplastic and thermosetting materials, lignin is capable of contributing its inherent properties as modulus-builder and slow-degrading organic matter that is considered pre-humus. These characteristics have attracted the attention of such industrial polymer users and producers as IBM, for printed circuit boards [26]. However, the limited availability of isolated, water-insoluble lignins from industrial operations has deterred potential users. This situation, and the quest for greater reliance on sustainable resources, is beginning to change.

The modification of lignin with propylene oxide (i.e., the formation of hydroxypropyl lignin [HPL] derivatives), which commenced in the early 1970s, transforms lignin into a thermoplastic (melt-deformable), (organic) solvent-soluble, functionally uniform aromatic polymer of (mostly) small size [32-50]. Its surprising T_g-lowering and solubility-raising effect that initially seemed to contradict the conventional understanding of lignin as a crosslinked polymer is consistent with the recent view of lignin as a compact aggregate of molecules assembled on the basis of non-covalent ϖ-ϖ interactions [51,52]. Just as esterification separates cellulose molecules sufficiently to create solubility by disturbing crystallinity (i.e., by creating distance between polysaccharide chains), hydroxypropylation of lignin seems to separate stacked aromatic structures sufficiently to render the modified product soluble in organic solvents and compatible with other macro-molecules [46-50]. Simple modification reactions capable of resolving non-covalent aromatic interactions, such as oxyalkylation, methylation [43], or esterification [30,31] are thus appropriate strategies for converting isolated lignins into important components of thermoplastic materials.

MATERIALS AND METHODS

Lignin and polyester sources

Isolated kraft lignin was obtained from the Domtar Paper Company in Plymouth, NC, USA, (www. domtar.com/en/pulp/lignin/10387.asp), which uses primarily southern pine as wood feedstock. The lignin composition was listed as 63%–66% carbon, 5.7%–6.2% hydrogen, 2%–2.5% sulfur, and <1.0% ash. The lignin was used as received for modification.

The BASF-supplied biodegradable polyester product, ecoflex F Blend C1200, is described as a statistical, aliphatic-aromatic copolyester based on the monomers 1,4-butanediol, adipic acid, and terephthalic acid (PBAT) in the polymer chain (www.basf.com) [53].

Modification and structure analysis

The oxyalkylation reaction was carried out as previously described [37] with modification to accommodate needs associated with the scale-up to the tonnage scale [44]. The resulting HPL product was filtered and washed, and used in dry powder form. It was analyzed by hydrogen-nuclear magnetic resonance (H-NMR) spectroscopy in dimethyl sulfoxide (DMSO) solution, as described previously [54].

Compounding and melt blowing

Melt processing was performed using pelletized blends composed of 0%–40% HPL in PBAT in a compounder with screw designed for filler dispersion, which allowed for superior mixing. The material was all fed at room temperature (zone 0). The temperature of the zones then varied from 110°C (zone 1) to 140°C for zones 3–10. Actual melt temperature was reached between 185°C–190°C at a screw speed of 200 rpm. A noticeable release of objectionable odor typical of kraft pulping was recognized. Film blowing was performed on a small pilot film blowing line using an 80 mm die, a die gap of 0.8 mm, and a blow-up ratio of 3.5:1. Films were made in 12 μm, 25 μm, and 30–93 μm thicknesses. All films contained varying portions of gel (non-melt) particles that apparently resulted from incompletely fluidized HPL. These impurities created instability of the 12 μm film at higher HPL content, which tended to collapse.

Mechanical property testing

Film testing was performed at least 1 week after melt-blowing for the 12 μm films, according to ISO 527-3:1996 "Determination of tensile properties – Part 3: Test conditions for films and sheets," at 23°C and 50% humidity using preconditioned strips with an effective measured length of 50 mm and a width of 10 mm. The results reported represent the median of five samples. The visual detection of some gel particles in the blown films indicated that the HPL sample used for the prototype films was incompletely homogenized, resulting in an apparent reduction in tensile strength.

Biobased/degradation/composting evaluation

The determination of biobased as opposed to fossil carbon composition by carbon dating was performed by Xceleron (Germantown, MD, USA). The results of percent-biobased have an uncertainty of +/- 3%, according to ASTM D6866 "Standard test method for determining the biobased content of solid, liquid, and gaseous samples using radiocarbon analysis." The quantitative bio-disintegration of 43 μm film samples was evaluated by Organic Waste Systems (OWS; Gent, Belgium), in a pilot-scale aerobic composting test, according to ISO 16929 (2013) "Determination of the degree of disintegration of plastic materials under defined composting conditions in a pilot-scale test." In brief, a sample of blended polymer composed of about 25% modified lignin, 15% calcium carbonate, and 60% PBAT was processed on a laboratory blown film line to produce a 43 μm film. This film was cut into 10 cm × 10 cm pieces and added in 1% concentration to bins of pure biowaste. Conditions remained at optimum levels of >60°C and <75°C for 1 week before the temperature dropped to >40°C for the consecutive 5 weeks. Tests were performed in duplicate and lasted for 12 weeks. Disintegration results were determined by sieving, in accordance with ASTM D 6400-12 "Standard specification for compostable plastics" and ISO 17088 (2012) "Specifications for compostable plastics."

Film degradation by exposure to ultraviolet (UV) light radiation was conducted by BASF using an accelerated test protocol for 10 days.

Headspace analysis for volatiles

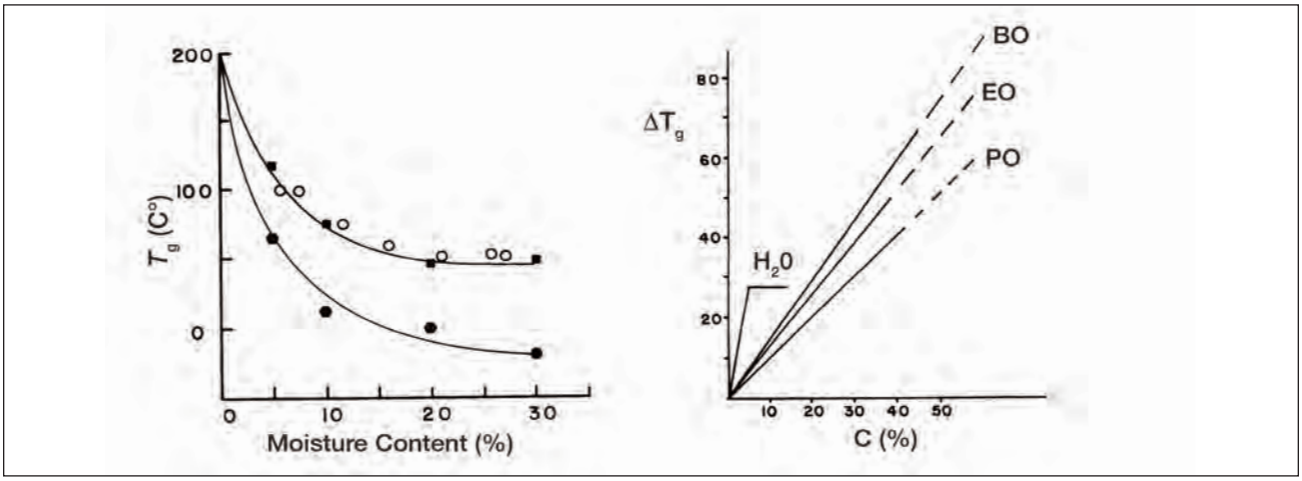
Headspace analysis was performed by the University of Dayton Research Institute (UDRI; Dayton, OH, USA) using the system for thermal diagnostic studies (STDS). This analysis is based on a temperature-programmable test section connected to an inline gas chromatography-mass spectrometer (GC-MS). An added sorbent trap was swept with about 10 mL/min of dry helium heated to 250°C at 20°C/min and held at 250°C for 10 min. Desorption of the trap produced a gas stream that was guided through the GC-MS. The resulting total ion chromatogram was analyzed using the National Institute of Standards and Technology (NIST) mass spectral library.

RESULTS AND DISCUSSION

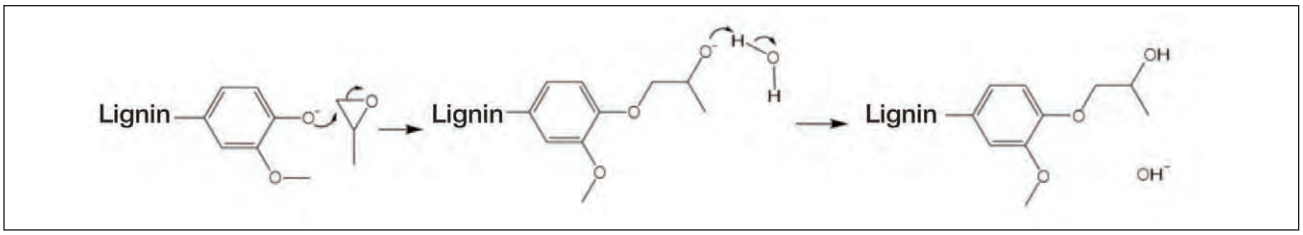
Lignin modification

In dry state, all isolated lignins have high glass transition temperatures, often at or near the thermal degradation temperature of the polymer. However, thanks to their multi-functionality, lignins respond to plasticization (**Fig. 2**). Water (Fig. 2, left), which serves as such an effective plasticizer for non-crystalline polysaccharides (hemicelluloses), also has a great effect on lignin's T_g, but its effect is limited to only the first 5–10 (wt.) % moisture (platicizer) content. The alternate option to T_g-reduction is chemical modification, which amounts to internal plasticization (Fig. 2, right).

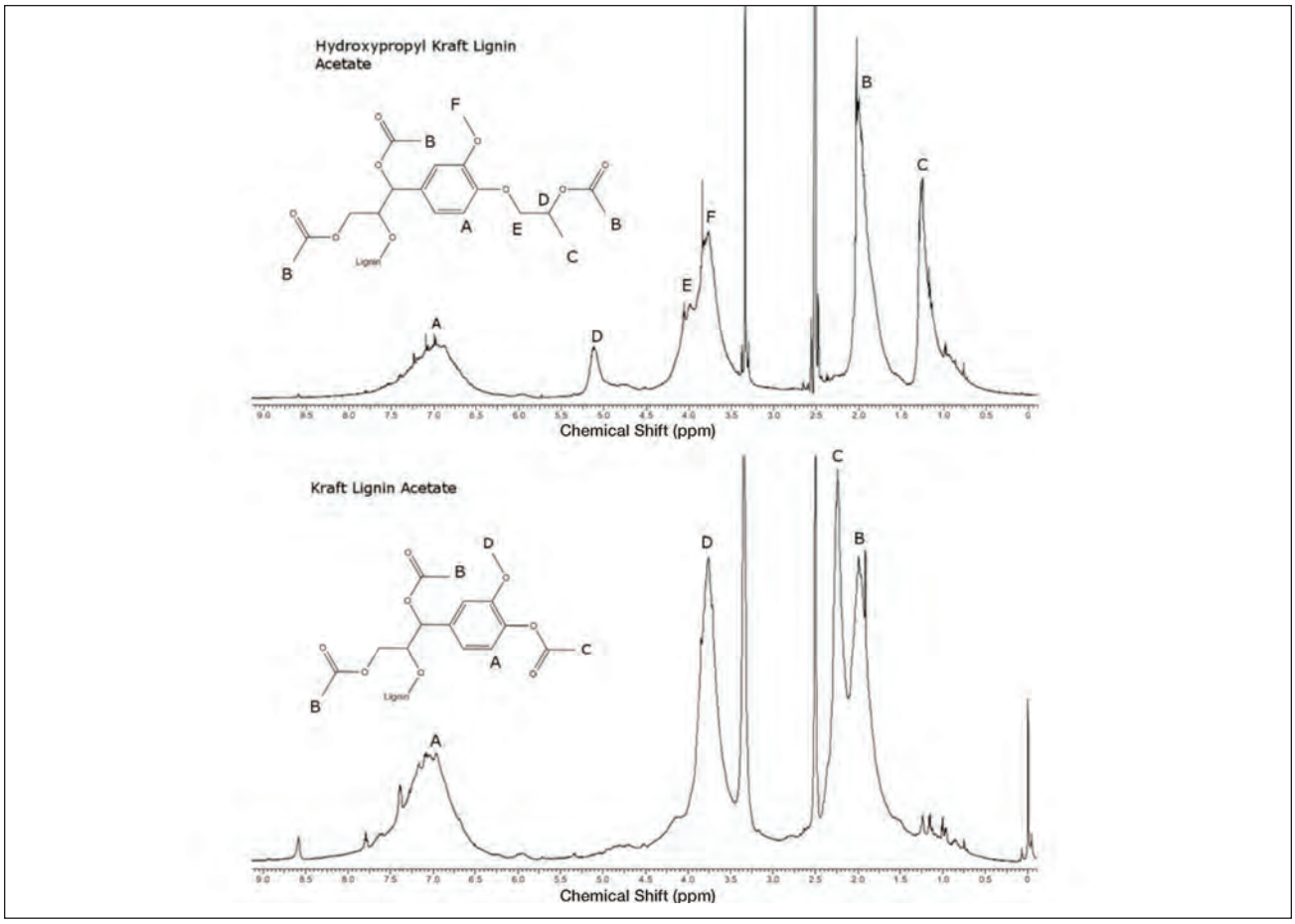
One of the most effective methods of altering the properties of lignin in terms of solubility and thermal properties involves reaction with alkylene oxides (**Fig. 3**) [32-37]. This reaction, which was first used in the early 1970s to synthesize lignin-based polyols for polyurethane foams [32-34], has evolved over several decades into a convenient technique for incorporating water-insoluble (non-sulfonated) lignins into



2. The plasticization effect of water (left) and hydroxyalkyl ether substituent content (C) (right) on the glass transition temperature of lignin (afterLora and Glasser [8]). ΔT_g represents T_g –change in relation to control (i.e., unmodified lignin) according to the equation by Fujita-Nishimoto [8].



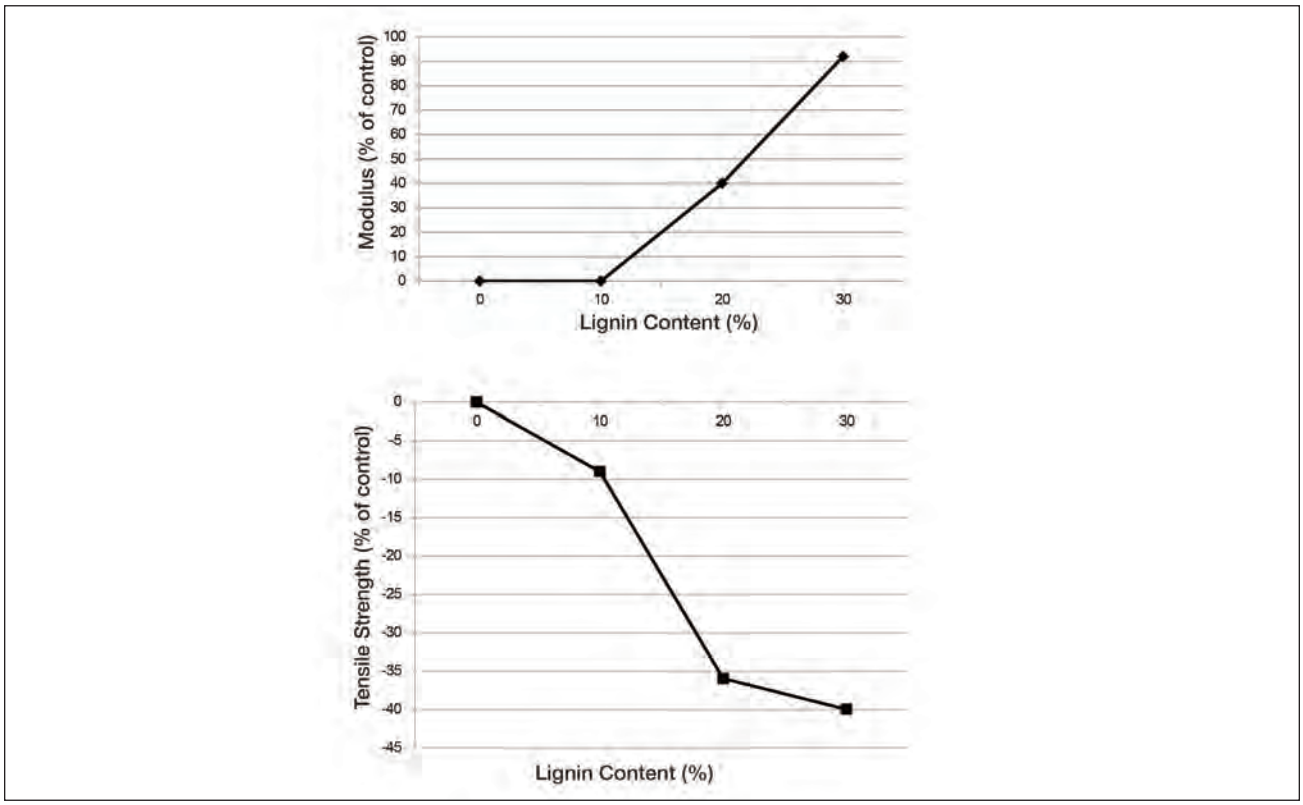
3. Schematic reaction of phenolic model substance representing lignin with alkylene oxide.



4. Hydrogen-nuclear magnetic resonance (H-NMR) spectra of acetylated kraft lignin before (A) and after (B) reaction with propylene oxide, showing the disappearance of the aro-OAc peak at 2.2 ppm and the formation of a larger ali-OAc peak and the CH_3-peak of propylene oxide (PO) at 1.2 ppm as a consequence of propoxylation.

polymeric materials with significant phase compatibility vis-à-vis a range of manufactured thermoplastic and thermosetting polymers [8].

Several factors, including reactivity, boiling point, and ease of handling, have contributed to a preference for propylene oxide (PO) as the modifying agent, although other epoxides were tested as well [31-33,54]. This chemistry has been the subject of considerable optimization throughout the research and development effort and the scale-up process [44]. Currently, the hydroxypropyl kraft lignin is manufactured economically in a batch process that produces multiple tons per batch. The resulting lignin derivatives proved to have glass transition temperatures that are 1.0°C–2.5°C/ % weight gain lower than the starting material. They were virtually monofunctional and soluble in and compatible with a range of solvents and polymers of common use, and their polydispersity was reduced over the starting material [37,54]. The complete removal of all phenolic functionality results in a derivative with a degree of substitution with PO of about 0.2 to 0.7 per phenylpropane lignin-repeat unit, depending on initial phenolic hydroxide content and reaction conditions. H-NMR spectroscopy reveals a transformation of the phenolic hydroxyl groups (approximately 45% of total hydroxide groups in kraft lignin [24,25]) into aliphatic hydroxide and methyl groups (**Fig. 4**). Variability in degree of modification may result from a range of reaction parameters, especially pH, temperature,



5. Mechanical properties of 12-14 µm films in relation to lignin content.

time, and concentration, as well as product character, especially syringyl (S) and guaiacyl (G) ratio and functionality of the lignin source. This modification and analysis has developed into a state-of-art that is practiced in many laboratories and institutions world-wide. The resulting effects on solubility and thermoplasticity are well-documented.

Compounding and melt-processing

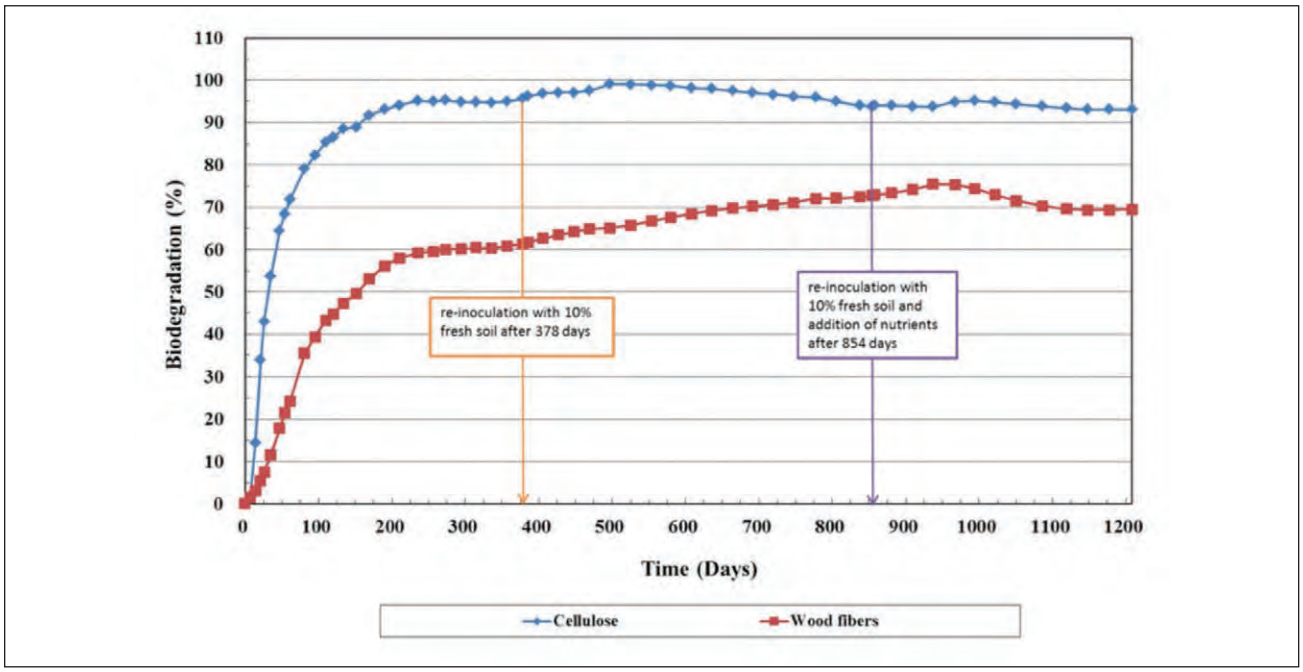
HPL in powder form was compounded in a 40 mm twin-screw extruder with the aliphatic-aromatic biodegradable polyester (PBAT) into pellets containing of 10%, 20%, and 30% HPL. The pellets were subsequently melt-blown into films of 12–14 μm (and greater) thickness. All melt-processing operations functioned without difficulties, except that the bubble became too unstable at the highest HPL concentration of 30% to allow for stable blowing operations. This was unique to the 12–14 μm films. At greater film thickness (60–90 μm), greater lignin contents were tolerated. Pellets with HPL contents as high as 50% were successfully melt-processed by injection molding without difficulties. Visually, the films provided no signs of separated phases; all (thin) films appeared transparent and with undiminished elongation at break-values. None of the films exhibited the embrittlement typical of blends with unmodified lignins.

Mechanical properties

The resulting films had the expected properties of increased modulus (and slightly enhanced elongation at break) and reduced tensile strength (**Fig. 5**) with HPL content. The degree to which modulus responded to HPL content proved to be somewhat dependent on degree of substitution of the lignin with propylene oxide. Desired properties were subject to film thickness and HPL content. Overall, the 12–14 μm films with HPL contents of up to 20% exhibited adequate performances during processing (compounding and melt-blowing) and mechanical testing. All required performance standards were met, especially if the lignin content remained below approximately 25%–30%.

Biodegradation

The analysis of biodegradation was performed in a simulated industrial composting test according to ISO 16929 (2013). The resulting data showed that under composting conditions, lignin and modified lignin (HPL) are essentially the same with regard to carbon dioxide (CO_2) production. The two degradation experiments were performed under very similar conditions. The results are consistent with wood biodegradation tests (provided by OWS, the contract laboratory), which revealed that wood with a 30% lignin content degraded quickly and reached a CO_2 production level of 70%–75% under conditions under which standard cellulose converts to CO_2 levels of 90%–100% (**Fig. 6**). These results indicate that, even given 1200 days of composting, the lignin content of the wood does not decompose into significant amounts of CO_2. Lignin in compost is degraded, but not primarily into CO_2. This is consistent with experiments with radio-labeled lignin [55] that



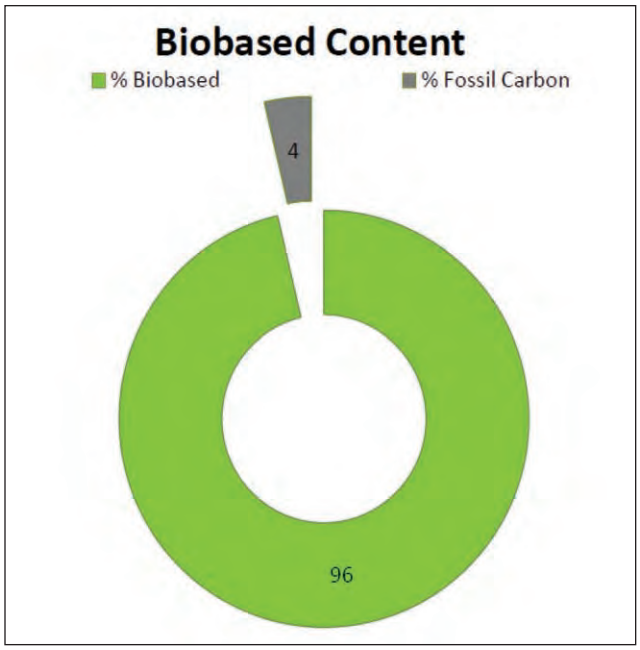
6. Biodegradation results of cellulose and lignin under simulated composting conditions.



7. Illustration of the results of simulated composting tests with 93 µm-thick films. H3070E refers to sample designation by the contractor (Organic Waste Systems).

have shown that much of lignin is converted into carbon-14 labeled water-soluble fragments instead of CO_2. Tuomela et al. [56,57] observed that lignin inhibits the degradation of carbohydrates and generates water-soluble degradation products that are mineralized or bound to humic substances and incorporated into humin or other insolubles.

In separate experiments, HPL in inoculated slurry designed to simulate a composting environment also produced a significant portion of dissolved aqueous lignin solids. After 33 days in an aqueous slurry at 60°C (at an initial pH of 7.5), along with cellulose and a commercial soil inoculant, 15.8% of the HPL sample had degraded into soluble lignin fragments, indicating that the modified lignin behaves comparably to unmodified lignin in a compost environment. The disintegration of the 10 cm × 10 cm film pieces into smaller particles proceeded well. After 10 weeks of composting the average size of the remaining pieces was approximately 1 cm × 2 cm. After 12 weeks the whole content of the bins, in which the simulated soil test was carried out, was used for sieving, sorting, further isolation and analyses, and a disintegration percentage was calculated. Disintegration is defined as a size reduction to <2 mm. Only some rather small pieces of film could be retrieved in the different fractions (**Fig. 7**). The major parts of these pieces were dark brown and fragile. By far the major part of the test material had disappeared. An average disintegration percentage of 94.0% was determined. This is well above the 90% pass level required by the ASTM D6400-12, EN 13432 (2000) "Requirements for packaging recoverable through composting and biodegradation-test scheme and evaluation criteria for the final acceptance of packaging," and ISO 17088 (2012) standards for compostable plastics. Figure 7 gives a visual comparison of the <10 mm



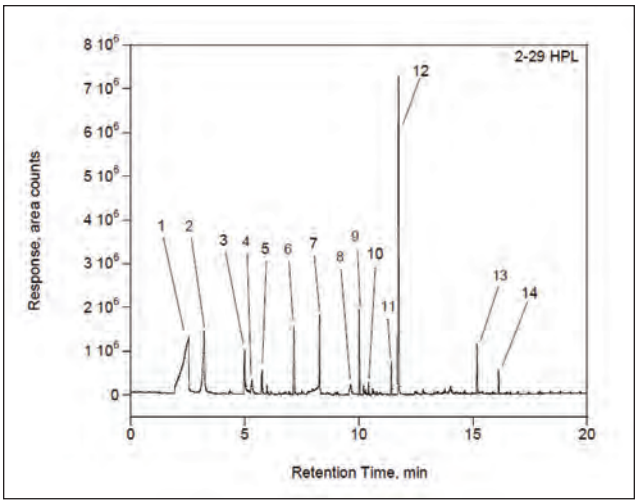
8. Determination of biobased and fossil carbon in hydroxypropyl lignin. Test conducted in accordance with test standard ASTM D6866-12 that has an uncertainty of +/- 3%.



9. Hydroxypropyl lignin-containing polyester film (12–14 µm) following photo-irradiation in test chamber illustrating the photo-bleaching effect in the exposed film area. The fringe area remained shaded by clamping.

fraction of film subjected to test compost after 12 weeks. As a consequence of these results, the 30% HPL/polyester blend films have already been successfully certified in the United States as compostable materials according to ASTM D 6400-12.

The designation of compostable material hinges on both (or either) conversion to CO_2 (within time limits) and natural polymer source. Neither lignin nor HPL (nor wood, for that matter) fully meet those criteria. However, experiments involving radiocarbon analysis produced results distinguishing bio-based from fossil-based carbon in materials. The results shown in **Fig. 8**, which were obtained according to test standard ASTM D6866-12, reveal a bio-based carbon content



10. Headspace analysis results of lignin film by system for thermal diagnostic studies and gas chromatography-mass spectrometry. Partial peak identification is given in Table I. (Peak no. 12 represents a contaminant from the vacuum oven used for gas collection and was not a product of hydroxypropyl lignin off-gassing.)

Peak No.	Assignment	Relative Area, %
2	Dimethyl sulfide	11.4
5	Propylene sulfide	1.7
6	Dimethyl disulfide	4.4
8	Dimethyl trisulfide	2.0
12	Tributylamine	23.1

I. Sulfur-containing volatiles identified in headspace films.

of >95% for the HPL produced by cycleWood Solutions, Inc., and used in the tests described in this report. The missing designation as natural polymer prevents the film blends from being so-far recognized as compostable in Europe (according to EN 13432).

Photo-degradation

The initial evaluation of exposure of a prototype film (with 20% HPL content) to UV radiation was carried out in a test chamber simulating intense irradiation for 10 days. The film sample initially (within the first 7 days) responded well by displaying similar elongation at break compared with the pure polyester control sample, but the films showed distinct signs of photo-degradation by becoming totally colorless and transparent (**Fig. 9**) and severely brittle. It was obvious that the lignin component protected the polyester from being degraded until it lost its protective capacity by being degraded itself. This behavior parallels lignin's function in the process of wood weathering [58,59], in which it serves as a guardian of the highly degradable (non-crystalline carbohydrate) portions of the biocomposite until the lignin itself has been converted



11. Illustration of several prototype and (semi-) commercial products made from lignin-containing melt-blown and injection molded polymer blends.

to volatile (vanillin) and water-soluble degradation products, and its protective capacity has been exhausted.

Analysis of volatiles

Native lignin is an odorless polymer that protects the wood composite in many ways. Among them is a thermally induced charring at high temperature that involves some volatilization [60]. When lignin is removed from pulp fibers during kraft pulping, it is modified with reduced sulfur that results in a low level (<2.5% sulfur) of mercaptan (thiol) formation [2] at the benzylic carbon position. Exposure of kraft lignin and its derivatives to temperatures typically used in some melt-processing operations might therefore result in the release of malodorous volatiles. This was apparent with the melt-blown film samples, but much less so with more solid products generated by injection-molding at HPL contents as high as 50%. An analysis of the headspace of film samples stored in a closed container for an extended period for sulfur-containing volatiles produced the results summarized in **Fig. 10** and **Table I**. The analysis identified the usual compounds known to be associated with kraft pulping, plus a minor ingredient, propylene sulfide (#5 in Table I), that might originate from the release of propoxylated thiol groups.

CONCLUSIONS

The use of commercially available kraft lignin in melt-processed thermoplastics was demonstrated successfully on industrial scale following a well-known chemical modification procedure with propylene oxide (**Fig. 11**).

In melt-blown film products, lignin contributed to moderate increases in modulus while providing compostability and a definite (but exhaustible) protection against photo-degradation.

Like native lignin, the modified lignin failed to degrade substantially to CO_2 in favor of the formation of water-soluble degradation products and solids usually found in humus.

Processing and material characteristics represent the first promising demonstration of the production (on commercial scale, in multiple tons) of compostable thermoplastics with (modified) lignin.

The source of lignin as byproduct of kraft pulping, the only source currently available in tonnage quantities, represents the limitation to wider commercial success because of the release of trace amounts of objectionable volatiles with reduced sulfur functionality when melt-blown. This release of volatiles is less noticeable during injection molding, and it is virtually unnoticeable in injection-molded solid parts, even at lignin contents as high as 50%.

The technology developed and tested on industrial scale is ready for adoption by biorefineries that convert plant biomass into glucose and other cellulosic products using a sulfur-free fractionation process [60]. **TJ**

LITERATURE CITED

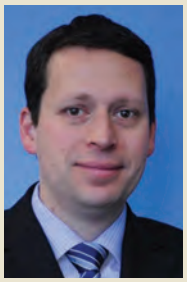
1. Sarkanen, K.V. and Ludwig, C.H., *Lignins – Occurrence, Formation, Structure and Reactions*, Wiley-Interscience, New York, 1971, p. 916.
2. Glasser, W.G. and Kelley, S.S., in *Encyclopedia of Polymer Science and Engineering*, Vol. 8, Wiley-Interscience, New York, 1980, pp. 39-111.
3. Gargulak, J.D. and Lebo, S.E., *ACS Symp. Ser.* 742: 304(2000).
4. Tomani, P., *Cellul. Chem. Technol.* 44(1-3): 53(2010).
5. Lake, M., "What are we going to do with all this lignin?" *Frontiers in Biorefining Conf.*, Center for Renewable Carbon, University of Tennessee, Knoxville, TN, USA, October 2014. Available [Online] http://www.frontiersinbiorefining.org/2014/Documents/Session_4B/What%20To%20Do%20With%20All%20This%20Lignin_MichaelLake.pdf <27March2017>.
6. Doherty, W.O.S., Mousavioun, P., and Fellows, C.M., *Ind. Crops Prod.* 33(2): 259(2011).
7. Ragauskas, A.J., Beckham, G.T., Biddy, M.J., et al., *Science* 344(6185): 1246843(2014).
8. Lora, J.H. and Glasser, W.G., *J. Polym. Environ.* 10(1/2): 39(2002).
9. Kelley, S.S., Rials, T.G., and Glasser, W.G., *J. Mater. Sci.* 22(2): 617(1987).
10. Olsson, A.-M. and Salmén, L., *ACS Symp. Ser.* 489: 133(1992).
11. Glasser, W.G., *ACS Symp. Ser.* 742: 216(2000).
12. Košiková, B., Zákutná, L., and Joniak, D., *Holzforschung* 32(1): 15(1978).

13. Koshijima, T. and Watanabe, T., *Association between Lignin and Carbohydrates in Wood and Other Plant Tissue*, Springer-Verlag, Berlin, 2003.
14. Ohara, S., Hosoya, S., and Nakano, J., *Mokuzai Gakkaishi* 26(6): 408(1980).
15. Leary, G., Miller, I.J., Thomas, W., et al., *J. Chem. Soc. Perkin Trans.* 2(13): 1737(1977).
16. Hemmingson, J.A., Leary, G., Miller, I.J., et al., *J. Chem. Soc., Chem. Commun.* 3: 92(1978).
17. Glasser, W.G., *Sven. Papperstidn.* (84)6: R25(1981).
18. Iversen, T. and Waennstroem, S., *Holzforschung* 40(1): 19(1986).
19. Giummarella, N. and Lawoko, M., *ACS Sustainable Chem. Eng.* 4(10): 5319(2016).
20. Baer, E., Cassidy, J.J., and Hiltner, A., *ACS Symp. Ser.* 489: 2(1992).
21. Altgen, M. and Militz, H., *Holzforschung* 70(10): 971(2016).
22. Fratzl, P., Burgert, I., and Gupta, H.S., *Phys. Chem. Chem. Phys.* 6(24): 5575(2004).
23. Fratzl, P. and Weikamer, R., *Prog. Mater. Sci.* 52(8): 1263(2007).
24. Glasser, W.G., Barnett, C.A., Muller, P.C., et al., *J. Agric. Food Chem.* 31(5): 921(1983).
25. Glasser, W.G., Barnett, C.A., and Sano, Y., *Appl. Polym. Symp.* 37: 441(1983).
26. Kosbar, L.L., Gelorme, J.D., Japp, R.M., et al., *J. Ind. Ecol.* 4(3): 93(2001).
27. Glasser, W.G., in *The Polymeric Materials Encyclopedia* (J.C. Salamone, Ed.), CRC Press, Boca Raton, FL, USA, 1996, pp. 3623-3631.
28. Stewart, D., *Ind. Crops Prod.* 27(2): 202(2008).
29. Wang, C., Kelley, S.S., and Venditti, R.A., *ChemSusChem* 9(8): 770(2016).
30. Thielemans, W. and Wool, R.P., *Biomacromolecules* 6(4): 1895(2005).
31. Dehne, L., Vila, C., Saake, B., et al., *J. Appl. Polym. Sci.* (2016), DOI:10.1002/aap.44582.
32. Hsu, O.H.-H. and Glasser, W.G., *Wood Sci.* 9(2): 97(1976).
33. Glasser, W.G., Hsu, O.H.-H., Reed, D.L., et al., *ACS Symp. Ser.* 172: 311(1981).

ABOUT THE AUTHORS



Glasser



Loos



Cox



Cao

Lignin is Earth's most underutilized sustainable organic resource. It is separated from plant biomaterials in delignification processes leading, among others, to pulp and paper and cellulosic ethanol products. Its isolation as aromatic (brown) polymer of high purity has become technically and economically feasible worldwide. When repurposed on the molecular level in such plastic commodity products as packaging films, it retains its native properties of high modulus (stiffness builder), bio-degradability, and photo-degradability. This has been demonstrated in a series of commercial products described in this paper.

The first author (Wolfgang Glasser) has worked for 40+ years on the use of lignin in structural materials, mostly thermosetting and thermoplastic polymers of all types. One focus of this work was the understanding of (a) lignin's glass-to-rubber transition at target temperature levels by chemical modification, and (b) its flow, solubility, and compatibility properties in association with other macromolecules, natural and synthetic.

The major obstacle to lignin use in structural materials has been its notorious intractability. This required (a) the development of an in-depth understanding of the structure-property-performance relationship that makes melt-blowing and blend compatibility possible, and (b) finding a modification method that is sufficiently simple and affordable to be used on tonnage scale.

One of the interesting challenges of this study was the process of transferring research explored (and demonstrated) on laboratory bench-scale to industrial scale within a short time.

Pulp and paper mills that are often limited by chemical recovery capacity can profitably extend this capacity by the recovery of isolated lignin (or its modified derivatives), which are useful in sustainable and biodegradable components of polymeric materials.

The next step in this research is to incorporate the process of isolation/modification into existing mill operations on-site, and to extend product use to other polymeric materials, thermosets (such as phenolics, epoxies and polyurethanes), and thermoplastics (other than biodegradable polyesters, such as polyolefins and PVC).

Glasser is professor emeritus, Department of Sustainable Biomaterials, Virginia Polytechnic Institute and State University, Blacksburg, VA, USA. Loos is senior scientist, Biopolymers, at BASF SE, Ludwigshafen, Germany. Cox is rocket scientist, Orbital ATK, Dulles, VA, USA. Cao is CEO, CycleWood Solutions, Fayetteville, AK, USA. Email Glasser at wglasser@vt.edu.

34. Glasser, W.G., Wu, L.C.-F., and Selin, J.-F., in *Wood and Agricultural Residues: Research on Use for Feed, Fuels, and Chemicals* (E.J. Soltes, Ed.), Academic Press, New York, 1983, pp. 149-166.
35. Wu, L.C.-F. and Glasser, W.G., *J. Appl. Polym. Sci.* 29(4): 1111(1984).
36. Kelley, S.S., Glasser, W.G., and Ward, T.C., *ACS Symp. Ser.* 397: 402(1989).
37. Jain, R.K. and Glasser, W.G., *Holzforschung* 47(4): 325(1993).
38. Chen, P., Zhang, L., Peng, S., et al., *J. Appl. Polym. Sci.* 101(1): 334(2006).
39. Gandini, A. and Belgacem, M.N., in *Monomers, Polymers and Composites from Renewable Resources*, Elsevier Science, Kidlington, UK, 2008, pp. 273-288.
40. Cateto, C.A., Barreiro, M.F., Rodrigues, A.E., et al., *Ind. Eng. Chem. Res*. 48(5): 2583(2009).
41. Ahvazi, B., Wojciechowicz, O., Ton-That, T.-M., et al., *J. Agric. Food Chem.* 59(19): 10505(2011).
42. Xue, B.-L., Wen, J.-L., Xu, F., et al., *J. Appl. Polym. Sci.* 129(1): 434(2013).
43. Cui, C., Sadeghifar, H., Sen, S., et al., *BioResources* 8(1): 864(2013).
44. Cao, N., Oden, K., Glasser, W. G., U.S. pat. 9,000,075 (2013).
45. Kuehnel, I., Podschun, J., Saake, B., et al., *Holzforschung* 69(5): 531(2015).
46. Kelley, S.S., Glasser, W.G., and Ward. T.C., *J. Wood Chem. Technol.*, 8(3): 341(1988).
47. Saraf, V.P., Glasser, W.G., Wilkes, G.L., et al., *J. Appl. Polym. Sci.* 30(5): 2207(1985).
48. De Oliveira, W. and Glasser, W.G., *J. Appl. Polym. Sci.*, 37(11): 3119(1989).
49. Chen, P., Zhang, L., Peng, S., et al., *J. Appl. Polym. Sci*. 101(1): 334(2006).
50. Wei, M., Fan, L., Huang, J., et al., *Macromol. Mater. Eng.* 291(5): 524(2006).
51. Chen, Y.-R. and Sarkanen, S., *Phytochemistry* 71: 453(2010).
52. Falkehag, S.I., *Appl. Polym. Symp.* 28: 247(1975).
53. Siegenthaler, K.O., Künkel, A., Skupin, G., et al., in *Synthetic Biodegradable Polymers: Advances in Polymer Science* (B. Rieger, A. Künkel, G.W. Coates, et al., Eds.), Springer-Verlag, Berlin, 2011, pp. 91.
54. Glasser, W.G., Barnett, C.A., Rials, T.G., et al., *J. Appl. Polym. Sci.* 29(5): 1815(1984).
55. Tuomela, M., Hatakka, A., Raiskila, S., et al., *Appl. Microbiol. Biotechnol*. 55(4): 492(2001).
56. Tuomela, M., Vikman, M., Hatakka, A., et al., *Bioresour. Technol.* 72(2): 169(1999).
57. Kluczek-Turpeinen, B., Tuomela, M., Hatakka, A., et al., *Appl. Microbiol. Biotechnol*. 61(4): 374(2003).
58. Hon, D.N.-S., in *Wood and Cellulosic Chemistry* (D.N.-S. Hon and N. Shiraishi, Eds.), Marcel Dekker, New York, 2001, pp. 513-546.
59. Evans, P.L., *Wood Mater. Sci. Eng.* 4(1-2): 2(2009).
60. Overend, R.P., Milne, T.A., and Mudge, L.K., Eds., *Fundamentals of Thermochemical Biomass Conversion*, Elsevier Applied Science Publishers, New York, 1985, pp. 1159.

Accelerated aging of bio-oil from lignin conversion in subcritical water

HUYEN NGUYEN LYCKESKOG, CECILIA MATTSSON, LARS OLAUSSON, SVEN-INGVAR ANDERSSON, LENNART VAMLING, AND HANS THELIANDER

ABSTRACT: Accelerated aging of bio-oil derived from lignin was investigated at different aging temperatures (50°C and 80°C) and times (1 hour, 1 day, 1 week, and 1 month). The bio-oil used was produced by the hydrothermal liquefaction of kraft lignin, using phenol as the capping agent, and base (potassium carbonate and potassium hydroxide) and zirconium dioxide as the catalytic system in subcritical water. Elemental composition, molecular weight (by using gel permeation chromatography), and chemical composition (by using gas chromatography–mass spectrometry and 2D nuclear magnetic resonance [18.8 T, DMSO-d_6]) of the bio-oil were measured to gain better understanding of the changes that occurred after being subjected to an accelerated aging process. The lignin-derived hydrothermal liquefaction bio-oil was quite stable compared with biomass-pyrolysis bio-oil. The yield of the low molecular weight fraction (light oil) decreased from 64.1% to 58.1% and that of tetrahydrofuran insoluble fraction increased from 16.5% to 22.2% after aging at 80°C for 1 month. Phenol and phenolic dimers (Ar–CH_2–Ar) had high reactivity compared with other aromatic substituents (i.e., methoxyl and aldehyde groups); these may participate in the polymerization/condensation reactions in the hydrothermal liquefaction bio-oil during accelerated aging. Moreover, the 2D heteronuclear single quantum coherence nuclear magnetic resonance spectra of the high molecular weight fraction (heavy oil) in the aged raw oil in the aromatic region showed that the structure of this fraction was a combination of phenol-alkyl patterns, and the guaiacol cross-peaks of Ar_2, Ar_5, and Ar_6 after aging indicate that a new polymer was formed during the aging process.

Application: Pulp mill personnel can use this information when considering technology to extract lignin from black liquor and process it further into bio-oil.

Discovering viable alternatives to fossil fuels is imperative because of their shortage and environmental impact. It is, therefore, not surprising that a number of different thermal conversion processes, such as gasification, pyrolysis, and liquefaction [1], have been suggested for the production of bio-oil from various types of biomass. In the investigations of these conversion processes, it has been concluded that these bio-oils are promising supplements or alternatives to fossil fuels [2]. However, because of the varied methods and raw materials used, there are differences in composition and properties of the bio-oils produced.

In many applications, bio-oil requires storage for a long period at an elevated temperature; therefore, it is important that it be able to retain its original properties under these conditions. A number of studies can be found pertaining to the storage properties of various bio-oils in the literature [2-16]. It can be concluded that the properties of the majority of the bio-oils studied change considerably. The viscosity, molecular weight (mol. wt.), water, and insoluble fraction contents of biomass-pyrolysis bio-oil often increase significantly during aging. The changes in the physicochemical and chemical properties of this type of bio-oil were a function of aging temperature and time [5-8]. The increase in water content and mol. wt. after accelerated aging was mainly due to polymerization/condensation reactions leading to the formation of large molecules [9-12]. Joseph et al. [2] reported there was a major decrease in the ether soluble fraction and a substantial increase in both the low and high mol. wt. fractions during aging. Regarding changes in the chemical structure, Ben and Ragauskas [4] revealed that an increase in alkyl groups and a decrease in aromatic and methoxyl groups in the structure of biomass-pyrolysis bio-oil after aging was caused by the condensation reactions initiated by instable organic peroxides via a radical mechanism. Structural information of bio-oil can be characterized using Fourier transform infrared spectroscopy (FTIR), gas chromatography–mass spectrometry (GC–MS), and nuclear magnetic resonance (NMR) [4]. They also showed that, by using ^{1}H–^{13}C heteronuclear single quantum coherence (HSQC) NMR analysis, deeper insight into the chemical structures of bio-oil with very high mol. wt. could be obtained as well as better understanding of the aging mechanism of bio-oil.

One promising bio-oil is obtained from the liquefaction of lignin using subcritical water [14-18], in which the catalytic system is a combination of base (potassium carbonate [K_2CO_3] and potassium hydroxide [KOH]) and solid zirconium oxide

(ZrO_2), with phenol used as a capping agent. For this system, the yield of bio-oil and char were 69%–87% and 16%–22%, respectively. Furthermore, this bio-oil has the characteristics of low oxygen (15%–21%) and water (11%–19%) contents, making the oil advantageous for fuel application. Nguyen Lyckeskog et al. [14] investigated the storage stability (room temperature, 2 years) of this type of bio-oil (lignin-derived hydrothermal liquefaction [HTL] bio-oil) and reported some promising results. This type of bio-oil was found to be relatively stable: its low mol. wt. fraction (light oil) was found to be very stable. It was also suggested that the removal of the tetrahydrofuran (THF) insoluble fraction could be beneficial in enhancing the stability of the HTL bio-oil. However, to the best of the authors' knowledge, few studies have been published on lignin-derived HTL bio-oil in a scientific journal. Therefore, it is important that the stability of lignin-derived bio-oil is evaluated, using elevated temperature to accelerate the aging process, so that the mechanisms of aging and ways of improving the quality of the oil can be identified.

The current work investigated the effects of temperature (50°C and 80°C) and time (up to 1 month) during the accelerated aging of lignin-derived HTL bio-oil. The properties of the HTL bio-oil were measured (i.e., water content, elemental composition, mol. wt. distribution, volatiles, and functional compositions) before and after aging. GC–MS and high-resolution ^1H–^{13}C HSQC NMR (800 MHz, dimethyl sulfoxide-d_6 [DMSO-d_6]) analyses were used to provide new insights into the structural changes that occur in HTL bio-oil during an accelerated aging process.

MATERIALS AND METHODS

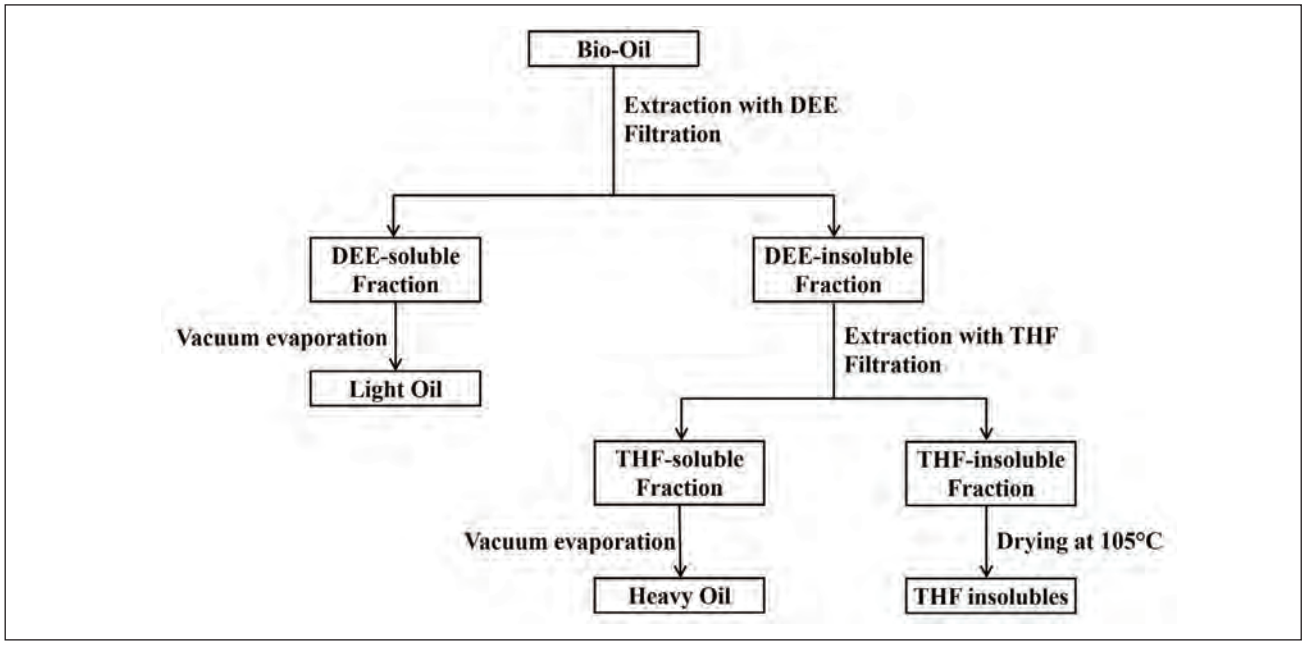
These method cannot fully address safety issues that might arise. The user is responsible for assessing potential safety issues associated with the given methods at its point of use and must consider all general laboratory safety precautions. In particular, the user must identify and implement suitable health and safety measures and comply with all pertinent regulations.

Production of the bio-oil

The bio-oil samples were obtained from the continuous conversion of LignoBoost (Invenntia AB; Stockholm, Sweden) kraft softwood lignin in subcritical water and have been characterized elsewhere [14-18]. In the experiment where the lignin-derived bio-oil was produced, the reactor temperature and pressure were kept at 350°C and 25 MPa, respectively. The dry lignin content was about 5.6% and the mass ratio of phenol to dry lignin was 0.70; the contents of K_2CO_3 and KOH were 1.6% and 0.4%, respectively. The heterogeneous catalyst used in this process was ZrO_2, manufactured by Saint-Gobain NorPro (Stow, OH, USA). The feed flow rate was 2 kg/h, the recycle-to-feed ratio was 4/5, and the steady-state period for sampling was 2 h and 40 min. Further details of the apparatus and procedure related to the production of lignin-derived bio-oil can be found in previous work by Nguyen et al. [17,18] and Belkheiri et al. [15,16].

Fractionation of the bio-oil

Figure 1 is a block diagram of the various steps involved in the solvent fractionation of lignin-derived bio-oil; the fractionation was performed according to a method described elsewhere [14]. The bio-oil (about 5 g) was first extracted by diethyl ether (DEE) using a solvent-to-feed ratio (S/F) of 20/1 and separated into DEE-soluble fraction (light oil) and DEE-insoluble fraction. The latter was extracted further by THF, with an S/F ratio of 20/1, into THF-soluble fraction (heavy oil) and THF-insoluble fraction (THF insolubles).



1. Block diagram of the solvent fractionation of the lignin-derived bio-oil. DEE = diethyl ether; THF = tetrahydrofuran.

Accelerated aging of the bio-oil

The lignin-derived bio-oil produced by HTL was used in the investigation of accelerated aging at elevated temperatures (i.e., 50°C and 80°C). At 80°C, the large change in the properties of pyrolysis bio-oil can be expected [5,13], while at 50°C, the change can be used in comparison. The bio-oils were subjected to accelerated aging for periods of 1 hour, 1 day, 1 week, and 1 month. The aged bio-oil was fractionated into aged raw oil_light oil (aRO_LO), aged raw oil_heavy oil (aRO_HO), and aged raw oil_THF insolubles (aRO_TIS). The stability test was performed according to a procedure in Elliott et al. [19]; about 10 g of bio-oil were put into 10 mL Schott Duran bottles (with screw caps) and placed in a heating oven at different temperatures for different residence times. All bio-oil samples were weighed before and after accelerated aging to ensure there was no significant loss of water or other volatiles. The results showed that the samples of bio-oil were able to maintain a uniform phase, with only a minor loss in weight (~0.18%).

Characterization of the bio-oil

Water content

The water content of the bio-oil was determined in triplicate according to the ASTM E203-08 method [12]. About 0.5 g oil was dissolved in THF with an S/F about 20/1, and the water content was measured by using Karl Fischer volumetric titration using Hydranal-Composite 5 (Honeywell; Morris Plains, NJ, USA) and methanol. The titrant concentration was determined using the Honeywell Hydranal Water Standard 10.0.

Elemental analysis

The elemental composition of the bio-oil was determined at Mikroanalytisches Laboratorium Kolbe (Germany), which uses a CHNOS Analyzer (Elementar Analysensysteme GmbH; Langenselbold, Germany) to measure the contents of carbon and hydrogen, and an ion chromatography system (Metrohm; Herisau, Switzerland) to measure the sulfur content. The content of ash in the bio-oil was measured in triplicate according to the ASTM E1755-01 method [20], using a Labotherm Program Controller S27 (Nabertherm; Lilienthal, Germany). The oxygen content was calculated by difference; the higher heating value (HHV) was calculated using an elemental analysis by applying Doulong's formula [7], as in Eq. (1):

$$HHV\ [MJ/kg] = [338.2 \times \%C + 1{,}442.8 \times (\%H - \%O/8)] \times 0.001 \quad (1)$$

Molecular weight of the light oil, heavy oil, and THF insolubles (GPC analysis)

About 30 mg of each fraction of raw oil (light oil, heavy oil, and THF insolubles) at fresh state (LO, HO, and TIS) and aged state (aRO_LO, aRO_HO, and aRO_TIS) were dissolved in the mobile phase DMSO/LiBr (10 mM) and filtered with a 0.2 µm syringe filter. The sample solutions were analyzed for mol. wt. and mol. wt. distribution by means of gel permeation chromatography (PL-GPC 50 Plus, Agilent Technologies; Alpharetta, GA, USA) connected to refractive index and ultraviolet detectors (280 nm, Polymer Laboratories, Varian Inc.; Palo Alto, CA, USA). Two Agilent PolarGel-M columns and a guard column (300×7.5 mm and 50×7.5 mm, 8 µm) were coupled in series. A 10-point calibration curve with Pullulan standards (PL 2090-0100 polysaccharide calibrations kit, Varian) was used to determine the mol. wt. of the samples. The analyses were repeated in triplicate and the average value was reported. All of the samples were found soluble in the mobile phase (DMSO/LiBr). The same systematic error obtained from all of the samples (i.e., same concentration, solvent, analysis time) allows the average value of the mol. wt. determined by GPC for the oil to be compared.

Chemical composition of the light oil (GC–MS analysis)

About 0.5 g of raw oil in fresh and aged states were dissolved in DEE with an S/F of 30, and mixed with a known amount of internal standard (IST, syringol in DEE). This mixture was filtered through a 0.2 µm syringe filter and injected in the GC–MS system. The Agilent 7890A gas chromatograph used is coupled to an Agilent 5975C mass spectrometer operating in electron ionization mode. The analysts are separated in a chromatographic column HP-5MS (length: 30 m; internal diameter: 0.25 mm; thickness of stationary phase: 0.25 µm) by injecting 1 µL of sample via an Agilent7693A auto-sampler, using helium at 1 mL/min as the carrier gas. The injector temperature was set at 300°C and the temperature program of the gas chromatograph oven was 45°C for 2.25 min, 2°C/min up to 300°C, 300°C for 10 min. The mass spectrometer source and quadrupole temperatures were set at 250°C and 150°C, respectively. Spectral interpretation was carried out using the NIST MS Search program (version 2.0) operating on the NIST/EPA/NIH Mass Spectral Database 2011 (NIST 11). The contents of the main components were determined semi-quantitatively: each sample was analyzed in triplicate and the average value was then used.

Functional groups of the light oil, heavy oil, and THF insolubles (2D HSQC NMR analysis)

About 100 mg of each samples (LO, HO, TIS, aRO_LO, aRO_HO, and aRO_TIS) were dissolved in 0.75 mL DMSO-d_6 using a small vial equipped with a stirring bar overnight to ensure that the samples were dissolved completely. The sample solutions were then analyzed by means of ^{1}H–^{13}C HSQC NMR (Bruker, 800 MHz). The correlation spectra were recorded at 25°C on a Bruker Advance III HD 18.8 T NMR spectrometer (Rheinstetten, Germany) equipped with a 5 mm TXO cryoprobe. The HSQC spectra were recorded using a standard Bruker pulse sequence "hsqcedetgpsisp2.3" with a 0.25-s 1H acquisition time, 5.3 ms 13C acquisition time, 3 s interscan delay, and ^{1}JC–H coupling constant of 145 Hz, 8 scans; each spectrum was recorded for 4 h. The spectra were processed and analyzed using the default processing template of Mestrenova version 10.0.0 software (Mestrelab Research; Escondido, CA, USA), along with automatic phase and baseline correction.

RESULTS

Fractionation and yields of the bio-oil

The raw bio-oil obtained from the lignin conversion in subcritical water was aged using a heating oven at 50°C and 80°C for periods of 1 hour, 1 day, 1 week, and 1 month. After aging, the raw bio-oil was fractionated into light oil, heavy oil, and THF insolubles to assess the compositional changes of the bio-oil. **Table I** presents the yield of each fraction after aging at different temperatures and periods, measured on a dry basis.

The yield of light oil decreased after aging whereas that of THF insolubles increased. In general, a higher aging temperature (80°C) and a longer aging time (1 month) result in larger changes in the yields of the bio-oils fractions; this is consistent with the findings of Jiang et al. [7], who studied the aging of biomass-pyrolysis bio-oil. In particular, the light oil decreased from 64.1% to 62.3% after 1 month of aging at 50°C and to 58.1% after 1 month of aging at 80°C. The THF insoluble, on the other hand, increased from 16.5% to 20.9% after 1 month of aging at 50°C and to 22.2% after 1 month of aging at 80°C. Various oligomerization/polymerization reactions of reactive compounds must thus have occurred not only in the light oil during aging, leading to a decrease in the yield of light oil and an increase in that of heavy oil, but also in the heavy oil, leading to a decrease in the yield of heavy oil and an increase in that of THF insolubles. The yield of heavy oil did not change significantly, which indicates that both the increase and decrease occurred simultaneously during aging. Compared with biomass-pyrolysis bio-oil [3,12], lignin-derived bio-oil from HTL is more stable at 80°C for up to 1 month.

Elemental composition of the bio-oil

Table II shows the water content and elemental composition of fresh and aged bio-oil at different aging temperatures and times, measured on a dry basis. The contents of water and oxygen of the lignin-derived bio-oil used in this study was about 4.8% and 14.1%, respectively, which is low compared to conventional biomass-pyrolysis bio-oil [21]. After aging, the water content of this bio-oil showed no systematic change; this indicates that the total water content had no dramatic effect on chemical reactions that are typical for producing water (i.e., condensations), and thereby differs to the biomass-pyrolysis bio-oil [12,15]. Moreover, the changes in the elemental composition of the bio-oil before and after aging were rather small. These results indicate that the chemical composition of the lignin-derived HTL bio-oil is very stable during the aging at 80°C for up to 1 month.

Determination of molecular weight of the bio-oil

The mol. wt. distribution curves of different fractions of fresh raw oil (light oil, heavy oil, and THF insoluble) are

Aging Temperature, °C	Fresh	50				80			
Aging Time		1 Hour	1 Day	1 Week	1 Month	1 Hour	1 Day	1 Week	1 Month
Light oil	64.1	63.5	60.0	59.9	62.3	62.9	58.4	61.7	58.1
Heavy oil	19.4	17.0	19.6	19.7	16.8	18.1	21.5	17.2	19.7
THF insolubles	16.5	19.5	20.4	20.4	20.9	19.0	20.1	21.1	22.2

I. Yield (%) of each fraction before and after accelerated aging at different temperatures for different periods, measured on a dry basis.

Aging Temperature, °C	Fresh	50				80			
Aging Time		1 Hour	1 Day	1 Week	1 Month	1 Hour	1 Day	1 Week	1 Month
Water content, %	4.8	4.2	4.3	4.5	4.2	4.2	4.2	4.3	4.5
Elemental composition, %									
Carbon	74.4	74.1	74.2	74.2	73.5	73.6	73.9	74.1	73.7
Hydrogen	6.2	6.2	6.3	6.6	6.5	6.2	6.4	6.5	6.4
Sulfur	0.3	0.3	0.3	0.3	0.3	0.3	0.3	0.3	0.3
Ash	5.0	4.5	3.8	5.0	3.7	4.3	4.3	4.7	6.6
Oxygen*	14.1	14.8	15.3	13.8	15.9	15.5	15.0	14.3	12.9
HHV (MJ/kg)**	31.6	31.3	31.4	32.1	31.4	31.0	31.5	31.9	31.8

* Oxygen was calculated by difference.
** HHV (higher heat value) was calculated using Doulong's formula.

II. Water content and elemental composition of the fresh and aged bio-oil, measured on a dry basis.

shown in **Fig. 2a**. The mol. wt. distribution of the fresh light oil comprises a high amount of monomers (peak 1, ~60 dalton) and small amounts of dimers (peak 2, ~200 dalton) and oligomers (peak 4, ~2000 dalton). The mol. wt. distribution of the fresh heavy oil contains mainly oligomers with a low amount of peak 3 (~400 dalton) and a higher amount of peak 4 and 5 (~3600 dalton). The mol. wt. distribution of the fresh THF insolubles consists mainly of highly polymerized oligomers (peak 6, ~8600 dalton). The mol. wt. distribution curves of light oil, heavy oil, and THF insolubles at aged state (aRO_LO, aRO_HO, and aRO_TIS, respectively) are shown in Fig. 2c–d. The mol. wt. distribution of all the aged raw oil fractions (aRO_LO, aRO_HO, and aRO_TIS) showed no major changes when compared with the fresh raw oil fractions (LO, HO, and TIS) after aging at 50°C for up to 1 month (1 hour, 1 week, and 1 month) and at 80°C for up to 1 week (1 hour, 1 day, and 1 week).

However, when the bio-oil was stored for 1 month at 80°C, changes in the mol. wt. distribution of the bio-oil fractions could be detected. The mol. wt. distribution curve of the aged raw oil_heavy oil at 80°C for 1 month of aging (aRO_HO_80_1m) in particular differed noticeably from the other curves (Fig. 2c); it shows a significant shift toward signals characteristic of higher mol. wt. species. The weight-average molecular $(\overline{M_w})$ of peak 5 increased from 3600 dalton to 5500 dalton after aging for 1 month at 80°C; this change was combined with a simultaneous reduction of the lower mol. wt. distribution fractions (peaks 1 and 3, Fig. 2c) in the aged raw oil_heavy oil (1 month, 80°C). Also, the mol. wt. distribution curve of aged raw oil_THF insolubles at 80°C for 1 month of aging (aRO_SS_80_1m) shows a major change (Fig. 2d), where the mol. wt. distribution curve shifts toward the higher mol. wt. region. In detail, $\overline{M_w}$ the of peak 6 increased from 8600 dalton to 13700 dalton after aging at 80°C for up to 1 month. This indicates that the severest condition (80°C and 1 month) can alter the mol. wt. distribution of the bio-oil and thereby induce polymerization of the low-mol. wt. materials in the light oil and heavy oil to form high-mol. wt. materials (heavy oil and THF insolubles). Compared with pyrolysis bio-oil obtained from biomass [1,9,10,12], these changes are nevertheless small and indicate that the lignin-derived HTL bio-oil is more stable than biomass-pyrolysis bio-oil after aging at 80°C for 1 month.

GC–MS analysis of the DEE solubles of bio-oil

GC–MS analysis was performed to provide more detail of the chemical composition of the DEE soluble fraction. **Table III** shows the yield of the GC–MS compounds identified in the

Aging Temperature, °C	Fresh	50				80			
Aging Time		1 Hour	1 Day	1 Week	1 Month	1 Hour	1 Day	1 Week	1 Month
Anisole	5.84	6.31	6.33	6.22	6.07	6.35	6.28	6.12	5.67
Phenol	15.96	14.90	14.98	14.81	14.13	15.04	14.93	14.67	14.14
Alkyl anisoles	0.67	0.62	0.63	0.62	0.63	0.63	0.62	0.62	0.59
Alkyl phenols	3.62	3.42	3.45	3.41	3.34	3.45	3.41	3.40	3.37
Guaiacol	2.29	2.16	2.16	2.14	2.09	2.16	2.13	2.11	2.07
1,2-Dimethoxylbenzen	0.20	0.19	0.19	0.19	0.18	0.19	0.19	0.18	0.18
2-Acetylphenol	0.18	0.17	0.17	0.17	0.16	0.17	0.17	0.17	0.17
Alkyl guaiacols	0.70	0.66	0.67	0.66	0.65	0.67	0.66	0.66	0.66
Catechol	0.06	0.07	0.07	0.07	0.05	0.07	0.07	0.07	0.06
Xanthene	0.24	0.23	0.23	0.22	0.23	0.23	0.22	0.23	0.22
Phenolic dimers* (Ar–CH_2–Ar)	2.25	2.17	2.20	2.16	0.13	2.18	2.11	2.12	0.13
Phenolic dimers* (Ar–CH_2–CH_2–Ar)	0.46	0.43	0.45	0.44	0.20	0.43	0.42	0.46	0.21
Retene	0.10	0.09	0.09	0.10	0.10	0.09	0.09	0.09	0.10
* Ar = aromatic ring.									

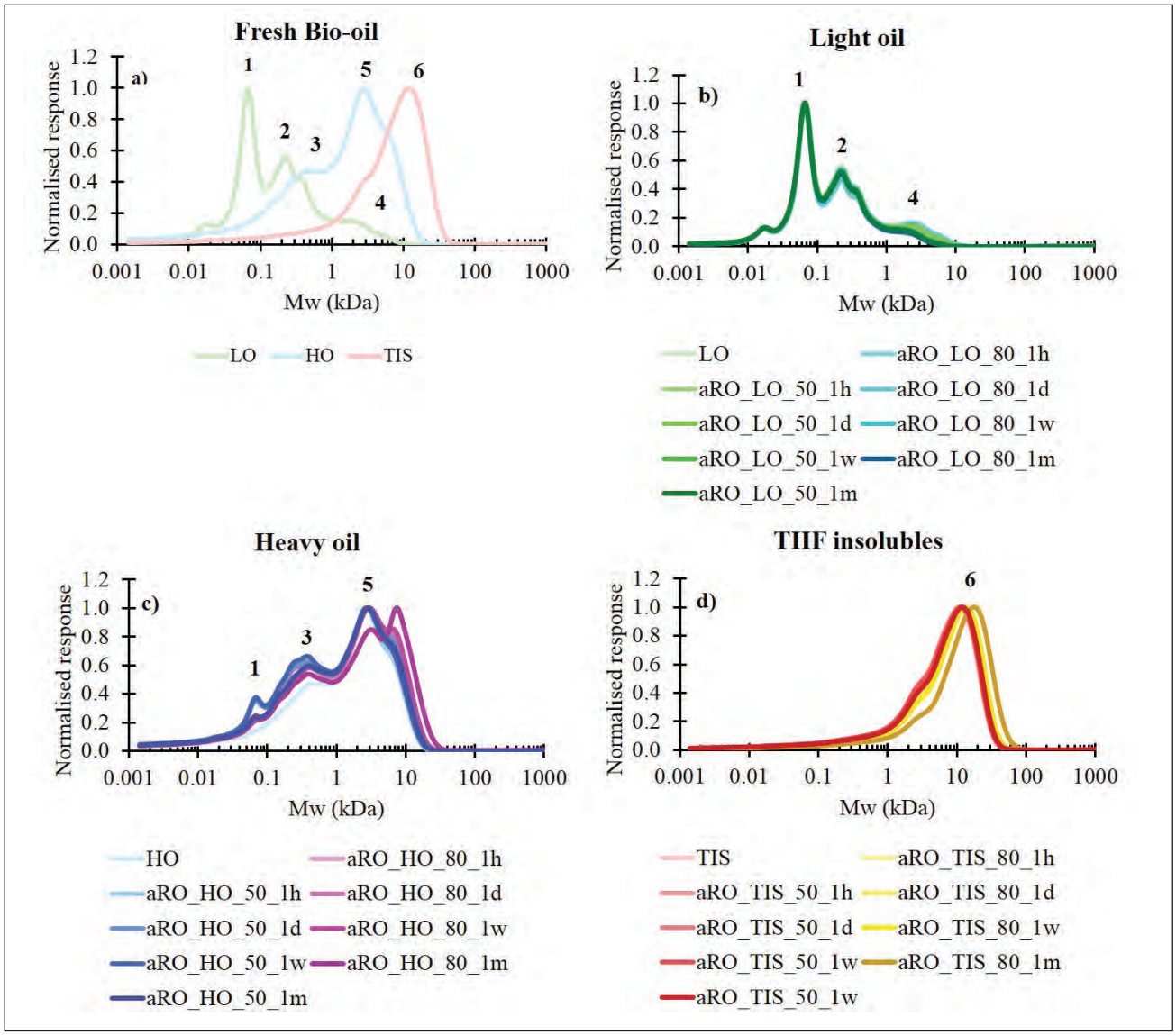
III. Yields (%) of gas chromatography–mass spectrometry compounds identified from the diethyl ether solubles in the fresh and aged raw oil, measured on a dry basis.

fresh and aged light oil, measured on a dry basis. The compounds were classified on the basis of structure, such as phenols (phenol and alkyl phenols), anisoles (anisole and alkyl anisoles), guaiacols (guaiacol and alkyl guaiacols), and catechols (catechol and alkyl catechols). As shown in Table III, the components that were detected include anisoles, phenols, guaiacols, catechols, phenolic dimers (Ar–CH_2–Ar) and some others, including 1,2-dimethoxylbenzene, 2-acetylphenol, xanthene, and retene (7-isopropyl-1-methyl phenanthrene).

The results in Table III show that the only notable changes in yields are found for anisole, phenols, guaiacol, and phenolic dimers. For all other compounds, the changes in yield are small. After 1 hour of aging, the yield of anisole increased slightly from 5.8% to 6.3% (an increase of about 8.4%), whereas phenol decreased slightly from 16.0% to 15.0% (a decrease of about 6.2%) irrespective of aging temperature (50°C and 80°C). The clear simultaneous increase in anisole and decrease in phenol after 1 hour of aging may be explained by the formation of anisole from phenol. No other large changes in the yields of monomers were detected in the two shorter time samples (1 hour and 1 week) by using GC–MS.

At the severest condition in this study (1 month and 80°C), both the yields of anisole (6.3% to 5.7%) and phenol (16.0% to 14.1%) were found to be reduced. One possible explanation is that these monomers react with THF insolubles and that phenol, having no side groups, has a higher reactivity than other monomers (see Table III). Besides, the yield of guaiacol was decreased from 2.3% to 2.1% at this severest condition.

The yield of phenolic dimers with methylene (Ar–CH_2–Ar)



2. Molecular weight distribution of the fresh bio-oil: (a) fresh light oil (LO) and aged raw oil_light oil (aRO_LO); (b) fresh heavy oil (HO) and aged raw oil_heavy oil (aRO_HO); (c) fresh THF insolules (TIS) and aged raw oil_THF insolubles (aRO_TIS); and (d) at different aging temperatures (50°C [50] and 80°C [80]) and times (1 hour [1h], 1 day [1d], 1 week [1w], and 1 month [1m]).

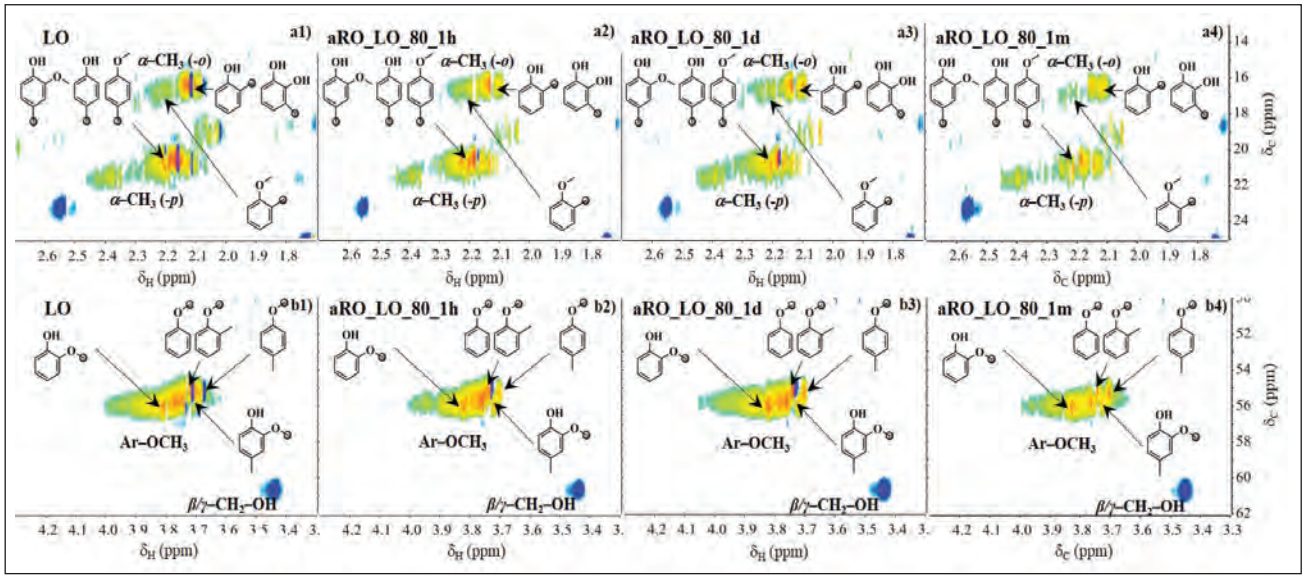
and ethylene (Ar–CH_2–CH_2–Ar) groups showed a large decrease in yield after being aged for 1 month: from 2.3% to 0.1% (a decrease of about 94.2%) and from 0.5% to 0.2% (a decrease of about 60.0%), respectively. This change was found to be independent of aging temperature (50°C and 80°C) and shows that the bridging phenolic structures have a high reactivity at the investigated conditions during aging. There are at least two possible routes these reactions can take: (1) the condensation reaction at the oligomerization/polymerization positions on the phenolic rings and (2) the nucleophilic substitution at the benzylic bridging methylene group [22]. Furthermore, our results indicate that an aromatic bridging methylene group (-CH_2-) has a higher reactivity compared with an ethylene group (-CH_2–CH_2-) during the accelerated aging of lignin-derived HTL bio-oil.

Consequently, the activity of the compounds identified by GC–MS in the bio-oil was in the following order: phenolic dimers (Ar–CH_2–Ar) > phenol > anisole > phenolic dimers (Ar–CH_2–CH_2–Ar) > guaiacol > alkyl phenols, alkyl anisoles, alkyl guaiacols, xanthene, catechol, and retene after aging at 80°C for 1 month. This trend in reactivity was found to differ slightly from our previous study of the long-term storage of lignin-derived HTL bio-oil at room temperature [14]. Xanthene in particular, having the methylene group (-CH_2-) in its structure but without a hydroxyl substituent, was shown to have a low reactivity in the present study. The reason for this is not fully understood, but a possible explanation might be that several different reaction paths occur in parallel and the influence of temperature on the reaction kinetics for the involved reactions differs. Summarizing, the GC–MS results indicate that lignin-derived HTL bio-oil is quite chemically stable at 80°C for up to 1 month.

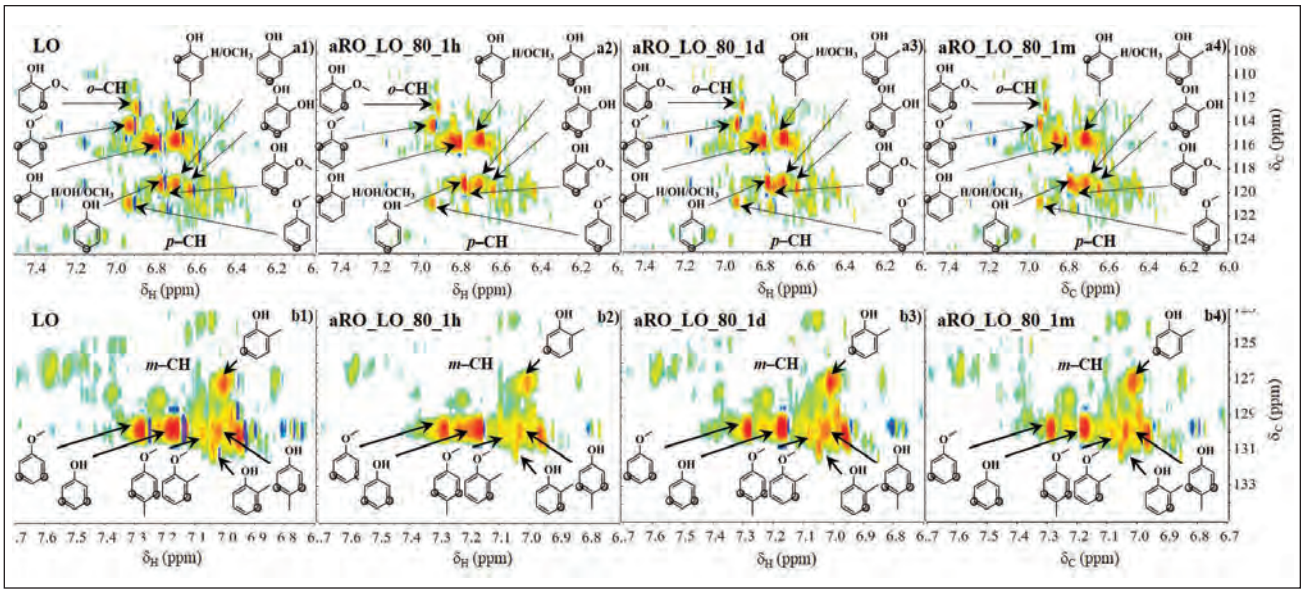
^{1}H–^{13}C HSQC NMR analysis of the bio-oil

To gain deeper insight into the chemical changes that occur during the aging of raw bio-oil, the ^{1}H–^{13}C HSQC NMR spectra obtained for the bio-oil before and after it was subjected to the accelerated aging process were analyzed. The interpretation of NMR spectra is difficult for complex mixtures of bio-oil, so the NMR analysis was performed using different fractions, namely light oil, heavy oil, and THF insolubles. To achieve a more precise elucidation, 23 model compounds identified from GC–MS were recorded using ^{1}H–^{13}C HSQC NMR (800 MHz, DMSO-d_6) (**Table A1** and **Fig. A1** in the Appendix) together with NMR assignments found in the literature [23–30]. **Figures A2–A4** in the Appendix show the aliphatic and aromatic regions in the ^{1}H–^{13}C HSQC NMR spectra of fresh bio-oil fractions: light oil, heavy oil, and THF insolubles. Signals corresponding to the aliphatic region, including aliphatic and ether/nonether connected groups, were observed between δ_C/δ_H 10–70/0–5 ppm. The chemical shift region belonging to the aromatic region of the respective subunits were detected in the range of δ_C/δ_H 105–135/5.7–6.2 ppm.

The major cross-peaks in the aliphatic region of the fresh light oil correspond to the alkyl groups (Ar–CH_3, Ar–CH_2–CH_3, Ar–CH_2–CH_2–CH_3), methoxyl groups (Ar–OCH_3), methylene and ethylene bridging groups (Ar–CH_2–Ar and Ar–CH_2–CH_2–Ar), aliphatic methylene groups (α/β–CH_2), and methylene groups adjacent to alcohol groups (β/γ–CH_2–OH/OR). The major cross-peaks in the aromatic region of the fresh light oil correspond to the aromatic C–H bonds at the *o*-, *m*-, and *p*-positions on aromatic rings. These findings are consistent with the results found in the GC–MS analysis of light oil. The fresh heavy oil and THF insolubles



3. Aliphatic region in the ^{1}H–^{13}C heteronuclear single quantum coherence (HSQC) nuclear magnetic resonance (NMR) spectra (800 MHz, dimethyl sulfoxide-d_6 [DMSO-d_6]) of the fresh light oil (LO) (a1 and b1) and aged raw oil_light oil at 80°C for 1 hour (aRO_LO_80_1h) (a2 and b2), 1 day (aRO_LO_80_1d) (a3 and b3), and 1 month (aRO_LO_80_1m) (a4 and b4), and the highlighted characteristic signals. Ar = aromatic ring; α- = the aliphatic carbon from the aromatic ring.



4. Aromatic region in the $^{1}H–^{13}C$ HSQC NMR spectra (800 MHz, DMSO-d_6) of the fresh light oil (LO) (a1 and b1) and aged raw oil_light oil at 80°C for 1 hour (aRO_LO_80_1h) (a2 and b2), 1 day (aRO_LO_80_1d) (a3 and b3), and 1 month (aRO_LO_80_1m) (a4 and b4), and the highlighted characteristic signals.

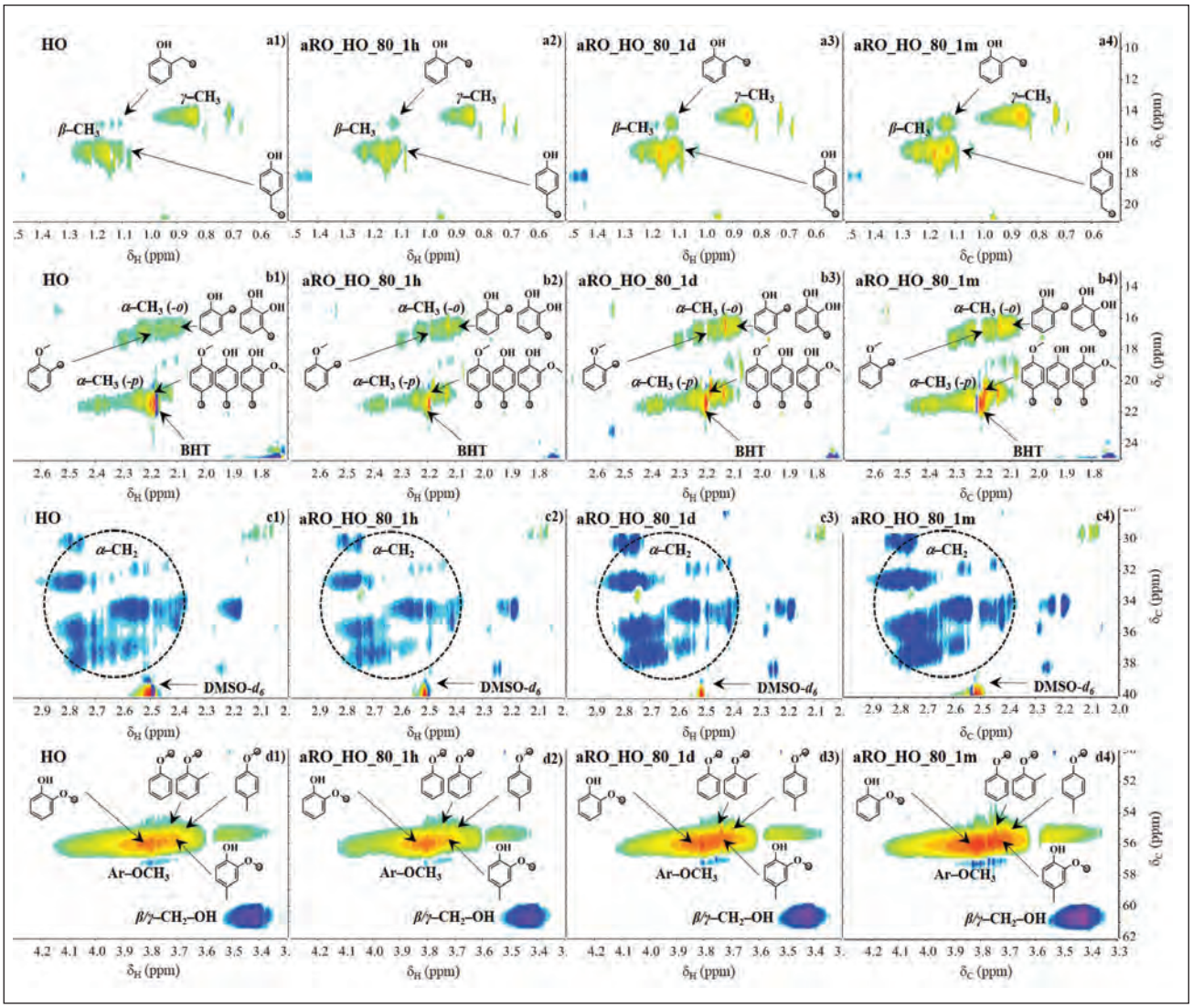
structures, on the other hand, differ slightly from the structural motifs published previously by Mattsson et al. [26], in which the polycyclic aromatic hydrocarbon (PAH)-like structures (δ_C/δ_H 123–135/7.2–8.3 ppm), branched β–methyl groups (i.e., *tert*–butyl *t*–C_4H_9 or *iso*–propyl *i*–C_3H_7, δ_C/δ_H 29.7–30.9/1.1–1.3 ppm), and alkenes groups conjugated with aromatic structures were detected. Because heavy oil and THF insolubles contain higher mol. wt. structures, a lower signal intensity and peaks broader than that of light oil were found in the NMR spectra.

Light oil

The $^{1}H–^{13}C$ HSQC NMR spectra of the fresh light oil (LO) and aged raw oil_light oil for 1 hour (aRO_LO_80_1h), 1 day (aRO_LO_80_1d), and 1 month (aRO_LO_80_1m) samples were analyzed for the aliphatic (δ_C/δ_H 10–70/0–5 ppm) and aromatic (δ_C/δ_H 105–135/5.7–8.2 ppm) regions of light oil (**Figs. 3** and **4** and **Figs. A5** and **A6** in the Appendix). In the aliphatic region, no new cross-peaks were obtained; there was just a slight reduction in the existing structural motifs after aging at 80°C for 1 month. The aromatic substituents methyl (Ar–CH_3, Fig. 3a), methoxyl (Ar–OCH_3, Fig. 3b), and aldehyde (Ar–CHO, Fig. A6) groups were found to have a slight decrease in signal intensity after aging at 80°C for 1 month. This indicates that the aromatic rings, with substituents such as methyl (-CH_3), methoxyl (-OCH_3), and aldehyde (-CHO), have a higher tendency for participating in reactions during the accelerated aging of bio-oil at 80°C. Using our model compounds for $^{1}H–^{13}C$ HSQC NMR database makes it possible to detect nonoverlapping regions for the most dominating phenolic structures in the light oil [30]. For instance, the chemical shifts of the aromatic *m*–CH in phenol and anisole do not overlap with those of guaiacols and can thus be used to determine the changes in these structures (i.e., anisole with δ_C/δ_H 130.0/7.3 ppm, phenol with δ_C/δ_H 130.0/7.2 ppm, alkylated phenols [-CH_3, -CH_2–CH_3], and phenolic dimers Ar–CH_2–Ar with δ_C/δ_H 6.9–7.1/125.6–127.8 ppm). Also, the chemical shifts of the guaiacol aromatic *o*–CH (Ar_2) with δ_C/δ_H 112.6/6.9 ppm are found not to overlap with those of other phenolic structures. Comparing fresh light oil with aged raw oil_light oil $^{1}H–^{13}C$ HSQC NMR spectra in the aromatic region (1 hour, 1 day, and 1 month), it can be concluded that phenol and anisole decreased slightly after aging at 80°C for 1 month, which corresponds well with the GC–MS data obtained in this study (Section 3.4). Previous studies on guaiacol and anisole structures have shown that the bond energy of the C–O bond in O–CH_3 (methoxyl groups) is low and reactions can therefore occur at this substituent during aging [23]. However, in the aged raw oil_light oil at the severe condition (i.e., 80°C and 1 month), it was possible to observe an increase in a cluster of peaks in the region with δ_C/δ_H 118–122/6.4–6.6 ppm and a specific cross-peak with δ_C/δ_H 117/6.6 ppm. In previous publications, this region has been interpreted as being catechol compounds [26], and our two examples of model catechol structures (i.e., catechol and 3-methylcatechol, Table AI and Fig. A1) also have resonance here [30].

Heavy oil and THF insolubles

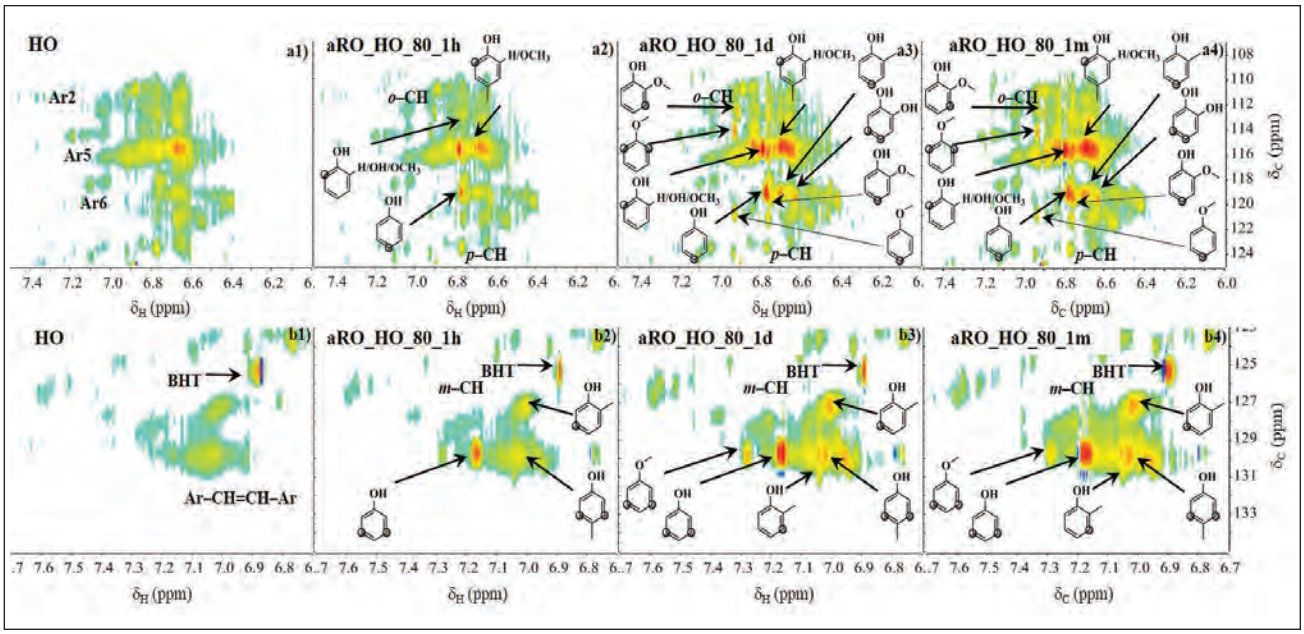
Figures 5 and **6** and **Figs. A7** and **A8** show the $^{1}H–^{13}C$ HSQC NMR spectra of the fresh heavy oil (HO) and aged raw oil_ heavy oil at 80°C (aRO_HO_80) for 1 hour, 1 day, and 1 month. When the fresh and aged raw oil_heavy oil are compared, the chemical changes that have occurred in the heavy oil structure can be clearly observed in the aromatic region; new cross-peaks, with a high signal intensity, are obtained (Fig. 6). In the fresh heavy oil fraction, the peak with the high-



5. Aliphatic region in the ^{1}H–^{13}C HSQC NMR spectra (800 MHz, DMSO-d_6) of the fresh heavy oil (HO) (a1, b1, c1, and d1) and aged raw oil_heavy oil at 80°C for 1 hour (aRO_HO_80_1h) (a2, b2, c2, and d2), 1 day (aRO_HO_80_1d) (a3, b3, c3, and d3), and 1 month (aRO_HO_80_1m) (a3, b4, c4, and d4), and the highlighted characteristic signals. BHT = 3,5-Di-tert-4-butylhydroxytoluene; Ar = aromatic ring; α-, β-, and γ- = the aliphatic carbon from the aromatic ring.

est intensity is found in the region corresponding to the combined guaiacol Ar_5/general region for aromatic C–H structures (δ_C/δ_H 114.7–116.3/6.6–6.9 ppm). However, in the aged raw oil_heavy oil, cross-peaks with δ_C/δ_H 115/6.7–6.8 ppm, 115/6.6–6.7 ppm, 119/6.6–6.8 ppm, 127/7.0 ppm, 130/7.1–7.2 ppm, and 131/6.9–7.0 ppm appear; this new pattern of peaks has clear similarities to that of the light oil monomeric fraction (Fig. 4). Correlation of our findings to the monomeric light oil fraction and the model database (Fig. A1) shows that these peaks correspond to *m*–CH in anisole (δ_C/δ_H 130/7.3 ppm), phenol (δ_C/δ_H 130/7.2 ppm), alkyl phenols (-CH_3, -CH_2–CH_3), and phenolic dimers (δ_C/δ_H 126–131/6.9–7.1 ppm) [30]. Also, correlations of the unselective cross-peaks with δ_C/δ_H 115/6.6–6.9 ppm and 119/6.6–6.8 ppm correspond to aromatic *o*- and *p*- substituted phenol/guaiacol-like structures. The intensity of this new phenol-alkyl pattern in the aromatic region increased when the raw oil was aged at 80°C for a longer time (1 hour to 1 month) (Fig. 6). This new pattern was observed with a high signal intensity, thus indicating the formation of a new polymer based on other aromatic ring structures. This is also in good agreement with the changes in the aliphatic ^{1}H–^{13}C HSQC NMR region (Fig. 5) where aromatic substituents, such as methoxyl (Ar–OCH_3) and methyl (Ar–CH_3) groups, were found to be increased. This confirms that anisole, guaiacol, and alkylated phenolic structures are parts of a newly formed phenolic polymer.

Furthermore, another aliphatic structural motif was also found to increase in the heavy oil at 80°C for 1 month (i.e., α/β–CH_2, β/γ–CH_3). A new group of peaks, with δ_C/δ_H 24–26/1.1–1.2 ppm and interpreted as branched β–CH_3 group-like structure, was found. Moreover, other cross-peaks, such as the aldehyde groups (-CHO, δ_C/δ_H 190–194/9.7–10.3 ppm),



6. Aromatic region in the $^{1}H–^{13}C$ HSQC NMR spectra (800 MHz, DMSO-d6) of fresh heavy oil (HO) (a1 and b1), and aged raw oil_heavy oil at 80°C for 1 hour (aRO_HO_80_1h) (a2 and b2), 1 day (aRO_HO_80_1d) (a3 and b3), and 1 month (aRO_HO_80_1m) (a4 and d4), and the highlighted characteristic signals. BHT = 3,5-Di-tert-4-butylhydroxytoluene; Ar = aromatic ring.

were found to reduce in intensity with longer aging time, and finally disappeared in the aged raw oil_heavy oil after 1 month. This indicates that the aldehyde groups are involved in aging reactions, which is in agreement with the previous findings [2].

The new phenol-alkyl pattern signals obtained in the aged raw oil_heavy oil imply the formation of a new phenolic-polymer, the origin of which was investigated in another study by Nguyen Lyckeskog et al. [30]. In that study, the fresh bio-oil was separated into light oil and heavy oil fractions and these fractions were then aged at 80°C for 1 week. After aging, a small amount of the insolubles (DEE insolubles and THF insolubles) were separated and analyzed using $^{1}H–^{13}C$ HSQC NMR. It was confirmed that DEE insolubles (from aged light oil fraction) have a pattern similar to a phenolic-polymer found in the aged raw oil_heavy oil fraction detected in the present study.

Polymerization of the small phenolic structures (light oil) was shown to take place and a phenolic-polymer structure is, therefore, formed in the HTL bio-oil. This new phenolic-polymer is soluble in THF and can thus be found in the THF soluble fraction (heavy oil). On the other hand, the fresh heavy oil fraction is also polymerized during accelerated aging; the THF insolubles structures that are formed end up in the THF insolubles because of the increase in mol. wt. The THF insolubles formed in the heavy oil were found to give the same structural pattern as the THF insolubles in the fresh bio-oil (**Figs. A9** and **A10** in the Appendix); that is, a more condensed network of aromatic structures, such as PAH and di-substituted ether aromatic structures (i.e., guaiacol-like structures) with alkene and aliphatic bridges [26,30].

Consequently, the structure of the aged raw oil_heavy oil obtained in the accelerated aging process used in this study is a combination of the DEE insolubles (from aged light oil) and THF solubles (from aged heavy oil) structures. This explained the observations made in this study of a new pattern of structural peaks in the aged raw oil_heavy oil (see Fig. 6). These findings were also supported by the results of the yield obtained of the various fractions after aging.

The THF insolubles (TIS) that were formed during aging at 80°C for different periods (1 hour, 1 day, 1 week, and 1 month) were found to be soluble in DMSO-d_6 and investigated using $^{1}H–^{13}C$ HSQC NMR to discover any structural changes (Figs. A9 and A10). It was revealed that no structural changes could be observed during aging at the conditions used in this study.

Suggestions regarding the aging mechanism

On the basis of the GC–MS and $^{1}H–^{13}C$ HSQC NMR data, different pathways of the polymerization/condensation reactions that might occur in the HTL bio-oil can be proposed. One possibility is that the -CH_2- group between two phenolic rings reacts to form a new carbon–carbon bond. No increase in Ar–CH was, however, found in the aliphatic region $^{1}H–^{13}C$ HSQC NMR spectra of the light oil and heavy oil (Figs. 3–6). Full substitution to quaternary carbon could nevertheless proceed; these types of carbon cannot be detected in $^{1}H–^{13}C$ HSQC NMR. Another possible pathway is the formation of new carbon–carbon linkages at the *o*- and *p*- positions in the phenolic nucleus, leading to a large network of phenolic structures. The findings of both an increase in the aliphatic methylene groups (Ar–CH_2–Ar and

α–CH_2) and a significant increase in aromatic intense peaks from phenol, anisole, and alkylated phenolic structures indicate that this reaction pathway takes place.

The facts that the content of water did not increase and that the content of acid compounds in the lignin-derived HTL bio-oil was found to be low result in a low level of acid-catalyzed mechanism of polymerization/condensation reactions during the accelerated aging of HTL bio-oil. The main mechanism of these reactions might, therefore, be a radical mechanism. It is possible that the radicals were generated either in the HTL process or by the stereo-electronic effect of the aromatic ring [4,31].

Combining the studies carried out on the thermal stability of the bio-oil fractions (i.e., light oil and heavy oil) [30] at elevated temperature (80°C) and the raw bio-oil in the present study, it can be concluded that the aging mechanism in the medium with and without THF insolubles/residues differs. When the separated light oil fraction without THF insolubles present was aged, a low turnover to higher mol. wt. structures was detected; the light oil yield decreased 0.5% after aging 1 week at 80 °C [30]. However, when the raw oil with THF insolubles present was aged, it gave the higher turnover rate in the light oil yield (i.e., a decrease of 2.4%) shown in this study. The same trend could also be seen for the heavy oil fraction. Accelerated aging of raw bio-oil could, therefore, be assumed to be catalyzed by the THF insolubles and a higher change can thus be observed in the aged raw bio-oil than in the aged bio-oil fractions.

CONCLUSIONS

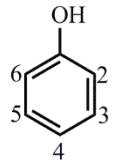
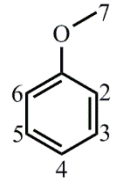
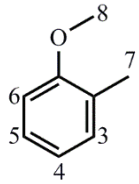
The accelerated aging of lignin-derived bio-oil was investigated at different temperatures (50°C and 80°C) and periods (1 hour, 1 day, 1 week, and 1 month). The lignin-derived HTL bio-oil was observed to be quite stable when aged at 80°C for 1 month compared with the biomass-pyrolysis bio-oil. In this study, phenolic dimers with methylene bridge (Ar–CH_2–Ar) were found to be more reactive than corresponding ones with ethylene bridge (Ar–CH_2–CH_2–Ar). Xanthene, having a methylene group was, however, found to be relatively stable during aging. The fact that phenol and phenolic dimers (-CH_2-group) were found to be mostly decreased indicates that the polymerization/condensation reactions differ in the oil during the accelerated aging in the presence of char/THF insolubles. The structure of the heavy oil fraction in the aged raw oil was found to be a combination of the light oil insolubles structures (phenolic polymers) that were formed and the heavy oil structures. **TJ**

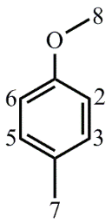
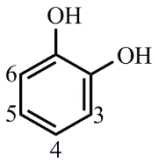
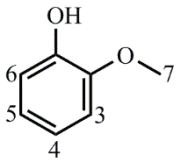
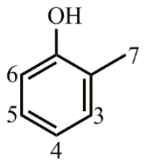
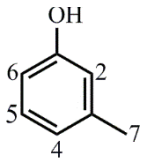
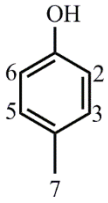
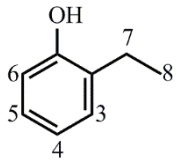
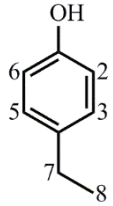
ACKNOWLEDGEMENTS

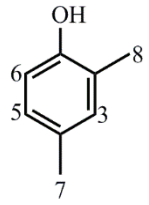
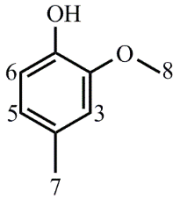
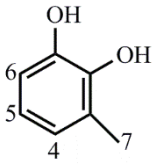
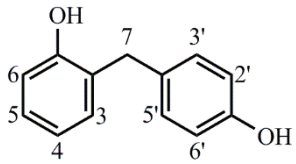
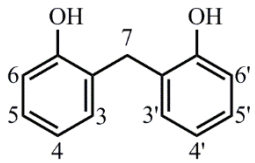
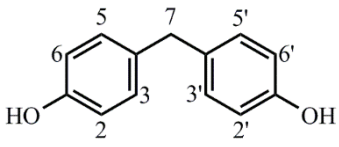
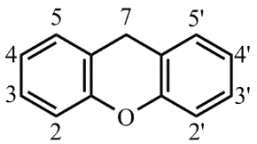
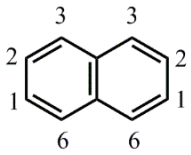
The authors gratefully acknowledge financial support from Chalmers Energy Initiative-LignoFuel Project, Valmet Power AB, the Swedish Energy Agency, and Ångpanneförenings Forskningsstiftelse. The authors thank Maxim Mayzel for the NMR analysis at Swedish NMR Centre of Gothenburg University, Lars-Erik Åmand for the experimental support, and Tommy Friberg for the technical assistance.

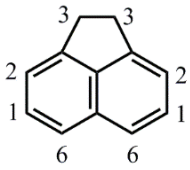
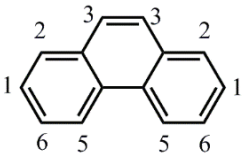
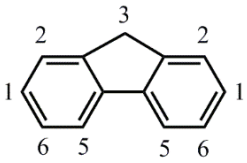
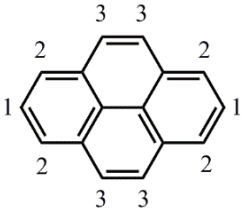
APPENDIX

This appendix includes Table A1 and Figs. A1-A10.

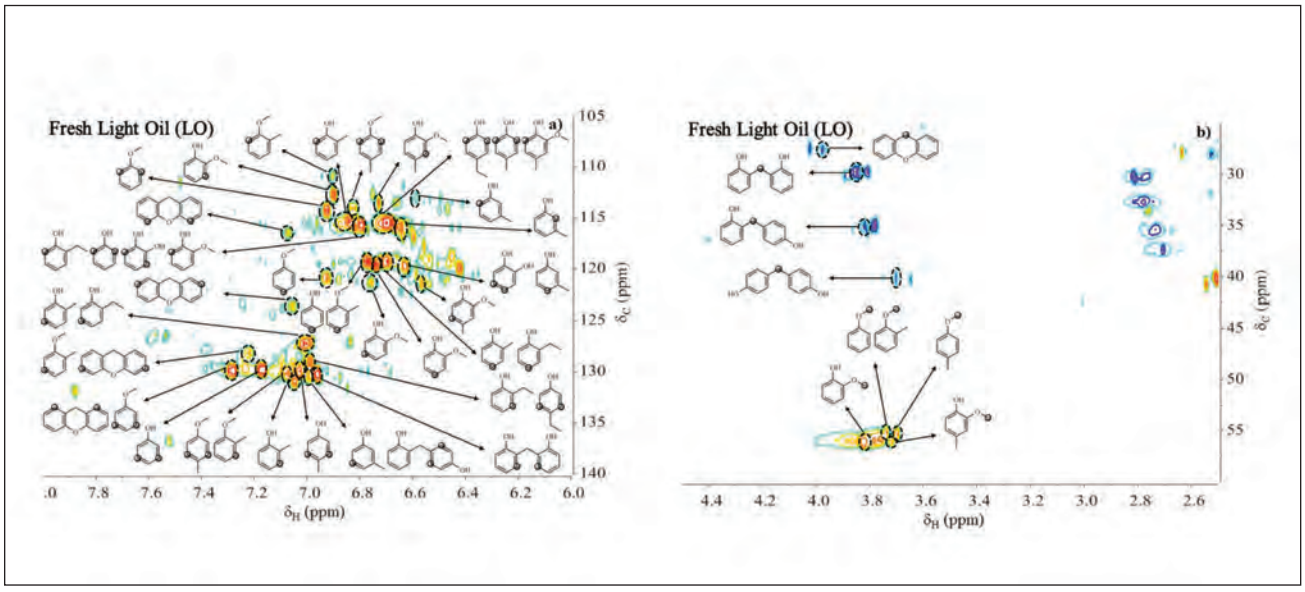
Compounds	Structures	Positions	Chemical Shift δ_C/δ_H (ppm)
Phenol		2,6 3,5 4	115.8/6.8 130.0/7.2 119.4/6.8
Anisole		2,6 3,5 4 7	114.4/6.9 130.0/7.3 121.0/6.9 55.4/3.8
2-Methylanisole		3 4 5 6 7 8	130.7/7.1 120.5/6.8 110.6/6.9 16.5/2.2 55.5/3.8

Compounds	Structures	Positions	Chemical Shift δ_C/δ_H (ppm)
4-Methylanisole		2,6 3,5 7 8	114.1/6.8 130.2/7.1 20.5/2.2 55.4/3.7
Catechol		3,6 4,5	116.3/6.8 119.9/6.6
Guaiacol		3 4 5 6 7	112.9/6.9 119.8/6.7 121.5/6.8 116.2/6.8 56.1/3.8
o–Cresol		3 4 5 6 7	131.1/7.1 119.3/6.7 127.2/7.0 115.1/6.8 16.6/2.1
m–Cresol		2 4 5 6 7	116.4/6.6 120.2/6.6 129.7/7.0 112.9/6.6 21.6/2.2
p–Cresol		2,6 3,5 7	115.6/6.7 130.3/7.0 20.7/2.2
2-Ethylphenol		3 4 5 6 7 8	129.3/7.0 119.3/6.7 127.0/7.0 115.2/6.8 23.2/2.5 14.7/1.1
4-Ethylphenol		2,6 3,5 7 8	115.6/6.7 129.1/7.0 27.9/2.5 16.6/1.1

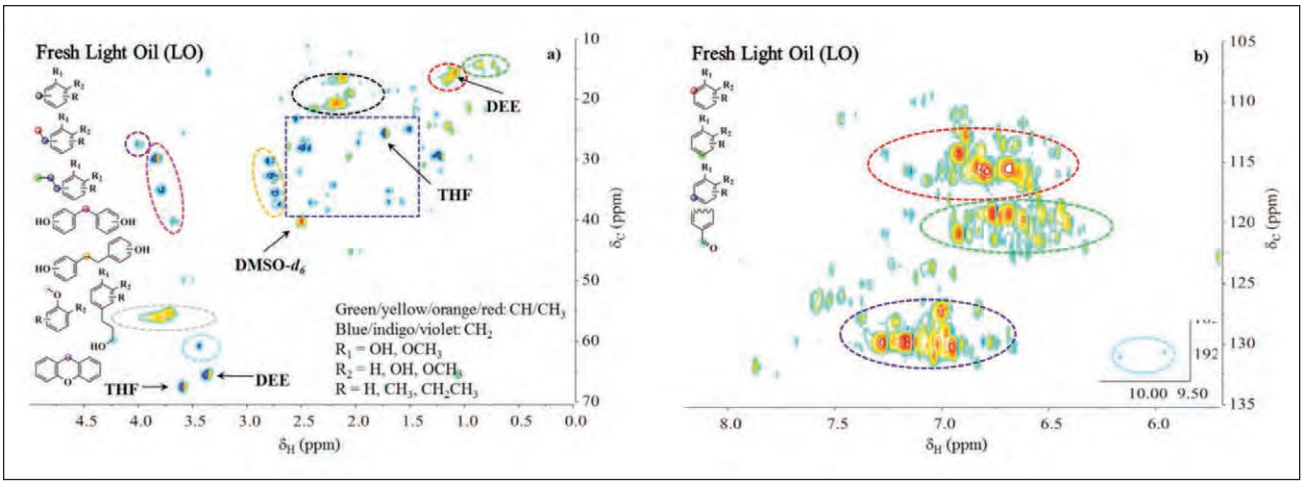
Compounds	Structures	Positions	Chemical Shift δ_C/δ_H (ppm)
2,4-Dimethylphenol		3 5 6 7 8	131.7/6.9 127.4/6.8 115.0/6.7 20.7/2.2 16.5/2.1
4-Methylguaiacol		3 5 6 7 8	113.7/6.7 121.5/6.6 115.9/6.7 21.1/2.2 56.0/3.7
3-Methylcatechol		4 5 6 7	121.6/6.5 119.1/6.5 113.6/6.6 16.6/2.1
2,4′-Methylenediphenol		3 4 5 6 7 2′,6′ 3′,5′	130.7/7.0 119.5/6.7 127.5/7.0 115.5/6.8 34.9/3.8 115.5/6.7 130.2/7.0
2,2′-Methylenediphenol		3,3′ 4,4′ 5,5′ 6,6′ 7	130.7/6.9 119.4/6.7 127.4/7.0 115.4/6.8 29.8/3.8
4,4′-Methylenediphenol		2,6,2′,6′ 3,5,3′,5′ 7	115.7/6.7 130.0/7.0 40.1/3.7
Xanthene		2,2′ 3,3′ 4,4′ 5,5′ 7	116.6/7.1 128.3/7.2 123.8/7.1 129.7/7.3 27.5/4.0
Naphthalene		1,2 3,6	126.4/7.5 128.2/7.9

Compounds	Structures	Positions	Chemical Shift δ_C/δ_H (ppm)
Acenaphthene		1 2 3 6	128.3/7.5 119.7/7.3 30.3/3.3 122.5/7.6
Phenanthrene		1 2 3 4 6	127.3/7.6 129.0/8.0 127.3/7.8 123.3/8.8 127.3/7.7
Fluorene		1 2 3 5 6	127.2/7.3 125.6/7.6 36.9/3.9 120.4/7.9 127.2/7.4
Pyrene		1 2 3	126.6/8.1 127.8/8.2 125.5/8.3

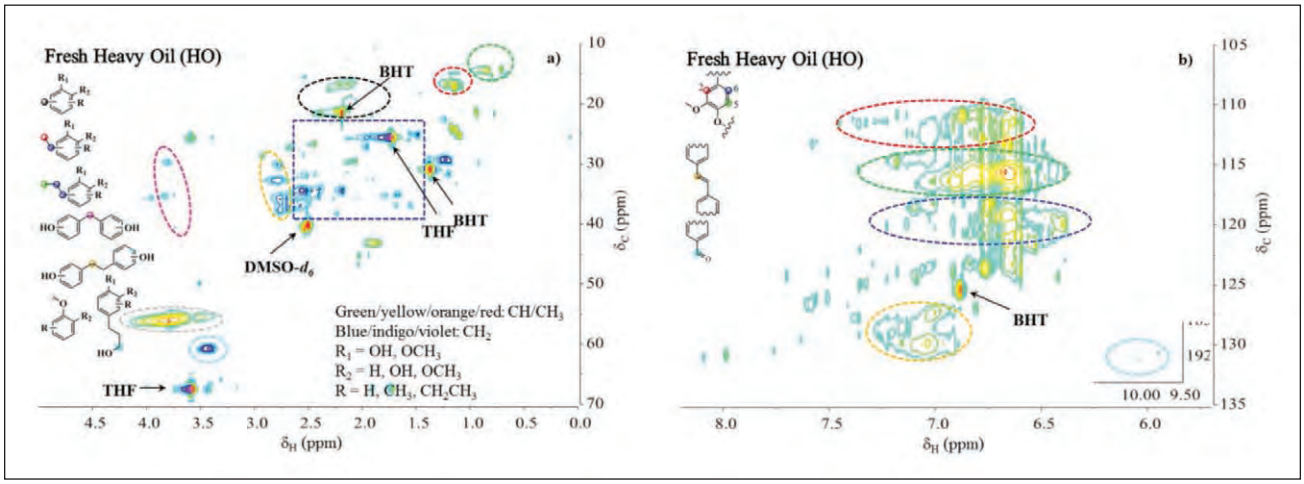
AI. ^1H–^{13}C HSQC NMR (800 MHz, DMSO-d_6) data of the model compounds.



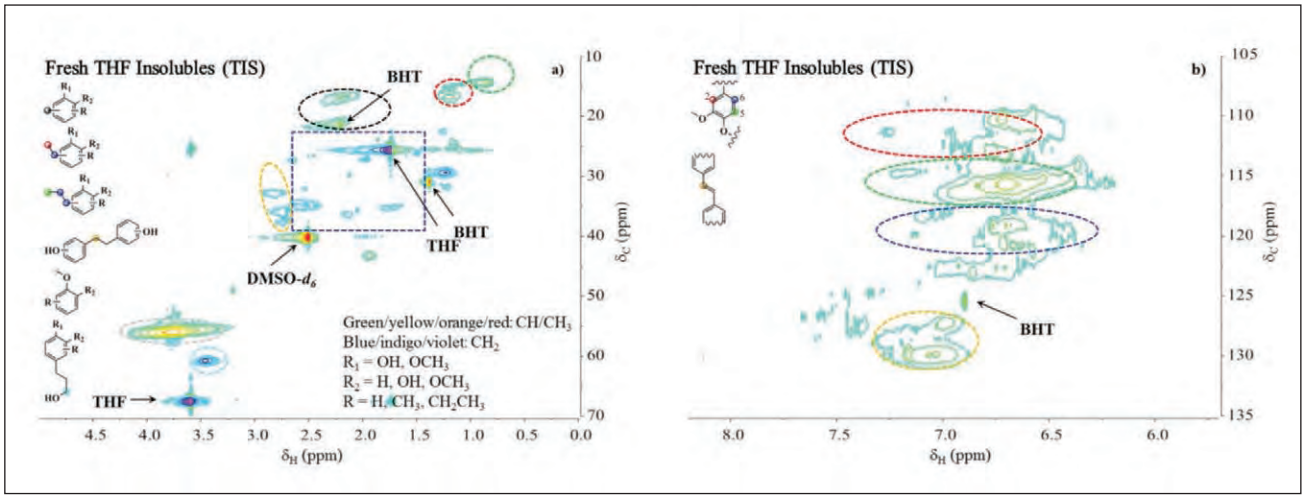
A1. ^1H–^{13}C HSQC NMR assignments (800 MHz, DMSO-d6) of the model compounds.



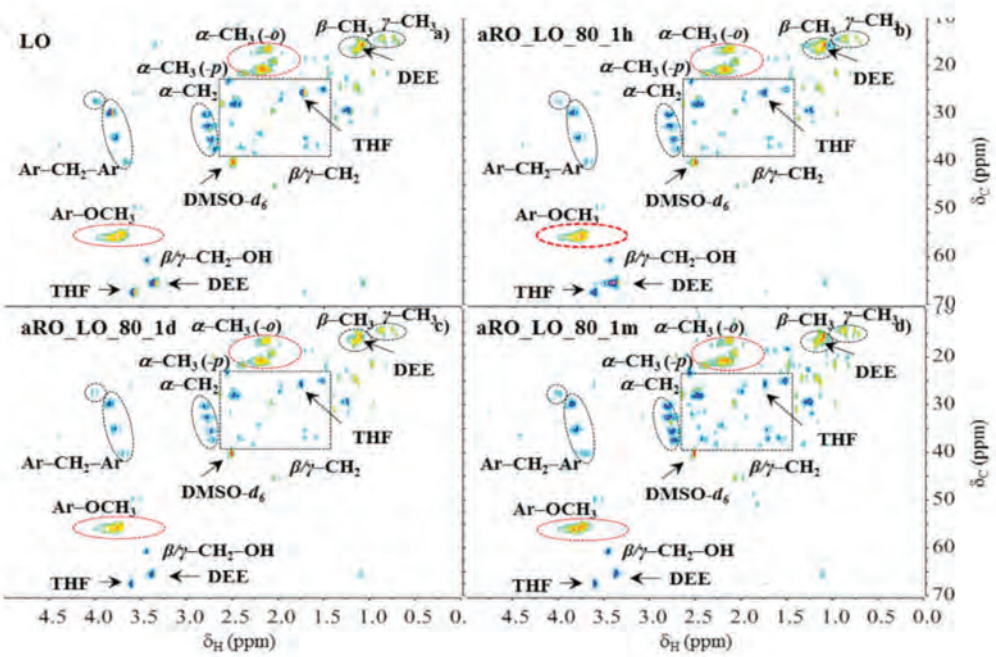
A2. Aliphatic (δ_C/δ_H 10–70/0–5 ppm) and aromatic (δ_C/δ_H 105–135/5.7–8.2 ppm) regions in the ^1H–^{13}C HSQC NMR spectrum (800 MHz, DMSO-d6) of the fresh light oil (LO), and the highlighted characteristic signals. DEE = diethyl ether; THF = tetrahydrofuran.



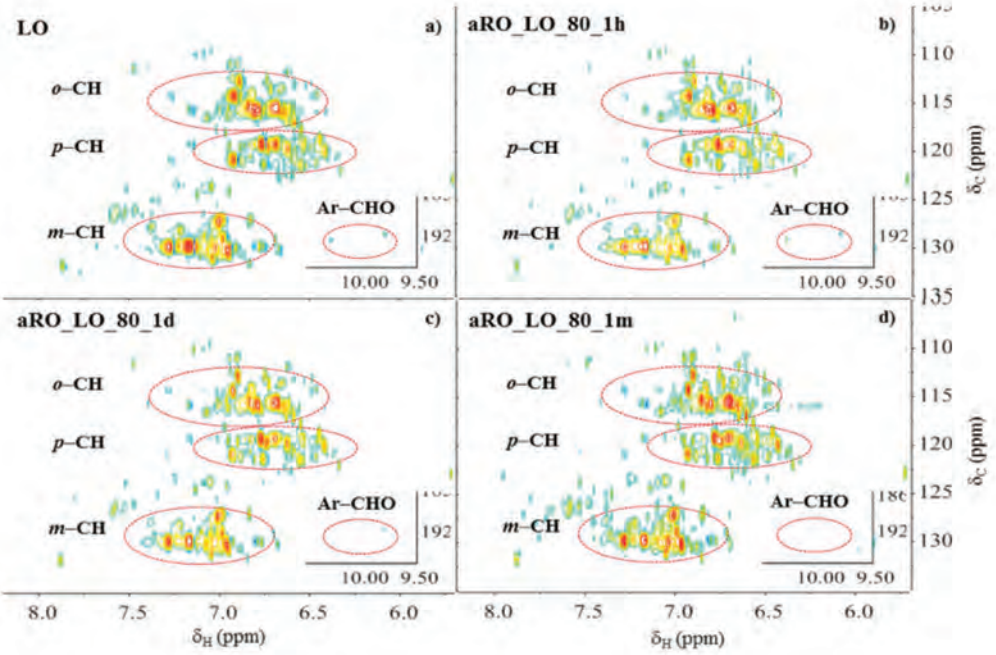
A3. Aliphatic (δ_C/δ_H 10–70/0–5 ppm) and aromatic (δ_C/δ_H 105–135/5.7–8.2 ppm) regions in the ^1H–^{13}C HSQC NMR spectrum (800 MHz, DMSO-d_6) of the fresh heavy oil (HO), and the highlighted characteristic signals. BHT = 3,5-di-tert-4-butylhydroxytoluene; THF = tetrahydrofuran.



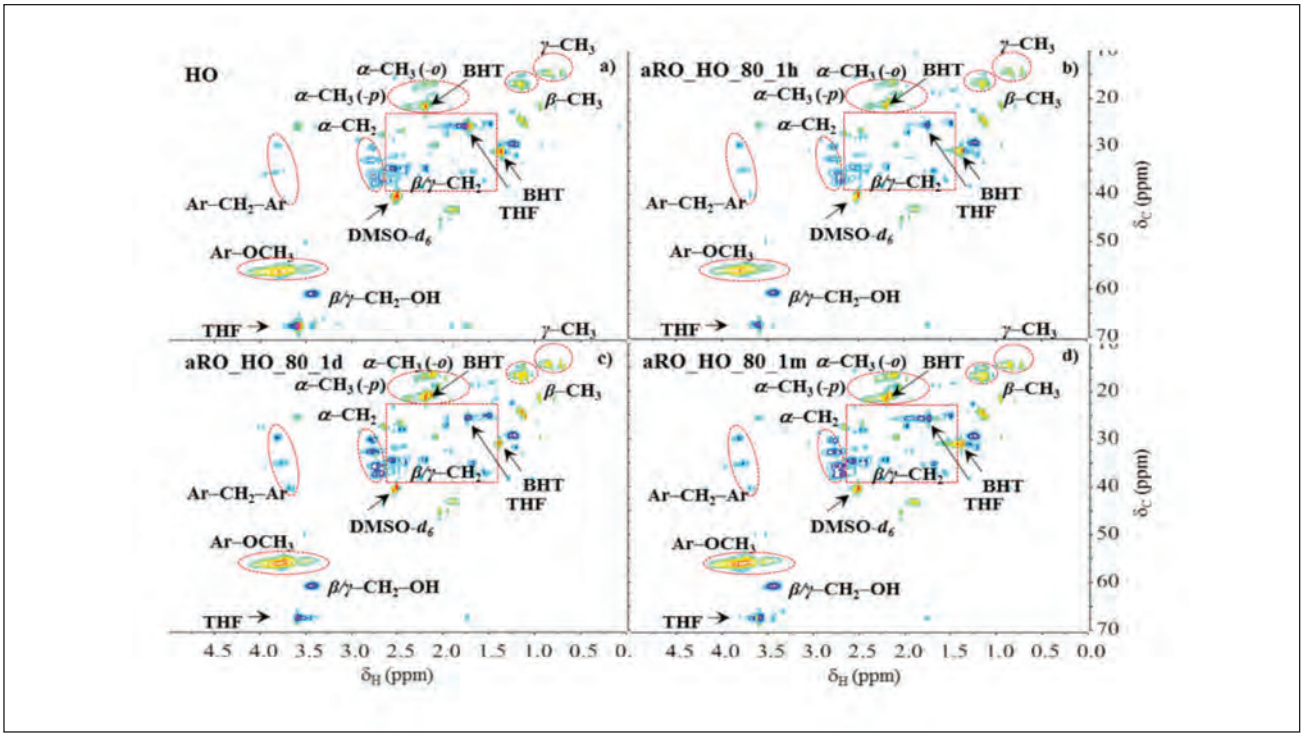
A4. Aliphatic (δ_C/δ_H 10–70/0–5 ppm) and aromatic (δ_C/δ_H 105–135/5.7–8.2 ppm) regions in the ^1H–^{13}C HSQC NMR spectrum (800 MHz, DMSO-d_6) of the fresh THF insolubles (TIS), and the highlighted characteristic signals. BHT = 3,5-di-tert-4-butylhydroxytoluene; THF = tetrahydrofuran.



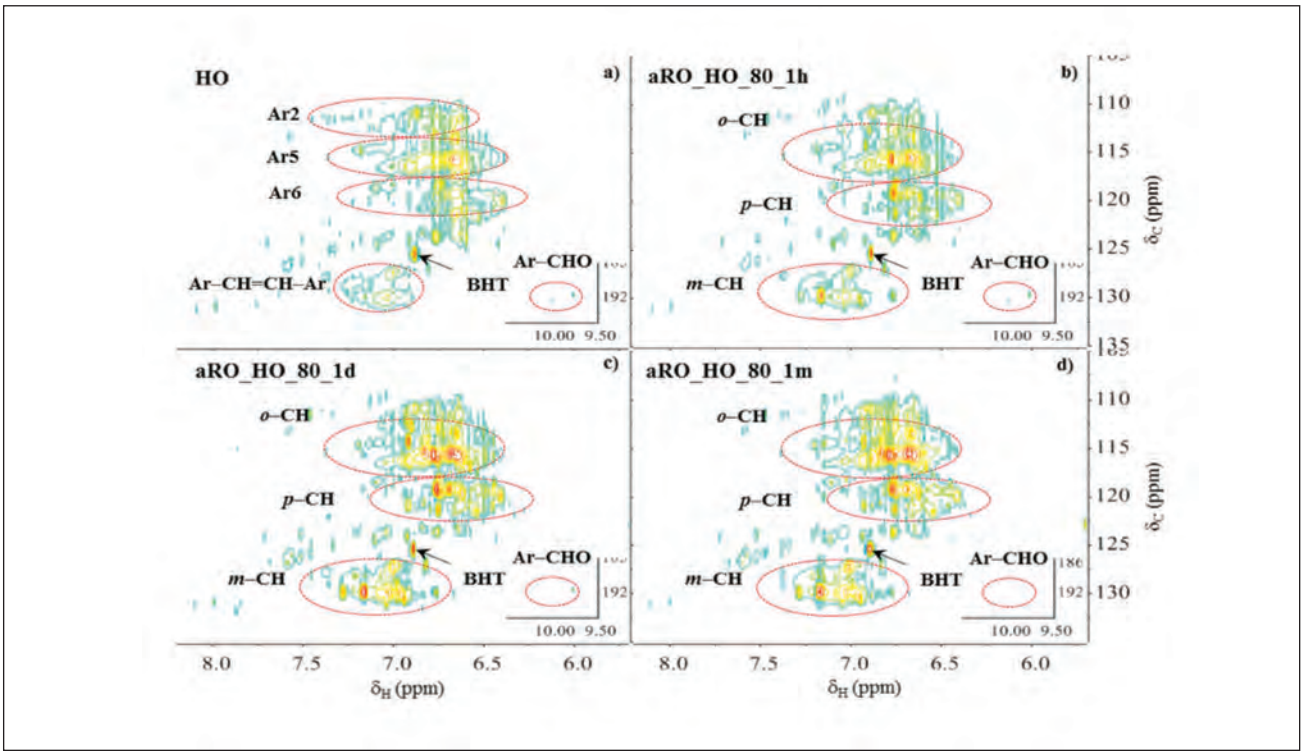
A5. Aliphatic regions (δ_C/δ_H 10–70/0–5 ppm) in the ^1H–^{13}C HSQC NMR spectra (800 MHz, DMSO-d_6) of the (a) fresh light oil (LO), (b) aged raw oil_light oil at 80°C for 1 hour (aRO_LO_80_1h), (c) 1 day (aRO_LO_80_1d), and (d) 1 month (aRO_LO_80_1m), and the highlighted characteristic signals. DEE = diethyl ether; THF = tetrahydrofuran; Ar = aromatic ring; α-, β-, and γ- = the aliphatic carbon from the aromatic ring.



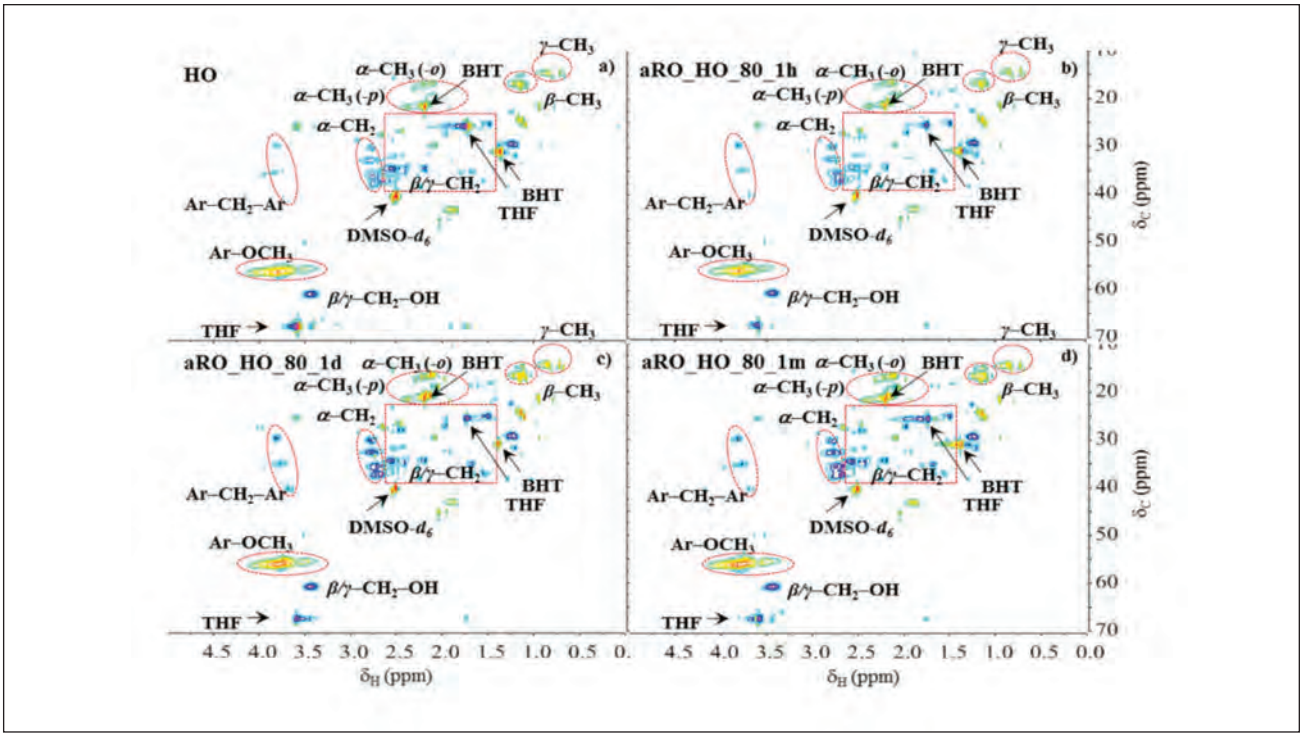
A6. Aromatic regions (δ_C/δ_H 105–135/5.7–8.2 ppm) in the ^1H–^{13}C HSQC NMR spectra (800 MHz, DMSO-d_6) of the (a) fresh light oil (LO), (b) aged raw oil_light oil at 80°C for 1 hour (aRO_LO_80_1h), (c) 1 day (aRO_LO_80_1d), and (d) 1 month (aRO_LO_80_1m), and the highlighted characteristic signals. Ar = aromatic ring.



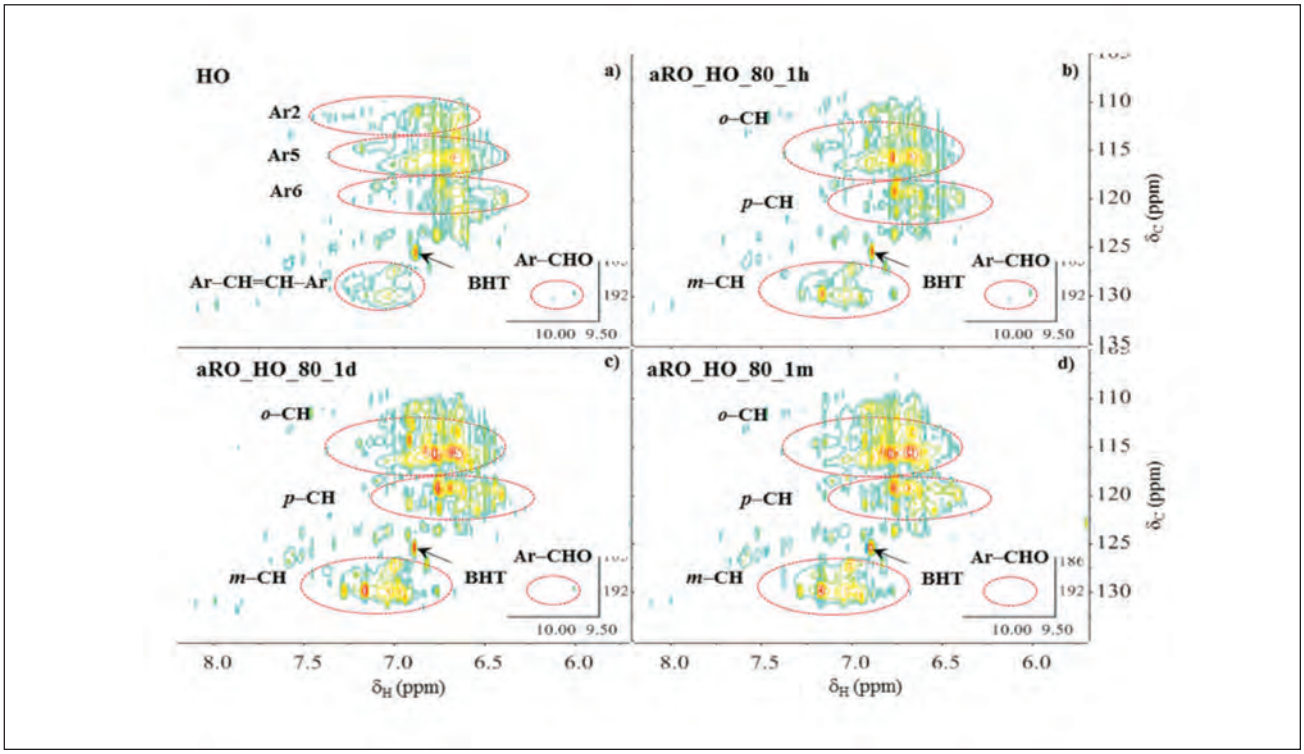
A7. Aliphatic regions (δ_C/δ_H 10–70/0–5 ppm) in the ^1H–^{13}C HSQC NMR spectra (800 MHz, DMSO-d_6) of the (a) fresh heavy oil (HO), (b) aged raw oil_heavy oil at 80°C for 1 hour (aRO_HO_80_1h), (c) 1 day (aRO_HO_80_1d), (d) 1 month (aRO_HO_80_1m), and the highlighted characteristic signals. BHT = 3,5-di-tert-4-butylhydroxytoluene; THF = tetrahydrofuran; Ar = aromatic ring; α-, β-, and γ- = the aliphatic carbon from the aromatic ring.



A8. Aromatic regions (δ_C/δ_H 100–160/5–10 ppm) in the ^1H–^{13}C HSQC NMR spectra (800 MHz, DMSO-d_6) of the (a) fresh heavy oil (HO), (b) aged raw oil_heavy oil at 80°C for 1 hour (aRO_HO_80_1h), (c) 1 day (aRO_HO_80_1d), (d) 1 month (aRO_HO_80_1m), and the highlighted characteristic signals. BHT = 3,5-di-tert-4-butylhydroxytoluene; Ar = aromatic ring.



A9. Aliphatic regions (δ_C/δ_H 10–70/0–5 ppm) in the ^1H–^{13}C HSQC NMR spectra (800 MHz, DMSO-d_6) of the (a) fresh THF insolubles (TIS), (b) aged raw oil_THF insolubles at 80°C for 1 hour (aRO_TIS_80_1h), (c) 1 day (aRO_TIS_80_1d), (d) 1 month (aRO_TIS_80_1m), and the highlighted characteristic signals. BHT = 3,5-di-tert-4-butylhydroxytoluene; THF = tetrahydrofuran; Ar = aromatic ring; α-, β-, and γ- = the aliphatic carbon from the aromatic ring.



A10.Aromatic regions (δ_C/δ_H 105–135/5.7–8.2 ppm) in the ^1H–^{13}C HSQC NMR spectra (800 MHz, DMSO-d_6) of the (a) fresh THF insolubles (TIS), (b) aged raw oil_THF insolubles at 80°C for 1 hour (aRO_TIS_80_1h), (c) 1 day (aRO_TIS_80_1d), (d) 1 month (aRO_TIS_80_1m), and the highlighted characteristic signals. BHT = 3,5-di-tert-4-butylhydroxytoluene; Ar = aromatic ring.

LITERATURE CITED

1. Bridgwater, A.V., *Environ. Prog. Sustainable Energy* 31(2): 261(2012).
2. Joseph, J., Rasmussen, M.J., Fecteau, J.P., et al., *Energy Fuels* 30(6): 4825(2016).
3. Alsbou, E. and Helleur, B., *Energy Fuels* 28(5): 3224(2014).
4. Ben, H. and Ragauskas, A.J., *ChemSusChem* 5(9): 1687(2012).
5. Boucher, M.E., Chaala, A., Pakdel, H., et al., *Biomass Bioenergy* 19(5): 351(2000).
6. Chaala, A., Ba, T., Garcìa-Pèrez, M., et al., *Energy Fuels* 18(5): 1535(2004).
7. Jiang, X., Zhong, Z., Ellis, N., et al., *Chem. Eng. Technol.* 34(5): 727(2011).
8. Jiang, X., Naoko, E., and Zhong, Z., *Chin. Sci. Bull.* 56(14): 1417(2011).
9. Li, H., Xia, S., Li, Y., et al., *Chem. Eng. Sci.* 135(10): 258(2015).
10. Garcìa-Pèrez, M., Chaala, A., Pakdel, H., et al., *Energy Fuels* 20(2): 786(2006).
11. Meng, J., Moore, A., Tilotta, D., et al., *ACS Sustainable Chem. Eng.* 2(8): 2011(2014).
12. Meng, J., Moore, A., Tilotta, D.C., et al., *Energy Fuels* 29(8): 5117(2015).
13. Samanya, J., Hornung, A., Jones, M., et al., *Int. J. Renewable Sustainable Energy* 1(3): 66(2011).
14. Nguyen Lyckeskog, H., Mattsson, C., Åmand, L.-E., et al., *Energy Fuels* 30(4): 3097(2016).
15. Belkheiri, T., Vamling, L., Nguyen, T.D.H., et al., *Cellul. Chem. Technol.* 48(9–10): 813(2014).
16. Belkheiri, T., Mattsson, C., Andersson, S.-I., et al., *Energy Fuels* 30(6): 4916(2016).
17. Nguyen, T.D.H., Maschietti, M., Belkheiri, T., et al., *J. Supercrit. Fluids* 86(2): 67(2014).
18. Nguyen, T.D.H., Maschietti, M., Åmand, L.-E., et al., *Bioresour. Technol.* 170(10): 196(2014).
19. Elliott, D.C., Oasmaa, A., Meier, D., et al., *Energy Fuels* 26(12): 7362(2012).
20. Mante, O.D. and Agblevor, F.A., *Waste Manage.* 32(1): 67(2012).
21. Chen, D., Zhou, J., Zhang, Q., et al., *Renewable Sustainable Energy Rev.* 40(12): 69(2014).
22. Yangfei, C., Zhiqin, C., Shaoyi, X., et al., *Thermochim. Acta* 476(1–2): 39(2008).
23. Ben, H. and Ragauskas, A.J., *Energy Fuels* 25(12): 5791(2011).
24. Giummarella, N., Zhang, L., Henriksson, G., et al., *RSC Adv.* 6(48): 42120(2016).
25. Huang, X., Korányi, T.I., Boot, M.D., et al., *Green Chem.* 17(11): 4941(2015).
26. Mattsson, C., Andersson, S.-I., Belkheiri, T., et al., *Biomass Bioenergy* 95(12): 364(2016).
27. Sudasinghe, N., Cort, J.R., Hallen, R., et al., *Fuel* 137(12): 60(2014).
28. Narani, A., Chowdari, R.K., Cannilla, C., et al., *Green Chem.* 17(11): 5046(2015).
29. Yue, F., Lu, F., Ralph, S., et al., *Biomacromolecules* 17(6): 1909(2016).
30. Nguyen Lyckeskog, H., Mattsson, C., Olausson, L., et al., *Biomass Convers. Biorefin.,* 2016, doi:10.1007/s13399-016-0228-4.
31. Wright, J.S., Shadnia, H., and Chepelev, L.L., *J. Comput. Chem.* 30(7): 1016(2009).

ABOUT THE AUTHORS

Lignin valorization is an important step toward renewable liquid fuel and can simultaneously increase profit for the kraft mill. Our work differs from previous studies because we investigated a higher storage temperature. The biggest challenge we had to overcome was to conduct a proper analysis of the high molecular weight lignin-derived bio-oil structure.

We found that the stability of the lignin-derived bio-oil we investigated is very good. This information can help pulp mill personnel determine whether to investigate technology to extract lignin from black liquor and process it further to liquid bio-oil. Our next step is to refine the bio-oil further.

Nguyen Lyckeskog is a doctoral candidate, Mattsson is a post-doctoral student, and Andersson, Vamling, and Theliander are professors at Chalmers University of Technology, Department of Chemistry and Chemical Engineering, Gothenberg, Sweden. Olausson is with Valmet Power AB, Gothenberg, Sweden. Email Theliander at hanst@chalmers.se.



Nguyen Lyckeskog



Mattson



Andersson



Vamling



Theliander



Olausson

An easy and reliable method for syringyl:guaiacyl ratio measurement

RAQUEL PRADO, LISA WEIGAND, SHIKH M.S.N.S. ZAHARI, XABIER ERDOCIA, JASON P. HALLETT, JALEL LABIDI, AND TOM WELTON

ABSTRACT: Lignin structure elucidation is one of the main targets for biorefinery related research. Because of its complexity, obtaining reproducible results in a straight-forward way is very important. One of the values that is used to compare different lignins is the syringyl:guaiacyl (S/G) ratio, which has been measured in different ways. The most reliable result is obtained for nitrobenzene oxidation, but this involves a complex process. In this work, the S/G ratios measured by pyrolysis-gas chromatography mass spectrometry (py-GCMS) and heteronuclear single quantum coherence-nuclear magnetic resonance (HSQC-NMR) spectroscopy were compared with attenuated total reflection infrared (ATR-IR) spectroscopy results to establish a reliable, quick, and simple method for the measurement. To achieve this, two mathematical models were applied with multivariate data analysis software. A partial least squares regression model for py-GCMS gave the best result.

Application: This study describes an easy way to characterize lignin.

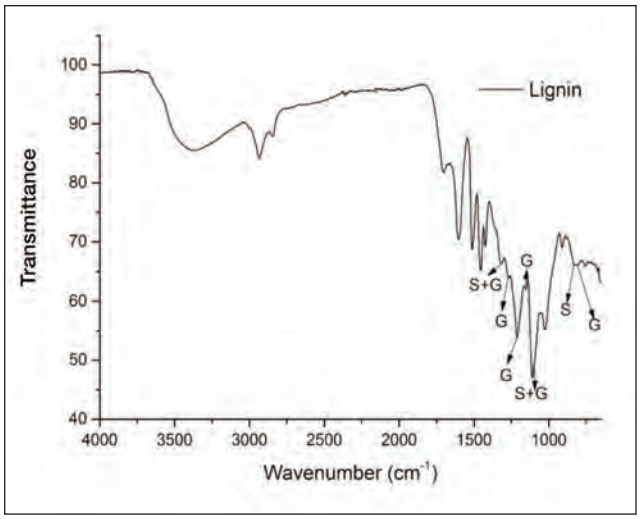
Lignin structure elucidation is an important but difficult task for biorefinery research. Lignin has a complex structure composed of a variety of substituted aromatic rings and is the only known renewable source of aromatic compounds. When lignin is depolymerized, the obtained products can be valuable as platform chemicals for numerous processes and lignin itself can be used for many applications [1]. Lignin is biosynthesised by dehydrogenative polymerization from L-phenylalanine via coumaril alcohol, coniferil alcohol and sinapyl alcohol, whereupon phenoxyl radicals are created, initiating a radical reaction that finally forms the lignin [2]. This radical mechanism is responsible for the variability of final lignin structures that can be different for every unit. Several authors have also demonstrated that lignin structure changes during its extraction [3,4,5]. However, there are certain similarities among the types of biomass, such as the proportion of the types of linkages and the phenolic monomers. For example, the coniferil alcohol proportion is 90%–95% in softwood, around 50% for hardwood, and around 75% for grasses, and the proportion of β-O-4 linkages is around 46% for softwood and 60% for hardwood [6].

The syringyl (S):guaiacyl (G) ratio is one of the most widely measured characteristics for lignin samples, and it is indicative of its composition. It has been measured successfully by thioacidolysis [7], permanganate oxidation, and alkaline oxidation with nitrobenzene, commonly known as nitrobenzene oxidation [8,9]. These techniques take a long time and have complex processes, which involve lignin oxidation with dioxane or nitrobenzene (highly harmful chemicals), and the final step is a chromatographic technique, either gas chromatography (GC) or high performance liquid chromatography (HPLC), to determine and quantify the composition of the lignin. In the search for easier ways to determine the S/G ratio, spectroscopic techniques such as Fourier transform-infrared (FT-IR) and nuclear magnetic resonance (NMR) have been investigated, not only for saving reaction time but also to decrease the use of harmful chemicals following one of the principles of green chemistry [10], but this has proven difficult because of sensitivity problems with these spectroscopic techniques. With quantitative heteronuclear single quantum coherence-nuclear magnetic resonance (HSQC-NMR) spectroscopy, good agreement with the measurements obtained by the nitrobenzene oxidation technique was achieved [11]. Finally, pyrolysis-gas chromatography mass spectrometry (py-GCMS) is a promising alternative. It gives results very close to those obtained by nitrobenzene oxidation, and it is a well-established, reliable, and reproducible technique [12].

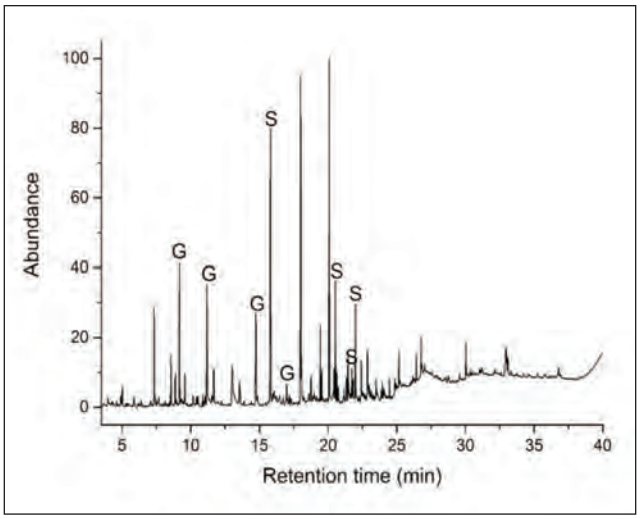
Chemometrics is a part of chemical science that uses algebraic calculation methods to extract quantitative or qualitative information from chemical data, particularly to identify trends. It is most commonly applied to spectral data [13]. Multivariate regression methods, such as principal component regression (PCR) and partial least squares regression (PLSR), have been designed to tackle situations in which there are many predictor variables and relatively few samples. They are widely applied, for example, in near infrared spectroscopy where the bands overlap and it is difficult to obtain quantitative information from the spectra. It is important to discard all the variations that are not related with the measurement conditions. When chromatography and spectral profiles are analyzed, it is necessary to normalize these to avoid the influ-

Sample	Biomass	Treatment	Conditions	Py-GCMS	NMR
1	Willow	Ionosolv	0.5 h, 120°C $[Et_3NH][HSO_4]$	1.28	1.59
2	Willow	Ionosolv	1 h, 120°C $[Et_3NH][HSO_4]$	1.52	1.55
3	Willow	Ionosolv	2 h, 120°C $[Et_3NH][HSO_4]$	2.06	1.92
4	Willow	Ionosolv	4 h, 120°C $[Et_3NH][HSO_4]$	2.62	3.1
5	Willow	Ionosolv	8 h, 120°C $[Et_3NH][HSO_4]$	2.49	2.76
6	Willow	Ionosolv	12 h, 120°C $[Et_3NH][HSO_4]$	2.24	3.15
7	Willow	Ionosolv	0.5 h, 150°C $[Et_3NH][HSO_4]$	1.93	1.35
8	Willow	Ionosolv	1 h, 150°C $[Et_3NH][HSO_4]$	1.38	1.27
9	Willow	Ionosolv	1.5 h, 150°C $[Et_3NH][HSO_4]$	1.73	1.42
10	Willow	Ionosolv	2 h, 150°C $[Et_3NH][HSO_4]$	2.33	2.34
11	Willow	Ionosolv	4 h, 150°C $[Et_3NH][HSO_4]$	2.41	2.48
12	Willow	Ionosolv	8 h, 150°C $[Et_3NH][HSO_4]$	2.53	2.11
13	Willow	Ionosolv	0.33 h, 170°C [Et3NH][HSO4]	2.81	2.26
14	Willow	Ionosolv	0.5 h, 170°C $[Et_3NH][HSO_4]$	1.86	2.25
15	Willow	Ionosolv	0.66 h, 170°C $[Et_3NH][HSO_4]$	1.83	2.48
16	Willow	Ionosolv	1 h, 170°C $[Et_3NH][HSO_4]$	0.73	2.33
17	Willow	Ionosolv	2 h, 170°C $[Et_3NH][HSO_4]$	2.56	2.35
18	Willow	Ionosolv	1 h, 150°C $[Et_3NH][HSO_4]$	2.81	3.04
19	Willow	Ionosolv	1 h, 150°C $[Et_3NH][HSO_4]$	2.14	1.97
20	Willow	Ionosolv	1 h, 150°C $[Hbim][HSO_4]$	2.24	2.28
21	Willow	Ionosolv	1 h, 150°C $[Hbim][HSO_4]$	2.06	2.11
22	Willow	Ionosolv	1 h, 150°C $[Et_3NH][HSO_4]$	2.51	2.40
23	Willow	Ionosolv	1 h, 150°C $[Et_3NH][HSO_4]$	1.88	2.30
24	Willow	Ionosolv	1 h, 150°C $[Hbim][HSO_4]$	2.20	2.09
25	Willow	Ionosolv	1 h, 150°C $[Hbim][HSO_4]$	0.91	0.99
26	Willow	Ionosolv	1 h, 150°C $[Hbim][HSO_4]$	0.88	0.88
27	Rice straw	Ionosolv	4 h, 120°C $[Et_3NH][HSO_4]$	1.37	1.32
28	*Mischantus*	Ionosolv	6 h, 120°C $[Et_3NH][HSO_4]$	1.43	1.43
29	*Mischantus*	Ionosolv	1 h, 150°C $[Et_3NH][HSO_4]$	1.39	1.40
30	Pine	Ionosolv	0.5, h 170°C $[Et_3NH][HSO_4]$	0.90	0.90
31	Pine	Ionosolv	0.5 h, 170°C $[Et_3NH][HSO_4]$	0.09	0
32	Pine	Ionosolv	0.5 h, 170°C $[Et_3NH][HSO_4]$	0.04	0
33	Pine	Ionosolv	0.5 h, 170°C $[Hbim][HSO_4]$	0.03	0
34	Pine	Ionosolv	0.5 h, 170°C $[Hbim][HSO_4]$	0.01	0
35	Pine	Ionosolv	0.5 h, 170°C $[Hbim][HSO_4]$	0.01	0
36	Pine	Ionosolv	0.5 h, 170°C $[Et_3NH][HSO_4]$	0.06	0
37	Pine	Ionosolv	0.5 h, 170°C $[Et_3NH][HSO_4]$	0.13	0
38	Pine	Ionosolv	0.5 h, 170°C $[Et_3NH][HSO_4]$	0.14	0
39	Baggasse	Ionosolv	2 h, 120°C $[Et_3NH][HSO_4]$	2.77	2.77
40	Baggasse	Ionosolv	4 h, 120°C $[Et_3NH][HSO_4]$	1.99	1.99
41	Willow	Organosolv	1.5, h 180°C EtOH	2.03	1.73
Py-GCMS = pyrolysis-gas chromatography mass spectrometry; NMR = nuclear magnetic resonance.					

I. Samples used for the calibration.



1. Attenuated total reflection infrared (ATR-IR) spectrum of willow lignin sample obtained by ionosolv process (120°C for 22 h).



2. Pyrolysis-gas chromatography mass spectrometry (py-GCMS) chromatogram of lignin sample.

ence of the size of the objects [14].

PCR and PLSR have been successfully applied to extract information in many instances. They are frequently used in medical chemistry, as in tumor classification and spatial analysis of brain images [15,16]. There is little difference between the use of PLSR and PCR; in most situations, similar results are achieved. However, PLSR normally requires fewer latent variables, so the model is better described and it is able to analyze correlated and noisy data, which can be very useful when spectral and chromatographic data are treated.

In this work, lignin from different sources (hardwood, softwood, and grass) and extracted by different processes (ionosolv and organosolv) from biomass were characterized to establish a model that relates attenuated total reflection infrared (ATR-IR) spectra with the S/G ratio measured by HSQC-NMR and py-GCMS. We compared both methodologies with the goal of finding a reliable, simple, and quick method to elucidate this ratio. This study will advance lignin structure elucidation and address the potential application of lignins as a source of process chemicals.

EXPERIMENTAL

Lignins from different species (willow varieties, pine, bagasse, rice husk, and *Mischanthus*), 41 different samples in total, obtained by different delignification processes (organosolv and ionosolv at different temperatures) (**Table I**) were characterized by ATR-IR, HSQC-NMR, and py-GCMS. The lignins were characterized and the data were analyzed with The Unscrambler software (CAMO Software; Oslo, Norway).

Organosolv process

The organosolv pulping was carried out under the following conditions: 60% (v/v) aqueous ethanol solution, solid:liquid ratio of 1:4 at 180°C for 90 min. The resultant solutions were filtered and washed with distilled water. Lignin was precipitated from the black liquor by adding water acidified to pH 2 by adding H_2SO_4. Then the mixture was centrifuged at 4000 rpm for 15 min. Lignin was washed with acidified water and dried at 70°C for 16 h.

Ionosolv process

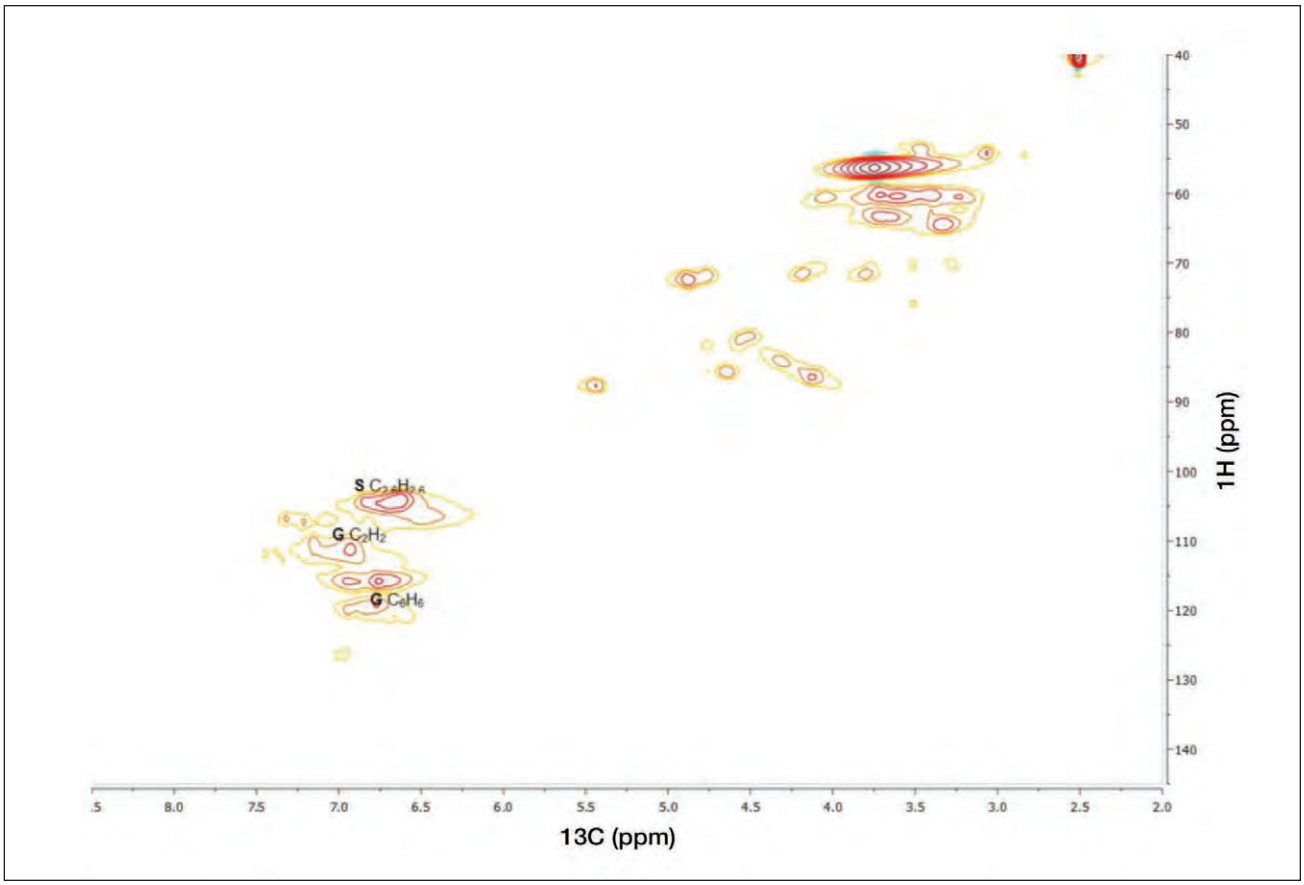
For the ionosolv process, biomass, water and ionic liquid (IL) were mixed in a mass ratio 1:2:8. Triethylamonium hydrogen sulfate $[Et_3NH][HSO_4]$ and butylimidazolium hydrogen sulfate $[Hbim][HSO_4]$ were used as the ionic liquids and mixtures were treated at different temperatures (120°C–170°C) and different times (0.5-22 h). Then the resultant solutions were filtered with Whatman 542 filter paper and washed with three volumes of ethanol (30 mL). The ethanol of the black liquor was removed by evaporation. Lignin was precipitated by adding 2 volumes of distilled water (20 mL) and then centrifuging at 4000 rpm for 15 min. Lignin was washed with distilled water and dried at 70°C for 16 h.

The ATR-IR spectra were collected by placing a particle of each sample onto the window of the ATR device. A background spectrum was measured before the sample spectrum in all cases (**Fig. 1**) [17].

S/G ratio calculation

The S/G ratio from py-GCMS was calculated by dividing the sum of the area of the syringol-related peaks (syringol, 4-ethylsyringol, 4-vinylsyringol, and 4-propenylsyringol) against the sum of the area of guaiacol-related peaks (guaiacol, 4-methylguaiacol, 4-vinylguaiacol, and vanillin) (**Fig. 2**) [12]. The $G_{(C_2H_2)}$ signal was used as an internal standard, with the following equation:

$$(1)\ \frac{S}{G} = \frac{S_{(C_{2,6}H_{2,6})}}{(G_{(C_2H_2)} + G_{(C_6H_6)})} \qquad (1)$$



3. Heteronuclear single quantum coherence-nuclear magnetic resonance (HSQC-NMR) spectroscopy of lignin sample.

Figure 3 shows the HSQC-NMR of a representative lignin sample where S and G ring signals are detected. Where $G_{(C_2H_2)}$ was assigned to the 6.93-110.10 ppm peak, $G_{(C_{2,6}H_{2,6})}$ was assigned to the 6.64–104.21 ppm peak, and $G_{(C_6H_6)}$ was assigned to the 6.77–119.13 ppm peak. All of these were integrated with $G_{(C_2H_2)}$ as the reference [18,19].

For the ATR-IR

The Unscrambler multivariate analysis software was used to establish the relationship between the ATR-IR spectra and the S/G ratio calculated by HSQC-NMR and py-GCMS. PLR and PLSR models were chosen for the multivariate analysis. **Table II** details the specifications of each model. Analysis of the data can lead to different conclusions as to which is the best model to be applied, if there is a good relation between IR spectra and S/G ratio, and which measurement has better correlation.

Instruments

All lignin samples were characterized by attenuated-total reflectance infrared spectroscopy (ATR-IR) by direct transmittance in a single-reflection ATR system (ATR top plate fixed to an optical beam condensing unit with a zinc selenide lens) with a Specac (Orpington, UK) Golden Gate ATR accessory. Spectral data were acquired over 10 scans in the range of 4000–650 cm^{-1} and 4 cm^{-1} resolution.

HSQC-NMR spectra were recorded at 30ºC on a Bruker (Karlsruhe, Germany) Avance 600 MHz NMR spectrometer equipped with a z-gradient BBI probe. Typically, 20 mg of sample was dissolved in 0.6 mL of dimethyl sulfoxide-d_6. The pyrolysis device was a CDS Analytical (Oxford, PA, USA) Pyroprobe 5150. The pyrolysis temperature was set at 600°C for 15 s with a heating rate of 2°C $msec^{-1}$. Helium was used as the carrier gas from the pyrolyzer to the GC.

GC-MS analysis was performed to identify the monomers in the lignin structure. After pyrolysis, the lignin monomers were transferred by the inner line and injected into an Agilent GC (7890A)-MS (5975C inert MSD with Triple-Axis Detector) (Agilent; Santa Clara, CA, USA) equipped with a HP-5MS capillary column ([5%-phenyl]-methylpolysiloxane, 60 m × 0.32 mm). The temperature program started at 50°C and was raised to 120°C at a rate of 10°C min^{-1}, held for 5 min, raised to 280°C at a rate of 10°C min^{-1}, held for 8 min, raised to 300°C at a rate of 10°C min^{-1}, and finally held for 12 min. Helium was used as the carrier gas.

RESULTS AND DISCUSSION

Figure 1 shows the ATR-IR spectrum of one representative lignin sample. The bands were assigned as shown in **Table III**. This lignin spectrum was chosen as a general example to show the assignments of the bands to the different

Principal Component Regression Model		Partial Least Squares Regression Model	
X-variables	Spectra	**X-variables**	Spectra
Y-variables	S/G	**Y-variables**	S/G
Number of components	10	**Number of factors**	10
Validation	Leverage correction	**Validation**	Leverage correction/Cross validation
Algorithm	NIPALS	**Algorithm**	NIPALS*
NIPALS = non-linear iterative partial least squares.			

II. Multivariate analysis conditions.

816	CH out of plane in positions 2, 5, and 6 of G units
824	CH out of plane deformation in 2 and 6 position on S ring and in all positions of H units
912	CH out of plane deformation
1031	C-O deformation, primary OH plus CO stretching in unconjugated ketones and aromatic CH in plane deformation
1075	CO deformation in secondary alcohols and aliphatic ethers
1114	Etherified G ring + S unit and secondary hydroxyl plus CO stretching
1153	Aromatic CH in plane deformation in the G ring
1213	G ring breathing plus C=O stretch
1268	G ring breathing with carbonyl stretching
1323	S ring and G ring condensed
1362	Phenolic OH and aliphatic CH in methyl groups
1425	Aromatic skeletal vibrations combined with CH in plane deformation
1456	CH deformation in methyl and methylene groups
1514	Aromatic skeletal vibrations
1603	Aromatic skeletal vibrations
1724	C=O stretch in unconjugated ketones, carbonyl, and ester groups
2851	CH stretching methyl and methylene
2921	CH stretching methyl and methylene
3380	OH stretching

III. Attenuated total reflection infrared (ATR-IR) spectroscopy bands.

aromatic structures present in the lignin and to highlight the bands specifically related to G and S rings. We observed that the bands assigned to G and S rings are found between 1400 cm^{-1} and 800 cm^{-1}. Other bands related to aromatic rings in general were seen in the range of 1700 cm^{-1} to 650 cm^{-1}.

In py-GCMS, the lignin is decomposed into its main monomers and other fragments that confirm its structure. The chromatogram is basically divided into three parts. The first is more related to the sugar fraction present in the lignin from 3 min to 11 min, the second is mainly composed of phenolic monomers from 9 min to 26 min, and the third is composed of complex aromatics and fatty acids from 26 min to 50 min. Figure 2 shows a typical lignin chromatogram, in which it can be observed that lignin is mainly composed of phenolic derived fragments. The peaks taken into account for the calculation of the S/G ratio have been marked. G itself is the peak at 9.78 min and S is the peak at 15.839 min, but other structures derived from these have been introduced in the calculation.

Figure 3 depicts a representative lignin HSQC-NMR spectrum. The signals needed for the calculation of S/G in accordance with Eq. (1) are marked in Fig. 3. The spectra can be divided into different sections for lignin, side chain region (δC/δH 50–95/2.5–6.0 ppm) and the aromatic region (δC/δH 95–160/5.5–8.0 ppm).

Spectra Range	Samples	Variable	Components	Modelled	Predicted
4000–650 cm^{-1}	Softwood, hardwood, grass	NMR	4	0.8636	0.8190
		GCMS	5	0.8986	0.8417
1825–650 cm^{-1}	Softwood, hardwood, grass	NMR	7	0.8976	0.8253
		GCMS	5	0.8909	0.8188
	Hardwood, grass	NMR	5	0.9680	0.9450
		GCMS	4	0.9673	0.9467

NMR = nuclear magnetic resonance; GCMS = gas chromatography mass spectrometry.

IV. Principal component regression (PCR) results.

Multivariate analysis

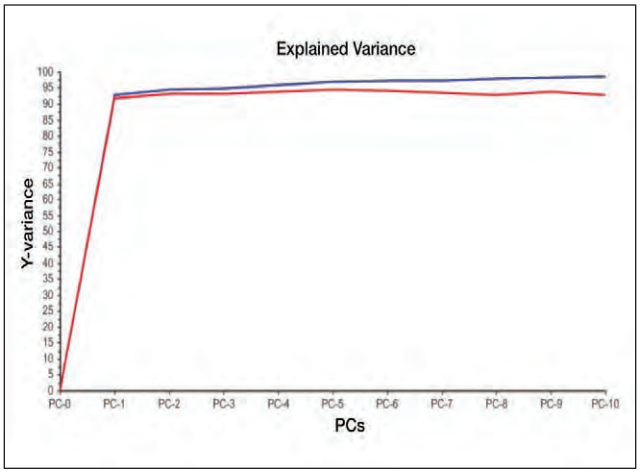
The data treatment was accomplished using The Unscrambler software, which is widely used for multivariate analysis and design of experiments. PCR and PLSR models were independently applied to the data to decide which gave the best approach. PCR is generally considered to be a more robust model, whereas PLSR is often a better approach for spectra data analysis.

The data matrix was composed of 41 rows that are the lignin samples disposed in rows, two columns with the S/G ratios calculated by py-GCMS and HSQC-NMR, which are the response variables, and 837 columns of spectral data that are the predictor variables. The best model result was chosen according to the regression coefficient, the number of components for PCR and factors for PLSR, and the explained variance curve. The target is a model with a high regression coefficient, a low number of components, and low variance.

First, PCR was chosen as the model to apply to the data matrix with all the samples and the whole IR spectra with the S/G ratio measurements. **Table IV** shows the results obtained from the PCR model. The first row shows results for the initial approach. The best regression coefficient was obtained for the py-GCMS measurement. However, more components were needed to define the calibration than for HSQC-NMR. The predicted curve also did not match the model curve very well for more than three components. Hence, it was discarded.

To improve the results, the spectral range was reduced to cover only the aromatic ring-related part and was set from 1825 cm^{-1} to 650 cm^{-1}. The second row of Table IV shows the results. Nevertheless, the result was contrary to that expected; more components were needed to have a good regression coefficient. Furthermore, the difference between the model curve and the predicted curve was higher; the predicted curve did not match the model at all. The obtained variance was not acceptable.

Finally, the softwood S/G ratio is very low because of the tiny concentration of syringyl in softwood lignin, making this ratio hard to measure, especially by NMR, resulting in outcomes with high standard deviations. The third row in Table IV shows the results of applying the PCR model to hardwood and grasses. As a result, the regression coefficient was substantially improved and the variance was acceptable up to five components (see **Fig. 4** in which the predicted curve is depicted). Similar regression coefficients were obtained for NMR and py-GCMS measurements of the S/G ratio, but more components were needed to define the NMR calibration curve. To have less modification of the data and to give a better prediction, the aim is to reduce the number of components that define the model.



4. Principal component regression (PCR) modelled and predicted curve.

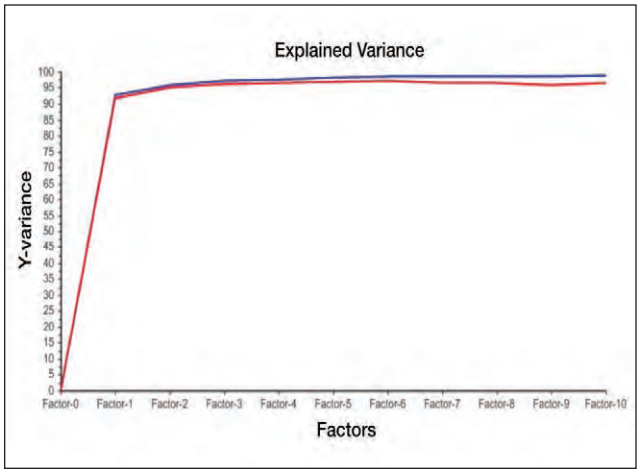
The PLRS model was applied in an attempt to improve on the results obtained by the PCR. The PLSR model was applied in the same way as the PCR to be comparable. The results of the application to the whole spectra are shown in the first row of **Table V**. The obtained regression coefficient improved in comparison to the ones obtained for the PCR model. The drawback was the number of factors needed in each case, which was eight for NMR and seven for py-GCMS. The best variance was obtained for two factors, as observed in the comparison of predicted curve with the modelled curve.

To reduce the number of factors in the final equation, the

Spectra Range	Samples	Variable	Factors	Modelled	Predicted
4000–650 cm^{-1}	Softwood, hardwood, grass	NMR	8	0.9560	0.9219
		GCMS	7	0.9484	0.9064
1825–650 cm^{-1}	Softwood, hardwood, grass	NMR	7	0.9470	0.9196
		GCMS	6	0.9454	0.9052
	Hardwood, grass	NMR	5	0.9815	0.9721
		GCMS	3	0.9778	0.9704

NMR = nuclear magnetic resonance; GCMS = gas chromatography mass spectrometry.

V. Partial least squares regression (PLSR) results.



5. Partial least squares regression modelled and predicted curve.

spectral range was reduced to 1823–650 cm^{-1} as this range is more related to the aromatic structure; the results are shown in the second row of Table V. After reducing the spectra, the best regression coefficient was obtained with less factors but the obtained regression coefficient was worse than for the previous modelling. In addition, the variance was not acceptable for any factor. This result was discarded.

Finally, when softwood samples were deleted, a huge improvement in the regression coefficient was observed as shown in the third row of Table V. The improvement was from 0.92–0.90 to 0.97 together with a decrease of factors needed to define the model. With only three factors, the calibration curve for the S/G ratio measured by py-CGMS was defined and very good regression coefficient was obtained. In addition, the variance was acceptable up to six factors (see **Fig. 5** in which the predicted curve is depicted). For the S/G ratio measured by NMR, the regression coefficient was slightly higher at 0.972, but five factors were needed to achieve this result. As mentioned before, the results obtained by py-GCMS seem to be more reliable for a calibration with IR spectra data as the integration is easier and less dependent on the human factor.

CONCLUSION

Lignin was characterized by ATR-IR, py-GCMS, and HSQC-NMR for the calibration of S/G ratios with ATR-IR spectra. Using multivariate analysis, it was determined that the results obtained by py-GCMS had better correlation with the IR spectra and the best approach was obtained with the PLRS model. The regression coefficient was 0.97. The curve was defined with only three factors, with a good variance result. Hence, py-GCMS is a good characterization technique to determine the S/G ratio. In addition, it does not require manipulation of the sample, no solvent is required, and the quantity needed for running the experiment is very small compared with other techniques. Although this method is robust and reliable, the quantity of the original sample is usually not known. Therefore, the method can only give relative amounts and should be considered semi-quantitative. We have also demonstrated that ATR-IR can be calibrated with py-GCMS to obtain the S/G result. This information can be very useful in developing a sensor able to have a quick response. Lignin from different sources and processes can be initially characterized by py-GCMS and calibrated with ATR-IR to obtain the algorithm relating the S/G ratio with the spectrum. Further, lignins can then be characterized by simple ATR-IR alone by applying the obtained algorithm to give the S/G ratio. **TJ**

ACKNOWLEDGEMENTS

We thank the UK Engineering and Physical Sciences Research Council (EP/K014676/1) for support.

LITERATURE CITED

1. Toledano, A., Serrano, L., and Labidi., J., *J. Taiwan Inst. Chem. Eng.* 44(4): 552(2013).
2. Vanholme, R., Demedts, B., Morreel, K., et al., *Plant Physiol.* 153(3): 895(2010).
3. Kumar, P., Barret, D.M., Delwiche, M.J., et al., *Ind. Eng. Chem. Res.* 48(8): 3713(2009).
4. Erdocia, X., Prado, R., Corcuera, M.A., et al., *J. Ind. Eng. Chem.* 20(3): 1103(2014)

5. Prado, R., Erdocia, X., and Labidi, J., *J. Chem. Technol. Biotechnol.* 88(7): 1248(2013).
6. Lanzalunga, O. and Bietti. M., *J. Photochem. Photobiol., B* 56(2-3): 85(2000).
7. Ona, T., Sonoda, T., Itoh, K., et al., *Holzforschung* 51(5): 396(1997).
8. Reeves, J.B., *J. Dairy Sci.* 69(1): 71(1986).
9. Sun, R., Lawther, J.M., and Banks, W.B., *Ind. Crops Prod.* 4(4): 241(1995).
10. Martínez, A.T., Almendros, G., González-Vila, F.J., et al., *Solid State NMR* 15(1): 41(1999).
11. Sette, M., Wechselberger, R., and Crestini. C., *Chem. – Eur. J.* 17(34): 9529(2011).
12. Nunes, C.A., Lima, C.F., Barbosa, L.C.A., et al., *Bioresour. Technol.* 101(11): 4056(2010).
13. Otto, M., *Chemometrics: Statistics and Computer Application in Analytical Chemistry*, Wiley-VCH, Weinheim, Germany, 2007.
14. Wold, S., Sjöström, M., and Eriksson. L., *Chemom. Intell. Lab. Syst.* 58(2): 109(2001).
15. Mevik, B.H. and Wehrens, R., *J. Stat. Software.* 18(2): 1(2007).
16. Depczynski, U., Frost, V.J., and Molt. K., *Anal. Chim. Acta* 420(2): 217(2000).
17. Skoog, D.A., Hooler, F.J., and Nieman, T.A., *Principles of Instrumental Analysis*, McGraw-Hill, Madrid, Spain, 2001.
18. Yuan, T.Q., Sun, S.N., and Xu, F., et al., *J. Agric. Food. Chem.* 59(19): 10604(2011).
19. Wen, J.L., Sun, S.L., Xue, B.L., et al., *Materials* 6(1): 356(2013).

ABOUT THE AUTHORS

We chose this topic to research because I (Welton) have been dealing with the complexity of lignin characterization. The study will ease the way of samples characterization.

The most difficult part of this study was organizing the data sheet. From the study, we learned that statistics are an important tool for characterizing complex structures. We were pleased to see a good correlation between py-GC-MS and ATR-IR.

We expect that mills will benefit from this new, facile way to characterize lignin. The next step could be the development of a new sensor.



Prado



Zahari



Welton



Hallett



Weigand



Erdocia



Labidi

Prado is researcher, Zahari is professor, and Welton is dean, Department of Chemistry; Hallett is senior lecturer, Department of Chemical Engineering; and Weigand is Ph.D. student, Department of Chemistry and Department of Chemical Engineering, Imperial College London, London, UK. Erdocia is doctor and Labidi is professor, Chemical and Environmental Engineering Department, University of the Basque Country, San Sebastian, Spain. Email Welton at t.welton@imperial.ac.uk.

Analysis of economically viable lignin-based biorefinery strategies implemented within a kraft pulp mill

CÉDRIC DIFFO TÉGUIA, ROD ALBERS, AND PAUL R. STUART

ABSTRACT: Many pulp and paper companies are considering implementing a lignin-based biorefinery to diversify their core business to new products and improve their longer-term competitiveness. The best strategy to achieve might not be obvious, considering the lignin extraction process and derivatives to be implemented over the longer term that meet market and business objectives, and provide competitive advantage. In this article, various lignin biorefinery strategies were considered in a case study involving lignin precipitation processes integrated within an existing kraft mill, and solvent pulping processes that would be implemented in parallel to the existing mill processes using additional hardwood. The analysis aimed to identify the conditions under which various strategies would represent suitable investments. Operating constraints in the case study mill limited lignin extraction to 85 metric tons/day from 15% of the mill's black liquor, whereas 260 metric tons/day lignin could be extracted by solvent pulping 1500 metric tons/day of hardwood. The preferred strategies identified by the study were lignin precipitation to phenolic resins production, and solvent pulping to carbon fiber production. The first product-process strategy requires lower investment, provides high returns (internal rate of return [IRR] of 39% to 43%), and is more easily implemented in the near term. Solvent pulping resulted in reasonable profitability (IRR of 18% to 25%), with higher production volumes and a diversified product portfolio, and was considered more suitable as a longer-term strategy. Business model robustness and long-term competitiveness can be better assured by combining both strategies. It was shown that 1) government support to offset capital cost, and 2) high derivatives market prices positively influence lignin valorization strategies, which are sensitive to technology and market maturity.

Application: This study illustrates how a technical and economic analysis could be used to identify lignin-based biorefinery strategies that represent an attractive investment.

In recent years, certain segments of the pulp and paper industry have experienced stable growth, led by emerging markets in Asia and Latin America [1,2]. The forecasted trend is for a timid growth going forward [3]. These global numbers overshadow a more difficult situation for certain geographic and market segments, and most forestry companies today are actively pursuing transformation through product diversification to procure their competitive position in the longer term.

Biorefinery strategies related to the improved management of hemicelluloses, and from the sale of lignin either found in black liquor or extracted by wood fractionation processes, offer good potential for diversification, especially for kraft pulp mills that have traditionally focused on the sale of cellulose. Lignin is interesting as a basic chemical because of its complex chemical structure with aromatics, methoxyl groups, and a variety of other functional units [4]. As a result, lignin is being explored for a wide range of market applications [5], either by partially using it in a formulation or by exploiting specific functionalities. However, investment in a lignin-based biorefinery strategy is not obvious because of a number of factors. These include 1) technology maturity – especially for the case of solvent pulping, 2) uncertainty in the understanding of the linkage that exists between lignin properties and specific market applications, and 3) uncertainty around the reproducibility of lignin-based product properties, etc.

The purpose of this paper is to evaluate lignin-based biorefinery strategies implemented in retrofit to an existing kraft pulp mill. The defined product-process strategies, implemented using a phased approach over several years, consider technology and market risk mitigation. A techno-economic analysis is performed to identify lignin-based biorefinery strategies that represent an attractive investment. In this project, we addressed the following objectives:

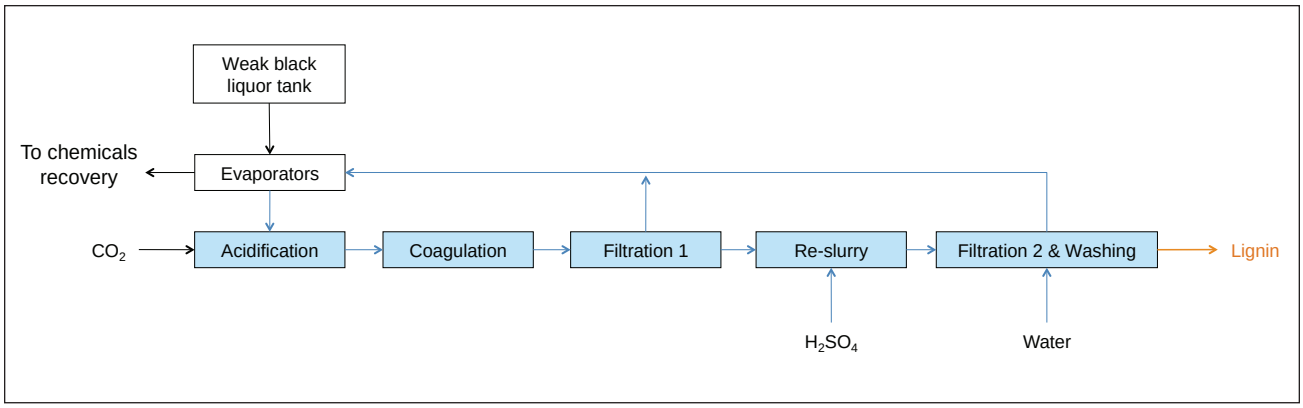
1. Characterize the lignin biorefinery in terms of extraction processes and downstream derivatives.
2. Define a set of promising product-process combinations that could be integrated to an existing kraft pulp mill using a phased implementation strategy.
3. Evaluate the economic performances of the strategies, and analyze critical factors for their success.

THE LIGNIN-BASED BIOREFINERY

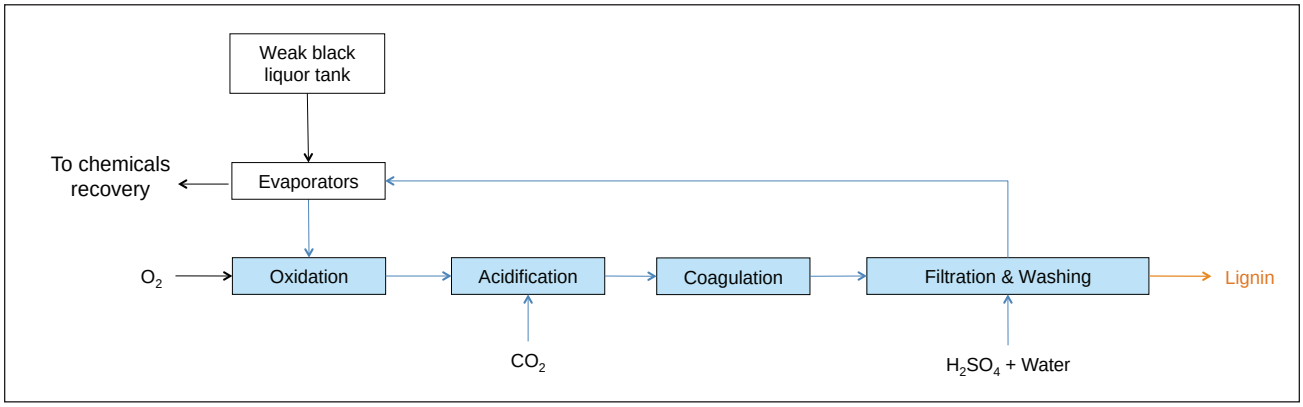
Lignin extraction processes

The common nomenclature used for generic lignin types recognizes the difference between native lignin, as it forms in

ECONOMIC ANALYSIS



1. Block flow diagram of the LignoBoost process.



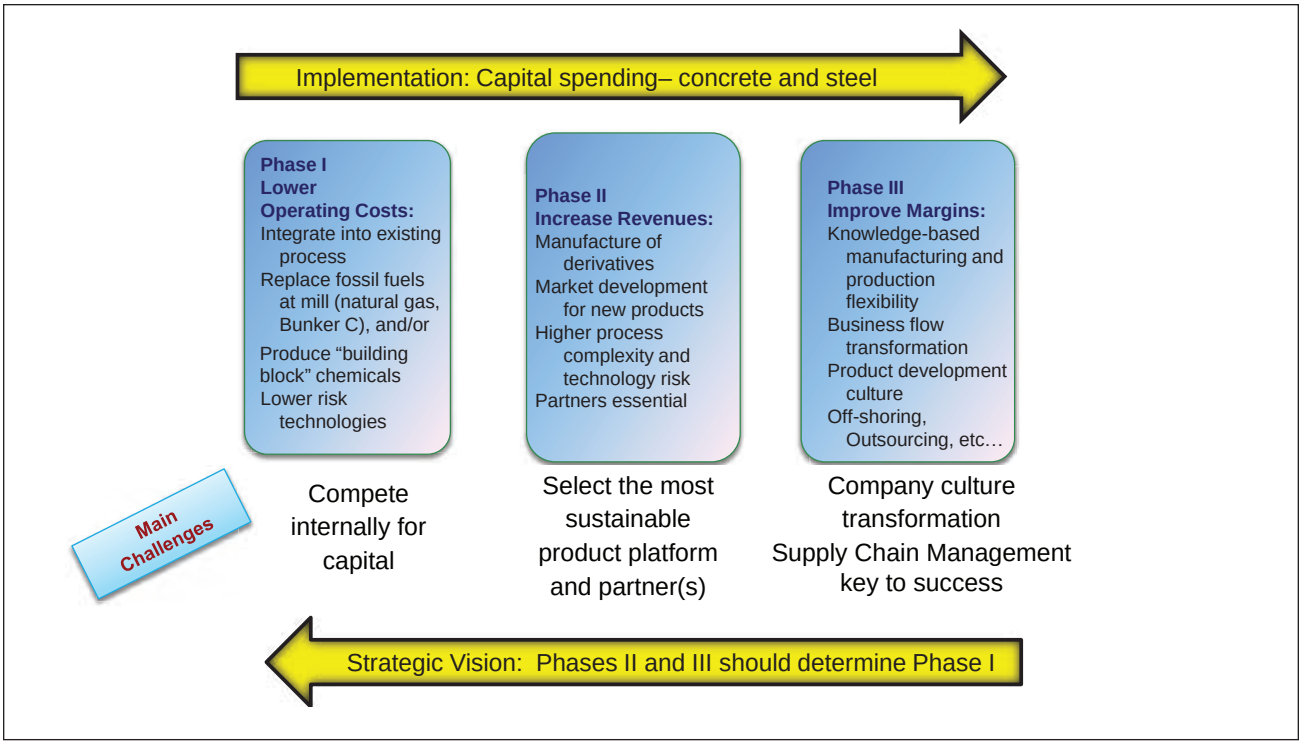
2. Block flow diagram of the LignoForce process.

plants, and technical lignins, as obtained from diverse industrial processes. It is practical to classify technical lignins based on physical and chemical conditions in the extraction processes that lead to the final structure and functionality of the lignin [6].

Agbor et al. [7] present an extensive review of existing biomass fractionation processes. They did not, however, define the technologies reviewed with the specific purpose of isolating lignin. Biomass fractionation processes can be classified according to comminution (i.e., mechanical size reduction) and biological, chemical, and physical-chemical characteristics. Comminution methods are mainly used to increase the specific surface area of wood before digestion. Biological processes are currently less practical at the industrial scale because of the long residence times required. Physical-chemical pretreatments include most of the fractionation processes that have been developed (steam explosion, dilute acid pretreatment, and ammonia fiber expansion) and the use of organic solvents (organosolv) for pretreatment, among others. In this category, organosolv pretreatment appears promising for lignin extraction, especially for those processes where the operating and separation conditions produce minimum damage to the lignin structure. The mixture of water and organic solvent (often ethanol) used in organosolv pulping leads to a purer lignin than do processes that use sulfurous solvents. Organosolv lignin is recognized as a high-purity, low molecular weight lignin [8,9].

Valuable products can be obtained from hemicelluloses and extractives present in pulping spent liquors. The low proportion of extractives renders economies-of-scale complex to establish, whereas hemicelluloses isolation can be achieved using membrane filters [10]. In kraft black liquor, lignin is kept in colloidal form by repulsion forces that the charged phenolic and carboxylic acid groups create between lignin particles. Disrupting black liquor's properties, such as pH, temperature, or ionic strength, can reduce repulsion forces and lead to lignin precipitation. The most common method consists of acidification using carbon dioxide, sulfuric acid, or a combination of both to lower the pH of the black liquor from 13–13.5 to 9–10. The resulting precipitated lignin must be filtered and washed [11,12].

The first commercial scale plant for lignin precipitation from black liquor was implemented by Domtar in its mill in Plymouth, NC, USA, using the LignoBoost technology developed by Innventia in association with Chalmers University of Technology and supplied by Valmet (**Fig. 1**) [13]. In this technology, the acidification is followed by an initial filtration of lignin. Following a re-slurry of the lignin cake in dilute sulfuric acid, a second filtration step is then performed. More recently, the LignoForce technology has been introduced by FPInnovations, commercialized by NORAM (Vancouver, BC, Canada) (**Fig. 2**), and recently implemented at the West



3. Phased-approach for the strategic implementation of a biorefinery [26].

Fraser mill in Hinton, AB, Canada [14,15]. This technology introduces an oxidation step before the acidification and uses a press filter in a single filtration washing step.

Lignin conversion into added-value derivatives

Black liquor is combusted in the kraft pulp mill recovery boiler to produce steam and green liquor. Lignin can be separated from the black liquor to the extent that acceptable combustion conditions can be maintained, or when lignin is produced by fractionating wood using an organosolv process. Lignin separated from black liquor can be used for numerous fossil-based products, among which phenol-formaldehyde (PF) resins and carbon fibers appear as promising [16,17].

Because of their affinity for wood and wood fibers, liquid phenolic resins are used for the specialty wood adhesives industry. Wood bonding applications such as particleboard, medium-density fiberboard, or waferboard/plywood have traditionally used phenolic resin binders. The interest in lignin for use in phenolic resins resides in its high substitution potential for phenol. The substitution level for phenol can potentially be higher than 50% [18], but 30% remains a practical maximum tested at the commercial scale to meet a range of board processing and product requirements (e.g., bond strength, hardening time, and the mechanical properties of panels). Lignin can essentially be directly mixed with phenol and formaldehyde to formulate PF resins. Currently, this method is limited to a relatively low percentage of lignin because of the amount of reactive sites in the lignin structure. A chemical modification of lignin, such as phenolation, can be used to overcome this limitation [19]. Phenolation requires mixing lignin with phenol to improve its reactivity, before blending with formaldehyde or additional phenol.

Lignin also has potential as an inexpensive and abundant replacement of polyacrylonitrile (PAN), which is the most conventionally used carbon fiber precursor. Higher production volumes and a wider use of carbon fibers are currently limited by the feedstock cost, which can contribute to more than half of production costs and has high market price volatility [20]. Recent research by Oak Ridge National Laboratory in the United States has focused on melt-spun PAN, polyolefins, and lignin as low-cost alternative precursors, targeting structural (e.g., vehicles, aerospace, infrastructure) and non-structural applications (e.g., thermal management, electronics). Lignin usage challenges remain regarding production at higher scales and the mechanical properties of the resulting fibers [21].

The conventional carbon fiber manufacturing process consists of four main steps: 1) fiber spinning, 2) stabilization, 3) carbonization, and 4) surface treatment. In some applications, carbonization is followed by a graphitization step [22]. A study by Kadla et al. [23] demonstrated the potential to manufacture carbon fibers via melt spinning using organosolv and hardwood kraft lignins. However, softwood kraft lignin failed to pass the spinning step (it charred at temperatures above 140°C). Eckert and Abdullah [24] demonstrated that charring could be prevented by acetylating lignin such that its acetyl content is at least 16% before spinning. Acetic anhydride is a suitable acetylating agent for that purpose. More recent work by Norberg [25] shows another alternative, which is to separate the kraft black liquor into two molecular weight fractions using an ultrafiltration membrane before

acidification, and to use the lower molecular weight fraction for carbon fiber manufacturing. This method has been successfully used with hardwoods, softwoods, and combinations of the two feedstocks.

Phased biorefinery implementation

Every biorefinery strategy implies technology and business risks to different extents, and should incorporate implementation approaches that mitigate risk to the extent possible. Such an approach has been introduced by Chambost et al. [26] and further applied by Jeaidi et al. [27] to the context of mechanical pulp mills (**Fig. 3**). They suggest a phased implementation of biorefinery strategies, nominally over three phases. The longer-term phases (II and III) are defined first, and these determine the near-term implementation phase. Phases I and II are where technology disruption mainly occurs, while phase III implies mainly business disruption. Phase II represents the longer-term evolution of the product portfolio, while phase I represents the risk mitigation stage(s) implemented to gradually achieve the longer-term goals.

To invest, companies expect that their biorefinery strategy should result in high returns and an enhanced competitive position, considering the integration of new bioproducts within the existing product portfolio. Phase I in the near-term (typically <5 years) should involve the implementation of low to no-risk technologies that would be part of the overall process in the long run. Ideally, these technologies lead to the production of building blocks or intermediate products to provide early profits in the development of the biorefinery. Besides technology and business risk mitigation, an advantage of the sequential implementation is that it can potentially provide flexibility to change the orientation of phase II as processes and markets evolve in the bioeconomy, in case a more valuable strategy is identified during the phase I implementation period.

The timeline for each phase is case-specific. In many cases, the timelines for the later phases will depend on the ability of the pulp and paper company to create partnerships, capture market share, and reach targeted production and sales volumes before switching from one phase to the next. The case study developed in this article focuses on the assessment of biorefinery implementation in phases I and II, with additional analyses of the effect of the length of phase I on the overall economic return of the project.

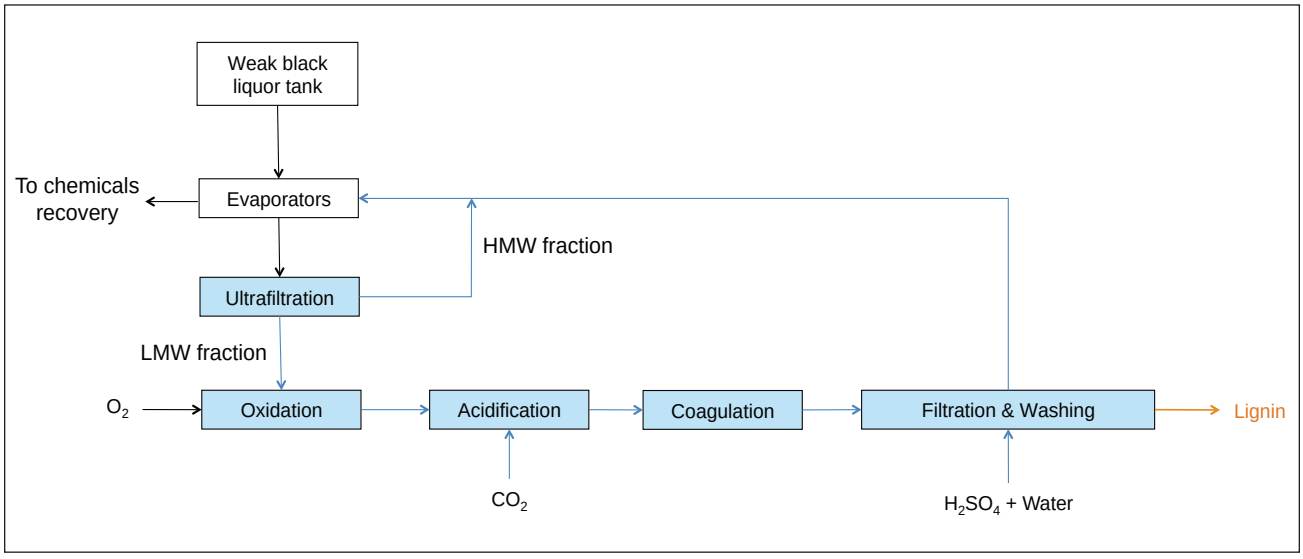
CASE STUDY

The case study considers an existing kraft pulp mill producing 1500 air-dried metric tons/day of softwood pulp. In addition to black liquor from the kraft process, potential feedstock for the biorefinery includes unused biomass in the forest management area owned by the mill, of approximately 1500 moisture-free metric tons/day of hardwood sawlogs. Lignin extraction from black liquor is limited to the extent that would maintain suitable burning properties of the black liquor, thus ensuring good operation of the recovery boiler. A major concern for the pulp mill was to maintain the quality and amount of pulp because of existing long-term agreements with customers.

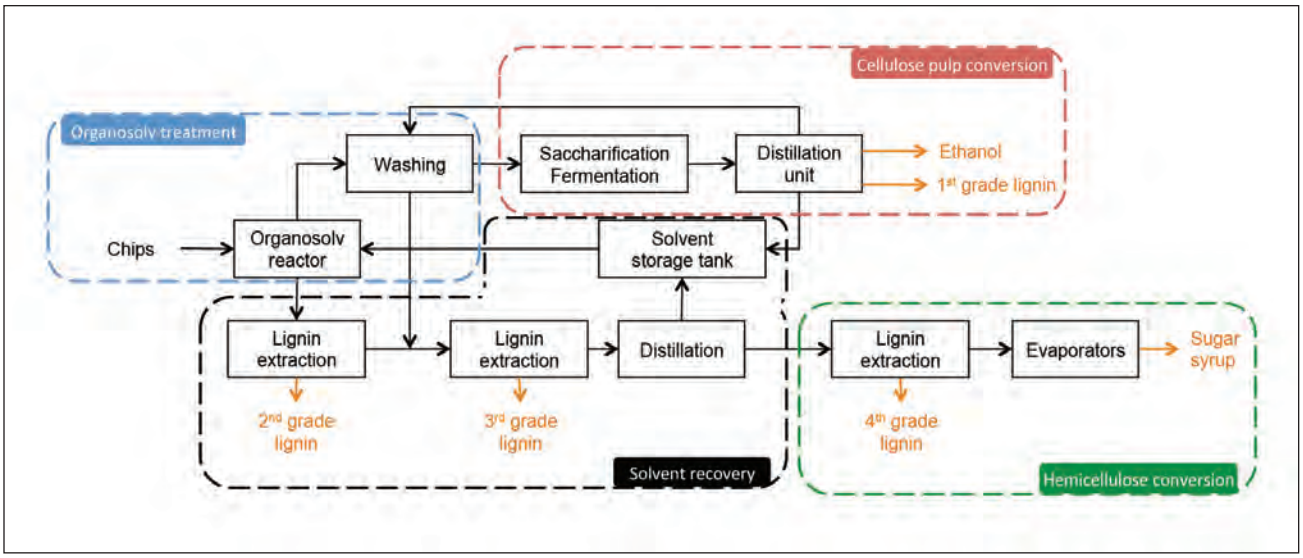
METHODOLOGY

Lignin-based biorefinery strategies were defined by combining process and product possibilities, as well as their phased-approach for implementation. To avoid affecting the existing mill pulping process by hardwood chips, strategies were separated into two categories: 1) integrated processes that would use black liquor as the main feedstock, defined as the lignin precipitation (LP) strategy, and 2) non-integrated hardwood conversion processes defined as the organosolv or more specifically, solvent pulping (SP) strategy.

Relevant information was collected for the completion of



4. Block flow diagram of the second lignin precipitation strategy (LP2), incorporating ultrafiltration (LMW = low molecular weight; HWM = high molecular weight).



5. Block flow diagram of the organosolv solvent pulping (SP) process base cast strategy.

mass and energy balances, and combined in a large-block analysis [28] to obtain comparable capital and operating costs estimates for each phase of the strategies defined. Energy balance simulations of some process units were carried out using Aspen Plus (AspenTech; Bedford, MA, USA) chemical process optimization software. Other calculations relative to mass balances, process economics, and cash flows were made using Microsoft Excel software.

Definition of product-process combinations

The LignoBoost process was considered the most mature of the lignin precipitation technologies and was selected as the base case (LP base case) (Fig. 1). The LignoForce process is the main comparison alternative (LP1), and differences in economics were estimated (Fig. 2). A second alternative consists of incorporating ultrafiltration technologies before black liquor acidification in conjunction with the LignoForce process (LP2), and using only the lower molecular weight fraction in subsequent operations (**Fig. 4**). This strategy is interesting because of its implication for the production of carbon fibers. Not having to pretreat the kraft lignin before spinning increases savings in capital and operating costs, and affects the overall profitability. For the LP process alternatives, estimates were based on a lignin production capacity of 85 metric tons/day. Lignin recovered in the first two strategies (LP base case and LP1) was defined as "kraft lignin" and lignin from LP2 was defined as "ultrafiltrated kraft lignin."

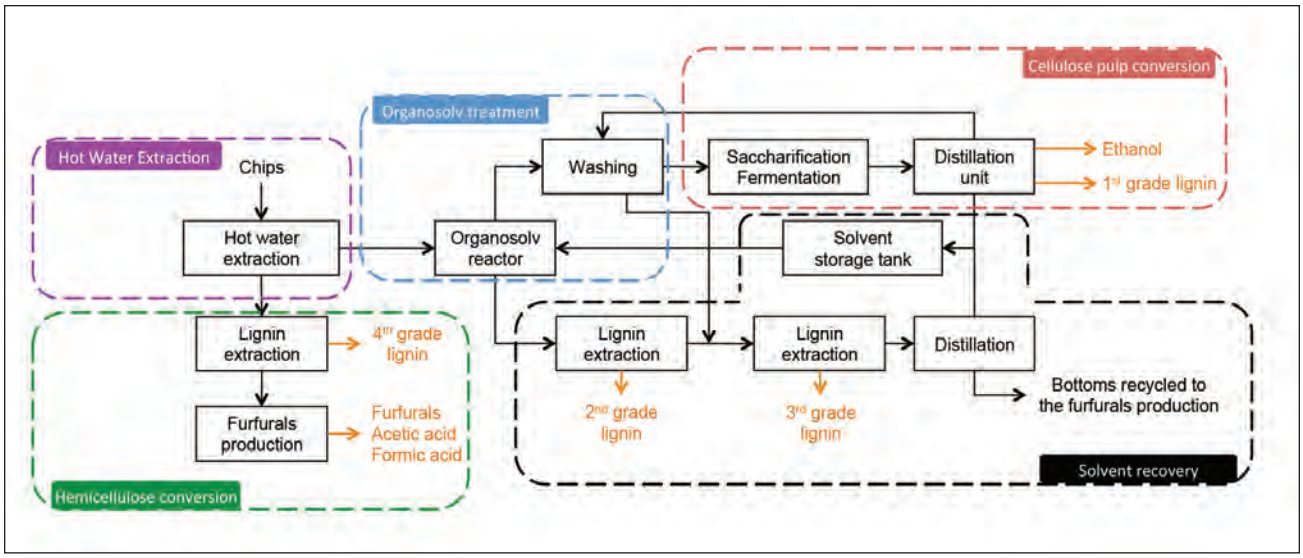
Phenolic resins and carbon fibers are the only two lignin derivatives assessed in the case study. They would be produced in phase II. Lignin was converted either into a PF resin or a carbon fiber precursor and sold to a manufacturer downstream on the value chain during phase I to mitigate market risks. For PF resin applications, lignin was phenolated before sale to resin manufacturers as a phenol replacement. For carbon fiber applications, kraft lignin was acetylated and sold as a PAN replacement; ultrafiltrated kraft lignin was sent to the market without any additional modification.

The organosolv process, as developed by Alcell and further improved by Lignol [29], was defined as the base case for solvent pulping (SP base case) (**Fig. 5**). Solvent-based fractionation and the conventional pulping of wood chips have many similarities. This makes it easier to adopt the new technology at the mill and mitigates certain risks associated with technology disruption. Although there are several potential lignin extraction spots along the SP process, the differentiation between lignin grades was not considered in the process evaluation. All the lignin collected was assumed to be mixed into a single stream identified as "organosolv lignin."

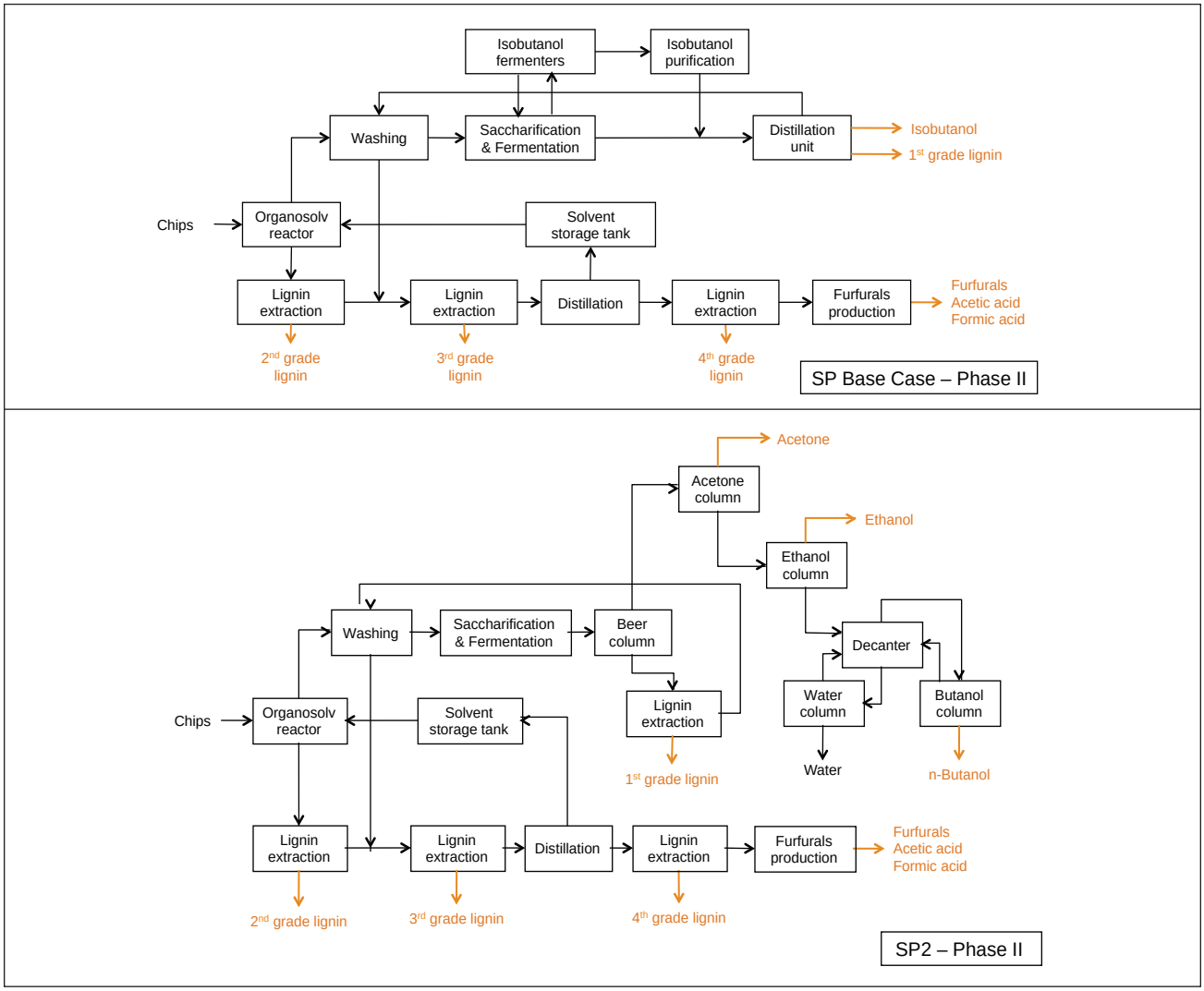
To make the biorefinery strategy comparisons consistent, the sequence of business phases for the sale of lignin derivatives is the same for the LP and SP alternatives. In the case of carbon fibers production, and similarly with ultrafiltrated kraft lignin, organosolv lignin was considered to not require any pretreatment and sold as-is during phase I. Because the focus of the case study is on lignin, products identified as "preferred derivatives" have been selected for cellulose and hemicellulose conversion, considering a minimum risk approach.

Although ethanol production through C6 sugar fermentation is well established in North America, the current trend is toward replacing ethanol with butanol, as the latter provides several advantages (e.g., higher energy content, better compatibility with automobile systems, higher blending potential with gasoline [30]). Companies such as Gevo and Butamax have developed processes for converting existing ethanol production plants into butanol plants [31], and several projects are expected in the coming years. Two approaches have been considered for butanol production: 1) implement the organosolv process for ethanol production in phase I and convert the cellulose line into a butanol plant during phase II, or 2) implement the acetone-butonal-ethanol (A-B-E) process [32] (com-

ECONOMIC ANALYSIS



6. Block flow diagram of SP1 strategy, incorporating hot water extraction.



7. Block flow illustrations of SP base case and SP2 strategies in phase II.

		SP Base Case	SP1	SP2	SP3
Phase I	C6 sugars	Ethanol		Acetone n-Butanol Ethanol	
	C5 sugars	Sugar syrup	Furfural	Sugar syrup	Furfural
	Lignin	Precursor of either PF resin or carbon fiber			
Phase II	C6 sugars	Isobutanol	Acetone	Acetone n-Butanol Ethanol	
	C5 sugars	Furfural			
	Lignin	PF resin or carbon fiber			

I. Summary of solvent pulping biorefinery strategies considered in the case study.

	Process Block	Lang Factor
Organosolv-related blocks	Organosolv treatment	2.80
	Ethanol/butanol production	
	Solvent recovery	
Non-organosolv blocks	Feedstock storage	1.97
	Product storage	
	New boiler(s)	
	Hot water extraction	
	Lignin conversion	
	Furfural production	2.01

II. Process blocks and associated Lang factors used for techno-economics of solvent pulping (SP) strategies.

monly used to produce butanol, with ethanol and acetone as byproducts) and start butanol production during phase I. Butanol from the A-B-E process (n-butanol) would be used for chemical applications; butanol from retrofitting ethanol processes (isobutanol) would target biofuel applications.

Furfural has been selected among possible hemicellulose derivatives for its market potential [33] and the maturity of processes for its manufacturing. Formic and acetic acids are co-products. The implementation approach proposed for this strategy consists of converting hemicellulose into a C5 sugar syrup to be sold as animal feed in phase I, before converting sugars into furfural during phase II. In the pulp and paper industry, hemicellulose extraction processes are increasingly used as pretreatment units to isolate C5 sugars and convert these into higher-value products [7, 34]. This strategy is considered as an alternative in the case study, by implementing a hot water extraction process [35] before the organosolv reactor (**Fig. 6**).

Overall, four strategies were defined for the SP category combining the implementation approaches for butanol and furfural (**Table I**). **Figure 7** represents the evolution of the SP base case to isobutanol and furfural production in phase II, and the alternative strategy producing n-butanol (SP2).

Process techno-economics

Techno-economic estimates involve determining a realistic value for capital and operating costs, and for expected revenues that depend on future market prices. The techno-economics for most biorefinery projects is most sensitive to the latter, around which there is high uncertainty.

Equipment costs were estimated by assessing comparable processes in the literature, including projects and equipment similar to those for which estimations were being made. Cost data were scaled to the capacity required for the case study and actualized using cost index factors. Commonly used design heuristics were used to estimate components of direct and indirect capital costs for the LP processes. For the SP processes, after equipment costs were obtained, the Lang method [36] was applied. This method uses factors to obtain order-of-magnitude estimates of capital investment from equipment

costs. This method was considered appropriate because detailed cost information on the organosolv process was scarce. Different Lang factors have been applied to operating units of the SP processes, as summarized in **Table II**. For cash flow calculations, a 2-year construction period was assumed for each of the implementation phases. Two cases were considered for the internal rate of return (IRR) calculations for each product-process strategy:

- IRR for phase I was calculated as though run for 20 years ("Phase I" in the figures).
- IRR for phase I was calculated for 5 years, then phase II is implemented and run for 20 years ("Phase I + Phase II" in the figures).

Table III summarizes other main assumptions of economic calculations. Regarding lignin derivatives, specific discounts were applied to assumed market prices to reflect market penetration strategies. Discounts applied vary from 10% to 20% for different lignin types and applications, based on judgement.

Scenarios definition and sensitivity analysis

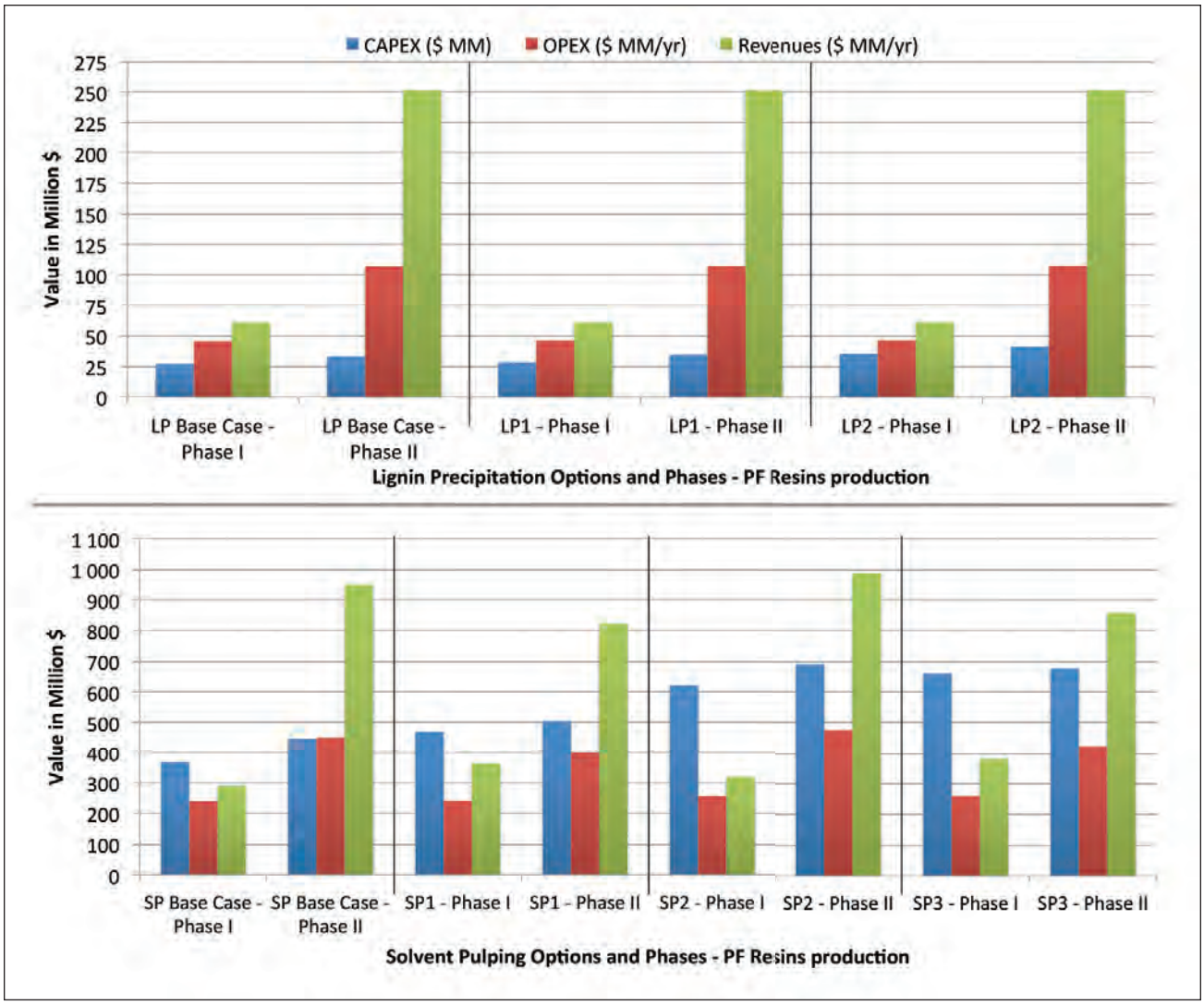
Based on the results of the preliminary profitability assessment, a scenario representing the preferred strategy was developed. A sensitivity analysis was performed on this scenario, considering five parameters identified as critical to the profitability of the case study strategies: 1) capital cost subsidy, 2) process scale, 3) the length of phase I, 4) the market price of phenol, and 5) the market price of carbon fiber.

Capital cost subsidy considered the minimum of 1) 50% of phase I capital requirements, and 2) $100 million. Subsidies are considered only for phase I.

The effect of process scale was assessed on the SP processes for biomass procurement capacities of 1) 500 metric tons/

Parameter	Assumptions / Values
Feedstock costs • Biomass • CO_2 • O_2 • H_2SO_4 • Caustic	• $100/moisture-free metric ton • $300/metric ton • $50/ metric ton • $180/metric ton • $430/metric ton
Product prices 1. Phenol, phenol-formaldehyde (PF) resin 2. Polyacrylonitrile (PAN), carbon fiber 3. Ethanol 4. n-butanol, isobutanol 5. Sugar syrup 6. Furfural	1. $1005/metric ton and $2000/metric ton 2. $2480/metric ton and $15,430/metric ton 3. $0.49/L ($1.84/gal) 4. $1.36/L ($5.15/gal, sold as a chemical); $0.81/L ($3.08/gal, sold as a fuel) 5. $170/metric ton 6. $1600/metric ton
Taxes	33% on net income
Depreciation	Accelerated method • Year 1: 25% of fixed capital investment (FCI) • Year 2: 50% of FCI • Year 3: 25% of FCI
Production ramp-up	• Year 1: 70% of nominal capacity • Year 2: 90% of nominal capacity • Years 3+: 100% of nominal capacity
Lignin usage	• Year 1: 80% burnt, 20% sold as derivative precursor • Year 2: 20% burnt, 80% sold as derivative precursor • Years 3-5: 100% sold as derivative precursor • Years 6+: 100% sold as final customer product
Discount on market price, per type of lignin	PF resin applications: 10% Carbon fiber applications • Kraft lignin: 20% • Ultrafiltrated kraft lignin: 15% • Organosolv lignin: 10%

III. Main assumptions for economic calculations.



8. Summary of techno-economics for lignin-based phenol-formaldehyde (PF) resins production.

day (i.e., the same lignin production capacity as lignin precipitation [LP] producing 85 metric tons/day of lignin), and 2) up to 2335 metric tons/day (inventory of pulp logs and sawlogs in the forest) on a dry basis.

The length of phase I was evaluated from 3 years (2-year construction + 1-year production) to 27 years (2-year construction + 25 years of the "Phase I + Phase II" scenario).

RESULTS

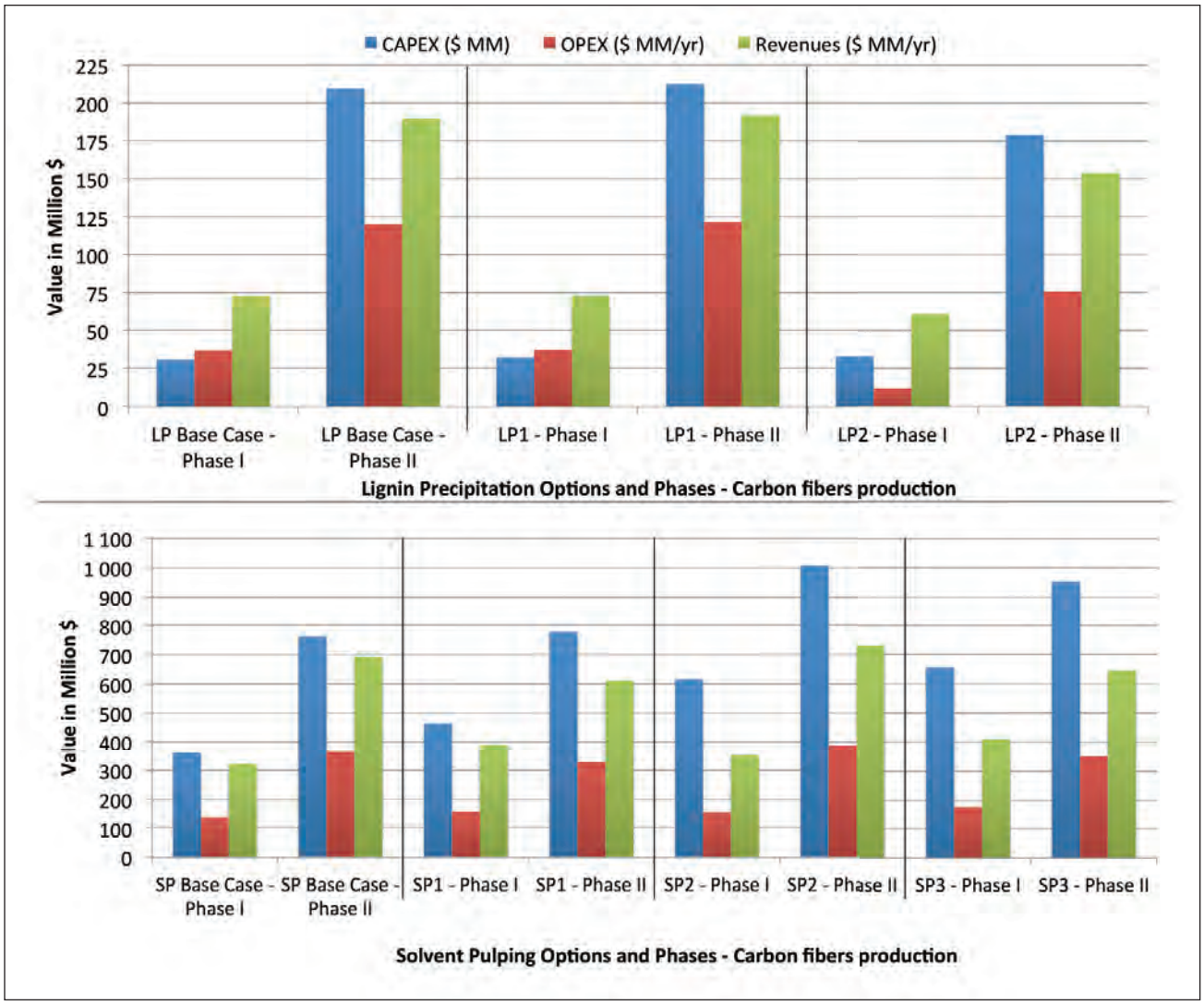
With 1500 metric tons/day of hardwood supply, 260 metric tons/day of lignin can be extracted for the SP base case process, whereas only 85 metric tons/day are recovered from the acidification of 15% of the mill black liquor. This amount of lignin results in the production of 178 metric tons/day of resin precursor in Phase I and 410 metric tons/day of PF resin in Phase II, for the case of LP strategies. The same conversion yields apply to organosolv lignin. In the case of carbon fibers production, a yield of 42% is estimated for organosolv lignin and ultrafiltrated kraft lignin, and a 53% yield is assumed for kraft lignin. This difference is because of the mass increase that occurs during acetylation of kraft lignin.

Techno-economic performance

Figures 8 and **9** summarize the results of cost and revenue estimates for each phase of the production of PF resins and carbon fibers, respectively. These results are specific only to the case study mill because they take into consideration integration and other costs that are related to the existing processes (e.g., materials handling, power island, and wastewater treatment plant). Costs and revenues are much lower for LP strategies than for SP processes; however, direct comparison between LP and SP categories is difficult because of the magnitude of the scale difference between the two types of processes. Regardless of the lignin extraction process, carbon fibers appear more costly to produce than PF resins.

Figures 10 and **11** present the IRR estimates for "Phase I" alone, and "Phase I + Phase II" for PF resins and carbon fibers production, respectively. For PF resins production, LP strate-

ECONOMIC ANALYSIS



9. Summary of techno-economics for lignin-based carbon fibers production.

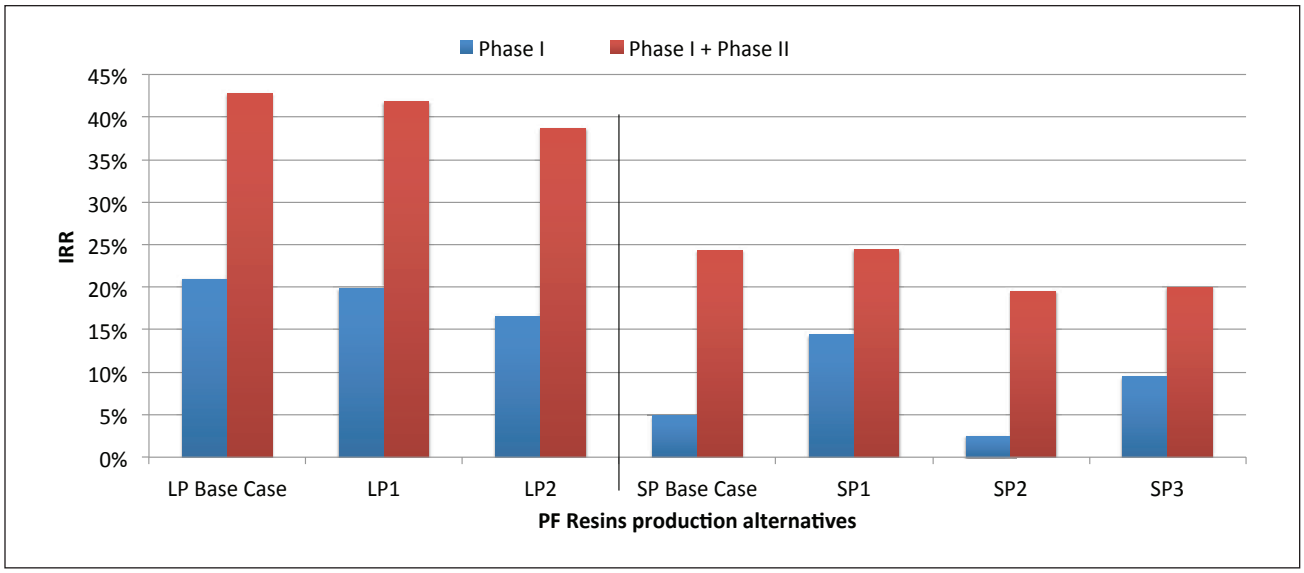
gies are generally more profitable than SP ones, at each phase of biorefinery implementation. Results are more balanced in the case of carbon fiber production, for which ultrafiltrated kraft lignin (LP2) presents substantially better results. The production of PF resins is more interesting in the "Phase I + Phase II" scenarios, while in the case of carbon fibers, the production of precursors ("Phase I" scenarios) are more profitable.

Scenarios analysis

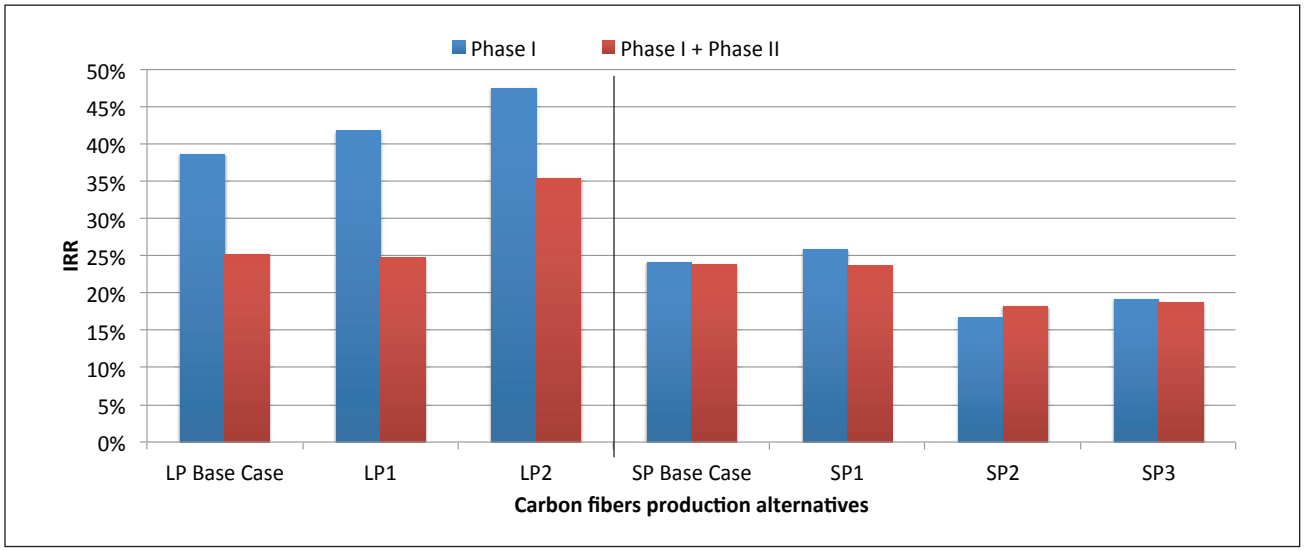
Lower investment requirements, a more mature technology, and a good IRR result in LP processes and PF resins production being the most promising in the short-term. In the longer term, SP processes will become preferred because higher production volumes are required for capturing market share and added-value lignin-based products are manufactured from differentiated lignin. Furthermore, SP processes result in a better IRR for carbon fibers production. Therefore, the strategy selected for the scenarios analysis combined LP and SP processes as follows:

- Phase I — Lower risk phase
  - LP2 integrated to existing mill, producing PF resins precursor.
  - SP base case demonstration plant (300 metric tons/day of hardwood) for carbon fiber development.
- Phase II — Commercial scale development
  - LP2 evolves to carbon fiber precursor production.
  - SP base case commercial scale plant implemented (1500 metric tons/day), producing carbon fiber precursors, ethanol, and sugar syrup.
- Phase III — Full implementation of the product portfolio
  - Carbon fiber manufacturing strategy evolves from precursors to carbon fiber production.
  - Ethanol and sugar syrup units evolve, respectively, to isobutanol and furfural production.

Figure 12 presents the results of the sensitivity analysis applied to this "LP+SP strategy." The allowance of capital cost subsidy, or a higher carbon fiber price, make the strategy



10. Profitability of phenol-formaldehyde (PF) resins production strategies.



11. Profitability of carbon fibers production strategies.

much more attractive. As well, a higher phenol price benefits short-term profitability. From another perspective, a low-capacity commercial scale or a longer-than-expected phase I reduces the profitability of the strategy.

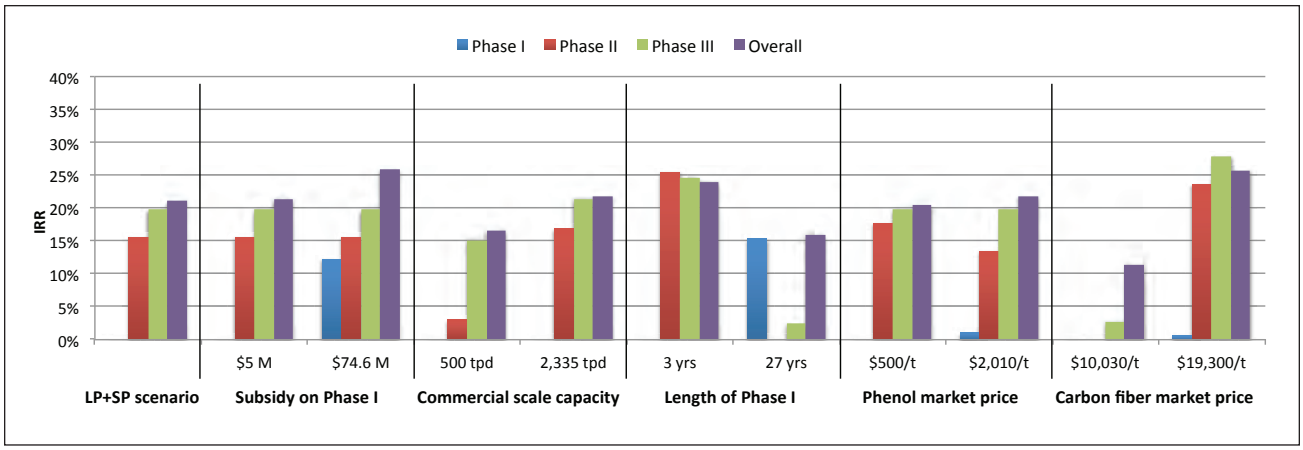
DISCUSSION

Although the estimates for biorefinery implementation are context-specific and have high uncertainty, some generalities can be extrapolated from the case study.

For this case study, obtaining PF resins from lignin precipitation processes was the preferred strategy for the short term. Revenue from this strategy is limited by capacity constraints of the kraft mill recovery cycle. SP strategies performed better when combined with carbon fiber production.

Solvent pulping processes are capital-intensive. Considering their level of risk, especially during scale-up, this is a significant discouraging factor to their implementation in the near term. Further, depending on the existing mill power island and the process steam demand, the integration of SP processes into existing mills might require the purchase of a new boiler and adapting the chip handling system or the wastewater treatment facility. Nonetheless, the resulting diversified product portfolio can potentially provide significant additional revenue streams in the early years of an implemented project if the market conditions are realized.

Combining LP and SP processes into a single strategy provides the opportunity to develop a unique competitive advantage regarding lignin markets, and the production of high-value derivatives in the longer-term. At the same time, short-term risks are mitigated by more developed applications



12. Sensitivity analysis for the "LP+SP" lignin-based biorefinery strategy.

such as phenol replacement in PF resins. A vertically integrated company that owns forest management areas, pulp mills, and plywood manufacturing plants would have a considerable advantage in this regard. Capital cost subsidy significantly enhances the profitability of the transformation strategy, and should be considered essential to mitigate short-term risk.

CONCLUSIONS

Beyond the need to generate positive cash flows in the short term, pulp and paper companies have the opportunity to define their long-term biorefinery strategy through substantial volumes of added-value product streams. In this project, the context of the lignin-based biorefinery implemented at a kraft pulp mill has been considered, for which integrated lignin precipitation and parallel solvent pulping strategies were assessed for the production of PF resins or carbon fiber. These strategies would be implemented using a phased approach, where phase II involves the manufacture of added-value products, and phase I is defined to mitigate short-term risks in a way that supports the transition to phase II. This analysis shows that 1) PF resins production from lignin precipitation and 2) carbon fibers production from solvent pulping are profitable strategies. Lignin precipitation, including ultrafiltration of black liquor before acidification, is a promising alternative for carbon fiber production. Two important drivers are technology maturity and the ability to match production volume with market demand, which will depend on the speed to market maturity. In this regard, combining lignin precipitation and solvent pulping for the production of PF resins in the short-term and carbon fiber in the longer term appears to be a competitive and robust strategy. **TJ**

ACKNOWLEDGMENTS

This work was funded by a Collaborative Research and Development (CRD) grant from the Natural Sciences and Engineering Research Council of Canada (NSERC). The authors would like to thank industrial partners in the project, who provided access to operating facilities, process and technology data, and expertise for the validation of assumptions and results.

LITERATURE CITED

1. Pöyry PLC, "Paper and paperboard market: demand is forecast to grow by nearly a fifth by 2030," Pöyry, Helsinki, 13 March 2015. Available [Online] http://www.poyry.com/news/paper-and-paperboard-market-demand-forecast-grow-nearly-fifth-2030 <10March2017>.
2. Hawkins Wright, "Market outlook," *PwC Global Forest and Paper Industry Conf.*, PricewaterhouseCoopers, New York, May 2015. Available [Online] https://www.pwc.com/ca/en/forest-paper-packaging/publications/20150506-pwc-roger-wright-market-outlook-fpp.pdf <10March2017>.
3. Macdonald, C., *Pulp Pap. Can.* 117(3): 9(2016).
4. Eudes, A., Liang, Y., Mitra, P., et al., *Curr. Opin. Biotechnol.* 26: 189(2014).
5. Zhang, Y.-H., *J. Ind. Microbiol. Biotechnol.* 35(5): 367(2008).
6. Bontems, P.-O., "Stratégie industrielle du bioraffinage de la lignine et méthode pour atténuer les risques dans le modèle d'affaires," M.Sc. thesis, École Polytechnique de Montréal, Montreal, QC, Canada, 2014.
7. Agbor, V.B., Cicek, N., Sparling, R., et al., *Biotechnol. Adv.* 29(6): 675(2011).
8. Arato, C., Pye, E.K., and Gjennestad, G., *Appl. Biochem. Biotechnol.* 121-124: 871(2005).
9. Pan, X., Gilkes, N., Kadla, J., et al., *Biotechnol. Bioeng.* 94(5): 851(2006).
10. Fatehi, P. and Chen, J., in *Production of Biofuels and Chemicals from Lignin* (Z. Fang and R.L. Smith, Jr., Eds.), Springer, Singapore, 2016, Chap. 2.
11. Öhman, F., Theliander, H., Tomani, P., et al., pat. WO 2006/031175 (March 23, 2006).
12. Kouisni, L. and Paleologou, M., U.S. pat. 2011/0297340 (Dec. 8, 2011).
13. Macdonald, C., *Pulp Pap. Can.* 117(5): 16(2016).
14. Kouisni, L., Holt-Hindle, P., Maki, K., et al. *Pulp Pap. Can.* 115(1): 18(2014).
15. Macdonald, C., "True north bioproducts," *Canadian Biomass*, 9 October 2015. Available [Online] http://www.canadianbiomassmagazine.ca/bio-products/its-time-to-check-in-on-how-the-industry-is-doing-on-its-forays-into-the-bio-economy-5357 <10March2017>.

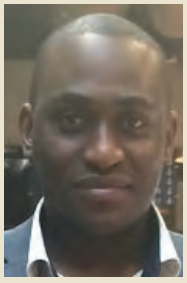
16. LigniMatch, "Future use of lignin in value added products." Available [Online] http://www.gmv.chalmers.gu.se/digitalAssets/1448/1448662_roadmap.pdf <10March2017>.
17. Smolarski, N., "High-value opportunities for lignin: unlocking its potential," Frost & Sullivan, San Antonio, TX, USA, 2012. Available [Online] http://www.greenmaterials.fr/wp-content/uploads/2013/01/High-value-Opportunities-for-Lignin-Unlocking-its-Potential-Market-Insights.pdf <10March2017>.
18. Wang, M., Leitch, M., and Xu, X., *Eur. Polym. J.* 45(12): 3380(2009).
19. Çetin, N.S. and Özmen, N., *Int. J. Adhes. Adhes.* 22(6): 477(2002).
20. Naskar, A.K., "Developing low cost carbon fiber for automotive lightweight composites," *32nd Annu. Meet. Counc. Chem. Res.*, Council for Chemical Research, Washington, D.C., 2011.
21. Eberle, C., "R&D on low-cost carbon fiber components for energy applications," *Harper International Carbon Fiber R&D Workshop*, Harper International Corp., Buffalo, NY, USA, 2013.
22. Huang, X., *Materials* 2(4): 2369(2009).
23. Kadla, J.F., Kubo, S., Venditti, R.A., et al., *Carbon* 40(15): 2913(2002).
24. Eckert, R.C. and Abdullah, Z., U.S. pat. 7,794,824 (Sept. 14, 2010).
25. Norberg, I., "Carbon fibres from kraft lignin," Ph.D. thesis, KTH Royal Institute of Technology, Stockholm, Sweden, 2012.
26. Chambost, V., McNutt, J., and Stuart, P.R., *Pulp Pap. Can.* 109(7): 19(2008).
27. Jeaidi, J. and Stuart, P.R., *J. Sci. Technol. For. Prod. Processes* 1(3): 62(2011).
28. Hytönen, E. and Stuart, P.R., *Pulp Pap. Can.* 110(5): T58(2009).
29. Hallberg, C., O'Connor, D., Rushton, M., et al., U.S. pat. 7,465,791 (Dec. 16, 2008).
30. Abbasi, J., "The fuel that could be the end of ethanol," *Fortune*, April 2013. Available [Online] http://tech.fortune.cnn.com/2013/04/12/the-fuel-that-could-be-the-end-of-ethanol/ <10March2017>.
31. Fountain, H., "Corn ethanol makers weigh switch to butanol," *New York Times*, October 2012. Available [Online]. http://www.nytimes.com/2012/10/24/business/energy-environment/weighing-butanol-as-an-alternative-to-ethanol.html <0March2017>.
32. Mariano, A.P., Keshtkar, M.J., Atala, D.I.P., et al., *Energy Fuels* 25: 2347(2011).
33. De Jong, W. and Marcotullio, G., *Int. J. Chem. React. Eng.* 8(1): A69(2010).
34. Mosier, N., Wyman, C., Dale, B., et al., *Bioresour. Technol.* 96(6): 673(2005).
35. Wang, H., Srinivasan, R., Yu, F., et al., *Energy Fuels* 25(8): 3758(2011).
36. Peters, M., Timmerhaus, K., and West, R., *Plant Design and Economics for Chemical Engineers* 5th edn., McGraw-Hill, Boston, MA, USA, 2003.

ABOUT THE AUTHORS

The lignin biorefinery is emerging as a business consideration, but companies need to consider strategies that are implemented incrementally to create competitive advantage over the long term. This report provides practical research intended to inspire mills considering the lignin-based biorefinery. The report organizes the conceptual ideas and provides a quantitative analysis as illustration for those in the field.

The most difficult part of developing this analysis was in making the broad assumptions needed for the techno-economic analysis. This was addressed through databases and discussions with experts.

As part of the study, we found that companies investing in the lignin-based biorefinery have ambitious long-term plans! We were impressed by the high rates of return possible with the lignin-based biorefinery, but also note the high level of uncertainty around this outcome. From here, we intend to extend these scenarios to a multi-criteria decision-making (MCDM) panel.



Diffo



Albers



Stuart

Diffo is post-doctoral fellow and Stuart is professor, Natural Sciences and Engineering Research Council of Canada (NSERC) Chair in Design Engineering, Department of Chemical Engineering, École Polytechnique de Montréal, Montréal, QC, Canada. Albers is manager, energy and bioproduct development, West Fraser Timber Company, Quesnel, BC, Canada. Email Stuart at paul.stuart@polymtl.ca.

TAPPI JOURNAL
WWW.TAPPI.ORG
THE PAPER AND PACKAGING INDUSTRIES' TECHNICAL RESOURCE
APRIL 2017 | VOL. 16 NO.4



NANOTECHNOLOGY 179
Novel thin functional coatings for paper by foam coating
Karita Kinnunen-Raudaskoski, Tuomo Hjelt, Ulla Forsström, Patrizia Sadocco, and Jouni Paltakari

PULPING 189
In-process detection of fiber cutting in low consistency refining based on measurement of forces on refiner bars
R. Harirforoush, J. Olson, and P. Wild

SPECIAL LIGNIN VALORIZATION CONTENT

LIGNIN PRODUCTS 203
Recent advances in lignin-based polyurethanes
Yun-Yan Wang, Charles M. Cai, and Arthur J. Ragauskas

LIGNIN PYROLYSIS 213
Toward valorization of lignin: characterization and fast pyrolysis of lignin recovered from hot-water extracts of electron-beam irradiated sugar maple
Derek Corbett, Ofei Mante, and Biljana Bujanovic

ECONOMIC ANALYSIS 229
Decision-making process for the identification of preferred lignin-based biorefinery strategies
Cédric Diffo Téguia, Sophie D'amours, Rod Albers, and Paul Stuart

April 2017

TABLE OF CONTENTS VOL. 16 NO. 4

175 EDITORIAL

TAPPI Journal 2016 Best Research Paper Award: Mining Big Data to improve pulping and papermaking operations

Monica Shaw

179 NANOTECHNOLOGY

Novel thin functional coatings for paper by foam coating

Karita Kinnunen-Raudaskoski, Tuomo Hjelt, Ulla Forsström, Patrizia Sadocco, and Jouni Paltakari

189 PULPING

In-process detection of fiber cutting in low consistency refining based on measurement of forces on refiner bars

R. Harirforoush, J. Olson, and P. Wild

203 LIGNIN PRODUCTS

Recent advances in lignin-based polyurethanes

Yun-Yan Wang, Charles M. Cai, and Arthur J. Ragauskas

213 LIGNIN PYROLYSIS

Toward valorization of lignin: characterization and fast pyrolysis of lignin recovered from hot-water extracts of electron-beam irradiated sugar maple

Derek Corbett, Ofei Mante, and Biljana Bujanovic

229 ECONOMIC ANALYSIS

Decision-making process for the identification of preferred lignin-based biorefinery strategies

Cédric Diffo Téguia, Sophie D'amours, Rod Albers, and Paul Stuart

»COVER CREDIT: Foams suitable for a thin layer coating process were produced by mixing a foaming agent and nanoparticles containing cellulose nanofibrils (CNF) with pressurized air in the mixing head of a foam generator (Kinnunen-Raudaskoski et al., p. 179).

TAPPI JOURNAL
WWW.TAPPI.ORG

Editor-in-Chief
Scott Rosencrance scott.rosencrance@kemira.com
+1 770 429-2753

Associate Editor
Brian N. Brogdon brian.brogdon@gmail.com
+1 678 581-9114

Editorial Director
Monica Shaw mshaw@tappi.org
+1 770 367-9534

Vice President, Operations
Eric Fletty efletty@tappi.org

PRESS Manager
Jana Jensen jjenson@tappi.org
+1 770 209-7242

Webmaster
Trina Heath theath@tappi.org
+1 770 209-7416

***TJ* EDITORIAL BOARD**

Brian N. Brogdon, FutureBridge Consulting & Training LLC
brian.brogdon@gmail.com, +1 678 581-9114

David A. Carlson, Carlson Consulting
dacarlson39@aol.com, +1 847 323-2685

Jere W. Crouse, JWC Consulting
cj522@inwave.com, +1 608 362-4485

Mahendra Doshi, Doshi and Associates
mahen@aol.com, +1 920 832-9101

Marc Foulger, GL&V USA Inc.
Marc.foulger@glv.com +1 315 767-2920

Peter W. Hart, WestRock
peter.hart@westrock.com, +1 409 276-3465

Carl J. Houtman, USDA Forest Products Laboratory
choutman@fs.fed.us, + 1 608 231-9445

John A. Neun, John A. Neun LLC
john.neun@gmail.com, +1 518 275-8139

Jim Niemiec, Verso Corporation
jim.niemiec@versoco.com, +1 715 422-7404

Steven P. Ottone, Omya
steven.ottone@omya.com, +1 919 641-7854

Gaurav Pranami, Imbed Biosciences
gpranami@imbedbio.com, +1 515 230-7005

Arthur Ragauskas, Oak Ridge National Laboratory
aragausk@utk.edu

Gerard J.F. Ring, University of Wisconsin—Stevens Point
gerrryring@wi-net.com, +1 715 592-3732

Scott Rosencrance, Kemira Chemicals
scott.rosencrance@kemira.com, +1 770 429-2753

Ricardo B. Santos, WestRock
ricardo.santos@westrock.com, +1 540 969-2426

Paul Wiegand, NCASI
pwiegand@ncasi.org, +1 919 941-6417

Junyong Zhu, USDA Forest Products Laboratory
jzhu@fs.fed.us, +1 608 231-9520

Join TAPPI *today!*

TAPPI JOURNAL is a free benefit of TAPPI membership, and is only available to members. To join TAPPI, to renew your TAPPI Membership, or to learn about other valuable benefits, visit www.tappi.org.

TAPPI, 15 Technology Parkway S., Suite 115, Peachtree Corners, GA 30092, publishes *TAPPI JOURNAL* monthly.

ATTENTION PROSPECTIVE AUTHORS: All papers published are subject to *TAPPI JOURNAL's* peer-review process. Not all papers accepted for review will be published. Before submitting, check complete author guidelines at http://www.tappi.org/s_tappi/doc.asp?CID=100&DID=552877.

Statements of fact and opinions expressed are those of individual authors. TAPPI assumes no responsibility for such statements and opinions. TAPPI does not intend such statements and opinions or construe them as a solicitation of or suggestion for any agreed-upon course of conduct or concerted action of any sort.

Copyright 2017 by TAPPI, all rights reserved. For copyright permission to photocopy pages from this publication for internal or personal use, contact Copyright Clearance Center, Inc. (CCC) via their website: www.copyright.com. If you have questions about the copyright permission request process, please contact CCC by phone at +1 978 750-8400. To obtain copyright permission to use excerpts from this publication in another published work, send your specific request in writing to Editor, TAPPI JOURNAL, 15 Technology Parkway S., Suite 115, Peachtree Corners, GA 30092, USA; or by fax to +1 770 446-6947. Send address changes to TAPPI, 15 Technology Parkway S., Suite 115, Peachtree Corners, GA 30092, USA; Telephone +1 770 446-1400, or FAX +1 770 446-6947. www.tappi.org

Editorial

MONICA SHAW | EDITORIAL DIRECTOR
mshaw@tappi.org



TAPPI Journal 2016 Best Research Paper Award: Mining Big Data to improve pulping and papermaking operations

TAPPI and the *TAPPI Journal* (*TJ*) Editorial Board would like congratulate the authors of the 2016 *TAPPI Journal* Best Research Paper Award: Jianzhong Fu and Peter W. Hart. Their paper, "Leveraging mill-wide big data sets for process and quality improvement in paperboard production," appeared on p. 309 of the May 2016 issue. This research was recognized by the Editorial Board for its innovation, creativity, scientific merit, and clear expression of ideas among the eight nominated papers.



Peter W. Hart (left) receives the 2016* TAPPI Journal *Best Research Paper Award from TAPPI President and CEO Larry N. Montague at the 2017 PaperCon Awards Dinner.

In their paper, Fu and Hart described how Big Data analytics were used to develop predictive models and critical insights regarding a long-term paper indents problem on a 1990s-era machine at the MWV (now WestRock) mill in Covington, VA, USA. The issue resulted in significant amounts of internal rejects and production downtime to the point that the machine was averaging just 50% of its capacity.

"We have absolute gold mines worth of information locked in our mill data historians, but we just don't know how to routinely turn the key and release that wealth of information so that it's useful." — PETER W. HART

The three-month Big Data project at Covington, led by Hart with seven other full-time team members, involved selecting 6,000 operating variables from mill process logs and 60,000+ PI data points from one of the data historians, amounting to 9 billion data points during an approximately three-year period. The data were then cleaned and classified, and software was used to develop decision trees for root cause analysis that led to specific projects for the pulp mill and paper machine that ultimately addressed the indents issue.

Fu is senior technical engineer for WestRock in Covington, and Hart is director of Fiber Science for the company. Hart accepted the *TJ* Best Research Paper Award from TAPPI President and CEO Larry N. Montague at the PaperCon Awards Dinner on April 25 in Minneapolis. *TJ* recently spoke with Hart about the Covington mill's use of Big Data analytics for the indents issues and in the future.

How long did it take you to narrow down the variables from over 60,000 to under 8,000? About how much data did you pull from the PI server as compared with what you collected from the manual mill logs?

It took the team around three weeks to select the 6,000 variables, and probably 80% of it came from the PI system. We then programmed 15 laptops to pull all the data from PI into Microsoft Excel, which was a convenient way to load it into the GE Intelligent Platforms Csense Troubleshooter to model the decision trees for analysis.

Your research paper noted that you relied a great deal on the in-depth process knowledge of your team for the data analysis. Had the people on your team been at the mill for a while?

We had a full range of people. We had young process engineers that had been at the mill two to three years, and then we brought back a few retired folks as consultants that had worked at the mill for over 30 years, along with my own industry experience as team lead. We also reviewed these steps with several other senior people within operations or who had extensive operational experience.

What was the biggest discovery in your use of Big Data analytics?

It was that no one particular thing caused the indents issue; it was always a combination of events, which is why we couldn't diagnose the problem with traditional tools in the first place. To solve it, we had to open up some of the operational windows, like operating the bleach plant in a better manner.

Did the bleach plant see the most changes after your analysis?

Of all the tweaks we made, the bleach plant was one of the biggest, because the pulp mill was much more responsive to change than the paper mill was. There were some issues around the wet end of the paper machine that were fixed, but the majority were in the bleach plant and approach flow systems, such as giving operators a better window to respond to brownstock washer carryover. Still, there were days when the bleach plant was running well but the paper machine would be a bit off and the problems would occur even though pulp quality was good. All of these changes resulted in providing the machine with a larger operational window to be successful.

You mentioned that the analysis and manipulation of Big Data sets was very difficult. Was sifting through the variables the worst part?

Cleaning up bad data and identifying good and bad timeframes that met our established criteria were quite difficult. For instance, if there was downtime or a sensor went bad, the variables were recorded as zeroes, throwing off your global average. The PI system provided data from every minute of the three years examined in the project, and there were many data points like these that you couldn't just randomly throw out.

We also had misunderstandings with less experienced team members doing the manual sifting work who weren't exactly sure what we were looking for. When we identified time periods of good versus bad data, there was to have been no downtime 24 hours before the beginning of the data set. On the first pass of generating this data, we didn't always get that level of detail in what was declared a good period of time.

What could have helped with the analysis and manipulation of the Big Data sets?

This was one of our first forays into Big Data analysis. Since that time, the software has come a long way. We've been looking at alternative software packages that will allow us to substantially improve our capability for data manipulation.

Right now, we are in a four-month beta test of Wedge software, which sits on top of your PI system and allows you to directly pull data from PI and manipulate it. We actually think we could have done the Covington project in three to four weeks instead of three months if we'd had this newer, more powerful software that is friendly enough for mill process engineers to use on a routine basis. If this beta test goes as we think, we'll consider it for all 13 of our chemical pulp mills.

My basic thought is we have absolute gold mines worth of information locked in our mill data historians, but we just don't know how to routinely turn the key and release that wealth of information so that it's useful. We can't repeat the Covington process where it takes a dedicated team of eight a full quarter of the year to solve a single problem. We've got to be able to mine this data much faster. What this Big Data project did prove is that there's tremendous value in the data for problem solving, but we just need better software to manipulate and understand it. **TJ**

For information on publishing in TAPPI Journal*, contact tjournal@tappi.org, mshaw@tappi.org, or an editorial board member in your field of expertise. You can submit your papers to our online peer review system at http://www.editorialmanager.com/tappi/.*

Novel thin functional coatings for paper by foam coating

KARITA KINNUNEN-RAUDASKOSKI, TUOMO HJELT, ULLA FORSSTRÖM, PATRIZIA SADOCCO, AND JOUNI PALTAKARI

ABSTRACT: Conventional coating methods are currently being challenged by newly developed technologies that can result in products with interesting properties and competitive prices. Versatile foam coating is one such promising technology. Foam coating is carried out using different foam application methods, and the viscoelastic nature of the foam allows the use of a large variety of materials. Paper was coated with nanomaterials on a pilot scale using a method based on slot die application combined with foam destruction by absorption and infrared drying. A thin layer of titanium dioxide/zinc oxide (TiO_2/ZnO) functionalized cellulose nanofibrils (CNF) creates antimicrobial properties in the paper, and a thin layer of CNF-TiO_2 alone has substantial ability to oxidize nitric oxide (NO) and nitrogen oxides (NOx). These results illustrate methods that can be used to create novel functional properties for different end-use applications. Thin functional layers could bring added value to current products and also create opportunities to introduce novel products for several industrial areas using web-type manufacturing processes.

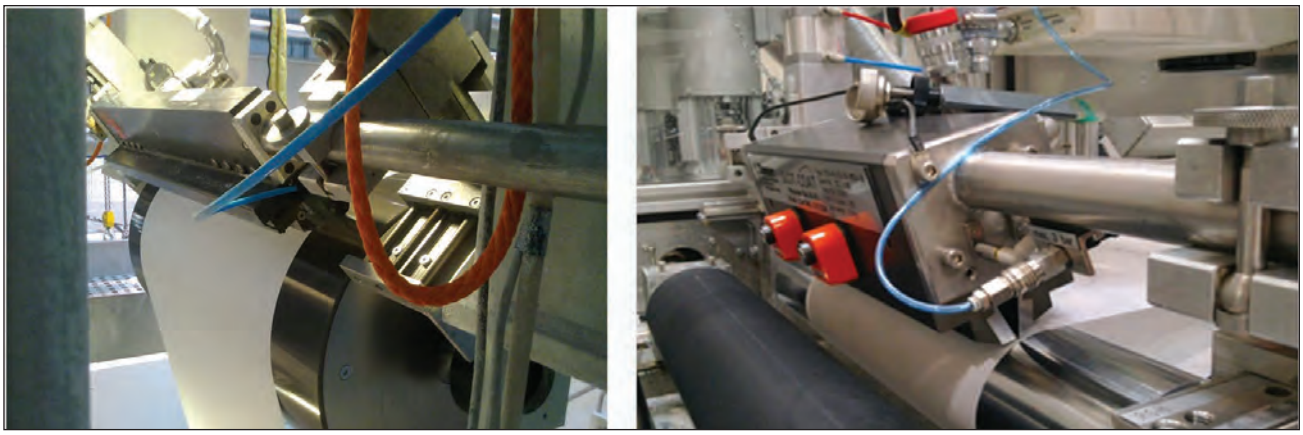
Application: The versatile foam coating method, using foam as a transferring media, allows manufacturers to modify web surfaces with a large variety of materials, from nanoparticles to highly viscous material such as cellulose nanofibers.

In foam coating, foam is commonly used as a carrier phase for applied chemicals or dispersions. In the textile industry, a wide variety of foam application techniques have been developed [1-9]. The foam application method reduces the problems caused by large amounts of liquid medium used in conventional treatments [10]. In paper applications, dispersions containing microcapsules with the natural foaming agents, gelatin, casein, and soybean extract have been applied [11]. Materials such as starch, wet strength resin, polyvinyl alcohol, wet end sizing agent, and direct dyes, as well as correction of an inherent curl in one-side-coated papers by water, have been applied using the foam coating method [12-14]. This system, referred to as the Foamcote system, is described in patents [15,16]. Eklund and Hobbs presented a more flexible application system for applying foamed starch to a paper web at high speeds [17].

Our earlier work [18-24] clearly shows that foam coating is a suitable method for applying nanoscale material to fiber-based substrates, and the method has several benefits compared with spray or film transfer technologies [21]. The technology offers a unique method for applying very light coat weights to the web surface with exceptional uniformity and absence of coating strike-in. Our earlier studies also showed that even a small amount of organic nanomaterial could change the surface properties of the paper [21]. The characterization of the coating layer having a small amount of material on the surface is challenging; however, in the case of inorganic particles, a combination of microscopic and spectroscopic procedures can be used for the analysis [23]. A thin layer of unmodified cellulose nanofibrils (CNF) increased hydrophilicity of paper and closed the paper surface, making it smoother and slightly less permeable [20,21].

Silver has been known to be an antimicrobial agent. Polycrystalline titanium dioxide (TiO_2) powders, on the other hand, have been intensively used as white pigments in diverse applications, including papermaking [25]. The photocatalytic properties of TiO_2 were first discovered 40 years ago [26]. TiO_2 is also a photoactive material with the ability to promote oxidation of organic adsorbates at the surface because of photogenerated electron-hole pairs after ultraviolet irradiation [27, 28]. The optical activity of TiO_2 has also been intensively exploited in the field of heterogeneous photocatalysis and solar energy conversion. Moreover, extended studies have been carried out on photodegradation of volatile organic compounds. More recently, there has been great interest in TiO_2 as a photoactive antimicrobial agent. In addition, the antimicrobial properties of zinc oxide were considered to be of interest [29].

In this paper we describe how the aforementioned properties of TiO_2 and zinc oxide (ZnO) were exploited for the first time in CNF-based products by foam coating of paper [24]. In addition, we tested the thin layer of CNF-TiO_2 alone for the oxidation of nitric oxide (NO) and nitrogen oxides (NOx).



1. The narrow slot-type foam applicator. The left side applicator has a labyrinth design, and the foam enters the applicator chamber in the middle of the unit. The right side applicator has a chamber design, and the foam enters the applicator from both ends.



2. Cellulose nanofibrils (CNF) with solid content 2.9 % (left), and foamed CNF containing 90% air (right).

EXPERIMENTAL

In the foam coating process, dry foam with air content greater than 80% and preferably 90%–95% (corresponding to foam densities of 50–200 g/L) is used as a carrier phase for the coating material. The coating material is located in the bubble pockets (vertices) and on the bubble surfaces. The main components in a foam coating line are a foam generator and a foam applicator. These trials used the Top-Mix type 60 foam generator (Hansa Industrie-Mixer GmbH & Co. KG; Stuhr, Germany). The starting material feeding capacity of the generator is 6–60 kg/h, and it can produce foam with densities of 50–400 g/L. The generator is connected to the compressed-air pipeline of the pilot plant. The coating material and foaming agents are mixed with pressurized air in a mixing head equipped with a rotor-stator unit.

For the application of the foam, two different Magnojet narrow slot-type applicators (J. Zimmer Maschinenbau GmbH; Klagenfurt, Austria) were employed and are shown in **Fig. 1**.

Foam coating trials

In the trials of CNF functionalized with nanoparticles, we used a noncontact, curtain-type foam application method, where foam collapses through the absorption of the paper web and through infrared (IR) drying. This method is suitable especially for small application amounts with hydrophilic substrates with fast absorption properties.

The trials were performed at the Zimmer coating line in Austria. The chamber-type applicator was used in the trials. A 400-µm gap between the slot and the moving web was used. The IR drying, with the dryers on both sides of the web, was followed by drying with hot-air ovens at a temperature of 150°C. The maximum speed of the line is around 180 m/min, but the coatings were applied at 100 m/min. This coating speed allowed for the low consistency of CNF coating to achieve the desired coat weights, while providing enough speed to obtain a good quality coating layer. The applied coat weights in trials at Zimmer were 0.4–1.8 g/m^2. The maximum speed we have obtained so far with the KCL pilot coater is 400 m/min (KCL Pilot Plant; Espoo, Finland). Technical improvements are nonetheless needed to increase the speed and to improve the evenness of the coating layer.

Property	±	TiO_2	ZnO
Concentration, %w/w	0.5	6.0	1.0
Density, g/cm³	0.05	1.20	1.12
Viscosity (25°C), mPa/sec	0.1	2.00	ND
Particle dimension, nm	-	40.0	45.0
Polydispersity index	0.05	0.25	0.20
pH	0.5	1.0	ND
Cationic surfactant, %w/w	0.05	0.1	-

I. Physicochemical characterization of inorganic nanoparticles (TiO_2 = titanium dioxide; ZnO = zinc oxide).

Materials

Functionalized cellulose nanofibrils

This work was carried out as part of the European SUNPAP (Scaling Up Nanoparticles in Modern Paper Making, 2009-2012) project targeting CNF applications. However, other nanomaterials, such as silica, can be used as a carrier for the functional materials. CNF are nanosized cellulose fibrils with a high aspect ratio (length-to-width ratio). The width of fibrils is typically 5–20 nanometers and the length ranges widely from tens of nanometers to several microns. The more nanoscale particles present in the CNF material, the more viscous and transparent the material will be. The benefit of foam coating is that high-viscosity CNF does not need to be diluted for the coating process. **Figure 2** shows the case where the starting CNF had a solids content of 2.9% and did not flow by itself into the screw pump. However, the foamed CNF from the generator (with an air content of 90%) was a suitable material for the coating process. The foamed CNF was pushed manually to the pump through the pipe (10 cm length and 4 cm diameter), combining the feeding tank and the screw pump.

The CNF for the trials was produced by the Centre Technique du Papier, Gières, France (CTP). The CNF fibers were produced by an initial enzymatic pretreatment of cellulose fibers followed by low consistency refining. Then, the pretreated and refined fibers were disintegrated to nanoscale particles by running them through a homogenizer several times. This produced CNF with a solids content of 2.3%, which was then functionalized by Innovhub (Milan, Italy). For functionalization of the CNF, inorganic nanoparticles TiO_2 and ZnO were produced by Colorobbia (Vinci, Italy). **Table I** shows the physicochemical characterization of inorganic nanoparticles.

The functionalization of CNF was achieved on the basis of direct physical adsorption of inorganic nanoparticles to CNF. The nanocomposites were prepared by mixing CNF (2.3% in water) with TiO_2 (6% in water) or ZnO (1% in ethylene glycol), or both, for 15 min. The mixtures were then washed three times with water followed by centrifugation to eliminate non-adsorbed inorganic fillers. CNF and inorganic nanoparticles suspensions were mixed together as supplied by an immersion mechanical blade stirrer. Centrifugations were performed and washings were carried out to eliminate excess TiO_2 or ZnO. After each washing, homogenization by stirring was carried out. The centrifuge took approximately 2 min to reach 7000 rpm, which was then maintained for 5 min. After centrifugation, the water supernatant was discarded. The pellet produced was suspended in the same volume of fresh water that had been removed by ultracentrifugation and then mixed with the mechanical stirrer. For the trials, 25 kg of CNF-TiO_2 (2.8% dry weight) and 15 kg of CNF-ZnO-TiO_2 (4.8% dry weight) were produced. The concentration of TiO_2 and ZnO in the final nanocomposites was determined by inductively coupled plasma analysis. **Table II** shows the mixing ratios and the contents of inorganic nanoparticles in the prepared composites.

The foams were produced by mixing the foaming agent and CNF containing nanoparticles with pressurized air in the mixing head of the foam generator. The air content of the foams was adjusted to 80%–90%, with foam density 100–200 g/L. The anionic foaming agent used was sodium dodecyl sulfate, in a ratio of 0.2% of CNF composite volume. The addition of a surface active agent was on the basis of the liquid volume.

Base paper and paperboard

The base paper used in the CNF trials was 80 g/m² uncoated and uncalendered fine paper produced from hardwood and softwood fiber without hydrophobic sizing agents with fast absorption properties.

Characterization

Using the paper samples coated by CNF-TiO_2 or CNF-ZnO, or CNF- TiO_2 and ZnO, the following tests were performed:

Nanocomposite	Solids Content, %	Initial Mixing Ratio of the Preparations, as dry weight	TiO_2 Content, % dry weight	ZnO Content, % dry weight
CNF-TiO_2	2, 8	1:1	24	-
CNF-ZnO and TiO_2	4, 8	10:1:10	42	2

II. Analysis of CNF/inorganic nanoparticles suspensions (TiO_2 and ZnO determined by inductively coupled plasma analysis).

Data Type	Counts
Image resolution	1024 by 1024
Image pixel size	1.06 µm
Map resolution	256 by 256
Map pixel size	4.24 µm
Alternating current (AC) voltage	12.0 kV
Magnification	100

III. The information of scanning electron microscopy analysis of TiO_2/ZnO modified CNF–containing paper.

- Antimicrobial activity (AATCC Test Method 100 "Quantitative assessment of antibacterial activity") toward gram-positive *Staphylococcus aureus* and gram-negative *Klebsiella pneumoniae* [24].
- Photocatalytic activity by using a device designed by Colorobbia Italy [24].

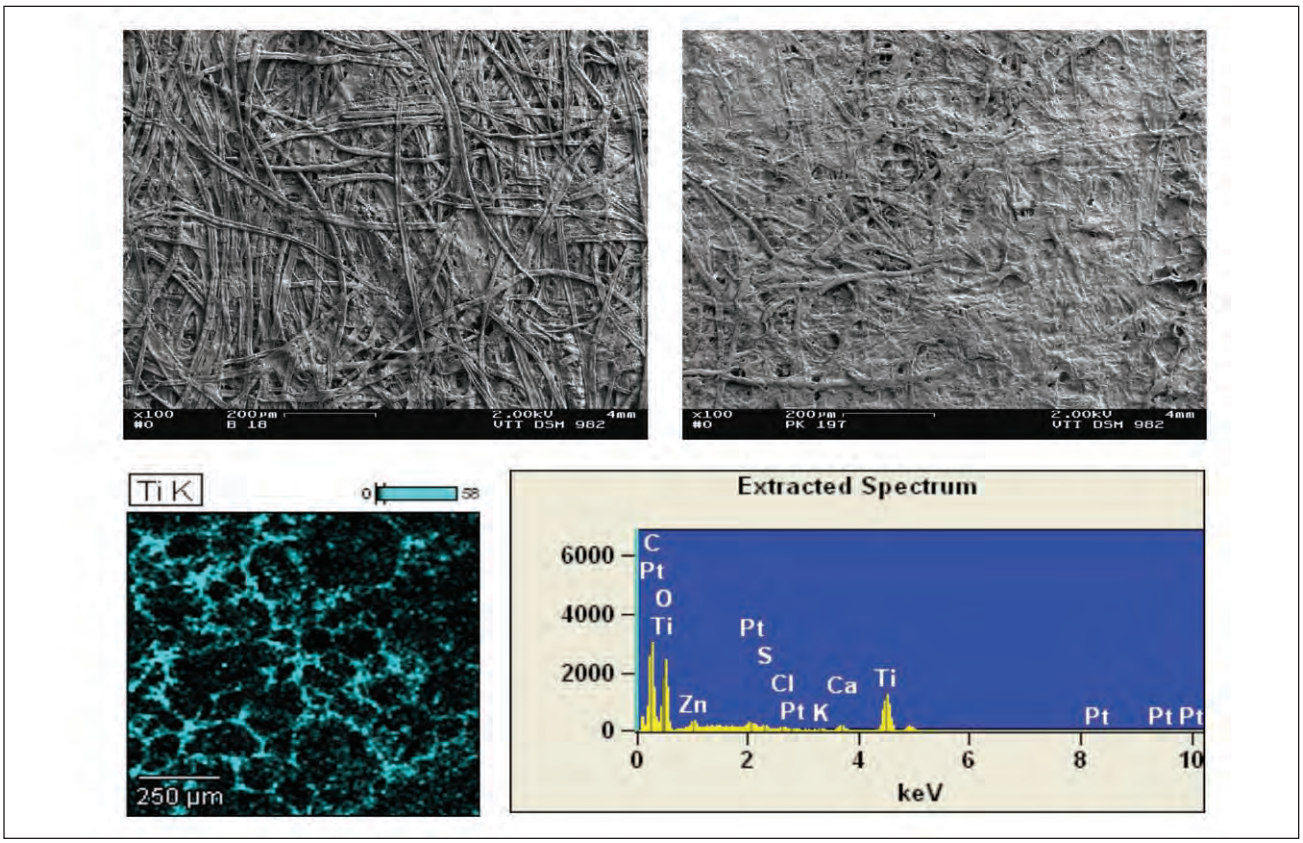
Before the tests, the TiO_2/ZnO modified CNF-containing papers were analyzed with scanning electron microscopy (SEM) imaging using a backscattered electron (BSE) detector and titanium element mapping. The information of SEM analysis is seen in **Table III**.

Titanium element maps show that material on a paper surface is attached on the fiber surfaces to form a structure that resembles a honeycomb (**Fig. 3**).

Antimicrobial activity of the foam-coated papers

Photoactivation

In the presence of TiO_2 and ZnO nanocomposites, the antibacterial tests were carried out on photoactivated samples as follows. The samples were sterilized before testing and the antibacterial tests were conducted by spreading a known number of living cells on the paper surface to yield a population of 10^5 colony forming units (CFU). The paper samples were subjected to light exposure (4 h by standard solar lamp 6000 lux) to induce photoactivation of inorganic nanoparticles (TiO_2 or ZnO, or both). Then the samples were incubated by adopting testing conditions (temperature and nutrients) that promote bacterial growth. In addition, some tests were also run in darkness. The inoculated paper samples were maintained 20 h under optimal nutrient and temperature conditions for bacterial growth. At the end of the test, the paper samples were extracted and the number of living cells determined by plating serial dilution on nutrient agar.



3. Titanium element scanning electron microscopy/energy-dispersive x-ray spectroscopy (SEM/EDS maps) from calendered TiO_2/ZnO modified CNF–containing paper showing that material on the paper surface is attached on the fiber surfaces (top left–base; top right–coated surface).



4. The photodegradation kinetics of nitrogen oxides (NOx) in gaseous phase by foam-coated papers were tested using a photoreactor equipped with chemiluminescence and gas chromatography–mass spectrometry.

Testing conditions

The tests were performed according to AATCC Test Method 100 under static conditions. The foam-coated paper samples were tested for antibacterial activity toward gram-positive *Staphylococcus aureus* and gram-negative *Klebsiella pneumoniae*. The inoculated samples were subjected to overnight incubation (about 18 h) at 30°C or 37°C, depending on the optimal temperature for microbial growth. After incubation, the bacteria were extracted from the samples under investigation by using a neutralizing solution. CFU, the number of living cells in the extracted suspension, was evaluated by the count plate agar method. The antibacterial activity of the sample, as bacteria log reduction, was calculated as follows in Eq. (1):

$$\text{log reduction} = \log \text{CFU } T_{18} \text{ blank (control)} - \log \text{CFU } T_{18} \text{ sample} \quad (1)$$

where CFU T_{18} is the colony forming number corresponding to the bacteria living cells at incubation of 18 h.

In general, two antibacterial effects can be distinguished:

1. Bactericidal — Reduction (killing) of the number of bacteria initially inoculated (CFU at time 0).
2. Bacteriostatic — Inhibition of bacteria growth under testing conditions favorable to bacteria proliferation, evaluated with respect to growth in the blank sample (CFU at time 18 h).

Untreated CNF was used as a blank untreated control (CNF control).

Photocatalytic activity of the foam coated papers

The catalytic activity of the treated paper samples was tested using a device developed by Colorobbia Italy consisting of a glass chamber with a quartz window, in which the treated samples were exposed. In the chamber, a NOx-polluted atmosphere was created and the NOx concentration, humidity, and temperature were measured at fixed sampling time intervals. The measurement of NOx concentrations was carried out by a Model 42i chemiluminescence apparatus (Thermo Fisher Scientific; Waltham, MA, USA) (**Fig. 4**). The samples were continuously irradiated by an Ultravitalux 300W mercury vapor lamp (Osram Light AG; Munich, Germany) to induce photoactivation. The measurements were made by passing the polluted air passed through a closed circuit, including the reaction glass chamber, a bag in which the polluted air was stored, and a pump. During the entire experiment, the lamp remained on for activation of the samples. The data collected were used to assess the kinetics of the photocatalytic process.

RESULTS AND DISCUSSION

Antibacterial activity of the foam coated papers

Table IV reports the results obtained with the different paper samples (logarithmic reduction of the number of living cells) for tests run under light exposure conditions. Bacteria grown on the untreated reference is at a level of 10^6–10^7 CFU (6–7 log). One sample from earlier trials at KCL, namely the CNF/ZnO (0.8 g/m^2) sample, was tested at the same time with these new samples because the preparation procedure of modified CNF and the base paper were the same.

The results reported in Table IV show substantial antibacterial activity for paper samples treated by CNF-TiO_2 for TiO_2 content around 0.3%, while for paper samples treated by CNF-ZnO, a much lower inorganic filler content is needed to obtain similar effects. In general, bacteriostatic activity was obtained while bactericidal activity was not detected with these amounts of inorganic particles. Bacteriostatic activity was also demonstrated for CNF-TiO_2 foam-coated papers under conditions of darkness with respect to *Staphylococcus aureus*, as reported in **Table V**. The results show that in the absence of light, TiO_2 or ZnO modified CNF coated papers had only a slight effect on bacteria growth; that is, they need light exposure to show antibacterial activity.

Photocatalytic activity of the foam coated papers

The paper samples foam coated by nanocomposites CNF-TiO_2, CNF-ZnO, and CNF-ZnO and TiO_2 were characterized for their photocatalytic efficiency. As shown in **Table VI**, paper samples foam coated by nanocomposites containing TiO_2 display

Paper Sample (coat weight)	ZnO, ppm	TiO_2, %	*Staphylococcus aureus*		*Klebsiella pneumoniae*	
			Bacteriostatic Activity, log reduction	Bactericidal Activity, log reduction	Bacteriostatic Activity, log reduction	Bactericidal Activity, log reduction
Untreated paper	-	-	0	0	0	0
CNF-TiO_2 (0.4 g/m^2)	-	0.034	0	0	0	0
CNF-TiO_2 (0.9 g/m^2)	-	0.167	1.3	0	0	0
CNF-TiO_2 (1.8 g/m^2)	-	0.291	Total bacteriostatic	1.0	1.8	0
CNF-ZnO and TiO_2 (0.6 g/m^2)	38.4	0.115	0.7	0	0	0
CNF-ZnO&TiO_2 (1.3 g/m^2)	104.6	0.307	Total bacteriostatic	0.1	0.2	0
CNF/ZnO (0.8 g/m^2)*	180	-	Total bacteriostatic	0.3	2.1	0

* A sample from KCL coating machine trials. The procedure of CNF/ZnO composite preparation and the base paper were the same as in Zimmer trial samples.

IV. Antibacterial activity of foam-coated paper samples, under conditions of light exposure.

Paper Sample (coat weight)	ZnO, ppm	TiO_2, %	*Staphylococcus aureus*	
			Bacteriostatic Activity, log reduction	Bactericidal Activity, log reduction
Untreated paper (control)	-	-	0	0
CNF-TiO_2 (1.8 g/m^2)	-	0.291	1.7	0
CNF-ZnO (0.8 g/m^2)	180	-	1.2	0

V. Antibacterial activity of foam-coated paper samples, under conditions of darkness. Bacteria grown on untreated reference: 106–107 (6–7 log).

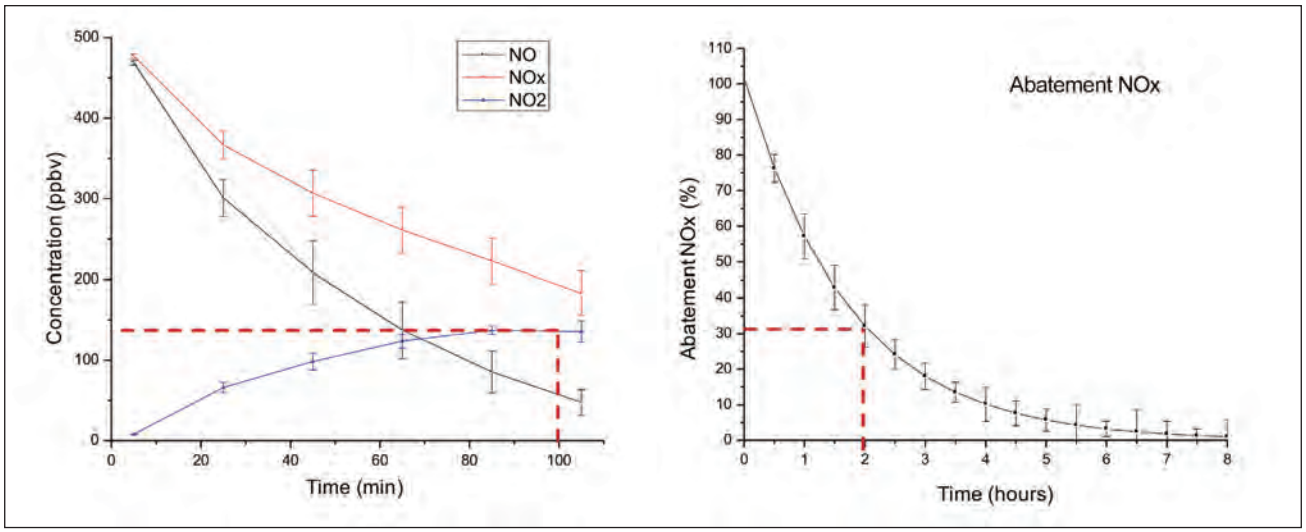
photoactivity for the degradation of volatile compounds at TiO_2 content higher than 0.1%. In contrast, ZnO presence seems to have little influence on the photoactivity of the paper. Photo-oxidation of volatile substances depends only on the TiO_2 content of the paper.

Figure 5 shows the NOx photodegradation in gaseous phase by CNF-TiO_2 foam-coated paper. Around 70% NOx oxidation occurred within 100 min, showing that foam-coated paper with CNF-TiO_2 had significant activity for the oxidation of NO and NOx. At a coat weight of 0.9 g/m^2, the corresponding TiO_2 dry weight on paper was 0.162%; this was enough to have an influence of 72.6% NO degradation after 105 min.

Photo-oxidation of NOx has important applications for the control of air pollution. In the case of active paper it could be used for wallpaper, for example, to control indoor pollution. However, the photo-oxidation by TiO_2 can also work to oxidize or breakdown organic volatile compounds (not only for inorganic materials such as NOx). These could include formaldehyde or other air pollution organic compounds (e.g., acetaldehydes) or ethylene produced by fruits that are responsible for the ripening and fast spoilage of fruits and vegetables in packaged produce systems.

CONCLUSIONS

Foam coating technology offers a unique opportunity to apply coating to a web surface thinly enough to be economically viable. The method is suitable for production of functional construction materials, filters, and disposable textile materials for hospital use or for active packaging solutions with antimicrobial, photoactivity, or barrier properties. The results ob-



5. NOx photodegradation in gaseous phase by CNF-TiO_2 foam-coated paper. Note: coat weight below 1 g/m².

Paper Sample (coat weight)	ZnODry Weight on Paper*, ppm	TiO_2Dry Weight on Paper*, %	NO Degradation (after 105 min), %	NO Degradation (after 105 min), %
Untreated paper	-	-	0	0
CNF-TiO_2 (0.4 g/m²)	-	0.008	16.8	12.6
CNF-TiO_2 (0.9 g/m²)	-	0.167	72.6	46.0
CNF-TiO_2 (1.8 g/m²)	-	0.291	79.9	61.6
CNF-ZnO and TiO_2 (0.6 g/m²)	38.4	0.115	81.7	64.9
CNF-ZnO and TiO_2 (1.3 g/m²)	104.6	0.307	90.9	78.5
CNF/ZnO (0.8 g/m²)	180	-	0	0
* From inductively coupled plasma analysis.				

VI. Nitric oxide (NO) and NOx degradation by foam-coated papers.

tained from the foam coating trials with TiO_2 and ZnO functionalized CNF show that it is possible to create antimicrobial and photocatalytic properties of paper and paperboard.

The results obtained from the foam coating trials with functionalized CNF showed that by using modified CNF, it is possible to activate properties on the paper surface even at extremely low coat weights (i.e., below 1 g/m²). For the foam coating trials, functionalized CNF was prepared using a physical absorption based method. Nanoscale inorganic particles TiO_2 and ZnO were mixed with CNF to create nanocomposites CNF-TiO_2, CNF-ZnO, and CNF-ZnO and TiO_2 .

The paper coated by the functionalized CNF showed antibacterial activity mainly depending on the TiO_2 or ZnO content, or both. The antibacterial activities obtained were mainly bacteriostatic. The bacteriostatic property of CNF-TiO_2 or CNF-ZnO, or both, was obtained even at low coat weights of modified CNF. The TiO_2 content was around 0.3% dry weight on paper, and ZnO content was even lower.

Regarding the photo-oxidation of NOx compounds in gaseous phases, only paper samples coated by CNF-TiO_2 showed efficient photoactivity. At a coat weight of 0.9 g/m², the corresponding TiO_2 dry weight on paper was 0.162%; this was enough to result in a 72.6% NO degradation after 105 min. The degradation depended strongly on the TiO_2 content, while the paper samples containing only CNF-ZnO nanocomposite did not show any photoactivity, indicating that this additive is not sensitive to photoactivation.

Further work with more defined targets for different end applications, including product and process development at high speeds, would serve to optimize the effects reported here. **TJ**

ACKNOWLEDGEMENTS

The authors thank the partners of the European SUNPAP project and the European Commission. The research leading to the results from application of functionalized CNF received funding from the European Community's Seventh Framework Programme under Grant Agreement No. 228802.

LITERATURE CITED

1. Hoechst AG, G.B. pat. 1,430,184 (Mar. 31, 1976).
2. Faber, L. and Carroll, C.J., U.S. pat. 1,948,568 (Feb. 27, 1934).
3. Faber, L. and Carroll, C.J., U.S. pat. 2,023,013 (Dec. 3, 1935).
4. Stritzko, V., U.S. pat. 3,697,314 (Oct. 10, 1972).
5. Abrahams, D.H. and Graham, A.D., U.S. pat. 3,762,860 (Oct. 2, 1973).
6. Hoechst AG, G.B. pat. 1,516,882 (July 5, 1978).
7. Schwemmer, M., Bors, H., and Götz, A., *Textilveredlung* 10(1): 15(1975).
8. Childers, B. and Fesperman, C.D. Jr., U.S. pat. 3,954,404 (May 4, 1976).
9. Von der Eltz, H-U., Gulden, W., and Wassner, R.B., U.S. pat. 3,990,840 (Nov. 9, 1976).
10. Gregorian, R.S. and Namboodri, C.G., G.B. pat. 1583246 (Jan. 21, 2981).
11. Robertson, N.G.D., G.B. pat. 1,476,787 (June 16, 1977).
12. Riddell, M.C. and Jenkins, B., *Pap. Technol. Ind.* 27(2): 80(1976).
13. Riddell, M.C. and Jenkins, B., *Pap. Technol. Ind.* 18(6): 176(1977).
14. Riddell, M. and Jenkins, B., *Symp., Chem. Papermaking*, EUCEPA, Warsaw, 1978, p. 234.
15. Jenkins, B., U.S. pat. 4,184, 914 (June 22, 1980).
16. Jenkins, B., G.B. pat. 1,551,710 (Aug. 30, 1979).
17. Eklund, R.W. and Hobbs, O.J., *Coat. Conf.*, TAPPI Press, Atlanta, 1986, p. 83.
18. Kinnunen, K., Hjelt, T., and Kenttä, E., "Thin nanoparticle layers applied on the paper by foam coating technique," *PTS Coat. Symp., 25th*, Papiertechnische Stiftung, Munich, 2011.
19. Kinnunen, K., Hjelt, T., and Kenttä, E., "Innovative surface treatment with foam coating technology," *EU Project SUNPAP (Scaling Up Nanoparticles in Modern Paper Making) Final Conf.*, 19 June 2012. Available [Online] http://sunpap.vtt.fi/pdf/final_conference/8 SUNPAP_Kinnunen_2012.pdf <10April2017>..
20. Kinnunen, K., Hjelt, T., Kenttä, E., et al., "Thin coatings for paper by foam coating," *PaperCon,* TAPPI Press, Atlanta, GA, USA, 2013.
21. Kinnunen, K., Hjelt, T., Kenttä, E., et al., *TAPPI J.* 13(7): 9(2014).
22. Kinnunen, K., Hjelt, T., Kenttä, E., et al., "Functional thin coatings for paper by foam coating," *TAPPI Int. Conf. Nanotechnol. Renewable Mater.*, TAPPI Press, Atlanta, 2013.
23. Kenttä, E., Kinnunen, K., and Hjelt, T., *TAPPI J.* 13(7): 21(2014).
24. Kinnunen-Raudaskoski, K., Hjelt, T., Kenttä, E., et al., "Thin barrier and other functional coatings for paper by foam coating," *PaperCon*, TAPPI Press, Atlanta, 2015.
25. Wienand, H. and Adel, J., in *Industrial Inorganic Pigments* (G. Buxbaum, Ed.), Wiley-VCH, Weinheim, 1998.
26. Fujishima, A. and Honda, K., *Nature* 238(5358): 37(1972).
27. Schiavello, M., *Heterogeneous Photocatalysis*, Wiley, Hoboken, 1997.
28. Beydoun, D., Amal, R., Low, G., et al., *J. Nanopart. Res.* 1(4): 439(1999).
29. Yousef, J.M. and Danial, E.N., *J. Health Sci.* 2(4): 38(2012).

ABOUT THE AUTHORS

The paper and board industry needs new tools for renewal. We chose this research topic because foam based technologies in several application areas are such promising tools. This research is a continuation of earlier foam coating research focusing on the application of unmodified cellulose nanofibrils.

The most difficult aspect of this work was finding the facilities for starting the research at pilot scale. It was difficult because no relevant laboratory scale facilities exist. The most interesting finding was that the foam coating technology was able to transfer the effectiveness of the functionalized cellulose nanofibrils to the paper surface. The research shows that the foam based coating technology is very versatile. It allows the use of a wide variety of materials, which might challenge the conventional coating technologies.

For this author (Kinnunen-Raudaskoski), the next step is to continue product development based on foam technologies at Paptic Ltd., a spinoff company of VTT.

Kinnunen-Raudaskoski is co-founder and research director, Paptic Ltd., Espoo, Finland. Hjelt is senior scientist and Forsström is principal scientist, VTT Technical Research Centre of Finland, Espoo, Finland. Sadocco is director with Innovhub SSI Paper Division, Milan, Italy. Paltakari is a professor, School of Chemical Technology, Aalto University, Aalto, Finland. Email Kinnunen-Raudaskoski at karita.kinnunen@paptic.fi.



Kinnunen-Raudaskoski



Hjelt



Forsström



Sadocco



Paltakari

In-process detection of fiber cutting in low consistency refining based on measurement of forces on refiner bars

R. HARIRFOROUSH, J. OLSON, AND P. WILD

ABSTRACT: A major drawback of low consistency refining is the degradation of mechanical properties due to fiber cutting at high refining energies. Conventional strategies to avoid fiber cutting are based on post-refining measurement of pulp properties and, typically, this does not enable rapid adjustment of refiner operation in response to the onset of fiber cutting. The objective of this study is to detect the onset of fiber cutting by using custom-designed piezoelectric force sensors that measure shear and normal forces applied to pulp fibers by the refiner bars. Trials are performed in an AIKAWA/Advanced Fiber Technologies Inc. 16-in. single-disc low consistency refiner. The trials are run using mechanical softwood SPF (spruce, pine, and fir) pulp with 378 ml CSF at 2.5% and 3.5% consistency at rotational speeds of 800 rpm, 1000 rpm, and 1200 rpm. Distributions of the peak normal and shear forces and peak coefficient of friction are determined for each operating condition, and a two-parameter Weibull function is fit to each of these distributions. The scale parameter, which is one of the key parameters of the Weibull function, is calculated, and length-weighted fiber length is plotted as a function of this parameter. The results show that the onset of fiber cutting consistently corresponds to a distinct transition in the plot of length-weighted fiber length versus scale parameter. This transition is believed to be caused by a fundamental transition in the fiber-bar interaction. Moreover, frequency analysis of the sensor data shows that the magnitude of the dominant frequency remains relatively constant while the plate gap is reduced, up to a threshold value, which corresponds to the onset of fiber cutting. These results suggest that these sensors have potential to be used for in-process detection of the onset of fiber cutting.

Application: The application of this study is in-process detection of fiber cutting in low-consistency mechanical refining.

Mechanical pulping is an energy intensive process. For example, in British Columbia (BC), 78 refiners consume 5400 GWh/yr or 11% of BC's total electrical energy production [1], and the bulk of this energy is consumed in the mechanical pulping process. With the increasing cost of energy, the long-term survival of mechanical pulping may depend on reducing energy consumption of this process.

One method of diminishing energy consumption in mechanical pulping is to decrease the number of refining treatments at high consistency (HC) and increase the number of treatments at low consistency (LC). LC refining of mechanical pulp has been shown to be more energy efficient than conventional HC refining [2-5]. Moreover, LC refining is effective for removal of shives, external fibrillation of fibers, removal of latency, and improving fiber networking and bonding capabilities [6,7]. However, the degradation of mechanical properties due to fiber cutting at high refining energies has limited the widespread adoption of LC refining [1]. Understanding the relation between refiner operating conditions and resulting pulp properties is essential to reduce fiber cutting.

In mechanical refining, as the plate gap is closed, fibers are subjected to increasing compressive and shear forces that lead to an increase in net refiner power. Based on pilot and mill-scale LC refining studies, Luukkonen et al. found that the plate gap is a key link between the refiner process variables and resulting changes in pulp properties [1]. In a separate study, Luukkonen et al. [8] proposed a methodology to correlate operating conditions to pulp quality by relating the refiner operating conditions (i.e., power, flow rate, rotational speed, and plate gap) to fiber quality (i.e., fiber length and freeness) and then relating fiber quality to pulp handsheet quality (i.e., tensile, tear, and bulk). They also showed that pulp quality remains constant as the gap is closed, until a critical gap, which is characterized by the onset of significant fiber cutting, is reached. Beyond the critical gap, fiber cutting commences and paper strength is reduced. Moreover, beyond this point, the relationship between refining power and plate gap deviates from linearity [9].

Similar results were observed by Nugroho [10] for various mixes of softwood and hardwood chemical pulps in LC refining. Refining power increased as the plate gap decreased and, at a critical gap between 0.3 to 0.5 mm, the power sharply increased. Moreover, the fiber length and freeness decreased

when the plate gap reached the critical gap. This transition occurred for all of the trial conditions.

Elahimehr et al. [11] studied the relationship between fiber length and plate gap in a AIKAWA 16-in. pilot-scale LC refiner. Trials were run at three rotational speeds, with four refiner plate patterns, and at 3% consistency. They found that mean fiber length was unchanged until the plate gap reached a critical gap, near 0.25 mm. The mean fiber length significantly decreased for the plate gaps smaller than the critical gap. Results also showed that increasing the rotational speed increases the critical gap.

Berg et al. [12] found that power increases linearly as the plate gap is reduced over the range of 0.1–0.2 mm in a two-zone TwinFlo72 LC refiner. They calculated average forces applied to fibers using the expression developed by Kerekes [13]. Fiber cutting was defined as the point where the ratio of outlet to inlet fiber length was equal to 0.95. Plate gap, forces on fibers, and specific edge load (SEL), defined as the energy expended per unit refiner bar length over one bar-crossing event, were found to predict fiber cutting.

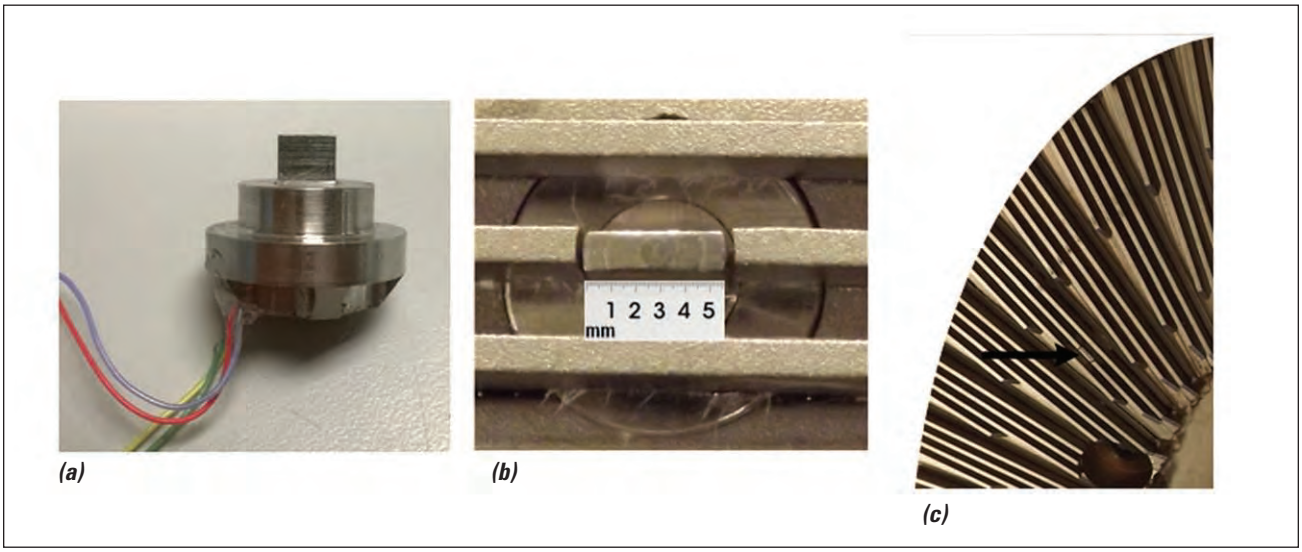
In all of the studies previously discussed here, fiber cutting is detected by post-refining measurement of pulp properties. Typically, this approach does not enable rapid in-process adjustment of refiner operation in response to the onset of fiber cutting. These studies also do not address the mechanical interactions between fibers and refiner bars. Kerekes [14] suggests that bar force (i.e., the force applied to pulp fibers by the refiner bars) is the key parameter between bars and fibers in refining that cause important changes in fiber properties.

A piezoelectric sensor has been developed to measure bar forces. The sensor uses the piezoelectric effect, which is the ability of certain materials to generate an electric charge in response to applied mechanical stress. This sensor, referred to here as the refiner force sensor (RFS), has a sensing probe that replaces a short length of a refiner bar, enabling measurement of forces normal to and tangential to the refiner bars. The RFS has been used in a number of studies in both low consistency [15,16] and high consistency refining [17,18]. In a recent study, Harirforoush et al. [19] investigated the relation between net power, gap, and forces on bars in LC refining using the RFS. They found that, as the plate gap is reduced, the length-weighted fiber length remains relatively constant while net refiner power and the mean peak normal and shear forces increase up to threshold values. Here, peak refers to the maximum value that occurs as a bar on the rotor passes over the sensor. Above these thresholds, the mean peak normal and shear forces continue to increase, but the length-weighted fiber length exhibits negative linear relationship with these forces.

The objective of this study is to investigate the onset of fiber cutting based on analysis of bar forces measured with the RFS at a wide range of rotational speeds at 2.5% and 3.5% consistency. Distributions of the peak normal and shear forces, and peak coefficient of friction (i.e., peak shear force divide by peak normal force) are determined for each operating condition. Distinct transitions occur in these distributions that correspond to the onset of fiber cutting. In addition, frequency analysis of the sensor data shows that the magnitude of the dominant frequency can be used as an indication of the onset of fiber cutting.

MATERIALS AND METHODS

Trials were conducted using the AIKAWA 16-in. single-disc refiner at the Pulp and Paper Center at the University of British Columbia (Vancouver, BC, Canada). The refiner is equipped with a power meter, plate actuation, and a variable speed drive. The plate used in these trials is manufactured by AIKAWA FINEBAR, which has bar edge length of 2.74 km/rev and bar angle of 15° from radial. The bar width, groove width, and groove depth of the plate are 1.6 mm, 3.2 mm, and 4.8 mm, respectively.



1. (a) Refiner force sensor (RFS) used at the Pulp and Paper Center, University of British Columbia (Vancouver, BC, Canada) trials, (b) a close-up of RFS installed in the stator plate, and (c) the location of the sensor in the stator plate [19].

An RFS-type sensor was custom designed and fabricated based on the design previously used in refiner trials [20]. A photograph of the RFS used in this work is shown in **Fig. 1a**. The sensor is installed in a custom recess that is machined into the back of the stator plate. The sensor wires pass from the back side of the sensor and through a custom gland located in the door of the refiner. The sensor recess is located so that the tip of the sensor replaces a short length of the refiner bar (i.e., 5 mm), as shown in Fig. 1b. The sensor measures force normal to the plate surface (i.e., parallel to the axis of the refiner bar) and the shear force perpendicular to the major axis of the refiner bar and normal to the bar edge. The sensor is positioned in the second bar of a three-bar cluster at a radius of 151 mm, as shown in Fig 1c. At this radius, the heads of the bolts do not pass over the sensor. The 144 bars on the rotor, grouped into 48 three-bar clusters, cross over the sensor in one revolution of the refiner.

Calibration and environmental tests were performed as described in [19,21]. Modal analyses were performed to ensure that the first natural frequency of the sensor is well above the bar-passing frequency of the refiner so that phase and magnitude distortion due to sensor resonance is avoided. The ratio of the first natural frequency of the sensor to the maximum bar-passing frequency is 8.2, which provides a sufficient margin above the bar passing frequency.

A custom charge amplifier converts the high impedance charge output of the sensors to a low impedance voltage signal that is read by a National Instruments (Austin, TX, USA) PXI 1042 Q high-speed board. National Instrument BNC-2110, Shielded Connector Blocks are used to connect the high-speed DAQ board to the charge amplifier. A custom LabVIEW (National Instruments; Austin, TX, USA) interface is used to control data acquisition. A sampling rate of 150 kHz is used, which is more than twenty times the maximum bar-passing frequency that occurs during the trials.

Mechanical SPF (40% spruce; 45% pine; 10% balsam fir and 5% Douglas fir) softwood pulp, produced at Quesnel River Pulp Mill, with 378 ml CSF at 2.5% and 3.5% consistency was used in all trials. The operating conditions for the trials are shown in **Table I**. The refining operating mode was mono-flo with one inlet perpendicular to the outlet. The refiner speed was set with a variable frequency drive (VFD). The plate gaps were adjusted using a controller from no-load position (3.5 mm) to the smaller plate gaps (0.25 mm). The flow rate was held constant at 250 L/min. Sensor signals were recorded using the LabVIEW interface for approximately 10 s once reaching stable condition at each target point. At each operating condition, the refiner was held steady for about 10 s to give the pulp time to move from the refining zone to the sample collection point. A 2-L pulp sample was collected over a 5 s interval. The process was repeated until all of the target points were achieved for one rotational speed. Then, the plate gap was increased to the no-load position and the refiner was adjusted to the next rotational speed using the VFD.

The length-weighted fiber length (L_W) was measured for all pulp samples using a Fiber Quality Analyzer (HiRes FQA, Optest Equipment Inc.; Hawkesbury, ON, Canada). Length-weighted fiber length is calculated based on Eq. (1) [22]:

$$L_w = \frac{\sum n_i L_i^2}{\sum n_i L_i} \quad (1)$$

where, n_i and L_i are the number of the fibers in the ith class and mean length of the ith class, respectively.

An algorithm was created in MATLAB (Mathworks; Natick, MA, USA) to identify bar-passing events in the force data. A bar-passing event is defined to occur when the passage of a rotor bar over the sensor results in a maximum or peak value in the force data that exceeds a predefined threshold value. The algorithm and its verification are described in [19].

For each bar-passing event, peak force is defined as the difference between the force at the base of the local valley that precedes the peak and the force at the peak [16]. The peak coefficient of friction is calculated by dividing the peak shear force by the peak normal force. The peak force and peak coefficient of friction data are assessed in the form of distributions to which the two-parameter Weibull distribution function is fit.

The Weibull distribution function is widely used because of its ability to characterize a wide variety of distributions, and

Parameter	Condition	
Refiner speed, rpm	800, 1000, 1200	1200
Consistency	3.5 %	2.5 %
Flow rate, L/min	250	
Plate gap, mm	3.5–0.25 (15 gaps)	3.5–0.25 (12 gaps)
Operating mode	Mono-flo	
Pulp type	Mechanical SPF softwood pulp, starting freeness at 378 ml CSF	

I. Operating conditions for the pilot-scale low consistency refining trials at the Pulp and Paper Center, University of British Columbia.

it has been used in previous HC and LC refining studies [15,17]. The Weibull distribution function is shown in Eq. (2) [23]:

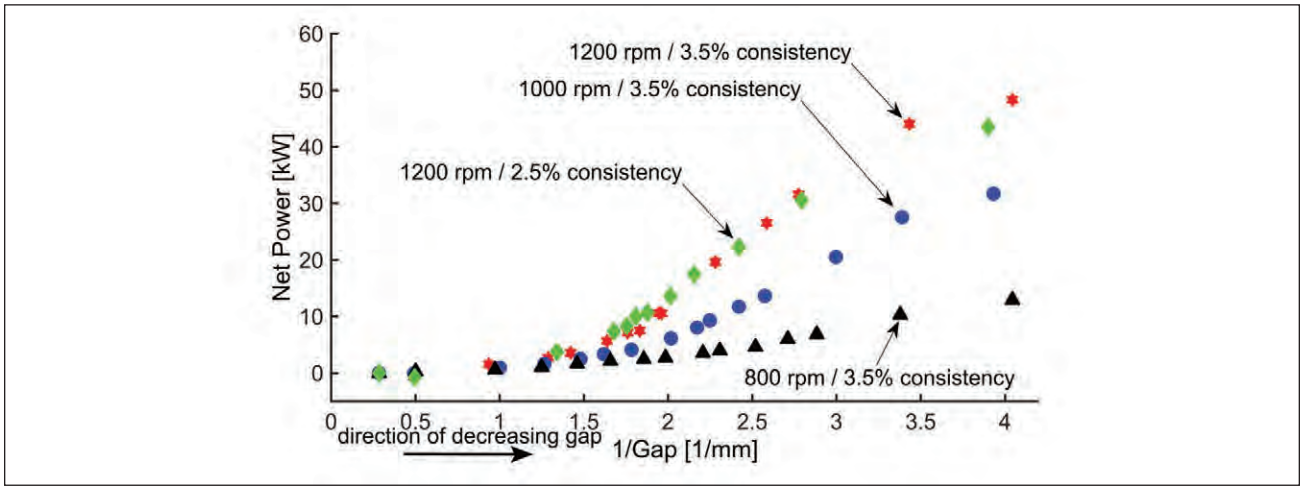
$$f(x) = \frac{\beta}{\eta}\left(\frac{x-\gamma}{\eta}\right)^{\beta-1} exp^{-\left(\frac{x-\gamma}{\eta}\right)^{\beta}} \quad (2)$$

where, β, η, and γ are shape, scale and location parameters, respectively. The effects of these parameters on the Weibull distribution are discussed by Lee [24]. The two-parameter Weibull distribution function is obtained by setting in Eq. (2). In this study, the Weibull scale and shape parameters of the peak normal, shear force, and peak coefficient of friction distributions are calculated for each operating condition. Each of these parameters are then correlated to both plate gap and L_W.

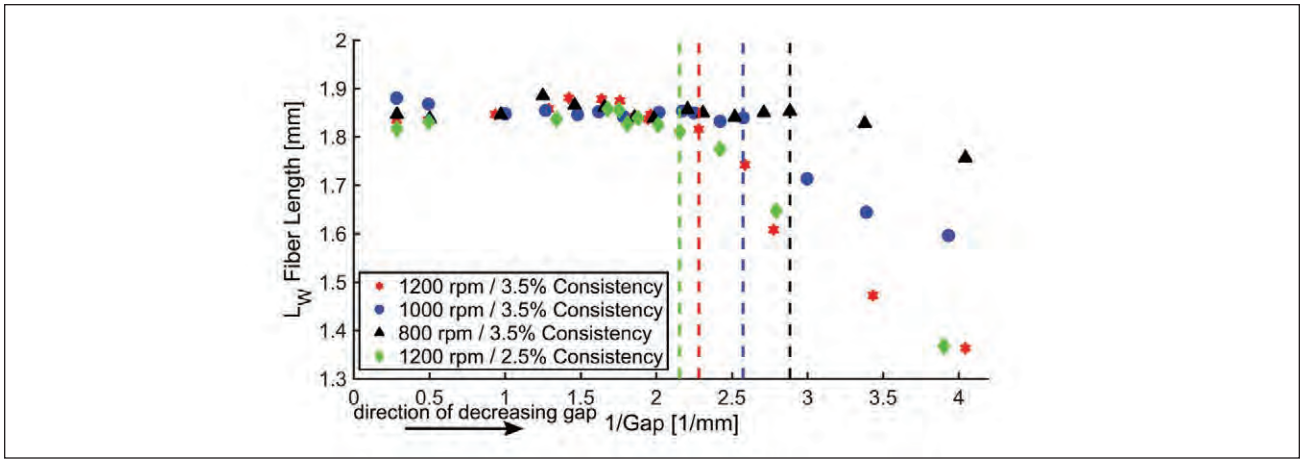
RESULTS

The relation between net power and the inverse of plate gap for three rotational speeds (i.e., 1200 rpm, 1000 rpm, and 800 rpm) at 3.5% consistency and 1200 rpm at 2.5% consistency is shown in **Fig. 2**. In all cases, the net power increases as the plate gap is reduced. However, a considerable increase in energy transferred to the fibers is seen for gaps of less than 0.5 mm (or more than 2 mm^{-1}). At a constant gap and consistency, increasing the rotational speed increases the net power. The relationships are similar to the results of Nugroho [10], Elahimehr et al. [11], and Harirforoush et al. [19]. Across the full range of gaps at 1200 rpm, the net power for 3.5% and 2.5% consistency are approximately equal.

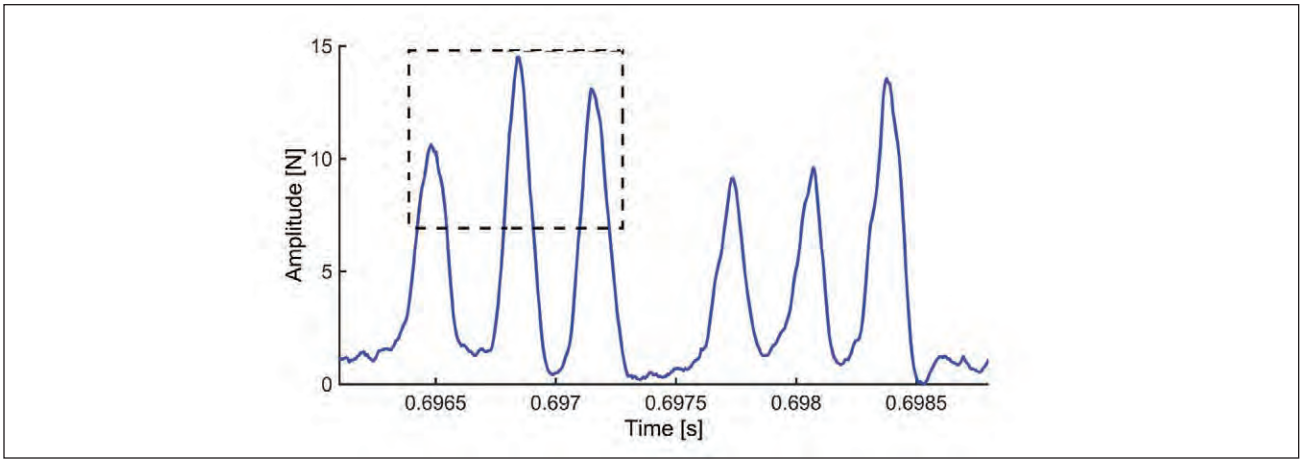
The relation between L_W and the inverse of plate gap for three rotational speeds (i.e., 1200 rpm, 1000 rpm, and 800 rpm) at 3.5% consistency and 1200 rpm at 2.5% consistency is shown in **Fig. 3**. In each case, L_W remains relatively constant as the plate gap is closed until the gap reaches the critical value, indicated by the dashed lines. The critical values are determined based on transitions in the plot of L_W versus the inverse of plate gap. For plate gaps smaller than the critical gap, L_W decreases in an approximately linear manner.



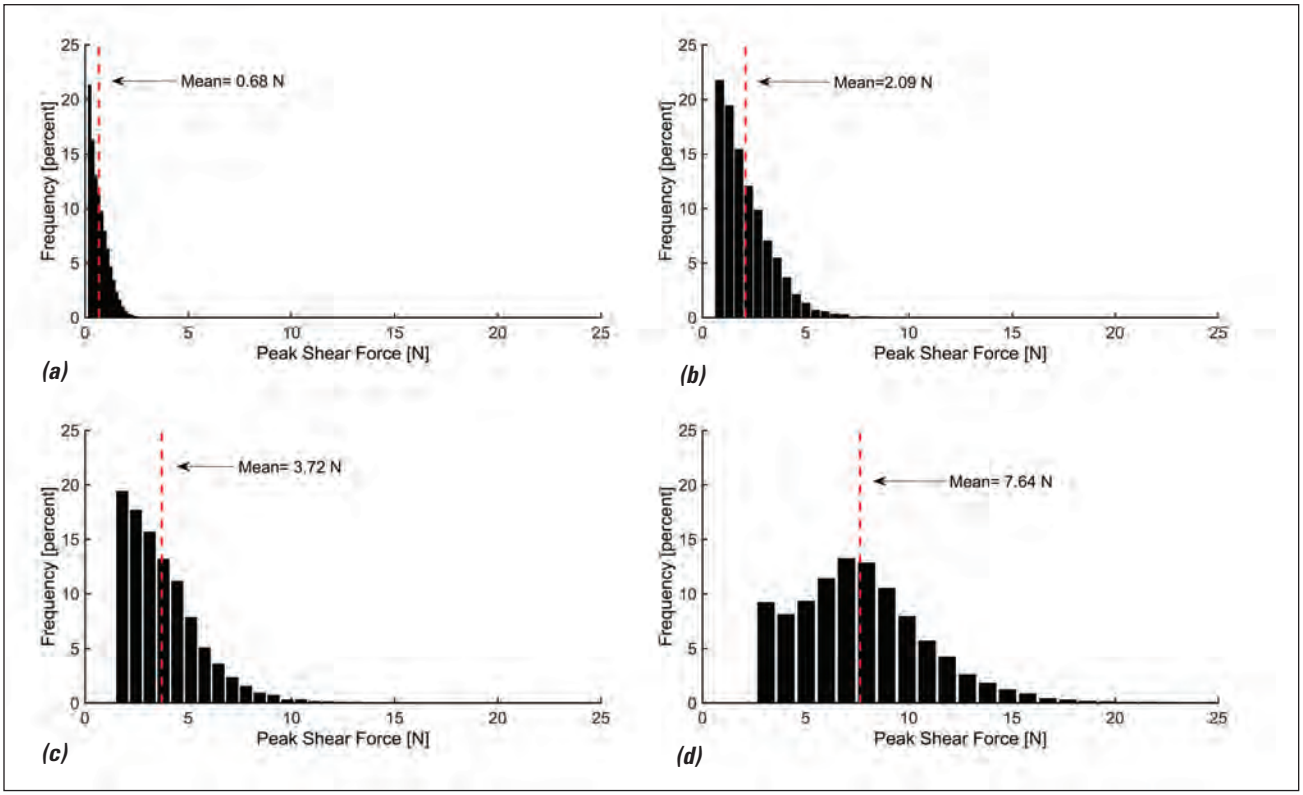
2. Net power versus the inverse of plate gap for three rotational speeds (i.e., 1200 rpm, 1000 rpm, and 800 rpm) at 3.5% consistency. Data is also shown for 1200 rpm at 2.5% consistency.



3. L_w versus the inverse of plate gap for three rotational speeds (i.e., 1200 rpm, 1000 rpm, and 800 rpm) at 3.5% consistency. Data is also shown for 1200 rpm at 2.5% consistency.



4. Typical unfiltered normal force data at 1000 rpm and 0.45 mm plate gap.

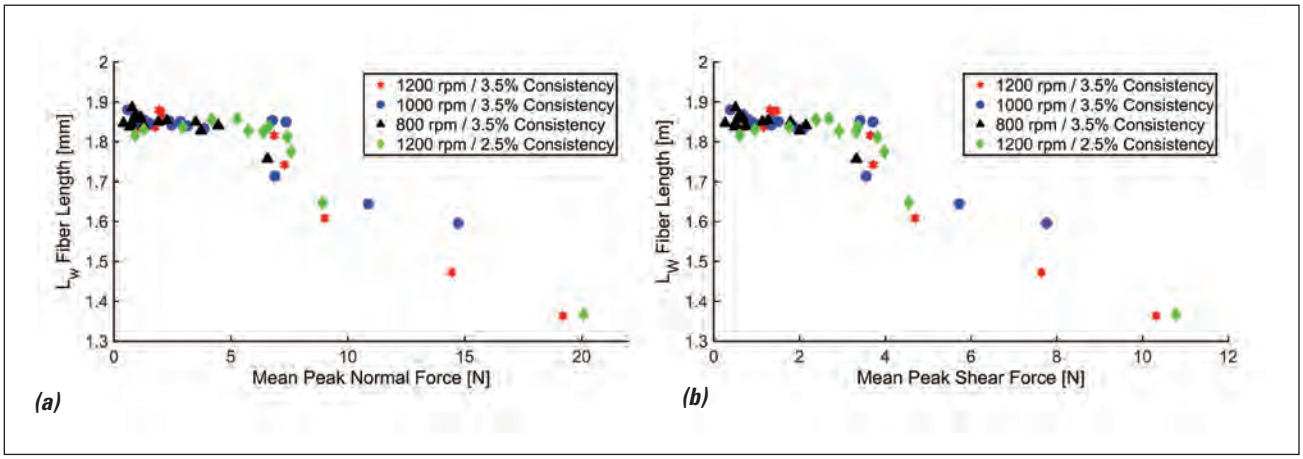


5. Normalized distributions of peak shear force for plate gaps of (a) 3.5 mm, (b) 0.55 mm, (c) 0.4 mm, and (d) 0.3 mm for rotational speed of 1200 rpm at 3.5% consistency.

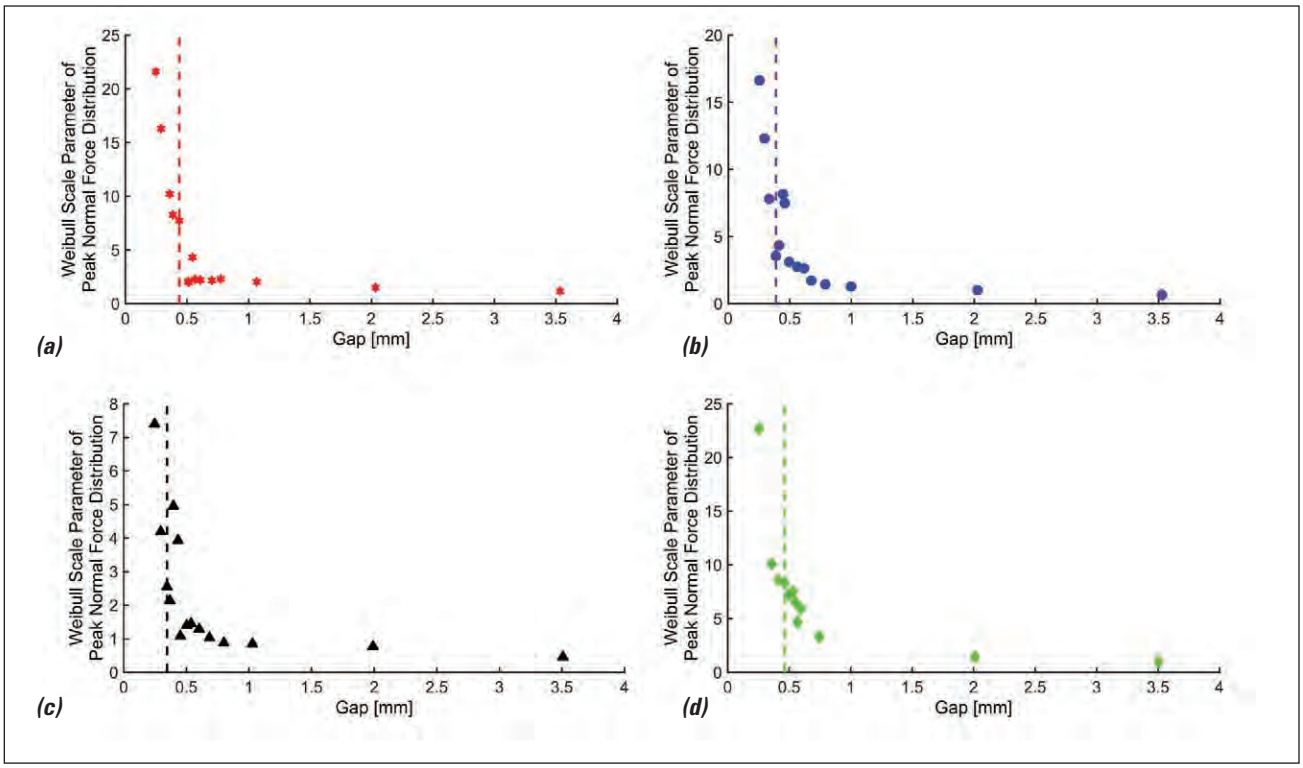
Figure 3 also shows that, at the same consistency (i.e., 3.5%), the critical gap decreases as rotational speed decreases. This finding is consistent with the results of Nugroho [10], Elahimehr et al. [11], and Harirforoush et al. [19]. Moreover, the red dashed line representing the critical gap for 1200 rpm at 3.5% consistency occurs where 1/Gap = 2.282 (or gap = 0.438 mm), while the green dashed line indicating the critical gap for 1200 rpm at 2.5% consistency occurs where 1/Gap = 2.155 (or gap = 0.464 mm). Thus, at the same rotational speed, decreasing the consistency from 3.5% to 2.5% slightly increases the critical gap. This trend is not in agreement with Lundin [25], who reported that decreasing the consistency from 6% to 3% decreases the critical gap from 0.27 mm to 0.2 mm.

Typical unfiltered normal force data, taken at 1000 rpm and a plate gap of 0.45 mm, is shown in **Fig. 4**. Each peak represents a bar-passing event. As highlighted by the dashed rectangle, bar-passing events appear as clusters of three peaks, since the bars of the rotor that cross over the force sensor are grouped in three-bar clusters.

Normalized distributions of peak shear force data for plate gaps of 3.5 mm (no-load), 0.55 mm, 0.4 mm, and 0.3 mm for 1200 rpm at 3.5% consistency are shown in **Fig. 5**. The mean



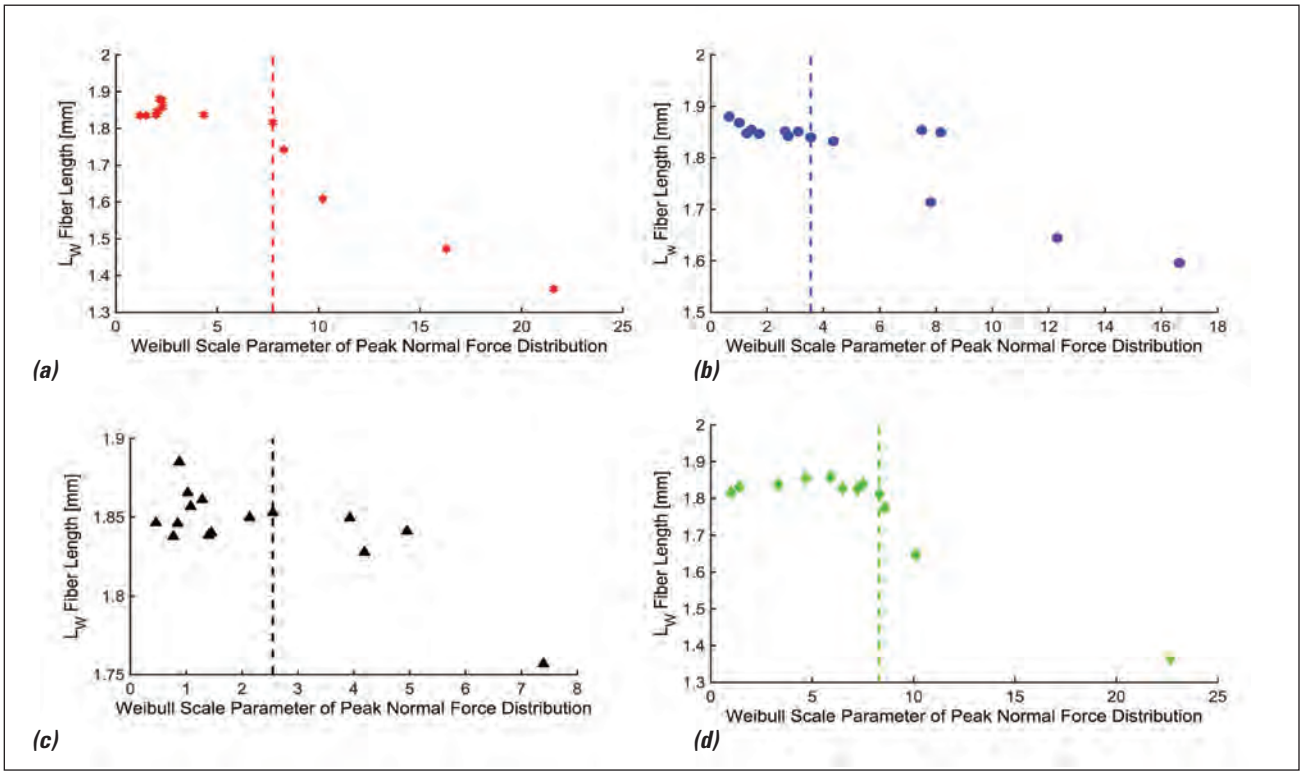
6. (a) L_w versus mean peak normal and (b) shear force for three rotational speeds (i.e., 1200 rpm, 1000 rpm, and 800 rpm) at 3.5% consistency. Data is also shown for 1200 rpm at 2.5% consistency.



7. The Weibull scale parameter of peak normal force distribution versus plate gap for rotational speeds of (a) 1200 rpm, (b) 1000 rpm, (c) 800 rpm at 3.5% consistency, and (d) 1200 rpm at 2.5% consistency.

value of the peak shear force distribution, highlighted by the dashed line, increases as the plate gap decreases, which is consistent with the increase in net refiner power. This result is in agreement with the results of Prairie et al. [15], who showed that the median forces increase with increasing specific edge load (SEL). Moreover, as the plate gap is closed, the distribution of peak shear forces is extended to the right, its height decreases, and the shape of the distribution changes from positively skewed to an approximately normal distribution. The truncation of the left-hand end of the distributions shown in Figs. 5b, 5c, and 5d is an artefact of the algorithm used to identify bar-passing events. This algorithm, which is described in [19], discards events that fall below a prescribed threshold.

Figure 6 shows the relationship between L_W and mean peak force for three rotational speeds (i.e., 1200 rpm, 1000 rpm, and 800 rpm) at 3.5% consistency and 1200 rpm at 2.5% consistency. As shown in Fig. 6a, L_W remains relatively unchanged as mean peak normal force increases up to a threshold value that corresponds to the critical gap. The L_W value decreases in an approximately linear manner beyond the critical gap threshold. The trend is consistent with the results of Harirforoush et al. [19]. The mean peak normal force at this



8. L_w versus the Weibull scale parameter of peak normal force distribution for rotational speeds of (a) 1200 rpm, (b) 1000 rpm, (c) 800 rpm at 3.5% consistency, and (d) 1200 rpm at 2.5% consistency.

threshold is relatively constant, approximately 7 N, for all rotational speeds at 3.5% consistency. Decreasing the consistency from 3.5% to 2.5% slightly increases this threshold value.

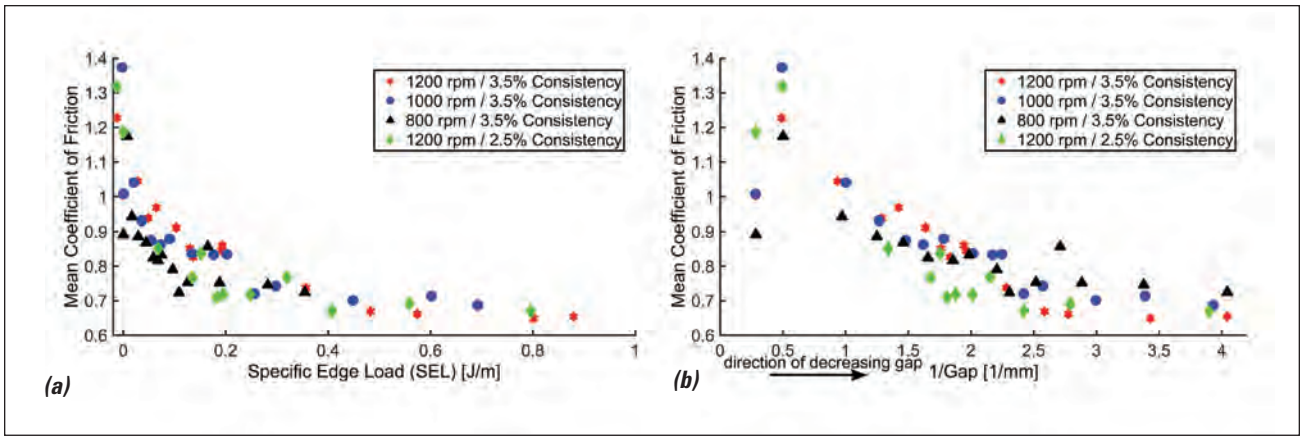
A similar trend is seen in the relationship between L_W and mean peak shear force (Fig. 6b). However, the threshold value at which the transition occurs is lower, approximately 3.8 N. For 800 rpm, possibly due to insufficient data for the plate gaps less than the critical gap, the trend cannot be seen.

To explore the relationship between the distribution of peak force and plate gap, the Weibull scale parameter of peak normal force distribution is plotted versus plate gap for three rotational speeds (i.e., 1200 rpm, 1000 rpm, and 800 rpm) at 3.5% consistency and 1200 rpm at 2.5% consistency. As shown in **Fig. 7a**, as the plate gap is decreased, the scale parameter remains relatively constant up to a threshold value. The threshold, highlighted by dashed line, corresponds to the transition seen in the plot of L_W versus the inverse of plate gap for 1200 rpm at 3.5% consistency, Fig. 3. This transition is in agreement with the onset of the fiber cutting. The trend also appears in Figs. 7b, 7c and 7d but is less definitive for 800 rpm at 3.5% consistency, Fig. 7c, and 1200 rpm at 2.5% consistency, Fig. 7d.

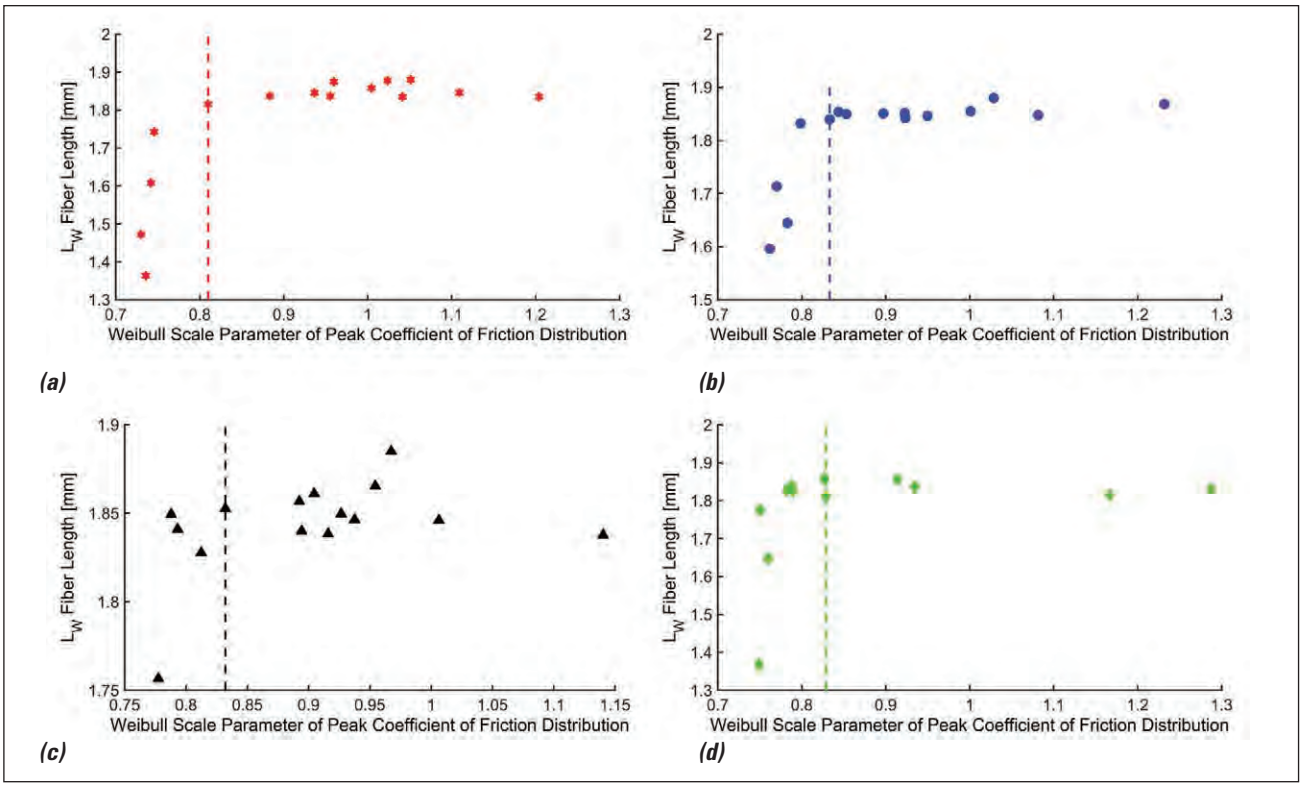
The relation between the distribution of peak forces and fiber length is investigated by plotting L_W versus the Weibull scale parameter of peak normal force distribution for three rotational speeds (i.e., 1200 rpm, 1000 rpm, and 800 rpm) at 3.5% consistency and 1200 rpm at 2.5% consistency. As shown in **Fig. 8a**, the length-weighted fiber length remains relatively constant as the scale parameter increases up to a threshold value, highlighted by dashed line. The dashed line corresponds to the transition seen in the plot of L_W versus the inverse of plate gap, Fig. 3, and it is at the same position as the dashed line shown in Fig. 7a. The L_W value decreases beyond this point. This point corresponds to the onset of fiber cutting. Similar trends occur in Figs. 8b, 8c, and 8d but are less definitive for 1000 rpm, Fig. 8b, and 800 rpm, Fig. 8c. At 800 rpm, pulp flow rate was observed to be unstable which may reflect unstable conditions in the refiner and may also be the cause of anomalous data at this speed.

The mean coefficient of friction is plotted in **Fig. 9a** as a function of SEL for three rotational speeds (i.e., 1200 rpm, 1000 rpm, and 800 rpm) at 3.5% consistency and for 1200 rpm at 2.5% consistency. Mean coefficient of friction decreases with increasing SEL. This result is consistent with Prairie et al. [15]. As shown in Fig. 9b, the mean coefficient of friction decreases as the plate gap is reduced. This finding is in accordance with Senger et al. [26]. The mean coefficient of friction varies from 0.65 to 1.37.

The relationships between L_W and the Weibull scale parameter of the distribution of peak coefficient of friction for three rotational speeds (i.e., 1200 rpm, 1000 rpm, and 800 rpm) at 3.5% consistency and 1200 rpm at 2.5% consistency are shown in **Figs. 10a-10d**. As shown in Fig. 10a, L_W remains relatively constant as the scale parameter decreases to a threshold, highlighted by a dashed line. The dashed line is at the same point as the dashed lines shown in Fig. 7a and Fig 8a, and it is



9. (a) Mean coefficient of friction versus specific edge load (SEL), and (b) mean coefficient of friction versus plate gap for three rotational speeds (i.e., 1200 rpm, 1000 rpm, and 800 rpm) at 3.5% consistency. Data is also shown for 1200 rpm at 2.5% consistency.

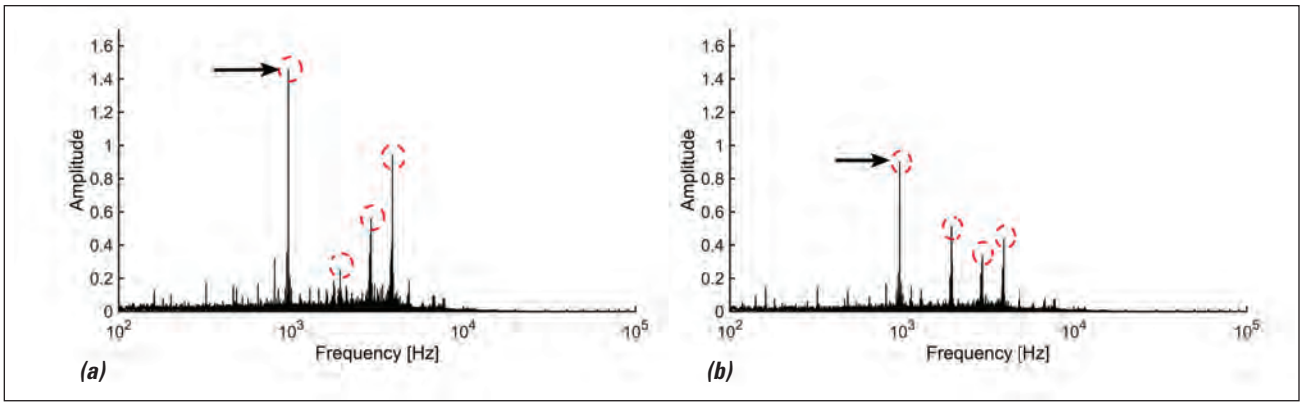


10. L_w versus Weibull scale parameter of peak coefficient of friction distribution for rotational speeds of (a) 1200 rpm, (b) 1000 rpm , (c) 800 rpm at 3.5% consistency, and (d) 1200 rpm at 2.5% consistency.

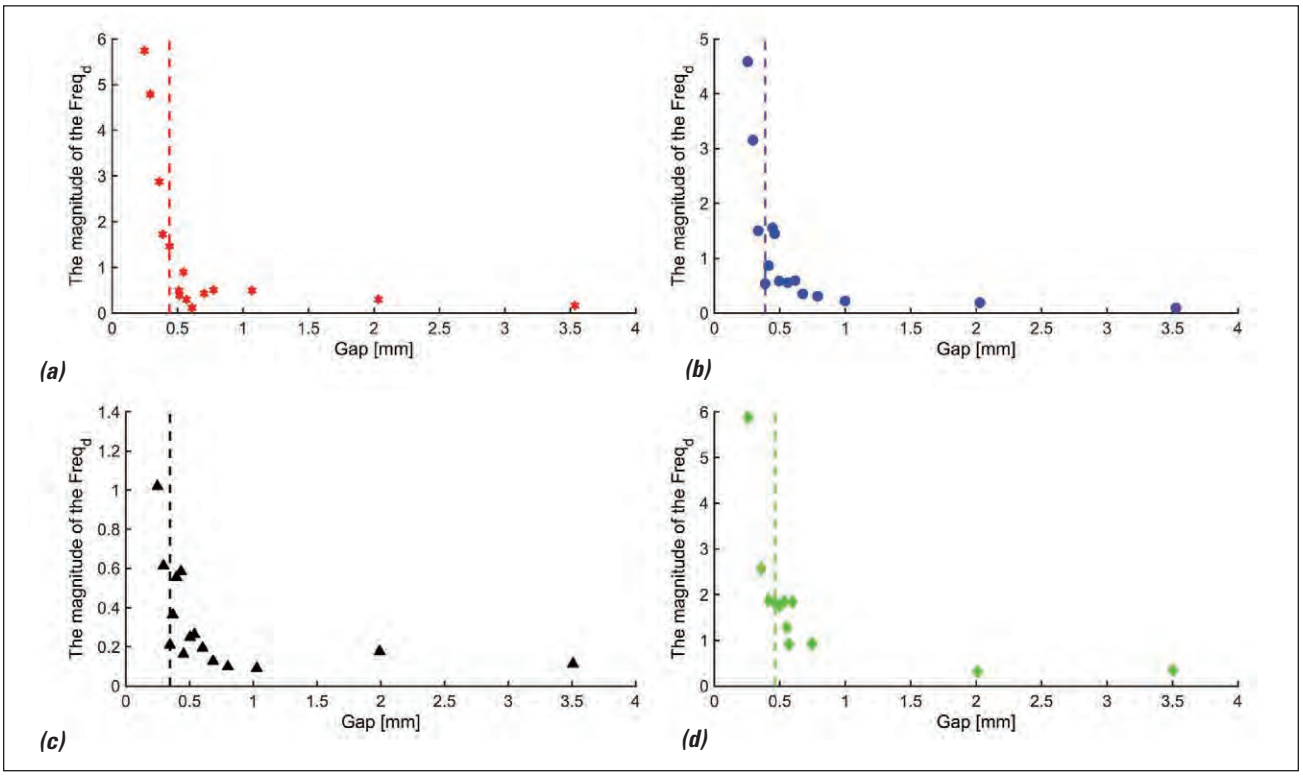
determined based on the transition seen in the plot of L_W versus the inverse of plate gap, Fig. 3. This point corresponds to the onset of fiber cutting. The L_W value decreases beyond this point. Similar transitions occur in Figs. 10b, 10c, and 10d.

The spectra of the normal force data at 1200 rpm, plate gaps of 0.45 mm and 0.55 mm, and 3.5% consistency show four maxima at frequencies of 3.82, 2.87, 1.90, and 0.95 kHz, highlighted by dashed circles, **Fig. 11**. The frequencies correspond to crossings of different bars within the three-bar clusters of the rotor, as described in [19]. The highest amplitude, marked by the arrow, corresponds to the passage of equivalent edges in adjacent three-bar clusters. This frequency, referred to here as the dominant frequency ($Freq_d$), appears in the frequency analysis for all of the operating conditions. Comparing Fig. 11a and Fig. 11b, it is apparent that the amplitude (magnitude) at this frequency is affected by the plate gap.

Figure 12 shows the magnitude of the dominant frequency, ($Freq_d$), versus plate gap for three rotational speeds (i.e., 1200 rpm, 1000 rpm, and 800 rpm) at 3.5% consistency and 1200 rpm at 2.5% consistency for normal force data. As shown in Fig. 12a, the magnitude remains relatively constant while the plate gap is reduced up to a threshold value, which



11. Spectrum of normal forces at plate gaps of (a) 0.45 mm and (b) 0.55 mm for rotational speed of 1200 rpm and 3.5% consistency.



12. The magnitude of the frequency corresponds to the passage of equivalent edges in adjacent three-bar clusters versus the plate gap for rotational speeds of (a) 1200 rpm, (b) 1000 rpm, (c) 800 rpm at 3.5% consistency, and (d) 1200 rpm at 2.5% consistency.

corresponds to the onset of fiber cutting, indicated by dashed lines. This trend is present but less definitive for 800 rpm, Fig. 12c, and 1200 rpm at 2.5% consistency, Fig. 12d.

The trends shown in Figs. 7, 8, and 12 also appear in the peak shear force distributions. This data is not included here in the interest of brevity.

DISCUSSION

The RFS measures normal force and shear force, perpendicular to the major axis of the refiner bar, in a single-disc LC refiner. The bar-passing events are characterized as distributions of event parameters such as peak normal and shear forces and peak coefficient of friction. These distributions are used to compare refining conditions on the basis of data taken at each operating condition. Distinct transitions are observed in parameters that characterize these distributions; in particular, mean peak force and the Weibull scale parameter. These transitions consistently correspond to the onset of fiber cutting.

As the plate gap is reduced, mean peak normal and shear forces increase but L_W remains relatively constant, up to a threshold value of mean peak normal and shear force. The L_W value decreases in an approximately linear manner beyond these threshold values, as shown in Fig. 6. These transitions correspond to the onset of fiber cutting. Above these thresholds, mean peak forces continue to increase but L_W exhibits a

negative linear relationship with force that mirrors the established relationship between L_W and the inverse of plate gap (Fig. 3). The trend is consistent with the results in [19].

The Weibull scale parameter of the peak force distributions and of peak coefficient of friction distributions are also candidates for in-process detection of fiber cutting. As shown in Fig. 8 and Fig. 10, transitions occur in length-weighted fiber length at the values of the scale parameters that correspond to the onset of fiber cutting. Note that the position of these transitions, indicated by the dashed lines, correspond to the transitions seen in the plot of L_W versus the inverse of plate gap shown in Fig. 3.

In addition to these indicators of fiber cutting found in the time domain data, the power spectrum of the sensor data can also be used to detect the onset of fiber cutting. As shown in Fig. 12, as the plate gap is reduced, the magnitude of the dominant frequency, which is equal to the bar-passing frequency, remains relatively constant up to a threshold value that corresponds to the onset of fiber cutting. Beyond this threshold, the amplitude increases. According to Parseval's theorem, the magnitude of the spectrum at a given frequency is equal to the energy transferred at that frequency. Therefore, this transition in the spectrum may be due to a fundamental change in the mode of energy transfer to the pulp at the onset of fiber cutting.

These results suggest that the RFS has potential to be used for in-process detection of fiber cutting in mill operations. In previous mill trials, the sensors have been shown to be sufficiently rugged [17] for industrial use. Key challenges to such an application are modification of refiner plates to accommodate the sensors and passage of signal wires from the sensor to the refiner exterior.

CONCLUSION

This study investigates in-process detection of the onset of fiber cutting using a custom designed piezoelectric sensor measuring normal and shear forces, perpendicular to the major axis of the refiner bars, in an AIKAWA/Advanced Fiber Technologies Inc. 16-in. single-disc LC refiner. Trials were run using mechanical SPF softwood pulp with 378 ml CSF at 2.5% and 3.5% consistency for three rotational speeds (1200, 1000, and 800 rpm) and a wide range of plate gaps. The pulp was sampled at regular intervals, and the length-weighted fiber length was determined for each sample. The data recorded from the sensors were processed and the distributions of the peak normal and shear forces and peak coefficient of friction are determined for each operating condition. A two-parameter Weibull function is fit to each of these distributions. The Weibull scale parameter is calculated and length-weighted fiber length is plotted as a function of this parameter. The results show that the onset of fiber cutting consistently corresponds to a distinct transition in the plot of length-weighted fiber length versus scale parameter. In addition, the power spectrum of the sensor data indicates that the magnitude of the dominant frequency can be used as an indication of the onset of fiber cutting. This result suggests that the sensor has potential to be used for in-process detection of the onset of fiber cutting. **TJ**

ACKNOWLEDGEMENTS

This work is funded by a Collaborative Research and Development grant provided by National Sciences and Engineering Research Council of Canada (NSERC) and the following partners, who we thank for their ongoing support: AB Enzymes, Alberta Newsprint Company, Andritz, BC Hydro, Canfor, Catalyst Paper, FPInnovations, Holmen Paper, Meadow Lake Pulp (Paper Excellence), Millar Western, NORPAC, West Fraser, Westcan Engineering, and Winstone Pulp International.

A special thanks to M. Miller, E. Jahangir, E. Trudel, G. Burton, and G. Soong for their assistance during the preparation and execution of the refining trials at the Pulp and Paper Center at the University of British Columbia.

LITERATURE CITED

1. Luukkonen, A., Olson, J.A., and Martinez, D.M., *J. Pulp Pap. Sci.* 36(1-2): 28(2010).
2. Muenster H., Ferritsius O., Lecourt M., et al., *Proc. Int. Mech. Pulping Conf.*, TAPPI Press, Atlanta, GA, USA, 2005, p. 213.
3. Zha, Q., Lanouette, R., Law, K.-N., et al., *Prepr. - PAPTAC Annu. Meet., 94th*, Pulp and Paper Technical Association of Canada, Montreal, 2008, p. B481.
4. Musselman, R., Letarte, D., and Simard, R., *Int. Refin. Conf., 4th*, Pira International, Leatherhead, UK, 1997, pp.139–148.
5. Sandberg., C., Sundström, L., and Nilsson, L., *Proc. Int. Mech. Pulping Conf.*, TAPPI Press, Atlanta, 2009, p. 186.
6. Kappel, J., *Mechanical Pulps: From Wood to Bleached Pulp*, TAPPI Press, Atlanta, 1999.
7. Smook, G.A., *Handbook for Pulp and Paper Technologists*, 2nd Edn., Angus Wilde Publications, Vanouver, BC, Canada, 1992.
8. Luukkonen, A., Olson, J.A., and Martinez, D.M., *J. Pulp Pap. Sci.*, 36(3-4): 107(2010).
9. Luukkonen, A., Ph.D. thesis, "Development of a methodology to optimize low consistency refining of mechanical pulp," University of British Columbia, Vancouver, 2011.
10. Nugroho, D.D.P., "Low consistency refining of mixtures of softwood and hardwood bleached kraft pulp: Effects of refining power," M.Sc. thesis, Asian Institute of Technology, Khlong Nung, Thailand, 2012.
11. Elahimehr, A., Olson, J.A., and Martinez, D.M., *Nord. Pulp Pap. Res. J.* 28(3): 386(2013).
12. Berg, J.E., Sandberg, C., Engberg, B., et al., *Nord. Pulp. Pap. Res. J.* 30(2): 225(2015).
13. Kerekes, R.J. and Senger, J.J., *J. Pulp Pap. Sci.* 32(1): 1(2006).
14. Kerekes, R.J., *Nord. Pulp Pap. Res. J.* 26(1): 14(2011).
15. Prairie, B., Wild, P., Byrnes, P., et al., *J. Pulp Pap. Sci.* 34(1): 1(2008).
16. Prairie, B., Wild, P., Byrnes, P., et al., *J. Pulp Pap. Sci.* 108(9): 34(2007).
17. Olender, D., Wild, P., Byrnes, P., et al., *J. Pulp Pap. Sci*. 33(3): 163(2007).

18. Olender, D., Wild, P., Byrnes, P., et al., *Nord. Pulp Pap. Res. J.* 23(2): 218(2008).
19. Harirforoush, R., Wild, P., and Olson, J., *Nord. Pulp Pap. Res. J.* 31(1): 71(2016).
20. Olender, D., Wild, P., and Byrnes P., *J. Process Mech. Eng.* 222(Part E): 115(2008).
21. Prairie, B.C., "Measurement of forces in a low consistency refiner," M.Sc. thesis, University of Victoria, Victoria, BC, Canada, 2005.
22. Graca Carvalho, M., Ferriera, P.J., Martins, A.A., et al., *TAPPI J.* 80(2): 137(1997).
23. Prabhakar Murthy, D.N., Xie, M., and Jiang, R., *Weibull Models*, John Wiley & Sons, Hoboken, NJ, USA, 2003.
24. Lee, S., *Int. J. Basic Appl. Sci.* 14(2): 18(2014).
25. Lundin, T., Ph.D. thesis, "Tailoring pulp fibre properties in low consistency refining," Laboratory of Fiber and Cellulose Technology, Abo Akademyi University, Turku, Finland, 2008.
26. Senger, J., Siadat, A., Ouellet, D., et al., *J. Pulp Pap. Sci.* 30(9): 247(2004).

ABOUT THE AUTHORS

Low consistency (LC) refining of mechanical pulp has been shown to be more energy efficient than conventional high consistency refining. However, degradation of mechanical properties due to fiber cutting at high refining energies has limited the widespread adoption of LC refining. In-process detection of the onset of fiber cutting is essential to reduce fiber cutting.

In 2016, we investigated relationships between local bar forces, plate gap, and fiber length in a single-disc low consistency refiner (Harirforoush et al. [19]). The results showed that the sensors have potential for the onset detection of fiber cutting.

Developing the sensor to withstand the harsh conditions inside the refiner was the most difficult aspect of the research here. Our results suggest that these sensors have potential to be used for in-process detection of the onset of fiber cutting.

The most interesting findings we observed were the distinct transitions in parameters that characterize the distributions of bar forces (forces applied to pulp fibers by the refiner bars). These transitions consistently correspond to the onset of fiber cutting. In addition, the power spectrum of the sensor data indicates that the magnitude of the dominant frequency can be used as an indication of the onset of fiber cutting.

For mills, detection of the onset of fiber cutting conditions is potentially beneficial in low consistency refining as it may reduce fiber cutting, optimize fiber quality improvements, and increase energy efficiency. Our next step is to understand the effect of pulp furnish on the distribution of bar forces and investigate the onset of fiber cutting by using the sensor data.


Harirforoush


Wild


Olson

Harirforoush is a Ph.D. candidate in the Department of Mechanical Engineering and the Institute for Integrated Energy Systems (IESVic), and Wild is professor of Mechanical Engineering and director of IESVic, at the University of Victoria, Victoria, BC, Canada. Olson is associate dean of Research and Industrial Partnership, Faculty of Applied Science; professor of Mechanical Engineering; and FPInnovations professor at the University of British Columbia – Point Grey Campus, Vancouver, BC, Canada. Email Harirforoush at rharirfo@uvic.ca.

Recent advances in lignin-based polyurethanes

YUN-YAN WANG, CHARLES M. CAI, AND ARTHUR J. RAGAUSKAS

ABSTRACT: Given the rise in demand for sustainable renewable biofuels and promising developments in cellulosic ethanol, the valorization of lignin has become essential for biorefining operations, especially with today's low-cost energy production state of affairs. In the past 40 years, numerous efforts have been devoted to incorporate lignin and lignin derivatives into commercial polymeric materials. One of the promising strategies is to utilize multifunctional lignin macromolecules or oligomers as the replacement of polyols during polyurethane synthesis. In this review, recent advances in fabricating polyurethane foams, films, and adhesives with modified or unmodified lignins are examined. The mechanical and thermal properties of these lignin-based polyurethanes were correlated to their formulations, lignin molecular weight, and polydispersity, as well as the structural features of different lignin preparations. Recalcitrance and strong intermolecular interactions of lignin macromolecules are known to prevent them from effective incorporation into other polymeric materials, covalently or noncovalently. Therefore, this review intends to summarize the methods that improve the reactivity of lignin through chemical modification such as depolymerization, demethylation, and chain extension. Future developments and applications will be examined with a special emphasis on tailoring lignin structure to specific applications.

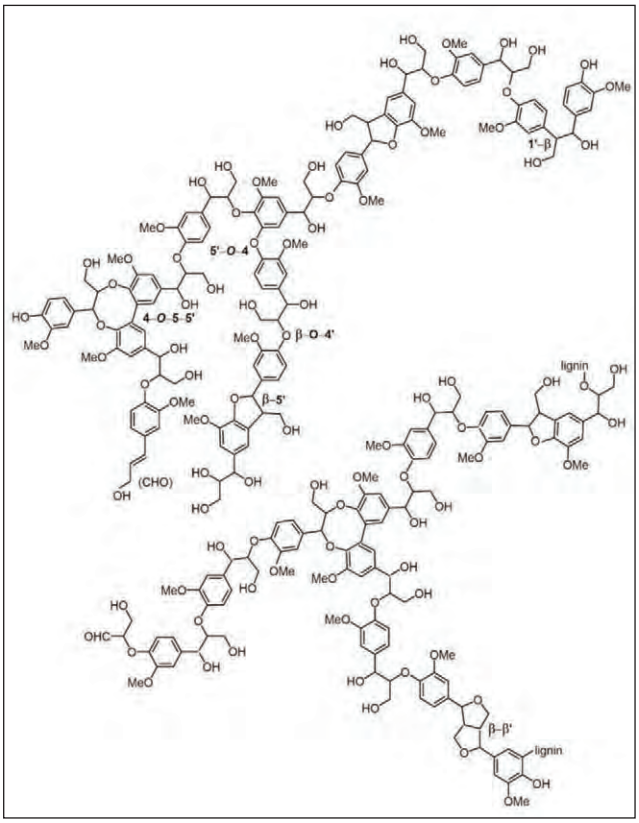
Application: Lignin can be used as polyols to produce polyurethane foams, films, and adhesives.

As the second most abundant renewable biopolymeric material in nature, lignin represents 15%–35% dry weight of plant lignocellulose. During lignin biosynthesis, lignin macromolecules are assembled to form hydroxyphenyl (H), guaiacyl (G), and syringyl (S) subunits through dehydrogenative coupling of three primary monolignols: p-coumaryl alcohol, coniferyl alcohol, and sinapyl alcohol. The contents of these subunits vary depending on the plant species (**Table I**) [1]. **Figure 1** depicts a model of macromolecular softwood lignin structure [2] with six predominant substructures, including *β*–*O*–4, *β*–5, *β*–1, 5–5, 4–*O*–5, and *β*–*β*.

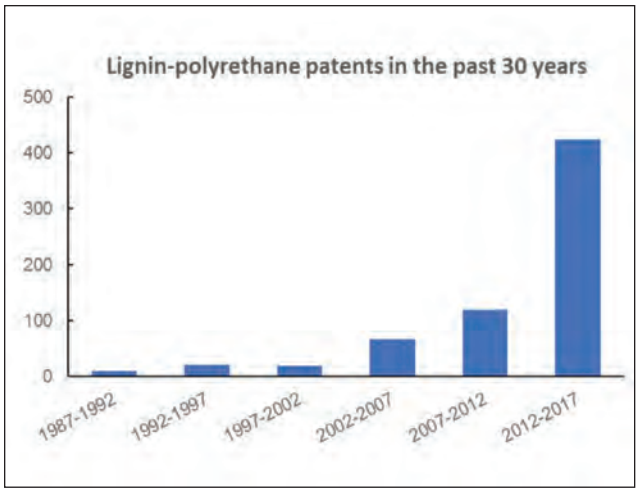
In the paper and pulping industry, the largest application of technical lignins that were considered a waste material is

Sample	S, %	G, %	H, %	S/G
Poplar	61.9	37.8	0.3	1.64
Pine	ND	98.3	1.7	ND
Corn	58.9	38.3	2.8	1.54
Arabidopsis	20.1	77.1	2.8	0.26
ND = none detected.				

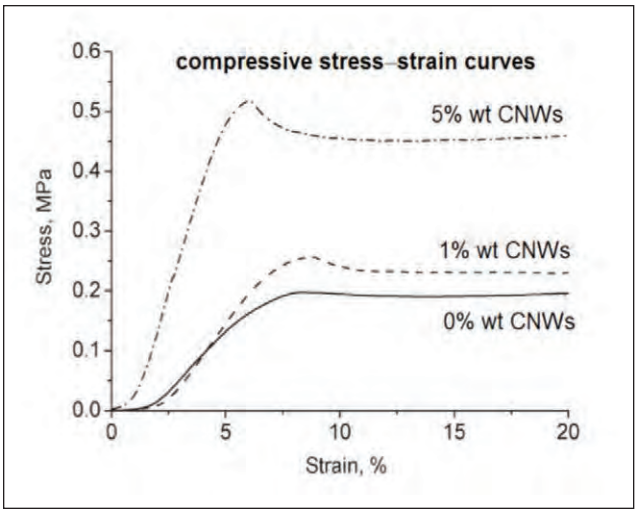
I. Molar % of syringyl (S), guaiacyl (G), and hydroxyphenyl (H) lignin subunits in the plant cell wall of different plant species as determined by two-dimensional nuclear magnetic resonance (2D NMR) spectroscopy [1].



1. An illustration of softwood lignin structure [2]. (Image adapted with permission of American Chemical Society, © 1998.)



2. Lignin-polyurethane patents published worldwide in the past 30 years.



3. Compressive stress-strain curves of lignin-based polyurethane foam reinforced by cellulose nanowhiskers (CNWs) [14]. (Image adapted with permission of Royal Society of Chemistry, © 2012.)

to combust them on site as a low-cost fuel and allow recovery of cooking chemicals; approximately 1%–2% of these technical lignins [3] are used as low-value additives for concrete admixtures, dust control, and oil well drilling muds [4].

These days, the growing demand for green energy has brought more attention to lignin utilization than ever before. The economic viability of converting lignocellulosic biomass to biofuel and commodity organic chemicals relies on the value-added coproduct lignins [5]. By 2022, about 62 million tons of lignin will be produced annually as a coproduct of second-generation biofuel generation in the United States [5], far exceeding the current lignin supply for the additives market worldwide. Therefore, robust commercial applications of lignin will be on the front burner for any lignocellulosic-related industries.

Petrochemical-based polyurethanes are polymerized with small blocks of polyesters or polyethers that are covalently connected through a urethane bridge (–NHCO–O–) [6]. The inherent versatility in polyurethane syntheses makes them a class of polymeric plastics that can be engineered to suit various industrial and residential applications such as rigid and flexible foams, adhesives, sealants, and elastomers. The total production of polyurethane in the United States was 2.4 billion tons with approximately $281 billion in revenues in 2014 [7]. Approximately 50% of the polyols in the North American market are used for the rigid polyurethane foams production annually [8].

The abundance of phenolic and aliphatic hydroxy (OH) groups allows macromolecular lignin to polymerize further in the presence of diisocyanate crosslinker to form the hard segments in polyurethane network [9]. As a heterogeneous polyol, one of key factors that governs the reactivity of lignin with isocyanate is the accessibility of OH groups. Higher conversion of isocyanate group (NCO) into urethane was found as content of aliphatic OH groups increased as a result of solvent fractionation [10].

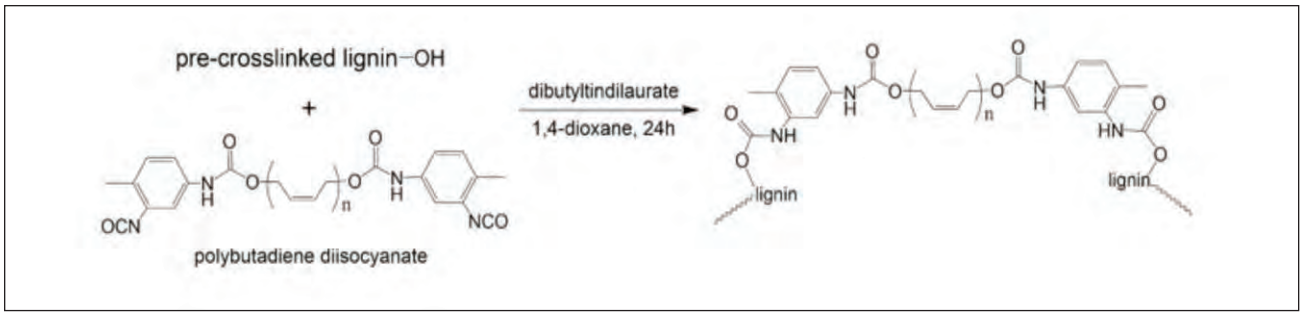
Over 600 patents related to polyurethane containing lignin have been published worldwide in the past 30 years; more than 60% of them were documented since 2012 (**Fig. 2**). It is well recognized that, as a green replacement for petrochemical polyols, the commercialized utilization of low-cost coproduct lignin will reduce the manufacturing cost of polyurethane products, including thermoplastics, foams, and coatings [11-13], and in return will support lignocellulosic biorefinery industries that eventually lead to affordable biofuels and bioproducts for end-use customers.

LIGNIN-BASED POLYURETHANE PRODUCTS

Rigid foams

Li et al. reported the reinforcing effect of cellulose nanowhiskers on a lignin-based rigid polyurethane foam [14]. The reaction between the oxylpropylated ethanol organosolv lignin (weight-average molecular weight, M_w = 3700 g/mol, PDI = 2.2) and polymeric methylene diphenyl diisocyanate (MDI) was catalyzed by dimethylcyclohexaneamine and a Mannich base catalyst. In the presence of 5% cellulose nanowhiskers, the density and compressive strain of the corresponding polyurethane foam increased significantly by 185% and 260%, respectively (**Fig. 3**). The lignin content in the foam is estimated to be less than 33%. Similarly, in the study of rigid polyurethane foam reinforced with pulp fiber, the compressive strength dropped dramatically as the content of alkaline lignin increased gradually to 37.2%, yet reinforcement of the additional 1%–5% pulp fiber was quite limited compared to the impact of lignin content [15].

Instead of using filler, monomeric 1,4-butanediol was examined as a bifunctional chain extender in a hardwood organosolv lignin-base (12%–36% w/w) rigid polyurethane foam [16]. It was found that when the ratio of NCO/OH was kept constant, additional 3.5% butanediol could improve foam compressive strength by 30%.



4. Lignin-based polyurethane film synthesized from the pre-crosslinked solvent-extracted lignin and oligomeric polybutadiene diisocyanante [18]. (Image reproduced with permission of Royal Society of Chemistry, © 2013.)

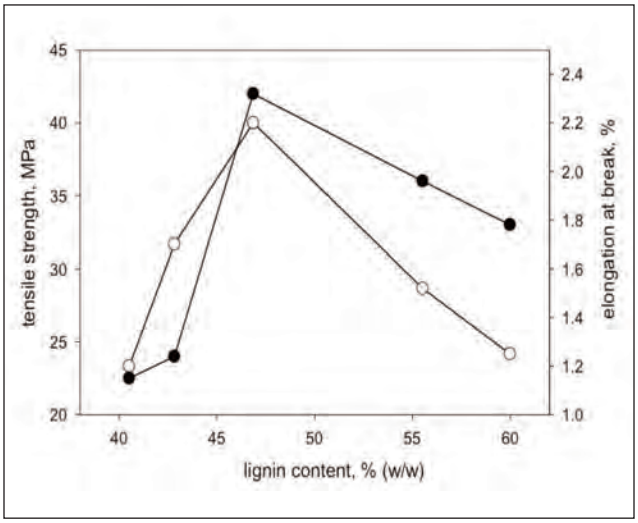
Films

A solvent-extracted hardwood lignin sample (equivalent to that of trademarked Alcell lignin) was pre-crosslinked through reaction with formaldehyde [17]. The pre-crosslinked lignin possessed a quite broad molecular weight distribution pattern with polydispersity index (PDI) of 61; meanwhile, its number-average molecular weight (M_n) increased from 1840 to 12500 g/mol [18]. A series of polyurethane films were synthesized by reacting the pre-crosslinked lignin (65%–80% w/w) with polybutadiene (PBD) (M_n ~2500 g/mol) ended with an isocyanate group on each side (OCN–PBD–NCO) as depicted in **Fig. 4**. It was expected that the rubbery polybutadiene segments would toughen lignin-based polyurethane thermoplastics. Phase separation was confirmed through differential scanning calorimetry (DSC) analyses as two distinct glass transition temperatures (T_g) representing PBD (-30ºC) and lignin (150ºC) were observed. The Young's modulus of lignin itself was reported to be 2.3~4.7 GPa [19]; however, the modulus of the rubbery plateau and tensile behaviors of the lignin-based polyurethane thermoplastics showed strong dependence on the crosslinking density rather than the amount of lignin present in the thermoplastics. When the lignin content reaches 80%, the resultant polyurethane became very brittle [18].

In another study that lignin was employed as the only source of hydroxyl groups, Jia et al. extracted a dilute hydrochloric acid pretreated spruce wood meal with 80% (w/w) 1,4-butanediol aqueous solution at 220ºC for 1 h [20]. The obtained lignin preparation exhibited a low molecular weight (M_n = 2483 g/mol) with narrow polydispersity pattern (PDI = 1.52). The monolithic polyurethane film was cast from dioxane at 85ºC; MDI and triethylamine were used as crosslinker and catalyst, respectively. Such a simple formulation produced polyurethane films containing more than 40% lignin, and the best tensile properties (**Fig. 5**) were achieved when the NCO/OH ratio reached 1.7 and the corresponding lignin content was 47%.

Adhesives and coatings

Griffini et al. conducted direct reactions of unmodified softwood kraft lignin with toluene diisocyanate (TDI) in 2-methyl tetrahydrofuran (MeTHF) [21]. In this work, the kraft lignin applied in polyurethane was MeTHF-soluble fraction (M_n = 1310 g/mol, PDI = 1.8, T_g = 92ºC) that accounted for approximately 50% of the crude kraft lignin sample. The highest T_g was observed as 143ºC when NCO/OH ratio reached 0.16, equivalent to 70% (w/w) lignin incorporated in the polyurethane. The adhesion strength of 80% (w/w) lignin-polyurethane adhesive was investigated by performing pull-off adhesive tests on different substrates such as glass, metal, and wood. It was found that the best application of this lignin-polyurethane adhesive would be on the woody surface due to the high nature affinity of lignin with wood. Moreover, another potential application of this adhesive would be on a glass surface, as the corresponding adhesive strength achieved 7.6 MPa. In addition, Nacas et al. converted a technical grade kraft lignin and MDI into polyurethane adhesive in tetrahydrofuran [22]. It was claimed that the presence of a greater amount of free isocyanate groups would contribute to the lap shear strength on wood, and the highest lap shear strength (6.3 MPa) was observed when NCO/OH was 1.2.



5. Effects of lignin content on the tensile strength (dark dot) and elongation of break (open dot) of 1,4-butanediol aqueous extracted lignin-based polyurethane films [20]. (Image reproduced with permission of Royal Society of Chemistry, © 2015.)

MODIFIED LIGNIN IN POLYURETHANE

Demethylation

The crosslinking density in lignin-based polyurethane is governed by the frequency of hydroxyl group in lignin components. Some studies [23-26] demonstrate that the aromatic methoxy groups can be substituted by hydroxyl group through demethylation. Wu et al. reported that sulfur dioxide-mediated demethylation could increase the contents of the phenolic hydroxyl group and carboxyl group by 54% and 55%, respectively [25]. The hydrobromic acid (HBr)-treated alkaline lignin exhibits a 28% increase in hydroxyl group compared to unmodified lignin sample [26], and subsequently, 6.5-fold increase in modulus was achieved due to higher crosslinking density of the resultant polyurethane network. However, the HBr-treated lignin-based polyurethane was too brittle, and an additional 40% polyethylene glycol (M_n = 200 g/mol) was needed during the polyurethane syntheses, which eventually lowered the lignin content to 17% (w/w).

Chain extension

Converting phenolic OH groups into long chain aliphatic ones has been considered an effective approach to improve the reactivity with NCO by reducing the steric and/or electronic constraints. A flexible linear chain polymer such as propylene oxide has been introduced to the lignin-based polyurethane system as the soft segments through oxyalkylation [27]. The chain-extended hydroxpropyl lignin exhibited better solubility in organic solvents and lower glass transition temperature compared to underivatized lignin. The toughness and elongation at break of a lignin-based polyurethane network can be further improved by incorporation of soft segments through blending [28].

Esterification is another effective method to incorporate soft segments into the lignin-based polyurethanes. Organosolv hardwood lignin produced from the Alcell process (M_n = 1000 g/mol, PDI = 2.28) was esterified with oleic acid by using a solvent-free and catalyst-free method [29]. A new hydroxyl group was added to the double bond of oleic acid via epoxidation followed by oxirane ring-opening reaction. The resultant lignin-fatty acid based macropolyol mixture was then reacted with an isocyanate prepolymer prepared with poly(propylene)glycol with different molecular weights to form the final biobased polyurethane with lignin content up to approximately 37% (w/w). Such lignin-fatty acid based polyurethanes are rubbery materials with elongation at break ranging from 170% to 360% and highest value of ultimate tensile strength reaching 9.6 MPa. Thermal analyses by DSC and dynamic mechanical analysis (DMA) indicated that the elastomeric properties arose from microphase separation [30].

The lignin-based polyurethanes containing soft segments in general exhibit multi-step thermal decomposition patterns, depending on the components in the network [31]. A typical example can be found in the study of the polyurethanes containing both xylaric acid-lignin ester and polyethylene glycol [32]. Four decomposition temperature ranges were observed when the samples were heated up to 700ºC. The decompositions occurring at 190ºC and 550ºC were correlated to the degradation of urethane bonds and aromatic moieties in lignin, respectively.

Depolymerization

Cinelli et al. [33] studied the syntheses flexible polyurethane foams with depolymerized Indulin AT lignin (MeadWestvaco Corp.; Richmond, VA, USA). The lignin was depolymerized in the presence of glycerol and polyethylene glycol (M_n = 400 g/mol) in a microwave oven at 180ºC for 3 min to form a liquefied mixture. However, such a mixture was not suitable for preparing flexible polyurethane foam due to its excessive viscosity and a very high OH value; therefore, additional polyols were added to reduce the viscosity and T_g of the final polyurethane foam as well. The lignin contents by weight in the resultant flexible polyurethane foams were always below 14%.

CONCLUSION

As the quest for high lignin content polyurethane systems continues, more attention will be placed on producing polyurethane using lignin as the main or sole hydroxyl group provider. The NCO/OH ratio, solubility of coproduct lignin in organic solvents, the interactions between lignin and non-lignin components, and between lignin macromolecules [2] will all affect the incorporation level of lignin in polyurethane in a synergistic way. Considering the production cost and environmental impact of lignin-based polyurethanes, minimal chemical modification on coproduct lignin will be preferred in the competition with conventional petrochemical polyols [34]. **TJ**

ACKNOWLEDGMENTS

We acknowledge support through U.S.D.A. National Institute of Food and Agriculture Grant no. 9008-004957 titled "Integrated Biorefinery to Produce Ethanol, High Value Polymers, and Chemicals from Lignocellulosic Biomass".

LITERATURE CITED

1. Mansfield, S.D., Kim, H., Lu, F., et al., *Nat. Protoc.* 7(9): 1579(2012).
2. Brunow, G., Kilpeläinen, I., Sipilä, J., et al., *ACS Symp. Ser.* 697(10): 131(1998).
3. Lora, J.H. and Glasser, W.G., *J. Polym Environ.* 10(1): 39(2002).
4. Berlin, A. and Balakshin, M., in *Bioenergy Research: Advances and Applications*, Elsevier, Waltham, MA, USA, 2012, pp. 315-336.
5. Ragauskas, A.J., Beckham, G.T., Biddy, M.J., et al., *Science* 344(6185): 709(2014).
6. Mahmood, N., Yuan, Z., Schmidt, J., et al., *Renewable and Sustainable Energy Reviews* 60: 317(2016).
7. American Chemistry Council, "The Economic Benefits of the U.S. Polyurethanes Industry 2015," American Chemistry Council – Economics & Statistics Department, Arlington VA, USA, September 2016.

8. Luo, N., Qian, J., Cupps, J., et al., in *Polyurethanes Technical Conference API*, American Chemistry Council, Arlington, 2008, pp. 801-808.
9. Saraf, V.P., Glasser, W.G., Wilkes, G.L., et al., *J. Appl. Polym. Sci.* 30(5): 2207(1985).
10. Arshanitsa, A., Krumina, L., Telysheva, G., et al., *Ind. Crops. Prod.* 92(12): 1(2016).
11. Zhang, Y., Yang, D.-Q., and Wang, X.-M., et al., *PCT Int. Appl.*, 2012, WO 2012113058 A1, CA 201200153.
12. Langlois, A. and Drouin, M., *PCT Int. Appl.*, 2015, WO 2015021541 A1, CA 2014050724.
13. Mukerjee, S., Rogers, K.A., Beatty, M.J., et al., U.S. Pat. Appl., 2016, US 20160208044 A1.
14. Li, Y. and Ragauskas, A.J., *RSC Adv.* 2(8): 3347(2012).
15. Xue, B.-L., Wen, J.-L., and Sun, R.-C., ACS Sustainable Chem. Eng. 2(6): 1474(2014).
16. Pan, X. and Saddler, J.N., *Biotechnol. Biofuels* 6: 12(2013).
17. Satio, T., Brown, R.H., Hunt, M.A., et al., *Green Chem.* 14(12): 3295(2012).
18. Saito, T., Perkins, J.H., Jackson, D.C., et al., *RSC Adv.* 3(44): 21832(2013).
19. Elder, T., *Biomacromolecules* 8(11): 3619(2007).
20. Jia, Z., Lu, C., Zhou, P., et al., *RSC Adv.* 5(66): 53949(2015).
21. Griffini, G., Passoni, V., Suriano, R., et al., *ACS Sustainable Chem.* Eng. 3(6): 1145(2015).
22. Nacas, A.M., Ito, N.M., De Sousa Jr., R.R., et al., *J. Adhesion* 9(1-2): 18(2017).
23. An, X.N., Schroeder, H.A., and Thompson, G.E., *Chemistry and Industry of Forest Products* 15(3): 36(1995).
24. Hu, L., Pan, H., Zhou, Y., et al., *BioResources* 6(3): 3515(2011).
25. Wu, S.B. and Zhan, H.Y., *Cellul. Chem. Technol.* 35(3): 253(2001).
26. Chung, H. and Washbum, N.R., *ACS Appl. Mater. Interfaces* 4(6): 2840(2012).
27. Kelly, S. and Glasser, W.G., *J. Appl. Polym. Sci.* 36(4): 759(1988)
28. Kelly, S.S., Glasser, W.G., and Ward, T.C., *ACS Symp. Ser.* 397(31): 402(1989).
29. Laurichesse, S., Huillet, C., and Averous, L., *Green Chem.* 16(8): 3958(2014).
30. Xu, Y., Petrovic, Z., Das, S., et al., *Polymer* 49(19): 4248(2008).
31. Sen, S., Patil, S., and Argyropoulos, D.S., *Green Chem.* 17(11): 4862(2015)
32. Pohjanlehto, H., Setälä, H.M., Kiely, D.E., et al., *J. Appl. Polym. Sci.* 131(8): 39714(2013)
33. Cinelli, P., Anguillesi, I., Lazzeri, A., *Eur. Polym. J.* 49(6): 1174(2013).
34. Hatakeyama, H. and Hatakeyama, T., in *Biopolymers: Lignin, Proteins, Bioactive Nanocomposites* (A. Abe, K. Dušek, and S. Kobayashi, Eds.), Springer, Berlin, 2010, pp. 1-63.

ABOUT THE AUTHORS

We created this review because valorization of co-product lignin is currently a frequently mentioned research topic, and converting lignin into polyurethane is widely studied.

One of the most difficult aspects of research in this area is how to increase the lignin content in the polyurethane, while maintaining its mechanical properties. Consequently, various modification approaches have been reviewed in the paper.

One finding in the review is that lignin-based polyurethanes can be synthesized by using lignin as the sole resource for phenolic and aliphatic hydroxy (OH) groups.

If lignin-based polyurethane can be commercialized, mills can make profit from co-product lignin instead of burning it as low-cost fuel. The next step is to explore the feasibility of producing polyurethane containing very high amounts of lignin, as well as studying lignin's solubility in organic solvents so that its reactivity is improved.



Wang



Cai



Ragauskas

Wang is postdoctoral research associate in the Department of Forestry, Wildlife, and Fisheries and Center for Renewable Carbon, University of Tennessee Institute of Agriculture, Knoxville, TN, USA. Cai is an assistant research engineer and adjunct professor, Department of Chemical and Environmental Engineering, University of California – Riverside, Riverside, CA, USA. Ragauskas is professor/Governor's Chair in Biorefining, Oak Ridge National Laboratory; Department of Chemical and Biomolecular Engineering; Department of Forestry, Wildlife, and Fisheries; and Center for Renewable Carbon; University of Tennessee, Knoxville, TN, USA. Email Ragauskas at aragausk@utk.edu.

Toward valorization of lignin: characterization and fast pyrolysis of lignin recovered from hot-water extracts of electron-beam irradiated sugar maple

DEREK CORBETT, OFEI MANTE, AND BILJANA BUJANOVIC

ABSTRACT: This paper provides an analysis of lignin-rich (>80%) solids recovered as a byproduct of hot-water extraction (HWE) pretreatment performed on sugar maple (*Acer saccharum*) (autohydrolysis at 160°C for 2 h). The effects of electron beam irradiation (EBI) pretreatment before HWE were assessed with regard to lignin removal during HWE and selected features of the recovered lignin. The results of catalytic fast pyrolysis – gas chromatography-mass spectrometry (Py-GCMS) are also discussed. EBI of sugar maple increased lignin removal (delignification) during subsequent HWE; however, recovery of dissolved lignin and lignin degradation products from the hot water extract was hindered. Variation of EBI energy dosages before HWE had little effect on lignin recovered from extracts, except for a slightly reduced molecular weight, as evidenced by size exclusion chromatography. The recovered lignin was hypothesized to have advantages for Py-GCMS compared with common technical lignins, such as kraft or dilute acid hydrolysis lignin, because of lower ash and sulfur content and fewer condensed structures (i.e., increased reactivity). The Py-GCMS results showed that the hot water-extracted lignin-rich samples produced less residual char than kraft and commercial dilute acid hydrolysis lignin samples; however, yields to simple phenols were reduced compared with kraft lignin results, mostly because of the high syringyl-unit content of the hardwood-derived lignin.

Application: This research could benefit a mill's research and development efforts toward developing products other than paper from lignocellulosic material.

Concerns about climate change and the long-term sustainability of the fossil fuel industry have increased the interest in improved fractionation and use of lignocellulosic biomass to produce renewable and bio-based products. Lignocellulosic biomass has considerable potential to replace fossil resources for the production of biofuels and biochemicals because of its abundance, low value as food, and renewable nature. However, the inherent resistance to fractionation of lignocellulosic biomass (LCB) hinders its efficient use. To tackle the substantial barrier of biomass recalcitrance, many pretreatment methods, such as steam explosion, dilute acid, ammonia fiber explosion (AFEX), liquid hot water, wet oxidation, and carbon dioxide explosion, have been suggested and studied [1-9] Among these, hot water extraction (HWE) (160°C, 2 h), a hydrothermal (autohydrolytic, mild acidolysis) pretreatment, has been shown to relatively selectively dissolve hemicelluloses/xylans to produce a valuable sugar solution from xylan-rich lignocellulosics (*Angiosperms*) with limited inhibitor production [10,11]. At the same time, this pretreatment increases the susceptibility of the remaining biomass to further treatments, such as enzymatic hydrolysis, pelletizing, or pulping [11-14]. Additionally, electron beam irradiation (EBI) has been proposed as an LCB pretreatment method to improve the enzymatic hydrolysis of in-situ cellulose [4,5,9,15,16]. EBI effectively reduces cellulose crystallinity, substantially improving enzymatic hydrolysis efficiency. The effect of EBI on lignin is not well understood, although some studies have shown that free radicals produced during EBI lead to the occurrence of competing cleavage and cross-linking reactions in lignin [9,17].

The HWE pretreatment process results in three main product streams: 1) pretreated solids with reduced resistance to further treatment, 2) extract containing predominantly dissolved hemicelluloses (mostly oligomers), and 3) a lignin-rich solid precipitated or ultrafiltered from the extract. During HWE, initial cleavage of acidic functional groups, such as acetic acid (deacetylation of acetylated glucuronoxylans), results in a decrease in pH. This facilitates cleavage of acid-labile bonds (e.g., glycosidic bonds) and dissolution of resulting low molecular-weight hydrophilic molecules/fragments of polymers (e.g., xylose-based carbohydrates such as water-soluble shorter chains of xylans, xylooligomers, and xylose) [11]. The final pH of the hot water extract is ~3.5 (sugar maple) [11].

HWE results in the dissolution of a large percentage of hemicelluloses from *Angiosperms*. For example, ~80% of hemicelluloses were removed from sugar maple (*Acer saccharum*) in previous HWE studies [18].

In addition to hemicelluloses, a portion of relatively easily accessible lignin is also dissolved. In earlier studies, 9.4% and 15.7% of the original lignin was solubilized from sugar maple and foxglove tree/princess tree (*Paulownia tomentosa*) chips, respectively [13]. Depending on the LCB type and HWE conditions (particle size and water-to-biomass ratio), delignification degree can be even higher; sugar maple: 30%, apricot pit shells: 24%, wheat straw: 28% (Parr reactor, 30 mesh, 50:1 water-to-biomass ratio) [13,19]. EBI with HWE has been studied as a two-step pretreatment for further improvement of enzymatic hydrolysis efficiency [5,9,20]. It was shown that EBI increases mass removal from sugar maple during HWE. In addition, EBI and HWE both enhanced enzymatic hydrolysis efficiency, although HWE had a stronger effect than did EBI [20]. However, isolation and chemical characterization of the lignin dissolved during this two-step EBI-HWE process was not performed in those studies.

Removal of dissolved lignin from the hot water extracts is necessary before further processing, especially hydrolysis and fermentation, because dissolved lignin fragments are responsible for enzyme deactivation and inhibit biological growth [21-23]. Reduction of the pH of the hot water extract to 2.0 facilitates precipitation of a portion of the dissolved lignin. The solids can then be recovered by membrane filtration (retentate lignin) or centrifugation (precipitate lignin) [24]. It has been reported that greater than 60% of the total lignin dissolved can be recovered from the extract using membrane ultrafiltration (~1.8% based on the total ovendry mass of starting sugar maple) [23]. The rest of the dissolved lignin may be recovered in an acid hydrolysis stage conducted to hydrolyze any remaining hemicellulose oligomers.

Even though a relatively small percentage of the original lignin in wood is recovered from hot water extracts, in a biorefinery using HWE for sugar production, a considerable quantity of lignin would be produced. In a plant processing 100 tons of sugar maple biomass per day, ~375 tons of lignin would be produced per year (based on 25% lignin in biomass, 10% lignin dissolved, 60% of the dissolved lignin recovered, and 252 business days per year).

In an economically viable integrated biorefinery producing relatively low-value biofuels, each of the co-product streams resulting from pretreatment must be effectively used in a high-value application. Therefore, attempts have been made to understand the properties of the lignin recoverable from hot water extracts and to find applications for its use [25-27]. A good understanding of the effect of EBI on lignin removal during HWE and the chemical nature of the dissolved lignin is important for determining the viability of the process and determining potential applications for the lignin produced. The present study expands on past work and presents results obtained in our recent experiments aimed at recovery and characterization of lignin-rich solids (precipitate lignin) removed from sugar maple and electron beam-irradiated sugar maple by HWE.

Many options for the use of lignin in high-value applications have been proposed, including production of fuels, polymeric macromolecules, and low molecular weight, aromatic type compounds [28]. This paper presents an initial assessment of the potential for valorization of HWE precipitate lignin by fast pyrolysis. Fast pyrolysis, involving the thermochemical depolymerization of high-carbon solids, is an attractive technology for the production of valuable low molecular weight chemicals. During fast pyrolysis of lignin, thermal energy is used to break inter-unit lignin bonds while maintaining the native aromatic structure of the polymer. However, fast pyrolysis of lignin is difficult because lignin is highly prone to char formation from condensation reactions and typically suffers from low yields.

Catalysis has therefore been applied to improve the yield and purity of desired compounds [29]. Zeolite catalysts have generally been the focus of catalytic fast pyrolysis studies. HZSM-5 has been more effective at producing aromatic hydrocarbons from lignin than have similar catalysts [29,30]. However, pore exclusion, dealumination, and catalytic coke formation resulting in deactivation are significant issues with zeolite catalysts [30]. In addition, zeolites tend to be extremely aggressive and destroy the potentially valuable phenolic structure of the lignin monomers. Metal oxide minerals such as titanium dioxide (TiO_2), zirconium oxide (ZrO_2), and iron oxide (Fe_2O_3) have been studied as a less severe alternative to zeolites [31-33]. Metal oxides have shown promise as catalysts for the thermal degradation of organic compounds while maintaining aspects of the native structure [31-33]. In this study, HZSM-5 and TiO_2 (anatase) powdered catalysts were investigated for the production of low molecular weight phenols from lignin-rich solids derived from HWE-based biorefinery processes.

For the pyrolysis studies in this work, we hypothesized that the HWE precipitate lignin would behave differently from common technical lignins, such as kraft lignin, considering the fact that the HWE precipitate lignin has lower inorganic content (including lower sulfur content) and might be more reactive (higher content of aryl ether bonds and less condensed structure). Preliminary evaluation of hot water-extracted precipitate lignin for valorization by fast pyrolysis was performed along with an analysis of the effects of EBI treatment before lignin removal (by HWE) on pyrolysis results. Softwood kraft lignin and hardwood (sugar maple) dilute acid hydrolysis (DAH) lignin were included in the study for comparison, as these are two currently available technical lignins.

EXPERIMENTAL

Materials

Sugar maple was the primary biomass species investigated in this work because of its potential for application in an HWE-based biorefinery in the northeastern United States [12]. In

addition to sugar maple, two technical lignins were used as references: softwood kraft lignin purchased from Sigma-Aldrich (St. Louis, MO, USA) (CAS: 8068-05-1) and a DAH lignin produced during treatment of sugar maple shavings provided by Pure Lignin Environmental Technologies (Kelowna, BC, Canada). Kraft lignin was used for comparison in pyrolysis studies only. Although the chemical character of different kraft lignins can vary, characterization of softwood kraft lignin in general has been covered previously [34,35].

Electron beam irradiation

EBI was performed at IBA Industrial in Edgewood, NY, USA, using a 250 kW, 3.0 MeV IBA Dynamitron E-beam accelerator. Total energy dosages were 250 kGy, 750 kGy, and 1000 kGy. Bars (~2 ft. × ~1 in. × ~1 in.) were passed under the EB accelerator on a conveyer belt running at 3 m/min and exposed to a uniform energy of 125 kGy per scan [9]. Samples were treated multiple times to reach the final total irradiation energies. The irradiation dose was measured using a thin film dosimeter, which showed that the dose entering the sample was approximately equal to the dose leaving the sample, indicating that the energy was applied evenly throughout the sample. Bars of EBI-treated sugar maple (identified by irradiation dosage as I_{250}SM, I_{750}SM, and I_{1000}SM) were supplied by the Department of Chemistry at the State University of New York College of Environmental Science and Forestry (Syracuse, NY, USA). For HWE, bars were first cut into cubes, then each cube was manually chopped using a hammer and knife to produce consistent wood fragments of about the same size as a typical wood chip (10-30 mm × 3-6 mm).

HWE and lignin recovery

HWE experiments of sugar maple and electron beam irradiated sugar maple were performed in a 6 L M/K digester: deionized water; ~600 g air-dried wood chips; water-to-oven dry wood ratio = 4:1; ramped temperature increase to 160°C (~25 min); 2 h at 160°C; *p*-factor = 543.7 (*p*-factor as described by Sixta [36]). Liquor was circulated with a centrifugal pump through an electric heat exchanger. Temperature was controlled with a proportional-integral-derivative (PID) controller. Hot water-extracted chips were washed twice with water for 20 min at 80°C. Material removed during water washes was not used in this work. HWE was performed in duplicate side-by-side digesters (standard deviations of digester yields were less than 1%). Moisture content measurements of wood chips before and after HWE (air-dried for 1 week) were taken to ensure accurate water-to-ovendry biomass ratios and to determine digester yields. Final pH of extract was recorded at room temperature.

HWE precipitate lignins ("maple extract precipitate:" ME_p, and "irradiated maple extract precipitates:" $I_{250}ME_p$, $I_{750}ME_p$, and $I_{1000}ME_p$) were recovered from the hot water extract by pH adjustment to 2.0 ± 0.02 with sulfuric acid (20%) followed by cold-settling, centrifugation, and decantation. Lignin was transferred to pre-weighed vessels and dried in the vacuum oven at 40°C. After weighing, lignin samples were ground with a mortar and pestle and stored in 20 mL scintillation vials.

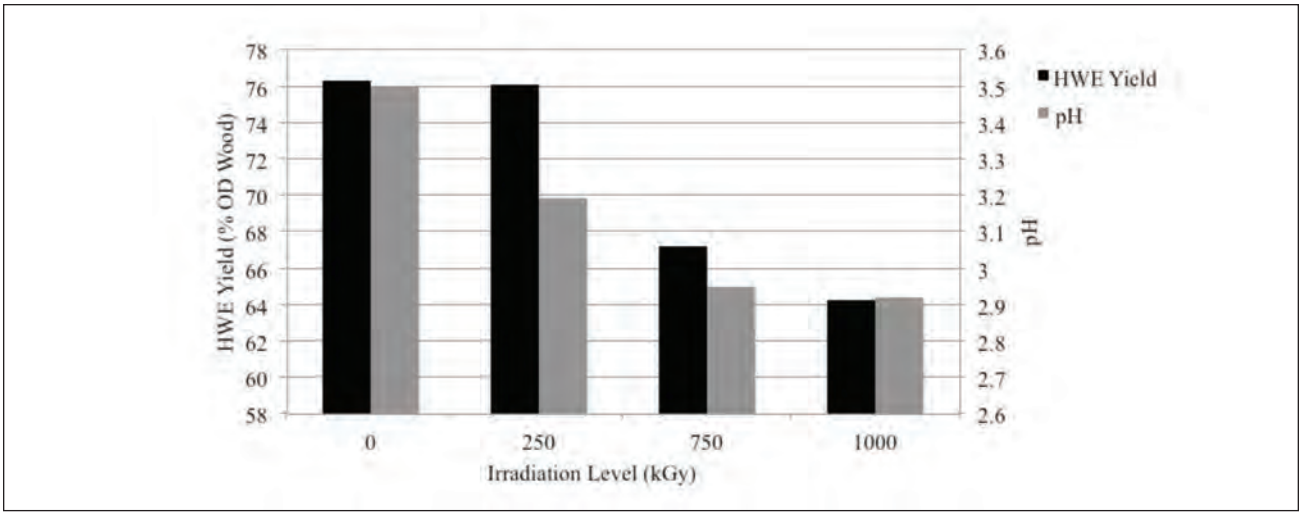
Lignin characterization

Moisture content was determined as the mass loss at 105ºC during thermogravimetric analysis (TGA) in air. Ash content was determined in accordance with TAPPI Standard T413 om-93, "Ash in wood, pulp, paper and paperboard: combustion at 900ºC." Lignin content (including acid soluble content) was determined by a modified Klason lignin method involving ultrasonication in 72% sulfuric acid for 1 h (Branson 3510 ultrasonic bath, Branson Ultrasonics Corporation; Danbury, CT, USA) and autoclaving at 120ºC in 4% sulfuric acid for 1 h (Saniclave 200, Revolutionary Science; Shafer, MN, USA) [37]. Acid-soluble lignin content was determined using an ultraviolet-visible (UV-Vis) spectrophotometer at 205 nm (Genesys 10S, ThermoScientific; Waltham, MA, USA) [37]. A pre-extraction with organic solvents was not performed for the precipitate lignins because low molecular weight organic compounds remain mainly soluble after acidification of hot-water extracts [24].

Carbohydrate content was determined via acid hydrolysis and high performance liquid chromatography (HPLC) analysis following a slightly modified National Renewable Energy Laboratory (NREL) procedure (initial hydrolysis was done for 2 h at 20ºC) [38]. Sugars other than xylose were found to be below the detection limit of the method. Because a large amount of xylan remaining in lignin might be converted to furfural during autohydrolysis under these conditions [39], results likely underestimate the actual carbohydrate content. Overall mass balances for the IME_p and DAH lignins (lignin + ash + carbohydrates) were between 84% and 88%.

Free phenolic hydroxyl group (PhOH) content was determined by the periodate oxidation method [40] and a UV-Vis method [41]. The periodate oxidation method measures methanol released during the formation of an *ortho*-quinone structure through oxidation with aqueous sodium periodate solution. This method can only detect PhOH groups with an adjacent (*ortho*) methoxyl group. The amount of methanol produced at the end of the periodate oxidation was determined by ^{1}H nuclear magnetic resonance (NMR) spectroscopy. The UV-Vis method is based on the absorbance change that occurs when PhOH groups are ionized. Unlike the periodate method, the UV-Vis method can detect PhOH units that do not have adjacent methoxyl groups [41]. It is therefore expected that the UV-Vis results will be higher than the periodate results, particularly if the lignin samples contain *p*-hydroxyphenylpropanoid or catechol units [41].

TGA was performed using a Q5000 series thermogravimetric analyzer (TA Instruments; New Castle, DE, USA) with a temperature ramp of 10ºC/min to 700ºC in nitrogen. Air was used for moisture content determination. UA 2000 software from TA Instruments was used for data analysis. Samples were not run in duplicate.



1. M/K digester hot water extraction results. "HWE yield" refers to the mass of ovendry chips remaining after hot-water extraction (HWE) pretreatment as a percent of the starting ovendry chip weight (digester yield).

All heteronuclear single quantum coherence experiments (HSQC) spectroscopy experiments were acquired at 30°C on a Bruker AVANCE III 600 spectrometer (600 MHz 1H frequency, Bruker Biospin Corporation; Billerica, MA, USA) equipped with a 5 mm BBO cryo-cooled Prodigy probe with a z-gradient. Sample size was ~15 mg lignin, in 0.5 mL dimethyl sulfoxide-d_6 (DMSO-d_6) solvent. Data were processed with Topspin v. 3.2 processing software from Bruker Biospin. The distortionless enhancement by polarization transfer-edited HSQC had the following parameters: acquired from 11.8 ppm to −0.2 ppm in F2 (^{1}H) using 1024 data points (acquisition time of 71 ms), 220 ppm to 0 ppm in F^1 (^{13}C) using 400 increments, 32 scans with 1.5 s interscan delay, total acquisition time of 2 h and 48 min, or 5 h and 40 min. Processing used typical squared sine-bell apodization in F2 and F1. 2D ^{13}C-^{1}H correlation HSQC NMR spectroscopy data were used to determine the S:G ratio of the lignin samples based on the integral volume of S2/6 and G2 from the aromatic region (G2 integral value was multiplied by two) [26,42].

Size exclusion chromatography was used for determination of molecular weight distribution. Acetylated samples were dissolved in tetrahydrofuran (1 mg/mL) and filtered through 0.45 μm polyvinylidene fluoride filters before analysis. The columns used were Waters (Milford, MA, USA) Styragel HR 0.5, HR 3, and HR 4E. Absorption was measured at 280 nm by a UV spectrophotometer. Polystyrene standards were used for calibration and a third order polynomial equation was used for quantification. Acetylation was achieved by adding a minimal amount of 1:1 pyridine:acetic anhydride. After 24 h, pyridine and excess acetic acid were removed by repeated co-distillations with ethanol in a rotary evaporator.

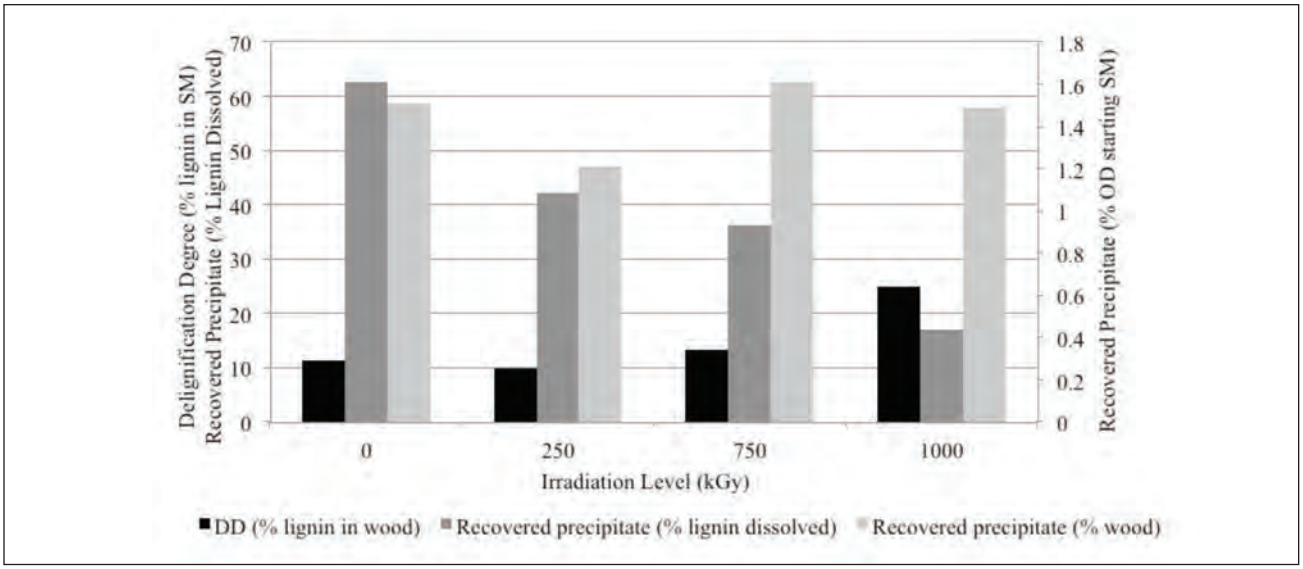
Pyrolysis-gas chromatography mass spectrometry

Before pyrolysis, lignins were manually ground to powder using a mortar and pestle; particle sizes were not determined. Pyrolysis-gas chromatography mass spectrometry (Py-GCMS) studies were performed at the Energy Technology Division of RTI International (Research Triangle Park, Durham, NC, USA). The pyrolysis system was a cup-style tandem micro-reactor micropyrolyzer (Rx-3050 TR, Frontier Laboratories; Fukushima, Japan). A 0.5 ± 0.02 mg sample was added to a pre-weighed steel cup and dropped into the first micro-reactor, which was pre-heated to the pyrolysis temperature. Heating rate was 1000°C/sec.

Volatile pyrolysis products were carried via helium carrier gas (flow rate: 90 mL/min) to an inline GCMS for pyrolysis oil compositional analysis (capillary column: 60 m × 0.25 0 mm and 0.250 µm thickness). The gas chromatography oven was programmed to hold for 3 min at 40ºC before beginning a 52 min ramp to 250ºC at a rate of 5ºC/min. Separated products were analyzed with a 5975C Agilent Technologies (Santa Clara, CA, USA) mass spectrometer. Non-condensable products were not analyzed. Char yields were determined gravimetrically. All non-catalytic pyrolysis results are averages of at least two replicates. Pearson correlation coefficients were calculated to assess the correlations (if any) between the lignin properties and the char yield during non-catalytic Py-GCMS. Data analysis in this work was performed using Microsoft (Redmond, WA, USA) Excel software, and the Analysis ToolPack in Excel was used to determine the Pearson correlation coefficients.

The catalysts used in this study were HZSM-5 (CBV2314 with SiO_2:Al_2O_3 ratio of 23:1; Zeolyst International; Conshohocken, PA, USA), anatase titanium (IV) oxide (TiO_2; 99.7%, <25 nm particle size; Sigma-Aldrich), and iron(III) oxide (Fe_2O_3; ≥99%, <5 µm particle size; Sigma-Aldrich). Before use, the catalysts were calcined at 550°C (heating rate of 5°C/min) in a muffle furnace for 5 h [43,44].

In-situ catalytic Py-GCMS was performed in this study. The correct mass of catalyst was added directly on top of the preweighed lignin sample in the micropyrolyzer cup to form a



2. Delignification degree (DD) and lignin recovery results. *DD = lignin removed by hot-water extraction as a percent (by weight) of lignin in wood; SM = sugar maple.

layer of catalyst on top of the lignin. The sample was then pyrolyzed exactly as described in the previous section. Gravimetric determination of char yield during catalytic studies is not presented because data were extremely inconsistent, likely because of catalyst entrainment in the carrier gas.

RESULTS AND DISCUSSION

Quantitative aspects of EBI: effects on HWE

EBI treatment of sugar maple performed before HWE had a marked effect on HWE yield (extracted wood in % ovendry wood) and final pH (**Fig. 1**). Higher irradiation levels resulted in an increased dissolution of biomass (24% to 36% of ovendry wood) and a lower final pH (3.50 to 2.92), indicating more advanced degradation through prior EBI treatment. This finding is consistent with the reported effect of EBI on biomass [9].

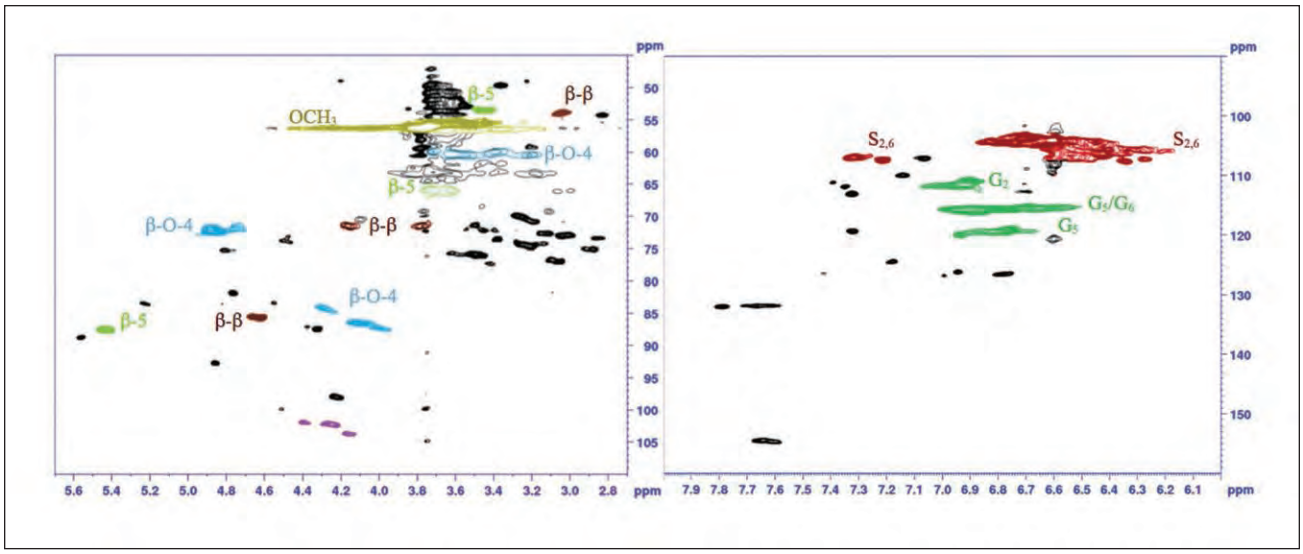
EBI resulted in an increase in the removal of lignin (delignification degree; DD) during HWE from ~10% (sugar maple) to ~25% (I_{1000}SM) (as a percent of lignin in wood; **Fig. 2**). The increase in lignin removal by HWE after EBI treatment is in accordance with an increased accessibility through disruption of wood composite structure, including lignin, that is believed to occur during EBI [9,45,46].

On the other hand, the percentage of the lignin removed that could be recovered from the hot water extract (by acidification/precipitation and centrifugation) decreased dramatically from ~63% (MEP) to ~17% ($I_{1000}ME_P$) because of EBI treatment. This might be attributed to EBI-modified lignin structures, which result in the release of smaller, more hydrophilic fragments during HWE that do not precipitate at pH 2 and that demonstrate occurrence of lignin cleavage reactions during the prior EBI treatment [45,46]. This explanation is supported by size exclusion chromatography (SEC) results, which indicated that the IME_P lignins have a lower average molecular weight than ME_P. In addition, earlier studies of liquid-liquid extraction of permeates produced by membrane separation of hot water showed an increased yield of low molecular weight compounds from EB-irradiated sugar maple compared with non-irradiated sugar maple [27]. These findings provide evidence that cleavage reactions of either lignin bonds or lignin-carbohydrate complex (LCC) bonds are the dominant reactions for at least a portion of the lignin in wood during EBI.

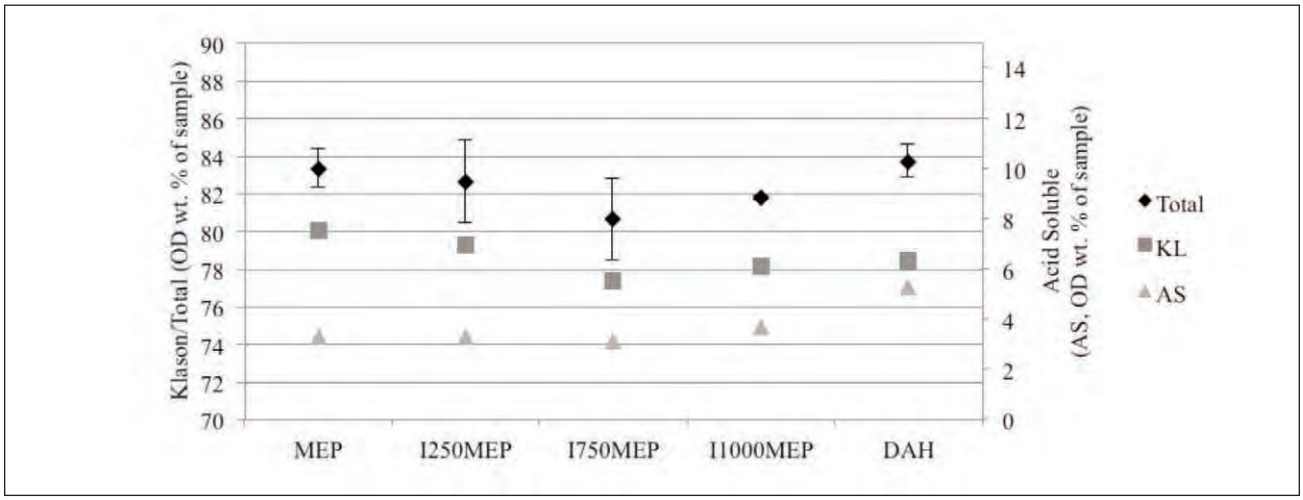
Characterization of sugar maple precipitate lignin

Solid material recovered from hot water extract of sugar maple by precipitation (pH 2) and centrifugation (precipitate lignin; ME_P) was found to contain ~83% lignin (Klason + acid soluble). The remaining solids consisted of carbohydrates (as demonstrated by HSQC studies), predominantly xylans (as demonstrated by HPLC studies of acid hydrolysates of the ME_P) that are believed to be covalently bonded to lignin and represent LCCs that can be isolated from wood using water at high temperatures. For example, LCCs have been recovered from poplar wood using water at 140°C [47]. The ash content of ME_P was found to be relatively low (~0.7%) in comparison to typical unwashed technical lignins (ash content in unwashed kraft lignin can be as high as 25% [34,35] and as low as 1% for LignoBoost process kraft lignin [48]). Low ash content is an advantage for valorization in thermal processes (gasification, pyrolysis) because ash can cause catalyst deactivation and slagging.

The PhOH content of ME_P was quite high (1.83 and 2.73 mmol/g lignin by periodate and UV-Vis analysis, respectively) compared with that of native lignin (0.5-0.75 mmol/g lignin [49]; sugar maple milled wood lignin: 0.624 mmol/g lignin [26]). This result corroborates evidence supporting cleavage



3. Side-chain (a) and aromatic (b) regions of the two-dimensional heteronuclear single-quantum correlation (2D-HSQC) spectrum of sugar maple hot-water extract precipitate (ME_P) lignin.

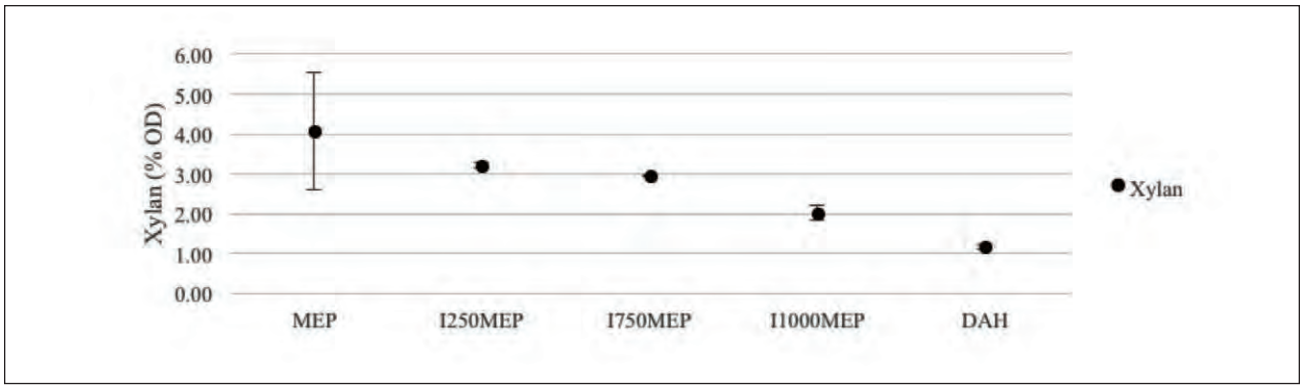


4. Klason (KL; acid insoluble), acid soluble (AS; secondary vertical axis), and total lignin content of the precipitate lignins and dilute acid hydrolysis lignin. Error bars represent ± 1 standard deviation.

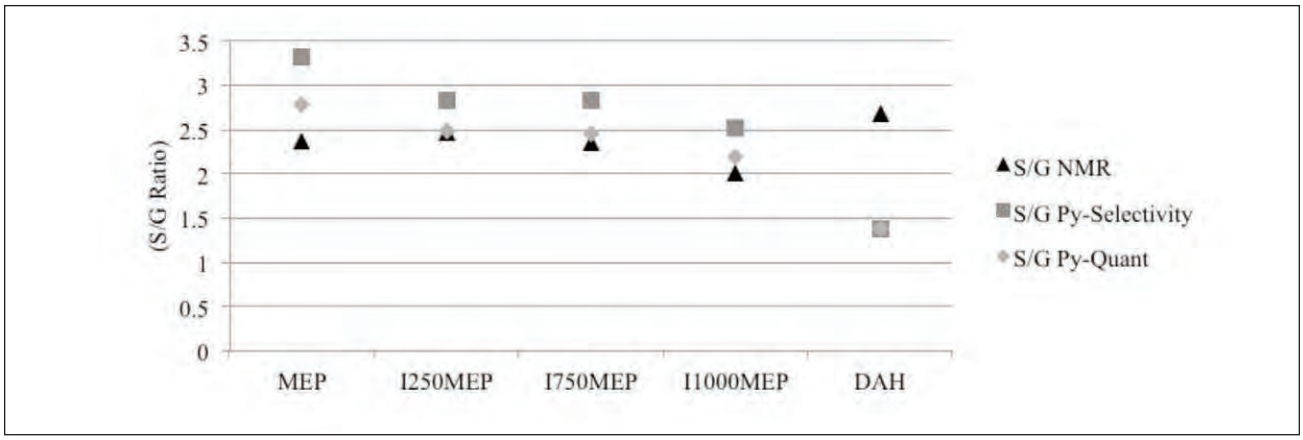
of inter-unit lignin bonds during HWE, which has been previously postulated to proceed via cleavage of aryl-ether (α–O–4 or β–O–4) bonds [23]. The cleavage of LCC bonds, including benzyl-ether and phenyl-glycosidic bonds in mild acid conditions of HWE might also be expected [50,51]. Consequently, the resulting smaller fragments of lignin with higher PhOH content than original lignin dissolve in hot water and are recovered in our studies as lignin precipitate.

Because HWE is preferentially performed using xylan-rich lignocellulosics (*Angiosperms*), which contain lignin characterized by syringyl (S) and guaiacyl (G) phenylpropanoid units (SG lignin in hardwoods) or *p*-hydroxy (H), syringyl, and guaiacyl phenylpropanoid units (HSG lignin in agriculture residues and grasses), lignin dissolved during HWE is expected to be SG (hardwoods) or HSG (agriculture residues, grasses) lignin [52]. The S:G ratio (two-dimensional heteronuclear single-quantum correlation [2D-HSQC]: 2.36) was higher for precipitate lignin than for native lignin (sugar maple milled wood lignin: 1.04 [26]), indicating that HWE promotes dissolution of lignin enriched in S-units more than lignin enriched in G-units. Earlier studies have revealed that S-enriched lignin is present in fibers, and vessels contain G-enriched lignin [49]. Accordingly, we can propose that precipitate lignin more likely originates predominantly from fibers than from vessels (sugar maple: fibers: 61% by volume; vessels: 21% by volume [53]).

The 2D-HSQC NMR analysis (**Fig. 3**) of ME_P showed typical lignin correlations (β–O–4: blue; β–β: brown; β–5: bright green, OCH_3: yellow) as well as correlations associated with carbohydrate contamination, mainly xylans (anomeric C_1/H_1: purple) [26,50], as further documented by HPLC analysis.



5. Xylan content of the precipitate lignins and dilute acid hydrolysis (DAH) lignin. Error bars represent ± one standard deviation of duplicates.



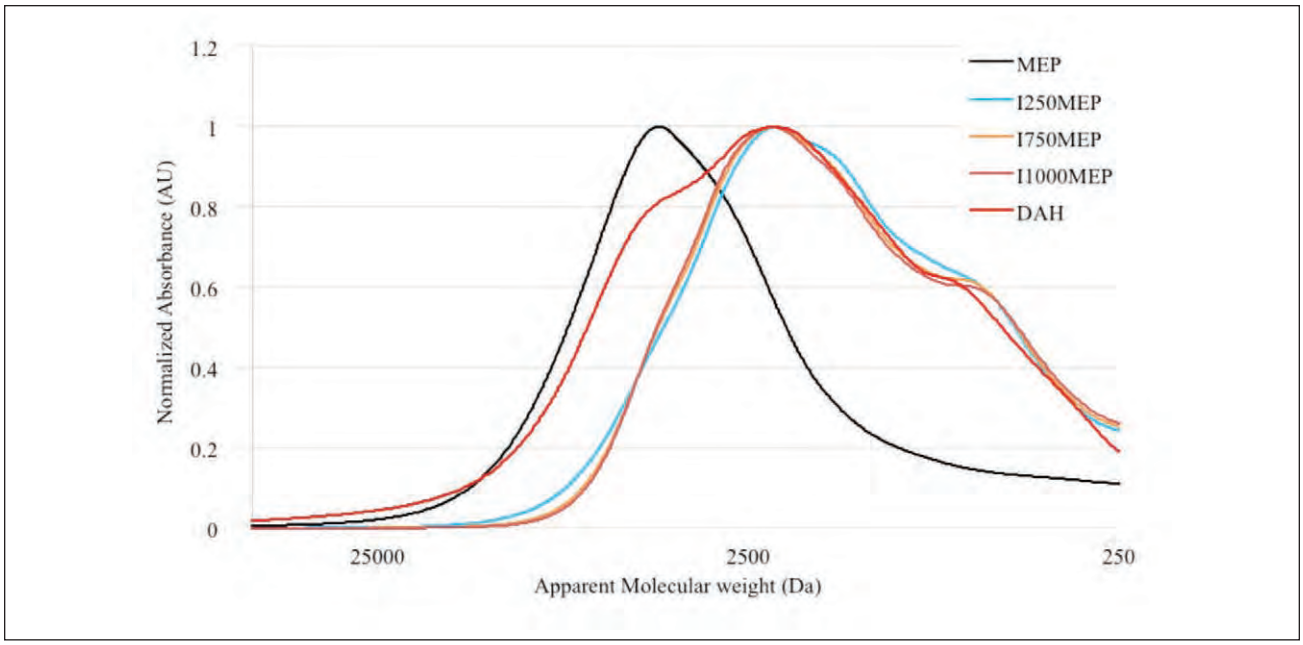
6. Syringyl:guaiacyl (S:G) ratio of the precipitate lignins and DAH lignin. Determined by 2D-HSQC nuclear magnetic resonance spectroscopy (NMR) (▲), non-catalytic pyrolysis-gas chromatography mass spectrometry (Py-GCMS) using selectivity (■; sum of selectivity to all S-derived products divided by sum of selectivity to all G-derived products), and non-catalytic Py-GCMS using yield results (◆; sum of yield to all S-derived products divided by sum of yield to all G-derived products).

Characterization of precipitate lignin from EB-irradiated sugar maple

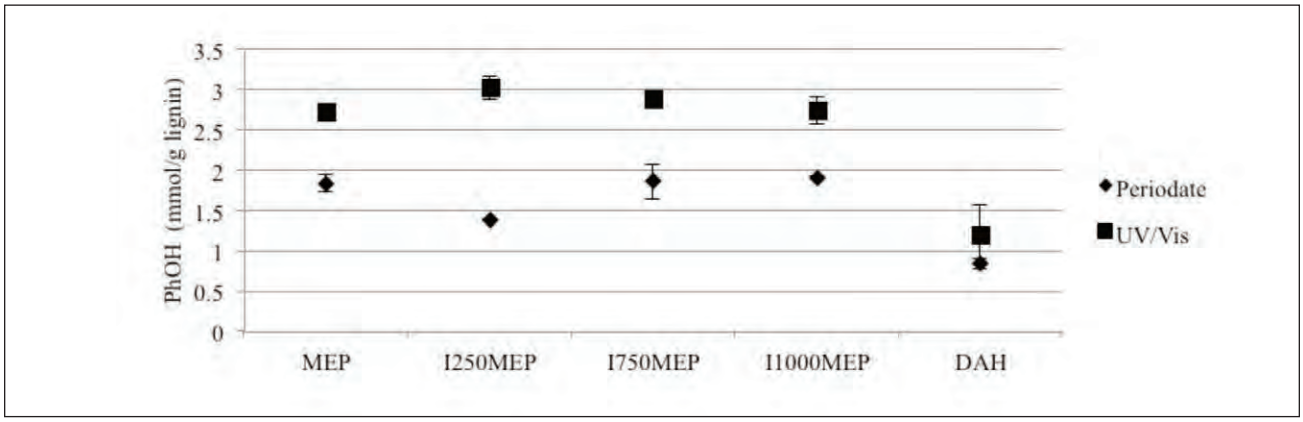
EBI treatment of sugar maple before HWE appeared to have a minimal effect on the chemical nature of the recovered precipitate lignins with regard to lignin content (average: 82.7%; standard deviation: 1.15; **Fig. 4**). DAH had a similar lignin content to the sugar maple precipitate lignins (83.7%; standard deviation: 0.86). Xylan was the only detectable carbohydrate component during HPLC analysis and represented less than 5% of the ovendry weight for any of the lignins (**Fig. 5**). As mentioned, this result might be an underestimate resulting from the tendency of xylose to degrade into furfural under strong acid conditions. However, a noted decrease in xylan content was observed as EBI energy level increased.

The S:G ratio results, calculated from NMR and non-catalytic Py-GCMS data (**Fig. 6**), correlated relatively closely with one another for the sugar maple precipitate lignins, with a slight decrease observed at higher EBI energy levels. This finding implies that EBI treatment leads to an increased release of G-containing lignin, probably originating from vessels, during HWE. The correlation between NMR and non-catalytic Py-GCMS results for DAH samples was not as evident. Past research has indicated that Py-GCMS and 2D-HSQC NMR analysis can be used to determine S:G ratios in lignin [27,42,54,55]. The present results, while somewhat informative, indicate a need for further development of these methods and underline the continued relevance of standard methods such as nitrobenzene oxidation [56]. Pyrolysis of lignin results in the production of a significant amount of char, which poses a challenge for the application of Py-GCMS as an analytical tool. The use of 2D-HSQC NMR for S:G ratio determination is challenging as well because the specific integration boundaries used to calculate S:G ratio influence the results, which has been noted in previous reports [27].

Size exclusion chromatography results indicated that the IME_p lignins were of lower average molecular weight than ME_p lignin, although increased irradiation above 250 kGy did not appear to lead to further reduction of molecular weight (**Fig. 7**). As mentioned earlier, the lower molecular weight of the IME_p lignins corroborates the hypothesis that the reduced lignin recovery from hot water extract of highly irradiated sugar maple is a consequence of smaller lignin fragments



7. Size exclusion chromatography curves for the ME_P and irradiated ME_P (IME_P) lignins.

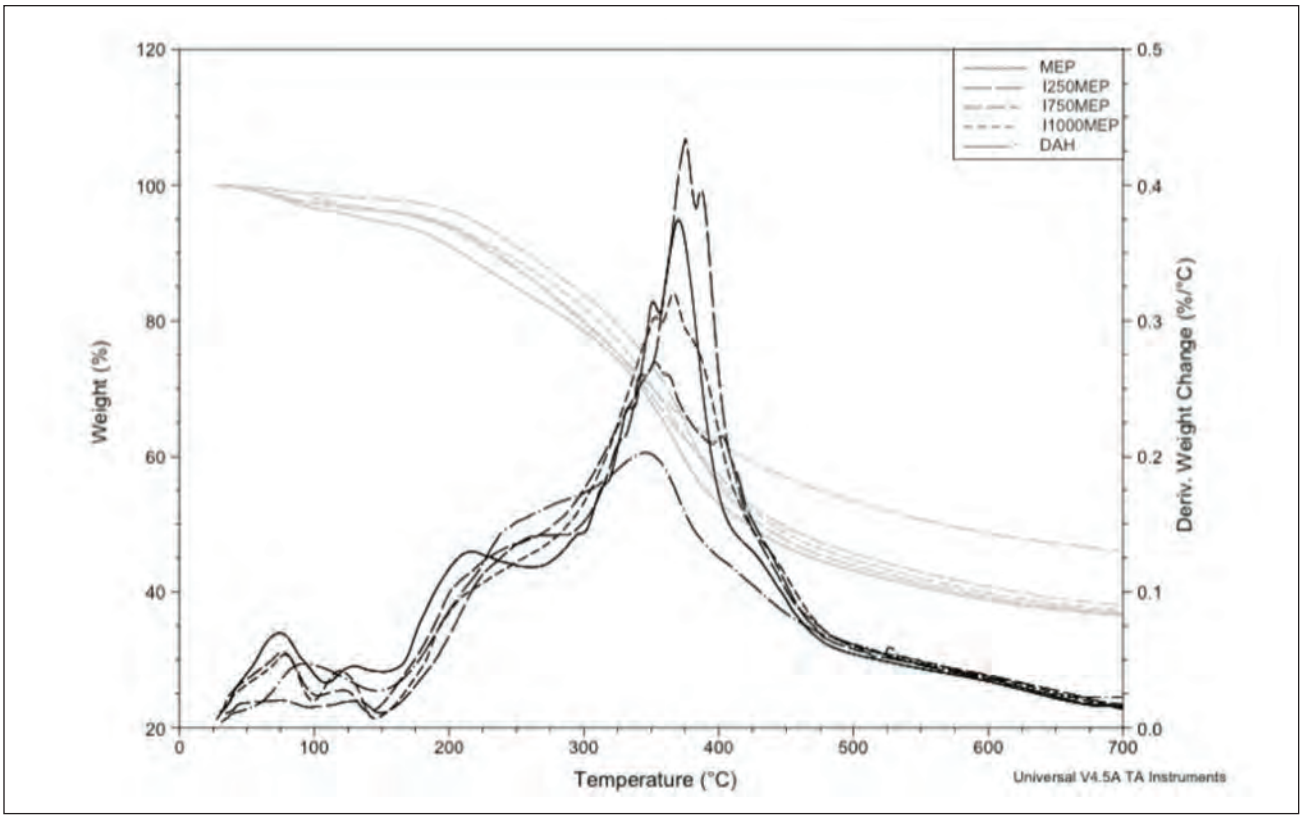


8. Free phenolic hydroxyl group (PhOH) content of the precipitate lignins and DAH lignin determined by the periodate oxidation and ultraviolet-visible spectrophotometry (UV/Vis) methods. Error bars represent ± 1 standard deviation.

being released during HWE. Reduction in molecular weight resulting from aryl-ether and phenyl glycosidic bond cleavage is expected to be associated with an increase in PhOH content. A slight increase in PhOH content was observed for $I_{250}ME_P$ lignin by the UV-Vis method, but not by the periodate oxidation method (Fig. 8). The discrepancy between the two methods might be because of an increased presence of structures formed by demethoxylation/demethylation during EBI treatment (e.g., catechol and *p*-hydroxyphenylpropanoid units) [57] that cannot be detected by the periodate method. Demethoxylation of S-units would result in an increased concentration of G-units. This is consistent with (and might provide a second explanation for) the generally decreasing S:G ratios observed at higher EBI energy levels. Above 250 kGy, the PhOH results do not change substantially, in accordance with the relatively constant average molecular weights of the IME_P lignins (SEC results) (Fig. 7). However, the lignin recovery yields still decreased at EBI energy levels above 250 kGy (Fig. 2), indicating that along with degradation via aryl-ether bond cleavage, other pathways (e.g., cleavage of LCC and benzyl ether bonds) might be important and even more prevalent at higher EBI energy levels. EBI-induced LCC cleavage would result in a lower xylan content in precipitate lignin, which was observed in our studies (Fig. 5).

Thermogravimetric analysis

Typically, thermal decomposition of lignin occurs slowly over a broad range of temperatures (120°C-600°C) and involves many cleavage and defunctionalization reactions [58-60]. The differential thermogravimetric analysis (D)TGA curves of the four precipitate lignins (**Fig. 9**) are similar and feature four notable decomposition events. The decomposition event



9. Differential thermogravimetric analysis ([D]TGA) curves of the ME_P lignin.

below 100°C results from evaporation of water and other low molecular weight volatiles. Initial lignin decomposition producing formic acid, formaldehyde, and carbon dioxide is reported to occur around 120°C, which might account for the small decomposition event observed at that temperature [60]. Although mass loss from lignin decomposition begins occurring below 200°C, decomposition of carbohydrate contaminants is the likely source of the mass loss at 200°C [4]. The major lignin decomposition event is a relatively sharp peak at ~380°C. The small shoulder at 420°C might be the result of decomposition of lignin that is more condensed (indicating cleavage of C-C bonds) [59]. DAH lignin lost mass at a relatively slow rate compared with the precipitate lignins. The sharp (D)TGA peak for the precipitate lignins (indicating a relatively high rate of decomposition) is generally not observed for lignin and is evidence that the precipitate lignins might be more chemically uniform than most lignins.

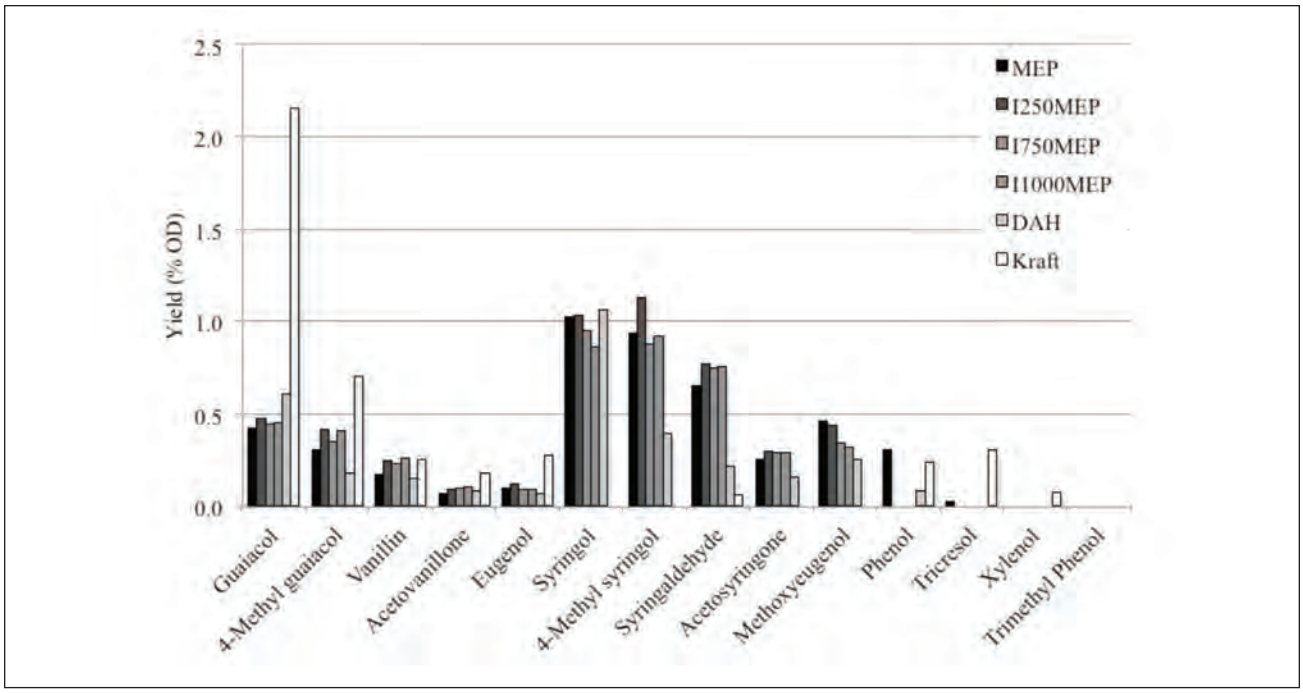
For the precipitate lignins, just under 40% of the original mass remained as char at 700°C in nitrogen (Fig. 9). This is high compared with the char formed during pyrolysis of carbohydrates, but fairly typical for lignin, particularly with a slow heating rate [59]. High char yields result from condensation reactions that take place simultaneously with degradation reactions. In addition to being dependent on the feedstock, char yields are highly dependent on conditions such as heating rate, atmosphere, and final temperature [58,61]. In comparison, char yield from DAH lignin was ~45%.

While small differences in the chemical character of lignin recovered from sugar maple treated at different EBI energy levels were observed, the changes were not particularly profound considering the substantial amount of energy used (up to 1000 kGy). The effect on lignin character is small in comparison with previously reported effects of EBI treatment on enzymatic hydrolyzability of cellulose, for example [9]. It appears that while EBI treatment has a great effect on HWE digester yields and lignin recovery yields, the chemical nature of solids that are recovered by the precipitation/centrifugation method is not affected as greatly.

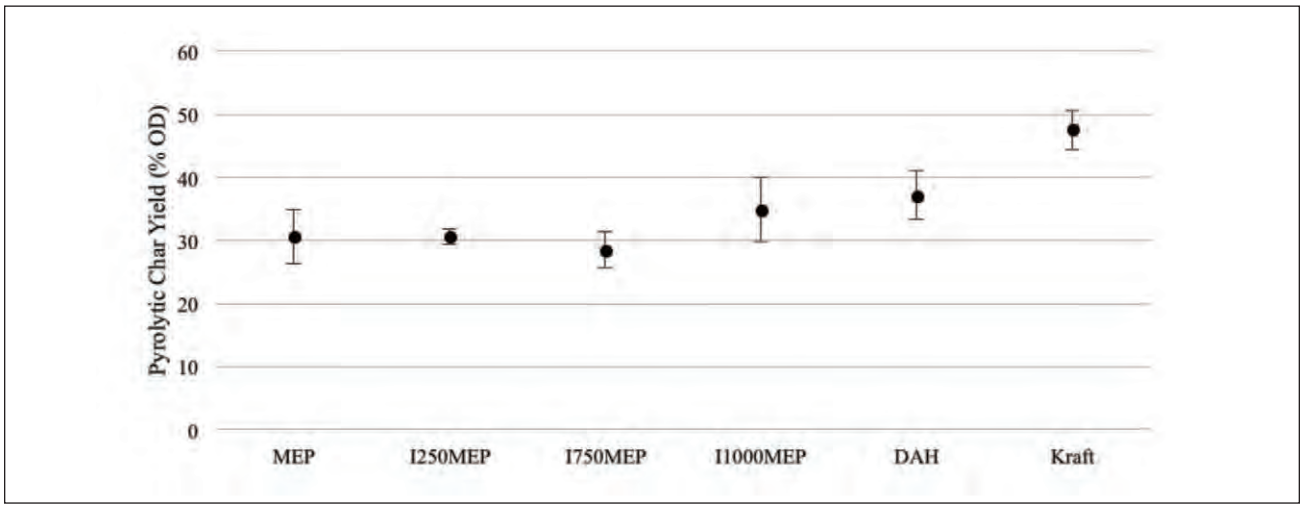
Fast Py-GCMS analysis

Fast Py-GCMS of the recovered precipitate lignins, DAH lignin, and kraft lignin was initially performed in the absence of catalyst. Py-GCMS experiments were not optimized to improve product yields. Experiments were instead intended to provide a comparison between the different lignins in the context of their different pretreatments and recovery techniques. The intent was to show whether or not hot-water precipitate lignin gives improved yield or selectivity to valuable lignin derivatives during fast pyrolysis compared with current technical lignins.

The main products identified during Py-GCMS analysis of the precipitate lignins included derivatives of S and G monomers. S derivatives (syringol, 4-methyl syringol, syringaldehyde, acetosyringone, and methoxyeugenol) were the domi-



10. Approximate quantified yield to various main products of non-catalytic Py-GCMS spectrometry.



11. Non-catalytic fast pyrolysis char yields for the precipitate lignins, DAH lignin, and kraft lignin. Values are an average of three replicates. Error bars indicate ± 1 standard deviation.

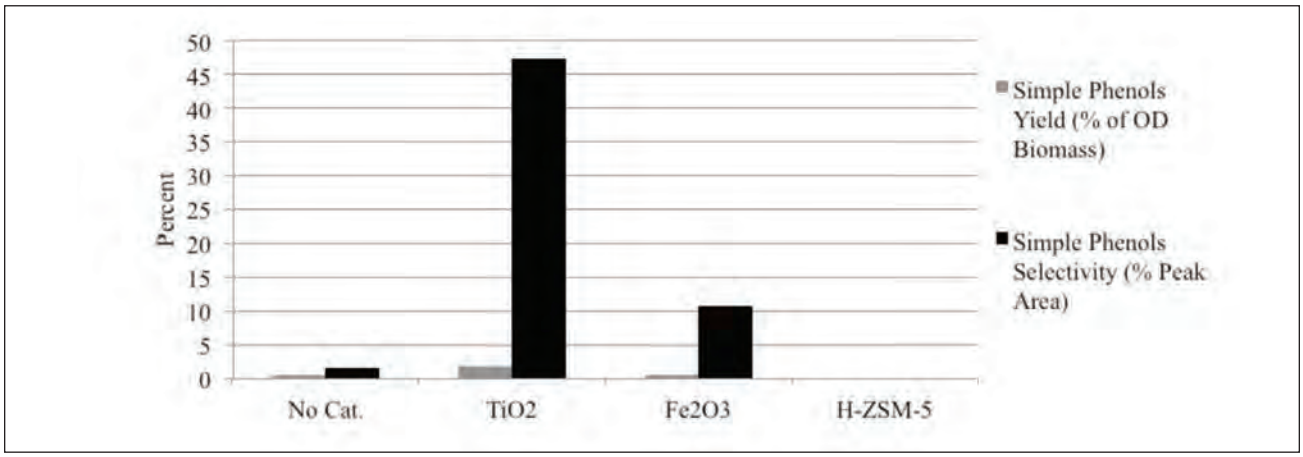
nant pyrolysis products for the precipitate lignins and for DAH lignin, in accordance with their hardwood origin and their high S:G ratio observed during HSQC experiments. As expected, softwood kraft lignin yielded no S-derived compounds, but yielded major products derived from G units (guaiacol, 4-methyl guaiacol, vanillin, acetovanillone, and eugenol) (**Fig. 10**). All major pyrolysis products observed and positively identified had been previously reported in the literature [31,62,63].

The char yields (residual solid after pyrolysis; determined gravimetrically) for the precipitate lignins were lower than for kraft technical lignin and about the same as the DAH lignin (**Fig. 11**). Many factors could affect pyrolysis char yield. The most obvious explanation is the lignin content (carbohydrate content), as none of the samples were 100% lignin. Higher lignin content is expected to result in higher char yields, as has been shown in past studies [59]. Other possible factors that were measured in this study include free PhOH content, S:G ratio, ash content, and molecular weight. The chemistry occurring during fast pyrolysis is very complex, so it is difficult to be confident that any one of the tested properties is solely responsible for increased char production. Char yield is likely to depend on a combination of factors. However, by using a Pearson correlation matrix, relationships

				PhOH		S:G		
Correlation:	Lignin	Xylan	Ash	Periodate	UV/Vis	NMR	Py-Selectivity	Py-Quantity
	0.924	-0.834	**0.909**	-0.619	-0.792	**-0.855**	**-0.956**	**-0.967**

PhOH = phenolic hydroxyl group, S:G = syringyl:guaiacyl, UV-Vis = ultraviolet-visible spectrophotometry, NMR = nuclear magnetic resonance, Py = pyrolysis.

I. Pearson correlation coefficients indicating relationships between various lignin properties and yield of residual char produced during non-catalytic pyrolysis-gas chromatography mass spectrometry (Py-GCMS). Bold values indicate $p \leq 0.05$.



12. Effect of catalyst type on simple phenol production during Py-GCMS experiments at same conditions (500°C, 20:1 catalyst loading, ME_P lignin).

between various lignin characteristics and pyrolysis char yields have been determined (**Table I**). There is evidence that lower lignin content, increased xylan content, increased PhOH content, lower ash content, and lower S:G ratio all lead to reduced residual material after pyrolysis.

EBI before HWE appeared to have very little effect on residual char yield during Py-GCMS, which is not surprising based on the minimal variation between the lignins observed during characterization studies. The average pyrolytic char yield for the precipitate lignins was 31.1% (standard deviation: 2.73; ~10 percentage points lower than the char yield during TGA).

Figure 10 shows the approximate yields to various main pyrolysis products for the precipitate lignins tested including DAH and kraft lignin. EBI pretreatment before HWE appeared to have a slight effect on the production of certain compounds during pyrolysis. Syringol, 4-methyl syringol, and methoxyeugenol production decreased slightly with increasing EBI level above 250 kGy. No phenol was produced from IME_P lignins at all.

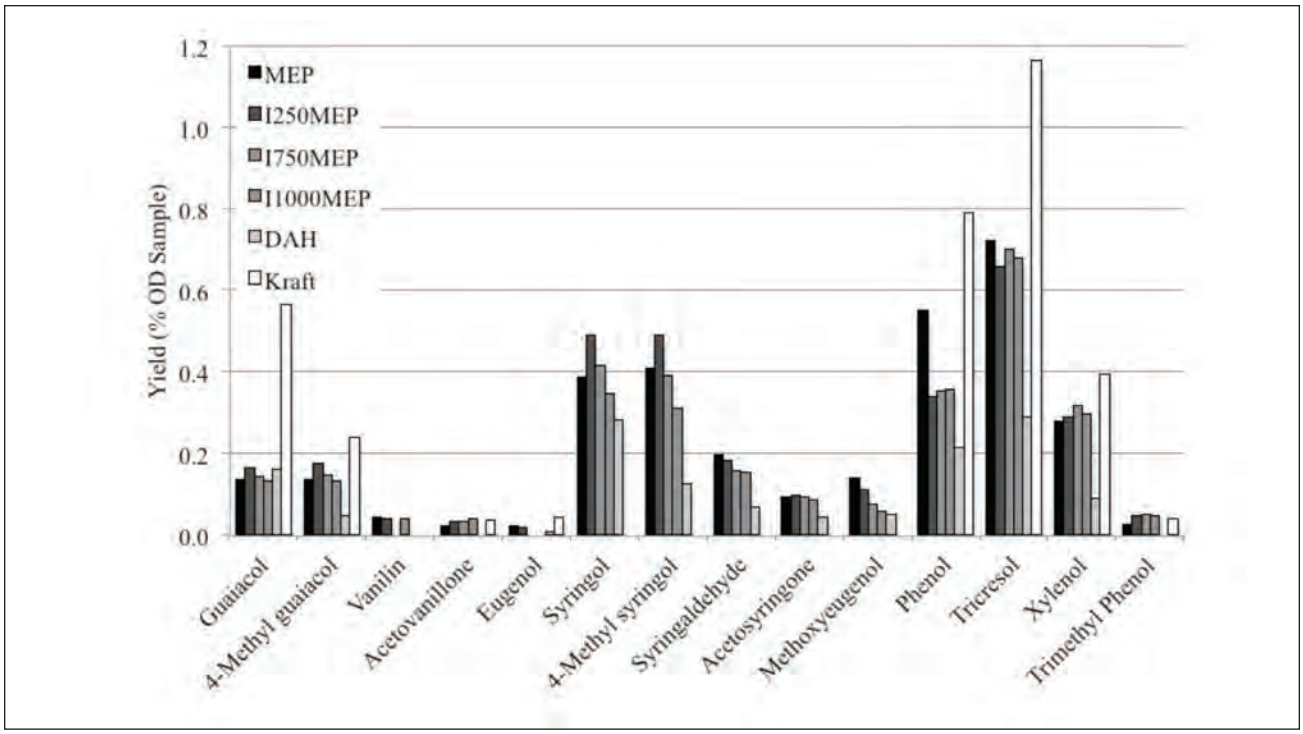
Overall yields were very low and neither yield nor selectivity was improved by prior EBI treatment. The hardwood origin of the lignins tested resulted in a large proportion of S-based monomers, increasing the diversity of the pyrolysis products. DAH showed similar results to the precipitate lignins but kraft lignin resulted in relatively higher yields and of solely G-derived products.

Titanium dioxide (TiO_2; anatase), iron oxide (Fe_2O_3), and zeolite (HZSM-5) catalysts were studied to improve selectivity and yield to high-value simple (non-methoxylated) phenols (phenol, tricresol, xylenol, and trimethyl phenol). **Figure 12** shows the catalytic Py-GCMS yield and selectivity to simple phenols for the catalysts studied. TiO_2 resulted in the greatest increase in selectivity and yield compared to control condition (no catalyst). HZSM-5 resulted in the production of no simple phenols at all, but was effective at production of aromatic compounds such as benzene, toluene, xylenes, and naphthalenes.

Figure 13 shows the approximate yields to various major products of TiO_2 catalytic pyrolysis for the precipitate lignins and DAH lignin. Selectivity to simple phenols was substantially improved compared with non-catalytic Py-GCMS. However, mass yields from precipitate and DAH lignins were still below 1% for any individual product and dimethoxylated S-derived compounds still made up a substantial portion of the total condensable liquid products. Kraft lignin had the highest yield and selectivity to simple phenols, of the lignins tested.

CONCLUSIONS

A lignin-rich material of relatively high lignin content (~80%) was removed and recovered from sugar maple and electron beam irradiated sugar maple as a byproduct of a relatively simple and non-hazardous HWE process. Electron beam irradiation (EBI) substantially enhanced delignification during HWE, but a lower percentage of the dissolved lignin could be recovered from the extract. EBI also had only a small



13. Approximate quantified yield to various main products of titanium dioxide catalytic Py-GCMS.

effect on the resulting lignin chemical character other than a slight decrease in S:G ratio and a decrease in molecular weight, as revealed by SEC. The recovered precipitate lignin had low ash content, low sulfur content, was fairly uniform (based on TGA results), and had relatively high reactivity (high PhOH and S:G ratio, compared with that of native lignin, indicating a relatively low degree of condensation). These factors make hot water-extracted precipitate lignin an attractive lignin for further upgrading and valorization technologies such as catalytic fast pyrolysis.

Although there was some evidence that hot water-extracted precipitate lignin resulted in less char formation during pyrolysis compared with kraft and dilute acid hydrolysis lignins, the reasons for the lowered char formation were not clear. A combination of factors likely contributed to the observed lower residual char yield. Non-catalytic Py-GCMS studies showed that the relatively high S content of the hardwood-derived lignin strongly affected the nature of the pyrolysis products. Therefore, simple, non-methoxylated phenolic compounds were not the major Py-GCMS products and were produced at very low yield. Pyrolysis with TiO_2 (anatase) improved the selectivity to simple phenols substantially, but yields were still very low. Any improvement in yield as a result of lignin properties was negatively affected by the highly S/G-nature of the hardwood-derived precipitate lignins compared with the G-rich softwood kraft lignin. Further work on pyrolytic decomposition of hardwood-derived lignin should focus on less selective catalysts such as zeolites for production of non-phenolic aromatic compounds. **TJ**

ACKNOWLEDGEMENTS

The authors thank RTI International for allowing Derek Corbett to perform Py-GCMS analysis; Thomas Amidon for all of his continued support of the biorefinery research at the State University of New York College of Environmental Science and Forestry; Dave Kiemle and Art Stipanovic for their invaluable assistance with NMR and TGA studies, respectively; Mark Driscoll for providing EBI-treated sugar maple; the North Carolina State Department of Forest Biomaterials for the use of their facility for carbohydrate analysis; and Aditi Nargardeolekar for performing the UV-Vis PhOH analysis.

LITERATURE CITED

1. Taherzadeh, M.J. and Karimi, K., *Int. J. Mol. Sci.* 9(9): 1621(2008).
2. Carvalheiro, F., Duarte, L.C., and Gírio, F.M., *J. Sci. Ind. Res.* 67(11): 849(2008).
3. Narron, R.H., Kim, H., Chang, H., et al., *Curr. Opin. Biotechnol.* 38: 29(2016).
4. Sundar, S., Bergey, N.S., Salamanca-Cardona, L., et al., *Carbohydr. Polym.* 100: 195(2014).
5. Driscoll, M.S., Stipanovic, A.J., Cheng, K., et al., *Radiat. Phys. Chem.* 94: 217(2014).
6. Zheng, Y., Lin, H.-M., Wen, J., et al., *Biotechnol. Lett.* 17(8): 845(1995).
7. Mosier, N., Wyman, C., Dale, B., et al., *Bioresour. Technol.* 96(6): 673(2005).
8. Alvira, P., Tomás-Pejó, E., Ballesteros, M., et al., *Bioresour. Technol.* 101(13): 4851(2010).

9. Cheng, K., Barber, V.A., Driscoll, M.S., et al., *J. Bioprocess Eng. Biorefinery* 2(2): 143(2013).
10. Mittal, A., "Kinetics of hemicellulose extraction during autohydrolysis of sugar maple wood," Ph.D. thesis, State University of New York College of Environmental Science and Forestry, Department of Paper and Bioprocess Engineering, Syracuse, NY, USA, 2006.
11. Amidon, T.E. and Liu, S., *Biotechnol. Adv.* 27(5): 542(2009).
12. Amidon, T.E., Wood, C.D., Shupe, A.M., et al., *J. Biobased Mater. Bioenergy* 2(2): 100(2008).
13. Gong, C. and Bujanovic, B.M., *Energies* 7(2): 857(2014).
14. Gong, C., Goundalkar, M.J., Bujanovic, B.M., et al., *J. Wood Chem. Technol.* 32(2): 93(2012).
15. Bak, J.S., Ko, J.K., Han, Y.H., et al., *Bioresour. Technol.* 100(3): 1285(2009).
16. Karthika, K., Arun, A.B., and Rekha, P.D., *Carbohydr. Polym.* 90(2): 1038(2012).
17. Fischer, K., *Macromol. Symp.* 12(1): 303(1987).
18. Duarte, G.V., Ramarao, B.V., Amidon, T.E., et al., *Ind. Eng. Chem. Res*. 50(17): 9949(2011).
19. Corbett, D.B., Kohan, N., Machado, G., et al., *Energies* 8(9): 9640(2015).
20. Cheng, K., "An investigation of lignocellulosic biomass including: compositional modeling, novel pretreatments, and extraction of cellulose nanocrystals," Ph.D. thesis, State University of New York College of Environmental Science and Forestry, Department of Chemistry, Syracuse, 2010.
21. Liu, T., Lin, L., Sun, Z., et al., *Biotechnol. Adv.* 28(5): 602(2010).
22. Amidon, T.E., Bujanovic, B., Liu, S., et al., *Forests* 2(4): 929(2011).
23. Ye, P., Cheng, L., Ma, H., et al., in *The Role of Green Chemistry in Biomass Processing and Conversion*, (H. Xie and N. Gathergood, Eds.), John Wiley & Sons Inc., New York, 2012, pp. 135-180.
24. Goundalkar, M.J., Bujanovic, B., and Amidon, T.E., *Cellul. Chem. Technol.* 44(1): 27(2010).
25. Dongre, P., Driscoll, M., Amidon, T., et al., *Energies* 8(8): 7897(2015).
26. Goundalkar, M.J., Corbett, D.B., and Bujanovic, B.M., *Energies* 7(3): 1363(2014).
27. Goundalkar, M.J., "Investigating the effect of hot-water extraction on phenolic constituents of selected hardwoods: a study aided by 2D NMR and GC-MS," Ph.D. thesis, State University of New York College of Environmental Science and Forestry, Department of Paper and Bioprocess Engineering, Syracuse, 2014.
28. Holladay, J.E., Bozell, J.J., White, J.F., et al., "Top value-added chemicals from biomass. Vol. II – results of screening for potential candidates from biorefinery lignin," National Technical Information Service, U.S. Department of Commerce, Springfield, VA, USA, 2007. Available [Online] https://www1.eere.energy.gov/bioenergy/pdfs/pnnl-16983.pdf <18April2017>.
29. Zakzeski, J., Bruijnincx, P.C.A., Jongerius, A.L., et al., *Chem. Rev.* 110(6): 3552(2010).
30. Bulushev, D.A. and Ross, J.R.H., *Catal. Today,* 171(1): 1(2011).
31. Mante, O.D., Rodriguez, J.A., and Babu, S.P., Bioresour. Technol. 148: 508(2013).
32. Lu, Q., Zhang, Y., Tang, Z., et al., *Fuel* 89(8): 2096(2010).
33. Kamwilaisak, K. and Wright, P.C., *Energy Fuels* 26(4): 2400(2012).
34. Brodin, I., "Chemical properties and thermal properties of kraft lignins," Licentiate thesis, KTH Royal Institute of Technology School of Chemical Sciences and Engineering, Stockholm, Sweden, 2009.
35. Mansouri, N.-E.E. and Salvadó, J., *Ind. Crops Prod.* 24(1): 8(2006).
36. Sixta, H. (Ed.), *Handbook of Pulp, Vol. 1*, Wiley-VCH, Weinheim, Germany, 2006.
37. Lin, S.Y. and Dence, C.W. (Eds.), *Methods in Lignin Chemistry*, Springer, Berlin, Germany, 1992.
38. Sluiter, A., Hames, B., Ruiz, R., et al. "Determination of structural carbohydrates and lignin in biomass," Laboratory Analytical Procedure, National Renewable Energy Laboratory, Golden, CO, USA, 2008.
39. Shin, S.-J. and Cho, N.-S., *Cellulose* 15(2): 255(2007).
40. Lai, Y.-Z. and Guo, X.-P., *Wood Sci. Technol*. 25(6): 467(1991).
41. Gartner, A., Gellerstedt, G., and Tamminen, T., *Nord. Pulp Pap. Res. J.* 14(2): 163(1999).
42. Stewart, J.J., Akiyama, T., Chapple, C., et al., *Plant Physiol.* 150(2): 621(2009).
43. Abu El-Rub, Z., Bramer, E.A., and Brem, G., *Ind. Eng. Chem. Res.* 43(22): 6911(2004).
44. Wang, K., Johnston, P.A., and Brown, R.C., *Bioresour. Technol.* 173: 124(2014).
45. Argyropoulos, D.S. and Sun, Y., *Photochem. Photobiol.* 64(3): 510(1996).
46. Chuaqui, C.A., Rajagopal, S., Kovács, A., et al., *Tetrahedron* 49(43): 9689(1993).
47. Koshijima, T. and Watanabe, T., *Association Between Lignin and Carbohydrates in Wood and Other Plant Tissues*, Springer-Verlag, Berlin, 2003.
48. Tomani, P.E.R., *Cellul. Chem. Technol.* 44(1): 53(2010).
49. Sjöström, E., *Wood Chemistry: Fundamentals and Applications*, Academic Press, London, 1993.
50. Balakshin, M., Capanema, E., Gracz, H., et al., *Planta* 233(6): 1097(2011).
51. Zoia, L., Orlandi, M., and Argyropoulos, D.S., *J. Agric. Food Chem.* 56(21): 10115(2008).
52. Ralph, J., Brunow, G., and Boerjan, W., "Lignins," in *Encyclopedia of Life Sciences*, John Wiley & Sons Ltd., Chichester, UK, 2007.
53. Isenberg, I.H., Harder, M.L., and Louden, L., *Pulpwoods of the United States and Canada, Vol. II - Hardwoods*, The Institute of Paper Chemistry, Appleton, WI, USA, 1981.
54. Ohra-aho, T., Gomes, F.J.B., Colodette, J.L., et al., *J. Anal. Appl. Pyrolysis* 101: 166(2013).
55. Rodrigues, J., Meier, D., Faix, O., et al., *J. Anal. Appl. Pyrolysis* 48(2): 121(1999).
56. Chen, C.-L., in *Methods in Lignin Chemistry* (S.Y. Lin and C.W. Dence, Eds.), Springer-Verlag Berlin, 1992, pp. 301–321.
57. Skvortsov, S.V., *Chem. Nat. Compd.* 26(1): 1(1990).
58. Kubo, S. and Kadla, J.F., *J. Appl. Polym. Sci.* 98(3): 1437(2005).

59. Gardner, D.J., Schultz, T.P., and McGinnis, G.D., *J. Wood Chem. Technol.* 5(1): 85(1985).

60. Fenner, R.A. and Lephardt, J.O., *J. Agric. Food Chem.* 29(4): 846(1981).

61. Laurichesse, S. and Avérous, L., *Prog. Polym. Sci.* 39(7): 1266(2014).

62. Mu, W., Ben, H., Ragauskas, A., et al., *BioEnergy Res.* 6(4): 1183(2013).

63. Ralph, J. and Hatfield, R.D., *J. Agric. Food Chem.* 39(8): 1426(1991).

ABOUT THE AUTHORS

Lignin characterization and use is challenging, interesting, and important for advancing sustainable products production. Understanding the nature of lignin produced by biorefinery processes is an important aspect of producing value from this byproduct by various methods in an integrated biorefinery.

A challenge in conducting this study is that analytical catalytic fast pyrolysis requires very advanced instrumentation, which is difficult to obtain. We partnered with RTI International to conduct that aspect of the research.

An interesting discovery from the study is that electron beam irradiation had a remarkably small effect on the character and subsequent valorization of the hot water extracted lignin.

Biorefinery processes producing products other than paper from lignocellulosic material are a logical extension of the pulp and paper industry. This research could benefit a mill's R&D efforts toward that end.

Based on this work, selective catalysts are not as useful for lignin of high S-content. Less selective catalysts such as zeolites for producing non-phenolic (BTX) compounds should be preferred.



Corbett



Mante



Bujanovic

Corbett (who completed this work as a graduate student at State University of New York [SUNY] College of Environmental Science and Forestry) is research analyst/Ph.D. student, North Carolina State University, College of Natural Resources, Department of Forest Biomaterials, Raleigh, NC, USA. Mante is research chemical engineer, RTI International, Energy Technologies Division, Durham, NC, USA. Bujanovic is associate professor, SUNY College of Environmental Science and Forestry, Department of Paper and Bioprocess Engineering, Syracuse, NC, USA. Email Corbett at dbcorbet@ncsu.edu.

Decision-making process for the identification of preferred lignin-based biorefinery strategies

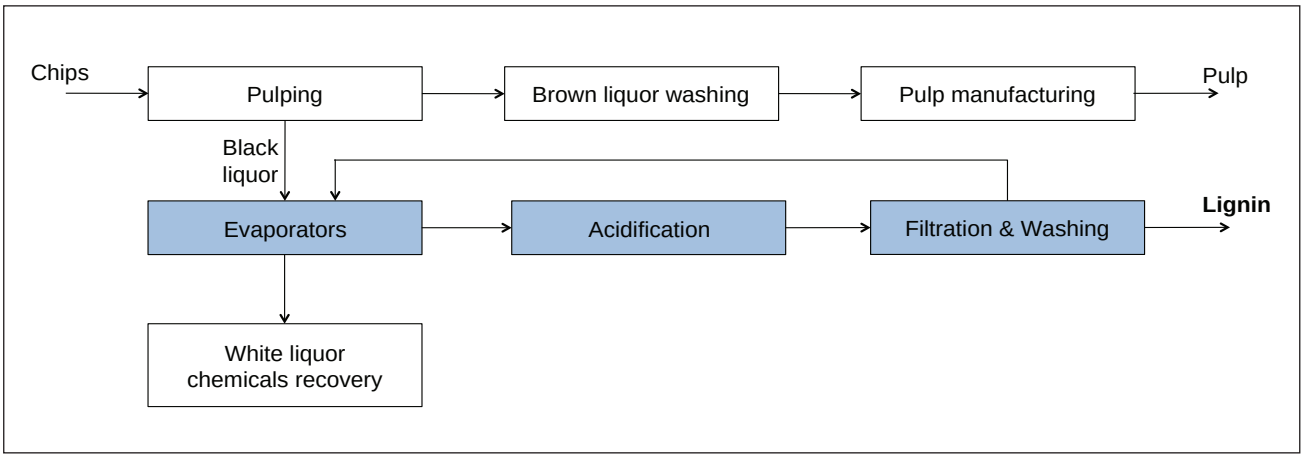
CÉDRIC DIFFO TÉGUIA, SOPHIE D'AMOURS, ROD ALBERS, AND PAUL STUART

ABSTRACT: The lignin biorefinery is emerging; there has been significant progress in recent years regarding lignin extraction and conversion processes, their implementation at the commercial scale, and the validation of lignin substitution potential in various applications. In this paper, seven strategies for implementing the lignin-based biorefinery into a kraft pulp mill were considered, and different performance metrics for these strategies were calculated in order to identify the "most preferred". The different options addressed two distinctly different objectives that companies can consider regarding their biorefinery strategy, either (1) a near-term mill-level profitability improvement vision, or (2) a longer-term revenue growth-oriented vision. A phased-implementation approach was systematically defined for each option in order to mitigate technology and market risks. Lignin product applications that were considered included phenol replacement in phenol-formaldehyde (PF) resins, polyols replacement in polyurethane (PU) foams, and polyacrylonitrile (PAN) replacement in carbon fiber.

A Multi-Criteria Decision-Making (MCDM) panel was executed for evaluating the seven lignin-based biorefinery strategies, using a set of economic, market risk, and competitiveness criteria. Although the panel selected Internal Rate of Return (IRR) as the most important criterion, Competitiveness on Production Costs (CPC) appeared to be the most important factor for distinguishing between lignin strategy options. CPC reflects the robustness of the biorefinery strategy relative to an aggressive price-cutting strategy from the competition. Overall, strategies involving lignin precipitation were more attractive economically, while those involving larger-scale solvent pulping processes and the associated larger revenue streams were considered better long-term strategies. The most preferred strategy considered by the panel was for precipitated lignin sold for both PF resin and PU foam applications. The next preferred strategy considered lignin sales to the same market segments, but at larger volumes. The next closely-ranked strategy considered the production of a lignin-based PF resin at the host mill. These three strategies were identified as "preferred," for further, more detailed assessment.

Application: This paper provides an evaluation of lignin-based biorefinery strategies in the context of retrofit implementation within a market kraft pulp mill. The evaluation is made though a Multi-Criteria Decision-Making panel, whose members considered a set of profitability, market, and risk-based criteria.

Lignin is burnt as black liquor in the recovery boiler to produce steam and electricity for the pulp manufacturing process, but it could also be separated and comprise the feedstock for new "green" revenue streams. Although the lignin chemical structure is dominated by aromatics and methoxyl groups, it also includes a variety of other functional units, which makes it potentially valuable in a wide range of applications [1,2]. Recent progress in lignin extraction from black liquor has resulted in the emergence of the first commercial plants in the United States, Canada, and Sweden, using either the LignoBoost process [3] or the LignoForce process [4]. Both of these processes are based on the use of carbon dioxide to lower the black liquor pH to 9-10, and causing lignin to precipitate [5,6]. **Fig. 1** illustrates operational steps of a generic lignin precipitation process. Alternatively, lignin can be extracted directly from wood through various biomass fractionation processes [7], as generically illustrated in **Fig. 2**. A solvent-based technology can be employed for that purpose, which has a less damaging effect on the lignin structure compared to the kraft pulping process. The cases of lignin precipitation units integrated within an existing kraft-pulping mill and of lignin extraction within a stand-alone organosolv plant have been systematically treated by Diffo Téguia et al. from a techno-economic perspective [8]; nevertheless, extracting and/or producing lignin is only the first step of a successful biorefinery transformation. Companies face the complex choice of identifying the right applications to which they should sell their lignin, knowing that each option implies unique technical and market challenges, while the precise understanding of the linkage between lignin properties, derivative product performance, and



1. Simplified lignin precipitation process from black liquor.

market supply/demand growth remains uncertain.

Considering this context, this paper aims to assess different strategies for the deployment of the lignin-based biorefinery. Risk mitigation using a phased implementation approach is considered, taking into consideration technology and market uncertainties associated with the business model. The following objectives were addressed in this project:

1. Generalize the market and technology landscape associated with the conversion of lignin into added-value derivatives.
2. Define a set of lignin-based biorefinery strategies, potentially suitable for implementation within an existing kraft pulp mill.
3. Define a set of technology, market and risk-based criteria, and consider these in a panel methodology, in order to identify the "most preferred" lignin-based biorefinery strategies.

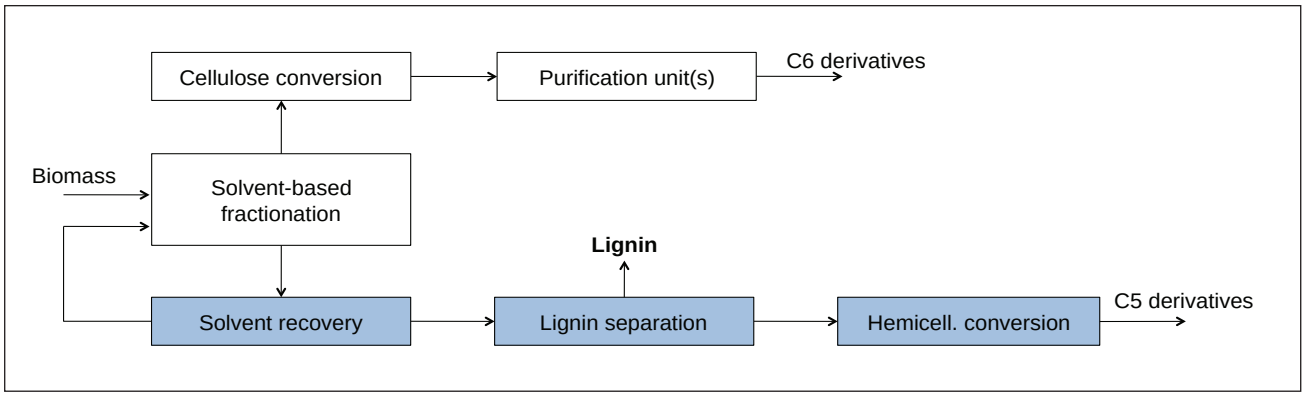
LIGNIN DERIVATIVES AND MARKET APPLICATIONS

The spectrum of products that can potentially be synthesized from lignin is fairly diversified. Holladay et al. [9] generally described this spectrum as including power, fuel, and syngas products, macromolecules, and aromatics, which can further be classified as near-term, medium-term, and long-term opportunities.

Lignosulfonates obtained from the sulfite pulping process are the most widely used today among technical lignin types; for example, they are used as concrete and animal feed additives, for dust control, or as a precursor in the production of vanillin, dimethyl sulfide (DMS), and dimethyl sulfoxide (DMSO). Phenol-formaldehyde (PF) resins, polyurethane (PU) foams, and carbon fibers are emerging as promising near-term opportunities for kraft and organosolv lignins [10-12], the category of lignins considered in this paper. For example, lignin can theoretically replace more than 50% of phenol used in resin formulations [13]; however, high levels of substitution are not recommended yet due to the lower performance of the resulting resin (bond strength, hardening time, mechanical properties of panels) [14]. In practice, at the present time the substitution potential of essentially unmodified lignin in PF resins is limited to 25%, and it can increase to 40% if the lignin is pre-treated, as by phenolation prior to resin manufacturing, for example [15].

With regards to PU foams manufacturing, lignin can be used as a replacement of polyols and is more suitable for rigid foams applications. Lignin depolymerization to obtain polyols can be realized with high yields (80%-90%) but this process remains embryonic for the moment [16]. A level of substitution of 15% has been achieved using a mechanically ground lignin (without chemical modification), while chemically modified lignin can replace up to 30% of polyols in PU foams [12], achieved through an oxyalkylation process.

The opportunity to produce carbon fiber from lignin is arguably one of the most attractive potential applications. Carbon fiber exhibits unique physical and mechanical properties that make it suitable for replacing metals in various applications, including in the automobile and aerospace industries [17]. Despite growing demand, carbon fiber production volumes remain low due to its high cost, which is related in good part to the cost of precursors. Lignin can potentially be a much cheaper alternative to polyacrylonitrile (PAN), which is currently the most common precursor used in the industry [18]. The conventional carbon fiber manufacturing process includes four steps: fiber spinning, stabilization, carbonization, and surface treatment. The lignin substitution potential varies with the type of spinning employed, ranging from 50% in the case of wet spinning to a full replacement when melt spinning is used [19]. Past studies have highlighted some difficulties for the spinning step using softwood kraft lignin, which charred at high temperature. Recent developments have overcome that limitation by separating the black liquor into distinct molecular weight fractions using an ultrafiltration membrane prior to lignin precipitation and using only the low-molecular weight fraction as a carbon fiber precursor [20]. Nevertheless, the current performance of lignin-based carbon fibers are not yet equivalent to PAN-based ones, especially for high-strength applications [17].



2. Simplified solvent-based biomass fractionation process.

MITIGATING BIOREFINERY RISKS THROUGH PHASED IMPLEMENTATION

Despite risks associated with lignin product performance and market growth, several forest product companies seek to have significant strategic advantages to being first- or early-to-market with the manufacture of lignin. A practical approach to mitigating these risks is through phased implementation. Chambost et al. [21] suggest a nominal three-phase approach.

Various factors influence the definition of phases from the perspective of mitigating risk, including (1) the product point-of-entry on the existing value chain, (2) the market characteristics and associated penetration needed, and (3) the technology development approach for the deployment of the strategy [22]. For the example of lignin use in phenolic resin applications, the first factor would consider whether lignin is sold as phenol replacement for resin manufacture, or whether it is mixed/converted into the PF resin. The penetration rate for a given position on the value chain, which is dependent on the substitution potential, leads to defining the design capacity of the process over several phases. Will the lignin be sold internally, or sold and re-purchased from the PF resin supplier? The third element considers whether the company is open to horizontal or vertical integration. Is the company open to vertical integration, as well as increasing risk and added value from manufacture of the downstream phenolic resin, requiring that their strategy brings them closer to the final user? What would be the company's competitive position to achieve this goal, relative to others?

EVALUATION AND SELECTION OF BIOREFINERY OPTIONS

The problem of biorefinery strategy selection has been addressed in various studies, and several methods have been developed to address the evaluation and decision-making regarding individual projects or project portfolios [23-26]. The success of a biorefinery initiative is dependent on a wide range of factors identified using different perspectives, among which the most important must be identified and taken into account during the biorefinery selection process. A committee of decision-makers rather than a single individual is typically responsible for capital investment recommendations in the company, and the committee must respectfully consider a range of technology, market, and risk issues. This emphasizes the need for a decision-making method that is practical for summarizing critical information, and using this to aggregate the perspectives of stakeholders in order to reach a balanced decision. Multi-criteria methods suitable for this purpose have been successfully employed to solve biorefinery decision problems in past studies [27-30]. Among these, multi-criteria decision-making (MCDM) aggregates the panel member preferences systematically and in an interactive context, resulting in an outcome that is readily interpretable, which facilitates alignment between stakeholders regarding "preferred" strategies.

In the MCDM process, the definition of the set of evaluation criteria is critical. Significant care is needed to define important criteria that reflect the values of the company [31]. Criteria can be defined using top-down [32] or bottom-up approaches [33], ultimately resulting in a consistent family of attributes, which should be exhaustive, monotonic, minimal, legible, and operational [34].

OBJECTIVE

This study considers the implementation of a lignin-based biorefinery at a North-American forest product company that owns sawmills and panel board mills, as well as kraft pulp and paper mills. The company seeks to diversify its product offering, starting with one of its market pulp mills. The mill produces 1500 air dried (a.d.) metric tons of kraft softwood pulp per day and is adjacent to a sawmill also owned by the company. Two recovery boilers and one hog fuel boiler are running under normal operating conditions, and the mill has enough cogenerated power to be energy self-sufficient. With regards to the integration of biorefinery processes with the existing pulping process, there is a reasonable capacity for a certain additional steam production, whereas spare capacity at the wastewater treatment plant is more limited. Additional biomass of approximately 1500 bone dry (b.d.) metric tons/day of hardwood saw logs is

available as potential feedstock for the biorefinery from the mill-owned forest management area (FMA).

It is assumed that in the base case, a lignin precipitation unit producing 30 b.d. metric tons/day of lignin from black liquor has been implemented at the mill. The objective of the project was to assess the different strategies available to the mill and to maximize the value of the lignin-based biorefinery.

Candidate biorefinery strategies

A preliminary screening of lignin applications was made considering (1) technology and market readiness for different lignin products, and (2) the potential to create competitive advantage in the near and longer terms. This analysis led to retaining polyols replacement in PU foams among immediately achievable alternatives to PF resins applications, while PAN replacement in carbon fibers was retained among the longer-term applications. All strategies were defined as extensions of the Base Case situation, considering phased implementation. The first strategy, referenced as "Ligno 90•PF," aims to improve market position by increasing production volume. It considers tripling the capacity of the lignin precipitation unit from 30 metric tons/day to 90 metric tons/day, still having minimal impact on recovery boiler operations. Two strategy alternatives emerge from this: (1) a mill-centric strategy that focuses on improving the competitive position of the host mill at the current scale (Group 1 strategies), and (2) strategies that seek larger manufacturing scales and greater impact in terms of revenue diversification (Group 2 strategies).

Ligno 90•PF PU and Ligno 90•PF CF strategies consider commercializing lignin for PU foams and carbon fiber applications, respectively. In both cases, 7% of the production would be used in company owned panel board mills, 60% would be sold for PF resin applications, and 33% for either PU foams or carbon fiber applications. A vertical integration approach is represented through the strategy Resin 90, which considers on-site manufacturing of a lignin-phenol-formaldehyde resin. In this case, the acquisition of an existing resin manufacturer is considered in order to facilitate the integration of resin production, as well as access to distribution channels.

In the second group of strategies, a joint venture is considered for the implementation of a standalone solvent pulping plant in parallel to the existing process. It would convert the available supply of hardwood into a portfolio with isobutanol (sold as a biofuel), a hemicellulose-rich sugar syrup (sold as animal feed), and lignin derivatives. The non-lignin products were selected using minimum technology and market risk considerations and remain fixed for all scenarios. The first lignin strategy, Ligno 90 + SP•PF, considers additional sales with the main lignin application. The last two, Ligno 90 + SP•PF PU and Ligno 90 + SP•PF CFs, consider product diversification into PU foams and carbon fiber applications. **Table I** summarizes the Phases for each of the seven strategies.

ANALYSIS METHODOLOGY

Information relative to mass and energy balances for the design of processes associated with the lignin-based biorefinery strategies was collected from the literature. A large-block analysis approach [35] was employed to obtain capital and operating costs estimates for each implementation phase of each strategy.

Techno-economic analysis

Considering retrofit implementation, the specifics of the case study host mill were taken into account for integration potential. This analysis emphasized the materials handling system, the inventory of unused equipment, the energy island and the wastewater treatment plant with the purpose of (1) identifying technology risks and additional costs for their mitigation, as well as (2) the potential for cost reduction resulting from synergies with the existing process.

In order to determine realistic values for capital expenses, capital costs were first estimated considering information in the literature on comparable processes, in a manner consistent with Diffo Téguia et al. [8]. Equipment with similar functions were identified, then data were scaled up to the case study design capacities and actualized using proper cost index factors. Common design heuristics were used to extrapolate components of direct and indirect capital costs for the integrated precipitation units, while the Lang method was employed for the case of standalone solvent pulping plants. Design heuristics were also employed for estimating fixed components of operating costs.

The basis for feed material costs and product prices involved making projections over the period of the project lifetime. Correlations were made between historical feed costs or product prices and energy commodities (crude oil, natural gas, and/or electricity). Average, minimum and maximum values of projections for energy commodities in reports from the International Energy Agency (IEA) [36] and the U.S. Energy Information Administration (EIA) [37] were used to extrapolate to future values for feed materials and products. For materials not directly linked to energy commodities, only historical values were used as the main basis for pricing. **Table II** summarizes feed material unit costs, and **Table III** summarizes product prices considered in this study.

Conservative discounts have been considered for the first three years following the market launch of derivative lignin products. These were nominally set based on the maturity of the targeted applications at: 10% for the replacement of PF resin, 20% for the replacement of phenol and polyols, and 30% for the replacement of PAN. For cash flow calculations, a 1-year construction period was assumed for capacity increase of the precipitation unit and for the solvent pulping demonstration plant, while a 2-year period was assumed for construction of the full-scale solvent pulping plant. In order to compare the impacts of each strategy, cash flow values were actualized to the year of the capacity increase occurring in Phase I of all strategies.

<table>
<tr><th rowspan="2">Strategic Orientation</th><th>Lignin Biorefinery Strategies</th><th>Phase 0
Year 0 – Year 4</th><th>Phase I
Year 5 – Year 9</th><th>Phase II
Year 10 – Year 30</th></tr>
<tr><td>Base Case 30 metric tons/day lignin precipitation</td><td colspan="3">• Year 0: 100% lignin burnt
• Year 1: 28 metric tons/day burnt, 2 metric tons/day to board mills
• Year 2: 24 metric tons/day burnt, 6 metric tons/day to board mills
• Year 3: 18 metric tons/day burnt, 6 metric tons/day to board mills, 6 metric tons/day to PF resin market
• Year 4: 12 metric tons/day burnt, 6 metric tons/day to board mills, 12 metric tons/day to PF resin market
• Year 5: 6 metric tons/day burnt, 6 metric tons/day to board mills, 18 metric tons/day to PF resin market
• Year 6+: 6 metric tons/day to board mills, 24 metric tons/day to PF resin market</td></tr>
<tr><td rowspan="4">Group 1: Improve mill competitive position</td><td>Ligno 90•PF</td><td rowspan="7">Same as Base Case</td><td colspan="2">Increase of lignin precipitation capacity to 90 metric tons/day
• Year 5: 6 metric tons/day burnt, 6 metric tons/day to board mills, 48 metric tons/day to PF resin market
• Year 6: 6 metric tons/day to board mills, 84 metric tons/day to PF resin market</td></tr>
<tr><td>Ligno 90• PF PU</td><td colspan="2">Same as Ligno 90•PF, excepting:
• Year 5: 33 metric tons/day to PF resins, 15 metric tons/day to PU foams
• Year 6: 54 metric tons/day to PF resins, 30 metric tons/day to PU foams</td></tr>
<tr><td>Ligno 90•PF CFs</td><td colspan="2">Same as Ligno 90•PF, excepting:
• Year 5: 33 metric tons/day to PF resins, 15 metric tons/day to carbon fibers
• Year 6: 54 metric tons/day to PF resins, 30 metric tons/day to carbon fibers</td></tr>
<tr><td>Resin 90</td><td>Same as Ligno 90•PF</td><td>Acquisition of a resin producer
• Year 10: 290 metric tons/day of resin produced
• Year 11: 435 metric tons/day of resin produced</td></tr>
<tr><td rowspan="3">Group 2: Larger-scale revenue diversification</td><td>Ligno 90 + SP•PF</td><td>Same as Ligno 90•PF + Solvent pulping demo plant[1]</td><td>Increase of solvent pulping to full capacity[2]</td></tr>
<tr><td>Ligno 90 + SP•PF PU</td><td colspan="2">Same as Ligno 90 + SP•PF, excepting lignin distribution: 6 metric tons/day to board mills, 220 metric tons/day to PF resins, 124 metric tons/day to PU foams</td></tr>
<tr><td>Ligno 90 + SP•PF CFs</td><td colspan="2">Same as Ligno 90 + SP•PF, excepting lignin distribution:
6 metric tons/day to board mills, 220 metric tons/day to PF resins, 124 metric tons/day to carbon fibers</td></tr>
</table>

[1] The demo plant extracts 9 b.d. metric tons/day of lignin from 50 b.d. metric tons/day of hardwood.
[2] There is a capacity ramp up of the full-scale plant from Year 10-12 resulting in 220, 270, and 350 b.d. metric tons/day of lignin extracted.

I. Summary of lignin-based biorefinery strategies and phased implementation (PF = phenol-formaldehyde; PU = polyurethane; CF = carbon fiber).

ECONOMIC ANALYSIS

Feed Material	Assumed Unit Cost ($/metric ton)		Basis for Assumed Cost
	Nominal	Maximum	
Phenol	1 005	1 905	Correlation identified with the price of crude oil.
Sulfuric acid	180	240	Pricing based on historical trends dictated by phosphate fertilizers and copper industries.
Carbon dioxide	300	390	Case-specific values.
Oxygen	50	65	
Caustic	430	810	Correlation identified with the price of crude oil.
Enzymes	2 270	2 500	Latest available price in literature. A 5% increase was considered for the maximum, as prices are expected to considerably decrease with more economical technologies.
Yeast	1 875	2 060	
Biomass	100 (dry)	127 (dry)	30% of the delivery costs were attributed to transportation, which was assumed to be varying with crude oil.
Formaldehyde	210	400	Formaldehyde is produced on-site. Methanol represents around 80% of production costs, and its price is correlated to both crude oil and natural gas.
Electricity	7.9 ¢/kWh	14.8 ¢/kWh	Values adjusted to mill location based on historical trends.
Natural gas	4.35 $/GJ	7.15 $/GJ	

II. Assumed unit costs for feed materials to process.

Product	Assumed Market Price ($/metric ton)		Basis for Assumed Price
	Nominal	Minimum	
Phenol	1 005	690	Correlation identified with the price of crude oil.
Polyols	2 970	2 035	Correlation identified with the price of propylene, which is conjointly influenced by prices of crude oil and natural gas.
PAN	2 480	1 700	Based on target carbon fiber prices between 5-7 $/lb. Minimum value based on variations of acrylonitrile, therefore of propylene.
PF resin	2 000	1 485	Average price among different providers. Minimum value linked to variations of phenol and formaldehyde.
Sugar syrup	170	155	Molasses price in cattle industry-intensive U.S. states.
Isobutanol	3.08 $/gal	2.11 $/gal	Correlation identified with the price of propylene.

III. Assumed market prices for lignin-based biorefinery products

Definition of a minimal and necessary set of decision criteria

For the purposes of the case study, a database of MCDM panel criteria from many previous panels was considered. There were two criteria triage steps, (1) considering the pertinence of individual criteria, and (2) considering the family of criteria as a whole. In the first step, criteria judged not relevant, important, representative, or discriminative were screened [38]. The panel members judged the reliability of criteria based on information and assumptions used to calculate criteria metrics. The set of criteria resulting from the first step was then enhanced, by assessing that it formed a consistent family of criteria [34]. Certain criteria were combined into a single one to make a set of workable criteria for the panel, with a maximum of eight.

A set of six criteria were identified in close collaboration with panel members, a majority being related to market risk and competitiveness. **Table IV** summarizes the criteria and their interpretations as established by the panel members.

Decision-making for the "preferred" lignin-based biorefinery strategy

An MCDM panel method was employed for decision-making. Preferences regarding relative criteria importance (weights) were obtained through a pair-wise tradeoff process between criteria with the one considered most important by panel members. Biorefinery strategies could then be compared based on their overall scores, which were calculated using a weighted sum as defined by Eq. (1):

$$\text{Score}_{\text{candidate j}} = \sum_{i=1}^{N} W_i \times U_i(x_j) \quad (1)$$

where N is the number of criteria, W_i is the weight of criterion i, U_i is the utility function associated with criterion i, and x_j is the value obtained by evaluating biorefinery candidate j under criterion i. The utility function serves the purpose of bringing criteria with different units to a common basis. In this case, a linear normalization was employed, using lower and upper bounds determined by panel members based on the results of criteria evaluation.

The panel was composed of seven members, including four representatives of the forest products company, and three external members. External members are usually facultative but were included in this case at the request of the company. Quintero-Bermudez demonstrated that consistent decisions – different criteria weights but similar alternatives scores and ranking – are generally achieved even with different panel compositions [39]; however, in order for the decision to adequately reflect the company's vision, its representatives must be people with authority on project approval, which in this case was an accountant and three managers.

RESULTS

Techno-economic estimates

The techno-economic analysis results are summarized in **Table V**. The "company contribution" considers the joint venture approach used for the solvent pulping (SP) strategy.

Although these techno-economic results are mill-specific, there is an order-of-magnitude difference between costs and revenues associated with integrated (Group 1) and larger-scale (Group 2) strategies. The Group 1 strategies require relatively low capital and operating expenses, but also generate lower annual revenues compared to larger scale strategies. On the other hand, strategies in Group 2 rely on the availability of subsidies and economies-of-scale for attractive returns. Although they generate higher annual margins, the associated NPV's are lower than those of Group 1 strategies with similar lignin derivative products. Higher profitability could be expected if higher value derivatives from cellulosic sugars were to be considered; however, it was not the focus of this case study. The profitability of the Resin 90 strategy is impressive, but implies more economic uncertainties compared to other strategies.

Assessment of decision criteria

Decision-making for corporate transformation to a new product portfolio, such as the case for the lignin-based biorefinery, should not rely on profitability metrics alone. Technology and market risks are critical for this long-term diversification decision, and thus a more complete set of decision-making metrics was considered in the present study. The values for the 6 decision-making criteria identified and defined in Table IV are presented in **Table VI**. (Note: Considering a sustainability perspective, environmental, and other criteria would typically also be considered in an MCDM panel; however, the focus of the current work was on technology and market risks in addition to profitability.)

The two economic criteria (IRR and CFCE) display a similar trend, and strategies involving integrated processes are more profitable than those involving larger scale processes. Group 2 strategies have a greater impact on revenue diversification and are less vulnerable to fluctuations in energy and chemical costs. RPMC displays a unique profile that makes a direct comparison between strategies of the two groups less obvious. Considering the global picture, no candidate strategy results in criteria evaluation that are higher than all other candidates for the criteria considered. This justifies the need to allocate weights to criteria using an MCDM panel, alongside other benefits of MCDM panels, such as alignment of stakeholders.

MCDM panel outcome

IRR was selected by the panel as the most important criterion in the context of the case study, considering the importance of profitability for ensuring competitiveness of the overall site over the long term. Panel members set the target value of IRR at 25%, and an ambitious value of 75% for the upper limit of

Category	Criterion	Interpretation	Metric
Economic Risk	Internal Rate of Return (IRR)	Measure of **project profitability under normal market conditions**, considering all phases of the biorefinery strategy. The hurdle rate was set at 20%, considering the risk level expected in Year 5 of the project.	Discount rate at which NPV equals zero. $NPV = \sum_{t=0}^{25} \frac{\text{Cash flow}_t}{(1 + \text{IRR})^t} = 0$
	Cash Flow on Capital Employed (CFCE)	Ability to generate cash flows from the capital investment over the life of the project, and thereby **to improve the value of the company by lowering its debt**.	• Discount rate for future EBITs: 20% • Discount rate for capital investments: 6% $CFCE = \frac{\sum \text{present value of future EBITs}}{\sum \text{present value of capital investments}}$
Market Risk and Competitiveness	Revenue Diversification (RD)	Potential to meet revenue growth targets from new bioproducts, over the revenue from the mill in its current situation. It indicates an ability to mitigate market risk by being **less dependent on pulp sales**, due to a more **diversified source of revenues**.	RD = Importance of new revenues × Importance of new products
	Competitiveness on Production Costs (CPC)	**Robustness** of the biorefinery strategy relative to an **aggressive price-cutting strategy from the competition**, based on assumptions of a low-end production price for the competition.	$CPC = \frac{(\text{Total portfolio revenue})_{\text{minimum market prices}} - \text{Operating costs}}{(\text{Total portfolio revenue})_{\text{minimum market prices}}}$
	Resistance to Energy and Chemicals Market Uncertainty (RECMU)	Vulnerability of the strategy to **production cost volatility due to the volatility of feed material costs** (product transportation and logistics not included).	$RECMU = 1 - \frac{\text{Costs of (energy + chemicals)}}{\text{Total variable costs}}$
	Robustness to Poor Market Conditions (RPMC)	Ability to **afford process operation under poor market conditions** for a 6-month period, expressed by EBITDA as a percentage of the capital investment.	$RPMC = \frac{(\text{monthly EBITDA under poor market conditions}) \times 6}{\text{Total capital costs}}$

IV. Summary of decision criteria used for decision-making panel (NPV = net present value; EBIT = earnings before interest and tax; EBITDA = earnings before interest, taxes, depreciation and amortization).

the normalization range. The latter was justified by the need to encompass uncertainty of parameters that influence IRR, given especially uncertainty of data for Year 5 and beyond of the project timeline. Criteria weights and ranking that resulted from tradeoff activities are summarized in **Fig. 3**, and the overall scores obtained when combining the weights with normalized calculated outcomes for each strategy criteria are presented in **Fig. 4**.

After IRR, Competitiveness on Production Costs (CPC) was attributed the second highest weighting among the criteria, mainly due to the impact that pricing strategy has on the potential to penetrate and capture early market share. The relatively high weight of the Revenue Diversification (RD) criterion was linked with the objective of diversifying sources of revenues as part of the long-term vision of the forest product company. Cash Flow on Capital Employed (CFCE) and Resistance to Energy and Chemicals Market Uncertainty (RECMU) criteria received similar weights as indicators of profitability and robustness. Since all biorefinery strategies had positive margins under poor market conditions, panel members decided not to attribute Robustness to Poor Market Conditions (RPMC) a significant weight.

As per Fig. 4, the application of criteria weights to the different biorefinery strategies did not lead to scores disparate enough that they were easily distinguished. Criteria weights influenced strategies scores in diverse ways. Strategies involving integrated processes were preferred due their performance on economic indicators, while strategies involving larger-scale processes were preferred due to their diversification potential and robustness. The strategy Ligno 90•PF PU, ranked first, adequately combines economic and strategic advantages, being the best performer for IRR, CFCE, and CPC. Overall, strategies involving PU foams were more preferred than strategies using similar processes but promoting carbon fiber. The strategy Resin 90 also had an interesting position, with a profile distinct to other strategies of comparable scores.

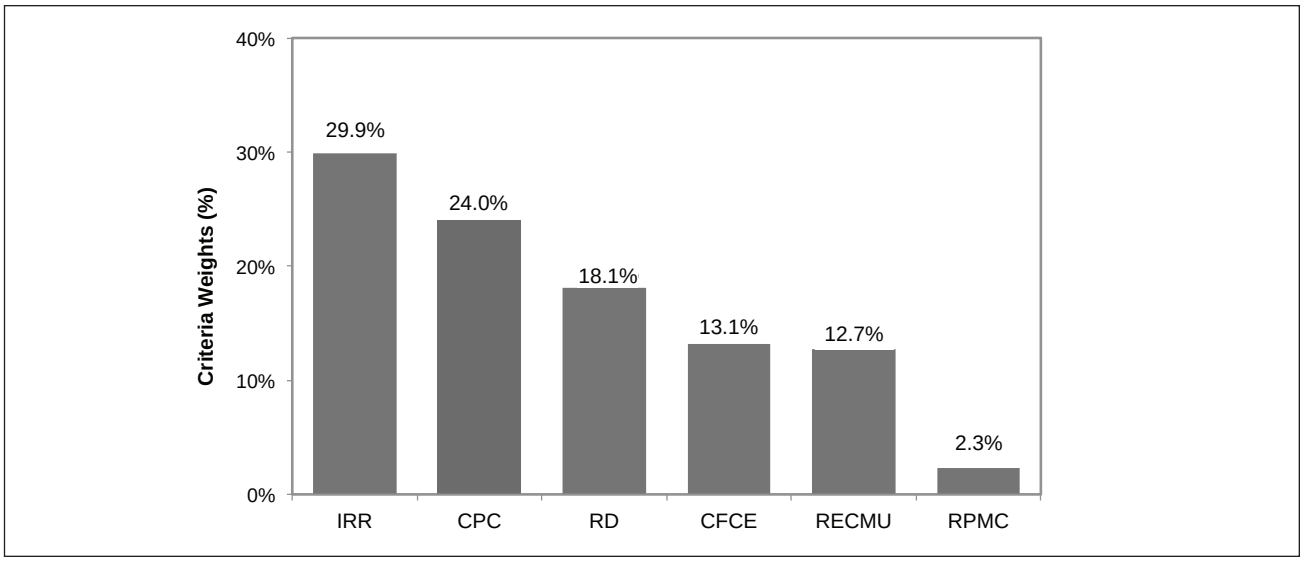
		Group 1 Improve mill competitive position				Group 2 Larger-scale revenue diversification		
Indicator		Ligno 90•PF	Ligno 90•PF PU	Ligno 90•PF CFs	Resin 90	Ligno 90 + SP•PF	Ligno 90 + SP•PF PU	Ligno 90 + SP•PF CFs
Lignin production capacity		90 metric tons/day	90 metric tons/day	90 metric tons/day	90 metric tons/day 435 metric tons/day resin	350 metric tons/day	350 metric tons/day	350 metric tons/day
Capital Investment	Total project cost	32 M$	33 M$	39 M$	146 M$	432 M$	438 M$	436 M$
	Company contribution					153 M$	156 M$	154 M$
Annual Operating Costs (Phase II)	Total costs	6 M$/year	7 M$/year	7 M$/year	104 M$/ year	123 M$/ year	127 M$/ year	126 M$/ year
	Company contribution					60 M$/year	62 M$/year	61 M$/year
Annual Revenues (Phase II)	Total revenues	21 M$/year	41 M$/year	36 M$/year	287 M$/ year	222 M$/ year	305 M$/ year	284 M$/ year
	Company share					120 M$/ year	162 M$/ year	151 M$/ year
Annual EBITDA (Phase II)		15 M$/year	34 M$/year	29 M$/year	183 M$/ year	60 M$/year	100 M$/ year	90 M$/year
NPV (Phases I and II combined)		17 M$	70 M$	49 M$	164 M$	6 M$	50 M$	37 M$

V. Summary of techno-economic results.

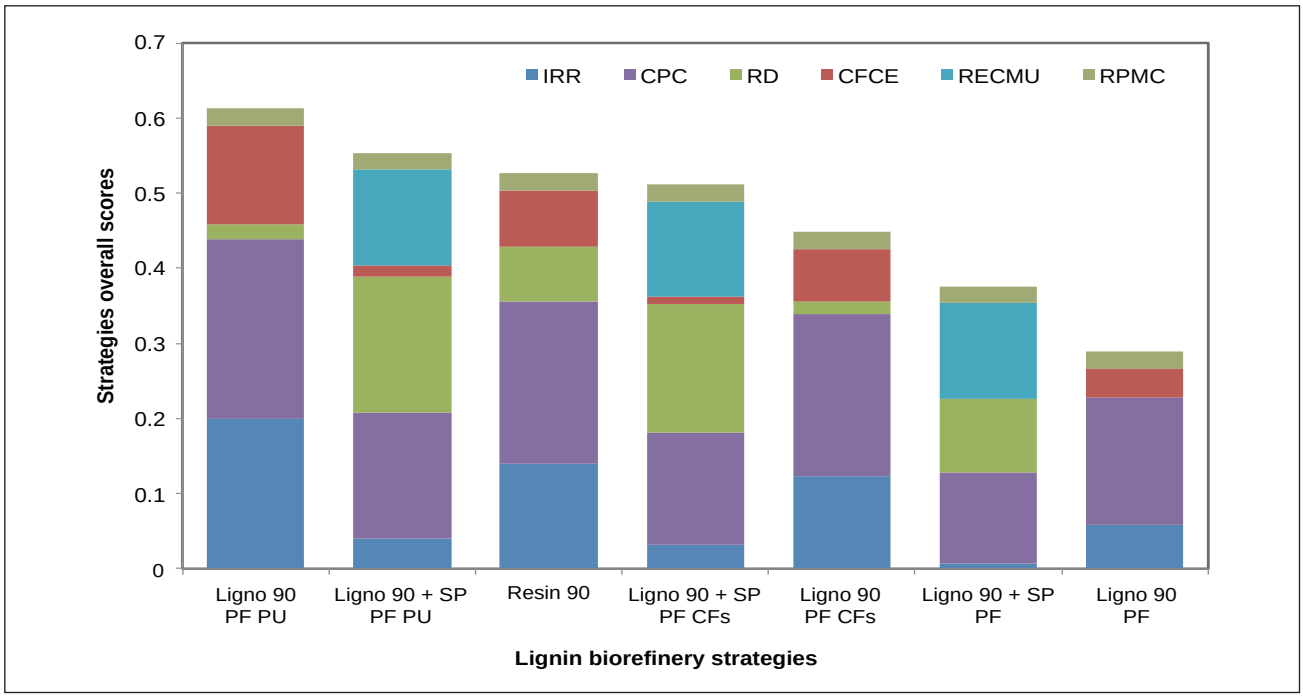
	Group 1 Improve mill competitive position				Group 2 Larger-scale revenue diversification		
Criterion	Ligno 90•PF	Ligno 90•PF PU	Ligno 90•PF CFs	Resin 90	Ligno 90 + SP•PF	Ligno 90 + SP•PF PU	Ligno 90 + SP•PF CFs
Internal Rate of Return (IRR)	31%	57%	43%	46%	21%	28%	26%
Cash Flow on Capital Employed (CFCE)	2.0	4.5	2.9	3.0	1.0	1.4	1.3
Revenue Diversification (RD)	2%	7%	7%	22%	29%	51%	48%
Competitiveness on Production Costs (CPC)	46%	65%	59%	58%	33%	45%	41%
Resistance to Energy and Chemicals Market Uncertainty (RECMU)	21%	30%	28%	14%	82%	83%	83%
Robustness to Poor Market Conditions (RPMC)	7%	22%	13%	4%	4%	11%	8%

VI. Summary of results of criteria evaluation.

ECONOMIC ANALYSIS



3. Criteria weights resulting from the Multi-Criteria Decision-Making (MCDM) tradeoff panel.



4. Scores for lignin-based biorefinery strategies resulting from the MCDM panel.

Based on these results, the panel identified the top three strategies as "most preferred" for implementing the lignin-based biorefinery. The following two could eventually be reconsidered if market conditions become more favorable for their implementation. The last two candidate strategies were rejected.

DISCUSSION

A marginally profitable strategy is unlikely to be preferred. On the other hand, the IRR criterion weight is surprisingly low compared to others, due in large part to the upper bound of normalization set at 75% by the panel, as in high profitability expectations from a lignin-based biorefinery strategy by panel members.

CPC has an important impact for distinguishing between strategies and is the most important contributor for five of seven strategies. Product pricing, which is dependent on both process economics and the comparability of lignin-derived with existing products, is a determining factor for the endorsement of the lignin-based biorefinery by forestry companies.

From the perspective of distinguishing between strategies, RPMC did not play a distinctive role, as all strategies had good

performance. For the assumptions of the study, the lignin-produced products from the mill have good potential to be cost-competitive compared to similar derivative products that use fossil-based feedstocks.

It is clear that the larger volume strategies are preferred due to their more significant revenue growth and their diversified product portfolio for mitigating price volatility. Combining the best two candidates, a forest product company could: (1) increase its lignin precipitation capacity and diversify the targeted lignin applications including higher value derivatives in the midterm, prior to (2) implementing a larger scale process, such as solvent pulping leading to a diversified product portfolio to simultaneously improve its market position and its robustness.

Emphasizing vertical integration by entering into the resin-manufacturing segment was also a preferred lignin-based biorefinery strategy. The score of the Resin 90 strategy shows that it can potentially create unique competitive advantage for the forestry company. Because it can partially absorb unsold volumes of lignin or eventually lignin-based resin by using it in its own board mills, such a company has the opportunity to demonstrate the application, optimize the application, and clearly identify the value proposal for lignin-based phenolic resins.

Finally, the ranking and score of the Ligno 90•PF strategy demonstrates that minimal risk strategies are unlikely to lead to a sustainable competitive position. Market demand is expected to increase as the usage of lignin derivatives for diverse applications gets mature, and a strategy relying solely on increasing the production capacity would be insufficient from a competitive point of view.

CONCLUSIONS

Recent progress towards the emergence of the lignin-based biorefinery motivated this study, which aims at the identification of promising strategies considering particularly the context of a retrofit implementation of the lignin-based biorefinery within a forest products company. This has been achieved through a case study considering seven candidate strategies for implementation at an existing kraft pulp mill where a 30 metric tons/day lignin precipitation unit is already in place. Company-specific drivers and barriers led to retaining PF resins, PU foams, and carbon fiber applications as potential market segments for lignin positioning.

The assessment of candidate strategies was made using a set of economic and market criteria. Results showed that strategies involving integrated (lignin precipitation) processes were more profitable than those involving larger scale (solvent pulping) processes, while the latter was more attractive in terms of revenue diversification and were more robust to price volatility on energy and chemical markets.

Criteria weighting was made using a Multi-Criteria Decision-Making (MCDM) panel, during which Internal Rate of Return (IRR) received the highest weight. Nevertheless, the criterion representing price competitiveness was the highest contributor to strategy scores. Price competitiveness relative to competing fossil-based products is expected to be critical to the development of lignin biorefinery, both for market penetration and positioning. The MCDM panel members identified that the top three lignin-based biorefinery strategies should be retained as "preferred". The first-ranked strategy would sell lignin for PF resins and PU foams at a low volume and resulted in strong economic returns, cash flow generation and cost competitiveness. The second-ranked strategy considered the same applications for lignin but at a larger scale, and the third-ranked strategy considered on-site manufacturing of a lignin-based PF resin. **TJ**

ACKNOWLEDGMENTS

This study was funded by a grant from the Natural Sciences and Engineering Research Council of Canada (NSERC). The authors would like to thank the industrial partners in the project that provided data and contributed to validating assessment results, as well as panelists who participated in MCDM sessions.

LITERATURE CITED

1. Ragauskas, A., "Lignin Overview," Institute of Paper Science and Technology, Atlanta, GA, USA. Available [Online] http://www.ipst.gatech.edu/faculty/ragauskas_art/technical_reviews/Lignin%20Overview.pdf <18April2017>.
2. Zhang, Y.-H., *J. Ind. Microbiol. Biotechnol.* 35(5): 367(2008).
3. Macdonald, C., *Pulp Pap. Can.* 117(5): 16(2016).
4. Kouisni, L., Gagné, A., Maki, K., et al., *ACS Sustainable Chem. Eng.* 4(10): 5152(2016).
5. Öhman, F., Theliander, H., Tomani, P., et al., pat. WO 2006031175 A1 (March 23, 2006).
6. Kouisni, L. and Paleologou, M., pat. US20110297340 A1 (Dec. 8, 2011).
7. Agbor, V.B., Cicek, N., Sparling, R., et al., *Biotechnol. Adv.* 29(6): 675(2011).
8. Diffo Téguia, C., Albers, R., and Stuart, P., *TAPPI J.* 16(3): 157(2017).
9. Holladay, J.E., Bozell, J.J., White, J.F., et al., *Top Value-Added Chemicals from Biomass Volume II—Results of Screening for Potential Candidates from Biorefinery Lignin*, U.S. Department of Energy, Oak Ridge, TN, USA, 2007.
10. Smolarski, N., "High-Value Opportunities for Lignin: Unlocking its Potential," Frost & Sullivan, San Antonio, TX, USA, 2012. Available [Online] http://www.greenmaterials.fr/wp-content/uploads/2013/01/High-value-Opportunities-for-Lignin-Unlocking-its-Potential-Market-Insights.pdf <12April2017>.
11. LigniMatch, "Future use of lignin in value added products," Chalmers University of Technology/University of Gothenburg, Gothenburg, Sweden. Available [Online] http://www.gmv.chalmers.gu.se/digitalAssets/1448/1448662_roadmap.pdf <12April2017>.
12. Gosselink, R., "Future perspectives of organosolv lignins," DLO-BIOCORE, Wageningen, Netherlands, 2014. Available [Online] http://www.biocore-europe.org/file/2_1%20BIOCORE%20R%20Gosselink%20DLO%20Organosolv%20lignins.pdf <18April2017>.
13. Wang, M., Leitch, M., and Xu, X., *Eur. Polym. J.* 45(12): 3380(2009).

14. Çetin, N.S. and Özmen, N., *Int. J. Adhes. Adhes.* 22(6): 477(2002).
15. Matsushita, Y., *J. Wood Sci.* 61(3): 230(2015).
16. Mahmood, N., Yuan, Z., Schmidt, J., et al., *Eur. Polym. J.* 68: 1(2015).
17. Naskar, A.K., "Developing low cost carbon fiber for automotive lightweight composites," *32nd Annu. Meet. Counc. Chem. Res.*, Council for Chemical Research, Washington, D.C., 2011.
18. Nordström, Y., Norberg, I., Sjöholm, E., et al., *J. Appl. Polym. Sci.* 129(3): 1274(2013).
19. Kadla, J.F., Kubo, S., Venditti, R.A., et al., *Carbon* 40(15): 2913(2002).
20. Norberg, I., "Carbon fibres from kraft lignin," Ph.D. thesis, KTH Royal Institute of Technology, Stockholm, 2012.
21. Chambost, V., McNutt, J., and Stuart, P.R., *Pulp Pap. Can.* 109(7): 19(2008).
22. Diffo Téguia, C., Chambost, V., Sanaei, S., et al., in *Forest Value Chain Optimization and Sustainability* (S. D'Amours, Eds), CRC Press, Boca Raton, FL, USA, 2016, Chap. 3.
23. Archer, N.P. and Ghasemzadeh, F., *Int. J. Proj. Manage.* 17(4): 207(1999).
24. Henriksen, A.D. and Traynor, A.J., *IEEE Trans. Eng. Manage.* 46(2): 158(1999).
25. Verbano, C. and Nosella, A., *Eur. J. Innovation Manage.* 13(3): 355(2010).
26. Thamhain, H.J., *Eng. Manage. J.* 6(3): 3(2014).
27. Papalexandrou, M.A., Pilavachi, P.A., and Chatzimouratidis, A.I., *Process Saf. Environ. Prot.* 86(5): 360(2008).
28. Sacramento-Rivero, J.C., *Biofuels Bioprod. Biorefin.* 6(1): 32(2012).
29. Posada, J.A., Patel, A.D., Roes, A., et al., *Bioresour. Technol.* 135: 490(2013).
30. Niekamp, S., Bharadwaj, U.R., Sadhukhan, J., et al., *J. Ind. Prod. Eng.* 32(1): 23(2015).
31. Vincke, P., *Multicriteria Decision Aid*, John Wiley and Sons, New York, 1992.
32. Keeney, R.L. and Raiffa, H., *Decisions with Multiple Objectives: Preferences and Value Trade-Offs*, Cambridge University Press, New York, 1993.
33. Roy, B., *Méthodologie multicritère d'aide à la décision*, Economica, Paris, 1985.
34. Roy, B. and Bouyssou, D., *Aide multicritère à la décision: Méthodes et cas*, Economica, Paris, 1993.
35. Hytönen, E. and Stuart, P.R., *Pulp Pap. Can.* 110(5): T58(2009).
36. International Energy Agency, "World Energy Outlook 2015 - Chapter 1: Introduction and scope," 2015. Available [Online] http://www.worldenergyoutlook.org/media/weowebsite/2015/WEO2015_Chapter01.pdf <18April2017>.
37. U.S. Energy Information Administration, "Annual Energy Outlook 2015 with Projections to 2040," 2015. Available [Online] https://www.eia.gov/outlooks/aeo/pdf/0383(2015).pdf <18April2017>.
38. Bouyssou, D., in *Readings in Mutiple Criteria Decision Aid* (C.A. Bana e Costa, Ed.), Springer Verlag, Berlin, Germany, 1990, pp. 58-80.
39. Quintero-Bermudez, M.A., Janssen, M., Cohen, J., et al., *TAPPI J.* 11(11): 9(2012).

ABOUT THE AUTHORS


Téguia


Stuart


D'Amours


Albers

We chose to study this topic because the decision about long-term lignin-based biorefinery strategies that meet company needs and values is not obvious. We have previously conducted research on Multi-Criteria Decision-Making (MCDM) methodology, including several papers published in *TAPPI Journal*.

The most difficult aspect of this research was assembling an interested industry panel willing to invest their time in becoming familiar with the MCDM methodology. We did enhance our ability to conduct effective MCDM panels through this exercise. Our most interesting finding was that companies are more concerned about downside risk than they are about making money!

Through this research, mills can better appreciate (a) long-term lignin-based biorefinery strategies, and (b) their relative strengths and weaknesses, especially regarding risk. The next step will be for our industry partner to decide on their longer-term lignin-based biorefinery strategy.

Diffo Téguia is post-doctoral student and Stuart is professor at Polytechnique Montréal, Montréal, QC, Canada. D'Amours is professor, Université Laval, Quebec City, QC, Canada. Albers is manager, Energy and Bioproduct Development, West Fraser Timber Co. Ltd., Quesnel, BC, Canada. Email Stuart at paul.stuart@polymtl.ca.

TAPPI JOURNAL
WWW.TAPPI.ORG
THE PAPER AND PACKAGING INDUSTRIES' TECHNICAL RESOURCE
MAY 2017 | VOL. 16 NO.5



PULPING 253
Determining wash loss levels in the brownstock pulp washing line using different methods
Riku Kopra and Olli Dahl

BLEACHING 263
Generalized steady-state model for chlorine dioxide brightening of hardwood kraft pulps
Brian N. Brogdon

PULPING 275
Impact of dissolved matter in the oxygen delignification stage
Caroline Wilke, Niclas Andersson, and Ulf Germgård

BIOREFINERY 287
Process for producing acetic acid in hardwood kraft pulp mills
Ravikant Patil, Joseph Genco, Hemant Pendse, and Adriaan van Heiningen

FEATURING SPECIAL CONTENT FROM THE:
2016 PEERS Conference

May 2017

TABLE OF CONTENTS VOL. 16 NO. 5

249 GUEST EDITORIAL
Professional networking in the nonwovens and technical textiles sector
Seshadri Ramkumar

253 PULPING
Determining wash loss levels in the brownstock pulp washing line using different methods
Riku Kopra and Olli Dahl

263 BLEACHING
Generalized steady-state model for chlorine dioxide brightening of hardwood kraft pulps
Brian N. Brogdon

275 PULPING
Impact of dissolved matter in the oxygen delignification stage
Caroline Wilke, Niclas Andersson, and Ulf Germgård

287 BIOREFINERY
Process for producing acetic acid in hardwood kraft pulp mills
Ravikant Patil, Joseph Genco, Hemant Pendse, and Adriaan van Heiningen

»COVER CREDIT: Receptacles for collecting liquid acetic acid and caustic solutions generated in the University of Maine's laboratory bipolar membrane electrodialysis (BPMED) apparatus, which was used by Patil and co-authors to obtain the data for their research (p. 287).

TAPPI JOURNAL
WWW.TAPPI.ORG

Editor-in-Chief
Scott Rosencrance scott.rosencrance@kemira.com
+1 770 429-2753

Associate Editor
Brian N. Brogdon brian.brogdon@gmail.com
+1 678 581-9114

Editorial Director
Monica Shaw mshaw@tappi.org
+1 770 367-9534

Vice President, Operations
Eric Fletty efletty@tappi.org

PRESS Manager
Jana Jensen jjenson@tappi.org
+1 770 209-7242

Webmaster
Trina Heath theath@tappi.org
+1 770 209-7416

***TJ* EDITORIAL BOARD**

Brian N. Brogdon, FutureBridge Consulting & Training LLC
brian.brogdon@gmail.com, +1 678 581-9114

David A. Carlson, Carlson Consulting
dacarlson39@aol.com, +1 847 323-2685

Jere W. Crouse, JWC Consulting
cj522@inwave.com, +1 608 362-4485

Mahendra Doshi, Doshi and Associates
mahen@aol.com, +1 920 832-9101

Marc Foulger, GL&V USA Inc.
Marc.foulger@glv.com +1 315 767-2920

Peter W. Hart, WestRock
peter.hart@westrock.com, +1 409 276-3465

Carl J. Houtman, USDA Forest Products Laboratory
choutman@fs.fed.us, + 1 608 231-9445

John A. Neun, John A. Neun LLC
john.neun@gmail.com, +1 518 275-8139

Jim Niemiec, Verso Corporation
jim.niemiec@versoco.com, +1 715 422-7404

Steven P. Ottone, Omya
steven.ottone@omya.com, +1 919 641-7854

Gaurav Pranami, Imbed Biosciences
gpranami@imbedbio.com, +1 515 230-7005

Arthur Ragauskas, Oak Ridge National Laboratory
aragausk@utk.edu

Gerard J.F. Ring, University of Wisconsin—Stevens Point
gerrryring@wi-net.com, +1 715 592-3732

Scott Rosencrance, Kemira Chemicals
scott.rosencrance@kemira.com, +1 770 429-2753

Ricardo B. Santos, WestRock
ricardo.santos@westrock.com, +1 540 969-2426

Paul Wiegand, NCASI
pwiegand@ncasi.org, +1 919 941-6417

Junyong Zhu, USDA Forest Products Laboratory
jzhu@fs.fed.us, +1 608 231-9520

Join TAPPI *today!*

TAPPI JOURNAL is a free benefit of TAPPI membership, and is only available to members. To join TAPPI, to renew your TAPPI Membership, or to learn about other valuable benefits, visit www.tappi.org.

TAPPI, 15 Technology Parkway S., Suite 115, Peachtree Corners, GA 30092, publishes *TAPPI JOURNAL* monthly.

ATTENTION PROSPECTIVE AUTHORS: All papers published are subject to *TAPPI JOURNAL's* peer-review process. Not all papers accepted for review will be published. Before submitting, check complete author guidelines at http://www.tappi.org/s_tappi/doc.asp?CID=100&DID=552877.

Statements of fact and opinions expressed are those of individual authors. TAPPI assumes no responsibility for such statements and opinions. TAPPI does not intend such statements and opinions or construe them as a solicitation of or suggestion for any agreed-upon course of conduct or concerted action of any sort.

Copyright 2017 by TAPPI, all rights reserved. For copyright permission to photocopy pages from this publication for internal or personal use, contact Copyright Clearance Center, Inc. (CCC) via their website: www.copyright.com. If you have questions about the copyright permission request process, please contact CCC by phone at +1 978 750-8400. To obtain copyright permission to use excerpts from this publication in another published work, send your specific request in writing to Editor, TAPPI JOURNAL, 15 Technology Parkway S., Suite 115, Peachtree Corners, GA 30092, USA; or by fax to +1 770 446-6947.

Send address changes to TAPPI, 15 Technology Parkway S., Suite 115, Peachtree Corners, GA 30092, USA; Telephone +1 770 446-1400, or FAX +1 770 446-6947. www.tappi.org

Guest Editorial



SESHADRI RAMKUMAR
Chair, TAPPI NET Division

Professional networking in the nonwovens and technical textiles sector

Nonwovens and technical textiles (NWTT) is a relatively a young field within the textiles sector and has tremendous growth opportunity. In fact, the growth in this sector has historically performed well above or on par with the gross domestic product (GDP) of nations, specifically in developed economies. Particularly, in developing nations such as India, good growth is expected for the next few years.

Unlike commodity and conventional textiles, which are predominantly determined by aesthetics, fashion and consumer appeal, NWTT is determined by its functional and high-performance properties. Therefore, this industry is heavily dependent on research and development and, in particular, on the development of new and innovative products.

NWTT's need for global platforms, organizations

In general, the functional textiles sector to which the nonwovens and technical textiles belongs can be conveniently grouped into three major segments: 1) consumer, 2) institutional, and 3) government procurement-based products. Within these three broad categories, specific products like filtration, geotextiles, hygiene and medical, coated textiles, etc., can be easily grouped. These sectors are burgeoning, and therefore not much product know-how and process information are available to new entrants, small businesses, and startups. This necessitates the need for global platforms and organizations to disseminate timely and relevant technical information. Also, for the sake of key players, such platforms are needed to exchange ideas and market their products.

The NWTT sector is blessed to have associations such as the Nonwovens Engineers & Technologists (NET) Division of TAPPI, INDA, EDANA, IFAI, and the Materials Interest Group of AATCC. The NET division of TAPPI is the only professional home for individual professionals in the field of nonwovens, which makes it an extremely necessary group to advance the interest of the industry and more importantly, individual professionals working in the field. Due to the nature of the industry, which is heavily driven by new products and competitive pricing, free exchange of technical information is vital for individual professionals in this sector for both individual career growth and the advancement of the sector.

Groups like TAPPI provide necessary resources for professionals and industry in the growing field in many different ways. A noteworthy effort is the annual nonwovens conference hosted by the NET Division, the NETInc Innovative Nonwovens Conference, along with many technical webinars and regular committee gatherings offered throughout the year. These avenues provide opportunities to create professional friendships among people in the sector, which may come handy in terms of career moves and advancements.

Due to the nature of the industry, which is heavily driven by new products and competitive pricing, free exchange of technical information is vital for individual professionals in this sector for both individual career growth and the advancement of the sector. — SESHADRI RAMKUMAR

As the nonwovens and technical textiles sector is truly interdisciplinary, involving scientific disciplines such as chemistry and materials science, manufacturing technologies such as mechanical and chemical engineering, and management disciplines, the way to move forward is to provide interactions with allied disciplines like tissue and paper, nanotechnology, advanced manufacturing, functional finishes, etc. To provide such multidisciplinary avenues, TAPPI has in the past few years co-located NETInc with the largest gathering of the pulp and paper science industry, the PaperCon conference. This year's event was held in April in Minneapolis, which provided an opportunity for nonwo-

vens professionals to interact with tissue and paper scientists and also gather new information from leading players in fields like chemical manufacturers, machinery makers, and testing organizations.

Moving forward, interactions with groups dealing with chemical and functional finishes, nanotech industry, international professional organizations such as the UK-based Textile Institute, Brussels-based EURATEX, China Nonwovens Technical Association (CNTA), and Mumbai-based Textile Association (India), to name a few, will benefit nonwovens industry professionals through enhancing their contact base and exchanging technical information on a global scale.

As part of advancing the industry and creating more opportunities for industry professionals and businesses in the field of nonwovens and technical textiles, it is important to create international cooperation and knowledge transfer forums. **TJ**



GET CONNECTED WITH YOUR NWTT PEERS

Professionals in the field of nonwovens and technical textiles can find out more about TAPPI's NET Division at: http://www.tappi.org/Members/Divisions-Committees/NET/

Seshadri Ramkumar is a professor in the Nonwovens & Advanced Materials Laboratory at Texas Tech University in Lubbock, TX, as well as Chair of the TAPPI NET Division. Email him at s.ramkumar@ttu.edu. Dr. Ramkumar was the lead author of the runner up to the 2016 TAPPI Journal *Best Research Paper titled "Preparation and characterization of bioactive and breathable polyvinyl alcohol nanowebs using a combinational approach,"* TAPPI Journal *15(10): 655(2016).*

For information about publishing nonwovens research in TAPPI Journal*, please contact* TJ *Editorial Board Member Gaurav Pranami, gpranami@gmail.com, or submit your content at www.editorialmanager.com/tappi.*

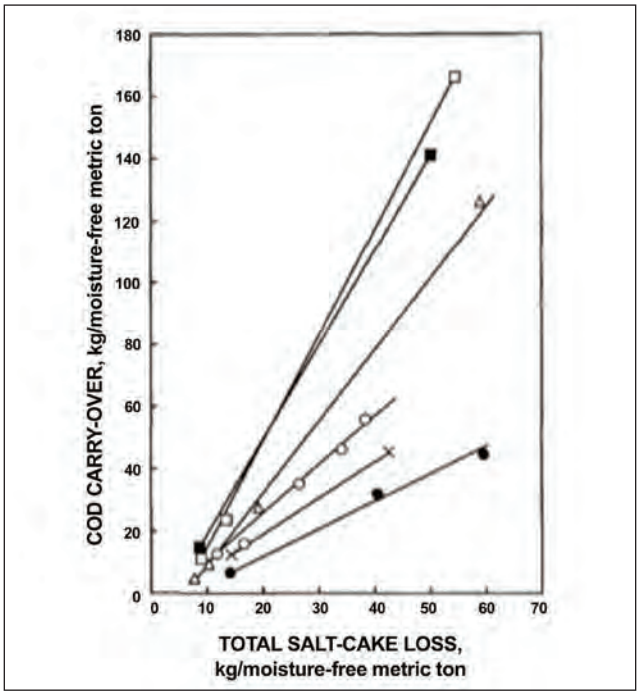
Determining wash loss levels in the brownstock pulp washing line using different methods

RIKU KOPRA AND OLLI DAHL

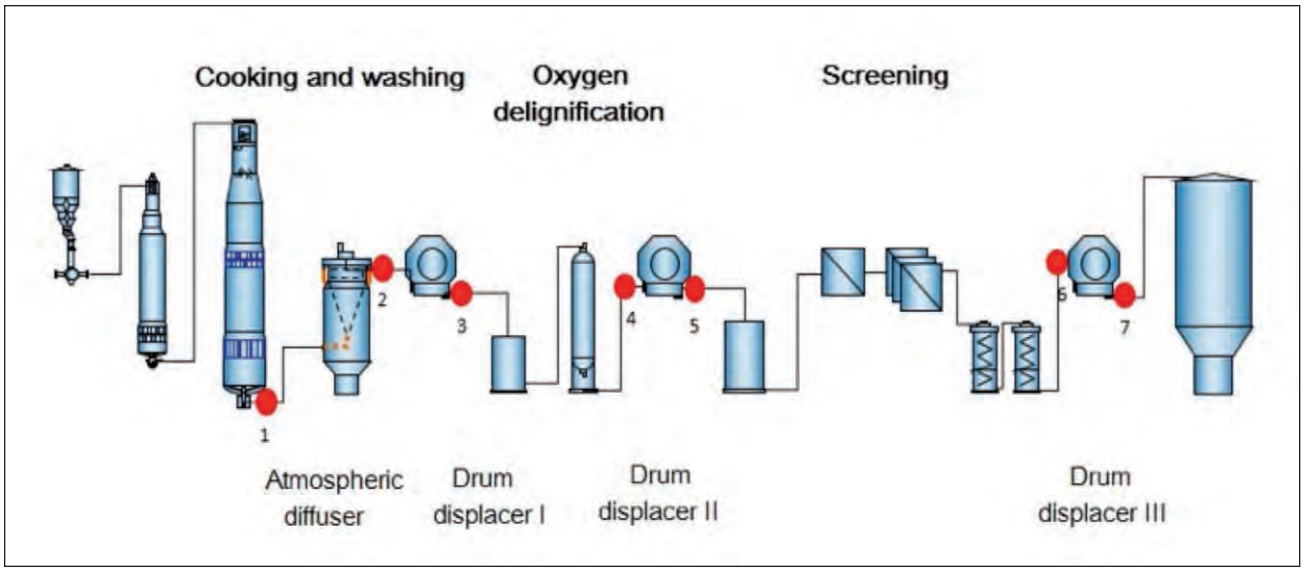
ABSTRACT: The purpose of brownstock pulp washing is to recover the maximum amount of dissolved inorganic and organic material using a minimal amount of water. Brownstock washing is a notable subprocess in chemical pulping because it has effects on the subsequent treatments of the pulp and is also the first step in the chemical recovery cycle. Without effective washing, the economic viability of chemical pulp production is affected. The performance of washing can be described in two main ways: using wash loss, which describes the amount of washable compounds in the pulp suspension that could have been removed in washing; or the dilution factor, which represents the net amount of water that is added during washing. The amount of sodium in the pulp suspension after washing has typically been used as an indicator of wash loss, usually expressed as kg sodium sulfate/ovendry ton of washed pulp. Other common measurement methods are conductivity, chemical oxygen demand (COD), total organic carbon (TOC), dissolved dry solids (DDS), and lignin concentration. Scandinavian pulp mill softwood and hardwood fiber lines were investigated using various measurement methods in the pulp phases to gain better understanding of wash loss. The concentration of DDS in the streams was measured using a refractometer and laboratory scale. The pH, conductivity, lignin content, TOC, and COD were measured to look for any correlations. Using different methods, the level differences remain constant, but it is difficult to control the washing process with sufficient precision using individual measurements. The measurement methods must also be continuous and reliable to be used to monitor and control washing.

Application: Proper measurement techniques can help mills detect a wash line's problem areas; predict wash efficiency in real-time; and control washers' operation, water usage, and chemical consumption, which have a direct impact on the economics of other processes.

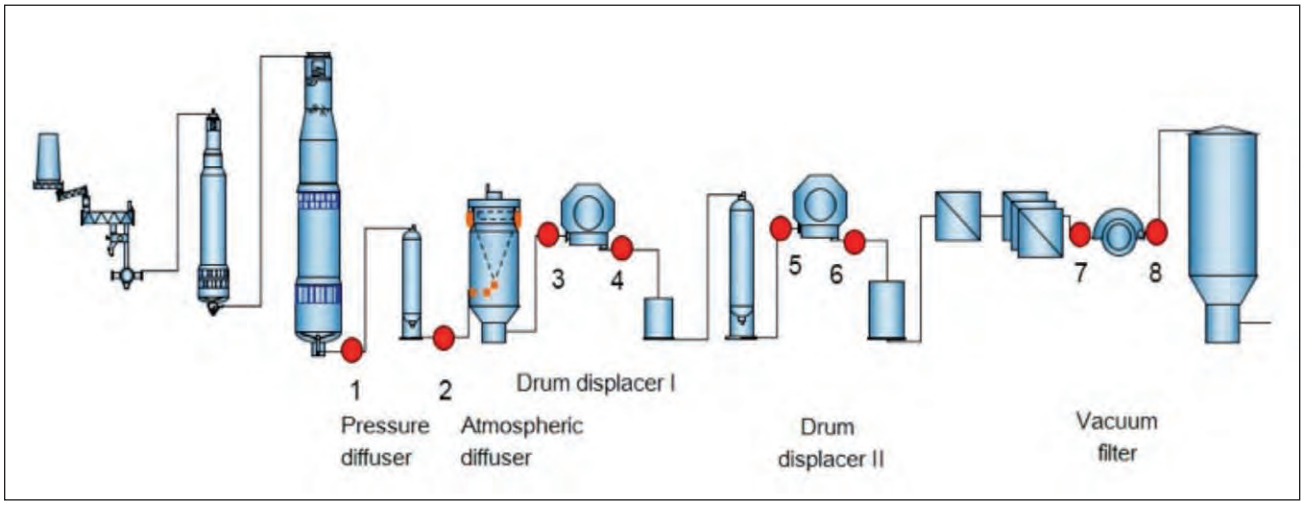
Wash loss (or carryover) is the amount of soluble (washable) inorganic and organic compounds that remain in the pulp suspension after washing. Wash loss can originate from the pulp itself (reaction products) or from the wash water used (e.g., condensates, recirculated washing filtrates). Traditionally, wash loss is measured on a laboratory scale as the amount of sodium that leaves the washer with the pulp. The method for evaluating wash loss in brownstock washing as the amount of sodium (SCAN-C 30:73 "Sodium content of wet pulp") was considered obsolete in 2003 and is no longer a standard method. Nowadays, wash losses are evaluated by measuring individual parameters such as chemical oxygen demand (COD), total organic carbon (TOC), sodium content, and conductivity [1]. Of these, COD has partly replaced sodium measurement as an indicator in both brownstock washing and bleaching as the most-used wash loss method; this is because the constituents of COD are totally dissolved in water [2]. In bleaching, COD is a better way to measure wash loss than amount of sodium because organic compounds causing wash loss may also have an effect on the consumption of bleaching chemicals [3]. The most important chemical compounds causing COD in filtrates are lignin, carbohydrates, methanol, low molecular weight organic acids, and extractives [4].



1. Correlation between chemical oxygen demand (COD) carryover and salt-cake loss for washed pulp from six kraft mills.



2. Hardwood pulp fiber line; 650,000 a.d. metric tons/year. Sample points: red circle indicates pulp sample.



3. Softwood pulp fiber line; 250,000 a.d. metric tons/year. Sample points: red circle indicates pulp sample.

Figure 1 presents the wash loss correlation between COD and salt-cake loss from six different kraft mills [3]. The ratio of salt-cake loss and COD wash loss can vary greatly from mill to mill. Variations of this magnitude complicate the estimations of bleaching chemical consumption on the basis of salt-cake wash loss, especially in a new mill or after major process or equipment changes. Dissolved sodium and dissolved organic material also behave differently in the wash line. Therefore, changes in a mill's operations, such as to the production ratio, dilution factor, and kappa number target, can affect the ratio between sodium and COD. Nowadays, the recommendation is to measure either all dissolved solids as a sum parameter, for example with a refractometer, or the organic and inorganic matter separately.

The traditional online method is to measure the filtrates' conductivity, which has an acceptable correlation with the amounts of sodium [5]. The recently generalized online method involves measuring dissolved dry solids (DDS) using a refractometer. From a practical standpoint, the evaluation of washing efficiency on the basis of dissolved solids is simple and repeatable and has been used widely by washer manufacturers and researchers for experiments on and troubleshooting of brownstock washing systems [6]. All methods have their advantages and disadvantages. For example, measuring the amount of sodium or conductivity does not take into consideration other substances retained in the pulp suspension, such as lignin and other organic compounds. In brownstock washing, disadvantages of using the COD method include the complexity of the test, which makes it less attractive for the continuous monitoring of operations, and the difficulty of repeating results accurately, especially at the low end of the range (less than 10 kg/ton COD) [7].

Studies [8-12] investigating the composition and certain components of wash loss have shown that several compounds cause organic load (COD) in the wash waters, but only some

of them are detrimental or harmful to the process. In oxygen delignification, kraft lignin and inorganic sulfur compounds (sodium thiosulfate and sodium hydrogen sulfide) could be mentioned as real wash loss compounds. Real wash loss compounds are certain chemical compounds that have an impact on the pulp quality responses (i.e., kappa number, brightness, and viscosity). Similarly, low molecular weight organic compounds such as methanol (which cause a high COD load) were harmless compounds in the washing and following bleaching stages. Thus, in the future, several of the measurements might have to be used. For example, DDS could be measured by refractometer and inorganic compounds by conductometer; regarding the remaining organic materials, possible dissolved lignin could also be measured separately. New measurements would increase costs, but a combination of measurements would open up new possibilities for more accurate monitoring and controlling of washing.

MATERIALS AND METHODS

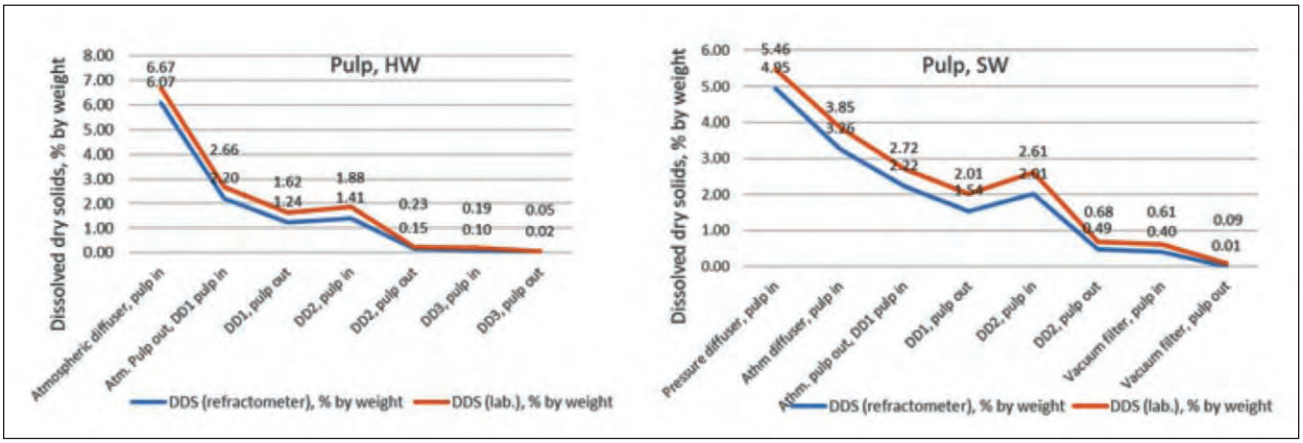
The research was carried out in the hardwood (HW) and softwood (SW) pulp brownstock washing lines at a Scandinavian kraft pulp mill. The HW pulp brownstock washing line consists of high-heat washing, an atmospheric diffuser, one DD-washer before 1-stage oxygen delignification, and two DD-washers after the oxygen stage. Production was about 2000 a.d. metric tons/day during research; kappa number targets were 17 after digester and 11 after oxygen delignification. The SW pulp brownstock washing line consists of high-heat washing, a pressure diffuser, an atmospheric diffuser, one DD-washer before 1-stage oxygen delignification, a second DD-washer after the oxygen stage and the last washer before bleaching is a vacuum filter. The SW pulp line production was 700 a.d. metric tons/day; kappa number targets were 32 after digester and 22 after oxygen delignification. Pulp samples were taken from the washer's inlet and outlet pulp. Three sample laps were taken from both lines. The fiber lines and sample points are shown in **Figs. 2** and **3**.

From the pulp lines, the filtrate sample was extruded from the pulp through wire gauze about 15 min after sampling. The pH, conductivity, and amount of DDS of all samples were determined using a refractometer on the spot. In the refractometer analysis, the temperature of the samples was controlled to 40°C using a thermostat. The DDS by laboratory standard, COD, TOC, and dissolved lignin of all samples were determined afterwards in the laboratory. The consistency and kappa number of the pulp samples were also determined afterwards. The COD and dissolved lignin were determined from the HW line samples 3 weeks after sampling and from the SW line samples 2 weeks after sampling. This could reduce the COD analysis results slightly according to the presence of volatile organic compounds and easily degradable organic material.

Analytical determinations

Analyses were made to define the chemical situation of the washing line. The samples were analyzed using the following methods:

- Determination of dry matter content (analytical) (ISO 638 "Paper, board and pulps—determination of dry matter content—oven-drying method")
- Determination of dry matter content (on site), refractometer
- Conductivity (on site), conductometer (Mettler Toledo; Columbus, OH, USA)
- COD liquor, COD liquor samples were filtrated using 1000 µm paper and then analyzed in a COD analyzer (ISO 15705 "Water quality determination of the chemical oxygen demand index [ST-COD] small-scale sealed-tube method")
- TOC, total organic carbon analyzer (Shimadzu Corp.; Kyoto, Japan) (ISO 8245:1999 "Water quality—guidelines for the determination of total organic carbon [TOC] and dissolved organic carbon [DOC]")
- Dissolved lignin, ultraviolet (UV) measurement at 280 nm, UV 2550 Spectrophotometer (Shimadzu Corp.) using an absorptivity value of 19.8 L/(g·cm)
- Pulps (ISO 302 "Determination of kappa number")



4. Hardwood (HW) and softwood (SW) pulp filtrate fractions of dissolved dry solids (DDS) measured by refractometer and standard methods in whole brownstock washing line.

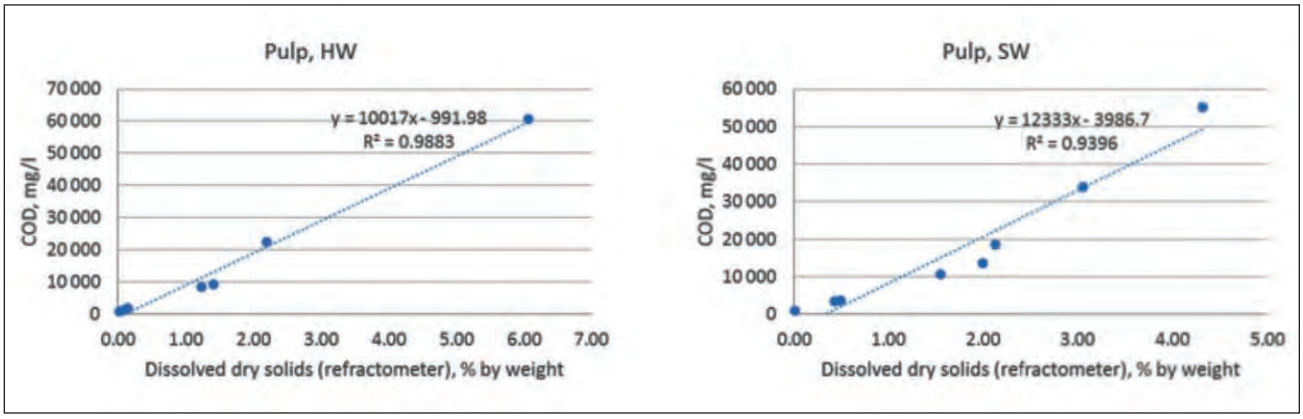
RESULTS AND DISCUSSION

Brownstock washing works well in both fiber lines. The washing loss to bleaching in the HW line was about 5 kg COD/a.d. metric tons of pulp and in the SW line about 6 kg COD/a.d. metric tons of pulp, both at the target level. However, the measurement results showed differences between the washing of different fractions. The results for both washing lines are presented in the following.

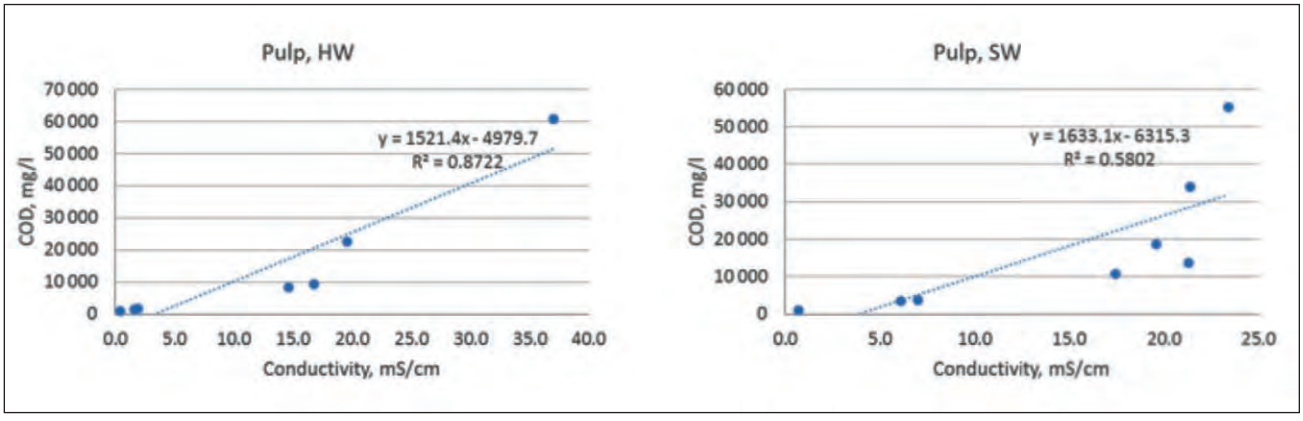
Figure 4 represents the level changes in the pulp suspensions' real-time DDS, measured by refractometer and laboratory standard. The refractometer results are regularly lower than the standard results. This is caused by the lack of field calibration of the refractometer. When using the refractometer, calibrations should be done for the wood species and the specific installation location, while considering the concentration of the solution. Oxygen delignification occurs between drum displacer 1 and 2, which explains the increase at sample point DD2, pulp in, in Fig. 4. Otherwise, the pulp logically becomes cleaner as it moves forward through the fiber line.

Figure 5 presents the relation between COD content and DDS content measured in real time by a refractometer for HW and SW pulp filtrates. **Figure 6** shows the correlation between COD and conductivity. **Figure 7** shows the correlation between COD and lignin content. **Figure 8** shows the correlation between COD and TOC. The results indicate that measurement of dissolved organics and inorganics by a refractometer has excellent correlation to COD (HW 0.9883 and SW 0.9396) because of the high portion of organic matter present in the filtrates. Conductivity's correlation with COD is satisfactory with HW (0.8722) and weak with SW (0.5802). The reason for the difference in wood species in this case is unknown. This phenomenon can perhaps be explained by the different proportions of potassium chloride or potassium hydroxide concentration in the measured solution, as the pH was equal in both cases. TOC has a naturally excellent correlation with COD (HW 0.9996 and SW 0.9998). Lignin, which caused significant organic load, also followed the COD value levels (HW 0.9947 and SW 0.9969). For the COD and dissolved lignin analysis, the samples must be diluted with plenty of water, which in turn can cause measurement errors and make real-time measurements difficult to implement. Components measured with COD or conductivity or dissolved solids wash away differently.

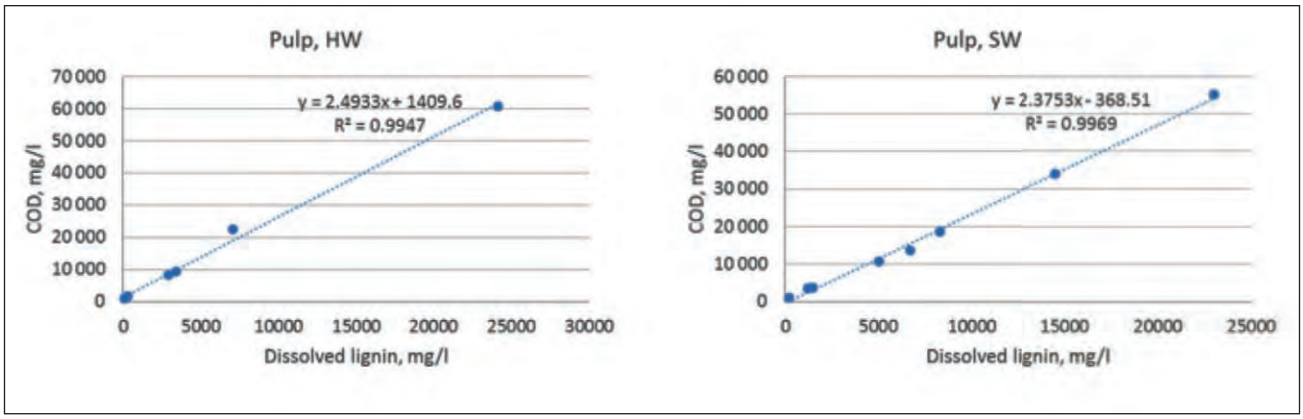
According to Shackford [6], it is important to measure dissolved organic wash loss because it has detrimental effects on viscosity, delignification efficiency, chemical consumption, and organochlorine formation in the bleach plant. Otherwise, measuring inorganic content using conductivity is important



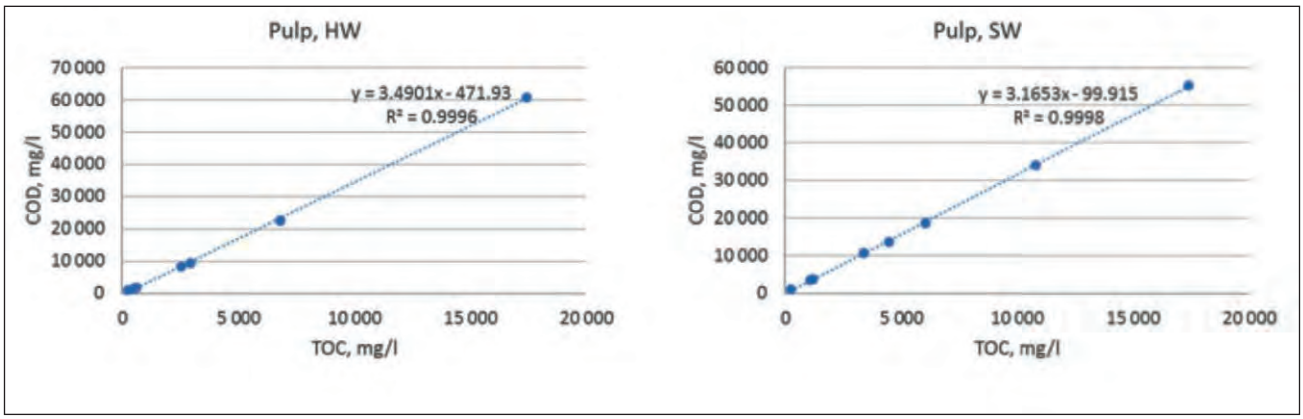
5. COD content of HW and SW pulp filtrate fractions analyzed in laboratory versus DDS measured by a refractometer.



6. COD content of HW and SW pulp filtrate fractions analyzed in laboratory versus conductivity.



7. COD content of HW and SW pulp filtrate fractions analyzed in laboratory versus dissolved lignin analyzed in laboratory.



8. COD content of HW and SW pulp filtrate fractions analyzed in laboratory versus total organic carbon (TOC) analyzed in laboratory.

because of the chemical recovery system. Targets for washing efficiency generally are based on conductivity because simple, robust sensors have not been available to monitor the wash loss of dissolved organics.

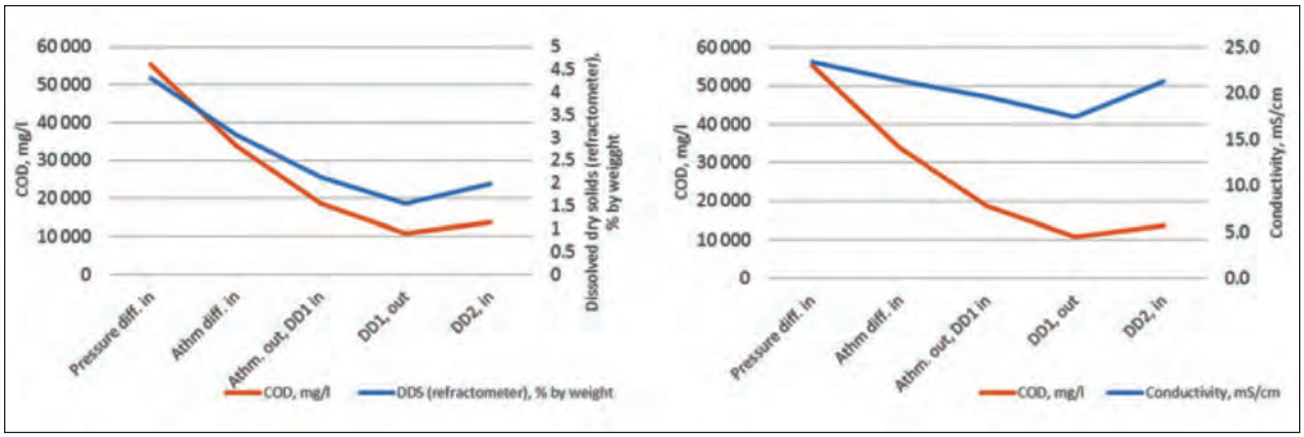
Nowadays, total dissolved solids (TDS) is of interest for several reasons, as concluded by Brown and Hart [5]. Most methods to evaluate the efficiency of brownstock washing use dissolved solids in their calculations. All washer material balance calculations must use dissolved solids mass, and it is a relatively easy test to run. Furthermore, knowing the dissolved solids losses at the washers can help account for changes in daily solids burned in the recovery boiler and even the steam used to evaporate the water associated with those solids. As discussed in the following, the results confirm that measurement of either organic or inorganic material does not give a holistic view of washing.

Figure 8 shows that COD and TOC values follow each other relatively, as they should. Carbon combustion consumes oxygen at the ratio of 2.667, so the COD/TOC ratio should be at this level. Experimentally, it has been stated that the ratio is usually between 2.6 and 3.2. Most of our measurement results were between 2.9 and 3.4. A partial explanation for the larger variation can be found from the TOC analyzed. The analysis also oxidizes some of the inorganic matter.

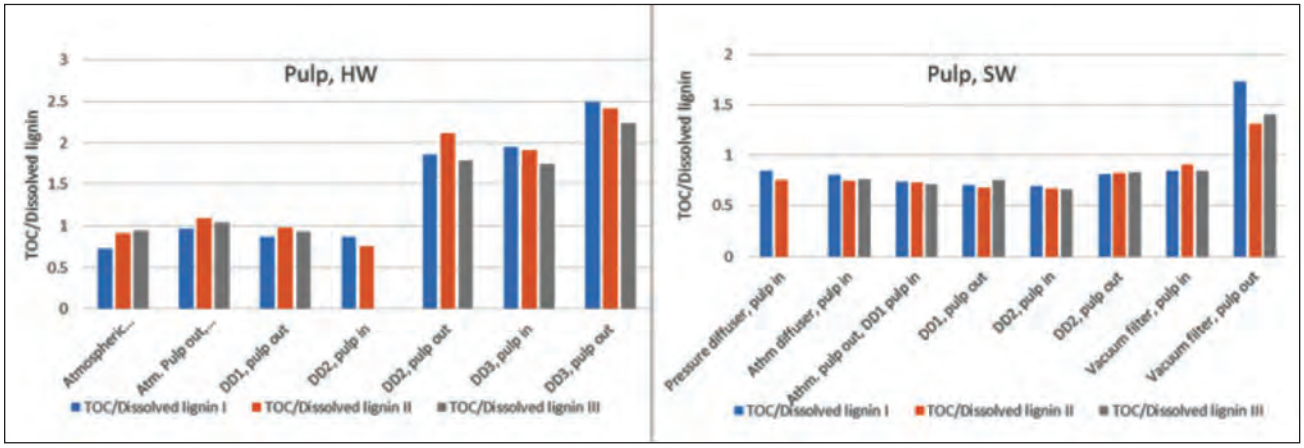
From the results, it can also be stated that organic materials (COD) wash away relatively faster than inorganic material (conductivity) at the beginning of the washing line. Relative efficiency can be a function of process variables, e.g. pH, and washer type, as well. Especially at the beginning of the SW line, inorganic material washes away inefficiently from the diffuser washers (**Fig. 9**).

The measurements were repeated three times and results were codirectional/repeatedly consistent, thus eliminating any measurement errors. Insufficient wash results arise from low feed consistency to the diffuser. It was not possible to completely understand a clear reason for the better washability of the organic matter. However, the organics were in a soluble form and in a higher proportion relative to the inorganics, whereas inorganic matter could be adsorbed in the surface of the fibers because of the charges. This being so, conductivity would not give representative wash result information and COD would also give good wash results and be influenced by the nonwashable components. Measurement by a refractometer shows the TDS content of washable compounds in the filtrate, which describes washing success relatively well.

Figure 10 represents the TOC values per dissolved lignin from every three sample laps. The closer the ratio is to 0.7, the



9. COD content of SW pulp filtrate fraction compared with DDS measured with a refractometer and conductivity at the beginning of the line.



10. HW and SW pulp filtrate fractions of laboratory-analyzed TOC per laboratory-analyzed dissolved lignin.

more lignin represents a significant part of the organic carbon. Regarding the results, a clear change of ratio occurs after oxygen delignification, especially in HW. This is probably because the oxygen stage removes more hemicellulose (sugars) than lignin when using HW, whereas with SW, the ratio of hemicellulose and lignin is more even. Furthermore, with SW, magnesium sulfate is used to limit the loss of hemicellulose.

The results present the one precise occasion and give the direction of the performance of the washing. However, the choice of sampling time has a major impact on the values obtained. In addition, the dilution of the samples and the measurement errors caused errors in the results. Reliable monitoring of the washers' effectiveness required real-time measurements.

CONCLUSIONS

The results indicated that when using different methods for measuring wash loss, the level differences remain quite constant. The results also showed clear differences between, for example, how organic and inorganic materials are washed away and how the oxygen stage affects soluble materials. The wash results for the HW and SW lines also differed from each other at the pulp mill. Using a range of measurements would allow more information on the washing status to be obtained. Conductivity alone does not give an accurate account of the washing lines, and COD cannot be measured in real time; therefore, TDS could be one potential way to measure the performance of brownstock washing. In the future, different types of measurement might be combined and used more frequently for adjustment purposes. It is difficult to properly control the washing process using individual measurement. The measurement methods must also be continuous and reliable to be used to monitor and control the washing.

These types of study on the basis of a hand-picked samples will necessarily include both sampling and analysis errors. Furthermore, the results represent a temporary status when the process itself might have momentarily deviated significantly from the mean value. **TJ**

ACKNOWLEDGMENTS

This study was initiated under a contract between the Mikkeli University of Applied Sciences, Aalto University School of Chemical Technology, Department of Forest Products Technology, K-Patents Oy, and Stora Enso Oyj. This work was financed partially by the South Savo Center for Economic Development,

Transport and the Environment (ELY Center). The authors thank Liz Dexter for revising the English of the manuscript and Anu Pihlajaniemi and Sakari Toivakainen (Toihan Ltd.) for help with the analysis. The authors are grateful to all participants.

LITERATURE CITED

1. Lunn, R., *Pulp Pap. Can.* 102(3): 46(2001).
2. Shackford, L.D., *Bleach Plant Operations Short Course*, TAPPI Press, Atlanta, GA, USA, 1992, p. 147.
3. Strömberg, B., *Tappi J.* 74(10): 113(1991).
4. Herstad-Svärd, S., Basta, J., Jour, P., et al., *Papel* 59(3): 52(1998).
5. Brown, M. and Hart, P., *TAPPI J.* 16(2): 65(2017).
6. Shackford, L.D., "Unraveling the mystery of washing efficiency determination," *TAPPI Pulping Conf.*, TAPPI Press, Atlanta, 1997.
7. Bottan, G., *Pulp Pap. Int.* 35(3): 51(1993).
8. Viirimaa, M., Dahl, O., Niinimäki, J., et al., *Appita J.* 55(6): 484(2002).
9. Sillanpää, M., Sankari, M., Dahl, O., et al., *TAPPI J.* 2(9): 18(2003).
10. Sillanpää, M., Sankari, M., Dahl, O., et al., *Appita J.* 56(5): 397(2003).
11. Sankari, M., Ala-Kaila, K., Dahl, O., et al., *Nord. Pulp Pap. Res. J.* 19(2): 264(2004).
12. Sankari, M., Sillanpää, M., Ala-Kaila, K., et al., *Pulp Pap. Can.* 105(5): 36(2004).

ABOUT THE AUTHORS

Without efficient brownstock washing, kraft pulp production is not economically viable. Because effective brownstock washing requires reliable and real-time monitoring and controlling equipment, we compared several types of available measurements. We have studied brownstock washing for a number of years, published articles in several journals, and presented our findings at conferences. However, this study has helped us to understand the benefits and advantages of different measurement techniques. In particular, each measurement technique detects very different components in the washable matter and provides different information on washing performance.

The most difficult aspect of this study was to find the causes for certain behaviors of different measurements. For example, we noticed that one of the measurement techniques gave deviant results when comparing hardwood and softwood lines. Drawing conclusions required research and understanding of process chemistry. The results indicate that inorganic and organic matter can be washed out with different methods. Thus, a single measurement, be it focusing on the inorganic or organic, can reflect a very diverse image of washing success.

Mills can benefit from the comparison of several different types of available measurements or tests to predict brownstock washing performance. In addition, the data were comprehensively collected and tested, bringing distinct value to the readers. For the next step, we will focus on the performance of oxygen delignification by using total dissolved solids measurements and on how dissolved solids behave when process conditions change.



Kopra



Dahl

Kopra is RDI scientist at the Fiber Laboratory, South-Eastern Finland University of Applied Sciences, Savonlinna, Finland. Dahl is a professor at Aalto University School of Chemical Engineering, Department of Bioproducts and Biosystems, Clean Technologies Research Group, Espoo, Finland. Email Kopra at Riku.kopra@xamk.fi.

Generalized steady-state model for chlorine dioxide brightening of hardwood kraft pulps

BRIAN N. BROGDON

ABSTRACT: A generalized, steady-state model for the first chlorine dioxide brightening (D_1) stage is proposed for North American hardwood kraft pulps. The model predicts the post-D_1 brightness obtained for a given chlorine dioxide (ClO_2) charge based on three equation parameters. Data from laboratory D_1 studies were examined with the model to determine the relationships of the parameters to extracted pulp properties. The asymptotic D_1 brightness limit at extremely high bleach charges was ~93% ISO for most hardwood pulps. This parameter can be calculated from the limiting light absorption coefficient of D_1 kinetic studies (≈ 0.10 m^2/kg) and the unbeaten light scattering coefficient of the pulp. A second parameter was linearly correlated to the extracted kappa number of the hardwood pulp. This relationship seems to be affected by the chosen kraft pulping process (e.g., liquor or dissolved solids profiling). The final parameter is the extracted pulp brightness. The hardwood D_1 model forecasted the brightness values of laboratory pulps that differ from measured values of ±0.5 to ±0.6 points. Daily averages of bleach plant data for a southeastern U.S. hardwood fiber line were examined with the model. Predictions were generally 0.5 points higher than the measured mill brightness values. This observation implied that the D_0(EOP) pulp contained a small amount of extraction washer carryover (~0.4 kappa units on pulp) that was consuming ~1.2 kg ClO_2/ton pulp, which was not accounted for in the hardwood D_1 model.

Application: These models are simple and can be easily programmed into computer spreadsheets, which can be used to calculate optimum bleach set points and to minimize manufacturing costs.

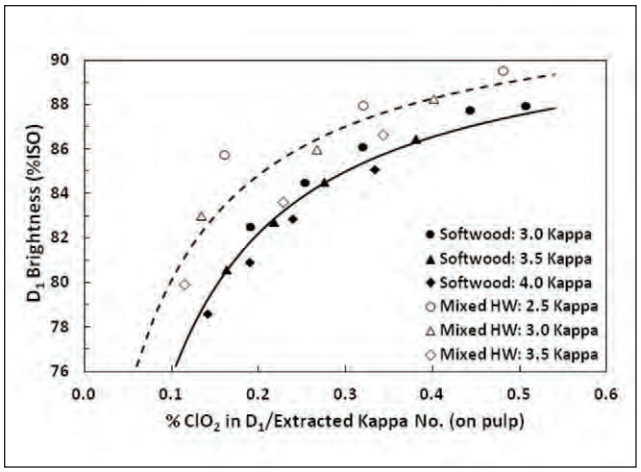
In North America, elemental chlorine-free (ECF) bleaching is the dominant process used to delignify and brighten brownstocks and oxygen-delignified pulps. Chlorine dioxide delignification (D_0) and brightening (D_1 and D_2) stages are major components in these bleach sequences [1]. It is important to balance the amount of chlorine dioxide used in these stages with the kappa number of the softwood or hardwood pulp entering the bleach plant [2-10]. Unbalanced proportioning of chlorine dioxide for delignification and brightening can lead to higher bleach usage and cost.

Multistage ECF sequence models [3-16] can be used to help estimate the optimum proportioning of chlorine dioxide among the various stages based on the kappa number and washer carryover entering the bleach plant, as well as other constraints. Previous works [11-15] have proposed generalized expressions for bleaching stages of softwood kraft pulps. These steady-state models can predict bleach consumption, extracted kappa numbers, and final brightness values based on inputs and constraints, such as brownstock kappa number, washer stage carryover, extraction stage conditions, and entering and exiting pulp brightness. Similar expressions for chlorine dioxide delignification have been proposed for hardwood pulps [16]. Nonetheless, generalized models for chlorine dioxide brightening stages for hardwoods are lacking. Thus, one objective of this study was to extend a softwood model for a chlorine dioxide brightening (D_1) stage [13,15] to apply to hardwood pulps. A second objective was to test the veracity of the hardwood model by examining actual bleach plant data.

BACKGROUND

Most laboratory studies have focused on bleaching softwood kraft pulps. It was assumed that the findings and conclusions obtained from these investigations would be equally applicable to hardwoods. In some cases, however, the extrapolation of these results can yield incorrect conclusions. Hardwoods have noteworthy differences. Among the softwood species as a group, the tracheids tend to be somewhat similar in their morphological characteristics [17,18], such as fiber length, width, and wall thickness. In contrast, the various hardwood species have greater heterogeneity regarding these characteristics and fiber types (e.g., fibers, parenchyma cells, and vessel elements) [17,18]. Hardwood brownstocks entering the bleach plant typically contain lower lignin and higher hexenuronic acid (HexA) levels than do their softwood counterparts.

These factors result in different delignification and brightening responses for the two types of pulps. For example, using aggressive (EO) or (EOP) stages increases the delignification of D_0 softwoods, whereas applying the same approach to D_0



1. D_1 brightness versus D_1 multiple (% ClO_2/extracted kappa number) plot for softwood (solid symbols) and mixed hardwood (open symbols) pulps. Solid and dotted lines denote the normalized brightening responses of softwood and hardwood pulps, respectively, for the range of extracted kappa numbers. D_1 data are from the $D_0(EO)D_1$ bleaching of softwood pulp [21] and $D_0(EOP)D_1$ bleaching of mixed hardwood pulp [22,23].

hardwoods affords marginal to negligible benefits [7,9,19,20]. Generally, for softwoods, plotting D_1 brightening versus D_1 multiple yields a normalized brightening response for a range of extracted kappa numbers (**Fig. 1**). Similar plots for mixed hardwood pulps, on the other hand, often do not exhibit a well-defined brightening response. This phenomenon might be related to the post-extracted brightness values of hardwood pulps, which are typically higher than softwoods [3-5,7,9,12,19-25]. This phenomenon also might be related to the higher levels of hexenuronic acids in post-extracted hardwood pulps [9,10,19,20].

Most laboratory D_1 studies of hardwoods [3-5,24-31] have examined single species pulps, such as sugar maple (*Acer saccharum*), red oak (*Quercus falcate/Q. rubra*), sweetgum (*Liquidambar styraciflua*), birch (*Betula papyrifera*), and eucalypt (*Eucalyptus globulus*). Reeve and Weishar [26] reported that brownstock and oxygen-delignified pulps made from either sugar maple or sweetgum required less bleach in the D_1 stage to bleach to 86% ISO than did red oak pulps. McDonough and co-workers [3-5,30,31] performed several D_1 bleach studies with oak kraft pulps. These authors examined pulps produced using different pulping conditions and quantified their D_1 bleachability by using steady-state models. Rawat and McDonough [24,25] used similar techniques to characterize the D_1 bleachability of birch and maple kraft pulps produced by various pulping conditions. Germgård and co-workers [27,28] reported that hardwood kraft pulps (e.g., birch and eucalypt) at a given E_1 kappa number required more bleach in the $D_1E_2D_2$ sequence than did softwoods to reach 90% ISO [26]. Ragnar [20] observed similar results for the D_1 bleaching of mixed hardwood and softwood pulps. Barroca and Castro [29] developed a dynamic model to describe the D_1 stage bleaching of eucalypt kraft pulps.

Several D_1 investigations have been conducted using mixed hardwood pulps. Parthasarathy et al. [22,23] examined the D_1 bleaching of a mixed hardwood pulp produced at a kraft mill. The pulp was predominantly composed of North American oaks and hickories. These investigators developed a statistical response surface model that related how D_1 brightness was influenced by D_0 kappa factor charge, D_0 consistency, (EOP) temperature, and D_1 bleach charge. Hart and Connell [32] examined how D_1 stage brightening was affected by stage pH for mixed hardwood kraft pulps produced at various North American mills. Brogdon used statistical response surface models [9], which were developed from various ECF bleaching datasets [4,5,22,23,26], to study how various process variables influenced bleach sequence optimization for hardwood kraft pulps.

Previous D_1 models are able to predict the amount of chlorine dioxide needed to reach a targeted D_1 brightness for hardwood kraft pulps [3-5,9,22-25,30,31]. Nevertheless, these steady-state expressions have limitations. The statistical response-surface models do not explicitly express how kappa numbers and brightness values of extracted pulps affect D_1 brightness for applied bleach charges. The steady-state D_1 models of McDonough et al. [3-5] are based on kraft pulps made from a single hardwood species. The mathematical expressions could be used to model other hardwood pulps made from other species or species mixes. However, additional bleaching experiments are required to determine and tune the model parameters for each hardwood kraft pulp. An alternative approach would be to develop a more generalized steady-state model for the D_1 stage where the tunable parameters can be determined by measured properties of the post-extracted hardwood pulp. Such an approach was undertaken in this study.

DATA ANALYSIS

Brightness versus bleach consumption data were obtained from various D_1 laboratory studies for single and mixed hardwood species [3,4,22,23-26,30,31,33-35]. In these investigations, the kraft or oxygen delignified pulps were treated with a D_0 stage, which was followed by an (EO), (EOP), or (EP) alkaline extraction stage. Individual data sets were fitted to D_1 model and regressions were analyzed using the curve-fitting program CurveExpert Professional (Daniel G. Hyams, version 2.5.1; Madison, AL, USA). The software calculated the values of the equation parameters of the models and the corresponding 95% confidence intervals (CIs). Regressions made to models containing three and two tunable parameters were statistically compared with one another using the *F*-test, where the F_0 ratios and critical *F*-values were calculated by the software program.

After a generalized D_1 model was finalized, a second curve-fitting analysis was conducted on the data sets collectively. These computations were performed in a spreadsheet program (Microsoft Office Excel 2007; Microsoft, Redmond, WA, USA), which used the software's Solver routine. Simulta-

neous regressions minimized the sum of squares errors (SSE) of the model when fitted to the data sets, while simultaneously regressing one of the model's parameters to the post-extracted kappa number of the pulp. The calculated 95% SSE limits were calculated from the SSE of the pooled datasets and the *F*-test. The elliptical 95% CI bounds for the slope and y-intercept values of the linear regression were determined from 95% SSE limits.

RESULTS

Chlorine dioxide brightening stage model for hardwoods

A generalized D_1 model for softwoods [13,15] has been successful at forecasting the chlorine dioxide needed to reach a desired brightness and vice versa for extracted pulps with a range of extracted kappa and brightness values. The model is a modification of an earlier steady-state expression that McDonough et al. [4,5] used to numerically quantify the bleachability of oak kraft pulps. The revised model is denoted as follows:

$$y_1 = c_{01} - \frac{\beta_{11}}{x_1 + \beta_{21}} \quad (1)$$

where x_1 is the chlorine dioxide consumed in D_1 (as % ClO_2 on pulp), y_1 is the post-D_1 brightness (% ISO), c_{01} is the asymptotic D_1 brightness limit, and β_{11} and β_{21} are fitted equation parameters. The β_{21} parameter is a function of post-extracted brightness (B_E), c_{01}, and β_{11}:

$$\beta_{21} = \frac{\beta_{11}}{c_{01} - B_E} \quad (2)$$

For softwood kraft pulps, the β_{11} parameter is a linear function of the extracted kappa number ($Kappa_E$) of the pulp entering the D_1 stage [13]. Eq. (1) and Eq. (2) can be combined into a single expression:

$$y_1 = c_{01} - \frac{\beta_{11}}{x_1 + \frac{\beta_{11}}{c_{01} - B_E}} \quad (3)$$

whereby D_1 data sets can be fitted by nonlinear regression to determine B_E, c_{01}, and β_{11} simultaneously. An important distinction of the modified model to the earlier model of McDonough et al. [4,5] is that Eq. (1) uses the chlorine dioxide consumed in D_1 (x_1) rather than the chlorine dioxide multiple (i.e., % ClO_2 applied in D_1/extracted kappa no.). As shown in Fig. 1 for a mixed species hardwood pulps, plots of D_1 brightening versus

Pulp	Pulp Kappa No.	Bleaching Delignification*	Extracted		Model D_1 Asymptotic Brightness, c_{01}	SE of c_{01}	95% CI of c_{01}
			Kappa No.	Brightness			
Oak [30] – modified kraft cook w/ black liquor	15.5	D_0(EO); 0.20 KF	2.7	56.9% ISO	91.1% ISO	±1.2% ISO	±14% ISO
Oak [30] – modified kraft cook (low solids/alkali profiled)	15.0	D_0(EO); 0.20 KF	2.4	64.9% ISO	92.6% ISO	±0.9% ISO	±11% ISO
Red oak [4] – high effective alkali batch kraft cook	14.0	D_0(EO); 0.20 KF	4.4	71.2% ISO	90.5% ISO	±1.4% ISO	±18% ISO
Red oak [4] – low effective alkali batch kraft cook	14.0	D_0(EO); 0.20 KF	3.6	68.8% ISO	90.7% ISO	±1.9% ISO	±24% ISO
Sweetgum [26] – batch kraft cook	12.1	OD_0(EO); 0.16 KF	4.7	71.2% ISO	90.7% ISO	±0.3% ISO	±3.8% ISO
Maple – high effective alkali batch kraft cook [24]	20.3	D_0(EO); 0.20 KF	2.8	74.9% ISO	94.6% ISO	±0.3% ISO	±3.4% ISO
Maple – intermediate effective alkali batch kraft cook [25]	15.0	D_0(EO); 0.20 KF	4.0	74.3% ISO	92.6% ISO	±1.2% ISO	±16% ISO
Southeastern U.S. mixed hardwood kraft pulp [35]	12.4	D_0(EP); 0.22 KF	4.4	64.0% ISO	93.6% ISO	±0.8% ISO	±9.6% ISO
Northeastern U.S. mixed hardwood kraft pulp [34]	12.0	OD_0(EOP); 0.21 KF	3.3	71.2% ISO	92.2 % ISO	±0.4% ISO	±1.1% ISO
Midwestern U.S. mixed hardwood kraft pulp [22,23]	15.0	D_0(EOP); 0.26 KF	2.8	65.9% ISO	91.8% ISO	±1.3% ISO	±17% ISO
* Sequence and kappa factor (KF).							

I. Calculated D_1 asymptotic brightness values, c_{01}, of Eq. (3) from the nonlinear regression of various laboratory bleaching data sets [4,22-25,34,35] with Eq. (3) with the standard errors (SE) and 95% confidence intervals (CIs) of c_{01}. In all cases, the coefficient of determination (r^2) values for the regressions were greater than 0.994.

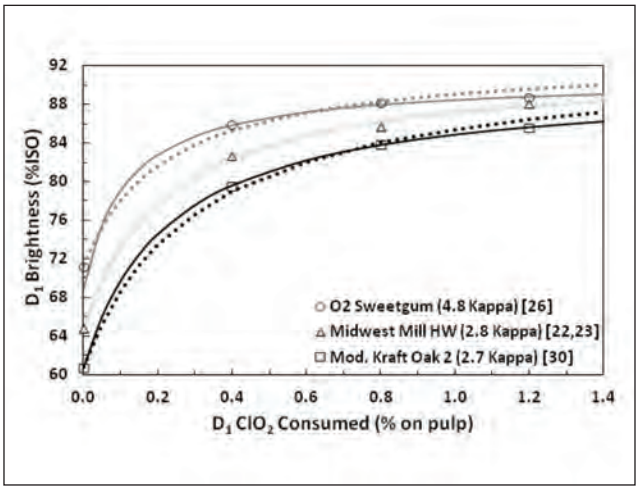
Pulp	Unbeaten Light-Scattering Coefficient, *s*	Estimated Asymptotic Brightness, c_{01}
Southern U.S. oaks	29 to 33 m²/kg	92.0% to 92.5% ISO
Sweetgum	32 to 37 m²/kg	92.4% to 92.9% ISO
Maple	45 to 53 m²/kg	93.6% to 94.0% ISO
Aspen	~41 m²/kg	~93.3% ISO
Birch	36 to 38 m²/kg	92.8% to 93.0% ISO
Southeastern U.S. mixed hardwood	38 to 42 m²/kg	93.0% to 93.3% ISO
Northeastern U.S. mixed hardwood	38 to 45 m²/kg	93.0% to 93.6% ISO
Midwestern U.S. mixed hardwood	36 to 39 m²/kg	92.8% to 93.1% ISO

II. Calculated D_1 asymptotic brightness values, c_{01}, for various single and mixed species hardwoods using Kubelka-Munk remission function with the limiting light absorption coefficient (k_∞) value of 0.10 m²/kg [29,36] and the appropriate unbeaten light scattering coefficient (s) value [38-42].

the chlorine dioxide multiple do not always afford a normalized response curve that is well defined.

Hardwood data from various investigations were analyzed [3,4,22-26,30,31,33-35]. These studies explored a range of bleach charges in the D_1 for pulps made from either single hardwood species or mixed hardwoods. These data sets were curve-fitted to Eq. (3) to evaluate the D_1 asymptotic brightness limit (c_{01}). The curve-fitted c_{01} values were scattered, ranging from 91% to 95% ISO. However, the c_{01} values for single species and mixed hardwood pulps in **Table I** are not statistically different from one another, based on their calculated 95% CIs. In most cases, the curve-fitted c_{01} values are indistinguishable from one another when their standard errors are considered. Similar results have been observed in the corresponding D_1 modeling study for softwood pulps [13].

An alternative approach was undertaken to obtain estimates of c_{01} based on the optical properties of the pulps. Kinetic D_1 studies for softwoods [36] and eucalypts [29] have shown an asymptotic light absorption coefficient (k_∞) at 457 nm to be ~0.10 m²/kg. This k_∞ value likely represents the light absorption coefficient (k) of the cellulose and hemicelluloses in the nearly lignin-free pulps, which has been noted by Middleton and Scallan [37]. A c_{01} value can be estimated from this k_∞ if the light-scattering coefficient (s) of the unbeaten pulp is known. Light-scattering coefficients for most unbeaten softwood pulps range from 26 m²/kg to 33 m²/kg, whereas the s values of unbeaten North American hardwood pulps range from 30 m²/kg to 53 m²/kg [38-42]. For softwoods, a c_{01} value of ~92% ISO can be calculated using the Kubelka-Munk remission function [13]. The c_{01} values of single and mixed hardwood species pulps have been determined similarly (**Table II**). The c_{01} value for oak, ~92% ISO, was similar to that of softwoods, whereas the values for maple, sweetgum, and various mixed hardwoods were ~94%, ~93%, and ~93% ISO, respectively. In the 1960s, Rapson [43] showed that mixed hardwood kraft pulps, when bleached with multiple chlorine dioxide stages, had an upper brightness limit that was 1 to 2 points higher than softwood kraft pulps. Rapson's observations seem consistent with the c_{01} values calculated from k_∞ and s.

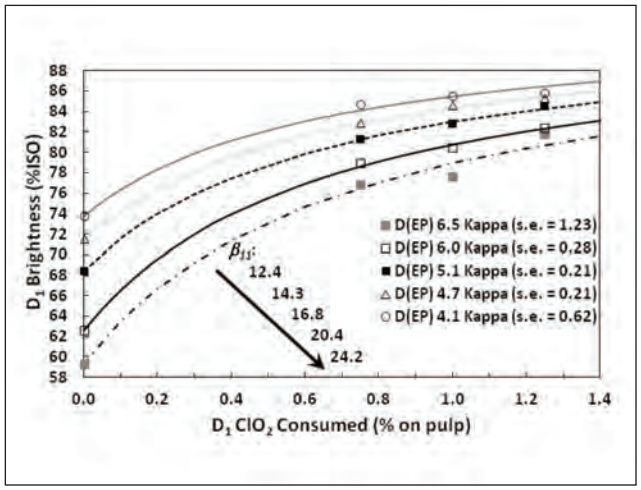


2. Nonlinear regression with selected D_1 data sets [22,23,26,30] of Table I to Eq. (3). Solid lines denote regression analysis to determine the values of c_{01}, B_E, and β_{11} simultaneously (Model 1). Dotted lines denote nonlinear regression analysis to determine the values of B_E and β_{11} only (Model 2); c_{01} set constant to 93% ISO for $OD_0(EO)$ sweetgum and $D_0(EOP)$ mixed hardwood pulps, and to 92% ISO for $D_0(EO)$ oak (Table II).

Figure 2 plots Eq. (3) where the c_{01} was determined by nonlinear regression (Model 1) and by Kubelka-Munk (Model 2). Visually, both models fit the D_1 data well over the dosage range of 0.4% to 1.2% ClO_2, regardless of how c_{01} was determined. The two models were compared with one an-

Pulp	Computed F_0 Ratio	*p*-value	Critical *F* value	Critical *p*-value	Accepted Model
Oak [30] – modified kraft cook w/ black liquor	0.516	0.603	161.448	0.05	Model 2
Red oak [4] – high effective alkali batch kraft cook	0.991	0.501	161.448	0.05	Model 2
Sweetgum [26] – batch kraft cook	48.304	0.0910	161.448	0.05	Model 2
Maple [24] – high effective alkali batch kraft cook	5.447	0.257	161.448	0.05	Model 2
Southeastern U.S. mixed hardwood kraft pulp [35]	0.547	0.594	161.448	0.05	Model 2
Northeastern U.S. mixed hardwood kraft pulp [34]	4.282	0.107	7.709	0.05	Model 2
Midwestern U.S. mixed hardwood kraft pulp [22,23]	16.929	0.152	161.448	0.05	Model 2

III. Statistical comparisons of Model 2, where c_{01} is calculated from the Kubelka-Munk remission function, versus Model 1, where c_{01} is determined from nonlinear regression. Examples are presented for several of the data sets from Table I. Inferences are based on a 95% confidence level (i.e., p-value ≤ 0.05) that Model 2 is an adequate representation of a generalized D_1 brightening model for hardwood kraft pulps.



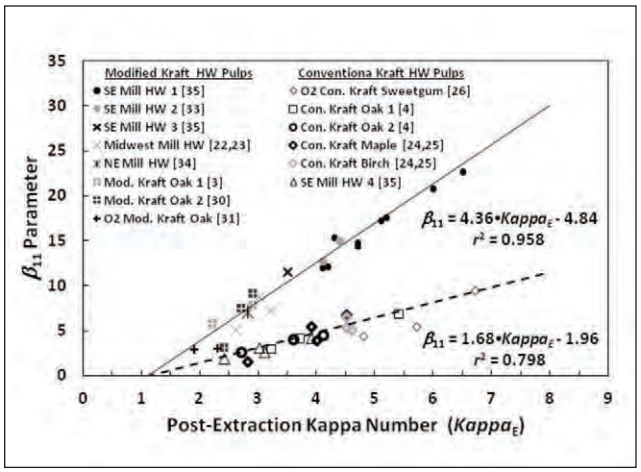
3. Predicted brightness values from Eq. (3) (various lines) compared with experimental D_1 data (symbols) for a southeastern U.S. mixed hardwood pulp [35]. Model's standard error usually ranged from 0.2% to 0.6% ISO units and r^2 ranged from 0.990 to 0.999. Hardwood kraft brownstock (12.4 kappa) was delignified by the D_0(EP) sequence.

other using the analysis of variance from the nonlinear regression provided by the curve-fitting software program. The null hypothesis (H_0) was defined as c_{01} being equal to the Kubelka-Munk calculated value (i.e., Model 2), whereas the alternative hypothesis (H_1) was defined as c_{01} is not equal to the Kubelka-Munk value (i.e., Model 1). **Table III** shows the summarized results. The null hypothesis could not be rejected at the 95% confidence level. Thus, Eq. (3) could be simplified to two tunable equation parameters, namely β_{11} and B_E, whereas the c_{01} value can be determined from the pulp's *s* and k_∞ values, provided that reasonable estimates are known for these intrinsic pulp properties.

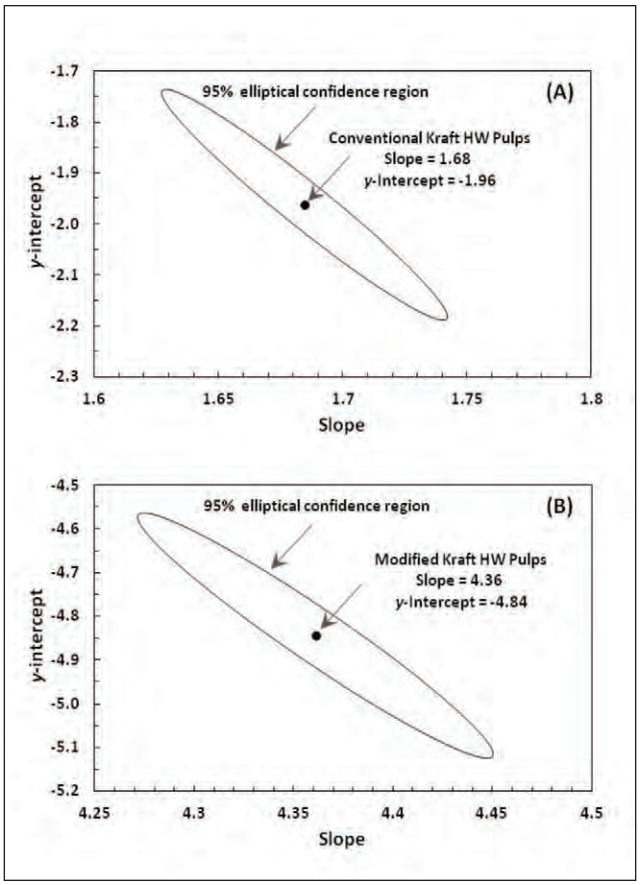
Relationships of D_1 model parameters to extracted kappa number

Figure 3 shows the fitting of the model to the D_1 bleaching data for a mixed hardwood kraft pulp from a southeastern U.S. mill [35]. This 12.4 kappa brownstock was delignified by the D_0(EP) sequence using various D_0 kappa factors (0.15 to 0.30) and peroxide levels in the (EP)-stage (0.2% to 0.8%). Curve fittings to the model were performed with c_{01} set to 93% ISO, which was based on the pulp's unbeaten *s* value of 38 m²/kg. The model represents the D_1 brightening data well, with an $r^2 \geq 0.990$. The curve fits for this mixed hardwood kraft pulp have standard error values that generally range from 0.2% to 0.6% ISO units. The β_{11} values seem to vary in accordance with the extracted kappa of the D_0(EP) pulp.

Data from the other D_1 studies were curve-fitted to the model where the c_{01} values were calculated and the B_E values were set to the measured values. These studies investigated kraft pulps that were produced either in the laboratory or at the mill and were treated with D_0 and D_1 stages that used multiple bleach charges. The rationale was to determine if there was a correlation between the pulp's β_{11} parameter and its extracted kappa number, which has been observed for softwood kraft pulps [13]. The curve-fitted β_{11} values decreased linearly as the extracted kappa ($Kappa_E$) of the hardwood pulp decreased (**Fig. 4**). Two different linear trends were observed. Pulps produced where the digesters used alkali profiling, dissolved solids profiling, or black liquor impregnation showed a linear correlation with a larger slope value, as well as a high r^2. The other linear relationship, which exhibited a lower slope and r^2, had digesters that used conventional kraft or older modified kraft pulping technology (i.e., pre-1990s). Both trends had a common *x*-intercept that approached an extracted kappa of 1.1 to 1.2. The slopes and *y*-intercepts that related the β_{11} values to extracted kappa numbers for the two groups were statistically different from one another (**Fig. 5**).



4. Relationship of the β_{11} parameter of Eq. (3) to the post-extraction kappa number (Kappa$_E$) for various hardwood kraft pulps [3,4,22-26,30,31,33-35]. The β_{11} values were determined by nonlinear regression of the model to the D_1 brightening data with c_{01} values calculated by the Kubelka-Munk remission function. β_{11} values typically had standard errors of ±0.8.



5. Slope and y-intercepts values from the linear regression of the β_{11} parameter to the extracted kappa number from Fig. 4: (A) conventional and (B) modified hardwood kraft pulps. Ellipses represent the 95% confidence region for paired slope and y-intercept values, whereas the central points represent the regressed values. The two groups of kraft pulps have statistically different linear regression parameters.

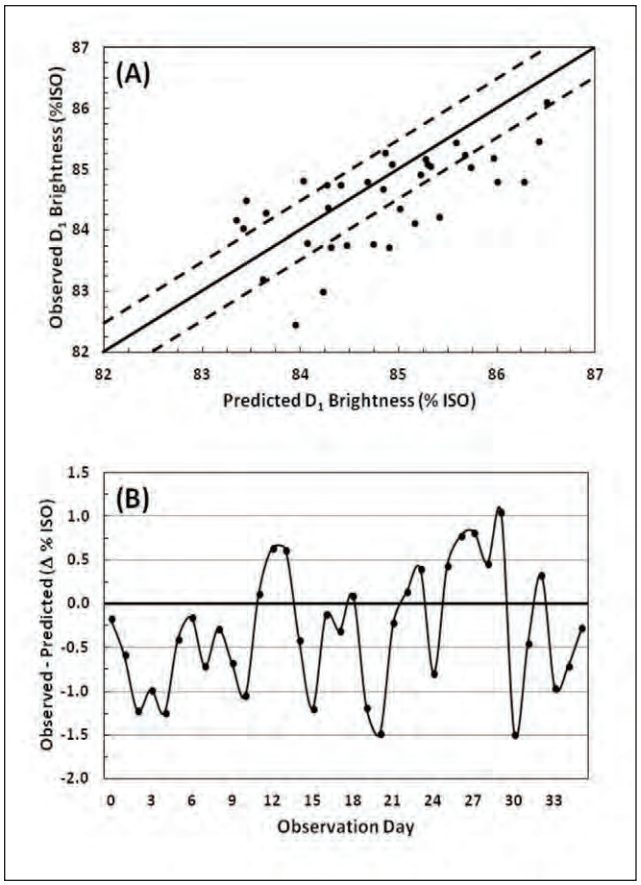
The curve-fitted β_{11} parameters for the conventional kraft pulps were also plotted versus the extracted pulp brightness (not shown). As a group, the β_{11} values showed a weak linear correlation to the extracted brightness ($r^2 = 0.696$). When the β_{11} values versus extracted brightness for each individual pulp were examined, the β_{11} value was linearly correlated to the pulp's brightness ($r^2 > 0.93$). However, no generalized relationships were discerned that related the slope, abscissa intercept, or ordinate intercept values among the pulps as a group.

Testing the D_1 model with mill data

The generalized D_1 model for hardwood kraft pulps was tested against actual bleach plant data to evaluate its veracity. Process data from a southern U.S. hardwood kraft mill were obtained. This mill bleaches a mixed hardwood pulp, which is made primarily from southern U.S. red and white oaks and sweetgum with small amounts of poplar and maple species. The pulp is produced using a Lo-Solids continuous digester (Andritz; Graz, Austria). Daily averages were calculated from the hourly process data over a 1-month period. **Table IV** presents the prevailing conditions at the bleach plant. The mill uses a D_0(EOP)D_1 sequence to brighten the hardwood pulp to an 84% ISO target. The bleachery did not monitor the (EOP) washer carryover into the D_1 stage. However, previous bench-

Condition	Monthly Range	Monthly Average	Monthly Standard Deviation
Brownstock kappa No.	9.5 to 17.8	14.1	0.7
D_0(EOP) kappa No.	2.85 to 4.21	3.60	0.29
D_0(EOP) brightness, % ISO	68.4 to 77.3	71.3	1.8
D_1 ClO_2, % on o.d. pulp	0.60 to 1.03	0.80	0.10
D_1 vat pH	3.6 to 5.3	4.6	0.4
D_1 brightness, % ISO	82.5 to 86.6	84.6	0.8

IV. Hardwood bleach plant conditions during the data collection over a 1-month period.



6. D_1 brightness values calculated by Eq. (3) based on mill data for x_1, $Kappa_E$, and B_E inputs over a 1-month period: (A) mill measured versus predicted model brightness values and (B) differences between the values for each observation day. Model's β_{11} value is based on modified kraft pulp relationship of Fig. 4 and c_{01} = 93% ISO. Dotted lines represent ±0.5% ISO units difference of the model's values from mill measured values.

marking studies have indicated this fiber line operates with very low bleach chemical consumption when compared with similar ECF fiber lines. The mill runs the D_1 with a low post-stage bleach residual (~0.1 g to 0.2 g ClO_2/L).

Daily bleach charges (x_1), extracted kappa numbers ($Kappa_E$), and extracted brightness values (B_E) were used as the input variables into the model. The c_{01} parameter was set to 93% ISO. This parameter was estimated from the Kubelka-Munk remission function, which used an unbeaten light scattering coefficient (s) of 38 m²/kg and asymptotic light absorption coefficient (k_∞) of 0.10 m²/kg. The β_{11} parameter was determined from the correlation shown in Fig. 4 for modified hardwood kraft pulps, which was verified with laboratory D_1 bleaching data on the mill's pulp (not shown).

Figure 6 compares the predicted brightness values to the bleach plant data. Forecasted values were relatively close to the measured values for this hardwood fiber line. However, the generalized D_1 model consistently over-predicted the brightness, usually by ~0.5 points over the mill-measured value. This discrepancy was somewhat anticipated. Similar results have been observed when using the softwood D_1 model to analyze data from a bleach plant that had extraction stage carryover [15].

One item that was not considered with the brightness (D_1) model was the bleach consumed by extraction washer carryover. Most bleach plants do not monitor the entrained dissolved solids entering the D_1 stage. This carryover can be approximated by measuring the well-washed and the unwashed (or "wet") kappa numbers of the pulp mat leaving the extraction washer [44,45]. The difference between these two tests provides an estimate of the entrained dissolved solids expressed as kappa units on pulp (i.e., 1 mL of 0.1 N potassium permanganate/g pulp). The hardwood mill data were re-analyzed with the model by using similar techniques developed for analyzing softwood bleach plant data [15] to estimate the carryover contained in the hardwood pulp mat. The analysis indicated that pulp mat leaving the (EOP) washer contained, on average during this 1-month period, 0.4 kappa units of carryover. This (EOP) carryover was consuming ~0.12% ClO_2 on pulp (1.2 kg ClO_2/o.d. ton pulp).

DISCUSSION

The generalized steady-state model for the D_1 stage accurately predicts the brightening of hardwood kraft pulps produced from single or mixed wood species delignified by chlorine dioxide sequences such as D_0(EOP), OD_0(EO), etc. For well-washed extracted pulps, the predicted brightness values from the hardwood model are generally within ±0.6 points from the laboratory measurements. These observations with the D_1 model are similar to observations noted in an earlier report for a softwood D_1 model [13]. Predicted versus measured differences are close to the 95% CIs observed with well-controlled D_1 laboratory studies (±0.7 points).

The model is defined by three equation parameters. The first parameter is asymptotic or upper brightening limit, c_{01}. It can be calculated with the Kubelka-Munk remission function. This calculation uses the asymptotic k value of 0.10 m²/kg and the *s* for of the unbeaten hardwood pulp, which can vary considerably depending on species comprising the pulp ($s \approx 32$ m²/kg to 53 m²/kg). For many North American pulps made from mixed hardwood species, this c_{01} value is ~93% ISO. The c_{01} values determined by this method are close to the c_{01} values from nonlinear regression, usually within the calculated standard errors of the parameter. Additionally, this simplification eliminates one tunable equation parameter without sacrificing the accuracy of the D_1 model.

The next parameter is β_{21}. It is a function of the extracted pulp brightness (B_E), c_{01}, and β_{11}. Extracted pulp brightness tends to be linearly related to the $Kappa_E$ of the pulp for a fixed set of extraction stage conditions. This relationship is affected by the oxidant-reinforced conditions of the extraction stage, such as peroxide dosage, as well as the pulping process (e.g., modified kraft) and cooking conditions (e.g., effective alkali) used. Generalized expressions of B_E versus $Kappa_E$ considered for softwood kraft pulps [12] were not explored in this hardwood study. Determination of this rela-

tionship would be needed if the hardwood D_1 model is to be coupled with other steady-state models to simulate a hardwood ECF bleach sequence. Further work is needed to establish generalized expressions of B_E versus $Kappa_E$ if B_E is not measured.

The final parameter is β_{11}. Its value is linearly related to $Kappa_E$. This correlation appears to be influenced by the kraft pulping process used. Hardwood pulps produced with the modified kraft process have β_{11} values that are affected more by small changes in $Kappa_E$. On the other hand, conventional hardwood pulps exhibit β_{11} values that are less sensitive to changes in $Kappa_E$. These distinctions might be related to the proportions of lignin and HexA structures in the pulp. Modified pulping tends to generate fewer HexA groups versus conventional pulping when compared with the same kappa number [46]. The conventional pulps would have less lignin content than the modified kraft pulps, although the kappa number measurement implies that both pulps have the same lignin content. McDonough et al. [5] noted D_1 bleachability differences for oak brownstocks that had the same kappa number entering the $D_0(EO)D_1$ sequence but different proportions of lignin and HexA groups. These differences in constituents likely persist after chlorine dioxide delignification and caustic extraction, which would then influence the β_{11} versus extracted kappa relationship. Additional research would be needed to verify this assertion.

The linear regression of β_{11} to the extracted kappa for modified hardwood pulps has a similar slope to that observed for softwoods (~4.4 vs. ~4.5) but differs with their x-axis intercepts (~1.2 vs. ~1.6) [13]. The x-axis intercepts are within the range of measured kappa numbers of hardwood pulps bleached by the D_1 to 80% to 86% ISO. The relationships shown in Fig. 4 are the trends observed for the laboratory and bleach plant data examined in this investigation. Further work is needed to confirm these trends with other single and mixed species hardwood pulps, such as eucalypt species.

The hardwood D_1 model can predict pulp brightness from bleach plant data when the bleach dosage (x_1), B_E, and $Kappa_E$ are known. Forecasted brightness values are typically higher than the measured mill brightness. This difference likely reflects the bleach consumption caused by washer carryover, which is not considered. This factor could be incorporated into the brightening model analogous to the corrections proposed to softwood D_1 model [15]. If extraction carryover is monitored, then this variable can be taken into account to improve the model's accuracy. Furthermore, if washer carryover is not measured, then this process variable can be approximated from the bleach plant data using the model (after other contributing factors, such as D_1 pH, chemical mixing, etc., have been eliminated). In the mill example, the monthly average carryover was estimated at ~0.4 kappa units (on pulp). The average amount of bleach consumed by this carryover was ~1.2 kg ClO_2/ton pulp. This level of carryover is low, which indicates good pulp washing efficiency after the extraction stage [15,44,45].

CONCLUSIONS

A generalized hardwood model for the first chlorine dioxide brightening (D_1) stage has been developed (Eq. [3]). The model predicts the D_1 bleaching response based on three parameters that are related to the properties of the extracted pulp.

At extremely high bleach charges, the asymptotic D_1 brightness limit (c_{01}) can be determined by the Kubelka-Munk remission function using the floor-level light absorption coefficient (k_∞) of 0.10 m²/kg and the light scattering coefficient (s) of the unbeaten hardwood pulp. The c_{01} calculated from these hardwood pulp properties are within the values calculated by the curve-fitting of D_1 bleaching data by nonlinear regression. Another equation parameter in the hardwood model is the brightness of the extracted pulp (B_E) entering the D_1 stage. The last parameter, β_{11}, defines the brightening response of the extracted hardwood pulp. This parameter is linearly correlated to extracted kappa number ($Kappa_E$) of the pulp. The relationship of β_{11} to $Kappa_E$ appears to be affected by the process conditions used in the digester to produce the hardwood kraft pulp. The predicted brightness values from the D_1 model are generally within ±0.5 to ±0.6 points of the measured laboratory value.

When the model was tested against bleach plant data for a southeastern U.S. hardwood fiber line, the forecasted brightness values were ~0.5 points higher than the mill's values. In this scenario, the bleach consumption caused by extraction washer carryover was not taken into account. It was estimated that the $D_0(EOP)$ pulp contained a small amount of carryover (~0.4 kappa units on pulp), which was consuming ~1.2 kg ClO_2/ton pulp. **TJ**

ACKNOWLEDGEMENTS

The author thanks Carl Houtman of the USDA Forest Products Laboratory for his insightful comments and suggestions regarding the regression analyses used to analyze the bleaching data. Portions of this work were presented at the 2016 TAPPI Pulping, Engineering, Environmental, Recycling, and Sustainability (PEERS) Conference in Atlanta, GA, USA (September 27, 2016; Session 2-1).

LITERATURE CITED

1. Rudie, A.W. and Hart, P.W., in *The Bleaching of Pulp* (P.W. Hart and A.W. Rudie, Eds.) 5th edn., TAPPI Press, Atlanta, GA, USA, 2012, Chap. 1.
2. Annergren, G.E., Boman, M., and Sandstrom, P., *Int. Pulp Bleaching Conf.*, SPCI, Stockholm, Sweden, 1998, pp. 99-110.
3. McDonough, T.J., Rawat, N., and Krishnagopalan, G.A., *Appita J.* 57(5): 381(2004).
4. McDonough, T.J., Uno, S., Rudie, A.W., et al., *TAPPI J.* 7(1): 4(2008).
5. McDonough, T.J., Uno, S., Rudie, A.W., et al., *TAPPI J.* 8(8): 10(2009).
6. Hart, P.W. and Connell, D., *TAPPI J.* 5(4): 23(2006).
7. Brogdon, B.N., *TAPPI J.* 9(8): 27(2010).
8. Brogdon, B.N., *TAPPI J.* 9(9): 47(2010).

9. Brogdon, B.N., *TAPPI J.* 12(10): 33(2013).
10. Brogdon, B.N., in *The Bleaching of Pulp* (P.W. Hart and A.W. Rudie, Eds.) 5th edn., TAPPI Press, Atlanta, 2012, Chap. 12.
11. Brogdon, B.N., *TAPPI J.* 11(3): 31(2012).
12. Brogdon, B.N., *TAPPI J.* 13(3): 29(2014).
13. Brogdon, B.N., *TAPPI J.* 13(3): 17(2014).
14. Brogdon, B.N., *TAPPI J.* 14(2): 93(2015).
15. Brogdon, B.N., *TAPPI J.* 15(3): 178(2016).
16. Brogdon, B.N., *TAPPI J.* 12(2): 17(2013).
17. Rydholm, S.A., in *Pulping Processes* (S.A. Rydholm, Ed.), Wiley & Sons, New York, 1965, pp. 42-68.
18. Reeves, R.H., in *Pulp and Paper Manufacture: Vol. 7 Paper Machine Operations* (B.A. Thorp, Ed.), The Joint Textbook Committee of the Paper Industry, Atlanta, 1991, pp. 26-53.
19. Süss, H.U., Schmidt, K., Davies D., et al., *Int. Papierwirtsch.* 11(5): 40(2006).
20. Ragnar, M., *Nord. Pulp Pap. Res. J.* 18(2): 162(2003).
21. Basta, J., Andersson, L., Blom, C., et al., *TAPPI Pulping Conf.*, TAPPI Press, Atlanta, 1992, pp. 547-553.
22. Parthasarathy, V., Rudie, G., Detty, A., et al., *TAPPI Pulping Conf.*, TAPPI Press, Atlanta, 1993, pp. 933-949.
23. Parthasarathy, V., Detty, A., and Steffy, J., "Elemental chlorine free and low chlorine bleaching of Chillicothe hardwood – extending delignification and bleaching of hardwood pulps," *Internal Report No. 16,136*, Mead Central Research, Chillicothe, OH, USA, October 1993.
24. Rawat, N. and McDonough, T.J., *TAPPI Pulping Conf.*, TAPPI Press, Atlanta, 1998, pp. 883-891.
25. Rawat, N. and McDonough, T.J., Unpublished data, Institute of Paper Science and Technology, Atlanta, 24 March 1998.
26. Reeve, D.W. and Weishar, K.M., *Tappi J.* 82(10): 136(1999).
27. Germgård, U. and Lundquvist, M., *Appita J.* 43(1): 63(1990).
28. Germgård, U., Klorat, A., and Karlsson, R.-M., *Nord. Pulp Pap. Res. J.* 3(4): 166(1988).
29. Barroca, M.J.M.C. and Castro, J.A.A.M., *Ind. Eng. Chem. Res.* 42(18): 4156(2003).
30. McDonough, T.J., Krishnagopalan, G.A., Rawat, N., et al., *Int. Symp. Wood Pulping Chem., 10th*, Japan TAPPI, Tokyo, Japan, 1999, pp. 296-301.
31. McDonough, T.J., Krishnagopalan, G.A, Rawat, N., et al., "Bleachability in oxygen-based ECF sequence of softwood and hardwood kraft pulps made with altered liquor concentration profiles 1: effect of oxygen delignification on the bleachability of conventional pulps," *Int. Pulp Bleaching Conf.*, PAPTAC, Montréal, 2000.
32. Hart, P.W. and Connell, D., *TAPPI J.* 7(7): 3(2008).
33. Connell, D. and Smith, S., "An evaluation of the effects of $Mg(OH)_2$ addition to the extraction stage," *TAPPI Eng., Pulping Environ. Conf.*, TAPPI Press, Atlanta, 2009.
34. Brogdon, B.N. and Bell, J.M., "Optimization of chlorine dioxide bleaching sequences for kraft pulps through improved oxidative alkaline extraction stage performance," *TAPPI Fall Tech. Conf.*, TAPPI Press, Atlanta, 2004, Session 18-3.
35. Brogdon, B.N., Unpublished data, June 2003.

ABOUT THE AUTHORS

This work continues the paper series on steady-state models for elemental chlorine-free (ECF) bleach sequences. It is the companion to the study that models D_1 stages for softwood pulps (*TAPPI J.* 13[3]: 17[2014]). It was anticipated that the findings from the softwood study could be extended to cover North American hardwoods. These models are simple and can be easily programmed into computer spreadsheets, which can be used to calculate optimum bleach setpoints and to minimize manufacturing costs.

This work builds on the earlier D_1 model proposed by Tom McDonough and co-workers of the Institute of Paper Science and Technology (IPST) (e.g., *TAPPI J* 7[1]: 4[2008]). One issue encountered when using the IPST model is establishing the tunable parameter values. These parameters are affected by the conditions used to produce the pulp. This restricts the generalization of the D_1 model because the parameters have to be determined experimentally. The goal of this study was to discover a more general D_1 stage model.

A problem encountered with the generalized D_1 model for hardwoods was establishing the asymptotic limit. Unlike softwoods, the brightness limits for hardwood pulps vary widely from 92% to 94% ISO. Nonetheless, it was discovered that this parameter can be estimated by the fundamental properties of the hardwood pulp by using Kubelka-Munk theory. After this was resolved, it was discovered that one of the tunable parameters could be correlated to the extracted kappa number of the pulp entering the D_1 stage, which is in turn influenced by the kraft pulping process used. This observation matches literature reports on D_1 bleachability differences for hardwood pulps produced by different pulping conditions. These differences reflected by the model might be related to the proportions of residual lignin and hexenuronic acid (HexA) groups in the pulp. However, this speculation will need to be verified by additional laboratory work.



Brogdon

Brogdon is president, Future Bridge Consulting Services LLC, Marietta, GA, USA. Email Brogdon at Brian.Brogdon@gmail.com.

36. Teder, A. and Tormund, D., *Trans. Tech. Sect. (Can. Pulp Pap. Assoc.)* 3(2): TR41(1977).

37. Middleton, S.R. and Scallan, A.M., *Nord. Pulp Pap. Res. J.* 7(1): 22(1992).

38. Nanko, H., Button, A., and Hillman, D., in *The World of Market Pulp* (C.E. Swann, Ed.), 3rd edn., WOMP LLC, Appleton, WI, USA, 2005, pp. 137-262.

39. Kibblewhite, R.P., Bawden, A.D., and Hughes, M.C., *Appita J.* 44(5): 325(1991).

40. Byrd, V.L. and Fahey, D.J., *Pap. Trade J.* 153(47): 54(1969).

41. Barker, R.G., *Tappi* 57(8): 107(1974).

42. Wilder, H.D., Unpublished data, Institute of Paper Chemistry, Appleton, 18 March 1964.

43. Rapson, W.H., in *The Bleaching of Pulp* (W.H. Rapson, Ed.), TAPPI Press, Atlanta, 1963, Monograph No. 27, pp. 130-179.

44. Pryke, D.W. and Nylen, K., *Pulp Pap. Can.* 109(1): 43(2008).

45. Steelreath, E., Earl, P.F., and Vanderheide, J., "Bleach plant optimization at the Resolute Forest Products Coosa Pines mill," *TAPPI PEERS Conf.*, TAPPI Press, Atlanta, 2014.

46. Brogdon, B.N., "A fundamental review and critical analysis of hexenuronic acids and their impact in elemental chlorine-free bleaching," *TAPPI Eng., Pulping Environ. Conf.*, TAPPI Press, Atlanta, 2009.

Impact of dissolved matter in the oxygen delignification stage

CAROLINE WILKE, NICLAS ANDERSSON, AND ULF GERMGÅRD

ABSTRACT: The presence of dissolved matter in the pulp suspension in an oxygen (O_2) delignification stage, consisting mainly of dissolved lignin, is normally considered to negatively affect the delignification rate due to the competing reactions between the fiber bound lignin and the lignin dissolved in the filtrate. Recirculated oxidized filtrate from the post-O_2 washing is usually considered to be less harmful to the delignification efficiency than unoxidized dissolved matter originating from the cooking stage. To develop a better understanding of the mechanisms of the dissolved matter's reactions and impact on the O_2 stage performance, laboratory oxygen delignification experiments with varying levels of unoxidized and oxidized dissolved matter were conducted.

The results showed that unoxidized dissolved matter had a negative impact on the delignification in the O_2 stage, whereas oxidized dissolved matter actually had a positive effect. The delignification efficiency of the laboratory experiments thus depends on both the amount of dissolved matter and its origin. The pulp viscosity decreased with increasing dissolved matter content irrespective of its origin but at higher COD levels; however, the viscosity drop was larger for the unoxidized dissolved matter. In terms of selectivity, the oxidized filtrate had a similar impact as additional NaOH charge. Both types of filtrates consumed hydroxide and the final pH decreased with increasing dissolved matter content. The final pH was significantly lower in the unoxidized filtrate experiments at higher COD levels, indicating a high reactivity between the unoxidized dissolved matter and the oxygen in the reactor.

Based on the results, further understanding is achieved about the relation between pre-O_2 washing performance and process configuration in an actual mill case, as well as the impact of dissolved matter on delignification. The importance of efficient removal of harmful unoxidized dissolved matter is verified, but the results also suggest that the oxidized dissolved matter that is recirculated from post-O_2 washing actually has a significant positive impact on the delignification and is not just a potential problem in case of carryover to the bleach plant. Subsequently, pulp washing efficiency is critical both pre- and post-O_2.

Application: The results from the study reinforce the importance of well-performing brownstock washing to minimize the carryover of unoxidized dissolved matter from the cooking stage. However, because the oxidized post-O_2 filtrate actually has a significant positive impact when recirculated, this can be exploited to improve delignification and reduce alkali consumption in the O_2 stage. Subsequently, optimum operation of pre- and post-O_2 washers will depend on the mill's washer configuration.

To accurately control the degree of delignification in a pulp mill fiber line, the most frequently used parameter is the fiber kappa number, especially in the beginning of the delignification, i.e., in the digester and the following oxygen (O_2) delignification stage. Studies [1-4] have shown, however, that the kappa number reduction is strongly influenced by the presence of dissolved matter in the pulp slurry, both in the cook and in the following O_2 delignification. This is clearly shown in the O_2 delignification stage, which was the target for this study. The dissolved matter generated in the digester and the O_2 stage is largely removed through washing of the pulp; however, an industrial washer is never 100% perfect. The remaining amount of dissolved matter in the pulp after washing is usually referred to as "wash loss" or "carryover," and it consists of both inorganic and organic dissolved matter. The carryover of dissolved matter is often characterized as the chemical oxygen demand (COD), and it is typically expressed as kg COD/ton of pulp. Good washing of the pulp before the O_2 stage minimizes the amount of unoxidized dissolved matter entering the O_2 stage with the pulp. Large carryover of unoxidized dissolved matter will reduce the O_2 delignification response and consume more oxygen and sodium hydroxide (NaOH) in the O_2 stage [5-10]. The higher chemical consumption is due to competing reactions between the dissolved lignin in the carryover and the lignin in the fibers [5,8,10]. Studies have shown that the alkali consumption by the dissolved matter can partly be counteracted for by adding more NaOH in the O_2 stage [7-10].

There are two kinds of dissolved matter that enter the O_2 stage: unoxidized dissolved matter originating from the digester and oxidized dissolved matter from post-O_2 washing. The degree of pre- and post-O_2 washing will not only deter-

mine the amount of dissolved matter carryover but also the distribution between unoxidized and oxidized dissolved matter [10]. According to previous studies, recirculated oxidized filtrate from post-O_2 washing is less harmful to the delignification efficiency than unoxidized filtrate originating from the cooking stage [5-9]. The unoxidized filtrate is more reactive than oxidized filtrate, and the competing reactions between dissolved lignin and the fiber bound lignin are thus more pronounced for the unoxidized filtrate. However, Miller et al. [10] claimed that oxidized dissolved matter was more harmful to the O_2 delignification stage than unoxidized dissolved matter due to its low content of alkali. All of the mentioned studies agree that dissolved matter indeed has an effect on the efficiency of the O_2 stage, but the size of the impact differs. Some of the studies [6,7,10] showed that small amounts of unoxidized dissolved matter could have positive effects on the O_2 delignification stage, while larger quantities always decreased the delignification. A study by Iijima and Taneda [5] indicated that oxidized dissolved matter was beneficial for delignification, but they only studied low COD levels, i.e., below 18 kg/ton. Miller et al. [9] showed that oxidized filtrate enhanced delignification at 130 kg COD/ton, but it was explained by the reactive nature of the pulp used. Bokström and Nordén [11] concluded that oxidized dissolved matter was beneficial for the viscosity-kappa number selectivity at COD levels up to 160 kg/ton.

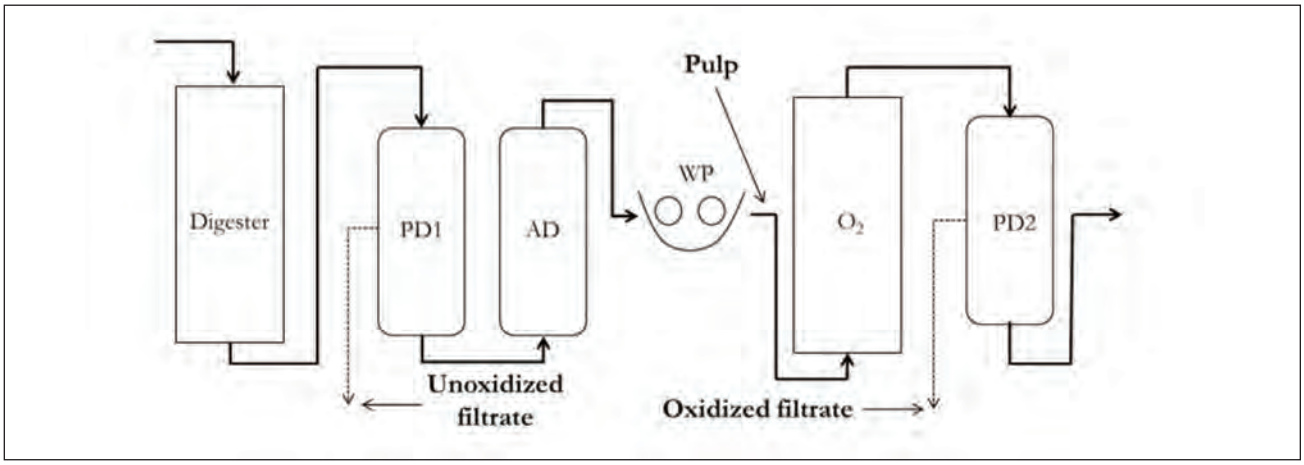
Hence, in the literature, there is no unanimous conclusion regarding the impact of dissolved matter, so the objective of this study was to further investigate the effects of carryover on the O_2 delignification responses. Three types of dissolved matter were used: unoxidized, oxidized, and mixtures of the two.

EXPERIMENTAL

This study was carried out in the laboratory on softwood kraft pulp taken from a Scandinavian pulp mill. As can be seen in **Fig. 1**, the pulp had been washed in a pressure diffuser (PD1) after the digester, followed by an atmospheric diffuser (AD) and a wash press (WP). The sampling position for the pulp was located at the screw after the wash press (WP). Filtrates from pre- and post-O_2 washing systems were also obtained from the mill. They were collected from the pressure diffusers before and after the O_2 delignification stage. The filtrate collected before the O_2 stage was assumed to contain primarily unoxidized dissolved matter, and filtrate collected after the O_2 stage was assumed to contain exclusively oxidized dissolved matter. The sampling positions were chosen so that the pulp sample represented the actual pulp entering the O_2 stage, whereas the filtrate samples were chosen to allow for the examination of the effect of the different types of dissolved matter. In reality, the pulp slurry entering the O_2 delignification stage contains both unoxidized and oxidized dissolved matter due to the recirculation of filtrates in the different washing stages. In the first set of experiments, the pulp samples were thoroughly washed in the laboratory, whereas in the second set of experiments, the pulp samples were unwashed. The sampling positions and the properties of the collected samples are depicted in Fig. 1 and **Table I**.

The O_2 delignification experiments were conducted in 2.5 L autoclaves immersed in a polyethylene glycol bath, and the laboratory conditions are listed in **Table II**. Filtrate was added to the pulp samples in most of the experiments in order to simulate various levels of dissolved matter. The filtrates were diluted with deionized water to achieve different levels of COD. In order to reach certain COD levels, the dilution for the unoxidized filtrates was much larger, thus causing their pH values to decrease more compared to the oxidized filtrates.

Some preparatory experiments were conducted in order to exclude any impact from suspected disturbance factors. The presence of metal ions can affect the pulp viscosity [12]. Oxygen delignification experiments were performed with ethylenediaminetetraacetic acid (EDTA), which acts as a chelating agent to negate the effect of metal ions. The results showed that there was no significant difference in pulp viscosity between the experiments with and without added ETDA. Furthermore, hydrogen sulfide ions are known to affect negatively pulp viscosity, and to some extent also delig-



1. Sampling positions in the pulp mill pulp mill (PD1, PD2 = pressure diffusers; AD = atmospheric diffuser; WP = wash press; O_2 = oxygen delignification).

	Viscosity, dm^3/kg	Kappa Number (of clean pulp)	COD, g/L	pH
Experiments with washed pulp (I)	**1247**	**26.8**	**0.0**	
Unoxidized filtrate			120.0	12.5
Oxidized filtrate			15.5	10.7
Experiments with unwashed pulp (II)	**991**	**27.3**	**56.5**	**10.5**
Unoxidized filtrate			135.5	12.1
Oxidized filtrate			35.0	11.8

I. The properties of the original samples used in the experiments.

Pulp, g	50
Consistency, %	10
COD, kg/ton pulp	25-360
NaOH, %	2
$MgSO_4$, %	0.2
Pressure, bar	5
Temperature, °C	90
Time, min	120

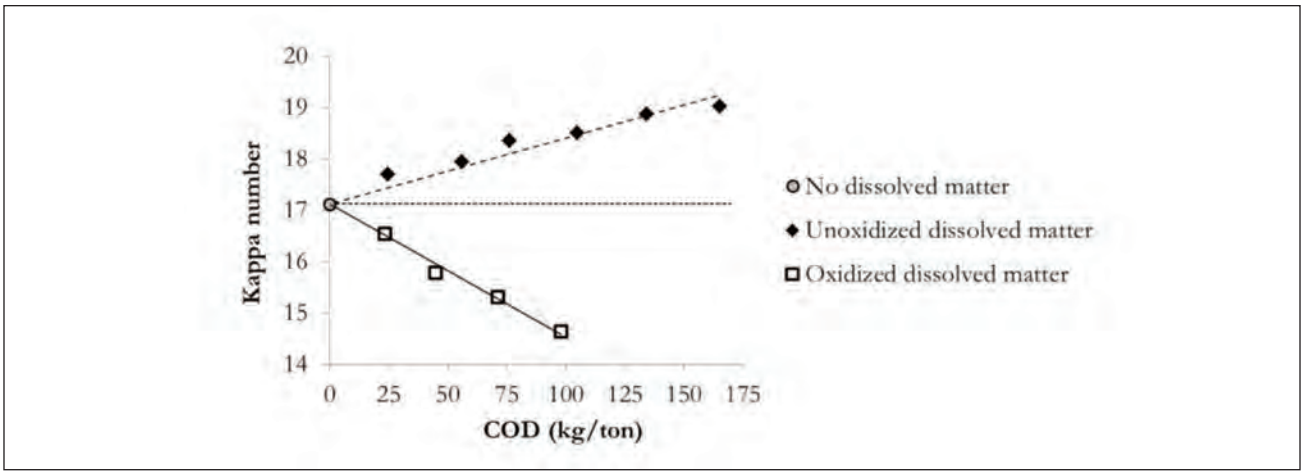
II. Laboratory conditions used, where the charges are calculated on dry pulp.

nification [13]. In order to ascertain that the hydrogen sulfide ions did not impact the experiments, a comparison was made between a thoroughly aerated unoxidized filtrate and the non-treated one. The differences in kappa number and pulp viscosity after the O_2 delignification stage were marginal. The hydrogen sulfide ion concentration was also determined by titration (SCAN-N 31:94 "Hydrogen sulfide ion concentration") and the very low level confirmed the observations (0.06 M HS^- for the raw unoxidized filtrate). Furthermore, the COD was measured before and after aeration, again showing no significant difference.

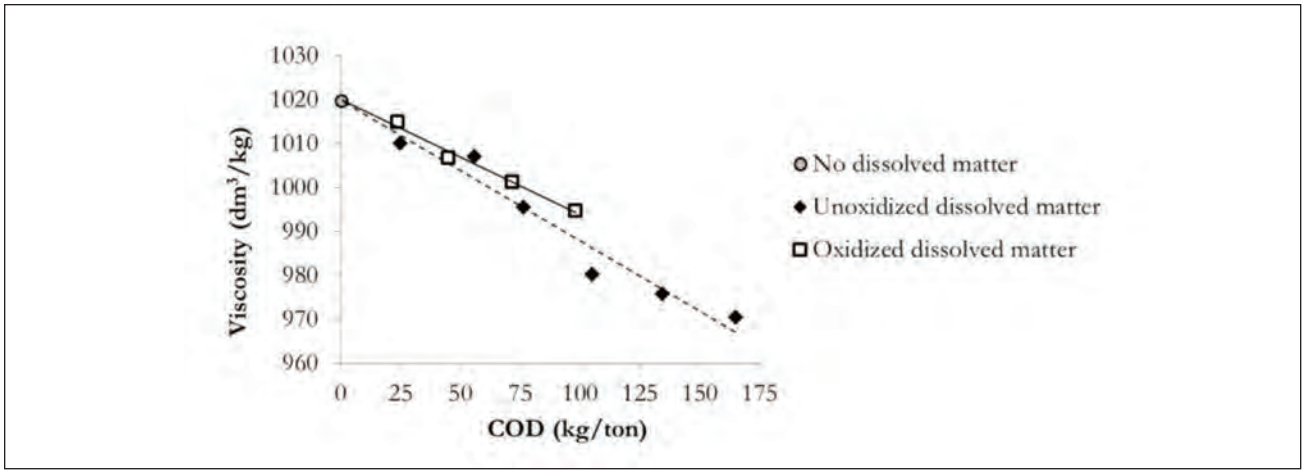
RESULTS AND DISCUSSION

Experiments with washed pulp

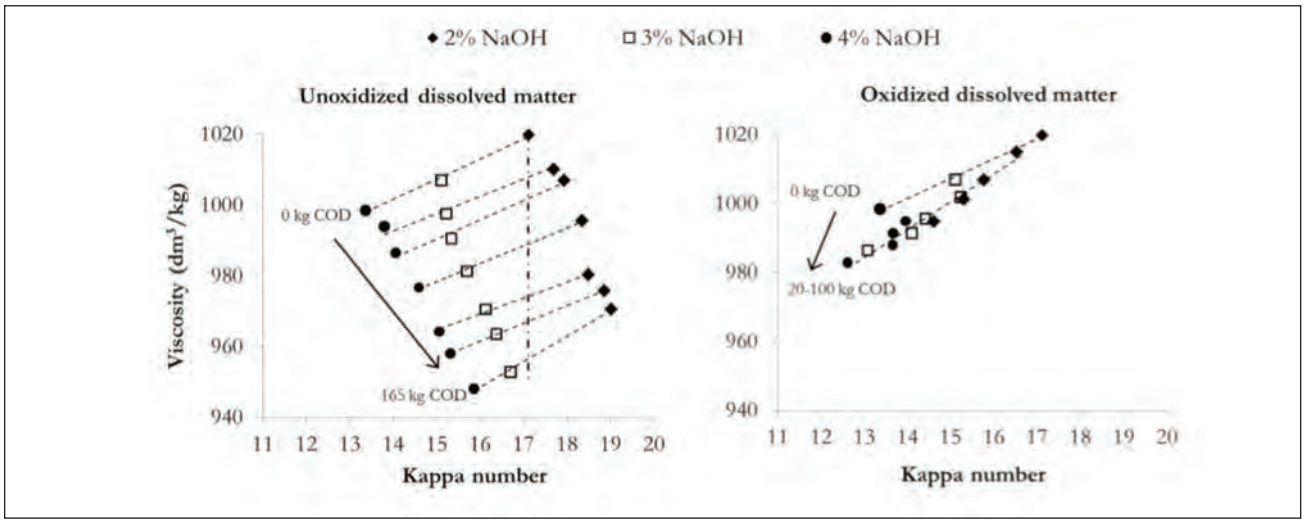
The first set of experiments were done on a well-washed pulp sample (pulp I in Table I). Laboratory O_2 delignification experiments were conducted on this pulp in order to investigate how varying contents of unoxidized and oxidized dissolved matter influenced lignin removal during the O_2 delignification. In **Fig. 2**, the resulting fiber kappa numbers after the O_2 delignification experiments are plotted vs. the COD in the samples prior to the O_2 stage. As can be seen, the experiment with the well-washed pulp sample (i.e., without dissolved matter) reached a kappa number of 17.1. It is evident that the presence of unoxidized dissolved matter had a relatively large negative impact on the delignification, with resulting kappa numbers up to 19.0 at the highest COD levels studied (i.e., 165 kg/ton). This result is in agreement with earlier studies [6-9]. The presence of oxidized filtrate, on the other hand, had a positive impact on delignification, and in this case, the resulting kappa number after the O_2 stage was down to 14.5



2. Fiber kappa number vs. chemical oxygen demand (COD) with unoxidized and oxidized filtrates.



3. Viscosity vs. COD with unoxidized and oxidized filtrates.



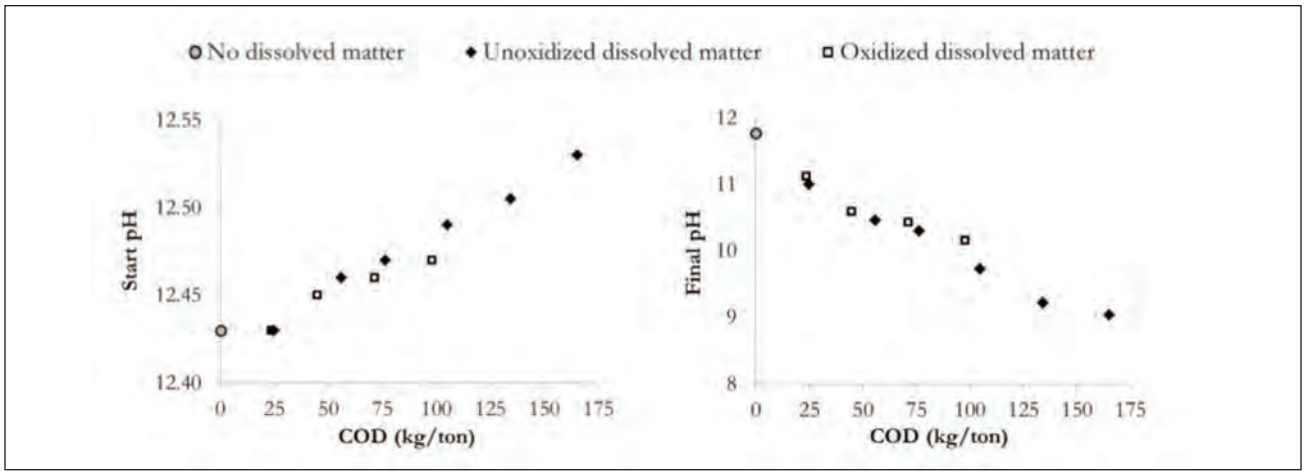
4. Viscosity vs. kappa number at different sodium hydroxide (NaOH) charges with unoxidized (left) and oxidized (right) filtrates.

at the highest COD level. Small positive effects of oxidized dissolved matter have previously been indicated by several investigators [5,9,11], but none have observed the significant impact presented by the current study.

The corresponding pulp viscosities after the O_2 delignification stage vs. COD were found to decrease in a similar manner for both types of filtrates, as shown in **Fig. 3**. The results with the unoxidized dissolved matter are somewhat scattered, but still indicated that the viscosity loss was slightly more than that of the oxidized dissolved matter.

The effect on selectivity by the two types of filtrates was investigated by additional experiments with 3% and 4% NaOH charges, and the results are shown in **Fig. 4**. It is evident that the additional NaOH charge yielded considerably lower kappa numbers, while the viscosities were rather moderately affected. The relative effect on delignification and viscosity degradation was principally independent of the COD level and was also independent of the type of dissolved matter (i.e., unoxidized or oxidized) with respect to the additional NaOH charge. However, as noted earlier, the presence of unoxidized dissolved matter itself had a very negative impact on the selectivity in the O_2 stage. One can also note that the addition of oxidized dissolved matter actually influenced the O_2 delignification in a similar way as a higher NaOH charge, resulting in just a slightly lower viscosity compared to the reference case (0 kg COD). The dash-dotted line in the left subplot, for unoxidized dissolved matter, can be used to approximate the additional NaOH charge required to counter effect the COD charge compared to the reference case with no COD. A rough assessment is that an additional 0.5% NaOH charge is required per 100 kg COD, or 0.05 kg NaOH per kg COD. Furthermore, note in the right subplot, for oxidized dissolved matter, that all points with any COD charge are on the same trend line. However, the symbols used are the same as for the left subplot, and for any NaOH charge, an increase in the COD charge will lower both kappa number and viscosity.

It has previously been suggested by investigators [5,8-10] that the alkali contribution from the filtrate could have a pos-



5. Start pH (left) and final pH (right) vs. COD with unoxidized and oxidized filtrates.

itive effect on the delignification and a negative effect on the pulp viscosity. However, the additional NaOH contribution from the filtrates at 100 kg COD/ton (determined with SCAN-N 33:94 "Residual alkali [Hydroxide ion content]") was only 0.14% NaOH (on pulp) for the unoxidized filtrate and 0.09% for the oxidized one. Such small NaOH contribution compared to the NaOH charges shown in Fig. 4 is thus not likely to be the reason for the differences observed for delignification and pulp viscosity.

The filtrate pH was determined at 25°C before and after the laboratory O_2 delignification, and the results can be seen in **Fig. 5**. The starting pH values were measured after the addition of 2% NaOH. The differences in initial pH were very small over the studied COD range due to the low alkali contribution from the filtrates, which was about 0.1% NaOH, as previously described. However, the differences in pH after the O_2 delignification were substantial, indicating that dissolved matter consumed a significant amount of alkali. The large consumption could have explained the poor delignification observed for the unoxidized filtrates, but not the beneficial delignification for the oxidized ones. Subsequently, according to the present study, hydroxide consumption and pH levels alone cannot explain the difference in delignification observed for unoxidized and oxidized matter, at least up to 100 kg COD/ton.

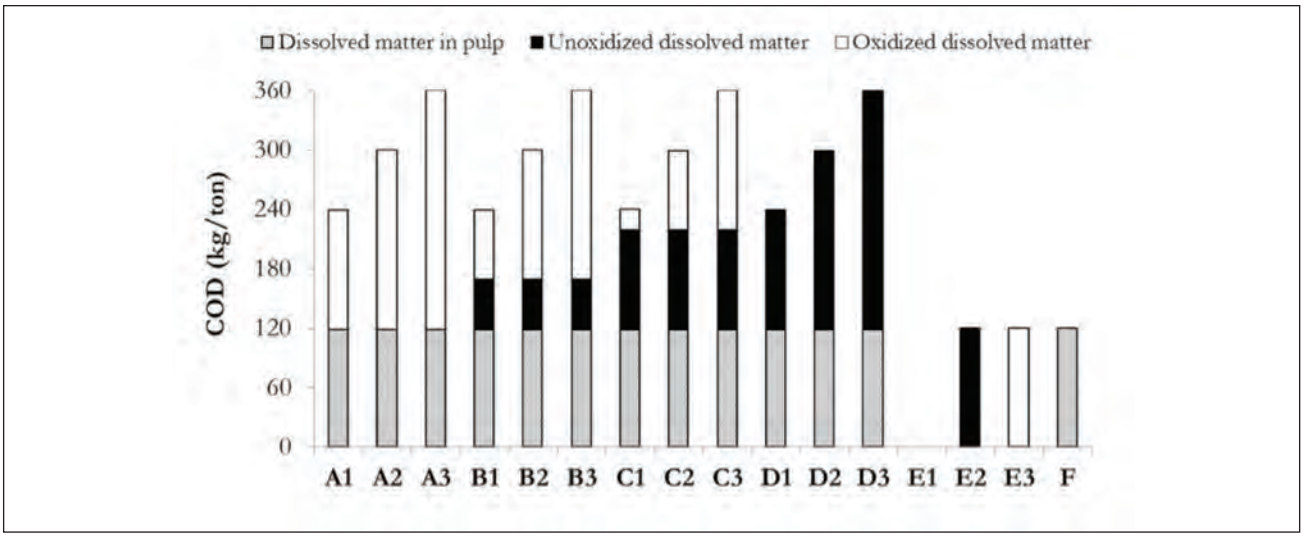
It has previously been reported [10] that unoxidized dissolved matter generates more organic acids than oxidized dissolved matter, thus resulting in lower final pH. The results in these experiments indicated, however, that the two types of filtrates have similar final pH up to 100 kg COD/ton. Other studies [8,9] have stated that oxidized dissolved matter had a higher carbon dioxide evolution, which resulted in a higher NaOH consumption. It may be that the larger organic acid generation from the unoxidized dissolved matter and the higher carbon dioxide evolution from oxidized dissolved matter affected the filtrates equally, thus resulting in similar final pH.

Experiments with unwashed pulp

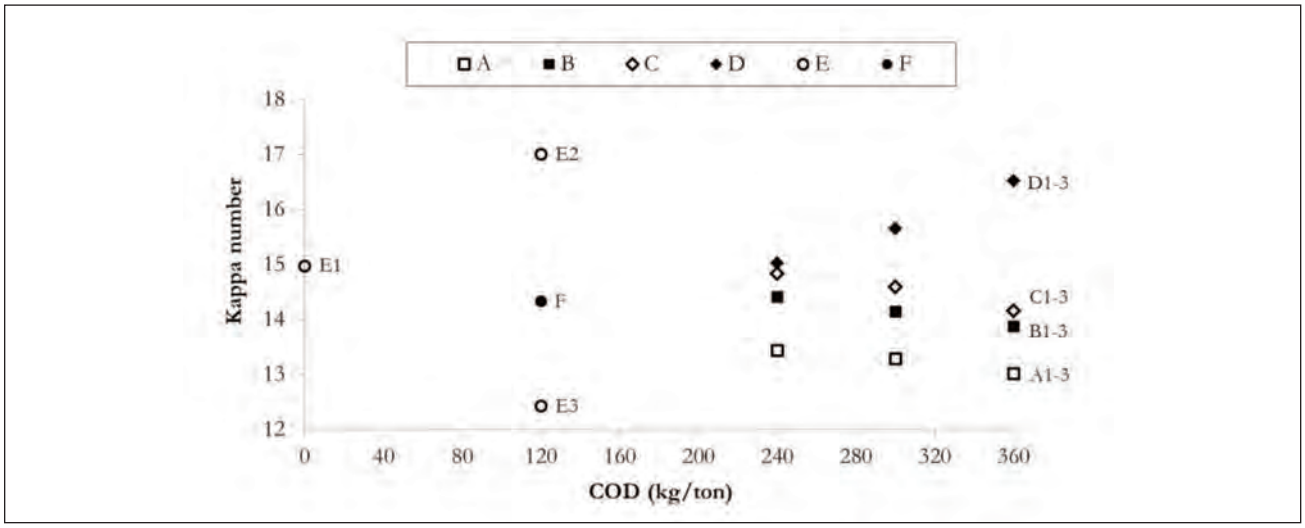
In order to ensure that the results in the previous experiments were not affected by the laboratory pulp washing, a further set of experiments was performed using unwashed pulp (pulp II in Table I), i.e., pulp sampled at the mill's wash press outlet in Fig. 1 (at approximately 30% consistency). Five series of experiments were performed where the additions of unoxidized and oxidized filtrates were altered according to **Fig. 6**. The unwashed pulp had a COD contribution of 120 kg/ton (sample F). The actual O_2 delignification feed at this mill corresponded to sample A3 at the time of collecting the pulp and filtrate samples. A previous study using an inline sensor for measurement of dissolved lignin in the O_2 delignification stage inlet at the same mill showed that the COD typically varied between 90 and 390 kg COD/ton [4].

The pulp (II) sample used in these experiments had a significantly lower pulp viscosity than the pulp (I) used in the experiments (see Table I). According to Miller et al. [9], lower pulp viscosity indicates that the fiber structure is more open and lignin reaction sites more accessible, thus making the pulp more reactive. Some pulp (II) was therefore washed and oxygen delignified for comparison. Note that sample E1 did not contain any dissolved matter; hence, the COD is 0 kg/ton in Fig. 6.

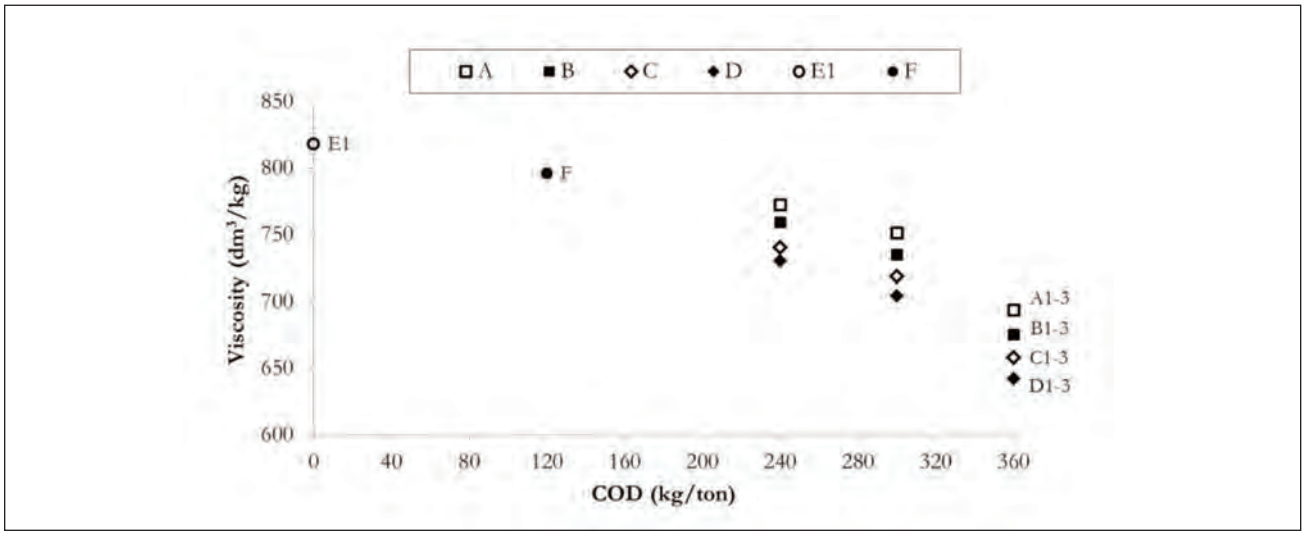
The kappa numbers after oxygen delignification of pulp (II) are shown in **Fig. 7**. The two washed samples with added unoxidized and oxidized filtrates (E2 and E3) resulted in kappa numbers that were in agreement with the previous studies with washed pulp samples. The kappa number for the sample containing only unwashed pulp (F) was 0.5 units lower than that of the washed sample (E1), indicating that slightly more than half of the pulp's dissolved matter was oxidized. Note that the oxygen delignification feed consisted of a mixture of unoxidized and oxidized filtrates, and this distribution varies from one mill to another mill. Results by Miller et al. [10] are in agreement with this, as the authors showed that 70%–92% of the dissolved matter entering the O_2 stage consisted of oxidized dissolved matter. Note that this percentage was the actual O_2 delignification feed, thus including the dilution with the oxidized filtrate as well.



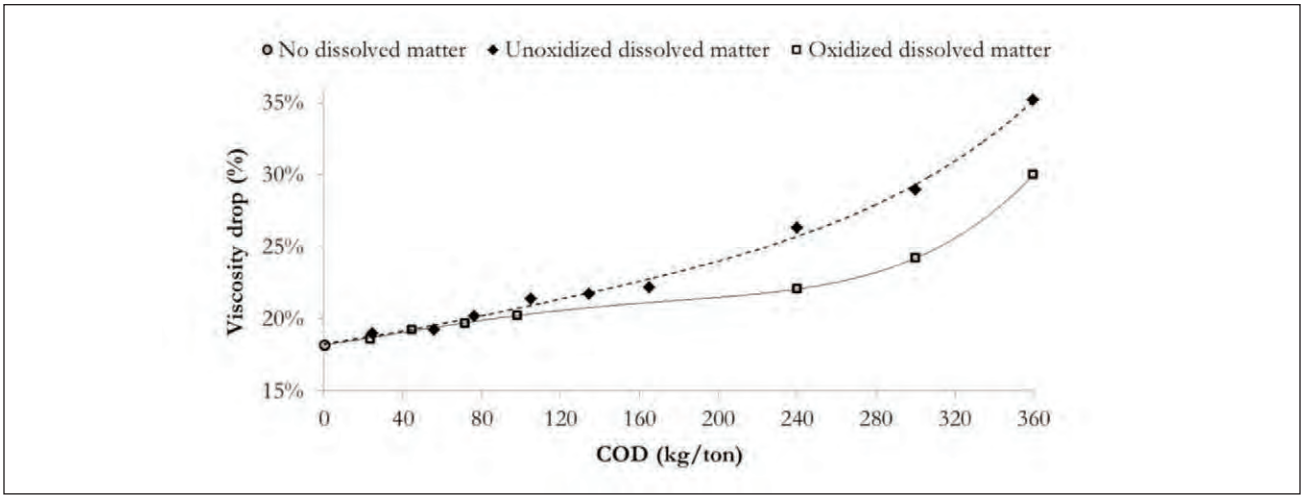
6. The amount and origin of COD in the experiments with unwashed pulp.



7. Kappa number vs. COD for the different experiments.



8. Viscosity vs. COD for the different experiments with unwashed pulp.



9. Viscosity drop vs. COD with unoxidized and oxidized filtrates. Pulp (I) is 0–165 kg COD/ton and pulp (II) is 240–360 kg COD/ton.

When comparing series A and D, it is clear that delignification benefited from increasing amounts of oxidized filtrate. The highest delignification was for sample A3, which resulted in a kappa number 1.5 units lower than that for the unwashed reference sample (F). From the kappa numbers of the D series, it is again evident that unoxidized filtrate had a negative impact on the delignification, which was more pronounced at high COD levels. Kappa numbers from the B and the C series further confirmed that the effect of additional unoxidized dissolved matter is always negative for delignification, while the effect of additional oxidized dissolved matter is always positive.

The results showed that good washing before the O_2 stage is important in order to remove as much as possible of the unoxidized dissolved matter. Oxidized filtrate is currently being used for dilution before the O_2 stage in mills, and the results indicate that this is very beneficial in order to exploit the positive effect of oxidized dissolved matter, at the same time minimizing the impact of any carryover of unoxidized dissolved matter.

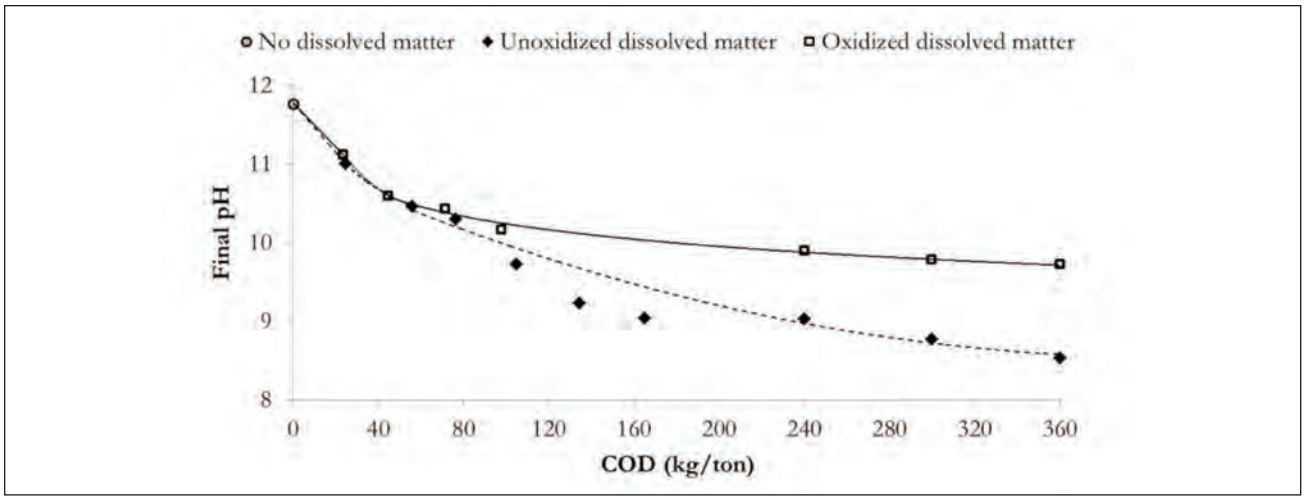
The pulp viscosities for series A to D, along with the reference samples E1 (washed pulp) and F (unwashed pulp), are shown in **Fig. 8**. It can be seen that the viscosity decrease was more pronounced at higher COD levels. It is also evident that there was a difference between unoxidized and oxidized dissolved matter that was not observed at lower COD levels in the previous experiments with washed pulp (I).

Since the starting viscosity prior to the O_2 stage was much lower for this pulp (pulp [II]) compared to the experiments with well washed pulp (pulp [I]), the percentage decrease of pulp viscosities is a better way to compare the results; this is shown in **Fig. 9** for comparison. All of the viscosities for the experiments with pulp (I) are shown, but only series A to D with pulp (II) are shown. The viscosity drop due to dissolved matter appeared rather moderate up to around 200 kg COD/ton, i.e., less than 5% relative; furthermore, the impact of unoxidized and oxidized filtrates was very similar. However, the viscosity decrease was more notable at the higher COD values, i.e., above 200 kg/ton, and the unoxidized filtrate showed a more detrimental impact than the oxidized filtrate.

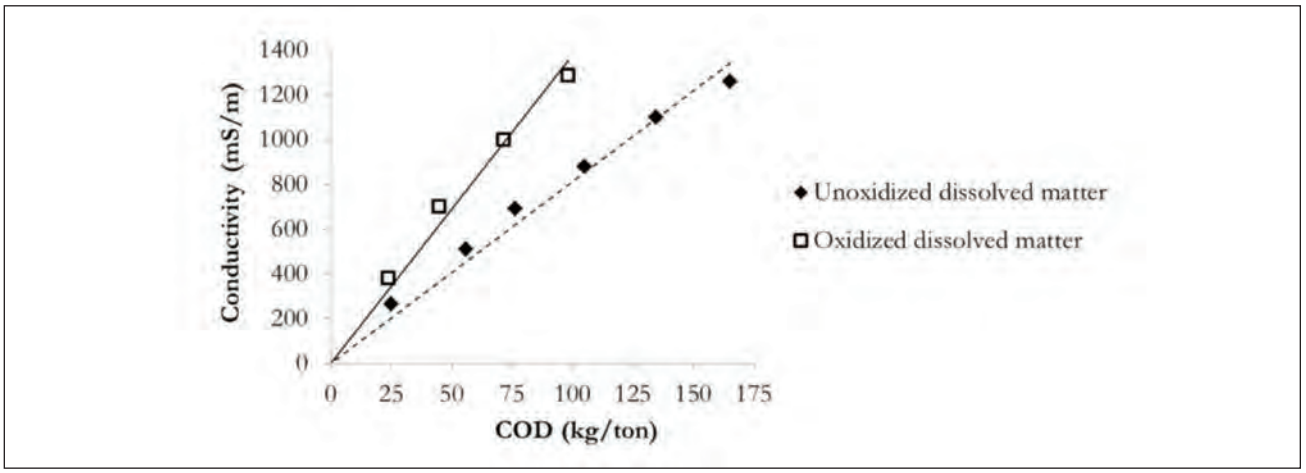
According to **Fig. 10**, there was a significant difference between the final pH values for additions of unoxidized and oxidized filtrates that were not observed in the experiments with pulp (I) using lower levels of oxidized dissolved matter. The final pH values for A and D series using pulp (II) are used for the comparison. It can now be seen that the unoxidized dissolved matter consumed significantly more hydroxide than the oxidized filtrate above 100 kg COD/ton. This is in agreement with a previous report [10], which stated that unoxidized dissolved matter has a higher chemical demand than oxidized filtrate, thus consuming more hydroxide and oxygen. Due to the dissolved matter, competing reactions between fiber-bound lignin and dissolved lignin occur, and hydroxide and oxygen are free to react with both types of lignin [7,8,10]. These reactions lower the delignification rate, and the poor delignification for the unoxidized filtrate could partly be explained by this.

Previous reports by Miller et al. [10] suggested that the viscosity loss was only significant when the final pH was below 9.7. The final pH for the oxidized filtrates remained at or above 9.7 at all COD levels, whereas the final pH dropped below this pH at COD levels above 100 kg/ton for the unoxidized filtrates. It can be seen in Fig. 9 that the viscosity drop was larger above 100 kg COD/ton for the unoxidized filtrate, which thus is in agreement with Miller et al. [10].

The oxidized filtrate contains a larger amount of carbonate ions than the unoxidized filtrate because of the previous exposure to oxygen, where dissolved organic matter was oxidized to carbonate [8,9]. A higher carbonate concentration will shift the equilibrium in Eq. (1) to the right, thus producing not only more bicarbonate or carbon dioxide, but also more NaOH. According to Miller et al. [8], the carbonate ion is a weaker base than the hydroxide ion and the rate would hence be hindered. However, the pulp delignification is significant-



10. Final pH vs. COD with unoxidized and oxidized filtrates. Pulp (I) is 0–165 kg COD/ton and pulp (II) is 240–360 kg COD/ton.



11. Conductivity vs. COD with unoxidized and oxidized filtrates.

ly improved with oxidized dissolved matter, and the presence of the carbonate ion could partly explain these results, as NaOH could potentially be produced. The carbonate ion could also act as a pH buffer in the oxidized filtrate [13], thus explaining the higher final pH compared to the unoxidized filtrate.

$$CO_3^{2-} + H_2O \leftrightarrow HCO_3^- + OH^- \leftrightarrow CO_2 + 2\ OH^- \qquad (1)$$

To assess the ionic strength of the respective filtrate, conductivity was measured. The results are plotted in **Fig. 11**. As expected, the oxidized filtrate had a substantially higher conductivity, and subsequently higher ionic strength, than the unoxidized filtrate. The difference in ionic strength or alkalinity could explain part of the differences in delignification and viscosity seen for the unoxidized and oxidized dissolved matter. Subsequently, the use of end pH alone may have limitations for an optimal O_2 stage control.

As described in the experimental section, tests comparing the addition of aerated and non-aerated unoxidized filtrates were made in order to rule out any impact of HS^- ions. However, another potential impact of sulfur species is $S_2O_3^{2-}$ ions, since they can be oxidized further to SO_4^{2-} in an O_2 stage and thus consume NaOH. The thiosulfate content of the filtrates was not determined in the study, but in case the content was higher in the unoxidized filtrate than in the oxidized one. This can also partly explain the relatively higher NaOH consumption thereof and the subsequently lower degree of delignification observed for experiments using filtrates with unoxidized dissolved matter. Further experiments are, however, required to confirm this hypothesis.

CONCLUSIONS

- Unoxidized and oxidized dissolved matter had different impacts on the delignification in a laboratory O_2 stage. Subsequently, the impact depended on the relative amount of these two types of filtrates in the pulp slurry. Unoxidized dissolved matter had a negative impact on the delignification, while oxidized dissolved matter had a positive impact.
- With the conditions employed in the laboratory experiments, any contribution of NaOH from either type of dis-

solved matter, unoxidized or oxidized, only had a very small impact on the delignification. This observation could not explain the positive impact due to oxidized filtrate nor the negative impact due to unoxidized filtrate.

- Both unoxidized and oxidized dissolved matter had a negative impact on the pulp viscosity. At higher COD levels, the unoxidized dissolved matter is more negative than the oxidized one.
- Both unoxidized and oxidized dissolved matter consumed hydroxide and the final pH after the O_2 stage decreased. At higher COD, the final pH when using unoxidized filtrate was significantly lower than that when using oxidized filtrate.
- The relative impact on delignification and viscosity degradation (i.e., selectivity) when using oxidized filtrate was very similar to that of using a higher NaOH charge. When using unoxidized filtrate, the selectivity was significantly impaired since the degree of delignification was low and the viscosity drop high.
- Good pre- and post-O_2 washing is important for high delignification and low chemical consumption, both in the O_2 stage and the subsequent bleach plant. The harmful unoxidized dissolved matter should therefore be removed as much as possible before the O_2 stage. The industrial standard to recirculate post-O_2 washing filtrate means the beneficial effect of the oxidized dissolved matter is utilized.
- Differences in the ionic strength of the unoxidized and oxidized dissolved matter in the filtrates may be related to their different impacts on delignification. It follows that using terminal pH for NaOH charge control may have some limitations for an optimal O_2 stage control at the industrial scale. **TJ**

ACKNOWLEDGEMENTS

This study was performed within the Industrial Graduate School VIPP (Values Created in Fiber Based Processes and Products) at Karlstad University, Sweden, with financial support from the Knowledge Foundation, Sweden.

LITERATURE CITED

1. Rydholm, S.A., *Pulping Processes*, Interscience Publishers, New York, 1965.
2. Genco, J.M., van Heiningen, A.R.P., and Miller, W., in *The Bleaching of Pulp* (A.W. Rudie and P.W. Hart, Eds.), TAPPI Press, Atlanta, GA, USA, 2012.
3. Hart, P.W., *TAPPI J.* 10(7): 37(2011).
4. Wilke, C., Andersson, N., Van Fleet, R., et al., *TAPPI J.* 15(3): 167(2016).
5. Iijima, J.F. and Taneda, H., *J. Pulp Pap. Sci.* 23(12): 561(1997).

ABOUT THE AUTHORS

In a previous study, we showed that dissolved lignin in the first chlorine dioxide stage consumed, per kappa number, approximately the same amount of bleaching chemicals as fiber-bound lignin. The aim of the current study was to investigate whether this was also the case in the oxygen (O_2) delignification stage.

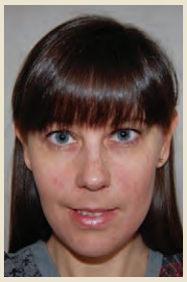
Many studies have been carried out on O_2 delignification over the years, and the results of these studies differ significantly with respect to the impact of dissolved matter. None of the previous studies has shown the same effects that we presented in our study, and our results are therefore unique.

The biggest challenge was to decide how to simulate, in a laboratory, the complex chemical reactions that take place in a commercial O_2 delignification stage, where temperature, pH, and dissolved matter influence each other in a very dynamic manner. We tried to solve this problem by using industrial filtrates from only one kraft pulp fiber line.

For us, the most interesting result was that the two different types of dissolved matter into the O_2 delignification stage had opposite effects on delignification. Despite different delignification, the pulp viscosities were affected similarly by unoxidized and oxidized dissolved matter.

For mills, good pre-O_2 washing is important for high delignification in the O_2 delignification stage, so it is important to maximize the washing efficiency. Recirculation of post-O_2 washing filtrate has beneficial effects due to the oxidized dissolved matter, so optimizing the recirculation could potentially increase the delignification.

In the future, we plan to further investigate the effects of carbonate ions and thiosulfate ions in the O_2 delignification stage.



Wilke



Andersson



Germgård

Wilke is development engineer at BTG Instruments AB, Säffle, Sweden, and post-graduate student at Karlstad University in Karlstad, Sweden. Andersson is head of R&D and Business Development at BTG Instruments AB, Säffle, Sweden. Germgård is professor of Pulp Technology at Karlstad University, Karlstad, Sweden. Email Wilke at caroline.wilke@btg.com.

6. Magnotta, V.L. and Courchene, C.E., "Process effects of entrained black liquor and oxygen stage filtrate solids on oxygen delignification," *TAPPI Pulping Conf.*, TAPPI Press, Atlanta, 1982.
7. Vuorenvirta, K., Fuhrmann, A., and Gullichsen, J., "Effect of black liquor carry-over on selectivity of oxygen delignification," *Int. Pulp Bleaching Conf.*, TAPPI Press, Atlanta, 2000.
8. Miller, W., Sullivan, D.P., Genco, J.M., et al., "Medium consistency oxygen delignification design using a two phase concept. Part 2. High solids carry-over," *TAPPI Pulping Conf.*, TAPPI Press, Atlanta,1998.
9. Miller, W.J., Kwon, H., Liukkonen, A., et al., "Medium consistency oxygen delignification design utilizing a two phase concept - Part I," *TAPPI Pulping Conf.*, TAPPI Press, Atlanta, 1995.
10. Miller, W.J., Shackford, L.D., Jiang, H., et al., *Tappi J.* 74(2): 117(1991).
11. Bokstrom, M. and Norden, S., "Extended oxygen delignification," *Int. Pulp Bleaching Conf.*, Gummerus Kirjapaino Oy, Helsinki, 1998.
12. Singh, R.P. and B.C. Dillner, "Oxygen delignification," in *The Bleaching Of Pulp* (R.P. Singh, Ed.), TAPPI Press, Atlanta,1979.
13. Sankari, M. and Dillner, B.C., *Nord. Pulp Pap. Res. J.* 19(2): 264(2004).

Process for producing acetic acid in hardwood kraft pulp mills

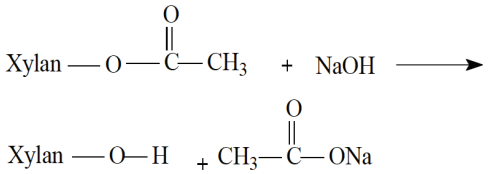
RAVIKANT PATIL, JOSEPH GENCO, HEMANT PENDSE, AND ADRIAAN VAN HEININGEN

ABSTRACT: To determine the economic feasibility of producing acetic acid from commercial hardwood chips in kraft pulp mills, laboratory experiments were conducted to obtain sufficient data to perform a preliminary economic analysis for a proposed acetic acid recovery process. The acetyl groups in northeast hardwood were hydrolyzed from the xylan polymers in the wood to obtain sodium acetate. The extraction experiments were performed by using 4%–6% sodium hydroxide at low temperature (50°C–80°C). Sodium acetate from the extract was concentrated and then converted into acetic acid and sodium hydroxide by salt splitting using bipolar membrane electrodialysis (BPMED). Flow diagrams were prepared and cost estimates made for the capital and operating costs for the proposed acetic acid recovery process. The discounted cash flow rate of return on investment was estimated for pulp mills in the range of 1000–2000 tons/day. A preliminary economic analysis showed that the discounted cash flow rate of return on investment is primarily a function of (1) the plant size, (2) the selling price of acetic acid, and (3) the content of acetyl groups present in wood species. The income for the process and thus the rate of return on investment increases with increasing acetyl content in the wood and selling price of the acetic acid. When food grade acetic acid is produced, for example, the rate of return varies between 9% and 16% depending upon the size of the pulp mill, assuming the wood contains 3.5% acetyl groups on a dry basis and the selling price of acetic acid is US$900/ton.

Application: A process to recover acetic acid or acetate salt as a byproduct of kraft pulp mills will be useful to scientists and engineers who are developing the biorefinery concept.

Technical grade acetic acid is widely used in the manufacture of vinyl acetate monomer; polyethylene terephthalate; and a host of other industrial chemicals including ethyl and butyl acetate esters, monochloroacetic acid, ketene and diketene derivatives, pharmaceuticals, and dyestuffs. The worldwide market for technical grade acetic acid was about 11.9 million metric tons in 2012 and is expected to grow to 15 million metric tons by 2022 [1]. The global market for food grade acetic acid and other organic acids (citric, lactic, and malic acids) grows at about 7% annually. The market for organic acids for use in foodstuffs is expected to reach US$5.2 billion by 2018 [2]. Paper companies can increase their revenue by producing acetic acid in addition to conventional pulp and paper products. Because the market for acetic acid is large and growing, production of acetic acid at kraft mills would be small relative to the total market and would not be disruptive.

Hardwoods contain approximately 3%–4% acetyl (CH_3CO-) groups on a dry weight basis. The acetyl groups are located in hemicelluloses, primarily the glucuronoxylan polymer [3]. In a conventional hardwood kraft pulp mill, the acetyl groups end up as sodium acetate in the black liquor and are burned for recovery of the sodium content and energy in the recovery boiler. Recent work by Patil [4] has shown that acetyl groups in wood hemicelluloses can be readily hydrolyzed by using dilute alkali at low temperature (50°C) before the pulping process to produce an aqueous solution containing approximately 15 g/L of sodium acetate [5], as in Eq. (1):



(1)

The results of semi-batch feed and bleed mode experiments performed using model sodium acetate solution have shown that up to 170 g/L of acetic acid and 30 g/L of sodium hydroxide can readily be produced using bipolar membrane electrodialysis (BPMED) [6]. Although higher concentrations of sodium hydroxide can be produced using BPMED, 30 g/L concentration of sodium hydroxide is an appropriate target for caustic recycle back to the extraction step for the deacetylation reaction to occur. The feed and bleed mode experiments also showed that the efficiency of the BPMED process can be improved if the sodium acetate in the raw wood extract and the accompanying chip wash liquid were concentrated to about 85 g/L.

Acetic acid is an attractive chemical for recovery at kraft mills for the following reasons. First, a significantly higher selling price for acetic acid can be achieved if acetic acid is

concentrated to about 99% by weight or converted into food grade reagent. A liquid-liquid extraction plant to produce food grade acetic acid from an effluent stream at a sulfite pulp mill is operated by A.G. Lenzing in Austria [7]. Second, depending upon the amount of sodium acetate removed from the wood, the use of BPMED allows recovery of most of the sodium hydroxide used in the extraction process at little additional cost. It has been shown that up to 90% of the acetyl groups present in the raw wood can be recovered by washing the extracted chips before adding effective alkali (EA) and completing the kraft pulping process. Finally, the proposed process can be fully integrated into an existing kraft mill. It has been shown that pulp obtained from the two-stage process has the same yield and physical properties as conventional kraft hardwood pulps provided white liquor is used in both the extraction and pulping stages [8].

The objectives of our work were to (1) demonstrate splitting of sodium acetate from hardwood caustic extract using BPMED and (2) present the results of a preliminary economic analysis for production of acetic acid in a two-stage kraft pulping process. In the present study, acetyl groups were extracted in the form of sodium acetate before pulping and subsequently converted into acetic acid and sodium hydroxide using BPMED. The preliminary economic analysis was performed using the data from the laboratory study.

BACKGROUND

Retsina and coworkers evaporated the acetic acid in wood hydrolysate and neutralized the condensate to form acetate salts that were subsequently separated using reverse osmosis [9]. Tertiary amine-type ion exchange resin was evaluated for separating acetic acid from activated charcoal–treated prehydrolysis liquor in kraft pulp mills [10]. The results showed that about 66%–84% of acetic acid could be recovered using this method. Reactive extraction using trioctylamine/octanol was also evaluated for separating acetic acid from kraft prehydrolysis liquor [11]. About 10%–15% acetic acid solution was produced when the ratio of masses of organic to aqueous phase was 40 and an equimolar amount of caustic was used to regenerate the solvent.

Kassotis and coworkers describe converting 6% solution of sodium acetate into 35% acetic acid and about 8% sodium hydroxide using a three-compartment BPMED cell at a current density of 109 mA/cm^2 [12]. In another laboratory-scale study using a three-compartment cell, 4%–12% solutions of sodium acetate were converted into 8%–12% acetic acid solution [13]. The membranes used in this study were synthesized using ion exchange resins. Eurodia Industry, Germany, commissioned a two-compartment pilot-scale BPMED unit that converted a byproduct stream of 22% sodium acetate into 18% acetic acid and 6% sodium hydroxide. The current efficiency was optimum and the payback period was less than two years [14]. Yu and coworkers used a two-compartment BPMED system to concentrate a dilute 0.2% solution of acetic acid in wastewater to as much as 70% [15].

BPMED technology has been previously applied to kraft mills. To overcome the high capital cost of the kraft recovery system for small pulp mills, BPMED was studied for recovering organic and inorganic salts from spent liquor [16]. A similar process has been developed for use in soda-anthraquinone pulping where lignin in the spent liquor was precipitated by the addition of acid; sugars were separated using ultrafiltration and sodium acetate was crystallized and converted into acetic acid and caustic using BPMED [17]. BPMED has been used to selectively remove chloride ion from the kraft recovery cycle to prevent corrosion problems [18]. Paleologou and Davis applied a BPMED process to split sodium sulfate originating from the chlorine dioxide generation system into caustic and sulfuric acid for internal use in the mill [19–21]. An economic analysis of this process showed the rate of return on investment was 24.6% when economic credit was given for both the sulfuric acid and caustic [22].

Process description

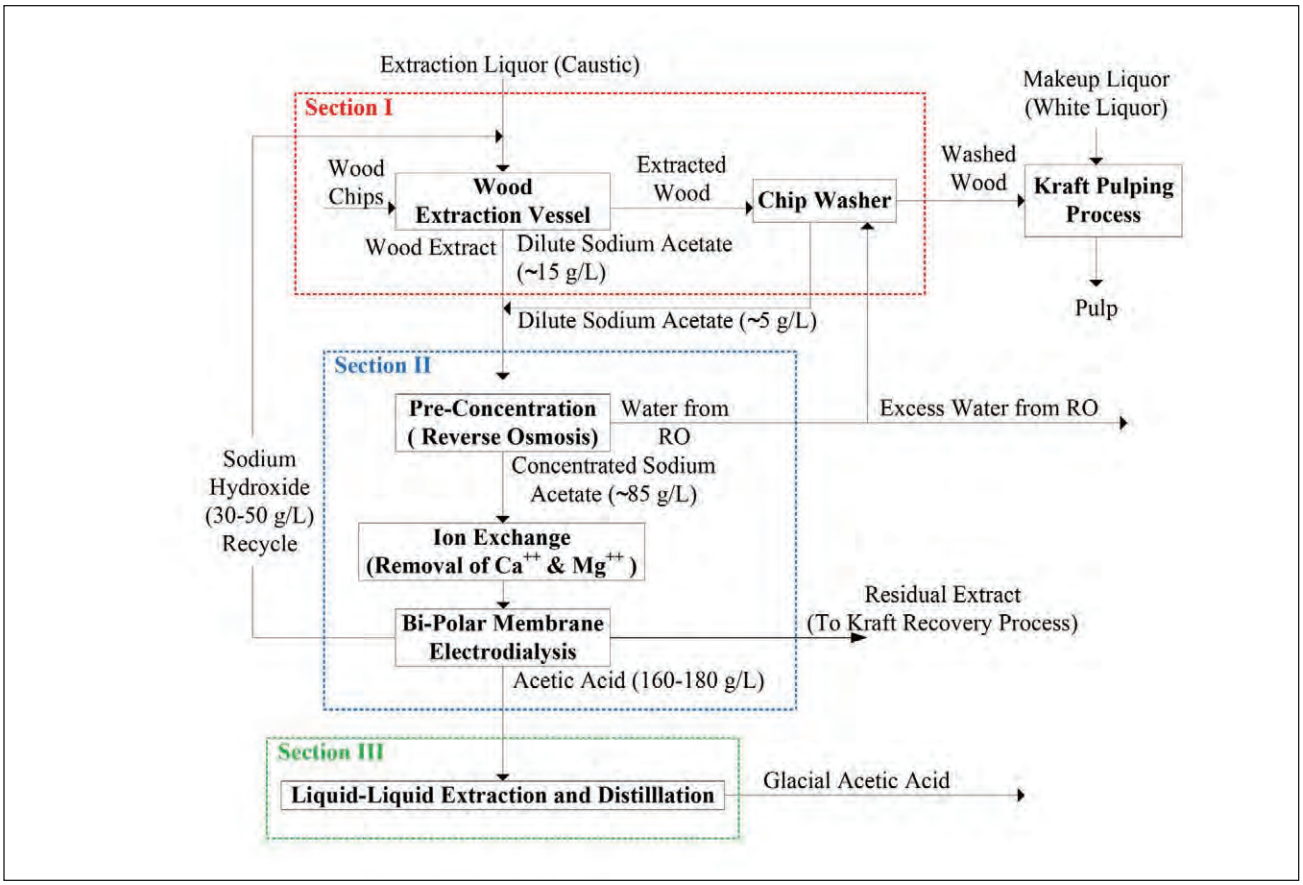
Figure 1 shows a block flow diagram of the overall process that consists of three sections; extraction and chip washing (section I), preconcentration and BPMED (section II), and product recovery by liquid/liquid extraction and distillation (section III). A detailed description of the important unit processes follows.

Sodium acetate extraction

Wood chips are presteamed in a steaming vessel for 15 min and conveyed to the extraction vessel where they are extracted using dilute sodium hydroxide solution for 2 h at low temperature. The extraction step is conducted at 50°C (6% EA) or 80°C (4% EA) at a liquid-to-wood (L/W) ratio of 3.5. The extraction can be performed in an atmospheric vessel because the extraction temperature is below 100°C. The extraction liquor is then drained from the partially macerated wood chips following the extraction step and the extracted wood chips are washed using warm recycled water in a chip washer. The chips are washed with sufficient water to remove approximately 85%–90% of the sodium acetate that was formed in the deacetylation reaction; the dilution factor is about 1. The dilute extract is sent for processing into acetic acid and caustic while the partially macerated wood chips are sent to the kraft digester for processing into brownstock pulp.

Kraft pulping

In the second stage of the kraft pulping process, the white liquor charge would be adjusted to maintain the pulp yield and properties equal to those in a conventional one-stage kraft pulping process. For pulping mixed northeast hardwoods, for example, the total alkali applied in the two-stage pulping process would be 14.9% EA white liquor (on a sodium oxide basis) at a L/W ratio of 3.5. The top temperature would be set at 160°C to give an H-factor of 780 h. The difference is simply that the alkali would be split between the two stages. For example, because 4% or 6% EA (sodium hydroxide) was applied in the



1. Modified kraft pulp mill for the production of acetic acid using bipolar membrane electrodialysis (BPMED).

extraction step, 8.9%–10.9% EA would be applied in the second stage. Thus, the total alkali applied would be the same in the two-stage process that would equal that in a conventional one-stage process. Using this strategy, Patil [8] has shown that brownstock pulp with equivalent properties can be obtained.

Converting sodium acetate into acetic acid and caustic

The combined drained extract and wash liquor are preconcentrated using reverse osmosis. The concentrated sodium acetate solution is then passed through an ion exchange column to remove multivalent ions. The resultant solution is then processed in the BPMED cells to produce acetic acid and sodium hydroxide, which is recycled back to the extraction process. The concentrated acetic acid is sent to liquid-liquid extraction and a series of distillation columns to produce glacial acetic acid. The concentrated acetic acid is converted into food grade acetic acid to achieve a higher selling price [7].

Purification of acetic acid

Acetic acid can be recovered using a combination of liquid-liquid extraction and fractional distillation [23]. A variety of solvents can be used for extracting acetic acid from water; notable among them are ethyl acetate, isopropyl acetate, and methyl tertiary butyl ether (MTBE) [24]. Reactive extraction using trioctylamine/octanol has also been proposed [11]. Special techniques are sometimes employed because acetic acid forms an azeotrope with water. Commercial acetic acid separation processes consist of (1) an extraction tower for removing acetic acid from the water phase, (2) a rectification tower for purification of the acetic acid and for recovery of the extraction agent, and (3) a water-stripping tower for removal of water and reclaiming residual solvent. Depending on the number of equilibrium stages in the extraction tower, the residual concentrations of acetic acid can be reduced to between 0.1% and 0.5 wt% acetic acid in the extraction tower. Because the aqueous phase leaving the extraction tower is simultaneously saturated with the extraction agent, the residual solvent is recovered in the downstream stripping tower, which can be operated either as a conventional distillation tower or as a steam stripper by the injection of live steam.

Bipolar membrane electrodialysis

Sodium acetate can be readily split into acetic acid and sodium hydroxide by application of an electrical field in a BPMED cell (Eq. [2]):

$$NaAc + H_2O + Energy_{Electrical} \rightarrow HAc + NaOH \quad (2)$$

Detailed information regarding the basic principles and general process guidelines for BPMED are available in the lit-

erature [25-27]. The current efficiency (η) for splitting or transferring a given mass of sodium acetate (W) is the ratio of the theoretical ($C_{Theoretical}$) to the actual (C_{Actual}) charge required to transform the sodium acetate into the corresponding acetic acid and sodium hydroxide (Eq. [3]):

$$\eta = \frac{C_{Theoretical}}{C_{Actual}} = \frac{W \cdot F}{E \cdot N \cdot C_{Actual}} \cdot 100 \quad (3)$$

where E = equivalent or molecular weight of sodium acetate (gm/equivalent), N = number of cell pairs, and F = Faraday's constant (96,485 coulombs/equivalent).

The actual charge (C_{Actual}) is simply the integral of the current (i) over the time that the voltage is applied across the cell pairs (Eq. [4]):

$$C_{Actual} = \int_0^t i \cdot dt \quad (4)$$

where i = current (A) and t = time (s).

The electric energy (E_{Elec}) is calculated by integrating the product of voltage (V) and current (i) with respect to time (t). E_{elec} is the sum of the energies required for transferring ions from one compartment to another and decomposing water molecules in the bipolar membranes (Eq. [5]):

$$E_{Elec} = \int_0^t V \cdot i \cdot dt \quad (5)$$

The degree to which a desired ion is selectively removed from the feed solution is a measure of the efficiency of the electrodialysis system. Conventional selectivity (S) is defined as the ratio of molar flow rate of the desired product (acetic acid) to that of an undesired product. However, conventional selectivity is not useful for characterizing efficiency when a reaction system leads to the formation of more than one undesired product. In such cases, the relative number of moles of each species transported (or split) is more useful. It is defined as the ratio of the number of moles of a given salt transported across the membranes to the total moles of all salts transported in the same direction (Eq. [6]):

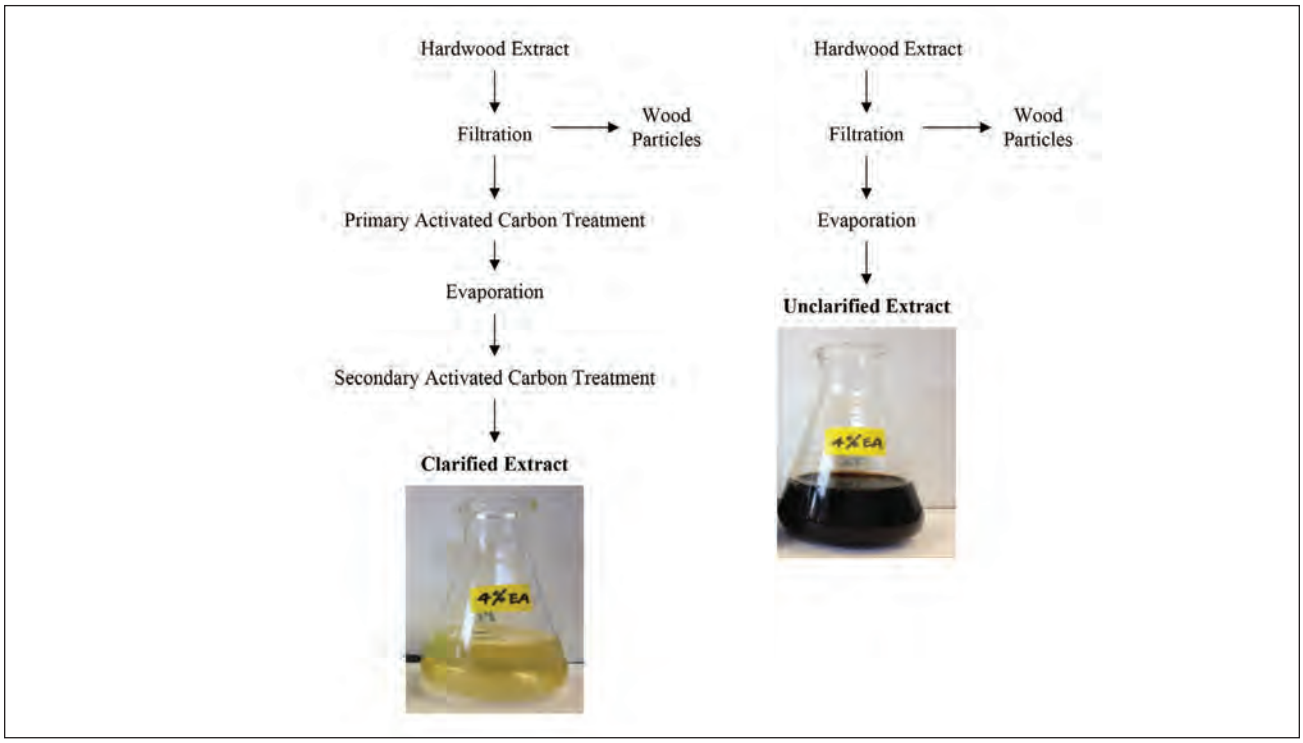
$$RM_i = \frac{V_F(0) \cdot C_{F,i}(0) - V_F(t) \cdot C_{F,i}(t)}{V_F(0) \cdot C_F(0) - V_F(t) \cdot C_F(t)} \quad (6)$$

where RM_i = relative number of moles of a given salt (sodium acetate) transported across membranes or split, V_F = volume of feed solution (m^3), $C_{F,i}$ = concentration of an ion in feed solution ($mol \cdot m^{-3}$) at time 0 and (t), and C_F = total concentration of all ions present in feed solution ($mol \cdot m^{-3}$) at time 0 and (t).

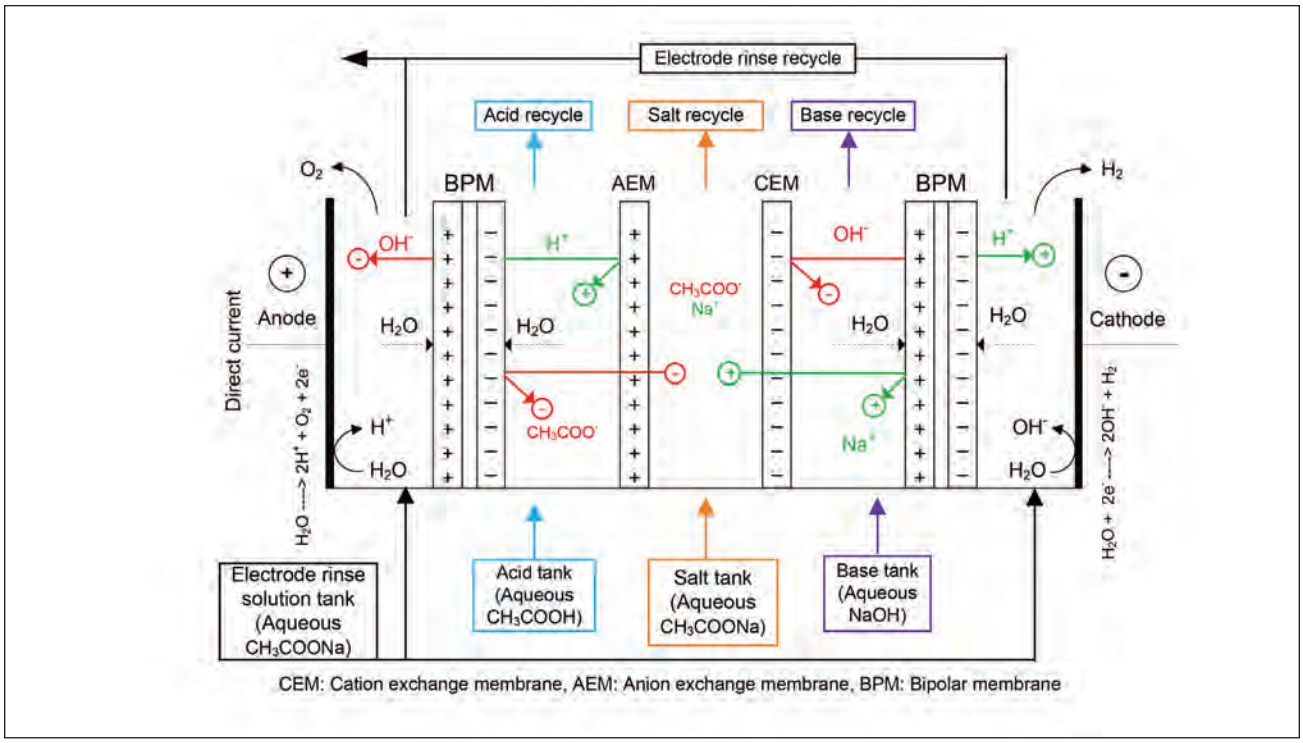
EXPERIMENTAL METHODS

Pretreatment of hardwood extract

Figure 2 illustrates the procedure used to prepare the pretreated hardwood extracts. Although reverse osmosis is the proposed method for the preconcentration of wood extract, evaporation was used in the present study to simplify the laboratory work. The concentration of sodium acetate in the pretreated extracts following evaporation was maintained at



2. Pretreatment of hardwood extract before use in the electrodialysis.



3. Arrangement of ion-exchange membranes in the BPMED cell.

47–57 g/L so that these solutions could be processed at a middle-level current density of about 40 mA/cm². The use of clarified solution allows the exclusive understanding of the effect of different salts present in the extract on the splitting of sodium acetate and protects ion exchange membranes from possible fouling due to the lignin. However, because the activated charcoal is not easily regenerated, such type of pretreatment is expensive and thus will adversely affect the economic viability of the process. Therefore, additional experiments were performed to demonstrate the processing of unclarified extract in BPMED. For practical applications, the effect of lignin on ion exchange membranes can be determined by performing long-term stability studies.

Detailed information about the equipment used in this study and the experimental procedure is given by Patil [8].

Experimental apparatus

The experimental BPMED cell was manufactured by PCCell/PCA GmbH, Heusweiler, Germany. **Figure 3** shows the arrangement of membranes for the unit cell pair of a three-compartment BPMED cell. The experimental cell consisted of five cell pairs of cation, anion exchange, and bi-polar membranes (Neosepta CMB/AHA/BP-1, Tokuyama America; Arlington Heights, IL, USA). The surface area of each membrane was 64 cm². Spacers were placed between adjacent membranes, which allowed the flow of solutions between the membranes. The maximum allowed voltage drop for the BPMED cell used in this study was 16.4 V. The equipment also consisted of a heat exchanger, which maintained the temperatures of all solutions below 25°C.

Experimental procedure

The BPMED process was operated at constant current mode. All experiments were conducted in the batch recycle mode. The feed solution was recirculated at a flow rate of about 550 mL/min, which corresponded to a superficial velocity of 5.1 cm/s. It is necessary to maintain the applied current density below its limiting value to avoid the loss of electric energy resulting from the decomposition of water at overlimiting currents. The limiting current density data for use with the equipment has been reported previously [6]. In the BPMED experiments, the initial liquid placed in the acid-receiving vessel was one liter of 17 g/L sodium acetate. The initial liquid placed in the base-receiving vessel and the liquid used as the electrode rinse solution consisted of one liter each of 6 g/L and 40 g/L of sodium hydroxide, respectively. Approximately the same amounts of electric energy and charge were applied in the BPMED experiments using pretreated extracts.

Small quantities of sodium formate, sodium lactate, and sodium glycolate would be expected to be present in the extract under alkaline conditions. The formate, lactate, and glycolate ions are byproducts of the extraction process resulting from alkaline peeling and stopping reactions that occur simultaneously with the alkaline cleavage of the acetyl groups from the xylan hemicellulose polymers [28]. The concentrations of sodium acetate, sodium formate, sodium lactate, and sodium glycolate were measured at the conclusion of each experiment following conversion to their corresponding acid forms using high performance liquid chromatography (HPLC). Thus, the total concentration of all acids present in the final acid solution was separately determined by titration with base. This inde-

Parameter	Value
Acetic acid selling price (reagent and food grade)	US$600–900/ton
Pulp mill size	500–2000 tons/day
Acetyl group content in wood	3%–4% (on dry basis)
Fractional recovery of acetic acid	90% (with chip washing)
Project life	10 years
Startup period	18 months
Operating factor	95%
Tax rate	35%
Working capital	5% of fixed capital investment
Depreciation	Modified accelerated cost recovery system
Financing	100% equity, no loan

I. Assumptions used in the economic analysis.

pendent check was thought necessary because HPLC measurements might not identify all the component acids present in the acid solution. Sodium hydroxide was analyzed by titrating a sample of synthetic extract with 0.1 N hydrochloric acid.

METHODOLOGY FOR PRELIMINARY ECONOMIC ANALYSIS

The economic analysis was performed by estimating the capital investment and operating cost using standard methods described by Turton and coworkers [29]. The viability of the project was determined by estimating the discounted cash flow rate of return and payback period for the process. **Table I** shows the major assumptions made in this analysis. It was also assumed that mills would have sufficient utilities (waste treatment and steam generating capacity) to accommodate the new acetic acid process and no new capital would be incurred for upgrading these facilities. Only costs associated with tying the new process into the mill utility system were included in the analysis. The size of the kraft pulp mill was considered a parameter in the economic analysis. The analysis was performed for four plant sizes: a small plant (500 tons/day), a medium size plant (1000 tons/day), and two large (1500 and 2000 tons/day) kraft pulp mills.

RESULTS AND DISCUSSION

Composition of extract

Table II summarizes the composition and volumes of the pretreated (feed) solutions used in the BPMED experiments, as well as the concentration of the raw hardwood extract. A variety of sodium compounds are present in the extract in addition to sodium acetate, even at the low temperature used in the extraction experiments (80°C). Notably among these lesser compounds found in the raw extract are sodium formate, sodium lactate, and sodium glycolate, as well as lignin and component sugars. Because sodium formate and sodium lactate were also present in the extracts, it was expected that smaller quantities of formic and lactic acids would be present in the acid compartment in addition to the desired acetic acid product. For the extraction experiments conducted at 50°C, a similar concentration of sodium acetate was obtained, but lesser quantities of sodium formate, sodium lactate, and sodium glycolate were present in the extract [8].

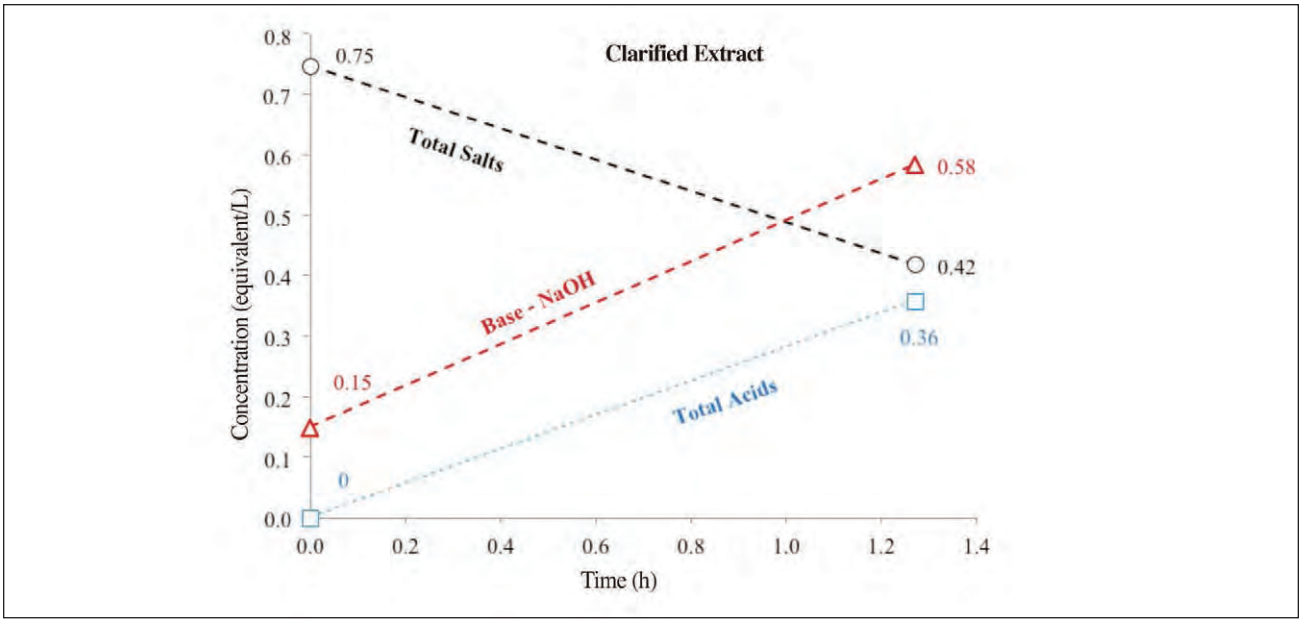
Salt splitting experiments using pretreated and concentrated extracts

Figures 4 and **5** show the variation in the concentrations of the salt feed solution and the acid and base product solutions for the BPMED experiments using the clarified and unclarified extracts, respectively. Only the initial and final concentration points were sampled and thus appear on the graphs. By comparing these figures, it can be seen that approximately the same amounts of salts were decomposed in both experiments. The total concentration of all acids present in the final acid solution from each experiment was about 0.36–0.38 equivalent/L. Similarly, the final base solutions contained about 0.56–0.58 equivalent/L of caustic.

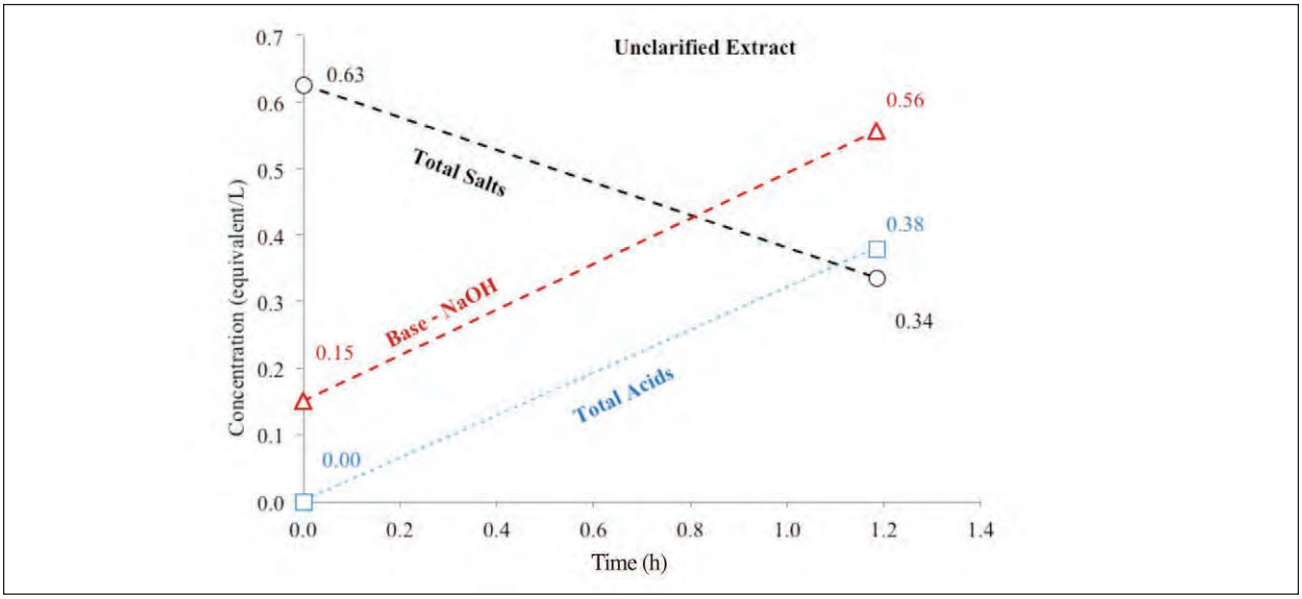
Tables III, **IV**, **V**, and **VI** summarize the composition data obtained in the BPMED experiments. Because both the clarified and unclarified feed solutions contained small amounts of sodium formate and sodium lactate, these salts were subsequently converted into the corresponding acids and sodium hydroxide in the BPMED electrochemical reactor. However, the total sugars and the lignin were predominately retained in the feed solutions and did not penetrate the membranes. The small amounts of sugars transferred from the salt to the acid and base solutions are thought to occur by diffusion because the component sugars are not charged. For the BPMED experiment performed using the clarified extract, the

Extract Type	Concentration, g/L						pH	Volume, L
	Sodium Acetate	Sodium Formate	Sodium Lactate	Sodium Glycolate	Total Lignin	Total Sugars		
Raw extract (dilute)	14.60	1.55	0.28	0.69	4.52	0.76	12.2	---
Concentrated unclarified extract	46.20	3.24	1.72	1.93	12.07	2.11	10.2	1.74
Concentrated clarified extract	56.50	3.28	1.18	1.09	0.62	0.25	10.5	1.64

II. Composition of pretreated hardwood extract (4% effective alkali [EA], 0% sulfidity, and 80°C; liquor-to-wood ratio [L/W] = 4).



4. Concentration profiles for the BPMED experiment performed using clarified extract.



5. Concentration profiles for the BPMED experiment performed using unclarified extract.

Concentrations, equivalents/L					Total Lignin, g/L	Total Sugars, g/L	pH	Volume, L
Solution	Sodium Acetate	Sodium Formate	Sodium Lactate	Sodium Hydroxide				
Initial salt	0.69	0.05	0.0105	0	0.62	0.25	10.5	1.64
Final salt	0.40	0.01	0.0060	0	0.48	0.23	11.5	1.54
Initial base	0	0	0	0.15	0	0	---	1.00
Final base	0.0012	0	0	0.58	0.0036	0.0040	---	1.11

III. Composition of salt and base solutions for the BPMED experiment performed using clarified extract (4% EA, 0% S, and 80°C; L/W = 4).

Solution	Concentrations, equivalents/L						Total Lignin, g/L	Total Sugars, g/L	Volume, L
	Sodium Acetate	Formic Acid	Lactic Acid	Acetic Acid	Total Acids, by HPLC*	Total Acids, by Titration			
Initial acid	0.21	0	0	0	0	0	0	0	1.00
Final acid	0.18	0.0450	0.0056	0.3075	0.3581	0.4040	0.26	0.043	1.16
Composition of Final Acid Solution, g/L									
	Formic Acid		Lactic Acid		Acetic Acid				
Final acid	2.1		0.5		18.5				
* HPLC = high performance liquid chromatography									

IV. Composition of acid solution for the BPMED experiment performed using clarified extract (4% EA, 0% S, and 80°C; L/W = 4).

Concentrations, equivalents/L					Total Lignin, g/L	Total Sugars, g/L	pH	Volume, L
Solution	Sodium Acetate	Sodium Formate	Sodium Lactate	Sodium Hydroxide				
Initial salt	0.56	0.05	0.0154	0	12.07	2.11	10.2	1.74
Final salt	0.32	0.01	0.0078	0	11.65	2.11	10.8	1.67
Initial base	0	0	0	0.15	0	0	--	1.00
Final base	0.0021	0	0	0.56	0.0034	0.004	--	1.11

V. Composition of salt and base solutions for the BPMED experiment performed using unclarified extract (4% EA, 0% S, and 80°C; L/W = 4).

Solution	Concentrations, equivalents/L						Total Lignin, g/L	Total Sugars, g/L	Volume, L
	Sodium Acetate	Formic Acid	Lactic Acid	Acetic Acid	Total Acids, by HPLC*	Total Acids, by Titration			
Initial acid	0.21	0	0	0	0	0	0	0	1.00
Final acid	0.18	0.0537	0.0113	0.3150	0.3800	0.3860	0.24	0.003	1.16
Composition of Final Acid Solution, g/L									
	Formic Acid		Lactic Acid		Acetic Acid				
Final acid	2.5		1.0		18.9				
* HPLC = high performance liquid chromatography									

VI. Composition of acid solution for the BPMED experiment performed using unclarified extract (4% EA, 0% S, and 80°C; L/W = 4).

total acid concentration determined using titration was about 10% higher than the HPLC measurement whereas, for the experiment with the unclarified extract, both values were almost equal.

Table VII shows the current efficiencies, the specific electric energy, the selectivity, and the relative number of moles of each species split in the BPMED experiments performed using pretreated extracts with compositions of about 45 g/L of sodium acetate in the feed. The current efficiencies and specific energies for the experiments performed with the pretreated extracts were similar to those of the experiments performed using model sodium acetate solution. The relative number of moles of each species split also indicates the fraction of the total useful electric energy spent for splitting the given salt molecule. Because the model sodium acetate solution contained only sodium acetate along with water, all of the useful electric energy was spent for splitting only sodium acetate. The pretreated extract contained additional salts such

Parameters	Type of Feed Solution*		
	Synthetic Sodium Acetate Solution	Clarified Extract	Unclarified Extract
Current efficiency for total acids (per HPLC** data), %	76	68	76
Current efficiency for base, %	80	81	81
Specific electric energy, kJ/equivalent of acid formed	382	424	411
Relative number of moles of each species split, %			
Sodium acetate	100	87.4	84.3
Sodium formate	------	11.1	12.9
Sodium lactate	------	1.5	2.8
Selectivity, moles of each acid formed per unit mole of formic and lactic acids formed			
Acetic acid	------	5.87	6.83
Formic acid	------	1.00	1.00
Lactic acid	------	0.21	0.12

* The concentrations of the sodium salts in the feed solutions are summarized in Tables III and V.

** HPLC = high performance liquid chromatography.

VII. Summary of the BPMED experiments performed using pretreated extracts (4% EA, 0% S, and 80°C; L/W = 4).

as sodium formate, sodium lactate, and sodium glycolate, which were also split along with sodium acetate. Hence, about 13%–15% of the useful electric energy was lost in splitting these additional salts.

Selectivity values shown in Table VII were calculated using Eq. (6). Selectivity data show that about 5–6 moles of acetic acid were formed for every mole of undesired product.

These experiments suggest that BPMED can be used to obtain a clear solution of concentrated acetic acid together with smaller quantities of formic acid and lactic acid, provided that the presence of lignin in the feed-salt solution does not lead to appreciable fouling of the membranes over extended run times. The mass balances for the major components of the extracts, such as sodium acetate, sodium formate, and lignin, could be close to 90%–100% depending upon the species.

Results of economic analysis

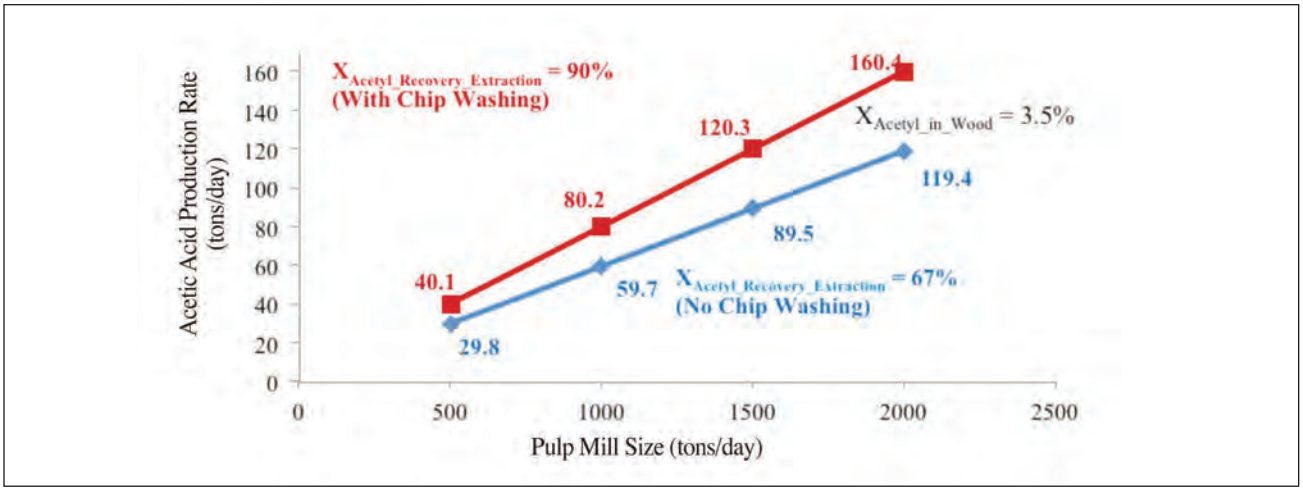
Acetic acid production rates

Figure 6 shows the rate of production of acetic acid as a function of pulp mill size. When chip washing is included in the process, about 40–160 tons/day of acetic acid can be produced depending upon the size of the pulp mill. If the extract is simply drained from the chips and no washing is performed, then only about 75% of these values can be obtained.

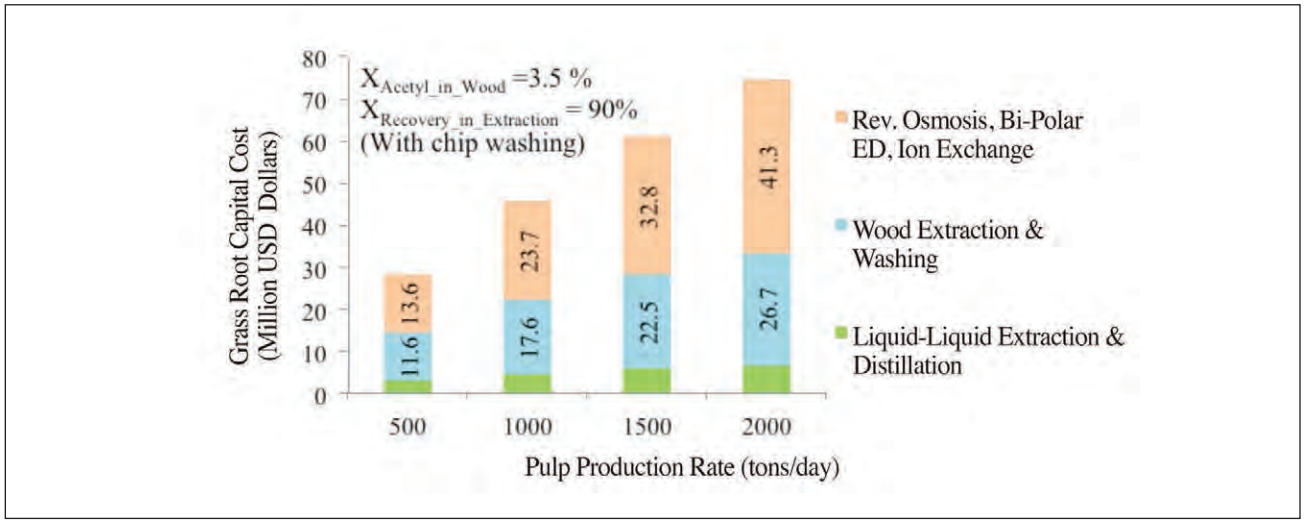
Estimation of capital cost

The capital cost for the process was estimated by using a combination of vendor estimates for the major pieces of equipment and estimates obtained from the CAPCOST cost estimating program for the less important equipment in the process [29]. CAPCOST presents a series of tables and graphs for estimating the capital cost of various pieces of process equipment in terms of what is called the bare module cost. The bare module cost program represents the sum of the direct and indirect costs associated with each piece of equipment. The direct costs involve the equipment FOB cost, as well as materials and labor for installation. The indirect costs involve freight charges, insurance, taxes, construction overhead, and contractor engineering expenses. The grassroots capital costs include the bare module cost plus all direct and indirect costs, contingency fees, and auxiliary cost for site development.

An estimate of the total bare module cost for the extraction vessel and chip washing system was obtained from Andritz Inc. (Alpharetta, GA, USA). The extraction reaction was assumed to be conducted in chip bins because the extraction temperature is below 100°C. To achieve a 2-h time, the chip flow was split between two chip bins operating in parallel. The total bare module cost for the reverse osmosis, ion exchange, and bipolar membrane electrodialysis equipment was obtained from the Ameridia Division of Eurodia Industrie (Somerset, NJ, USA). About half of the cost estimate from Ameridia is associated with the membranes used in BPMED cells. The cost estimates obtained from the vendors for both sections I and II were obtained for a 1000 tons/day and



6. Rate of production of acetic acid in kraft pulp mill using BPMED.



7. Grassroot capital cost as function of pulp mill size.

1500 tons/day pulp mill, respectively. These values were scaled to the other mill sizes using the power law scaling rule [29], as in Eq. (7):

$$C_A = C_A\left(\frac{P_A}{P_B}\right)^n \quad (7)$$

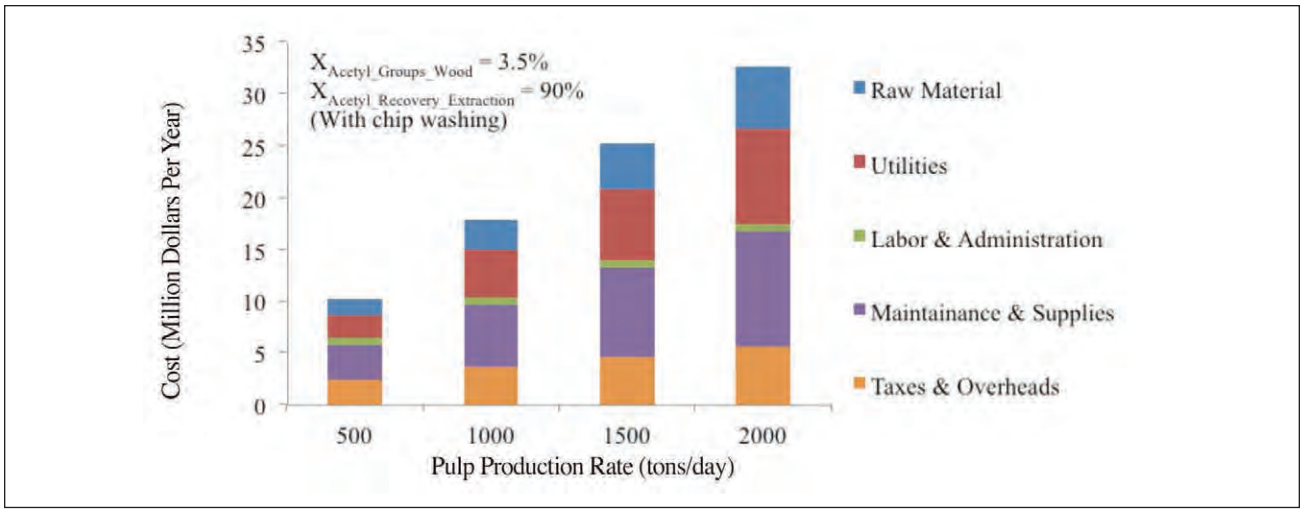
where P_A and P_B = size of pulp mills A and B; C_A and C_B = capital cost of process for mills A and B; and n = scaling cost exponent.

The scaling exponent (n) for section II (reverse osmosis, ion exchange, and BPMED) was taken to be 0.8 because the surface area of membranes increases linearly with increase in acetic acid production rate. The scaling factor for the remaining equipment in sections I and III of the process was scaled by using a scaling factor of 0.6. MTBE was used as the solvent in the liquid-liquid extraction process. The capital costs for the liquid-liquid extraction tower for removal of acetic acid from the solvent, the rectification tower for purification of acetic acid and solvent recovery, and the stripping tower for scalping residual solvent were obtained using CAPCOST.

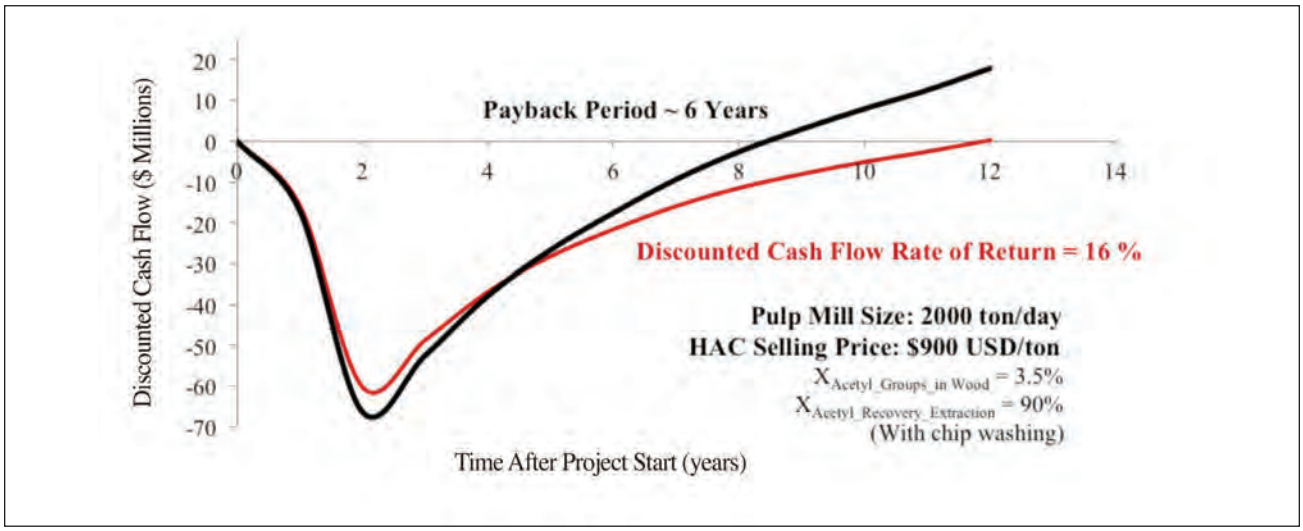
A contingency factor of 18% was applied to the total bare module cost (C_{BM}) when estimating the grassroot capital cost (C_{GR}) for the process. Another 20% of the total bare module cost was included for site development, auxiliary buildings, and utility connections. Thus, the grassroots cost for the process was assumed to be 38% greater than the total bare module or installed equipment cost (Eq. [8]):

$$C_{GR} = 1.38 \cdot \sum_{i=1}^{N} C_{BM,i} \quad (8)$$

Figure 7 shows the total grassroot capital cost for the acetic acid process. The project cost was estimated to be between US$28 million and US$75 million depending upon the size of the pulp mill (500–2000 tons/day).



8. Operating costs as a function of pulp mill size.



9. Example of discounted cash flow diagram (HAC = acetic acid).

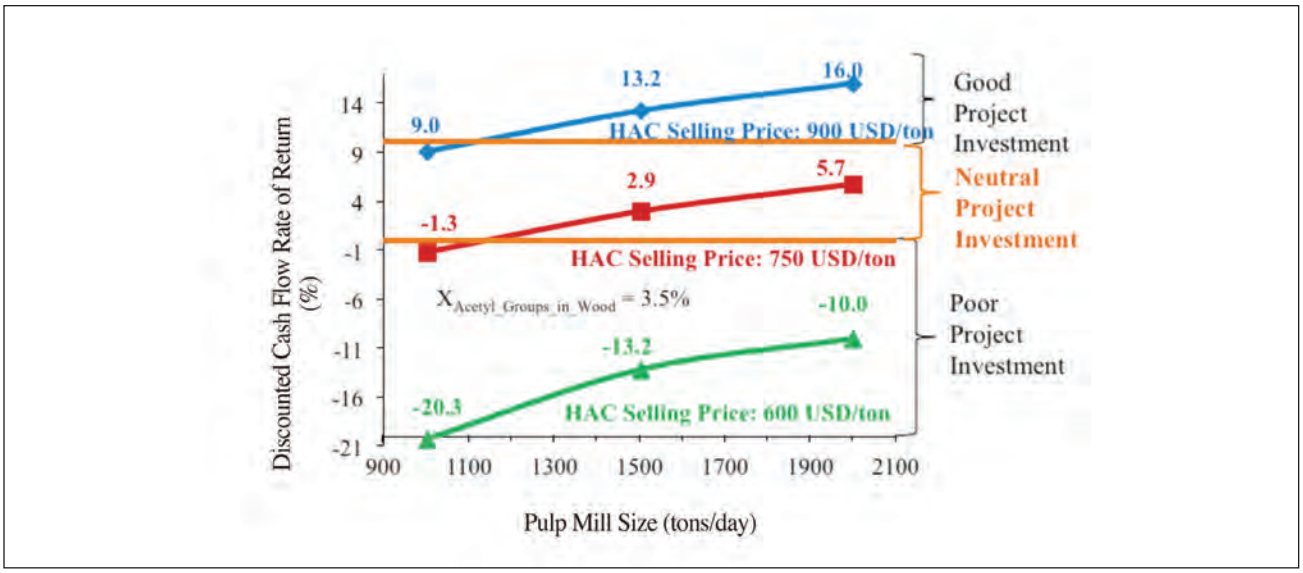
Estimation of operating costs

Because only 90% of the caustic used in the extraction process is recovered, the remaining 10% of the caustic requirements necessary for the extraction need to be purchased at a cost of US$530/ton. Because the BPMED process produces caustic, this is equivalent to extending the chemical recovery process. Utilities required by the process are water and electricity costs for the BPMED process. The number of operators required for this process was calculated by following the method described by Turton and coworkers [29]. It was assumed that this plant will have one shift supervisor, one laboratory technician, and 13 process operators. The major maintenance and supplies cost is due to the replacement of the membranes used in BPMED processes. The other maintenance costs, taxes, and overhead were calculated using the multiplication factors given by Turton and coworkers [29]. **Figure 8** shows the operating costs as a function of pulp mill size. The total operating cost varied from US$10 million to US$33 million per year, depending upon the pulp mill size.

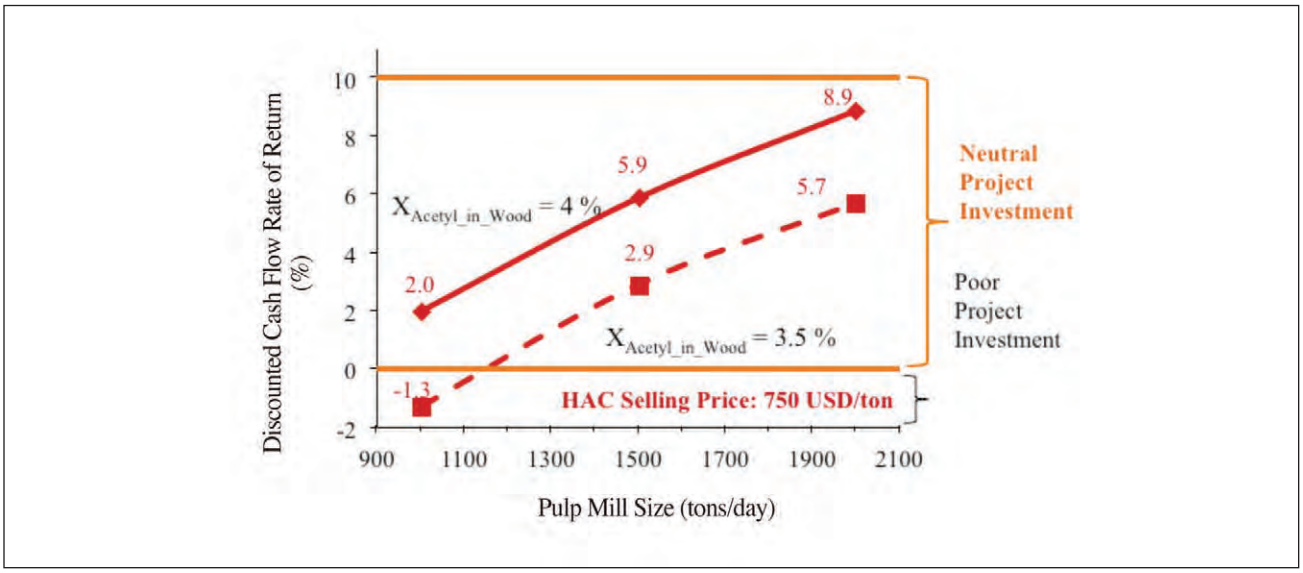
Discounted cash flow rate of return

In the discounted cash flow rate of return (DCFROR) method, the economic feasibility of a project is determined by comparing the calculated discounted rate of return with the cost of capital, which is considered to be the minimum acceptable rate of return. An example of the discounted cash flow diagram is illustrated in **Fig. 9** for the case of a 2000 tons/day pulp mill producing food grade acetic acid as a byproduct. In this analysis, the selling price for food grade acetic acid was assumed to be US$900/ton, and the rate of return on investment was estimated to be 16%. The payback period was estimated to be 6 years. This case was one of the best evaluated because of the large plant size and high selling price. **Figure 10** summarizes the results of the economic analysis for all of the cases evaluated.

As the pulp mill size increases, DCFROR increases because additional product is produced and the operating cost per unit of product is reduced. The highest DCFROR was 16%, which was



10. Discounted cash flow rate of return on investment (HAC = acetic acid).



11. Effect of acetyl group content on rate of return (HAC = acetic acid).

obtained for the case with the highest acetic acid selling price (US$900/ton) and for a large pulp mill size (2000 tons/day). However, the process did not prove it was profitable to install the acetic acid process if the selling price of acetic acid was below US$900/ton. Thus, food grade acetic acid must be produced for the process to be profitable.

Effect of acetyl group content on rate of return

The process becomes more profitable as the amount of acetyl groups in wood increases (**Fig. 11**). This figure shows the economic analysis when the selling price is US$750/ton for technical grade acetic acid. DCFROR increases for the 4.0% acetyl group case compared with the 3.5% case results from the increase in the rate of production of acetic acid, which in turn lowers the unit cost of production. White birch (4.4%), eucalyptus (3.9%), white elm (3.9%), beech (3.9%), and red maple (3.9%) contain high amount of acetyl groups [28,30]. The acetyl groups measured in this study using commercial mixed northeast hardwoods contain about 3.5% acetyl groups on a dry mass basis; therefore, some improvement in process economics is possible if wood with higher acetyl content is used.

Process uncertainties

Several uncertainties exist in the present analysis that warrant further investigation. First, the increase in manufacturing cost for producing food grade rather than technical grade acetic acid is associated with increased costs for product purification. These costs arise from the increase in steam and process water required in the distillation processes to meet

the higher purity requirements for the food grade acetic acid. No costs other than those associated with distillation were considered for removing formic, lactic, and glycolic acids. This is justified by conducting the extraction reaction at 50°C rather than 80°C, where experimentally it is seen that little if any sodium formate, sodium lactate, and sodium glycolate are formed. No credit was taken for any potential cost savings associated with the kraft process. Second, because caustic is being generated electrochemically in the BPMED unit, this could conceivably lead to cost reductions associated with the lime cycle and causticization process. Lastly, it should be possible to supply 85%–95% of the caustic requirements in the extraction step from the caustic recovered from the salt splitting process. The required L/W ratio in the extraction vessel to meet the concentration requirements to drive the deacetylation reaction would be satisfied by recycling extract back to the vessel, much like what is done with dilute black liquor in the kraft process.

CONCLUSIONS

The results of the BPMED experiments performed using pretreated extracts were similar to those obtained using model sodium acetate solution previously reported [6]. However, an increase of about 15% in the consumption of electric energy occurred when the real extract was used. This loss is caused by the transport of additional sodium salts present in the extract originating from sodium formate, sodium lactate, and sodium glycolate. The loss is expected to be smaller when extraction is performed at 50°C rather than at 80°C. Lignin and sugars were retained in the feed solution and the acetic acid recovered was not discolored. Hence, it was concluded that BPMPED can be used to obtain a clear solution of concentrated acetic acid, provided the presence of lignin in the feed solution does not lead to membrane fouling when the apparatus is operated over extended periods. If fouling occurs, then membrane life would be shortened and operating cost would be increased.

Possibly, the formic and lactic acids in the acetic acid product could be recovered and sold as additional byproducts. However, their concentration in the acetic acid solution is low and thus most likely not practical to separate and recover economically. In the present analysis, it was assumed that any formic, lactic, and glycolic acids were not recovered and hence no credit was taken as possible byproducts.

The rate of return on investment for the acetic acid process is a function of plant size, selling price of acetic acid, and amount of acetyl groups in the wood. The economic analysis showed that the acetic acid process is profitable for the large plants when food grade acetic acid is recovered and the wood contains appreciable quantities of acetic acid. The rate of return varies between 9% and 16% depending upon the size of the pulp mill (1000–2000 tons/day) for the case where the selling price of acetic acid is US$900/ton and the acetyl contained in the wood chips is 3.5% on dry weight basis. Although the rate of production of wood-based acetic acid is much smaller than in modern acetic acid plants, the process discussed here, if implemented, could lead to positive revenue for some hardwood kraft pulp mills. **TJ**

ACKNOWLEDGEMENTS

The authors acknowledge funding from the Forest Bio-Products Research Institute's NSF-SEP grant No. CHE-1230908 and are thankful to Brad Cort of Andritz Pulp & Paper and Daniel Bar of Ameridia, Division of Eurodia Industrie, for their assistance.

LITERATURE CITED

1. Grand View Research, "Acetic Acid Market Analysis by Application (VAM, Acetic Anhydride, Acetate Esters, PTA) and Segment Forecasts to 2022," Market Research Report, Grand View Research, San Francisco, CA, USA, July 2015. Available [Online] http://www.grandviewresearch.com/industry-analysis/acetic-acid-market <17May2017>.
2. Markets and Markets, "Acidity Regulators Market by Type (Acetic Acid, Citric Acid, Lactic Acid, Malic Acid, Phosphoric Acid), Application (Beverages, Sauces, Dressings and Condiments, Processed Foods, Bakery and Confectionery), and Geography—Global Trends and Forecasts to 2018," Market Report FB 1525, Markets and Markets Inc., Seattle, WA, USA, April 2013. Available [Online] http://www.marketsandmarkets.com/Market-Reports/food-acidulants-market-1072.html <17May2017>.
3. Sjöström, E., *Wood Chemistry—Fundamentals and Applications*, Academic Press, New York, 1993, pp. 62-65.
4. Patil, R., "Cleavage of acetyl groups for acetic acid production in kraft pulp mills," M.S. thesis, University of Maine, Orono, ME, USA, 2012.
5. Patil, R., Truong, C., Genco, J.M., et al., *TAPPI J.* 14(11): 695(2015).
6. Patil, R., Genco, J.M., Pendse, H., et al., *TAPPI J.* 15(3): 215(2016).
7. Sixta, H., "Zellstoffherstellung und Recycling von Rohund Hilfsstaffen nach dem Leninger Mg-Bisulfitverfahren," Lenzing AB, Lenzing, Austria, July 1986. Available [Online] https://www.lenzing.com/fileadmin/template/pdf/konzern/lenzinger_berichte/ausgabe_61_1986/LB_1986_01_Sixta.pdf <18May2017>.
8. Patil, R., "Production of acetic acid in kraft pulp mill biorefinery using bipolar membrane electrodialysis," Ph.D. thesis, University of Maine, Orono, 2016.
9. Retsina, T. and Pylkkanen, V., U.S. pat. 20110195468 (Aug. 11, 2011).
10. Ahsan, L., Jahan, M.S., Khan, M.I.H., et al., *BioResources* 9(1): 1588(2014).
11. Ahsan, L., Jahan, M.S., and Ni, Y., *Ind. Eng. Chem. Res.* 52(26): 9270(2013).
12. Kassotis, J., Harry, P., and Chlanda, F.P., *J. Electrochem. Soc.* 131(12): 2810(1984).
13. Trivedi, G.S., Shah, B.G., Adhikary, S.K., et al., *React. Funct. Polym.* 32(2): 209(1997).
14. Bar, D., "The 'Eurodia Industry' bipolar membrane electrodialysis unit for the conversion of sodium acetate into reusable acetic acid and caustic acid: More than five years of successful operation," *Membrane and Separation Technology News*, BCC Research, Wellesley, MA, USA, March 2006.
15. Yu, L., Guo, Q., Hao, J., et al., *Desalination* 129(3): 283(2000).

16. Mishra, A.K. and Bhattacharya, P.K., *J. Membr. Sci.* 33(1): 83(1987).
17. Gordon, O.W., Plattner, E., and Doppenberg, F., U.S. pat. 5,595,628 (Jan. 21, 1997).
18. Thompson, R., Paleologou, M., and Berry, R.M., *TAPPI J.* 80(6): 154(1997).
19. Paleologou, M., Wong, P.Y., and Berry, R.M., *J. Pulp Pap. Sci.* 18(4): J138(1992).
20. Paleologou, M., Thibault, A., Wong, P.Y., et al., *Sep. Purif. Technol.* 11(3): 159(1997).
21. Davis, S.M., "Electrochemical splitting of sodium sulfate," M.S. thesis, Georgia Institute of Technology, Atlanta, GA, USA, 2006.
22. Thompson, R., Paleologou, M., and Berry, R.M., *Tappi J.* 78(6): 127(1995).
23. Seader, J.D. and Henley, E.J., *Separation Process Principles*, John Wiley and Sons, Hoboken, NJ, USA, 2011.
24. DE Dietrich Process Systems, "Recovery of acetic acid by means of liquid-liquid extraction" Literature, DE Dietrich Process Systems GmbH, Mainz, Germany. Available [Online] http://www.dedietrich.com/en/recovery-acetic-acid-means-liquid-liquid-extraction<17May2017>.
25. Strathmann, H., in *Ullmann's Encyclopedia of Industrial Chemistry*, Vol. 21, Wiley-VCH, Weinheim, Germany, 2003, pp. 243-322.
26. Strathmann, H., in *Comprehensive Membrane Science and Engineering*, Vol. 2 (E. Drioli and G. Lidietta, Eds.), Elsevier Science, Oxford, UK, 2010, pp. 391-429.
27. Tanaka, Y., *Ion Exchange Membrane Electrodialysis*, Nova Science Publishers, New York, 2010.
28. Rydholm, S., *Pulping Processes*, Interscience Publishers, New York, 1965.
29. Turton, R., Bailie, R.C., Whiting, W.B., et al., *Analysis, Synthesis and Design of Chemical Processes*, Pearson Education, Upper Saddle River, NJ, USA 2012.
30. Inalbon, M.C., Mocchiutti, P., and Zanuttini, M., *BioResour. Technol.* 100(7): 2254(2009).

ABOUT THE AUTHORS

This work was an attempt to use the acetyl groups found in hardwoods. They are currently cleaved during the pulping process and are sent to the recovery boiler with the black liquor. Co-author Patil performed his doctoral research in this field. The current publication summarizes the basic data used in the process design for an acetic acid recovery process and summarizes the preliminary process economics.

The most difficult aspect of the research was coming up with realistic costs for the process. To address this challenge, we called vendors who helped us with estimates for the major equipment for a 1000 tons/day pulp mill. We then scaled the vendors' data to other pulp mill sizes.

An interesting aspect was minimizing the use of fresh caustic to the process. In theory, the process should not use any fresh caustic because the bipolar membrane process produces caustic in the same amounts that are used in cleaving the acetyl groups from the hemicelluloses in the wood.

Mills would benefit directly if management would make the capital investment and attempt to recover acetic acid for sale in the open market.


Patil


Genco


Pendse


van Heiningen

Patil is a postdoctoral student, Genco is a professor emeritus, Pendse is chair of the Chemical and Biological Engineering Department, and van Heiningen is a professor of Chemical Engineering at the University of Maine, Orono, ME, USA. Email Genco at JGenco@umche.maine.edu.

TAPPI JOURNAL
WWW.TAPPI.ORG
THE PAPER AND PACKAGING INDUSTRIES' TECHNICAL RESOURCE
JUNE 2017 | VOL. 16 NO.6



NONWOOD PULPING 313
Kinetics of sulfur dioxide-alcohol-water (SAW) pulping of sugarcane straw (SCS)
Asif Masih Sharazi and Adriaan van Heiningen

BLEACHING 331
Improving the efficiency of hydrogen peroxide bleaching of chemimechanical pulp by continuous replenishment of bleaching chemicals
Xianqi Sun, Qingxi Hou, Bingxu Zhang, and Guanting Zhao

PAPERMAKING 345
Finite element analysis of the thermal bending of a chilled cast thermo roll
Thomas Widmaier, Jukka Pirttiniemi, Esa Porkka, Panu Kiviluoma, and Petri Kuosmanen

NONWOOD PULPING 361
Pulping and bleaching of Malaysian oil palm empty fruit bunches
Robert W. Hurter and Medwick V. Byrd

June 2017

TABLE OF CONTENTS VOL. 16 NO. 6

309 EDITORIAL
Coating & Graphic Arts, Process Control papers honored at PaperCon
Monica Shaw

313 NONWOOD PULPING
Kinetics of sulfur dioxide-alcohol-water (SAW) pulping of sugarcane straw (SCS)
Asif Masih Sharazi and Adriaan van Heiningen

331 BLEACHING
Improving the efficiency of hydrogen peroxide bleaching of chemimechanical pulp by continuous replenishment of bleaching chemicals
Xianqi Sun, Qingxi Hou, Bingxu Zhang, and Guanting Zhao

345 PAPERMAKING
Finite element analysis of the thermal bending of a chilled cast thermo roll
Thomas Widmaier, Jukka Pirttiniemi, Esa Porkka, Panu Kiviluoma, and Petri Kuosmanen

361 NONWOOD PULPING
Pulping and bleaching of Malaysian oil palm empty fruit bunches
Robert W. Hurter and Medwick V. Byrd

»COVER CREDIT: Researchers Hurter and Byrd evaluated oil palm empty fruit bunches (EFB) as a raw material for caustic soda cooking, followed by elemental chlorine free and totally chlorine free bleaching sequences (p. 361). Their results indicated EFB could be a low-cost fiber resource for mills located near oil palm plantations.

TAPPI JOURNAL
WWW.TAPPI.ORG

Editor-in-Chief
Scott Rosencrance scott.rosencrance@kemira.com
+1 770 429-2753

Associate Editor
Brian N. Brogdon brian.brogdon@gmail.com
+1 678 581-9114

Editorial Director
Monica Shaw mshaw@tappi.org
+1 770 367-9534

Vice President, Operations
Eric Fletty efletty@tappi.org

PRESS Manager
Jana Jensen jjenson@tappi.org
+1 770 209-7242

Webmaster
Trina Heath theath@tappi.org
+1 770 209-7416

***TJ* EDITORIAL BOARD**

Brian N. Brogdon, FutureBridge Consulting & Training LLC
brian.brogdon@gmail.com, +1 678 581-9114

David A. Carlson, Carlson Consulting
dacarlson39@aol.com, +1 847 323-2685

Jere W. Crouse, JWC Consulting
cj522@inwave.com, +1 608 362-4485

Mahendra Doshi, Doshi and Associates
mahen@aol.com, +1 920 832-9101

Marc Foulger, GL&V USA Inc.
Marc.foulger@glv.com +1 315 767-2920

Peter W. Hart, WestRock
peter.hart@westrock.com, +1 409 276-3465

Carl J. Houtman, USDA Forest Products Laboratory
choutman@fs.fed.us, + 1 608 231-9445

John A. Neun, John A. Neun LLC
john.neun@gmail.com, +1 518 275-8139

Jim Niemiec, Verso Corporation
jim.niemiec@versoco.com, +1 715 422-7404

Steven P. Ottone, Omya
steven.ottone@omya.com, +1 919 641-7854

Gaurav Pranami, Imbed Biosciences
gpranami@imbedbio.com, +1 515 230-7005

Arthur Ragauskas, Oak Ridge National Laboratory
aragausk@utk.edu

Gerard J.F. Ring, University of Wisconsin—Stevens Point
gerrryring@wi-net.com, +1 715 592-3732

Scott Rosencrance, Kemira Chemicals
scott.rosencrance@kemira.com, +1 770 429-2753

Paul Wiegand, NCASI
pwiegand@ncasi.org, +1 919 941-6417

Junyong Zhu, USDA Forest Products Laboratory
jzhu@fs.fed.us, +1 608 231-9520

Join TAPPI *today!*

TAPPI JOURNAL is a free benefit of TAPPI membership, and is only available to members. To join TAPPI, to renew your TAPPI Membership, or to learn about other valuable benefits, visit www.tappi.org.

TAPPI, 15 Technology Parkway S., Suite 115, Peachtree Corners, GA 30092, publishes *TAPPI JOURNAL* monthly.

ATTENTION PROSPECTIVE AUTHORS: All papers published are subject to *TAPPI JOURNAL's* peer-review process. Not all papers accepted for review will be published. Before submitting, check complete author guidelines at http://www.tappi.org/s_tappi/doc.asp?CID=100&DID=552877.

Statements of fact and opinions expressed are those of individual authors. TAPPI assumes no responsibility for such statements and opinions. TAPPI does not intend such statements and opinions or construe them as a solicitation of or suggestion for any agreed-upon course of conduct or concerted action of any sort.

Copyright 2017 by TAPPI, all rights reserved. For copyright permission to photocopy pages from this publication for internal or personal use, contact Copyright Clearance Center, Inc. (CCC) via their website: www.copyright.com. If you have questions about the copyright permission request process, please contact CCC by phone at +1 978 750-8400. To obtain copyright permission to use excerpts from this publication in another published work, send your specific request in writing to Editor, TAPPI JOURNAL, 15 Technology Parkway S., Suite 115, Peachtree Corners, GA 30092, USA; or by fax to +1 770 446-6947.

Send address changes to TAPPI, 15 Technology Parkway S., Suite 115, Peachtree Corners, GA 30092, USA; Telephone +1 770 446-1400, or FAX +1 770 446-6947. www.tappi.org

Editorial

MONICA SHAW | EDITORIAL DIRECTOR
mshaw@tappi.org



Coating & Graphic Arts, Process Control papers honored at PaperCon

More than 1750 industry professionals met in Minneapolis, MN, this April for PaperCon, TAPPI's annual conference that features a multi-track technical program, seminars, networking, and exhibits. Technical program tracks included coating, papermaking, additives, process control, nonwovens, and fluid dynamics. There were also tracks on mill leadership perspectives and employee retention.

A highlight of this year's event was keynote speaker Marcus Shingles, CEO of the XPRIZE Foundation, who spoke about the benefits of disruptive change in his presentation, "Uber yourself before you get Kodaked." He noted that, in today's high-tech world of exponential, not linear, change, large companies – including traditional ones – are asking how to reach a 10X improvement instead of just 10% without needing ten times more people or resources. Shingles sees the answer in different management and planning. From quantum computing to "hyperloop" transport technology, he challenged attendees to consider a variety of disruptive changes.

Another event highlight was the annual PaperCon Awards Dinner, where Honghi Tran, professor in the Department of Chemical Engineering and Applied Chemistry at the University of Toronto, received the Gunnar Nicholson Gold Medal – the highest honor TAPPI bestows on an individual. Among other notable awards given at the dinner were four awards for best PaperCon 2017 and 2016 (assessed after the event) papers described in this column.

Coating & Graphic Arts Division Best Paper Award 2017

"The role of base substrate in barrier and convertibility properties of water based barrier coated (WBBC) paper board and paper"

P. Miettinen, M. Ahokas, T. Engstrom, J. Heinonen (CH-Polymers Oy)

S. Auvinen (Tampere University of Technology)

This paper studied the role of base substrate variables in dispersion coverage and barrier properties. The new generation WBBC solutions used in the study are partly based on bio materials and link together knowledge of both polymer dispersion chemistry and novelty special pigment development.

Also studied was the effect of how dispersion film coverage and surface structure affect the convertibility of dispersion coated packaging materials. Heat sealing of the dispersion coating layers against each other is usually easy, but problems can occur. Very high sealing temperatures where the dispersion coating is sealed against the uncoated surface can be lowered by closing the substrate structure before dispersion coating, as with a small layer of standard pigment coating. Pre-coating also makes the base material more dense and smooth, so in general, the dispersion coating coverage and barrier properties are assumed to improve.

The barrier properties analyzed were KIT test, grease and oil barrier, water vapor, oxygen barrier, and water resistance. The convertibility properties of dispersion coated paper materials were evaluated by creasing tests. The structure of base material was analyzed by different porosity and roughness measurements, such as optical profilometry, SEM, and other microscopy techniques.

Coating & Graphic Arts Division Best Student Paper Award 2017

"Conductive carbon-nanocellulose coatings on paper"

V. Kumar, S. Forsberg, A. Engstrom, M. Nurmi (Åbo Akademi University)

C. Dahlstrom, M. Toivakka (Mid Sweden University)

This work aims at demonstrating large scale production of flexible low-cost paper-based electrodes utilizing graphene, nano-graphite, and graphite coatings. The large aspect ratio of graphene limits the suspension solids content to very low values, which makes it challenging to create thick coating layers required for high conductivity. The combined use of nanocellulose as binder and viscosity modifier, together with a custom-built slot coating device, enabled roll-to-roll coating of thick conductive coatings on paper.

The rheological and water retention properties of carbon-nanocellulose suspensions were reported. The influence of coat weight, carbon black addition, and calendering on coating structure and the resulting conductivity of the coatings was investigated. The lowest surface resistivities obtained were in the range 1-2 Ohm/sq for 15 gsm coat weight.

Best Process Control Paper 2016

"Characterization of paperboard formation using soft X-radiography and image analysis"

D.S. Keller, H. Abedsoltan (Miami University)
G. Wood (Verity IA)

While the uniform distribution of fibers in the forming section is of paramount importance, imaging and subsequent analysis of paperboard formation has been difficult. Few systems have sufficient energy to penetrate paperboards with grammages values exceeding 120 g/m^2 with sufficient sensitivity to determine mass variation at the spatial dimensions useful for characterizing the inherent flocked structures.

To find a more precise imaging method with a higher spatial dynamic range, the researchers investigated the use of 6 keV soft X-radiography with both film and storage phosphor screens to obtain a continuous image of paper formation within a 70-mm^2 region of interest. This presentation describes the acquisition method for soft X-radiography that enables capture of images suitable for advanced statistical and spectral formation analysis. When using film and scanner, individual fibers throughout the board structure are discernable with high sensitivity and depth of field. Use of storage phosphor systems as the image detector 2 enables rapid imaging at more practical resolutions. From these images, grammages maps are subjected to statistical, spectral, and customized routines. These routines provided statistical pathways to correlate the formation images with other end use properties, such as surface topography and print quality.

Next year's PaperCon will be held April 15-18, 2018, in Charlotte, NC. Learn more about the 2017 program, sponsors, and exhibitors at www.papercon.org.

Jasper Mardon Memorial Prize for Best Papermaking Technology Paper 2016

"Innovations in plant-wide monitoring, diagnostics, & optimization"

R.C. Rice, D. Nash (Control Station Inc.)

From operations and engineering to maintenance and management, control loop analytics target the unique information needs of those groups that are tasked with maximizing uptime and achieving production goals. This presentation covers recent innovations in control loop performance monitoring (CLPM), specifically in context of the pulp and paper industry, to demonstrate the value of loop analytics.

The typical paper mill operates hundreds of PID control loops and maintains an even larger quantity of production assets. The typical plant historian stockpiles data, and extracting information that is actionable and relevant to performance can be a challenge.

Control loop analytics leverage the information stored in a production facility's data historian. Technologies like PlantESP actively evaluate PID control loops on a plant-wide basis, identifying issues that undermine production performance and lead to shutdown. These technologies also isolate root causes and recommend corrective actions. **TJ**

Kinetics of sulfur dioxide-alcohol-water (SAW) pulping of sugarcane straw (SCS)

ASIF MASIH SHARAZI AND ADRIAAN VAN HEININGEN

ABSTRACT: Pulping kinetics of sugarcane straw (SCS) using the sulfur dioxide (SO_2)-alcohol-water (SAW) system were investigated with different solvents (methanol, ethanol, and isopropanol) in order to evaluate the effect of the solvents. The methanol, ethanol, and isopropanol SAW pulps are identified as SMW, SEW, and SPW, respectively. The pulping experiments were carried out at 135°C, 145°C, and 155°C with cooking liquor (L/F = 4 L/kg feedstock) composition; SO_2/alcohol/water of 12/44/44 w%. The pulps were characterized in terms of yield, kappa number, viscosity, cellulose, and hemicellulose and lignin content. After a fast initial dissolution phase, two regimes of delignification were identified in all solvent systems: a bulk and a residual phase. Bulk delignification and xylan removal followed first order kinetics in residual lignin and xylan, respectively, while the cellulose hydrolysis rate was zeroth order in cellulose.

Linear relationships between Klason lignin content and kappa number were developed for each solvent system after correcting the acid insoluble lignin for ash and non-oxidizable matter. The corrected lignin content on original SCS was used to develop the bulk delignification kinetics. Rate constants and activation energies for bulk delignification, xylan removal, and cellulose hydrolysis were evaluated for each pulping system. In terms of degree of delignification, the pulping systems followed the sequence of: SMW <SEW <SPW. Bleachable grade pulps with acceptable intrinsic viscosity (>800 ml/g) were produced in SEW and SPW systems, while the lower rate of delignification and higher rate of cellulose hydrolysis in SMW yielded much lower viscosity pulps of higher kappa number at the same pulping temperature and time. The results are explained in terms of the effective acidity and lignin/carbohydrate dissolution properties of the pulping liquors.

Application: Based on the knowledge developed in this study, isopropanol can be considered in SAW pulping processes. The use of isopropanol will reduce the capital cost and safety regulations. However, recovery potential of isopropanol still needs to be evaluated.

Recovered paper and chemical wood pulps are preferentially used for paper manufacturing [1]. Pulp and paper demand varies depending upon the degree of development of the region. However, during the last decade, pulp demand in developed countries is stagnant or decreasing, while demand is still increasing in developing nations. The latter results in a shortage of wood and gradual deforestation in developing countries. For this reason, nonwoody materials are being considered as feedstock for pulping and papermaking products in those regions [2].

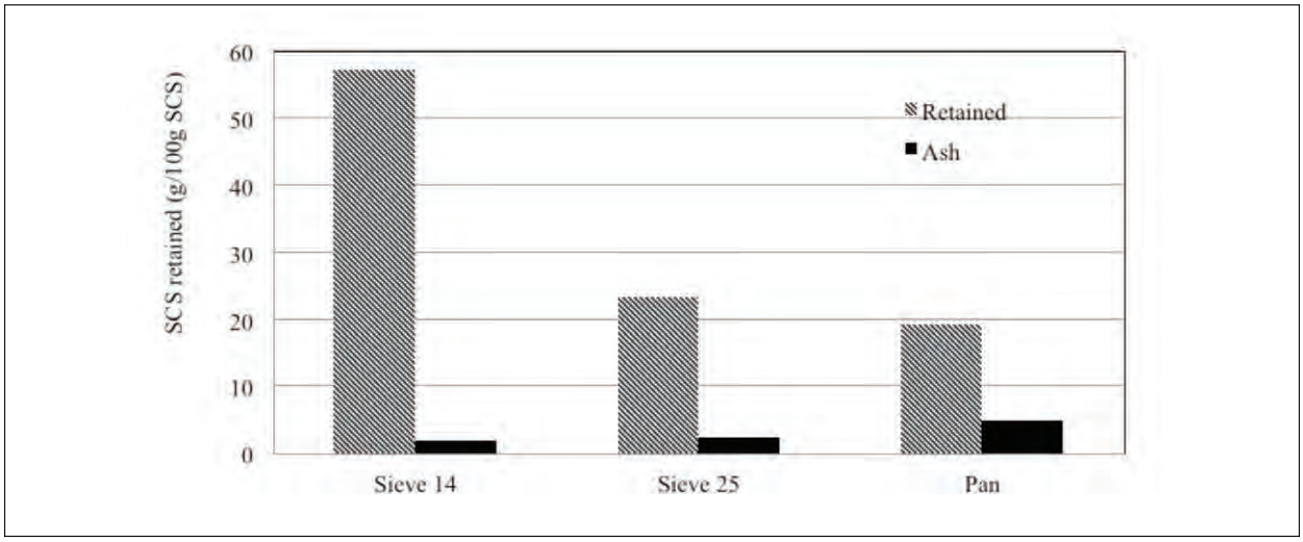
Agricultural residues are one nonwoody biomass that is abundantly available in many countries. The high growth rate and adaptability to various soil types makes agriculture fibers a good alternative to wood as raw material for pulping [3]. Sugarcane straw (SCS) is one of the abundantly available agriculture residues. The biomass that is removed before sugarcane is crushed is known as SCS [2,4]. It consists of fresh and dried leaves, including the tip of the plant [4,5]. According to the Food and Agriculture Organization, the annual production of sugarcane worldwide in 2014 was nearly 1900 million metric tons [6]. Also, 140–150 kg of SCS is produced from one metric ton of cultivated sugarcane [1]. So, nearly 285 million tons of SCS is produced annually around the world. Brazil is the foremost sugarcane producing country, with 84 million metric tons of SCS annual production [2]. Presently, it is only used as solid fuel and not for the manufacturing of chemicals [3]. However, it is traditionally burned in the field, thereby destroying a potential energy feedstock as well as causing environmental pollution. Nowadays in Brazil, burning of SCS is strictly controlled by a specific federal law (Decree 2661/98), and in the state of Sao Paulo, by an even more restrictive law (State law 11.241/02) [9]. Therefore, it is logical that SCS is being considered for production of renewable products such as pulps, biofuels and biochemicals.

Similar to woody biomass and other agricultural residues, SCS can also be fractionated into its basic components (cellulose, hemicellulose, and lignin) for further conversion into diverse grades of pulps, biofuels, and specialty products such as lignosulfonates, vanillin, xylitol, xylanase, and cellulose derivatives. Cellulose pulp is manufactured from woody and nonwoody feedstocks by chemical and mechanical methods [10]. Nowadays, chemical wood pulp is the second most used fiber furnish for paper manufacture, with recovered paper being the first [1]. Kraft (sulfate) and acid sulfite pulping are the two well-known chemical pulping processes. However, organosolv (mostly ethanol-water) pulping processes have also been tried, but none were eventually implemented at full scale. A variant of organosolv pulping, the so-called sulfur di-

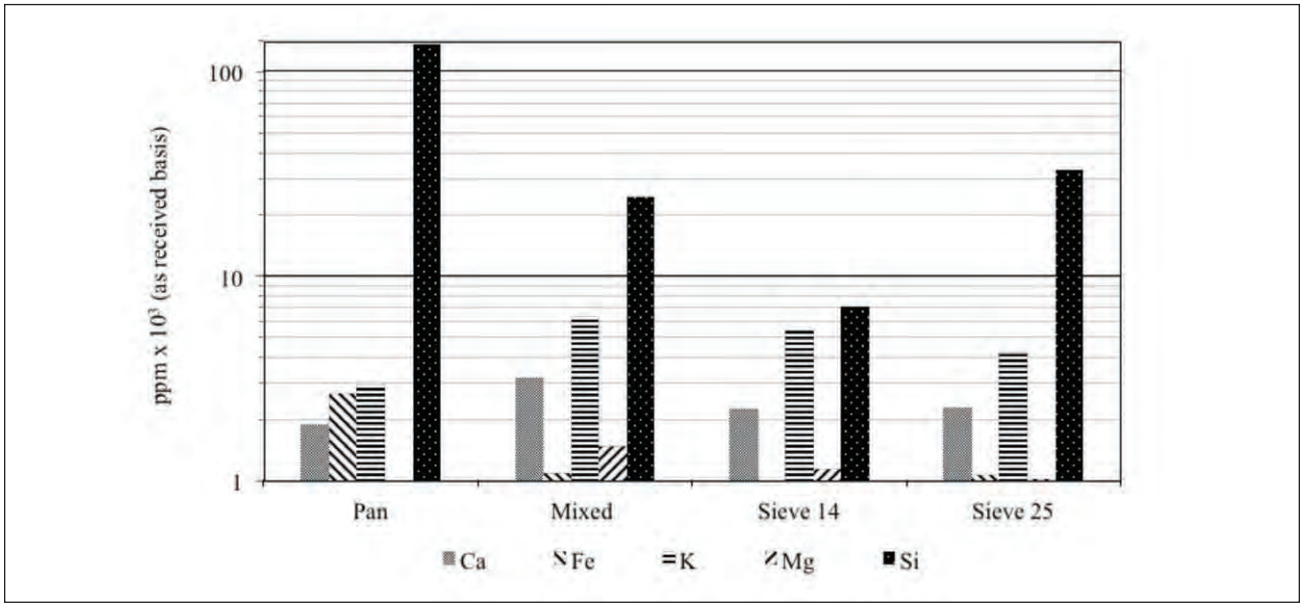
oxide (SO_2)-ethanol-water (SEW) process was recently studied in much detail at Aalto University in Finland [11,12,13,14]. This process, first introduced in 1950s by Schorning [15], was investigated by Iakovlev [11] for fractionation of spruce, beech, and wheat straw. It has distinct advantages of short cooking time, lower fractionation temperature than kraft pulping, less sulfur consumption than acid sulfite (AS), a simple recovery cycle, and reduced precipitation of sticky lignin [11,16]. Yamamoto [12] evaluated the enzymatic hydrolysis potential of SEW pulps produced from hardwood and softwood forest biomass. In two parallel studies, Sklavounos [13] and Jurgens et al. [17] determined the recovery pathway and ABE fermentation potential, respectively, of SEW spent liquors. Most recently, the SEW process was applied to SCS using a relatively low ethanol/water mass ratio of 22.5/65.5 [14]. First order xylan hydrolysis and zero order cellulose hydrolysis were reported in this study, with kinetic parameters similar to those of wood species. However, no clear delignification kinetics were presented because of high data scatter.

In the present study, we evaluated three SO_2-alcohol-water (SAW) pulping systems with methanol, ethanol, and isopropanol as solvents. During SAW pulping, hemicellulose and cellulose are degraded by acidic hydrolytic cleavage, while lignin degrades and dissolves due to sulfonation. Thus, it has been found that most of the hemicelluloses are dissolved as monomeric and oligomeric sugars [18] while leaving nearly all cellulose in the solid residue/pulp, albeit at a lower degree of polymerization. The dissolved sugars are degraded to hydroxymethylfurfural, furfural, formic acid, levulinic acid, humins, and other products only at severe cooking conditions [19,20]. In the SAW system, SO_2 and its hydrates and solvates are mainly responsible for lignin sulfonation, as the concentration of hydrosulfite anion is low due to the absence of a base [11,21]. The rate of sulfonation depends on the nucleophilicity of the sulfonating agent (hydrated SO_2 in this case), while the degree of sulfonation is not affected by the solvent concentration [22,23]. Although there is no direct correlation between sulfonation and rate of lignin dissolution, it seems reasonable that a lower degree of sulfonation is required for lignin dissolution in a solvent in which it has a high solubility [22,24]. A lower degree of lignin sulfonation in a solvent with good lignin solubility properties is advantageous from an economic and environmental point view. The lower degree of sulfonation in an ethanol environment as compared to that during acid sulfite (AS) pulping also suggests the possibility of lignin cleavage by alcoholysis [22]. However, in a similar manner alcohol can also react with carbohydrates to form furanosides and pyranosides [25]. Therefore, alcoholysis can potentially have a negative effect on solvent recovery economics in the SAW process. Short chain alcohols are more likely to form furanosides and pyranosides than long chain alcohols. It has been found that it is more difficult to produce propyl xylosides than methyl and ethyl xylosides [26]. Solvents also have considerable impact on carbohydrates degradation, especially cellulose [27,28,29]. For example, ethanol, propanol, and methyl ethyl ketone (MEK) increase cellulose degradation by affecting the hydronium ion reactivity. Similarly, gamma valerolactone (GVL) accelerates cellulose and hemicellulose hydrolysis by decreasing the activation energy. On the other hand, dimethyl sulfoxide (DMSO) suppresses the degradation of cellulose. Hence, delignification and carbohydrate degradation and dissolution kinetics may be optimized by employing different solvents to obtain desirable pulping characteristics such as high delignification/low carbohydrate degradation selectivity, while close to complete solvent recovery should be achieved in an economical and environmentally friendly way.

Low molecular weight aliphatic alcohols are the most commonly tried solvents used for pulping. The lower cost and ease of recovery makes methanol and ethanol solvents of high interest. Methanol is the lowest cost solvent (besides water), and because some methanol is created during pulping (about 0.5% on feedstock basis) [30] small losses in the pulping process



1. Ash in different sugarcane straw (SCS) fractionations.



2. Elemental ash analysis of SCS fractions (Ca = calcium, Fe = iron, K = potassium, Mg = magnesium, Si = silicon).

may be tolerated. On the other hand, the use of ethanol is advantageous in terms of lower toxicity, flammability, and volatility [31]. Ethanol losses may be compensated for by using sugars from pretreated biomass for bioethanol production. On the other hand, high pressures associated with these highly volatile alcohols increases the capital cost [19]. The use of isopropanol is not very common in pulping research, but it might be safer relative to methanol and ethanol. Also, it can be produced from lignocellulosic sugars by isopropanol butanol ethanol (IBE) fermentation [32,33].

All previously mentioned studies focus mostly on wood raw materials using ethanol in the SEW process. On the other hand, very few publications have appeared on fractionation/pulping of abundantly available agricultural residues, such as sugarcane straw. Therefore, the present study was undertaken to investigate the effect of two other fully water miscible alcohols, methanol and isopropanol, besides ethanol, on the fractionation potential of SCS using the SAW process.

MATERIALS AND METHODS

Lignocellulosic biomass and fractionation methods

SSCS was obtained from the Thomaston, GA, USA, biorefinery of API, who again obtained this material from its Brazilian partner, Granbio. The material was size reduced using a Munson mill grinder with a 6.35 mm screen. Then, the shredded material was screened through 1400 µm (sieve no. 14) and 710 µm (sieve no. 25) standard sieves on a mechanical Humboldt shaker. Straw fractions retained on each sieve and in the pan were analyzed for yield and ash (**Fig. 1**). The fraction collected in the pan was not included in the fractionation feedstock because of its high ash content. Each fraction was analyzed for calcium (Ca), iron (Fe), potassium (K), magnesium (Mg,), and silicon dioxide (SiO_2) by ICP-AES using the EPA 200.7 Method "Trace elements in water, solids, and biosolids by inductively coupled plasma-atomic emission spectrometry." Elemental ash analysis revealed that the fraction retained in the pan was mostly composed of silica (**Fig. 2**). SCS fractions retained on no. 14 and no. 25 standard sieves were mixed (Fig. 2), and this mixture was used for the pulping experiments. The chemical composition of SCS used in the fractionation experiments is shown **Table I**. The moisture content of the SCS is 6%.

Component	g/100 g o.d SCS
Arabinan	3.0 ± 0.2
Galactan	0.9 ± 0.1
Glucan	35.7 ± 0.4
Xylan	21.2 ± 0.6
Mannan	0.6 ± 0.2
Acid soluble lignin (ASL)	3.8 ± 0.4
Corrected Klason lignin (CKL)[1]	19.8 ± 0.2
4-OMGA	1.1 ± 0.0
Acetyl groups	2.9 ± 0.1
Ash	6.1 ± 0.2
Extractives	3.5 ± 0.4
Proteins	2.24
Total	**100.8± 2.6**

[1] Klason corrected for ash content.

I. Chemical composition of mixed fraction SCS.

Three water miscible alcohols, namely methanol, ethanol, and isopropanol, were used for pulping of SCS. SAW cooking liquors were prepared by injecting SO_2 in alcohol-water mixtures (50 w/w%). The concentration of SO_2 in each cooking liquor was 12% (by weight). Cooking digesters (220 ml) were filled with 22 g ovendry (o.d.) SCS, and cooking liquor was added at a feedstock ratio of 4 L/kg, which also accounts for the SCS moisture content. The digesters were immersed in a hot multi digester oil bath (MDOB) containing polyethylene glycol as a heating media at a temperature settings of 135°C, 145°C, or 155°C (±1°C). The digesters rotated 180° at 2 rpm during cooking. After completion of pulping, the digesters were put into an ice bath to quench and stop further reaction. The digester content was quantitatively transferred into a nylon bag (mesh size 75), and the solid pulp was obtained after manually squeezing out the spent liquor. The obtained pulp was washed twice with 50% (by weight) aqueous alcohol solution (L/F = 2 L/kg) at 60°C and then washed twice with deionized (DI) water (L/F = 20 L/kg) at room temperature. Finally, the pulp slurry was disintegrated, filtered through Whatman quantitative grade ashless filter paper, and transformed into a pulp pad. Pulp pads were dried overnight at room temperature and then stored in plastic bags for further analysis. Methanol-, ethanol-, and isopropanol-based pulps were designated as SMW, SEW, and SPW, respectively.

Chemical analysis of SCS and pulps

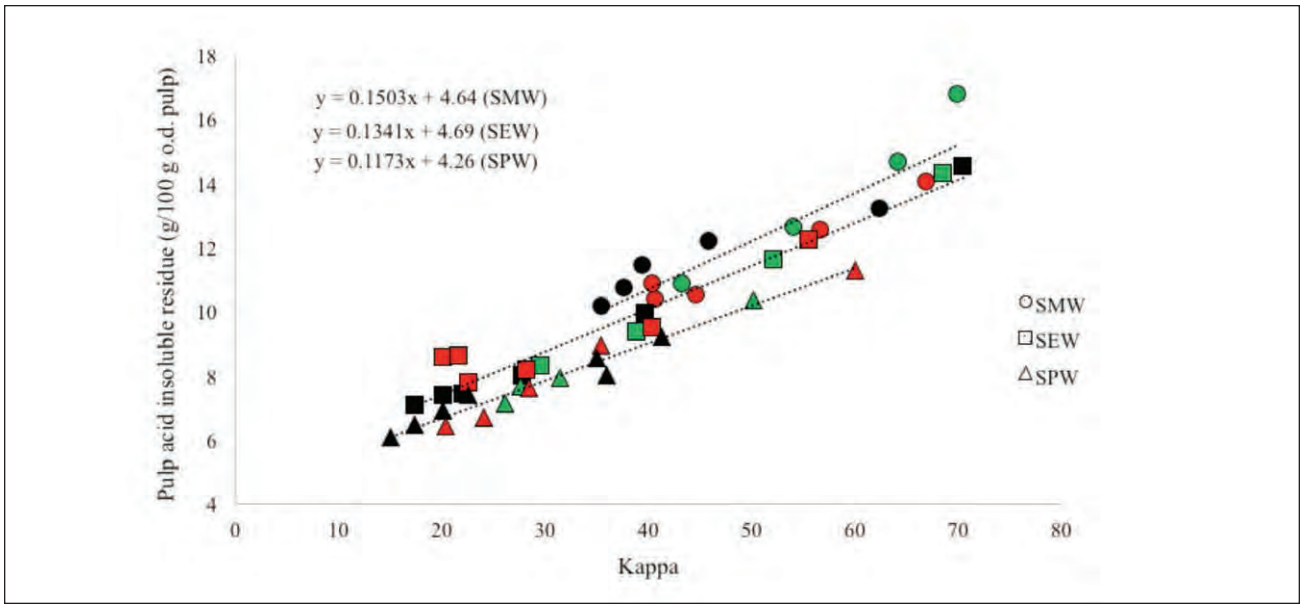
SCS and pulps were ground using a Wiley mill and analyzed for chemical composition. The acetone extractives in SCS were determined according to SCAN-CM 49:03 "Content of acetone-soluble matter." Kappa number and intrinsic viscosity of pulps in cupriethylenediamine (CED) solution were determined according to SCAN-C 1:00 "Chemical pulp: Kappa number" and SCAN-CM 15:99 "Pulps: Viscosity in cupriethylenediamine solution," respectively. All pulps were treated with sodium chlorite according to TAPPI Suggested Method T 230 su-66 "Viscosity of pulp (capillary viscometer method)" before viscosity determination. The pulp yield based on o.d SCS was determined with variability of less than ±1.0%. Lignin and carbohydrate content of Wiley mill ground SCS (extractive free) and pulps were determined according to NREL/TP 510-42618 "Determination of structural carbohydrates and lignin in biomass" after double stage hydrolysis. Klason lignin was corrected for ash by burning it at 525°C for 24±6 hours in a muffle furnace. Acid soluble lignin (ASL) was determined by measuring the ultraviolet (UV) absorbance of liquor (at 205 nm and extinction coefficient of 110 l/g.cm) from two-stage hydrolyzed (4% sulfuric acid [H_2SO_4], 1 h) SCS/pulp. Scott's method was employed for uronic anhydride determination and hence for the quantification of 4-OMGA [34]. A high performance anion exchange chromatography with pulse amperometric detection (HPAEC-PAD) was used for separation of the monosugars. Acetic acid in the SCS/pulp hydrolysate was determined by high performance liquid chromatography (HPLC) using a refractive index detector and BIO-RAD Aminex HPX-87K column (BIO-RAD Laboratories; Hercules, CA, USA). The mobile phase used was 0.6 ml/min 5 mM H_2SO_4, and the oven temperature was 45ºC. SCS and some selected pulps were analyzed for nitrogen content by dry combustion method. Protein content was determined by multiplying the nitrogen content by a factor of 5.6 [35]. The composition of the two mixed fractions of SCS used in the pulping experiments is shown in Table I.

The SCS compositional analysis shows that it is rich in carbohydrates, containing 61.4% anhydrous sugars. Xylan is the most abundant hemicellulose sugar, while galactan and mannan are present less than 1%. It contains 3.8% ASL and nearly same amount of acetone soluble extractives. Like other agriculture residues, it has a significant amount of ash that adds 6.1% to its dry weight. Ash free Klason lignin is 19.8%, and this value also likely includes a significant amount of protein, which is present in SCS at 2.24%. The composition of SCS depends on the collection site, climate conditions, stage of plant development, and variety [36,37]. The SCS in our study is from the same source as the SCS batch III that You et al. [14] employed in their study. It had 59.9% carbohydrates and 20.2% lignin, but less extractives (2.1%) and more ash (8.5%). A comprehensive description of the composition of sugarcane residues, including SCS, was reported by Costa et al. [38]. However, the authors did not provide information on protein content. In a more recent study [39], it is reported that SCS contains 3.72% proteins, with the rest of the composition very similar to that in Table I.

KAPPA-LIGNIN CORRELATIONS

SCS was subjected to fractionation at three different temperatures, 135°C, 145°C, and 155°C, with cooking duration ranging from 20 to 120 min. All cooking times include 8–10 min for heat-up of the biomass to reach pulping temperature. Pulps produced under these conditions did not have any apparent rejects except for some of the SMW pulps with kappa >70. Acid insoluble Klason lignin content of pulps after standard two-step hydrolysis was determined and corrected for acid insoluble ash, because SCS contains a significant amount of acid insoluble inorganics, mostly silica. Linear correlations between kappa number and ash free acid insoluble lignin content of SMW, SEW, and SPW pulps were obtained with intercepts of 4.64, 4.69, and 4.26, respectively, at zero kappa number as shown in **Fig. 3**. The results show that the lignin-kappa correlations are only a function of cooking solvent, but not of cooking temperature. The highest Klason lignin content at a fixed kappa number is seen for methanol, followed by ethanol and finally isopropanol.

Many correlations between kappa number and Klason/total lignin content of pulps have been reported in literature. However, no such correlation was ever reported for SCS. In a recent study on SEW fractionation of SCS [14], the kappa number and lignin content for various pulps were reported, but no correlation was presented due to large variability of the data. Iakovlev



3. Kappa vs. ash free acid insoluble lignin relation (unmodified) for methanol, ethanol, and isopropanol pulps. Color coding shows three different temperatures: green (135°C), black (145°C), and red (155°C).

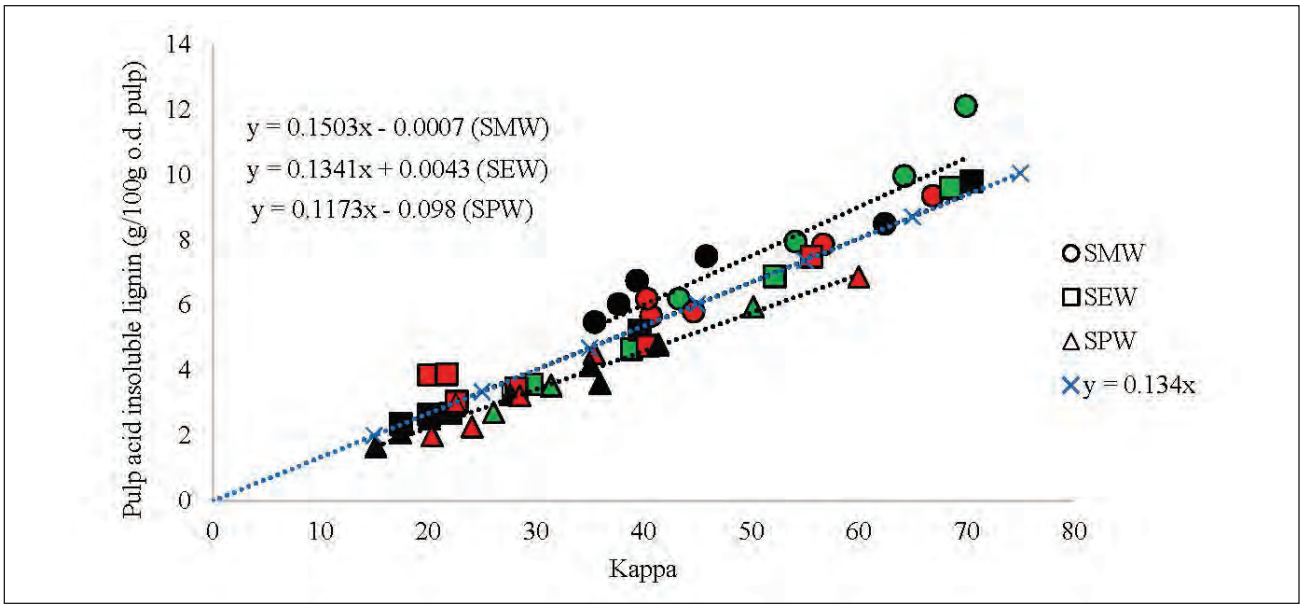
and van Heiningen [40] reported that the proportionality constant in the kappa vs. lignin correlations depends on species and fractionation process. Most of the correlations were developed for wood species, starting with Tasman and Berzins [41] in the late 1950s for beech, birch, spruce, and pine. In later studies [42,43], slightly different proportionality constants were found depending on wood specie and pulping process, but interestingly, the intercept was always found to be zero. However, for annual fiber biomass such as barley straw, a high intercept value (3.5–6.5) was found for the correlation between Klason lignin and kappa covering a narrow range of total lignin content [44]. The high value of the intercept in the latter study was attributed to the presence of shives, knots, and permanganate non-oxidizable components in the unscreened pulp. For SEW pulping of spruce, beach, and wheat straw, Iakovlev and van Heiningen [40] also reported intercepts of the Klason lignin-kappa correlations of nearly zero for wood species, while for wheat straw it was 1.27. Thus, it is apparent that pretreated/pulped annual fibers are characterized by Klason lignin-kappa correlations with a high intercept, even after correcting Klason lignin for the acid insoluble ash present in it. This may indicate the presence of a significant amount of permanganate non-oxidizable matter in acid insoluble ash-corrected Klason lignin. Recent studies show that there are 3.72% proteins [39] and significant amounts of lipids present in SCS [45]. Such components may possibly contribute to high intercept values in Klason lignin-kappa correlations in SAW pulping of SCS.

In order to investigate whether protein could be responsible for the permanganate non-oxidizable matter, different kappa number pulps were analyzed for protein content (a factor of 5.6 was used to convert nitrogen content to protein content according to [35]). The data in **Table II** shows that these pulps contain a significant percentage (8.7%–29.3%) of the protein present in the original SCS (2.24% on original SCS). Pulps with higher kappa number retain comparatively more protein. This suggests that a significant amount of protein ends up in the Klason lignin and may contribute (in part) to the permanganate non-oxidizable matter in SAW pulps. Lipids

	SMW		SEW		SPW	
Pulp kappa	45.8	44.7	27.8	22.6	22.6	20.4
Nitrogen, % pulp	0.26	0.22	0.21	0.11	0.12	0.09
Protein*, % pulp	1.46	1.24	1.15	0.62	0.66	0.51
Pulp yield, % SCS	45.1	41.1	42.3	38.3	41.4	37.9
Protein, % SCS	0.66	0.51	0.49	0.24	0.27	0.19
Protein retained in pulp, %	29.3	22.8	21.7	10.6	12.2	8.7

*A factor of 5.6 was used to calculate protein content [35].

II. Protein content of pulps based on nitrogen analysis (SMW = methanol, SEW = ethanol, SPW = isopropanol).



4. Kappa vs. lignin relation (modified) for methanol, ethanol, and isopropanol pulps. Color coding shows different temperatures: green (135°C), black (145°C), and red (155°C). Blue dotted line represents the average of the methanol (SMW), ethanol (SEW), and isopropanol (SPW) correlations.

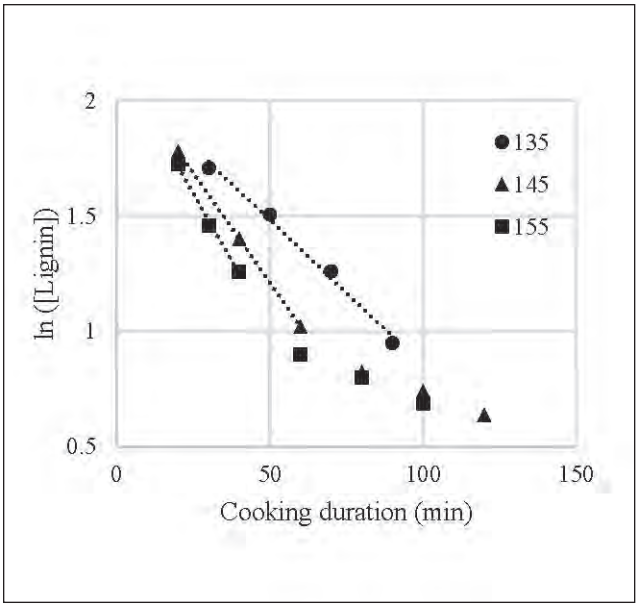
(not determined in this study) are the other possible contributing factor to high intercepts in lignin-kappa correlations.

Consequently, we corrected the acid insoluble Klason lignin content of pulps, not only for ash but also for permanganate non-oxidizable matter such as lipids and proteins. This is done by subtracting the intercept values at zero kappa in Fig. 3 from ash free Klason lignin for each corresponding pulp. The Klason lignin content corrected for ash and permanganate non-oxidizable matter for all pulps is plotted against kappa number in **Fig. 4**. It shows that the lignin content versus kappa relationship is not affected much by the type of solvent or pulping temperature. The intercepts of the modified correlations are now close to zero, similar to the kappa-Klason lignin correlations for wood species [40,42,43]. Hence this suggests that the ash and permanganate non-oxidizable matter (including protein) corrected Klason lignin represent the real amount of lignin in pulps. Considering the scatter in the data and that the correlations in Fig. 4 for the SMW, SEW, and SPW pulps do not differ much, it was considered appropriate to represent all the lignin-kappa data by a single straight-line correlation that passes through the origin with a slope of 0.134. This overall correlation of the data is also seen in Fig. 4.

DELIGNIFICATION KINETICS

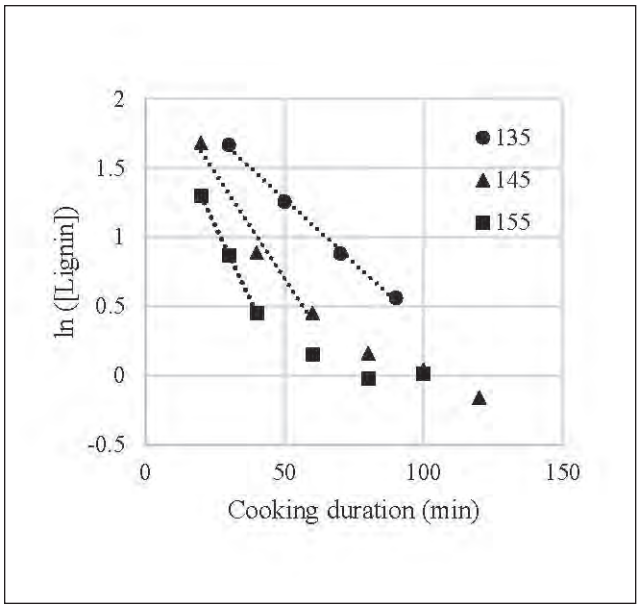
The delignification kinetics were determined for the three SAW pulping series with temperature (135°C–155°C) and time as variables. The lignin content of the pulps based on original SCS was calculated from the kappa number using Eq. (1):

$$[Lignin] = 0.134 \times kappa \times Pulp\ Yield \quad (1)$$

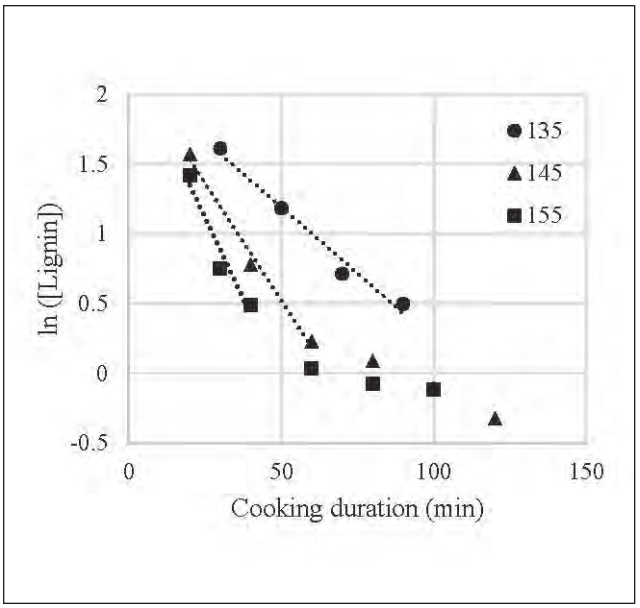


5. Natural logarithm of residual lignin (g/100 g SCS) vs. cooking duration for methanol (SMW) pulping.

Figures 5-7 show the calculated lignin expressed in % on original SCS plotted against cooking time for pulping with methanol (SMW), ethanol (SEW), and isopropanol (SPW), respectively. In accordance with first order delignification kinetics, a logarithmic scale is used for lignin on the vertical axis, while pulping time on the horizontal axis is a linear scale. This plot is selected based on pseudo first order delignification kinetics [46], which is valid during SAW cooking because the proton concentration is approximately constant during delignification as:



6. Natural logarithm of residual lignin (g/100 g SCS) vs. cooking duration for ethanol (SEW) pulping.



7. Natural logarithm of residual lignin (g/100 g SCS) vs. cooking duration for isopropanol (SPW) pulping.

$$-\frac{d[Lig]}{dt} = k'_{Lig}\,(T)\,[Lig]^a\,[H_3O^+]^b = k_{Lig}\,(T)\,[Lig] \qquad (2)$$

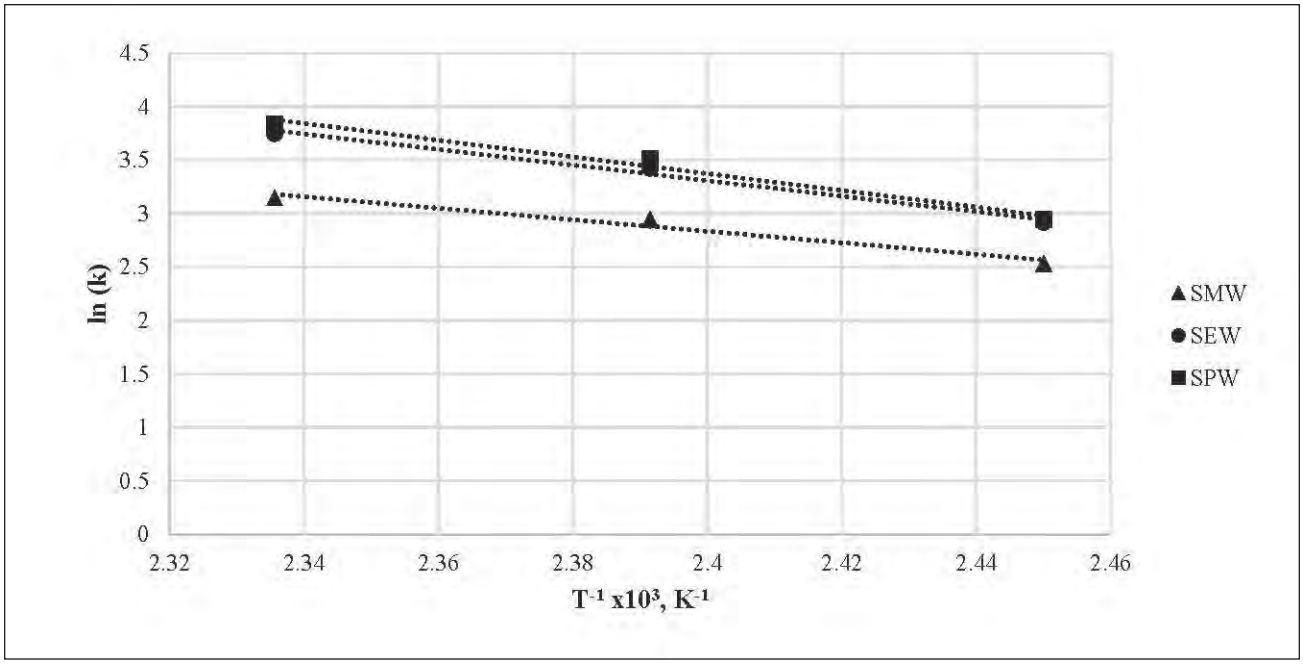
Only the first 3 to 4 data points were used to determine the first order delignification rate constant because these data points could reasonably be represented by straight lines of increasing slopes at increasingly higher temperature. The choice of 3 or 4 initial data points is somewhat arbitrary, and therefore the rate constants are subject to some uncertainty. However, it is clear that the data points obtained at longer cooking times and higher temperatures do not follow the same first order relationship, and thus are indicative of slower delignification during the residual kinetic phase. The onset of the residual delignification phase occurs at shorter cooking time at increasing temperature for all three SAW systems.

Since the lignin in SCS is 17.6% (after ash and protein corrections) while the extrapolated lignin at 10 min cooking time (i.e., after heat-up) is 7%–9% on original SCS, almost 50%–60% of the SCS lignin is dissolved during the heat-up time for SMW, SEW, and SPW. You et al. [14] also reported the same behavior during the initial phase of SCS delignification using SEW but at a different pulping liquor composition (12:22.5:65.5 w/w%) versus the present SAW composition of 12:44:44 w/w%. Iakovlev [11] identified two phases of delignification (bulk and residual phase), without an initial phase, when pulping spruce, beech, and wheat straw using SEW. In kraft and SEW delignification of wood species, most lignin is removed in the bulk phase [11]. However, for SCS delignification most lignin is removed during the initial phase. It is reported that the percentage of total lignin in the middle lamella and cell corners of annual fibers is much higher than for wood fibers [47]. Also, the structure of annual fibers is more porous than that of wood species, and these characteristics may explain the faster delignification rate during the initial cooking stage of annual fibers [48].

The delignification indicated in Figs. 5-7 by dotted lines is called bulk delignification. It follows pseudo first order kinetics as seen by the straight-line relationship between ln (lignin) and pulping time. At 135°C, the bulk phase extends to 90 min, while at higher temperatures (145°C and 155°C) it lasts for a shorter time before transition to the residual phase of delignification, which is characterized by a slower delignification rate. It can be seen that the residual phase for SEW and SPW starts when the lignin content reaches about 1.5%, while for SMW it starts at about 3% lignin (on SCS). At 145°C and 155°C, the residual phase begins after 60 min and 40 min of cooking (includes 10 min heat-up time), respectively, for both SEW and SPW. The onset of the residual delignification phase for SMW occurs after 60 and 50 min at 145°C and 155°C, respectively. Iakovlev and co-workers [49] showed that for beech and spruce, the SEW residual delignification phase appears when the lignin content decreases below 1% (on original wood), while the threshold for wheat straw is around 2.3% (kappa 30), the latter value without correcting for lipid/protein content. The onset of the residual phase at higher lignin content in SCS is not clear, but several differences between lignin structure in annual plants and wood could be responsible for the effect. The amount of lignin at the onset of residual delignification phase is higher for SMW than SEW and SPW (Figs. 5-7). The higher amount of lignin at the onset of residual delignification for SMW may be explained by the lower solubility of lignin in 50% methanol

	Rate Constant k_{Lig} x 10^3, min^{-1}			Activation Energy, kJ/mol
Temperature, °C	135°C	145°C	155°C	
SMW	12.6±0.1	19.0±0.0	23.3±0.2	44.7±1.4
SEW	18.5±0.2	30.7±0.9	42.5±0.0	60.5±0.7
SPW	19.0±0.4	33.6±0.3	46.5±2.8	65.1±1.3

III. Bulk delignification rate constants and activation energies (SMW = methanol, SEW = ethanol, SPW = isopropanol).



8. Arrhenius plot (delignification kinetics) for methanol (SMW), ethanol (SEW), and isopropanol (SPW) pulping based on rate constants from Table III.

compared to that in 50% ethanol and isopropanol based on their Hildebrand solubility parameters (δ values). Puumala [50] also reported that ethanol provides better delignification than methanol.

Bulk delignification rate constants were determined from the slopes of the straight lines in Figs. 5-7 and are shown in **Table III**. At each temperature, the delignification rate constants for SPW are highest, followed by SEW and SMW. The rate constants for each solvent system increase with increase in temperature. A 20°C increase in temperature (135°C to 155°C) results in 1.8, 2.3, and 2.4 times increase in delignification rate for SMW, SEW, and SPW, respectively. The maximum rate constant value achieved was 46.7±2.8 x 10^{-3} min^{-1} at 155°C for SPW delignification.

At similar pulping conditions, Iakovlev [11] reported a bulk delignification rate constant for three biomass species (at 135°C 30.9 x 10^{-3} min^{-1} for spruce; 39.9 x 1^{-3} min^{-1} for beech; and 31.1 x 10^{-3} min^{-1} for wheat straw; and at 145°C and 155 °C the values are 64 x10^{-3} min^{-1} and 135 x10^{-3} min^{-1} for spruce, respectively). At 135°C, the present SEW rate constants for SCS are a factor 1.7 lower than those of spruce and wheat straw, while at 155°C, the difference increases to a factor of 3.2. The low delignification rate constants in SAW pulping of SCS might be related to high ash content in SCS (6.1%, Table I), which lowers the effective acidity of the pulping system. The bulk delignification rate constants of the pulping solvents follow the sequence SPW > SEW > SMW. This sequence agrees with the lignin dissolution properties of cooking liquor of SPW > SEW > SMW. The lignin dissolution capacity of the cooking liquors may be estimated from the Hildebrand solubility parameter (δ) given by Eq. 3 [51]:

$$\delta = \sqrt{\left[\frac{(\Delta H - RT)\rho}{MW}\right]} \qquad (3)$$

where ΔH is heat of vaporization in J/mol, T is normal boiling point in Kelvin, MW is molecular weight in kg/mol, and ρ is density in kg/m^3.

Based on Eq. (3), the δ-values of fresh SMW, SEW, and SPW cooking solvents were calculated as 37.03, 36.46, and

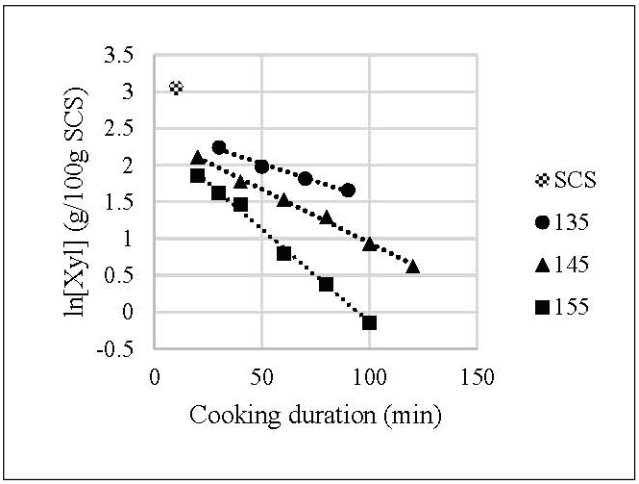
34.60 $(MPa)^{1/2}$, respectively. The presence of SO_2 in the cooking liquor had an insignificant effect on the δ-value. The δ-value of lignin can be determined based on knowledge of the atomic and functional group contributions in the phenylpropane unit. The δ-values of 27.73, 29.12, and 36.49 $(MPa)^{1/2}$ were obtained for typical structures of G, S, and H phenylpropane units respectively (see Appendix). Thus, the weighted average solubility parameter of SCS lignin (G:S:H of 68:28:4) [52] was 28.47 $(MPa)^{1/2}$. According to the Hildebrand solubility parameter theory, the closer the δ-values of the polymer and solvent are, the greater will be the polymer solubility in that solvent [53]. By comparing δ-values of the cooking liquors with δ-value of SCS lignin (28.47 $(MPa)^{1/2}$), it can be concluded that the SPW liquor is the best SCS lignin solvent, while SMW cooking liquor is the poorest solvent. It also shows that the H lignin units have a poorer solubility in the cooking liquors than the G and S units.

Rate constants at 135°C, 145°C, and 155°C from Table III were used to determine activation energies using the Arrhenius plot shown in **Fig. 8**. The activation energy values for SAW delignification (Table III) are much lower than those for SEW pulping of wood species like spruce (108 kJ/mol) and beech (102 kJ/mol) [49]. Many other researchers have also found low activation energies of delignification for different straws at different pulping conditions compared to those for wood species [48,54,55,56,57]. The lower activation energies may be explained by the high porosity of SCS where lignin is more easily accessible as compared to hardwood and softwood species.

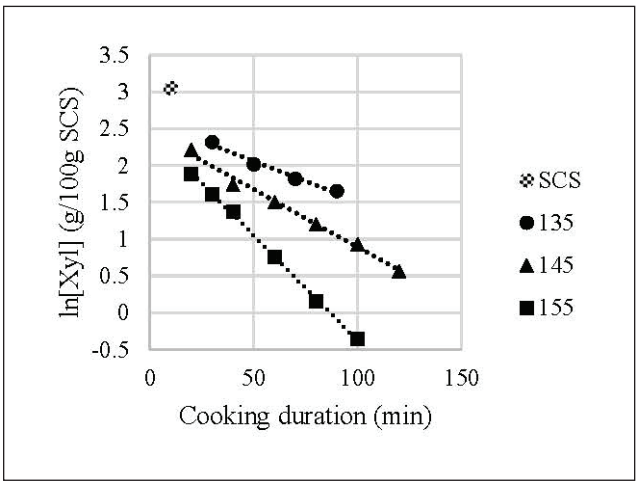
KINETICS OF XYLAN REMOVAL

Xylan is the most abundant hemicellulose in SCS, comprising nearly 22% of its total weight (Table I). Galactan and mannan are present in very small amounts, 0.9% and 0.6%, respectively. SCS also contains 3% arabinose, but these units are quickly removed during the initial cooking phase because of the high reactivity of the furanosidic bonds in an acidic environment [58]. Iakovlev [11] showed that 70% and 100% dissolution of arabinose took place during the heat-up period at 135°C and 165°C, respectively, in SEW pulping. Therefore, our study only addressed the kinetics of xylan removal.

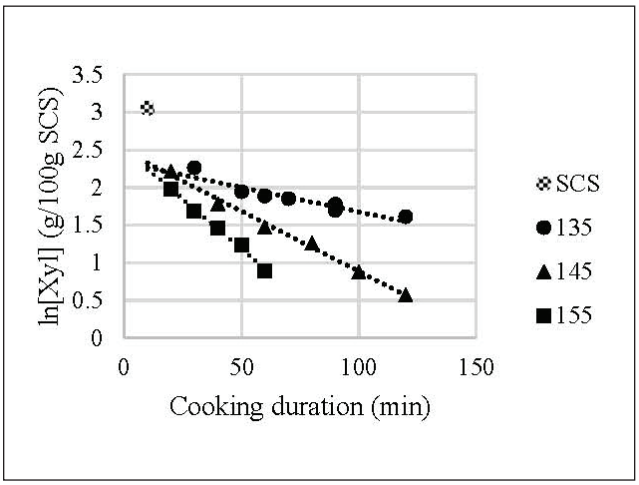
Two phases of xylan removal were observed in SMW, SEW, and SPW pulping of SCS; initial xylan dissolution proceeded by a first-order process, as can be seen in **Figs. 9-11**. By comparing the xylan content obtained by extrapolation to the heat-up time at 10 min with the xylan content in fresh SCS, it can be seen that about 50% of xylan is removed in the first phase (i.e., "initial phase"). You et al. [14] reported that two-thirds of SCS xylan was removed in the initial phase. The higher percentage xylan removal that was reported by You et al. [14] can be explained by the more acidic environment used due to a lower ethanol concentration (12:22.5:65.5 w/w% SO_2:ethanol:water). As 50%-60% of the SCS lignin was also removed during the initial phase, it seems likely that most of the xylan and lignin were removed as lignin-carbohydrate



9. Natural logarithm of residual xylan vs. cooking time for methanol (SMW) pulping of SCS.



10. Natural logarithm of residual xylan vs. cooking time for ethanol (SEW) pulping of SCS.



11. Natural logarithm of residual xylan vs. cooking time for isopropanol (SPW) pulping of SCS.

	Rate Constant k_{xyl} x 10^3, min^{-1}			Activation Energy, kJ/mol
Temperature, °C	135°C	145°C	155°C	
SMW	9.6±0.2	14.6±0.1	25.4±0.3	70.6±0.7
SEW	10.9±0.2	15.6±0.2	28.5±0.3	69.6±1.7
SPW	6.5±0.8	16.0±0.2	26.5±0.3	102.3±2.2

IV. Xylan removal (bulk phase) rate constants with activation energy data (SMW = methanol, SEW = ethanol, SPW = isopropanol).

complex (LCC) as described by Iakovlev [11]. The xylan content of the solid residue was calculated by taking into account the uronic anhydride (UA) content just as is done for hardwoods [59] as:

$$Xylan = Xylose\left(\frac{132}{150}\right) + UA\ (0.6)\left(\frac{132}{176}\right) \quad (4)$$

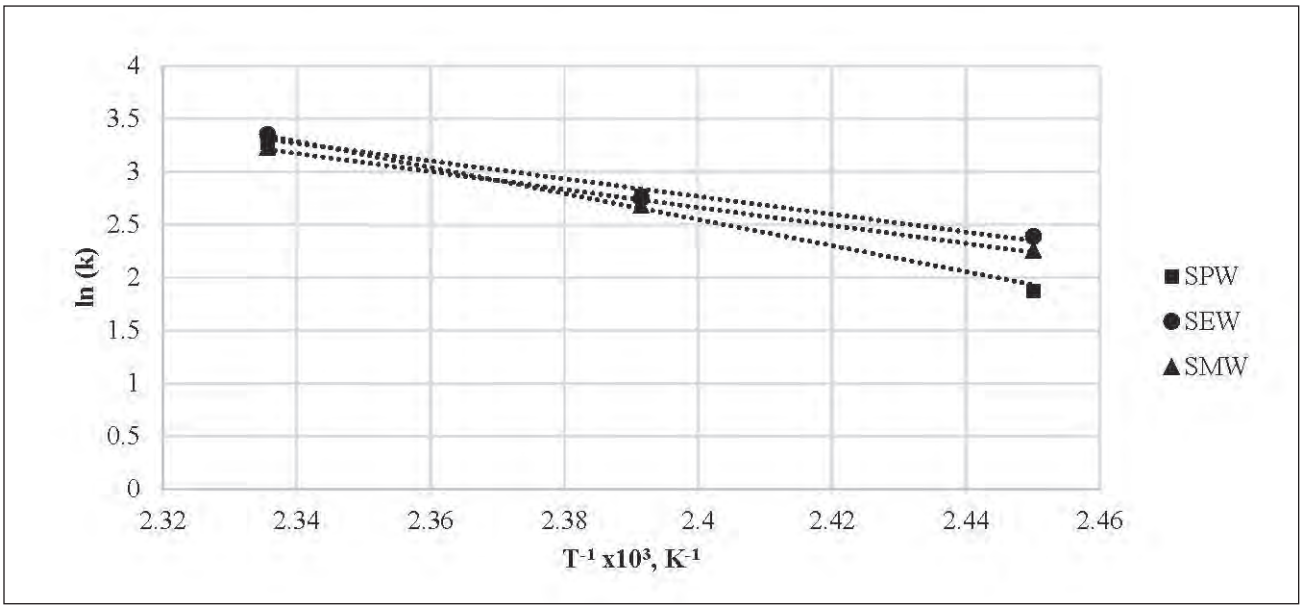
Because xylan dissolution occurs after acid hydrolysis following SN_1 substitution mechanism, the kinetics of xylan removal can be described by Eq. (5) [11]:

$$-\frac{d[Xyl]}{dt} = k'_{Xyl}\ (T)\ [Xyl]^a\ [H_3O^+]^b = k_{Xyl}\ (T)\ [Xyl] \quad (5)$$

where [Xyl] is xylan content of pulp (% SCS); k'_{Xyl} and k_{Xyl} are real and composite rate constants for xylan removal; $[H_3O^+]$ is hydronium ion concentration; T is reaction temperature; and a and b are reaction orders in xylan and hydronium ion concentration.

When the hydronium concentration is constant, and the reaction is first order in xylan, Eq. (5) implies a linear relationship between the natural logarithm of [Xyl] and cooking duration. This is seen for SMW, SEW, and SPW pulps in Fig. 9, Fig. 10, and Fig. 11, respectively.

The rate of xylan removal in the second phase, also called the bulk phase, is indicated by straight dotted lines in Figs. 9-11. Pseudo first order rate constants determined from their slopes are listed in **Table IV**. All the rate constants are nearly identical, indicating the same xylan removal rate for the three solvent systems at 145°C. This implies that the hydronium ion concentration in each pulping system is nearly the same, as was confirmed experimentally with spent liquors pH values ranging from 0.9 to 1.2. The maximum difference in pH values at similar pulping conditions was only 0.05 units. The present rate constant value at 135°C for SEW of 10.9 x 10^{-3} min^{-1} is in agreement with that of 11.6 x 10^{-3} min^{-1} determined by Iakovlev et al. [49] for SEW pulping of beech at the same temperature and fresh cooking liquor composition. This confirms the similar nature of xylan in SCS and hardwood species. Higher rate constant values for xylan removal were obtained by You et al. [14] for SEW pulping of SCS at a lower ethanol content (12:22.5:65.5 w/w% for SO_2:ethanol:water). The authors reported 8.74 x 10^{-3} min^{-1}, 20.5 x 10^{-3} min^{-1}, and 39.8 x 10^{-3} min^{-1} xylan removal rate constants at 135°C, 145°C, and 155°C, respectively. The higher rate



12. Arrhenius plot (xylan removal kinetics) for methanol (SMW), ethanol (SEW), and isopropanol (SPW) based on rate constants from Table IV.

	k_{Lig}/k_{Xyl}		
	135°C	145°C	155°C
SMW	1.3	1.3	0.9
SEW	1.7	2.0	1.5
SPW	2.9	2.1	1.8

V. Delignification selectivity over xylan removal in methanol (SMW), ethanol (SEW), and isopropanol (SPW) pulping systems.

constants can be explained by the higher effective acidity of the cooking liquor in the You et al. [14] study. Hence, it can be concluded that effective acidity of the pulping system significantly affects the xylan removal rate in SAW pulping.

The rate constants increase with temperature and were used to determine the activation energy through an Arrhenius plot seen in **Fig. 12**. The activation energies based on Arrhenius plot are listed in Table IV with rate constants. It can be seen from Table IV that activation energy values of SMW and SEW are nearly same (70 kJ/mol). Contrary to that, the SPW pulping system has significantly higher activation energy of xylan removal (102 kJ/mol). Iakovlev [11] reported a higher activation energy (110 kJ/mol) for xylan removal from spruce in SEW pulping. No activation energy data of xylan removal from beech and wheat straw was reported in that study. The high activation energy for spruce species may be related to the fact that softwood xylan contains twice the amount of 4-O-methylglucuronic acid units per xylose unit than that in hardwood xylan [60] and contains arabinose side chains [61]. It is known that the presence of 4-O-methylglucuronic acid partially stabilizes against xylan hydrolysis [62] at lower temperatures. You et al. [14] reported high rate constants and an activation energy of 106.6 kJ/mol for SEW pulping of SCS. The low activation energy for SEW (69.6 kJ/mol) in our case can be related to high ethanol concentration (22.5% vs. 44%), which ultimately affects the acidity of the pulping system and reaction rate.

The difference in activation energies of SPW (102 kJ/mol), SMW (70.6 kJ/mol), and SEW (69.6 kJ/mol) pulping systems might be related to extent of hydrolysis and alcoholysis in each system. In a recent study, Grisel et al. [63] employed methanol and ethanol for acid-catalyzed alcoholysis of wheat straw. It was interesting to note that the yields of glycosides and xylosides were significantly higher for methanol. Hu and co-workers [64] revealed that a high methanol-water ratio promoted methanolysis, resulting in faster conversion of xylose into methyl xylosides. According to Hu et al. [64], methanolysis of xylose dominates over its degradation at lower temperatures (i.e., 130°C vs. 150°C). Drouet and his team [26] synthesized alkyl-*ß-d*-xylosides employing different aliphatic alcohols, including methanol, ethanol, and propanol. They concluded that longer chain alcohols lowered the production of alkyl-*ß-d*-xylosides. Based on these studies, it can be concluded that a significant portion of SCS xylan might have been removed through formation of alkyl xylosides in SMW and SEW, resulting in low activation energies. On the other hand, alcoholysis of xylan in SPW pulping is less likely, and most of the xylan is removed just by hydrolysis. The formation of xylosides during SAW pulping will be reported in a future study that is based on chemical analysis of the spent liquors. The presence of xylosides in SAW fractionation is very important from the point of view of solvent recovery and thus for the economics of the process.

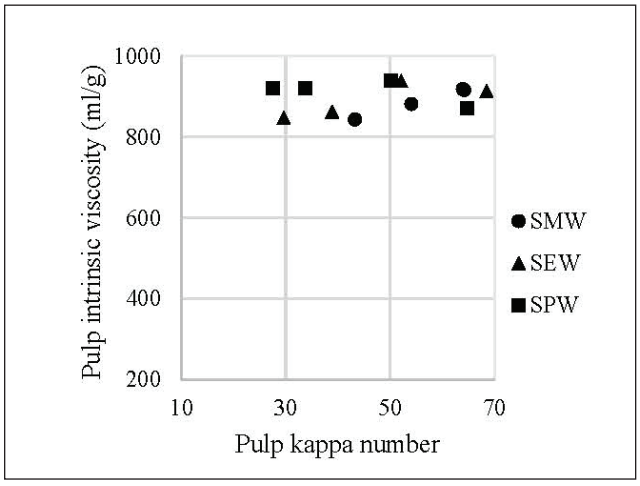
The ratio of the reaction rate constants for delignification and xylan removal are listed in **Table V**. It shows that that the delignification/xylan removal selectivity is highest for the SPW pulping system, and that the highest selectivity and thus yield at the same lignin content or kappa number can be obtained at low temperatures. This is in agreement with the finding of Iakovlev [11].

KINETICS OF CELLULOSE HYDROLYSIS

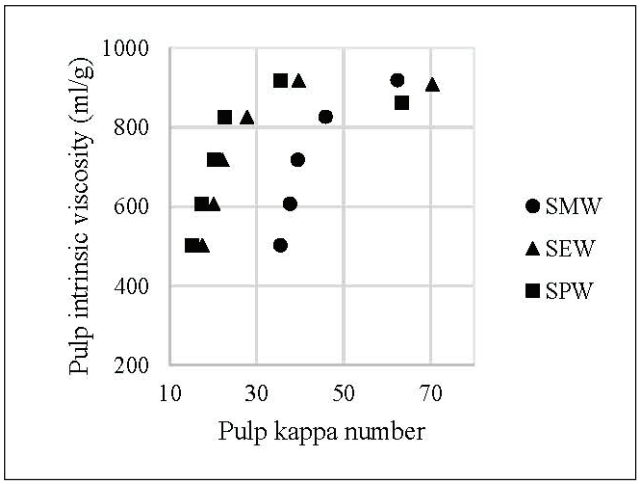
Cellulose degree of polymerization (DP) was calculated by measuring the intrinsic viscosity of the pulp in cupriethylenediamine (CED) solution. The viscosity-average DP of cellulose is nearly equal to the weight-average DP [65]. In the current study, we used the pulp viscosity ([η]), hemicellulose content ([Hemi]), and cellulose content ([Cel]) in the following correlation to determine the cellulose DP [66]:

$$DP_v = \left(\frac{1.65[\eta]-116[Hemi]_{pulp}}{[Cel]_{pulp}}\right)^{1.111} \quad (6)$$

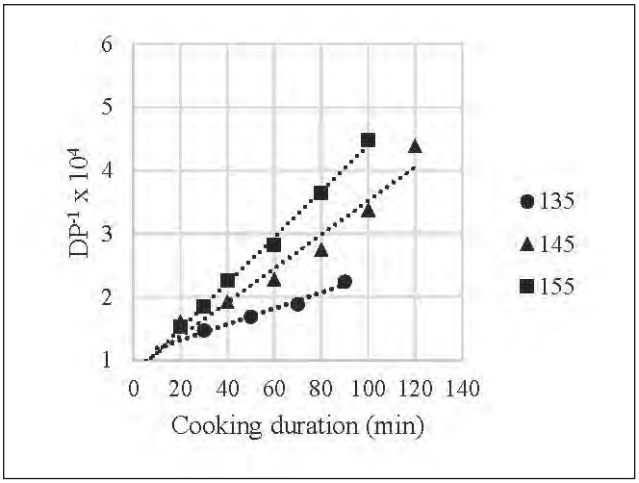
Kappa vs. viscosity relationships for SMW, SEW, and SPW pulps are shown in **Fig. 13**, **Fig. 14**, and **Fig. 15** at 135°C, 145°C, and 155°C, respectively. It can be observed that the intrinsic viscosity remains high (>800 ml/g) at 135°C down to a kappa number of 30 for SEW and SPW (Fig. 13). At 145°C



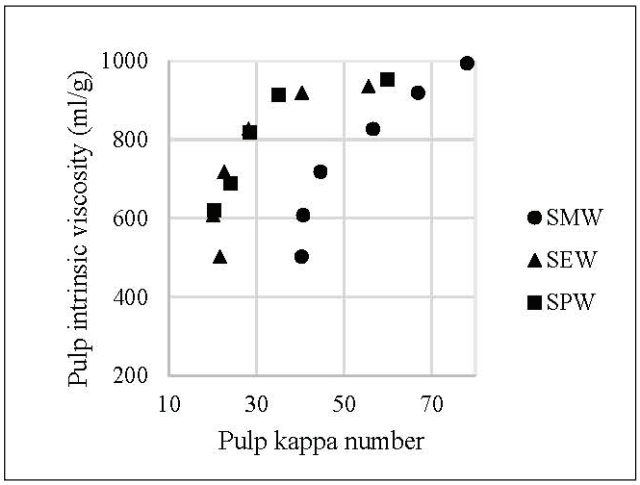
13. Methanol (SMW), ethanol (SEW) and isopropanol (SPW) pulps: viscosity at 135°C.



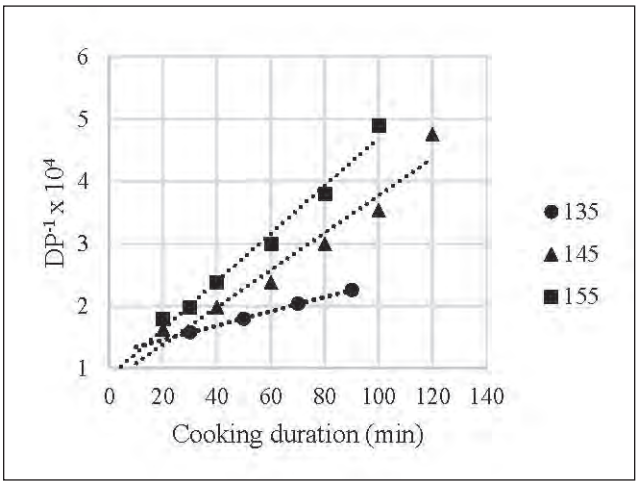
14. Methanol (SMW), ethanol (SEW), and isopropanol (SPW) pulps: viscosity at 145°C.



16. Cellulose hydrolysis kinetics in methanol (SMW) pulping system.



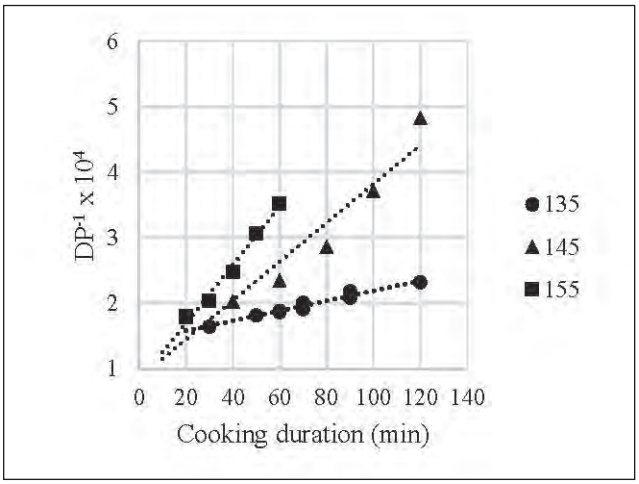
15. Methanol (SMW), ethanol (SEW) and isopropanol (SPW) pulps: viscosity at 155°C.



17. Cellulose hydrolysis kinetics in ethanol (SEW) pulping system.

in Fig. 14, however, the viscosity drops rapidly for SMW pulping below kappa 45, while the same occurs for SEW and SPW below kappa 25. At 155°C, these sharp drops occur at higher kappa numbers of 50 and 30, respectively (Fig. 15). Hence, at lower kappa numbers, SMW pulp shows the lowest viscosity while for SEW and SPW, the values are nearly equal. It has been reported that the use of non-swelling media like n-propanol-water (90/10 v/v%) and methylethylketone (MEK) increases the rate of cellulose chain cleavage [67]. Ethanol addition has a similar effect by decreasing the structural stress of the cellulose chains [27,67]. Addition of aprotic solvents, like GVL and THF, as well as p-dioxane, to water also accelerates the rate of hydrolysis [29]. These findings from literature studies imply that cellulose hydrolysis in SAW pulping will be higher than that in water.

The reciprocal of DP was plotted against cooking time to evaluate the rate of cellulose hydrolysis in the three different fractionation systems (**Fig. 16**, **Fig. 17**, **Fig. 18**). The linear



18. Cellulose hydrolysis kinetics in isopropanol (SPW) pulping system.

	Rate Constant k_{Cel} x 10^6, min^{-1}			Activation Energy, kJ/mol
Temperature	135°C	145°C	155°C	
SMW	1.26±0.03	2.68±0.13	3.64±0.04	77±4
SEW	1.14±0.01	2.99±0.15	3.84±0.08	88±8
SPW	0.76±0.03	2.96±0.24	4.46±0.09	130±10

VI. Rate constant and activation energy values for cellulose hydrolysis (SMW = methanol, SEW = ethanol, SPW = isopropanol).

relationship between DP^{-1} and time shows that cellulose hydrolysis is zero order in cellulose and obeys Eq. (7) under the assumption of constant hydronium ion concentration:

$$\frac{1}{DP} - \frac{1}{DP_0} = k'_{Cel}\,(T)\;[H_3O^+]\,t = k_{Cel}\,(T)\,t \qquad (7)$$

The convergence point of the straight lines reveals that the DP_0 of cellulose in original SCS is between 8000–10000. Rate constants for cellulose hydrolysis were calculated from the slopes of the straight lines and are shown in **Table VI**. The rate constants for SEW pulping are 1.14 x 10^{-6} min^{-1}, 2.99 x 10^{-6} min^{-1}, and 3.84 x 10^{-6} min^{-1} at 135°C, 145°C, and 155°C, respectively (Table VI). The corresponding rate constants reported by You et al. [14] for SCS at a lower ethanol concentration than in the present study (22.5 vs 44 w/w%) are 1.59 x 10^{-6} min^{-1}, 5.86 x 10^{-6} min^{-1}, and 17.0 x 10^{-6} min^{-1}, respectively; i.e., cellulose hydrolysis rate constants that are 1.4, 2.0, and 4.4 times higher, respectively. Again, this shows that the effective acidity is lower at higher ethanol concentrations. Iakovlev [11], who employed SEW liquor of essentially the same composition as the present study (12:43.5:44.5 vs. 12:44:44) for pulping of spruce and beech, found rate constants of 1.51 x 10^{-6} min^{-1} (135°C), 4.76 x 10^{-6} min^{-1} (145°C), and 15.4 x 10^{-6} min^{-1} (155°C) for spruce and 1.04 x 10^{-6} min^{-1} (125°C), 2.75 x 10^{-6} min^{-1} (135°C), and 7.80 x 10^{-6} min^{-1} (145°C) for beech. The mostly lower rate constants in the present SCS study compared to those obtained for wood species may be related to the presence of a significant amount of ash in SCS (6.1%; Table I), which decreases the effective acidity of the pulping system.

Arrhenius equation was applied to determine the sensitivity of the rate constants to reaction temperature. The activation energy of cellulose hydrolysis for SMW, SEW, and SPW were found to be 77±4, 88±8, and 130±10 kJ/mol, respectively (Table VI). These activation energies are similar to many other agricultural materials used for pulping; however, they are much lower than for wood species reported in the literature.

Generally, the low activation energies of SCS cellulose hydrolysis may be related to differences in the physical structure of biomass; i.e., degree of polymerization and crystallinity. Crystallinity values have been reported that vary from 73% for cotton linter to 23% for corn maize [68,69]. According to Millett et al. [70], wood cellulose hydrolyzes twice as quickly as cotton cellulose. Low activation energies of cellulose hydrolysis for agricultural biomass have been reported in literature that range from 34 kJ/mol for rice husk [71] to 80.34 kJ/mol for corn cobs [72]. For SEW pulping of spruce [46] and beech [49], activation energy values of 166 kJ/mol and 135 kJ/mol were reported, respectively. You et al. [14] also found an activation energy of 166 kJ/mol for SCS cellulose hydrolysis. Since the ethanol concentration in our cooking liquor (SEW) was 44% (by weight), which is almost twice that of You et al. [14] (22.5%), it appears that doubling the ethanol concentration reduces the activation energy for cellulose hydrolysis by about half.

	k_{Lig}/k_{Cel} x 10^3		
	135°C	145°C	155°C
SMW	10.0	7.1	6.4
SEW	16.2	10.3	11.1
SPW	25.0	11.4	10.4

VII. Delignification selectivity over cellulose hydrolysis (SMW = methanol, SEW = ethanol, SPW = isopropanol).

SPW pulping has a higher activation energy for cellulose hydrolysis compared to SMW and SEW (Table VI). This might be explained in terms of the effect of solvent on the activity of proton, which is responsible for the cellulose hydrolysis. It is known that the addition of an organic solvent changes the proton availability in acidic media and hence affects the hydrolysis kinetics [73]. Similarly, the addition of ethanol increases the cellulose degradation by decreasing the proton hydration [27]. In terms of polarity, the employed alcohols can be arranged in the order of their increasing polarity as isopropanol < ethanol < methanol. It suggests that isopropanol is the least favorable solvent for proton hydration, and thus increases the energy barrier for cellulose hydrolysis.

The delignification selectivity is listed in **Table VII**. It shows that pulping with isopropanol in the SAW process at low temperature provides the highest delignification relative to cellulose hydrolysis among the three employed solvents.

CONCLUSIONS

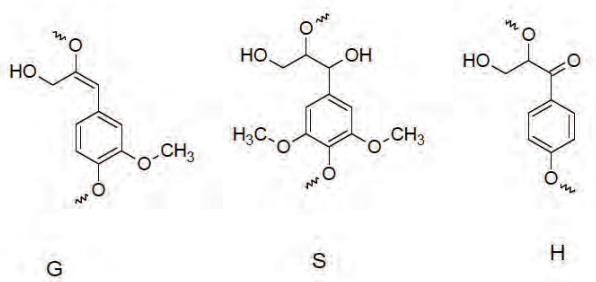
SCS was fractionated into cellulose, hemicellulose, and lignin by the SAW process using methanol, ethanol, or isopropanol. Delignification kinetics for SCS were developed for the first time by correcting Klason lignin for ash (mostly silica) and permanganate non-oxidizable material (proteins identified as one of the contributing factors). In terms of delignification, SPW is the most effective pulping system because it has the highest lignin dissolution capacity, while SMW has the lowest delignification rate. The low activation energy values for SCS relative to wood species indicate the ease of delignification for highly porous agricultural residues such as SCS. The residual delignification phase for SEW and SPW starts when the lignin content reaches 1.5% (on original SCS), while for SMW it starts at about 3%. This compares to less than 1% for beech and spruce using SEW fractionation. Thus, the lignin content of SAW produced SCS pulp is relatively high compared to SEW wood pulp. The rate of xylan removal is the same in all three solvent systems at 145°C, but it is suggested that a significant amount of xylan in SMW and SEW is removed by alcoholysis, as indicated by the higher activation energy of the SPW system. The possibility of significantly less alcoholysis reactions (especially with xylan) in SPW pulping may be an advantage over other solvents from a solvent recovery point of view. The cellulose hydrolysis rate is nearly the same for all three solvent systems at 145°C, but the activation energy is highest for the SPW pulping system. It is possible to produce a paper grade quality SCS pulp of 800–850 cP viscosity and kappa number of about 25 using SEW or SPW pulping at 145°C for 60 min, while SMW pulps have a much higher lignin content in this viscosity range. **TJ**

ACKNOWLEDGEMENTS

The authors are grateful to the University of Maine Ober Chair, which provided financial resources for this research. A special appreciation goes to American Process Inc. (API) in Thomaston, GA, USA, for providing feedstock material.

APPENDIX

Typical structures of G, S, and H phenylpropane lignin units.



LITERATURE CITED

1. FAO, "Forest Products Statistics: 2014 Global Forest Products Facts and Figures," Food and Agriculture Organization of the United Nations, Rome, 2014. Available [Online] http://www.fao.org/3/a-bc092e.pdf <20June2017>.
2. Moryia, R.Y., Goncalves, A.R., and Duarte, M.C.T., *Appl. Biochem. Biotechnol.* 136-140(7): 501(2007).
3. Rocero, M.B., Torres, A.L., Colom, J.F., et al., *Bioresour. Technol.* 87(3): 305(2003).
4. Saad, M.B.W., Oliveira, L.R.M., Candido, R.G.G., et al., *Enzyme Microb. Technol.* 43(2): 220(2008).
5. Neto, M.A.T., in *Biomass Power Generation: Sugarcane Bagasse and Trash* (S.J. Hassuani, M.L.R.V. Leal, and I.C. Macedo, Eds.) 1st edn., CTC, Piracicaba, Brazil, 2005, p. 24.
6. FAO, "FAOSTAT," Food and Agriculture Organization of the United Nations-Statistics Division, Rome, 2014. Available [Online] http://www.fao.org/faostat/en/#compare <6Nov2016>.
7. Canilha, L., Chandel, A.K., Milessi, T.S.d.S., et al., "Bioconversion of sugarcane biomass into ethanol: an overview about composition, pretreatment methods, detoxification of hydrolysates, enzymatic saccharification, and ethanol fermentation," *J. Biomed. Biotechnol.*, 2012. Available [Online] http://dx.doi.org/10.1155/2012/989572.
8. Goncalves, A.R., Benar, P., Costa, S.M., et al., *Appl. Biochem. Biotechnol.* 121-124(5): 821(2005).
9. Chagas, A.L.S., in *Biofuels in Brazil: Fundamental Aspects, Recent Developments, and Future Perspectives* (S.S. da Silva and A.K. Chandel, Eds.), Springer International Publishing, Cham, Switzerland, 2014, p. 79.
10. Bajpai, P., *Biotechnology for Pulp and Paper Processing*, Springer Science & Business Media, New York, 2012, pp. 7-13.
11. Iakovlev, M., "SO_2-ethanol-water (SEW) fractionation of lignocellulosics," Ph.D. thesis, Aalto University, Espoo, Finland, 2011.
12. Yamamoto, M., "SO_2-ethanol-water fractionation and enzymatic hydrolysis of forest biomass," Ph.D. thesis, Aalto University, Helsinki, 2014.
13. Sklavounos, E., "Conditioning of SO_2-ethanol-water (SEW) spent liquor from lignocellulosics for ABE fermentation to biofuels and chemicals," Ph.D. thesis, Aalto Unversity, Helsinki, 2014.
14. You, X., van Heiningen, A., Sixta, H., et al., *Bioresour. Technol.* 212: 111(2016).
15. Schorning, P., "Base-free sulfite pulping of wood," *Faserforsch. Textiltech.* 8: 487(1957).
16. Primakov, S., Tsarenko, I., and Zaplatin, V., "Delignification of wood by aqueous-alcohol solutions of sulfur dioxide," *Koksnes Kim.* 6: 39(1979).
17. Jurgens, G., Survase, S., Berezina, O., et al., *Biotechnol. Lett.* 34(8): 1415(2012).
18. Iakovlev, M. and van Heiningen, A., *ChemSusChem* 5(8): 1625(2012).
19. Aziz, S. and Sarkanen, K., *Tappi J.* 72(3): 169(1989).
20. Paszner, L. and Cho, H., *Tappi J.* 72(2): 135(1989).
21. Eliashberg, M.G., Parfenova, A.I., and Tikhomirova, E.V., "The theory of sulfite pulping and its practical importance. I. The sulfonation of lignin with aqueous sulfur dioxide solutions," *Bum. Prom-st.* 30(9): 9(1955).
22. Iakovlev, M. and van Heiningen, A., *RSC Adv.* 2(7): 3057(2012).

23. Tsypkina, M., Vishnevskaya, S., Boyarskaya, R., et al., "Sulfonation and dissolution of lignin in sulfite pulping. 1. Sulfonating agents," *Koksnes Kim.* 1: 19(1981).
24. Primakov, S., "Delignification of various wood species with aqueous-alcoholic solutions," *Nauchn. Tr. Vses. Nauchn.-Issled. Inst. Tsellyulozn.-Bumazhn. Prom.* 47: 69(1961).
25. Zhang, Z., Harrison, M.D., Rackemann, D.W., et al., *Green Chem.* 18(2): 360(2016).
26. Drouet, P., Zhang, M., and Legoy, M.D., *Biotechnol. Bioeng.* 43(11): 1075(1994).
27. Lai, Y.-Z., "Chemical degradation," in *Wood and Cellulose Chemistry* (D.N. Hon and N. Shiraishi, Eds.) 2nd edn., Marcel Dekker, New York, 2000.
28. Garves, K., *Cellul. Chem. Technol.* 18(1): 3(1984).
29. Mellmer, M.A., Martin Alonso, D., Luterbacher, J.S., et al., *Green Chem.* 16(11): 4659(2014).
30. Zhu, J.Y., Chai, X.S., and Dhasmana, B., *J. Pulp Pap. Sci.* 25(7): 256(1999).
31. Oliet, M., Garcia, J., Rodriguez, F., et al., *Chem. Eng. J.* 87(2): 157(2002).
32. Lee, J., Jang, Y.S., Choi, S.J., et al., *Appl. Environ. Microbiol.* 78(5): 1416(2012).
33. Papoutsakis, E.T., *Curr. Opin. Biotechnol.* 19(5): 420(2008).
34. Scott, R.W., *Anal. Chem.* 51(7): 936(1979).
35. Mariotti, F., Tome, D., and Mirand, P.P., *Crit. Rev. Food Sci. Nutr.* 48(2): 177(2008).
36. Gómez, E.O., Souza, R.T.G., Rocha, G.J.M., et al., in *Sugarcane Bioethanol: R&D for Productivity and Sustainability* (L. Cortez, Ed.) Edgard Blucher, São Paulo, Brazil, 2010, pp. 637-659.
37. Santos, F.A., Queiróz, J.H., Colodette, J.L., et al., *Quim. Nova* 35(5): 1004(2012).
38. Costa, S.M.D., Aguiar, A., Luz, S.M.d., et al., in *Polysaccharides* (K.G. Ramawat and J.M. Merillon, Eds.), Springer International Publishing, Cham, Switzerland, 2015, pp. 513-533.
39. Szczerbowski, D., Pitarelo, A.P., Zandona Filho, A., et al., *Carbohydr. Polym.* 114: 95(2014).
40. Iakovlev, M. and van Heiningen, A., *J. Wood Chem. Technol.* 31(3): 223(2011).
41. Tasman, J. and Berzins, V., *Tappi* 40: 699(1957).
42. Li, J. and Gellerstedt, G., *Nord. Pulp Pap. Res. J.* 13(2): 147(1998).
43. Kyrklund, B. and Strandell, G., *Pap. Puu* 51(4): 299(1969).
44. Oreopoulou, V., *Cellul. Chem. Technol.* 22(1): 53(1988).
45. del Río, J.C., Marquesa, G., Linoa, A.G., et al., *Ind. Crops. Prod.* 77: 992(2015).
46. Iakovlev, M., Paakkonen, T., and van Heiningen, A., *Holzforschung* 63(6): 779(2009).
47. Zhai, H.M. and Lee, Z.Z., *Wood Chem. Technol.* 9(3): 387(1989).
48. Huang, G., Shi, J.X., and Langrish, T.A., *Bioresour. Technol.* 98(6): 1218(2007).
49. Iakovlev, M., Sixta, H., and van Heiningen, A., *J. Wood Chem. Technol.* 31(3): 250(2011).

ABOUT THE AUTHORS

We chose this topic because sugarcane straw (SCS) is an abundantly available biomass residue that is being considered for pulping using the SO_2-ethanol-water (SEW or trademarked AVAP) process. We wanted to understand what the effect was when using methanol and isopropanol instead of ethanol during pulping.

Ethanol solvent system (SEW) follows the same reaction order for SCS as described for different lignocellulosic biomass described in the literature. However, the presence of the alcohols reduces the degradation of the dissolved sugars, and the delignification rate is improved when using isopropanol.

The most difficult aspect of this research was producing consistent kinetic data, as ash content varies for SCS, even within same batch. This problem was overcome by screening SCS through standard sieves and discarding the fraction (mostly silica) retained in pan.

We discovered that despite many obstacles, success and breakthroughs occur by perseverance and collaboration. It was surprising that the activation energy values for carbohydrates hydrolysis were higher with the isopropanol pulping system, but for delignification, the values were similar to the SEW system.

The use of isopropanol might be beneficial in mill pulping systems, as it offers better delignification than methanol and ethanol. Also, the use of isopropanol will reduce capital cost and the severity of safety regulations.



Sharazi



van Heiningen

Although the use of isopropanol and/or ethanol in SAW pulping offers distinctive advantages, research on solvent recovery is still needed. Also, these organosolv systems need to be evaluated for alcoholysis reactions, i.e., reaction with carbohydrates and lignin.

Sharazi is a doctorate student and van Heiningen is professor in the Department of Chemical and Biological Engineering at the University of Maine, Orono, ME, USA. Email Sharazi at asif.sharazi@maine.edu.

50. Puumala, R., "Organosolv pulping and a preliminary vapor-liquid equilibrium study of a sulfur dioxide, ethanol, water system," Master's thesis, Michigan Technological University, Houghton, MI, USA, 1991.
51. Schuerch, C.J., *J. Am. Chem. Soc.* 74(20): 5061(1952).
52. del Río, J.C., Lino, A.G., Colodette, J.L., et al., *Biomass Bioenergy* 81: 322(2015).
53. Hildebrand, J.H. and Scott, R.L., *The Solubility of Nonelectrolytes*, Reinhold, New York, 1950.
54. Huang, G. and Shi, Y., *Zhongguo Zaozhi* 5(3): 35(1986).
55. El-Sakhawy, M., Lonnberg, B., Ibrahim, A.A., et al., *Cellul. Chem. Technol.* 30(3-4): 281(1996).
56. Huang, G., Zhang, C., and Chen, Z., *Chin. J. Chem. Eng.* 14(6): 729(2006).
57. Ho, C.-L., Wu, K.-T., Wang, E.I.-C., et al., *Ind. Eng. Chem. Res.* 50(7): 3849(2011).
58. Shafizadeh, F., *Tappi* 46(6): 381(1963).
59. Genco, J.M., Busayasakul, N., Medhora, H.K., et al., *Tappi J.* 73(4): 223(1990).
60. Sjöström, E., *Wood Chemistry: Fundamentals and Applications*, Academic Press, New York, 1981.
61. Fengel, D. and Wegener, G., *Wood - Chemistry, Ultrastructure, Reactions*, Walter de Gruyter, Berlin, 1984.
62. Meier, H., *Sven. Papperstidn.* 65: 299(1962).
63. Grisel, R., van der Waal, J., de Jong, E., et al., *Catal. Today* 223: 3(2014).
64. Hu, X., Lievens, C., and Li, C.-Z., *ChemSusChem* 5(8): 1427(2012).
65. Evans, R. and Wallis, A.F.A, *J. Appl. Polym. Sci.* 37(8): 2331(1989).
66. da Silva Perez, D. and van Heiningen, A., *Cellulose* 22(6): 3967(2015).
67. Philipp, B., Jacopian, V., and Loth, F., in *Hydrolysis of Cellulose: Mechanisms of Enzymatic and Acid Catalysis* (R.D. Brown, Jr., and L. Jurasek, Eds.) Vol. 181, ACS, Washington, DC, 1979, pp. 127-143.
68. Aberuagba, F., "The kinetics of acid hydrolysis of wastes cellulose from maize cobs and groundnut shells," *Annu. Conf. Niger. Soc. Chem. Eng.*, Nigerian Society of Chemical Engineers, Ikeja, Nigeria, 1997.
69. Ghose, T.K., *Adv. Biochem. Eng.* 6: 39(1977).
70. Millett, M.A., Moore, W.E., and Saeman, J.F., *Ind. Eng. Chem.* 46(7): 1493(1954).
71. Ajani, A.O., Agarry, S.E., and Agbede, O.O., *J. Appl. Sci. Environ. Manage.* 15(4): 531(2011).
72. Eken-Saracoglu, N., Mutlu, S., Dilmac, G., et al., *Bioresour. Technol.* 65(1-2): 29(1998).
73. Mellmer, M.A., Sener, C., Gallo, J.M.R., et al., *Angew. Chem., Int. Ed.* 53(44): 11872(2014).

Improving the efficiency of hydrogen peroxide bleaching of chemimechanical pulp by continuous replenishment of bleaching chemicals

XIANQI SUN, QINGXI HOU, BINGXU ZHANG, AND GUANTING ZHAO

ABSTRACT: Hydrogen peroxide (H_2O_2) is commonly used to bleach chemimechanical pulp. A decrease in the concentrations of the bleaching reagents throughout the bleaching process results in low bleaching efficiencies. In this study, chemical solutions were continuously added into the pulp slurry during the bleaching process to maintain constant concentrations of H_2O_2 and total alkali in the bleaching system to improve bleaching efficiency. The results showed that when the H_2O_2 and total alkali concentrations were maintained at 4.5 g/L and 0.79 g/L, respectively, for 50 min, the bleaching efficiency reached 16.79 (Δ% ISO brightness/Δ% H_2O_2 consumed [on ovendry pulp]), which was significantly higher than 7.38 obtained by using the high-consistency bleaching method. The results confirmed that continuous replenishment of chemical solutions into the bleaching system to maintain the constant chemical concentrations improved the efficiency of H_2O_2 bleaching of the chemimechanical pulp.

Application: Continuous replenishment of H_2O_2 during chemimechanical pulp bleaching improves bleaching efficiency and reduces production costs.

Bleached chemimechanical pulp is an important fiber stock. It offers advantages of higher pulping yield, greater opacity, and higher bulk. It is commonly used in many kinds of paper products, including lightweight coated paper, supercalendered paper, and wallpaper [1]. Two primary processes for the production of bleached chemimechanical pulp are the pre-conditioning refiner chemical treatment, alkaline peroxide mechanical pulping process, and the bleached chemithermomechanical pulping process. Peroxide bleaching is used for brightening both types of pulps [2]. The advantages of peroxide bleaching include high brightening capabilities, less yellowing after bleaching, and low environmental impact of bleaching effluents. However, the bleaching efficiency, which can be defined as % ISO brightness/% hydrogen peroxide (H_2O_2) consumed (on ovendry pulp), is very low [3]. In the bleaching process, H_2O_2 is primarily consumed by two simultaneously competing reactions: 1) the self-decomposition of H_2O_2, and 2) the bleaching reaction of H_2O_2 with the chemimechanical pulp. The former reaction can consume a significant portion of the total H_2O_2 applied, which can result in low brightness gains [4,5]. Therefore, to improve the bleaching efficiency of H_2O_2, the bleaching reaction should be selected to minimize H_2O_2 decomposition. An important factor affecting the selectivity of the reaction is the chemical concentration in the bleaching system.

An H_2O_2 bleaching solution is comprised of various chemical constituents. During the bleaching process, the concentrations of various chemicals, especially H_2O_2 and total alkali, decline to various degrees. In the bleaching system containing high concentrations of chemicals, the rate of the brightening reaction is high, but the rate of H_2O_2 decomposition is also high [6,7]. In the conventional high-consistency peroxide bleaching process, the concentrations of H_2O_2 and total alkali at the beginning are approximately 20 g H_2O_2/L and 10 g sodium hydroxide (NaOH)/L (~12 pH or more), and the values at the end of the bleaching reaction are 5.0 g/L and 0.2 g NaOH/L (~ 9 pH) [8]. A previous study showed that the concentrations of these chemicals are not optimal for high bleaching efficiency (i.e., they are too high at the start and are too low at the end, which results in low bleaching efficiency) [9].

Reasonable control of the chemical concentration profiles during peroxide bleaching can be an effective method to improve brightening efficiency [3,10,11]. In the last stage of a traditional high-consistency peroxide bleaching process, a large amount of unreacted H_2O_2 often remains in the pulp because of insufficient alkali to activate the bleach. Zhao et al. [12] added additional NaOH midway during the bleaching process so that the residual H_2O_2 could be activated later during the bleaching stage. This study showed that the bleaching efficiency with the addition of NaOH increased by 0.61 (Δ% ISO brightness/Δ% H_2O_2 consumed) when compared

with that of the control. Wang [10] adopted the same method to bleach wheat straw pulp and observed similar results. The addition of extra alkali in the middle of the bleaching process enhanced the bleaching efficiency by increasing the alkali concentration in the latter portion of bleaching process. However, the alkali concentration in these bleaching systems still decreased when alkali was added midway through the bleaching stage, although it did result in a slight enhancement of bleaching efficiency (i.e., Δ% ISO brightness/Δ% H_2O_2 consumed).

Two-stage peroxide bleaching is also an effective method for promoting brightening reactions while minimizing undesired reactions. The initial alkali and peroxide concentrations of both stages are lower than those of a single peroxide stage, and chemical consumption was decreased by 10%–20% [13]. Although two-stage peroxide bleaching can solve the excessively high chemical concentrations at the beginning of bleaching, the issue of insufficient chemical concentrations toward the end of the bleaching stage remains unsolved.

Displacement bleaching has also been studied in peroxide bleaching of chemimechanical pulp [14,15]. Zhao [3] studied a single displacement bleaching stage with a chemithermomechanical pulp (CTMP). Zhao [3] showed that under optimized peroxide bleaching conditions, the bleaching efficiency reached 10.79 (Δ% ISO brightness/Δ% H_2O_2 consumed). The initial peroxide and alkali concentrations were lower in this process than those of conventional high-consistency peroxide bleaching.

Although the chemical concentrations in the peroxide bleaching system are balanced to a certain degree by these methods, the concentrations of bleaching reagents decrease throughout the reaction, which still results in low bleaching efficiencies. This study focused on improving bleaching efficiency by maintaining constant concentrations of bleaching reagents. We continuously replenished the chemicals to the bleaching stage to account for the chemicals consumed during the brightening reactions. We have termed this process as "continuous chemical supplement" (CCS) peroxide bleaching. CCS peroxide bleaching for poplar CTMP was studied. A response surface methodology was used for the experimental design to determine the optimum H_2O_2 and total alkali levels of the CSS peroxide bleaching process. The impact of this process on peroxide bleaching efficiency (i.e., Δ% ISO brightness/Δ% H_2O_2 consumed) was also assessed.

EXPERIMENTAL

Raw material

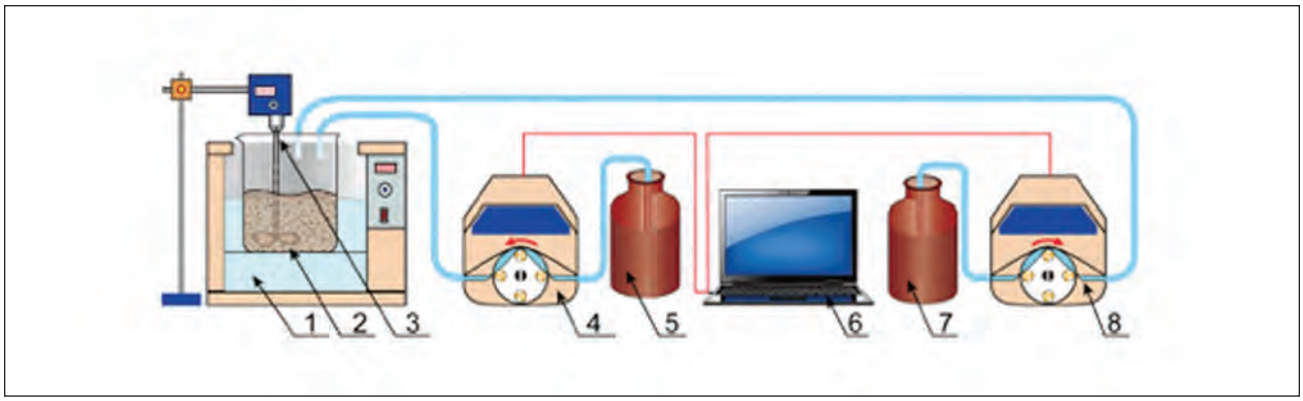
Unbleached poplar CTMP with an ISO brightness of 46.07% was obtained from a CTMP mill in Shandong Province, China. This pulp was first washed with deionized water, thickened to a consistency of about 30%, and stored in a cold room at approximately 4°C.

Chemicals

The following chemical reagents were used in this study: sodium silicate (Na_2SiO_3) (41° Bé) from China PQ (Tianjin) Silicates Technology Co. Ltd.; diethylenetriamine pentamethylenephosphonic acid (DTPMPA) from Chunjiang (Changzhou) Chemicals Co. Ltd., China; magnesium hydroxide ($Mg(OH)_2$) slurry (80 g/L) from Haililong Magnesium Technology Co. Ltd., China; and diethylenetriaminepentaacetic acid (DTPA) from Akzo Nobel N.V. (Amsterdam, Netherlands). Hydrogen peroxide and NaOH were purchased from Jiangtian Chemical Co., Tianjin, China. All chemicals used were of analytical grade unless otherwise specified.

CCS experimental apparatus and process control

Figure 1 illustrates the CCS peroxide bleaching apparatus used in the present study. A 2000 mL beaker was placed into a constant temperature water bath and used as a bleaching reactor. A mixer with a speed range of 50–2000 rpm was used to mix pulp and chemicals in the beaker. Two peristaltic pumps set to a flow rate of 20 μL/min continuously replenished the chemical solutions into the pulp slurry during the bleaching process. The bleaching chemicals that were replenished were stored in separate 500 mL plastic bottles. The flow rates of each peristaltic pump were controlled by a computer using the pump manufacturer's software.



1. Apparatus for the continuous chemical supplement (CCS) bleaching process.
Note: 1 = thermostatic bath; 2 = reactor; 3 = stirrer; 4 = peristaltic pump for hydrogen peroxide (H_2O_2); 5 = plastic container for H_2O_2; 6 = computer; 7 = plastic container for sodium hydroxide (NaOH); 8 = peristaltic pump for NaOH.

CCS experimental procedure

The entire CCS bleaching process was divided into two phases: 1) the constant chemical concentration phase, and 2) the residual peroxide consumption phase. In the first phase, 40.00 g of ovendried unbleached poplar CTMP was first placed in the reactor and then diluted to a pulp consistency of 5% at a stirring speed of 200 rpm. When the pulp reached a temperature of 75°C, the following bleaching chemicals were added to the pulp: 0.2% $Mg(OH)_2$, 0.3% DTPMPA, and 0.2% DTPA (on ovendried unbleached pulp). Subsequently, according to the initial chemical concentrations in the experimental design, Na_2SiO_3, NaOH, and H_2O_2 were successively added to the pulp. Finally, the pulp was diluted to a consistency of 4.0% with deionized water, and the peristaltic pumps immediately started to replenish the consumed peroxide and alkali with 60 g/L H_2O_2 and 30 g/L NaOH solutions at set flow rates. The initial concentrations of the H_2O_2 and total alkali in the bleaching system remained constant for 50 min. When the reaction time reached 50 min, the pulp in the reactor was transferred to a cloth bag and thickened to a consistency of about 30%. The residual H_2O_2 concentration of the filtrate and the yield of bleached pulp were then measured.

In the residual peroxide consumption phase, 60.00 g of wet pulp (equivalent to about 18.0 g of ovendried pulp) obtained in the CCS phase was immediately sealed in a plastic bag and quickly placed in a water bath at 90°C, and the bleaching reaction was continued for 70 min. After the bleaching reaction was completed, the concentration of the residual H_2O_2 and the pulp brightness were measured. The H_2O_2 consumption, S, was calculated according to the following equation:

$$S = \frac{40y\left(\frac{100}{c_1} - 1\right)\cdot(c_2 - c_3)\cdot 10^{-5} + v_1c_4 + 0.960c_5 - (0.960 + v_1 + v_2)c_2}{40} \times 100\% \quad (1)$$

where

c_1 = thickened pulp consistency at the end of constant chemical concentration phase, %
c_2 = peroxide concentration at the end of the constant chemical concentration phase, g/L
c_3 = peroxide concentration at the end of the residual peroxide consumption phase, g/L
c_4 = concentration of H_2O_2 solution for replenishment, g/L
c_5 = initial H_2O_2 concentration in the constant chemical concentration phase, g/L
y = pulp yield in the constant chemical concentration phase, %
v_1 = volume of H_2O_2 solution for replenishment, L
v_2 = volume of NaOH solution for replenishment, L

The constant value of 0.960 is the initial volume of bleaching solution (L) and the constant value of 40 is the weight of ovendried unbleached pulp (g). The bleaching efficiency was obtained by the following formula:

Bleaching efficiency = brightness gains (% ISO)/H_2O_2 consumption on pulp (%) (2)

Experimental design

We used a response surface methodology statistical software program, Design Expert 8.0.5b (State-Ease; Minneapolis, MN, USA), to optimize the parameters of the CCS bleaching process [16,17]. According to the results of preliminary experiments, the initial concentrations of H_2O_2 (x_i), NaOH (x_j), and Na_2SiO_3 (x_k) in the bleaching system were chosen as the independent variables. These variables were investigated at three levels. The response variables were the pulp brightness (Y_1) and bleaching efficiency (Y_2). According to a statistical Box-Behnken Design, there were a total of 17 experimental runs (**Table I**).

High-consistency peroxide bleaching experiment

To compare the effectiveness of the CCS peroxide bleaching process with that of a conventional high-consistency peroxide bleaching process, an experiment of high-consistency peroxide bleaching was made in the present work. The process conditions of the experiment were the same as those in the CTMP mill from which we obtained the CTMP sample. An equivalent of 40 g ovendried CTMP was mixed with the following bleaching chemicals: 5.5% H_2O_2, 2.75% NaOH, 3% Na_2SiO_3, and 0.2% DTPA on ovendried CTMP. The mixed pulp was adjusted to a consistency of 25% and sealed in a plastic bag. The bag was placed in a water bath at 90°C for 120 min [18].

Analysis and measurement

Brightness measurements were taken on bleached pulp samples made into handsheets in accordance with ISO Standard 3688: 1999 (E) "Pulps — Preparation of laboratory sheets for the measurement of diffuse blue reflectance factor (ISO brightness)." Brightness measurements were conducted on the handsheets according to ISO Standard 2470—1: 2009 "Paper, board and pulps — Measurement of diffuse blue reflectance factor — Part 1: Indoor daylight conditions (ISO brightness)." An AT-510 automatic titrator (Kyoto Electronics Mfg. Co. Ltd.; Kyoto, Japan) was used for the titration analyses of the chemical concentrations [19,20].

RESULTS AND DISCUSSION

Relationship between bleaching efficiency and pulp brightness

When the concentrations of H_2O_2 and total alkali in the bleaching system were maintained at constant values, the pulp brightness and bleaching efficiency varied significantly (**Table I**). The maximum bleaching efficiency was 18.00 (Δ% ISO brightness/Δ% H_2O_2 consumed) while obtaining an ISO brightness was 74.98%. However, the highest ISO brightness was 77.86%, with a bleaching efficiency of 10.83. A high pulp brightness was usually accompanied by a low bleaching efficiency value. The optimal bleaching efficiency, in fact,

Run	Independent Variables			Response Variables	
	x_i	x_j	x_k	Y_1	Y_2
	H_2O_2, g/L	NaOH, g/L	Na_2SiO_3, g/L	ISO Brightness, %	Bleaching Efficiency, Δ% ISO brightness / Δ% H_2O_2 consumed
1	1.78	1.02	2.50	72.76	14.62
2	1.78	0.51	3.75	72.00	16.65
3	3.57	0.51	2.50	74.98	18.00
4	3.57	1.02	3.75	75.84	13.84
5	3.57	1.53	2.50	75.80	10.18
6	1.78	1.02	5.00	73.04	15.05
7	1.78	1.53	3.75	72.60	12.93
8	5.35	0.51	3.75	76.36	13.84
9	3.57	0.51	5.00	74.32	13.69
10	3.57	1.53	5.00	75.98	13.63
11	3.57	1.02	3.75	75.16	13.63
12	5.35	1.02	5.00	77.29	12.96
13	5.35	1.53	3.75	77.86	10.83
14	5.35	1.02	2.50	77.53	13.02
15	3.57	1.02	3.75	75.52	12.91
16	3.57	1.02	3.75	75.92	13.72
17	3.57	1.02	3.75	75.46	12.25

H_2O_2 = hydrogen peroxide; NaOH = sodium hydroxide; Na_2SiO_3 = sodium silicate.

I. Results from the Box-Behnken design-of-experiments.

hinges on the gain of the pulp brightness. The higher the pulp brightness, the lower the bleaching efficiency (**Fig. 2**).

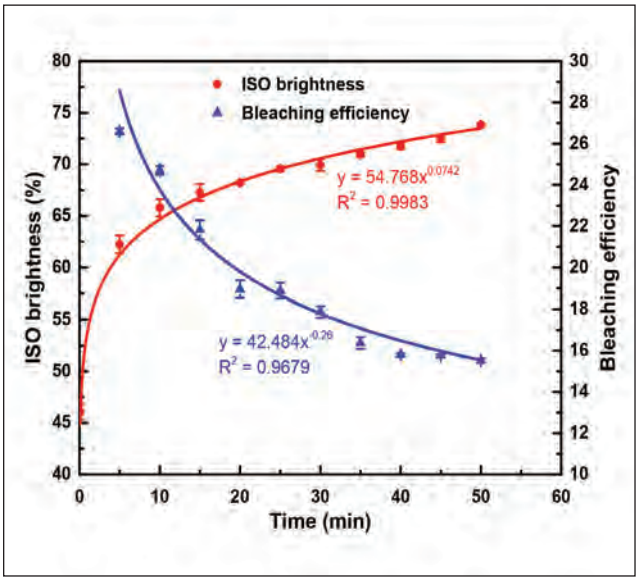
Establishment of the mathematical model for pulp brightness and bleaching efficiency

A second order multivariate regression analysis of the data in Table I was conducted, and two corresponding regression equations, Eqs. (3) and (4), with pulp brightness (Y_1) and bleaching efficiency (Y_2) as the response values were obtained (uncoded):

$$Y_1 = 68.46 + 2.38x_i + 1.99x_j - 0.51x_k + 0.25x_ix_j - 0.06x_ix_k + 0.32x_jx_k - 0.16x_i^2 - 1.46x_j^2 + 0.04x_k^2 \quad (3)$$

$$Y_2 = 31.23 - 0.60x_i - 15.69x_j - 2.96x_k + 0.19x_ix_j - 0.05x_ix_k + 3.04x_jx_k \quad (4)$$

The results of the analysis of variance (ANOVA) in **Tables II** and **III** show the significance of each factor and the degree of their influences on the response values. The p values of x_i and x_j elements were <0.0001 and 0.0005, respectively, which indicated a significant effect of H_2O_2 and NaOH concentrations on bleached pulp brightness. The influences of various factors on the pulp brightness were: H_2O_2 (x_i) > NaOH (x_j) > Na_2SiO_3 (x_k). The ANOVA result of the bleaching efficiency model in Table III revealed that the p values of x_j



2. Effect of bleaching time on the pulp brightness and bleaching efficiency.
Note: The bleaching conditions were as follows: 4.50 g/L H_2O_2, 0.50 g/L NaOH, and 2.50 g/L sodium silicate (Na_2SiO_3) in the bleaching system; 0.2% magnesium hydroxide ($Mg(OH)_2$), 0.3% diethylenetriamine pentamethylenephosphonic acid (DTPMPA), and 0.2% diethylenetriaminepentaacetic acid (DTPA) based on the weight of ovendried unbleached pulp; 75°C, and 4% pulp consistency.

Source	Sum of Squares	Degrees of Freedom	Mean Square	F-value	*p*-value
Model	48.2500	9	5.3600	79.1000	<0.0001
x_i	43.4312	1	43.4312	640.7807	<0.0001
x_j	2.6221	1	2.6221	38.6855	0.0004
x_k	0.0242	1	0.0242	0.3570	0.5690
x_ix_j	0.2025	1	0.2025	2.9877	0.1275
x_ix_k	0.0676	1	0.0676	0.9974	0.3512
x_jx_k	0.1764	1	0.1764	2.6026	0.1507
x_i^2	1.0317	1	1.0317	15.2214	0.0059
x_j^2	0.6080	1	0.6080	8.9704	0.0201
x_k^2	0.0206	1	0.0206	0.3044	0.5983
Residual	0.4745	7	0.0678		
Lack of fit	0.0969	3	0.0323	0.3420	0.7977
Pure error	0.3776	4	0.0944		
Total*	48.7282	16			
	R^2 = 0.9903			R_{adj}^2 = 0.9777	

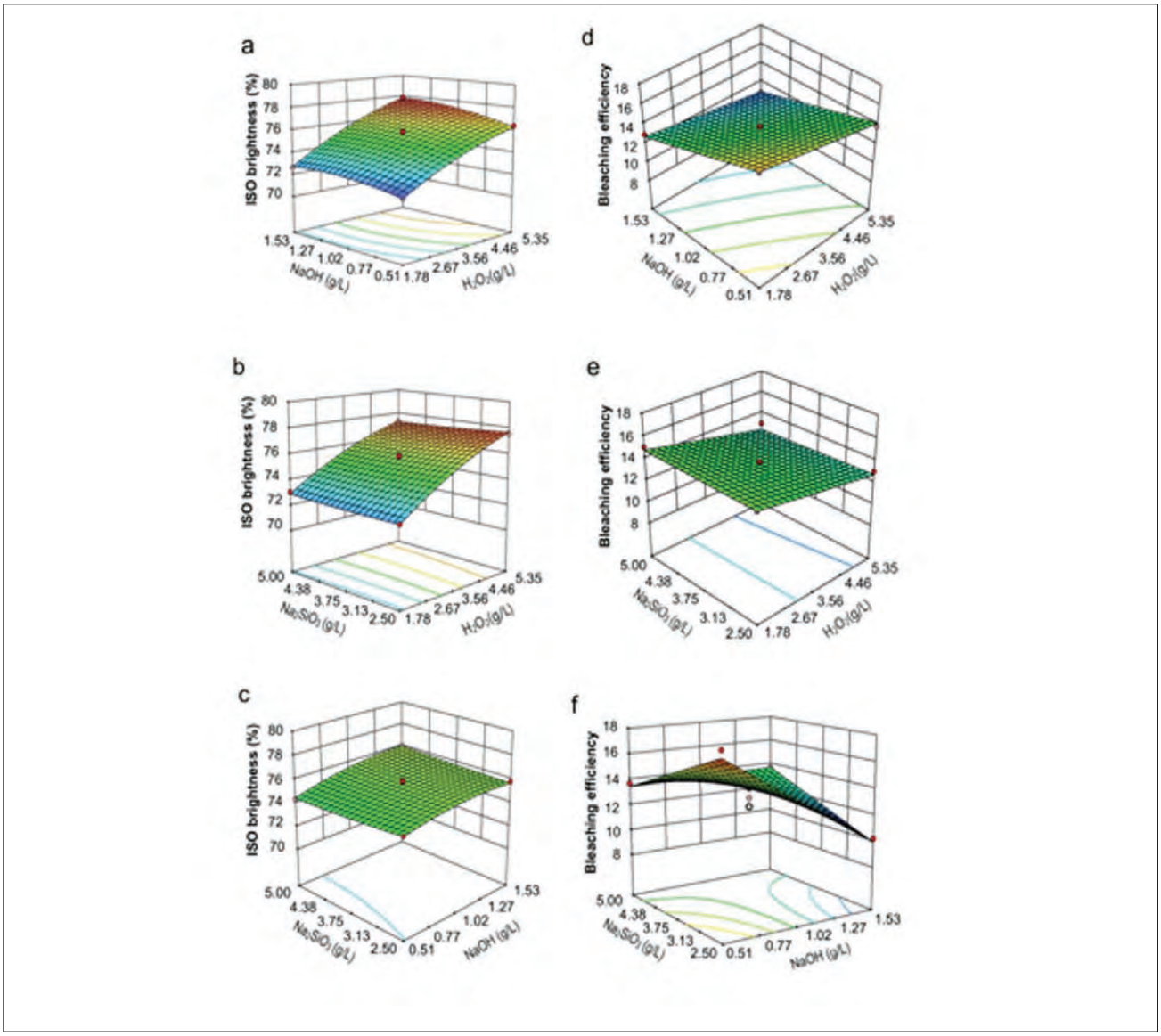
*Total corrected for the mean.

II. Analysis of variance (ANOVA) for the fitted quadratic polynomial model for bleached brightness. (Note: The responses were the mean values of three experiments with a relative deviation of ±0.6%–4.0%.)

Source	Sum of Squares	Degrees of Freedom	Mean Square	F-value	*p*-value
Model	51.2000	6	8.5300	23.7500	<0.0001
x_i	9.2450	1	9.2450	25.7311	0.0005
x_j	26.6815	1	26.6815	74.2611	<0.0001
x_k	0.0300	1	0.0300	0.0835	0.7785
x_ix_j	0.1260	1	0.1260	0.3508	0.5668
x_ix_k	0.0600	1	0.0600	0.1671	0.6913
x_jx_k	15.0544	1	15.0544	41.9001	<0.0001
Residual	3.5929	10	0.3593		
Lack of fit	1.7659	6	0.2943	0.6444	0.7001
Pure error	1.8270	4	0.4568		
Total*	54.7899	16			
	R^2 = 0.9344			R_{adj}^2 = 0.8951	

* Total corrected for the mean.

III. ANOVA for the fitted quadratic polynomial model of bleaching efficiency.



3. Response surfaces showing the effects of different bleaching parameters (x_1 = H_2O_2 concentration, x_2 = NaOH concentration, and x_3 = Na_2SiO_3 concentration) on the response brightness (Y_1) and bleaching efficiency (Y_2).

and x_i elements were also <0.0001 and 0.0005, respectively, which indicated that the NaOH and H_2O_2 concentrations had a significant effect on bleaching efficiency as well. The p value of the quadratic term $x_j x_k$ was <0.0001, which indicated significant interactions between the concentrations of NaOH and Na_2SiO_3 on the bleaching efficiency. The influences of various factors on the bleaching efficiency were: NaOH (x_j) > Na_2SiO_3 (x_k) > H_2O_2 (x_i).

The significance and goodness-of-fit of the established models were assessed, as shown in Tables II and III. The p values of the brightness and bleaching efficiency models were all <0.0001, indicating that a linear relationship generally existed between the independent variable expressed by these models and the response values. The coefficients of determination (R^2) for the brightness and bleaching efficiency models were 0.9903 and 0.9344, respectively, showing that these models effectively reflected the actual relationship between the factors and response values, and that they could be used to predict the optimal process conditions.

Effect of constant chemical concentrations on pulp brightness and bleaching efficiency

The mathematical model generated by response surface model revealed the effects of various concentrations of individual chemicals and their interactive effects on the brightness and bleaching efficiency (**Fig. 3**). Within the investigated range of chemical concentrations (NaOH: 0.51–1.53 g/L, Na_2SiO_3: 2.5–5.0 g/L, and H_2O_2: 1.78–5.35 g/L), the brightness of the bleached pulp rapidly increased with increasing H_2O_2 concentration (Figs. 3a and b) and slightly improved with raising NaOH concentration (Figs. 3a and c). However, the bleaching efficiency exhibited a slight down-

	H_2O_2, g/L	NaOH, g/L	Na_2SiO_3, g/L	Bleaching Efficiency, Δ% ISO brightness/ Δ% H_2O_2 consumed	ISO Brightness, %
Predicted value	4.50	0.52	2.50	16.86	75.99
Measured value	4.50	0.50	2.50	16.79	75.83

H_2O_2 = hydrogen peroxide; NaOH = sodium hydroxide; Na_2SiO_3 = sodium silicate.

IV. Comparison of the predicted model value and observed value obtained from validation experiment.

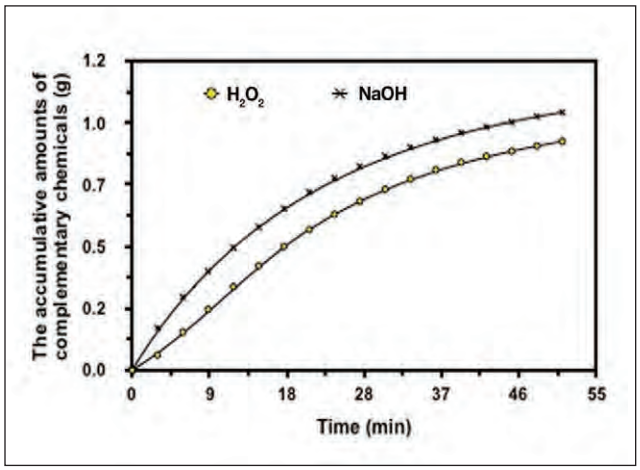
ward trend (Figs. 3d and e). These results can be explained by the fact that an increased H_2O_2 concentration accelerated the bleaching reaction rate because of the formation of the perhydroxyl anion (HOO^-) from H_2O_2, the specie that is responsible for the bleaching effect. Although this ion increases the pulp brightness, it also accelerates the decomposition of H_2O_2, which hinders bleaching efficiency [21]. Therefore, the concentrations of H_2O_2 and NaOH should be maintained at a certain level to achieve the brightness target with a bleaching efficiency as high as possible.

Figure 3c shows that the brightness of the bleached pulp did not change appreciably when the Na_2SiO_3 concentration was varied from 2.5 g/L to 5 g/L. When the NaOH concentration increased from 0.51 g/L to 1.53 g/L, the bleaching efficiency changed from decreasing rapidly to increasing rapidly as the Na_2SiO_3 concentration increased (Fig. 3f). The results indicated that a significant synergistic effect existed between Na_2SiO_3 and NaOH. One reason for this synergistic effect could be that Na_2SiO_3 acts as a buffer [1,2] that stabilizes the total alkalinity of the bleaching system while inhibiting H_2O_2 decomposition and improving bleaching efficiency. It should be noted that Na_2SiO_3 could form complexes with transition metal ions, together with magnesium ions, thus inhibiting catalytic peroxide decomposition [1].

Prediction and validation of the optimal process conditions

Maximum bleaching efficiency was dependent on the target brightness of bleached pulp. In the current work, an ISO brightness target of 76% was set while achieving maximum bleaching efficiency. According to the mathematical model (Y_2), we predicted the optimal process conditions, and the response values of brightness and bleaching efficiency (**Table IV**). Based on the predicted conditions, the experimental conditions set for a validation experiment was: 4.50 g/L H_2O_2, 0.50 g/L NaOH, and 2.50 g/L Na_2SiO_3 (with an initial total alkali concentration of 0.79 g NaOH/L). The result of the validation experiment showed that the bleaching efficiency and pulp brightness were very close to the predicted values (Table IV). These conditions were considered as the optimal ones to obtain the maximum bleaching efficiency.

Figure 4 shows the cumulative totals of H_2O_2 and NaOH versus time for the optimized CCS bleaching process. The cumulative amounts of added H_2O_2 and alkali gradually increased with time, and the addition rates decreased with increased bleaching reaction time toward the end of the bleaching stage.



4. Relationship between the accumulative amounts of complementary chemicals (on 40 g unbleached pulp) and bleaching duration.

Comparison between the CCS bleaching and high-consistency bleaching

Table V compares CCS bleaching and high-consistency bleaching (i.e., control). The pulp ISO brightness values in these two bleaching methods were relatively close. However, the bleaching efficiency of the CCS bleaching method was 16.79, which was much higher than the 7.38 of the high-consistency bleaching. Zhao [3] reported a bleaching efficiency of 10.79 with the displacement bleaching method. To our knowledge, Zhao's study produced the highest reported value. Thus, the CCS bleaching method exhibited the highest bleaching efficiency among the compared methods. The results confirmed that CCS bleaching was an effective method to improve hydrogen peroxide bleaching efficiency.

When the chemical concentrations and the H_2O_2 consumption in the bleaching system were compared, the initial H_2O_2 concentration and total alkali concentration in the CCS bleaching process were 4.50 g/L and 0.79 NaOH/L (pH 10.46). Those concentrations were significantly lower than the corresponding initial levels in the high-consistency bleaching process (H_2O_2 of 19.38 g/L and total alkali of 10.30 g NaOH/L). At the same time, the H_2O_2 consumption in the CCS bleaching process was only 1.77% on pulp, which was significantly

	Bleaching Process	
	CCS Bleaching	High-consistency Bleaching
ISO brightness of the unbleached pulp, %	46.07	46.07
ISO brightness of the bleached pulp, %	75.83	76.42
Bleaching efficiency, Δ% ISO brightness/Δ% H_2O_2 consumed (on ovendry pulp)	16.79	7.38
H_2O_2 concentration, g/L	4.50	19.50
Total alkali concentration, g/L	0.79	10.30
H_2O_2 consumption, %	1.77	4.11
NaOH consumption, %	2.69	2.71
Pulp consistency, %	4	25
Bleaching temperature, °C	75	90

H_2O_2 = hydrogen peroxide; NaOH = sodium hydroxide.

V. Comparison between the continuous chemical supplement (CCS) peroxide bleaching and high-consistency peroxide bleaching of poplar chemithermomechanical pulp.

lower than the 4.11% on pulp with the high-consistency bleaching process. We concluded that the low initial chemical concentrations in the CCS bleaching could result in a low H_2O_2 consumption, and therefore, the bleaching efficiency was enhanced.

When comparing the two bleaching methods, lower reaction temperatures (i.e., 75°C) and use of multiple peroxide stabilizers, DTPMPA and $Mg(OH)_2$, were used in the CCS bleaching process. However, both of these process conditions with the CCS bleaching played an important role in inhibiting unproductive hydrogen peroxide decomposition.

CONCLUSIONS

This study examined using the CCS bleaching process to improve H_2O_2 bleaching efficiency of poplar CTMP. The pulp brightness was enhanced with the constant addition of H_2O_2 and total alkali solutions over time, but the bleaching efficiency decreased. The synergistic effect of Na_2SiO_3 and NaOH significantly affected the bleaching efficiency. The optimized chemical concentrations for CCS bleaching were 4.50 g/L H_2O_2, 0.50 g/L NaOH, and 2.50 g/L Na_2SiO_3. Under these conditions, the bleaching efficiency reached 16.79 (Δ% ISO brightness/Δ% H_2O_2 consumed), which was significantly higher than the 7.38 of the high-consistency bleaching process (i.e., control). The low initial chemical concentrations in the CCS bleaching could result in low H_2O_2 consumption, and hence, the efficiency of the CCS bleaching was enhanced. In addition, low bleaching reaction temperature and the addition of multiple peroxide stabilizers could help improve bleaching efficiency. The CCS bleaching process can be an effective approach to improve the efficiency of peroxide bleaching of chemimechanical pulp. **TJ**

LITERATURE CITED

1. Sundholm, J., *Mechanical Pulping*, Papermaking Science and Technology, Book 5, Fapet Oy, Helsinki, 1999.
2. Ek, M., Gellerstedt, G., and Henriksson, G., *Pulp and Paper Chemistry and Technology: Pulping Chemistry and Technology*, Walter de Gruyter GmbH & Co., Berlin, 2009.
3. Zhao, Q., "Research on reinforced hydrogen peroxide bleaching of poplar CMP and bleaching mechanism," Ph.D. dissertation, Beijing Forestry University, Beijing, China, 2009.
4. Xu, E., *J. Pulp Pap. Sci.* 28(11): 379(2002).
5. Zhao, Q., Pu, J., Mao, S., et al., *BioResources* 5(1): 276(2010).
6. Fei, X., Yao, J., Du, J., et al. *Cellulose* 22(2): 1379(2015).
7. Zeinaly, F., Shakhes, J., Firozabdi, M.D., et al., *BioResources* 4(4): 1409(2009).
8. Behrooz, R., Ghasemi, S., Atoii, G.A., et al., *BioResources* 7(1): 161(2012).
9. Shen, K., "High-brightness bleaching of China fir CTMP pulp and its mechanism," Ph.D. dissertation, Chinese Academy of Forestry, Beijing, China, 2008.
10. Wang, R., "Studies on anaphase activation of peroxide bleaching of pulp," M.S. thesis, Northeast Forestry University, Harbin, China, 2004.
11. Hatam, A., Pourtahmasi, K., Resalati, H., et al., *Wood Sci. Technol.* 42(5): 353(2008).
12. Zhao, Q., Sun, D., Wang, Z., et al., *BioResources* 7(4): 4889(2012).
13. Suhr, M., Klein, G., Kourti, I., et al., *Best Available Techniques (BAT) Reference Document for the Production of Pulp, Paper and Board*, European Integrated Pollution Prevention and Control Bureau, Sevile, Spain, 2014. Available [Online] http://eippcb.jrc.ec.europa.eu/reference/BREF/PP_revised_BREF_2015.pdf <21June 2017>.

14. Li, Z., Ni, Y., and van Heiningen, A., *Pulp Pap. Can.* 97(9): 46(1996).
15. Li, X., "Studies on hydrogen peroxide displacement bleaching processes and mechanisms of *E. globulus* CTMP," Ph.D. dissertation, South China University of Technology, Guangzhou, China, 2000.
16. Singh, G., Ahuja, N., Batish, M., et al., *Bioresour. Technol.* 99(16): 7472(2008).
17. Perincek, S., Duran, K., and Korlu, A.E., *Ozone: Sci. Eng.* 35(4): 316(2013).
18. Liu, W., Han, S., Xu, N., et al., *Ind. Eng. Chem. Res.* 53(8): 2897(2014).
19. Hietanen, T.M., Ősterberg, M., and Backfolk, K.A., *BioResources* 8(2): 2337(2013).
20. Karlsson, A., and Agnemo, R., *Nord. Pulp Pap. Res. J.* 25(3): 256(2010).
21. Mota, S.F., Paulo, J.G., Zeller, C.A.V., et al., *Nord. Pulp Pap. Res. J.* 22(1): 17(2007).

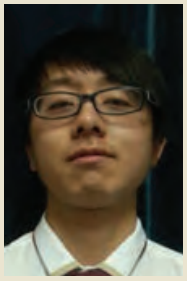
ABOUT THE AUTHORS



Sun



Zhang



Zhao



Hou

Hydrogen peroxide (H_2O_2) is widely used in bleaching chemimechanical pulp. However, its bleaching efficiency is not high because of the self-decomposition of H_2O_2 in bleaching. Much research has focused on improving bleaching efficiency by balancing the chemical concentration in the bleaching system. Although bleaching efficiency has been improved to some extent, much further improvement could be made.

In this study, the authors made a great effort to improve the bleaching efficiency of H_2O_2. A novel bleaching method was proposed by which constant chemical concentrations in the bleaching system were maintained.

How to maintain the chemical concentrations was the difficult aspect of this research. The authors used two peristaltic pumps to continuously supplement H_2O_2 and sodium hydroxide solutions into the bleaching system to maintain constant concentrations of H_2O_2 and total alkali. Flows of the peristaltic pumps were accurately controlled and changed by computer. A surprising find was that the bleaching efficiency gained in the study was extremely high.

To better understand the new bleaching method, the authors will further study the reaction kinetics and mechanism of peroxide bleaching under the conditions of constant chemical concentrations. Mills could use the bleaching method proposed in this study to reduce bleaching chemical costs. New equipment would be developed to meet the needs of practical production.

Sun, Zhang, and Zhao are students, and Hou is professor, Tianjin Key Laboratory of Pulp & Paper, Tianjin University of Science & Technology, Tianjin, China. Email Hou at qingxihou@tust.edu.cn.

Finite element analysis of the thermal bending of a chilled cast thermo roll

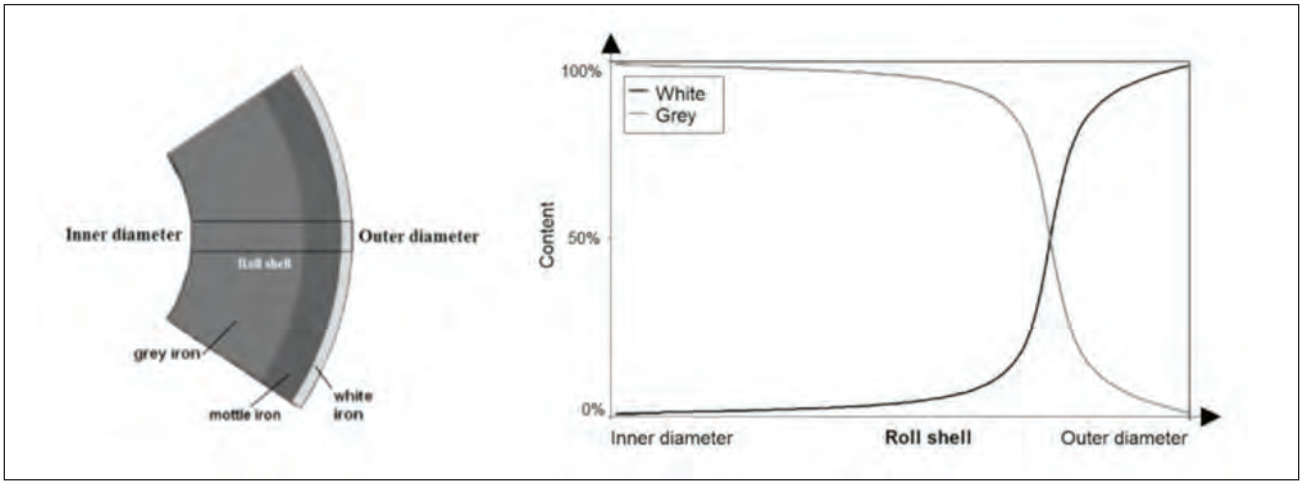
THOMAS WIDMAIER, JUKKA PIRTTINIEMI, ESA PORKKA, PANU KIVILUOMA, AND PETRI KUOSMANEN

ABSTRACT: A previously-created roll model based on the ultrasound measurements of a chilled cast iron thermo roll of a soft calender was used to create a finite element (FE) model of the same roll. The FE analysis was used to simulate the behavior of the roll when heated and in changing operating conditions. The main interest was to study the thermal bending of the roll model. The simulated behavior was consistent with known behavior of the thermo rolls in general, and when compared to actual measurements carried out in the calender, the results of the simulation showed similar behavior between the roll model and the actual roll. The main difference was in the absolute value of the bending, but the bending directions were practically the same. These results are promising for future research to develop methods to avoid or minimize the negative effects of the thermal deformations in thermo rolls.

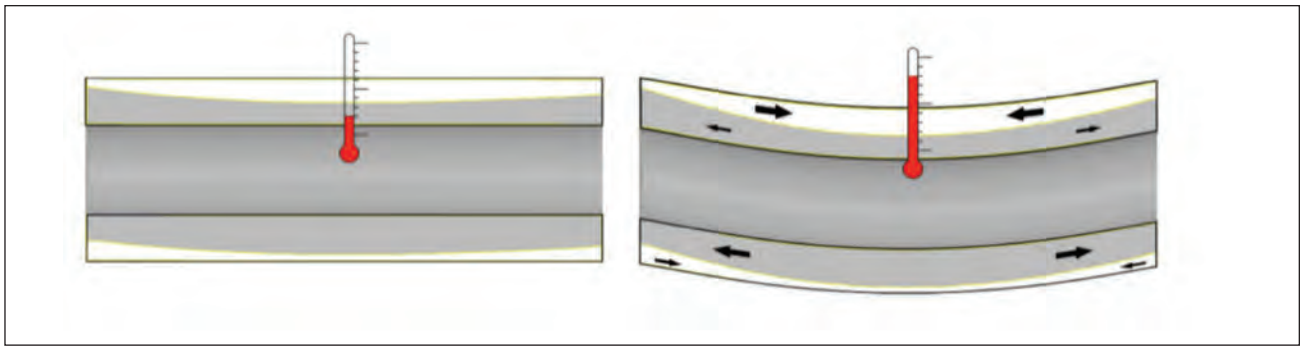
Application: This paper discusses some of the phenomena caused by temperature changes in paper machine thermo rolls. The studied phenomena include mainly thermal deformations, i.e., bending. This study is relevant to finding the cause for some calender-related problems, including thermo rolls.

The thermo rolls belong to the family of heated rolls in the paper industry. They are used to heat up the paper web passing through a calender. The heat improves the formability of the paper, thus improving the efficiency of the calendering. For many decades, chilled cast iron thermo rolls have been successfully used in calenders of paper machines. In 2004, the proportion of chilled cast iron thermo rolls amounted to 99% of all thermo rolls in the paper industry [1]. Even though the number of forged steel thermo rolls and other thermo roll types is slowly increasing, the number of the chilled cast thermo rolls is still dominant. Chilled cast iron has been used for roll shell material, mainly because of its good manufacturability and low material cost. Thermo rolls have an undesirable tendency to deflect when heated to the operating temperature. This temperature dependent deflection is also called thermal bending. Because of the inhomogeneous roll shell material, the chilled cast thermo rolls are more prone to this phenomenon than some other roll types.

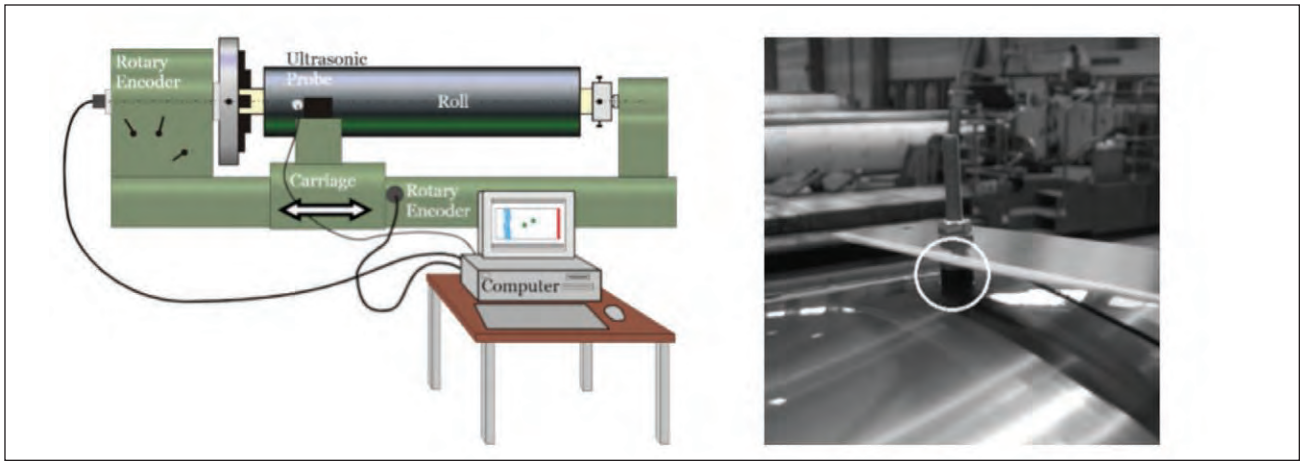
The bodies of the chilled cast thermo rolls have a layered structure with three different layers (**Fig. 1** [2,3], left). On the surface, they have a white iron layer and on the inside, a grey iron layer. Between the two main layers, there is an intermediate zone (also called mottle iron layer), where the content of mainly white iron changes to mainly grey iron (Fig. 1, left). The layered structure with varying layer thicknesses is a byproduct of the casting process [4]. The average thickness of the white iron layer in paper machine rolls is typically 8 to



1. Different layers of iron in the chilled cast iron roll body and their typical content as a function of depth in the roll body [2,3].



2. As temperature changes, thermal bending of the thermo roll is caused by the uneven layer thickness of white iron.



3. Principle of the ultrasonic measurement system (left) and the ultrasonic probe on the roll surface (right, circled). The rotary encoders give the coordinates of the ultrasound probe during measurement.

24 mm [5,6]. The mottle iron layer is thicker, but there are no clear boundaries between the layers, as it can be seen in Fig. 1 (right). The rest of the body is grey iron.

Thermal bending is caused by the uneven layer thickness of white iron. The thermal expansion coefficient of white iron is smaller than that of grey iron. If the roll is heated, it will deflect because of the forces that caused the uneven thermal expansion of the layers (**Fig. 2**). The direction and form of the deflection is determined by the layer distribution and temperature distribution in the roll body. Normally, there is no deflection in the rolls at room temperature.

There are several types of thermo rolls, and the most common types are center bore rolls, displacer type rolls, and peripherally drilled rolls. The working principle of these thermo rolls is based on hot heating fluid flowing through the roll body, i.e., the roll is heated from inside. Modern thermo rolls are mainly peripherally drilled rolls or displacer type rolls [7,8].

Peripherally drilled rolls have usually 15 to 50 bores that are 20 to 60 mm from the roll surface. The diameters of these bores are 25 to 50 mm [7]. The length of the bores is the same as the length of roll body, i.e., up to 12 m. There are many designs for the heating fluid passages, ranging from one bore per pass to three or more connected bores. The name of the design gives the number of the connected passages: mono-pass, duo-pass, tri-pass, etc. The heating fluids used with the thermo rolls are water, steam, or thermal oil. Some passage arrangements are presented in the book edited by Jokio [6], in the articles by Zaoralek [9,10] and Grosskreutz [11], and in the patent from von Schweinichen [12]. The heat transfer from the heating fluid to the roll can be made more effective if the turbulence of the fluid is increased. This can be done by special inserts in the passages. The inserts are called turbulators [8,12].

This study discusses the use of a previously-created roll model [4] in simulating the thermomechanical behavior of a chilled cast iron thermo roll. Ultrasonic measurements were used to acquire dimensions of the peripherally drilled bores in the shell of the roll body. Ultrasound was also used in measuring the layer thickness of the white iron layer on the roll surface. The ultrasonic measurement principle is shown in **Fig. 3**. This study is about the peripherally drilled chilled cast iron thermo rolls, but some of the results can be extended to other roll types, too.

METHODS

A chilled cast iron thermo roll (**Table I**) was used as a test roll and as a basis for the roll model. The test roll was the upper roll of a soft calender. The heating passage design was

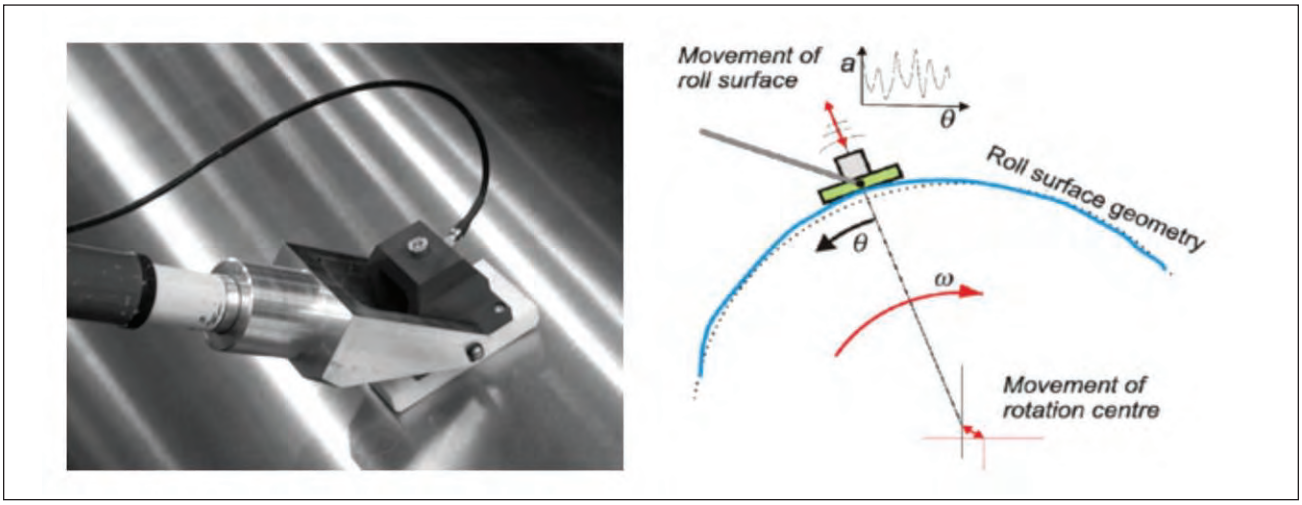
Total length	9810 mm
Body length	7690 mm
Maximum paper web width	6660 mm
Nominal diameter	1067 mm
Shell thickness of the roll body	198 mm
Bearing length	8400 mm
Peripheral bore diameter	32 mm
Layer thickness of white iron	9 mm
Layer thickness of mottle iron	42 mm
Heating fluid	thermal oil
Design temperature for oil	249°C
Heating capacity	695 kW
Balancing speed range	0 to 388 min^{-1}

I. Dimensions and properties of the test roll.

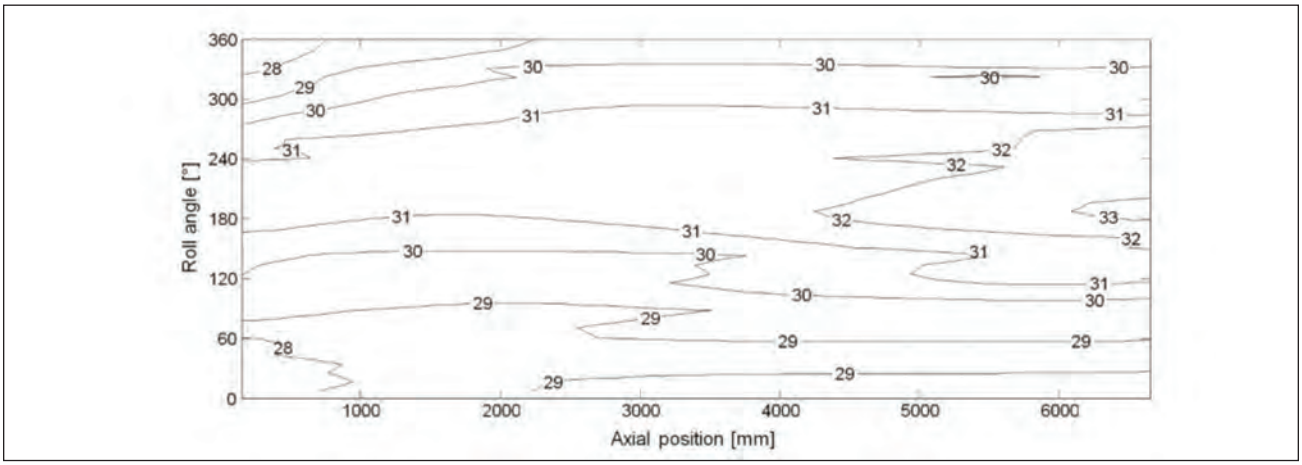
duo-pass, and the roll had 40 peripheral bores. The roll was measured during normal operation and during maintenance. The ultrasonic measurements were carried out at a roll shop on a roll grinder. The run-out measurements were carried out in the soft calender. The run-out measurement method is discussed in the dissertation of Kiviluoma [13], and it is based on a sliding pad with an accelerometer, as in **Fig. 4**. The run-out values were obtained by double integration of the acceleration signal.

The calculation of the distribution of the white iron layer in the roll body is explained in the article of Widmaier et al. [4]. It is based on the reverse ultrasonic measurement of the wall thickness of the roll body. To simplify the calculations, the layer structure is reduced to two layers, assuming that one half of the mottle iron layer behaves like grey iron and the other half like white iron. If not otherwise mentioned, in the rest of this study the white iron layer is defined this way. The thickness variation of the white iron layer was from 27.0 mm to 33.3 mm. The average layer thickness was 30.3 mm (**Fig. 5**).

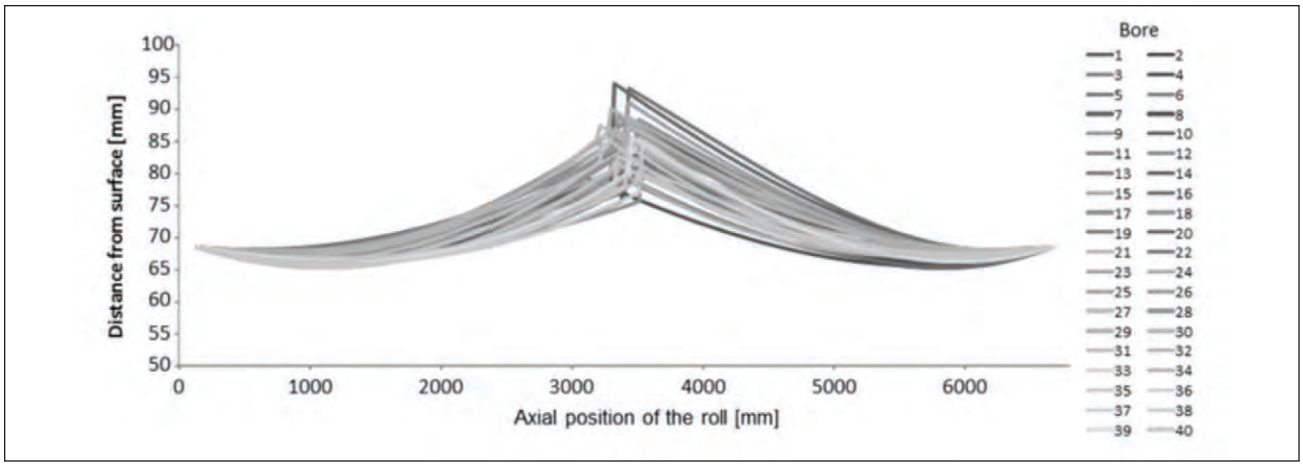
The depths of the peripheral bores in the roll were mea-



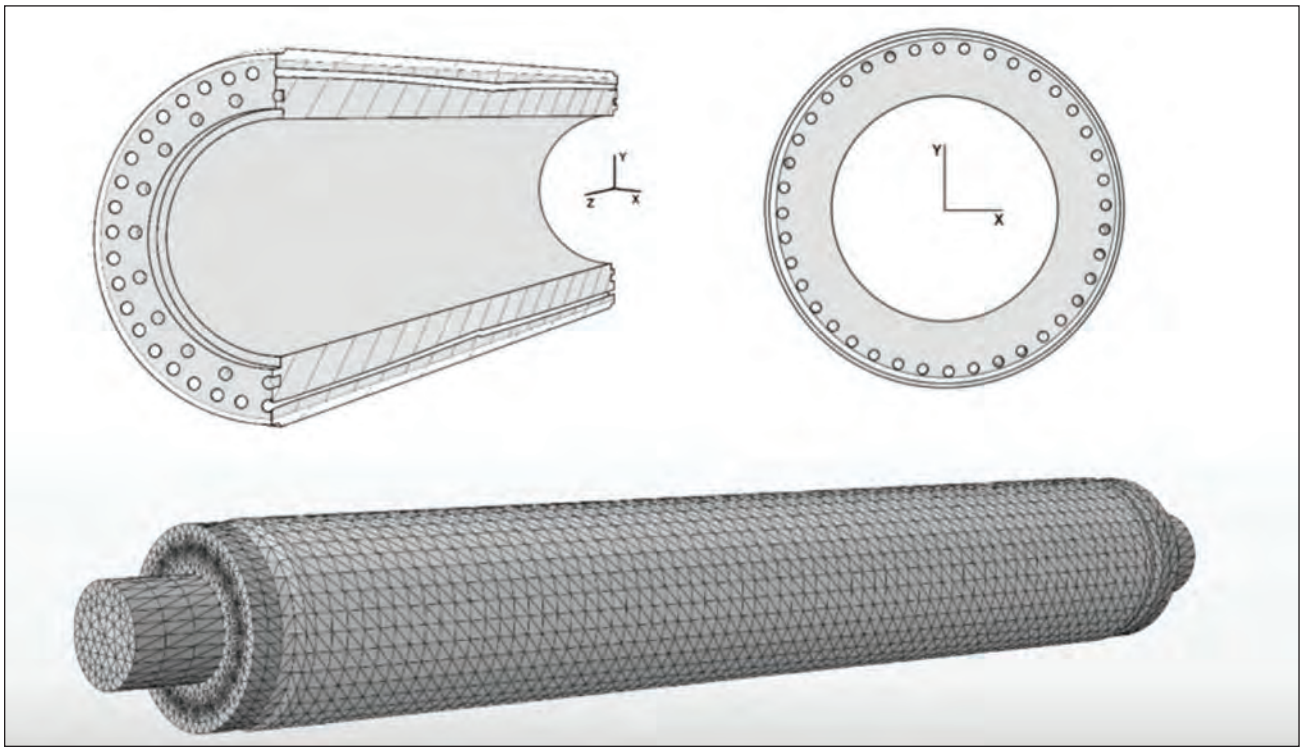
4. Left: in-situ run-out measuring device with accelerometer. Right: the measurement principle.



5. Map of the layer thickness variation (mm) of the white iron in the roll body of the test roll [4].



6. Bore depths of all the peripheral bores in the roll body [4].



7. Top: 3D model of the thermo roll body in cut-in-half state and shown from the end. Bottom: the finite element (FE) model of the roll with the modelled journal parts attached. The used element type is a 4 node tetrahedron.

sured with ultrasound. The measured values show some meeting difficulties in the bores and some scattering in the bore depths (**Fig. 6**) similar to the results found in the literature [14]. The measurement of the depths of the bore centerlines with ultrasound is described by Widmaier et al. [4].

Finite element model of the roll

The dimensions for roll model were taken from the test roll. The white and grey iron layer models were created with the help of the ultrasonic layer border (Fig. 5). The layer border surface was the outer surface of the grey part and the inner surface of the white part. The solid model with 40 protrusions of the peripheral bores was used to cut the fluid channels into the grey iron part. Each measured peripheral bore centerline was used as a trajectory of a protrusion for the bore model. The protruded section was a circle with the diameter of 32 mm. Two different roll journals of steel were added. The journals were also equipped with heating fluid passages. One of the journals was the service side journal and the other was the drive side journal. The journals were fastened with 20 simplified M32 x 200 bolts each. The part to simulate the heating oil in the model was created from the cut-out model for the bores.

The 3D model (**Fig. 7**, bottom) was exported to Abaqus

Material	E, GPa	ν	ρ, kgm^{-3}	k, Wm^{-1}K^{-1}	c_p, Jkg^{-1}K^{-1}
White iron	180	0.27	7694	20.76	586.6
Mottle iron	140	0.27	7583	31.15	544.6
Grey iron	120	0.27	7334	45.68	502.8
Steel	207	0.30	7835	48.17	628.5

II. Material values of the iron phases [2,8,15,16].

Temperature, °C	h, Wm^{-2}K^{-1}
40	405
100	980
150	1452
170	1632
200	1900
250	2300

III. Temperature-dependent oil-shell gap conductance (h) interaction [17].

Interaction	Interaction type	h, Wm^{-2}K^{-1}
Oil-insulated bores	Gap conductance	40
Body – journal	Gap conductance	5000
Paper web area	Surface film condition	73
Cylinder faces of journals	Surface film condition	72
Other surfaces of journals	Surface film condition	25

IV. Temperature-independent heat transfer coefficients of the interactions.

Nominal Oil Temperature, °C	Input Temperature, °C	Output Temperature, °C
100	100	98
150	150	147
170	170	165
200	200	197
249	249	240
250	250	246

V. Input and output temperature of the oil.

Unified FEA software (Dassault Systemes; Vélizy-Villacoublay, France) for the finite element (FE)-based thermomechanical analyses. The individual parts (shell, journals, bolts and oil) were meshed. The used element type was a solid 4 node linear tetrahedron. After the meshin,g the total number of the nodes was 77170, and the total number of the elements was 333174 in the FE model. The used element type is suitable for the calculation of the node displacements in the model, even though it is one of the simplest 3D element types, and thus can give distorted geometry changes in small scale. The reduced number of nodes reduces the calculation time of the analysis.

The used material values are in **Table II**. The mass of the model (Fig. 7, bottom) was 30385 kg, which is close to the given mass of the actual roll (30500 kg). In the FE analyses, the roll heating was simulated by changing the temperature of the nodes in the oil part to the desired operating temperature. The starting temperature was always the room temperature (20°C). This was done in heat transfer steps. After the analysis was run, the resulting database contained the temperatures of the nodes as a function of time. In the heat transfer steps, the elements in the model were of DC3D4 element type (4 node tetrahedron) of Abaqus software. During the heat transfer analysis, the parts of the model had several interactions. **Table III** lists the values of heat transfer from the oil to the roll body, which are defined as temperature dependent. Table IV lists the rest of the interactions, which are defined as temperature independent.

The gap conductance for the thermal oil-to-roll body interaction was calculated as the film coefficient in a pipe with turbulent oil flow. The used oil flow speed was 1.9 m/s. This calculation is explained in the article of Zwart and Farrell [16]. The use of a turbulator increases the heat transfer coefficient value. Based on the information provided by the thermo roll manufacturer, it was concluded that the used turbulators increase the heat transfer coefficient by a factor of two. The roll had also insulation around the bores at the roll shell ends. The heat transfer coefficient for this part of the oil-to-shell contact was taken also from Zwart and Farrel [16], but increased slightly from 34.4 to 40 W/m^{2}K to reduce the large temperature drop on the roll surface in the end area of the roll body.

The drop in the temperature distribution of the oil part was linearly distance dependent, i.e., the temperature dropped linearly from input to output. This simulated the cooling of the oil. **Table V** lists the input and output temperatures of the oil at the set oil temperatures. The temperature difference between input and output temperature for the 100°C, 150°C, 200°C, and 250°C oil temperatures is smaller than for the 170°C and for 249°C oil temperatures, because

Set Oil Temperature, °C	Heat Surface Flux, kWm^{-2}	Equivalent Heat Load per Roll Length, kWm^{-1}
170	9.0	30.1
190	10.5	35.2
249	15.5	51.9

VI. Heat surface fluxes and the corresponding heat loads used in the analyses.

the latter cases simulate paper production conditions where the temperature drop in the oil is larger.

The calculation of the film coefficient for the heat transfer into the air from the rotating roll surface is also explained in the same article of Zwart and Farrell [16]. For the calculations of the film coefficients, a rotation speed of 5.8 Hz of the roll was used. The calculation of the thermal contact conductance between the roll body and the journals is explained by Yovanovich [18]. Too many of the needed parameters for the calculation were missing (turning pitch, tool radius, etc.), so an estimate of the coefficient was made based on values found in several research papers.

The heat load during paper production was simulated by a surface heat flux from the paper web area of the roll. The magnitude of the heat flux was chosen so that the final surface temperature was close to measured temperatures and close to temperatures provided by the roll manufacturer. The heat flux values are listed in **Table VI**. The equivalent heat load in the same table tells how much of the heat was taken by the paper web per roll length. The total heat transferred through the roll is more than in Table VI, because the heat also escapes through the other parts of the roll. The standard heat transfer simulation analysis had 7 steps, with a total duration of 10 h of simulated operation. The steps were named: *StartTemperature, HeatOn, Heating, PaperWebOn, PaperProduction, NipOpen*, and *NoProduction*. The other analyses simulated the effect of the decreasing heat load of the paper web and the effect of the changing oil temperature. **Table VII** lists the names and main parameters of the individual steps.

After the temperature field in the roll was calculated in the heat transfer analyses, a displacement database was calculated for the same model, but without the oil and the bolt parts. The temperature field for this analysis was taken from the heat transfer analysis results database. The element type was changed to C3D4, which is a 3D stress element, and it can be used for displacement calculations. The node locations and the mesh did not change due to this.

The journal ends were tied to the roll body ends in a small ring around the bolt holes. The width of the ring was 40 mm. Otherwise, the journal-to-body contact was defined as a hard contact. The roll models were simply supported at the journal ends. This means that the center point of the axis end of the service side journal is locked in all directions and the axis end of the other journal is locked in radial directions (XY plane). A supplementary node in the service side journal axis end was locked in the radial direction (XY plane). These boundary conditions allowed the roll to axially expand and kept it from rotating, but did not prevent the bending of the roll.

The coefficients of thermal expansion used for the white and grey iron are shown in **Table VIII**. As the table shows, both iron layers had temperature-dependent thermal expansion coefficients, and in addition, the white iron layer had an orthotropic (direction-dependent) thermal expansion coefficient during the analyses.

Step Name	Duration	Heat	Heat load	Purpose/simulates what?
StartTemperature	60 s	no	no	Whole model set to 20°C
Heating	3 h			This period has 2 steps
HeatOn	10 min	yes	no	Oil heat is turned on
Heating	2:50 h	yes	no	Roll is heated
Paper production	6 h			This period has 2 steps
PaperWebOn	10 min	yes	yes	Paper production starts
PaperProduction	5:50 h	yes	yes	Paper production
Decreasing load	3 h	yes	yes	Heat load decreases slowly
Changing temperature	3 h	yes	yes	Temperature fluctuates
Nip open	1 h			This period has 2 steps
NipOpen	10 min	yes	no	Nip opens
NoProduction	0:50 h	yes	no	Conditions after production

VII. Durations of the analysis steps and heat conditions.

Temperature, °C	Grey iron, °C^{-1}	White Iron, °C^{-1}	
		Radial Direction (XY)	Axial Direction (Z)
50	10.0E-6	9.0E-6	7.5E-6
100	11.0E-6	9.3E-6	6.9E-6
150	11.0E-6	9.3E-6	6.2E-6
200	11.0E-6	9.3E-6	5.5E-6
250	11.0E-6	10.0E-6	6.6E-6
300	11.8E-6	10.8E-6	7.8-6

VIII. Temperature-dependent thermal expansion coefficients for the used iron layers. Grey iron thermal expansion coefficient is isotropic and white iron thermal expansion coefficient is orthotropic [2].

Fourier analysis

One of the most common Fourier analyses is done with the fast Fourier transform (FFT) algorithm originally developed by Cooley & Tukey [19]. The inverse FFT algorithm can be used to compose the original measurement signal in the time domain from these complex numbers. Filtering of some unwanted frequencies or components is straightforward. The complex number representing the unwanted frequency or component is set to zero before the inverse FFT, an example of which is shown by Mosier-Boss et al. [20]. In the analyzed measurement signals of our research, the FFT algorithm is used for both identifying certain harmonic components and for filtering purposes.

Analysis software

The FE analyses were solved with the Abaqus FEA software. The analysis procedure used was the Abaqus/Standard. For all the analysis steps, the step type was "static, general". The starting condition for each general analysis step is the ending condition from the last step, with the state of the model evolving throughout the history of the analysis steps. The FE analyses produced result files with all the results from each analysis. From these results, a report file was generated with the Abaqus CAE software. In the report file, all the node displacement and all the node temperature results were stored. One report file contained the results from all the simulation steps with their time increments from one analysis run. The presented results were calculated from the report file together with the analysis input file. The input file was used to locate the surface nodes in the nip area of the roll. During this work, over 200 individual FE analyses were run. The report file sizes ranged from ~400 megabytes to over 800 megabytes, depending on the extent of the analysis. A software program was developed to calculate the displacement of the surface nodes in the radial direction (XY plane) from nine cross sections of the roll body in all analysis time steps. At the same time, it calculated the average temperature of the all surface nodes in the nip area. The radial direction was chosen, because the axial direction (Z) was not relevant for the study of the thermal bending. Still, the thermal expansion in the axial direction was the most dominant expansion direction; e.g., at 200°C it was over 10 mm.

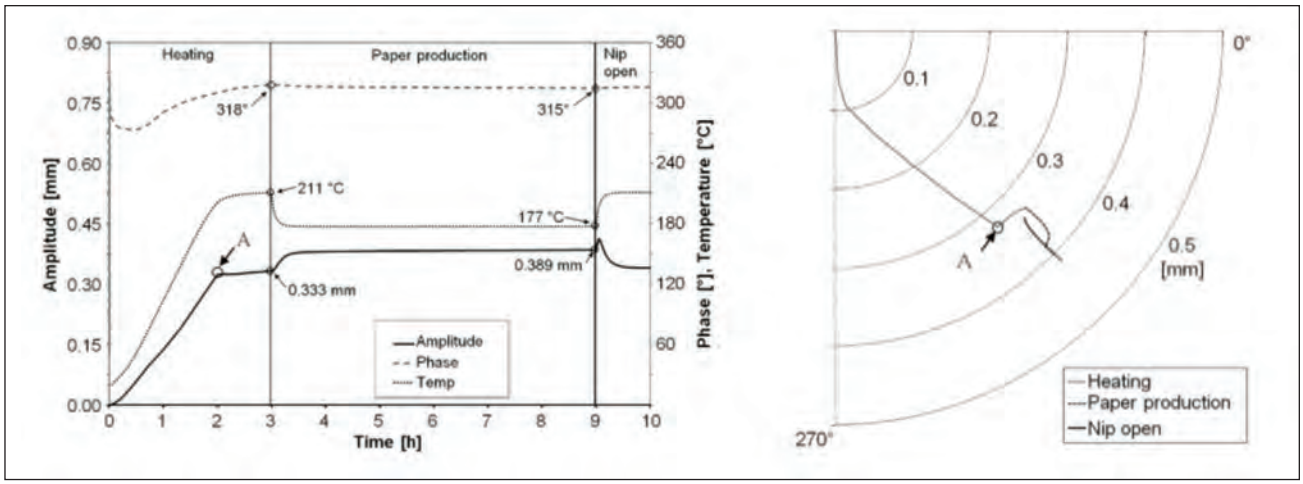
The same software performed an FFT analysis of the individual cross section profiles. From this FFT analysis, the overall thermal bending can be observed from the 1st FFT term of middle cross section if the ends of the roll shafts are fixed like in these simulations. The 1st term, also known as the 1st harmonic component, gives the amplitude and the direction of the bending.

RESULTS

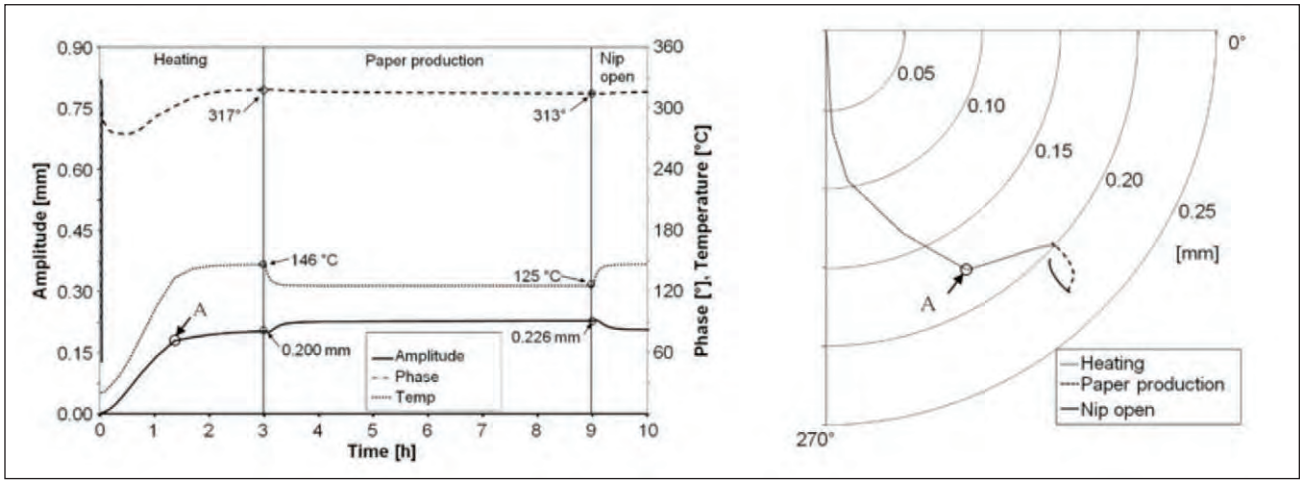
The results from the model analyses and simulations are presented as graphs. Some results are compared to measurements. Simulation results are presented as a function of time and as a polar plot. The presented results are the amplitude and the phase of the 1st harmonic component of the displacement of the circumferential surface nodes in the middle cross section. The time-based graphs also show the average temperature of the all surface nodes at the roll shell in the nip contact area. The time scale is divided into periods like heating, paper production, and nip open. These periods are explained in Table VII. If not otherwise stated, only during the paper production period is a heat load taken from the roll nip surface. During the heating period, oil temperature changed to operating temperature with a speed of 2°C/min. This value was found in the literature for modern thermo rolls [10,21]. Also, graphs from nine cross sections are presented to show the bending profile in the nip surface of the whole roll length.

Time based simulations

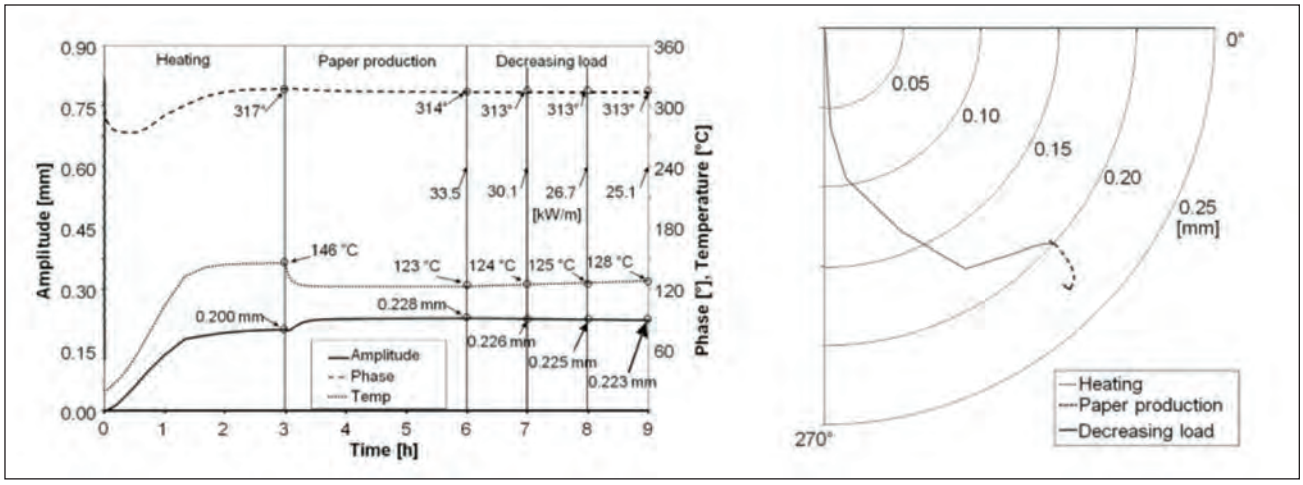
Figures 8-9 show the results from the standard simulation set. The first figure always shows the amplitude, phase angle,



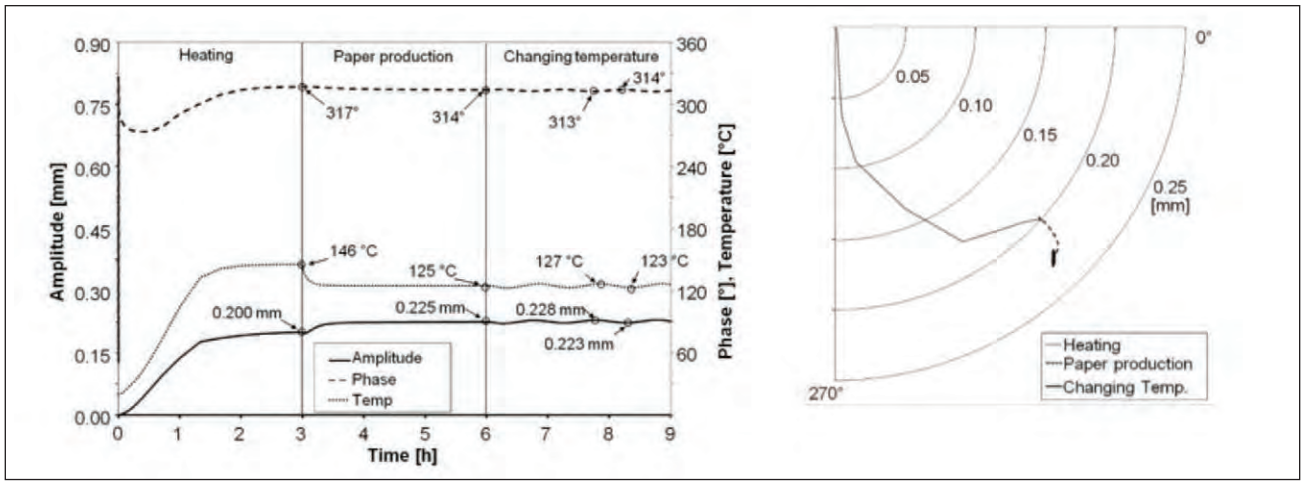
8. Left: thermal bending of the roll model and average surface temperature as a function of time, heating oil 249°C, and heat load 51.9 kW/m during production. Right: development of the left figure's thermal bending as a polar plot.



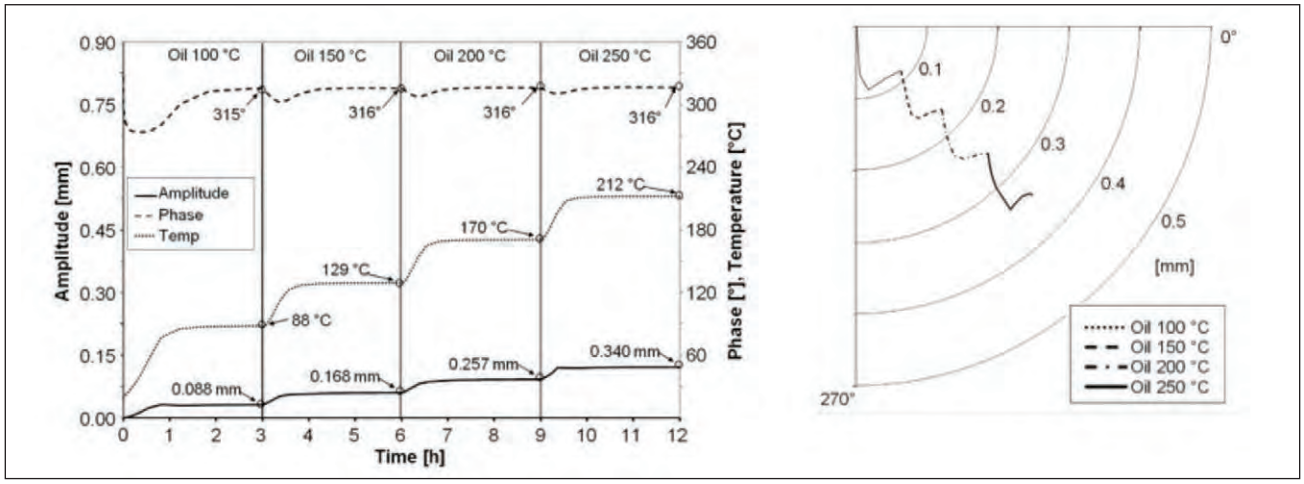
9. Left: thermal bending of the roll model and average surface temperature as a function of time, heating oil 170°C, and heat load 30.1 kW/m during production. Right: development of the left figure's thermal bending as a polar plot.



10. Left: effect of a slowly decreasing heat load (33.5 to 25.1 kW/m) with 170°C oil temperature. Right: development of the left figure's thermal bending as a polar plot.



11. Left: effect of a slowly changing oil temperature (±4°C) with 170°C oil temperature. Right: development of previous figure's thermal bending as a polar plot.



12. Left: heat up ramp, with four different oil temperature steps. Right: development of the left figure's thermal bending as a polar plot.

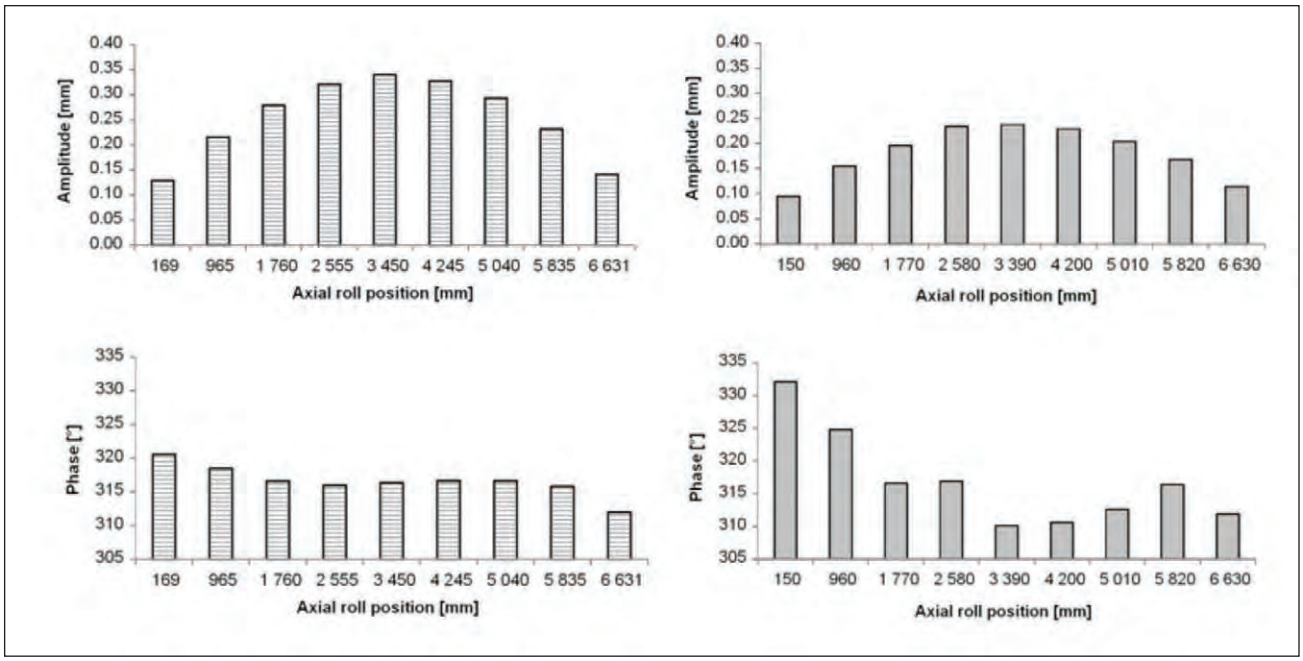
and temperature vs. time plot. This figure is then followed by a polar plot with the same bending data. The difference in the first two analyses was in the simulated oil temperature. The maximum temperature in the first analysis was 249°C. This temperature was chosen because it was the original design temperature of the roll (Fig. 8). In the second analysis, the maximum temperature was 170°C. This temperature was chosen because it is currently the temperature used in the paper mill (Fig. 9). The first two simulations present a simulation run with 3 h heat up time and 6 h production time. After the heat load is set to zero (simulates the nip open situation), the behavior was analyzed for 1 h. The polar plot shows the movement of the center point of the middle cross section during the simulation. A point A is shown in both graphs. This is provided to help visually synchronize both plots.

In **Fig. 10**, the nip open period was replaced by a slowly changing heat load period. The heat load changed from 33.5 to 25.1 kW/m in 3 h. The purpose of this simulation is to see effect of slight paper web variations like web speed, water content, bulk density, etc. **Figure 11** shows the effect of a slowly fluctuating oil temperature. This simulates the thermostat effect in the oil temperature control system of the roll. The temperature fluctuation was ±4°C. **Figure 12** presents a temperature ramp with four oil temperature steps. The roll model was heated with 100°C, 150°C, 200°C, and 250°C hot oil.

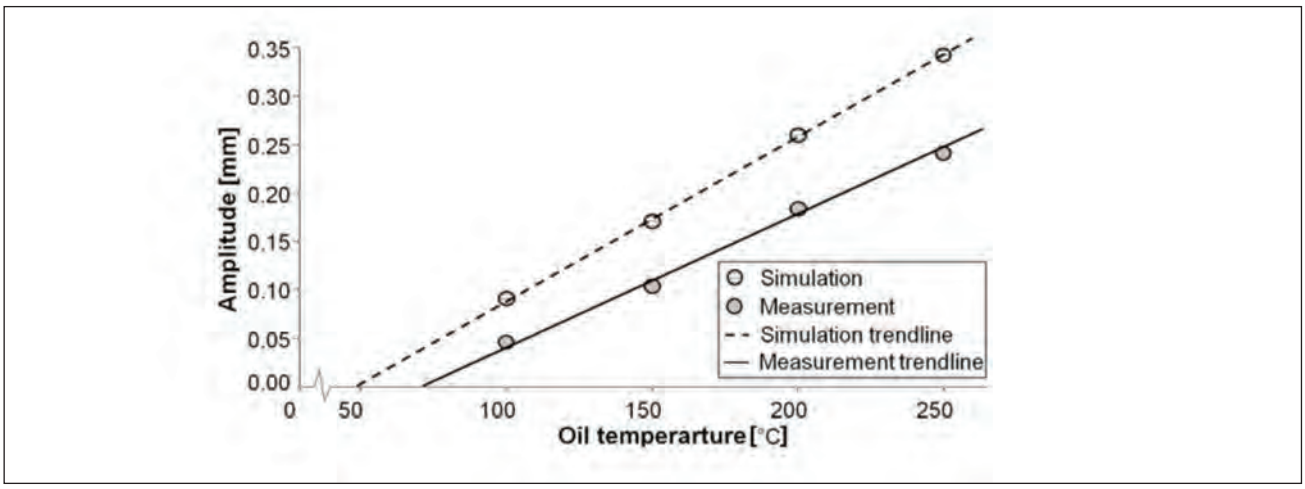
Comparison of simulated run-out and run-out measurements

The last set of results compares a range of simulated results with actual measurements. The first harmonic components of the node displacements from nine cross section profiles are presented in **Fig. 13**.

The simulation data is the same as in Fig. 12. The upper results are from the simulation, and they are taken from the end of the period with oil temperature of 250°C (after 12 simulated hours of heating). The lower graphs are from the



13. Amplitudes and phase angles of the 1st harmonic components from 9 cross sections. Left graph is from the simulation and right graph is from the run-out measurements.



14. Comparison between a measurement and a simulation with the same oil temperatures.

run-out measurement in the calender. The oil temperature during the measurement was set to 250°C, and the rotating speed of the roll was 6 Hz.

Figure 14 shows the amplitude of the 1st harmonic component of the run-out measurement of the middle cross section profile of the roll [22]. The same figure shows the amplitude of the 1st harmonic component of the displacement in the surface nodes of the middle cross section of the roll model. The amplitudes are from the same heat ramp simulation as in Fig. 12. The speed of the oil heat up in the simulation was 2°C/min. The speed of the oil heat up during the measurements is not known. The roll was rotating during the measurements (6 Hz), and the simulated roll model was static, but the thermal effects were calculated as if the roll was rotating with 5.8 Hz. The thermal effects were mainly the surface film condition parameters for the cooling effect by the surrounding air during rotation.

The actual measurement was performed so that the temperature was set from the operator panel. The roll was considered to have reached the set temperature when the surface temperature of the roll was steady for 10 min. The temperature of the roll surface was measured with a handheld IR-thermometer from Fluke (Everett, WA, USA). Fig. 14 shows the development of the amplitude of the 1st harmonic component in the middle cross section of the roll in correlation with oil temperature.

DISCUSSION

The results from the simulations are consistent with previous studies and common knowledge about the behavior of the chilled cast iron thermo rolls. When compared to actual measurements, the distinct difference is in the amplitude. The phase angles (direction) of the bending are more similar, although the roll had a service visit between the run-out measurements and the ultrasound measurements for the roll model creation. During the service visit, the journals were removed, machined, and reattached, so there is no absolute guarantee that zero position for the roll angle was the same during the measurements, but normally the positions of the journals are fixed.

The change in the direction of the bending during the heating period probably comes from the bore depth variation. The bore depths vary in the roll body, thus delaying the temperature increase in some parts of the body. When the temperature differences have time to even out, the bending direction determined by the layer thickness variation then becomes the main direction. The delay in the settling time of the bending direction can also explain the greater variation in the phase angles of the actual measurement in Fig. 13. The results from the simulation are calculated from the same simulation step; i.e., the simulation time is the same for the data. In the actual measurement, there is a small delay between the measurements of the individual cross sections. The roundness profile of the actual roll can also affect the run-out measurement results. The average bending direction of the actual roll and the roll model are almost identical: actual is 316.9°, and the roll model is 316.6°.

The cooling of the surface during paper production increased the thermal bending of the roll model during simulation. This kind of behavior was observed before from measurements made from actual thermo rolls [23]. This behavior comes from the increased stress between the layers in the roll body.

The simulations with the decreasing heat load and the small variation in the temperature were performed to see the effect of these changes on the thermal bending. There have been some reports from paper mills that the direction of the bending has suddenly changed, e.g., by 180°. The performed simulations gave no explanation as to these reports. In the case of one of the reported bending direction changes, the roll journals had valves to affect the speed of the heating fluid flow. These valves can delay the heat up of the roll body in some parts of the roll, and so provide an explanation for the sudden change of the thermal bending direction. This was not simulated in the performed FE analyses. From the results of all the simulations, it can also be seen that a temperature change causes a change in the bending direction and in its amplitude, but a change in the heat load mainly causes a change in the bending amplitude. The change in the heat load affects the temperature in the roll more slowly than the heating oil. The heat transfer rate of the white iron layer is much less than that of the grey iron layer; i.e., the white iron layer acts as an insulator.

The reason for the difference in the amplitudes between the actual measurements and the simulated behavior could be in the chosen material values. The material properties are chosen from different sources found in the literature. The size of the thermal deflection of the roll is very sensitive to the values of the heat expansion coefficients. Also, the simplified structure has an effect on the behavior of the model. The values for the used material properties were for pure white iron and for pure grey iron. As it can be seen in Fig. 1, the thickness of the pure white iron layer is almost nonexistent. This means that at least the main material values for the white iron layer are too high (as for E) or too low (as for α). A better value for these can be obtained by the integration over the depth of the white iron content in the outer layer. Because of the larger thickness of the grey iron layer, the content of the white iron in the grey iron layer can probably be neglected; i.e., no change in the values for the grey iron is necessary. The used element type was one of the simplest. The 4 node tetrahedron element type is easy to use, but the results are not always reliable. The thermal bending of the roll model, and especially the amplitude, should be otherwise checked, either analytically or with another element type.

The nip pressure is also neglected in the model. The other roll in the calender will have an effect on the measured thermo roll. This effect is very likely dependent of the magnitude of the nip pressure, although other measurements made during this work showed almost no correlation between the nip load and the deflection in the allowed nip load range. The measurements presented in this study were all made in the nip open condition.

The thermal deflection causes an unbalance in the roll. If the roll rotates (as during the run-out measurements or as during paper production), this unbalance can increase the total run-out. The roll model experienced no centrifugal forces during the simulation, so this can explain some of the differences in the amplitudes.

During the simulation, the nodes of the oil part had the same temperature distribution in the end of the heat up period, paper production period, and the nip open period. In the actual roll, the temperature drop in the oil will be larger during the paper production period than in the other periods. This can have an effect on the thermal deformations in the roll model.

Also, the boundary conditions of the FE model can have a strong effect on the simulated thermal bending. The center nodes at the end of the shafts of the journals were fixed. The actual roll has a bearing around the shaft. Even though the distance between the fixed nodes in the simplified journals of the model and the distance between the bearings of the actual roll were the same, the forces or torque caused by the bearings are not the same as in the roll model. The effect of the chosen boundary conditions and possibly better alternatives should be studied further. The exact material properties in the roll should also be measured. Normally, this cannot be done from a production roll, because the dismantling of the

roll is not allowed. Possible cooperation with the roll manufacturer can provide a solution to this problem.

CONCLUSIONS

The fact that the direction of the thermal bending of the roll and the roll model were almost identical gives the authors reason to believe that the roll modelling by ultrasound measurements can provide valuable information about the roll behavior, which would otherwise be very hard to obtain. The main difference between the simulated behavior of the roll model and the actual roll was in the magnitude of the bending. This was observable in the 1st harmonic component calculated from the cross-section profiles in the middle of the roll. The simulation was done by FE analysis. The service visit of the roll, where the journals were removed and reattached, is an unfortunate uncertainty factor in the results.

The presented case is from one roll only. The research should be expanded to cover several other rolls so that the correctness of the modelling method can be reliably assessed. Also, the correctness of the material properties should be assured.

Despite the previously mentioned factors, the results are promising and the research should be continued to validate these results. **TJ**

ACKNOWLEDGEMENTS

The main part of this work was carried out in the research project "Termo – Geometry control of the nip rolls in the paper machine environment," financed by the Technology Development Centre of Finland (TEKES) and the Finnish paper industry. The contributions and cooperation of the companies and their staff are gratefully acknowledged.

LITERATURE CITED

1. SHW Casting Technologies, "Steel Rolls?", Technical News Letter, Calender Rolls, No. 13, SHW Casting Technologies GmbH, Aalen-Wasseralfingen, Germany, December 2004
2. Jacot, A., Maijer, D., and Cockcroft, S., *Metall. Mater. Trans. A* 31A(4): 1201(2000).
3. Jacot, A., Maijer, D., and Cockcroft, S., *Metall. Mater. Trans. A* 31A(8): 2059(2000).
4. Widmaier, T., Pirttiniemi, J., Kiviluoma, P., et al., *DAAAM International Scientific Book*, DAAAM International, Vienna, Austria, 2011, pp. 347-364.
5. Rothenbacher, P. and Vomhoff, E., *Tappi J.* 68(7): 82(1985).
6. D'Amato, D., "Temperature controlled rolls design and application," *Prepr. Pap., Annu. Meet. - Can. Pulp Pap. Assoc., Tech. Sect., Part A*, CPPA/PAPTAC, Montreal, 1987.
7. Jokio, M., Ed., *Papermaking Science and Technology, Papermaking Part 3, Finishing,* Fapet Oy, Helsinki, 1999.
8. Wirtz, W., "Advanced thermo rolls for high speed modern calenders," *Int. Conf. New Available Technologies, 7th*, SPCI, Stockholm, 2002.
9. Zaoralek, M., "Hot rolls for soft calendering: Meeting the operator's needs," *TAPPI Finish. Converting Conf.*, TAPPI Press, Atlanta, GA, USA, 1990.
10. Zaoralek, M., "Improved high temperature calender roll," *Prepr. Pap., Annu. Meet. - Can. Pulp Pap. Assoc., Tech. Sect., Part B*, CPPA/PAPTAC, Montreal, 1991.

ABOUT THE AUTHORS

The basis of this paper was a research project in our department at the Aalto University School of Engineering. It complements well our previous research on paper machine rolls, although thermo rolls and their properties were unfamiliar to our research group. We interviewed thermo roll experts and gathered the required information from them and from previous research.

The most interesting aspect of this work was the unique behavior of the thermal effects on the thermo roll. Our most interesting finding was that the bending direction of the roll changes. Roll suppliers and mills will find this research useful in the manufacturing of better thermo rolls, and we plan to continue studying them.

Widmaier is a post-doctoral research scientist, Kiviluoma is senior university lecturer, and Kuosmanen is professor in the Department of Mechanical Engineering, Aalto University School of Engineering, Aalto, Finland. Pirttiniemi is CEO and Porkka is chief engineer, Dynator Oy, Helsinki, Finland. Email Widmaier at Thomas.Widmaier@aalto.fi.


Widmaier


Kiviluoma


Kuosmanen


Pirttiniemi


Porkka

11. Grosskreutz, M., "Thermo rolls – Different flow principles, design according to FKM and alternative materials for best performance in paper calenders," *Asian Paper 2010 – New Appl. Technol. (NAT) Conf.*, UBM, London, 2010.
12. Schweinichen, J., U.S. pat. 6793008 B2 (Sept. 21, 2004).
13. Kiviluoma, P., "Method and device for in situ runout measurement of calender thermo rolls," Ph.D. dissertation, Helsinki University of Technology, Espoo, Finland, 2009.
14. Zaoralek, M., "Higher precision for high temperature calender rolls," *Prepr. Pap., Annu. Meet. - Can. Pulp Pap. Assoc., Tech. Sect., Part B*, CPPA/PAPTAC, Montreal, 2004.
15. Brierley, P., Hopkins, H.G., and Peel, J.D., *Pap. Technol. Ind.* 18(7): 219(1977).
16. Zwart, J. and Farrel, W.R., *Pulp Pap. Can.* 93(2): T41(1992).
17. Neste Oil, "Thermal oil Neste S8," data sheet, Neste Oil, Espoo, Finland.
18. Yovanovich, M.M., "Thermal contact conductance of turned surfaces," *Aerosp. Sci. Meet., 9th*, American Institute of Aeronautics and Astronautics, Reston, VA, USA, 1971.
19. Cooley, J.W. and Tukey, J.W., *Math. Comput.* 19(90): 297(1965).
20. Mosier-Boss, P.A., Liebermann, S.H., and Newbery R., *Appl. Spectrosc.* 49(5): 630(1995).
21. Anderson, J., "Steps in the right direction," Customer Newsletter, SHW Casting Technologies GmbH, Aalen-Wasseralfingen, Germany, 2006, p. 21.
22. Porkka, E., Toiva, J., and Kuosmanen, P., "Run-out of a calender thermo roll at different speeds and temperatures," *Reports in Machine Design 4/2004*, Helsinki University of Technology, Espoo, Finland, 2004.
23. Pirttiniemi, J., Widmaier, T., Kiviluoma, P., et al., "Geometry control of the nip rolls in a paper machine environment - project report," TKK-K-3/09, Publications in Engineering Design and Production, Espoo, Finland, 2009.

Pulping and bleaching of Malaysian oil palm empty fruit bunches

ROBERT W. HURTER AND MEDWICK V. BYRD

ABSTRACT: Oil palm empty fruit bunch (EFB) was evaluated as a raw material for papermaking pulp production. The EFB was chopped, screened, and washed before cooking. Preliminary bench-scale trials were carried out using soda and soda-anthraquinone cooking followed by bleaching using elemental chlorine free and totally chlorine free sequences. Pilot-scale soda cooking was carried out in a 2300 L spherical digester using the soda process followed by a three-stage elemental chlorine free bleaching sequence. Unbleached and bleached EFB pulps were tested for physical and optical properties. Comparisons were made between the properties of the EFB pulps and bleached kraft eucalyptus pulp. The EFB unbleached and bleached pulps were acceptable for papermaking.

Application: For mills located near oil palm plantations, EFB could be a low-cost fiber resource for pulping.

Oil palm (*Elaeis guineensis*) is cultivated on a large scale as a source of edible oil in Central and West Africa, where it originated, as well as in Indonesia, Malaysia, and Thailand. Malaysia has about 4.7 million hectares of oil palm plantations that annually produce about 19 million metric tons of palm oil and 2 million metric tons of palm kernel oil. A typical plantation yields about 20 metric tons of fruit/ha/year but some new clones yield up to 28 metric tons/ha/year.

Oil palm plantations generate a significant amount of biomass in the form of fronds from harvesting and pruning, trunks and canopy from replanting, and empty fruit bunches (EFB). Fronds have no significant commercial uses and are typically returned to the soil as mulch. Trunks and canopy are typically pulverized and returned to the soil; some trunks are converted to plywood in combination wood veneers. Empty fruit bunches have been commercially used to produce low-value products such as construction materials, fiberboard, and molded fiber products. However, most EFB is returned to the plantations as mulch. Malaysian EFB production varies but is conservatively estimated at about 20 million metric tons/year, or about 4.3 metric ton/ha/year [1].

This study was carried out to establish pulping and bleaching conditions for EFB to produce paper grade pulps and to evaluate the pulp properties.

EXPERIMENTAL

All work was carried out at the North Carolina State University Department of Forest Biomaterials laboratory and pilot plant (Raleigh, NC, USA) under the direction of HurterConsult. All tests were conducted in accordance with TAPPI methods.

Materials

Malaysian EFB fiber strands were used for all experiments. The fiber strand raw material had been extracted from the EFB, thoroughly washed and cleaned, and then dried by forced air. The EFB fiber strands were tan in color and approximately 0.5–15 cm in length, with most fiber strands in the 5–12 cm range. The longer fiber strands were extensively intertwined in a manner similar to a bird nest. The EFB appeared to be free of stones and dirt, but dust and seed hulls were present.

Composite samples were taken from random boxes and tested for moisture content and hot water solubility. For the hot water solubility test, the samples were immersed in hot water (54°C) for 24 h. The hot water solubility was tested in this manner instead of using a standard test method (TAPPI T 207 "Water solubility of wood and pulp") because the delivered EFB fiber had been dried by forced air, which made it difficult to absorb cooking chemicals. We found that soaking EFB fiber in this manner allowed for better cooking and thus needed to measure the solubility losses.

EFB fiber preparation

Through trial and error, we found that the as-received EFB needed to be chopped, screened, and soaked overnight before cooking. The EFB fiber raw material was chopped to 2–3 cm lengths by running it twice through an Appleton pilot-scale wood chipper (Appleton Manufacturing Division; Neenah, WI, USA). The wood chipper featured a 24-in. flywheel equipped with two knives and driven by a 20-hp motor at 300 rpm. The EFB raw material was fed normal to the disk rotation and the resulting kinetic energy, along with the high volume of air flow produced by the flywheel, propelled the chopped material out of the discharge chute. The chopped material was dry screened using a vibrating screen and stored in drums for later use.

Before introduction to the digester, the chopped and dry screened EFB fiber was soaked in warm water (30°C) overnight and then drained.

Variable	Range	Optimum
Cooking apparatus	(a) Two 3-L stainless bombs placed on rotating rack in heated-air oven (b) 30-L batch digester, direct steamed	30-L batch digester, direct steamed
Sample size	200–1000 o.d. g total batch size	1000 o.d. g total batch size
Cutting/Dry screening	No cutting or cutting and dry screening	Cut empty fruit bunches (EFB) to 2–3 cm lengths, wash/screen EFB to remove nut hulls and fines
Soaking	No soaking or overnight soaking	Soaked in warm water overnight, drained
Sodium hydroxide on o.d. fiber	18%–23%	21%
Anthraquinone on o.d. fiber	0%–0.1%	0%
Liquor-to-fiber ratio	4:1–10:1	10:1 start
Maximum temperature	160°C–170°C	165°C–170°C
Time to maximum temperature	45–90 min	45 min
Time at maximum temperature	90–187 min	135 min
H-factor target	1490–1750	1750
Post-cooking treatment	Mixed, washed, and screened	Mixed, washed, and screened

I. Bench-scale cooking apparatus, procedures, and conditions.

Cooking

For the bench-scale trials, both the soda and soda-anthraquinone processes were tested using a range of test conditions (**Table I**) to determine optimum cooking conditions. A total of 11 cooks was carried out (five using 3-L bombs and six using a 30-L batch digester). Only the results for the optimum test conditions are reported in this paper.

Pilot-scale cooking was done in a 2300-L spherical digester, rotated at 10 rpm, using the soda process with the test conditions in **Table II**. Prepared EFB material was loaded into the digester, followed by caustic and adequate water to achieve the desired liquor-to-fiber ratio. The digester was then closed and heated with direct steam injection during rotation. When the target temperature and pressure were achieved, the digester was allowed to rotate, with periodic injections of steam, until the target H-factor was achieved. Rotation was then terminated, followed by depressurization (no blowing) and dumping. A sample of black liquor was obtained and saved for testing.

Pulp washing, screening, and cleaning

The bench-scale cooked material was drained of black liquor and then fiberized in cold tap water for 20 min using an immersion mixer. The slurry was screened using a 0.25-mm slotted screen.

The pilot-scale cooked material was collected in a catch box covered with fine mesh wire. Black liquor passed through the wire and was separated from the pulp. The pulp was then washed in the box to remove the bulk of the black liquor. The resulting brownstock was then pumped into a 9500-L tank and diluted to approximately 1% consistency. This slurry was passed through an Ahlstrom pressure screen (Ahlstrom; Helsinki, Finland) equipped with 0.25-mm slots. Material passing through the screen was collected in a separate tank. Rejects were directed back into the feed tank, to minimize good fiber loss. This process was continued until no more good fiber was observed in the accept stream. The screen accepts were cleaned using a Beloit Posi-Flow cleaner (Metso; Helsinki, Finland) with a feed pressure of 25 psig and an accept pressure of 10 psig. The cleaner accepts were dewatered in the wire-bottom catch box described previously.

Black liquor passing through the wire was collected and tested for residual alkali, to provide an estimate of alkali consumption during cooking. Screen accepts were tested for kappa number (TAPPI Standard Test Method T 236 "Kappa number of pulp"), total yield, fiber length distribution (optical instrument), 0.5% CED viscosity (TAPPI Method T 230 "Viscosity of pulp [capillary viscometer method]"), brightness (TAPPI Method T 525 "Diffuse brightness of paper, paperboard and pulp [d/0] – ultraviolet level C"), and Canadian Standard Freeness (TAPPI Method T 227 "Freeness of pulp [Canadian standard method]").

Bleaching

Bench-scale bleaching trials tested two sequences, DEDED and OZPP, both with a target brightness of 90% ISO. Medium-consistency bleaching with chlorine dioxide, caustic, and hy-

Variable	For Unbleached Pulp	For Bleached Pulp
Cooking apparatus	2300-L batch digester, direct steamed	2300-L batch digester, direct steamed
Number of cooks	3	5
Cook size	45–68 o.d. kg	68 o.d. kg
Cutting/dry screening	Cut empty fruit batch (EFB) to 2–3 cm lengths, wash/screen EFB to remove nut hulls and fines	
Soaking	Soaked in warm water (30°C) overnight, drained	
Sodium hydroxide on o.d. fiber	21%	22%
Anthraquinone on o.d. fiber	0%	0%
Liquor-to-fiber ratio	10:1 start	10:1 start
Maximum temperature	165°C–170°C	165°C–170°C
Time to maximum temperature	20–60 min	40–45 min
Time at maximum temperature	115–147 min	135–146 min
H-factor target	1800	1750
Post-cooking treatment	Mixed, washed, and screened	Mixed, washed, and screened

II. Pilot-scale cooking apparatus, procedures, and conditions.

Sequence	Stage	Time, min	Temperature, °C	Pressure, psi	Pulp Consistency, %
Bench Scale					
DEDED	D_0	60	70	--	10
	E_1	60	70	--	10
	D_1	180	70	--	10
	E_2	60	70	--	10
	D_2	180	70	--	10
OZPP	O	30	105	100	10
	Z	9	20 (room temperature)	--	3
	Pp	90	105	--	10
	P	240	90	--	10
Pilot Scale					
DEpD	D_0	60	70	--	10
	Ep	60	70	--	10
	D_1	180	70	--	10

III. Bleaching conditions.

Sequence	Stage	ClO_2	NaOH	H_2O_2	O_2	O_3	DTPA	DTMPA	$MgSO_4$	$NaSiO_3$	H_2SO_4
Bench Scale											
DEDED	D_0	18	--	--	--	--	--	--	--	--	--
	E_1	--	24	--	--	--	--	--	--	--	--
	D_1	14	7	--	--	--	--	--	--	--	--
	E_2	--	5	--	--	--	--	--	--	--	--
	D_2	5	--	--	--	--	--	--	--	--	--
OZPP	O	--	25	--	n/a	--	--	--	5	5	--
	Z	--	--	--	--	21	5	--	--	--	9.8
	Pp	--	40	40	--	--	--	2	5	5	--
	P		40	40	--	--	--	2	5	5	--
Pilot Scale											
DEpD	D_0	35	--	--	--	--	--	--	--	--	12
	Ep	--	30	10	--	--	--	5	5	--	14
	D_1	40	--	--	--	--	--	--	--	--	--

ClO_2 = chlorine dioxide; NaOH = sodium hydroxide; H_2O_2 = Hydrogen peroxide; O_2 = oxygen; O_3 = ozone; DTPA = diethylenetriaminepentaacetic acid; DTMPA = diethylene triamine penta (methylene phosphonic) acid; $MgSO_4$ = magnesium sulfate; $NaSiO_3$ = sodium silicate; H_2SO_4 = sulfuric acid.

IV. Bleaching chemical charges (kg/o.d. metric ton).

Moisture Content, %		Hot Water Solubility Losses, %	
Sample 1	6.6	Sample 1	13
Sample 2	6.1	Sample 2	7.2
Sample 3	6.7	--	--
Average	6.5	Average	11.1

V. Empty fruit bunches (EFB) raw material.

Material	% of Air-dried Mass by Weight		
	Trial 1	Trial 2	Average
Longer/coarser	64.0	73.2	68.6
Shorter/slender	22.4	10.9	16.6
Fines/dust	12.8	15.7	14.3
Hulls	0.8	0.2	0.5

VI. EFB chopped raw material dry screening analysis.

drogen peroxide was carried out in sealed plastic bags immersed in a heated water bath. Chemicals were mixed into the pulp using an industrial kitchen mixer fitted with a kneading blade. The pulp was then sealed into the bags. The bags were kneaded periodically during the reaction. Low-consistency bleaching using ozone (Z) was carried out by sparging ozone gas into a mixing vortex of pulp slurry. Bleaching with oxygen was carried out in 3-L pressure vessels placed on a rotating rack in a hot-air oven.

All pilot-scale bleaching was done at 10% consistency in a 950-L stirred tank. Bleaching was done using a three-stage elemental chlorine free sequence. After each stage, the slurry was tested for chemical consumption and then dumped into the wire-bottom catch box to separate most of the residual liquor.

After each bleaching stage, a liquor sample was collected and tested for residual chemical, to provide an estimate of chemical consumption. Washed pulp from each stage was tested for yield, brightness (TAPPI Method T 525), Canadian Standard Freeness (TAPPI Method T 227), and 0.5% CED viscosity (TAPPI Method T 230). **Tables III** and **IV** provide the bleaching conditions and bleaching chemical charges, respectively.

RESULTS AND DISCUSSION

EFB raw material

Table V shows the EFB raw materials. The moisture content of three random samples ranged from 6.1% to 6.7% with an average of 6.5%. The results show good uniformity between the samples; however, the moisture content was lower than one would expect from nonwood plant fiber raw materials. Over time, many lignocellulosic materials will achieve equilibrium of about 10% moisture content. The lower than expected moisture content was likely a result of the forced drying of the EFB fiber raw material.

The solubles losses in the two hot water solubility tests were 7.2% and 13.0% with an average of 11.1%. There was no evidence of oily residue in the filtrate, which was light tan in color, with a small amount of fine crill that settled out. It appeared there might be considerable variability in the hot water solubles content of EFB raw material; however, the samples were small, so it is likely that pulping larger samples will result in lower variability. That there was no evidence of oily residue in the filtrate indicates well-

Variable	Bench Scale	Pilot Scale							
		For Unbleached Paper			For Bleached Paper				
Cook no.	Optimum	13	14	15	16	17	18	19	20
Kappa number	18.4	20.3	21.4	24.8	28.0	26.7	28.5	29.8	26.8
ISO brightness	37.5%	36.1%	--	--	33.9%	34.4%	32.0%	30.9%	31.5%
Total yield	44.2%	42.6%			43.6%		50.9%		
Screened yield	43.6%	40.9%			41.2%		50.3%		
Screened rejects	1.53%	4.0%			5.5%		1.1%		
Black liquor terminal pH	11.8	12.5	--	--	10.9	10.8	10.8	10.9	10.9
Freeness, mL CSF	--	622	428	320	430	529	445	510	530
CED Viscosity, cp	--	20.3	--	--	16.5	15.8	--	--	--

VII. Cooking results.

washed material. The fine crill likely was residual dust from the fiber strand extraction process and would be mostly washed out in a good fiber preparation system in a commercial operation.

Fiber preparation

Table VI shows the fiber preparation. The wood chipper separated the EFB material and reduced the length of long strands well. It did not appear to excessively cut or damage fiber. There was, however, a large amount of dust produced. The average length of chopped EFB fiber was 2–3 cm.

Dry screening analysis shows that the chopped EFB contained a significant amount of fines and dust. The longer/coarser and shorter/slender fractions appeared suitable for pulping and papermaking. However, the fines/dust fraction was of concern, especially because it made up more of the material weight than anticipated. About half of this fraction was finely powdered material and dust and the other half was fine filaments and hairlike fibers. This combined fraction could be responsible for the high alkali consumption and lower yields obtained from bench-scale cooks 2 and 3. Bench-scale cooks 4 and 5 were carried out with dry screened EFB raw material and bench-scale cooks 6–11 were carried out using dry screened and washed EFB raw material.

Because the bench-scale cooking trials showed that the fines/dust fraction had a negative effect on alkali consumption, yield, and pulp quality, this fraction along with the hulls was not used in the pilot-scale cooks.

Cooking

Table VII shows cooking results. The optimum bench-scale cooking conditions resulted in a total and screened yield on o.d. raw material of 44.2% and 43.6%, respectively. The pulp had a kappa number of 18.4% and 37.5% ISO brightness. Alkali consumption was 99.1%.

An initial pilot-scale cook was carried out at the optimum bench-scale cooking conditions. The resultant pulp was not acceptable so the pilot-scale cooking conditions were adjusted accordingly.

A total of eight pilot cooks were carried out: three to produce pulp for unbleached papermaking and five to produce pulp for bleached papermaking. Pulp washing, screening, and cleaning were done in three batches:

- Group 1—for pulp for unbleached papermaking, cooks 13, 14 and 15
- Group 2—for pulp for bleached papermaking, cooks 16 and 17
- Group 3—for pulp for bleached papermaking, cooks 18, 19, and 20

The results from group 1 and 2 pilot cooks are reasonably comparable with the optimum bench-scale cook results in terms of yield, despite the lower kappa number of the optimum bench-scale cook, particularly with respect to group 2 cooks.

For group 1 and 2 pulps, the total yield was 42.6% and 43.6%, respectively, and the screened yield was 40.9% and 41.2%, respectively, even though the average kappa number was 22.2 for group 1 cooks and 27.4 for group 2 cooks. However, group 3 pulps had significantly higher total and screened yield, 50.9% and 50.3%, respectively. The average kappa number for the group 3 cooks was 28.3, similar to group 2. We have no explanation for the significant yield gain seen for group 3, other than the possibility that the EFB samples used might have been more heavily weighted toward the longer/coarser fraction than group 2 cooks.

Bench-scale bleaching

Table VIII shows bleaching results. For the DEDED sequence, the final brightness was 90.7% ISO, which met the target of 90% ISO. This was achieved using a total of 37 kg of

Stage	pH	Consumption			Residuals, kg/ o.d. metric ton	Yield, %	Freeness, mL CSF	Brightness, % ISO	Kappa Number	Viscosity, CP
		—	%	kg/ o.d. metric ton						
DEDED Sequence – Bench Scale										
D_0	2.4		100	18.0	0	n/a	n/a	44.4	n/a	n/a
E_1	12.5		n/a	n/a	n/a	92.3	577	56.9	3.8	16.6
D_1	4.5		89.2	12.5	1.5	95.6	555	84.0	1.1	13.6
E_2	11.6		n/a	n/a	n/a	n/a	n/a	84.2	n/a	n/a
D_2	4.5		85.4	4.3	0.7	96.7	540	90.7	0.5	12.0
					Overall Yield	85.3				
OZPP Sequence – Bench Scale										
O	10.9	NaOH	73.5	18.4	6.6	95.8	660	48.2	11.3	16.1
Z	1.5		2.1	21.0	nil	97.2	540	57.5	8.2	14.5
P_1	11.3	NaOH	86.9	34.8	5.2	93.1	510	80.1	4.1	8.7
		H_2O_2	94.8	37.9	2.1					
P_2	11.7	NaOH	80.3	32.1	7.9	94.4	430	85.5	3.3	8.3
		H_2O_2	59.5	23.8	16.2					
					Overall Yield	81.2				
DEpD Sequence – Pilot Scale										
D_0	3.3		97.1	34.0	1.0	92.6	250	62.0	2.7	12.9
Ep	10.8		98.0	29.4	0.6	94.1	210	68.5	2.0	12.8
D_1	3.6		78.5	31.4	8.6	98.4	201	85.1	1.4	10.4
					Overall Yield	85.7				

VIII. Bleaching results.

chlorine dioxide per o.d. metric ton of unbleached pulp. Because 100% of the chlorine dioxide was consumed in the D_0 stage, increasing the chlorine dioxide charge in this stage likely would allow for achieving an 86% ISO brightness after the D_1 stage. The viscosity decreased from 20.3 cp for the unbleached pulp to 12.0 cp for the fully bleached pulp. Although this is a significant drop in viscosity, the final pulp viscosity is still reasonably good. The final kappa number of 0.5 is in the range expected for fully bleached wood pulps. Overall, pulp freeness after bleaching is high, which indicates good drainability of the pulps. The overall total bleaching yield was 85.3%.

For the OZPP sequence, the final brightness was 85.5% ISO, well below the target of 90% ISO despite using 80 kg of hydrogen peroxide per o.d. metric ton of unbleached pulp. Peroxide consumption in the first pressurized P stage was 94.8% but only 59.5% in the second unpressurized P stage. It is possible that better brightness results might have been achieved with a second pressurized P stage rather than an unpressurized stage. The viscosity decreased from 20.3 cp for the unbleached pulp to 8.3 cp for the fully bleached pulp. It appears that most of the drop in viscosity occurred in the oxygen delignification and pressurized peroxide stages. It is possible that using a second pressurized peroxide stage would result in a further viscosity drop. Further process optimization might reduce the drop in viscosity. Although this is a significant drop in viscosity, the final pulp viscosity is still in an acceptable range. The final kappa number of 3.3 is much higher than expected for fully bleached pulp. Overall, pulp freeness after bleaching is high, which indicates good drainability of the pulps. The overall total bleaching yield was 81.2%.

The overall total bleaching yield was lower than expected for both bleaching sequences. Our previous R&D and commercial observations indicate that typically, for nonwood fibers starting with an unbleached kappa number of about 15, a total bleaching loss in the order of 6%–7% is anticipated. For an unbleached pulp with a kappa number of 20, one could expect a yield loss in the order of 9%–11%. However, the total bleaching yield for both sequences shows higher losses than

Sequence	Brightness, % ISO	Brightness After Aging, % ISO_{1h}	Brightness Reversion, % ISO_{1h}	Brightness After Aging, % ISO_{3h}	Brightness Reversion, % ISO_{3h}
Bench Scale					
DEDED	89.2	88.5	-0.7	88.1	-1.1
OZPP	85.5	84.5	-1.0	83.9	-1.6
Pilot Scale					
DEpD	85.1	84.5	-0.6	84.3	-0.8
Note: The final brightness for the DEDED sequence was 90.7% ISO immediately after the bleaching trial. Some natural reversion (-1.5% ISO) took place during the time between the completion of the bleaching trial and the brightness reversion test.					

IX. Brightness reversion after final bleaching stage.

Pulps	Rev	Average Fiber Length (w/w), mm	Average Fiber Width, µm	Fines Content by Number, %
Bench Scale				
Unbleached Pulp	0	0.684	18.9	24.79
DEDED	0	0.822	18.3	28.06
OZPP	0	0.918	18.4	34.20
Pilot Scale				
Unbleached Pulp	0	0.720	19.4	25.76
DEpD	0	0.862	18.4	32.55
DEpD	4000	0.744	18.6	39.02

X. Fiber length analysis.

typically anticipated. We have no explanation for the high bleaching losses.

Pilot-scale bleaching

On the basis of the bench-scale bleaching results, we decided to use a DEpD sequence for the pilot-scale bleaching. The final brightness was 85.1% ISO, which met the target of 85% ISO. This was achieved using a total of 65 kg of chlorine dioxide per o.d. metric ton of unbleached pulp. The viscosity decreased from 16.1 cp for the unbleached pulp to 10.4 cp for the fully bleached pulp. Although this is a significant drop in viscosity, the final pulp viscosity is still reasonably good. The final kappa number of 1.4 is in the range expected for 85.1% ISO bleached pulp, but is still on the high side.

The freeness of the bleached pulp dropped substantially versus the unbleached pulp. This is an indication that mechanical action on the pulp using pilot-scale equipment during bleaching had a significant negative effect on the pulp and likely was the source of fines generation. Minimizing mechanical action in the commercial mill will be important for good quality bleached EFB pulp.

Overall bleaching yield of 85.7% is low but is similar to that experienced with the bench-scale testing. Even though the average kappa number of the unbleached pulp from the five cooks was 28.0, the total yield is still lower than what we would have anticipated. We have no explanation for the high bleaching losses.

Brightness reversion

Table IX shows brightness reversion results. For the bench-scale bleaching sequences, the DEDED sequence had brightness reversion ranging from 0.9 to 2.6 units if the natural reversion is included. The OZPP sequence experienced higher brightness reversion. Brightness reversion for the pilot-scale DEpD bleached pulp was the lowest at 0.8 units

Fiber length analysis

Table X shows results of fiber length analysis. For the bench-scale pulps, the average unbleached pulp fiber length on a weight/weight basis is 20%–30% shorter than that of the bleached pulps with no refining.

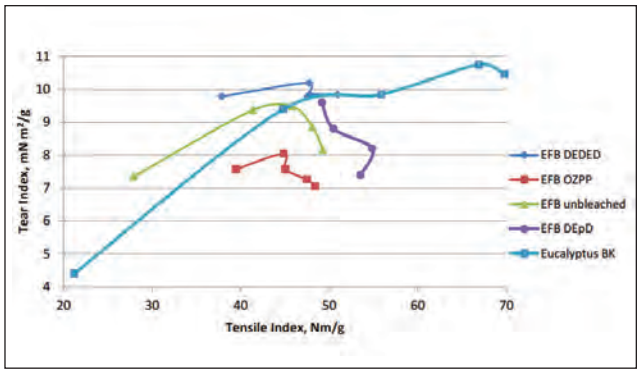
For the pilot-scale pulps, the average unbleached pulp fiber length on a weight/weight basis is 16.5% shorter than that of the bleached pulp with no refining. Even with significant re-

Test	Units	DEDED Bleached Pulp					OZPP Bleached Pulp				
Beating	rev	0	500	1000	1500	2000	0	300	500	1000	1500
Freeness	CSF, ml	540	423	364	306	252	430	300	248	195	143
Basis weight	g/m^2	67.5	66.9	65.9	66.6	65.9	66.6	66.5	65.3	65.2	65.5
Thickness	µm	123.2	102.6	95.4	91.2	84.6	107	94.6	91.4	82	76.8
Bulk	cm^3/g	1.83	1.53	1.45	1.37	1.28	1.61	1.45	1.4	1.25	1.17
Density	g/cm^3	0.546	0.654	0.690	0.730	0.781	0.621	0.690	0.714	0.800	0.855
Tear index	mN·m^2/g	9.78	10.19	9.77	9.84	9.84	7.57	8.04	7.57	7.26	7.05
Burst index	kPa·m^2/g	3.12	3.78	4.39	4.58	5.05	3.66	3.92	3.98	4.00	4.29
Tensile index	Nm/g	37.85	47.75	47.55	47.81	50.95	39.49	44.85	45.05	47.47	48.42
Fold		48	115	203	340	700	67	131	177	312	652
Stiffness	mN	7.3	6.6	6.1	5.8	5.8	5.42	5.16	5.03	4.35	4.83
TEA	J/m^2	111.9	195.5	153.8	125.6	140.5	113.3	130.2	122.3	119.6	88.1
Stretch	%	5.61	7.83	6.25	5.02	5.31	5.26	5.43	5.48	4.77	3.49
Smoothness	Sheffield, s	357	273	258	250	240	287	274	269	246	238
Porosity	Gurley, s	2.26	6.87	15.68	27.72	79.04	11.4	44.46	76.14	226.44	639.38
Notes: 1. Tear Index based on 4 ply. 2. Fold test based on M.I.T. Double Fold (2.5P). 3. Stiffness test based on Gurley 1 in. * 1-1/2 in. test.											

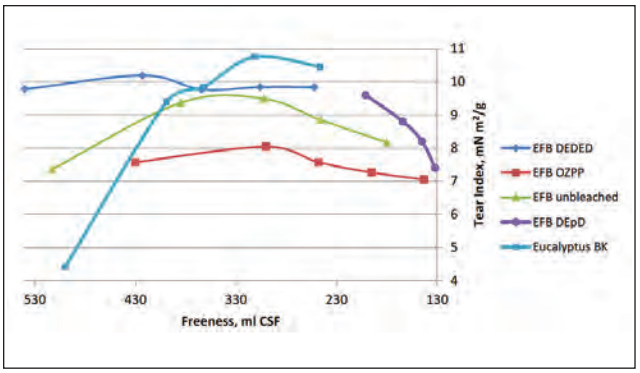
XI. Bleached pulp properties (bench-scale pulps).

Test	Units	Unbleached Pulp					DEpD Bleached Pulp			
Beating	rev	0	750	1500	2250	3000	0	1000	2000	3000
Freeness	CSF, ml	513	385	302	246	180	201	164	145	132
Basis weight	g/m2	65.0	66.2	66.9	66.2	62.7	65.2	65.3	64.9	64.9
Thickness	µm	151.8	116.6	109.8	97.0	83.2	96.8	80.2	80.4	79.6
Bulk	cm^3/g	2.34	1.76	1.64	1.47	1.33	1.50	1.20	1.20	1.20
Density	g/cm^3	0.427	0.568	0.610	0.680	0.752	0.667	0.833	0.833	0.833
Tear index	mN·m^2/g	7.35	9.37	9.49	8.85	8.17	9.6	8.8	8.2	7.4
Burst index	kPa·m^2/g	1.75	3.54	4.21	4.25	4.72	4.1	4.4	4.5	4.6
Tensile index	Nm/g	27.95	41.38	45.76	48.11	49.29	49.19	50.48	54.86	53.52
Fold		13	51	122	368	570	310	946	1397	1238
Stiffness	mN	7.1	6.8	6.8	5.7	4.1	n/a	n/a	n/a	n/a
TEA	J/m^2	51.3	138.2	166.2	138.1	115.0	156.0	108.5	120.0	85.3
Stretch	%	3.60	6.34	6.85	5.50	4.72	5.95	4.10	4.20	3.23
Smoothness	Sheffield, s	387	344	302	280	228	322	241	226	n/a
Porosity	Gurley, s	0.88	5.59	9.99	27.94	74.87	3.45	18.7	101.0	n/a
Notes:1. Tear Index based on 4 ply. 2. Fold test based on M.I.T. Double Fold (2.5P). 3. Stiffness test based on Gurley 1 in. * 1-1/2 in. test.										

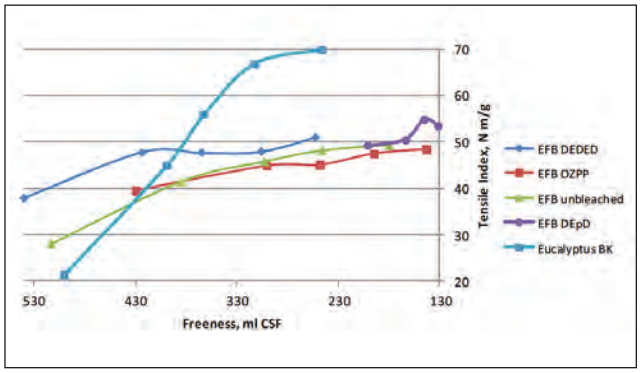
XII. Bleached pulp properties (pilot-scale pulps).



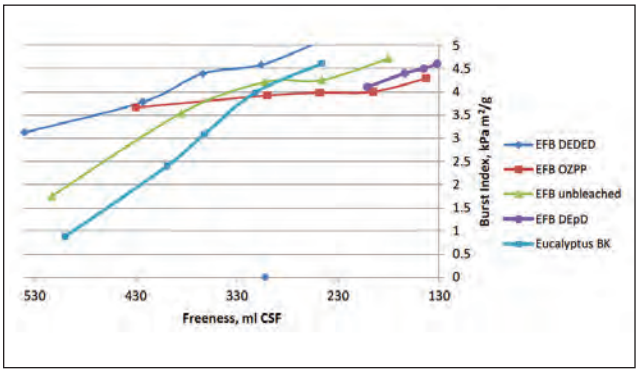
1. Tear index vs. tensile index.



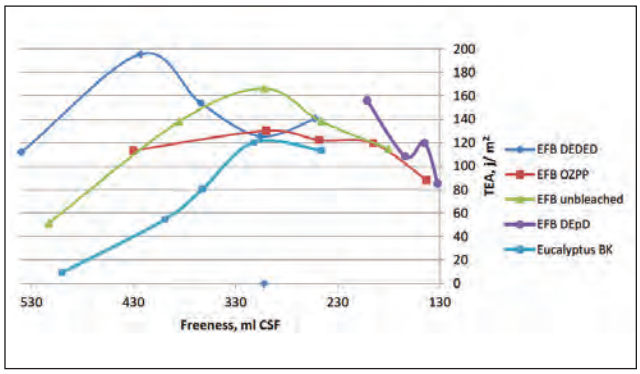
2. Tear index vs. freeness.



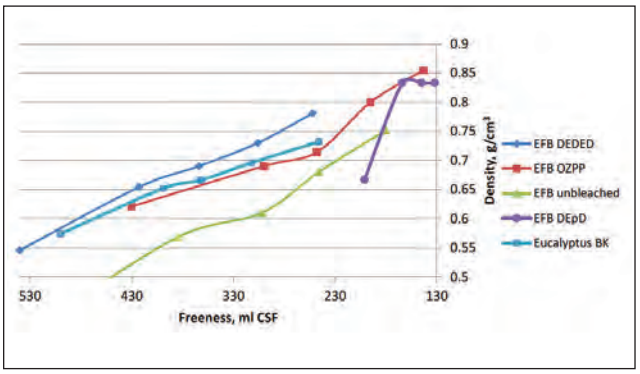
3. Tensile index vs. freeness.



4. Burst index vs. freeness.



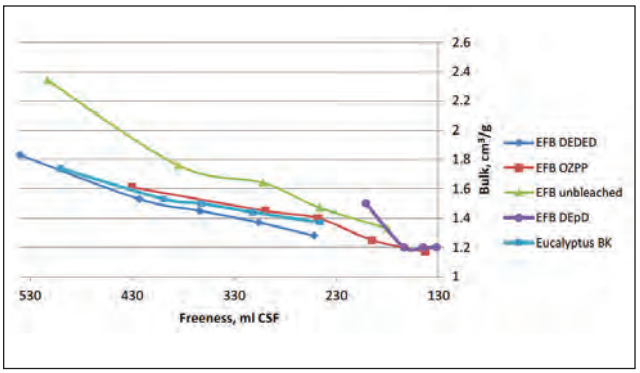
5. Tensile energy absorption (TEA) vs. freeness.



6. Density vs. freeness.

fining, the bleached pulp still has a longer average fiber length. However, the average fiber width of the unbleached and bleached pulps for all pulps is not significantly different.

Given the high fines content of the unbleached pulp, one would have thought that bleaching might reduce the fines content, thus giving the higher average fiber length for the bleached pulps. However, the fines content of the bleached pulps exceeds that of the unbleached pulp in all cases. One possible reason for the fiber length discrepancy might be the EFB samples used for the respective pulping and bleaching trials. Data are insufficient to determine whether this is the reason and more work needs to be done for a definitive answer.



7. Bulk vs. freeness.

Foelkel [2] provides a selected list of some important eucalyptus fiber/pulp characteristics and their range of variation for eucalyptus pulps. In this list, the weighted average fiber length is provided as 0.6–0.85 mm for eucalyptus. This places the EFB pulp in the range of good quality eucalyptus pulp in terms of average fiber length.

Bleached pulp properties

The properties of bench-scale soda cooked EFB DEDED and OZPP bleached pulps are provided in **Table XI**, and the properties of pilot-scale soda cooked EFB unbleached and DEpD bleached pulps are provided in **Table XII**. Selected physical properties of the EFB pulps are compared with eucalyptus bleached kraft pulp in **Figs. 1–7**.

Bench-scale EFB DEDED and OZPP bleached pulps (Table XI) both exhibited similar tensile index and burst index. However, the EFB DEDED bleached pulp had significantly higher tear index, tensile energy absorption (TEA), and bulk than the OZPP pulp.

Compared with eucalyptus bleached kraft pulp:

- EFB DEDED and DEpD bleached pulps achieved a tear index close to the maximum for eucalyptus pulp but with significantly less energy input (i.e., in a PFI mill, reaching maximum tear index required 3000 revolutions for eucalyptus versus 500 revolutions for EFB DEDED and 0 revolutions for EFB DEpD pulps).
- Tensile index for all EFB pulps was significantly lower.
- Burst index and TEA for all EFB pulps was higher.
- Bulk for the EFB bleached pulps was lower (especially for the OZPP bleached pulp).
- Bulk for the unbleached EFB pulp was higher.

CONCLUSIONS

Malaysian oil palm EFB can produce acceptable quality unbleached or bleached papermaking pulps using the soda process and either elemental chlorine free or totally chlorine free bleaching. For a commercial facility, bleaching using a three-stage DEpD sequence would reduce both capital and operating costs. Given the vast EFB resource, further study of this interesting fiber raw material is warranted. **TJ**

LITERATURE CITED

1. Daud, W.R.W. and Law, K-N., *BioResources* 6(1): 901(2011).
2. Foelkel, C., "The eucalyptus fibers and the kraft pulp quality requirements for paper manufacturing," *Eucalyptus Online Book & Newsletter*, ABCTP, Sao Paolo, February/March 2007. Available [Online] at www.eucalyptus.com.br/capitulos/ENG03_fibers.pdf <27June2017>.

ABOUT THE AUTHORS

This research was part of a 3-year project carried out during 2004-2007 for a HurterConsult client that was looking for new sources of low cost fiber. HurterConsult retained the copyright of all of the work and the client did not proceed with a project using EFB. Therefore, we decided to publish the work so that others could possibly benefit from it.

This research was similar to other work we have carried out at North Carolina State University (NCSU) on other nonwood fiber raw materials such as sisal, wheat straw, oat straw, flax, and industrial hemp. Only the raw material differed.

At the outset of the project, we were given cooking conditions for EFB fiber developed in Malaysia. However, using these conditions, we could not duplicate the cooking results at NCSU on the EFB fiber sent from Malaysia. It took some time to discover that the fiber had been dried by forced air before shipping. This appeared to have hornified the material to some extent, making it react differently in the digester. We found that soaking EFB fiber in hot water overnight allowed it to cook properly. We do not believe that this would be required in a commercial mill using fresh EFB fiber.

Interestingly, we found that totally chlorine free bleaching was less effective than elemental chlorine free bleaching. Also, elemental chlorine free bleached EFB pulps were almost as good as bleached eucalyptus pulp.



Hurter



Byrd

Mills that could benefit from this work will be location specific; that is, they need to be located near the source of EFB fiber as it cannot be shipped long distances cost effectively. For these mills, EFB fiber could be a low cost fiber resource as it is a waste from the palm oil industry.

As the next step, at PEERS 2017, November 5-8 in Norfolk, VA., we plan to report on unbleached and bleached pilot papermaking trials using high EFB pulp furnishes, which were done as part of the project.

Hurter is president, HurterConsult Inc., Ottawa, ON, Canada. Byrd is associate teaching professor, North Carolina State University, Raleigh, NC, USA. Email Hurter at bob@hurterconsult.com.

TAPPI JOURNAL
WWW.TAPPI.ORG
THE PAPER AND PACKAGING INDUSTRIES' TECHNICAL RESOURCE
JULY 2017 | VOL. 16 NO.7



PROCESS CONTROL **383**
Reduction of alkali loss in an ash leaching system
Carla Célia Rosa Medeiros, Flávia Azevedo Silva, Saulo Godoy Pignaton, Estanislau Victor Zutautas, and Kleverson Figueiredo

Progress in Paper Recycling

RECYCLING **397**
How old are fibers in paper for recycling and what is their life expectancy? A contribution to the life cycle assessment of wood fiber-based products
Gert Meinl, Lydia Tempel, Mike Schiefer, and Constanze Seidemann

LIGNIN **409**
Evaluation of the particle size of organosolv lignin in the synthesis of resol resins for plywood and their performance on fire spreading
Electra Papadopoulou, Sotiris Kountouras, Konstantinos Chrissafis, Mikelis Kirpluks, Ugis Cabulis, Pavla Švíglerová, and Bouchra Benjelloun-Mlayah

PULPING **419**
Low consistency refining of mechanical pulp — system design
Christer Sandberg, Jan-Erik Berg, and Per Engstrand

July 2017

TABLE OF CONTENTS VOL. 16 NO. 7

383 EDITORIAL
The Laboratory of Soft Materials & Green Chemistry at North Carolina State University
Monica Shaw

383 PROCESS CONTROL
Reduction of alkali loss in an ash leaching system
Carla Célia Rosa Medeiros, Flávia Azevedo Silva, Saulo Godoy Pignaton, Estanislau Victor Zutautas, and Kleverson Figueiredo

Featuring Exclusive Content from
Progress in Paper Recycling

397 RECYCLING
How old are fibers in paper for recycling and what is their life expectancy? A contribution to the life cycle assessment of wood fiber-based products
Gert Meinl, Lydia Tempel, Mike Schiefer, and Constanze Seidemann

409 LIGNIN
Evaluation of the particle size of organosolv lignin in the synthesis of resol resins for plywood and their performance on fire spreading
Electra Papadopoulou, Sotiris Kountouras, Konstantinos Chrissafis, Mikelis Kirpluks, Ugis Cabulis, Pavla Švíglerová, and Bouchra Benjelloun-Mlayah

419 PULPING
Low consistency refining of mechanical pulp — system design
Christer Sandberg, Jan-Erik Berg, and Per Engstrand

»COVER CREDIT: To minimize alkaline losses while controlling the recovery cycle's chloride level, researchers Medeiros et al. at the Veracel mill in Brazil adjusted the ash leaching system control loops, mainly on slurry density and purge control (p. 383). Cover image shows purge without decanting before the adjustments (top), purge decanted for 5 min before the adjustments (middle), and purge decanted for 5 min after the adjustments (bottom).

TAPPI JOURNAL
WWW.TAPPI.ORG

Editor-in-Chief
Scott Rosencrance scott.rosencrance@kemira.com
+1 770 429-2753

Associate Editor
Brian N. Brogdon brian.brogdon@gmail.com
+1 678 581-9114

Editorial Director
Monica Shaw mshaw@tappi.org
+1 770 367-9534

Vice President, Operations
Eric Fletty efletty@tappi.org

PRESS Manager
Jana Jensen jjenson@tappi.org
+1 770 209-7242

Webmaster
Trina Heath theath@tappi.org
+1 770 209-7416

***TJ* EDITORIAL BOARD**

Brian N. Brogdon, FutureBridge Consulting & Training LLC
brian.brogdon@gmail.com, +1 678 581-9114

David A. Carlson, Carlson Consulting
dacarlson39@aol.com, +1 847 323-2685

Jere W. Crouse, JWC Consulting
cj522@inwave.com, +1 608 362-4485

Mahendra Doshi, Doshi and Associates
mahen@aol.com, +1 920 832-9101

Marc Foulger, GL&V USA Inc.
Marc.foulger@glv.com +1 315 767-2920

Peter W. Hart, WestRock
peter.hart@westrock.com, +1 409 276-3465

Carl J. Houtman, USDA Forest Products Laboratory
choutman@fs.fed.us, + 1 608 231-9445

John A. Neun, John A. Neun LLC
john.neun@gmail.com, +1 518 275-8139

Jim Niemiec, Verso Corporation
jim.niemiec@versoco.com, +1 715 422-7404

Steven P. Ottone, Omya
steven.ottone@omya.com, +1 919 641-7854

Gaurav Pranami, Imbed Biosciences
gpranami@imbedbio.com, +1 515 230-7005

Arthur Ragauskas, Oak Ridge National Laboratory
aragausk@utk.edu

Gerard J.F. Ring, University of Wisconsin—Stevens Point
gerrryring@wi-net.com, +1 715 592-3732

Scott Rosencrance, Kemira Chemicals
scott.rosencrance@kemira.com, +1 770 429-2753

Paul Wiegand, NCASI
pwiegand@ncasi.org, +1 919 941-6417

Junyong Zhu, USDA Forest Products Laboratory
jzhu@fs.fed.us, +1 608 231-9520

Join TAPPI *today!*

TAPPI JOURNAL is a free benefit of TAPPI membership, and is only available to members. To join TAPPI, to renew your TAPPI Membership, or to learn about other valuable benefits, visit www.tappi.org.

TAPPI, 15 Technology Parkway S., Suite 115, Peachtree Corners, GA 30092, publishes *TAPPI JOURNAL* monthly.

ATTENTION PROSPECTIVE AUTHORS: All papers published are subject to *TAPPI JOURNAL's* peer-review process. Not all papers accepted for review will be published. Before submitting, check complete author guidelines at http://www.tappi.org/s_tappi/doc.asp?CID=100&DID=552877.

Statements of fact and opinions expressed are those of individual authors. TAPPI assumes no responsibility for such statements and opinions. TAPPI does not intend such statements and opinions or construe them as a solicitation of or suggestion for any agreed-upon course of conduct or concerted action of any sort.

Copyright 2017 by TAPPI, all rights reserved. For copyright permission to photocopy pages from this publication for internal or personal use, contact Copyright Clearance Center, Inc. (CCC) via their website: www.copyright.com. If you have questions about the copyright permission request process, please contact CCC by phone at +1 978 750-8400. To obtain copyright permission to use excerpts from this publication in another published work, send your specific request in writing to Editor, TAPPI JOURNAL, 15 Technology Parkway S., Suite 115, Peachtree Corners, GA 30092, USA; or by fax to +1 770 446-6947. Send address changes to TAPPI, 15 Technology Parkway S., Suite 115, Peachtree Corners, GA 30092, USA; Telephone +1 770 446-1400, or FAX +1 770 446-6947. www.tappi.org

Editorial

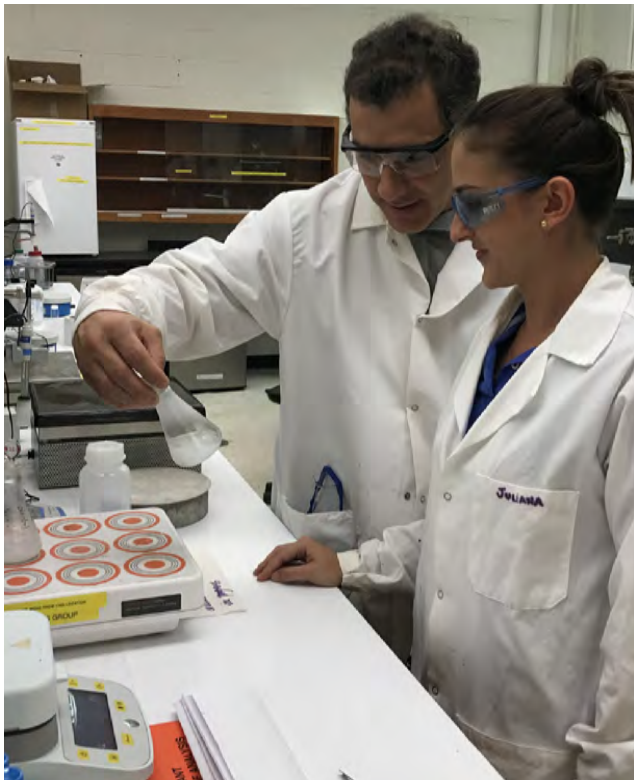
MONICA SHAW | EDITORIAL DIRECTOR
mshaw@tappi.org



The Laboratory of Soft Materials & Green Chemistry at North Carolina State University

This is the first in a series of columns featuring research and researchers from pulp, paper, biorefinery and related schools and institutions. In this column, TAPPI Journal spoke with Dr. Lucian A. Lucia about his laboratory, *The Laboratory of Soft Materials & Green Chemistry*, at North Carolina State University (NCSU) in Raleigh, NC. This lab's efforts are in materials science topics focused on the green chemistry of renewable polymers such as cellulose and lignin.

Lucia currently serves as an associate professor in the Departments of Forest Biomaterials (Wood & Paper Science) and Chemistry and as a faculty in the programs of Fiber & Polymer Science and Environmental Sciences. He received his Ph.D. in organic chemistry from the University of Florida for modeling photoinduced charge separation states of novel Rhenium (I)-based organometallic ensembles as a first order approximation of photosynthesis. Lucia began his professional career as an Assistant Professor at the Institute of Paper Science and Technology (IPST) at the Georgia Institute of Technology examining the mechanism of singlet oxygen's chemistry with lignin and cellulose. Here, *TAPPI Journal* speaks with Lucia about his recent work in bacterial cellulose, as well as his thoughts on traditional pulp and paper studies, and the industry at large.



Dr. Lucia working in The Laboratory of Soft Materials & Green Chemistry at North Carolina State University with Juliana Jardim, a M.Sc. student from Brazil who intends to become a Ph.D. student there next spring.

How did your previous training and studies influence your current work at The Laboratory of Soft Materials and Green Chemistry?

Cellulose is the common thread for me, from my past into my more recent work attempting to re-engineer it as a smart material, which goes back to when I studied energy storage in plants. I was trained as a photochemist to examine how matter uses sunlight to store energy in such things like lignocellulose. I later learned how various chemistries could break down lignocelluloses, which led me to understand how materials from plants could provide us with significant material chemical advantages. I have always been interested in the work of researchers like Vincenzo Balzani of the University of Bologna, who has long advocated the idea of developing supramolecular systems that can take on the characteristics of energy storage devices, transistors, diodes, machines, and logic circuits. This idea of supramolecular systems intrigues me because they work in a cleverly designed way to do the same things their macro counterparts do, but at a much smaller scale.

While we typically think of cellulose as plant based, some strains of bacteria also make cellulose, and they make it much faster than plants do. We can also tweak them much more easily than plants to generate cellulose with targeted functionality. By changing conditions, food sources, and other variables, we can constrain the living bacteria systems to

change the chemical and physical properties of the cellulose.

In my laboratory, we have examined electrical capacitance using bacterial cellulose. Some of the recent work is to engineer bio-based batteries by combining bacterial cellulose with graphene oxide to provide an overall structural asymmetry to potentially store charge. We found that bacteria can absorb or ingest many chemicals, graphene being one of them, whose precursor, graphene oxide, is reduced to graphene in their environment. Graphene is a functionally rich material in physics, material science and engineering, and chemistry because of its mechanical, electrical, optical, and associated properties.

Cellulose itself has many opportunities to take the place of today's plastics and electronics in their existing forms, as say, polyethylenes, PMMAs, or even some solid-state electronics. We can take a soft material like cellulose and engineer it to display the functional properties of hard solid-state electronics or tough nanocomposites.

Does bacterial cellulose compete with the potential of the lignocellulose in the paper industry?

Even though it has the same chemical composition as lignocellulose, bacterial cellulose is of much higher quality. However, it doesn't compete in the same markets as lignocellulose as it's more of a specialty product because it can't be produced in comparatively huge volumes. However, it can be engineered faster than normal engineering pathways in trees because you control the bacteria's living conditions.

To grow bacterial cellulose, biofermentation is done in a reactor through the control of temperature, pressure, reagents, nutrients, etc. It's processed differently than normal pulp from a tree, but once you are done, it has tremendous advantages that normal wood doesn't have. These are found in its physical properties, like strength, hydrophilicity, overall purity, and degree of crystallinity. It is a unique cellulose with enormous commercialization potential. In the overall published literature, there may be more patents than publications on it.

What is an example of a specialty end-product made with bacterial cellulose?

Bacterial cellulose can make a film of any dimension in the z direction (thickness) that provides an excellent cover for burn victims because it is transparent, allowing medical personnel to monitor healing. In today's health care market, opaque gauze or similar materials must be removed to check progress, which can interrupt healing and cause pain, but bacterial cellulose can stay in place because it is see-through and provides a uniform sealed and moist barrier to speed up healing and prevent infection. Its hydrophilicity, porosity, and favorable gas permeation for carbon dioxide transpiration and oxygen delivery also make it an excellent cover for burns. In addition, it has witnessed tremendous success as a cosmetic moisturizer.

How many students work in The Laboratory of Soft Materials and Green Chemistry?

We have 10 students. Of those 10, four are Ph.D. students and one is a Master's, and the remainder are visiting scientists, technicians, or undergraduates. At NCSU, we are very focused on recruiting and graduating Ph.D.'s.

Do you see students gravitating more toward biomaterials or toward traditional paper science?

We have been dealing with this issue for about 10 years now. There isn't enough funding for traditional pulp and paper science, or we might have a much more robust traditional graduate program because the post-graduate curriculum is really driven by funding. At IPST at its peak in 2000, we had unrestricted funding and we had 80 students, most of which were studying for a Ph.D. Even today, we could have the same number if the market would support it, but some calculations say the market could only support 30 Ph.D. graduates globally. There is much more of a demand for Bachelor's and Master's degrees in this current economic climate.

The funding today is in non-traditional biomaterial, bioenergy, and biorefinery areas. These are great areas, but they aren't as abundant in terms of careers as the existing pulp and paper and allied industries. In the last five years, I am not aware of an NCSU Ph.D. student who has done a traditional pulping project; they have done pulping, but more for pretreatment to explore pulp deconstruction into glucose for bioethanol or other fuel.

How do you feel about the potential for nanotechnology in our industry?

As with any research area, we must evaluate its merits. If nanotechnology passes the muster as a usable, and needed technology, it will stay and we'll figure out how it complements paper. Today, we are marrying the two in incredible ways, like using lignocellulosic scaffolds to introduce nanomaterials in industries like biomedical (tissue engineering),

pharmaceutical (drug delivery), electronic (sensors), food (antimicrobial), cosmetics (nutrients), etc. So, there's a way nanotechnology can evolve with the help of paper, but I don't think it will replace what we do with paper now. Even with nanocellulose, there are wonderful things to be done, but it's tough to envision it as a massive industry. I think it can be a niche industry and address some needs, but I don't see it addressing the needs of society the way paper does.

How do you feel about the future of the traditional pulp and paper industry in context of new developments like biomaterials?

I feel it would be a disservice to the world if we didn't continue to focus on existing traditional industries like pulp and paper. This industry needs institutions like NCSU to continue producing top-quality graduates. We realize that someday we will have a much more entrenched biomaterials industry -- bioenergy, bacterial cellulose, nanocomposites, and whatever that ends up meaning, but we can't stop serving this glorious industry. People will always need some form of lignocellulosics.

The threat to our industry may actually be its core character – sustainability. Can we continue to grow enough trees in a sustainable way? Can we treat mill effluent sustainably? Can we economically replace equipment in a mill after depreciation? Will we have enough people that understand mill processes to serve the industry?

Our industry should aggressively work together to better communicate the value of paper and this industry to the public, because people take for granted the many things they need that come from lignocellulose. Wood is a quintessential part of art, culture, civilization, and everyday life. **TJ**

Reduction of alkali loss in an ash leaching system

CARLA CÉLIA ROSA MEDEIROS, FLÁVIA AZEVEDO SILVA, SAULO GODOY PIGNATON, ESTANISLAU VICTOR ZUTAUTAS, AND KLEVERSON FIGUEIREDO

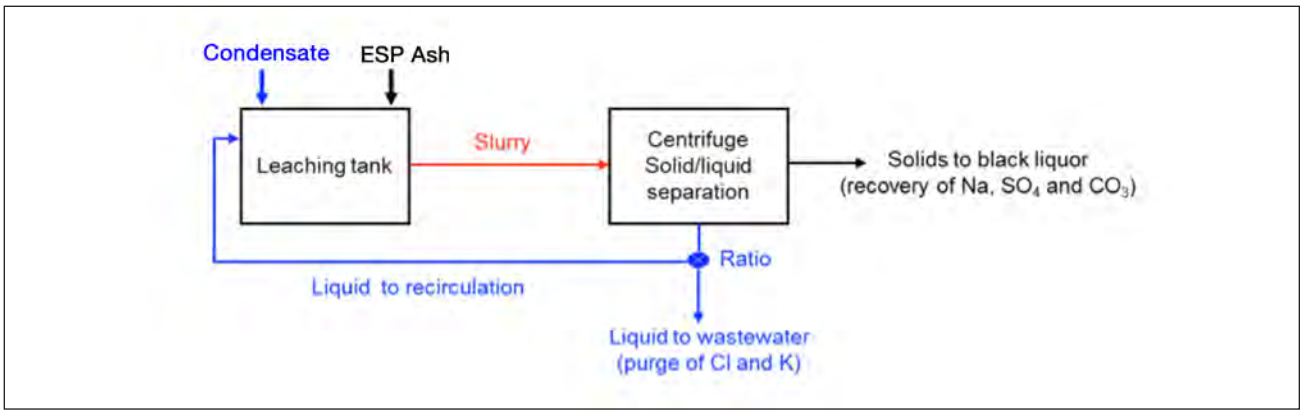
ABSTRACT: There are many points in a kraft mill where the alkaline compounds are purged from the process. Several effluents, solid waste, and air emissions contain alkali, which leads to the necessity of chemical makeups to maintain the liquor balance. The main loss of alkali at the Veracel mill is present in the wastewater from the recovery boiler; more precisely, it is from the ash leaching system, which represents 80% of the total losses.

To minimize the alkaline losses while keeping the chloride level in the recovery cycle under control, a project was developed at Veracel. Key actions were taken by adjusting the control loops of the ash leaching system, mainly on the slurry density and purge control. These adjustments led to a decrease in alkali losses and to an increase of treated ash, and kept the chloride level of the recovery boiler dust at 2.6%.

Application: This research demonstrates how alkaline losses can be reduced by automation solutions in the ash leaching system.

The Veracel mill has an ash leaching system to control the chloride (Cl) and potassium (K) level in the recovery boiler ash. This system has undergone many changes since it was installed. During previous work, a decrease in chloride level of the recovery cycle was achieved. This was pursued because the high levels of chloride in the recovery boiler ash lower the melting temperatures of carryover deposits and contribute to plugging problems, causing unscheduled shutdowns to clean the boiler [1]. The decreased level of chloride in electrostatic precipitator (ESP) dust to under 3% opened the possibility to study the alkaline losses, in order to minimize the cost for chemical makeup.

An ash leaching system follows a basic scheme, as shown in **Fig. 1**. Ash from the ESP, which consists of sodium sulfate (Na_2SO_4) with a small amount of sodium carbonate (Na_2CO_3) enriched in K and Cl [1], along with condensate from the evaporation, are fed into a tank where they are mixed, resulting in two phases of slurry: liquid and solid. The higher solubility of sodium chloride (NaCl) and potassium chloride (KCl) than Na_2SO_4 keeps chlorides in solution while Na_2SO_4 precipitates [2]. The phases are subsequently separated in a centrifuge. The liquid, which is essentially the saturated solution of the ash, contains a higher level of Cl and K and a lower content of the ions sulfate (SO^{2-}_4), carbonate (CO^{2-}_3), and sodium (Na^+) than the solid phase. Part of the liquid is purged to remove Cl and K, while the solid phase returns to the mill liquor in the mix tank for Na and sulfur (S) recovery [3]. Thus, the alkaline losses in the ash leaching are due to the sodium content of the liquid reject. According Gonçalves et al. [3], at a given degree of solid-liquid separation, a higher removal degree of Cl and K will normally generate a lower recovery degree of Na, CO_3, and SO_4. This is expected, as Na and SO_4 are also present in considerable quantities in the liquid. There-



1. Basic schematic of the ash leaching system (Cl = chlorine; K = potassium; Na = sodium ion; SO_4 = sulfate ion; CO_3 = carbon ion).

fore, the more the liquid is separated and discarded, the more Cl, K, Na, and SO_4 will be removed, and therefore the less Na and SO_4 will be recovered.

To obtain lower alkaline losses through the purge, the mill had to minimize the concentration of alkaline compounds and the flow of purge. Therefore, the aim of this project was to lower these parameters as far as possible. Further on, improvements in the density control of the tank and a new purge control were developed.

EXPERIMENTAL

This case study of the ash leaching at the recovery boiler was conducted at Veracel mill during 2015. The normal load in the recovery boiler is 5100 tons of dry solids per day, and the ash leaching load before this work was around 150 tons of ash per day.

This project opportunity was identified when the alkali losses, normally represented as mass of Na_2SO_4 (kg) per tons of air dry pulp (a.d. ton), started to increase. Then, a team of technical assistants and specialists in the recovery process and automation was created.

The team gathered input data from lab analyses and online process program, collected from the Aspen Process Explorer Version 2006.5 (AspenTech; Bedford, MA, USA). The main physical analyses were density and solids content of the purge, the slurry, and the solid phase. The chemical analyses were Na, K, Cl, sulfate, and carbonate content. The analysis of Cl and Na was based on standard methods from the American Public Health Association [4]. The sulfate analysis was performed according to an internally developed procedure.

Analyzing the data, the team observed that a way to reduce the alkali losses was to decrease the amount of solid in the liquid phase by improving the separation in the centrifuge, which could be made adjusting the torque's centrifuge. Further analysis comparing the torque with the slurry density showed that the density had an impact in the torque, which led to a change of the density control loops. Another improvement idea was to fix the volume of the purge, seeking its reduction, which was possible due to the previous stability of the chloride.

Minitab (Minitab; State College, PA, USA) charts were created to analyze the project results, such as time series and interval plots.

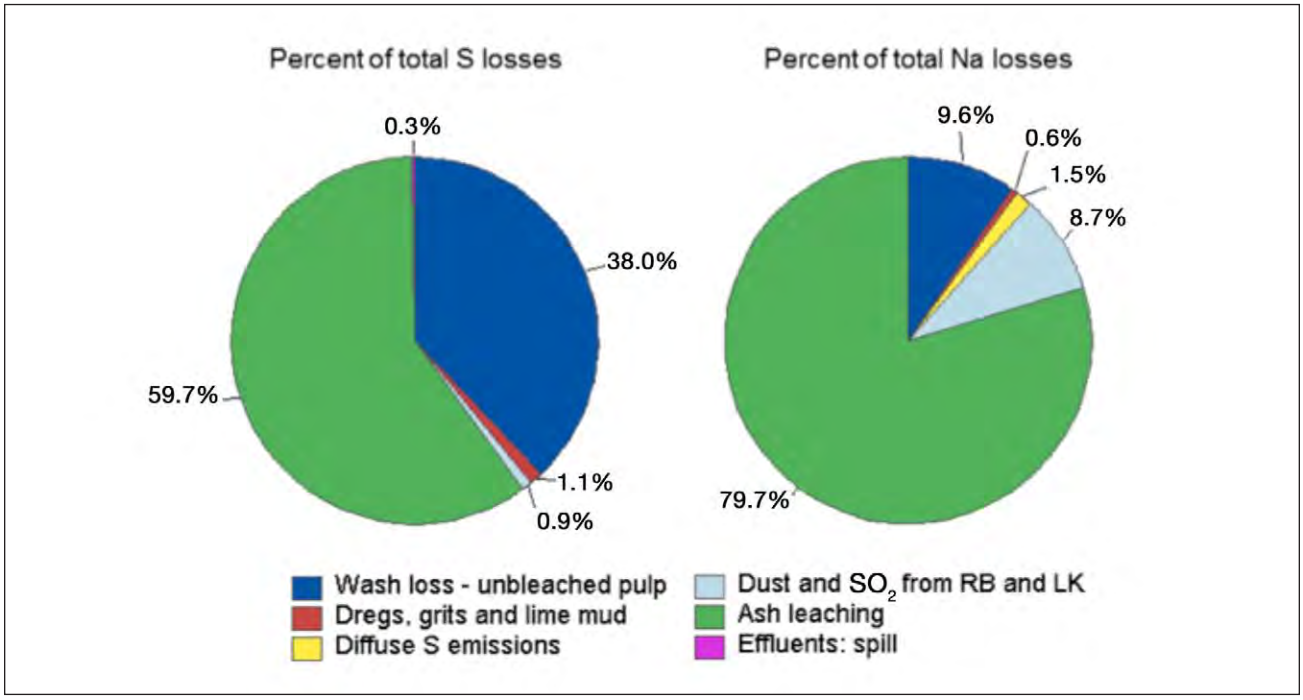
RESULTS AND DISCUSSION

The ash leaching was found to be the main cause of sodium and sulfur losses in the mill, which is shown in the comparison of losses from different process areas (**Fig. 2**). As can be seen, losses from ash leaching constituted 79.7% and 59.7 % of the Na and S losses, respectively.

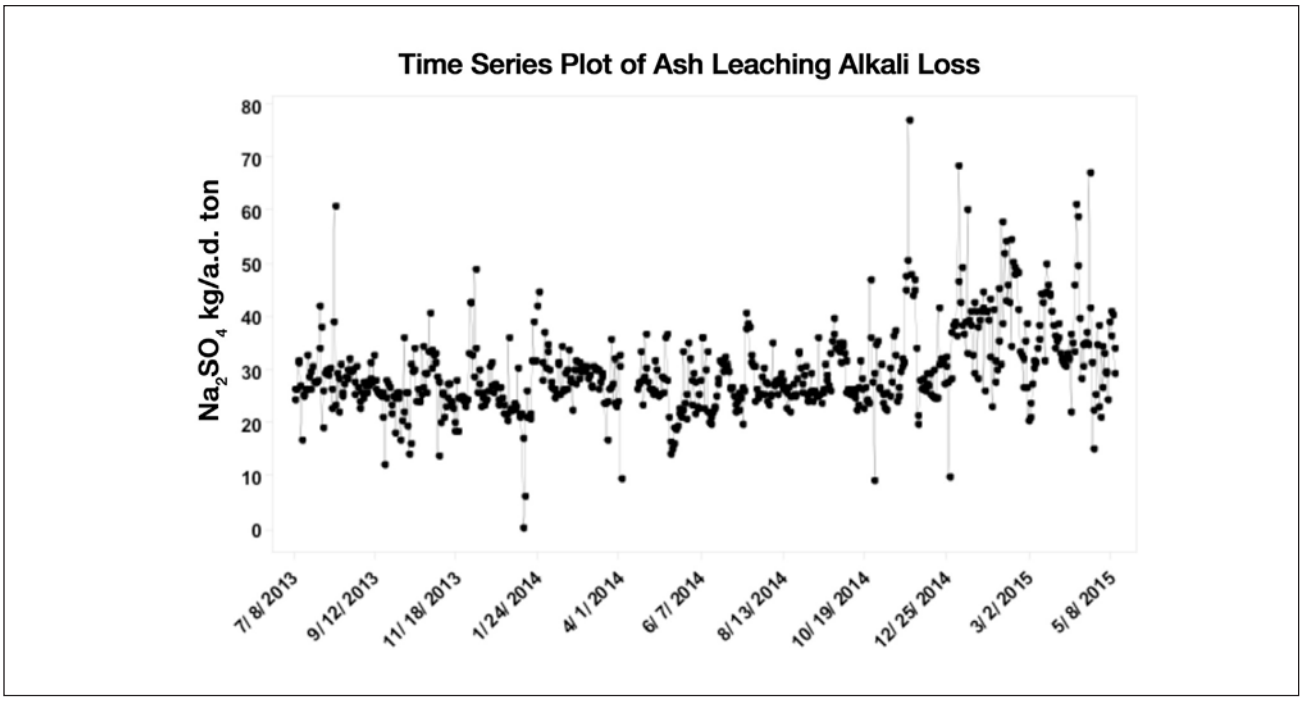
The alkali loss from the ash leaching system started to increase in November of 2014. The results of it from July 2013 to May 2015 are presented in **Fig. 3**.

Analyzing the data from Fig. 3, the following statistical values were obtained: the standard deviation was 10.04 kg Na_2SO_4/a.d. ton, the mean was 36.35 kg Na_2SO_4/a.d. ton, and the maximum and minimum value were 76.95 kg Na_2SO_4/a.d. ton and 9.7 kg Na_2SO_4/a.d. ton, respectively.

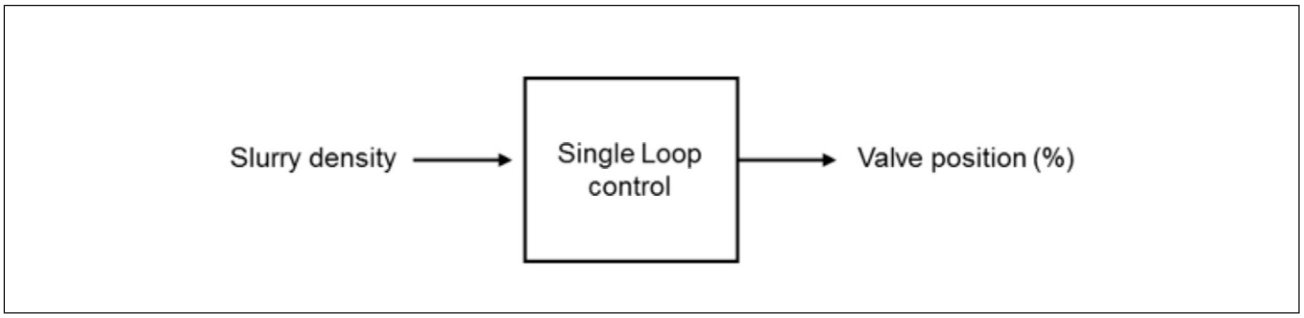
As the cost to make up all these chemical losses was quite high since November 2014, a study to decrease the alkali loss in the ash leaching system was initiated. The aim was to minimize the Na_2SO_4 concentration and the flow of the purge and



2. Percent of total sulfur (S) and sodium (Na) losses in the process based on kg sodium sulfate (Na_2SO_4)/a.d. ton.



3. Ash leaching alkali loss plot (Na_2SO_4 kg /a.d. ton) as a function of time, 2013-2015.



4. Basic schematic of the old control.

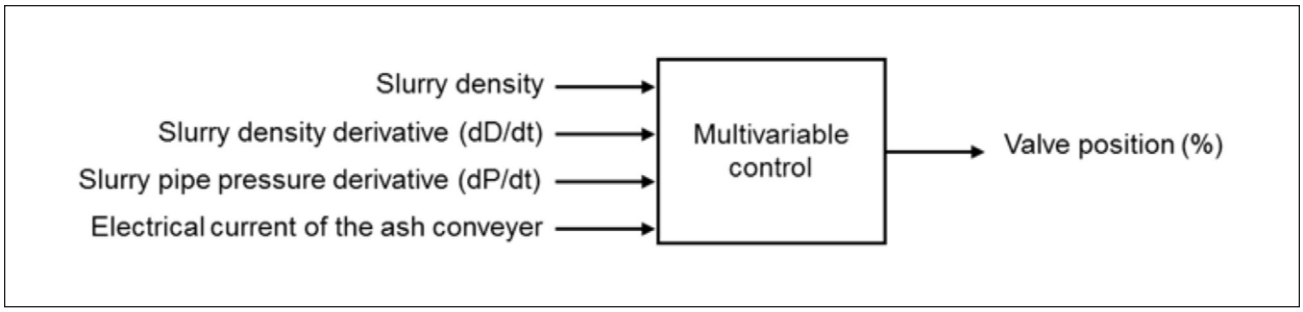
their variation, which are compounds of the alkali loss.

The purge concentration is quite linked with the degree of separation in the centrifuge. An important variable to enhance the separation of solid and liquid phases is the torque of the centrifuge, as a high torque on the machine lowers the carryover in the liquid. The torque is related to many machine variables, such as the rotation, the speed difference between the drum and the screw, and the slurry density. High density, which is related to the increase of ash content in the slurry, leads to high torque during normal operation. Thus, the first action was to evaluate a way to enhance the slurry density by improving its control loop.

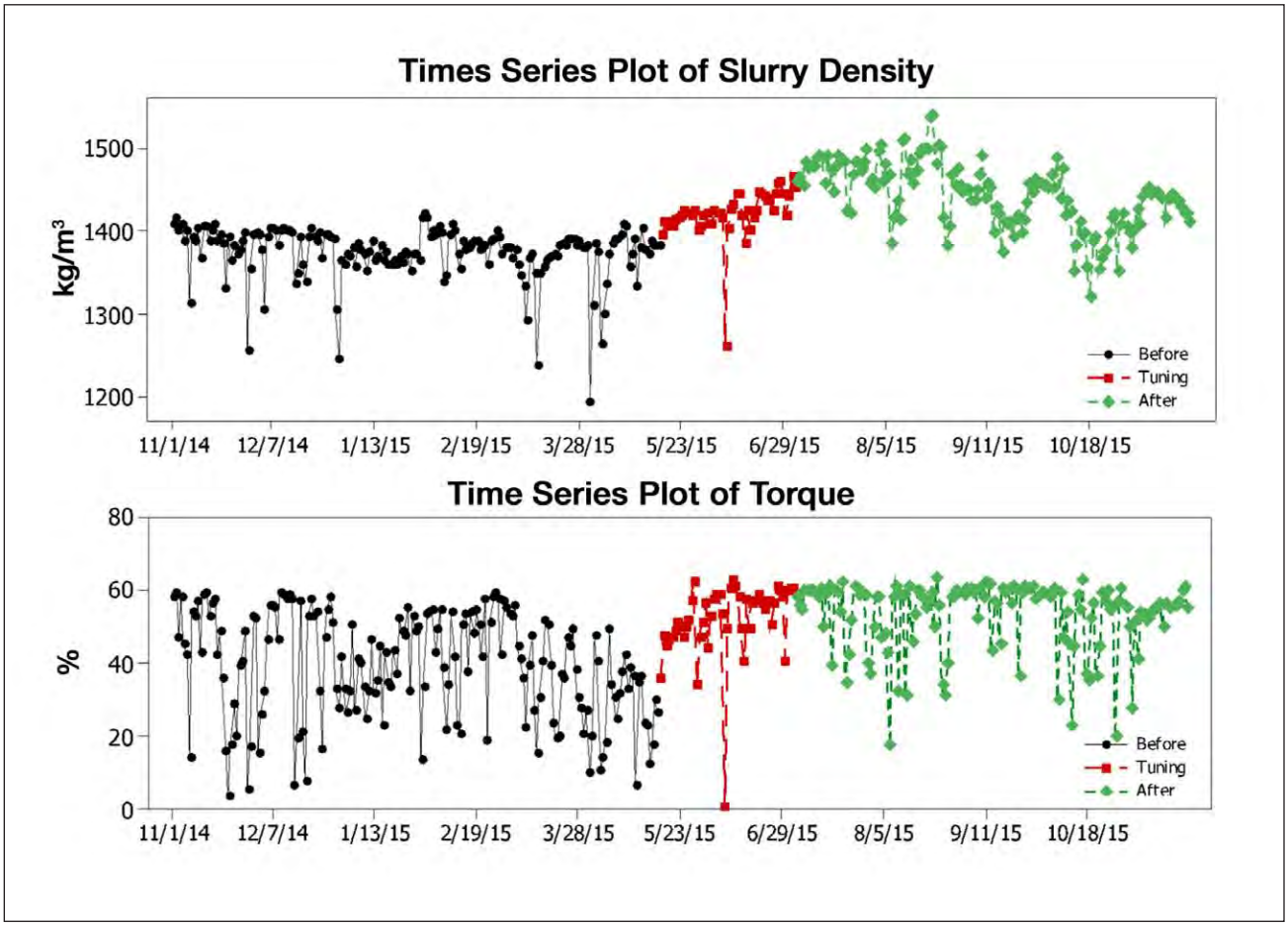
Before the project, the control was a single loop based only on the read of the slurry density (**Fig. 4**). This control then would act on the opening of the ash valve, allowing more or less ash to enter the tank, keeping the density on the setpoint. The ash for the ash leaching tank comes from the ESP in an unequal amount, meaning that for the same ash valve opening, a different amount of ash went to the tank. Due to the variation in the amount of ash, this control loop was unable to minimize the density variability.

Thus, a multivariable control was developed, adding new parameters in the control loop in order to minimize the change in ash amount to the tank, and consequently improve density control (**Fig. 5**). The first variable added was the electrical current of the ash conveyer to predict the volume of ash into the tank as a feedforward control. It was implemented as a feedback control: the rate of change of the slurry pipe pressure, and the density derivative (dD/dt). In other words, when the derivative of pressure or of the density start to decrease, the ash valve opens slowly. These improvements contributed to an increase in the density and the torque, as shown in **Fig. 6**.

The increase in the slurry density and torque led to the improvement of the purge quality in terms of carryover, which can be proven by the aspect of the purge and the re-



5. Basic schematic of the new control.



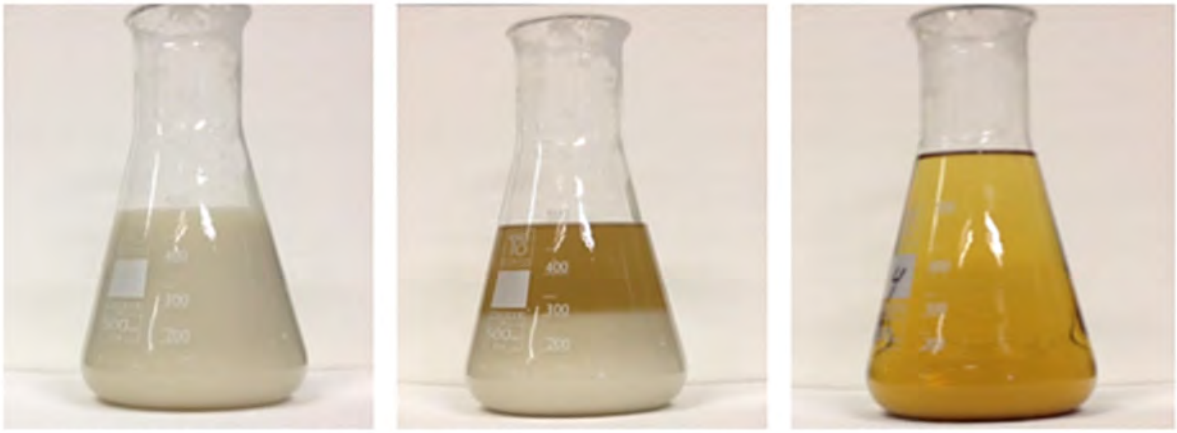
6. Time series of slurry density and centrifuge torque before the project, during the tuning phase, and after all adjustments.

duction of density and solids content in the purge before and after the improvements (**Fig. 7** and **Fig. 8**).

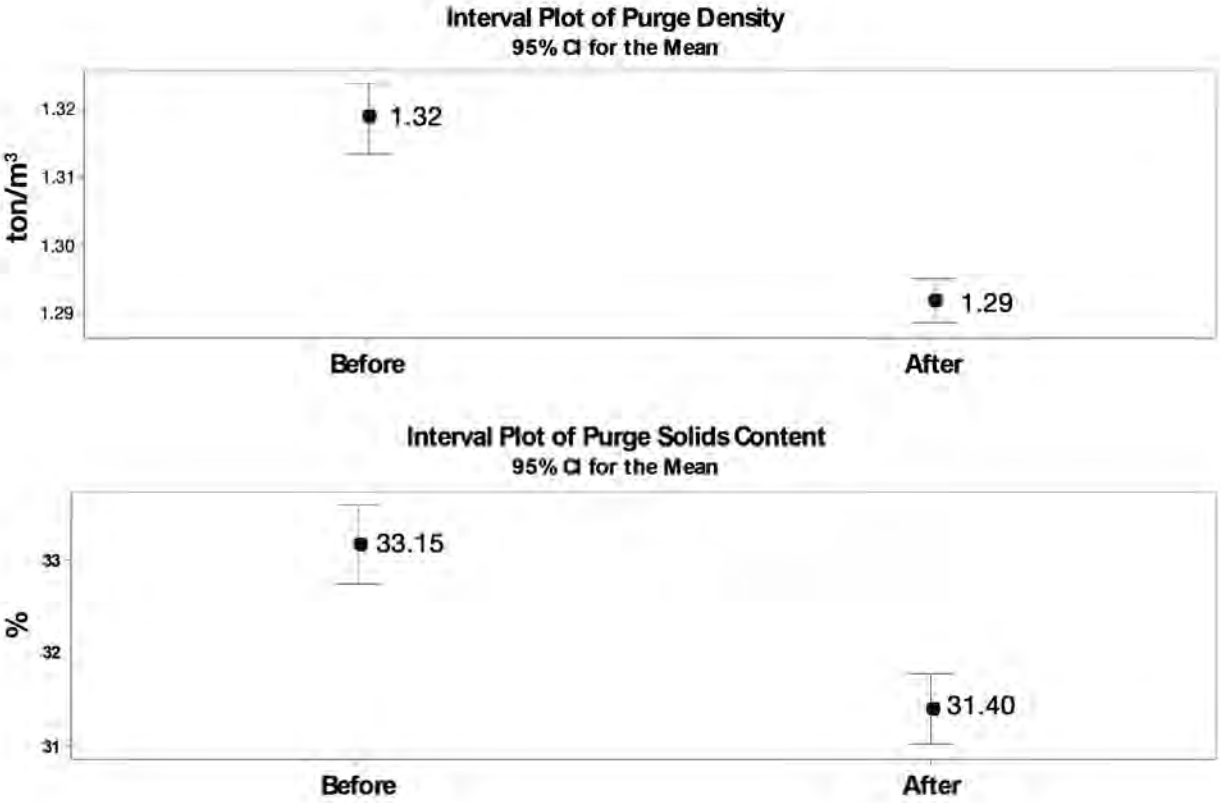
While a reduction in solids content in the purge was observed, an increase of it in the cake from 66.5% to 71.5% was seen. It means that the dryness in the cake has increased, which can be explained by the increase of the torque in the centrifuge as shown in the Fig. 6. The main benefit of increased dryness in the cake is the reduction of chloride once the liquid is enriched with this element.

Running with a higher density, the amount of treated ash was enhanced from 150 to 180 tons/day. This led to a reduction of the chloride content in the ESP ash (**Fig. 9**) from 3.0% to 2.6%. The high result during April 2015 was caused by the mill's annual shutdown and is considered an outlier.

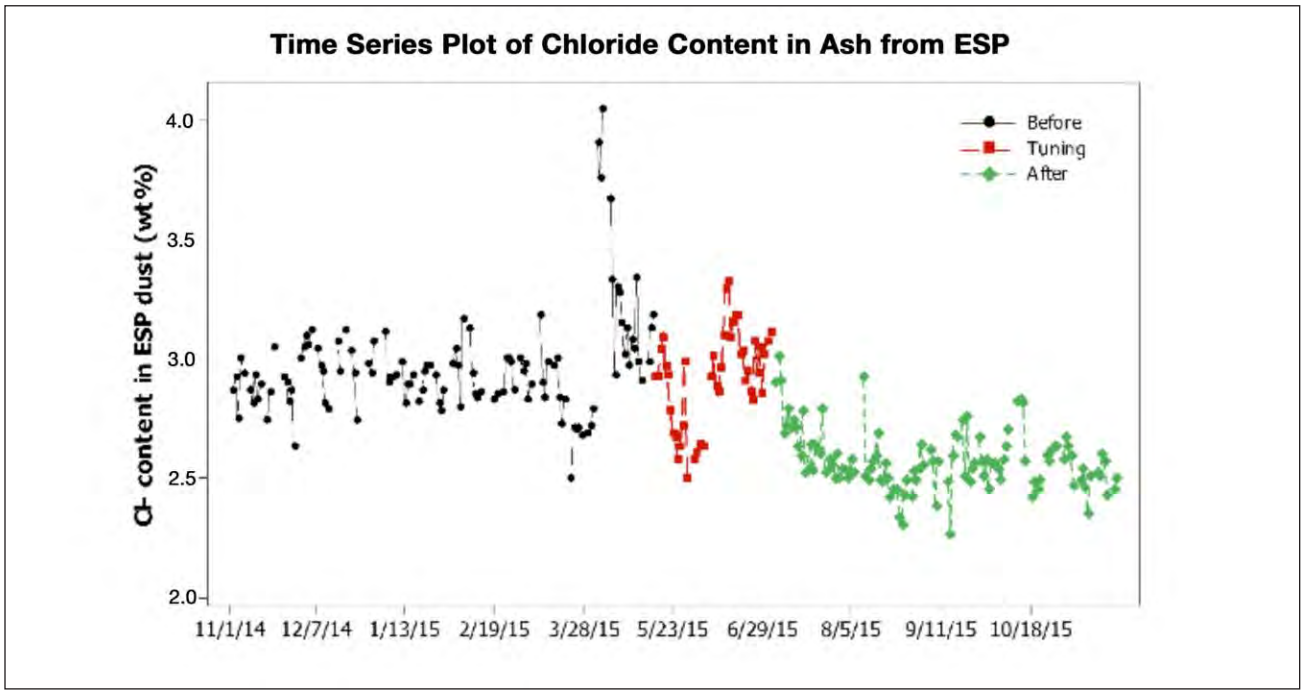
Once the carryover in the purge was minimized by the density and torque control, the next step was to develop a strategy to stabilize the purge volume. The purge flow used to change according to a fixed ratio between the purge and the recirculation flow. In order to fix the purge volume per day, since it is a main parameter, the variability was transferred to the ratio. **Figure 10** demonstrates the flow and ratio variation before and after the control. The ratio is represented based on the percentage of the purge and recirculation flow. The purge flow unit is m^3/h.



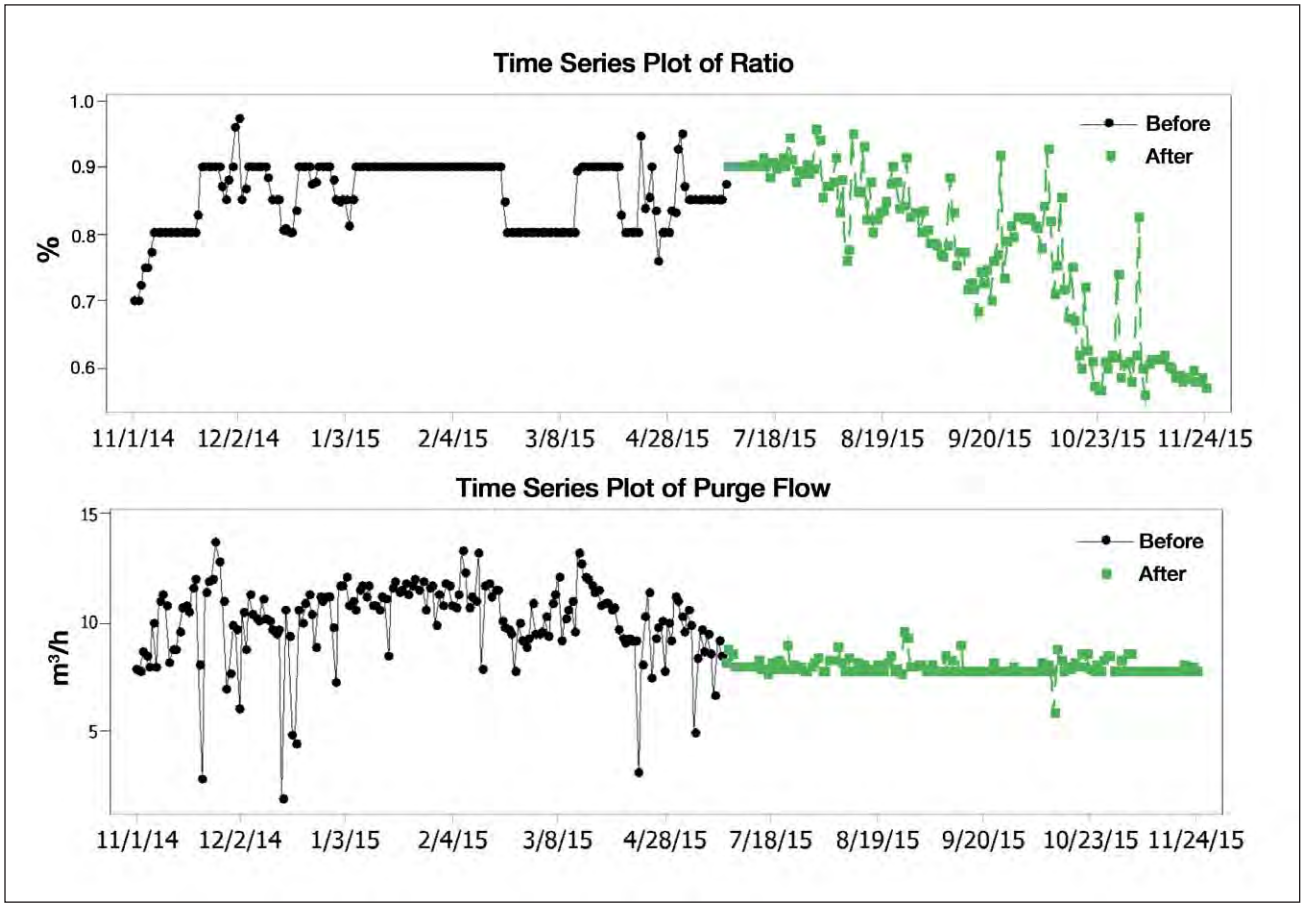
7. Pictures of the purge before and after improvements.



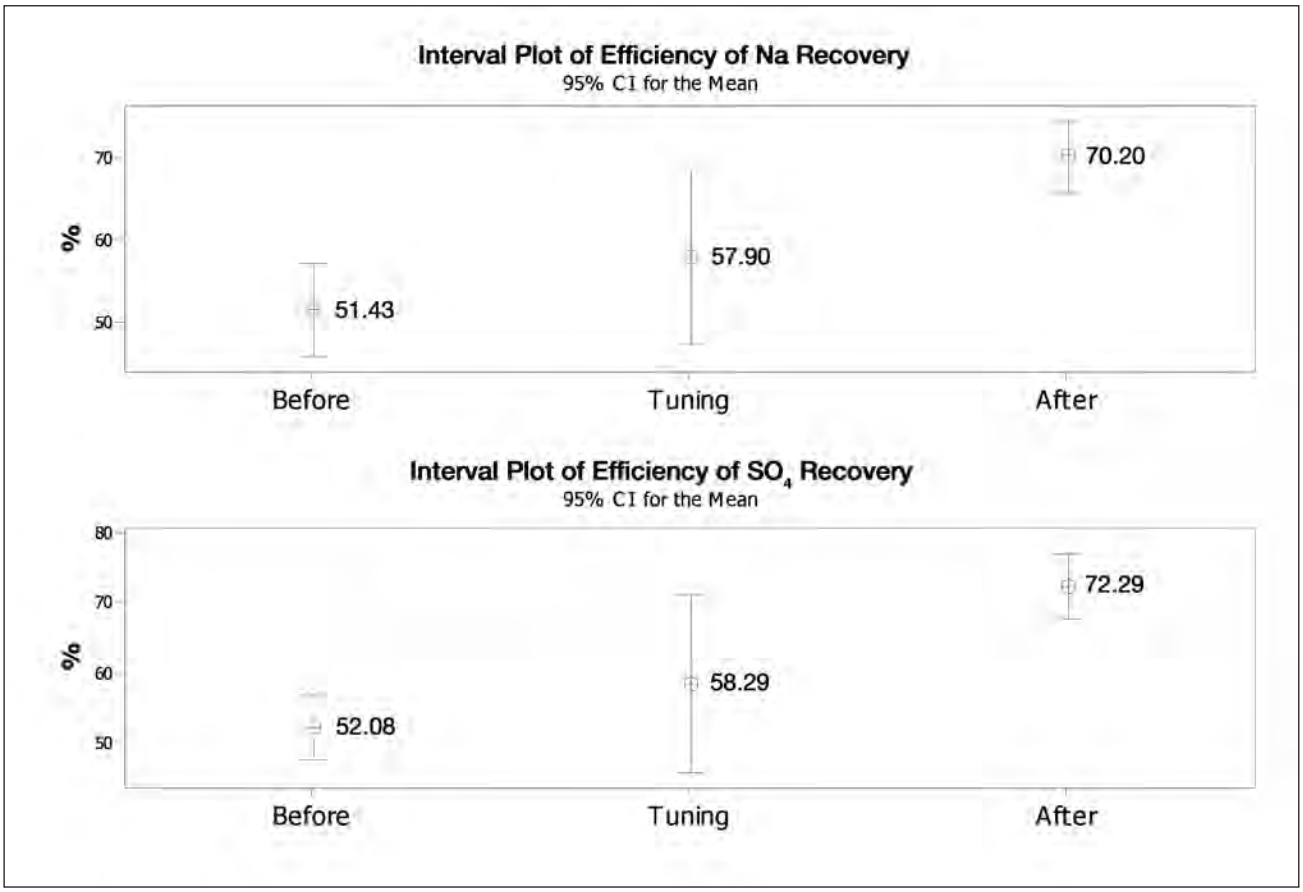
8. Interval plot of density and solids content of the purge before and after the improvements (CI = confidence interval).



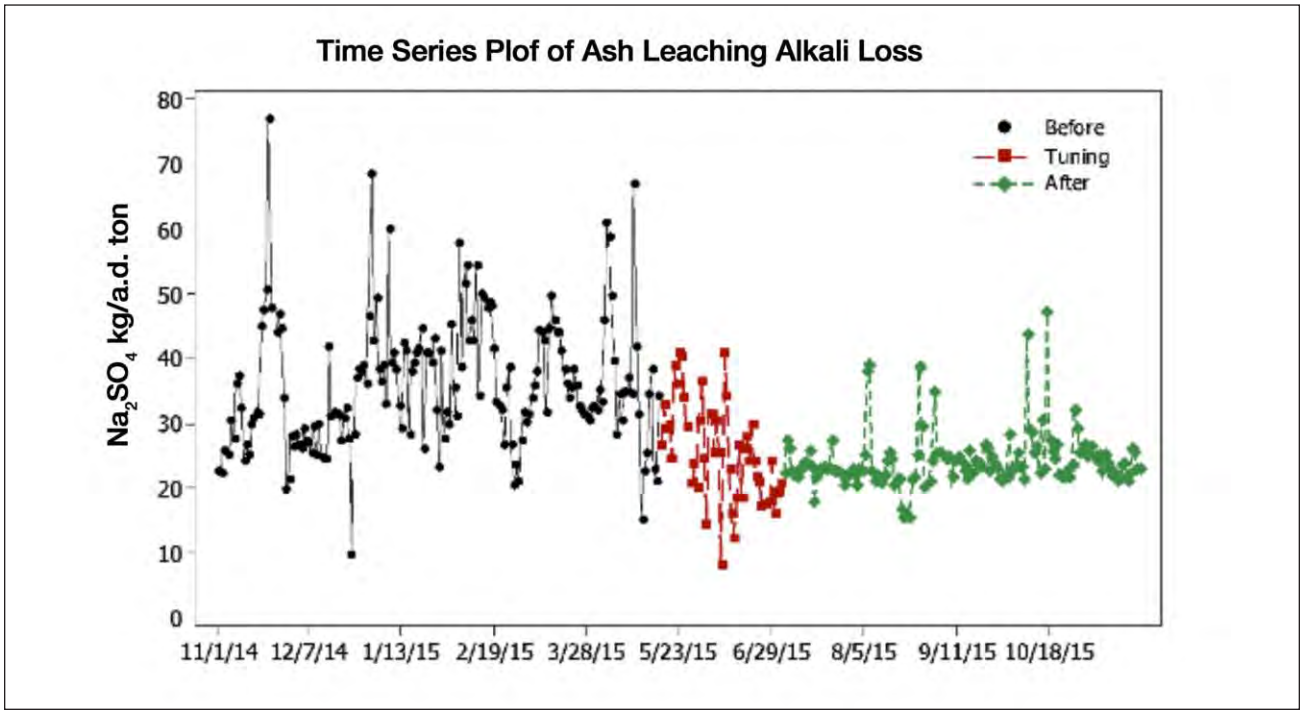
9. Time series of chloride (Cl) content in the ash from electrostatic precipitator before the project, during the tuning phase, and after all adjustments.



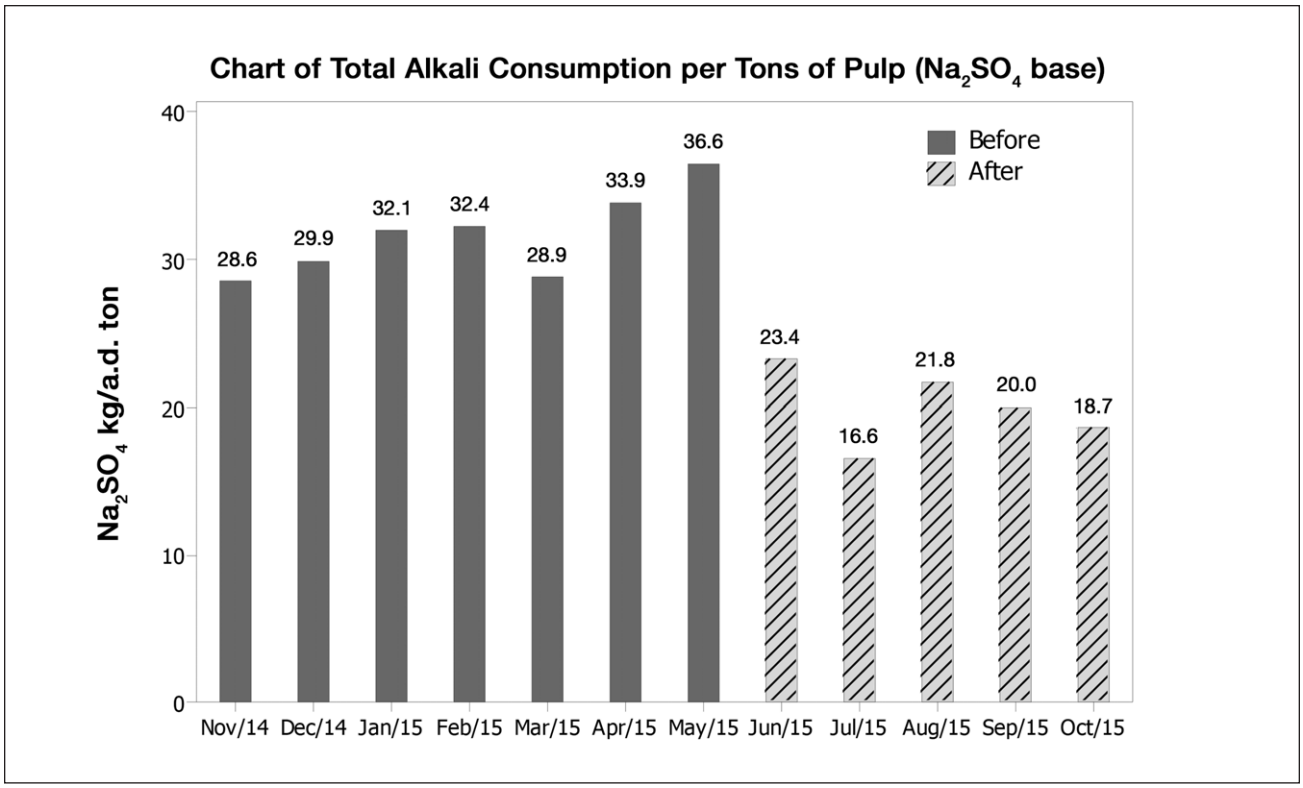
10. Time series of ratio and purge flow before and after the project. The variability of the main parameter (purge flow) was transferred to the less important one (ratio) in order to keep a fixed volume of purge per day.



11. Interval plot of sodium (Na) and sulfate (SO_4) recovery efficiency before the project, during the tuning phase, and after all adjustments (CI = confidence interval).



12. Time series of alkali loss from the ash leaching before and during the tuning phase and after all adjustments.



13. Chart of sodium hydroxide (NaOH) and sodium sulfate (Na_2SO_4) makeup consumption based on Na_2SO_4/a.d. ton before and after all the improvements.

After all these actions, the Na and SO_4 recovery in the ash leaching system increased from 51.4% to 70.2% and from 52.1% to 72.3%, respectively (**Fig. 11**). As expected, the chloride removal efficiency was reduced from 73.9% to 61.9%, since it is a tradeoff with the recovery efficiencies, as explained previously. However, as mentioned, the possibility to treat more ash and the increase of the dryness in the cake resulted in decreased chloride levels. The gain in the recovery efficiency is demonstrated in the alkali loss, which was reduced from 35.9 kg Na_2SO_4/a.d. ton to 24.0 Na_2SO_4/a.d. ton (**Fig. 12**).

The specific consumption of the makeup chemicals before and after the project is presented in **Fig. 13**. As can be seen, the use of makeup chemicals decreased, and the economic benefits were estimated to be in the order of US$2.5 million/year.

CONCLUSIONS

Alkali losses from the ash leaching unit of the Veracel mill were decreased in this study. The key to obtaining this reduction was to reduce the purge's carryover and improve the control of the purge flow. This was possible by tuning the torque control with a new strategy developed to control the slurry density and the pressure of the slurry pipe, combined with the creation of a flow control in order to limit the total purge volume per day. These actions have contributed to achieving a significantly better economy of chemical makeup, as a consequence of the ash leaching alkali loss reduction from 35.9 kg Na_2SO_4/a.d. ton to 24.0 Na_2SO_4/a.d. ton. As the improvements allowed the mill to enhance the amount of treated ash, it was also possible to reduce the chloride level from 3.0% to 2.6% in the ESP ash. **TJ**

LITERATURE CITED

1. Tran, H.N., in *Kraft Recovery Boilers* (T.N. Adams, Ed.), TAPPI Press, Atlanta, GA, USA, 1997, Chap. 9.
2. Johansson, U., "Different methods for the purge of chlorides and potassium from electrostatic precipitator dust in the kraft mill," M.Sc. thesis, Lund Institute of Technology, Lund, Sweden, 2005.
3. Gonçalves, C., Tran, H., and Shenassa, R., "Factors affecting chloride and potassium removal efficiency of a recovery boiler precipitator ash treament system," *Int. Chem. Recovery Conf.*, PAPTAC/TAPPI, Montreal/Atlanta, 2007.
4. Eaton, A.D., Clesceri, L.S., Greenberg, A.E., et al., Eds., *Standard Methods for the Examination of Water and Wastewater*, 20th edn., American Public Health Association, Washington, DC, 1998, pp. 3-98, 4-66.

ABOUT THE AUTHORS

The ash leaching system is a relevant research topic because it is related to chloride (Cl) and potassium (K) control and alkali loss. Chloride and K in the recovery boiler ash is associated with plugging problems and alkali loss and also with makeup costs. This study is a real case from a modern pulp mill, and the improvements mentioned in this paper could be applied in other similar systems.

The most difficult aspect of this research was keeping the Cl level under control during the tuning phase of the project. Interestingly, the recovery efficiency of sodium (Na) and the removal efficiency of Cl and K are a tradeoff in the ash leaching system. With the improvements, it was possible to increase the recovery efficiency of Na and decrease the Cl and K levels, even with the decrease in the removal efficiency of Cl and K. The decrease of Cl and K was possible because the improvements enabled the increase of the treated ash amount.

Our next step is to develop an efficient maintenance program that guarantees the availability of the ash leaching system.

Medeiros is Recovery & Utilities (R&U) specialist; Silva is technical control manager; Pignaton is R&U technical assistant; and Zutautas is R&U technical coordinator, at Veracel Celulose S.A., Eunápolis, Brazil. Figueiredo is process optimization specialist, Andritz, Eunápolis, Brazil. Email Medeiros at carla.medeiros@veracel.com.br.



Medeiros



Silva



Pignaton



Zutautas



Figueiredo

How old are fibers in paper for recycling and what is their life expectancy? A contribution to the life cycle assessment of wood fiber-based products

GERT MEINL, LYDIA TEMPEL, MIKE SCHIEFER, AND CONSTANZE SEIDEMANN

ABSTRACT: Mean fiber age (i.e., the mean number of production cycles that fibers in a given paper material have undergone so far) can be calculated theoretically on the basis of mass flows in a given paper recycling loop. Mean fiber age distributions can be calculated in multiple, connected recycling loop systems, which are typical of countries and regions with high recovered paper utilization and recycling rates. The calculation uses a graph theory approach. The same approach shows there is a second important value that highlights another aspect of the circular economy – the number of future material uses. This value quantifies how often the fibers in a given paper product will be used on average till their end of life. Put simply, the fiber age describes the past and the number of future material uses describes the future of the fibers in a paper or board product. Calculated results for the European region are presented and compared for fiber age and number of future material uses. Both values add up to a total number of material uses and should be used together.

Application: Mills will have information for comparing resource efficiency of their wood fiber-based paper products with those of other mills and other sectors. This will help solve allocation problems in life cycle assessment.

Every fiber in a paper product has a past and a future. The past starts with the extraction of the fiber from wood and extends to the current paper product. During this period, the fiber could have been used in different paper products a varying number of times. The future is the time from the fiber's use in the current paper product until the end of its life. Again, a single fiber will be used multiple times in multiple paper or other fiber-based products. Both periods together form the lifespan of a fiber. It would be of fundamental importance for all stakeholders along the value chain to know how many times a fiber is used and if possible in which paper product.

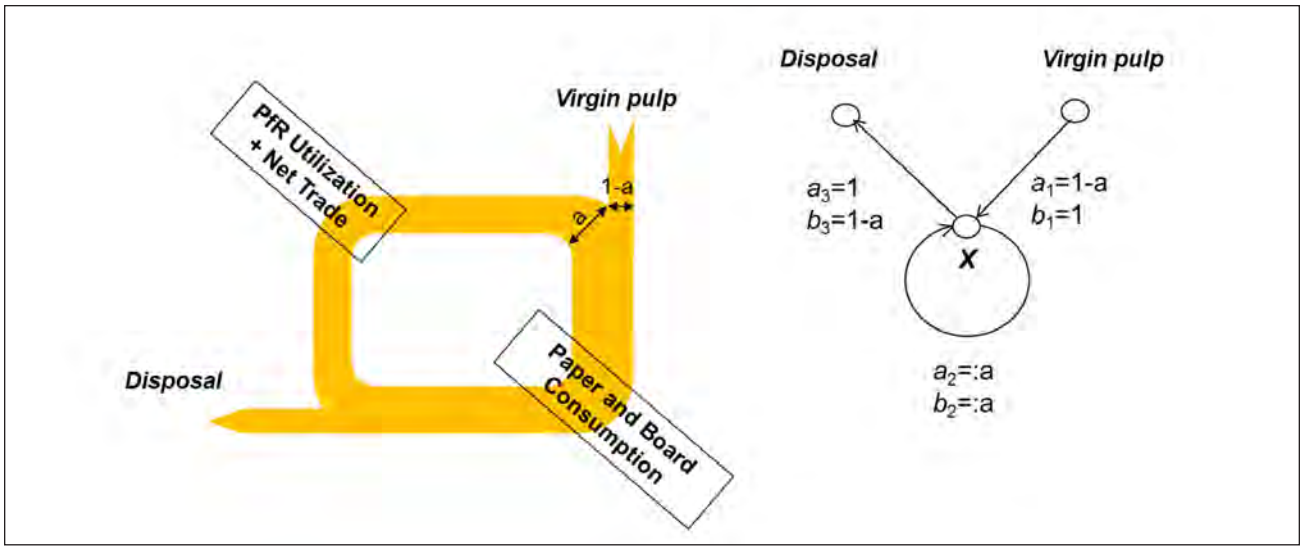
Unfortunately, no measuring procedure is available that provides an exact number in a direct way. An alternative approach is needed. In the 1990s, Hunold and Göttsching [1] started a detailed analysis of recycling systems and provided some useful formulas for calculating fiber age values. However, these calculations are incomplete because they only refer to the past life of the fibers. Nevertheless, their work was valuable because they provided the basic mathematical approach. Surprisingly, no substantial progress has been made since the work of Hunold and Göttsching [1] and Göttsching and others in the 1990s [2,3], and it seems that their work has been forgotten. The only exception is a paper published by Schabel and Putz in 2005 [4], who applied the approach to recent data to compare them with the predictions made by Hunold and Göttsching.

The recycling rates of paper are increasing in all countries, and it is becoming increasingly crucial to know the actual numbers of fiber uses and limits of recycling, at least for life cycle assessment (LCA). It is time to remember Hunold and Göttsching's work again.

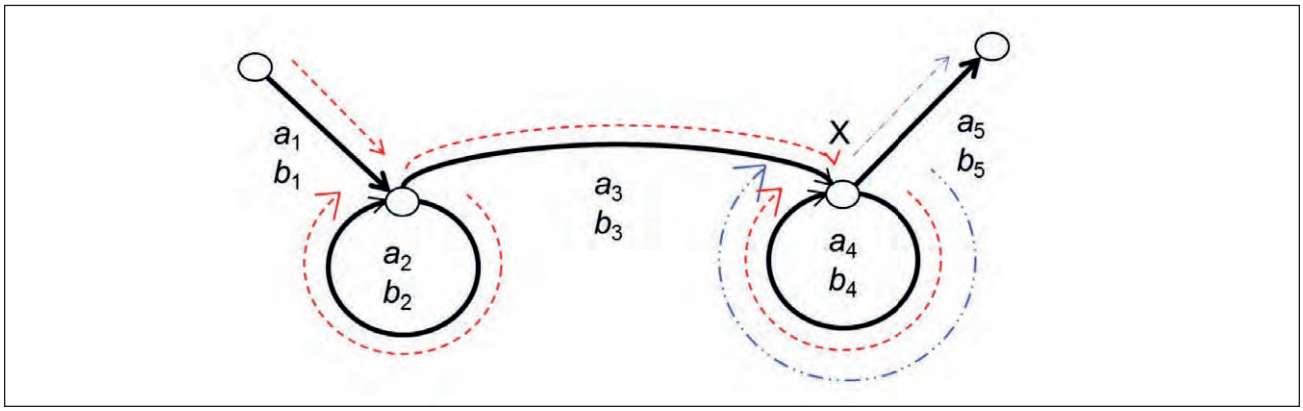
KEY PARAMETERS

For an individual fiber in a certain paper product, the first important parameter is the fiber age (*FA*). This is the number of repeated uses of a fiber from its beginning as a virgin fiber until its use in the current paper product. Accordingly, the *FA* of fibers in a graphic paper that is based totally on virgin fibers is 1. The second important parameter is the number of future uses (*NU*). This is the number of repeated uses of the fiber from now until the end of its life (e.g., incineration, landfill). The *NU* of fibers in a tissue paper is 1 if we assume that the tissue paper will not be recycled.

Obviously, the value *FA*+*NU*-1 is the total number of fiber uses during the lifespan of a fiber. This value should not be confused with the maximum number of fiber uses, (i.e. the number of uses as long as a sufficient bonding strength can be guaranteed). The latter value can be much higher than *FA*+*NU*-1.



1. One-parameter model as maximal simplification of a paper recycling system (left: Sankey diagram, right: oriented graph with entry weights a_i and exit weights b_i).



2. A network containing two inner nodes, one source, one sink, and five edges with entry weights a_i and exit weights b_i. All paths of the length FA=3 and ending at node X are marked with dashed lines. All paths of the length NU=3 and starting at node X are marked with a dotted line.

FA and *NU* of all fibers in a paper product or in an entire paper sector form a distribution. The mean value of the fiber age distribution is called mean fiber age (*MFA*), and the mean value of the distribution of the number of future uses is called mean number of future uses (*MNU*). The value *MFA*+*MNU*-1 is the mean total number of fiber uses that all fibers in a given paper product will experience during their lifetime. To calculate *MFA* and *MNU*, we need a mass balance of the fiber mass flow in the recycling system.

Fiber mass flow model

Figure 1 illustrates a fiber mass flow model. Sankey diagrams (left) are typically used to visualize mass flows. However, we represent the mass flow on a weighted and ordered graph referred to as network (right). Transferring data from a Sankey diagram to a network is simple. Every network consists of nodes (the paper grades or paper sectors), oriented edges (the mass flow directions) between the nodes, and a set of weights for every edge. The starting point and end point of an edge can be the same node, which is called an (oriented) loop.

Special nodes (the outer nodes) are those that have no precursor or no successor. These nodes are called source or sink and represent the extraction of fibers from wood or their final disposal (e.g., landfill, incineration). All other nodes (the inner nodes) represent the various paper products during the lifespan.

We want to consider recycling systems only under steady-state conditions; that is, all fiber masses entering the system equal the fiber masses exiting the system and the same yields at every node. Instead of using fiber mass as the weight of an edge, we introduce a pair of weights for every edge, named entry weight and exit weight. The entry weight is the ratio of the mass represented by the edge to the sum of all masses that enter the node where the edge is directed. The exit weight is the ratio of the mass represented by the edge to the sum of all

masses that exit the node where the edge comes from. Assuming steady-state conditions, the sum of the entry weights at all nodes equals 1 and the same yields for the exit weights at all nodes. Therefore, the entry nodes or the exit nodes can also be interpreted as the likelihood that a fiber in a given paper product has originated from another certain paper product or will be transferred to another certain paper product as a result of recycling.

Calculation of MFA *and* MNU

For an arbitrary inner node X, which represents a certain paper product, we want to calculate *MFA* and *MNU*. To denote the dependency on the node X, we write *MFA(X)* and *MNU(X)* further on. First, we need the portions G_{FA} and U_{NU} of fibers for a given *FA* value and for a given *NU* at node X. As far as *FA* is concerned, we have to find all paths of the length *FA* in the network starting from an arbitrary source and ending at the inner node X. An example of a network with two inner nodes is given in **Fig. 2**.

There are two different paths of the length *FA*=3 ending at node X in Fig. 2. The likelihood that a fiber will follow a certain path can be calculated by means of the entry weights and multiplication. Path 1 has a likelihood of $L_1 = a_1 \cdot a_2 \cdot a_3$ and path 2 a likelihood of $L_2 = a_1 \cdot a_3 \cdot a_4$. Portion G_3 of all fibers in the paper product X of *FA*= 3 is the sum of the likelihoods $G_3 = L_1 + L_2$.

In the same example, there is only one path of length *NU*=3 starting at node X and its likelihood is $L_3 = b_4 \cdot b_4 \cdot b_5$, which yields the portion $U_3 = L_3$.

Similarly, we have to calculate portions G_1, G_2, G_4, … as well as U_1, U_2, U_4, … . The mean values *MFA(X)* (Eq. [1]) and *MNU(X)* (Eq. [2]) finally equal:

$$MFA(X) = \sum_{FA=1}^{\infty} FA \cdot G_{FA} \qquad (1)$$

$$MNU(X) = \sum_{NU=1}^{\infty} NU \cdot U_{NU} \qquad (2)$$

A special infinite series can be applied to Eq. (1). If the portions G_i and U_i follow a geometric rule (i.e., $G_i = c \cdot d^{i-1}$ and $U_i = e \cdot f^{i-1}$ where c, d, e, and f are constants with $|d|<1$ and $|f|<1$), then the infinite series for the calculation of *MFA* and *MNU* is as follows:

$$MFA = c \sum_{i=1}^{\infty} i \cdot d^{i-1} = \frac{c}{(1-d)^2}$$
$$MNU = e \sum_{i=1}^{\infty} i \cdot f^{i-1} = \frac{e}{(1-f)^2} \qquad (3)$$

A proof of this series is provided by Taylor [5].

The more nodes a network has, the more complex the calculation of *MFA(X)* and *MNU(X)* becomes. Nevertheless, a recursive scheme can be applied to calculate the portions $G_{FA}(X)$ and $U_{NU}(X)$ for all nodes X and all numbers *FA* and *NU*:

1. Find all paths of length *FA*=1 or *NU*=1 for all nodes. Calculate the portions G_1 and U_1.
2. Assume that the portions $G_{FA\text{-}1}$ and $U_{NU\text{-}1}$ are known at all nodes. To calculate the portions G_{FA} and U_{NU} for a given node X:
   a. Find all precursor nodes to node X. We assume that these are the nodes $X_1,..,X_m$. Keep in mind that X itself might also be an element of the set $\{X_1,..,X_m\}$ if there is a loop at X. The corresponding entry weights of the edges connecting $\{X_1,..,X_m\}$ with X are $\{a_1,\ldots,a_m\}$.
   b. This yields $G_{FA}(X) = a_1 \cdot G_{FA\text{-}1}(X_1) + \ldots + a_m \cdot G_{FA\text{-}1}(X_m)$
   c. Find all successor nodes to node X. We assume that these are the nodes $Y_1,..,Y_m$. Keep in mind that X itself might also be an element of the set $\{Y_1,..,Y_m\}$ if there is a loop at X. The corresponding exit weights of the edges connecting X with $\{Y_1,..,Y_m\}$ are $\{b_1,\ldots,b_m\}$.
   d. The portion $U_{NU}(X) = b_1 \cdot U_{NU\text{-}1}(Y1) + \ldots + b_m \cdot U_{NU\text{-}1}(Y_m)$
3. Repeat step 2 to infinity

Per definition, *MFA(X)* and *MNU(X)* are calculated as an infinite row from *FA*=1 or *NA*=1 to infinity. In some special cases, it is possible to give a closed formula explicitly. In all other cases, we simply interrupt the calculation (i.e., the above recursion scheme) from a certain value of *FA* or *NU* onward. The deviation from the exact result is only minor if *FA* or *NU* values are high enough. In many recently calculated practical cases, the portions $G_{FA}(X)$ and $U_{NU}(X)$ at all nodes nearly vanished beginning with *FA*=*NU*=10 at the latest.

EXAMPLES

One-parameter model

The simplest fiber mass flow model of a recycling system is one that contains only one loop with one entry, one exit, and one inner node (Fig. 1). This model does not distinguish between different paper grades so we have only one paper grade (or paper in general) and only one inner node X. This type of model was also used by Hunold and Göttsching [1]. Because the model is fully described by only one parameter (the entry weight or exit weight a, which is also known as the recycling rate of the system), Hunold and Göttsching called it the one-parameter model. The proportions G_{FA} for each *FA* value at node X are:

$G_1 = 1\text{-}a$
$G_2 = a(1\text{-}a)$
…
$G_i = a^{i\text{-}1}(1\text{-}a)$

Applying the special infinite series, Eq. (3), to Eq. (1) yields:

$$MFA(X) = (1-a) \sum_{i=1}^{\infty} i \cdot a^{i-1} = \frac{1}{1-a}$$

The portions U_{NU} for each *NU* value at node *X* are:
U_1=1-*a*
U_2=*a*(1-*a*)
…
U_i=a^{i-1}(1-*a*)

The portions *Gi* and *Ui* are obviously the same, and it follows with Eq. (2) that:

$$MNU(X) = MFA(X) = \frac{1}{1-a}$$

In the one-parameter model the mean total number of fiber uses is:

$$MFA(X) + MNU(X) - 1 = \frac{1+a}{1-a}$$

Table I summarizes the *MFA*, *MNU*, and *MFA+MNU*-1 values of world regions on the basis of known recycling rates and a one-parameter model approach.

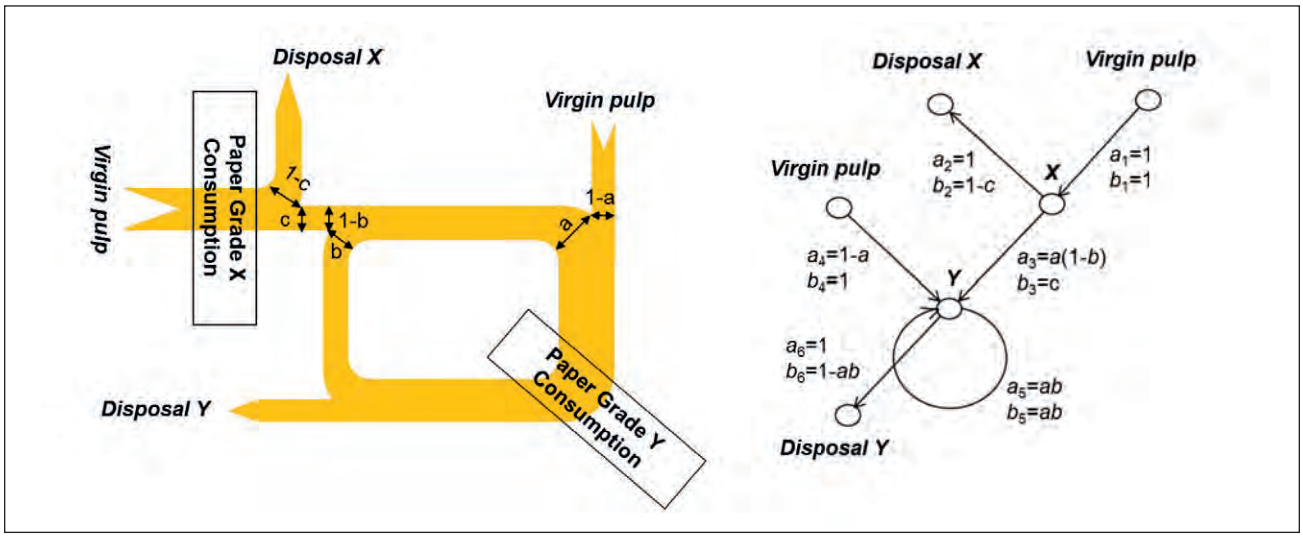
Two-parameter model

Hunold and Göttsching [1] then analyzed what has become known as the two-parameter model (**Fig. 3**) with two different paper grades *X* and *Y* (i.e., two inner nodes *X* and *Y*), two sources, two sinks, and one loop. As we can see, it is in fact a three-parameter model with the parameters *a* (utilization rate of paper for recycling for grade *Y*), *b* (share of grade *Y* in paper for recycling), and *c* (the recycling rate of paper grade *X*). But the researchers only focused on the fiber age distribution at node *Y*, on which the third parameter *c* has no influence. This type of model distinguishes between two different paper grades: a primary grade *X* that is based on virgin pulp and a secondary grade *Y* that uses partially recycled papers from both grades as the fiber source.

Using the portions G_{FA} and U_{NU} given in **Table II** for each node in the two-parameter model, *MFA* and *MNU* can be derived (**Table III**) according to Eqs. (1) and (2) by means of the infinite series (Eq. [3]). Obviously, *MFA* and *MNU* can be very different at the same node in the two-parameter model approach. Further on, the distributions of the *FA* and *NU* can vary from node to node (**Fig. 4**).

World Region	A	MFA=MNU	MFA+MNU-1
European Union + Norway and Switzerland	72.0%	3.6	6.1
Asia	52.8%	2.1	3.2
North America	64.3%	2.8	4.6
Latin America	4.1%	1.8	2.6
Africa	33.5%	1.5	2.0
World Total	**57.7%**	**2.4**	**3.7**

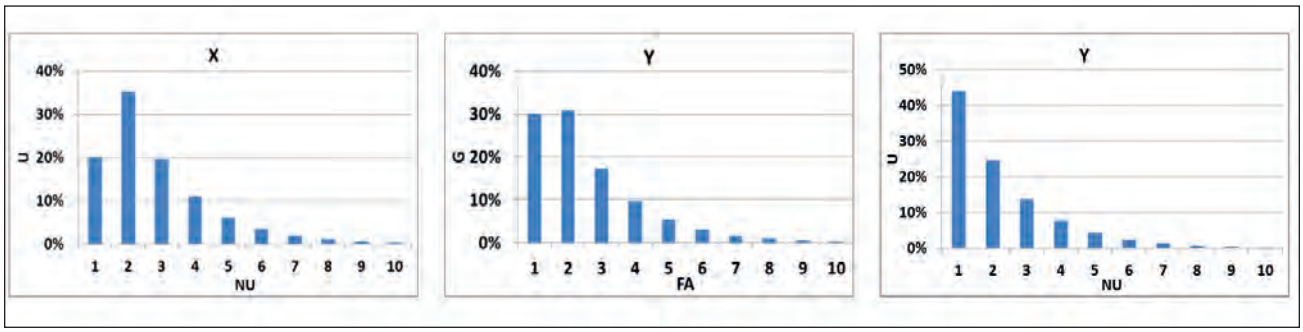
I. Recycling rate* A *(according to [6]), mean fiber age* (MFA), *mean number of future uses* (MNU), *and total number of uses* (MFA+MNU-1) *according to a one-parameter model for world regions.



3. Two-parameter model by Hunold and Göttsching (left: Sankey diagram, right: the same as an ordered and weighted graph).

	Node X	Node Y
Fiber age portions	$G_1 = 1$ $G_2 = 0$ ... $G_i = 0$	$G_1 = 1 - a$ $G_2 = a(1 - ab)$ ... $G_i = a^{i-1}b^{i-2}(1 - ab)$
Number of use portions	$U_1 = 1 - c$ $U_2 = c(1 - ab)$ $U_2 = c(1 - ab)ab$ ... $U_i = c(1 - ab)a^i b^i$	$U_1 = 1 - ab$ $U_2 = ab(1 - ab)$ ... $U_i = a^{i-1}b^{i-1}(1 - ab)$

II. Portions G_{FA} and U_{NU} at nodes X and Y in the two-parameter model.



4. Distributions of the number of future uses at node X (left), fiber age at node Y (center), and number of future uses at node Y (right) for a=0.7, b=0.8, and c=0.8.

	Node X	Node Y
MFA	$MFA(X) = 1$	$MFA(Y) = 1 + \frac{a}{1 - ab}$
MNU	$MNU(X) = 1 - c + \frac{c}{ab}\left(\frac{1}{1 - ab} - 1 + ab\right)$	$MNU(Y) = \frac{1}{1 - ab}$

III. MFA and MNU at the nodes X and Y of a two-parameter model.

Multiparameter model

Hunold and Göttsching [1] also provided fiber age distributions for more complex recycling systems. Another fiber flow model was the focus of the REFFIBRE project [7]. This model contains the following major paper grades produced in Europe and their recycling interactions: newsprint (*NP*); other graphic papers, including uncoated woodfree and mechanical coated papers (*OGP*); case materials for corrugated board manufacturing (*CM*); other paper and board for packaging, such as carton board, wrappings, and other (*OP*); sanitary and household (*SH*); and other paper and board for industrial and special purposes (*OPB*).

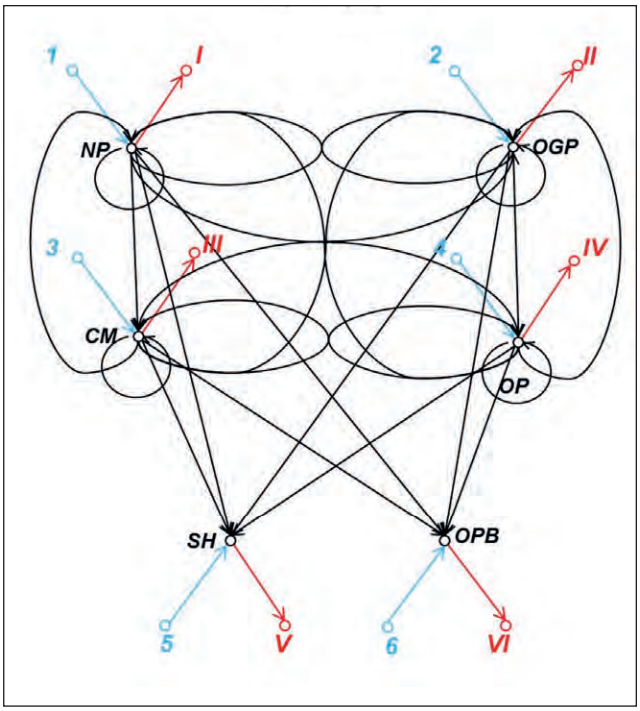
Paper products of the first four grades (*NP*, *OGP*, *CM*, and *OP*) were collected and recycled. Paper products of the two paper sectors (*SH* and *OPB*) are not yet recycled and are assumed to be unwanted paper components in paper for recycling.

Further details about the process of establishing the mass

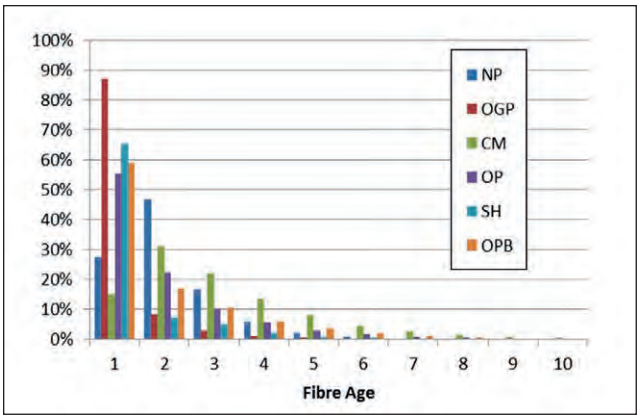
Nodes		Weights	
Start Node	End Node	Exit Weight	Entry Weight
NP	I	1.00	0.38
1	NP	0.27	1.00
NP	NP	0.26	0.26
NP	OGP	0.04	0.12
NP	CM	0.03	0.08
NP	OP	0.05	0.08
NP	SH	0.08	0.07
NP	OPB	0.03	0.01
OGP	II	1.00	0.47
2	OGP	0.87	1.00
OGP	NP	0.44	0.16
OGP	OGP	0.08	0.08
OGP	CM	0.12	0.12
OGP	OP	0.16	0.10
OGP	SH	0.04	0.07
OGP	OPB	0.09	0.01
CM	III	1.00	0.40
3	CM	0.15	1.00
CM	NP	0.00	0.00
CM	OGP	0.00	0.00
CM	CM	0.47	0.47
CM	OP	0.15	0.09
CM	SH	0.02	0.01
CM	OPB	0.20	0.03
OP	IV	1.00	0.46
4	OP	0.55	1.00
OP	NP	0.02	0.01
OP	OGP	0.01	0.01
OP	CM	0.23	0.39
OP	OP	0.09	0.09
OP	SH	0.02	0.01
OP	OPB	0.10	0.02
5	SH	0.65	1.00
SH	V	1.00	1.00
6	OPB	0.59	1.00
OPB	VI	1.00	1.00

NP=newsprint; OGP=other graphic papers, including uncoated woodfree and mechanical coated papers; CM=case materials for corrugated board manufacturing; OP=other paper and board for packaging, such as carton board, wrappings, and other; SH=sanitary and household; OPB=other paper and board for industrial and special purposes.

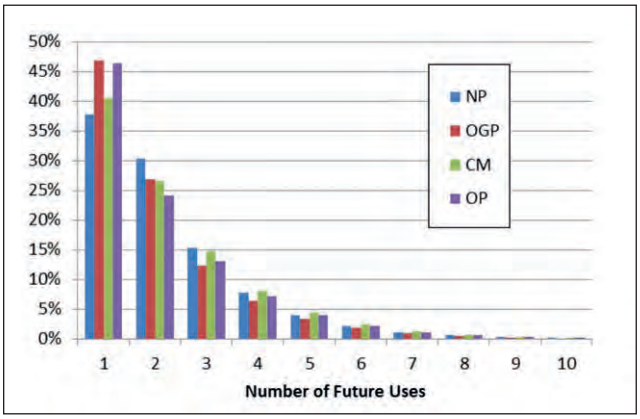
IV. Exit and entry weights of the fiber flow model.



5. Multiparameter model as oriented graph for the Confederation of European Paper Industries (CEPI) region. Arabic numerals represent the sources and Roman numerals the sinks.



6. Fiber age (FA) *distributions.*



7. Number of future uses (NU) *distributions.*

flow model are available in the public deliverables and workshop presentations from the REFIBRE project [7]. The corresponding oriented graph is shown in **Fig. 5**. The entry and exit weights for every edge resulting from the mass flow model are summarized in **Table IV**.

The nodes in **Fig. 5** representing the paper sectors *NP*, *OGP*, *CM*, and *OP* are obviously interconnected; that is, the network takes into account that (more or less) recycled paper products from all four paper sectors can be found in the raw materials used for production but also in the other sectors *SH* and *OPB*.

Applying the recursive procedure from to the network in Fig. 5 yields the distributions of *FA* and *NU* at all nodes (**Fig. 6** and **Fig. 7**). *MFA* and *MNU* are summarized in **Table V**.

Comparing the data in Table V with the data in Table I shows the difference when changing from an one-parameter approach to a more detailed multiparameter approach. But the differences between various paper grades are also remarkable. Not surprisingly, the total numbers of uses (*MFA*+*MNU*-1) for *NP* and *CM* are the highest in Europe. The utilization rates of paper for recycling are high for both paper grades, and collection systems are available for used paper products. For *OGP* or *OP*, the total number of uses is remarkably lower. Both

Paper Sector	MFA	MNU	MFA+MNU-1
NP	1.97	2.13	3.10
OGP	1.14	1.84	1.98
CM	2.98	2.25	4.23
OP	1.84	2.07	2.91
SH	1.24	1	1.24
OPB	1.86	1	1.86

NP=newsprint; OGP=other graphic papers, including uncoated woodfree and mechanical coated papers; CM=case materials for corrugated board manufacturing; OP=other paper and board for packaging, such as carton board, wrappings, and other; SH=sanitary and household; OPB=other paper and board for industrial and special purposes.

V.* MFA, MNU, *and* MFA+MNU-1 *according to the multiparameter model for the Confederation of European Paper Industries (CEPI) region in 2014.

paper grades use higher portions of virgin pulp and further, products of both grades are typically used over a longer period before being recycled. For *SH* and *OPB*, the *NU*=1 because no recycling is assumed for these paper grades.

To illustrate the meaning of *MFA* and *MNU*, a fiber in newsprint, for example, has a mean fiber age *MFA* of 1.97; that is, on average the fiber has been used 1.97 times from the beginning until its use in the current newsprint product. The *MNU* of the same fiber will be 2.13 times on average; that is, the fiber will be used 2.13 times from now until its end of life (including its use in the current newsprint product). The total number of uses is the sum of *MFA* and *MNU* minus one (because use in the current newsprint product is counted twice); that is, 3.10 on average. In other words, a fiber used at least once in newsprint has an average life span of 3.10 production cycles.

Within the scope of the REFFIBRE project, the *MFA* and *MNU* values from Table V were used to allocate the burdens to different production systems in LCA according to ISO 14041 "Environmental management—life cycle assessment—goal and scope definition and inventory analysis." Further details are available at the REFFIBRE website [7].

CONCLUSIONS

Fiber age and number of uses quantify the different phases within the lifetime of a fiber. Both characteristics are distributed within a paper product or a paper sector. The higher the recycling rates or utilization rates of paper for recycling, the higher the mean values *MFA* and *MNU* distributions are, which will finally lead to an increase in the mean total number of fiber uses (*MFA*+*MNU*-1).

The results for *MFA* and *MNU* depend on how many parameters are used to characterize a given recycling system or on the reliability of the parameters. Before using them for LCA purposes and comparison of different materials, a standardization process is necessary.

Even the complex network in Fig. 5 is only a simplification of reality. This network does not take into account the import or export of paper products and paper for recycling from or to other regions that have different recycling systems. For this purpose, the networks of individual regions have to be combined to form a global network. **TJ**

ACKNOWLEDGMENTS

This research received funding from the European Community's Seventh Framework Programme under grant agreement N° 604187.

LITERATURE CITED

1. Hunold, M. and Göttsching, L., *Papier (Bingen, Ger.)* 77(10A): 57(1993).
2. Göttsching L., Hamm U., Patzer E., et al., "Analysis of waste paper recycling and disposal options in Germany," Paper Cycle Report 15, Institut für Papierfabrikation, Technische Hochschule, Darmstadt, Germany, 1996.
3. Göttsching, L. and Pakarinen, H., *Recycled Fiber and Deinking, Papermaking Science and Technology* (Book 7), Fapet Oy, Helsinki, 2000, pp. 389-398.

ABOUT THE AUTHORS

This research was in response to a growing demand in life cycle assessment (LCA) for paper products to quantify the number of cycles a fiber was used or will be used. Previous research in this area was focused on the relationship between paper for recycling characteristics and the resulting paper properties. Because of the repeated use of fibers, their papermaking potential declines.


Meinl


Tempel


Schiefer


Seidemann

The most difficult aspect of this work was generating a valid mass balance for fiber flow. During the research, we had the cooperation of the Confederation of European Paper Industries (CEPI) in getting the necessary figures. We discovered that it is possible to combine LCA with established mathematical models.

An interesting finding was that fiber age and number of uses for individual paper sectors are far below 6, which is assumed to be the maximum number of possible uses of a fiber. The information will support the mills in comparing their paper products with products of other mills and other sectors in terms of resource efficiency.

Until now, research in this area was done on a regional level (Europe). In the next step, the shipment relationships between world regions (Europe, Canada and the United States, East Asia, and Russia) will be taken into account. More complex mass balances are necessary.

Meinl, Tempel, Schiefer, and Seidemann are scientists at Papiertechnische Stiftung, Munich, Germany. Email Meinl at gert.meinl@ptspaper.de.

4. Schabel, S. and Putz, H., *Wochenbl. Papierfabr.* 133(3–4): 103(2005).

5. Taylor, A.E., *Advanced Calculus*, Blaisdell, Boston, 1955, p. 603.

6. CEPI, K*ey Statistics 2014: European Pulp and Paper Industry*. Confederation of European Paper Industries, Brussels. 2015. Available [Online] http://www.cepi.org/system/files/public/documents/publications/statistics/2015/Key%20Statistics%202014%20FINAL.pdf <12July2017>.

7. Meinl, G., Tempel, L., Ringman, J., et al., "D1.4 European Fibre Flow Model," REFIBRE Project, http://reffibre.eu/, 15 December 2016. Available [Online] http://reffibre.eu/publications/european-fibre-flow-model.pdf/@@download/file/European%20fibre%20flow%20model.pdf <14July2017>.

Evaluation of the particle size of organosolv lignin in the synthesis of resol resins for plywood and their performance on fire spreading

ELECTRA PAPADOPOULOU, SOTIRIS KOUNTOURAS, KONSTANTINOS CHRISSAFIS, MIKELIS KIRPLUKS, UGIS CABULIS, PAVLA ŠVÍGLEROVÁ, AND BOUCHRA BENJELLOUN-MLAYAH

ABSTRACT: Scientists today are intensively seeking alternatives to petrochemical materials. Among others, lignin is a promising candidate because it is available in large quantities while its chemical structure makes its use possible in a variety of chemical reactions. Lignin, received by numerous methods from various feedstocks, is a promising material for the synthesis of many products like active carbon, thermosetting and thermoplastic polymers, surfactants, phenolic chemicals, etc.

In this paper, the potential of using Biolignin – a trademarked organosolv lignin from straw prepared by Compagnie Industrielle de la Matière Végétale (CIMV; Neuilly-sur-Seine, France) – in the synthesis of phenol-formaldehyde (PF) resins was studied by CHIMAR HELLAS S.A. (Kalamaria, Greece). Before its use, Biolignin was further purified and subjected to mechanical treatment for the reduction of its particle size in order to increase its reactivity. The effectiveness of the treatment was verified by atomic force microscopy (AFM) measurements that were carried out by SYNPO Company (Pardubice, Czech Republic). Resol phenolic resins were prepared with various substitution levels of phenol up to 80%. However, their synthesis process was smooth only up to the substitution level of 50%. The properties of the resins were determined with typical lab analysis. Their thermal behavior was studied with differential scanning calorimetry (DSC) and thermogravimetric analysis (TGA) measurements that were conducted by the Aristotle University of Thessaloniki in Greece. Their bonding ability was evaluated by CHIMAR HELLAS via their application in the production of plywood panels of three layers that were prepared following a simulation of the industrial process. The panels were tested for their properties according to the relevant European standards, while their performance relative to fire was studied with cone calorimetry measurements that were performed by the Latvian State Institute of Wood Chemistry (LIWC; Riga, Latvia).

All results were compared with that of a typical PF resin. It was found that the particle size of lignin affects the performance of the resins, while lignin-based PF resins are suitable for the production of plywood panels and have somewhat better performance relative to fire than typical PF resins. This study has been performed within the framework of the European project BIOCORE (biocommodity refinery for biofuels, chemical intermediates, polymers and materials).

Application: This study informs readers that the performance of organosolv lignin in the synthesis of PF resins may be improved with adjustments to its particle size. Lignin-based PF resins render to plywood panels better performance to fire.

Lignin is an amorphous, heterogeneous phenolic polymer found in all vascular plants (trees, plants and agricultural crops), mostly between the cells, but also within the cells, and in the cell walls. It is covalently linked to the polysaccharides and contains several functional chemical groups, such as hydroxyl (phenolic or alcoholic), methoxyl, carbonyl and carboxyl groups, in various amounts, depending on the origin of the material and the separation process applied [1].

Lignin has attracted the interest of scientists and business because it is derived from abundant, renewable sources while it is non-toxic and versatile in performance due to its complex nature and highly functional character. Among the top players in the industry involved in lignin business are Borregaard LignoTech, Sappi, MeadWestvaco, Tembec, Domtar, UPM, Asian Lignin Manufacturing, Northway Lignin Chemical, Green Value, etc. Until today, lignin has been used as raw material for the synthesis of various bio-based products like carbon fibers, cosmetics, foams, dust control systems, batteries, thermosetting and thermoplastic binders, polyolefin-based products, concrete admixtures (as rheology modifier), etc. [2,3].

Especially in the case of phenol–formaldehyde (PF) binders, lignin has been extensively studied as a phenol substitute. However, the phenol substitution levels are usually low. The

reason is that the various lignin types have very large and non-uniform molecular weights (Mw) that affect both the average molecular weight and the polydispersity of the resins, resulting in products with low performance in the various applications [4,5]. Scientists have confronted this by applying various treatments to lignin either before its use or during the formation of the lignin-based products. These methods include fragmentation (pyrolysis, oxidation by chemicals and enzymes), functionalization of its hydroxyl groups (esterification, etherification, phenolation, urethanization), synthesis of new chemical active sites (alkylation/de-alkylation, hydroxyalkylation, amination, nitration) [6] or even employing novel methods to separate lignin, like acid hydrolysis or organosolv process, etc. [3]. However, most of these treatments and processes are quite expensive and thus economically unprofitable for use in industrial scale production.

A more economical processing of materials, well known in the industry, that could also be applied in the case of lignin is mechanical treatment by various methods, like ball milling, which facilitates the reduction of particle size. Generally, the mechanical treatment of raw materials offers easy handling, increase in surface area per unit volume, and separation of entrapped components, while the mechano-chemical reaction, which is induced by the input of mechanical energy by grinding in ball mills, allows reactions to occur under simplified and solvent-free conditions at room temperature. The notion of structural change of lignin in the ball milling process can be traced back to the 1920s, but the majority of the related studies are focused on the particle size reduction of milled wood or the synthesis of new products by treating lignin and other chemicals together.

Ikeda et al. [7] studied the structures of milled wood lignin (MWL), cellulolytic enzyme lignin (CEL), and residual lignin (REL) from a loblolly pine, using a modified derivatization followed by reductive cleavage (DFRC) method developed to allow the quantitative determination of three different structural monomeric products originating in lignin: phenolic beta-O-4, alpha-O-4, and etherified beta-O-4 structures. Their study showed that dry vibratory ball milling under a nitrogen atmosphere causes substantial structural changes, including condensation, whereas vibratory ball milling in toluene had little effect on the lignin structure.

Kleine et al. [8] studied a base-assisted ball milling treatment of lignin model compounds and demonstrated that a cleavage process takes place that predominantly involves the breaking of β-O-4 linkages.

Vlček [9], in the patent WO2014/044234A1, discloses the reduction of particle size of lignin powder to nanometers and micrometers in a dispersion device-like ball milling. The resulting lignin is suitable to be dispersed without the use of solvents in a pre-polymer terminated by reactive isocyanate groups upon preparation of single–component polyurethane materials. This method gives a solution to the problem of the insolubility of lignin in polyols that prevents the reaction of OH^- groups of lignin with isocyanate leading to the formation of a polymer network.

Qu et al. [10] applied wet ball milling (WBM) and ionic liquid pretreatment to industrial lignin samples and evaluated their effect on the average molecular weight and polydispersity, surface morphology, and functional groups changes. The results showed that lignin pretreated by WBM with phosphoric acid presented a dramatic decrease of polydipersity (23%) and an increase of phenolic hydroxyl content (9%).

Kandula et al. [11] treated kraft lignin with ball milling and poly-esterified it with ε-caprolactone, in order to create hydroxyl groups that are more easily available to further reactions. The resulted copolymer was still soluble in several organic solvents and suitable for use in various chemical reactions like, for example, in the synthesis of polyurethane.

Guo et al. [12] prepared oleated organosolv lignin (OL) by transesterification between OL and methyl oleate. The oleation reaction was conducted effectively in a ball milling process. The oleated OL displayed improved thermoplasticity, while when blended with PLA, it exhibited improved dispersion, suggesting increased compatibility.

In the current study, organosolv lignin of various particle sizes that resulted from the application of mechanical treatment was evaluated as a substitute for phenol in the synthesis of PF resins for the production of wood-based panels. The effect of the ball milling was verified by observation with atomic force microscopy (AFM), while the resins were studied for their properties with lab analysis, differential scanning calorimetry (DSC), and thermogravimetric analysis (TGA). Their adhesive ability was evaluated via their application in the production of lab scale plywood panels that were tested for their mechanical and wet properties according to the European Union (EU) standards in force. Moreover, the performance of the resins to the spread of fire was evaluated via cone calorimetry tests of the plywood panels prepared with these resins. All results were compared with that of a typical PF resin.

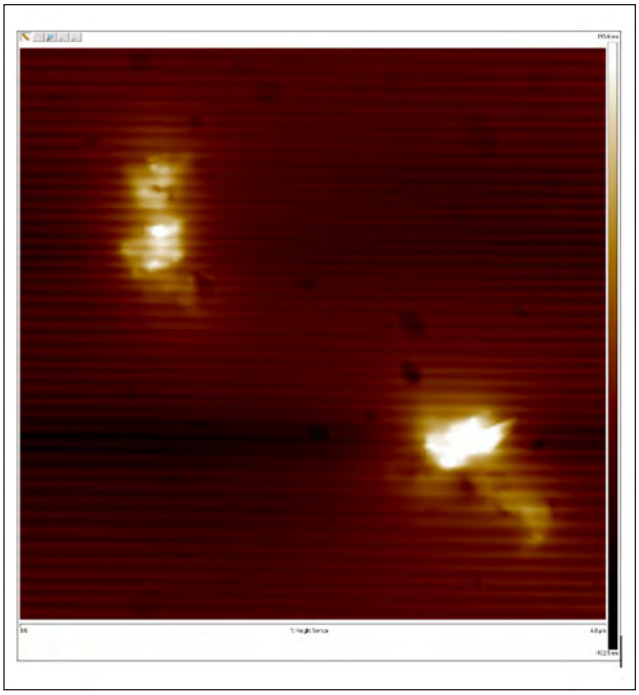
EXPERIMENTAL

Raw materials

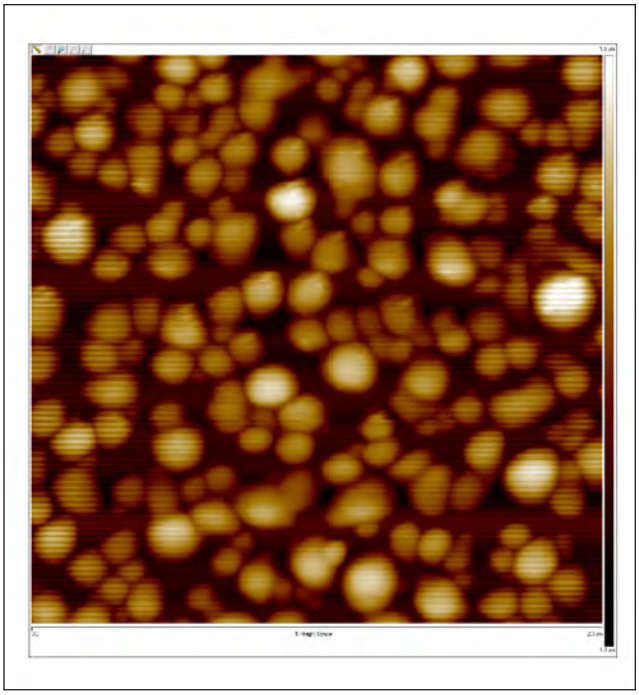
Thermosetting polymers of PF type were prepared using the following raw materials of technical grade in the form of water-based solutions: phenol 90% w/w, formaldehyde 37%w/w, and sodium hydroxide (NaOH) 50% w/w. Experimental resins were prepared by replacing phenol with organosolv lignin from straw provided by Compagnie Industrielle de la Matière Végétale (CIMV; Neuilly-sur-Seine, France) in the form of powder under the trademarked name Biolignin (45%w/w DM).

Lignin treatment

Biolignin, as initially provided by CIMV, was inefficient in the synthesis of resins, and CHIMAR HELLAS S.A. (Kalamaria, Greece) subjected it to treatment in order to increase its reactivity. This treatment consisted of a purification step followed by a particle size reduction step. In this study, this treatment will be named "CH-treatment". The purification step was applied in order to remove any acids and water soluble residues contained in Biolignin that may reduce its performance in the



1. Atomic force microscopy (AFM) image of untreated Biolignin from CIMV. Scan 4 µm and 2.3 µm, map of topology. There are agglomerates with diameter approximately up to 1 µm and height up to about 1 µm.



2. AFM image of CH-treated Biolignin. Scan 2.3 µm, map of topology. There are particles with diameter approximately up to 200nm. This sample is nicely dispersed.

polymerization reactions taking place during the synthesis of the PF type resins. The particle size reduction step was applied in order to make its reactive groups more readily accessible during the chemical reactions and thereby increase its activity. For the implementation of the CH-treatment, a quantity of lignin was initially immersed into tap water bath at room temperature (20°C–25°C) for 1 h, under slight stirring. Next, the water was removed by application of filtering using a Büchner funnel (purification step). The water extract was found to be of acidic pH (2–3) that verified the removal of acidic components. The resulting material was oven dried for about 20 h at 70°, and then it was ground in ball milling (particle size reduction step) in order to increase its surface area per unit volume and make more chemical units available for further reactions. In this study, Biolignin resulting from the previously described CH-treatment will be named "CH-treated" Biolignin.

SYNPO Company (Pardubice, Czech Republic), a partner of the BIOCORE project, carried out AFM measurements on treated and untreated Biolignin samples in order to evaluate the result of the ball milling process. The measuring unit was a Fritsch Laser Particle Sizer (Analysette 22, Fritsch GmbH; Idar-Oberstein, Germany). The samples were diluted in EtOH. CH-treated Biolignin was diluted without problem, but this was not the case for the untreated sample. The untreated Biolignin formed agglomerates with diameter approximately up to 1 µm and length of about 1 µm (**Fig. 1**). Such agglomerations were too big to be seen by AFM. On the contrary, the CH-treated Biolignin had particles with diameter approximately up to 200 nm and was nicely dispersed (**Fig. 2**).

Untreated Bioliognin, CH-treated Biolignin, as well as Biolignin, were subjected to some mechanical treatment from CIMV in order to receive material of two different average particle sizes (<500 µm and <10 µm), which were studied in the synthesis of PF resins.

Synthesis and analysis of resins

Initially, CHIMAR tried to use untreated Biolignin in the synthesis of a PF type resin. However, the sample performed insufficient dispersion into the resin mixture, which created problems during the manufacturing of plywood panels with the viscosity measurements during the synthesis of the resin and later on with the application of the glue mixture onto the wood veneers. CHIMAR proceeded to use a lignin that consisted of washing and lab-scale ball milling of lignin, as described previously (CH-treatment). This treatment was found to improve its performance, since the resulting material was now successfully incorporated into the resin mixture.

Although PF resins with phenol replacement level up to 80%w/w by CH-treated Biolignin were synthesized, the higher the substitution level the more irregular was the synthesis process. Therefore, only the resin with 50% phenol substitution was selected for a more thorough study because it had the highest phenol replacement level with the smoothest synthesis process. Together, CIMV provided CHIMAR with two Biolignin samples of different particle sizes prepared at pilot scale on CIMV premises. These samples were also used

Properties	PF Resin	Experimental Resins
Water content, %	53–55	53–55
Viscosity, %	250–500	250–500
pH @25°C	10.0–13.0	10.0–13.0
Gel time at 130°C, s	180–350	60–250
Alkalinity, %	7.1–7.7	6.0–8.0
Water tolerance, ml/ml	>1/10	>1/10
Conductivity, mS/cm	~20	~20
Free formaldehyde, %	<0.5	<0.5

I. Properties of the resins (PF = phenol–formaldehyde).

in the synthesis of PF resins with 50%w/w phenol substitution in order to evaluate their performance in comparison with the CH-treated Biolignin. A typical PF resin was also included in the tests.

All resins were subjected to typical lab analysis for the determination of their physicochemical properties, like water content, viscosity, pH, alkalinity, conductivity, water tolerance, gel time and free formaldehyde (**Table I**).

The thermal properties of the resins were determined with DSC and TGA measurements (Figs. **3a**, **3b** and **3c**). The TGA measurements were carried out with a SETSYS 16/18 TGA-DTG device (Setaram; Caluire-et-Cuire, France). The samples (6.0 ± 0.2mg of liquid resin) were placed in aluminum crucibles while an empty alumina crucible was used as reference. The samples were heated from ambient temperature to 1000°C in flow of air (in order to have an environment representative of the real conditions that resins are used), with a heating step 20°C/min.

The DSC measurements were carried out with a Setaram DSC141 calorimeter. The samples (6.0 mg ± 0.2mg of liquid resin) were placed in stainless steel sealed crucibles while an identical empty crucible was used as reference in each measurement. The samples were heated from ambient temperature (25°C) to 250°C in a 50 ml/min flow of nitrogen gas (N_2), with a heating rate of 10°C/min.

Production of plywood panels

The adhesive ability of the resins was evaluated via their application in the production of plywood panels. The panels were prepared at lab scale following a simulation of the industrial practice. Panels of 3 layers were produced using a veneer of poplar wood for the core and veneers from okume for the two face layers (okume/poplar/okume). Their testing and classification was carried out according to the following European standards:

- EN 314-1:2004 "Plywood – Bonding quality – Part 1: Test methods"
- EN 314-2:1993 "Plywood – Bonding quality – Part 2: Requirements"

Although these standards are valid for industrial production, they also give a good indication of the performance of lab scale panels.

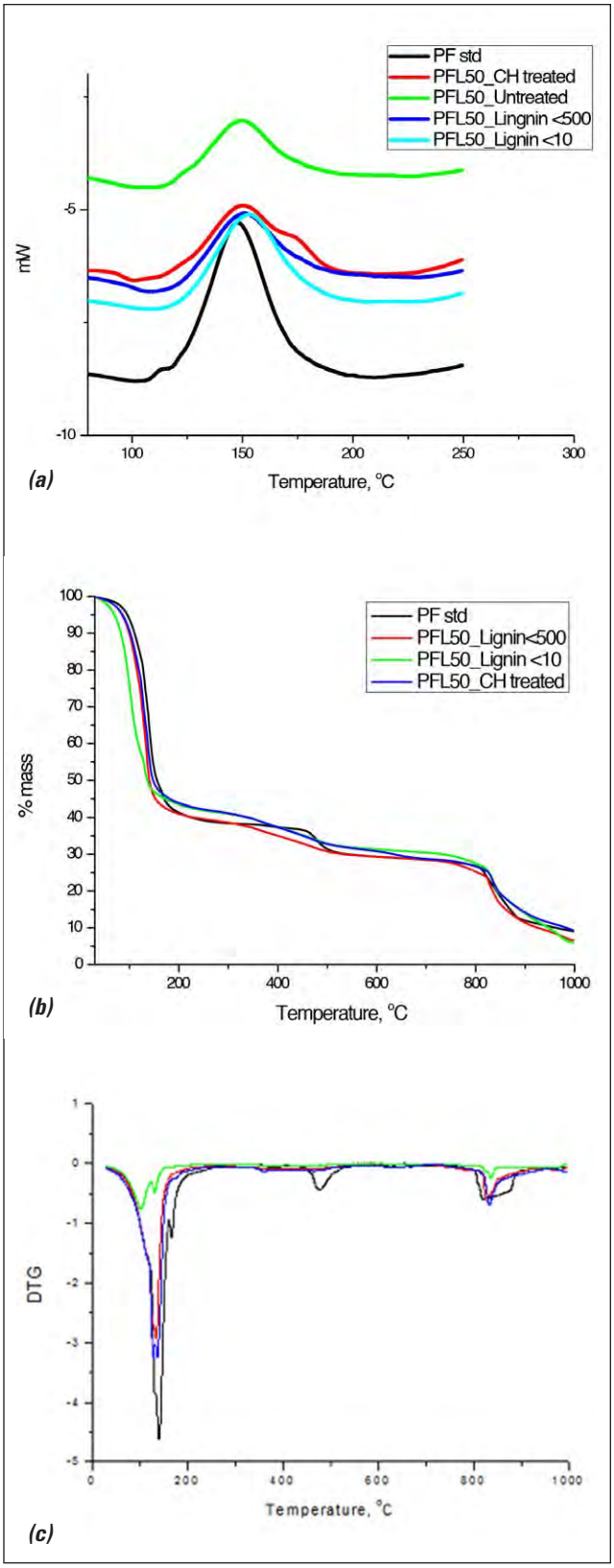
The standard EN 314-1:2004 describes the methods for the testing of the plywood panels, while the standard EN314-2:1993 categorizes the plywood panels and sets threshold values for their mechanical and wood failure performance. In particular, the standard EN314-2:1993 specifies requirements for bonding classes of veneer plywood according to their end use. The designated categories are:

- Class 1 - Dry Conditions: interior applications with no risk of wetting (12% or less moisture content, at 20°C and 65% relative humidity).
- Class 2 - Humid Conditions: protected exterior conditions (20% or less moisture content, at 20°C and 85% relative humidity).
- Class 3 - Exterior Conditions: unprotected exterior conditions (above 20% moisture content).

For all bonding classes, each glue line must satisfy two criteria: the values of mean shear strength and mean apparent cohesive wood failure must have the correlation described in **Table II**. The previously mentioned threshold values stand for any class of plywood panels, but according to their intended application, the panels are subjected to different pretreatments before their testing (EN314-1:2004).

The formaldehyde emissions were determined with the desiccator method (ISO 12460-4 "Wood-based panels – Determination of formaldehyde release – Part 4: Desiccator method"). Moreover, samples of all plywood panels were subjected to cone calorimetric flammability testing according to the ISO/TR 5660-3:2003 Standard "Reaction-to-fire tests – Heat release, smoke production and mass loss rate – Part 3: Guidance on measurement," which was performed by another partner of the BIOCORE project, the Latvian State Institute of Wood Chemistry (LIWC).

The parameters of the measurement are cited in **Table III**. Samples of the panels were measured for their heat release rate (HRR) and smoke production rate (SPR). The results are presented in **Figs. 4** and **5**.



3. a) Differential scanning calorimetry (DSC) graph of resins, b) thermogravimetric analysis (TGA) graph of resins, and c) differential thermal analysis (DTA) graph of resins (PF = phenol–formaldehyde).

Mean Shear Strength fv, N/mm²	Mean Apparent Cohesive Wood Failure w, %
0.2 ≤ fv < 0.4	≥ 80
0.4 ≤ fv < 0.6	≥ 60
0.6 ≤ fv < 1.0	≥ 40
1.0 ≤ fv	No requirement

II. Standard bonding performance requirements for European Standard EN 314-2:1993.

Heat flux	35 kW/m²
Test time	2 min
Ignition source	Electrical spark
Sample dimensions	10 cm x 10 cm x ~ 0.5-0.6 cm
Orientation	Horizontal

III. Parameters of the cone calorimetry measurements.

RESULTS AND DISCUSSION

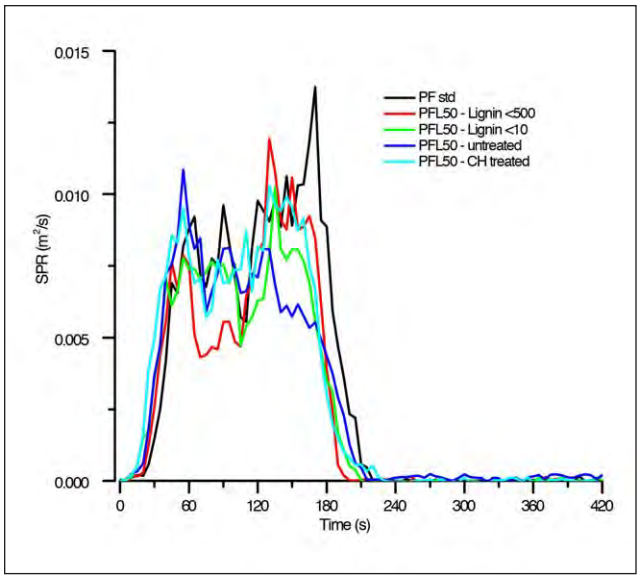
Characterization of resins

The physicochemical properties of the resins are cited in **Table I**.

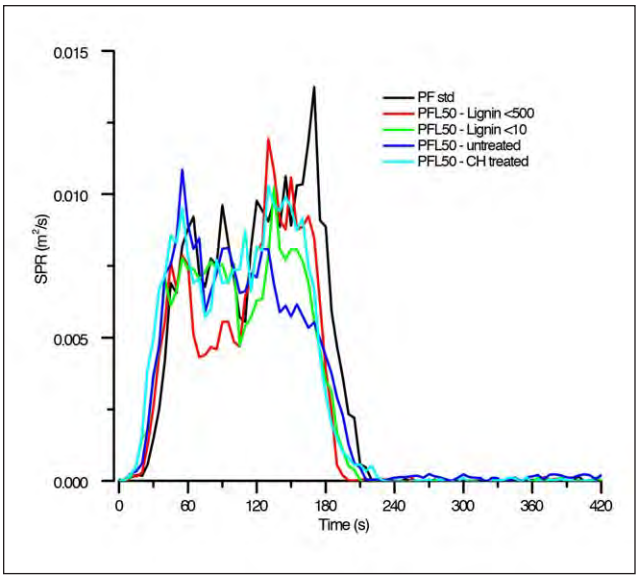
The lab analysis results show that the experimental resins have properties that fall within the limits of a typical PF resin and thus may be used in the production of wood-based panels. Furthermore, it is worth noting that the lignin-based resins have shorter gel time and thus develop their crosslinking network and set faster than typical PF resins.

The TGA measurements of the resins reveal their performance during thermal degradation. As the temperature increases, the resins lose mass at various steps. The first step from room temperature up to about 200°C is due to the loss of water and small molecules like free formaldehyde as well as further crosslinking and loss of byproducts [13]. After 200°C, the thermal degradation of the polymer starts. Until about 450°C, the control resin seems to be the most stable one, while the lignin based resins lose mass at a faster rate. At this region of temperatures, the pyrolytic degradation of polymers takes place while inter-unit linkages break down and release small chemical moieties, like monomeric phenol, for example, into the vapor phase. After about 450°C, the decomposition of aromatic rings takes place [14]. The resin with the CH-treated lignin leaves the highest percentage of ash at the end of the heating, up to 1000°C. According to literature references, the high ash content prevents the spread of fire.

The DSC thermographs show that all resins perform an exothermic phenomenon at around 150°C and thus it can be said that they have similar curing performance. However, in the case of lignin-based resins, the exothermic peak is shifted somehow to higher temperatures, which is in accordance



4. Smoke production rate (SPR).



5. Heat release rate (HRR).

with literature references [15]. The peak temperature of the resin prepared with CH-treated Biolignin is the closest to the control resin (**Table IV**).

The results of the bonding quality tests of the plywood panels are presented in **Table V**. All lignin-based resins have performance slightly lower than the control. Among the experimental resins, the one with lignin of particle size <500 µm as well as the CH-treated sample are the best performed after the severest pre-treatment (5.1.3) and meet the requirements of the standard EN314-2:1993 (Table I) for use in exterior applications. Between these two resins, the one prepared with the CH-treated Biolignin gave panels with significantly lower formaldehyde emissions.

The results of the cone calorimetry measurements of the plywood panels (**Figs. 4** and **5**) show that the control PF resin gives somewhat more smoke than the lignin-based resins, no matter the particle size of the lignin. Furthermore, the typical PF resin is burned more vigorously and emits more heat during the burning process. The three peaks of each plywood sample on the HRR test (Fig. 5) are attributed to their delamination during the burning process. When the layer of plywood is delaminated, a larger surface of the sample is exposed to flame, and hence more heat is released. The peak heat release rate was 268.6 kW/m² for the typical PF resin and 233.8–228.5 kW/m² for the lignin-based resins. All samples were burned for about 420 s until the material was fully charred. The cone calorimeter shows the kinetics of a material when it is burned under constant heat flux, and in the case of the typical PF resin, they were comparably faster. When materials burn at a slower rate, there is more time to put out a fire or evacuate people from a burning building. Among the experimental resins, there are no big differences, although it seems that the lower the particle size, the better the performance of the resin (lower HRR and SPR values). These findings are in accordance with other literature references where it is noted that lignin contributes to a material's resistance to the spread of fire due to a high charring ability and a low heat release when burning [16].

All the previous findings show that CH-treated Biolignin has advanced performance compared to the other lignin sam-

Resins	Onset Temperature, °C	Peak Temperature, °C	Endset Temperature, °C
PF std	105.753	146.457	202.253
PFL50-Lignin<500	110.671	150.109	190.004
PFL50-Lignin<10	113.138	152.607	205.019
PFL50-untreated	114.369	150.880	197.205
PFL50-CH treated	102.474	150.172	199.766

IV. Differential scanning calorimetry (DSC) characteristic temperatures for resins.

Resin	PF std	PFL50	PFL50	PFL50	PFL50
Biolignin particle size	-	<500μm	<10μm	untreated	CH treated
EN 314-1:2004 Tests					
Pre-treatment 5.1.1:	*Immersion in water at 20°C for 24 h*				
Shear strength, N/mm²	1.28	1.17	0.75	0.84	0.98
Wood failure, %	85	40	25	25	70
Pre-treatment 5.1.3:	*4 h boiling – 16 h drying at 60°C – 4 h in boiling water – 1 h in cool water*				
Shear strength, N/mm²	1.13	0.81	0.57	0.60	0.78
Wood failure, %	75	45	35	30	60
Formaldehyde emissions/ Desiccator values, mg/L	0.083	0.114	0.061	0.041	0.044

V. Bonding quality test results of plywood panels produced with Biolignin from CIMV.

ples tested in this study and verify the consideration that reduction of lignin particle size by the ball milling process (CH-treated Biolignin) can increase its reactivity. The CH-treated Biolignin not only made possible synthesis of the resin, contrary to the untreated sample, but the resin prepared from it also had the closest curing temperature to the control resin (DSC results) and gave acceptable mechanical properties and the lowest free formaldehyde emissions when applied to the production of plywood panels of all samples tested. It can be justified by the fact that the ball milling treatment enables more reactive sites on lignin to become available for reaction with formaldehyde, resulting in the creation of more cross-links between lignin and formaldehyde and thus faster curing and lower free formaldehyde emissions. Based on cone calorimeter results, plywood panels with lignin-based resins burn at a slower rate than that prepared with a typical PF resin. Also, according to the TGA results, the resin prepared with the CH-treated Biolignin gave the highest percentage of ash, signifying that this resin has the highest ability to prevent spreading of fire compared to all other lignin samples studied.

CONCLUSIONS

The results show that organosolv Biolignin from the CIMV process may be used in the synthesis of PF resins as phenol substitute. The treatment applied by CHIMAR (CH-treatment) improved its performance and resulted in resins with a clear advantage over the other experimental resins of this study. Such resins are suitable for the manufacturing of plywood panels and offer slightly improved performance to the spread of fire compared with a typical PF resin. However, in order to establish the CH-treatment as a general method for lignin improvement, more thorough studies are needed for determination of the optimum limits of the particle size of each type of lignin and its application. **TJ**

ACKNOWLEDGEMENTS

This work was carried out within the EU FP7 project BIOCORE (Biocomodity refinery), that was supported by the European Commission through the Seventh Framework Programme for Research and Technical development under contract no FP7-241566 (01/09/2009 - 30/09/2013).

LITERATURE CITED

1. Gosselink, R.J.A., Snijder, M.H.B., Kranenbarg, A., et. al., *Ind. Crops Prod.* 20: 191(2004).
2. Agrawal, A., Kaushik N., Biswas, S., *The Scitech J.* 1(7): 30(2014).
3. Derek, S., *Ind. Crops Prod.* 27(2): 202(2008).
4. Turunen, M., Alvila, L., Pakkanen, T.T., et. al., *J. Appl. Polym. Sci.* 88: 582(2003).
5. Wang, M., Leitch, M., Xu, C., *Eur. Polym. J.* 45(12): 3380(2009).
6. Laurichesse, S. and Avérous, L., *Prog. Polym. Sci.* 39: 1266(2014).
7. Ikeda, T., Holtman, K., Kadla, F.J., et. al., *J. Agric. Food Chem.* 50(1): 129(2002).
8. Kleine, T., Buendia J., Bolm, C., *Green Chem.* 15(1): 160(2013).
9. Vlček, T., WO pat. 2014/044234A1 (Mar. 27, 2014).
10. Qu, Y., Luo, H., Li, H., et. al., *Biotechnol. Rep.* 6: 1(2015).
11. Kandula, M., Schwenke, T., Friebel, S., et. al., *Holzforschung* 69(3): 297(2014).
12. Guo, X., Junna, X., Wolcott, P.M., et.al., *ChemistrySelect* 1: 3449(2016).
13. Chao, C.T., Sarmah, K.S., Burns, T.G., et. al., "Flammability studies of silicone and phenolic resins and their composite laminates," *International Fire and Cabin Safety Research Conference*, Federal Aviation Administration Fire Safety, Atlantic City International Airport, NJ, USA, 1998, p.16.
14. Mansouri, N.E.E., Yuan, Q., Huang, F., *BioResources* 6(3): 2647(2011).
15. Sarkar, S. and Adhikari, B., *J. Adhes. Sci. Technol.* 14(9): 1179(2000).
16. Ferry, L., Dorez, G. Taguet, A., et. al., *Polym. Degrad. Stab.* 113: 135(2015).

ABOUT THE AUTHORS



Papadopoulou



Kountouras



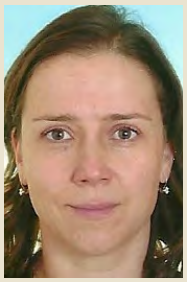
Chrissafis



Kirpluks



Cabulis



Švíglerová



Benjelloun-Mlayah

We chose this research topic because it was the subject of a European Union (EU) project where co-author Papadopoulou was the principal investigator on behalf of the company CHIMAR HELLAS S.A. In our study, a special treatment of lignin was developed that enabled this material's use in the synthesis of resins for wood-based panels. It was a novel approach in the field that promoted the state-of-the-art in lignin-based thermosetting resins.

The most difficult aspect of the research was to find a way to use the available lignin in the synthesis of resins. It was addressed by the development of a lignin treatment that enabled its successful utilization. A major discovery in this research was that the mechanical treatment of lignin leads to the reduction of its particle size and improves its performance.

Our most interesting finding was that an easy and low-cost treatment of lignin can change its performance and that lignin-based resins are more resistant to fire than typical PF resins.

Mills can apply this simple treatment method to lignin and make it usable when it otherwise cannot be used. Our next step is a scale up of the process.

Papadopoulou is senior researcher and Kountouras is researcher at CHIMAR HELLAS S.A., Kalamaria, Thessaloniki, Greece. Chrissafis is professor in the School of Physics, Solid State Department, at the University of Thessaloniki in Thessaloniki, Greece. Kirpluks is researcher and Cabulis is director at the Latvian State Institute of Wood Chemistry, Polymer Laboratory, in Riga, Latvia. Švíglerová is researcher at SYNPO A.S., Pardubice, Czech Republic. Benjelloun-Mlayah is R&D director at Compagnie Industrielle de la Matière Végétale (CIMV) in Labège, France.

Low consistency refining of mechanical pulp — system design

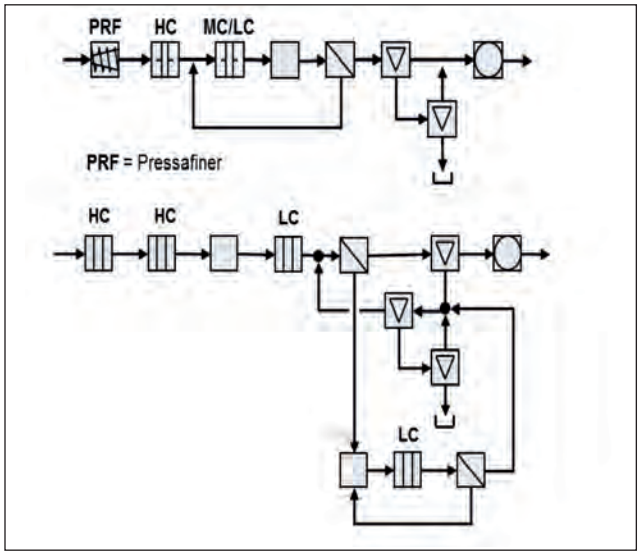
CHRISTER SANDBERG, JAN-ERIK BERG, AND PER ENGSTRAND

ABSTRACT: Many mechanical pulping mills use low consistency (LC) refining for energy efficient fiber development. In this study, energy efficiency and pulp quality were evaluated for six processes, of which four included LC refining. We studied two different types of chip refiners – single disc (SD) and double disc (DD) – with LC refining in the main and reject lines. All process combinations have been used in the Holmen Paper Braviken mill, Sweden, to make thermomechanical pulp for printing papers. LC refining was more energy efficient than high consistency (HC) refining at certain tensile index increases in all evaluated combinations. LC refining in the main line had somewhat higher energy efficiency than did LC refining in the reject line. The type of chip refiner (DD or SD) did not affect the efficiency or pulp property development in LC refining. The process with a combination of DD chip refining and LC refining had the highest energy efficiency (tensile index at certain specific energy consumption). All processes with LC refining produced pulp with somewhat lower light scattering and fiber length than did the corresponding system with only HC refining. Thus, for printing papers, the best combination was LC refining with DD chip refining. LC refiners seem to have a narrow range in specific energy for maximum energy efficiency and a good balance between tensile index increase and fiber length reduction. Much higher specific energy was applied on reject pulp. However, the reject share was only around 30%. The LC refining specific energy, based on main line production, was around 80 kWh/air-dried metric ton (a.d. metric ton), whereas up to 180 kWh/a.d. metric ton was applied in main line.

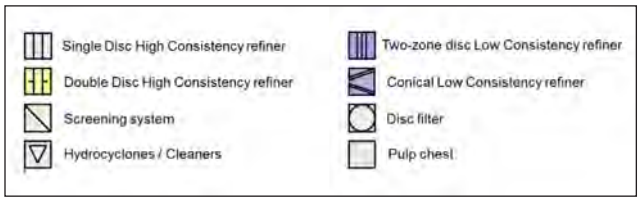
Application: LC refining can improve the process efficiency for mechanical pulping, but it is important to optimize HC and LC refining together to achieve the best combination of pulp quality and energy efficiency.

Low consistency (LC) refiners (consistency ranges of 3%–5%) have been used for a long time in mechanical pulping lines, first as reject or post refiners in stone groundwood mills [1,2]. The main purpose of post refining was to reduce shives and adjust the freeness level. The specific energy was limited to around 50 kWh/metric ton. Above that level, loss in strength properties and fiber length was observed. Kurdin [1] stated that LC refining was not able to develop fibers (i.e., to increase bonding properties such as tensile index). On the other hand, Gavelin [3] showed that when older types of refiners (attrition refiners) were substituted with disc refiners, groundwood rejects could be refined to strength levels higher than screen accept pulp. Two different strategies seem to have prevailed at the time. In one, high specific energy was applied, up to 1000 kWh/a.d. metric ton (more common in North America), turning the reject into wood dust. The other applied more gentle refining with 70–100 kWh/a.d. metric ton (more common in Europe), which produced a material that contributed to strength properties. In either case, at that time, LC refining only contributed marginally to the final pulp strength level. Based on the total production, specific energy applied in LC refining was around 10–50 kWh/metric ton.

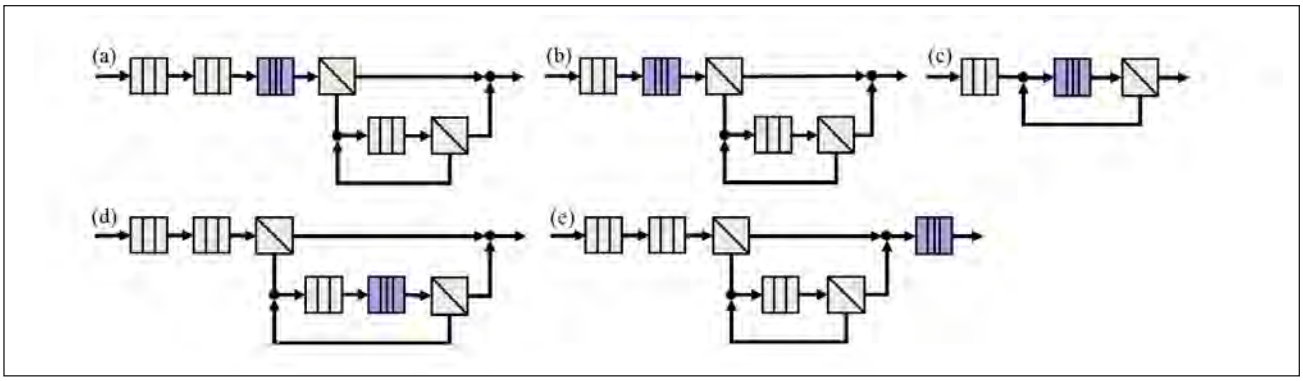
When refiner mechanical pulping (RMP) was introduced during the 1950s, LC refining was used in the main line and for reject refining [3,4]. **Figure 1** shows two examples of RMP-LC process configurations. **Figure 2** is a key to symbols used in Fig. 1 and other figures.



1. System design of two refiner mechanical pulping lines from 1950s, redrawn from [3,4] (see Fig. 2 for key to symbols).



2. Key to symbols used in Figs. 1 and 3-5.



3. Some positions where low consistency (LC) refining can be installed in thermomechanical pulping lines (see Fig. 2 for key to symbols; LC refiners are darker blue).

When the thermomechanical pulping (TMP) process was established in the 1970s, a rapid growth in production capacity and machine size started [5]. This trend continued into the 1980s. During these two decades, few LC refiners were installed in TMP lines. This was probably because very good quality was achieved with pressurized high consistency (HC) refiners (consistency range >30%), and because of the small size and rather poor performance of LC refiners at that time.

During the 1980s, several studies showed that high yield pulps require considerably lower refining intensity than do softwood chemical pulps to maintain fiber length and improve tensile index [6-10]. (Intensity is used in a broad sense in this paper – higher intensity indicating a harsher refining for HC and LC refining.) This led to a rapid development of segment designs toward more narrow bars and grooves. With segment designs adapted for mechanical pulp fibers, and new refiner designs with increased surface area, it became possible to perform a larger part of fiber development in LC refiners [11,12]. Pilot-scale work has shown that the specific energy needed to reach a certain tensile index or freeness can be reduced up to 30% by replacing HC refining with LC refining [12-15]. In those trials, however, fiber length reduction was rather large. Reported reductions of specific energy in mill installations are usually lower, around 10% [12,16-18].

LC refining system design

Figure 3 shows the most common positions where LC refiners have been installed in TMP lines. The motive for installation of LC refiners in TMP lines has usually been to reduce energy consumption, increase production, or improve pulp quality. During the early 1990s, many mills, especially in North America, installed third-stage main line LC refiners (Fig. 3a), mainly to increase production [19]. This has been the most common position at which to install LC refiners in TMP lines. The investment cost for moderate capacity increases – around 10% – is rather low, and the specific refining energy is reduced to a certain tensile index or freeness compared with a two-stage single disc (SD) HC TMP line [8,12,16].

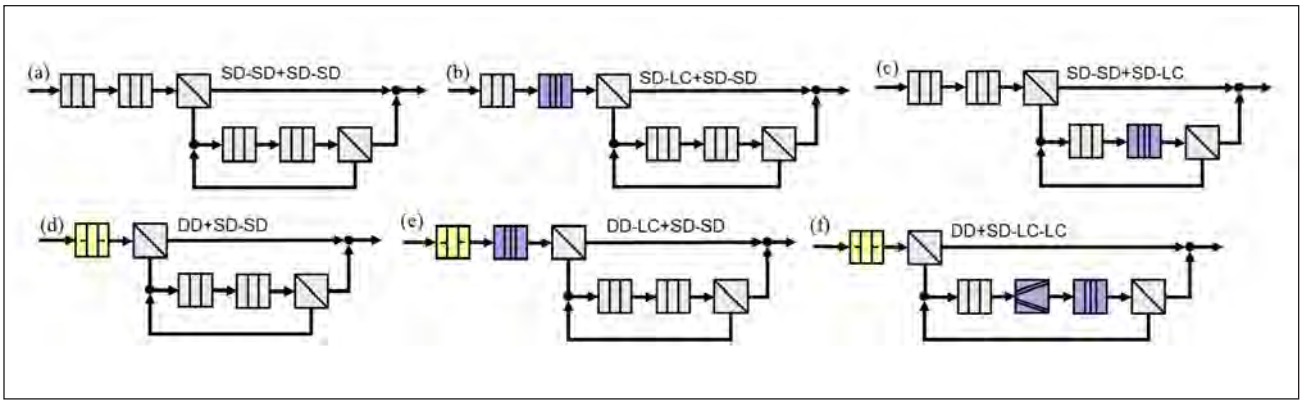
Second stage LC refining (Fig. 3b) is not so common. To our knowledge, the only installation for printing paper pulp production is at Holmen Paper, Braviken, Sweden [20]. An early installation at the Boyer mill in Tasmania used LC refining as a combined second stage and reject refining with a configuration similar to the process in Fig. 3c (called post refining in the papers) [7,21]. This concept was also evaluated, but never in continuous operation, at Stora Enso Kvarnsveden, Borlänge, Sweden, in the early 1990s [22].

At the end of the 1980s, Engstrand et al. [10] showed how the second stage LC refining process can be improved. By performing LC refining at high temperature, pH around 7, and at low intensity, a relatively high specific energy could be applied in LC refining without reducing the fiber length too much. Second stage LC refiners have also been installed in new hardwood chemithermomechanical pulp lines [23,24].

LC refining can also be applied in TMP reject lines (Fig. 3d), either as second stage combined with HC refining, [25-27] or as pure LC reject refining [28]. Of course, LC refining can be installed in main and reject lines both [29], but that is not so common. A special process solution, mentioned previously, has been used in a few cases where LC refining is operated as a combined main line refiner and reject refiner (Fig. 3b) [7,20,30].

LC refiners are also installed as post refiners (Fig. 3e). We define post refining as LC refining after the pulp mill, either on final pulp or in the paper machine stock preparation area. The applied specific energy in post refiners is normally 30–100 kWh/metric ton (net specific energy) [31]. It can be a means for fast adjustment of pulp quality, but the range is limited by the relatively low specific energy. However, this is not the best use of LC refiners for optimal energy efficiency. LC refiners have a rather narrow optimum in gap [32] and should preferably be running at the optimal load all the time. Another drawback with using LC refiners for post refining is that paper machine systems operate at lower temperatures than do pulping lines. Lower temperature increases the risk for more fiber length reduction [10,33].

LC refiners are relatively small compared with HC refiners, which limits the possibility to replace a large share of the HC refining in TMP lines today. Replacing one large second stage HC refiner, such as a CD82 (Metso; Helsinki, Finland) or TX68



4. Studied process configurations (see Fig. 2 for key to symbols).

(Andritz; Graz, Austria), with a load of 20 MW, would require around six LC refiners with a load of 1.7 MW each, assuming 50% lower refining energy.

Fiber development

Compared with HC refining, LC refining normally consumes 40%–50% of the energy needed to reach a similar tensile index or freeness (CSF) [8,10,13,27,34]. Tensile index increases in HC refining and in LC refining, but the increase in LC refining seems to partly be the result of straightening of fibers (latency removal) [35,36]. This means that if an LC refiner is running at low specific energy, the effect of fiber straightening is probably predominant.

When LC refining is made with low fiber length reduction, light scattering increase is lower at certain tensile index increases than for HC refining [13,20,27,36]. One driving force for installations of LC refiners has been the reported higher shive removal than with HC refining at certain specific refining energies [8,12]. This is not always true. The reduction of large shives, measured by a Somerville screen or similar device, is normally high in LC refining, but the large shives can be reduced to smaller shives passing a Somerville screen [7,30]. Thus, refiner segment design has to be optimized to defibrate and not cut shives in LC refining. Because of those considerations, care is needed in building a system with LC refining.

Scope

We compared HC-LC processes with those using only HC refining. All processes are, or have been, in continuous operation in the Holmen Paper Braviken mill, Norrköping, Sweden, during different periods over the years. We gathered and compared mill data to evaluate energy efficiency and pulp quality for the processes.

EXPERIMENTAL

In all figures, tables, and discussions, specific energy consumption (SEC) is based on gross power, including no-load. Production rate and specific refining energy is based on air-dried metric ton (a.d. metric ton) in all figures and tables. Wood raw material was Norway spruce (Picea abies), of which around 30% was sawmill chips and 70% roundwood (thinnings and top logs) from the Norrköping area.

We compared six process configurations for mechanical pulp production, of which four contain LC refining and two use only HC refining. Two types of HC refiners were studied: single disc (SD) and counter rotating double disc (DD) refiners. **Figure 4** shows the process configurations and **Table I** contains basic data, such as refiner types, production rate, etc. The six configurations have been used for different paper grades over the years.

The data shown are averages either from the mill data system (>100 measurements) or from pulp line surveys (5-10 sampling occasions). Pulp samples were taken after each stage in main lines and on final pulps. **Figure 5** shows an example of sampling positions (crosses). No data are presented from reject lines.

We have included data from a refining curve made with the second stage reject refiner (Fig. 4f), to illustrate the importance of running LC refiners at optimum conditions. The flow through the refiner was 100 L/s and flow forward 35 L/s, corresponding to a recirculation rate of 65%. Pulp feed consistency was 4.0% and temperature was 84°C. **Table II** shows additional process data for the refining curve. All those pulps were double-tested.

For the LC refiners, most of the data are based on operation with the 58TC111/112 (Andritz; Gratz, Austria) plate segment design, which has a 1.5 mm bar width.

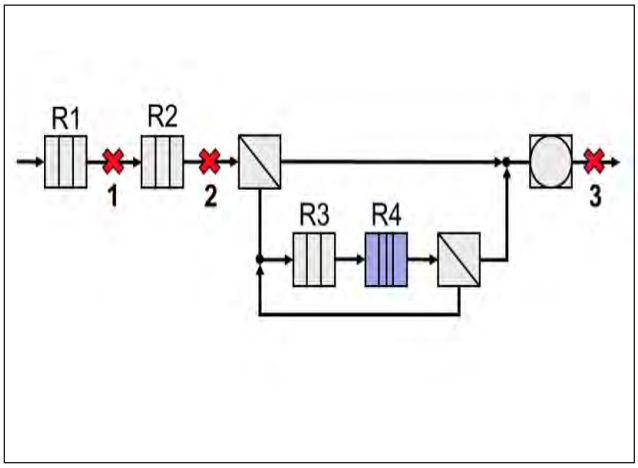
Energy efficiency

Energy efficiency for mechanical pulping has no standard definition. The energy consumption in a pulping process has to be related to a property of the produced pulp to make sense. In the literature, energy consumption has been related to different properties. A process that is energy efficient for one pulp property might not be efficient for another. In this work, we have related the efficiency to tensile index. The efficiency for second stage main line refining and for the whole reject systems are defined as the tensile index (TI) increase divided by specific refining energy: (Nm/g)/(MW/a.d. metric

	Refiner Type					Production, a.d. metric tons/h		SEC*, kWh/a.d. metric ton		
	Main		Reject			Total	Reject	Primary	Secondary	Reject**
Line	1st	2nd	1st	2nd	3rd					
SD-SD+SD-SD	4 RLP58	3 RL 58	RGP 262	RGP 262		16	7	1400	600	250+190
SD-SD+SD-LC	4 RLP58	3 RL 58	RGP 262	TF58		18	7	1300	600	220+80
SD-LC+SD-SD	4 RLP58	TF72	RGP 262	RGP 262		16	7	1370	1540	220+160
DD+SD-SD	2 RGP68DD		RGP 262	RGP 262		21	8	1660		170+150
DD-LC+SD-SD	2 RGP68DD	TF72	RGP 262	RGP 262		21	8	1550	130	180+150
DD+SD-LC-LC	3 RGP68DD		RGP 262	RF5	TF58	36	10	1540		170+40+40

* Specific energy consumption (SEC) does not include auxiliary drives, such as pumps, presses, etc.
** Specific energy is based on main line production rate, not reject production.
Note: RLP58, RL58, RGP68D, RGP262 and RF5 (Valmet; Espoo, Finland). TF58 and TF72 (Andritz; Gratz, Austria).

I. Refiner data for six mechanical pulp production process configurations.



5. Sampling points in the SD-SD+SD-LC process (SD = single disc, LC = low consistency), shown as an example (see Fig. 2 for key to symbols).

ton). As examples, the efficiency for the second stage refiner in Fig. 5 is (TI2 – TI1)/SECR2 and for the reject system is (TI3 – TI2)(SEC R3+SEC R4).

Pulp analysis

All pulps were analyzed at the Braviken mill laboratory. The following methods were used:

- Hot disintegration before pulp testing (ISO 5263-3 "Pulps – Laboratory wet disintegration – Part 3: Disintegration of mechanical pulps at > 85 degrees C")
- Laboratory sheets made with a Rapid-Köthen sheet former (ISO 5269-2 "Pulps – Preparation of laboratory sheets for physical testing – Part 2: Rapid-Köthen method")
- Tensile index (ISO 1924-2 "Paper and board – Determination of tensile properties – Part 2: Constant rate of elongation method [20 mm/min]")
- Specific light scattering coefficient at an effective wave-

	Power, MW	SEC, kWh/a.d. metric ton	SEL, J/m	CSF, mL	Fiber Length, mm	Tensile Index, Nm/g
Feed				241	1.28	46.9
				243	1.25	44.6
1	1.2	212	0.41	166	1.22	54.1
				169	1.23	55.2
2	1.4	248	0.52	159	1.19	57.1
				154	1.19	56.8
3	1.6	283	0.62	143	1.08	56.3
				143	1.12	57.1
4	1.8	319	0.73	118	1.05	55.2
				117	1.06	54.6

II. Process data and pulp properties for OptiFiner RF5 refiner (Valmet, Espoo, Finland). SEC = specific energy consumption; SEL = specific edge load.

	CSF, mL	Tensile Index, Nm/g	Light Scattering Coefficient, m^2/kg	Fiber Length,mm	Shives Sum, #/g	Long Shives, #/g
SD-SD+SD-SD						
Primary	290	36	44	1.31	2000	535
Secondary	100	48	49	1.27	800	96
Final pulp	58	54	53	1.24	43	0
SD-SD+SD-LC						
Primary						
Secondary	110	46	46	1.30	908	576
Final pulp	65	52	52	1.24	181	118
SD-LC+SD-SD						
Primary	284	36	44	1.28	1142	410
Secondary	175	45	46	1.16	966	213
Final pulp	90	51	49	1.07	205	29
DD+SD-SD						
Primary	120	46	57	1.01	320	64
Final pulp	72	50	58	0.97	193	35
DD-LC+SD-SD						
Primary	141	41	53	1.02	386	–
Secondary	97	48	54	0.94	220	–
Final pulp	66	52	56	0.92	118	–
DD+SD-LC-LC						
Primary	135	45	55	0.99	218	98
Final pulp	85	51	57	0.94	76	11

III. Pulp properties from the six mechanical pulp production process configurations studied.

length of 557 nm (ISO 9416 "Paper – Determination of light scattering and absorption coefficients [using Kubelka-Munk theory]")

- Canadian standard freeness (ISO 5267-2 "Pulps – Determination of drainability – Part 2: 'Canadian Standard' freeness method").

Length weighted average fiber length and shives content were analyzed with a PulpEye (PulpEye; Örnsköldsvik, Sweden).Shives are defined as particles longer than 0.3 mm and wider than 0.075 mm. Long shives are defined as all particles longer than 1.5 mm.

RESULTS

We evaluated six process configurations with LC refining in different positions with two types of chip refiners (DD or SD) at Holmen Paper Braviken. Tensile index, fiber length, light scattering coefficient, and shives content are reported in this paper. Tensile index is shown versus SEC to evaluate energy efficiency whereas other properties are shown versus tensile index. **Table III** shows the pulp properties.

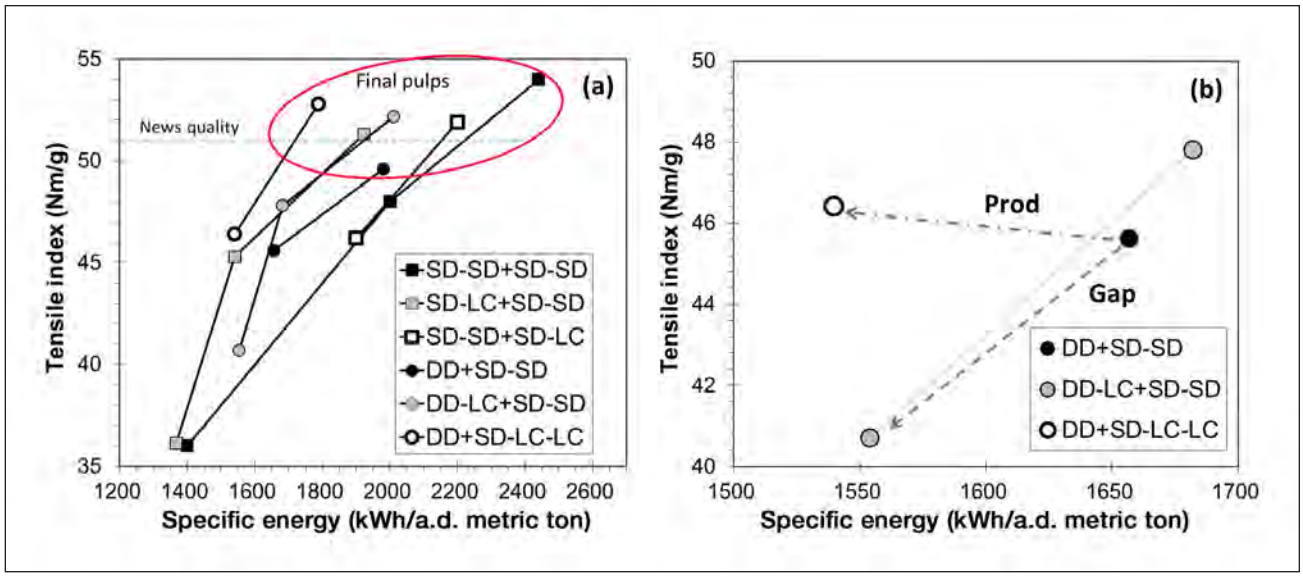
In all figures, the legend explains the process configurations. The left part of the notation in the legend is the main line and the right part is the reject line, separated by a + sign. Thus, the process configuration in Fig. 4c is SD-SD+SD-LC. This denotes two-stage single disc HC refining in series in the main line and single disc HC refining followed by LC refining in the reject line.

Main line refining

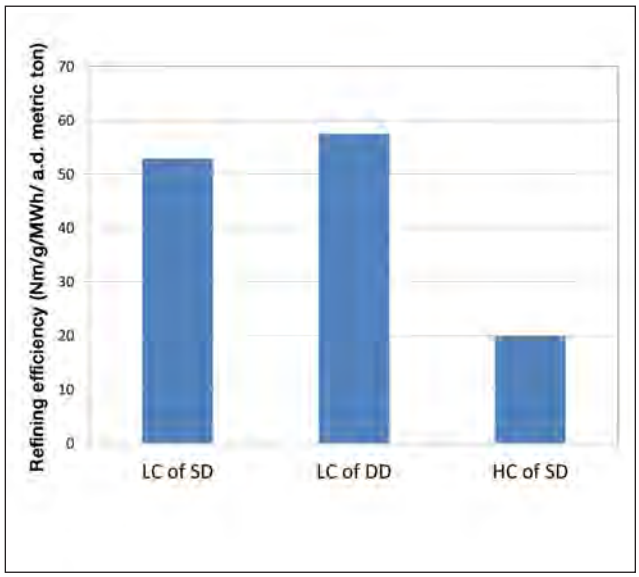
The configurations SD-SD+SD-SD and SD-SD+SD-LC used the same type of main line refiners; therefore, primary pulp properties are only shown for one of these configurations in **Figs. 6-10**. First, we present the four different main line configurations:

- Two-stage single disc HC refining (SD-SD) refining
- One-stage single disc HC followed by second stage LC refining (SD-LC)
- One-stage HC double disc refining (DD)
- One-stage HC double disc refining followed by second stage LC refining (DD-LC)

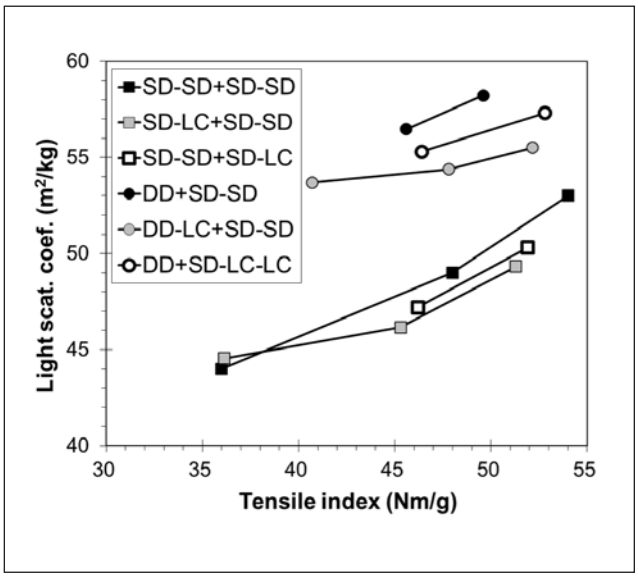
Figure 6a shows tensile index versus specific energy for all six processes, with final pulps circled. As can be seen, the



6. Tensile index along the pulping lines for (a) all processes and (b) the double disc (DD) refiners, enlarged picture. Tensile index was measured on Rapid-Köthen handsheets, which give a tensile index around 8 Nm/g higher than ISO handsheets.



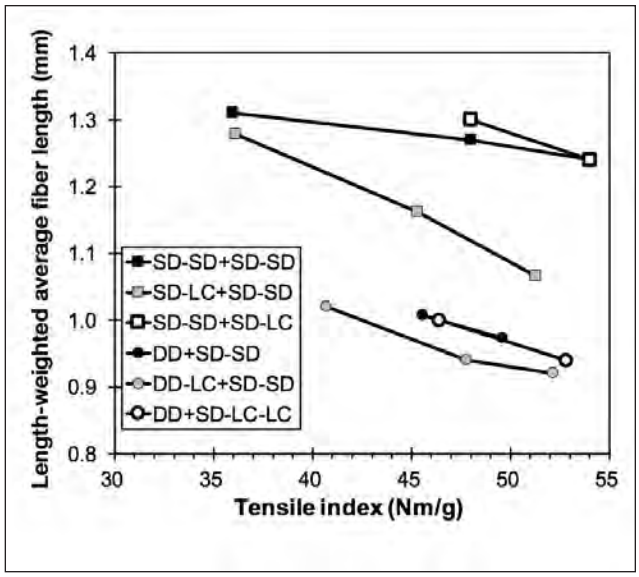
7. Energy efficiency (defined as tensile index increase divided by specific energy) for second stage main line low consistency (LC) refining of single disc (SD) and double disc (DD) pulp compared to second stage high consistency (HC) refining.



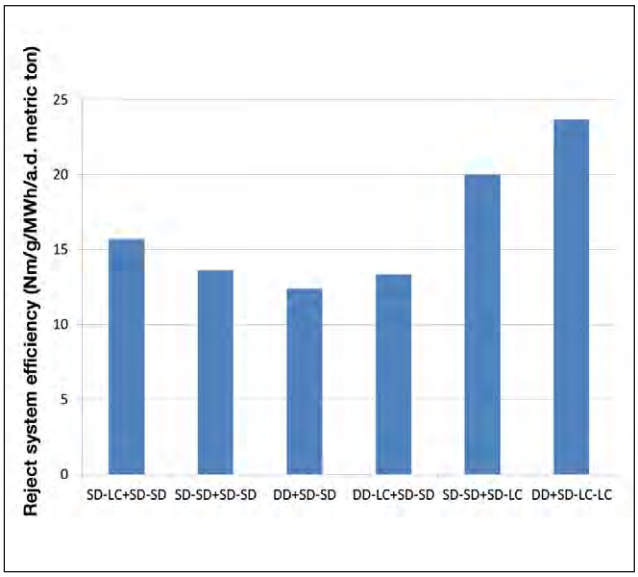
8. Specific light scattering coefficient along the whole process vs. tensile index.

energy needed to reach certain tensile indexes varies greatly. The six configurations have been used for different paper grades over the years, which explains the different tensile index levels of final pulps.

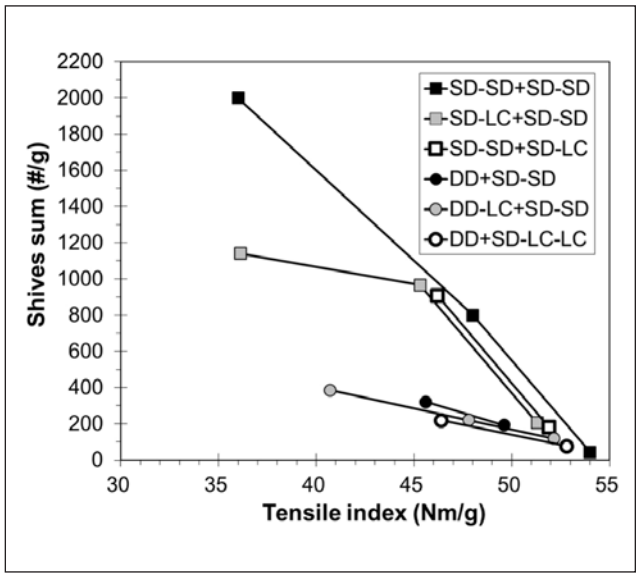
After installation in 2008, the DD refiners were running at the point represented by the filled circle in Fig. 6b. The energy consumption to tensile index is 46 Nm/g, which is a normal level for latency pulp in Braviken, was around 250 kWh/a.d. metric ton lower for the DD refining compared with the two-stage SD line. Together with the DD refiners, a prototype Andritz TwinFlo TF72 LC refiner was installed as the second stage in the main line. At that time, the mill had no need for higher pulp production and reduced the load of the DD refiners (disc gap was increased) when the LC refiner was running, indicated by the dashed arrow in Fig. 6b. After LC refining, the pulp reached somewhat higher tensile index compared with only DD refining. The efficiency was only marginally better for the DD-LC process. The TMP mill in Braviken was restructured a few years ago, which initiated work to increase the production of the DD refiners from around 10 a.d. metric ton/h to 12–13 a.d. metric ton/h, mainly based on segment design development. This clearly improved the energy efficiency, as shown by the dash-dotted



9. Length-weighted average fiber length along the whole process vs. tensile index.



11. Reject system efficiency (defined as tensile index increase divided by specific energy) for all configurations.



10. Shives content along the whole process vs. tensile index.

arrow in Fig. 6b. Today, the DD refiners are running as single stage chip refiners in the DD+SD-LC-LC configuration, represented by the unfilled circle in Fig. 6b

The TF 72 LC refiner (Andritz; Graz, Austria) is now operating as a second stage in the SD-LC+SD-SD line, replacing three old RL58 refiners (Valmet; Espoo, Finland). The SD-LC main line has almost the same energy efficiency as the single stage DD refiners today. However, the light scattering is much higher and shives content much lower for the DD refining, as described below. Figure 7 shows energy efficiency for second stage LC and second stage HC SD refining of primary SD pulp and second stage LC refining of primary DD pulp. The energy efficiency was 2.5 times higher for LC refining.

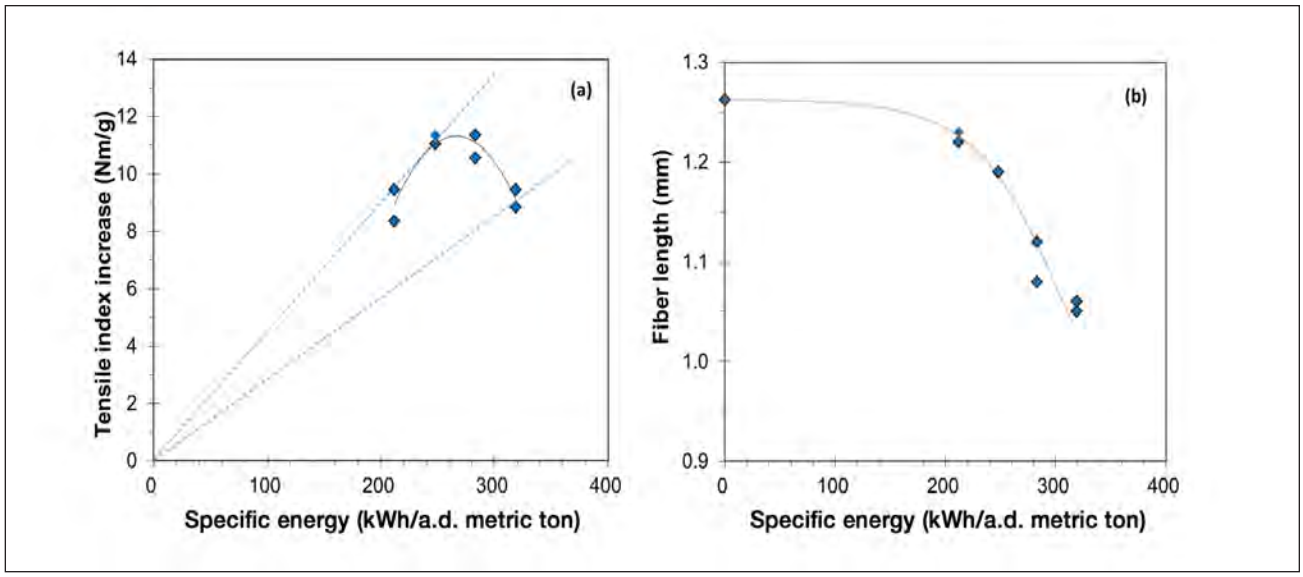
Figure 8 shows light scattering coefficient versus tensile index for the processes. The highest light scattering was attained with single stage DD refining (DD+SD-SD). The SD-LC process had the lowest light scattering. Low light scattering can be a problem for low grammage papers, so the SD-LC main line process is probably not the best choice for such products. The DD-LC process had a lower light scattering compared with the single stage DD processes, but higher than the SD-SD process. Light scattering increased marginally over LC refining, for both SD and DD pulps.

Figure 9 shows fiber length for the pulps from all process configurations. The DD configurations had the lowest fiber length. The low fiber length has not caused any problems with paper runability in Braviken or at printers. DD refining produces a different fiber property profile than does SD refining [18,37]. That profile probably compensates for the low fiber length. The fiber length reduction over LC refining depends very much on refining intensity, which has been shown in several studies [8,10,33]. The TF72 LC refiner in Braviken is usually running at rather high intensity, with specific edge load of around 0.8 J/m to be able to get as high a tensile index increase as possible. That is why the fiber length reduction is somewhat higher compared with the second stage SD HC refining in Fig. 9.

Shives content, which was much lower for the DD processes than for the SD processes, is another important pulp property (Fig. 10). The shives reduction over the LC refining in the SD-LC process was rather low. This is probably because of low reduction of small shives, which usually are the largest share of the total number of shives.

Reject systems

Keep in mind that even though screen room configurations were similar, the reject rates differed in the processes we studied, which can affect the results somewhat.



12. (a) Tensile index increase and (b) fiber length over OptiFiner RF5 low consistency refiner (Valmet; Espoo, Finland). The specific energy is based on reject line production.

Figure 11 shows the efficiency of the reject systems. The efficiency is defined as tensile index increase from latency chest to final pulp divided by reject refining specific energy based on whole line production.

All the SD-SD reject refining systems had similar energy efficiencies, around 14 (Nm/g)/(MWh/a.d. metric ton). The preceding main line system did not significantly affect the energy consumption of the reject system. The HC-LC-LC system had the highest energy efficiency, 24 (Nm/g)/(MWh/a.d. metric ton), which is around 70% higher than that of the lines with HC-HC reject refining.

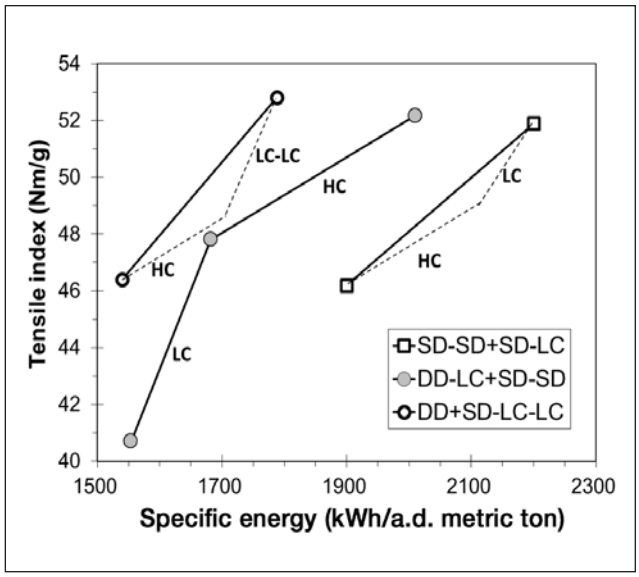
The increase in light scattering was lower over the reject systems (HC and HC-LC) for DD processes, compared with the corresponding reject systems for SD main line configurations (Fig. 8). This might be an effect of the already high scattering level before the reject system. Light scattering increase for reject systems containing LC refining did not differ significantly from that of systems with only HC refining. The DD-LC configuration had higher light scattering than did the process with only SD HC refining.

Fiber length (Fig. 9) and shives content (Fig. 10) over the reject systems are difficult to compare because the reductions depend much on reject rates and condition of screen baskets. The fiber length reduction over the reject systems was similar for all systems though. The shives content before screening was much lower for the DD processes, but after screening, the difference was small when compared at certain tensile indexes (Fig. 10). There was a large difference in SEC (750 kWh/a.d. metric ton), though, at the same shives content for the DD+SD-LC-LC and the SD-SD+SD-SD process.

Optimal refining conditions

A refining curve for the second stage reject refiner in the DD+SD-LC-LC line was made to illustrate the LC refiner behavior (**Fig. 12**). Process data and some pulp properties are shown in Table II. In Fig. 12a, tensile index increase is shown versus SEC for the refiner. The dashed lines highlight the large variation in efficiency, from 28 to 45 (Nm/g)/(MWh/a.d. metric ton). The maximum efficiency at around 240 kWh/a.d. metric ton corresponds to a refiner power around 1.4 MW. The maximum in tensile index increase is at a somewhat higher specific energy, 250 kWh/a.d. metric ton. Around the maximum efficiency, fiber length starts to drop faster (Fig. 12b). The differences between any two operation points is 0.2 MW, which also seems to be an acceptable range for power variation to maintain high efficiency. Thus, the optimum range is rather narrow. Of course, the optimum might not be so narrow for other LC refiners, but there seems to always be one [32]. As the refiner gap is closed, power increases, resulting in an increase in specific energy and intensity (at constant throughput). The increase in intensity (reduced gap) results in higher forces on fibers [38] and fibers are cut. This is a somewhat simplified description. More details on the effect of operation conditions on refiner performance have been presented by Luukkonen et al. [32] and Elahimehr et al. [39].

Our conclusion is that LC refiners should always be running at the point of maximum efficiency to maintain a good balance between tensile index increase and fiber length reduction. It is also important to run HC refiners at optimal conditions. As shown in Fig. 6b, increased gap in the DD refiners plus LC refining only marginally improved main line energy efficiency. It would have been better to increase production at maintained DD refiner load to get the best energy efficiency for the DD-LC process. Increased production often improves the energy efficiency of HC refiners [22].



13. Theoretical splitting of the reject development according to the applied energy in HC and LC reject refining is symbolized by the dashed lines.

DISCUSSION

One obvious question is, where is the best position to install LC refining in a mechanical pulping line? Unfortunately, in the studied processes, the LC refining specific energy in the reject lines and main lines differ for the SD and DD configurations. SEC was around 150 kWh/a.d. metric ton for LC refining in the main lines and around 80 kWh/a.d. metric ton for reject lines (based on main line production). These were the normal specific energies in those positions. If the specific energy would have been reduced in the main line applications to the level of the reject applications, the energy efficiency would have been poor because of the large plate gap [32]. However, the efficiency of the reject LC refiners can be calculated if we assume that the HC reject refining efficiency is similar to the efficiency of the pure HC reject refining lines, which was 13.8 (Nm/g)/(MWh/a.d. metric ton) on average. The increase in tensile index over the SD-LC-LC reject system is 6.0 Nm/g. The specific refining energies are 0.17 MWh/a.d. metric ton for HC and 0.08 MWh/a.d. metric ton for LC reject refining, which gives (6.4-13.8*0.17)/0.08 = 51 (Nm/g)/(MWh/a.d. metric ton). Corresponding estimation for the SD+LC line results in 33 (Nm/g)/(MWh/a.d. metric ton). The dashed lines in **Fig. 13** visualize these calculations. Both calculated efficiencies for LC reject refining are lower than the corresponding main line efficiencies, which makes it reasonable to conclude that LC refining in the main line has a somewhat higher efficiency than in the reject line.

Given our findings, if a large share of the fiber development should be made in LC refining, it should primarily be made in the main line. The difference between application of an LC stage in the main line or in the reject line can be illustrated by an example: 200 kWh/a.d. metric ton is supposed to be applied in LC refining in a 700 a.d. metric ton/day TMP line. That corresponds to around 6 MW applied power to a pulp flow of 180 L/s at 4% consistency. Four TwinFlo 58 refiners (Andritz; Gratz, Austria), or similar, are needed for that specific energy, preferably installed two-by-two in series [38]. If the same refiners would be installed in the reject system in the same TMP line, with a reject production of 280 a.d. metric tons/day (40% of main line production), the specific energy would be more than 500 kWh/a.d. metric ton at a pulp flow around 70 L/s. This would probably be too high of an SEC to maintain fiber length and the low flow would require recirculation. Thus, application in the main line is the only reasonable choice. It also would be possible to install two LC refiners in the main line and two on the reject line, with flow recirculation over the reject refiners, to get stable operation [34].

As shown in Fig. 8, the light scattering increase was low for all LC refining applications. If LC refining is made with a large fiber length reduction (cutting), light scattering can be increased though [12,14,15]. Because of the low increase of light scattering in LC refining, high intensity refining, such as DD or RTS (low retention time, higher temperature, higher refining speed), is preferable as primary stage refining before LC refining. Sufficient specific energy has to be applied in HC refining to reach the desired light scattering.

The increased production over the DD refiners improved the energy efficiency without loss of pulp quality, except for a slight reduction in light scattering. We then ask, can the production and energy efficiency be further increased by combining optimized DD refining with LC refining? We have initiated such a study and results will be presented in the near future.

The lowest energy efficiency was attained with HC refining in the reject systems. Thus, to reach the highest energy efficiency, as much of the fiber development as possible should be done in the main line, reject rates should be kept low, and reject refining made with a combination of HC and LC refining. It is also clear from this work that it is advantageous for energy efficiency, light scattering, and shives content to combine LC refining with high intensity HC chip refining. An important factor to consider when LC refining is installed in a TMP line is that the efficiency of the HC refiners is maintained (which usually happens if production is increased).

Recommendations for system design

When LC refining is installed in a TMP system for printing paper production, a few things require attention. Somewhat different issues have to be considered, depending on whether LC refining will be installed in an existing process or if a completely new line is planned.

For a new line:

- The best energy efficiency and pulp properties are attained if LC refining is combined with high intensity chip refining.
- If high SEC should be applied in LC refining, the largest share has to be in the main line.

For LC refining installed in an existing line for energy reduction:

- Do not unload preceding HC refiners; rather, increase production at maintained load.

For all installations of LC refiners:

- LC refiners preferably should operate just before the maximum tensile index increase, which seems to correspond with the point of maximum efficiency, to maintain a good balance between tensile index increase and fiber length reduction.
- Segment design has to be thoroughly worked with to get good reduction of small shives.

CONCLUSIONS

Evaluation of mill data from processes with two HC chip refiner types (SD and DD), with and without LC refining in the main line and reject line, has shown the following:

- LC refining improved the total energy efficiency to certain tensile indexes when applied both in the main line and in the reject line. LC refining in the main line had slightly higher efficiency.
- The best system energy efficiency was achieved with a combination of DD chip refining and LC refining.
- The type of chip refiner (DD or SD) did not affect the efficiency or pulp property development in LC refining.
- Processes with LC refining had somewhat lower light scattering and fiber length than did the corresponding process with only HC refining.
- The combination of DD and LC refining rendered higher light scattering than did the combination of SD and LC refining.
- LC refiners should always be running near the point of maximum efficiency to maintain a good balance between tensile index increase and fiber length reduction.
- The efficiency of HC reject systems was lower than the efficiency of HC main line refining.
- If LC refining is installed in a TMP line to reduce the specific energy to a given quality, it is important to maintain efficiency in the preceding HC refiners (which is usually attained if production is increased). **TJ**

ACKNOWLEDGEMENTS

The authors are most grateful to the Swedish Energy Agency, Knowledge Foundation, and Holmen Paper AB for financial support and to Jan Hill for valuable comments on the manuscript. This work was performed within the research program "Energy Efficient Mechanical Pulping – Research Profile," at Mid Sweden University, Sundsvall, Sweden.

ABOUT THE AUTHORS

Low consistency (LC) refining has always had its place in mechanical pulping for printing papers and in chemimechanical pulping for paperboard. Before refiner mechanical pulp was developed, LC refiners were mainly used for reject refining in groundwood production. When the thermomechanical pulp process started to dominate the market, the proportion of fiber development performed by means of LC refining decreased until the mid-1990s. At that time, the number of installed LC refiners increased again.

Now the question is, has LC refining a place in the future mechanical pulping process?

High consistency (HC) refiners of different types produce pulp with different pulp property profiles, and the fiber development is quite different in HC and LC refining. Thus, it is important to increase the understanding of how to optimize the combination of LC refiners and HC refiners to improve efficiency and optimize pulp quality for different products. Very little effort has been made in this area. The challenge in this respect is to be able to compare all interesting HC-LC combinations, preferably in mill-scale, with different wood raw materials. Holmen Paper Braviken is a unique mill in that the process has changed dramatically over the years. This has given us the possibility to evaluate at least some of the combinations that would be interesting for the future.

We believe that LC refining has a position in the highly efficient mechanical pulping lines of the future, but there is more work needed. Another challenge in this respect is the rather small size of LC refiners in comparison with HC refiners. We have continued to work with optimization of the combination of double-disc chip refining and LC refining within the e2mp (energy efficient mechanical pulping) research program at Mid Sweden University, which will be published soon.



Sandberg



Berg



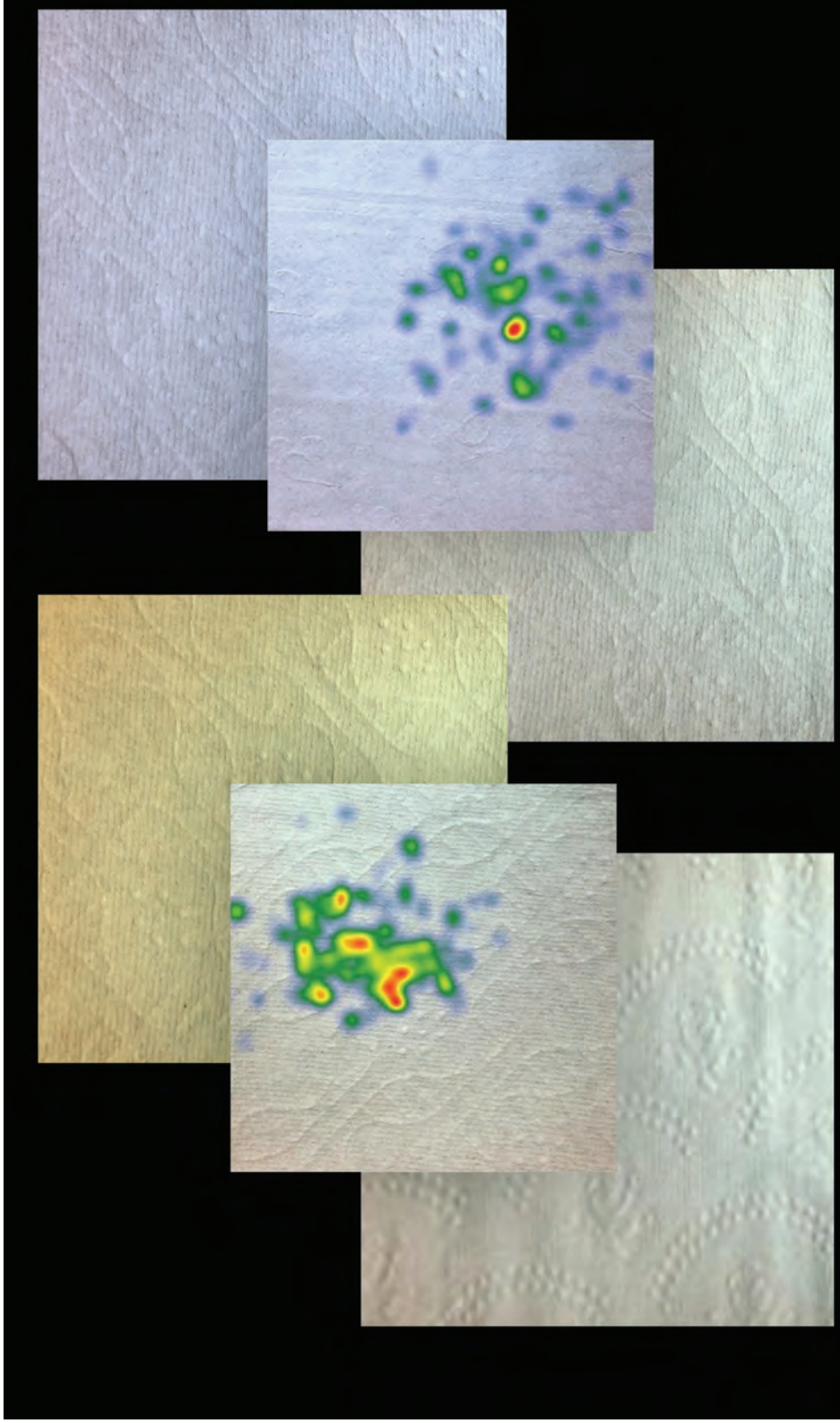
Engstrand

Sandberg is R&D specialist (part-time), Holmen Paper, Norrkoping, Sweden, and project manager (part-time), Mid Sweden University, Sundsvall, Sweden. Berg is project secretary and researcher, Fiber Science and Communication Network (FSCN), Mid Sweden University, Sundsvall, Sweden. Engstrand is professor, FSCN, Mid Sweden University, Sundsvall, Sweden. Email Sandberg at christer.sandberg@holmenpaper.com.

LITERATURE CITED

1. Kurdin, J.A., *Pulp Pap.* 48(3): 92(1974).
2. Klemm, K.H., *Modern Methods of Mechanical Pulp Manufacture*, Lockwood Trade Journal Co., New York, 1958.
3. Gavelin, N.G., in S*cience and Technology of Mechanical Pulp Manufacture*, Lockwood, New York, 1966, pp. 190-218.
4. Eberhardt, L., *Pap. Trade J.* 139(37): 26(1955).
5. Leask, R.A., *Pulp Pap. Can.* 85(3): 14(1983).
6. Levlin, J.-E., *Trans. Tech. Sect. (Can. Pulp Pap. Assoc.)* 6(4): TR94(1980).
7. Bonham, J.S., Flowers, A.G., and Schofield, A.J., *Appita J.* 36(6): 466(1983).
8. Berger, T.H., *Int. Refin. Conf., 3rd*, Pira International, Leatherhead, UK, Vol. 1, paper 11, 1995.
9. Robinson, D.H., Defoe, R.J. and Fredriksson, B., *Pulp Pap. J.* 59(5): 69(1985).
10. Engstrand, P., Hammar, L.Å., Sjögren, B., et al., Pat. WO 1991006700 A1. EP 0500674 A1 (May 16, 1991).
11. Kirchner, E.C. and Defoe, R.J., U.S. Pat. 4,619,414 (Oct. 28, 1986).
12. Cort, J.B., Sabourin, M.J., and Mussman, R.L., *TAPPI Pulping Conf.*, TAPPI PRESS, Atlanta, GA, USA, 1994, p. 987.
13. Hammar, L.-Å., Htun, M., and Svensson, B., *Int. Mech. Pulping Conf.*, SPCI, Stockholm, 1997, p. 257.
14. Sabourin, M., Aichinger, J., and Eksteen, R., "Minimizing TMP energy consumption using a combination of chip pre-treatment, RTS, and multiple stage low consistency refining," *TAPPSA J.*, July 2007. Available [Online] https://www.tappsa.co.za/archive3/Journal_papers/Minimizing_TMP_Energy_Consumpt/minimizing_tmp_energy_consumpt.html <21July2017>.
15. Gorski, D., Luukkonen, A., Sabourin, M., et al., *Appita J.* 65(3): 244(2012).
16. Musselman, R., Letarte, D., Simard, R., et al., *Appita Annu. Gen. Conf. Proc., 50th*, APPITA, Carlton, Victoria, Australia, 1996, p. 363.
17. Vaughn, J.W., Mitchell, G.W., and Musselman R.L., *TAPPI Pulping Conf.*, TAPPI PRESS, Atlanta, 1998, Book 1, p. 379.
18. Andersson, S., Sandberg, C., and Engstrand, P., *Appita J.* 65(1): 57(2012).
19. Cannell, E., *Solutions People, Processes Pap.* 85(12): 30(2002).
20. Sandberg, C., Berg, J.-E., and Engstrand, P., *Int. Mech. Pulping Conf.*, TAPPI Press, Atlanta, 2016, p. 485.
21. Flowers, A., Pearson, A., and Tyler, A., *Appita J.* 33(3): 195(1979).
22. Strand, B.C., Falk, B., Mokvist, A., et al., *Int. Mech. Pulping Conf.,* 1993, p. 143.
23. Mudri, J.L., Teubner, D., Zattoni, S., et al., *Int. Mech. Pulping Conf.*, SPCI, Stockholm, 2009, p. 169.
24. Xu, E.C., *Int. Mech. Pulping Conf.*, China Light Industry Press, Beijing, 2011, p. 9.
25. Danielsson, K.O., Falk, B.G.S., and Jackson, M., U.S. Pat. 5,145,010 (Sept. 8, 1992).
26. Viljakainen, E., Huhtanen, M., and Heikkurinen, A., *Int. Mech. Pulping Conf.*, SPCI, Stockholm, 1997, p. 173.
27. Sandberg, C., Sundström, L., and Nilsson, L., *Int. Mech. Pulping Conf.*, SPCI, Stockholm, Sweden, 2009, p. 186.
28. Moqvist, A., Russell, G., and Lauritzen, J., *Int. Mech. Pulping Conf.,* 2005, p. 209.
29. Radhuber, C., Ernet, C., and Bräuer, P., *Int. Mech. Pulping Conf.,* TAPPI Press, Atlanta, 2016, p. 732.
30. Mörseburg, K., Imppola, A., Johansson, L., et al., "Effects of inlet pulp quality and specific energy consumption in mill scale low-consistency refining of mechanical pulp," *8th International Fundamental Mechanical Pulp Research Seminar,* Mid Sweden University, Sundsvall, Sweden, 2013.
31. Pitkänen, M., Mannström, M., and Lumiainen, J., in *Mechanical Pulping* (B. Lönnberg, Ed.), Book 5, Paper Engineers' Association (PI)/Paperi ja Puu Oy, Helsinki, Finland, 2009, pp. 399-418.
32. Luukkonen, A., Olson, J.A., and Martinez, D.M., *J. Pulp Pap. Sci.* 36(1-2): 28(2010).
33. Hammar, L.A., Salmén, L., Sandberg, C., et al., *Appita J.* 63(5): 377(2010).
34. Sandberg, C. and Berg J.-E., *Nord. Pulp Pap. Res. J.* 30(2): 230(2015).
35. Welch, L.V.S., "Low consistency refining of mechanical pulps," Ph.D. thesis, University of British Columbia, Vancouver, BC, Canada, 1999.
36. Ferritsius, R., Sandberg, C., Ferritsius, O., et al., *Int. Mech. Pulping Conf.*, TAPPI Press, Atlanta, 2016, p. 609.
37. Ferritsius, R., Reyer, S., and Ferritsius, O., *Nord. Pulp Pap. Res. J.* 27(5): 860(2012).
38. Kerekes, R.J. and Senger, J.J., *J. Pulp Pap. Sci.* 32(1): 1(2006).
39. Elahimehr, A., Olson, J.A., and Martinez, D.M., *Nord. Pulp Pap. Res. J.* 30(4): 609(2015).
40. Luukkonen, A., "LC refining of high freeness CTMP," *Int. Mech. Pulping Conf.,* Paper Engineers' Association (PI), Espoo, Finland, 2014.

TAPPI JOURNAL
WWW.TAPPI.ORG
THE PAPER AND PACKAGING INDUSTRIES' TECHNICAL RESOURCE
AUGUST 2017 | VOL. 16 NO.8



TISSUE 439
Visual discrimination of hygiene tissue softness in the absence of haptic feedback
Jessica Carette, Pierre-Majorique Léger, and Sylvain Sénécal

BIOENERGY 453
Operating parameters affecting the thermal performance of biomass boilers
Naz Orang, Honghi Tran, Andy Jones, and F. Donald McCabe

BIOENERGY 465
Drying characteristics of biosludge from pulp and paper mills
Geanna Hovey, D. Grant Allen, and Honghi Tran

PAPERMAKING 477
Modeling the influence of forming fabric structure on vacuum box dewatering
Björn Sjöstrand, Christophe Barbier, and Lars Nilsson

August 2017

TABLE OF CONTENTS VOL. 16 NO. 8

435 GUEST EDITORIAL
The next act for nonwovens
Seshadri Ramkumar

439 TISSUE
Visual discrimination of hygiene tissue softness in the absence of haptic feedback
Jessica Carette, Pierre-Majorique Léger, and Sylvain Sénécal

453 BIOENERGY
Operating parameters affecting the thermal performance of biomass boilers
Naz Orang, Honghi Tran, Andy Jones, and F. Donald McCabe

465 BIOENERGY
Drying characteristics of biosludge from pulp and paper mills
Geanna Hovey, D. Grant Allen, and Honghi Tran

477 PAPERMAKING
Modeling the influence of forming fabric structure on vacuum box dewatering
Björn Sjöstrand, Christophe Barbier, and Lars Nilsson

»COVER CREDIT: When haptic (tactile stimuli) feedback is absent, as in an online context, consumers can only use visual perception to evaluate tissue softness. Researchers Carette et al. (p. 439) evaluated how manufacturers can manipulate color, embossing pattern, and digital images to influence consumer perception of tissue softness, as with blue and yellow color tones (leftmost cover images). They used oculometry to track study participants' attention to images of hygiene tissue (middle images) like away-from-home and facial tissue (rightmost images).

TAPPI JOURNAL
WWW.TAPPI.ORG

Editor-in-Chief
Scott Rosencrance scott.rosencrance@kemira.com
+1 770 429-2753

Associate Editor
Brian N. Brogdon brian.brogdon@gmail.com
+1 678 581-9114

Editorial Director
Monica Shaw mshaw@tappi.org
+1 770 367-9534

Vice President, Operations
Eric Fletty efletty@tappi.org

PRESS Manager
Jana Jensen jjenson@tappi.org
+1 770 209-7242

Webmaster
Trina Heath theath@tappi.org
+1 770 209-7416

***TJ* EDITORIAL BOARD**

Brian N. Brogdon, FutureBridge Consulting & Training LLC
brian.brogdon@gmail.com, +1 678 581-9114

David A. Carlson, Carlson Consulting
dacarlson39@aol.com, +1 847 323-2685

Jere W. Crouse, JWC Consulting
cj522@inwave.com, +1 608 362-4485

Mahendra Doshi, Doshi and Associates
mahen@aol.com, +1 920 832-9101

Marc Foulger, GL&V USA Inc.
Marc.foulger@glv.com +1 315 767-2920

Peter W. Hart, WestRock
peter.hart@westrock.com, +1 409 276-3465

Carl J. Houtman, USDA Forest Products Laboratory
choutman@fs.fed.us, + 1 608 231-9445

John A. Neun, John A. Neun LLC
john.neun@gmail.com, +1 518 275-8139

Jim Niemiec, Verso Corporation
jim.niemiec@versoco.com, +1 715 422-7404

Steven P. Ottone, Omya
steven.ottone@omya.com, +1 919 641-7854

Gaurav Pranami, Imbed Biosciences
gpranami@imbedbio.com, +1 515 230-7005

Arthur Ragauskas, Oak Ridge National Laboratory
aragausk@utk.edu

Gerard J.F. Ring, University of Wisconsin—Stevens Point
gerrryring@wi-net.com, +1 715 592-3732

Scott Rosencrance, Kemira Chemicals
scott.rosencrance@kemira.com, +1 770 429-2753

Paul Wiegand, NCASI
pwiegand@ncasi.org, +1 919 941-6417

Junyong Zhu, USDA Forest Products Laboratory
jzhu@fs.fed.us, +1 608 231-9520

Join TAPPI *today!*

TAPPI JOURNAL is a free benefit of TAPPI membership, and is only available to members. To join TAPPI, to renew your TAPPI Membership, or to learn about other valuable benefits, visit www.tappi.org.

TAPPI, 15 Technology Parkway S., Suite 115, Peachtree Corners, GA 30092, publishes *TAPPI JOURNAL* monthly.

ATTENTION PROSPECTIVE AUTHORS: All papers published are subject to *TAPPI JOURNAL's* peer-review process. Not all papers accepted for review will be published. Before submitting, check complete author guidelines at http://www.tappi.org/s_tappi/doc.asp?CID=100&DID=552877.

Statements of fact and opinions expressed are those of individual authors. TAPPI assumes no responsibility for such statements and opinions. TAPPI does not intend such statements and opinions or construe them as a solicitation of or suggestion for any agreed-upon course of conduct or concerted action of any sort.

Copyright 2017 by TAPPI, all rights reserved. For copyright permission to photocopy pages from this publication for internal or personal use, contact Copyright Clearance Center, Inc. (CCC) via their website: www.copyright.com. If you have questions about the copyright permission request process, please contact CCC by phone at +1 978 750-8400. To obtain copyright permission to use excerpts from this publication in another published work, send your specific request in writing to Editor, TAPPI JOURNAL, 15 Technology Parkway S., Suite 115, Peachtree Corners, GA 30092, USA; or by fax to +1 770 446-6947. Send address changes to TAPPI, 15 Technology Parkway S., Suite 115, Peachtree Corners, GA 30092, USA; Telephone +1 770 446-1400, or FAX +1 770 446-6947. www.tappi.org

Guest Editorial



SESHADRI RAMKUMAR
Chair, TAPPI NET Division

The next act for nonwovens

What drives the nonwovens sector? Consumer goods that enhance health and improve lifestyles. Products such as diapers, wipes, and hospital goods have been the main pillars of the industry. In addition, nonwovens are used in semi-durable and durable goods, such as products for construction, infrastructure, and automobiles, to name a few.

The single-use nonwovens sector is volume oriented and therefore depends on its consumer base. Population growth and the economy of nations are the drivers here. The industry has performed well because of these drivers and is predicted to have an optimistic future.

Historically, the nonwovens industry's annual growth rates have surpassed the GDP growth of nations in their respective regions. According to Brad Kalil, director of Market Research and Statistics at Cary, NC-based INDA, the Association of the Nonwoven Fabrics Industry, global growth is forecast to be about 5.7%. This figure is based on INDA and EDANA Worldwide Outlook for the Nonwovens Industry. Asia will lead the global growth, with China and India projected to have annual growth rates of about 7% and 8%, respectively.

Growth numbers are encouraging in regions where growth is happening from a small base, and consumer acceptance and consumer goods are the key drivers there. In well-established and mature markets like North America and Europe, finding new markets for nonwovens by developing products that have functional and high-performance properties and varied applications will be the driver. Therefore, having strategies that focus on regional expectations throughout the world, as well as on consumer trends in terms of products and cost, will benefit our industry.

Double-digit growth in India

In developing markets like India and the Middle East, demographics, population numbers, and economic scenarios will influence nonwovens growth. For example, India's technical textiles sector, with which the nonwovens industry is grouped, will have double-digit growth, as I predicted in this report, "India Rising: Opportunities in Nonwovens and Technical Textiles." Major global organizations in the field of technical textiles now accept that the growth in India will be in double digits due to a rising middle class population and government policy, such as the National Mission on Technical Textiles.

So far, the growth in India has been pushed by investments in spunbond and spunlace technologies with a few European lines and a number of spunbond lines from China, predominantly feeding to the packaging sector. However, future growth will be fueled by developing the "converting sector," which consumes the roll goods to develop products that are available for consumer consumption at retail outlets.

The cost factor in developing countries

An important aspect for our industry to consider, if they choose to penetrate into developing markets, is the cost factor. Converted nonwoven products that can be absorbed by lower- and upper-middle class populations in growing regions of the world will provide opportunities for our industry. Demographics, rising income levels, and growing awareness about health needs and hygiene will support the industry, which necessitates the need to work with governments and non-government organizations (NGOs) to promote the usefulness of nonwoven products.

Outside parties recognize potential in nonwovens

Interestingly, technocrats from other disciplines are turning their attention to nonwovens and technical textiles. Venkatakrishnan Ramanujan is a Chennai, India-based IT specialist who founded WELLGRO Tech to develop products for the nonwovens sector. According to him, "with the current economic scenarios and political situations affecting the growth of IT sector in those markets where there are layoffs, I was looking to start a new venture and consulted with industrial advisors as to where I should stand-up uniquely among industries with affordable investments, and they advised to choose nonwovens. I considered nonwovens after a self-study, which led me to go into developing fibers and products for the nonwovens industry."

Considerations for developed economies

Turning attention to the diversification of the nonwovens sec-

tor in developed economies, the industry has to focus its effort to move the industry into becoming an engineered fabrics sector. New products for applications in performance apparel, automotive, energy and defense sectors have to be considered and developed. Borrowing ideas and technologies from allied and science disciplines like bioengineering, nanotechnology, and advanced manufacturing will help. For example, plasma surface processing can bring some functional properties to nonwovens. According to Rory Wolf, business unit manager at ITW Pillar Technologies, "atmospheric pressure plasma, surface cleaning, etching, deposition, cross-linking, surface roughening, and grafting are possible using non-polymerizable gases or gas mixtures to introduce additional value-added surface properties to nonwovens."

The next phase of the nonwovens sector should have different strategies based on location and consumer expectations. Certainly, investments in research and development that can lead to both incremental and disruptive technologies and products are needed. Industry-institute cooperation is the need of the hour, which is a cost-effective way to advance the field. **TJ**

Seshadri Ramkumar is a professor in the Nonwovens & Advanced Materials Laboratory at Texas Tech University in Lubbock, TX, as well as Chair of the TAPPI NET Division. You may contact Dr. Ramkumar for the full version of his report, "India Rising: Opportunities in Nonwovens and Technical Textiles." Email him at s.ramkumar@ttu.edu.

For information about publishing nonwovens research in TAPPI Journal*, please contact* TJ *Editorial Board Member Gaurav Pranami, gpranami@gmail.com, or submit your content at www.editorialmanager.com/tappi.*

Visual discrimination of hygiene tissue softness in the absence of haptic feedback

JESSICA CARETTE, PIERRE-MAJORIQUE LÉGER, AND SYLVAIN SÉNÉCAL

ABSTRACT: Our perception of the softness of materials is dominated by the subjective interpretation of haptic stimuli — touch. Although softness is defined by the way a material deforms when force is applied, other sensorial inputs, such as vision and hearing, can be used to complement haptic feedback or when the material cannot be touched. Surface and bulk softness elements of hygiene tissue, such as surface roughness, embossing pattern, and bulk can be assessed visually. Softness is reported as the number one desired quality of hygiene tissue. So, it is of paramount importance to understand the criteria a consumer uses to judge softness visually. Consumers must rely on these other non-tactile senses at point-of-purchase or in e-commerce because they cannot interact with a product to judge the softness. This study proposes that a consumer can accurately gauge softness by sight alone, and that factors such as color tone, embossing, and image quality all affect the perception of softness. Stiffness and mechanical properties of the sheet cannot be observed by eye and can contribute to errors in visual judgement. We conducted an experiment using a complete pair ratio (round-robin) type comparison to evaluate the perceived softness of altered images of hygiene tissue with unaltered images. Images of hygiene tissue were altered to represent different lighting conditions or product color and digital image degradation. Our results suggest that yellow hygiene tissue is perceived as less soft than blue, and un-embossed tissue as less soft that embossed tissue. Reducing the image resolution to 10% of the original did not negatively affect the perception of softness.

Application: In product development, color and embossing pattern can be manipulated to influence the consumer's perception of product softness. Images displayed digitally can be optimized in a similar manner.

Softness is the most important quality in hygiene tissue, as judged by consumers who did not select price as the number one criteria in purchasing decisions [1]. Softness can be defined as "the subjective impression of the physical compressibility and deformability of objects" [2]. Thus, our perception of softness is dominated by the sense of touch. Surface softness of tissue paper can be influenced by the stiffness and coarseness of fibers [3], the number of fibers that stick out [4], the creping frequency and shape of the crepes [5,6], roughness profile [7], and characteristics of the embossing or sheet molding. Bulk softness is influenced by the density and stiffness of the sheet and can be inferred by the resistance to flexing or compressing the sheet. Stiffness is the in-plane resistance to bending and is influenced by the sheet strength via chemical bonding or mechanical modification of the fibers (refining) and fiber type.

Softness is the subjective interpretation by a human brain of a complex set of sensorial stimuli [8]. Haptics, the study of tactile stimuli, can explain much of the differences in human perception of softness of tissue products, yet we use a broad range of senses to judge the world around us. Vision, hearing, and touch work together to give a subjective representation of the materials with which we interact [9]. When we rub our hands over the surface of sandpaper, a sound is generated; the finer the grain, the quieter the sound produced. Likewise, crumpling a stiff tissue will produce a louder sound than a supple one. Vision and hearing have been calibrated with our tactile information through repeated interaction of soft and not soft materials.

In the absence of haptic feedback, as in an online context, customers can only rely on visual perception to evaluate softness. Global e-commerce sales are growing at a rate of 15% annually [10], and the ability for hygiene tissue manufacturers and distributors to make their product visually appeasing will be a key differentiator. To do so, it is crucial to develop a richer understanding of how images of hygiene tissue influence softness perception. Several studies have been conducted to understand the influence of vision on the sense of touch and how the two senses work together. For instance, Cellini et al. [11] found that the addition of visual information when pressing a button, greatly increased one's ability to estimate the softness or resistance of the object. Ernst and Banks [12] concluded that visual and haptic information work together to provide an accurate interpretation of physical characteristics of an object. Tiest and Kappers [13] found that subjects generally were good at estimating surface roughness of everyday materials, but that different subjects ordered the samples using different criteria. Norman et al. [14] found that vision and touch have functionally overlapping, but not necessarily equivalent, representations of three-dimensional shapes.

To our knowledge, no studies have yet to investigate the

extent to which a consumer can visually discriminate hygiene tissue softness when they cannot physically interact with the product, or which image characteristics influence a customer's perception. Our hypotheses for this study were as follows:

1. A consumer can visually discriminate and correctly sort images of high, medium, and low softness hygiene tissues.
2. A consumer can differentiate between a large difference in softness and a small difference through visual observation.
3. The disparity in softness between two samples is inversely proportionate to the decision time.
4. A consumer interprets images of hygiene tissue that are yellowish as less soft than images with a pure white or bluish tone.
5. The quality (resolution) of the image of hygiene tissue is inversely proportionate to the subject's interpretation of softness.
6. The subject's inherent precondition for tactile interaction, known as need for touch, will influence their decision time to visually discriminate softness.

To investigate these issues, we conducted a laboratory experiment with 17 participants who visually examined altered and unaltered images of hygiene tissue and selected the softest looking image in pairs. Information from their selections was analyzed to test our hypotheses about the influence of color, image resolution, and embossing on the perception of softness and decision time.

METHOD

Experimental design

We used a within-subject experimental design to evaluate 14 different combinations of visual and physical stimuli. These included three softness ranges (high, medium, and low) combined with four resolutions (unaltered, blueish, yellowish, and low resolution), plus two un-embossed samples of high and low softness. **Table I** lists the images and corresponding characteristics. Paired-comparison (or round-robin) type experiments were used to assess the perception for each stimulus by each participant. The set of 91 pairs (each image displayed in a pair with every other image) was presented to participants twice for control purposes. Participants were asked to make a choice of which image appeared to be softest in each pair. They were then asked to qualify their response by indicating the relative magnitude of the difference in softness between the two presented stimuli. The softness selections and differences in magnitude were converted into a visual softness scale.

Experimental stimuli

Three embossed retail bath tissues were chosen to represent high, medium, and low softness (two national brands and one private label corresponding to two conventional sheets and one through-air-dried product). An away-from-home, flat sheet, un-embossed jumbo roll bath tissue was used as the medium softness un-embossed sample. A high softness facial tissue was used as the high softness un-embossed sample. Samples were selected to fit into one of three softness brackets, as determined by the handfeel value using the "TPII" algorithm from the tissue softness analyzer (TSA) from Emtec Electronic GmbH (Leipzig, Germany).

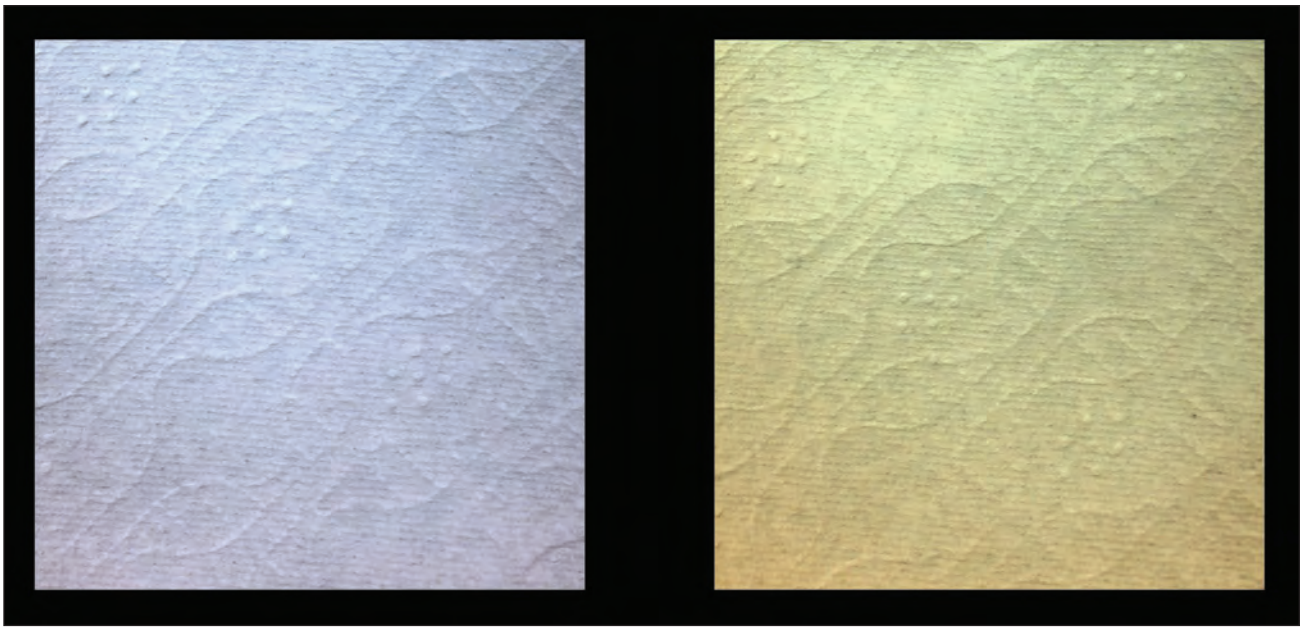
Sample Identifier	Sample Description
A	High softness – unaltered
B	High softness – low resolution
C	High softness – bluish
D	High softness – yellowish
E	Medium softness – unaltered
F	Medium softness – low resolution
G	Medium softness – bluish
H	Medium softness – yellowish
I	Low softness – unaltered
J	Low softness – low resolution
K	Low softness – bluish
L	Low softness – yellowish
M	High softness, un-embossed
N	Medium softness, un-embossed

I. Fourteen stimuli of high, medium, and low softness were presented to the participants.

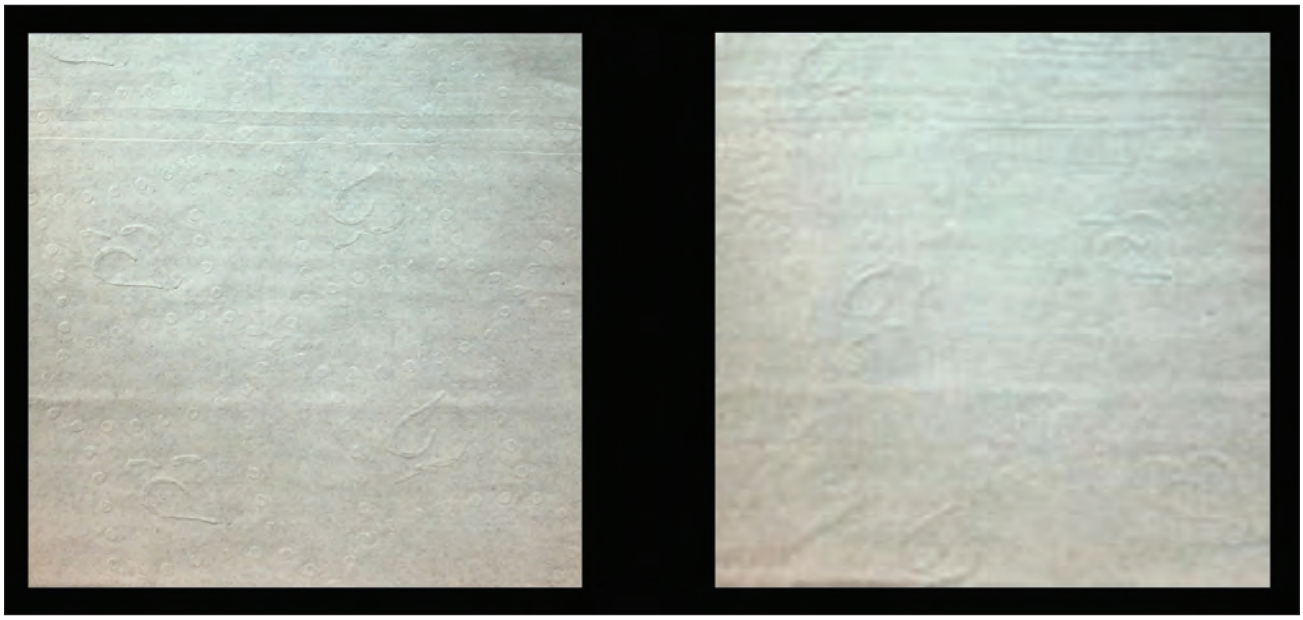
The advantage of presenting stimuli on a digital monitor instead of displaying the physical samples in front of the participants is that the images can be altered to reflect different conditions, such as lighting and image quality (resolution). The products were photographed on a black background with constant lighting conditions and then digitally altered in three ways:

1. The color tone was shifted to the blue region, as seen in **Fig. 1** (Adobe Photoshop's express temperature adjustment -15).
2. The color tone shifted to the yellow region (Adobe Photoshop's express temperature adjustment +15).
3. The image resolution was reduced ×10 by reducing the size of the image to 10% of the original size, as seen in **Fig. 2**.

The un-embossed samples were unaltered. The images were digitally cropped to 9 cm × 9 cm, with no edges or perforations visible, and presented two at a time, side-by-side on the monitor (**Fig. 3**).



1. Image altered to be more bluish on the left and yellowish on the right.



2. Original unaltered image on the left and 10% reduction in resolution on the right.

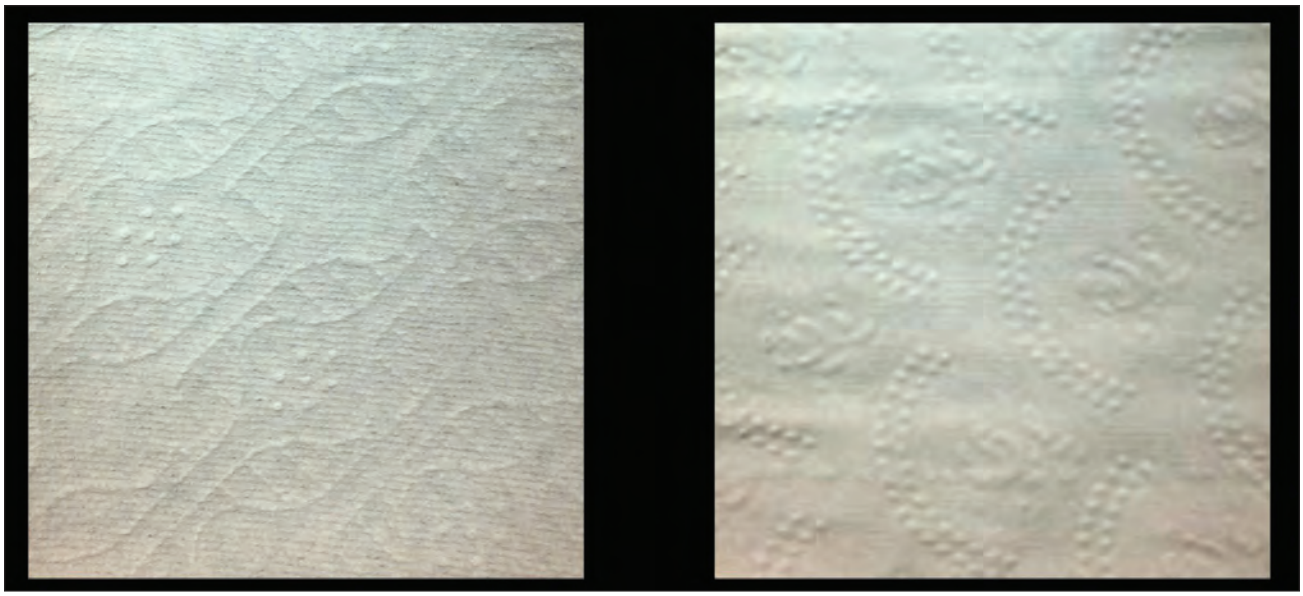
Participants

Participants were solicited from the research panel of our institution from among more than 3600 students, staff, and members of the public. Participants were compensated for their participation with a gift certificate of $20 for the university bookstore. To exclude confounding effects, the following exclusion criteria were used for subject recruitment:

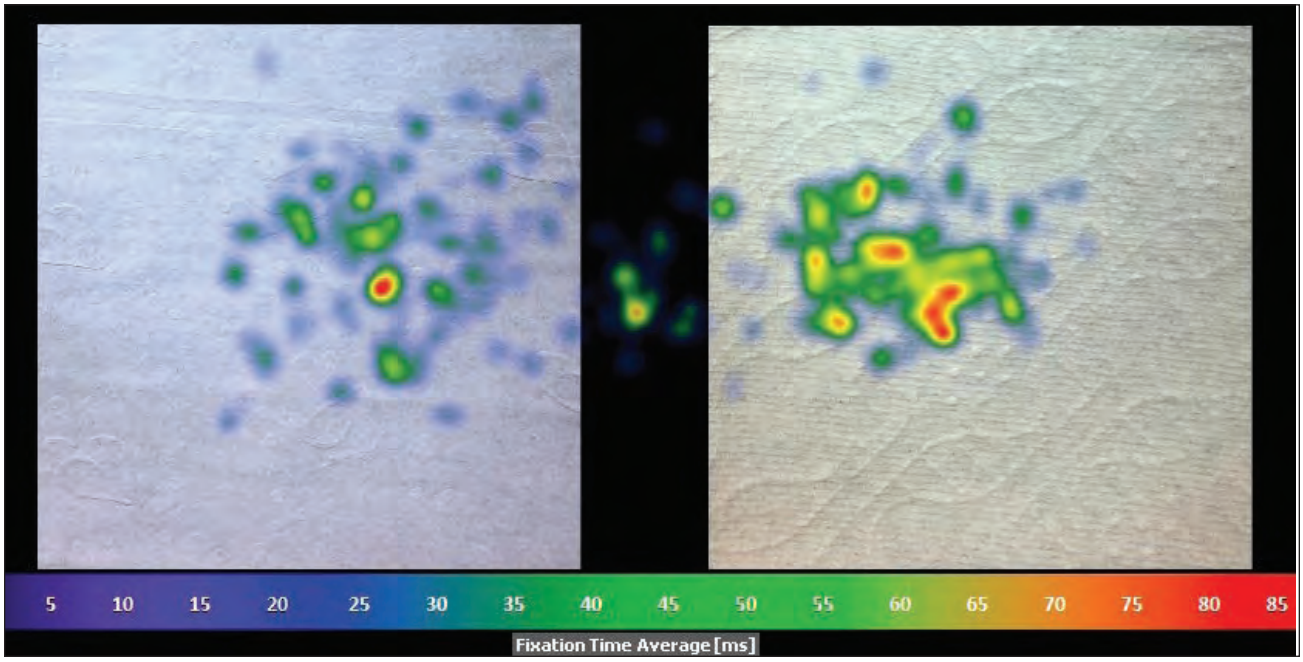
- The participant can work at a computer without the need of corrective lenses or contact lenses.
- The participant has not been diagnosed with color blindness.
- The participant does not have a cardiac stimulator.
- The participant has not been diagnosed with a neurological or psychiatric disorder.
- The participant has not undergone laser vision correction.
- The participant does not have astigmatism.
- The participant does not suffer from epilepsy.
- The participant has no diagnosed health problems.

Instruments and measures

We used oculometry (i.e., eye tracking) to track the attention of participants when presented with images of hygiene tissue. Oculometry records the eye position or point of gaze



3. Participants viewed all pair combinations of the 14 stimuli (91 pairs) arranged on a black background. Participants were asked to look at the images and then decided which image appeared to be the softest.



4. Heat maps were used to discover how much of the image the participants looked at before deciding. In this typical example, participants explored less than one quarter of the image before deciding about the softness. The concentration on fixation in the center between the two stimuli is an artifact of the gaze being directed to the center of the screen before each stimulus presentation.

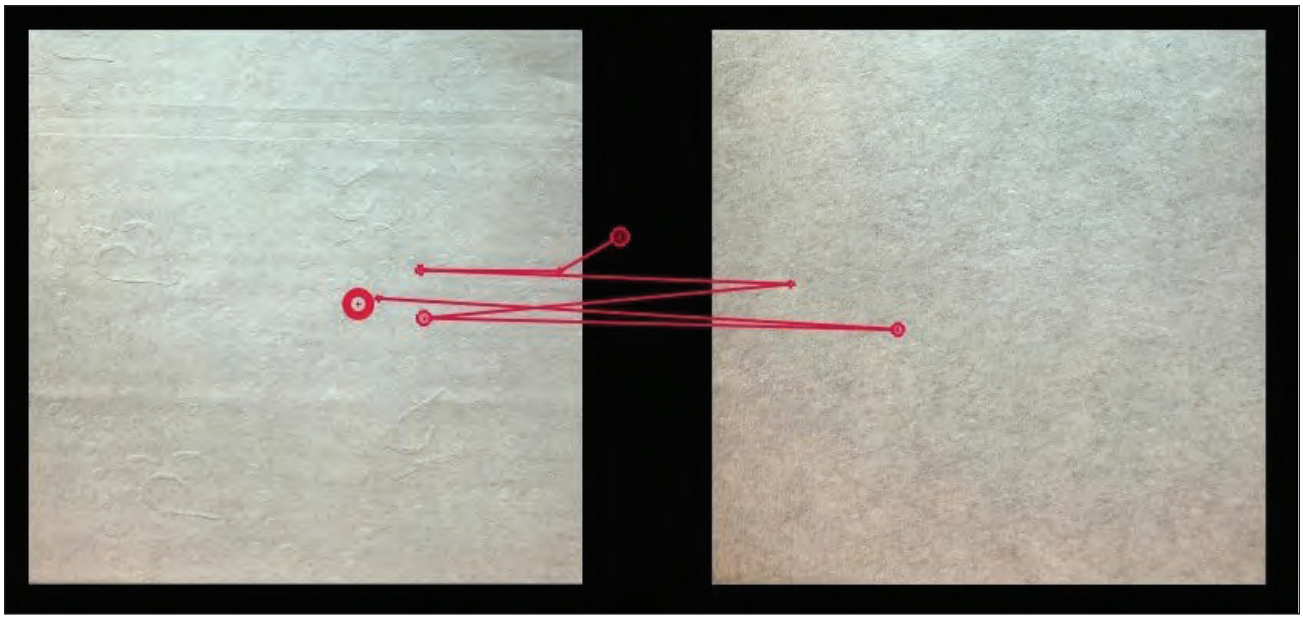
and movement on a monitor [15]. Near infrared light is shined into the pupils of the observer and the reflections off the cornea are tracked by a high-resolution camera. We used passive oculometry, where an instrument is mounted onto a monitor and the observer is stationary. We measured the amount of time a participant looked at each image, to identify what areas the participant spent the most time viewing, and to count how many times the participant scanned between images. **Figures 4** and **5** show the visual attention results of a typical pair of images.

PROCEDURE

The study was broken into five parts:

1. Calibration
2. Paired comparisons block 1
3. Break
4. Paired comparisons block 2
5. Questionnaire

To start, participants sat in front of a monitor fitted with an



5. This scan path image of a pair of stimuli is typical for all the pairs. Participants looked back and forth between the two images several times in the same areas before deciding.

SMI RED250 mobile oculometer (SensoMotoric Instruments; Berlin, Germany). The chair was positioned so that the participant's eyes were in the middle of the screen and 60-70 cm away from the oculometer. Positioning of the participant was aided by visual feedback displayed on the monitor. A pre-programmed eight-point calibration associated the position of the participant's cornea with their gaze on the screen. Calibrations were repeated until an error of less than 0.5° was noted in both eyes. Most participants required only one calibration, but two needed to repeat the exercise three times. The calibration is sensitive to the position of the participant's eyes; therefore, throughout the experiment, participants were observed and reminded to sit up straight in the chair, if required.

Participants were instructed to look at the images presented and indicate which image in each pair appeared softest. Participants were not given further instruction on how to identify the stimuli or given a definition of softness; therefore, each participant used a personal preference to guide their perception of softness. Participants were not presented the stimuli physically; their only interaction with the products was visual inspection. A participant indicated his or her choice by selecting a number on a numerical keypad provided. The participant selected 1 to indicate that the image on the left as the softest and 3 to select the image on the right as softest.

After selection of the softest image, a second screen was presented to the participant. For that, each participant was asked to qualify their answer by indicating the difference in softness between the two previously observed images. The options were: small, medium, and large. The participant selected 1 on the keypad to indicate there was a small difference in softness between the two previous images, a 2 for a medium difference, or a 3 for a large difference. The participants used the same keys on a number pad to select which image appeared softest (left or right with number keys 1 and 3) and to qualify the difference in softness (1 for small, 2 for medium, and 3 for large). Using the same set of keys eliminated the need for the participants to move their hands and look at the keyboard and then reposition their view for each screen. The effect of parity was accounted for in the qualifying step in which a response of 1 returned a null result for both stimuli. In the first block, 91 pairs of images were presented, followed by a short pause of 3 min, during which videos played and the participants could relax their eyes and arms. The pairs of images were then presented a second time, in random order, with the left and right orientation of the images reversed (block 2).

The procedure was followed by a questionnaire asking about participants' purchasing household habits and personal demographics. Responses were also used to assess the participant's "need for touch" (NFT). NFT is described as the "preference for the extraction and utilization of information obtained through the haptic system" [16,17]. Previous research has used this scale in an online context [18]. Participants report to what degree they agree with 12 statements about interacting and purchasing products. NFT is composed of two dimensions: autotelic and instrumental. The autotelic dimension relates to touch as the activity viewing shopping as a hedonic activity seeking sensory stimulation and enjoyment [19]. A person with a high autotelic NFT would agree with statements such as, "Touching products can be fun and I like to touch products even if I have no intention of buying them." The second dimension, instrumental, relates pre-purchase touch as a goal-oriented activity. A person who has a high instrumental NFT touches products to evaluate their quality and would agree with statements such as, "I place

x_{ij}	A	B	C	D	E	F	G	H	I	J	K	L	M	N	Geometric Mean $\bar{x}_i$	Ratio Geometric Mean RGM_i	Linear Non-standard ln RGM_i	Scaled Standard Values
A	1	1	2	1	1	2	1/2	1/2	1/3	1/3	1/3	1/3	1/2	3	0.75	0.050	-3.0	95.2
B	1	1	1	1	1/2	1/2	1/2	1/2	1/3	1/3	1/3	1/3	1/2	1/3	0.53	0.035	-3.4	114.4
C	1/2	1	1	1	1/2	1/2	1/2	1/3	1/3	1/3	1	1/3	1/2	1/3	0.53	0.035	-3.4	114.4
D	1	1	1	1	1/2	1/2	1/2	1/2	1/3	1/3	1/3	1/3	1/3	1/3	0.51	0.034	-3.4	116.0
E	1	2	2	2	1	1	1	1	1	1/2	1/2	1/2	1	1	1.00	0.066	-2.7	79.8
F	1/2	2	2	2	1	1	1	1	1/2	1/2	1/2	1/2	2	1	0.95	0.063	-2.8	82.5
G	2	2	2	2	1	1	1	1	1/2	1/2	1/2	1/2	1	1	1.00	0.066	-2.7	79.8
H	2	2	3	2	1	1	1	1	1/2	1/2	1/2	1/2	1	1	1.03	0.068	-2.7	78.3
I	3	3	3	3	1	2	2	2	1	1	1	1	1	1	1.59	0.105	-2.3	54.9
J	3	3	3	3	2	2	2	2	1	1	1	1	1	1	1.67	0.110	-2.2	52.2
K	3	3	1	3	2	2	2	2	1	1	1	1	2	1	1.62	0.107	-2.2	53.7
L	3	3	3	3	2	2	2	2	1	1	1	1	2	1	1.75	0.115	-2.2	49.5
M	2	2	2	3	1	1/2	1	1	1	1	1/2	1/2	1	1	1.08	0.071	-2.6	75.6
N	1/3	3	3	3	1	1	1	1	1	1	1	1	1	1	1.17	0.077	-2.6	71.4

II. Example of comparison matrix. The 14 image identification letters are inscribed in the columns and rows and the result of the difference magnitudes are entered into the matrix. An entry above 1 indicates that the row was selected as softer than the column; the inverse is true for numbers between 0 and 1. An insignificant difference between the softness of two stimuli results in an entry of 1. Note that columns and corresponding rows are reciprocals of each other. For the pair AC, the participant indicated that A was softest with a medium difference (2). For the pair CH, H was selected as softest with a large difference (3). The geometric mean or the nth root of the product of all entries in the row is inversely proportionate to the participant perceived softness. The ratio geometric mean normalizes the results to between 0 and 1 so the logarithm can be taken and produce a linear result. The final scaled standard values are achieved from the slope, m, and intercept, b, of a calibration curve between the scaled standard values and the tissue softness analyzer results.

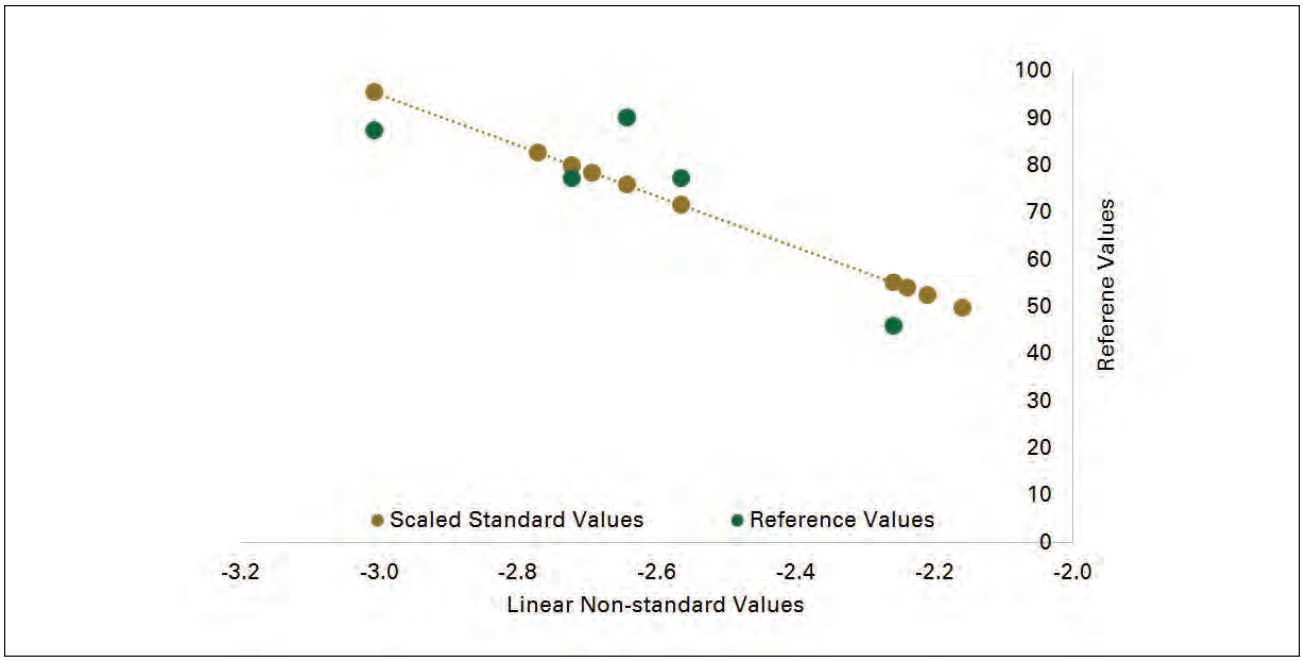
more trust in products that can be touched before purchase," and "If I can't touch a product in the store, I am reluctant to purchase the product" [20].

Measurement

We used numerical inputs to quantify the softness perceptions of each participant. We built a comparison matrix to calculate the visual softness of each image on a ratio scale. The analytic hierarchy process [21] was used on the scaled, paired comparisons [22]. An n × n matrix was built for each participant, where n is the number of stimuli (14 in this case). The 14 images were given codes A-N, corresponding to each row and column of the matrix. The softness preference selected by the participants was scaled by asking the participant to qualify his or her answer by announcing the degree of difference on a 3-point scale in the evaluated attribute (softness) [23]. The preference and magnitude estimation data x_{ij} are mapped into the n × n matrix. The diagonal is attributed the value of 1 because pairs of the same have minimum difference in softness. For each matrix entry, if the stimulus in the row was chosen as softest, the qualification rating was entered as is. If the column was selected as softest, the inverse fraction of the qualification was entered.

To convert the softness selection and magnitude estimations into the same scale as the TSA data, the geometric mean of the pair values was calculated, converted into a linear scale, and a calibration curve was built. The geometric mean of all the entries in a row was calculated by finding the n^{th} root of the product of the row.

The geometric mean of the participant selected preferences and difference magnitudes are used to convert the participant data into a visual softness scale (Eq. [1]):



6. Calibration curve to convert linear non-standard values to the 0-100 tissue softness analyzer scale. The slope and intercept are individual to each participant.

$$Geometric\ Mean = \bar{x}_i = \left(\prod_{j=1}^{14} x_{ij}\right)^{1/14}$$

The geometric means are then normalized between 0 and 1 by dividing by the sum of all the geometric means. (This can also be achieved by dividing by the maximum geometric mean in the series.)

The ratio of the geometric mean is used to normalize data to between 0 and 1 (Eq. [2]):

$$Ratio\ Geometric\ Mean = RGM_i = \bar{x}_i / \sum_{i=1}^{14} \bar{x}_i$$

The ratio geometric mean can then be converted into a linear scale by taking the natural logarithm. The linear scaled values are referred to as the linear non-standard values (see **Table II**). The linear non-standard values are converted to the same scale as the TSA data by building a calibration curve with the linear non-standard values on the x-axis and TSA values on the y-axis (**Fig. 6**). A linear regression curve was fitted to each participant's data and scaled standard values were calculated from the slope and intercept.

The analytical hierarchy process also allows us to track participant performance. Some basic assumptions are made about stimuli, such as:

- Each stimulus is presented without variation to each participant.
- Handfeel value of a product can be expressed by a single real number.
- Participant accurately reports their preference and selection.

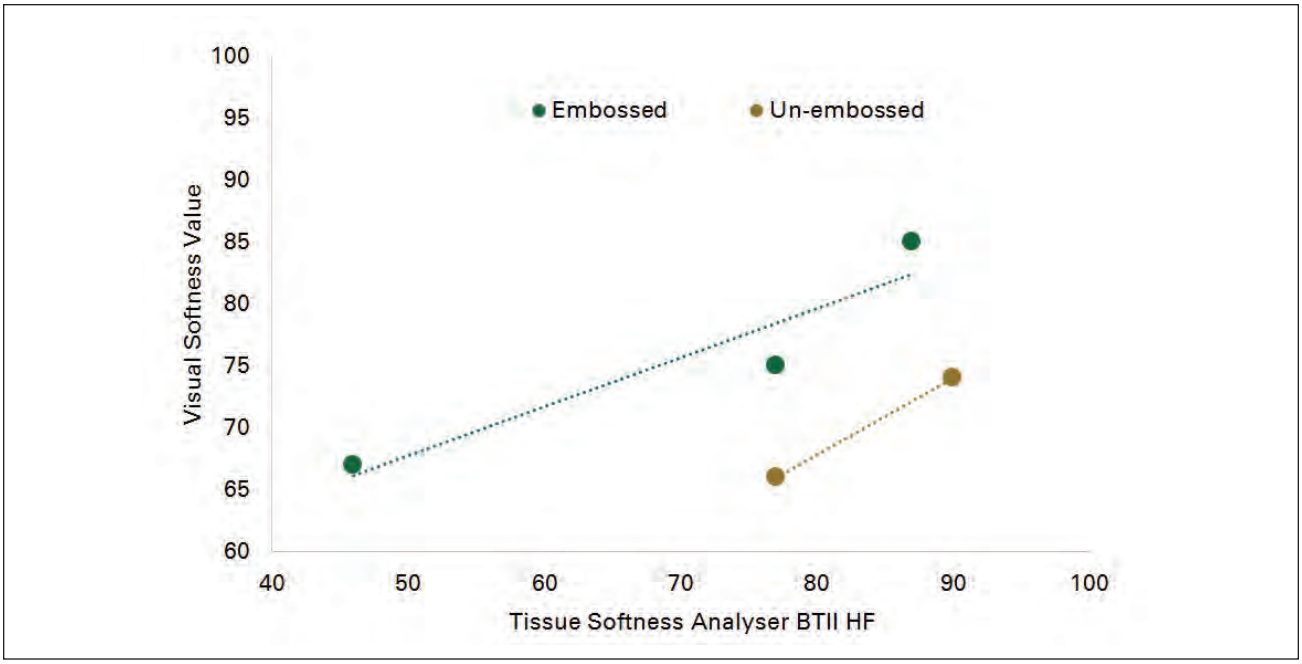
A perfectly consistent comparison matrix would have an eigenvalue equal to the number of stimuli. All panel-type tests have some level of inconsistency because of the subjectivity of the test. Thus, the largest real eigenvalue of the comparison matrix is proportionate to the inconsistency of the participant, while the minimum eigenvalue (λ) is equivalent to the number of stimuli [24]. One participant with an inconsistency significantly higher than the group was removed from calculations. In our case, the first participant had $\lambda = 15$ and the average was 14.5, with a standard deviation of 0.3; thus, participant 1 was excluded from all further analysis.

Participants were also evaluated on discordance or how well they agreed with the group. Discordance is the relative distance between a person's responses and the group's average. It is expressed as the sum of squares of the difference between a value, x, and the average, $\bar{x}$, divided by the number of stimuli, n, in Eq. (3):

$$discordance = \frac{\sum(x - \bar{x})^2}{n}$$

RESULTS AND DISCUSSION

Our first and second hypotheses were confirmed with the comparison data of the unaltered embossed stimuli. Participants rated the three unaltered embossed stimuli in the correct order and with a relative magnitude similar to the TSA softness (**Fig. 7**; **Table III**). With only three points, the fit-



7. Unaltered embossed stimuli were ranked with a similar magnitude as the tissue softness analyzer (TSA) handfeel (HF) value; the regression coefficient is 82%. The un-embossed stimuli were perceived as less soft than the embossed samples for equivalent TSA HF values.

Softness	Visual Characteristic	Tissue Softness Analyzer "TPII" Handfeel Value	Visual Softness Value	Standard Deviation	Significance
High	Bluish		90	9	
	Unaltered	87	85	5	A
	Yellowish		88	10	B
	Low resolution		88	9	AB
	Un-embossed	90	74	10	
Medium	Bluish		74	5	C
	Unaltered	77	75	4	
	Yellowish		72	3	
	Low resolution		74	4	C
	Un-embossed	77	66	3	
Low	Bluish		68	7	DE
	Unaltered	46	67	6	D
	Yellowish		66	8	E
	Low resolution		68	7	DE

III. Softness comparison results. Results with a significant difference in response populations are represented with the connected letter method. Stimuli not connected by the same letter are significantly different per the non-parametric Wilcoxon two-tailed test with a confidence level of 0.1. For example, the high softness unaltered and low-resolution visual softnesses were not significantly different, with results of 85 and 88, respectively.

ness of the linear regression is artificially high, with a regression coefficient of 88%. The reported visual softness of three embossed samples were significant, with p-values between high (H) and medium (M) = 0.0005, high and low = 0.0004, and medium and low = 0.01, with n = 16.

Opacity might play an important role in visual perception of softness. The low softness samples, both embossed and unembossed, were noticeably less opaque than the medium and high softness samples. Basis weight has an indirect effect on softness and can be inferred from the opacity of the sheet. For equivalent bulks, a high basis weight sheet will have a higher caliper and therefore deform more under stress, resulting in a higher handfeel value. We concluded that the participants associated thin, low basis weight as not soft. Most low basis weight, away-from-home, one-ply bath tissues are indeed much less soft than any two-ply retail brand.

Our third hypothesis was inconclusive. The decision time for stimuli pairs was not proportionate to the perceived difference in softness. We hypothesized that a smaller difference in softness would result in a longer decision time. The only significant difference was for pairs with a large difference in softness (**Table IV**). It took participants more than 1 s longer ($p = 0.004$) to decide for large difference pairs than for medium difference pairs.

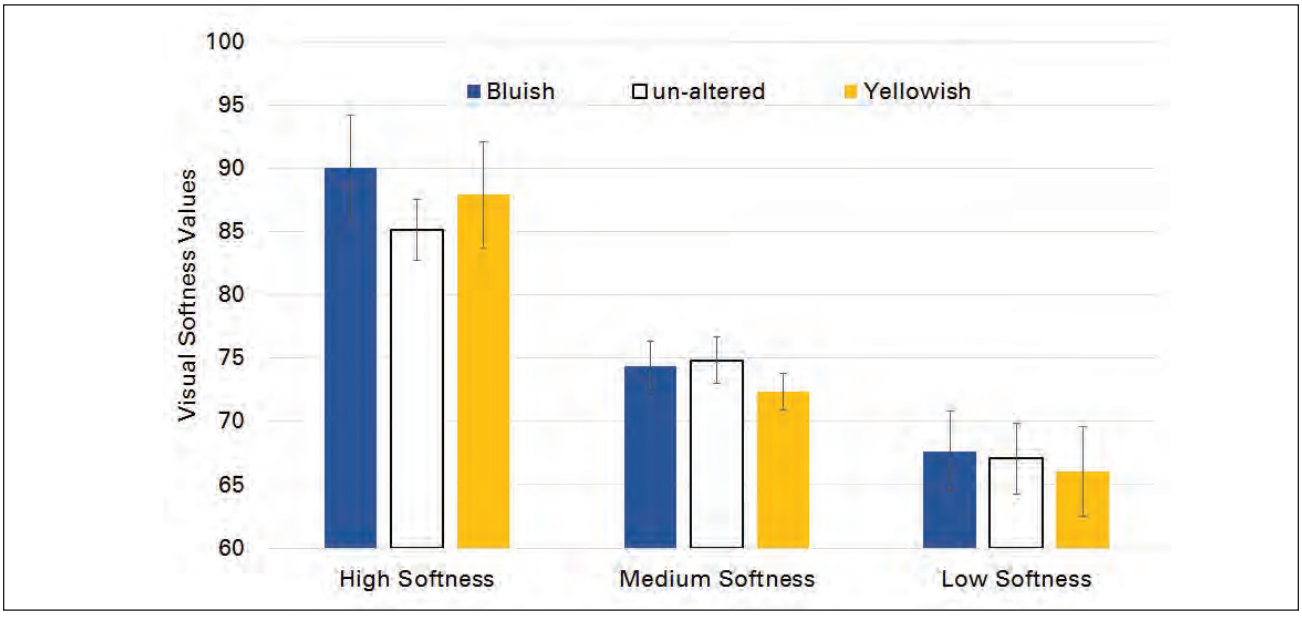
Participants perceived the yellowish stimuli as less soft than the bluish stimuli, supporting the fourth hypothesis (i.e., a consumer interprets images of hygiene tissue that are yellowish as less soft than images with a pure white or bluish tone). The yellowish images were perceived as 2 points less soft than the bluish images (Table II; **Fig. 8**). Only the results for the high and medium samples were significant, with p-values of 0.003 and 0.01, respectively. Color, having no physical effect on fiber or sheet structure, does not directly affect softness. The results of the color comparison seem to show that the participants have a positive color bias toward blue. Premium and ultra-premium hygiene tissue is bleached, and some even contain optical brightening agents to shift the emitted spectrum toward blue. Consumers have been habituated to associate this color with quality and softness and the contrary for yellow-toned tissues. Psychologically, yellow induces negative feelings associated with unpleasant feelings of sickness [25,26].

Some of this calibration is culturally acquired through the availability of materials. In North America, document paper

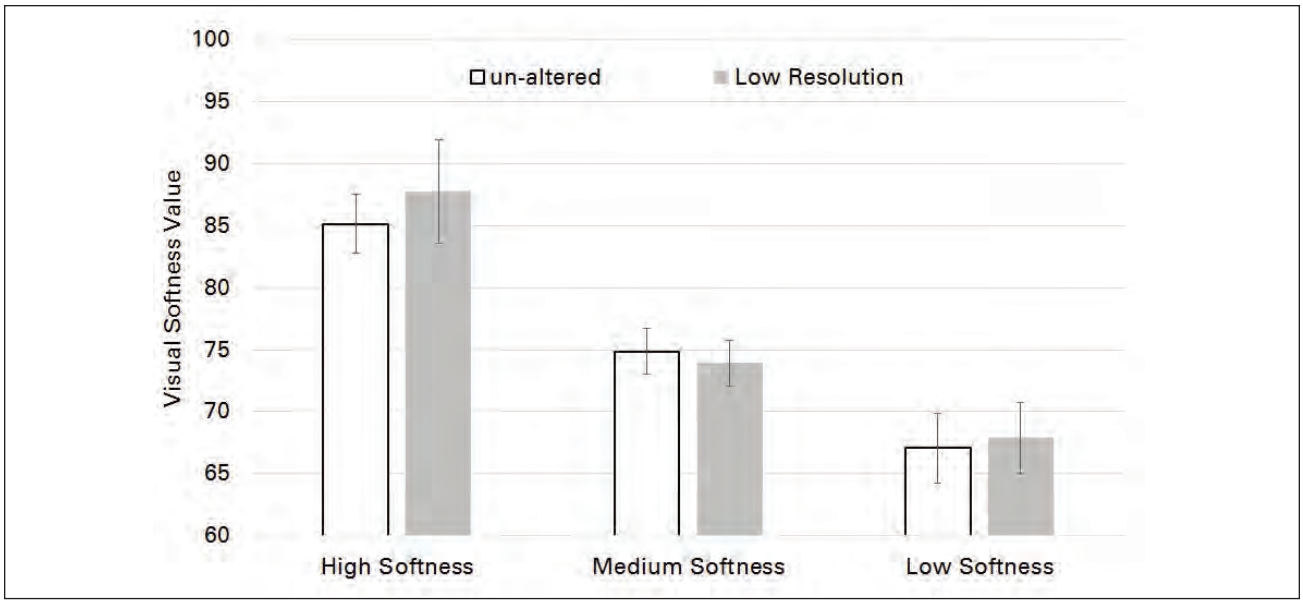
Difference in Perceived Softness of Stimuli Pairs	Determination Time, ms	Standard Deviation	No.	Significance*
Small	4243	1154	582	A
Medium	4316	1220	544	A
Large	5251	1630	295	

*Stimuli not connected by the same letter are significantly different per the non-parametric Wilcoxon two-tailed test with a confidence level of 0.1.

IV. Stimuli pairs with a large difference in perceived softness had a longer decision time than medium or small difference softness pairs. The difference was insignificant between small differences and medium differences.



8. Yellowish was perceived as less soft than bluish stimuli; however, the unaltered image was in one case perceived as softer than blue, and less soft in two other cases.



9. The effect of resolution was small, between one and three handfeel points.

	Determination Time, ms	Standard Deviation	No.
Low NFT (≤4)	3389	705	6
High NFT (<4)	3858	1125	10
Mann–Whitney U test	p-value	0.5	

V. A high or low "need for touch" (NFT) did not influence the participants' decision time.

and some hygiene papers are treated with optical brightening agent to shift the reflected light spectrum toward blue, which is viewed as true white or bright white. In Asia, yellow tones are preferred. Other sensorial associations may be made with tissue products because the materials used have an inherent softness component. Chemically bleached virgin fibers are preferred for soft tissue because of their low coarseness compared with recycled fibers, high yield pulp, agricultural fibers, or unbleached chemical fibers. Deinked pulp has specks of unremoved ink and the color is greyer than bleached pulps and high yield pulps, and agricultural fibers are often more yellow than bleached kraft. After repeated exposures, consumers might associate yellow or grey as less soft than pure white.

The fifth hypothesis can be altered to read that decreasing the resolution of an image of hygiene paper to 10% its original size does not negatively influence visual softness perception. The lower resolution stimuli were perceived as soft or softer than the full resolution images (**Fig. 9**). The loss in detail blurs any angular structures and smooths out the noise and apparent roughness.

Participants were divided into two groups of high and low NFT average scores. We might assume that a person who has a high NFT might take longer in making decisions about tactile quantities than someone who does not put much importance on such factors. However, contrary to our sixth hypothesis (i.e., the consumer's need for touch will influence their decision time to visually discriminate softness), results showed no correlation between decision time and NFT ($p = 0.5$) (**Table V**).

CONCLUSIONS

Our sense of softness, although dominated by haptic feedback, is also influenced by the other senses. Through repeated exposure to tissue products of varying softness, humans have been trained to associate certain aspects of the material (e.g., color, embossing, transparency, fuzziness) with softness. In this way, we can correctly identify the softness of a narrow set of stimuli by visual inspection only. Manufacturers and retailers can use this information to better present and market their products to reflect the desired attributes. The participants of this study perceived yellow-hued images of hygiene paper as less soft than blue-hued images. A reduction in resolution quality to 10% of the original size did not negatively affect softness perception.

The techniques used in this study can be applied to reveal the relationship between different sensorial stimuli and determine the criteria by which humans judge materials. Toyota, for example, used similar techniques to help develop leather for luxury automobile interiors that looks soft [27]. To further confirm these findings, the effects of dirt count, greyness, broader ranges of softness, more embossing patterns, and the difference between structured and conventional sheets should be examined, along with handfeel panel data and consumer preference panel data. **TJ**

ACKNOWLEDGEMENTS

The authors would like to thank Carl St-Pierre and the staff of Tech3lab for their help.

LITERATURE CITED

1. Bennett, J., and Blamey, R., *The Choice Modelling Approach to Environmental Valuation*, Edward Elgar Publishing Ltd., Cheltenham, England, 2001.
2. Di Luna, M., *Multisensory Softness*, Springer, London, England, 2014, p. xi.
3. Weißenbach, A., "Benchmark of pulps combined with softness measurements," Heinzel Group, Vienna, Austria, 2010.
4. Raunio, J. and Ritala, R., *Meas. Sci. Technol*. 24(12): (2013).
5. Stitt, J. and Richardson, H., *Tissue World Mag.* 60(5): 62(2014).
6. Kuo, L. and Cheng, Y., *TAPPI J.* 83(12): 61(2000).
7. Tiest, W.M.B. and Kappers, A.M.L., *Acta Psychol.* 121: 1(2006).
8. Hollmark, H., *Tappi J.* 66(2): 97(1983).
9. Peck, J. and Terry, C.L., *J. Marketing* 67(2): 35(2003).
10. U.S. Census Bureau, "Monthly & annual retail trade - annual retail trade survey historical data," U.S. Census Bureau, Suitland, MD, USA. Available [Online] https://www.census.gov/retail/arts/historic_releases.html <08Aug2017>.
11. Cellini, C., Kaim, L., and Drewing, K., *Iperception* 4(8): 516(2013).
12. Ernst, M.O. and Banks, M.S., *Nature* 415(6870): 429(2002).
13. Tiest, W.M.B. and Kappers, A.M.L., *Acta Psychol.* 124(2): 177(2007).
14. Norman, J.F., Norman, H.F., Clayton, A.M., et al., *Perception Psychophysics* 66(2): 342(2002).
15. Riedl, R. and Léger, P.M., *Fundamentals of NeuroIS*, Springer, Berlin, Germany, 2016.
16. Holbrook, M.B. and Hirschman, E.C., *J. Consumer Res.* 9(2): 132(1982).
17. Peck J. and Childers, T.L., *J. Consumer Res.* 30(3): 430(2003).
18. Sénécal, S., Léger, P-M., Fredette, M., et al., "Touch screen as input device: does it influence memory retrieval?", *2013 ICIS Conf.*, AIS, 2013.
19. Johansson, R.S., *J. Physiol.* 281(2): 101(1978).
20. Spreen, O. and Strauss, E., *A Compendium of Neuropsychological Tests: Administration, Norms, and Commentary*, Oxford University Press, New York, 1991, p. 334.
21. Saaty, T.L., *The Analytic Hierarchy Process*, 2nd edn., RWS Publications, Pittsburgh, PA, USA, 1990.
22. David, H.A., No. 12, Griffin's Statistical Monographs & Courses, 2nd edn., Charles Griffin & Company, London, 1969.
23. Torgerson, W.S., *Theory and Methods of Scaling*, John Wiley and Sons, Hoboken, NJ, USA, 1958.
24. Budescu, D.V., Zwick, R., and Rappoport, A., *Applied Psychol. Meas.* 10(1): 69(1986).
25. Valdez, P. and Mehrabian, A., *J. Exp. Psychol.* 123(4): 394(1994).
26. Kaya, N. and Epps, H.H., *College Student Journal* 38(3): 396(2004).
27. Kubota, T., Wada, T., and Matsuda, M., *Transactions of the Society of Instrument and Control Engineers* 35(8): 989(1999).

ABOUT THE AUTHORS

Our senses work in synergy to help us perceive the world around us. We undertook this study because we wanted to understand how our vision changes the perception of a dominantly tactile quality to help the industry design products so that the quality of softness is apparent before physical interaction.

Much of previous work on understanding the perception of softness has concentrated wholly on the tactile aspect. The rise in popularity of virtual reality and increasingly sophisticated haptic technology may beacon a new era in which we consider stimuli from all senses to describe an object.

The most difficult aspect of our study was ensuring that the participants were judging the variables presented to them and no other environmental factors. We therefore designed the study around digital images.

I was personally very surprised by the speed of determination. Participants took less than 5 s to look at a pair of images and decide which was the softest. The oculometry data also showed that participants looked at a very narrow area of the sample and scanned back and forth repeatedly in that short time span.

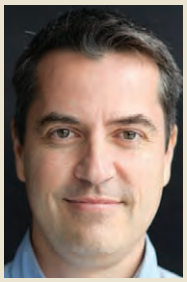
We hypothesized that the effect of the blue/yellow color change would have a much larger effect on softness perception. Having worked with optical brightening agents in the past on fine paper, we assumed that the participants would rate the yellowish samples as much less soft.



Carette



Léger



Sénécal

The key take-home message for mills and manufacturers is that first impressions count. Customers are making very rapid judgements of your product's quality based on appearance alone. Embossing, color, and presentation are drivers for first-time purchasers.

For future studies, we would like to extend the list of variables to cover other common tissue characteristics and add a tactile component to see if changing the visual appearance influences the tactile perception of softness.

Carette is innovation manager, Cascades Tissue Group, Candiac, QC, Canada, and a former MBA student at HEC Montréal, Montréal, QC, Canada. Léger is professor, Department of Information Technologies, and Sénécal is professor, Department of Marketing, at HEC Montréal, Montréal, QC, Canada. Email Carette at jessica_carette@cascades.com.

Operating parameters affecting the thermal performance of biomass boilers

NAZ ORANG, HONGHI TRAN, ANDY JONES, AND F. DONALD MCCABE

ABSTRACT: Operating data of a bubbling fluidized bed (BFB) boiler and three stoker grate (SG) biomass boilers from different pulp mills were analyzed over a 2-year period. The results show that in all cases, the thermal performance decreases markedly from 5.5 to 4 lb steam/lb dry biomass as the feedstock moisture content increases from 40% to 60%. The BFB boiler had better thermal performance, although it operated in a higher moisture content range compared with the SG boilers. Multivariate analysis was also performed on one of the SG boilers to determine operating parameters that affect thermal performance. The results show that furnace temperature, oil flow rate, and induced draft fan current positively correlate with thermal performance, while the feedstock moisture content, total air flow, and excess oxygen (O_2) negatively correlate with thermal performance. This implies that when making modifications to improve thermal performance, it is important to take into account correlations among various parameters. In some cases, one positively correlated parameter might cause an increase in a negatively correlated parameter. The net effect might be a decrease in thermal performance.

Application: Mills can find the most suitable way to optimize boiler operation with minimal process upsets.

Biomass (hog fuel) boilers in kraft pulp mills in Canada and the United States typically provide about one third of the mill's energy requirement. Hog fuel, which is a mixture of wood waste, bark, and biomass-based rejects from different parts of the pulping process, is burned in the biomass boiler and the heat of combustion is used to produce superheated steam [1]. The most common types of boilers are fixed bed boilers or stoker grates (SG) and bubbling fluidized bed (BFB) boilers. In SG boilers, the feedstock is fed onto the bottom grate where burning takes place. In BFB boilers, the biomass is delivered onto a hot fluidized sand bed. The biomass is vaporized in lean conditions and burns above the bed where air is introduced. BFB boilers are typically more versatile than SG boilers, operate with a wider range of fuel qualities, and are well suited for burning high moisture fuels. SG boilers, on the other hand, are susceptible to process upsets caused by small changes in fuel characteristics.

The variability of biomass boiler feedstock makes maintaining constant steam generation a challenge. The hog fuel quality, in terms of wood species, shape, size, and moisture content (MC), changes constantly as different wood waste sources are mixed. If the biomass feedstock is stored outside and exposed to rain or snow, MC can reach 70%. A portion of the heat content of the biomass might also be lost because of exposure to long durations of sunshine or biological decay. Depending on dry calorific value of the fuel, the biomass might reach an as-fired net calorific value of zero at high moisture and require auxiliary fuel firing.

The constant change in fuel quality and therefore steam production rate can make quantifying boiler performance difficult. For this reason, thermal performance (TP) values are typically used to provide an overall estimate for the quality of combustion and boiler operation. TP is a measure of how much steam with the required temperature and pressure, or enthalpy, is produced per unit mass of dry biomass. TP values are greatly influenced by boiler design and operation, as well as feedstock quality and consistency.

To optimize the TP of any boiler, first the interaction of the operating parameters needs to be studied. In this work, a systematic investigation was performed on three SG boilers and one BFB boiler to better understand the interaction and interconnectivity of operating parameters and their effect on TP. This paper first discusses the relationship of TP and feedstock MC, and then presents a statistical model for one of the SG boilers to determine the most influential operating parameters using multivariate analysis (MVA).

METHODOLOGY

Two years of daily average operating data were collected from three SG boilers and one BFB boiler. **Table I** lists the average operating data used in this study for each mill. To quantify biomass boiler operation, TP values were calculated using Eq. (1):

$$TP = \frac{F_{steam,T,P}}{F_{biomass,dry}} \quad (1)$$

where $F_{steam,T,P}$ is the flow rate of steam produced from burning biomass at the required superheated temperature and pressure, $F_{biomass,dry}$ is the feed flow rate of dry biomass, and TP is

a dimensionless value. Theoretical TP values were calculated from an energy and material balance. The data collected for each biomass boiler were used to calculate TP values.

Multivariate analysis was used to study the interaction of mill A hourly average operating parameters and to find the most influential ones. Multivariate analysis is an effective statistical method to summarize data tables with many variables by creating several new variables containing most of the information [2]. These new latent variables are then used for problem solving and display (i.e., classification, relationships, control charts, and more). The new variables, called the scores, denoted by t, are created as weighted linear combinations of the original variables and each observation has a t value.

Multivariate analysis has been used by our research group to analyze factors affecting ring formation in lime kilns [3], multi-effect evaporator performance [4], recovery boiler fouling and plugging [5], and recovery boiler smelt spout failures [6]. The main challenge associated with MVA and working with a large number of data is dealing with data dimensionality, multicollinearity, noise, and missing data. Principal component analysis (PCA) and orthogonal partial least squares analysis (OPLS) methods are suitable for handling this challenge [7].

In this study, a commercially available software package SIMCA 14 (Umetrics; Umeå, Sweden) was used to construct an MVA model from mill A operating data. The program uses PCA and OPLS for MVA and to summarize the information in the observations as t scores, which are the new latent variables. The group of points in a K dimensional space, where K is the number of variables, is approximated by a hyperplane and the points are projected on that plane [2].

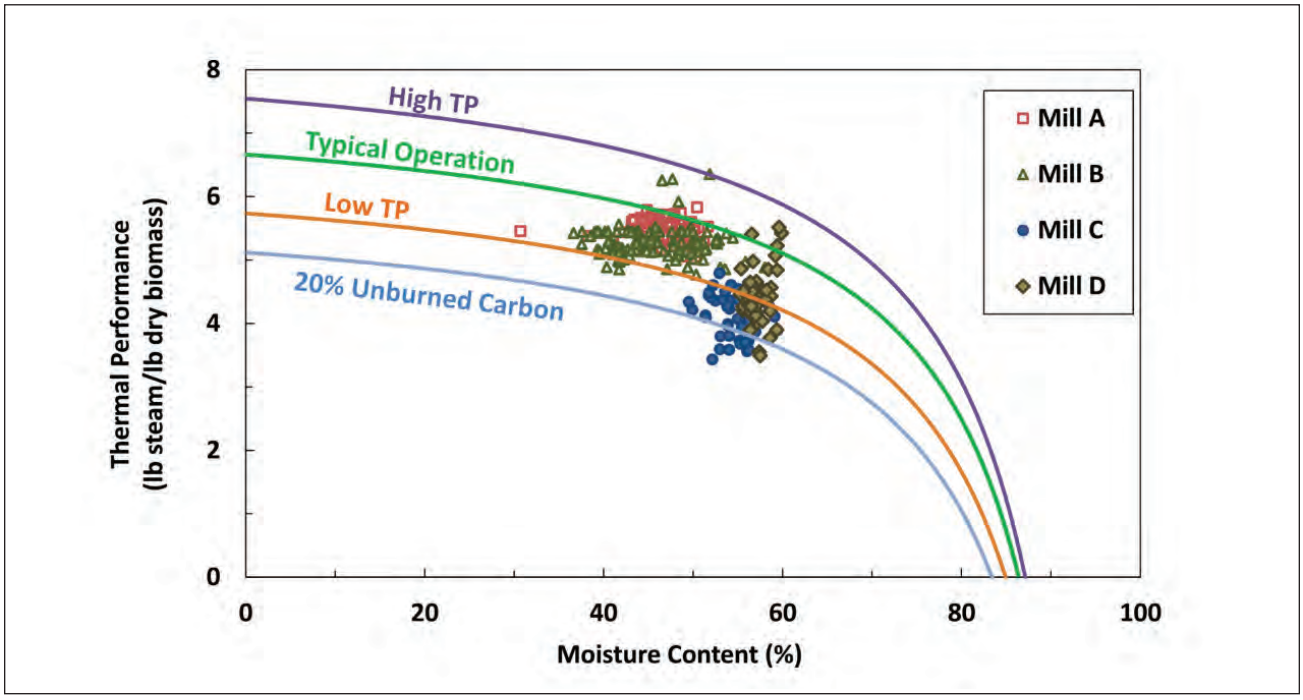
RESULTS AND DISCUSSION

Effect of moisture content on thermal performance

In this study, 2 years of daily average operating data from four biomass boilers at different pulp mills were analyzed, and the results are shown in **Fig. 1**. The boilers at mills A, B, and C are fixed bed, SG-type boilers and the boiler at mill D is a BFB boiler. The MC values for each boiler were either from batch oven-dried values provided by the mill or back calculated from other operating parameters.

To compare steam flow from different boilers with different fuel characteristics, combustion air conditions, and steam enthalpies, all steam flow values are normalized to the steam condition at 820°F and 900 psig. The data points shown on Fig. 1 are instances of normal operation. The steam flow rate, biomass flow rate, total air flow rate, and furnace temperature value ranges are average ± 1 standard deviation. The theoretical TP values were divided into high TP, typical operation, and low TP and calculated from energy and material balance. **Table II** summarizes the parameters used to calculate the theoretical values in Fig. 1.

As shown in Fig. 1, the TP decreases with increasing MC and becomes zero as the MC exceeds 85%. Comparing the calculated values with actual values obtained from each mill, it is evident that the SG boilers were operated at an average feedstock MC of 50%, ranging from 40% to 55%, and the BFB boiler was operated at higher moisture content, 55% to 60%. In both types of boilers, the maximum operable MC (55%–60%) was much lower than the theoretical maximum value (85%), even with auxiliary fuel firing. This was presumably because of the decrease in furnace temperature and the in-



1. Thermal performance (TP) versus moisture content.

Parameter	Mill A	Mill B	Mill C	Mill D
Boiler Type	Stoker Grate			Bubbling Fluidized Bed
Biomass feed rate, tons/h	29	30	62	50
Moisture content, %	38	40	58	56
Air flow rate, kpph	461	307	587	356
Undergrate air flow rate, kpph	177	170	159	176
Inlet air temperature, °F	192	293	349	219
Natural gas flow rate, scfm	30	124	124	-
Fuel oil flow rate, kpph	2.2	-	-	11.2
Flue gas temperature, °F	416	341	355	329
Excess O_2, %	7.7	5.5	7.3	5
Steam flow rate, kpph	214	266	285	182
Steam temperature, °F	820	827	738	871
Steam pressure, psig	900	915	652	1,178
Steam enthalpy, 1000 Btu/h	301	374	391	259

I. Operating data average values.

Parameter	Low Thermal Performance	Typical Operation	High Thermal Performance
Excess air, %	40	30	10
Radiation and unaccounted heat losses, %	10	5	0
Feedwater temperature, °F	250	300	350

II. Parameters for calculating theoretical thermal performance (TP) values.

crease in water vapor content in the combustion gas as a result of increased moisture content of biomass feedstock. These conditions might have resulted in unburned carbon in the fly ash or bottom ash or prevented some volatiles from burning [8]. Both unburned carbon and volatile loss mean that not all of the heat content of the feedstock is used. To demonstrate this adverse effect, a value of 20% is assumed for unburned carbon and TP values are calculated and shown in Fig. 1.

The results shown in Fig. 1 are representative of normal operation only; however, during biomass boiler operation, it is rare for all operating parameters to be at average conditions. It is also evident that TP is influenced by many different factors, not just MC. To address these challenges and investigate the simultaneous change of all parameters and their effects on TP, MVA was carried out to statistically study the simultaneous change of all the independent operating variables and to quantify the interaction and effect they have on several key dependent variables.

Multivariate analysis

Hourly average operating data from mill A were used in this study to build a statistical model. **Table III** lists main model parameters and their abbreviations. For MVA, an OPLS model was built, where TP and excess oxygen (O_2) were set as output or Y variables and all other process inputs, including moisture content, were set as X variables. The model uses all X variables to explain and predict the changes in Y variables.

Figure 2 shows the score scatter plot for the OPLS model built from mill A operating data from a total of 1400 data points. Each data point on the scatter plot represents one instance for all variables, in this case average hourly values for all operating parameters. The ellipse represents a 95% confidence interval (CI) of the data and the origin of the graph represents the average value across all variables. The further away a point is from the origin (shown by X), the greater it deviates from the average. Points clustered together on the scatter plot on each quadrant have similar collective characteristics and can be connected back to specific operating con-

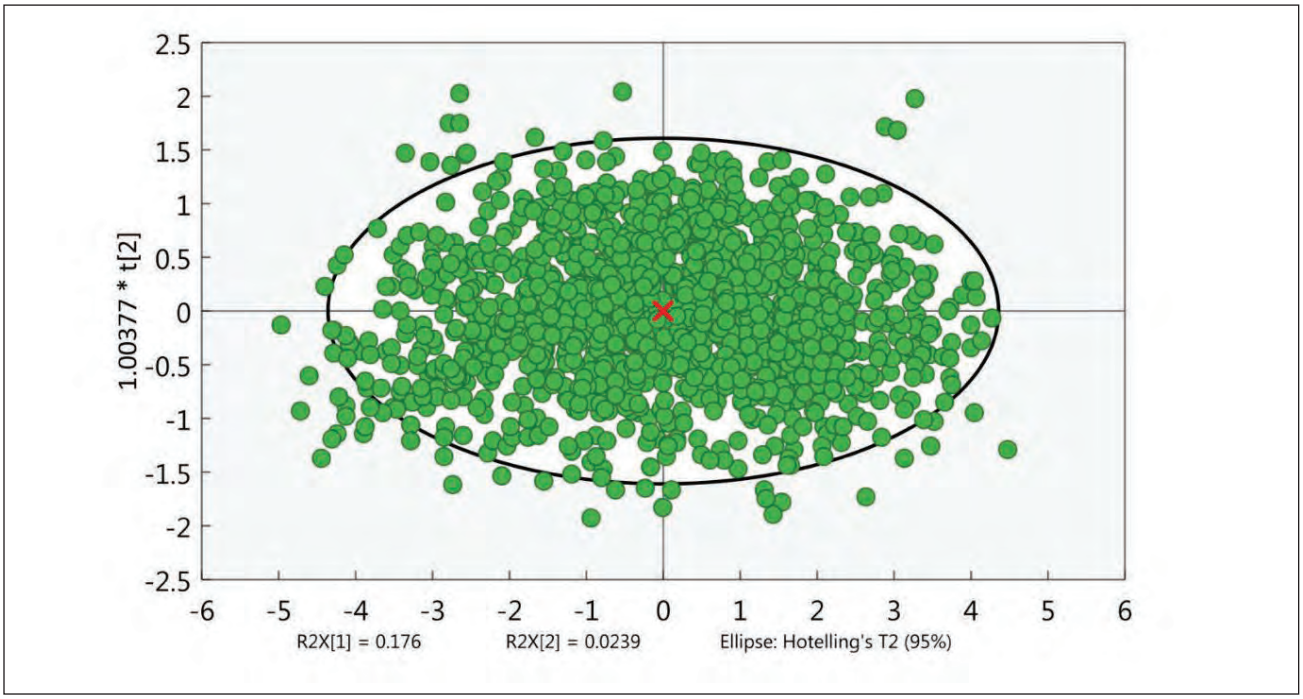
Abbreviation	Parameter
ArchAirFlw	Arch air flow rate
BarkAirFlw	Bark air flow rate
BurnerAirFlw	Gas burner air flow rate
DeAirT	Deaerator temperature
ExcessO2	Outlet excess O_2
GasFlow	Gas flow rate
IDFanCurr	Induced draft fan current
IDFanT	Induced draft fan outlet temperature
InAirT	Inlet air temperature
LowerFurnT	Lower furnace (bed) temperature
MC	Feed moisture content
OilFlow	Oil flow rate
TotalAirFlw	Total air flow rate
TP	Thermal performance
UGAirFlw	Undergrate air flow rate
WindboxAir	Windbox air flow rate
WindsweptAirFlw	Windswept spout air flow rate

III. Model parameters.

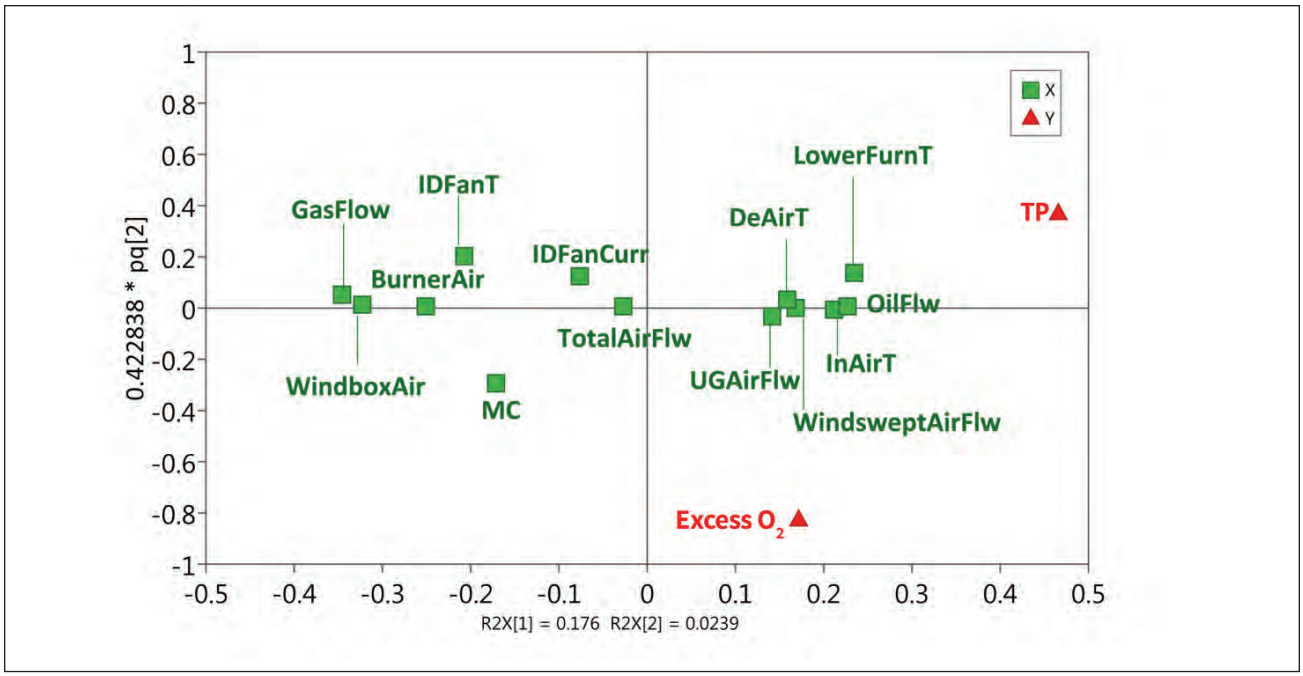
ditions [7]. It is clear from Fig. 2 that most of the data points fit within the 95% CI, meaning that the model explains the data well. On the other hand, the spread of the data points on the scatter plot demonstrates there are many instances where operating parameters are far from average.

The loading plot shows which variables are influential and how they are correlated. Variables placed further away from the origin are more influential in the model and variables grouped together in the loading plot are directly correlated with one another. **Figure 3** shows the loading scatter plot for the mill A model. Note the two Y variables in this model, TP and excess O_2, are situated in opposite quadrants. This means they have a negative correlation (i.e., TP is high when excess O_2 is low). Excess O_2 is sometimes used as an indicator for combustion quality. If this value suddenly increases, it means there is either more air than fuel at that moment, if the combustion quality is the same, or if the air/fuel ratio is the same, it means the combustion quality is poor; both cases lead to lower heat flux in the furnace area. This translates to less steam produced, which would decrease the TP value as well. To understand the correlation between any operating parameters, their locations in Fig. 3 can be used; if they are found in the same quadrants, they have a positive correlation and if they are situated in opposite quadrants, they are negatively correlated.

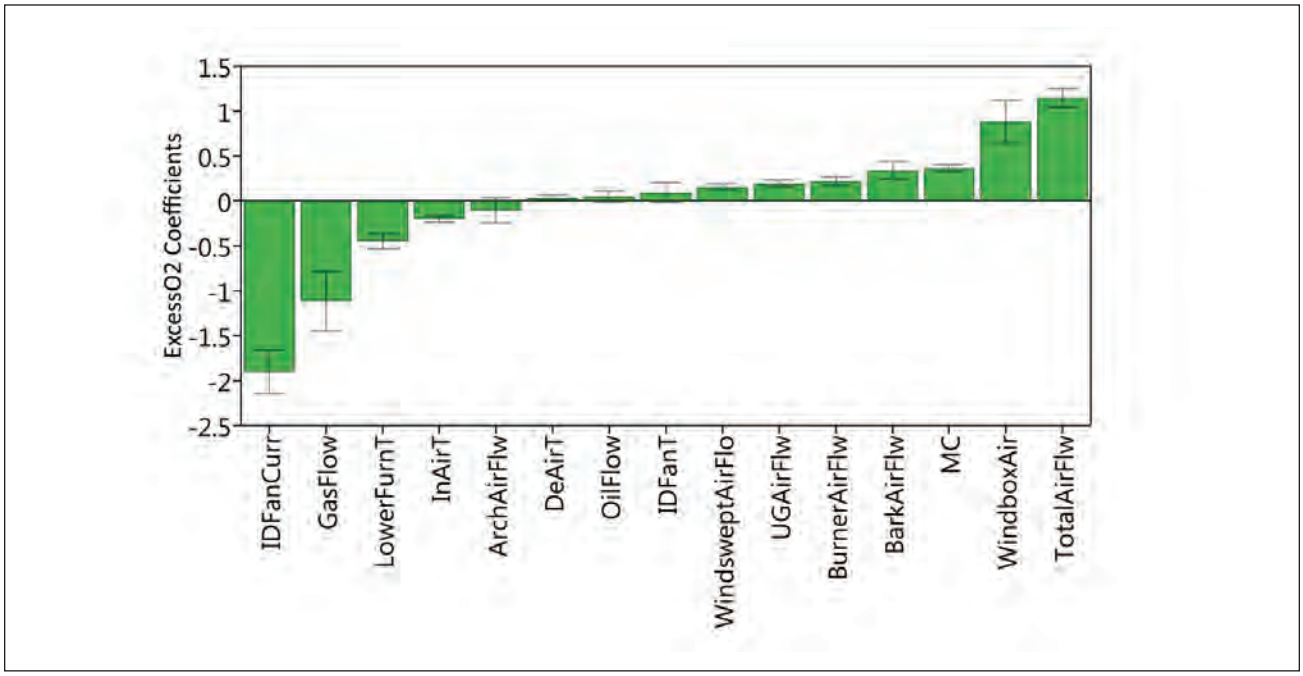
To determine the effect of each X variable on the Y variables separately, a coefficient plot is used where the contribution of each X variable on the corresponding Y variable is determined by a positive or negative coefficient. **Figure 4** shows the coefficient plot for excess O_2 from the OPLS model built for mill A operating data. Induced draft (ID) fan current, gas flow, and lower furnace temperature have the highest



2. Score scatter plot for mill A data.



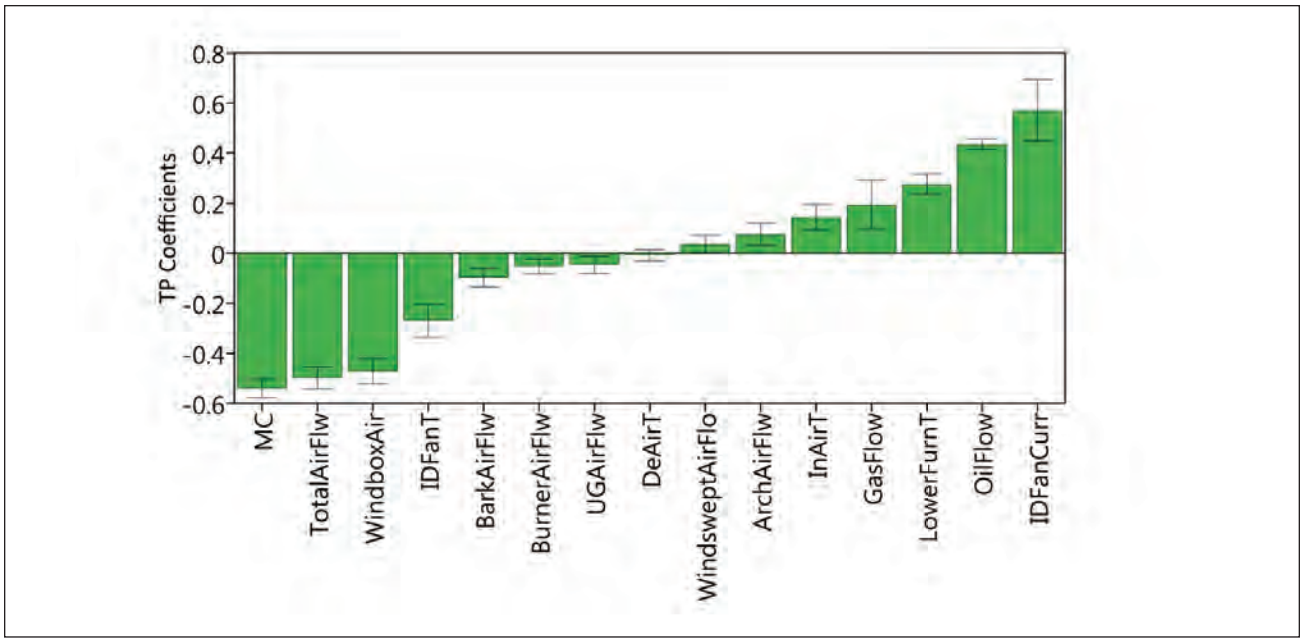
3. Loading scatter plot for mill A data.



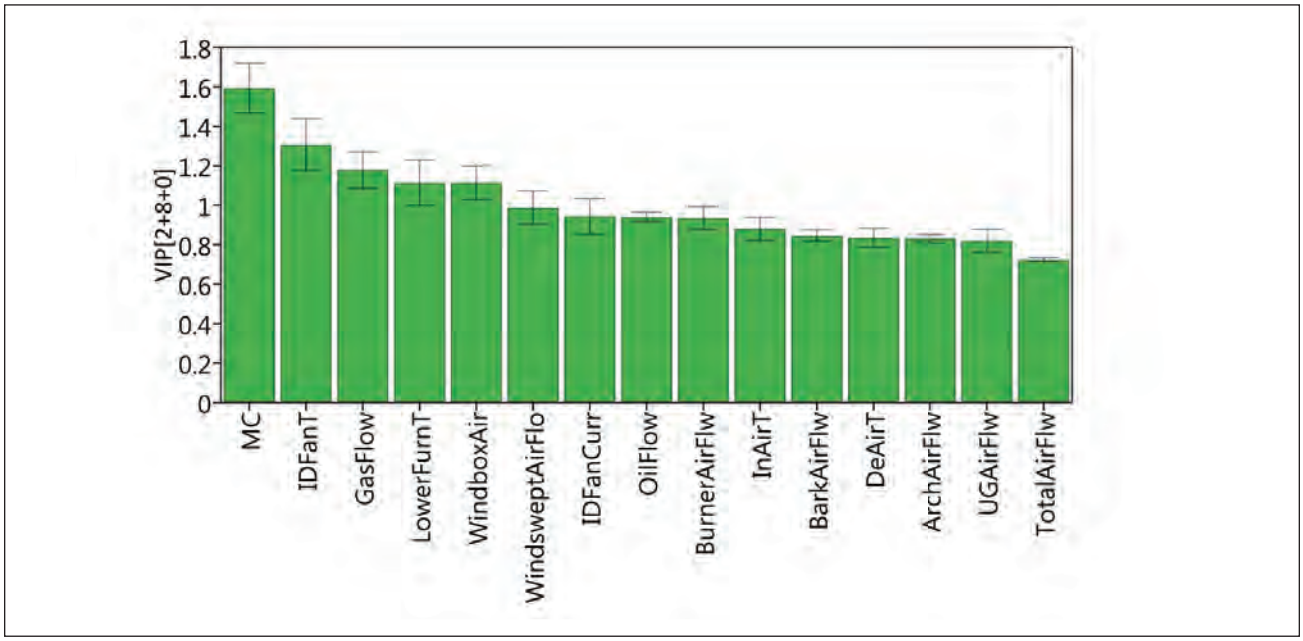
4. Coefficient plot for excess O_2.

negative coefficients, whereas total air flow and windbox air flow rate have the most significant positive effect on excess O_2. The positive effect of air flow rate on excess O_2 is intuitive; the negative coefficients could also be explained by process characteristics.

Low excess O_2, as explained earlier, is a good indicator for combustion quality provided that adequate air is provided for stoichiometric combustion. Also, when the biomass feedstock burns completely, more flue gas is produced and the ID fan current increases to remove the increased amount of flue gas to maintain the negative draft inside the boiler. The relationship between gas flow and excess O_2 could be explained by the same principle: burning more biomass would produce more flue gas and at the same time consume more O_2, resulting in less excess O_2. Furthermore, better combustion would increase the furnace temperature which, in turn, would improve combustion and result in more fuel being burned and less excess O_2 at the boiler exit.



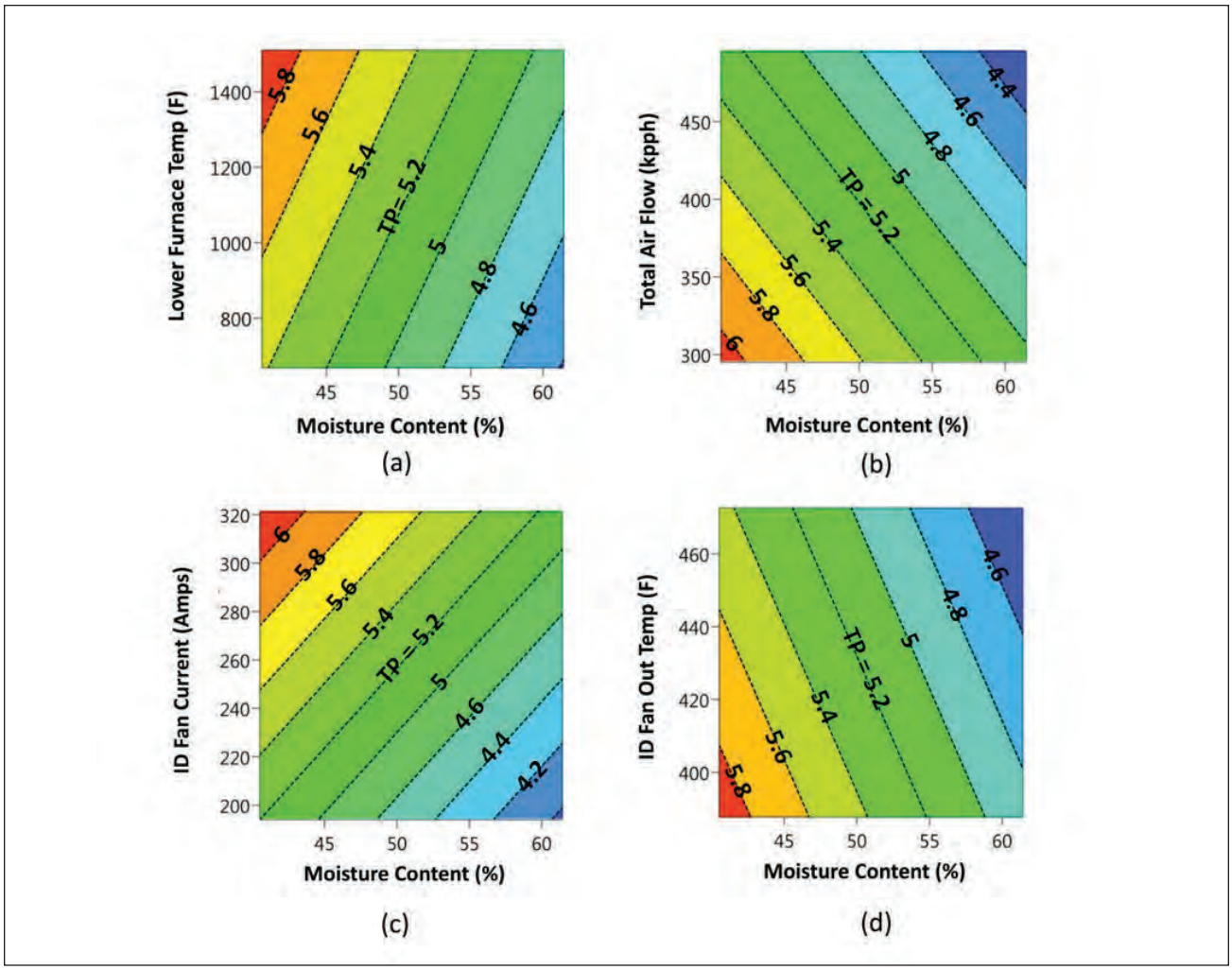
5. Coefficient plot for TP.



6. Variable importance for projection plot for orthogonal partial least squares analysis model.

Figure 5 shows the coefficient plot for TP. The positively correlated parameters with TP are ID fan current, lower furnace temperature, and oil flow. When more fuel is burned, whether biomass or oil, furnace temperature increases and more flue gas is produced, which results in more steam and an increase in TP. The negative coefficients for TP are MC, windbox air, and total air flow. The negative correlation between MC and TP will be explained in more detail in the following sections. Increase in air flow rate has a negative impact on TP because high air flow rate dilutes the flue gases and reduces the heat content available for steam production.

To choose the parameters that need to be followed closely for optimizing the performance of biomass boilers, the variable importance for projection (VIP) plot needs to be studied. The VIP plot for this model is shown in **Fig. 6**, where variables with VIP value larger than 1 have considerable impact on the model. The VIP plot for the OPLS model built for mill A clearly indicates that MC has the most significant impact on the model. This is also evident from Figs. 4 and 5, where MC is among the top three contributing variables to changes in excess O_2 and the most significant variable with the highest coefficient for TP.



7. TP response contour for changes in moisture content and (a) lower furnace temperature, (b) total air flow, (c) induced draft (ID) fan current, and (d) ID fan outlet temperature.

Because moisture content is the most influential variable in this model, a more in depth analysis is needed for the effect of MC on TP while considering other influential variables to help better understand their interaction. **Figure 7** shows response contours for TP with changes in MC. Each graph looks at TP response contours while considering changes in MC, shown on the x-axis, and one other influential parameter, shown on the y-axis.

Figure 7a shows the effect of lower furnace temperature and MC on TP, and the highest TP is for high furnace temperature and low MC. This is in agreement with the findings from the four boilers investigated (see Fig. 1) where it was speculated that lower furnace temperature has a significant impact, especially for high MC values. Figure 7b shows total air flow and MC with TP. High TP values occur for low total air flow and low MC. This shows that increasing total air flow results in diluting the flue gases and decreases the heat content available for steam production and therefore lowers TP. Induced draft fan current and temperature are representatives of flue gas flow rate and temperature, respectively. As mentioned previously, increase in flue gas flow rate is an indication of more fuel burned in the boiler and therefore more heat available for steam production, which results in higher TP if combustion takes place efficiently (Fig. 7c). The flue gas temperature, on the other hand, shows a negative correlation with TP (Fig. 7d). When the temperature of the flue gas is high, it means the heat content of the flue gas has not been used to its fullest at the superheaters, economizer, or heat exchangers, and the result is lower TP.

The response contours in Fig. 7 clearly show that regardless of the y-axis variable, TP decreases with increasing MC. However, to predict TP values more accurately, other influential variables shown must be taken into consideration.

IMPLICATIONS

When the TP of a biomass boiler decreases (e.g., due to variability in the fuel), a combination of operating parameters could be changed to optimize boiler operation and bring the TP back to the desired value. Only a handful of process parameters are independent variables, especially those that

could be changed without adverse effects on the rest of the process. For this reason, the interconnectivity of process variables and net effects on process outputs must be taken into consideration.

For example, a common practice is to increase the undergrate air flow rate when the operator is aware of wet biomass entering the boiler. This is thought to facilitate drying of high moisture material on the grate and expedite combustion to minimize process upset. The adverse effects of changing this parameter must also be considered. Depending on the air temperature, increasing the undergrate air might cause the lower furnace area to become cooler. It also results in an increase in total air flow entering the boiler, which in turn causes an increase in excess O_2. All of these lower the TP; therefore, the net effect must be considered beforehand to determine the maximum degree of change allowable.

The MVA results discussed here, as for any other statistical model, show correlations only and causality should not be concluded; when two parameters are closely correlated, one does not necessarily cause the occurrence of the other. Therefore, optimization methods for each boiler must be derived from individual assessment of boiler design, operation, and fuel types.

CONCLUSIONS

Optimized operation of biomass boilers depends on many factors, including fuel quality, operating conditions, and mill steam demand. The interaction of these parameters was investigated in a multivariate model to find which parameters have the most significant effect on TP. The most influential parameter on TP is MC, and excess O_2 and TP are negatively correlated. Induced draft fan current, gas flow, and lower furnace temperature have negative coefficients in relation to excess O_2, and windbox air and total air flow have positive coefficients in relation to excess O_2. Finally, ID fan current, lower furnace temperature, and oil flow have the most significant positive impact on TP, and the negative coefficients for TP are MC, windbox air, and total air flow. **TJ**

ACKNOWLEDGEMENTS

This work was conducted as part of the research program Increasing Energy and Chemical Recovery Efficiency in the Kraft Process—III, jointly supported by the Natural Sciences and Engineering Research Council of Canada (NSERC) and a consortium of the following companies: Andritz, AV Nackawic, Babcock & Wilcox, Boise, Carter Holt Harvey, Celulose Nipo-Brasileira, Clyde-Bergemann, DMI Peace River Pulp, Eldorado, ERCO Worldwide, Fibria, FPInnovations, Internation-

ABOUT THE AUTHORS


Orang


Jones


Tran


McCabe

Biomass combustion for the purpose of steam production is a viable solution for handling wood waste. Biomass is a carbon neutral fuel and therefore, finding ways to efficiently burn this type of sustainable fuel in biomass boilers has great potential. The main challenge, which is the variability of fuel quality, needs further research and exploration so that biomass boiler performance can be optimized.

Many researchers have developed numerical models for boiler optimization. However, we wanted to develop a practical solution for improving boiler operation using multivariate analysis as well as case studies to complement these statistical tools.

The most difficult aspect of this research was finding a suitable way to compare different biomass boilers. Boiler type, design, operation, and steam demands vary from mill to mill. To address this issue, we defined the thermal performance (TP) parameter with normalized steam properties to draw meaningful conclusions.

The power of statistical analysis was the main discovery for me (Orang) from this research. Specifically, multivariate analysis can be used to solve today's complex problems. The operating parameters that affect TP negatively were an interesting finding. Also, it was interesting to see the complexity in finding the desired balance between positively and negatively correlated parameters to improve TP.

The main takeaway from this work is that each boiler needs to be studied closely and in detail to find the most suitable way to optimize boiler operation with minimal process upsets. The next step is to conduct more case studies and develop a generalized guideline for biomass boiler operation and optimization.

Orang is a Ph.D. candidate; Jones is an adjunct associate professor; and Tran is Frank Dottori Professor of Pulp and Paper and director of the Pulp and Paper Centre, Department of Engineering and Applied Chemistry, University of Toronto, Toronto, ON, Canada. McCabe is senior process engineer, Irving Pulp and Paper Ltd., Saint John, NB, Canada. Email Tran at honghi.tran@utoronto.

al Paper, Irving Pulp & Paper, Kiln Flame Systems, Klabin, StoraEnso Research, Suzano, Tembec, Tolko Industries, Valmet, and WestRock.

LITERATURE CITED

1. Gavrilescu, D., *Environ. Eng. Manage. J.* 7(5): 537(2008).
2. Erikson, L., Johansson, E., Kettaneh-Wold, N., et al., *Multivariate and Megavariate Data Analysis Basic Principles and Applications (Part I)*, Umetrics, Umeå, Sweden, 2006.
3. D'Souza, T., Repka, J., and Tran, H.N., "Effects of process variability on ring formation in lime kilns," *TAPPI Eng., Pulping Environ. Conf.*, TAPPI Press, Atlanta, GA, USA, 2006.
4. Hajiha, H., Tran, H.N., Holik, D., et al., "Multivariate analysis of variables affecting thermal performance of black liquor evaporators," *TAPPI Eng., Pulping Environ. Conf.*, TAPPI Press, Atlanta, 2009.
5. Versteeg, P. and Tran, H.N., *TAPPI J.* 8(11): 22(2009).
6. Jones, A.K., Wagoner, J., Michaelson, T., et al., "Use of multivariate analysis to understand the root causes of premature smelt spout failures on recovery boilers," *Int. Chem. Recovery Conf.*, TAPPI Press, Atlanta, 2014.
7. Hoeskuldsson, A., *J. Chemom.* 9(8): 91(1995).
8. Orang, N. and Tran, H.N., *TAPPI J.* 14(10): 629(2015).

Drying characteristics of biosludge from pulp and paper mills

GEANNA HOVEY, D. GRANT ALLEN, AND HONGHI TRAN

ABSTRACT: Handling and disposal of biosludge has been a persistent problem for many pulp and paper mills primarily because of the material's high moisture content and poor dewatering and drying characteristics. Most biosludge is landfilled or incinerated, and some is used as a soil amendment. To incinerate biosludge, the mills mix it with primary sludge, mechanically dewater the mixture to 15%–30% solids, and burn it with hog fuel in biomass boilers. For biosludge to burn effectively, however, it must be dewatered or dried to at least 30%–35% solids. A systematic study was conducted to examine the drying characteristics of biosludge collected from pulp and paper mills at various temperatures using a thermogravimetric dryer. The drying behavior of the tested biosludges was similar, adding fillers such as wood fines and biomass boiler fly ash to biosludge up to 30 wt% did not significantly affect the drying rate, higher organic content might make biosludge more difficult to dry, and increasing drying temperature significantly increases the drying rate as expected.

Application: Mills can optimize their biosludge handling and disposal practices by understanding the material's drying characteristics.

Two types of sludge are produced from the wastewater treatment process of pulp mills: primary and secondary. Primary sludge is generated in the primary clarifier and is composed mainly of wood fibers. Secondary sludge (biosludge) is a colloidal suspension of small solids particles produced in the secondary clarifier. Biosludge is typically composed of microbes, undigested wood fibers, and organics, and it has a low solids content of about 2 wt% [1]. A portion of this sludge is recycled back into the wastewater treatment process to maintain the microbial community, and the remainder is disposed. The amount and composition of the sludge varies among mills and even among days at the same mill. Approximately 10–100 m^3 water is required per ton of paper produced [2], and with it 0.2–0.6 wet sludge per ton of pulp is produced [3]. Furthermore, the production of paper mill sludge is projected to increase between 48% and 86% from the amount produced in 2000 [4].

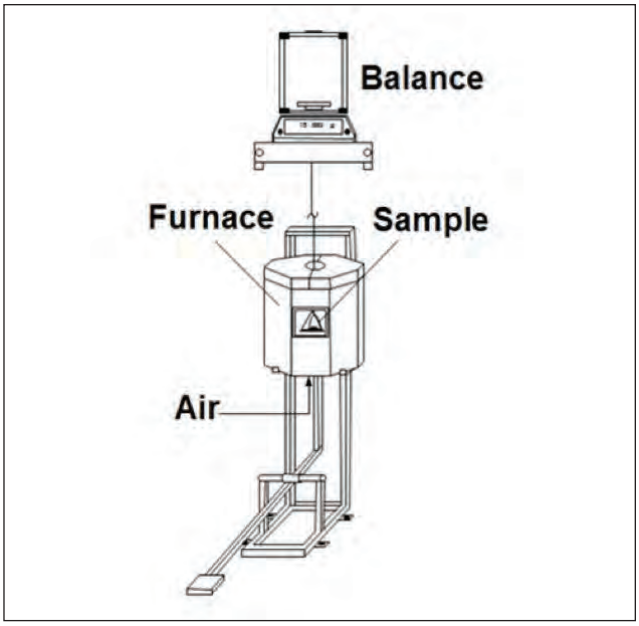
Most sludge is either landfilled or burned in biomass boilers, and some is used as a soil conditioner. Over the past decade, it has become more common for mills to burn the sludge as landfill space declines. To successfully burn wasted biological sludge, the solids content must be increased to at least 30%–35%. The challenge is to remove sufficient water so that the sludge can sustain combustion with no net thermal loss incurred by the boiler because of the high moisture content.

Drying is considered as a key step in the disposal of biosludge where waste heat from mill processes can be harnessed. Drier sludge is less costly to handle and easier to burn. Although much research has been done on the drying behavior of municipal sludge [5,6], not much work has been done on the drying behavior of pulp and paper mill biosludges. It is not known how biosludges from different mills compare or how biosludge contrasts with municipal sludge. It is also not clear whether drying can be facilitated with the addition of solids. The objective of this research was to investigate the fundamental drying characteristics of pulp and paper mill biosludge and methods to facilitate drying.

EXPERIMENTAL

The biosludge samples in this study were collected from a sulfite mill in Ontario and a kraft mill in Alberta, Canada. The samples were different in appearance and odor. The raw sulfite mill biosludge was dark brown (almost black) and contained 1.7% solids, whereas the kraft mill biosludge contained 3.3% solids, was brown and much thicker, and had a stronger odor. The samples were mixed with a 0.5 wt% solution of polymer (Zetag 8165, BASF; Ludwigshafen, Germany) to flocculate the solids, filtered by gravity, and pressed using a crown press to 13% solids. Assorted wood fines and biomass boiler fly ash, which were dried in an oven overnight at 105°C, were added to the dewatered sludge cakes in amounts of 10 wt%, 20 wt%, and 30 wt% to determine the effect of additives on the drying rate. The samples were molded into cylinders approximately 3.2 cm in diameter with heights varying from 1.2–3.0 cm depending of the amount of solids added. All tests were done using mechanically dewatered biosludge.

A thermogravimetric furnace (**Fig. 1**) was used to isothermally dry the samples. The apparatus can continuously measure and record the sample mass during drying, using a high-precision balance capable of measuring up to 200 g with a readability of 1 mg. Details of this apparatus have been previ-



1. Laboratory-scale thermogravimetric furnace.

ously described [7]. In this study, a weighing dish containing a sludge cake sample was hung from the balance directly above the opening of the furnace. The sample was then inserted into the furnace. By stepping on the pedal to lift the entire furnace assembly, the weighing dish and sample were situated in the center of the furnace chamber. Air was passed through the furnace from the bottom at a flow rate of 1 L/min to remove water vapor. The drying temperature varied from 110°C to 220°C at 1 atm. The changes in sample appearance and physical conditions were monitored using a high speed video camera focused through a viewing glass window at the side of the furnace.

	Sulfite Mill	Kraft Mill
Proximate (wt%), Dry Basis		
Volatiles	71.8	56.7
Fixed carbon	17.8	18.7
Ash	14.0	25.0
Higher heating value, MJ/kg	20.5	17.5
Ultimate (wt%)		
Carbon	44.7	39.8
Hydrogen	5.5	4.6
Nitrogen	6.0	3.2
Sulfur	2.1	2.4
Oxygen	31.3	27.0

I. Composition of biosludge from a sulfite mill and a kraft mill.

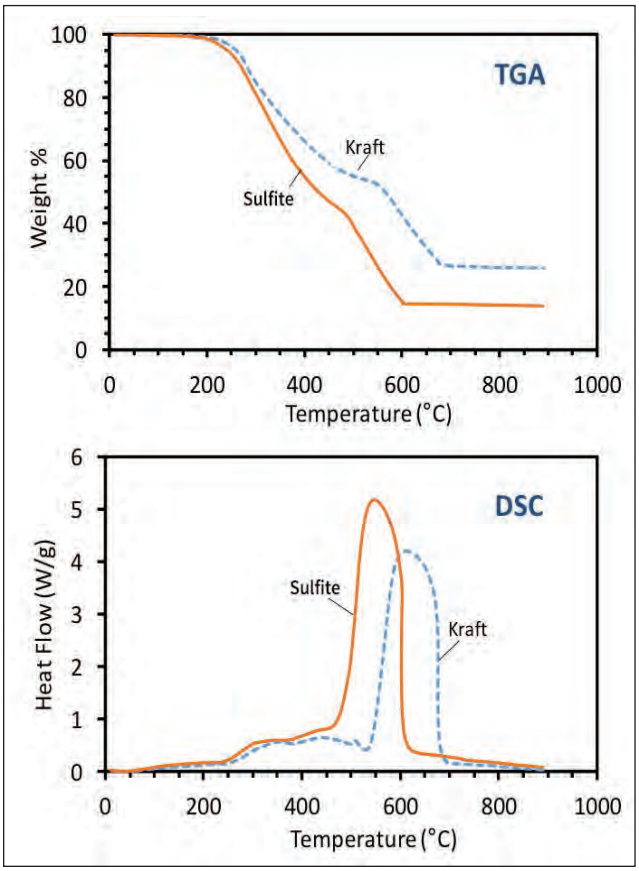
RESULTS AND DISCUSSION

Sludge analysis

The compositions of sulfite mill and kraft mill biosludges are shown in **Table I**. On a dry basis, the sulfite mill biosludge had a higher volatile content, higher heating value, and lower ash content than the kraft mill biosludge. After dewatering, a solids content of 13% could be achieved for both types.

A simultaneous thermogravimetric analysis/differential scanning calorimetry (TGA-DSC) analyzer was used to examine the combustion behavior of the sludge samples, which were first dried overnight at 105°C. The samples were heated in the analyzer from room temperature to 900°C at a heating rate of 20°C/min. The results are depicted in **Fig. 2**. Both samples have no change in weight up to about 180°C, at which point they began to lose weight. At 250°C, the heat flow rate and weight loss rate increase for both samples as volatiles are emitted and burned. This is followed by a continuing decrease in weight and a slight decrease and plateau in heat flow, indicating that the rate of heat absorbed equals the rate of heat released. This is a result of continued volatile burning occurring simultaneously with the heating of the solid particles.

At 460°C for sulfite mill biosludge sludge and 535°C for kraft mill biosludge, there is a large exothermic peak accompanied by a sharp reduction in sample weight as the solids



2. Thermal behavior of kraft and sulfite mill biosludges: thermogravimetric analysis (TGA, upper), and differential scanning calorimetry (DSC, lower).

burn (char burning). The amount of fixed carbon was similar for both biosludge types. The total heat flow during combustion was determined by calculating the area under the exothermic peaks. The total heat flow was found to be 1324 kJ/kg for sulfite mill biosludge and 1242 kJ/kg for kraft mill biosludge. This difference is most likely a result of the higher heating value of the sulfite mill biosludge, which contains more organic matter and less ash (Table I). After the char burning, the heat flow decreases for both samples and no changes in sample weight are observed. The plateau of the weight loss curve at high temperatures indicates the combustion is complete. Ash contents of the kraft mill biosludge and sulfite mill biosludge were 25 wt% and 14 wt%, respectively.

Drying rates

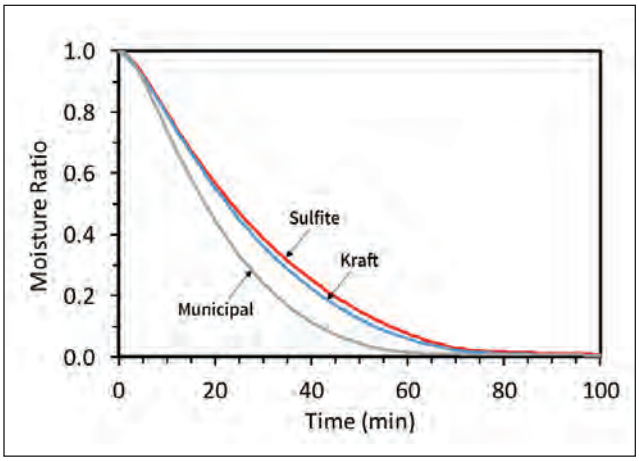
Upon drying, sludge samples lose weight as their moisture contents decrease. In this study, the change in sample weight during drying is expressed as moisture ratio to account for the difference in initial weight, as in Eq. (1):

$$\text{Moisture Ratio} = \frac{M - M_{Final}}{M_{Initial} - M_{Final}} \quad (1)$$

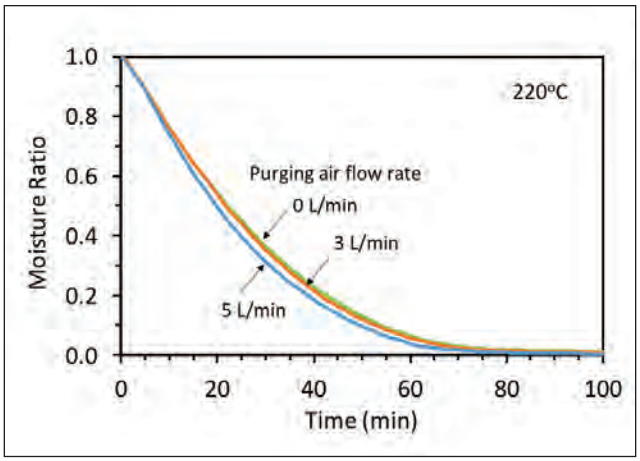
where M is the moisture content at time t (g H_2O/g dry solids), $M_{Initial}$ is the initial moisture content (g H_2O/g dry solids), and M_{Final} is the final moisture content (g H_2O/g dry solids).

Figure 3 indicates the drying curves for sulfite and kraft mill biosludges, which were mechanically dewatered to 13% solids, and municipal sludge, which could only be mechanically dewatered to 10% solids. The samples were dried at 220°C, with air flow rate of 1 L/min. The results indicate that the drying trends for sulfite and kraft mill biosludges are nearly identical and are similar to municipal sludge. The difference in drying rates can be attributed to the higher water content in the municipal sludge before drying.

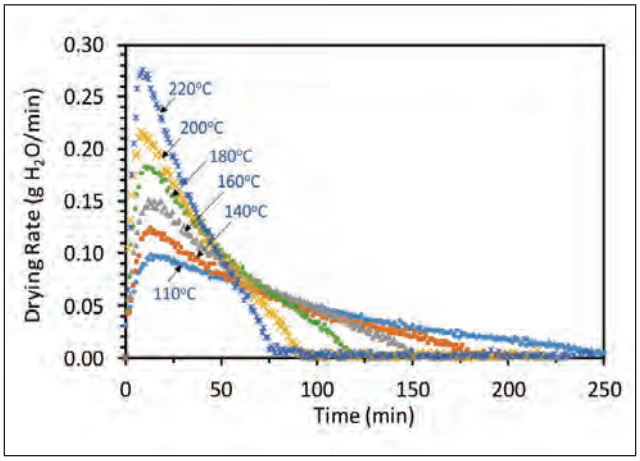
Figure 4 shows the effect of air flow rate on the drying of sulfite mill biosludge at 220°C. As expected, the biosludge drying rate increases as the air flow rate increases. This is because the greater velocity is more effective at removing the vaporized water from the sample, thus maintaining a concentration gradient.



3. Drying curve at 220°C and 1 L/min purging air flow rate for mechanically dewatered sulfite and kraft mill biosludges and municipal biosludge.



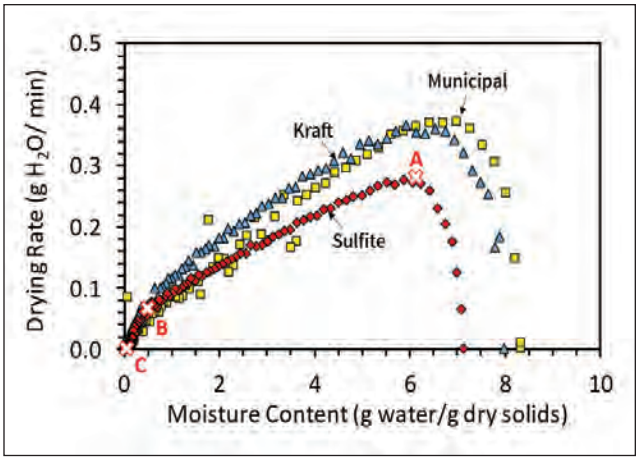
4. Effect of air flow rate on the drying curve of sulfite mill biosludge at 220°C.



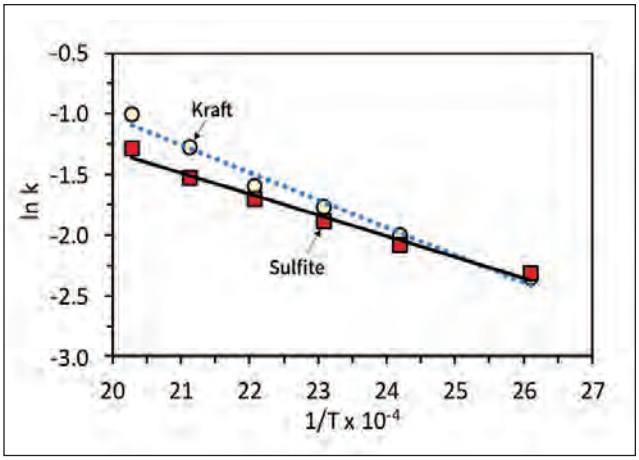
5. Drying rate curves of sulfite mill biosludge at temperatures between 110°C and 220°C and 1 L/min purging air flow rate.

The drying rate of sulfite mill biosludge dried at various temperatures from 110°C to 220°C is indicated in **Fig. 5**. The drying rate was determined by calculating the moisture content on a dry solids basis from the experimental data and then determined as the difference between two moisture contents in 1-min time intervals.

The drying rate at 220°C reached a maximum of 0.28 g H_2O/g dry solids at 9 min. During this time, the sample material undergoes heating as most of the thermal energy is absorbed by the water on the surface. Once enough thermal energy has been absorbed, the water on the sample surface will vaporize. The mass transfer rate will increase at the point where the initial vaporization briefly occurs. Once the maximum drying rate is reached, there is a sudden decrease in drying rate as the moisture content decreases. This is because the outer layer of the material has dried, forming a crust, and the water vapor must migrate from the sample interior to the sur-



6. Krischer curves showing the first and second falling rate periods for sulfite mill and kraft mill biosludges and municipal sludge at 220°C and 1 L/min purging air flow rate.



7. Arrhenius plot of sulfite and kraft mill biosludge at various temperatures with 1 L/min purging air flow rate.

face to escape. Because the distance the water must travel increases throughout the drying process, the rate is controlled by the diffusion of water toward the sample surface. Eventually, the drying rate reaches zero at 75 min because the moisture content is approximately zero and the concentration gradient between the sample and the hot air no longer exists.

Figure 6 shows the drying rates at 220°C of sulfite and kraft biosludges and municipal sludge as a function of moisture content. These curves, known as Krischer curves [8], suggest that the sulfite biosludge drying rate is lower than the rate for the kraft mill biosludge. This might be a result of the higher organic content in the biosludge, as suggested by Tuncal [9].

As suggested in previous studies [6,10], drying occurs primarily during two falling rate periods at two critical moisture contents. For the sulfite biosludge, for example, the first period is from A to B when the moisture content decreases from 5.8 to 0.3 g H_2O/g dry solids. The second period is from B to C when the moisture content decreases further from about 0.3 to 0 g H_2O/g dry solids. **Table II** summarizes the critical periods for all three types of sludge examined in this study.

The second critical moisture content of the pulp mill biosludges agrees with values reported in literature (0.4–0.8 g H_2O/g dry solids) [11]. However, the experimental value for municipal sludge is outside of this range and falls into the gelatin and gel category (>80 g H_2O/g dry solids). The critical moisture content is not solely a material property, but also

Critical Moisture Content	Sulfite Mill, g H_2O/g dry solids	Kraft Mill, g H_2O/g dry solids	Municipal, g H_2O/g dry solids
First (Point A)	5.8	6.5	6.7
Second (Point B)	0.4	0.4	0.4

II. Critical moisture contents of the tested biosludge.

depends on the drying conditions such as the temperature, drying rate, and humidity.

The rate constant for the drying process can be obtained by considering drying to be first order as follows in Eq. (2):

$$\frac{dM}{dt} = M_o e^{-kt} \quad (2)$$

where M is the moisture content at time t (g H_2O/g dry solids), M_o is the initial moisture content (g H_2O/g dry solids), t is time (min), and k is the rate constant.

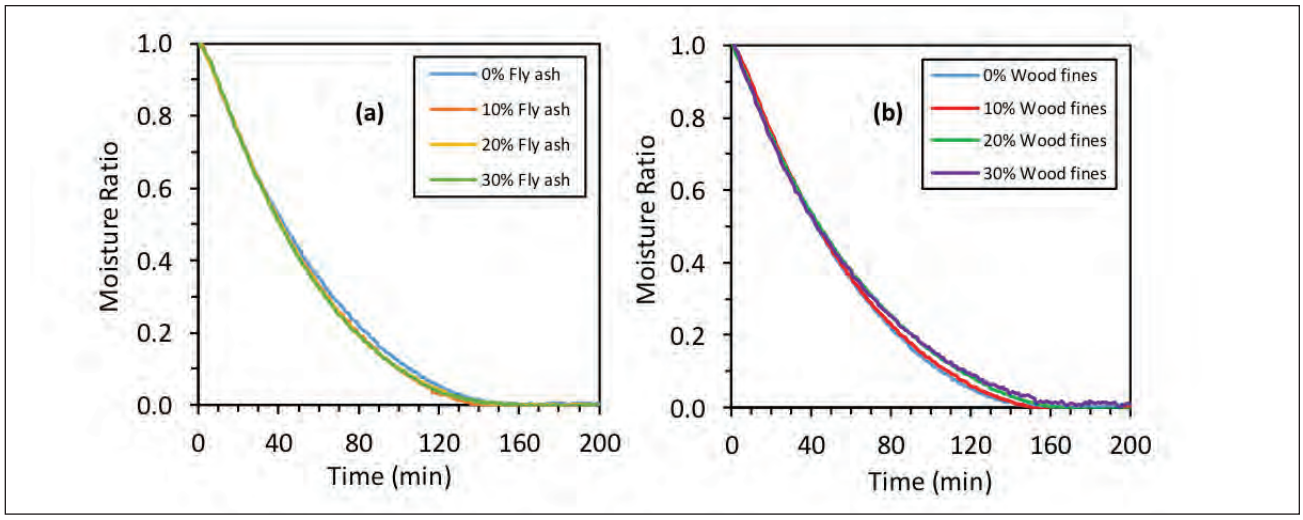
To obtain the drying rate constant for the sulfite biosludge, the natural logarithm of the maximum drying rate value for each temperature shown in Fig. 5 was plotted versus 1/T, where T is absolute temperature in °K. This Arrhenius plot was developed for both sulfite and kraft mill biosludges (**Fig. 7**).

Drying temperature clearly has a significant effect on the drying rate. The slope of this curve represents the activation energy, which is the minimum energy required for the process to proceed. The activation energy was determined to be 1742 kJ/mol for the sulfite mill biosludge and 2268 kJ/mol for the kraft mill biosludge.

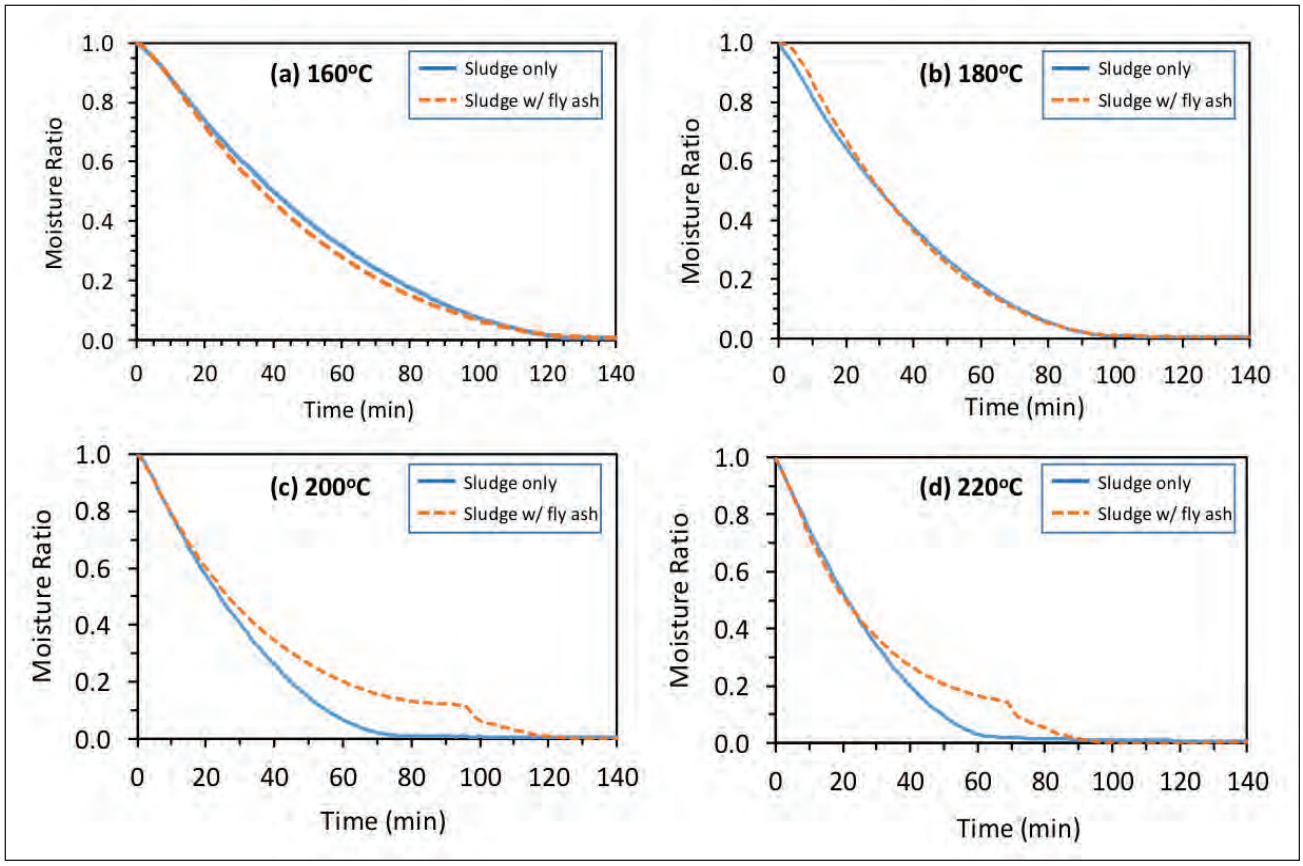
Effects of fly ash and wood fines addition

Fly ash and wood fines, common solid waste products at pulp mills, were added to the dewatered sludge mixture to test whether their addition can improve biosludge drying. These materials were oven dried and added to 10 g of biosludge in amounts of 10 wt%, 20 wt%, and 30 wt%. These tests were conducted at 140°C because higher temperatures would cause volatile burning of the wood fines.

Figure 8 shows the effect of fly ash and wood fines on the drying of biosludge. Fig. 8a indicates that the addition of fly ash has no effect. This could be caused by the low temperature (140°C), which did not allow the fly ash particles to reach high enough temperatures to alter the drying rate of biosludge. Fig. 8b indicates that the addition of wood fines adversely affects the drying of biosludge. This might be a result of the moisture-free wood fines absorbing moisture from



8. Effects of (a) fly ash and (b) wood fines on biosludge drying at 140°C with 1 L/min purging air flow rate.

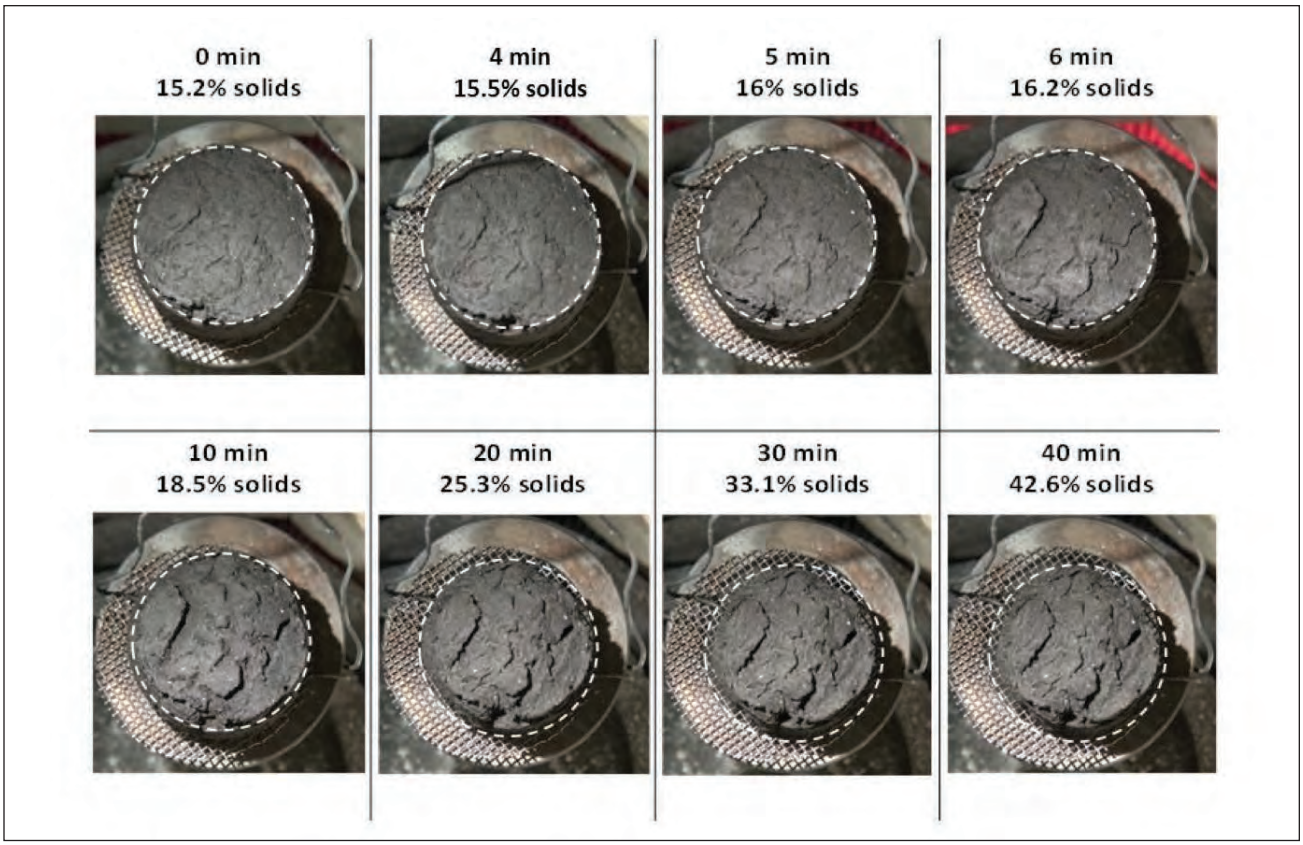


9. Effect of temperature on drying of biosludge mixed with 20 wt% fly ash with 1 L/min purging air flow rate.

the biosludge, as well as slower moisture transfer out of the wood fines than moisture transfer out of the biosludge. This agrees with findings on municipal sludge that suggest an increase in the organic content of the sludge adversely affects the drying potential [9].

From the results presented in Fig. 8, drying the sample at a low temperature was likely the reason the fly ash did not affect the drying behavior of biosludge. To test whether the drying temperature has an effect, 10 g of biosludge with 20 wt% fly ash were dried at various temperatures in the 140°C–220°C range. The results (**Fig. 9**) confirm that the fly ash does not have a significant impact on the drying behavior of biosludge.

At higher drying temperatures, 200°C and 220°C, sudden drops in the moisture content occur at 98 min and 70 min, respectively. This is caused by devolatilization of the sample,



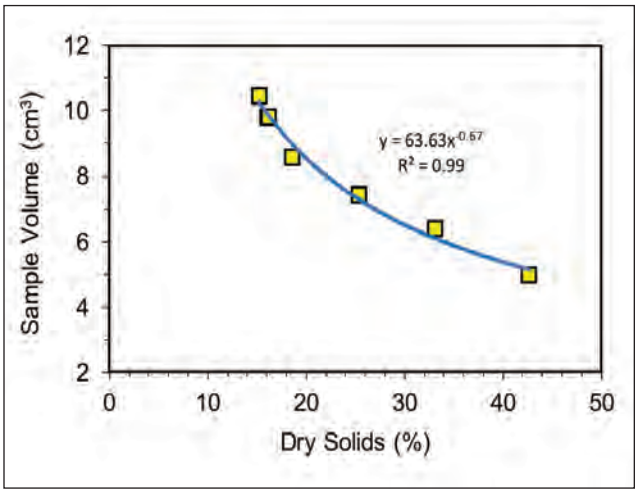
10. Crack development and shrinkage of the sulfite mill sludge during first 40 min of drying at 220°C with 1 L/min purging air flow rate.

where smoke was emitted. Devolatilization occurs initially at the surface and is reflected by the sudden weight loss indicated in Fig. 9c and Fig. 9d. Once the surface volatiles have escaped, the rate decreases as devolatilization occurs in the interior of the sample. In addition, the drying rates of the samples with fly ash at 200°C and 220°C were slower than the samples without fly ash, possibly because of the fly ash coating the sludge particles and preventing vaporization.

Sludge shrinkage during drying

The samples were prepared with dewatered sulfite mill biosludge, which had been molded into a cylinder using a cutout. During drying, the sludge passes through several physical stages and undergoes extensive cracking and shrinkage. **Figure 10** shows the shrinkage and cracking progression of biosludge during the first 40 min of drying at 220°C. After this, crack formation and shrinkage are difficult to notice visually.

Initially, the dewatered sludge is deformable with a soft pastelike consistency and shear thinning behavior. This was also noticed by Markis et al. in their study of biosludge rheology [12]. The drying behavior was comparable for all tests and sludge types. During the initial 5 min, a thin porous crust developed and the surface changed from slippery and shiny to rough and dull. As the moisture content decreases, the sludge cake shrinks and cracks form. Once the surface is no longer wet the thin porous crust develops into a hard impermeable



11. Change in volume of the sulfite mill sludge cake during the first 40 min of drying at 220°C with 1 L/min purging air flow rate.

layer, which continues to expand toward the center of the sample. The interior remains wet and malleable.

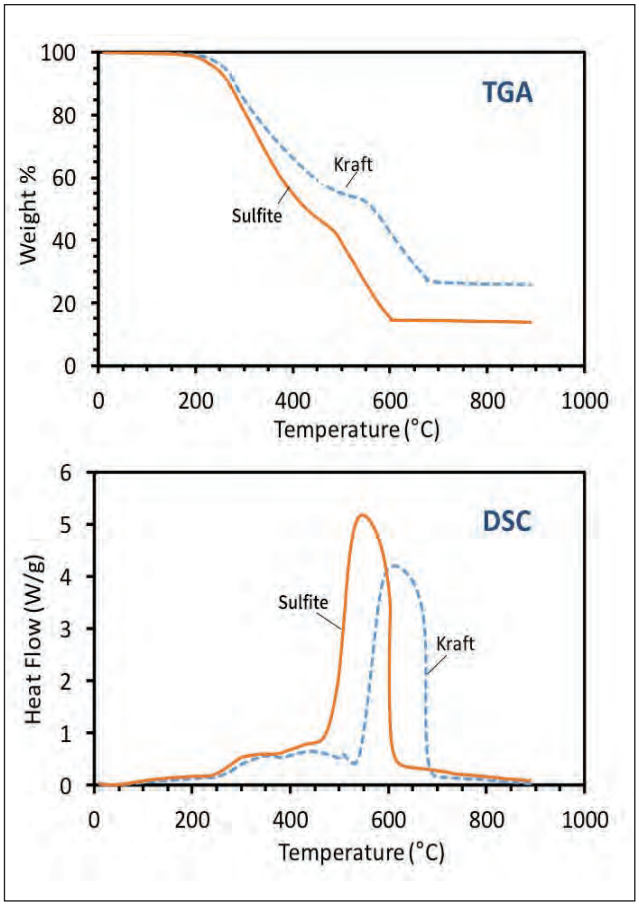
The top surface of the sample (the portion visible in Fig. 10) shrunk faster and had more crust growth than the bottom surface. Cracking accelerates crust growth and drying because it exposes more surface area to the hot air. The edges dry faster because they have greater contact with the air flowing past. Significant shrinkage and cracking are observed up

to 40–50 min at 55%–50% moisture, with only minor changes observed after this. These changes are random and unpredictable and can alter heat and mass transfer. Cracking is caused by nonuniform thermal stresses and an imbalance of surface capillary tension caused by shrinking [10,12]; it often begins in areas with superficial blemishes or low water content. Shrinkage occurs because of increasing particle-particle attraction as the water content decreases. Spalling, which results from tensile stresses and causes the sludge to lift, can also be observed. After approximately 100 min, the second drying period occurs and no shrinking is observed. As the sludge sample dries it became rigid, but brittle. The dried sample has many cracks and crevices, which can accelerate the drying process depending on their location and depth.

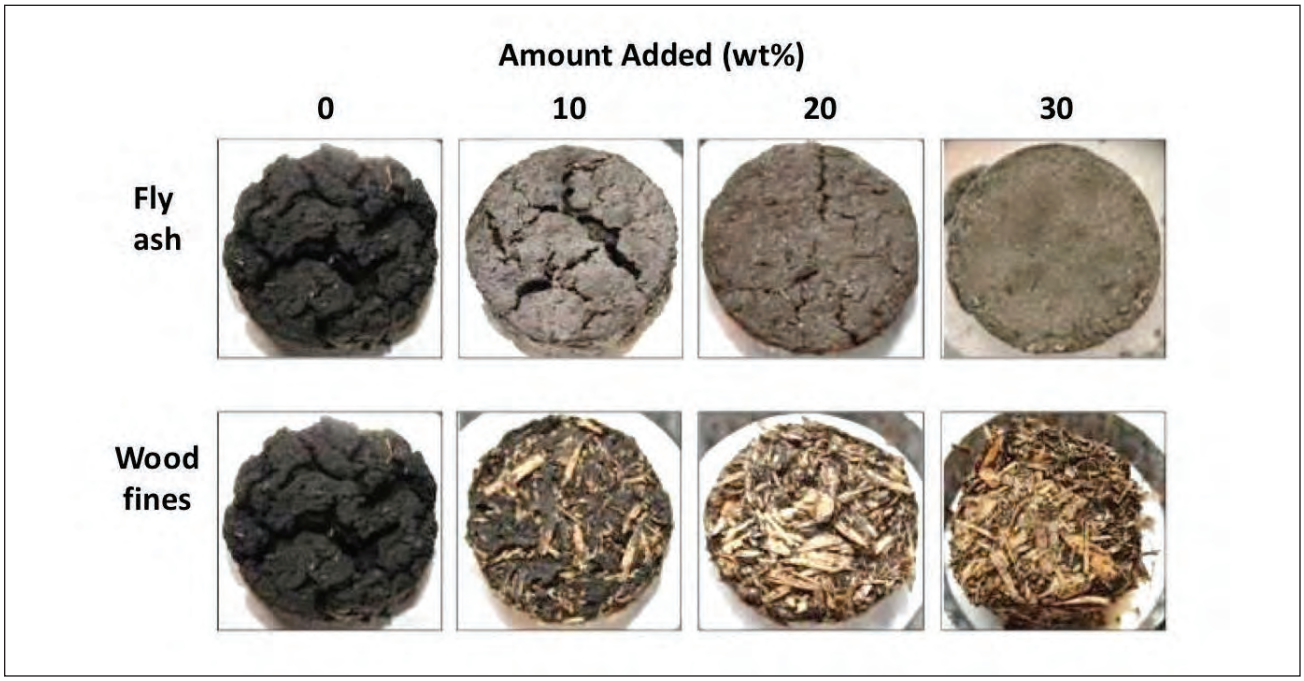
Figure 11 is based on the change in sample dimension shown in Fig. 10. The sample volume over the first 40 min of drying was estimated and plotted against the dry solids content of the sulfite mill sludge cake. The results indicate a rapid decrease in sample volume during the early stages of the drying process, when the sample is at higher moisture content, and corresponds to a higher drying rate. As the moisture content decreases, the rate of change of the sample volume also decreases because less water fills the voids within the sludge cake. This continues until the voids within the sample cake are empty.

Effect of fly ash and wood fines on shrinkage and cracking

We hypothesized that the addition of solids would support the solid sludge structure, increase available surface area, and reduce shrinkage. **Figure 12** shows the percentage de-



12. Effect of adding fly ash and wood fines on sludge shrinkage during drying at 220°C with 1 L/min purging air flow rate.



13. Comparison of crack formation between biosludge and biosludge mixed with various amounts of fly ash and wood fines. Samples were dried at 220°C with 1 L/min purging air flow rate.

crease in volume between samples of sludge with and without solids added. As expected, the sample shrinkage decreases as the amount of added solids increases. The samples mixed with wood fines shrink less than those with fly ash. The wood fines are much lighter than the fly ash, so for a given mass more wood fine particles would be present than fly ash. In addition, the wood fines have a larger volume and thus interact more with one another to form a stronger structure that is more resistant to shrinkage.

As indicated in **Fig. 13**, the addition of solids reduces cracking of the sample during drying. The cracking is further reduced as more solids are added to the sludge sample; this reduction is observed for both fly ash and wood fine additions. More cracking occurs in the samples with fly ash than those with wood fines, which are larger and more rigid and thus provide more support for the sludge.

CONCLUSIONS

A systematic study was performed to investigate the drying behavior of biosludges from a sulfite mill and a kraft mill. The results show that the drying behavior of sulfite and kraft mill biosludges is nearly identical, and the drying behavior is similar to that of municipal sludge. The drying rate of biosludge with low solids content increases initially and then decreases mostly linearly with an increase in solids content. Increasing the drying temperature increases the drying rate as expected, and the addition of fly ash and wood fines does not facilitate drying but reduces shrinkage and cracking. Fly ash facilitates devolatilization of sludge at temperatures greater than 200°C, and higher organic content may decrease the drying potential of biosludge. These findings provide a better understanding of how pulp and paper mill biosludge behaves as it is dewatered and dried. **TJ**

ACKNOWLEDGEMENTS

This work was conducted as part of the research program Increasing Energy and Chemical Recovery Efficiency in the Kraft Process—III. The program is jointly supported by the Natural Sciences and Engineering Research Council of Canada (NSERC) and a consortium of the following companies: Andritz, AV Nackawic, Babcock & Wilcox, Boise, Carter Holt Harvey, Celulose Nipo-Brasileira, Clyde-Bergemann, DMI Peace River Pulp, Eldorado, ERCO Worldwide, Fibria, FPInnovations, International Paper, Irving Pulp & Paper, Kiln Flame Systems, Klabin, StoraEnso Research, Suzano, Tembec, Tolko Industries, Valmet, and WestRock.

LITERATURE CITED

1. Mowla, D., Tran, H.N., and Allen, D.G., *Biomass Bioenergy* 58: 365(2013).

ABOUT THE AUTHORS

For many mills, biosludge disposal is a problem that will only worsen as landfill space declines. We wanted to explore the fundamentals of biosludge drying and provide insights into making biosludge a more attractive fuel for combustion in biomass boilers

Previous research focused primarily on mechanically dewatering biosludge. Although drying is used at some mills as part of the disposal process, a fundamental understanding of the drying process is lacking. This research aims to characterize this process and provide insight into improving biosludge disposal.

One of the more challenging aspects of the research was the length of some of the experiments. We addressed this by preparing a detailed experimental plan and extending working hours as needed. One of the researchers was a new graduate student with limited knowledge of the pulp and paper industry and waste water systems. This research served as an introduction to both subjects that also provided a new appreciation for the industry.

It was interesting to see the similarities between the drying curves of biosludge from pulp and paper mills and sludge from municipal waste water treatment systems. The sudden decarbonization of biosludge when mixed with fly ash and dried at higher temperatures was also surprising.



Hovey



Allen



Tran

For mills, this research provides additional insight into biosludge disposal, in particular the use of biosludge as a fuel in biomass boilers. Possible next steps would be to dry biosludge in a laboratory-scale dryer to better simulate industrial drying processes and to test biosludge from different mill types to observe any differences.

Hovey is a graduate student; Allen is professor and chair; and Tran is Frank Dottori Professor of Pulp and Paper and director of the Pulp and Paper Centre, Department of Chemical Engineering and Applied Chemistry, at the University of Toronto, Toronto, ON, Canada. Email Tran at honghi.tran@utoronto.ca.

2. Forest Products Association of Canada, "2009 FPAC sustainability report," FPAC, Ottawa, ON, Canada, 2009. Available [Online] at http://www.fpac.ca/wp-content/uploads/Sustainability_Report_2009-e.pdf <15Aug2017>.
3. Kantardjieff, A. and Jones, J., "Pulp and paper sludge to energy: preliminary assessment of technologies," Canmet Rept. #34-0173-471.1, CanmetEnergy, Varennes, QC, Canada, 2005.
4. Rashid, M., Barry, D., and Gross, M., *Soil Environ.* 25(2): 85(2006).
5. Arlabosse, P., Chavez, S., and Prevot, C., *Braz. J. Chem. Eng.* 22(2): 227(2005).
6. Reyes, A., Eckholt, M., Troncoso, F., et al., *Drying Technol.* 22(9): 2135(2004).
7. Orang, N. and Tran, H.N., *TAPPI J.* 14(10): 629(2015).
8. Krischer, O. and Kast W., *Die wissenschaftlichen Grundlagen der Trocknungstechnik*, Springer, Berlin, 1978.
9. Tuncal, T., *Water Environ. Res.* 83(5): 405(2011).
10. Mujumdar, A. and Devahastin, S. in *Mujumdar's Practical Guide to Industrial Drying* (S. Devahastin, Ed.), Exergex Corporation, Montreal, 2000, Chap 1.
11. Markis, F., Baudez, J., Parthasarathy, R., et al., *Chem. Eng. J.* 253: 526(2014).
12. Leonard, A., Blacher, S., Pirard, S., et al., *Drying Technol.* 21(8): 1507(2003).

Modeling the influence of forming fabric structure on vacuum box dewatering

BJÖRN SJÖSTRAND, CHRISTOPHE BARBIER, AND LARS NILSSON

ABSTRACT: This investigation used numerical models to describe forming section sheet dewatering at the high vacuum suction boxes. Three different fabric structures were examined with numerical models for single-phase flow of air and for two-phase flow of air and water. This was done to evaluate how forming fabric structure influences sheet dewatering. The numerical models were compared with an experimental study of the same fabrics investigated on a laboratory suction box. The small differences in dewatering rate in the experimental study could be simulated with the models, which confirmed the validity of the models. This implies that these numerical models can be used to describe new fabrics and how they will respond in the papermaking process.

Application: This article explains how numerical models can be used by manufacturers of paper machine clothing to obtain insights into how forming fabrics influence dewatering processes without investments in laboratory equipment and time-consuming experimental work.

Sheet dewatering is an important step of paper manufacturing. It demands huge amounts of energy over several unit operations, including dewatering by vacuum suction, pressing, and drying. An understanding of the mechanisms of dewatering in the different unit operations is fundamental to finding ways to reduce the energy requirements of paper manufacturing. This article focuses on sheet dewatering at the high vacuum suction boxes, and especially the forming fabrics' role in sheet dewatering. By using numerical models, the industry can obtain insights and vital information about dewatering processes without huge investments in laboratory equipment or costly manufacturing processes.

In the 1950s, Ergun [1] investigated single-phase flow through porous media and derived a calculation of flow rate as a result of pressure drop and material properties. We used Ergun's work as a foundation for calculations of flow of water and air through sheet and fabric in this study. Ergun's work combines the theory of high and low flow rates and is valid for a large interval of Reynolds numbers.

Li and Green [2] developed numerical models of the more complex system of fibers suspended in water and dewatered on a simple forming fabric. The fibers are added individually with random orientation to the simulated single sine-wave fabric. Surface roughness is measured as the topological differences of the resulting fiber mat. The bending stiffness of the fibers is considered, but Li and Green ultimately connected the greatest effect (over 50%) of surface roughness to the forming fabric structure. The dewatering velocity affects the bending of fibers and, therefore, the surface roughness [2].

Rezk et al. [3] described the dewatering of sheet and fabric structure in two-dimensional numerical models. They showed that two-phase flow simulations could be used to describe the dewatering of a sheet with fast initial dewatering and a certain amount of water being left in the sheet and steady state airflow toward the end. The calculated dewatering rate was twice as high as measured values, but the airflow matched the researchers' experimental data [3]. In a later article, Rezk et al. [4] concluded that the fabric structure was best described by using a combination of solid fabric yarns and flow resistance compared with only using flow resistance. After thus improving the description of the forming fabric, calculated and measured dewatering rates were in better agreement.

In the forming section, the forming fabric is known to affect sheet dewatering by its general design at the gravitational dewatering [5] and also more specifically by caliper, void volume, and air permeability at the high vacuum suction boxes [6]. Helmer et al. [5] used a high-speed digital imaging system to analyze dewatering during sheet forming and connected sheet properties and drainage behavior to fabric structure. The drainage velocity was different for different fabrics, and also for fabrics of identical weave pattern but different yarn diameter. The dewatering velocity was shown to affect sheet properties. Indirectly, the fabric structure is responsible for sheet properties and dewatering velocity [5].

According to Granevald et al. [6], the fabric parameters that affect sheet dewatering are fabric caliper, void volume, and air permeability. When these parameters are kept constant and the open area profiles of different fabrics are changed during high vacuum dewatering, Sjöstrand et al. [7] showed that different dewatering rates were obtained for different fabric structures. This difference in dewatering rate is seen at short dwell times (0–2.5 ms) and high pressure drops (40 kPa). The experimental work of Sjöstrand et al. [7] other-

wise shows the same development of dewatering with dwell time in a suction box as previous studies [8,9].

This article builds and expands on previous experimental work [7] by performing a deeper study of measurement uncertainty and by using numerical models to simulate single-phase airflow through forming fabrics and two-phase flow of water and air through sheet and fabric. This article explains how numerical models can be used by the paper industry to obtain insights into the mechanisms of dewatering processes without huge investments in laboratory equipment or costly breaks in manufacturing.

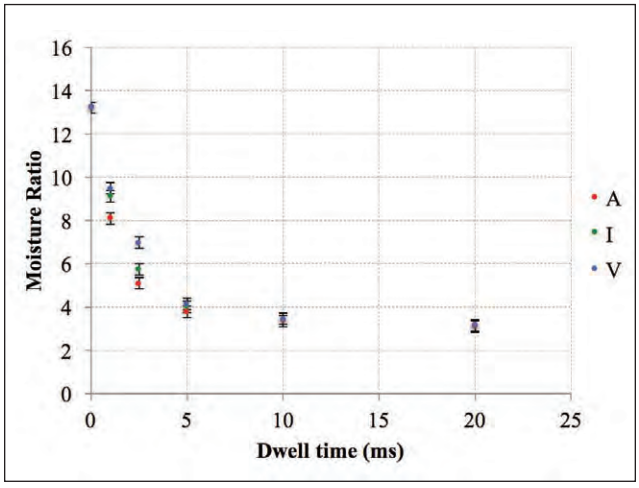
METHOD

All previous dryness measurements [7] were performed in triplets by the same researcher and on the same equipment. We therefore used pooled variance (Eq. [1]) on all measurement points to get the measurement uncertainty instead of using the variance on each separate triple measurement point.

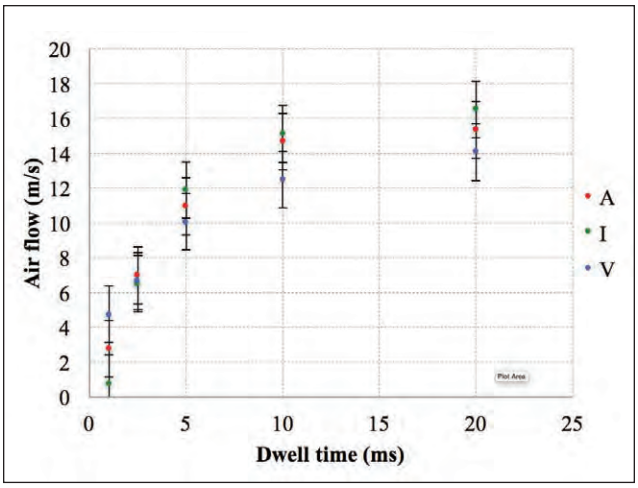
$$s^2 = \frac{\sum_{i=1}^{k}(n_i-1)s_i^2}{\sum_{i=1}^{k}(n_i-1)} \quad (1)$$

where the measurement series are numbered from 1 to k, s^2 is pooled variance, n_i is sample size of measurement series i, and s_i is standard deviation of measurement series i.

Figures 1 and **2** show results from the previous study [7], with the updated measurement uncertainty. This and the previous study [7] used the same fabrics in the experimental work presented by Sjöstrand et al. [7]. The fabrics had similar values for the caliper, void volume, and air permeability. They did, however, have different structures. The structures were defined by the open area profiles and were given the letters A, V, and I. The letters are based on the open area in the two bottlenecks where fabric A has a low open area in the sheet side bottleneck and high open area in the wear side bottle neck. Fabric V has a high open area in the sheet side bottleneck and low open area in the wear side bottleneck. Fabric I has an open area with values between those of fabrics A and V in sheet and wear sides.



1. Moisture ratio versus dwell time for the three fabrics of different open area profiles denoted as A, V, and I.



2. Airflow versus dwell time for the three fabrics of different open area profiles denoted as A, V, and I.

The open area profiles were obtained from the fabric manufacturer (**Fig. 3**). These were determined with x-ray microtomography. **Table I** shows more information regarding the three fabrics used. Moisture content of the sheets is expressed as moisture ratio (MR) and defined by Eq. (2):

$$MR = \frac{mass\ of\ water}{mass\ of\ dry\ content} \quad (2)$$

Single-phase numerical model

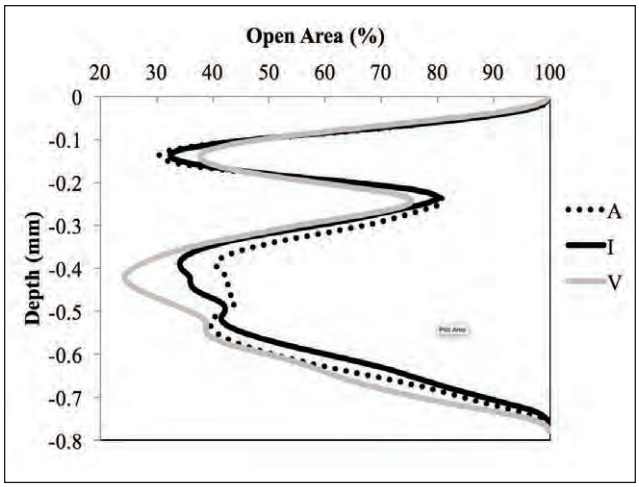
Ergun [1] developed an equation, Eq. (3), for flow through porous media, which can be used to formulate representative flow resistances of forming fabrics and paper sheets:

$$\frac{\Delta P}{L} g_e = 150 \frac{(1-\epsilon)^2}{\epsilon^3} \frac{\mu U_m}{{D_p}^2} + 1.75 \frac{1-\epsilon}{\epsilon^3} \frac{G U_m}{D_p} \quad (3)$$

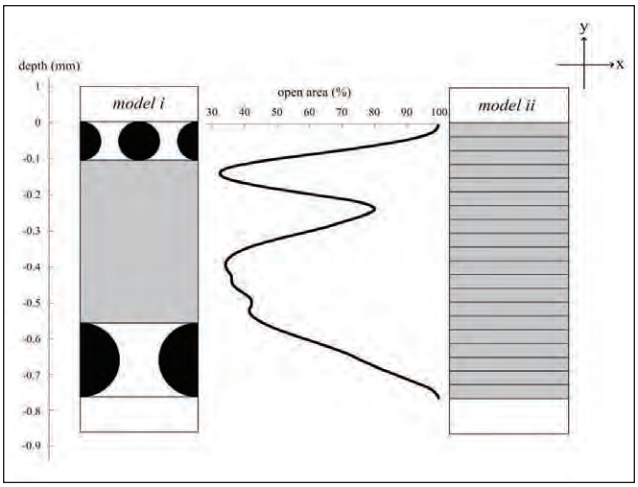
where ΔP is the pressure difference (Pa), L is the caliper (m), g_e is a gravitational constant (kg×m/N×s²), ϵ is volume fraction solid, μ is the dynamic viscosity (Pa×s), U_m is fluid velocity (m/s), D_p is yarn/fiber diameter (m), and G is the mass flow rate (kg/s×m²).

The flow resistance of the fabrics was evaluated experimentally at room temperature by applying different pressure drops between 30 Pa and 500 Pa and measuring the airflow through one of the fabrics (Fabric I). Fabric I was then modeled in two ways, model *i* and model *ii* (**Fig. 4**), both based on the open area curves (Fig. 3) of the fabric. The most basic way of modeling this is to use Eq. (3) for flow through porous media (model *iii*) [1].

Models *i* and *ii* were used in the modeling software COMSOL Multiphysics (COMSOL; Burlington, MA, USA), with size parameters from Table I and the stationary laminar single-phase flow



3. Open area profiles of the three fabrics.



4. Two ways of describing forming fabrics (i and ii).

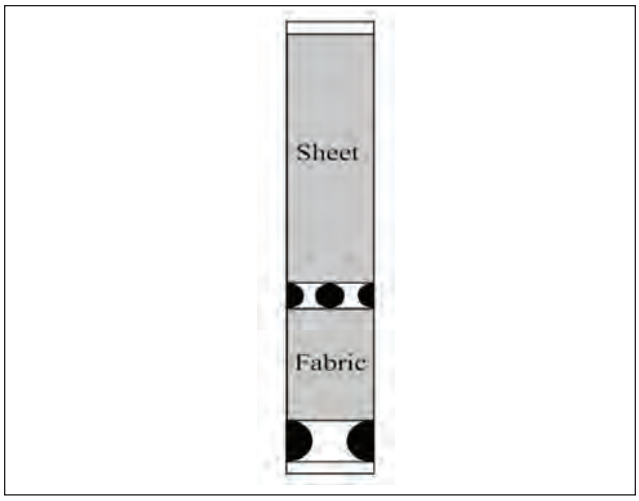
study. Both models are 0.32 mm wide and have a caliper of 0.76 mm. Each model has two additional rectangles, with y = 0.1-0 mm for one and y = 0.76-0.86 mm for the other. The purpose of the rectangles is to avoid flow issues at the corners and to provide an initial interface. They do not contribute to any flow resistance. The horizontal inlet boundaries (y = 0.1 mm) (Fig. 4) are set to atmospheric pressure and the horizontal outlet boundaries (y = -0.86 mm) to a pressure corresponding to the structure's varying pressure drop, according to the experimental data. The pressure difference between inlet and outlet drives the flow. The vertical boundaries are symmetry lines ($u_x = 0$) and the fabric yarn surfaces of model *i* are solid, no-slip walls where no flow can penetrate ($u_x = 0$; $u_y = 0$), where u is flow velocity. The flow is assumed to be incompressible and the temperature is set to 293.15 K. The flow resistances are built from [1] with yarn diameter and volume fraction solid from the actual values of the fabrics (**Table II**). The geometry of model *i* was also defined with yarn diameter and openness in sheet side and wear side and mean flow resistance between these yarn segments. Model *ii* was defined only by flow resistance and was divided into 20 layers with individually calculated mean volume fraction solid from the open area profiles (Fig. 3). For each layer, flow resistance was calculated from Eq. (3). Finally, the average volume fraction solid and average yarn diameter were used to model the flow according to the original form of the Ergun equation (Eq. [3]) without using any software. These three models were compared with the experimental data. For the first two models (*i* and *ii*), the resulting flow rates were not mesh-sensitive in the software and converged fast. The third model (*iii*) was solved analytically.

Profile	Caliper, mm	Void Volume, mm^3/cm^2	Permeability, cfm	Open Area Sheet Side, %	Open Area Wear Side, %	Sheet Side Yarn Diameter, mm	Wear Side Yarn Diameter, mm
A	0.78	47.5	356	30.5	39.5	0.11	0.18
V	0.78	43.6	330	37.7	24.4	0.13	0.21
I	0.76	45.9	362	32.4	34.1	0.11	0.18

I. Characteristics of the three versions of forming fabrics studied.

Dimension	Fabric A		Fabric V		Fabric I	
	Real	Model	Real	Model	Real	Model
Sheet side yarn diameter, mm	0.11	0.11	0.13	0.13	0.11	0.11
Sheet side openness, %	30.5	30.5	37.7	37.7	32.4	32.4
Wear side yarn diameter, mm	0.18	0.18	0.21	0.16	0.18	0.21
Wear side openness, %	39.5	43.1	24.4	23.3	34.1	35.5

II. Fabric dimensions for real fabrics and corresponding models.



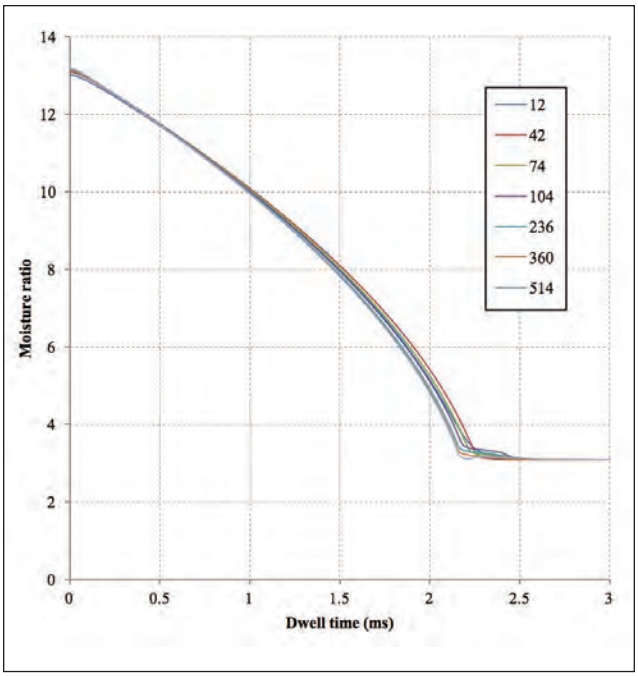
5. Picture of the model of fabric and sheet used in the COMSOL Multiphysics program. This model has two rectangles, as do the previous models. Their purpose is to avoid flow issues that might affect the corners of the fabric models.

To take full advantage of symmetry lines in the simulation, the models' wear sides were slightly modified according to Table II. Fabric A, V, and I are simulated according to Table II in two-phase flow models.

Two-phase numerical model

The structure of the fabric was thereafter described with model *i* with a sheet added on top of the fabric structure. The geometry of this numerical model (**Fig. 5**) was also built in COMSOL Multiphysics with size parameters from Table I modified according to Table II. This time, the study was a time-dependent laminar two-phase flow, otherwise with identical model structure except for the addition of the sheet and 40 kPa pressure drop over the structure. Two interface tracking methods were available in the software: level set and phase field. The phase field method uses two transport equations. It is more exact and demands more computational power than does the level set method, which uses one transport equation. We used the phase field method because we needed the interface calculations to be as detailed as possible, even though the calculation time increased with this. The flow resistance of the sheet was based on measured fiber width. The volume fraction solid was set to 0.45 to fit the experimental data. The wood fibers were characterized with a Lorentzen & Wettre fiber tester (ABB Process Automation Division; Kista, Sweden). The length-weighted mean width was 31 μm, with approximately 95% of the fibers ranging between 20 μm and 40 μm.

We evaluated the moisture ratio for the sheet during the dewatering by integrating volume fraction water over time for the sheet. After this, the model was used with the same geometry and basic settings and compressible steady state single-phase airflow to compare with the experimental data. The velocity was calculated by integrating over the outlet boundary with respect to flow velocity.



6. Mesh sensitivity of dewatering of the two-phase model. The numbers 12-514 indicate the number of mesh elements in the small rectangle on top of the model; 12 is the coarsest and 514 is the finest mesh.

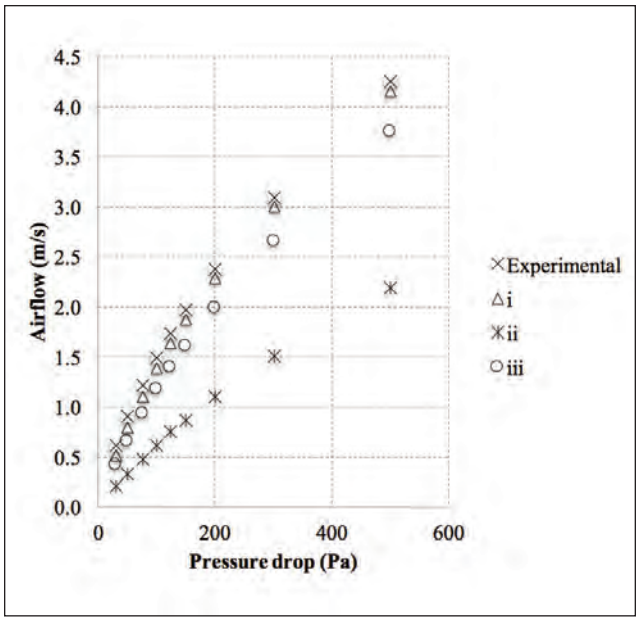
The model was mildly sensitive to the mesh (**Fig. 6**). The mesh of the model was varied between 12 and 514 mesh elements in the rectangle above the model. Figure 6 shows that the moisture ratio dependence on dwell time is almost exactly the same for the different mesh settings. The differences decline with every step of increasing mesh complexity. The largest time difference to reach a moisture ratio of 4 was 0.08 ms, which is negligible. The differences in mean dewatering rate are extremely small between the different mesh configurations.

Finer mesh leads to longer computation time. The mesh denoted "514" took about 8 h to run on an ordinary desktop computer. With respect to the appearance of Fig. 6 and the computational time, the results presented in this study are performed with the coarsest mesh.

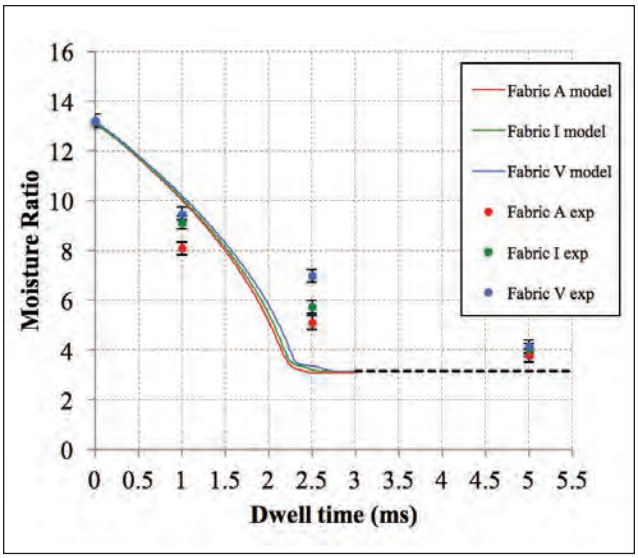
Fabric model *i* was based on the dimensions of the yarns in the actual fabrics. We needed to keep the dimensions in the sheet side intact and alter the wear side to fully use symmetry and thereby reduce the computation time. The wear side alteration was chosen over sheet side alteration because of sheet side influence on dewatering and paper properties [5]. Wear side geometry mainly affects machine runnability and is designed with higher yarn diameter than the sheet side [10].

The dewatering velocity was calculated for the experiments as the slope between the moisture ratio values of 0 ms and 2.5 ms (Fig. 1). The models' dewatering rates were calculated as the mean velocity for the entire dewatering process, which is approximately 2.5 ms.

Eq. (3) is suitable for a large interval of Reynolds numbers



7. Airflow versus pressure drop for the three ways of modeling the fabric and the experimental data.



8. Dewatering velocity versus dwell time for each model.

(N_{RE}), the highest N_{RE} in each model was calculated according to Eq. (4). The highest values of N_{RE} were 10 for the single-phase model with air (only fabric), 20 for the two-phase model with air, and 30 for the two-phase model with water.

$$N_{RE} = \frac{D_p \rho U_0}{4(1-\epsilon)\mu}, \quad (4)$$

where D_p = yarn/fiber diameter (m), ρ = density (kg/m^3), U_0 = velocity (m/s), ϵ = volume fraction solid, and μ = dynamic viscosity (Pa×s).

RESULTS AND DISCUSSION

Single-phase numerical model

Figure 7 shows the three single-phase models of the fabric and the experimental values of the pressure drop over the fabric.

Model *i* is in excellent agreement with the experimental data in Fig. 7. A fabric model similar to model *i* was previously shown to yield dewatering rates in fair agreement with experimental data [4]. The comparison between measured and calculated airflow further demonstrates that this type of model is useful, especially because no fitting parameters were needed to obtain the excellent agreement with experimental data. Initial work started with *i* based on results of Rezk et al. [4]. Model *i* involves partly describing the structure based on actual yarn diameters and local open area percentages and partly based on average flow resistance. The other two models (*ii* and *iii*) are not as capable of modeling the airflow as *i*, and based on Rezk et al. [4].

Looking at Fig. 7, it is challenging, at first, to understand why the third model (*iii*) is more efficient in describing the experiments than the more advanced numerical model (*ii*), which is based on flow resistance by the same equation. This can be explained by the nature of the equation. Eq. (3) describes the porous material as a continuum that is defined by two parameters, characteristic diameter and volume fraction solid. The equation was built with large amounts of data from materials that are much thicker than the characteristic diameter. Model *ii* is divided into 20 pieces that make every layer thinner than the yarn diameter; the thickness is about 30% of the yarn diameter in the example from Fig. 4. This can be one of the explanations why *iii* is closer to the experimental values than is *ii* in Fig. 7. The results of Fig. 7 show that even the simplest model can accurately model the actual airflow of fabrics.

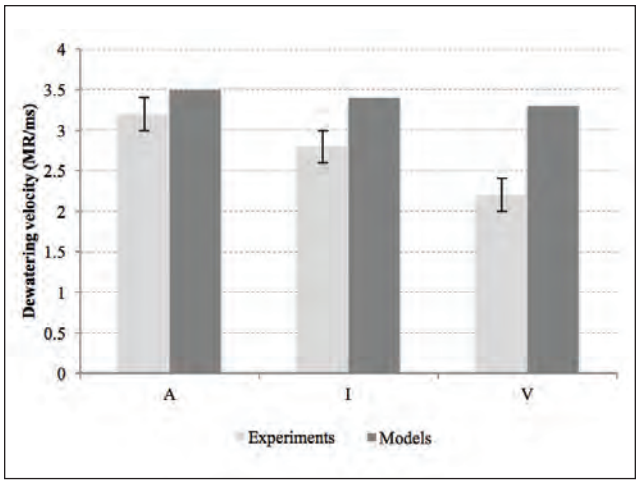
Two-phase numerical model

Figure 8 shows the moisture ratio for the dewatering for models and experiments. **Figure 9** compares the mean velocities.

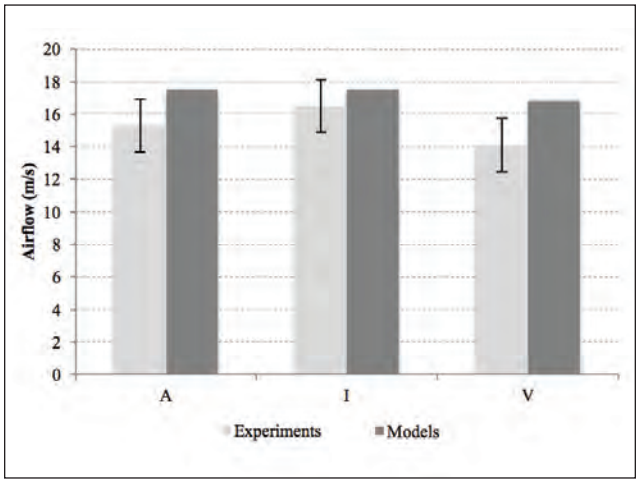
The curves in Fig. 8 differ. The dewatering velocity in the experimental data is fastest in the beginning and decreases toward the final moisture ratio. The models are slow in the beginning because of acceleration of the entire water column and speed up toward the end because of the absence of opposing forces such as capillary forces and other forces bonding water to the fibers. This makes it harder to compare dewatering velocity between the two than if the curves were more similar in shape.

The steady state airflow is almost identical for the models and lies within the confidence interval for the experimental values (**Fig. 10**). This is expected because of the small flow resistance the fabrics create, compared with the sheet. When the fabrics also are very similar, it seems natural that the airflow should be the same experimentally and from the numerical models.

The fabrics tested by Sjöstrand et al. [7] were very similar to each other. The results from the experimental study show



9. Mean dewatering velocities for experiments and models for the three fabrics.



10. Measured and calculated steady state airflow for the fabrics.

very little variation between the three. The fabric structure alone is only responsible for small differences in dewatering rate at certain conditions, such as the 40 kPa pressure drop and high flow resistance of the pulp [7]. All three fabrics are woven in the same fashion and the major parameters (caliper, void volume, and air permeability) are the same.

The geometry of the models was modified to enable symmetry lines. This gives dissimilar values for the wear side yarn diameter and open area compared with the real fabrics (Table II). It can be hard to draw conclusions on how and why the experiments by Sjöstrand et al. [7] turned out as they did, based on these models alone. That is not the most important reason for performing this study, however. The models are still very accurate. They can detect the minute differences between the fabrics that the experimental study show. The different dewatering rates in the experimental results could be seen in the numerical models. Figures 9 and 10 show almost identical dewatering velocity and airflow results for the numerical models and the experimental data. The model could be expanded to include some extreme fabrics that have different open area profiles or yarn diameter in the sheet side and wear side. The numerical models could in that case be used to find out how new fabric designs affect the dewatering.

CONCLUSION

Computational fluid dynamics flow models were made of forming fabrics with flow of air and water driven by pressure drop simulating high vacuum suction box dewatering. The models were based on previously performed experiments of vacuum dewatering with three different forming fabrics. The influence on dewatering by forming fabric structure was investigated. Single-phase models of the forming fabrics were in excellent agreement with the experimental results. Models of paper sheet and forming fabrics showed the same magnitude of the experimental results for both air velocity and dewatering rate. The small differences in dewatering rate that the experimental results showed between the different fabrics structures could be detected with the models. This implies that these numerical models can be used to test how new fabric designs will respond in the papermaking process. **TJ**

LITERATURE CITED

1. Ergun, S., *Chem. Eng. Progr.* 48(2): 89(1952).
2. Li, J. and Green, S.I., *TAPPI J.* 11(8): 39(2012).
3. Rezk, K., Nilsson, L., Forsberg, J., et al., *Chem. Eng. Sci.* 101: 543(2013).
4. Rezk, K., Nilsson, L., Forsberg, J., et al., *Drying Technol.* 33(5): 605(2015).
5. Helmer, R., Covey, G.H., Raverty, W.D., *Appita J.* 59(3): 202(2006).
6. Granevald, R., Nilsson, L.S., and Stenström, S., *Nord. Pulp Pap. Res. J.* 19(4): 428(2004)
7. Sjöstrand, B., Nilsson, L., and Barbier C., "Influence on sheet dewatering by structural differences in forming fabrics," *PaperCon*, TAPPI Press, Atlanta, GA, USA, 2016.
8. Neun, J.A., *Tappi J.* 77(9): 133(1994).
9. Norman, B., *The Fundamentals of Papermaking Materials, Transactions of the 9th Fundamental Research Symposium*, Mechanical Engineering Publications, London, 1989, p. 73.
10. Räisänen, K., in *Papermaking Part 1, Stock Preparation and Wet End*, Vol. 8: Papermaking Science and Technology (J. Gullichsen and H. Paulapuro, Eds.), Finnish Paper Engineers Association, Helsinki, Finland, 2000, p. 417.

ABOUT THE AUTHORS

The goal of this study was to investigate how the open area profile of forming fabrics affects the dewatering at high vacuum suction boxes and to expand the knowledge of how fabrics influence dewatering at the forming section.

This research builds on previous experimental work and adds the dimension of numerical models. A challenge in conducting the study was learning how to use the software. The software was previously unknown for me (Sjöstrand), which added some difficulties. I attended seminars and practices with colleagues.

A result of the study was learning how useful tools such as numerical modelling can be when designing forming fabrics. An interesting finding was that the equation from Ergun (1952) was accurate when modeling single-phase airflow through forming fabrics.

A benefit to mills and other researchers is that no expensive laboratory equipment is needed to perform simple investigations of flow of air and water through fabrics and sheets.



Sjöstrand



Nilsson



Barbier

Future studies might further develop the numerical models, perhaps to include rewetting and more complex sheet models.

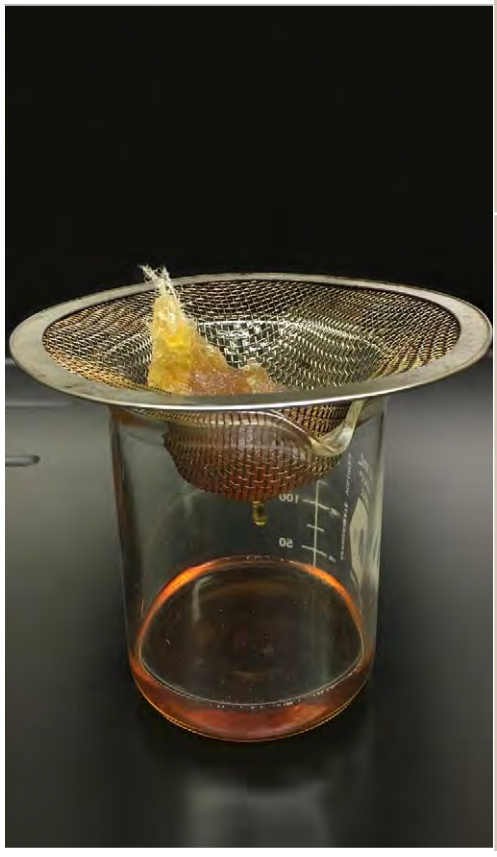
Sjöstrand is a Ph.D. student and Nilsson is professor, Department of Engineering and Chemical Sciences, Karlstad University, Karlstad, Sweden. Barbier is paper physics specialist, R&D Gruvön, BillerudKorsnäs AB, Sweden. Email Sjöstrand at bjorn.sjostrand@kau.se.

TAPPI JOURNAL
WWW.TAPPI.ORG
THE PAPER AND PACKAGING INDUSTRIES' TECHNICAL RESOURCE **SEPTEMBER 2017** | VOL. 16 NO.9









BIOREFINERY **495**
Addition of corn stover arabinoxylan into hardwood during pulping for improved physical properties
Anurag Mandalika and Troy M. Runge

NONWOVENS **507**
Oil absorption and desorption by polypropylene fibers
Praveen Kumar Yegya Raman, Akshay Jain, and Seshadri Ramkumar

PAPERMAKING **519**
Three-dimensional pore structure visualization and characterization of paper using X-ray computed tomography
Yves Defrenne, Vasili Zhdankin, Sahana Ramanna, Shri Ramaswamy, and Bandaru V. Ramarao

RECYCLING **535**
Effect of surface treatment with biodegradable materials on properties of linerboard made from old corrugated containers (OCC)
Somayeh Heydari, Ahmad Reza Saraeyan, and Alireza Shakeri

September 2017

TABLE OF CONTENTS VOL. 16 NO. 9

491 EDITORIAL
Multifaceted research at the University of Maine
Monica Shaw

495 BIOREFINERY
Addition of corn stover arabinoxylan into hardwood during pulping for improved physical properties
Anurag Mandalika and Troy M. Runge

507 NONWOVENS
Oil absorption and desorption by polypropylene fibers
Praveen Kumar Yegya Raman, Akshay Jain, and Seshadri Ramkumar

519 PAPERMAKING
Three-dimensional pore structure visualization and characterization of paper using X-ray computed tomography
Yves Defrenne, Vasili Zhdankin, Sahana Ramanna, Shri Ramaswamy, and Bandaru V. Ramarao

535 RECYCLING
Effect of surface treatment with biodegradable materials on properties of linerboard made from old corrugated containers (OCC)
Somayeh Heydari, Ahmad Reza Saraeyan, and Alireza Shakeri

»COVER CREDIT: Researchers Yegya Raman, Jain, and Ramkumar (p. 507) used a modified ASTM F726-12 test for the oil sorption study with non-detergent motor oil. Top images show a bundle of polypropylene fibers (left) and then fibers floating, with oil absorption initiated (right). Bottom images show fibers absorbing the oil (left) and oil being drained for recovery (right). Photos courtesy of Brad Thomas, Texas Tech University.

TAPPI JOURNAL
WWW.TAPPI.ORG

Editor-in-Chief
Scott Rosencrance scott.rosencrance@kemira.com
+1 770 429-2753

Associate Editor
Brian N. Brogdon brian.brogdon@gmail.com
+1 678 581-9114

Editorial Director
Monica Shaw mshaw@tappi.org
+1 770 367-9534

PRESS Manager
Jana Jensen jjensen@tappi.org
+1 770 209-7242

Webmaster
Trina Heath theath@tappi.org
+1 770 209-7416

***TJ* EDITORIAL BOARD**

Brian N. Brogdon, FutureBridge Consulting & Training LLC
brian.brogdon@gmail.com, +1 678 581-9114

David A. Carlson, Carlson Consulting
dacarlson39@aol.com, +1 847 323-2685

Jere W. Crouse, JWC Consulting
cj522@inwave.com, +1 608 362-4485

Mahendra Doshi, Doshi and Associates
mahen@aol.com, +1 920 832-9101

Marc Foulger, GL&V USA Inc.
Marc.foulger@glv.com +1 315 767-2920

Peter W. Hart, WestRock
peter.hart@westrock.com, +1 409 276-3465

Carl J. Houtman, USDA Forest Products Laboratory
choutman@fs.fed.us, + 1 608 231-9445

John A. Neun, John A. Neun LLC
john.neun@gmail.com, +1 518 275-8139

Jim Niemiec, Verso Corporation
jim.niemiec@versoco.com, +1 715 422-7404

Steven P. Ottone, Omya
steven.ottone@omya.com, +1 919 641-7854

Gaurav Pranami, Imbed Biosciences
gpranami@imbedbio.com, +1 515 230-7005

Arthur Ragauskas, Oak Ridge National Laboratory
aragausk@utk.edu

Gerard J.F. Ring, University of Wisconsin—Stevens Point
gerrryring@wi-net.com, +1 715 592-3732

Scott Rosencrance, Kemira Chemicals
scott.rosencrance@kemira.com, +1 770 429-2753

Paul Wiegand, NCASI
pwiegand@ncasi.org, +1 919 941-6417

Junyong Zhu, USDA Forest Products Laboratory
jzhu@fs.fed.us, +1 608 231-9520

Join TAPPI *today!*

TAPPI JOURNAL is a free benefit of TAPPI membership, and is only available to members. To join TAPPI, to renew your TAPPI Membership, or to learn about other valuable benefits, visit www.tappi.org.

TAPPI, 15 Technology Parkway S., Suite 115, Peachtree Corners, GA 30092, publishes *TAPPI JOURNAL* monthly.

ATTENTION PROSPECTIVE AUTHORS: All papers published are subject to *TAPPI JOURNAL's* peer-review process. Not all papers accepted for review will be published. Before submitting, check complete author guidelines at http://www.tappi.org/s_tappi/doc.asp?CID=100&DID=552877.

Statements of fact and opinions expressed are those of individual authors. TAPPI assumes no responsibility for such statements and opinions. TAPPI does not intend such statements and opinions or construe them as a solicitation of or suggestion for any agreed-upon course of conduct or concerted action of any sort.

Copyright 2017 by TAPPI, all rights reserved. For copyright permission to photocopy pages from this publication for internal or personal use, contact Copyright Clearance Center, Inc. (CCC) via their website: www.copyright.com. If you have questions about the copyright permission request process, please contact CCC by phone at +1 978 750-8400. To obtain copyright permission to use excerpts from this publication in another published work, send your specific request in writing to Editor, TAPPI JOURNAL, 15 Technology Parkway S., Suite 115, Peachtree Corners, GA 30092, USA; or by fax to +1 770 446-6947. Send address changes to TAPPI, 15 Technology Parkway S., Suite 115, Peachtree Corners, GA 30092, USA; Telephone +1 770 446-1400, or FAX +1 770 446-6947. www.tappi.org

Editorial



MONICA SHAW | EDITORIAL DIRECTOR
mshaw@tappi.org

Multifaceted research at the University of Maine

Editor's Note: *This column is a continuation of* TAPPI Journal*'s column series featuring research and researchers from pulp, paper, biorefinery and related schools and institutions*
– Monica Shaw, Editorial Director

In this column, *TAPPI Journal* spoke with Dr. Adriaan van Heiningen of the University of Maine about current research activities there. He is the J. Larcom Ober Professor of Chemical Engineering, and his research interests include fundamental chemical engineering aspects of pulp production and forest biomass conversion processes. In particular, van Heiningen studies pulping, bleaching, recovery of pulping chemicals, and production of bio-based chemicals and biomaterials like acetic acid, biofuels, and nanocellulose. He studied at the State University of Groningen in the Netherlands and holds a Ph.D. from McGill University in Montreal, Canada. Here, we discuss van Heiningen's areas of research, as well as biorefinery projects at the university and his thoughts on the industry at large.

One of the research areas you are involved in at UMaine is increasing kraft pulp yield, a project that is funded by Agenda 2020. Can you describe some of your efforts in the area?

We're working to increase kraft pulp yield by more than 5% for both hardwood and softwood, although presently mostly softwood, by using a pretreatment step that includes an additive derived from the black liquor waste stream. So, it is an integrated process and wouldn't require new chemical purchases. We do attain an increase in yield and reduce the load on the recovery boiler, which is generally the bottleneck for increasing pulp production. We aren't quite at our ultimate goal yet, but we're getting closer. I believe it has near-term potential with very big economic consequences.

What is another area of research for you with a traditional pulp and paper focus?

We are working to extend oxygen delignification to 80% for softwood—a significant improvement from the current maximum of 60%—which we can now get in two stages. We plan to use additives and achieve this goal while maintaining acceptable pulp strength. As far as the impact, going from 60% for softwood delignification to 80% means you have 50% less lignin or kappa no. to be removed during bleaching, which reduces the impact and the cost of bleach plant by a factor of two.

The oxygen delignification work is funded by International Paper (IP) and is therefore proprietary. The company is funding a Ph.D. student for four years. In addition to pursuing the process improvements, IP is also interested in fostering more U.S./homegrown Ph.D. students, so there is an educational aspect to the work as well.



Dr. Adriaan van Heiningen with members of his University of Maine research group, from left to right: Asif Sharazi (Ph.D. graduate), Etienne Montet (M.S. student), Magriet van Heiningen, Dr. van Heiningen, Azadeh Pahlevanzadeh (Ph.D. student), Sefik Tunc (former laboratory manager), and Ravikant Patil (research scientist).

UMaine's Forest Bioproducts Research institute (FBRI), located at the former Old Town mill, focuses on creating and commercializing new forest-based bioproducts. What are some of your efforts there?

Acetic acid production from an alkaline pretreatment step that is integrated into kraft pulping to make regular kraft

pulp is an area of focus for me, Dr. Joe Genco, emeritus professor, and Dr. Hemant Pendse, who leads the FBRI research team. Another area of research is modified Biofine treatment of lignocellulosic biomass to produce levulinic acid, which I work on with Dr. Clayton Wheeler and Dr. Pendse.

The Biofine process is a 1 ton/day pilot plant, operated in partnership with Biofine Technologies, that treats biomass with sulfuric acid that converts the C6 sugars (glucose and mannose) into levulinic acid, a platform chemical that can be used in the chemical industry to make all kinds of value-added products. Dr. Wheeler developed an additional process whereby the levulinic acid stream is converted together with calcium formate into a crude oil that can be distilled and hydrogenated to produce liquid transportation fuels. It is a very simple dry pyrolysis process, and it is of interest for the industry because the calcium recovery can be integrated with the lime cycle of the kraft pulp mill.

In addition to bioproducts, another non-traditional area of work in which UMaine is involved is nanocellulose. What are some of your activities in this field and how do you see its potential?

We're working on nanocellulose in several applications, including as a papermaking additive, coating additive, and as a building materials component. The persons involved include Mike Bilodeau, head of the UMaine Process Development Center (PDC), and Drs. Doug Bousfield and Mike Mason. I also study the use of nanocellulose as a structural component in polymer composites, with the focus to overcome the energy obstacle to remove the large amount of water from a nanocellulose suspension of about 3%.

Many paper companies ask us to test nanocellulose as a papermaking additive in our PDC mechanical refining pilot plant, and Drs. Bousfield and Bilodeau have obtained a significant grant for the application of nanocellulose in several important products. I believe nanocellulose will be an important future product for our industry. An important breakthrough was the reduction in energy requirement for producing nanocellulose by mechanical refining pioneered by the UMaine PDC. A number of companies are getting involved by producing their own nanocellulose, including Sappi. Because of its special properties, I think nanocellulose has an important future as a new product or papermaking and coating additive for the industry.

You have described both traditional and non-traditional pulp and paper studies at UMaine. Which of these areas receives the most research funding? Do students gravitate more toward traditional or non-traditional studies?

Our funding is about 50/50, meaning that both traditional and non-traditional areas of study are significant. As for students, they probably gravitate more towards the biorefinery side.

I am so grateful that a number of companies are stepping forward to fund traditional research at the universities—in this case through Agenda 2020, but also direct funding to involve the university in developing new technologies. Most funding for traditional pulp and paper projects is coming from companies and most of the funding for the biorefinery project comes from federal government organizations.

In Maine, the pulp and paper industry used to be very strong, but not so much today. Has that changed the kind of students you have? Are they from all over the world or from the U.S.?

Yes, the industry has changed significantly in Maine, and a number of mills have closed because generally they were making products for which the market is shrinking. However, kraft mills have stayed and expanded. I also hope we could get a large investment and replace some these closed mechanical pulping operations by one huge softwood kraft pulp mill like they have just completed in Finland and Sweden. This hope is based on the knowledge that Finland and Sweden have a similar climate as Maine and we have the wood resources available. Unfortunately, so far this hasn't happened.

Regarding undergraduate students, we still get many local students but also now more from other states, attracted by the Pulp and Paper Foundation. It is true that most of them won't necessarily be employed in Maine, but they go all over the U.S., and most of them have jobs before they graduate. The pulp and paper educational program supported by the Pulp and Paper Foundation is still going very strong.

On the graduate, post-graduate and post-doctoral levels, we have about 25 students/researchers. We have a number of American graduate students, but most of the post-graduate research is done by international students from all over the world.

What are the primary pulp and paper related laboratories at UMaine?

We have bench-scale labs in the main building for chemical and biomedical engineering in Jenness Hall, and then we have the pulp and paper facilities in the PDC at the back of Jenness Hall, which has been there for around thirty years. We also have the Technology Research Center (TRC), which is a 40,000-ft^2 facility located in the former warehouse of the pulp mill in Old Town, Maine, and which was established about five years ago funded by a large grant of the Maine Technology Institute and by private contributions. The TRC houses floor scale testing equipment, including the very large Biofine pilot plant. The TRC allows us to take the research out of our Jenness Hall labs and demonstrate and validate it at industrially relevant scales to help rapid commercialization for the industry.

How do you feel about the overall direction of the pulp and paper industry, especially in developed areas like the U.S. and Europe where digital technologies are the norm?

I am actually quite optimistic about the industry. Printing and writing products will continue to decrease, although they won't disappear, but other products will become much more important, such as packaging and hygiene products. In a way, the industry will become more competitive, because we make kraft pulp at larger and larger scales, have become very energy efficient and are a net energy/electricity exporter, and transform a renewable resource into biodegradable products. Thus, the industry is changing its product mix, and at the same time becoming more efficient by increasing scale and using improved technology. This is happening both here and in Europe, although Scandinavia is moving a bit more quickly, as they tend to upgrade more regularly than we do. **TJ**

Addition of corn stover arabinoxylan into hardwood during pulping for improved physical properties

ANURAG MANDALIKA AND TROY M. RUNGE

ABSTRACT: Agricultural residues, such as corn stover, are being considered for biofuels and bioproducts. They represent inexpensive, pentosan-rich feedstock that are available in abundance. These materials are typically pretreated to make them more amenable to biological processes such as fermentation. One such treatment involves extraction using alkali to remove the hemicellulose, leaving the cellulose more accessible for chemical or enzymatic hydrolysis. Extracted xylan hemicellulose may be considered for use in pulp and paper, or for providing a potential value stream from cellulosic ethanol biorefineries. To be useful, the extracted xylan should be concentrated and adsorbed into the pulp using existing equipment or a minimal number of new unit operations. In this work, we explored the concept of size-exclusion membrane-filtration to concentrate xylan that was extracted from corn stover in mild alkaline conditions. We examined hollow-fiber and tangential-flow filtration types and achieved a nearly two-fold increase in the xylan concentration using the former with a 50 kDa molecular weight cut-off (MWCO) membrane. Cassette-type tangential-flow filtration resulted in slightly greater xylan concentration with the use of a 10 kDa MWCO membrane. Hemicellulose extracts were then used as an additive during kraft pulping of hybrid poplar to show that the xylan could be adsorbed onto pulp fibers and retained even after washing. Pulp tensile strength improved after xylan addition following refining. An average of 33% of the xylan added in this method was retained, with xylan loading between 5 wt% and 20 wt%, compared with the control pulp sample that did not have added xylan. These results suggest potential for further exploration of biorefinery extracts use as additive feedstock for pulping. The study, being an evaluation of the proof-of-concept, aims to push research and optimization in this area that will lend well to scale-up and commercialization.

Application: This work benefits mills in demonstrating that adjunct hemicelluloses may be incorporated into their pulp products, and if obtained from a low-cost source, could provide an increase in sellable pulp mass. This work also underlines the importance of hemicellulose content on pulp properties.

Most bioprocessing operations involving the use of plant material are based on the use of cellulose. These include pulping, the production of cellulosic ethanol and other high-value cellulosic products and solvents. Access to the valuable cellulosic material, is however, impeded largely by the presence of the lignin, and to a smaller extent, the hemicellulose fractions. Physical associations between the carbohydrate and lignin fractions, and extensive hydrogen-bonding networks, render the feedstock recalcitrant. Removal of hemicellulose and lignin generally improves access to cellulose for chemicals and, more so, for enzymatic conversions. Several researchers have documented improvement in enzymatic cellulose digestibility resulting from removal of lignin and hemicelluloses, and the techniques for affecting this [1,2].

Delignification and solubilization of the hemicellulose sugars are also the basis for chemical pulping, of which the alkaline kraft process is the most prominent. It frees up the cellulose fibers from the rest of the plant material so they can be laid into paper. The approach is similar in modern-day biorefineries where the extraction and separation of cellulose is imperative for the production of cellulose-derived chemicals and fuels. By the same token, researchers have explored the utility and advantages of extracting the hemicelluloses before pulping and bioprocessing, and finding value-added conversion processes to produce bioproducts from hemicellulose sugars, such as furfural [3,4], furfuryl alcohol [5], γ-valerolactone [6], etc. This is seen as a promising way of adding value to existing cellulose-dependent bioprocessing operations, and to add value to the currently underused hemicellulose fraction of biomass.

In the development of modern biorefineries centered on the use of cellulose for products such as cellulosic ethanol, considerable value is lost by failing to realize the utility of hemicellulose-derived carbohydrates. The hemicellulose that can be recovered from agricultural residues represents a valuable source of inexpensive carbohydrates, the potential of which must be adequately realized.

The primary deterrent to the use of the hemicellulose carbohydrates, arabinoxylans from grasses in this instance, is a problem of efficient separations. Realizing value from hemicelluloses has been impeded by traditional bioprocessing op-

erations, which accumulate these carbohydrates in the reaction mixture, with a focus on increasing access to the cellulose fraction of lignocellulosic biomass. Improving hemicellulose recovery and valorization is key to furthering the concept of the biomass-based integrated biorefinery, where the majority of lignocellulosic constituents are used toward the production of value-added products. Efficient separation strategies in the preliminary stages of the bioprocessing operations are, therefore, key to preserving the chemical and biological fidelity of the substrate that can enable its conversion into these chemicals and fuels. It is with this objective that we explored membrane filtration as a means to extract, purify, and concentrate corn stover-derived arabinoxylan. A potential application of this product to the integrated pulp biorefinery is then explored as an additive to improve the strength properties of hybrid poplar pulp.

LITERATURE REVIEW

Alkaline extraction of hemicelluloses from Gramineae

Extraction and removal of hemicellulose sugars from plant feedstock using alkali is accomplished by the peeling reaction mechanism, where reducing end sugars are slowly "peeled off," leading to the generation of oligomeric hemicelluloses. This is in sharp contrast to the mechanism in acid where the sugars are cleaved randomly, leading to shorter-chained oligomers and monomers. Xylans, being the primary hemicellulosic oligosaccharide, have conventionally been extracted in high yield in alkaline conditions. Even though the concentration of the alkali used affects the amount of xylans extracted, there are theoretical limits to the amount that can be extracted, due in part to the interactions of the hemicelluloses with the lignin and cellulose fractions in biomass.

Lignins present in species of the *Gramineae* are structurally different and more heterogeneous than hardwood and softwood lignins. Straw lignins present higher alkaline solubility, rendering this treatment as a way to increase their digestibility [7]. Along with removal of hemicelluloses, alkaline treatment also delignifies the biomass and yields a feedstock that is richer in cellulose (by proportion). The hemicellulose carbohydrates that are liberated in the process are also chemically and structurally different than those obtained from softwoods and hardwoods. The primary hemicellulose oligomers in cereal crops and grasses are arabinoxylans, whereas galactoglucomannans and glucuronoxylans are characteristic of softwood and hardwood hemicelluloses, respectively [8].

Additionally, a fraction of the hemicellulose sugars is more easily removed from the plant lignocellulosic matrix than the remainder, which are tightly embedded and cross-linked to the lignin present in plants. Studies on hardwoods have shown that glucomannans are the first type of hemicellulose sugars to rapidly degrade via the peeling mechanism, followed by the xylans, which are extracted in the oligomeric form [9]. When considering the optimum conditions for hemicellulose extraction, it is imperative to design for the removal of the more labile sugar moieties and render the extraction more efficient to reduce process conditions and cellulose degradation to cater to digestibility considerations.

Sun et al. [10] reported improved xylan extraction in alkaline-methanol solvent aided by ultrasound treatment. The same group has also studied lignin solubilization in alkaline-methanol solvent aided by ultrasound treatment and extracted up to 78.5% of the original lignin contained in wheat straw [11]. Oliveira et al. [12] have reported delignification of up to 80% of the original lignin in sugarcane bagasse in an alkaline ethanol solvent system, subsequently extracting 55% of the hemicellulose. These studies take into account improved dissolution of the lignin in the organic solvents, thereby liberating the hemicellulose.

The present study does not focus on optimization of the alkaline extraction process because that aspect has been extensively investigated. Instead, we decided to outline a separation and concentration strategy to valorize hemicellulose from agricultural residues and have used mild alkaline extraction to evaluate the concept.

The principal hemicellulose type in corn stover is arabinoxylan, which essentially consists of a xylan backbone with arabinose substituents. A series of experiments were constructed to extract arabinoxylans from corn stover over a range of alkaline conditions by varying the temperature and the time of extraction. Mild extraction conditions were chosen to reflect scale-up and implementation into biorefineries from a green chemistry perspective.

Membrane filtration pertaining to bioprocessing

In contrast with conventional depth filtration, most membrane filters operate primarily on the superficial scale, accomplishing filtration on the surface and sub-surface [13]. The field of membrane filtration is classified primarily based on the particle size of the materials being separated. For the separation of macromolecules such as monosaccharides and polysaccharides, ultrafiltration is needed, operating in the range of 0.001 to 1 μm.

Ultrafiltration has previously been considered as a way to concentrate biopolymers, such as polysaccharides, over other techniques such as centrifugation and precipitation, primarily because ultrafiltration can be carried out at room temperature, and has greater scalability. From the perspective of generating concentrated hemicellulose extracts, membrane filtration affords a convenient way to separate hemicellulosic oligomers based on molecular weight, while preventing their degradation or chemical modification, because the unit operation can be undertaken at ambient conditions. The latter aspect also makes the technique attractive for implementation in larger-scale settings, because process conditions are not likely to be a limiting factor.

Jorda et al. [14] have studied the effect of filtering arabinoxylan and rhamnogalacturonan solutions. They found that a hollow fiber membrane with a molecular weight cut-off (MWCO) of 6 kDa provided the best results for arabinoxylan

purification. To improve pulp properties via addition of hemicellulosic oligomers to the kraft pulping mix of hybrid poplar, the oligomeric sugars were concentrated using membrane filtration as a less intensive and ambient temperature technique. This also provided the advantage of screening the sugar fractions based on their MWCO values.

Schlesinger et al. [15] used ultrafiltration and nanofiltration to separate and retain near-quantitative hemicellulose oligomers at sizes over 1000 g/mol. When it comes to preserving and retaining hemicelluloses, research efforts have shown progress using membrane separation techniques to separate galactoglucomannan oligomers from pulping liquors [16]. Wang et al. [17] have tried to retain hemicelluloses in a different fashion, by agglomerating the various interfering lignin macromolecular entities and then destabilizing them to separate these from hemicellulose-derived oligosaccharides. Similarly, Krawczyk and Jonsson [18] have studied microfiltration of thermomechanical pulp liquor, achieving a galactoglucomannan yield of ~50% using microfilters of various pore sizes.

Wallmo et al. [19] used a combination of precipitation and membrane filtration to study the role that kraft black liquor hemicelluloses play in the separation of lignin. Their findings, which show a considerable reduction in filtration resistance of the liquor when the hemicellulose content was reduced, clearly allude to an interference effect enacted by the carbohydrates. This finding raises interesting consequences for separations operations that need to account for the hemicellulose and the lignin fractions.

Li et al. [20] explored extraction of hemicelluloses from a kraft dissolving pulp preparation of three different hardwood chips in an acidic pre-hydrolysis stage before pulping. Inevitably, the authors noted conversion of the hemicellulose sugars into their respective hydrolysis monomers, and their subsequent degradation into small amounts of furfural. Although such a technique can be used for hemicellulose removal to convert into xylose-derived value-added products, it also strips off yield, which is already a matter of concern in the conventional kraft pulping operation. Interestingly, the presence of hemicelluloses that leads to their precipitation onto the cellulose fibers during kraft pulping is seen as an operational hindrance that leads to quality issues.

During alkaline kraft pulping, the glycosidic bond linking the uronic acid groups (4-O-methyl glucuronic acids) to the xylan backbone attached to it are preferentially cleaved. Release of the uronic acids results in a decrease of the solubility of the xylan, causing it to precipitate out of solution and subsequently adsorb onto the surface of the cellulose fibers [21]. Evidence for this re-precipitation of xylan oligomers onto cellulose (from bacterial, cotton, and dissolving pulp sources) was observed using atomic force microscopy and light scattering measurements [22]. Moreover, there is evidence that some of the hemicellulose oligomers in the alkaline cooking liquor act as sacrificial candidates to the peeling reaction, thereby preserving cellulose from small amounts of degradation. Extracting the hemicellulose before the alkaline pulping process can reduce pulp yield by way of cellulose degradation.

To reduce the possibility of degrading cellulose by extracting the hardwood hemicellulose before pulping, we made use of the observation that extracted xylan can re-precipitate onto cellulose fibers during pulping by adding corn stover hemicellulose to increase bonding between pulp fibers. This strategy allows for the preservation of pulp yield, while providing a new application to an overlooked and underused resource. The fact that there is easily recoverable hemicellulose present in lignocellulosic feedstocks is exploited by the use of mild conditions that do not lead to full recovery, but enable better implementation into a cellulosic ethanol pretreatment regime, opening up the pathway to integration with a pulp biorefinery.

METHODS AND MATERIALS

Feedstock and chemicals

Dried and baled corn stover (*Zea mays*) composed primarily of stalk and very little cob, was sourced from the Arlington Agricultural Research Station (University of Wisconsin-Madison; Arlington, WI, USA) for performing the corn stover hemicellulose extraction experiments. Hybrid poplar (*Populus maximowiczii x nigra*) was harvested from northern Wisconsin after 10 years of age, and hand-debarked, chipped, and screened (2–8 mm) before air-drying to a moisture content of ~5%. Sodium hydroxide pellets (>97% purity) were sourced from DOT Scientific (Burton, MI, USA). Commercial grade arabinoxylan from corn cobs was procured from Shanghai Yuanye Bio-Technology Co. (Shanghai, China). The received material was analyzed independently and found to be 85.8% arabinoxylan, which was factored into experiments. Avicel PH-101 was procured from Fluka Analytical (Cork, Ireland) and was used to account for a correction factor during the measurement of carbohydrates on the corn stover and pulp samples.

Alkaline extraction

Small-scale extractions were performed in duplicate using 10 g samples of dried, baled, and ground (1.8-2 mm) corn stover in sodium hydroxide (NaOH) solution in 500 mL media bottles at a liquor-to-wood (L/W) ratio of 20:1. The sparse nature of the material necessitated the use of the high L/W ratio. Temperature control and stirring of the sample was accomplished using a shaker incubator set at the conditions being employed. For screening analysis, temperature conditions were selected at 20°C, 40°C, and 60°C. The sodium hydroxide concentration was set at 1 wt%, 2 wt%, and 3 wt%. The extraction times were varied between 1 h, 3 h, and 5 h.

Larger-scale extractions were carried out using 500 g of corn stover (ground and screened to 1.8-2 mm particle size) at conditions derived from the small-scale results in a large 20 gal pail mounted under a stirrer motor. The temperature was controlled by using a feedback-loop immersion heater maintained at 60°C for 5 h at an alkali concentration of 2 wt%. After extraction, the solid and liquid portions were separated. The latter was filtered to separate the undissolved solids in a Buchner funnel and concentrated using membrane filtration.

Membrane filtration

Corn stover extract derived from the large-scale extraction was fractionated into the permeate and retentate portions using a membrane filtration apparatus (Demofilter, Koch Membrane Systems; Wilmington, MA, USA) to separate the oligomeric hemicellulose sugars and concentrate them in the latter fraction. A hollow fiber membrane (Romicon HF UF cartridge, Koch Membrane Systems) with a pore size of 50 kDa was used to accomplish the filtration.

Tangential flow filtration was accomplished by using a Vivaflow 200 setup (Sartorius; Bohemia, NY, USA) with a 10 kDa MWCO cassette filter made of polyether sulfone membrane. Less than 1 L of the alkaline extract was filtered for 60 min; the retentate fraction measured about 100 mL. Tangential flow filtration with the 10 kDa MWCO cassette was also used to concentrate 6955 g of the corn stover alkaline hemicellulose extract to produce ~2056 g of the retentate for use in the large batch kraft cook. This gave rise to an effective concentration of 3.38-fold. Because of the large volume involved, this step was performed in multiple batches.

Kraft pulping

Preliminary experiments testing the addition of pure compound xylan to hybrid poplar kraft cooks were tested at a constant H-factor of 1200–1300 and an L/W ratio of 5:1. The effective alkali was 16 and the target sulfidity was set at 20. The cooks were carried out at the 30 g scale in pressurized reactors heated in a temperature-controlled oil bath, with frequent rotation. Xylan loadings were tested at the 5%, 10%, 20%, and 50% levels in duplicate by adding arabinoxylan from corn cobs. No xylan was added to the control cook. After pulping, the pulp was separated from the black liquor by decantation, washed with copious amounts of water to reduce the pH, and air-dried.

The large batch cook was conducted using 280 g (dry mass) hybrid poplar chips, with 2163.4 g of neutralized and concentrated corn stover hemicellulose extract that contained ~56 g xylan by mass, giving rise to a L/W ratio of 6.44:1. The cook was performed in a 20 L circulating flow reactor with a Tmax of 165°C, an H-factor of 1200, a L/W ratio of 5:1, an effective alkali of 16, and sulfidity of 20.

Chemical analysis

Kappa numbers of pulps produced were determined using the micro-kappa method (TAPPI UM 246 "Micro kappa number") in duplicate. Carbohydrate analyses for the corn stover feedstock, hybrid poplar pulps, and the extracted liquors were performed using ion-exchange chromatography using a Dionex ICS-3000 system (Thermo Fisher Scientific; Waltham, MA, USA) on a CarboPac PA-20 column (Thermo Fisher Scientific) equipped with a pulsed amperometric detector over a disposable gold electrode. This is according to a modified version of a previously described method [23] incorporating a correction factor based on Avicel conversion to calculate the final carbohydrate concentrations.

RESULTS

Carbohydrate content of corn stover

Extractive-free (acetone) samples of the corn stover were characterized for the carbohydrate content using high-performance liquid chromatography to account for the five prominent sugars, giving a total carbohydrate content of 62.8%. **Figure 1** shows the distribution, and these values were used to calculate xylan yields in subsequent sections.

Extracted liquor characterization

The percent solids (g/100 g) in the original extracted material and the membrane-separated fractions were determined by freeze-drying and weighing the dry material. This quantity allowed us to account for the separation of (primarily) the hemicellulosic sugars as a result of the membrane separation. The original extracted, unfiltered material contained ~8.27% solids (dissolved and undissolved). The undissolved materials were separated using a size 4 qualitative filter to yield a solids content of ~5.48%. The membrane separation resulted in a retentate solids content of ~7.51%. The permeate contained ~3.43% dissolved solids. Estimating the solids content makes it possible to quantify the oligomers as percent solids (rather than individual sugar oligomers), which can be useful for studying the effects of adding concentrated hemicellulose solutions to improve pulp properties.

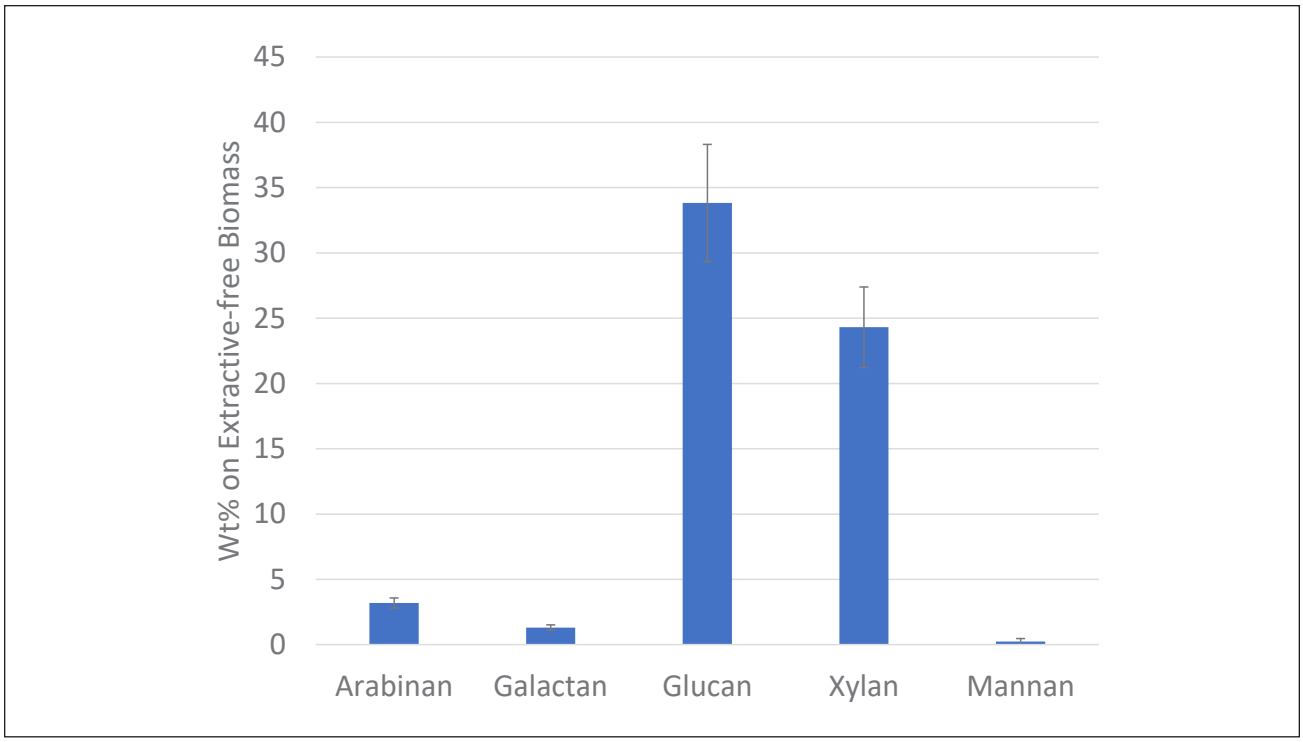
Small-scale extraction

Small-scale runs were conducted to identify optimal conditions to extract arabinoxylans. **Figure 2** shows the carbohydrate concentrations obtained from these experiments. As anticipated, xylan was preferentially extracted into the alkaline liquor at these mild conditions, whereas much of the cellulose was preserved in the stover solids. Run 8 with extraction conditions of 2 wt% NaOH for 5 h at 60°C yielded the highest xylan concentration at 8.76 g/L. Assuming complete recovery of the liquor, this xylan concentration corresponded with an extraction amount of 17.4 wt% on a dry solids basis, and 71.5 wt% based on the xylan amount present in the original feedstock; glucan extraction was minimal. The mannan concentration for the small-scale extraction runs were very dilute (this data has not been included in the figure). However, after concentration using membrane filtration, these were able to be detected (**Figs. 3 and 4**).

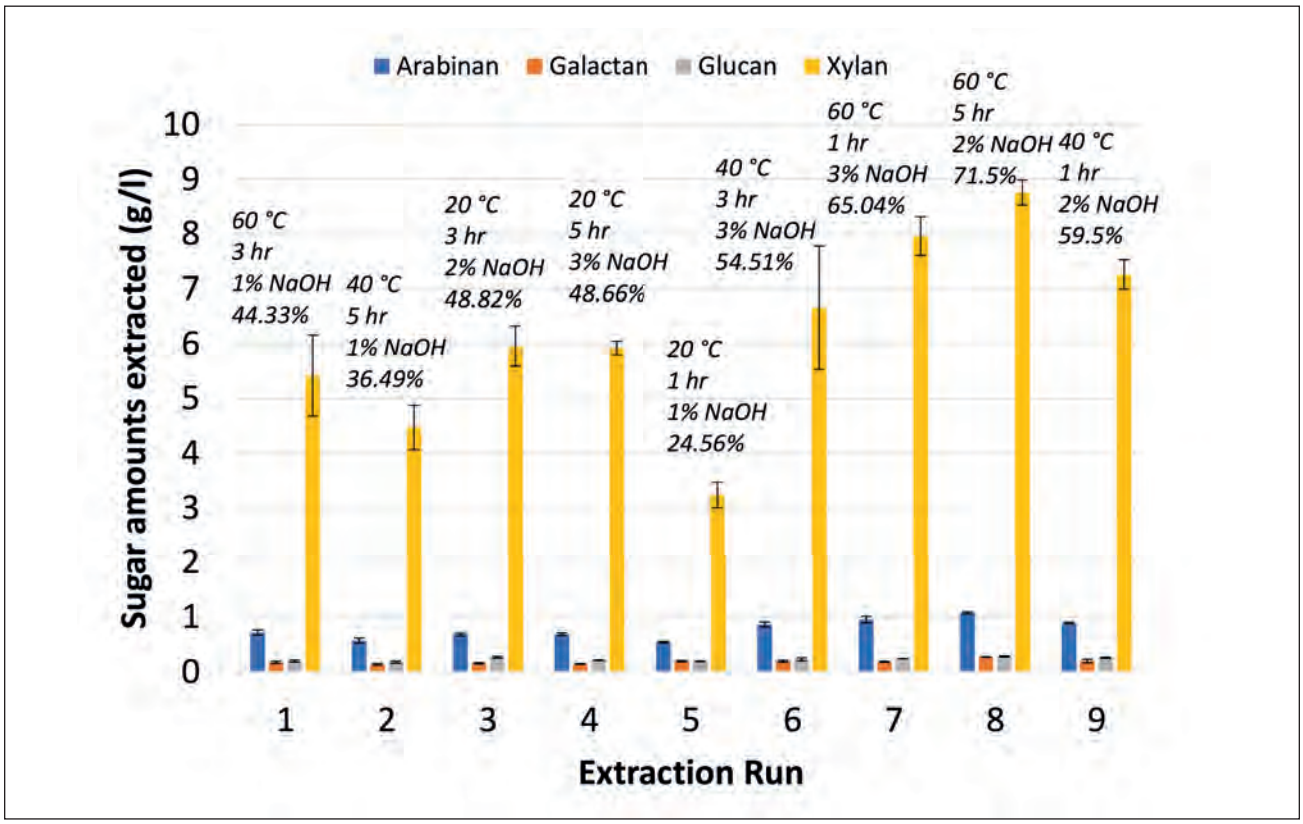
Large-scale extraction

Based on results from the small-scale extraction, the conditions that resulted in the greatest amount of arabinoxylans extracted were scaled up to extract 500 g of corn stover (in 2 wt% NaOH at 60°C for 5 h). Membrane ultrafiltration using hollow-fiber and tangential filters concentrated the xylan amount present in alkaline corn extract, accompanied by a reduction in total volume.

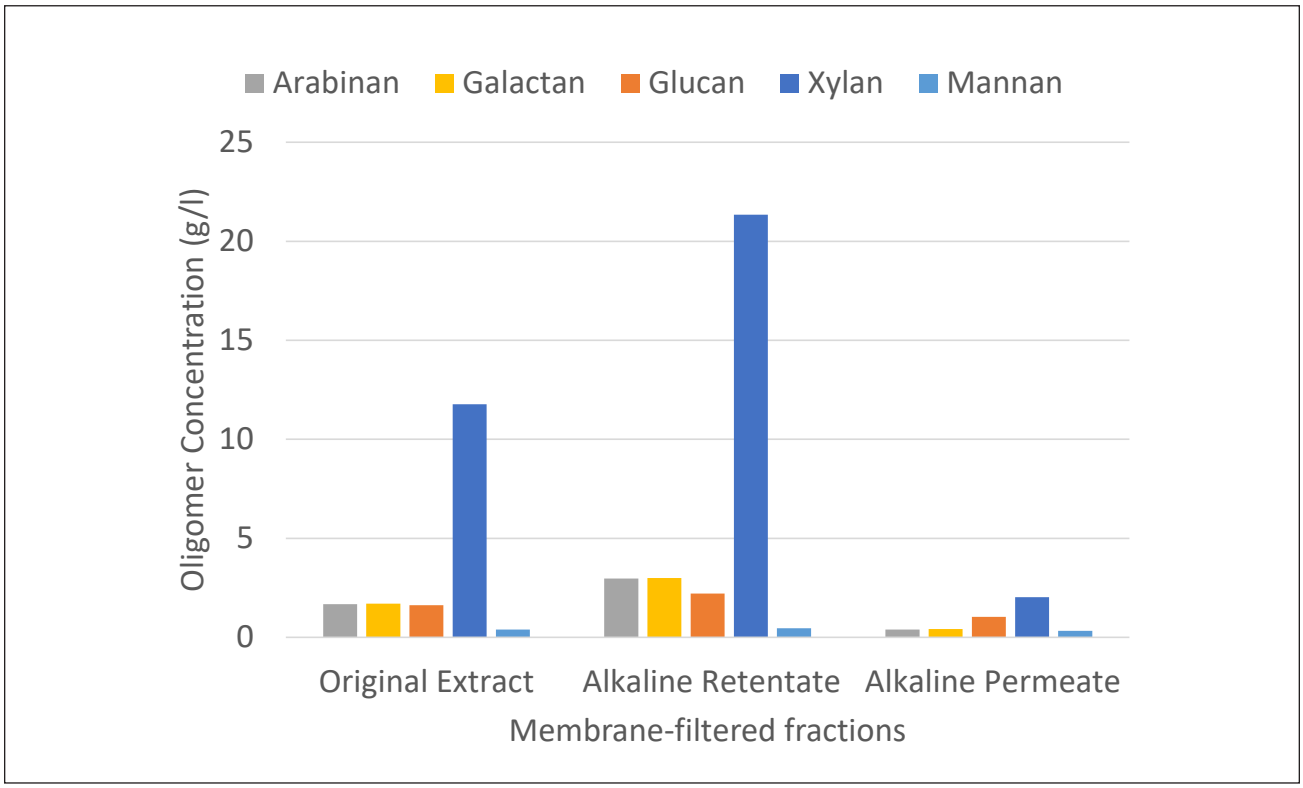
Based on the carbohydrate analysis performed (Fig. 3), ~11.7 g/L of xylan was extracted into the alkaline liquor extract when we replicated the conditions found during the



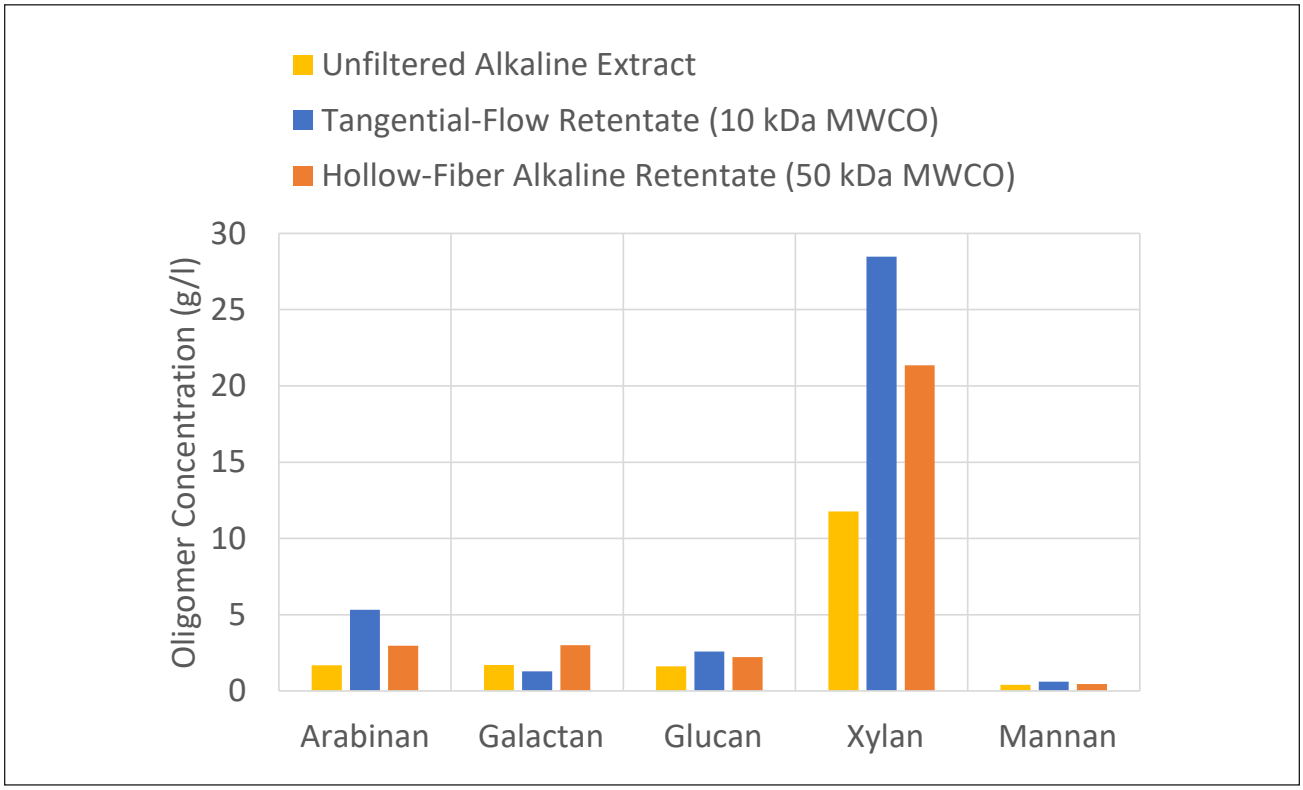
1. Carbohydrate content of the corn stover feedstock, as determined by high-performance liquid chromatography; error bars are shown as standard error for duplicate measurements.



2. Carbohydrate oligosaccharides extracted using mild alkali conditions (error bars showing the standard error for duplicates). The conditions used for the extraction runs, along with the yield of xylan (in percentages) based on the original amount in the corn stover is also reported (NaOH = sodium hydroxide).



3. Carbohydrate content showing the extent of oligomers extracted and separated using hollow-fiber membrane filtration (50 kDa molecular weight cut-off [MWCO]) in the original extract (unfiltered sample) and the membrane separated permeate and retentate fractions.



4. Comparison of the oligomer concentrations obtained by concentrating the corn stover alkaline extract using hollow-fiber and tangential membrane filtration processes, as determined by acidic hydrolysis followed by ion-exchange chromatography. The unfiltered extract is shown alongside for comparison.

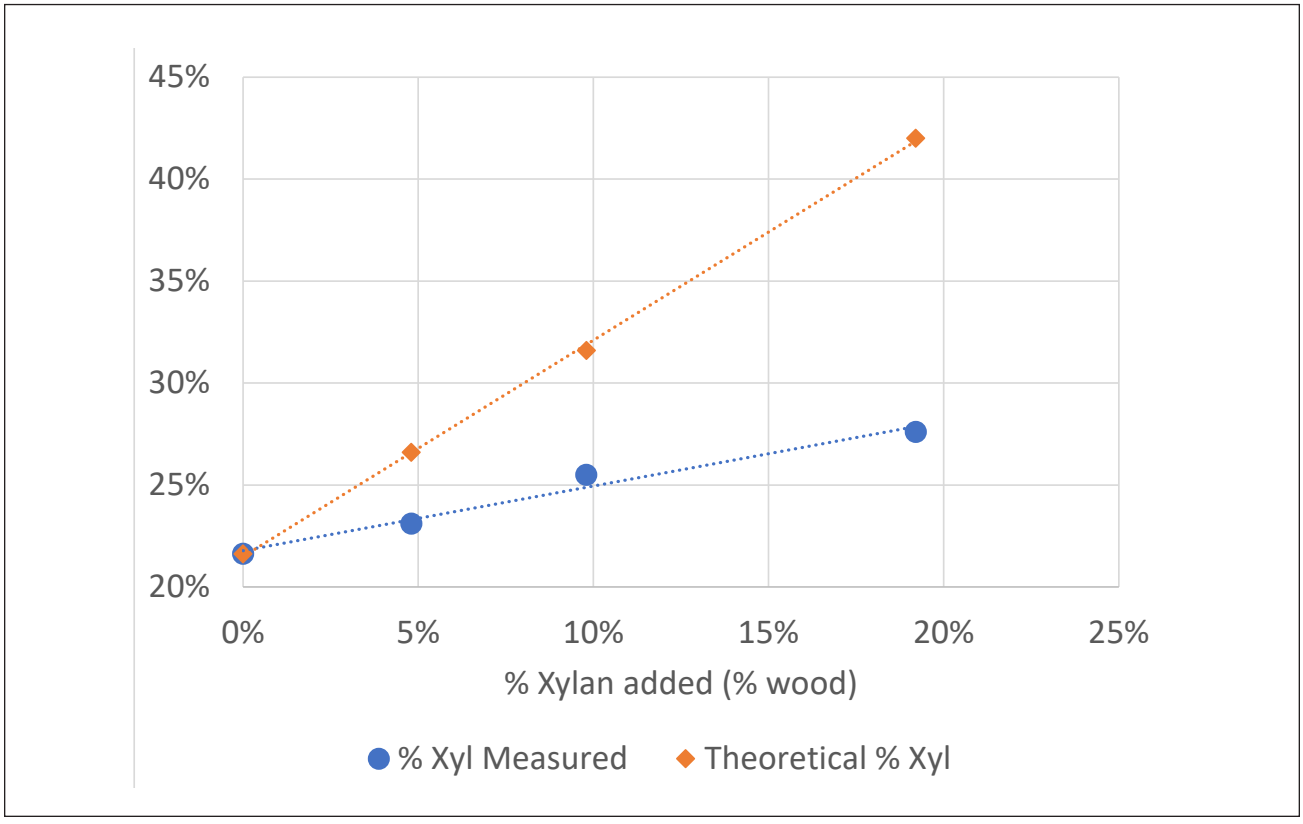
screening study (90.81% of the original xylan). This was greater than the xylan amount obtained in the screening study, and could be attributed to better mixing that was accomplished in the large batch extraction. Similar to the small-scale extraction runs, very small amounts of glucan (though greater than the small-scale) and other carbohydrates were extracted. Monomeric sugars were very low in concentration, and those of xylose and mannose were not detected in any of the fractions generated.

When filtered using the 50 kDa hollow-fiber membrane, the xylan concentration was increased almost two-fold, to 21.3 g/L. Slightly greater xylan and arabinan concentrations (28.5 g/L and 5.3 g/L, respectively) were obtained using the 10 kDa tangential flow membrane filtration apparatus (Fig. 4). For the tangential filtration system, 72.8% of the xylan contained in the feed was retained and concentrated during the filtration unit operation. Smaller oligomers and monomers would not have been retained, and 10.2% were collected in the filtrate. Although the smaller arabinoxylan oligomers and monomeric sugars are lost in the filtration operation, the goal of the study was to concentrate larger oligomers, which will translate well into improved bonding with pulp fibers. The concentration results suggest that a smaller MWCO might be a better size for concentrating the xylan oligomers than the 50 kDa hollow-fiber membrane, where there might be greater yield losses.

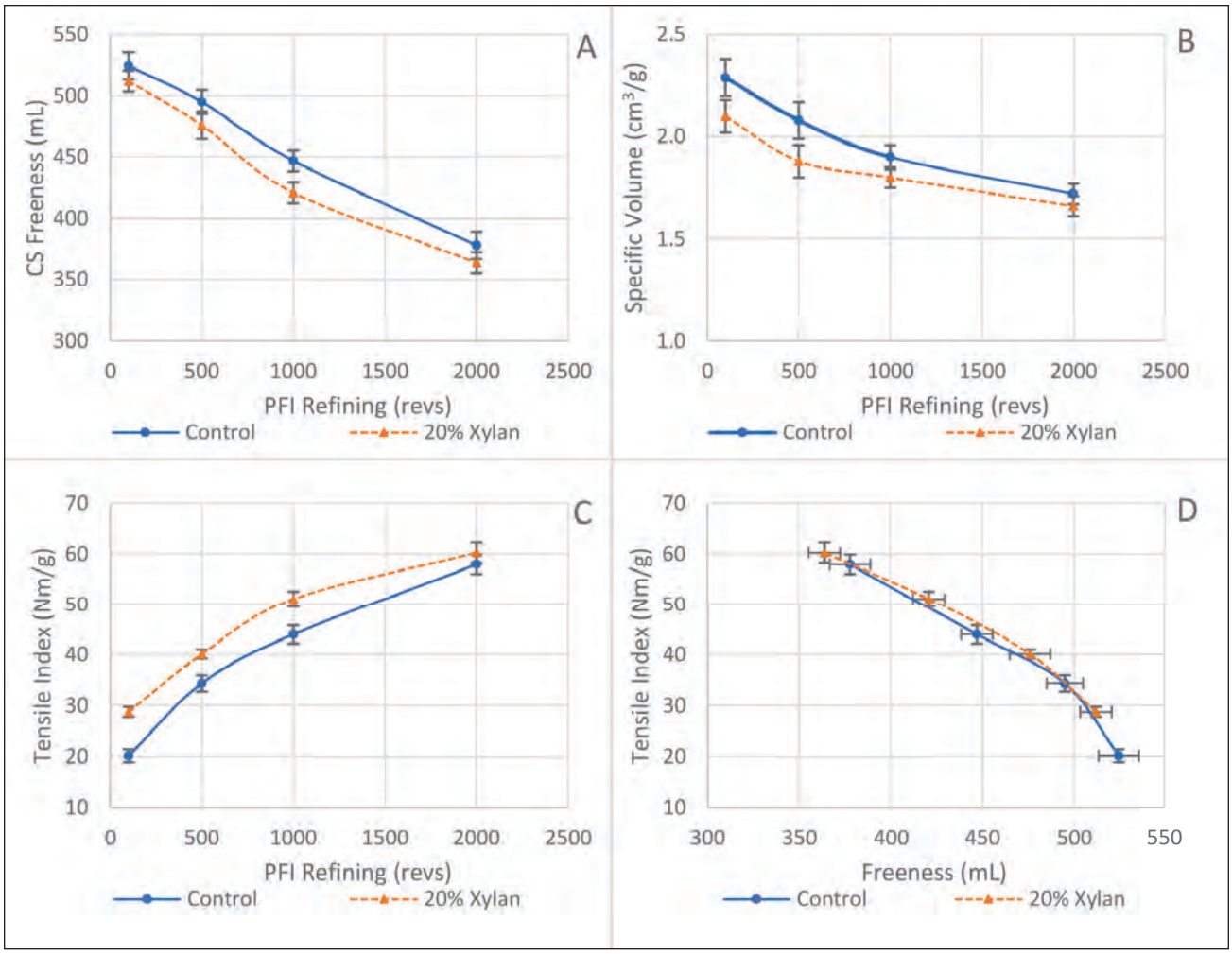
Kraft pulping with xylan addition

Small-scale kraft pulping experiments were performed using conditions mentioned in the experimental section to derive insights into the effect of xylan addition in the kraft cooks. The pulps produced in this study all had kappa numbers ranging from ~21.7 to ~30.4, so that they could all be compared on the basis of similar residual lignin content. Carbohydrate analysis on kraft pulp with xylan addition provided evidence of xylan adsorption on the pulp fibers, as predicted. Of the five wood sugars (arabinose, galactose, glucose, xylose, and mannose) tested for, only glucose and xylose were detected as monomers. The analysis calculated the measured mass percent xylan and the theoretical mass percent xylan, assuming that all the xylan added would be adsorbed (**Fig. 5**). Increased retention was measured for increased xylan loading, as expected. Interestingly, the adsorption linearly increased as a function of arabinoxylans added to the pulp between 5 wt% and 20 wt%, with approximately 1/3 of the xylan added being retained in the final product, regardless of the amount of arabinoxylans added.

Hybrid poplar pulps produced with xylan addition of 0% (control) and 20% charges were refined, measured for Canadian Standard Freeness (CSF), and then used to produce handsheets to measure physical properties of tensile index and specific volume. The resulting charts (**Fig. 6**), display a marked strength improvement for the arabinoxylans-modified



5. Kraft pulp carbohydrate analysis showing the amount of xylan adsorbed and how much there theoretically should be if 100% was retained with increasing amounts of xylan loading; control sample represented lack of xylan addition.



6. Handsheet physical properties comparing control to 20% xylan experimental pulps. Error bars denote standard error of handsheet replicates (n=3).

pulp, primarily for low refining levels, with the effect diminishing at 2000 PFI revolutions. Pulp strength increase from higher hemicellulose levels in pulps is well known, though typically the result of retaining the native hemicellulose from the wood, not from addition during pulping. Hemicellulose strength increase has been attributed to increased hydrogen bonding from surface hemicellulose and from an increase in fiber swelling because of the modification.

In conventional papermaking that includes the use of dry-strength additives such as cationic starch or polyacrylamide, the strength increase in the paper product could be attributed to bonding interactions between the strength agent and the pulp fibers. In this situation, as the dry-strength additives are generally added to the papermaking furnish, before forming the paper, the polyelectrolyte additives are retained on the surface. Being of large molecular mass, there is greater probability that these modifiers are retained on the surface through charge interactions, giving rise to greater surface hydrogen bonding [24]. In contrast, when the pulping is performed in conjunction with the hemicellulose modifiers (arabinoxylan, in this case), the modifiers are hypothesized to be adsorbed into the interior of the fiber, instead of being excluded to just the surface.

The freeness (as measured by CSF in milliliters) decreases with increasing refining, as expected [25]. As this is ideal laboratory refining in a PFI mill, the refining effect increased drainage resistance in pulps. This effect is primarily due to fiber swelling, not an increase in fines. Interestingly, the arabinoxylans-modified pulp sample had a consistently lower freeness throughout the refining range than did the control pulp (Fig. 6A), alluding to increased fiber networks in the latter, and consequently, greater strength. Figures 6B and 6C also support the hypothesis that the arabinoxylans-modified pulps were initially more swollen. The modified pulp has a greater density (inverse of the specific volume) and greater tensile index at the lower levels of refining, but approaches the control at 2000 revolutions, where the effect of refining on swelling overcomes the effect of hemicellulose content on swelling. Swollen fibers are known to provide more strength but lower density after drying because of their im-

proved wet fiber flexibility. Figure 6D shows a correlation between the tensile index and the CSF, displaying both samples on the same strength-freeness curve. As expected, they share an inverse relationship, with increased strength from swelling resulting in decreased freeness. Interestingly, the arabinoxylans-modified pulp appears to be "pre-refined." Unfortunately, this also suggests the arabinoxylans-modification does not provide greater strength than can be accomplished in pulps through refining.

DISCUSSION

The authors believe that the strategy proposed and evaluated in this paper outlines advantages and limitations to incorporating extracted hemicelluloses into the kraft pulping of poplar wood to incorporate a potentially low-cost material into the pulp and improve pulp strength properties at low refining levels. Such a strategy seeks to address multiple challenges in the current status of the biomass-based industry, add value to concentrated hemicellulose solutions, and demonstrate that they can be incorporated into a high-value pulp product.

Other researchers have studied the alkaline extraction of xylan from graminaceous plants and hemicellulose-rich agricultural residues. Generally, these studies have incorporated harsher extraction conditions, namely alkali concentration, time, and temperature. Chanliaud et al. [26] have reported that 10%–30% of the heteroxylans (arabinan, xylan, galactan, and glucuronic acids) in corn bran could be extracted using mild alkali conditions (1 M NaOH at 25°C for 24 h). Those results are similar to the results obtained in the current study. Greater yields (up to 90%) were also reported by the same authors by using different sources of the hydroxyl anion (KOH) and a temperature of 100°C. Cheng et al. [27] found optimum xylan extraction yields of 90% from depithed corn stover at NaOH concentration of 10% and 75°C, extracted for 2 h. Those authors also reported a slight decrease in the yield and physical strength properties of the soda-anthraquinone pulp as a result of the extraction. Under similar conditions, but over a much greater time, Xiao et al. [28] recovered between ~72% of the original hemicellulose sugars from corn stems, while simultaneously removing more than 7% of the glucan present in the material.

Our experimental results show that significant amounts of easily cleavable and recoverable arabinoxylans can be extracted in mild alkali to avoid degradation of the oligomers, and then concentrated to higher xylan concentration using hollow-fiber membrane filtration. Adding this material as a pulping additive allows approximately 33% of the material to be retained while also increasing pulp strength properties. This approach has the potential to improve the pulp yield and possibly improve profitability if hemicellulose extracts from agricultural resources can be made at low-enough cost. Future research will be required that focuses on concentrating polymeric hemicellulose extracts from agricultural residues and understanding the limitations of retention of the arabinoxylans during kraft pulping.

CONCLUSIONS

This work shows that hemicelluloses from inexpensive feedstock such as agricultural residues (corn stover) can be effectively recovered in mild alkaline conditions, concentrated and purified using membrane filtration, and blended into a kraft pulping cook to improve the strength properties of the pulp produced. This allows for the evaluation of a kraft pulping based biorefinery that integrates use of agricultural residues with novel separation strategies to produce pulp with improved properties. The present study did not address optimization of the various process parameters considered, but serves to illustrate the proof of concept of the implementation of concentrated hemicellulose from waste streams to expand the integrated kraft pulp biorefinery. We used mild alkali extraction that is common in pilot-scale cellulosic ethanol processes to recover easily extracted hemicellulose oligosaccharides and concentrate them to deliver a readily implementable blend to improve the strength properties of hybrid poplar pulp. The extracted residues are now more suited as substrate in a bioprocess that focuses on cellulose use, such as the production of bioethanol, as cellulose accessibility has now been improved. Future work should focus on optimization of the alkaline extraction process through a greater understanding of hemicellulose extractability and a study of the digestibility of the solid residues produced. The membrane filtration unit operations need to be optimized, targeting the parameters that encourage scale-up and commercialization (permeate flux and retentate concentration). **TJ**

ACKNOWLEDGMENTS

This material is based on work supported by the United States Department of Agriculture (USDA) National Institute of Food and Agriculture, under ID number WIS01800. The authors thank Carl Houtman and Roland Gleisner of the USDA Forest Products Laboratory (Madison, WI) for their assistance with this research. The authors credit Graeme Jacobson of Univeristy of Wisconsin-Madison for assistance with analysis and testing, and Elena Nikitina of Didion Ethanol (Cambria, WI) for assistance with hollow-fiber membrane filtration and Kevin Shinners of UW-Madison for the supply of the corn stover material.

LITERATURE CITED

1. Liu, C. and Wyman, C.E., *Bioresour. Technol.* 96(18): 1978(2005).
2. Yang, B. and Wyman, C.E., *Biotechnol. Bioeng.* 86(1): 88(2004).
3. Hayes, D.J., Fitzpatrick, S., Hayes, M.H.B., et al., in *Biorefineries—Industrial Processes and Products*, Wiley-VCH Verlag GmbH, Berlin, 2005, pp. 139-164.
4. Mandalika, A. and Runge, T., *Green Chem.* 14(11): 3175(2012).
5. Mandalika, A., Qin, L., Sato, T.K., et al., *Green Chem.* 16(5): 2480(2014).
6. Bui, L., Luo, H., Gunther, W.R., et al., *Angew. Chem., Int. Ed.* 52(31): 8022(2013).
7. Scalbert, A., Monties, B., Guittet, E., et al., *Holzforschung* 40(2): 119(1986).

8. Sjostrom, E., in *Wood Chemistry Fundamentals and Applications*, Academic Press Inc., San Diego, CA, USA, 1993.
9. Ban, W. and Van Heiningen, A., *Cellul. Chem. Technol.* 45(1): 57(2011).
10. Sun, R.C., Sun, X.F., and Ma, X.H., *Ultrason. Sonochem.* 9(2): 95(2002).
11. Sun, R., Sun, X.F., and Xu, X.P., *J. Appl. Polym. Sci.* 84(13): 2512(2002).
12. Oliveira, L.R.M., Nascimento, V.M., Corso, D.L.S., et al., *Investigaciones Aplicadas* 7(1): 1(2013).
13. Brock, T.D., *Memberane Filtration: A User's Guide and Reference Manual*, Science Tech Publishers, Madison, WI, USA, 1983.
14. Jorda, J., Marechal, P., Rigal, L., et al., *Desalination* 148(1-3): 187(2002).
15. Schlesinger, R., Götzinger, G., Sixta, H., et al., *Desalination* 192(1): 303(2006).
16. Al Manasrah, M., Kallioinen, M., Ilvesniemi, H., et al., *Bioresour. Technol.* 114: 375(2012).
17. Wang, Z., Wang, X., Fu, Y., et al., *Sep. Purif. Techno*l. 145(5): 1(2015).
18. Krawczyk, H. and Jönsson, A.S., *Sep. Purif. Technol.* 79(1): 43(2011).
19. Wallmo, H., Theliander, H., Jönsson, A.-S., et al., *Nord. Pulp Pap. Res. J.* 24(2): 165(2009).
20. Li, H., Saeed, A., Jahan, M.S., et al., *J. Wood Chem. Technol.* 30(1): 48(2010).
21. Sixta, H., in *Handbook of Pulp*, Wiley-VCH Verlag GmbH, Berlin, 2006, pp. 1009-1067.
22. Linder, Å., Bergman, R., Bodin, A., et al., *Langmuir* 19(12): 5072(2003).
23. Zhou, S. and Runge, T.M., *Carbohydr. Polym.* 112(2): 179(2014).
24. Hubbe, M.A., *BioResources* 1(2): 281(2007).
25. Taipale, T., Österberg, M., Nykänen, A., et al., *Cellulose* 17(5): 1005(2010).
26. Chanliaud, E., Saulnier, L., and Thibault, J.F., *J. Cereal Sci.* 21(2): 195(1995).
27. Cheng, H., Zhan, H., Fu, S., et al., *BioResources* 6(1): 196(2010).
28. Xiao, B., Sun, X.F., and Sun, R., *Polym. Degrad. Stab.* 74(2): 307(2001).

ABOUT THE AUTHORS

We chose this topic to study because, like many others, we have an interest in creating value from biomass hemicellulose, which could be a potential residual stream from cellulosic biorefineries. This led to the question: "Could agricultural residual, such as corn stover hemicelluloses, be incorporated into pulp to improve the economics of both systems, and if so, what would the resulting properties be?"

Previous research by our group has shown that co-cooking woods and nonwoods results in higher hemicellulose pulps. However, this is impractical from a digester loading standpoint. Therefore, we wanted to explore the incorporation of extracted grass hemicelluloses into hardwood pulps.

Determining a practical way of reacting the extracted hemicellulose oligomers with the wood chips for pulping was challenging, because the hemicellulose liquor was very dilute to begin with. Several methods of concentration were explored. Membrane filtration to concentrate the hemicellulose liquor was finally chosen as a promising unit operation for this purpose. Experimenting with different configurations and molecular-weight cutoffs helped us pick the appropriate filtration device for this aspect.

Being new to the field of pulp and paper science, we were fascinated by the number of theoretical conditions that needed to be taken into account when studying the adsorption of hemicelluloses into pulp fibers. An observation that could be practically taken for granted has a very interesting underlying theory that needed exploration.



Mandalika



Runge

It is surprising to note that the added hemicellulose oligomers were incorporated into the pulp with a somewhat consistent ratio, regardless of the amount added. We were expecting higher adsorption at low levels and diminishing adsorption as we added more of the oligomers. This is a facet of the work that needs to be further explored.

This work benefits mills in demonstrating that adjunct hemicelluloses may be incorporated into their pulp products, and if obtained from a low-cost source, could provide an increase in sellable pulp mass. This work also underlines the importance of hemicellulose content on pulp properties.

Our next step will be to study the polysaccharide interactions in more detail, and to try and substantiate the mechanism of the arabinoxylans incorporation into the pulp.

Mandalika is graduate student and Runge is associate professor, Department of Biological System Engineering, University of Wisconsin-Madison, Madison, WI, USA. Email Runge at trunge@wisc.edu.

Oil absorption and desorption by polypropylene fibers

PRAVEEN KUMAR YEGYA RAMAN, AKSHAY JAIN, AND SESHADRI RAMKUMAR

ABSTRACT: Oil spill is a threat to the ecosystem, and there is a need for the development of highly efficient oil sorbents for environmental remediation. In this study, four different types of polypropylene fibers were evaluated for their oil absorbency and desorption characteristics. These fibers varied in their fineness and structural characteristics, i.e., hollow or solid. A modified ASTM methodology was used in the study to better represent the oil sorption capacity of a sorbent. To the best of our knowledge, this is the first study to present the effect of fiber fineness and structure on the oil desorption behavior of polypropylene fibers. Results showed that finer fibers had higher oil sorption capacity (g/g) than the coarser fibers. There was no statistical difference in the rate of desorption among the solid fibers; however, the hollow fiber had a statistically higher rate of desorption than the solid fibers.

Application: This study will help with the development of efficient sorbents, which will have high oil sorption capacity and ease of transportation.

Economic growth and an increase in the world's population have caused an increase in the consumption of oil [1]. The increase in the consumption of oil has resulted in the increase in oil spill volumes and instances, with an estimated 224,000 tons of oil being released into the marine environment across the globe from 2000 to 2011 [2]. The 2010 Deepwater Horizon oil spill, for example, was responsible for the release of 4.9 million barrels of oil into the ecosystem, causing an influx of hydrocarbons into the Gulf of Mexico's ecosystem [3,4].

The contamination of water due to oil is caused during production, refining, transport, and general use. Oil spills have proven to take a toll on the ecosystem, and the impact can be understood by the fact that one liter of Benzene can effectively make millions of gallons of water unfit for human consumption [5]. Studies, such as the one conducted by Sabir, point to the transfer of oil compounds along the food chain via oil-contaminated marine food like fish and seaweed [2]. Laboratory testing programs have also shown the effects of oil on soil, including reduction in soil permeability, maximum dry density, optimum water content, and strength due to oil exposure [6]. Hence, there is a need to control the damage due to oil spills in an efficient and economically feasible way.

Existing technologies for the cleanup of oil include in-situ burning, use of chemical dispersants, sorbents, and physical methods [7,8]. Among these, the sorption processes and the use of sorbents provide the lowest economic cost, simple operational procedures, and high oil removal efficiency for the oil spill cleanups [9,10]. There are three classes of sorbents available: synthetic, natural, and inorganic mineral sorbents [11]. Oil sorbents have seen an increasing market share in the recent past, and the consumption of oil sorbents has also been predicted to expand, due to sales growth in allied industries such as automotive and manufacturing [1]. Consequently, there has been a great interest in recent times to develop a cost-effective and efficient sorbent for the absorption of oil in water due to ecological disasters and strict environmental policies worldwide [2]. An ideal sorbent should be economically feasible, readily available, oleophilic and hydrophobic in nature, and have high sorption capacity [8,12]. There has been wide research about the use of both natural and synthetic fibers for potential use in sorbents [2]. Researchers have extensively investigated natural fibers as oil sorbents and have successfully produced novel solutions [8].

The development of natural fiber-based sorbents, as well as introducing functionality onto the natural fibers, has been a great source of academic interest [9,13-16]. More recently, there has been an interest in the use of cotton as an oil sorbent [8,17-19]. A study by Vinit et al. found that low micronaire cotton showed higher sorption values due to higher surface area and increased fineness [17]. Micronaire of cotton fibers is regarded as an indicator of fiber fineness (linear density) and maturity (degree of cell wall development). A follow-up study by Vinit et al. presented a cotton-based novel sorbent with sorption capacity of 50.27 g/g, using low micronaire raw cotton [8]. However, in a recent study, the same group has comprehensively compared the sorption capacity of greige cotton hydroentangled and needle-punched nonwovens versus loose greige cotton fibers. The loose cotton fibers were found to have more oil sorption capacity as compared to the cotton nonwoven substrates [19]. Cortese et al. [20] proposed diamond like carbon (DLC) coated cotton textiles for the oil-water separation application, by the process of plasma-enhanced chemical vapor deposition of carbon, and reported super-

hydrophobicity, while Ge et al. [21] developed a fabrication method in their study for a hydrophobic fiber for the oil absorption—a graphene coated cotton. Lee et al. [22] fabricated a hydrophobic silicon dioxide (SiO_2) coated cotton fiber for potential application in oil spill cleanup. These methods do provide an insight into the oil absorption research on natural fibers; however, work still needs to be done to make multistep production and manufacturing of these sorbents scalable as well as commercially and economically viable.

Agricultural byproducts and wastes as potential oil sorbents have been worked on lately. Bazargan et al. [23] discussed an oil absorbent made after the treatment of rice husks, an agricultural waste. Suni et al. [24] have compared the oil sorption properties of cotton grass against commercially available synthetic sorbent for absorbing petrol, synthetic oil, diesel oil, mineral oil, and heavy fuel oil. Cotton grass is a major byproduct obtained when peat is excavated from wetlands. The oil sorption capacity (g/g) of cotton grass was observed to be the highest of all the previously-mentioned sorbents.

Synthetic fibers, on the other hand, provide a lower cost, are commercially and economically feasible, and can be produced regardless of the demography—unlike the natural fibers. Researchers have worked extensively on developing a sorbent consisting of polypropylene (PP) as at least one of the constituents. Zahid et al. [25] have investigated the removal of oil from the surface of seawater by the PP matrices. Zhao et al. [26] have used PP as a constituent in their work, presenting a thorough study of three nonwoven materials: PP; PP/poly(butylmethacrylate-co-hydroxyethylmethacrylate) (PBMA-co-HEMA; 6 wt%); and PP/poly(butylmethacrylate-co-hydroxyethylmethacrylate) (PBMA-co-HEMA; 20 wt%). The addition of PBMA-co-HEMA was reported to increase the oil sorption capacity, consequently reducing the strength of the material. The authors pointed out the dependence of oil viscosity on the oil absorption capacity; higher viscosity of crude oil as compared to diesel and toluene resulted in higher absorption of crude oil. Li et al. [27] discussed the fabrication of melt electrospinning based PP fibers, reporting an oil sorption capacity of 129 g/g—significantly higher than that of a PP nonwoven, which is attributed to the finer fiber diameter and porous structure. Lin et al. [28] proposed a composite material consisting of waste tire powder and recycled PP fiber, observing the cumulative oil sorption capacity after repeated use to be higher than that of PP fiber. Zhou et al. [29] introduced a new type of PP sorbent material obtained by UV-radiation induced graft polymerization of octadecyl acrylate monomer on the PP fiber and PP nonwoven matrices. The grafted PP fiber and PP nonwoven both were observed to have a significantly better oil retention capacity, even after 10 cycles. Wei et al. have presented a study with five different types of commercial nonwoven PP sorbents using different (stitch-bonded, needle-punched, melt-blown) manufacturing techniques, producing varying properties (processing, GSM, porosity, and fiber diameter) to determine and compare the retention ratio for oil sorption [30].

The wide array of research about PP does point out the importance of the PP fiber as a cornerstone in oil spill cleanup, an ideal sorbent [30], and as a widely used sorbent material for cleanup [8]. Batzargan et al. [23] argued that good oleophilicity and the ability of a sorbent to withhold the oil under gravitational force are desirable characteristics for a good sorbent. Bazargan et al. [31] have highlighted the importance of retention behavior of oil sorbents in the oil spill application, validating their model for sixty sorbent-sorbate systems. One of the factors that determine the suitability of a sorbent for an oil spill application is the retention of oil after the sorption, as long duration of handling and transportation is required.

The ever-increasing demand and potential expansion of the oil sorbent market calls for an in-depth study of the mechanism of the oil sorption by individual PP fibers. More importantly, the need for a cost-effective sorbent to enhance human health and protect the environment necessitates such a study. Accordingly, this study was conducted to better understand the oil sorption capacity, desorption behavior, and the rate of desorption of the PP fibers for oil spill cleanup application. We have used four different types of PP fibers with varying fiber fineness, as it influences the available surface for oil sorption. The dependence of the oil sorption and desorption behavior of PP fiber on the structure (hollow or solid) has also been studied. The sorption capacity of PP fibers was observed to decrease with increase in the fiber fineness, which agrees with the findings of other researchers [12,27]. The desorption performance and the rate of desorption values have been presented and statistically analyzed to better understand the retention capacity of the PP fibers.

MATERIALS AND METHODS

Polypropylene samples

Four different types of PP fibers having fiber fineness 1.5 denier (den), 2.2 den, 4 den, and 7 den were used in this study. The PP fibers were provided by FiberVisions (Covington, GA, USA). **Table I** provides the information about the fibers used in the study. Fibers with 1.5 den, 2.2 den and 4 den were solid in cross section, and the fibers with 7 den were hollow.

Fiber Fineness, den	Cross-section	Staple Length, mm	Crimp, crimps/mm	Surface Finish, TiO_2 Level*
1.5	Round	38.1	0.89	High level
2.2	Round	38.1	0.98	Low level
4	Round	47.62	0.83	Low level
7	Hollow	47.62	0.55	None

* The amount of titanium dioxide (TiO_2) influences (increases) the surface roughness and opacity of the fiber along with the dullness of the fiber surface. The TiO_2 is mixed in the PP resin during the extrusion process.

I. Polypropylene (PP) fiber properties

Type	Viscosity, cP	Density, g/cm³	Surface Tension, mN/m
Non-detergent motor (NDM) oil	139.8	0.925	31.44

II. Oil property [19].

Oil used

A non-detergent motor oil was used as a sorbate for the study. The properties of the non-detergent motor (NDM) oil are presented in **Table II**. According to the ASTM F726-12 "Standard test method for sorbent performance of adsorbents," the density of NDM oil used in the study satisfies the density requirement (0.860 to 0.970 g/cm³) for the medium oil.

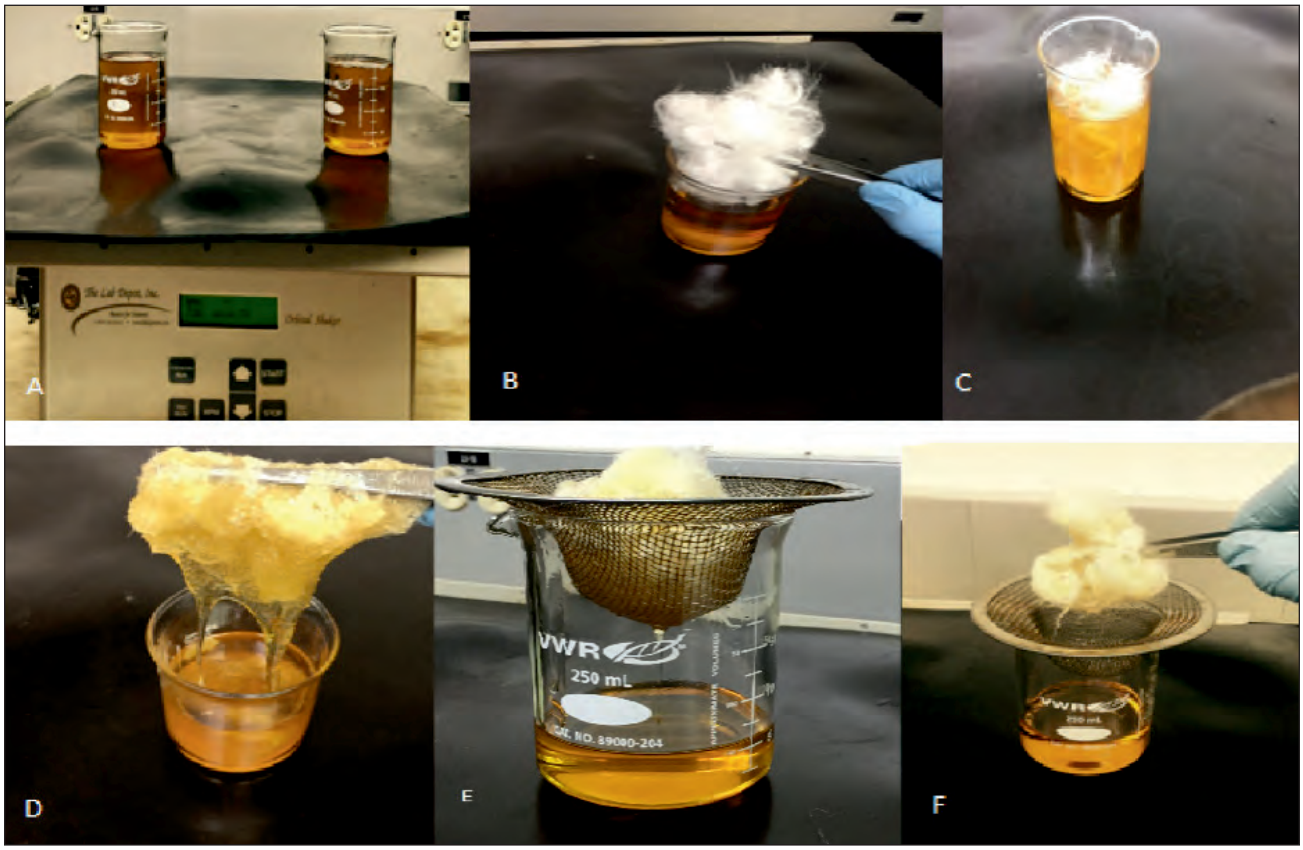
EXPERIMENTAL SETUP

The tests were carried out according to a modified ASTM F726-12 Standard (**Figs. 1A - 1F**). To perform the tests, 250 ml beakers containing 200 ml of NDM oil were used. The PP fiber samples, 5 grams in weight, were dropped in flasks containing oil. The beaker was then installed on the orbital shaker table, which was used to create a dynamic environment set at 75 rpm. The test was run for 15 min ± 3 s. The oil soaked samples were removed from the beaker and subsequently placed in a mesh for drainage. The gravimetric drainage process was used, and the weight of the sorbent was measured every 10 min ± 3 s, until reaching a cumulative time of 60 min ± 3 s. Researchers have observed a high desorption rate for the initial 10 min [8,32]. The values for the sorption capacities (**Fig. 2**) would be much higher if the measurements were taken after draining for 30 s rather than draining for 10 min. However, during an oil spill cleanup, the sorbents are spread onto the oil spill and then collected once the oil is absorbed. Accordingly, citing the high initial desorption, along with the delay in removal of the sorbents from the oil spill, we adopted a method for this study that measures the oil sorption after 10 min of gravimetric dripping, rather than the 30 s mentioned in ASTM F726-12, which to our understanding would reflect the oil sorption values mimicking real world application [8,17,19].

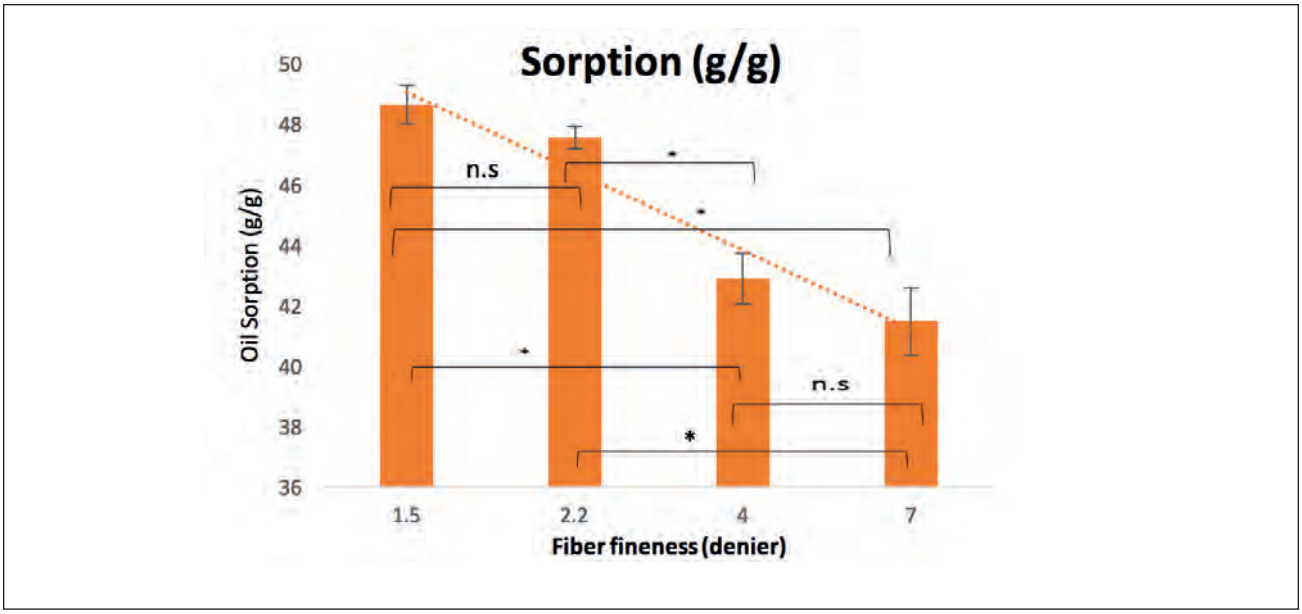
The oil sorption capacity was calculated as shown in Eq. 1:

$$\text{Oil sorption capacity} = (S_{st} - S_o)/S_o = S_s/S_o \quad (1)$$

where S_o = initial dry sorbent weight (g), S_{st} = weight of the oil sorbed sample (g) after 10 min of gravimetric dripping, and $S_s = (S_{st} - S_o)$ = net oil sorbed (g).



1. Modified ASTM F726-12 test standard for oil sorption study. A: Experimental setup for oil sorption study. B: Polypropylene (PP) fiber being immersed in the oil beaker. C: Oil sorption process: fiber getting fully immersed. D: Oil soaked PP fiber during the sorption process. E: Gravimetric oil dripping setup. F: PP fiber after oil draining for 10 min.



2. Sorption capacity (g/g). Statistical analysis was performed using two-sample t-tests for a sample size of 10 for all the possible pairs. Cross bars represent standard error of means, n=10; the region denoted by an asterisk (*) represents significance (P < 0.05), and "n.s" represents non-significance (P > 0.05).

RESULTS AND DISCUSSION

Oil sorption and desorption

The rationale for conducting both oil sorption and desorption study is provided here. There have been a wide range of studies about numerous materials for oil spill cleanup applications. The importance of sorption capacity (g/g) and the oil retention property of the sorbent have been stressed by researchers [16,17,33]. To the best of our knowledge, there has been no prior study on the desorption characteristics of polypropylene fibers and the effect of fiber fineness on the desorption of oil. The desorption study is critical for the design of oil sorbents, as once the oil is taken up, the expectation is that the sorbent does not lose the oil quickly so that it can be transported to a convenient site without causing any additional environmental problems. However, for recovery, after transporting the oil soaked sorbent to a safe environment, the oil must be recovered. The desorption behavior of the PP sorbent was evaluated using the gravimetric dripping process.

As reported in **Table III**, average oil sorption capacity (g/g) for PP fiber with fiber fineness (1.5 den, 2.2 den, 4 den, and 7 den) was found to be 48.65, 47.55, 42.89, and 41.48, respectively. As seen in **Fig. 2**, 1.5 den fiber had statistically higher oil sorption capacity than 4 den and 7 den fibers; however, there was a non-significant difference with 2.2 den fiber. The 2.2 den fiber had significantly higher oil sorption capacity than 4 den and 7 den fibers. There was no statistical difference between the oil sorption values of fibers with 4 den and 7 den.

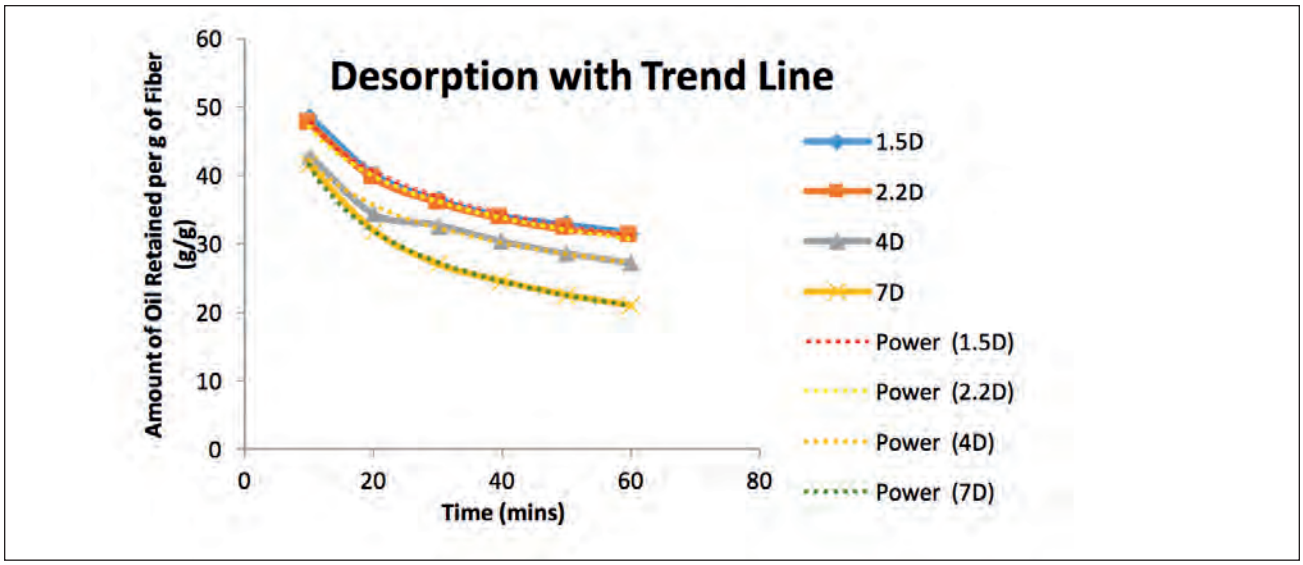
Fiber Fineness, den	Sorption, g/g
1.5	48.65 (0.63)
2.2	47.55 (0.38)
4	42.89 (0.83)
7	41.48 (1.12)

III. Mean sorption values (sample size =10) after gravimetric drainage for time of 10 min with standard error values in parentheses.

The fiber fineness, which represents the thickness of the fiber, was observed to have a significant effect on the oil sorption capacity of PP fibers. The oil sorption by PP fibers can be attributed to adsorption on the fiber surface and absorption by fibers [17]. It was seen, as a general trend from Fig. 2, that as the fiber becomes coarser, its sorption capacity decreased, as is the case with 7 den fiber compared with 1.5 den fiber. This means coarser fibers showed less oil sorption capacity than their finer counterparts. The high oil sorption, due to low fineness, corroborates with the results reported by other researchers [27,34]. Low fineness corresponds to higher specific surface area, which contributes to high oil sorption (g/g) [12,17]. Higher specific surface area would provide more surface for the sorbate to adsorb onto the surface, which is the initial mechanism for the oil sorption process.

Oil retention behavior

To analyze the oil retention behavior of the sorbent, the sorption test was performed in oil medium. As can be seen from the experimental curves (**Fig. 3**), all the fibers followed a similar oil retention behavior. The oil retention ratio (g/g) of the PP sorbent, presented in **Table IV**, underwent three stages. As soon as the sorbent was removed from the test, a high dripping rate was observed, accounting for the loosely



3. Amount of oil retained per gram of fiber (g/g) for PP fiber with fiber fineness (1.5 den, 2.2 den, 4 den, and 7 den) versus time.

adsorbed oil. In the second stage (from 10 to 30 min), a lower dripping rate was observed in all the evaluated fibers. The last stage (from 30 min until the end of the test) signified a stable and low dripping rate region. To further analyze the oil retention behavior, the desorption curve was plotted empirically. The desorption curve fit well with the power equation, as shown in **Table V**, with strong R^2 values. Higher R^2 values (all above 98%) provide evidence for the good fit of the experimental data to the derived power equation.

Rate of desorption

The rate of desorption for PP fibers is presented in **Table VI** with different fiber fineness (1.5 den, 2.2 den, 4 den, and 7 den) and were found to be 0.22, 0.24, 0.27, and 0.38, respectively. Statistical analysis was performed using a two-sample t-test for a sample size of 10 for the possible pairs. Cross bars in **Fig. 4** represent standard error of means, n=10; the region denoted by an asterisk (*) represents $P < 0.05$ and "n.s" represents non-significance.

Fiber Fineness, den	10 min	20 min	30 min	40 min	50 min	60 min
1.5	48.65 (0.62)	40.25 (0.47)	36.4 (0.60)	33.97 (0.57)	32.75 (0.51)	31.57 (0.52)
2.2	47.55 (0.38)	39.54 (0.37)	35.98 (0.31)	33.56 (0.36)	32.02 (0.4)	31.23 (0.26)
4	42.89 (0.83)	34.39 (0.59)	32.74 (0.77)	30.35 (0.63)	28.59 (0.57)	27.23 (0.48)
7	41.48 (1.12)	32.00 (1.09)	27.06 (1.18)	24.55 (1.15)	22.56 (1.03)	21.02 (0.96)

IV. Mean sorption values (g/g) with standard error in parenthesis (sample size =10) for different times under gravimetric dripping.

Fiber Fineness, den	Equation for Desorption Y: desorption, g/g X: time, min	R^2 Value
1.5	Y = 83.95X-0.242	0.994
2.2	Y = 81.355X-0.238	0.995
4	Y = 74.07X-0.244	0.986
7	Y = 99.332X-0.38	0.999

V. Desorption equations derived with their R^2 values.

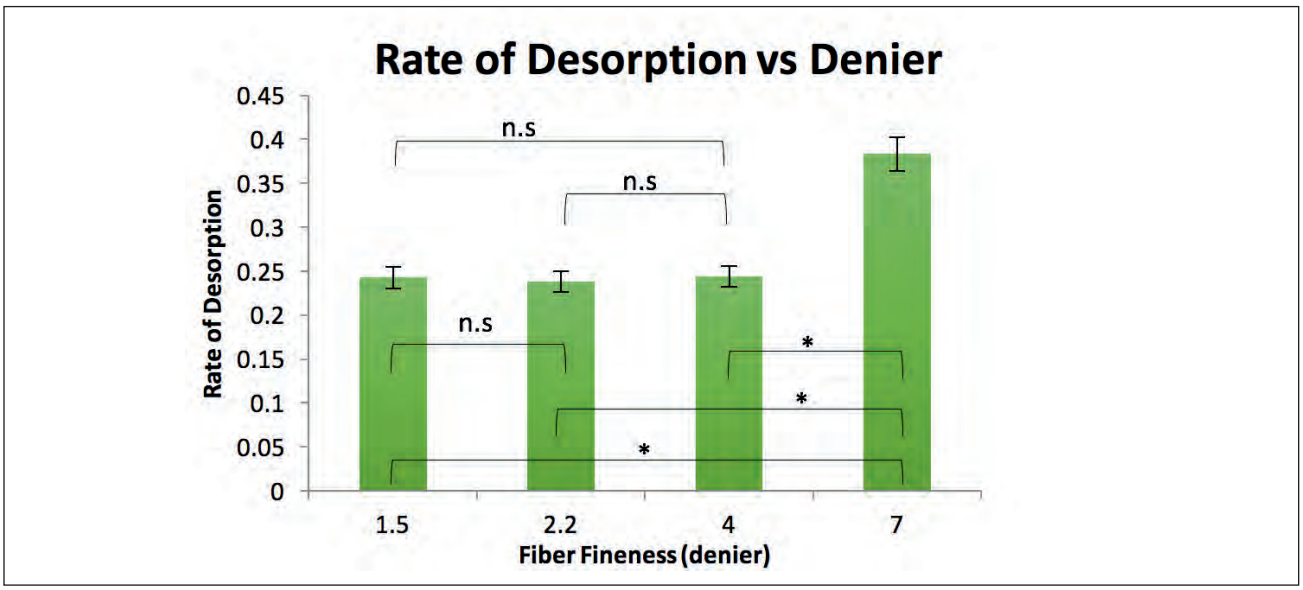
Fiber Fineness, den	Rate of Desorption (S.E.)
1.5	0.243 (0.008)
2.2	0.238 (0.007)
4	0.244 (0.007)
7	0.384 (0.021)

VI. Fineness versus the mean rate of desorption values (sample size =10) with standard error (S.E.) in parentheses.

The rate of desorption was calculated using the power equation for each of the samples used in this study (Fig. 4). The desorption rate, as discussed earlier, would provide a better understanding of the oil retention behavior of the fibers. Low rate of desorption is a desired attribute, as it signifies the tendency of the fibers to hold oil. Structure (i.e., solid or hollow) of the fibers was observed to play a role in the desorption rate. The fiber types with 1.5 den, 2.2 den, and 4 den, which are all solid in cross-section, have a statistically significant difference in rate of desorption with 7 den fiber. This can be explained by the solid structure of 1.5 den, 2.2 den, and 4 den fibers and hollow structure of 7 den fiber. To the best of our understanding, the absence of core in the hollow fibers is responsible for a statistically higher rate of desorption as compared to the solid fibers. As has been discussed by Vinit et al. [17], oil is diffused into the fiber through the micropores on the fiber, although this effect will be relatively less. However, in the case of hollow fibers, in the absence of the core, oil retention by individual fibers will be relatively less compared to regular fibers. In addition, the non-statistical significance of the difference in rate of desorption for fibers (1.5 den, 2.2 den, and 4 den) with solid structure supports this explanation, as fiber fineness does not have any significant effect on the rate of desorption. The higher rate of desorption in hollow fibers and non-dependence on fiber fineness are interesting takeaways from this study, and it would help in the selection of an appropriate fiber with maximum oil sorption and desired desorption.

CONCLUSIONS

A detailed analysis of PP fibers as oil sorbents, including the testing of fibers with fiber fineness 1.5 den, 2.2 den, 4 den, and 7 den, has been presented in this paper. In addition, the dependency of the fiber structure (i.e., hollow or solid) on the oil sorption was also investigated. The oil sorption capacity was observed to decrease (48 g/g to 42 g/g) with an increase in the fiber fineness (from 1.5 den to 7 den). The desorption, which is an important attribute for the oil sorbents, showed a similar trend for all the fiber types—high desorption followed by a decrease in the desorption. Strong statistical evidence suggested power equation as the best fit for time dependent desorption under gravimetric dripping. The rate of desorption was statistically insignificant within the solid fiber types (1.5 den, 2.2 den, and 4 den). However, the rate of desorption was significantly higher for the hollow fiber in comparison with other solid fiber types. In conclusion, the finer the fiber is, the higher is the oil sorption. However, in the case of desorption, the rate of desorption was shown to be influenced by the structure of the fiber rather than the fineness, which needs further investigation. Such a study would involve fibers with different cross-sections, different structure (i.e., solid or hollow), and varying fiber fineness. We hope that the results from this study would be valuable



4. Rate of desorption versus fiber fineness. Statistical analysis was performed using two-sample t-tests for a sample size of 10 for all the possible pairs. Cross bars represent standard error of means, n=10; the region denoted by an asterisk (*) represents significance (P < 0.05), and "n.s" represents non-significance (P > 0.05).

for designing a suitable oil sorbent with necessary oil sorption and desorption capabilities. **TJ**

ACKNOWLEDGEMENT

The authors gratefully acknowledge John Wolhar, Fiber Visions, Covington, GA, USA, for graciously providing the fibers used in this study.

LITERATURE CITED

1. Senanurakwarkul, C. and Chavarnakul, T., *International Journal of Research in Management & Technology* 2(6): 603(2012).
2. Sabir, S., *Crit. Rev. Environ. Sci. Technol.* 45(17): 1916(2015).
3. Reddy, C.M., Arey, J.S., Seewald, J.S., et al., *Proc. Natl. Acad. Sci. U. S. A.* 109(50): 20229(2012).
4. Orcutt, B.N., Joye, S.B., Kleindienst, S., et al., *Deep Sea Res., Part II* 57(21-23): 2008(2010).
5. Syed, S., Alhazzaa, M.I., and Asif, M., *Chem. Eng. J.* 167(1): 99(2011).
6. Khamehchiyan, M., Charkhabi, A.H., and Tajik, M., *Eng. Geol.* 89(3-4): 220(2007).
7. Seddighi, M. and Hejazi, S.M., *Mar. Pollut. Bull.* 96(1): 286(2015).
8. Singh, V., Jinka, S., Hake, K., et al., *Ind. Eng. Chem. Res.* 53(30): 11954(2014).
9. Wahi, R., Chuah, L.A., Choong, T.S.Y., et al., *Sep. Purif. Technol.* 113: 51(2013).
10. Carmody, O., Frost, R., Xi, Y., et al., *J. Colloid Interface Sci.* 305(1): 17(2007).
11. Al-Majed, A.A., Adebayo, A.R., and Hossain, M.E., *J. Environ. Manage.* 113: 213(2012).
12. Ying, Q., Lili, Z., Haixiang, S., et al., *IOP Conf. Ser.: Mater. Sci. Eng.* 62: 012032(2014).
13. Khan, E., Virojnagud, W., and Ratpukdi, T., *Chemosphere* 57(7): 681(2004).
14. Lim, T.T. and Huang, X., *J. Hazard. Mater.* 137(2): 820(2006).
15. Abdullah, M.A., Rahmah, A.U., and Man, Z., *J. Hazard. Mater.* 177(1-3): 683(2010).
16. Nyankson, E., Rodene, D., and Gupta, R.B., *Water, Air, Soil Pollut.* 227(1): (2015).
17. Singh, V., Kendall, R.J., Hake, K., et al., *Ind. Eng. Chem. Res.* 52(18): 6277(2013).
18. Singh, V. and Ramkumar, S., *Ind. Eng. Chem. Res.* 53(8): 3412(2014).
19. Singh, V., Sawhney, P., Reynolds, M., et al., *AATCC J. Res.* 4(2): 1(2017).
20. Cortese, B., Caschera, D., Federici, F., et al., *J. Mater. Chem. A* 2(19): 6781(2014).
21. Ge, B., Zhang, Z., Zhu, X., et al., *Compos. Sci. Technol.* 102: 100(2014).
22. Lee, J.H., Kim, D.H., Han, S.W., et al., *Chem. Eng. J.* 289: 1(2016).
23. Bazargan, A., Hui, C.W., and McKay, G., *Cellulose* 21(3): 1997(2014).
24. Suni, S., Kosunen, A.L., Hautala, M., et al., *Mar. Pollut. Bull.* 49(11-12): 916(2004).
25. Zahid, M.A., Halligan, J.E., and Johnson, R.F., *Ind. Eng. Chem. Process Des. Dev.* 11(4): 550(1972).
26. Zhao, J., Xiao, C., and Xu, N., *Environ. Sci. Pollut. Res.* 20(6): 4137(2013).
27. Li, H., Wu, W., Bubakir, M.M., et al., *J. Appl. Polym. Sci.* 131(7): n/a(2014).
28. Lin, C., Hong, Y.J., and Hu, A.H., *Waste Manage.* 30(2): 263(2010).
29. Zhou, X., Wei, J., Li, S., et al., *Desalin. Water Treat.* 53(3): 727(2013).
30. Wei, Q.F., Mather, R.R., Fotheringham, A.F., et al., *Mar. Pollut. Bull.* 46(6): 780(2003).
31. Bazargan, A., Sadeghi, H., Garcia-Mayoral, R., et al., *J. Colloid Interface Sci.* 450: 127(2015).
32. Qi, P.S., Lin, N., Liu, Y.Z., et al., *J. Donghua Univ.* 29(3): 233(2012).
33. Teas, C., Kalligeros, S., Zanikos, F., et al., *Desalination* 140(3): 259(2001).
34. Wu, J., Wang, N., Wang, L., et al., *ACS Appl. Mater. Interfaces* 4(6): 3207(2012).

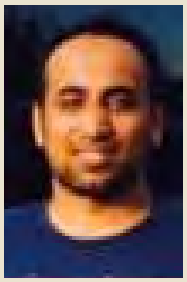
ABOUT THE AUTHORS

We studied this topic to find remedial solutions for environmental pollution and contamination using fibers and nonwovens. This topic furthers the research being done in our laboratory that focuses on understanding the use of a common fiber from the nonwovens industry for applications in oil spill remediation.The most difficult aspect of this study was to establish a reliable test protocol, as we had to use a small sample size, so it was important to focus on basic science that can lead to applications. Our most interesting finding was that fibers in loose form are the best candidates for use in oil spill remediation.

Toxic chemical and oil spills are common in many manufacturing industries, in addition to being a major issue in oil transport. So, our research highlights the use of fibers and nonwovens in saving the environment. The next step is to transfer these results so that practical products can be developed.



Yegya Raman



Jain



Ramkumar

Yegya Raman was research assistant, Jain was graduate research assistant, and Ramkumar is professor at the Nonwovens and Advanced Materials Laboratory, Texas Tech University, Lubbock, TX, USA. Email Ramkumar at s.ramkmuar@ttu.edu.

Three-dimensional pore structure visualization and characterization of paper using X-ray computed tomography

YVES DEFRENNE, VASILI ZHDANKIN, SAHANA RAMANNA, SHRI RAMASWAMY, AND BANDARU V. RAMARAO

ABSTRACT: Porous biomaterials such as paper and board have a complex structure that influences their mechanical, optical, and transport properties and thereby their performance during manufacturing and end uses. Reconstruction of the three-dimensional (3D) pore spaces in paper was obtained by X-ray computed tomography and used to study the structure and its impact on properties. A set of laboratory-made paper samples of varying freeness was prepared, and the 3D structures of the samples were visualized and characterized. Tomographic reconstruction images were processed using techniques such as anisotropic diffusion, minimum error thresholding, and isolated voxel removal to enhance image quality. The pore structures were analyzed to determine porosity, fiber-pore interfacial surface area, geometric tortuosity, and pore size distributions (using a sphere growing algorithm). These properties were compared with experimental data and were found to be in good agreement. The results from 3D visualization and characterization were then compared with experimental data of various samples using conventional pore structure characterization techniques, such as mercury intrusion porosimetry.

Application: Image processing techniques can help mills better understand the complex structure of porous biomaterials that influences properties and performance of manufactured products.

Porous biomaterials such as wood and paper have a complex three-dimensional (3D) structure consisting of interconnected pores and cellulose fibers. The understanding of this structure is important in determining the structural characteristics and properties of such materials. Previously, conventional characterization techniques, such as microscopy, energy dispersive X-ray spectroscopy [1,2], and mercury intrusion porosimetry (MIP) [3,4], were used. These techniques concentrate mainly on the 2D structure visualization; they are invasive and do not provide complete structural information. Mercury intrusion porosimetry is a conventional intrusive experimental technique used to characterize the porous materials. Hence, 3D characterization techniques were explored. X-ray computed tomography (XRCT) is one such technique that provides excellent visualization at micron and submicron scale [5-9]. X-ray computed tomography has been used increasingly to characterize the structure of porous materials [9-12]. Bloch et. al. have used XRCT to evaluate structural properties such as porosity, permeability, and effective thermal conductivity in paper and other porous materials [5,9,12]. Van Den Bulcke et al. and Mayo et al. used XRCT to investigate the structure of wood [7,8,13]. Antoine et al. used phase contrast X-ray tomography to obtain high quality images of paper structures [14]. Noninvasive techniques such as XRCT make it possible to visualize and characterize the structure of materials without any potential changes during the measurement. The principle of computed tomography is based on capturing a series of images of the object by rotating along a single or a dual-tilt axis. Using the tilt series, a 3D reconstruction is carried out by a back-projection technique [15].

In our previous work, low resolution XRCT images were used to visualize the 3D structure of paper and determine its pore characteristics [16-18]. The current work focuses on high resolution XRCT images of different paper samples acquired from the European Synchrotron Radiation Facility (ESRF; Grenoble, France). A series of effective image processing steps was applied to ensure maximum noise reduction while preserving the essential features of the images. Techniques such as anisotropic diffusion, minimum error thresholding, and isolated voxel removal were used to yield high quality images with clear distinction between the pore and fiber phases. A noninvasive method to determine the 3D pore size distribution and porosity, fiber-pore interfacial surface area, and geometric tortuosity is presented. The results from 3D visualization and characterization are then compared with experimental data of various samples using conventional techniques such as MIP.

MATERIALS AND METHODS

Paper samples

A large pool of samples of different varieties of paper was selected for our analysis. They included 300 g/m^2 paper handsheets made using softwood bleached kraft pulp (SWBK) fiber refined to different levels according to TAPPI T-205

"Forming handsheets for physical tests of pulp"; these were characterized by CSF levels in the range of 220–670 mL. Other samples consisted of varying types of fiber furnish with fibers obtained from different raw material sources (e.g., hardwood and softwood). Finally, commercial paper samples were subjected to calendering (mechanical densification of a dry paper sample) treatment and those that contained inorganic fillers (denoted as samples 1, 2, and 3).

X-ray computed tomography

High resolution XRCT images were obtained at ESRF using the ID 19 beamline (http://www.esrf.eu/home/UsersAndScience/find-a-beamline.html). This beamline was specifically designed for parallel beam applications by placing the very small (<100 µm) source 145 m away from the sample being scanned. Monochromaticity is ensured by a multilayer coated X-ray optical device with a narrow bandwidth. The pixel size was chosen to be 0.7 µm to provide a large enough field of view that would still retain a balance of high resolution in the scanned sample. The energy of the X-rays was 20 keV. With a resolution of 2048 x 2048 pixels, the samples to be scanned were about 1.4 mm wide and 1.4 mm tall. In about 20 min, a total of 1500 radiographs, over 180°, were taken. In the sample preparation process, a thin acrylic capillary tube was dipped into a hot adhesive and then instantly applied to the front of a cut piece of a sticky note with the same dimensions as the sample to be scanned. The sticky side was then gently pressed onto the sample. The reconstruction was done by a back projection technique [19].

Image processing

Even though the fibers are clearly identifiable (**Fig. 1**), the lack of sufficient contrast in XRCT images makes the automated recognition of each of these fibers difficult to implement. To enable the automated separation and identification of these two phases, an algorithm based on the following image processing techniques was developed and implemented in the following sequence:

1. Smooth only the regions of similar grayscale intensities.
2. Preserve edges or interfaces between different phases in the material.
3. Conduct adaptive smoothing, taking into account surrounding local image characteristics.
4. Generate a binary image.

Anisotropic diffusion

The technique of anisotropic diffusion filtering is an adaptive smoothing technique that preserves the edges or interfaces between two different phases in the material [9,20]. It is based on simulating the diffusion of a tracer inside an anisotropic medium, and the diffusivity is represented by a direction dependent tensor [20]. The rate of change of the voxel intensity, I, is given by the divergence of the local intensity gradient (Eq. 1):

$$\frac{\partial I}{\partial t} = div(c(x,y,z,t)\nabla I) = c(x,y,z,t)\Delta I + \nabla c.\nabla \mathrm{I} \quad (1)$$

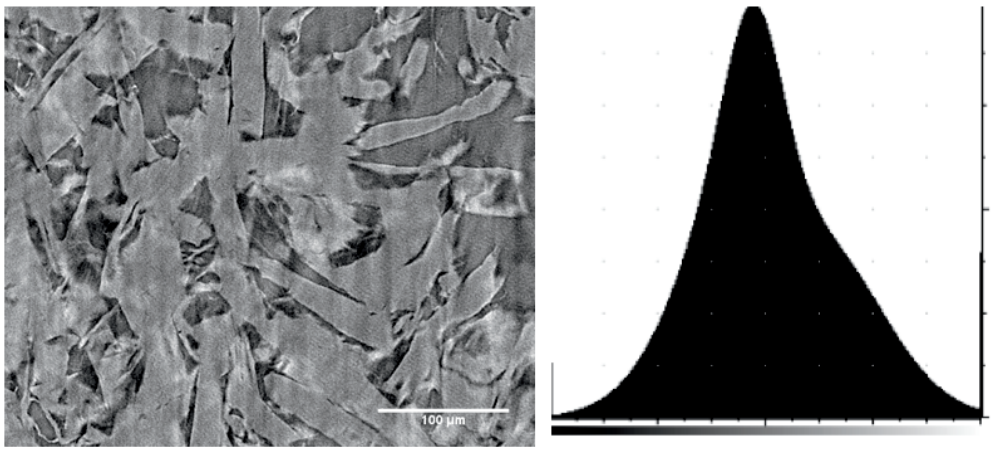
where I is the voxel intensity, c represents the diffusion coefficient, t is the time during iteration, and ∇I is the grayscale gradient.

The grayscale intensities between two consecutive iterations of the filter are related by [19] (Eq. 2):

$$I(x,y,z,t+1) = I(x,y,z,t) + \frac{1}{n}\sum_i \sum_j \sum_k w(i,j,k)\, c3\big(\nabla I(i,j,k)\big)\, \nabla I(i,j,k) \quad (2)$$

where w is the weighing coefficient, if implemented; n is the number of voxels taken into account; and i, j, and k are integers in a certain interval [-d, +d] such that the length of the vector (i,j,k) is lesser than the mask radius.

The diffusion coefficient $c3$ was chosen to be directly proportional to the grayscale gradient given by the following exponential function (Eq. 3):



1. Zoomed-in region (left) and histogram of a slice from a high resolution raw image stack.

$$c3 = exp\left[-\left(\frac{\|\nabla I\|}{K}\right)^4\right] \quad (3)$$

K was chosen as 60 and 30 for the first and second iterations, respectively, to ensure quick denoising without affecting the edges. For the rest of the iterations, K was constant and chosen to be 14. The value of K is dependent on the image to be processed. The convergence criterion employed for ending the filtering process for classifying voxels was less than 5% between successive iterations.

The anisotropic diffusion filter resulted in a histogram with two distinct Gaussian distributions corresponding to the two phases. The surface plots also revealed noise elimination and smoothing while retaining the features of the interface.

Thresholding

Once the anisotropic diffusion resulted in a histogram where two different peaks could be identified, a minimum error thresholding method was used to classify the pore and fiber phases [21,22]. The minimum error threshold method fitted two normal distributions to the overall histogram data. The point of intersection of these two curves was chosen as the threshold, as shown in **Fig. 2**. The threshold value ensured that the sum of the misclassified voxels in either phase was minimal. The misclassified voxels are located in the area under the curve on either side of the threshold value.

Final filtering steps

Even with the anisotropic diffusion method, some voxels that have unusually large or small grayscale values as compared with their neighbors cannot be smoothed out and could end up being misclassified. Hence, an isolated voxel removal algorithm was applied to detect and label all of the disconnected or isolated groups of voxels; their volumes were compared with a predetermined threshold volume. The threshold volume (512 μm^3) (8 μm x 8 μm x 8 μm) was chosen because all the fiber voxels were expected to be connected and the smallest isolated cellulose fiber particle (i.e., fines) was defined to be about 75 μm. If the isolated voxel volume was below the threshold volume (512 μm^3), then it was removed.

After the isolated voxels were eliminated, a morphological operator was applied to compensate for potential surface roughness misrepresentation caused by noise. The dilation and erosion algorithms were applied [22] and combined to yield either an open or a closed filter. It was found that five consecutive dilate steps followed by five erode steps were optimal in the current work. Once these final filtering steps were completed, the images were ready to be used for the determination of structural and transport characteristics.

Determination of pore structural characteristics

Once the images were filtered and binarized, pore structural characteristics such as porosity, fiber-pore interfacial specific surface area (SSA), geometric tortuosity and 3D pore size distribution could be determined.

Porosity

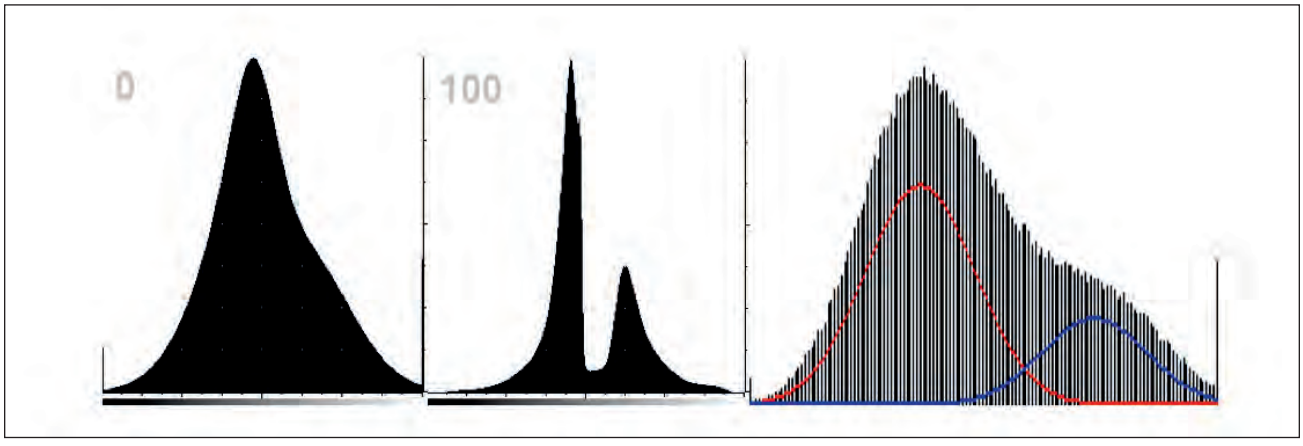
Porosity was one of the simplest measurements because the images contained two separate phases that have been identified. The porosity of the sample was calculated as (Eq. 4):

$$\varepsilon = \frac{number\ of\ pore\ voxels}{total\ number\ of\ voxels} \quad (4)$$

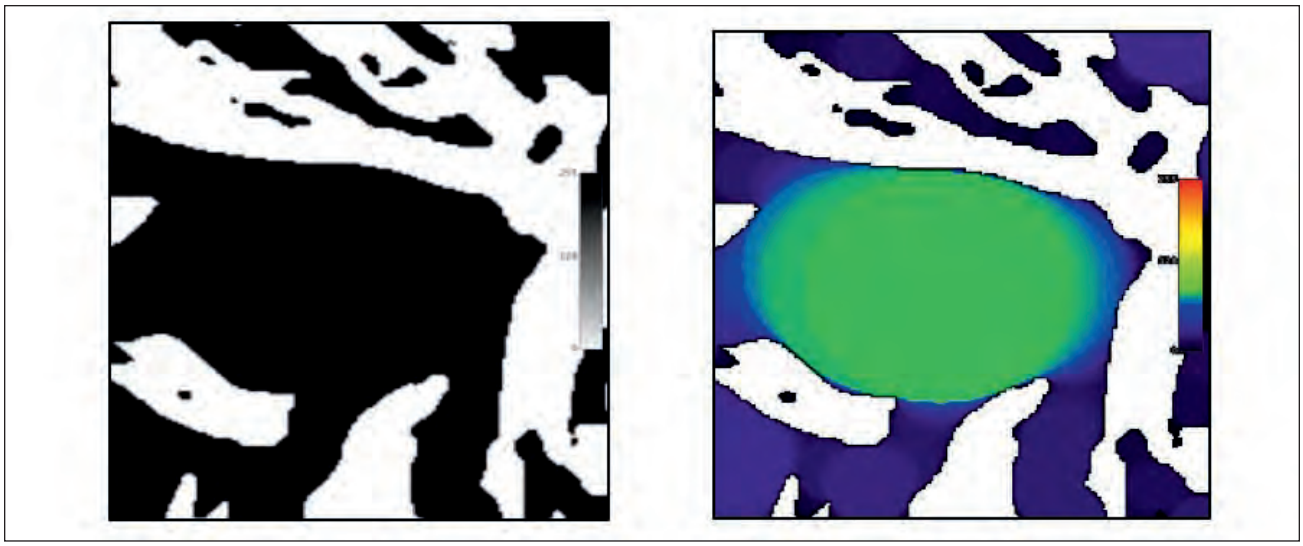
The porosity obtained from XRCT images of paper samples was verified with the experimentally obtained porosity based on sheet thickness (caliper) and basis weight (weight per unit area) measurements and also by MIP. The basis weight measurements were obtained by taking a sample of rectangular shape, measuring its dimensions (x,y), determining thickness using a caliper (z), and weighing the sample. Basis weight was calculated as follows (Eq. 5):

$$Basis\ weight = \frac{Weight}{A_{total}} \quad g/m^2 \quad (5)$$

The apparent density was calculated as follows (Eq. 6):



2. Histogram before (left) and after anisotropic diffusion (middle) and minimum error thresholding method (right).



3. Cross section of the processed image before (left) and after (right) fitting spheres.

$$\rho_a = \frac{Basis\ weight}{z} \qquad g/m^3 \tag{6}$$

The cell wall density of the cellulose fiber (ρ_f) was taken to be 1.55 g/cm³ under normal conditions [23]; hence the volume of fiber was calculated as follows (Eq. 7):

$$V_{fiber} = \frac{weight}{\rho_f} \tag{7}$$

The porosity is then calculated as follows (Eq. 8):

$$\varepsilon = \frac{V_{total} - V_{fiber}}{V_{total}} = \frac{(1/\rho_a - 1/\rho_f)}{1/\rho_a} \tag{8}$$

Specific surface area

The total interfacial area, S_t, was determined by counting the number of voxels that correspond to the pore-fiber interface and then multiplying that by the face area (square) of a cubic voxel. The SSA or the interfacial area per unit mass, S_W (m²/g), and specific area per unit volume, S_V (m²/m³), can be given by (Eqs. 9 and 10):

$$S_W = \frac{S_t}{(1-\varepsilon)\rho_f} \qquad m^2/g \tag{9}$$

$$S_V = \frac{S_t}{1-\varepsilon} \qquad m^3/g \tag{10}$$

where S_t is the total interfacial area, ε is the porosity, and ρ_f is the fiber density.

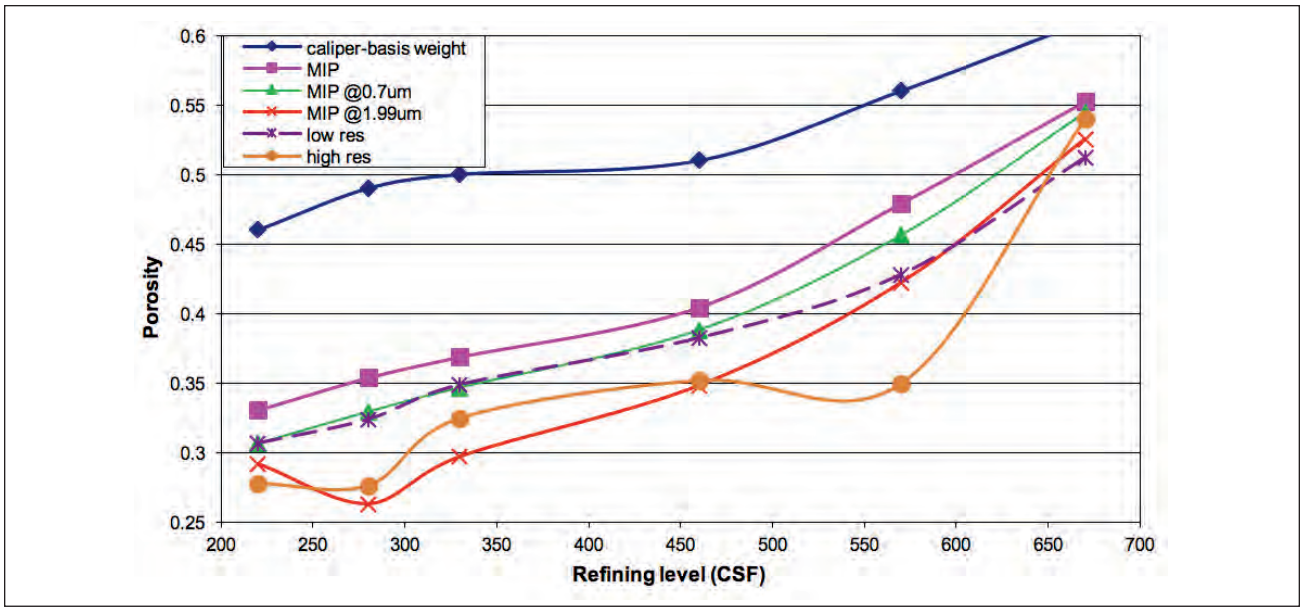
3D pore size distribution

Given that fibrous, porous materials have complex 3D structures, characterizing them using 2D approximations have inherent limitations. In the 2D model, long narrow pores are approximated using equivalent circular pores and their equivalent pore dimensions are then calculated. Also, 2D methods do not take into account important structural information in the third dimension. Hence, to get a more complete and accurate characterization of the porous network, a 3D characterization of the pore size distribution is necessary. This was achieved using a sphere growing algorithm.

In the sphere growing algorithm, a diameter map was created for the porous structure. This involved fitting a sphere of maximum size at every pore voxel location. Spheres were grown inside the pore space starting with a diameter of one and incrementing the diameter until it encountered a fiber voxel. This will give the maximum sphere diameter at that location and is then repeated for the entire volume. Once the diameter map was obtained, full spheres were grown starting from the smallest diameter and ending at the largest. As larger spheres are grown, they take over any voxels they overlap from previously grown smaller spheres. Then, the volume of pore space corresponding to the maximum sphere at a given location and its distribution gives the pore size distribution for the structure. **Figure 3** shows the cross section of the processed image before and after fitting spheres.

Tortuosity

In addition to classical structural parameters such as porosity, surface area, and pore size distribution, another important structural characteristic is tortuosity. In porous materials such as paper and board, the interfiber capillaries can be highly tortuous. There are two different aspects of tortuosity: (1) geometric tortuosity, defined by geometric features, and (2) transport (i.e., diffusion) tortuosity, deduced from resistance offered to fluid flow and mass transport in porous media. In this paper, we report a method to characterize the geometric tortuosity using the actual 3D structures of porous materials. Geometric tortuosity is defined as the ratio of the actual length of the pore space (capillaries between the fibers) to the straight line (or



4. Effect of refining level on porosity of softwood bleached kraft (SWBK) handsheets obtained by different methods

the shortest length) of the capillary [24]. It is more meaningful to determine the overall average geometric tortuosity for an entire volume. The algorithm we developed is based on allowing walkers (particles) to pass through the pores in a 3D image of the sample. Starting off on one face of the sample image, the tracers are allowed to traverse through the structure predominantly in one direction (i.e., in-plane and transverse directions). It is thus possible to obtain independent measurements of in-plane and transverse geometric tortuosity.

Mercury intrusion porosimetry

Pore structure characterizations using XRCT and image analysis were compared with experimental data obtained with MIP. Mercury intrusion porosimetry is a common, invasive method used to evaluate structural characteristics such as pore volume and pore size distribution of porous materials [25,27]. The method is based on the principle that the pressure required to force a nonwetting liquid to fill the pores inside the material is inversely proportional to the diameter of the pores [28]. The relationship between the pore diameter and pressure was established using the Lucas Washburn equation [29]. Using the Lucas Washburn equation and the known values of surface tension and contact angle for mercury, the relationship between pore diameter (D, m) and applied pressure (P) can be given as (Eq. 11):

$$D = \frac{213}{P} \quad (11)$$

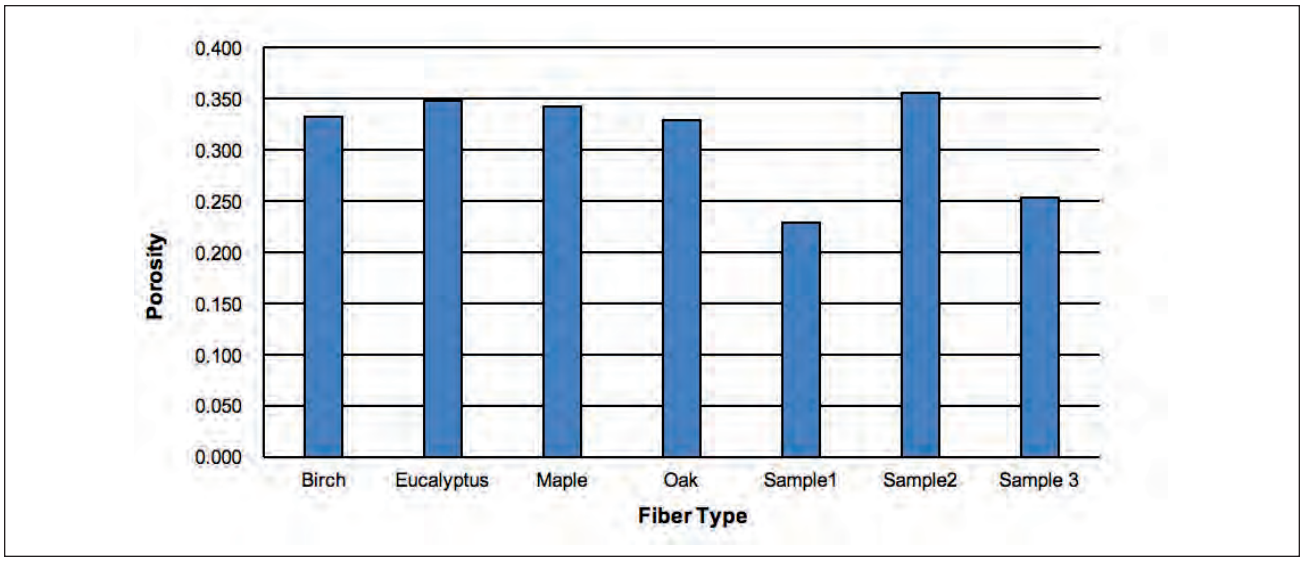
RESULTS AND DISCUSSION

For the pool of paper samples, various structural properties such as porosity, SSA, 3D pore size distribution, and tortuosity were determined with the help of XRCT images of the corresponding samples, as well as experimental methods.

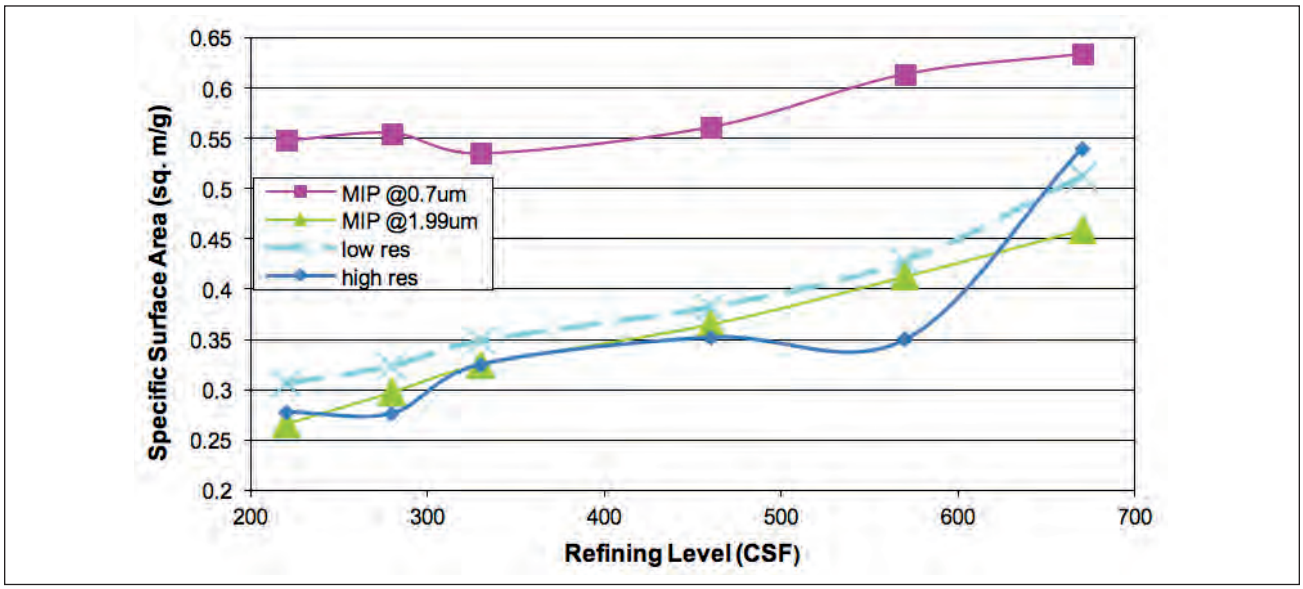
Porosity and specific surface area

Porosity results obtained from image analysis of XRCT images taken at high resolution (0.7 µm), were compared with porosity measurements based on sheet thickness and basis weight as well as mercury intrusion porosimetry, for paper samples with varying mechanical treatment or refining levels as measured by freeness (CSF, mL) . The results were also compared with low resolution XRCT images (2 µm) that were used in the previous work [30]. CSF is a measurement of the extent of mechanical treatment given to cellulose fibers prior to papermaking. The level of mechanical treatment or refining the pulp has undergone influences the swelling of fibers, strength, surface area, density, and amount of open space between the fibers when formed into a sheet [31]. The CSF of a paper sample decreases with the amount of mechanical treatment. With increase in the extent of refining, fiber cell walls are separated (defibrillation), which extends the fibrils on the fiber surface. When formed into a sheet, this causes an increase in the density and hence lowers the porosity as freeness decreases. The densification of the structure as evidenced by a decrease in porosity is shown by all the methods studied (**Fig. 4**). Apparent density measured by sample basis weight and thickness is a gross measurement; as expected, this exhibited the highest value for all the samples. MIP porosity values were greater than those obtained by image analysis. This could be because of the ability of MIP to detect pores much smaller than the resolution capability of XRCT.

Given the heterogeneity of paper structures and small sample volumes used on XRCT, there is an inherent variability in the structural characteristics [32]. To obtain a reasonable average for a larger sample, it is thus necessary to evaluate a number of regions within a sample volume. Whenever possible, three repeats of the sample scans from different locations were conducted. As shown in **Fig. 5**, the average varia-



5. Porosity comparison for different fiber furnishes (laboratory handsheets) and commercial samples.



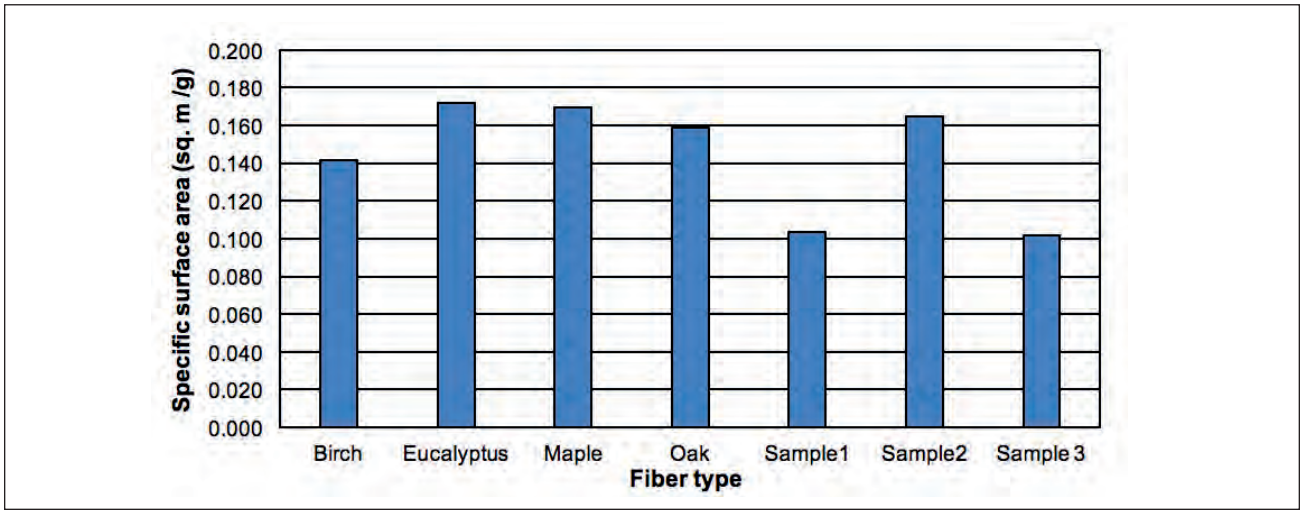
6. Effect of refining on specific surface area of SWBK handsheets obtained by different methods.

tion in structural characteristics measured using XRCT and image analysis for a given sample taken from various locations (normally three to five locations for a given sample) is about ±1%–14%. Taking this into consideration, the noninvasive XRCT technique does capture the changes in porosity as a result of mechanical treatment of fibers.

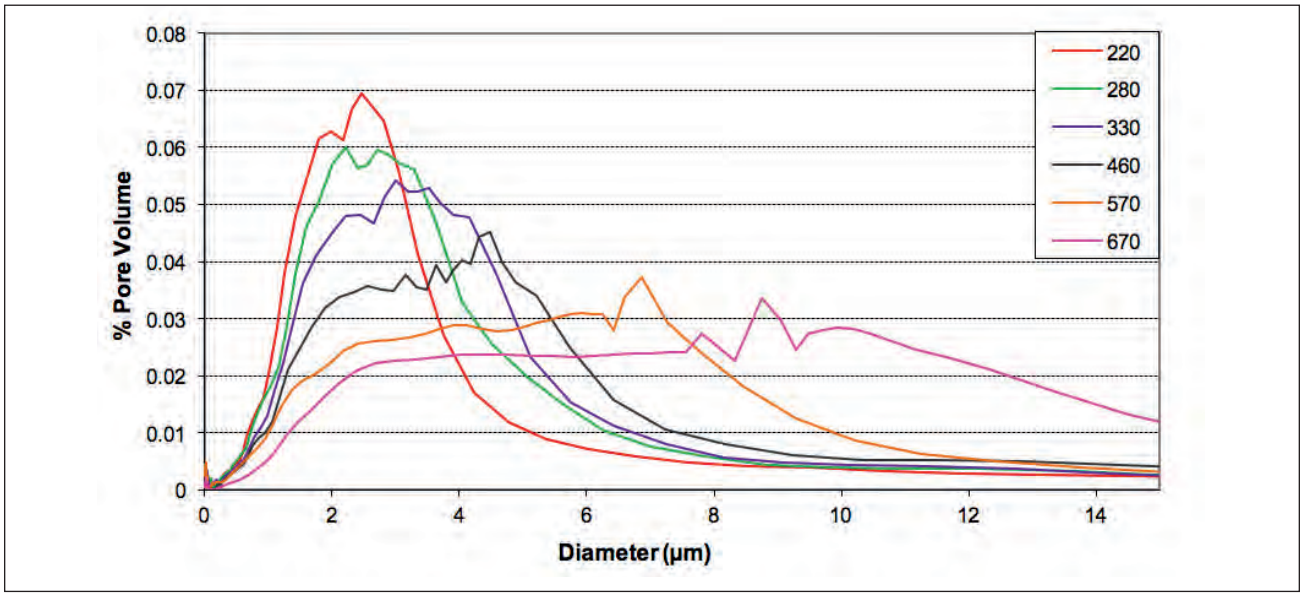
Figure 5 shows a similar comparison of paper structures made using cellulose fibers from different wood species, such as oak, birch, eucalyptus, and maple, and three commercially made fine paper samples, identified as samples 1, 2, and 3. It is again observed that the commercially made samples subjected to standard densification processes of wet pressing and calendering mostly exhibited a lower porosity than laboratory-made handsheets.

The SSA results for paper samples of different refining levels obtained by image analysis were compared with results obtained by MIP. As in the case of porosity, SSA results by MIP were much larger than those by image analysis. However, when the total MIP results were analyzed, considering only up to pore sizes of 0.7 μm and 1.99 μm, they were closer to the image analysis results. Even though the surface area of individual fibers increases with increases in the level of mechanical treatment due to defibrillation, the trend is opposite in the case of dry paper samples (**Fig. 6**). This is because the individual fibers are compacted and collapsed to form paper sheets, which increases the density and reduces the porosity as well as the exposed nonbonded interfacial area.

Similar comparisons for different fiber species and commercial samples also show a decrease in SSA with a higher degree of densification and consolidation (**Fig. 7**). The commercially made paper samples mostly show a lower surface



7. Specific surface area comparison for different fiber furnishes (laboratory handsheets) and commercial samples.



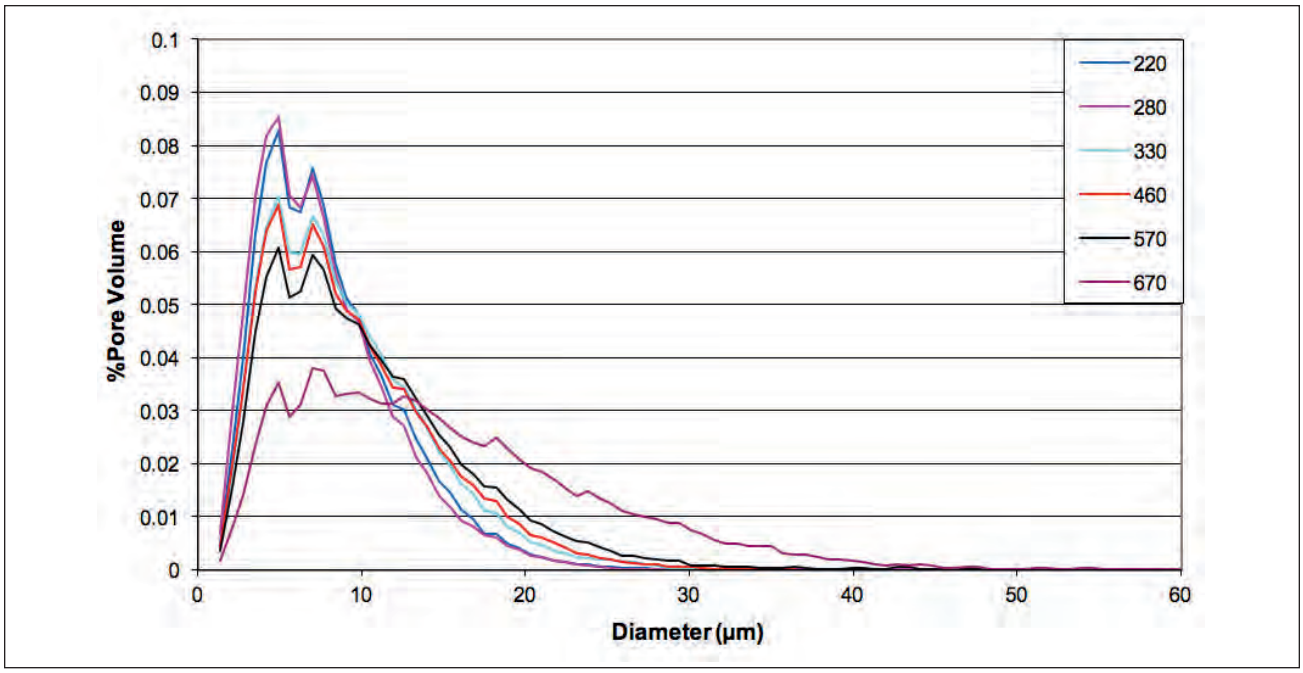
8. Three-dimensional pore size distributions of SWBK handsheets at different refining levels obtained from mercury intrusion porosimetry (MIP).

area compared with the laboratory-made handsheets, which is consistent with the porosity data.

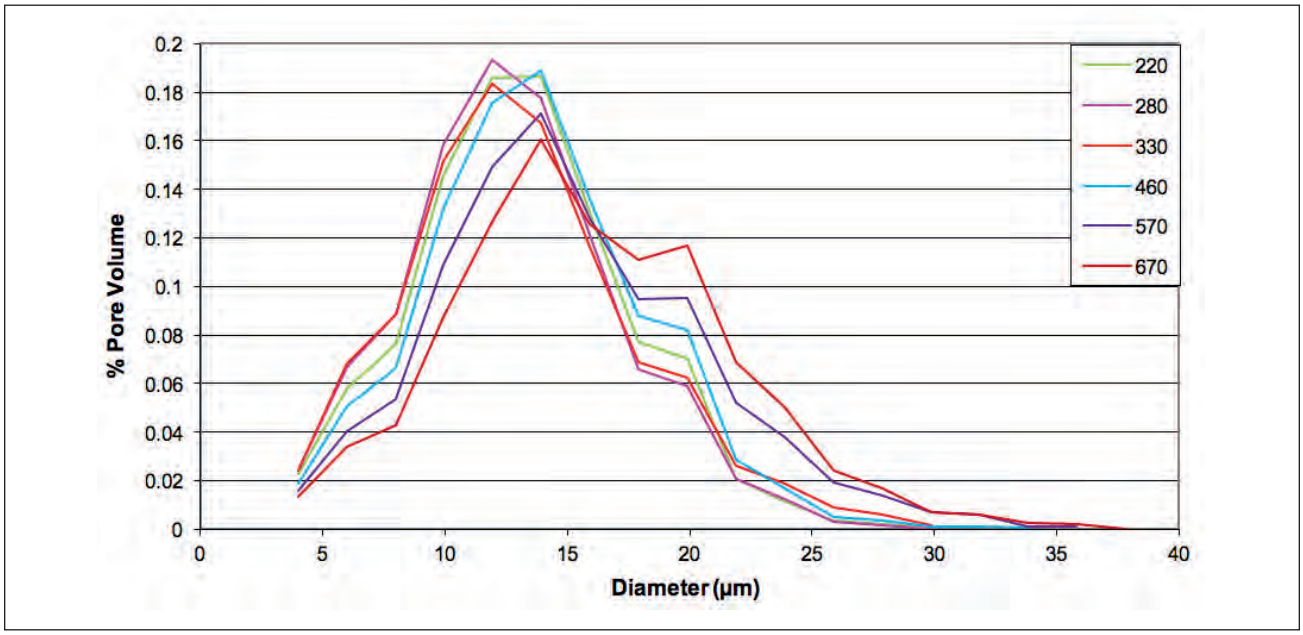
3D pore size distribution and tortuosity

The sphere growing algorithm was used to compute the 3D pore size distributions from high and low resolution XRCT images and compare them with the results obtained from MIP. **Figure 8** shows the pore size distributions obtained from MIP for samples with different levels of refining. As shown in Fig. 8, as the degree of mechanical refining of fibers is increased, the initially larger pores with wider distribution shift toward smaller pores and narrower distribution. This is expected because of the densification and consolidation of the structure, as shown by the porosity data. Because of the nature of the MIP technique, there is also a significant contribution to the size distribution from very small pores. In addition to being able to access really small pores, part of the volume from small pores can also be attributed to potential misinterpretation because of the ink-bottle effect [27].

A similar effect of refining on the pore size distribution is also observed with results from XRCT images obtained using the high resolution and low resolution methods as shown in **Figs. 9 and 10**. In the case of XRCT images, because of the limits of resolution and pixel size, pore diameters below 0.7 µm and 4 µm cannot be detected for the high and low resolution images, respectively. Hence the high peak near smaller diameters that was observed in the case of MIP is not visible here. Similar to MIP, with increasing refining and consolidation of the structure, there is a shift toward smaller pores and narrower mean pore diameter.



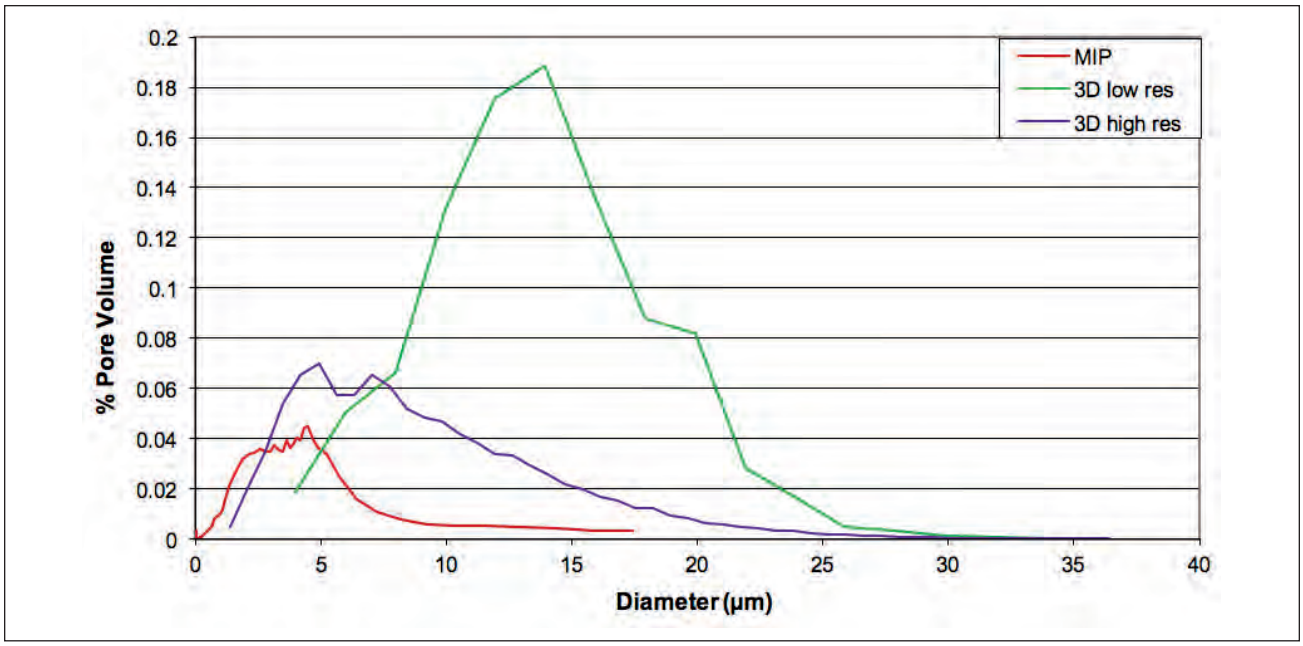
9. Three-dimensional pore size distributions of SWBK handsheets at different refining levels for high resolution X-ray computed tomography (XRCT) images computed by sphere growing method.



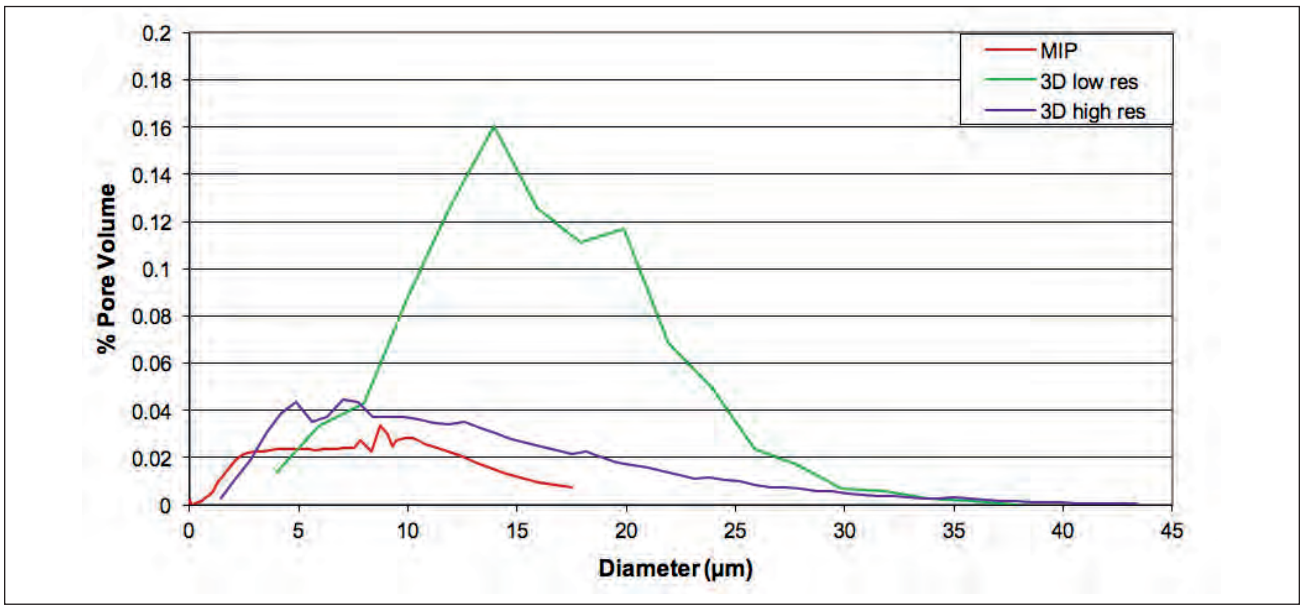
10. Three-dimensional pore size distributions of SWBK handsheets at different refining levels for low resolution XRCT images computed by sphere growing method.

The lower resolution images show a much bigger and broader pore size distribution. Even though decreasing mean pore size with increasing refining can be observed, in general the average pore size for low resolution images is about twice that of high resolution images for the same samples. The low resolution technique is quite coarse and only capable of capturing larger pores and hence might not be suitable for some of the end uses of paper. **Figures 11 and 12** show the comparison of pore size distributions obtained using different techniques (i.e., MIP and high and low resolution XRCT) for the same refining level (460 and 670 CSF, respectively). The MIP technique shows pore size distribution in the smallest pore size range followed by 3D high and low resolution XRCT images (**Fig. 13**).

Two-dimensional in-plane and transverse pore size distributions using the equivalent hydraulic diameter approach

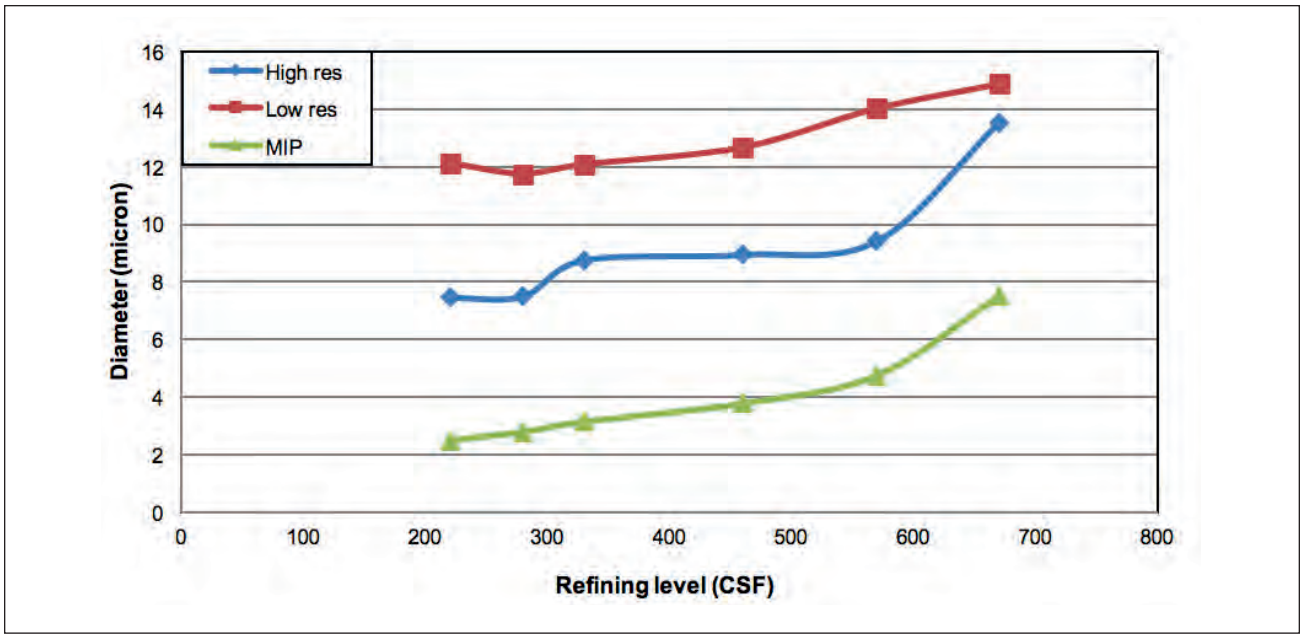


11. Comparison of 3D pore size distribution results for 460 CSF sample obtained by MIP and high resolution and low resolution XRCT images.



12. Comparison of 3D pore size distribution results for 670 CSF sample obtained by MIP and high and low resolution XRCT images.

were also determined for the high and low resolution XRCT images for comparison. In comparison with 3D pore size distribution results, 2D results showed bigger pore sizes. This is because the third dimension is not taken into account, which might contribute to decreasing the pore size. Moreover, the 3D pore size distributions are a combination of the in-plane and transverse pore size distributions. It was observed that the equivalent pore sizes in the plane (in-plane) direction were always lower than those in the transverse direction because the fibers are mostly aligned horizontally during papermaking and then formed layer by layer. Even though the pore sizes in the in-plane direction appear to be smaller than those in the transverse direction, it has been experimentally shown that in-plane liquid permeability in paper samples is always greater than transverse permeability [33]. This apparent anomaly can be explained further by studying the geometric tortuosity, which is also known to contribute to the overall resistance to flow. On the basis of these discussions, the 3D pore size distribution method is preferred for characterizing pore size distribution



13. Comparison of mean diameters of pores for samples of varying refining levels by different methods.

in porous materials such as paper and board.

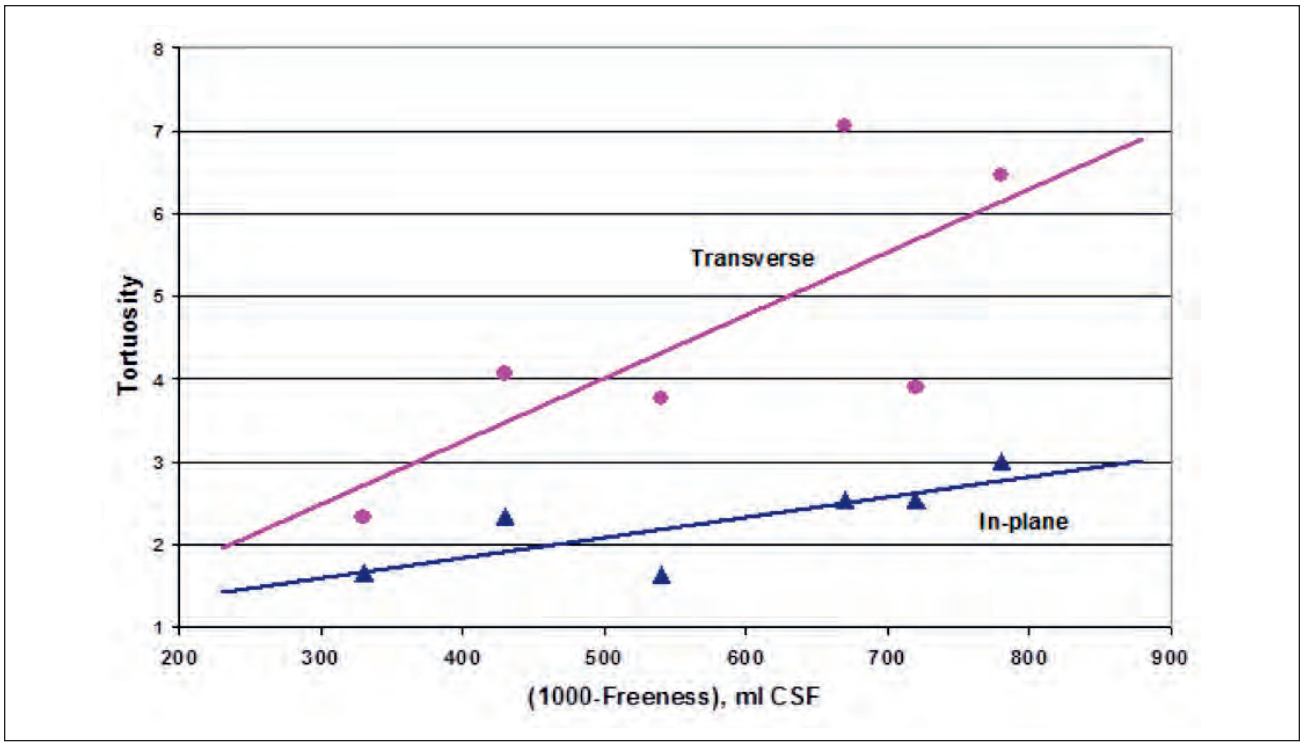
Tortuosity

Figure 14 shows the effect of refining on in-plane and transverse geometric tortuosity in paper samples using actual 3D sample volumes. The in-plane tortuosity is lower than the transverse tortuosity in all of the samples because of the layered structure of paper. As the mechanical treatment of fibers is increased, the pores become more tortuous and the geometric tortuosity increases in both the in-plane and transverse directions. The difference in tortuosity between the two orthogonal directions increased with increased refining and sheet consolidation. This could have significant effects on the overall transport and properties of the material and is in agreement with previous work [33].

CONCLUSIONS

X-ray computed tomography is an effective tool to visualize the complex internal 3D microstructure of porous materials. In the current work, paper samples made using different levels of refining or mechanical treatment and from different fiber species are visualized and structural characteristics are determined. The 3D XRCT images at two different resolutions (0.7 μm and 2 μm) were used. To improve the quality of the images and more accurately identify the different material components, a fully automated image processing technique using anisotropic diffusion, minimum error thresholding, isolated voxel removal, and binarization was developed. This technique was applied to paper samples of varying structures and shown to give higher quality images while retaining the essential structural features. Structural characteristics such as porosity, SSA, and 3D pore size distribution were determined using the high resolution XRCT images and compared with experimental methods as well as the low resolution XRCT images reported earlier [30]. Porosity was determined experimentally by sheet caliper and basis area weight measurements. Pore structure characteristics, SSA, and 3D pore size distribution were determined experimentally by MIP. A sphere growing method was developed to compute the 3D pore size distribution using the actual 3D images of sample volumes. This technique is an improvement over the previous 2D pore size distribution technique because it is a combination of the in-plane and transverse pore size distribution and information from neighboring voxels in all three directions is also accounted for.

Porosity results indicate that as the level of refining is increased and the samples are more consolidated, the densities of the paper samples are increased and hence the porosity is decreased. This trend is seen with both experimental data and XRCT image analysis methods. Likewise, the SSA in the dry paper samples containing bonded cellulose fibers is also decreased with an increase in the level of mechanical treatment. Three-dimensional pore size distribution comparisons showed that as the degree of mechanical refining of fibers is increased, the initially larger pores with a wider distribution shift toward smaller pores and narrower distribution. This is expected because of densification and consolidation of the structure and as shown by the porosity data. The MIP technique, which is able to penetrate smaller pore sizes and potential artifacts, showed the smallest pore size distribution followed by 3D high resolution and low resolution XRCT images. In many of the commercial manufacturing and end use applications, structural features from high resolution XRCT images might be adequate in explaining the overall performance. The geometric tortuosity, another important structural characteristic, was also shown to be affected by the



14. Effect of refining on in-plane and transverse geometric tortuosity.

mechanical treatment of fibers. As the mechanical treatment of fibers was increased, with more consolidation and densification of the structure, the pores become more tortuous and the geometric tortuosity increased in both in-plane and transverse directions. The transverse tortuosity was always found to be greater than the in-plane tortuosity, and this could have a significant influence on liquid and vapor transport in the two orthogonal directions.

Given the heterogeneous nature of porous materials such as paper and the relatively small sample volumes used to probe in XRCT technique, it is important to evaluate the material at numerous locations to obtain a more representative characterization. **TJ**

ACKNOWLEDGEMENT

The authors acknowledge the funding support provided by the Minnesota Agriculture Experiment Station and the U.S. Department of Energy.

LITERATURE CITED

1. Modgi, S., Mcquaid, M.E., and Englezos, P., *Nord. Pulp Pap. Res. J.* 21(5): 659(2006).
2. Yang, D., Moran-Mirabal, J.M., Parlange, J.Y., et al., *Biotechnol. Bioeng.* 110(11): 2836(2013).
3. Abrams, L., Favorite, C.W., Capano, P.J., et al., *TAPPI Coat. Conf.*, TAPPI Press, Atlanta, GA, USA, 1996, p. 185.
4. Johnson, R.W., Abrams, L., Maynard, R.B., et al., *TAPPI J.* 82(1): 239(1999).
5. Bloch, J.F., Decain, M., Geindreau, C., et al., *Appita J.* 61(4): 286(2008).
6. Chinga-Carrasco, G., Kauko, H., Myllys, M., et al., *J. Microsc.* 232(2): 212(2008).
7. Van den Bulcke, J., Boone, M., Van Acker, J., et al., *J. Coat. Technol. Res.* 7(2): 271(2010).
8. Mayo, S.C., Chen, F., and Evans, R., *J. Struct. Biol.* 171(2): 182(2010).
9. Du Roscoat, S.R., Bloch, J.F., and Thibault, X., *J. Phys. D: Appl. Phys.* 38(10A): A78(2005).
10. Chinga-Carrasco, G., Axelsson, M., Eriksen, Ø., et al., *J. Pulp Pap. Sci.* 34(1): 13(2008).
11. Samuelsen, E.J., Gregersen, O.W., Houen, P.J., et al., *J. Pulp Pap. Sci.* 27(2): 50(2001).
12. Du Roscoat, S.R., Decain, M., Thibault, X., et al., *Acta Mater.* 55(8): 2841(2007).
13. Van den Bulcke, J., Masschaele, B., Dierick, M., et al., *Int. Biodeterior. Biodegrad.* 61(3): 278(2008).
14. Antoine, C., Nygård, P., Gregersen, Ø.W., et al., *Nucl. Instrum. Methods Phys. Res. Sect. A* 490(1): 392(2002).
15. Saghi, Z. and Midgley, P.A., *Annu. Rev. Mater. Res.* 42: 59(2012).
16. Ramaswamy, S., Huang, S., Goel, A., et al., *12th Fund. Res. Symp.*, The Fundamental Paper Research Society, Bury, U.K., 2001, p. 1281
17. Huang, S., Goel, A., Ramaswamy, S., et al., *Appita J.* 55(3): 230(2002).
18. Goel, A., Tzanakakis, M., Huang, S., et al., *TAPPI J.* 84(5): 72(2001).
19. Defrenne, Y., "Three dimensional structural analysis of porous materials via micro-tomography image processing," Ph.D. dissertation, University of Minnesota, Minneapolis, MN, USA, 2008.

20. Perona, P. and Malik, J., *IEEE Trans. Pattern Anal. Mach. Intell.* 12(7): 629(1990).
21. Kittler, J. and Illingworth, J., *Pattern Recognit.* 19(1): 41(1986).
22. Toriwaki, J. and Yoshida, H., *Fundamentals of Three-dimensional Digital Image Processing*, Springer, New York, 2009, p. 194.
23. Stone, J.E., Scallan, A.M., and Aberson, G.M.A., *Pulp Pap. Mag. Can.* 67(5): T263(1966).
24. Cussler, E.L., *Diffusion: Mass Transfer in Fluid Systems*, Cambridge University Press, New York, 1997, p. 191.
25. Leon, C., *Adv. Colloid Interface Sci.* 76: 341(1998).
26. Romero Morales, E.E., Musso, G., and Jommi, C., in *ALERT Doctoral School 2012: Advanced Experimental Techniques in Geomechanics*, ALERT Geomaterials, Grenoble, 2012, pp. 125-156.
27. Abell, A.B., Willis, K.L., and Lange, D.A., *J. Colloid Interface Sci.* 211(1): 39(1999).
28. Bandyopadhyay, A. and Bose, S., *Characterization of Biomaterials*, Elsevier, Waltham, MA, USA, 2013, p. 41.
29. Washburn, E.W., *Phys. Rev.* 17(3): 273(1921).
30. Goel, A., "Numerical methods and image analysis to predict the transport properties of porous media," Ph.D. thesis, University of Minnesota, St. Paul, MN, USA, 2003.
31. Biermann, C.J., *Handbook of Pulping and Papermaking*, Academic Press, San Diego, CA, USA, 1996, pp. 158-188.
32. Gupta, M.K., "Modeling of simultaneous diffusion in heterogeneous porous media," M.S. thesis, University of Minnesota, St. Paul, 2004.
33. Lindsay, J.D. and Brady, P., "Studies of anisotropic permeability with applications to water removal in fibrous webs," *Nonwovens Conf.*, TAPPI Press, Atlanta, 1992.

ABOUT THE AUTHORS

Three-dimensional (3D) structure of paper and board plays an important role during the manufacturing process and during end-use applications. This study is part of ongoing research on structure-property relationships in porous materials such as paper and board.

In this study, we confirmed that the 3D structure of paper and board is indeed very important and that using the latest scientific developments can help us better understand and "engineer" paper for specific applications. The computational aspects of this work are quite challenging, and we have very good students who helped solve these and other complicated problems.

The most interesting aspect of our study is that it is possible to quantify the 3D internal structure of paper and board and use it for benchmarking products, as well as new process and product development. Mills can use the information here for those purposes, as the technique developed here is already being commercially used.

Our next step is to let mills and technical departments know about the capabilities of this technique and to assist in its widespread use.

Defrenne is process engineer at Appvion Inc., Appleton, WI, USA. Zhdankin is staff engineer at Segate Technology, Shakopee, MN, USA. Ramanna is a doctoral candidate and Ramaswamy is a professor and head of the Department of Bioproducts and Biosystems Engineering, at the University of Minnesota, St. Paul, MN, USA. Ramarao is professor and director, Empire State Paper Research Institute, at the State University of New York College of Environmental Science and Forestry (SUNY-ESF), Syracuse, NY, USA. Email Ramaswamy at shri@umn.edu.


Defrenne


Zhdankin


Ramanna


Ramaswamy


Ramarao

Effect of surface treatment with biodegradable materials on properties of linerboard made from old corrugated containers (OCC)

SOMAYEH HEYDARI, AHMAD REZA SARAEYAN, AND ALIREZA SHAKERI

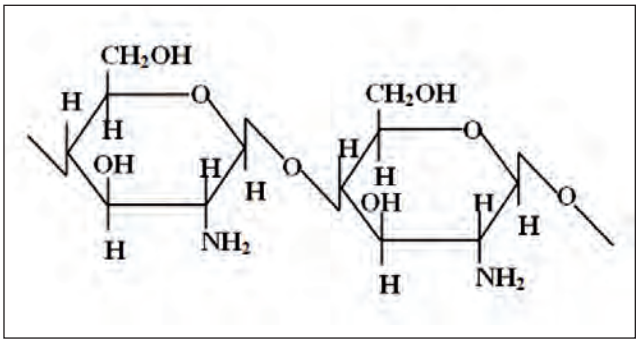
ABSTRACT: Linerboard produced from old corrugated containers (OCC) shows lower strength properties in comparison with linerboard produced from virgin fibers. This study determined the influence of surface treatment with polyvinyl alcohol (PVOH), ethylene vinyl alcohol (EVOH) (as synthesized biodegradable polymers), chitosan, and anionic starch (as biobased and biodegradable polymers) on properties of sheets produced from OCC. The polymers were applied from aqueous biodegradable dispersion, by using a laboratory-scale coater. This research investigated the burst index, tensile index, stiffness, water resistance, air resistance, and water absorption. The results showed that paper surfaces treated with water-soluble polymers increased the mechanical properties. In addition, PVOH increased the burst index value 136% and EVOH increased the tensile index, tear index, and stiffness values by 84.3%, 108.6%, and 22.43%, respectively. The anionic starch increased air resistance to 34.7% and chitosan decreased water absorption to 12.3%.

Application: Surface treatments with biopolymers can increase the strength properties of linerboard produced from old corrugated containers.

The use of secondary fiber for paper production is increasing all over the world. About 40% of the total paper production in the world was based on the secondary fiber in 2006 [1]. Paper recycling has many advantages. Every ton of recycled fiber saves an average of 17 trees plus related pulping energy, and for every ton of paper for recycling, the savings are at least 30000 L of water, 3000–4000 KW•h of electricity, and 95% of air pollution [2]. Therefore, recycled fibers have a very important role in the paper industry.

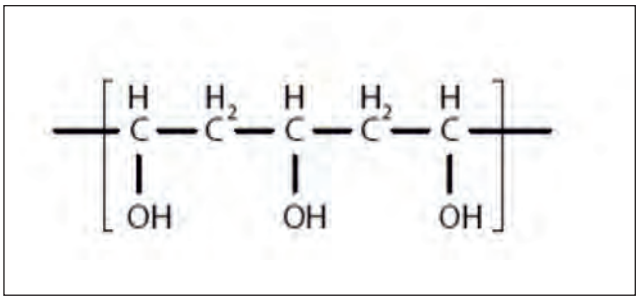
Linerboard is produced from virgin fiber, usually called kraft liner, whereas linerboard containing recycled fiber is called test liner. The major problem with recycling of old corrugated containers (OCC) is the loss of strength properties [3]. By increasing the number of cycles in the fiber recycling, the strength of papers is gradually reduced because of the decrease in interfiber bonding strength compared with virgin wood pulp fibers through the hornification phenomenon [4]. The strength of recycled fiber is not sufficient to meet the industry's demand; thus, the strength should be improved. Many polymers are used in paper manufacture to improve or enhance the strength and printability of paper. A number of these polymers are nonbiodegradable and might cause environmental problems, and some pose occupational health and safety risks to paper industry workers.

Chitosan, a natural polysaccharide, is a modified biopolymer (derived from the shells of certain crustaceans). It comprises an unbranched chain consisting of ß (1→4)-linked 2-Acetamido-2-deoxy-ß-D-glucopyranose [5]. The primary structure of chitosan is similar to cellulose except that the C-2-hydroxyl group of cellulose is replaced by an amino group (**Fig. 1**). Chitosan is insoluble in water under alkaline conditions, but it is soluble in acidified water because of its primary amino groups. It is a unique basic linear polysaccharide that has shown potential to improve both the strength and the printing properties of papers. Chitosan has been found to be effective as dry- and wet-strength agents [6], as well as in coatings [7] and sizing [8].



1. Chemical structure of chitosan.

Polyvinyl alcohol (PVOH) is a water soluble and biodegradable synthetic polymer available in both fully hydrolyzed and



2. Chemical structure of polyvinyl alcohol (PVOH).

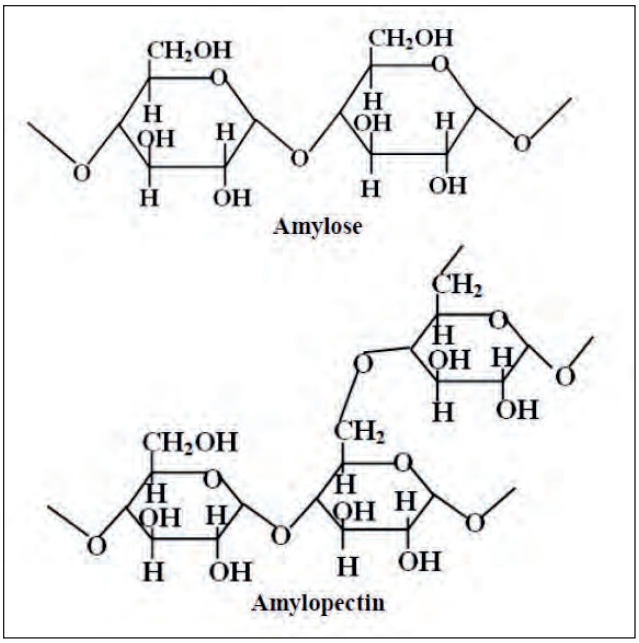
partially hydrolyzed grades (**Fig. 2**). It is an adhesive with superior bonding strength, film forming, and emulsifying properties. PVOH has been extensively used in the textile industry for warp sizing and resin finishing; in the paper industry for surface sizing and pigment coating; in the production of PVOH emulsion as a protective colloid; in the suspension polymerization of polyvinyl chloride as a dispersion agent; and as a binder for ceramics, magnet, foundry cores, and pigments [9].

Because of the presence of hydroxyl groups in every repeating unit of PVOH, it appears to be one of the best polymers to reinforce cellulose fibers [10]. In papermaking, PVOH is used for surface sizing to form films with very high tensile strength and a high degree of transparency, flexibility, and oil resistance [11]. PVOH can also be mixed with starch and applied at a size press [12].

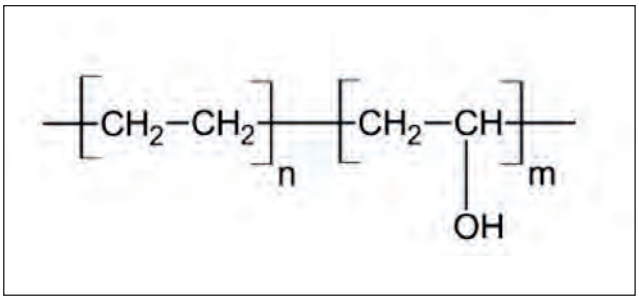
The other most abundant natural polymer is starch, regenerated from carbon dioxide and water by photosynthesis in plants [13]. Starch is a cheap, renewable, and completely biodegradable polymer [14] and thus is a promising candidate for developing sustainable materials. Starch is a semicrystalline polymer comprising two repeating units of 1, 4-α-D-glucopyranosyl: amylose and amylopectin (**Fig. 3**).

Ethyl-vinyl alcohol (EVOH) is used in conjunction with paper, foil, and other plastics for flexible and semirigid containers [15]. The properties of EVOH vary with the relative amounts of the two components, PVOH and polyethylene (PE) (**Fig. 4**). As the mol% of ethylene increases, the properties of EVOH become more like that of PE; conversely as mol% ethylene decreases, the material behaves more like PVOH. Similarly, materials with higher ethylene content resemble properties of PE. EVOH is a semicrystalline copolymer [16]. The repeating unit of EVOH has the following chemical structure. The copolymer composition (i.e., relative amounts of ethylene and vinyl alcohol) affects properties of EVOH copolymers (e.g., gas barrier, mechanical properties, and water vapor transmission) and hence influences EVOH processing and end use applications. EVOH resins are commercially available in a range of compositions, most commonly encompassing vinyl alcohol contents of about 52–76 mol% (Fig. 4)

One drawback of corrugated board is its hydrophilic character. Corrugated board usually absorbs water from the environment, especially when being stored under high humidity



3. Chemical structure of starch.



4. Chemical structure of ethylene vinyl alcohol (EVOH).

conditions or when coming into contact with high-moisture products such as fresh agricultural produce or frozen foods. Absorption of water reduces the physical and mechanical strength of corrugated board, causing corruption of the flute structures and failure of the corrugated package during storage and distribution. Surface treatments such as sizing, coating, and laminating are usually used on the kraft liner to improve the physical strength as well as water barrier properties [17,18].

This study was carried out to investigate strength properties, water, and air resistance of liner paper made from OCC surface treated with PVOH, EVOH, chitosan, and anionic starch.

MATERIALS AND METHODS

The materials used in this work were PVOH (98%–99% hydrolyzed, average mol. wt. 31000–50000), chitosan (medium mol. wt., 75%–85% deacetylated), EVOH, and anionic starch. The EVOH and anionic starch were purchased from Sigma Aldrich (St. Louis, MO, USA). Also, the samples used in this work were untreated linerboard made of OCC with a weight of 120±5 g/m^2 obtained from a local recycling paper mill.

Treatment	Biopolymer	Coated Weight, g/m²	Burst, Kpam²/g	Tensile, N.m/g	Tear, mN.m²/g	Stiffness, N/mm	Air Resistance, s/100 mL air	Water Absorption, g/m²
R	Reference	–	0.92±0.11	2.67±0.27	5.18±0.15	385.33±14	9.16±0.06	119±10.6
C	Chitosan	4.43±1.27	1.49±0.04	3.66±0.16	5.88±0.12	447.15±16.07	12.57±0.1	102±5.44
S	Anionic starch	5.56±0.84	1.31±0.08	3.35±0.34	5.74±0.06	435.07±35.4	20.77±0.17	144.26±10.65
P	Polyvinyl alcohol	5.27±1.38	2.17±0.02	4.55±0.38	5.63±0.23	477.5±33.8	10±0.67	152.46±7.65
E	Ethylene vinyl alcohol	4.43±1.45	1.92±0.05	4.92±0.27	6.02±0.08	490.73±35.55	10.7±0.06	217.21±4.51

I. Properties of sheets surface treated with different biodegradable polymers.

Solubilization of materials

The starch coating solution was prepared by gelatinizing 2% (w/w) of anionic starch at 90°C for 20 min. The chitosan solution was obtained by dispersing chitosan 1% (w/w) in aqueous acetic acid under continuous stirring for 2 h. The PVOH solution was prepared by dissolving it in distilled water and heating it on a hot plate with a magnetic stirrer at 90°C for 30 min. The EVOH solution was prepared by dissolving it in distilled water and heating it at 90°C for 20–30 min.

The untreated linerboard was used as substrate to apply the dispersion coating. The polymer coatings were applied from aqueous biopolymer dispersion using a laboratory coater (Auto BAR coater, BMIK Co.; Jeonmin-dong, Korea).

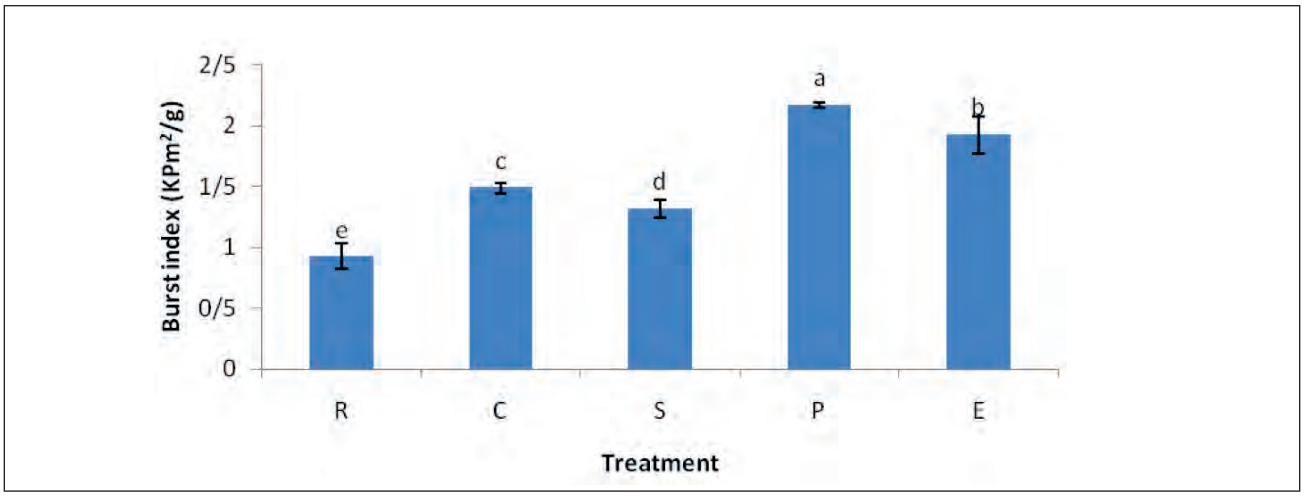
Determination of strength properties

For determination of strength properties, the samples were conditioned at 50±2% relative humidity (RH) and 23±1°C according to TAPPI Standard Test MethodT 402 sp-98 "Standard conditioning and testing atmospheres for paper, board, pulp handsheets, and related products" for at least 4 h. Dry-strength properties of sheets were tested according to the following TAPPI Standard Test Methods: tensile and stiffness (T 451 cm-84 "Flexural properties of paper [Clark stiffness]"), burst index (T 403 om-02 "Bursting strength of paper"), tear index (T 414 om-04 "Internal tearing resistance of paper [Elmendorf-type method]"), air resistance (T 460 om-98 "Air resistance of paper [Gurley method]"), and water absorption (T 441 om-09 "Water absorptiveness of sized [non-bibulous] paper, paperboard, and corrugated fiberboard [Cobb test]").

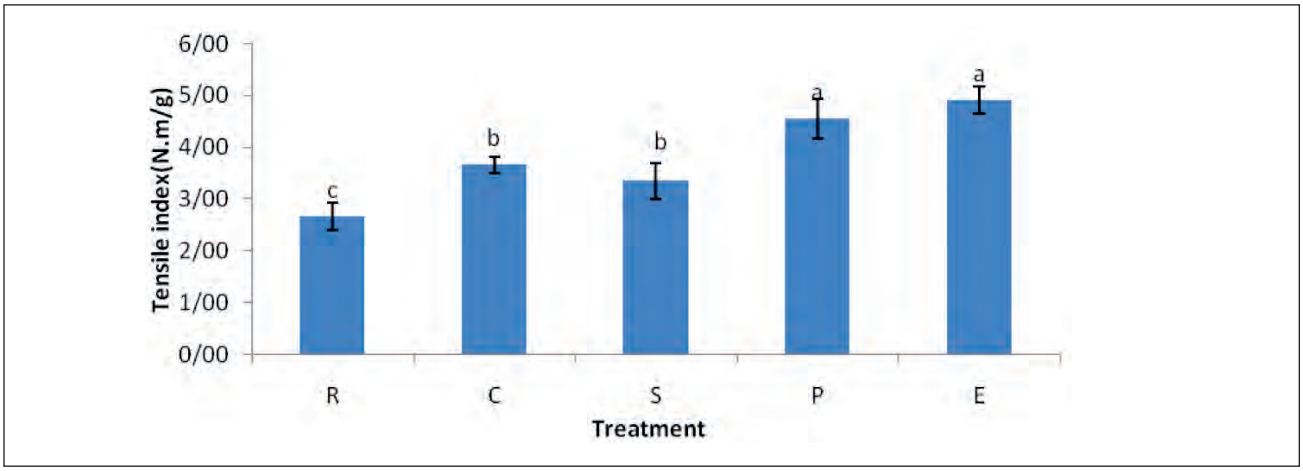
Analysis of variance was conducted using a randomized design. Mean values were compared using Duncan's test.

RESULTS AND DISCUSSION

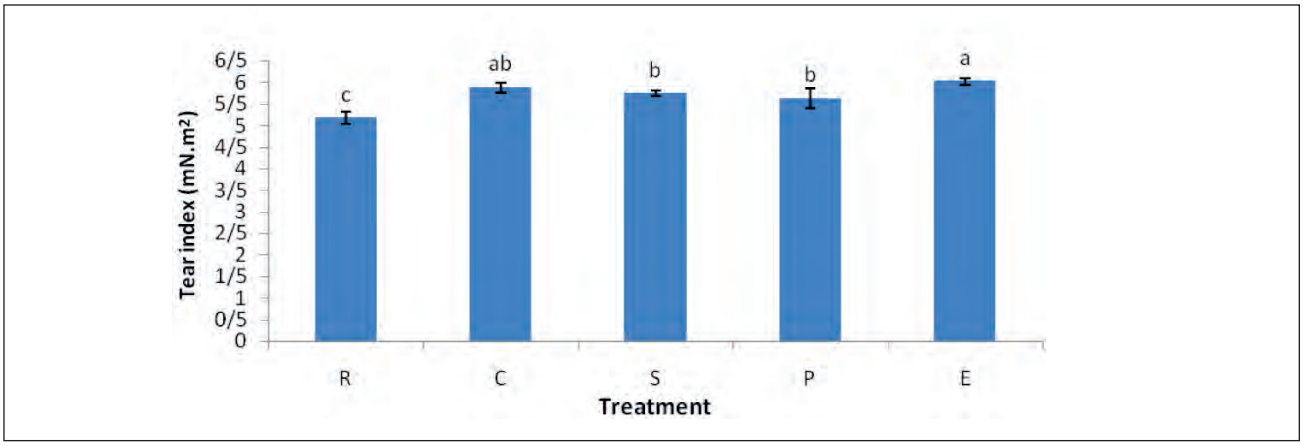
Data on burst index, tensile index, tear index, stiffness, air resistance, and water absorption of sheets surfaces treated by four biodegradable polymers are presented in **Table I**.



5. Average burst index of different surface treatments with biodegradable polymers. (Letters indicate significant difference at α = 0.05.)



6. Average tensile index of different surface treatments with biodegradable polymers. (Letters indicate significant difference at α = 0.05.)



7. Average tear index of different surface treatments with biodegradable polymers. (Letters indicate significant difference at α=0.05.)

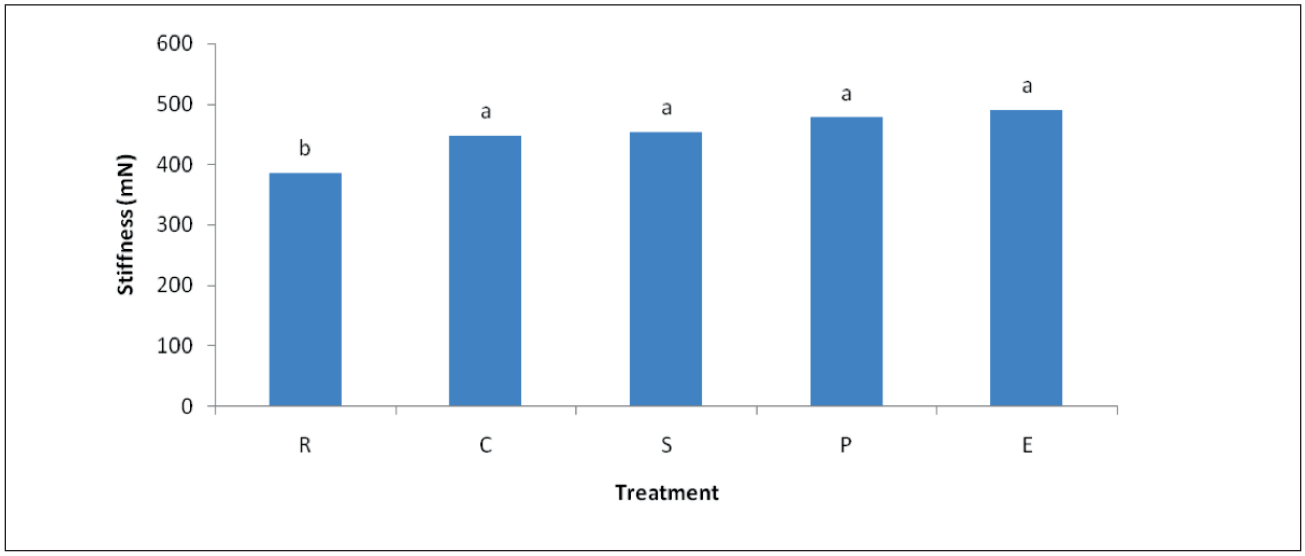
Strength properties

Figures 5, 6, and 7 show the effects of surface treatment with the biodegradable polymers on strength properties compared with controls. The results demonstrate that chitosan, anionic starch, PVOH, and EVOH increased burst, tensile, and tear indices. The surface treatment with PVOH and EVOH had a unique effect on the strength properties compared with surface treatment with anionic starch and chitosan. PVOH and EVOH enhanced tensile index of sheets 70.41% and 84.27%, respectively. PVOH is a biocompatible petroleum-based polymer. It is also one of the rare polymers with a carbon-carbon single-bond backbone that is fully biodegradable. Because of the hydroxyl (-OH) groups on the alternating carbon atoms, PVOH is strongly hydrophilic and soluble in water, which promotes its degradation and acetyl linkages with other materials such as cellulose and aldehydes [19]. This may be due to the formation of hydrogen bonding between the hydroxyl groups of cellulose and those of PVOH. There were interactions between cellulose and PVOH that involved the formation of interchange hydrogen bonds between hydroxyl groups of PVOH and ether oxygen in cellulose [20]. This polymer fills the paper pores and forms a dense layer at the paper surface. Hydrogen bonds that formed between the polar groups of EVOH mainly explain the high cohesive energy density of this film. However, these polar groups lead to the hydrophilic character of the polymer, and the different charges of the chitosan and cellulose can be expected to yield good adhesion between a chitosan and a cellulose-based substrate [21]. As the ionized amino groups of chitosan come into contact with fibers, they can form ionic and amino bonds in the presence of water.

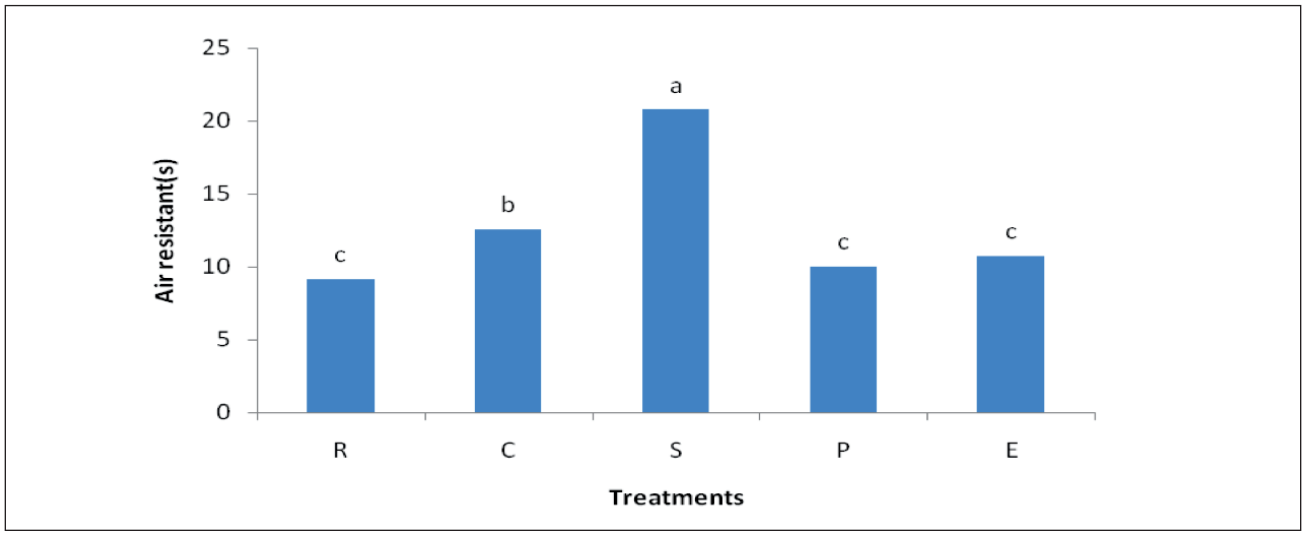
The results of stiffness are shown in **Fig. 8**. Stiffness is usually achieved through an increase in paper basis weight or densification of a sheet of some prescribed basis weight wet pressing. Both means involve high cost. Surface treatment with biodegradable polymers showed increased stiffness of sheets [22].

Air resistance

Effects of the surface treatment with biodegradable polymers on the air resistance of the sheets are shown in **Fig. 9**. The results indicated that anionic starch had a positive effect on air resistance of the sheets and the air resistance values were higher than for the other biopolymers. Starch seals the pores



8. Average stiffness index of different surface treatments with biodegradable polymers. (Letters indicate significant difference at α = 0.05.)

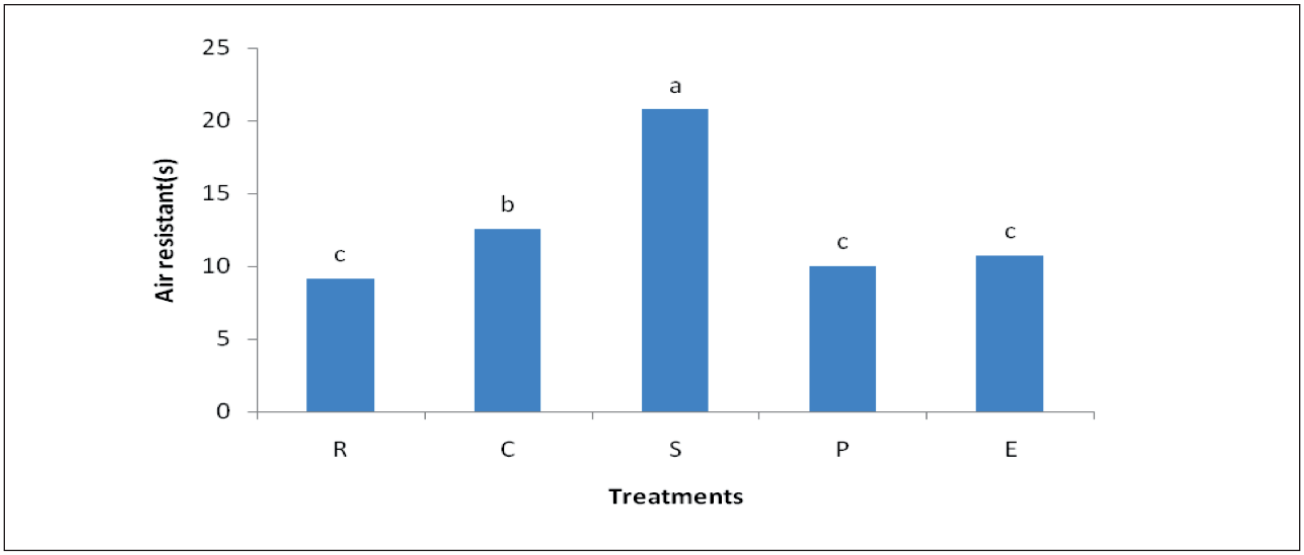


9. Average air resistant of different surface treatments with biodegradable polymers. (Letters indicate significant difference at α = 0.05.)

in the base papers. The air resistance is indicative of porosity, and this result suggests that either the numbers of pores in the paper surface treated with starch is reduced or their size is diminished. Chitosan coating showed change in the air resistance, but PVOH and EVOH showed no change in the air resistance compared with the uncoated control. A reason might be that PVOH and EVOH penetrated into the fibers and did not reduce the size of the pores.

Water absorption

Among the many properties of paper, one of the most important is its ability to control the penetration of various liquids, particularly those that are water based [23]. A water barrier can be formed by changing the wettability of the paper surface with sizing agents or through coating with hydrophobic materials [24]. **Figure 10** shows effects of the surface treatment with biodegradable polymers on the water absorption of the sheets. The lower the Cobb value, the less water penetrates into the sample. Starch, PVOH, and EVOH surface treatments did not provide any barrier against water, and their water sorption was found to be greater than the fiber sorption in the base paper. Hydrogen bonds formed between the polar groups of EVOH and PVOH. These polar groups are also the origin of the hydrophilic character of the polymers at high relative humidity [21]. The chitosan surface treatment reduced the Cobb60-values for the base paper. The results show that the chitosan surface treatment provided a barrier against water absorption. This might be due to the intrinsic chemical nature of chitosan [25]. A reduction in water absorption of chitosan may provide more appropriate absorbency characteristics in paper for improving printability. These properties make chitosan an attractive polymer for the barrier coating of cellulose-based materials for food packaging purposes [7].



10. Average water absorption of different surface treatments with biodegradable polymers. (Letters indicate significant difference at α = 0.05.)

CONCLUSIONS

Surface treatment of linerboard with biodegradable polymers has the potential to provide quality paper packaging. PVOH and EVOH have more effect on strength, whereas chitosan showed less absorption of water. Surface treatment with chitosan provided the strongest barrier against water. **TJ**

LITERATURE CITED

1. Sixta, H., in *Handbook of Pulp* (H. Sixta, Ed.), Wiley-VCH, Weinheim, Germany, 2006, pp. 2-19.
2. Bajpai, P., *BioResources* 5(2): 1(2010).
3. Mousa, M., Nazhad, M., and Sodtivarakul, S., *TAPPI J.* 3(1): 35(2004).
4. Hamzeh, Y., Najafi, S.M.H., Hubbe, M.A., et al., *Holzforschung* 66(2): 155(2012).
5. Dutta, P.K., Dutta, J., and Tripathi, V.S., *J. Sci. Ind. Res.* 63: 20(2004).
6. Laleg, M. and Pikulik, I., *Nord. Pulp Pap. Res. J.* 6(3): 99(1991).
7. Kjellgren, H., Gällstedt, M., Engström, G., et al., *Carbohydr. Polym.* 65(4): 453(2006).
8. Laleg, M. and Pikulik, I., *Nord. Pulp Pap. Res. J.* 7(4): 174(1992).
9. CCP, "PVA," Chang Chun Group, Taipei. Available [Online] at www.perrychem.com/files/PVA_English_2009_.pdf <18Sept2017>.
10. Pelton, R., *Appita J.* 57(3): 181(2004).
11. Briscoe, B. and Luckham, P., *Polymer* 41(10): 3851(2000).
12. Zakrajsek, N., *TAPPI J.* 7(11): 23(2008).

ABOUT THE AUTHORS

Linerboard produced from old corrugated containers (OCC) has lower strength properties than linerboard produced from virgin fibers. Previous research investigated dry additives for improved linerboard made from OCC. This research focused on coating with biopolymers to improve strength.

Our research showed that it is possible to increase the strength of recycled paper. Most surprising was the effect of polyvinyl alcohol (PVOH) and ethylene vinyl alcohol (EVOH) on burst strength. Mills producing linerboard with OCC can use biopolymers to increase mechanical properties. The next step is to investigate whether coating can improve printability as well as physical properties of linerboard.

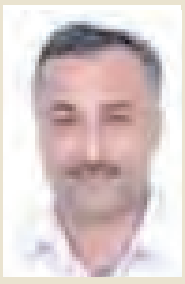
Heydari is a Ph.D. student and Saraeyen is an associate professor of Pulp and Paper in the Department of Wood and Paper Engineering, Gorgan University of Agricultural Sciences and Natural Resources, Gorgan, Iran. Shakeri is an associate professor of polymer engineering in the School of Chemistry, University of Tehran, Tehran, Iran. Email Heydari at somayeh_heydari88@yahoo.com.



Heydari



Saraeyan



Shakeri

13. Teramoto, N., Motoyama, T., Yosomiya, R., et al., *Eur. Polym. J.* 39: 255(2003).
14. Zhang, J-F. and Sun, X.Z., *Biomacromolecules* 5: 1446(2004).
15. Armstrong, R.B., "New EVAL® EVOH resins for flexible packaging," *PLACE Conf.*, TAPPI Press, Atlanta, GA, USA, 2004.
16. Iwanami, T. and Hirai, Y., *Tappi J.* 66(10): 85(1983).
17. Falat, L. and Sasthav., M., U.S. pat. 6,245,395 (Jun. 12, 2001).
18. Rhim, J.W., Lee, J.H., and Hong, S.I., *LWT—Food Sci. Technol.* 399(7): 806(2006).
19. Qiu, K. and Netravali, A.N., *Compos. Sci. Technol.* 72(13): 1588(2011).
20. Sawatari, C. and Kondo, T., *Macromolecules* 32(6): 1946(1999).
21. Zhang, Z., Britt, I.J., and Tung, M.A., *J. Polym. Sci., Part B: Polym. Phys.* 37: 691(1999).
22. Popil, R., *BioResources* 5(4): 2738(2010).
23. Micale, F.J., Iwasa S., Lavelle J., "The role of wetting in printing", *Proc.—TAGA*, Printing Industries of America/Technical Association of the Graphic Arts, Warrendale, PA, USA, 1989.
24. Khwaldia, K.H., Arab-Tehrany, E., and Desobry, S., *Compr. Rev. Food Sci. Food Saf.* 9(1): 82(2010).
25. Arvanitoyannis, I., Nakayama, A., and Aiba, S., *Carbohydr. Polym.* 37(4): 371(1998).

TAPPI JOURNAL
WWW.TAPPI.ORG
THE PAPER AND PACKAGING INDUSTRIES' TECHNICAL RESOURCE
OCTOBER 2017 | VOL. 16 NO.10



SPECIAL FEATURE 553
Lignin value prior to pulping (LVPP): An advanced pulping concept
Thomas T. Kwok, Christopher O. Luettgen, Matthew J. Realff, and Andreas S. Bommarius

WASTEWATER TREATMENT 559
Degradation of 2,4-dichlorophenol by melamine amine cellulose-immobilized lacasses
Zhen Wang, Pingping Bin, Ying Liu, Yu Liu, Guihua Yang, and Lucian Lucia

PAPERMAKING 567
Effect of conductivity on paper and board machine performance—a review and new experiences
Lebo Xu, Przemyslaw E. Pruszynski, and Peter W. Hart

BLEACHING 583
Techno-economic analysis of ECF bleaching and TCF bleaching for a bleached eucalyptus kraft pulp mill
Tiago de Assis, Jordan Perrin, Hasan Jameel, Richard Phillips, Dominique Lachenal, Adrianna Kirkman, and Ronalds Gonzalez

RECOVERY CYCLE 597
Formation mechanisms of "jellyroll" smelt in kraft recovery boilers
Honghi Tran and Andrew K. Jones

October 2017

TABLE OF CONTENTS VOL. 16 NO. 10

549 EDITORIAL
To paper and beyond at the University of Minnesota
Monica Shaw

553 SPECIAL FEATURE
Lignin value prior to pulping (LVPP): An advanced pulping concept
Thomas T. Kwok, Christopher O. Luettgen, Matthew J. Realff, and Andreas S. Bommarius

559 WASTEWATER TREATMENT
Degradation of 2,4-dichlorophenol by melamine amine cellulose-immobilized lacasses
Zhen Wang, Pingping Bin, Ying Liu, Yu Liu, Guihua Yang, and Lucian Lucia

567 PAPERMAKING
Effect of conductivity on paper and board machine new experiences
Lebo Xu, Przemyslaw E. Pruszynski, and Peter W. Hart

583 BLEACHING
Techno-economic analysis of ECF bleaching and TCF bleaching for a bleached eucalyptus kraft pulp mill
Tiago de Assis, Jordan Perrin, Hasan Jameel, Richard Phillips, Dominique Lachenal, Adrianna Kirkman, and Ronalds Gonzalez

597 RECOVERY CYCLE
Formation mechanisms of "jellyroll" smelt in kraft recovery boilers
Honghi Tran and Andrew K. Jones

»COVER CREDIT: A jellyroll smelt blob "sitting" on a spout trough. The formation of this type of potentially dangerous smelt has puzzled mills for years, so researchers Tran and Jones (p. 597) isolated three mechanisms for its formation based on mill observations and results from a recent study. Mills can use the information to identify their main causes for jellyroll smelt and devise a solution.

TAPPI JOURNAL
WWW.TAPPI.ORG

Editor-in-Chief
Scott Rosencrance scott.rosencrance@kemira.com
+1 770 429-2753

Associate Editor
Brian N. Brogdon brian.brogdon@gmail.com
+1 678 581-9114

Editorial Director
Monica Shaw mshaw@tappi.org
+1 770 367-9534

PRESS Manager
Jana Jensen jjensen@tappi.org
+1 770 209-7242

Webmaster
Trina Heath theath@tappi.org
+1 770 209-7416

***TJ* EDITORIAL BOARD**

Brian N. Brogdon, FutureBridge Consulting & Training LLC
brian.brogdon@gmail.com, +1 678 581-9114

David A. Carlson, Carlson Consulting
dacarlson39@aol.com, +1 847 323-2685

Jere W. Crouse, JWC Consulting
cj522@inwave.com, +1 608 362-4485

Mahendra Doshi, Doshi and Associates
mahen@aol.com, +1 920 832-9101

Marc Foulger, GL&V USA Inc.
Marc.foulger@glv.com +1 315 767-2920

Peter W. Hart, WestRock
peter.hart@westrock.com, +1 409 276-3465

Carl J. Houtman, USDA Forest Products Laboratory
choutman@fs.fed.us, + 1 608 231-9445

John A. Neun, John A. Neun LLC
john.neun@gmail.com, +1 518 275-8139

Jim Niemiec, Verso Corporation
jim.niemiec@versoco.com, +1 715 422-7404

Steven P. Ottone, Omya
steven.ottone@omya.com, +1 919 641-7854

Gaurav Pranami, Imbed Biosciences
gpranami@imbedbio.com, +1 515 230-7005

Arthur Ragauskas, Oak Ridge National Laboratory
aragausk@utk.edu

Gerard J.F. Ring, University of Wisconsin—Stevens Point
gerrryring@wi-net.com, +1 715 592-3732

Scott Rosencrance, Kemira Chemicals
scott.rosencrance@kemira.com, +1 770 429-2753

Paul Wiegand, NCASI
pwiegand@ncasi.org, +1 919 941-6417

Junyong Zhu, USDA Forest Products Laboratory
jzhu@fs.fed.us, +1 608 231-9520

Join TAPPI *today!*

TAPPI JOURNAL is a free benefit of TAPPI membership, and is only available to members. To join TAPPI, to renew your TAPPI Membership, or to learn about other valuable benefits, visit www.tappi.org.

TAPPI, 15 Technology Parkway S., Suite 115, Peachtree Corners, GA 30092, publishes *TAPPI JOURNAL* monthly.

ATTENTION PROSPECTIVE AUTHORS: All papers published are subject to *TAPPI JOURNAL's* peer-review process. Not all papers accepted for review will be published. Before submitting, check complete author guidelines at http://www.tappi.org/s_tappi/doc.asp?CID=100&DID=552877.

Statements of fact and opinions expressed are those of individual authors. TAPPI assumes no responsibility for such statements and opinions. TAPPI does not intend such statements and opinions or construe them as a solicitation of or suggestion for any agreed-upon course of conduct or concerted action of any sort.

Copyright 2017 by TAPPI, all rights reserved. For copyright permission to photocopy pages from this publication for internal or personal use, contact Copyright Clearance Center, Inc. (CCC) via their website: www.copyright.com. If you have questions about the copyright permission request process, please contact CCC by phone at +1 978 750-8400. To obtain copyright permission to use excerpts from this publication in another published work, send your specific request in writing to Editor, TAPPI JOURNAL, 15 Technology Parkway S., Suite 115, Peachtree Corners, GA 30092, USA; or by fax to +1 770 446-6947.

Send address changes to TAPPI, 15 Technology Parkway S., Suite 115, Peachtree Corners, GA 30092, USA; Telephone +1 770 446-1400, or FAX +1 770 446-6947. www.tappi.org

Editorial

MONICA SHAW | EDITORIAL DIRECTOR
mshaw@tappi.org



To paper and beyond at the University of Minnesota

Editor's Note: *This column is a continuation of* TAPPI Journal*'s column series featuring research and researchers from pulp, paper, biorefinery and related schools and institutions.*
– Monica Shaw, Editorial Director

In this column, *TAPPI Journal* spoke with Dr. Shri Ramaswamy of the University of Minnesota, where he is a professor in the Department of Bioproducts and Biosystems Engineering (BBE). He holds an M.S. and a Ph.D. in Paper Science and Engineering from the State University of New York (SUNY) in Syracuse, as well as an M.S. in Chemical Engineering from Syracuse University and a B.S. in Physics and Pulp and Paper Engineering from the University of Roorkee, India. Dr. Ramaswamy also has more than nine years of experience in the paper industry in various capacities, including process engineering, chemical applications technology development, and process research and development.

Since joining the University of Minnesota in 1995, Ramaswamy has seen significant growth in what was then the Department of Forest Products, with Paper Science and Engineering as one of the areas, and is now the Department of Bioproducts and Biosystems Engineering. Here, he discusses the evolution of this department and his personal research interests in the areas of bioproducts from lignocellulosic biomass, as well as structure-property relationships in porous media, especially bio-based materials.



Professor Shri Ramaswamy and his team of students and researchers at the University of Minnesota pursue innovative integrated forest biorefinery solutions and explore the feasibility of converting wood and other lignocellulose to pulp and paper, biofuels, plastics, and renewable energy. From left to right, Dr. Peter Huajiang Huang (research assistant professor), Dr. Shri Ramaswamy (professor), Lucas Stolp (scientist and graduate student), Sahana Ramanna (Ph.D. candidate), Sudhanya Banerjee (Ph.D. candidate), and Leonard Reynolds (scientist). Photo courtesy of Nkauj Vang.

How did paper-related studies evolve into the Department of Bioproducts and Biosystems Engineering at the University of Minnesota?

Around 14 years ago, we changed from a wood and paper science department to a broader bioproducts department. We were the first ones in the country to do so by envisioning how this field and research—and ultimately the industry—would evolve. Being a frontrunner can be difficult, because people always wonder and question your strategy, but we really wanted to position our department towards the future and continue to attract high quality students, as well as increase research opportunities and opportunities for students and graduates.

From a scientific and technical viewpoint, we realized that with wood, paper, and forest products, we were essentially dealing with lignocellulosic biomass and its conversion to various products, along with their end-use applications. At the time, however, the forest products department primarily focused on wood products and pulp and paper—the focus of our forest products community for 100-plus years. As discussions about the future of oil prices and alternative energy forms increased, the U.S. Government began recognizing and investing in bio-based

products as an emerging area, especially new products made from biological resources. So, we broadened our paper science and engineering program and curriculum to Bio-based Products Engineering and later to Bioproducts and Biosystems Engineering as we merged with the Biosystems and Agricultural Engineering Department and embraced broader renewable resources and their sustainable utilization. This opened up even greater opportunities for our students and graduates.

Pulp, paper, and wood products and composites are still a big component of what we do, but our motivation for the change is to be more forward thinking and discovering innovative approaches and sustainable solutions for new value-added products. Paper consumption is decreasing in the U.S. in markets like printing and writing papers, while tissue and packaging are growing.

Since the University of Minnesota transitioned its paper-oriented program to one focused on bioproducts and biosystems engineering, there has been proliferation of such changes among traditional pulp and paper schools. What would you say is unique about the University of Minnesota's approach?

For one, it was unique to be a front runner, but secondly, Minnesota has strong agricultural and forest-based industries, and we combined the two areas to address both agriculture-based and natural resource-based systems, processes, products, and solutions to create the Department of Bioproducts and Biosystems Engineering. Our department is affiliated with the College of Food, Agricultural and Natural Resource Sciences as well as the College of Science and Engineering. Our engineering students matriculate from the College of Science and Engineering.

How did becoming Department of Bioproducts and Biosystems Engineering eventually impact your student population?

Working with a range of renewable resources—wood, agricultural residues, algae, etc.—gave us more breadth in areas of study. Within the Bioproducts and Biosystems Engineering major, we have three areas of focus: bioproducts engineering (formerly paper science and engineering), food engineering (food can also be considered a bio-based product) and environmental and ecological engineering (addressing environmental and ecological aspects of biological resources, systems, and processes). As a result of the broadened scope, our undergraduate enrollment has grown within the engineering major from just 18 undergraduate students in the Paper Science and Engineering program in 1995 to 190 students in the BBE undergraduate major today.

Along the same lines, there has been more funding available to study biomass utilization and conversion, biological resources and systems, as well as to address environmental sustainability. This has helped us attract more graduate students. Within our department, our faculty advises around 100 graduate students in a variety of graduate programs. There are also about 50 post docs and researchers, and a total of about 250 people, including faculty, staff, and researchers.

One of your own primary research areas is the study of lignocellulosic biomass for second-generation biofuels, bioenergy, and bioproducts. What it your main focus in these studies?

In our research group, one of the primary focus areas is process modeling, simulation, design, and their applications in an integrated biorefinery. Here, we study the feasibility of producing multiple products from biomass, including fiber, cellulosic ethanol, chemicals, polymers, and energy. The first step was to model the entire pulp and paper process, including the chemical and energy recovery systems. With these efforts, we showed that it is possible to effectively separate the low molecular weight sugars and convert them into biofuels or bioplastics, integrated with the overall pulp and paper process.

We've shown that we can extract some of the hemicellulose present in wood prior to the pulping process and use it to make biofuels or value-added bioproducts. Currently, some of the removed sugars are being burned along with black liquor. When the extracted low molecular weight sugars are combined with waste cellulose fines from the mill and converted to bioethanol or bioplastics, the process becomes more economically feasible. We have shown that for a large mill (2000 tons/day) in the U.S., it is possible to produce about 30 million gallons of ethanol per year from these two sources—without adversely affecting pulp and paper quality.

Do you feel there is a good chance for success with the biorefinery concept, given there are certain political and market forces that could impact it, especially when it comes to fuel prices, as well as concerns from the pulp and paper industry about pulp yield and end-product quality?

It is very possible, but, yes, there are many factors to consider. From a big picture point of view, there has been a policy in place in the U.S. for using second-generation biofuels made from lignocellulose (i.e., forest and agricultural residue), and it's already in the marketplace. For example, DuPont is implementing a major plant in Iowa that uses corn cobs or stover to make ethanol. Such plants are either standalone or in conjunction with a corn-based ethanol facility. Along the same lines, the wood products and pulp and paper industries are well suited to pursue such an approach, which could provide an additional revenue stream.

While a biorefinery is still a very viable option, the pulp and paper industry continues to face significant challenges, including increased global competition, facing the effects of digital technologies, and other factors, and the investments in this new technology have been very limited. Other industry sectors continue to invest in R&D in biofuels and bioplastics. And yes, fuel is a commodity product and there are nuances associated with it, but what if we make a value-added bioplastic instead of fuel from the waste sugars and other under-utilized streams? With plastic and other value-added products, the profit margin could be much higher, and hence provide a more viable option. As we look into the future, there are more opportunities for the pulp, paper and forest products industry to truly embrace the biorefinery concept and continue to be a significant part of the thriving bioeconomy.

Your other primary area of research is the study of three-dimensional (3D) structural characteristics of porous materials like paper using advanced techniques such as x-ray micro computed tomography (XRCT) and nano tomography and image analysis. How did your work in this area evolve?

Another focus area of our research group has been in the area of structure-property-performance of porous materials, especially bio-based materials. The internal structure of paper and board plays a critical role in the paper manufacturing process as we remove water on the paper machine by dewatering, wet pressing, and drying processes. Paper structure also plays an important role during various end-use applications. If we better understand the 3D internal structure of paper and quantify its relationship to water removal and end-use applications, we can more efficiently and effectively "engineer" the structure for a specific end-use application, like a coffee cup, packaging, or paper towels.

Our pursuit here has been to visualize and quantify the complex 3D structure of paper using advanced techniques such as x-ray computed tomography (XRCT). Working together with Professor B.V. Ramarao from SUNY College of Environmental Science and Forestry and other colleagues from around the world, we helped develop the use of XRCT for looking at paper's internal structure. The principle and use of XRCT is much like the way a doctor uses a CT scan. Specifically, we're looking at the interfaces between the fibers and the void spaces and characterizing the pore structures in 3D. So, if you are making the same product or two products on two different paper machines, it is possible, using this technique, to characterize the products and better understand how each machine or product is performing.

Initially, in order to do XRCT, one had to resort to synchrotron radiation facilities. Nowadays, there are commercial bench top units that can be used to do XRCT at reasonable resolutions (1–4 μm) and at a reasonable cost. Such units are currently used in many companies to benchmark their products and better understand their performance.

As we described in our recent *TAPPI Journal* paper (*TJ* 16[9]: 519[2017]), we've developed a sphere growing algorithm that takes the digital 3D volumes of paper and digitally grows spheres inside the void spaces to determine the pore size distribution of paper. Since the image is in 3D, we can visualize the complex fiber networks from multiple perspectives, as well as fly through the structure. In addition to fibers and pores, it is also possible to visualize and characterize the 3D structure in the presence of inorganic fillers or pigments, as well as how the fillers are distributed in the paper. This is important in writing and printing papers.

We have extended the above work to evaluate the transport (i.e., liquid, vapor, heat, and mass) and

mechanical properties of paper and biomaterials. Also, we are developing the use of nano scale computed tomography (nCT) using transmission electron microscopy (TEM) and scanning electron microscopy (SEM) to study the 3D ultrastructure and topochemistry of biomass and how they evolve during the biomass conversion process.

What is another promising area for our industry that is studied at the University of Minnesota?

There are number of other topics pertaining to wood and other lignocellulose that are currently being researched at the University of Minnesota. As an example, nanocellulose is yet another area that can provide a high value-added product for the industry. Some of our faculty are studying nanocrystalline cellulose (NCC), which can be stronger than steel, and how you can effectively separate it from wood and other biomass and use it in composites and other applications. This is an area where the industry is paying attention, but as with the biorefinery, success will take a great deal of long term, persistent effort. At the University of Minnesota, we are driven to discover innovative approaches, technologies and solutions for a thriving, sustainable bioeconomy, ensuring industry's long-term success. **TJ**

For more information about the University of Minnesota's Department of Bioproducts and Biosystems Engineering, please visit https://bbe.umn.edu/.

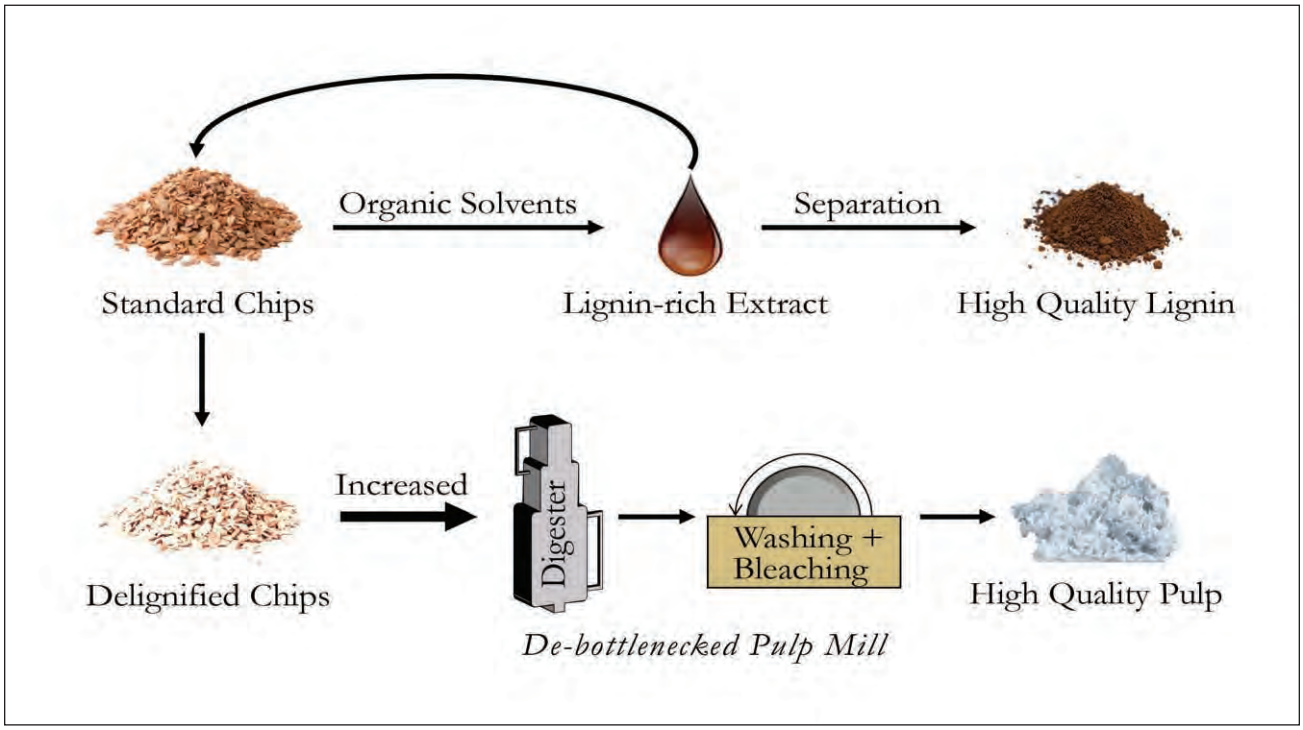
Lignin value prior to pulping (LVPP): An advanced pulping concept

THOMAS T. KWOK, CHRISTOPHER O. LUETTGEN, MATTHEW J. REALFF, AND ANDREAS S. BOMMARIUS

With an extensive infrastructure of kraft pulp mills, the United States pulp and paper industry is poised to take advantage of the scientific breakthroughs in lignocellulosic treatments. Volatility of oil prices and availability of ethanol subsidies have focused lignocellulosic research on the production of biofuels. Consequently, billions of dollars have been spent to convert biomass to ethanol, focusing primarily on converting cellulose from low recalcitrant, often grassy, feedstocks (e.g. corn stover, sugarcane bagasse, and wheat straw). Discoveries of effective pretreatments, which fractionate agricultural residues into lignin and carbohydrates, have spurred the forest products industry to pursue ethanol from woody biomass, a more recalcitrant feedstock. Though admirable as a concept, the idea of filling our nation's gas tanks with cellulosic ethanol from recalcitrant, woody biomass is naïve at best. The mass value of pulp is double that of fermentable sugars and yields of sugar and ethanol are detrimentally low when compared with pulping yields per ton of cellulose. Thus, from an economic perspective, pulpwood cellulose is best positioned towards pulp and paper products unless current fuel prices rise substantially.

A byproduct of lignocellulosic research is an enhanced understanding of lignin separation and valorization. Routes to valuable chemicals such as phenol, adipic acid, and vanillin are extensively studied, and lignin extraction techniques are numerous and diverse. We take this knowledge, combined with the understanding that cellulose is most valuable as a pulp, to describe an advanced pulping technology concept called lignin value prior to pulping (LVPP). This process utilizes organic solvent pretreatments to delignify woodchips prior to a kraft chemical pulping process. This advanced system provides an un-sulfonated lignin stream and has the potential to improve the governing economics of a pulp mill (**Fig. 1**).

While similar in concept to the value prior to pulping



1. Lignin value prior to pulping (LVPP): Organic solvent pretreatment increases pulp production and generates a new lignin stream.

(VPP) process introduced in the early 2000s, the extraction of lignin as opposed to hemicellulose has several distinct advantages [1,2]. The VPP process struggles to overcome the small margins that are imposed by pulp losses of 5%–15%, and the early extraction of hemicellulose contributes to significant pulp quality degradation [3-5]. LVPP addresses these issues by relieving bottlenecks to increase pulp yield and maintaining fiber quality with effective organic solvent delignifiers. Thus, LVPP can provide increased value by both increasing pulp throughput and creating an accessible lignin stream for chemical valorization.

The LVPP process will alter several kraft mill unit operations. Specifically, the recovery boiler, the digester, and the evaporator systems will be significantly affected. LVPP processes will also require several additional unit operations. First, a pressurized pretreatment vessel will mix an organic solvent with the wood chips to enable adequate solubilization of lignin. Second, counter-current washers will be employed to displace the organic solvent before the delignified chips are sent to the pressurized digester. Third, a precipitation step will isolate the lignin from the organic solvent. Finally, a separations unit will be added to recover the solvent. These changes will introduce new costs, but these costs are offset by the additional revenue streams.

A RENEWABLE BIOPRODUCTS INSTITUTE PROJECT

In a project supported by the Renewable Bioproducts Institute (RBI) at Georgia Tech and funded in part by Georgia-Pacific, Domtar, and Solenis, we are developing techno-economic models and performing initial lab-scale testing for the LVPP process.

The LVPP process hinges on an effective pretreatment step that isolates lignin from wood chips. An existing body of lignocellulosic research demonstrates how many organic solvents will isolate and modify native cellulose towards the production of cellulosic ethanol [6]. Several organic solvents are particularly good at solubilizing large quantities of lignin from biomass [7-11]. We are optimizing these organic solvent conditions and finding new solvents that quickly penetrate the wood chip, selectively solubilize lignin, maintain a wide liquid state temperature range, are straightforward to synthesize, and feature a low toxicity. After mapping delignification efficiency with cellulose swelling effects, we formulated an economic screening criterion that accounts for environmental impacts as well as for production capacity and separation efficiency [12].

Our techno-economic analyses demonstrate the importance of solvent recovery and determine several bounds on solvent loss. In a first-order economic analysis, we treat lost solvent as a feedstock in a lignin recovery system. With feedstocks accounting for 40% of process costs and a revenue margin set by comparing a lignin selling price with its heat value, we can show that the total solvent loss for our process must be less than 0.5% or 3.0% for a lignin selling price of $300 and $1000, respectively. To account for this loss, we research organic solvent recovery through chip washing, lignin precipitation, and solvent-water separations.

A chip washing unit operation differs from traditional brownstock washing due to the nature of the biomass. Modeled as a porous solid with entrapped liquids, the governing equations for the pore and free liquid solvent concentrations may be described by a linear combination of diffusion equations. These models can direct experiments and will enable the optimization of solvent loss due to chip entrapment.

Our organic solvents are effective delignifiers due to their strong affinity with lignin, so separation from lignin requires a strong anti-solvent or a significant change in conditions to affect the system's thermodynamics. The separation techniques we explore for our LVPP process are anti-solvent addition, membrane separation, and distillation. We use several anti-solvents for lignin, and we model both black liquor membranes and three-component distillation. The implementation of the latter techniques hinges on the extent of fouling caused by the precipitating lignin.

Once the lignin is precipitated and the chips are washed, the second stage of solvent recovery is the separation of the organic solvent from water. Our initial models suggest that distillation is the best option, with preliminary distillation energy loads on the order of 700 kJ/kg of solvent feed. These loads depend on the water content of the feed, the selected solvent, and the desired product streams, so we are still optimizing and exploring other separation techniques.

A CALL FOR RESEARCH

By modeling the pretreatment and solvent recovery, we are able to sufficiently define the LVPP process and test its feasibility. The treated wood chips are easily converted to fibers where yield and quality may be determined. However, it is necessary to quantify how the upstream modification of chip composition and structure impacts the downstream pulping process to realize LVPP's full potential.

Continuous digester models are needed to test our hypotheses that delignified chips will decrease the required cook severities, or H-factor, and decrease the equipment cost per unit volume without significantly impacting liquor flow and compaction due to lighter chips. Recovery boiler lifespan models are needed to understand the impacts of lower heat loads and altered cooking liquor-to-organics ratios. Additional considerations are needed due to the changing chemical compositions to the lime kiln, an altered black liquor to the evaporators, the new chip size distribution to the blow tanks and screens, the decreased lignin for brownstock washing and bleaching, and ultimately the different final pulp characteristics.

Understanding and quantifying LVPP's economic impact on a mill will enable comparison to lignin value after pulping (LVAP) processes. Current industrial lignin production recovers lignin after digester treatment. While easier to separate, this post-digester lignin has come into contact with harsh

alkali chemicals and does not provide bottleneck relief to the mills. The improved mill processes and un-sulfonated lignin streams will justify the increased difficulty of LVPP's lignin extraction. While there are still many parameters to understand, the LVPP process modifications promote a renewable chemical stream while decreasing the fixed cost per ton of pulp produced. A thorough pursuit of the LVPP process will ultimately provide a foundation for optimal utilization of our world's most renewable feedstocks. **TJ**

ACKNOWLEDGEMENTS

This work was funded in part by a PSE Fellowship from the Renewable Bioproducts Institute (RBI) at the Georgia Institute of Technology. Additional funding was provided through an RBI Member Project initiated by Agenda 2020, and supported by RBI, Georgia-Pacific, Domtar, and Solenis. Special thanks to "The Lignin Group" at Georgia Tech and the Georgia Tech TAPPI Student Chapter. Additional thanks to David N. Fogg Jr., Hannah E. Santillo, Matthew L. Wyatt, and Natasha J. Chrisandina for their experimental and modeling help.

LITERATURE CITED

1. van Heiningen, A., *Pulp Pap. Can.* 107(6): 38(2006).
2. Thorp, B. and Raymond, D., *Pap. Age* 120(7): 16(2004).
3. Yoon, S.H. and van Heiningen, A., *TAPPI J.* 7(7): 22(2008).
4. Duarte, G.V., Ramarao, B.V., Amidon, T.E., et al., *Ind. Eng. Chem. Res.* 50(4): 1847(2011).
5. Kautto, J., Saukkonen, E., and Henricson, K., *BioResources* 5(4): 2502(2010).
6. Shuai, L. and Luterbacher, J.S., *ChemSusChem* 9(2): 133(2016).
7. Kuo, C. and Lee, C., *Carbohydr. Polym.* 77(1): 41(2009).
8. Luterbacher, J.S., Rand, J.M., Alonso, D.M., et al., *Science* 343(6168): 277(2014).
9. Kang, Y., Realff, M.J., Sohn, M., et al., *Biotechnol. Progr.* 31(1): 25(2015).
10. Cai, C.M., Zhang, T., Kumar, R., et al., *Green Chem.* 15(11): 3140(2013).
11. vom Stein, T., Grande, P.M., Kayser, H., et al., *Green Chem.* 13(7): 1772(2011).
12. Kwok, T.T., Fogg, D.N., Realff, M.J., et al., *Cellulose* 24(6): 2367(2017).

ABOUT THE AUTHORS

Kwok is a post-graduate student in the School of Chemical and Biomolecular Engineering and the Renewable Bioproducts Institute; Luettgen is professor of practice in the School of Chemical and Biomolecular Engineering and an associate director of the Renewable Bioproducts Institute; Realff is professor in the School of Chemical and Biomolecular Engineering and an associate director of the Renewable Bioproducts Institute; and Bommarius is professor in the School of Chemical and Biomolecular Engineering, the School of Chemistry and Biochemistry, and the Renewable Bioproducts Institute at Georgia Institute of Technology, Atlanta, GA, USA. Email Bommarius at andreas.bommarius@chbe.gatech.edu.



Kwok



Luettgen



Realff



Bommarius

Degradation of 2,4-dichlorophenol by melamine amine cellulose-immobilized lacasses

ZHEN WANG, PINGPING BIN, YING LIU, YU LIU, GUIHUA YANG, AND LUCIAN LUCIA

ABSTRACT: Epoxidized dialdehyde cellulose (EDC) was prepared and grafted with melamine to obtain melamine grafted epoxidized dialdehyde cellulose (EDC-melamine); the products were characterized by various methods and were used as carriers to immobilize laccase. Results show EDC-melamine can immobilize laccase effectively and have higher enzymatic activity compared with EDC. Furthermore, the enzymatic activity of EDC-melamine was found to be as high as 865 U•mg^{-1}, compared with 140U•mg^{-1} for EDC. The removal efficiency of 2,4-dichlorophenol (2,4-DCP) for EDC-melamine immobilized laccase was about 71.5% at 40°C for 4 h at 10.0 mg•L^{-1} and dosage of laccase = 0.2 g/L. The removal efficiency can remain greater than 63%, even after six cycles.

Application: This topic provides a new method to immobilize laccases. The product can be used to treat wastewater polluted by phenol and shows excellent performance.

Laccases are among a class of extensively studied oxidoreductase enzymes [1,2]. Due to their prominent ability to oxidize a range of substrates, they have been broadly employed in several industrial sectors, such as decolorization of dyes [3], pulp delignification [4], oxidation of organic pollutants [5], development of biosensors [6], and construction of biofuel cells [7]. Among all the applications, laccase shows excellent performance in organic pollutants degradation, especially for phenolic compounds [8]. However, there were some factors that greatly limited its application in the field of phenolic pollutants removal, such as short service life, low stability, and low reusability. Surface covalent immobilization was considered as a promising method to overcome these problems. At present, the main traditional methods of enzyme immobilization include physical adsorption [9], embedding [10], cross-linking [11], and covalent binding [12].

However, each of these methods has disadvantages, so immobilization is rarely used as a standalone technology. At present, application of several methods in combination became the main method to immobilize laccase to reduce activity loss [13]. It is extremely important to select a suitable substrate to act as carrier materials. Some natural polymers, such as cellulose [14,15] and chitosan [16], have become the main substrates for enzyme immobilization because of low cost and reusability.

In this research, epoxidized dialdehyde cellulose (EDC) and melamine grafted epoxidized dialdehyde cellulose (EDC-melamine) were synthesized and were used as carriers to immobilize laccase to treat 2,4-dichlorophenol (2,4-DCP) in aqueous solution. The products may have great potential for the practical application of cellulose immobilized enzymes in the field of environmental protection.

MATERIALS AND METHODS

Materials

Microcrystalline cellulose was obtained from Sinopharm Chemical Reagent Co. Ltd. (Shanghai, China). Laccase Novozyme 51003 was provided by Novozymes A/S Co. (Tianjin, China; enzymatic activity was 1060 U/g) and 2,4-DCP was purchased from Aladdin Ltd. Co. (Shanghai, China). All other reagents were of analytical grade and used without pretreatment.

Preparation of epoxidized dialdehyde cellulose

A 6.0 g of microcrystalline cellulose was dispersed in 100 ml of 2.0 M sodium hydroxide (NaOH) under stirring, and 30 ml of epichlorohydrin was added while continuing stirring for 20 h at 25°C. The product was filtered and washed with distilled water and acetone until the pH reached approximately 7.0, and then dried at 90°C and stored.

The epoxidized cellulose suspension (50 ml with a concentration of 8%) was mixed with 50 ml of an aqueous solution of 7.9 g of sodium periodate ($NaIO_4$). The pH of the mixture was adjusted to 2.0 with 0.1 M H_2SO_4 in the dark to prevent the photo-induced decomposition of periodate. The reaction mixture was stirred at 35°C for 5 h, and then 4 ml of glycerol was added and continued to react for 1h. Finally, the product was filtered and washed several times with deionized water to remove iodine containing compounds, dried at 60°C, and then stored.

Preparation of EDC-melamine

A 0.5 g of oxidized cellulose was dissolved in 30 ml water while shaking at 80°C and pH was adjusted to 9.0 by 0.1 M NaOH. The 0.5 g of oxidized cellulose was added and allowed

to react for 12 h. Finally, 0.46 mmol sodium borohydride ($NaBH_4$) dissolved in 10 ml water was added and reacted for 4 h. The product was washed repeatedly to neutral pH and dried at 60°C.

Characterization

The Fourier transform infrared spectroscopy (FTIR) analyses of microcrystalline cellulose, epoxidized dialdehyde cellulose (EDC), and EDC-melamine were conducted using an FTIR spectrophotometer (Interspec 2020, Spectrolab Analytical; Newbury, UK) in the range of 4000–400 cm^{-1}. The surface morphologies of these samples were obtained by a scanning electron microscope (SEM) apparatus (Quanta 200, FEI; Hillsboro, OR, USA).

Laccase immobilization

Forty mg of EDC (or EDC-melamine) was dispersed in 10 ml acetic acid-sodium acetate buffer solution (pH=4.5), respectively, and then 20 µL 50% glutaraldehyde solution was added; the mixture was ultrasonicated for 10 min followed by the addition of a certain amount of laccase solution (2 mg/mL) under stirring for 3 h at 25°C. The laccase-immobilized carriers were repeatedly washed with the buffer solution until no laccase was found in the washing liquid. The laccase loading capacity was calculated using the following equation [17]:

$$\frac{M_0 - M_f - M_w}{M} \quad (1)$$

where M_0, M_f, and M_w are the amounts of laccase initially added, recovered in the supernatants, and recovered in the washing buffer, respectively; and M is the amount of carrier.

Enzyme assay

Laccase activity was measured at 420 nm by generation of ABTS radicals from the enzymatic oxidation of ABTS at 25°C using a CECIL 8600 spectrophotometer (Cecil Instruments Ltd.; Cambridge, UK). To determine the immobilized laccase activity, the assay mixture contained 0.2 mM ABTS, 100 mM sodium acetate buffer (pH=5.0) under shaking (100 rpm) at 30°C for 5 min [18]. After the incubation, the substrate oxidation by free and immobilized laccases was monitored at 420 nm (ε_{420}= 36.0 mM^{-1} cm^{-1}) using a UV-vis spectrophotometer [19]. One unit of laccase activity (U) was defined as the amount of enzyme needed to oxidize 1 µmol of ABTS per minute. The unit activity was defined by the following Eq. 2:

$$\frac{A \cdot V}{M_0 (t \cdot \varepsilon)} \times 10^6 \quad (2)$$

where A was the absorbance at 420 nm, V was the reaction volume, t was the reaction time, ε was the molar extinction coefficient for the ABTS oxidation, and M_0 was the mass of the immobilized laccase.

The total activity recovery R (percent) of the immobilized laccase was calculated according to the following Eq. 3 [20].

$$R(\%) = \frac{A_i}{A_f} \times 100 \quad (3)$$

where A_i and A_f were the activity of laccase immobilized on carriers and the starting activity of free laccase, respectively.

Removal of 2,4-DCP by immobilized and free laccases

The removal of 2,4-DCP by laccase was performed in a reaction mixture containing 50 ml of 10 mg/L 2,4-DCP in sodium acetate buffer solution (or NaOH). A suitable amount of carriers for immobilized laccase (5mg–30mg) was added and the mixture was shaken slowly for 4 h. Then, the upper solution was filtered, and the residual concentration of 2,4-DCP was exclusively measured by high performance liquid chromatography (HPLC) using a reversed-phase column (ODS-18, 150 mm × 4.6 mm) and methanol (chromatographic grade) as mobile phase at a flow rate of 0.8 ml•min^{-1}.

The effect of pH on the removal of 2,4-DCP was investigated within the pH range of 3.0–8.0 at 40°C, and the effect of temperature was investigated at pH 4.0 and 25°C–60°C. Blank test was also carried out to assess the effect of EDC, EDC-melamine, and free laccase on the removal efficiency of 2,4-DCP. Relative activity was used for laccase activity assay in this work, where laccase activities observed at the optimum conditions were defined as 100%.

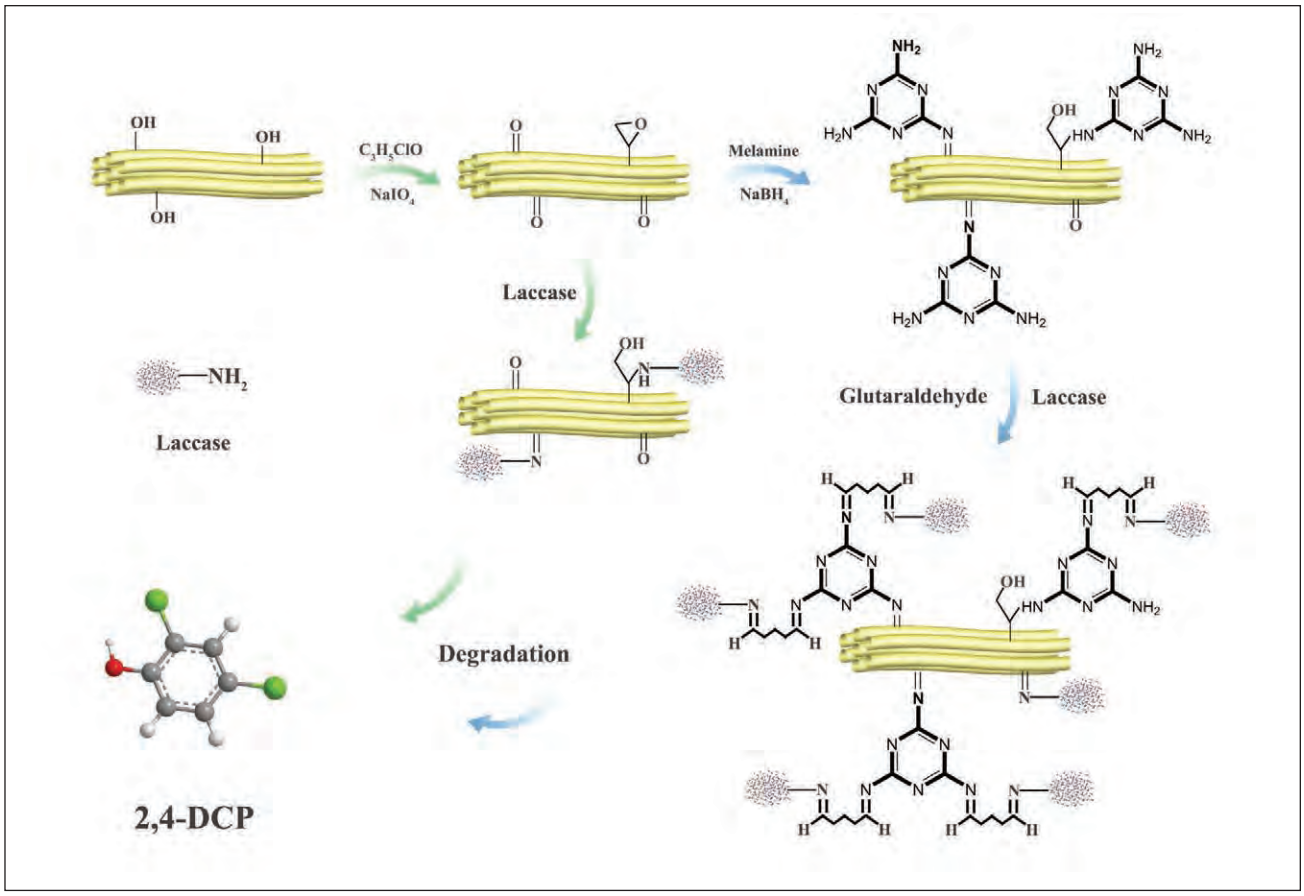
Reusability of immobilized laccase

The reusability of immobilized laccase was accessed using 2,4-DCP as a substrate. After each reaction run, the laccase-immobilized carriers were washed with the previously described buffer solution until no 2,4-DCP was detected in the wash solution.

RESULTS AND DISCUSSION

Synthesis mechanism

Figure 1 illustrates the synthesis process of EDC-melamine and the immobilization of laccase. The hydroxyl groups of cellulose reacted with microcrystalline cellulose to produce oxidized cellulose, since the steric hindrance of the hydroxyl groups at C_2 and C_3 was relatively large and microcrystalline cellulose mainly reacts with the hydroxyl group of C_6 under alkaline conditions. The aldehyde was introduced in epoxidized cellulose by partial oxidation with periodate, which promoted cleavage of the C_2-C_3 bond, thus forming two aldehyde groups per anhydroglucopyranose unit, and EDC was produced. Thereafter, amino groups reacted with epoxy groups through a nucleophilic reaction. Meanwhile, a Schiff base reaction occurred between melamine and the dialdehydes, and the EDC-melamine was synthesized. The products were stabilized by reduction with sodium borohydride. Fi-



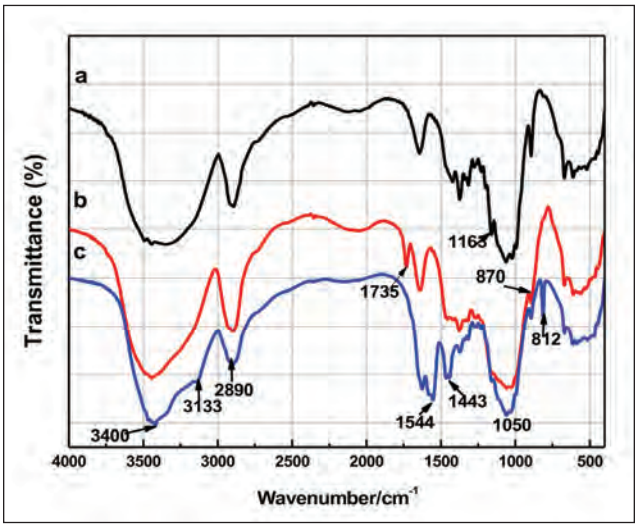
1. Reaction mechanism for the preparation of carriers immobilized laccase

nally, laccase covalently immobilized onto EDC-melamine (Fig. 1).

Properties of immobilized laccase

FTIR characterization

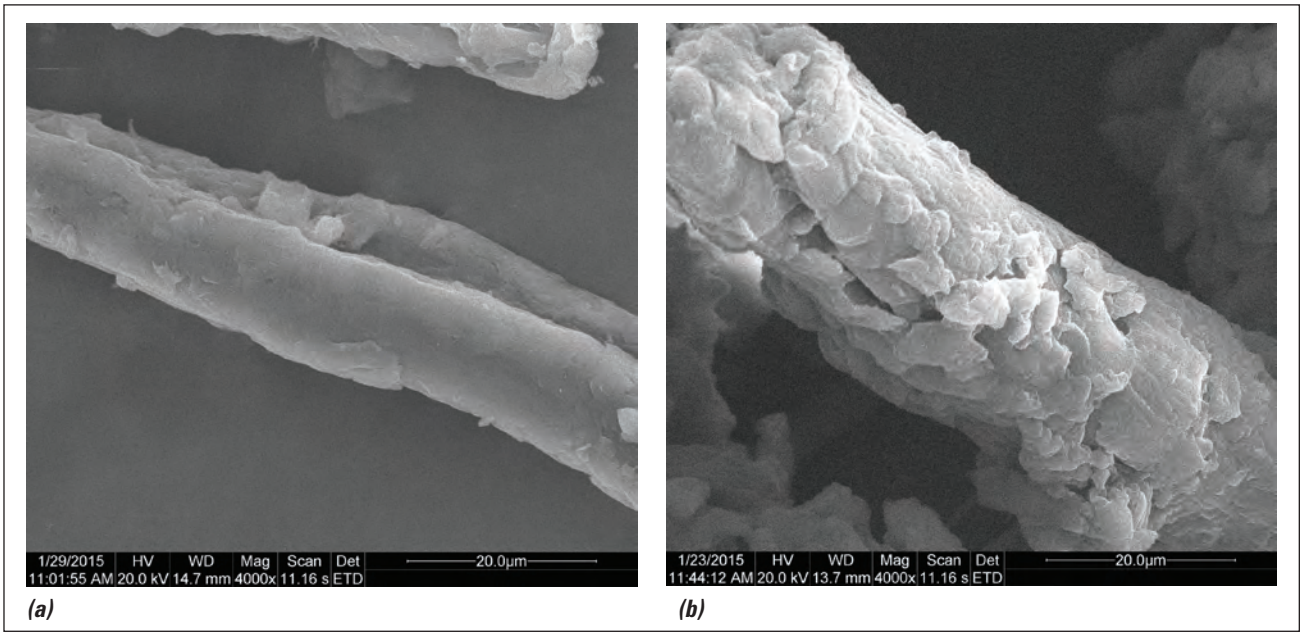
The FT-IR spectra of (a) microcrystalline cellulose, (b) oxidized cellulose, and (c) EDC-melamine are presented in **Fig. 2**. Compared with microcrystalline cellulose (Fig. 2, black line), the main changes in the FT-IR spectrum of oxidized cellulose (red line) is the new peak at 1735 cm^{-1}, a carbonyl stretching peak following oxidation [21]. The peak at 870 cm^{-1} in oxidized cellulose was due to the epoxy groups. Meanwhile, comparing EDC-melamine (blue line) and microcrystalline cellulose, the newly appeared peak at 3133 cm^{-1} in EDC-melamine may be attributed to the bending vibration of amine (N-H), while the stretching vibration peaks of C-N at 812 cm^{-1},1443 cm^{-1} and 1554 cm^{-1} indicate success of amine grafting onto the cellulose [22].



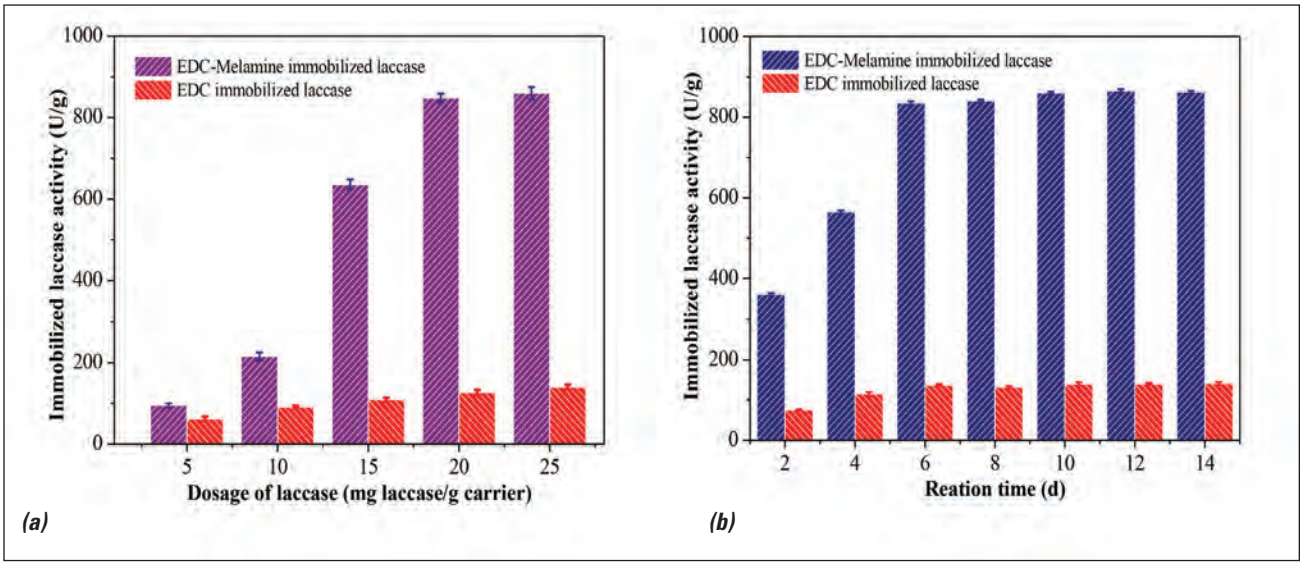
2. Fourier transform infrared spectroscopy (FTIR) analyses for (a) microcrystalline cellulose, (b) epoxidized dialdehyde cellulose (EDC), and (c) EDC-melamine.

SEM characterization

The SEM images of microcrystalline cellulose and EDC-melamine are shown in **Fig. 3**. It is obvious that the surface of cellulose changed significantly before and after modification. The surface of microcrystalline cellulose appeared smooth and simple, but the surface becomes rougher and displays a scaly appearance after modification (Fig. 3b). This increased the specific surface area of the product with much more functional groups exposed to the interface to enhance the reaction probability between laccase and the carrier.



3. Scanning electron microscope (SEM) images of (a) microcrystalline cellulose and (b) EDC-melamine.



4. Effect of (a) enzyme dosage and (b) reaction time on the activity of immobilized laccase.

Effect of enzyme dosage and reaction time on laccase immobilization

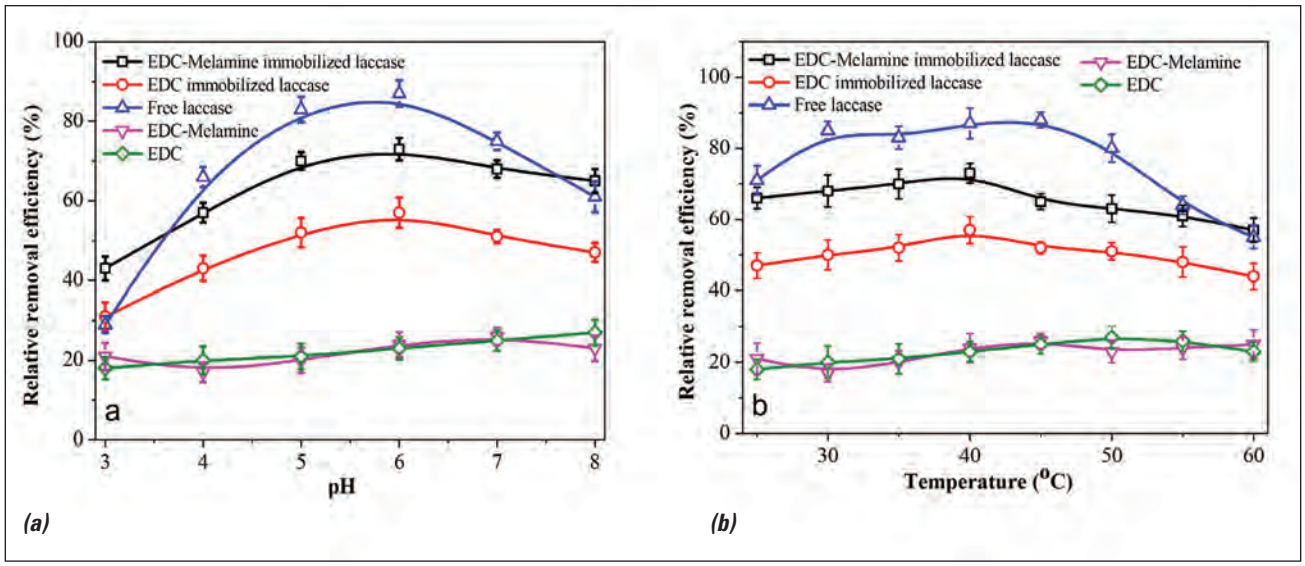
The relationship between laccase dosage and loading capacity of the carriers can be seen in **Fig. 4**. The activity of immobilized laccase increased with the increase of laccase dosage for both carriers (Fig. 4a), but the amount of increase reduced at high dosages. This may be due to the saturation of binding sites. Research found the optimal ratio were 20 mg•g^{-1} and 15 mg•g^{-1} for EDC-melamine and EDC, respectively. The optimal loading capacity of the carriers can be achieved under optimal ratio of 865 U•mg^{-1} for EDC-melamine and 140 U•mg^{-1} for EDC, respectively. Thus, EDC-melamine displays stronger binding ability for immobilized laccase than EDC.

The effect of reaction time was examined under the optimal laccase dosage. The immobilization time was set in a range of 2–14 h, and the interval time between each test was 2 h. As can be seen from Fig. 4b, the activity of immobilized laccase initially increased when time increased from 2 h to 6 h, but showed no significant change thereafter, due primary to steric constraints [23].

Removal of 2,4-DCP

Effect of pH on the degradation of 2,4-DCP

As can be seen from **Fig. 5a**, the highest removal efficiency was achieved at pH = 5.0–6.0 for the laccase immobilized laccase and free laccase. The highest removal efficiency for free



5. Effect of (a) pH and (b) temperature on relative removal efficiency of 2,4-dichlorophenol (2,4-DCP).

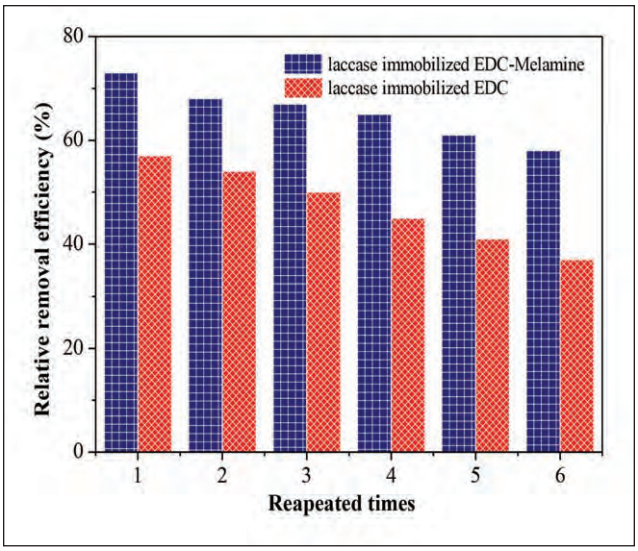
laccase was about 87%, while it was 71.5% and 57% for EDC-melamine immobilized laccase and EDC immobilized laccase. Compared with the free laccase, the immobilized laccase showed better stabilities to environmental change. The suitable pH range for removal of 2,4-DCP was 5.0–8.0 for carriers immobilized laccase. To the carriers, the total removal efficiency was attributed to both adsorption caused by the blank carrier and the degradation caused by the immobilized laccase. Both carriers have adsorption effect on laccase, and there was no obvious difference between them. The adsorption effect was perhaps mainly from physical adsorption. The specific surface of the carriers plays a key role during the physical adsorption. The adsorption removal efficiency by the two carriers was minimum because of the small variations in the specific surfaces between these two carriers.

Effect of temperature on the degradation of 2,4-DCP by laccase

The effect of temperature on removal of 2,4-DCP by immobilized laccase is shown in Fig. 5b. As can be seen from the figure, the optimum temperature was about 40°C for EDC-melamine and EDC immobilized laccase, and 45°C for free laccase. For the immobilized laccase, the impact of temperature was not obvious; for example, the range was about 12% when temperature increased from 30°C to 55°C for EDC-melamine immobilized laccase, while it was 21% for the free laccase. The suitable range of temperatures for oxidation of 2,4-DCP by the immobilized laccase was wider than that for the free laccase.

Reusability of immobilized laccase

Reusability was a significant feature for the immobilized enzyme. As shown in **Fig. 6**, the removal efficiency of 2,4-DCP by EDC-melamine immobilized laccase remained 63% even after six runs. The decrease in removal efficiency may come from two reasons: 1) the decrease or destroy of the grafted functional groups, and 2) the decrease of adsorption ability due to the wreck of the surface structure.



6. The reusability of laccase immobilized EDC and EDC-melamine for the removal of 2,4-DCP.

CONCLUSIONS

EDC and EDC-melamine were synthesized and were used as laccase carriers. Results show EDC-melamine has a strong binding ability for laccase and the immobilized laccase has high enzymatic activity. The enzymatic activity was 865 U•mg^{-1}, while it was about 140 U•mg^{-1} for EDC. EDC-melamine immobilized laccase showed a high removal efficiency for 2,4-dichlorophenol of 73% at 40°C for 4 h at 10.0 mg•L^{-1}, while it was 57% for EDC immobilized laccase. Both carriers showed better stability for pH and temperature compared with free laccase. Furthermore, the EDC-melamine

immobilized laccase also showed excellent reusability. The products have great application potential in the field of immobilized laccase. **TJ**

ACKNOWLEDGEMENTS

The authors are grateful to be supported in part by the Natural Foundation of Shandong province (ZR2013EMM011), the twelfth-year National Key Technology R&D Program (2014BAC13B04), provincial scientific and technological project (2011GGB01165), and the Taishan Schoars Program of Shandong Province.

LITERATURE CITED

1. Armstrong, A. and Wilson, S., *Electrochim. Acta* 45(16): 2623(2000).
2. Sheldon, A., *Adv. Synth. Catal.* 349(8-9): 1289(2007).
3. Barrière, F., Kavanagh, P., and Leech, D., *Electrochim. Acta* 51(24): 5187(2006).
4. Mayer, A.M. and Staples, R.C., *Phytochemistry* 60(6): 551(2002).
5. Solomon, I., *Chem. Rev.* 96(7): 2563(1996).
6. Abadulla, E., Tzanov, T., Costa, S., et al., *Appl. Environ. Microbiol.* 66(8): 3357(2000).
7. Freire, R.S., Duran N., and Kubota, L.T., *Anal. Chim. Acta* 463(2): 229(2002).
8. Thurston, F., *Microbiology* 140(1): 19(1994).
9. Rogalski, J., Dawidowicz, A., Jóźwik, E., et al., *J. Mol. Catal. B: Enzym.* 6(1-2): 29(1999).
10. Khani, Z., Jolivalt, C., Cretin, M., et al., *Biotechnol. Lett.* 28(22): 1779(2006).
11. Jiang, D.S., Long, S.Y., Huang, J., et al., *Biochem. Eng. J.* 25(1): 15(2005).
12. D´Annibale, A., Stazi, R.S., Vinciguerra, V., et al., *J. Biotechnol.* 77(2-3): 265(2000).
13. Fernández-Fernández, M., Sanromán, M.Á., and Moldes, D., *Biotechnol. Adv.* 31(8): 1808(2013).
14. Sathishkumar, P., Kamala-Kannan, S., Cho, M., et al., *J. Mol. Catal. B: Enzym.* 100(2): 111(2014).
15. Endry, N.P., Stefan, S., Nyanhongo, G.S., et al., *React. Funct. Polym.* 97: 12(2015).
16. Krajewska, B., *Enzyme Microb. Technol.* 35(2-3): 126(2004).
17. Xu, R., Zhou, Q., Li, F., et al., *Chem. Eng. J.* 222: 321(2013).
18. Nicolucci, C., Rossi, S., Menale, C., et al., *Biodegradation* 22(3): 673(2011).
19. Wolfenden, B.S. and Wilson, R.L., *J. Chem. Soc., Perkin Trans. 2* 11(7): 805(1982).
20. Ai, Q., Yang, D., Li, Y., et al., *Biochem. Eng. J.* 83: 8(2014).
21. Fan, Q.G., Lewis D.M., and Tapley, K.N., *J. Appl. Polym. Sci.* 82(5): 1195 (2001).
22. Zhai, F., "Study on the preparation and performance of oxidized micro-crystalline cellulose and its derivatives," M.S. thesis, Qilu University of Technology, Jinan, Shandong, China, 2016, p. 42.
23. Cristóvão, R.O., Tavares, A.P.M., Brígida, A.I., et al., *J. Mol. Catal. B: Enzym.* 72(1-2): 6(2011).

ABOUT THE AUTHORS

My (Wang's) research field is related to the modification of biomaterials and their application in wastewater treatment. The research here differs from previous research in this area in that the amount of the immobilized laccase was much lower.

The most difficult aspect of this research was how to tightly keep the laccase on the modified cellulose. To overcome this, we modified the cellulose with different groups and finally found the optimal way. One personally interesting discovery was that the modified cellulose has excellent performance on binding laccase and can maintain its activity. A surprising aspect of the research was that the immobilized laccase can provide higher enzymatic activity and can effectively treat phenol-polluted wastewater.

This research can provide a new way for mills to approach the treatment of phenol-polluted water. Our next step is to find a more effective way to realize the modification process.

Wang is professor and director of Environmental Science, School of Environmental Science and Technology; Bin and Ying Liu are M.S. students; and Yu Liu and Yang are professors at the Key Laboratory of Pulp & Paper Science and Technology, Ministry of Education, Qilu University of Technology, in Jinan, Shandong, China. Lucia is associate professor, Department of Forest Biomaterials, North Carolina State University, Raleigh, NC, USA, and is also distinguished professor of Green Chemistry for Qilu University of Technology. Email Wang at wangzhenyft@126.com.


Wang


Bin


Ying Liu


Yu Liu


Yang


Lucia

Effect of conductivity on paper and board machine performance—a review and new experiences

LEBO XU, PRZEMYSLAW E. PRUSZYNSKI, AND PETER W. HART

ABSTRACT: The current trend to further reuse water within paper mills has resulted in more accumulated salts, as reflected by increased conductivity values. Although conductivity measurement is widely used in paper mills, its fundamental principles and interpretation are not often fully understood. This keeps papermakers from reaching the full benefits of using conductivity measurements to help manage the wet end chemistry of paper or board machines. High and variable conductivity affects the intrinsic properties of pulps, the performance of chemical additives, and the interaction between them. This paper reviews principles of conductivity; its measurement; its effect on important aspects of papermaking operations, such as retention, drainage, sizing, strength development and deposit control; and the fundamentals behind the effects of conductivity on the papermaking process. Specific mill examples are also provided. Potential solutions for operating a mill under high and variable conductivity conditions are discussed.

Application: Understanding the principles of conductivity measurement and its limitations can help mills interpret the effect of high ion concentration on the papermaking processes. It will also help papermakers gain insight into issues associated with increased and changing conductivity for troubleshooting.

Originally, the papermaking process relied solely on the physical process to filter fiber slurries, fines, and mineral additives, forming a paper sheet. Today, the papermaking process increasingly relies on the application of chemical additives to enhance the performance of the paper machine and final paper products. Higher machine speeds, stronger shear in the forming section, more restriction on fresh water consumption, and significantly more closure of machine water systems lead to higher concentrations of dissolved and colloidal substances and bring the system closer to the point of potential destabilization.

These increasingly difficult machine conditions coincide with technological and market trends that require finely tuned operating conditions, frequent grade changes, and stringent quality expectations. Alkaline conversion introduced chemically reactive fillers (calcium carbonates) and hydrolysable sizing molecules, such as alkyl ketene dimer (AKD), low melting point alkylene ketene dimer (AIKD), and alkenyl succinic anhydride (ASA). Use of those additives requires better control over such conditions as pH, temperature, hardness, alkalinity, cationic demand, and conductivity than was required in the past. New, advanced, high performance and multicomponent retention programs and sophisticated strength programs require strict control over paper machine conditions to avoid variability in their performance, assuring machine efficiency and product quality.

Many studies have been published recently to describe the effects of various factors on the performance of retention and drainage programs. Factors that affect the performance of these drainage and retention programs have been well reviewed by several authors [1-5]. Those findings and others justify the need for reviewing the effects of important wet end chemistry components and their effects on machine operations. This paper focuses on the effects of ionic contamination, collectively represented by measurement of conductivity. Brown and Hart [6] recently reviewed the relevance of conductivity in the pulping process. This paper will focus entirely on the wet end of the paper machine. Because many of the consequences of increased or variable ionic strength are general in nature, they apply to paper, board, and tissue applications, although the relevance of individual effects might differ from grade to grade. In addition to the general effect of conductivity, we will briefly review the specific effects of calcium ions (Ca^{+2}) and magnesium ions (Mg^{+2}) associated with hardness.

This paper is a literature review that includes several of the authors' real-world experiences intermixed. Although the effects of conductivity, at a general concept level, are well understood by skilled and experienced wet end chemists, the authors realize that reviewing this topic to provide fundamental principles and bring practical examples with potential solutions could help papermakers better understand the relevance of conductivity and consider it as a very important wet end chemistry parameter. This becomes increasingly important now, as many mills plan to reduce fresh water consumption, either voluntarily or otherwise.

DISCUSSION

Conductivity fundamentals

In general, detrimental substances that accumulate in the papermaking systems are either inorganic or organic. This review considers the effect of inorganic dissolved solids, in general terms of conductivity, and the specific effect of Ca^{+2} and Mg^{+2} ions that contribute to water hardness.

When an electrical potential is applied to a pair of electrodes immersed in an aqueous solution containing ions, positive ions (cations) migrate toward the cathode, and negative ions (anions) migrate toward the anode. The conductivity (ability to conduct an electrical current) of the solution is a function of the rate of charge movement in the potential field. The conductivity value can be affected by the migration speed of individual ions, the charges and concentrations of the ions, and interactions among individual ions.

Conductivity can be expressed as the reciprocal of the resistivity normalized to a 1 cm cube of a liquid at a specified temperature, which is reported in micro-Siemens per centimenter (μS/cm). The term specific conductance is used in this paper when measurements are made at or corrected to the standard temperature of 25°C. In simple terms, conductivity is a function of ionic concentration and specific conductance. Without getting into details, the ability of ions to impart conductivity depends on their charge and mobility. Thus, not all ions contribute to conductivity to the same degree, as illustrated in **Table I** [7].

Although hydrogen (H^+) and hydroxide (HO^-), originating from water, have the highest specific conductance, they have only a small contribution to the total conductivity of a solution unless the solution is at an extremely high or low pH value. At near neutral pH conditions, the concentrations of H^+ and HO^- are low, resulting in only a small effect on total conductivity. In typical papermaking conditions, most conductivity and its variations come from contributions of other ions.

Conductivity increases with temperature at a rate of 2% to 3% per degree Celsius above 0°C. This is because of the effect of temperature on liquid viscosity and density. The viscosity of water decreases by about 2% per 1°C when heated, resulting in reduced resistance to flow, thus increasing conductivity. Both direction and magnitude of the temperature effect on viscosity closely match its effect on conductivity. Conductivity correlates with the concentration of ions and its change with temperature should lead to a decrease of concentration from temperature expansion of water by 0.025% per 1°C. Because the change in conductivity caused by temperature is not related to a change in the ionic strength of solution, it is not expected to correlate with paper machine performance. Because not all conductivity meters have temperature compensation, it is recommended to collect temperature data together with conductivity to check the effect of temperature on conductivity trends.

Ion	Specific Conductance, $\Omega^{-1}cm_2mol^{-1}$	Ion	Specific Conductance, $\Omega^{-1}cm_2mol^{-1}$
H^+	349.8	1/2 Ca^{+2}	59.50
HO^-	197.8	1/2 Sr^{+2}	59.46
Na^+	50.11	1/2 SO_4^{-2}	80.0
K^+	73.52	Cl^-	76.35
1/2 Mg^{+2}	53.06	HCO_3^-	44.5

I. Specific conductance of selected ions.

Effect of mill closure

Paper mill water closure results in the accumulation of soluble materials that have a pronounced effect on paper machine operations and product quality. This buildup of ionic material is an unavoidable consequence of water closure and dictates how far mill water circuits can be closed. On the research level, the effect of ionic strength to the system is well understood. In practical application, ionic concentrations will continue to increase with reduced use of fresh water in paper and board production. Understanding, preferably in quantitative terms, the nature of this effect and the way to mitigate it might, therefore, open the way to further the progress of water closure projects in a mill. The degree of accumulation of any substance in the paper machine system depends on the nature of the contaminant, its influx level to the system, and the degree of system closure. Equation 1 represents the degree of concentration or enrichment factor (ER) of any substance that fully follows the water phase (shows no affinity to the fiber):

$$ER = \frac{1}{1-r} \quad (1)$$

where r is the recycle ratio, or the amount of white water recycled divided by the total amount of water to the headbox [8]. This equation can be used to predict the steady state concentration of the simple electrolyte, provided it has no or very low affinity for the sheet of paper [9]. This equation was also used to predict the degree of closure when final concentration of the accumulated tracer (lithium [Li^+]), added at a known concentration of tracer, was measured [10]. Equation 1 applies well to ions that contribute to conductivity. At the recycle ratio r = 0.9, the enrichment factor ER = 10 can be calculated for ions that are not removed with the sheet of paper. There is always some degree of removal of ionic species with the water entering the press section (if pressate is not reclaimed). Nevertheless, any source of salts undergoes significant enrichment with increasing recycle ratio. A lot of attention needs to be devoted to understanding sources of conductivity and their reduction.

Equation 1 does not account for the adsorption of dissolved solids onto the fibers. Xu [11] modified Eq. 1 to account for the adsorption of dissolved solids to the formed web

of paper (Eq. 2):

$$C_{r,eq} = \frac{(\frac{Y}{M})(1-r)}{[\frac{1}{1-K}]-r} \quad (2)$$

where:

$C_{r,eq}$ = equilibrium concentration
Y = sum of the concentration of species of interest in different water flows on machine at equilibrium
r = recycle ratio
K = percentage of species of interest removed by adsorption
M = total amount of water coming from outside sources

This model, validated by the authors through experimental evaluation of the buildup rates for sodium (Na^+) and Ca^{+2}, allowed prediction of the final concentration and time required to reach equilibrium for species with some adsorption ability to the fiber. Because of higher adsorption of Ca^{+2} to the fiber, its final concentration was lower and time to reach equilibrium shorter.

Mittal and coauthors [12] discussed buildup of dissolved solids related to mill water closure contributing to conductivity in a paper board mill. This work focused on critical substances such as chlorine (Cl^-), sulfate (SO_4^{-2}), Ca^{+2}, Mg^{+2}, silica (SiO_2), and Na^+.

Sources of conductivity

Papermaking raw material and additives can introduce ions to the process. Wood contains different ions, such as Ca^{+2}, Mg^{+2}, and barium (Ba^{+2}), depending on its growing environment. If wood is chemically pulped and bleached, pulping and bleaching chemicals will be a great source of ions. The amount of ion carryover is determined by the efficiency of the various washing processes. Brightness development of mechanical pulps is the biggest contributor to conductivity in grades such as newsprint, improved newsprint, mechanical pulp-based coated grades, and supercalendered grades. The application of brightening chemistries, typically hydrosulfite (Y), peroxide (P), or combined PY bleaching, often results in high levels of ionic contamination. The contamination level is proportional to the brightness target and depends on the available thickening stages acting as water blocks between bleaching stages and the paper machine. Additionally, reaching desired brightness levels often requires change of dosages of brightening chemicals, leading to significant variation in water chemistry, including but not limited to conductivity. The effect of water blocks such as twin-wire presses on system contamination and wet-end stability is well documented [13].

For paper mills using virgin pulps, one of the main sources of conductivity at the wet end is the pulp. Mills using unbleached pulps (brown mills) will experience conductivity swings that directly correspond to upsets in the brownstock washers. These mills typically receive some amount of inorganic sodium compounds (typically reported as equivalent sodium sulfate [Na_2SO_4]), which remain in the pulp after washing. Several organic sodium salts might also be present from dissolved lignin and carbohydrate fragments remaining in the washed pulp. As upsets occur in the brownstock washing, the concentration of these materials changes, resulting in conductivity spikes on the paper machine. Work has been performed to correlate dissolved sodium concentration in stock to conductivity measurements [14]. University investigators [15] reported a linear correlation between the measured conductivity and the inorganic levels found in black liquor filtrates of a brownstock washing system. Sodium, the most prevalent inorganic component of black liquor, usually represents all the inorganics. This implies that conductivity can be correlated to sodium content.

Conductivity affecting paper machines making bleached grades comes from the pulp leaving the last stage of bleaching. Often, there is a need to adjust pH of the stock leaving the bleach plant going to the paper machines. These adjustments are performed with either sulfuric acid or caustic soda. Both materials will increase wet-end conductivity. As with brown pulps, upsets in the last stage of bleach plant washing will also increase the amount of material being sent forward to the paper machines, thus increasing the amount of chemical required to adjust pH of the stock. Therefore, upsets in the last stage of bleach plant washing might impart a double effect on conductivity variability.

For recycled fiber, the amount of ionic material it contains is mainly determined by previous manufacture and consumer history, on which a mill generally has less control. One good practical control method is to sample and sort recycled material. This will not reduce the total amount of ion, but can decrease the variation of conductivity from time to time to minimize its effect on the papermaking process. Broke (internal recycled fiber) should be more manageable by a mill. Most wet-end and dry-end additives, such as surface treatment or coating, are returned to the wet end through repulped broke. If a mill is expected to use a fair amount of broke, materials used at the wet end and dry end should be carefully chosen, considering the ion accumulation effect through broke system.

Incoming fresh water contains ionic material, especially Ca^{+2}, if the water is hard. Acid and caustic soda for pH adjustment will add additional ions. Most papermaking additives are designed in a salt form for good water solubility. Rosin soap and surfactant of dispersed rosin size, AKD, and ASA give Na^+ or K^+. Aluminum species (alum or poly-aluminum-chloride [PAC]) introduce Al^{+3}. Most cationic polymer additives (strength agent, retention aid, drainage aid) are salts of polymeric acid and release ions after dissolving. Dye is usually a salt of organic acids as well, which contributes ions after disassociating in water. If coated broke is used, coating material might become an ion source. For example, acidic process water can dissolve calcium carbonate ($CaCO_3$) pigment to generate Ca^{+2}. Some additional contribution to the ionic strength of the system can come from starch, biocides, dyes, and optical brightening agents.

Effect of conductivity on papermaking process

Conductivity affects wet-end operations through general charge interactions and leads to changes in the conformation of charged additives (polymers, starches), fiber surface properties, and colloidal stability. Additionally, accumulation of specific ions contributing to conductivity often leads to issues such as scale formation, deposits, and strength and sizing losses. These specific ionic interactions are primarily associated with the ions related to hardness (Mg^{+2} and Ca^{+2}) and to Ba^{+2}, which often results in scale formation. For the Al^{+3} ion, because of its weak base character, its effect is from various hydrolysis products formed in all pH ranges of practical papermaking.

Conductivity or, in wider terms, ionic content of water can affect the papermaking process in several ways:

- Colloidal stability
- Fiber properties
- Performance of chemical additives
- Direct interactions between ions leading to scale formation

Colloidal stability is particularly important for paper machine wet-end operations. Electrical double-layer repulsive forces are fundamental in providing stability of colloidally dispersed matter. Increased ionic strength, or in practical terms, increased conductivity, compresses double layer thickness. This reduces repulsive forces between colloidal particles and leads to colloidal destabilization.

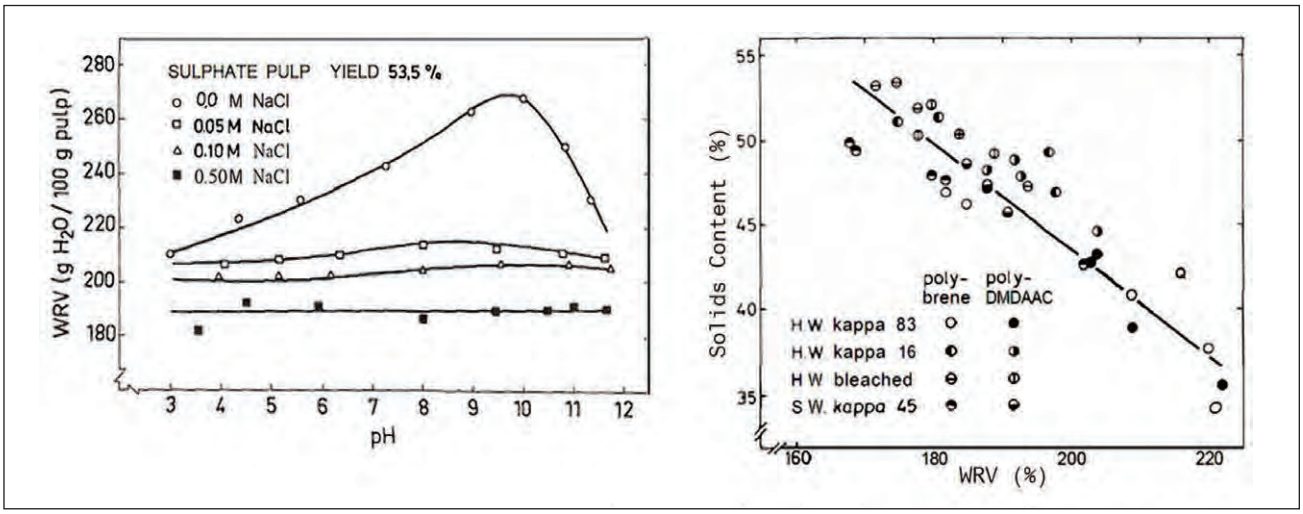
High conductivity and large variations of conductivity significantly affect the stability of wood pitch particles and make pitch control more difficult. This is especially important for pulps exposed to high pH in pulping or bleaching processes that are stripped of steric protection of sugars and rely solely on electrostatic stabilization. When troubleshooting pitch or stickies deposition problems, mills should consider conductivity shock, along with the traditionally culpable check points, such as temperature shock, pH shock, and shear.

Increased water closure, more aggressive bleaching processes, higher deinked pulp content, and higher shear at forming sections on new and modern paper machines result in increased levels of contamination at the wet end of a paper machine. Several studies have discussed the degree of the expected buildup of detrimental substances resulting from an increased degree of closure [16-21]. Several papers also reported on the effect of conductivity on formation of tacky sickies deposits on machines using recycled furnish [22-24].

Reduction of repulsive forces from high conductivity is not limited to colloidal material. **Figure 1** shows the effect of salt concentration (conductivity) on swelling of unbleached kraft pulp fiber, illustrated by water retention value changes with different salt concentration [25]. Higher conductivity (salt concentration) reduced repulsion between charges on the fiber and decreased its swelling, resulting in lower water retention value. Changes in water retention value also affected the water removal in the press section (Fig. 1, right side).

Dobbins [26] reported results from a pilot machine study of an effect of increased mill water closure on machine operation and paper quality. Furnish for the study contained a high content of groundwood pulp (75%). Varying degrees of machine closure were simulated by adding certain amounts of calcium chloride ($CaCl_2$), Na_2SO_4, sodium chloride (NaCl), potassium chloride (KCl), and magnesium sulfate ($MgSO_4$) to the white water system. Even at the highest degree of ionic contamination of 20,000 ppm of salts, which exceeded the electrolyte level of a mill recirculating 100% of its water, paper still could be produced. However, cationic retention aids were found to have limited effectiveness. Some strength losses were observed and associated with the sheet ash increase from incorporation of the salts after water was evaporated.

Davison [27] studied an effect of pH, ionic strength, calcium ion, and aluminum ion impurities on the retention of fines and fillers using a mixture of hardwood and softwood



1. Effect of pH and conductivity on water retention value (left) and solids content after presses (right) (reproduced with the permission of* Nordic Pulp and Paper Research Journal*).

kraft pulps blended in a 3:1 ratio. Anionic and cationic retention polymers were negatively affected by increased concentration of either Na_2SO_4 or NaCl. Conductivity of the system was adjusted between 200 μS/cm and 3000 μS/cm. An average drop of observed retention level between 5% and 18% was observed, at the same polymer dosage, for various retention polymers.

Lindstrom [28] studied the adsorption of cationic polyacrylamide polymers onto the surface of bleached softwood kraft pulp at different levels of simple electrolytes (NaCl, $CaCl_2$, and Na_2SO_4). Assuming the important role of fiber adsorption for the performance of polymeric retention additives, this paper provided fundamental answers about their performance under a high degree of ionic contamination. An increase in adsorption observed at the lower range of salt concentration was explained in terms of increased hydrodynamic size of polymer at more extended conformation. A further increase of salts concentration led to a decrease of adsorption and was attributed to ionic double layer compaction to reduce attractive forces between the polymer and fiber.

Buontempo [29] used a Britt jar technique to study the effect of ionic species on the performance of cationic flocculants with different charge densities. At a low starch dosage, all studied flocculants retained a high level of performance when conductivity was changed between 45 and 3000 μS/cm. For furnishes containing starch, all studied flocculants showed a marked decrease in performance when conductivity was increased. The authors concluded that the structure-performance relationship was not clear, and an empirical approach of screening a wide range of retention polymers and selecting the best program for given conditions was necessary in the process to select a retention program.

Because of the non-ionic character of the polyethylene oxide (PEO) molecule, PEO retention programs generally showed higher resistance to elevated conductivity and cationic demand that accompany increased water closure at a mill. A significant number of publications on water closure and contamination studied PEO – cofactor dual retention programs [3,4,30-33]. PEO-based programs typically showed strong performance of flocculation that might lead to sheet formation problems. Additionally, shear and chemical sensitivity (oxidizing agents, surfactants) contributed to the fact that PEO-based programs were not widely used.

Hulkko [23], Allen [3], Laivins [4,25], Polverari [24,26], and Trigylidas [25] reported negative effects of conductivity and cationic demand on retention programs using cationic polymers. In contrast, Miyanishi [34] reported that increasing levels of conductivity in wood-containing grades had little effect on the performance of cationic polymers (single, dual, and microparticle programs).

In principle, resistance of non-ionic polymers to increased levels of ionic contamination could be expected. However, the gap between non-ionic and cationic additives in the performance might be smaller than suggested in recent papers. This, plus the complexity of performance requirements (combination of retention, drainage, formation, and printability), made cationic polymers a viable option, even in highly closed mill systems. With increased use of recycled fibers and higher levels of fillers in newsprint production, cationic flocculants remained a major component of the retention program for this grade.

Brown and Hart [6] recently reviewed the principles of application of conductivity measurement in monitoring and inferring black liquor losses from brown stock washing. The paper provided fundamental information on conductivity measurement and its interpretation to pulp mill application.

To quantify the effect of increased ionic loading in the system, Pruszynski [5,35] studied the sensitivity of various types of retention programs in thermomechanical pulp furnish with varying levels of several different contaminants and two pH levels (pH 5 and pH 7). Free drainage measurement was selected as a response. Simplicity of this measurement allowed performing large numbers of experiments to provide statistically significant results. The contaminant data generated for Na_2SO_4 and NaCl were of special interest because observed performance could be attributed solely to the conformational changes of retention polymer (little surface modification) because of the low affinity of sodium ion to the fiber. Reduction of the radius of gyration, or in simple terms, folding of the polymer chain because of reduced repulsive forces between charges segments on the polymer backbone, led to less effective bridging capabilities at higher conductivity levels. The authors presented results in terms of the percentage loss of drainage benefited from the retention program in the clean system as a function of ionic contamination (Eq. 3):

$$\Delta_{var}(\%) = \left[{(V_{ct} - V_{00})}/{(V_{ot} - V_{00})} \right] \times 100 = {\Delta V_{ct}}/{\Delta Vot} \times 100 \quad (3)$$

where:

V_{00} - drainage for clean sample without retention program

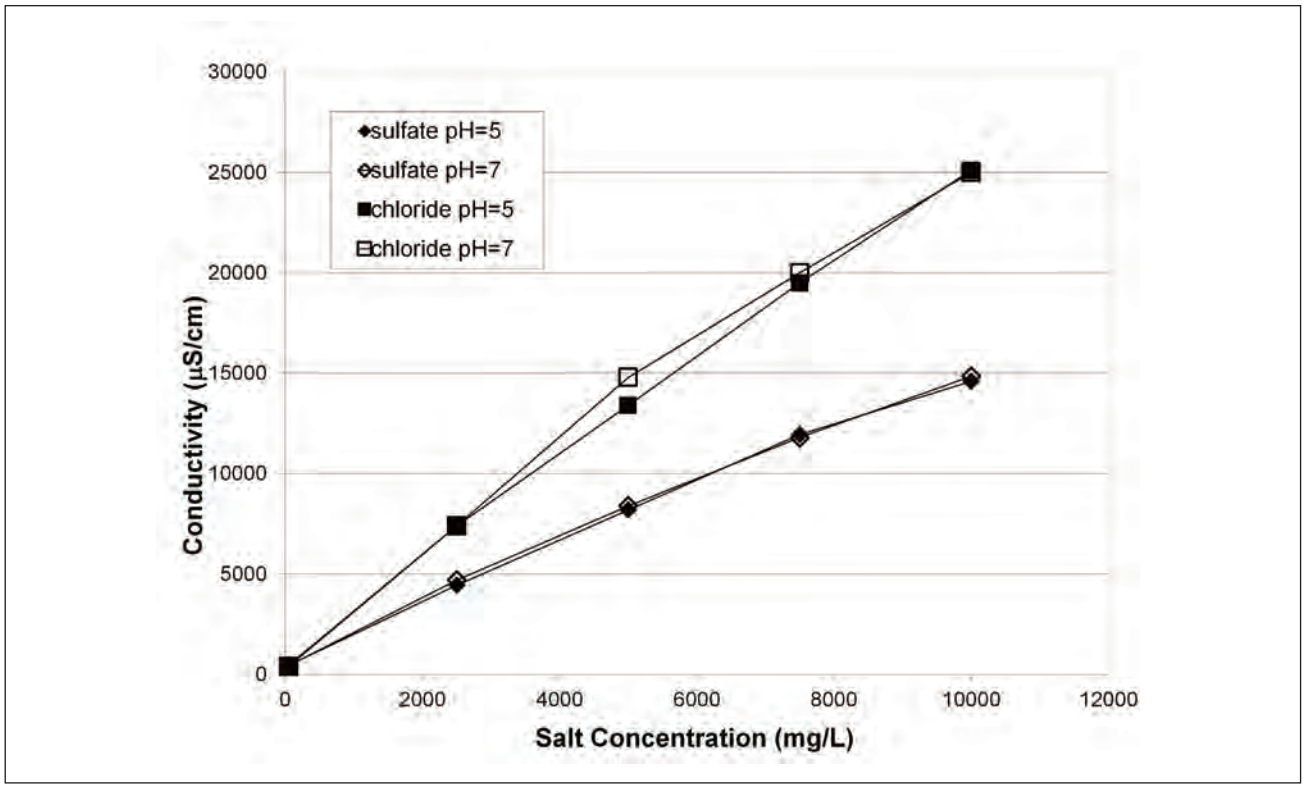
V_{0t} - drainage for clean sample treated with studied dosage of retention program

V_{ct} - drainage of sample with selected concentration of added contaminant and treated with studied dosage of retention program

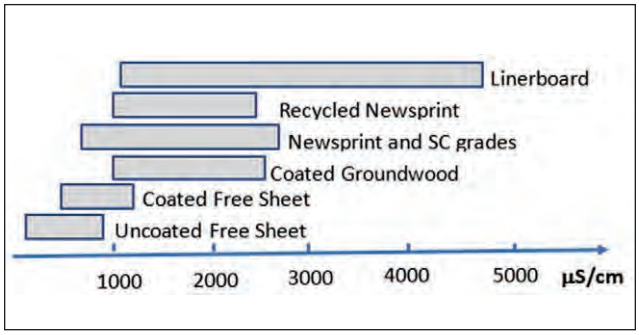
Figure 2 shows the relationship between the dosages of model salts in parts per million (ppm) and conductivity. Conductivities of samples were adjusted with NaCl at 460–25000 μS/cm and Na_2SO_4 at 460–15000 μS/cm, when the concentration of ions reached 10000 ppm.

These conditions exceed the level of ionic contamination typically found in most papermaking systems. **Figure 3** (based on the extensive experience of the authors) shows typical conductivity levels for major types of paper machines.

Figure 4 presents an observed relationship between performance of a typical dual polymer retention program, based on the coagulant and cationic flocculant, with various levels



2. Concentration of ionic contaminants and measured conductivity in pH 5 and pH 7.



3. Typical estimated conductivity levels for major grades of paper and board.

of ionic impurities at pH 7. Looking at the dotted lines representing experiments with NaCl and Na_2SO_4, the gradual loss of drainage gain from polymer application in a clean system (100%) could be observed.

Similar trends could be observed for a single polymer program and for a dual polymer program with both high and low charge density cationic flocculants at pH 5 and pH 7.

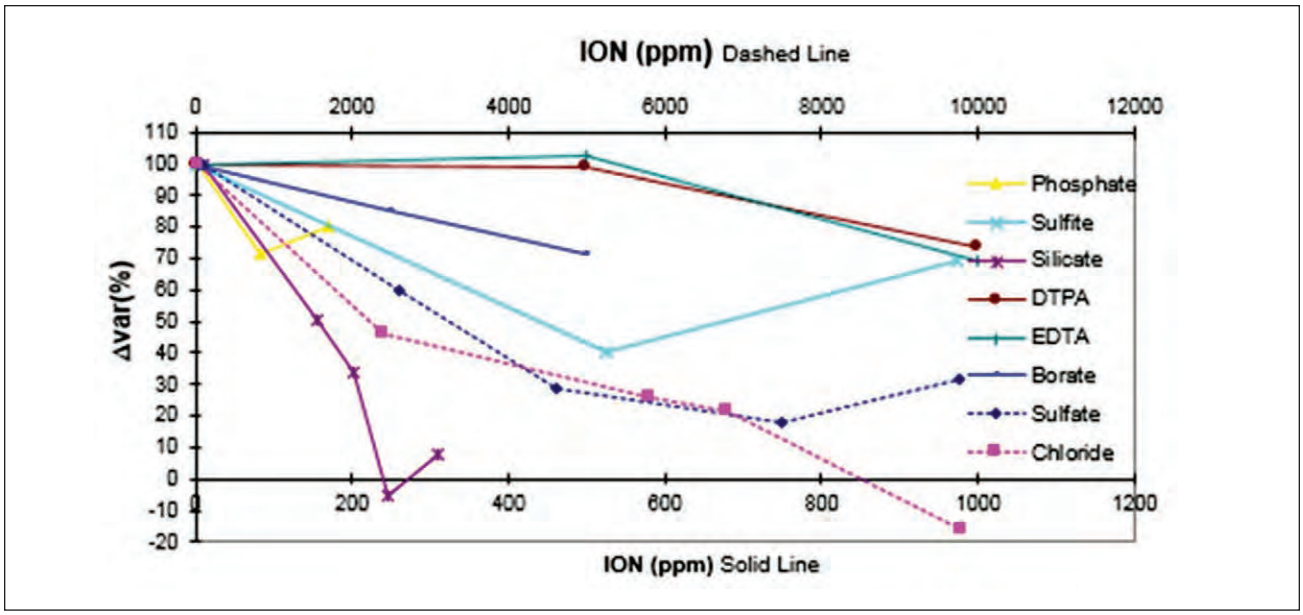
Although the range of conductivities covered by these experiments extended beyond the typical value at a paper mill, loss of drainage and retention because of increased conductivity was significant. These data were consistent with the earlier work of Lindstrom [21], who studied the effect of sulfate and chlorides on adsorption of cationic polyacrylamides. The observed loss of drainage could be a combination of changes to polymer adsorption and its conformation.

When bentonite was added before low charge density cationic flocculant, a significantly different response of drainage to conductivity was observed [36]. In this case, an initial increase in drainage was observed, followed by its reduction at the higher salt concentrations. This observation confirmed a proposed earlier mechanism [37-39] that involved interaction between flocculant and bentonite platelets to stiffen the network and prevent conformational changes impairing bridging capabilities. Changing the order of addition by adding cationic flocculant first significantly reduced resistance to conductivity increases. This suggested that interaction between flocculant and bentonite needed to occur before flocculant adsorbed onto the fiber.

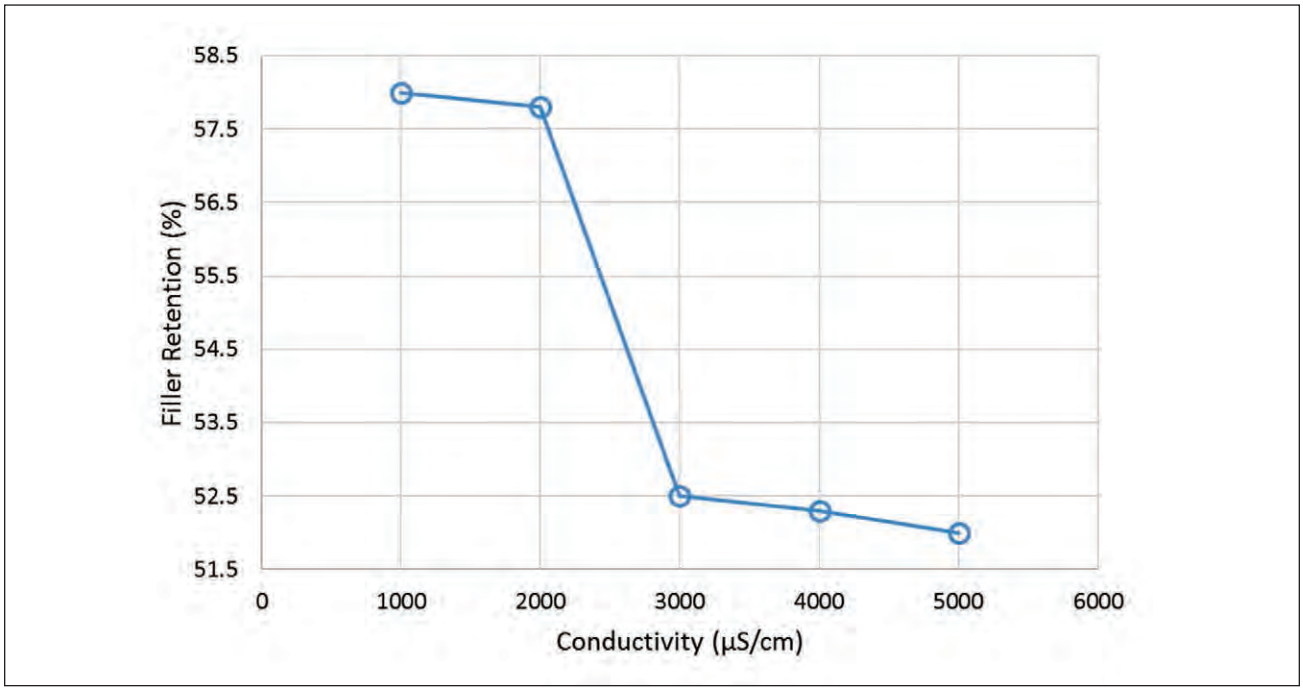
Based on results shown in Fig. 4, silicates are detrimental to single cationic flocculant and dual polymer programs. This effect is based mainly on their ability to act like ionic trash and to form complexes with cationic polymers rendering them inactive [40-42].

Gratton and coauthors [43] studied the effect of conductivity on retention and sizing. Several types of retention programs were evaluated in the laboratory. Observations from the laboratory were fully confirmed on a fine paper machine and indicated reduction of retention level, driven by lower filler retention (**Fig. 5**). At least in this paper machine system, a significant drop in retention was observed at conductivity changes of 2000–3000 µS/cm.

Reduced retention at the higher conductivity level was well illustrated by higher flow of cationic flocculant required to



4. Effect of ionic contamination on the drainage loss (%) for the dual polymer program, based on coagulant and cationic flocculant measured in pH 7.



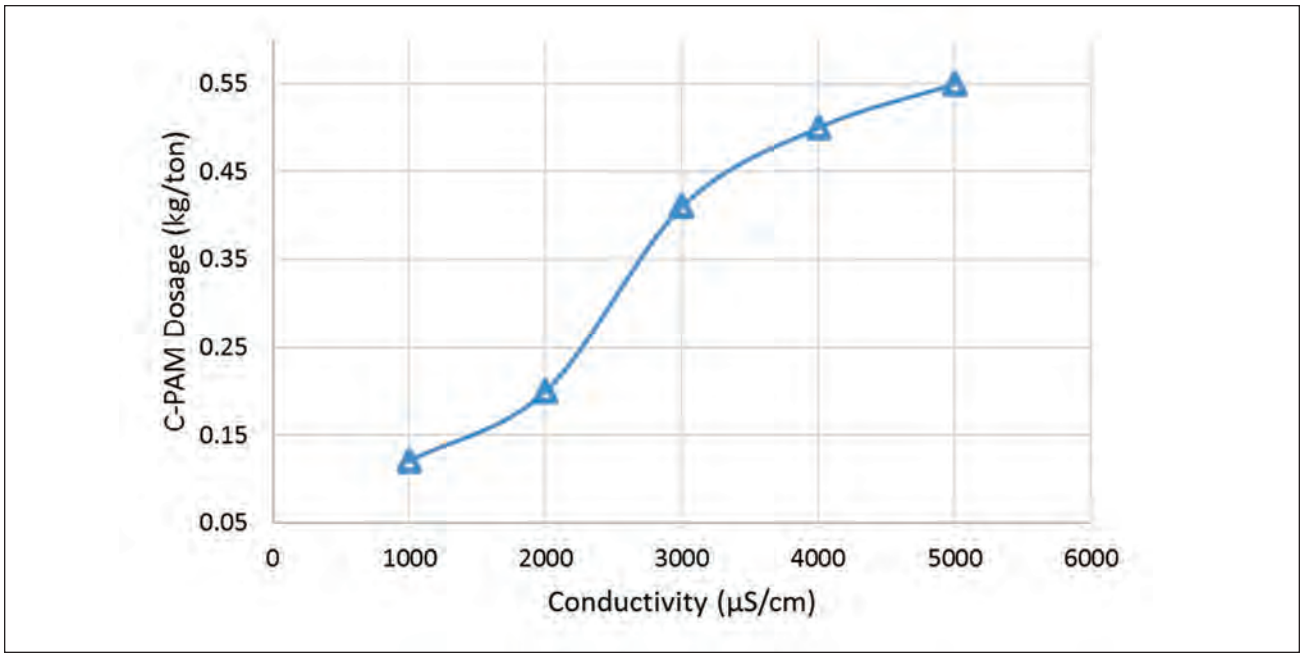
5. First pass filler retention as a function of conductivity.

maintain targeted white water consistency in the closed loop retention control application on the paper machine (**Fig. 6**).

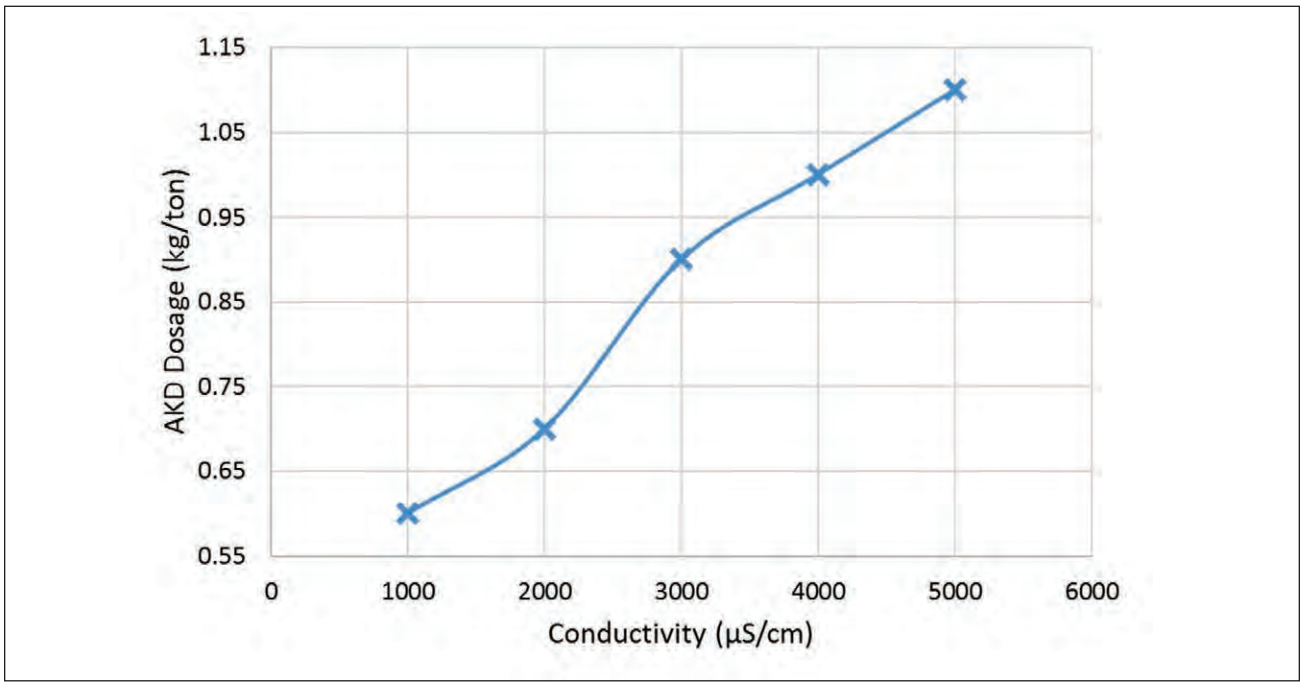
The authors observed a negative effect of conductivity on AKD sizing [43]. **Figure 7** illustrates an increase of AKD dosage required to meet sizing specification with increasing conductivity levels.

Similar results were observed in a study of the effect of conductivity on the performance of cationic starches (**Fig. 8**). In this work, cationic starches were used for ASA emulsification and sizing response was a measure of starch performance as emulsifier [44].

A negative effect of conductivity on various cationic starches was observed in terms of impaired sizing performance. Conductivity was varied in a wide range up to 5000 µS/cm. It was found that high levels of conductivity negatively affect the performance of cationic starches in terms of filler retention and internal sizing. All types of cationic starches, regardless of biological source, were affected. Starches with a high



6. Effect of conductivity on the dosage of cationic polyacrylamide (C-PAM) required to reach target white water consistency.

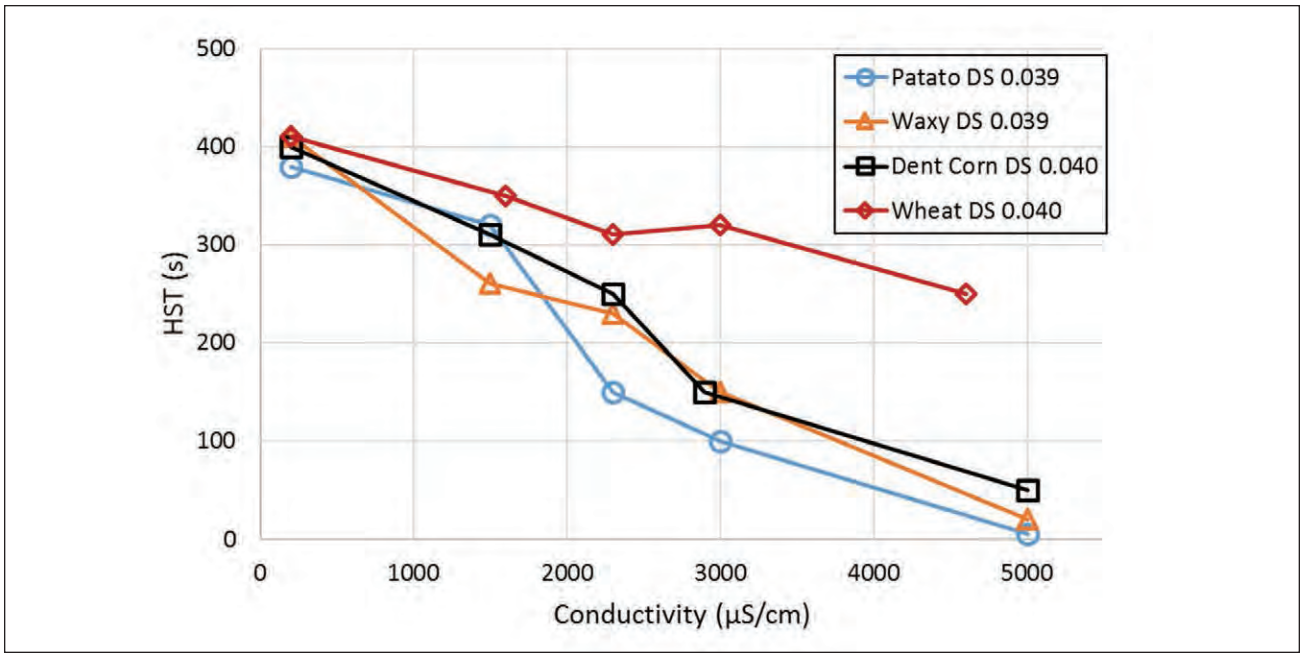


7. Effect of conductivity on dosage of alkyl ketene dimer (AKD).

degree of substitution (0.073) showed the best resistance to increased conductivity.

Zakrajsek [45] studied the effect of the level of dissolved and colloidal substances on paper sizing with a rosin/alum system. The effect of mill closure, conductivity, fresh water usage, and sulfate concentration were reported. Sizing response was expressed using $Cobb_{60}$ (g/m^2) value. The negative effect of a reduction in fresh water usage was studied in the range from 35 m^3/ton to 3 m^3/ton and was found to increase sharply when the fresh water usage was reduced to below 10 m^3/ton. Excellent relationships were observed between $Cobb_{60}$ value and conductivity, concentration of sulfate ion, and accumulation of unretained rosin sizing in the process water. In terms of conductivity, a change of 750–1050 μS/cm resulted in a 28.3–49.6 g/m^2 change of $Cobb_{60}$.

Conductivity affects water removal on the paper machine in various ways. By affecting the ability of retention aid to flocculate, conductivity reduces chemically induced free drainage



8. Effect of conductivity on performance of alkenyl succinic anhydride (ASA) emulsified with different starches.

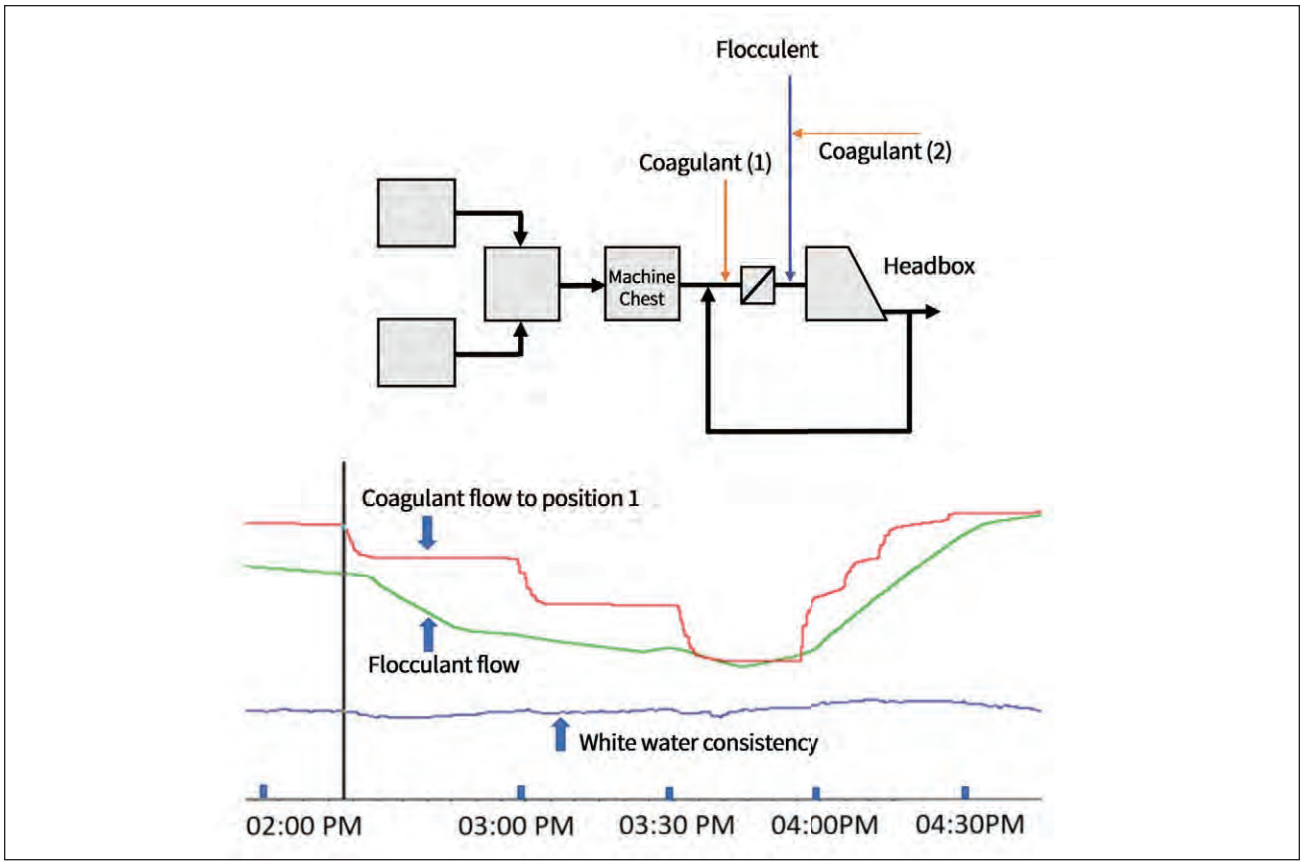
or chemically induced freeness of the stock. On the other hand, high conductivity reduces fiber swelling, as measured by water retention value, and this becomes relevant when water closely bound to the fiber is removed in the press section. Thus, when conductivity increases, mills might see slower drainage early in the forming section, but increased water removal through the presses. Because the amount of water removed in the early forming section, affected by flocculation, is by far greater than in the press section, we might expect that increased conductivity will have an overall negative effect on the combined water removal process.

For machines operating at high conductivity levels, some mechanical or chemical corrective options may be used to reduce the negative effects of high conductivity. For example, molecular weight or charge density of retention aids or starch can be adjusted. In some cases, the configuration of the feed points can be changed. Converting from the typical dual polymer retention program, based on consecutive addition of coagulant and cationic flocculant, to a pre-mix configuration improved retention and drainage at high conductivity conditions. Authors suggest [42-45] that repulsive interaction between cationic charges of coagulant and flocculant, either still in solution or after initial adsorption to the surface, delays conformational changes of polymer to the extent of allowing for more effective flocculation. This increases performance at any level of conductivity, but is especially important at high conductivity levels that drive polymer coiling processes faster. Considering how fast flocculation processes are at high turbulence levels, this delay in polymer coiling does not have to be large to noticeably boost performance. **Figure 9** shows results of the transition from consecutive addition to pre-mix configuration for a high brightness newsprint machine. With a total dosage of coagulant staying unchanged, the flow to the pre-screen position (1) was gradually reduced, with the balance mixed into the flocculant line (2). The paper machine operated with on-line consistency control, and because of improved performance, the dosage flocculant (3) gradually was reduced.

In addition, this paper machine producing high brightness supercalendered grade paper used a two stage (P-Y) brightening strategy—hydrogen peroxide followed by sodium hydrosulfite. This strategy required pH adjustment after alkaline hydrogen peroxide application, before application of sodium hydrosulfite. If the pH adjustment was not done properly, a significantly higher dosage of sodium hydrosulfite was required to reach the brightness target. The increased dosages drove system conductivity significantly higher than normal. Thus, conductivity variation from 800 µS/cm to 4000 µS/cm occurred and was observed to affect machine drainage and runnability. Although co-mixing coagulant to cationic flocculant brought an immediate relief to drainage problems, the mill also paid more attention to proper pH control between the two brightening stages.

Practical recommendations

Earlier discussion clearly illustrates that conductivity affects such fundamental aspects of paper machine performance as retention, drainage, and colloidal stability. It is therefore important that monitoring conductivity and developing response strategies should be a part of wet-end management. Understanding sources of conductivity and correcting its variability at the source will lead to improvement in paper machine stability. More closure unavoidably increases conductivity levels, but if the influx of electrolytes can be reduced, the



9. Improvement of performance of retention program with the move of coagulant feed point from pre-screen position to pre-mix with cationic flocculant.

conductivity increase at any given degree of closure will be minimized. Because simple ions have little affinity to the fiber, and through recirculation of machine water, conductivity levels tend to reach similar levels across the machine system. In the case of mechanical grades, with their integrated character, increasingly aggressive bleaching strategies, and limited pulp thickening opportunities, optimization of bleaching conditions to ensure the lowest possible usage of bleaching chemicals is the single most effective way to control conductivity levels. Monitoring conductivity on line in the headbox or tray should be a standard element of wet-end chemistry management. Changes in conductivity can provide an early warning of changes in drainage and press solid and draw variation, possibly allowing operators to prevent web breaks. Application of conductivity probes or frequent manual tests back in the system allow the mill to develop an understanding of the sources of conductivity and assist troubleshooting and improvement projects.

A conductivity probe is a simple, yet robust device that makes conductivity a common on-line measurement, even for older machines. If a mill does not have an on-line wet-end monitor or lacks staffing to run routine wet-end tests, conductivity measurement can be a useful tool to diagnose wet-end problems. For example, a containerboard mill running a mixture of unbleached kraft and recycled corrugated containers had an issue of losing strength and sizing. The mill only had on-line pH, temperature, and conductivity sensors around the machine. After reviewing these data, the mill noticed a strong correlation between increased conductivity of unbleached kraft pulp and quality issues. The increased conductivity indicated possible high pulp mill carryover. Based on this information, the mill checked the brownstock fiber line and found operational issues around the washer. After addressing the issues, conductivity on the paper machine returned to normal levels. The strength and sizing values were brought back to target. From this example, we see that the change of conductivity, rather than its absolute value, was valuable to gain insight into a wet-end issue.

Hardness

Because of their affinity to fiber surfaces and formation of insoluble salts, the hardness ions Ca^{+2} and Mg^{+2}, in addition to contributing to general conductivity levels, can also be responsible for very specific operational problems.

Several anions react with Ca^{+2} or Mg^{+2} to form insoluble calcium or magnesium salts that often trigger deposits or scale on the paper machine. Such precipitation processes take place only if the product of reacting ion concentration exceeds the solubility product (K_{sp}) for a given temperature. Typical examples of such salts are barium sulfate, calcium oxalate, cal-

cium carbonate, and calcium phosphate. These represent the most common scales formed in paper mills. The pH alters the forms of weak acid in solution and affects scale formation potential. For example, formation of calcium carbonate and calcium phosphate scale requires participation of CO_3^{-2} and phosphate (PO_4^{-3}) ions, both present only in the high pH environment. Similarly, calcium oxalate precipitation requires the presence of oxalate anion — $(COO)_2^{-2}$, which is formed in significant amount at greater than pH 3 [46]. Papermakers may reduce the risk for troublesome scale related issues by understanding the ionic composition of water circuits and mineral components from wood sources, optimizing the use of alum, understanding the effect of pH on scale formation, and operating peroxide bleaching in a way to reduce oxalic acid formation.

The ability of calcium and magnesium ions to form insoluble salts with carboxylic acids leads to other operational and quality problems, such as pitch and hydrolyzed ASA deposition, which is further discussed in the following. These problems typically are raised at greater than pH 6, when the carboxylic acid functionality exists in its anionic form.

A product of ASA hydrolysis, dicarboxylic acid, forms tacky and troublesome deposits. Magnesium-related deposits with ASA were particularly difficult. Avoiding ASA hydrolysis through proper emulsification conditions (low pH, low temperature) and carefully controlling hardness are necessary to ensure successful, deposit-free application of ASA. Limiting the time for ASA to circulate in the machine water loop through elevated first pass retention is another strategy to reduce the potential for hydrolysis and consequent deposits. A small amount of added alum, even in alkaline papermaking systems, provides competition for reaction with hardness ions and helps in preventing this deposition.

Calcium and magnesium ions also can form insoluble salts with the acidic components of natural pitch. Pitch deposition problems triggered by this precipitation mechanism are especially troublesome at levels greater than pH 6, at which a significant fraction of the carboxylic groups (-COOH) exist in their anionic form (-COO-). Reducing pH reduces the concentration of carboxylate anion, but in the case of systems using calcium carbonate fillers, hardness levels will increase. Identifying and minimizing sources of hardness should be part of every pitch control strategy. Variation of the calcium cation concentration could be caused by the following factors:

- Natural variation of the hardness level in the incoming fresh water
- Decomposition of calcium carbonate filler, as a function of pH
- Calcium in wood species and other incoming raw material, such as recycled board produced in high hardness systems

Yuan [47] discussed several aspects of hardness interaction with the fiber. The authors described an effect of accumulation of metals ions on the wet end of the paper machine. Despite the significant affinity of Ca^{+2} ions to the fiber surface, which loaded Ca^{+2} onto the paper product and removed it from the wet end, its concentration in the headbox often reached high levels. As discussed earlier, this is a function of the amount of hardness fed from short loop and system closure. Product (paper or board) manufactured in high hardness systems contains calcium salt after water is evaporated in the dryer section. When those products are recycled and repulped, the carryover calcium salt becomes an additional source of hardness for the upcoming papermaking process. The authors presented the isotherms of Ca^{+2} adsorption on kraft pulp and determined the exothermic and spontaneous character of this process (ΔH^0=-30.9 kJ/mol and $\Delta\Sigma^0$= -14.2J/molK). Thus, Ca^{+2} is easily adsorbed on the surface of the fiber and the bond is strong enough that it is not desorbed easily. Additionally, the amount of Ca^{+2} ion (0.0165-0.0167 mmol/g) was found to be close to half of the amount of carboxyl groups in the pulp used (0.0366 mmol/g), indicating 2:1 stoichiometry, with one Ca^{+2} ion reacting with two carboxylate functions. The negative effect of Ca^{+2} on the performance of cationic polyacrylamides in terms of retention and drainage was also reported and explained in terms of negative effect on available negative adsorption sites on the fiber. The same mechanism was also responsible for impaired strength development with cationic starch and sizing with AKD. The effect of Ca^{+2} on retention and drainage was also significantly higher than Na^+ at the same total conductivity levels. This indicates an additional contribution of fiber surface charge modification (in the case of Ca^{+2}) over general conformational changes related to conductivity.

SUMMARY

This report reviewed the effect of conductivity on the papermaking water system and on various aspects of paper machine operations. Conductivity can affect retention, drainage, press dewatering, sizing, strength, deposit formation, and scale. Based on the range of applications affected, conductivity needs to be closely monitored. Installation of conductivity probes in the tray should be an industry standard. Adding measures of conductivity to the paper machine distributed control system enables mills to build an understanding of how conductivity affects the paper machine performance and develop response strategies. For example, on-line measurement of conductivity might help operators predict changes in drainage, center roll release, pitch and stickies deposits, sizing, and strength. System conductivity profiles throughout the mill would allow engineers to identify major sources of conductivity and its variation. In most cases, conductivity is contributed by the pulp and bleaching chemicals, washing efficiency, and chemical additives for process and performance purposes. Opportunities for improvements in these applications should be reviewed to reduce their contribution to increased conductivity. Questions to consider include the following:

- Can required brightness level be reached with lower bleaching chemical consumption?

- Is my inter-stage bleaching pH control strategy effective in reducing unnecessary pH swings and the need for large pH corrections?
- Is my pH control accurate enough to prevent brightness losses (mechanical pulps) that would lead to excessive dosages of bleaching additives?

These are some of the questions that when addressed reduce conductivity levels and reduce overall cost of mills operations.

Two important factors affect the level of conductivity: 1) the amount of ionic materials added to the system and 2) the amount of fresh water used. Opening the mill system and adding more fresh water, in many cases, is not a best option to reduce conductivity. In fact, with many mills targeting reduced water usage for sustainable growth, the focus must remain on reduction of the amount of ionic materials introduced to the system, application of best practices of countercurrent water management, and generation of the waste stream with high levels of dissolved materials and low consistency.

Finally, with increased levels of mill closure, it is valuable to explore possible mechanical and chemical options to reduce negative effects of high conductivity on machine performance and sheet quality. The need to focus research in this area, to include conductivity and other contaminants, will continue. **TJ**

LITERATURE CITED

1. Gratton, R. and Pruszynski, P., "Potential incompatibilities in application of chemical additives in papermaking," Pira, Leatherhead, UK, 2005.
2. Gratton, R. and Pruszynski, P., "Potential incompatibilities in application of chemical additives in papermaking. What may go wrong…?" *Prepr. - PAPTAC Annu. Meet., 89th*, Pulp and Paper Technical Association of Canada, Montreal, QC, Canada, 2003, pp. 162-169.
3. Allen, L., Polverari, M., Levesque, B., et al., *TAPPI J.* 82(4): 188(1999).
4. Laivins, G., Polverari, M., and Allen, L., *J. Pulp Pap. Sci.* 27(6): 190(2001).
5. Pruszynski, P. and Jakubowski, R., *Appita J.* 59(2): 114(2006).
6. Brown, M.T. and Hart, P.W., *TAPPI J.* 16(2): 65(2017)
7. Harned, H.S. and Owen, B.B., "The physical chemistry of electrolyte solutions," 3rd edn., *ACS Monograph Series*, Reinhold Publishing, New York, 1964.
8. Alexander, S.D. and Dobbins, R.J., *Tappi* 60(12): 117(1977).
9. Pietschker, D., *TAPPI Papermakers Conf.*, TAPPI Press, Atlanta, GA, USA, 1996, p. 523.
10. Evans, B., Wright, R., Haskins, W.J., et al., "Filling SC paper with PCC; a holistic approach," *PIRA Conf.*, Pira, Leatherhead, UK, 2005.
11. Xu, Y. and Deng, Y., *TAPPI J.* 93(8): 17(2004).
12. Mittal, A., Iribarne, J., Rajan, K.G, et al., *Prog. Pap. Recycl.* 15(3): 19(2006).
13. Tomney, T., Pruszynski, P.E., Armstrong, J.R., et al., *Pulp Pap. Can.* 99(8): 66(1998).
14. Kemotron, "In-line measurements as the basis of process control systems in pulp mills," Kemotron Brochure No. 990.68/2, Kemotron A/S, Kongens Lyngby, Denmark (now Valmet Automation, Espoo, Finland), 2002.
15. Josephson, W.E., Krishnagopalan, G.A., and Cullinan, H.T., *Tappi J.* 76(9): 197(1993).
16. Linhart, F., Auhorn, W.J., Degen, H.J., et al., *Tappi J.* 70(10): 79(1987).
17. Webb, L., *Pulp Pap. Int.* 37(1): 44(1995).
18. Wearing, J.T., Huang, S., Piggott, A., et al., *Pulp Pap. Can.* 86(5): T139(1985).
19. Kotila, P.S. and Estes, T., *Prog. Pap. Recycl.* 3(4): 42(1994).
20. Pelton, R.H., Allen, L.H., and Nugent, H.M., *Pulp Pap. Can.* 81(1): 54(1980).
21. Hubbe, M.A., Rojas, O.J., and Venditti, R.A., *Nord. Pulp Pap. Res. J.* 21(2): 154(2006).
22. De Jong, R., *Prog. Pap. Recycl.* 14(3): 40(2005).
23. Doshi, M.R., *Prog. Pap. Recycl.* 9(3) 39(2000).
24. Haynes, D.R., *Prog. Pap. Recycl.* 16(2): 14(2007).
25. Lindstrom, T., *Nord. Pulp Pap. Res. J.* 7(4): 181(1992)
26. Dobbins, R.J. and Alexander, S.D., *Tappi* 60(12): 121(1977).
27. Davison, R.W., "Some effects of aqueous environment on fine particle retention in paper," *TAPPI Papermakers Conf.*, TAPPI Press, Atlanta, 1985, p. 171.
28. Lindstrom, T. and Wågberg, L., *Tappi J.* 66(6): 83(1983).
29. Buontempo, J.T., Sherman, L.M., and St. John, M.R., "The effects of salts on the performance of cationic flocculants used as retention aids for alkaline fine paper," *TAPPI Papermakers Conf.*, TAPPI Press, Atlanta, 1996, p. 49.
30. Hulkko, V.-M. and Deng, Y., *J. Pulp Pap. Sci.* 25(11): 378(1999).
31. Miyanishi, T. and Motegi, S., *TAPPI J.* 84(3): 58(2001).
32. Laivins, G., Polverari, M., and Allen, L., *J. Pulp Pap. Sci.* 27(6) 190(2001).
33. Polverari, M., Allen, L.H., Sithole, B., et al., *TAPPI J.* 84(1): 1(2001).
34. Miyanishi, T. and Shigeru, M., *TAPPI J.* 80(1): 262(2001).
35. Pruszynski, P and Jakubowski, R., "Impact of conductivity and cationic demand on drainage of TMP-based newsprint furnish," *Appita Annu. Conf. Proc., 56th*, Appita, Bundoora, Australia, 2002, pp. 323-331.
36. Pruszynski, P., "Impact of high yield pulps on wet end chemistry of typical fine paper applications—understanding and alternative corrective strategies," *Int. Mech. Pulping Conf.*, PAPTAC, Montreal, 2011.
37. Wågberg, L., Dispersions and Aggregation: *Fundamentals and Applications—Proceedings of the Engineering Foundation Conference*, Engineering Foundation, New York, 1994, p. 339.
38. Swerin, A. and Odberg, L., *Nord. Pulp Pap. Res. J.* 45(11): 22(1996).
39. Eklund, D. and Lindstrom, T., *Paper Chemistry: An Introduction*, DT Paper Science Publications, Grankulla, Finland, 1991.
40. Ali, T., Evans, T.D., Fairbank, M.G., et al., *J. Pulp Pap. Sci.* 16(6): J169(1990).

41. Ali, T., Fairbank, M.G., McArthur, D., et al., *J. Pulp Pap. Sci.* 14(2): J23(1988).
42. Ali, T., Fairbank, M.G., and McArthur, D., "Role of silicate in peroxide brightening of mechanical pulp. 6. Interactions of silicate and papermaking polymers," *Prepr. - CPPA Annu. Meet.*, PAPTAC/CPPA, Montreal, 1989, p. B209.
43. Gratton, R., Doiron, B., and Chen, G., "Impact of pulp mill contaminants on the wet end chemistry of a fine paper machine," *TAPPI Minimum Effluent Mills Symp.*, TAPPI Press, Atlanta, 1997.
44. Beaudoin, R., Gratton, R., and Turcotte, R., *J. Pulp Pap. Sci.* 21(7): J238(1995).
45. Zakrajsek, N., Zulc J., Moze, A., et al., *Acta Chim. Slov.* 52: 67(2005).
46. Rudie, A.W. and Hart, P.W., *Solutions People, Processes Pap.* 88(6): 45(2005).
47. Yuan, G., Dai, H., Ye, C., et al., *BioResources* 6(3): 2790(2011).

ABOUT THE AUTHORS

We did this review because papermakers might overlook the benefit of conductivity measurement. This study summarizes previous research and shares additional experience. The most difficult part of the research was finding mill examples that fit the theoretical areas we were discussing. Although we have seen them several times, finding well-documented examples was time consuming.

Although conductivity has been used for several years as a control parameter, it is not particularly well understood and not particularly exclusive to the properties it is being used to control. Stabilized conductivity is more manageable than low, yet varying conductivity.

Mills can benefit from this study by better understanding the principles of conductivity measurement and its limitations and make use of the information for better wet-end operation.

Our next step is to attempt to stabilize conductivity and reduce its overall effect on paper machine performance.


Xu


Pruszynski


Hart

Xu is senior R&D scientist/engineer, WestRock, Richmond, VA, USA. Pruszynski is global technical specialist, Nalco Water, Naperville, IL, USA. Hart is director, Fiber Technology and Innovation, WestRock, Richmond, VA, USA. Email Hart at peter.hart@westrock.com.

Techno-economic analysis of ECF bleaching and TCF bleaching for a bleached eucalyptus kraft pulp mill

TIAGO DE ASSIS, JORDAN PERRIN, HASAN JAMEEL, RICHARD PHILLIPS, DOMINIQUE LACHENAL, ADRIANNA KIRKMAN, AND RONALDS GONZALEZ

ABSTRACT: An early stage techno-economic analysis was performed to compare a traditional elemental chlorine free (ECF) sequence (O O D_0 [EOP] D_1 P) with the proposed totally chlorine free (TCF) sequence (O O A $[ZEO]_1$ $[ZEO]_2$ P)] for a bleached eucalyptus kraft pulp mill. Similar operating costs (ECF = US$465/a.d. metric ton; TCF = US$468/a.d. metric ton) and similar internal rate of return (ECF = 16.5%; TCF = 16.4%) were obtained. Although the TCF case has lower revenue with surplus steam, savings with chemicals (e.g., sodium chlorate and methanol) pays for the higher consumption of electricity. Probabilistic analyses were also performed to evaluate the financial risks associated with the variability of chemical costs and electricity price. Probabilistic analyses have shown that the price volatility of sodium hydroxide and sodium chlorate have a significant impact on the probability distribution of internal rate of return (IRR). Despite its promising potential, the new TCF sequence has only been tested in laboratory scale and further scaleup has to be performed to validate the technology. However, the techno-economic economic analysis shows that the proposed TCF technology has promising potential for future industrial application.

Application: Mills might consider the proposed TCF sequence as an alternative for bleached pulp manufacturing.

During the 1990s, governmental agencies developed new regulations for the pulp and paper industry because of environmental issues related to high emissions of persistent, bioaccumulative and toxic chlorinated organic compounds (COC) in water bodies. During that time, two bleaching technologies, elemental chlorine free (ECF) and totally chlorine free (TCF), were developed as alternatives to reduce COC emissions and several techno-economic studies were executed to compare the performance of both options.

Lancaster et al. [1] studied the capital costs, operating costs, and emissions of chlorinated compounds when an existing D_{50}→C_D delignification stage bleach plant was retrofitted to replace the elemental chlorine–based process with ECF, ozone-based ECF, and TCF bleaching. Despite the significant reduction of adsorbable organic halides (AOX) emissions, TCF bleaching presented lower pulp strength, higher capital, and higher operating costs. ECF bleaching presented the lowest total cost among all cases evaluated.

Homer and Govers [2] performed a cost estimation analysis to retrofit a C/D delignification stage bleach plant to ECF and TCF bleaching. The chemical costs between ECF and TCF bleaching were similar. However, TCF bleaching required more capital investment, resulting in higher total costs than ECF bleaching.

Brooks et al. [3] evaluated the retrofit of a chlorine bleached softwood pulp mill to ECF and TCF bleaching based on hydrogen peroxide and oxygen. TCF bleaching costs were about US$26–29/a.d. metric ton of pulp higher than ECF bleaching costs. Even the reductions made with the TCF case in caustic makeup, steam consumption, water use, and sewer loading were not sufficient to overcome wood and chemical costs when compared with ECF. Moreover, TCF bleaching based only on oxygen and hydrogen peroxide could not achieve the same brightness as ECF bleaching (90% ISO). Brightness values around 80%–85% ISO were obtained for TCF bleaching.

Parthasarathy [4] performed a cost-benefit analysis to retrofit an ECF bleached softwood pulp mill. Three different bleaching configurations were evaluated: (1) ozone-based ECF bleaching; (2) ECF bleaching based on Champion International's trademarked bleach filtrate recycle (BFR) process where the bleaching filtrate is recycled to the recovery area; and (3) closed-water-cycle TCF bleaching. Ozone-based ECF bleaching presented the lowest operating costs and best return on investment (ROI). The BFR process presented about 10%–11% higher operating costs and lower ROI than TCF bleaching.

Although the retrofit of existing plants makes more sense from a practical point of view, the costs to convert an existing bleached pulp mill to ECF or TCF bleaching are totally dependent on the existing assets (e.g., equipment availability, equipment specification, equipment size, and process configuration) and unlikely to be optimized. On the other hand, the design of greenfield (new) facilities has the potential to opti-

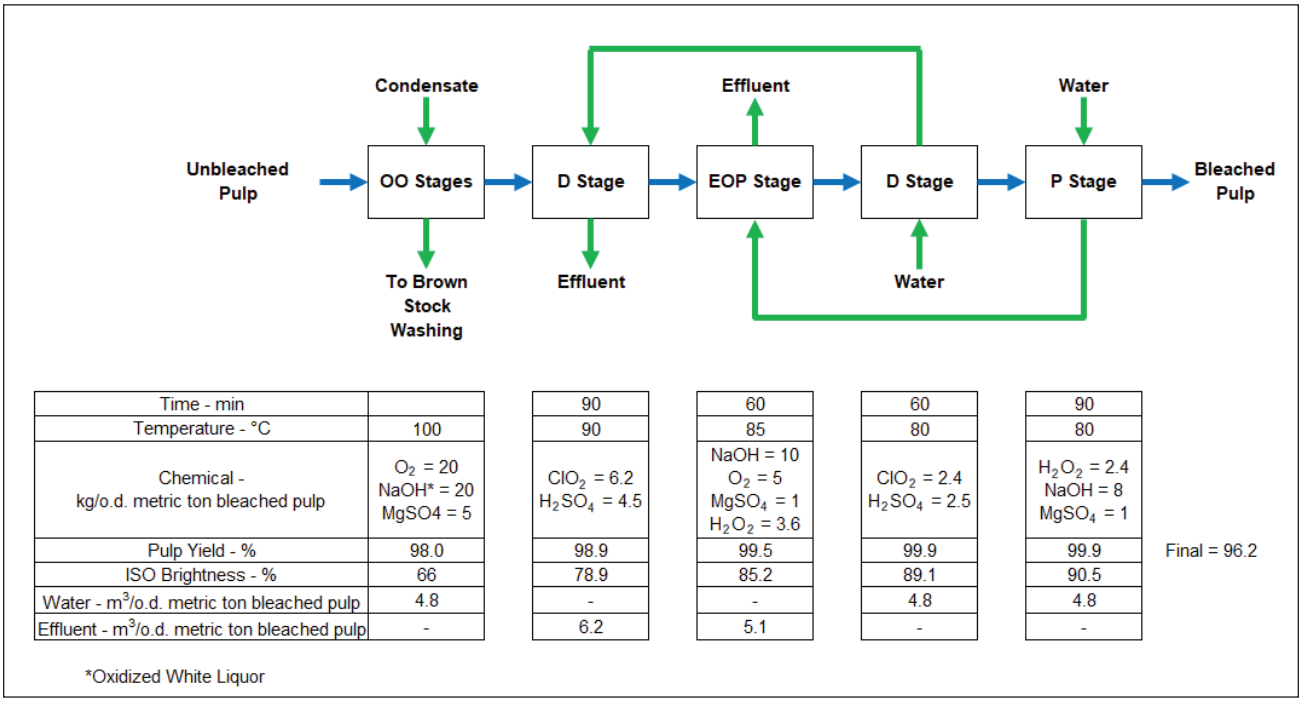
mize costs, capital investment, and product quality [5]. Therefore, techno-economic analysis of greenfield facilities can be used for an unbiased comparison between ECF and TCF technologies.

Brunner and Pulliam [6] performed a techno-economic analysis for a greenfield bleached softwood pulp mill to compare the performance among different bleach plants configurations (30% and 70% chlorine dioxide substitution, ozone-based ECF, and TCF bleaching). Capital investments for ozone-based ECF and TCF bleaching are similar. However, as a result of 7% higher operating costs, TCF bleaching presented 4% higher total costs (operating costs and depreciated capital) than ECF bleaching. Among all cases, TCF bleaching was the most expensive option, with total costs 10% higher than the least expensive case (30% chlorine dioxide substitution).

Albert [5] compared the techno-economic performance of ECF and effluent-free TCF bleaching for a greenfield bleached pulp mill. The effluent-free TCF bleached pulp mill presented lower capital and operating costs than the ECF bleached pulp mill. Main cost differences are related to a smaller water treatment plant and elimination of a wastewater treatment plant in the TCF case. Some of the conclusions presented by Albert [5] have been disputed on the basis that the chemical costs and process conditions used for the ECF case were overstated [7].

A critical factor for the success of closed-water-cycle bleach plants, with minimum or no effluent emission, is the control of nonprocess inorganic elements. If the nonprocess inorganic elements are not removed, their buildup in the process would cause corrosion, deposits, and undesired catalytic reactions with TCF bleaching chemicals that result in significant pulp quality issues [5]. Increased recycle of organics along the bleaching stages can also result in additional consumption of bleaching chemicals [8]. Although ECF bleaching can also be designed to operate within a closed-water cycle (BFR process) [9], partial or full closure of TCF bleaching might be more feasible. The closure of ECF bleaching will increase the corrosion rate of process equipment, such as evaporators and the recovery boiler, because of the recycle of chloride anions to the chemical recovery area [9]. Moreover, chlorinated byproducts will still be emitted with pulp, waste, and into the atmosphere in effluent-free ECF bleaching [5]. Although TCF bleaching generates lower amounts of AOX emissions than ECF bleaching, treated effluents originated from both bleaching options have very low levels of AOX emissions. Toxicity levels present in both effluents are safely below the levels that cause adverse environmental impacts [1].

Despite the long discussion in the literature about the economic, environmental, and technical aspects of each technology, ECF bleaching has become the dominant technology. ECF represents 90%–95% of the production of bleached chemical pulp in the world, whereas TCF bleaching has remained as a marginal technology. Reasons to justify the low participation in the market of bleached kraft pulp (less than 5%) are diverse. These reasons include (1) poor efficiency of combined oxygen and hydrogen peroxide reactions resulting in high costs and low brightness stability, (2) poor selectivity of ozone bleaching resulting in reduction of degree of polymerization of the cellulose [10], and (3) technical issues and inefficiency during the early years of ozone bleaching technology development.



Time - min		90	60	60	90	
Temperature - °C	100	90	85	80	80	
Chemical - kg/o.d. metric ton bleached pulp	O_2 = 20 NaOH* = 20 MgSO4 = 5	ClO_2 = 6.2 H_2SO_4 = 4.5	NaOH = 10 O_2 = 5 $MgSO_4$ = 1 H_2O_2 = 3.6	ClO_2 = 2.4 H_2SO_4 = 2.5	H_2O_2 = 2.4 NaOH = 8 $MgSO_4$ = 1	
Pulp Yield - %	98.0	98.9	99.5	99.9	99.9	Final = 96.2
ISO Brightness - %	66	78.9	85.2	89.1	90.5	
Water - m^3/o.d. metric ton bleached pulp	4.8	-	-	4.8	4.8	
Effluent - m^3/o.d. metric ton bleached pulp	-	6.2	5.1	-	-	

*Oxidized White Liquor

1. Process diagram and parameters of elemental chlorine free (ECF) sequence (O O D_0 [EOP] D_1 P). (O_2 = oxygen; NaOH = sodium hydroxide; $MgSO_4$ = magnesium sulfate; ClO_2 = chlorine dioxide; H_2SO_4 = sulfuric acid; H_2O_2 = hydrogen peroxide.)

However, the development of more efficient and reliable ozone generators, improved mixing technology [11,12], and better understanding of ozone chemistry [13,14] have contributed to reduce costs of equipment and energy, which increases the competitiveness of ozone bleaching technology. In addition, an efficient and selective TCF sequence, capable of producing bleached pulp with similar properties (e.g., beatability and tensile index strength) as ECF pulp, has been developed by Perrin et al. [10]. This sequence minimizes the production of hydroxyl radicals that can depolymerize or oxidize carbohydrates by eliminating hexenuronic acid groups by an acid hydrolysis stage and by splitting the ozone charge between two stages combined with an alkaline extraction to minimize the reaction of ozone with muconic acid structures. It also removes transition metal cations with an acid stage to avoid catalytic decomposition of TCF beaching chemicals and eliminates carbonyl groups with a hydrogen peroxide stage to improve pulp brightness stability.

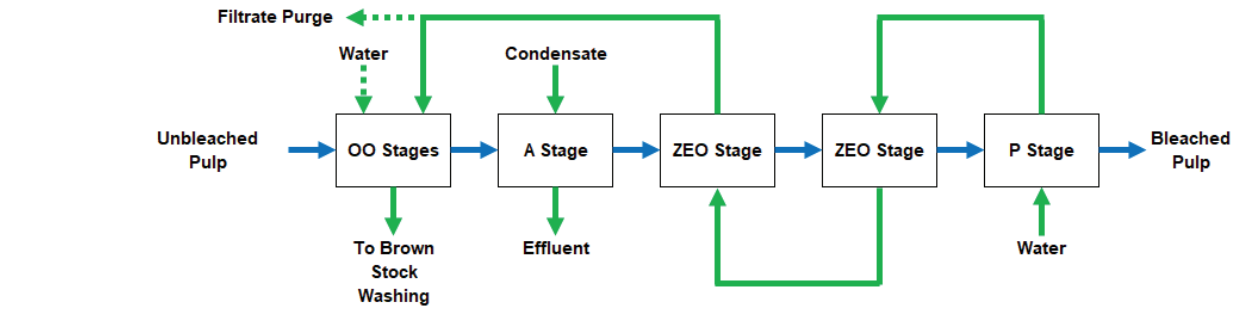
Therefore, the objective of this work is to execute an early stage techno-economic analysis for a greenfield bleached eucalyptus kraft pulp mill to compare the financial performance between an improved TCF sequence and a traditional ECF sequence.

MATERIALS AND METHODS

Process simulation and techno-economic analyses

Experimental data for the ECF (O O D_0 [EOP] D_1 P) (**Fig. 1**) and the TCF (O O A [ZEO]$_1$ [ZEO]$_2$ P) (**Fig. 2**) sequences have been provided by Perrin et al. [10]. These bleaching sequences were studied at the laboratory scale. Unbleached Brazilian eucalyptus pulp after oxygen delignification was used as the starting pulp. The properties of the unbleached and bleached pulps are given in the **Table I**.

Process simulation models were developed using the WinGEMS software to represent a bleached eucalyptus kraft pulp mill (1,000,000 a.d. metric tons/year) (**Fig. 3**). All bleaching stages were performed at 10% pulp consistency followed by a washing step using a press washer. The inlet consistency,



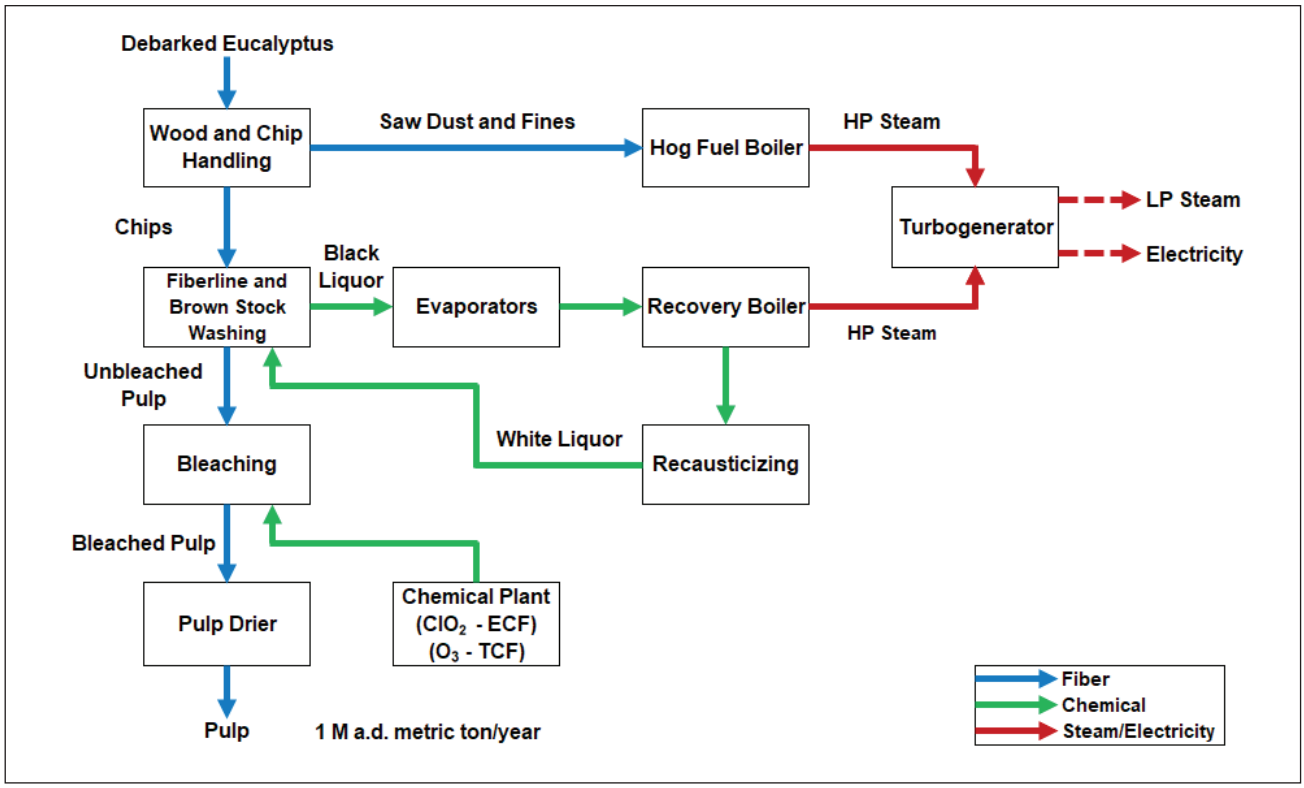
Time - min		180	60	60	120	
Temp - °C	100	90	70	70	80	
Chemical - kg/o.d. metric ton bleached pulp	O_2 = 20 NaOH* = 20 $MgSO_4$ = 5	H_2SO_4 = 6	O3 = 2.6 H_2SO_4 = 2.2 O_2 = 15 NaOH* = 11 $MgSO_4$ = 2	O_3 = 2.1 H_2SO_4 = 4.7 O_2 = 15 NaOH* = 10 $MgSO_4$ = 2	H_2O_2 = 6.6 NaOH = 8 $MgSO_4$ = 2.5	
Yield - %	98.0	99.0	99.6	99.8	99.8 (96.2)	Final = 96.2
ISO Brightness - %	66	66.9	78.2	85.9	90.5	
Water - m^3/o.d. metric ton bleached pulp	4.8	4.8	-	-	4.4	
Effluent - m^3/o.d. metric ton bleached pulp	-	5.0	-	-	-	

*Oxidized White Liquor

2. Process diagram and parameters of totally chlorine free (TCF) sequence (O O A [ZEO]$_1$ [ZEO]$_2$ P)-. (O_2 = oxygen; NaOH = sodium hydroxide; $MgSO_4$ = magnesium sulfate; H_2SO_4 = sulfuric acid; O_3 = ozone; H_2O_2 = hydrogen peroxide.)

Pulp Properties	Unbleached Pulp	ECF Bleached Pulp	TCF Bleached Pulp
Kappa	8.6	—	—
Hexenuronic acids, µmol/g	62.9	—	—
ISO brightness, %	66.0	90.5	90.5
Viscosity, mL/g	922	804	622
Tensile index, N.m/g at 400 mL CSF	—	66.4	63.0

I. Properties of unbleached and bleached eucalyptus kraft pulps.



3. Process diagram of a bleached eucalyptus kraft pulp mill.

discharge consistency, and Norden efficiency for each washing step were 5%, 30%, and 7, respectively [15].

The configuration of the TCF bleaching process was developed to minimize effluent emissions and water uptake by partially recycling the organic and inorganic compounds present in the bleaching filtrates to the recovery area, which would ultimately result in better economics. To save caustic soda, oxidized white liquor was used as a source of alkali for the O and EO stages. The vent gas leaving the ozone stages is rich in oxygen and can be used after ozone destruction in other mill applications, such as reinforced caustic extraction and white liquor oxidation. However, fresh oxygen is a preferred option for oxygen delignification [2,3,16]. The TCF bleaching mass balance showed that the oxygen content in the vent gas from ozone stages is enough to meet the oxygen demand for reinforced caustic extraction in (ZEO) stages and white liquor oxidation. Fresh oxygen was used for ozone generators and for oxygen delignification.

Three scenarios were evaluated for the TCF sequence. A TCF scenario (TCF 1) considers that all the bleaching filtrate coming from the $(ZEO)_1$ stage is recycled back to oxygen stages and brownstock washing. However, the high concentration of organic and inorganic compounds in the filtrate may cause a reduction of the delignification efficiency in the oxygen stages. To address this situation, two additional scenarios were evaluated. Scenarios TCF 2 and TCF 3 consider that a fraction of the filtrate (25% and 50%, respectively) is purged before the oxygen stages. The purged fraction of filtrate is replaced by fresh water.

After collecting process simulation data (i.e., mass and energy balance), capital investment and operating costs were calculated and a financial analysis was developed according to the financial assumptions presented in **Table II**. Capital investment was calculated using data collected from previous research projects executed at the Forest Biomaterials Department at North Carolina State University. Operating costs were calculated using prices and costs collected from a cost benchmarking software that is commonly used by the pulp and paper industry (Fisher Solve, Fisher International; South Norwalk, CT, USA). A sensitivity analysis was performed to evaluate the economic impact on internal rate of return (IRR) when the costs of chemicals (i.e., magnesium sulfate, sulfuric acid, sodium hydroxide, hydrogen peroxide, sodium sulfate, lime, sodium chlorate, methanol) and electrical price were varied. In addition, probabilistic analysis was performed using a specialized software (@Risk, Palisade Corporation; Ithaca, NY, USA) to aid understanding about the financial risks associated with the variability of the cost and revenue drivers. During the probabilistic analysis, the uncertainties of each economic driver are represented by a best-fit probability density function created from the available market data [17] or using data collected from the Fisher Solve software. The real value of each cost and revenue driver was adjusted to 2015 U.S. dollars using the respective producer price index [18] and inflation. The specialized software continuously samples the probability functions and continuously records the financial output (IRR). This approach allows the evaluation of the financial

Financial Assumptions	Values
Pulp selling price, US$/a.d. metric ton*	682.23
Operation, h/year	8400
Startup year	2015
Terminal year	2030
Capital spending year -3	5%
Capital spending year -2	15%
Capital spending year -1	30%
Capital spending year -0	50%
Annual increase in RAV**	2%
Annual inflation	2%
Capital investment in maintenance, % RAV	1%
Depreciation, years	15
Nominal capacity at year 1	90%
Nominal capacity at year 2	100%
Working capital, % (direct costs + revenue)	10%
Other fixed costs and overhead, % revenue	10%
Maintenance, % of RAV	2%
Tax	35%
Terminal value, multiple of EBITDA*** in year 15	5

* RISI list price, CIF Latin America. Price is adjusted by inflation.
** RAV = replacement asset value.
*** EBITDA = Earnings before interest, tax, and depreciation.

II. Financial assumptions for economic analyses.

impact associated with the variability of each input and provides a probability distribution for IRR.

RESULTS AND DISCUSSION

Chemical usage and liquid effluent

The TCF case requires 62% more magnesium sulfate to minimize viscosity losses that occur during the reinforced caustic extraction portions in the (ZEO) stages and 10% more hydrogen peroxide to achieve the same brightness when compared with the ECF scenario.

The TCF scenario requires 23% less sodium sulfate than the ECF scenario to account for the sulfur losses in the process. Because TCF bleaching filtrates are recycled to a chemical recovery area, the sulfate that is introduced for acidification of pulp (as sulfuric acid) for the ozone stages decreases the demand for sodium sulfate makeup. However, the ECF scenario is self-sufficient in sodium sulfate. A fraction of the sodium sulfate produced in the chlorine dioxide plant as a byproduct is consumed internally as makeup to account for the sulfur losses. Excess sodium sulfate is sold in the market, which represents additional revenue. On the other hand, all the sodium sulfate consumed in the TCF scenario has to be purchased, which represents an additional cost source.

The TCF case requires 17% less sulfuric acid than the ECF case. Although the consumption of sulfuric acid in TCF bleaching stages (12.9 kg H_2SO_4/o.d. metric ton of pulp) is higher than in ECF bleaching stages (7.0 kg H_2SO_4/o.d. metric ton of pulp), the chlorine dioxide plant consumes a considerable amount of sulfuric acid (8.5 kg H_2SO_4 /o.d. metric ton of pulp). Consumption of sodium hydroxide and lime are similar for both cases.

Liquid effluent discharged from ECF bleaching area is about 10.5–11.5 m^3/a.d. metric ton of pulp. On the other hand, the liquid effluent discharge from TCF bleaching area (4.5–5.5 m^3/a.d. metric ton of pulp) is around 55% lower than the ECF case. If we consider that the total liquid effluent from a modern bleached kraft pulp mill based on ECF bleaching is approximately 20 m^3/a.d. metric ton of pulp [8], then the TCF process would generate 30% less liquid effluent, which could represent savings in capital and operating costs (i.e., chemicals and energy).

Steam and power balances

As expected, the recycle of washing filtrate from P, $(ZEO)_1$, and $(ZEO)_2$ stages to the recovery system increases the recycle of dissolved organics by 0.5% in the case of TCF bleaching. However, TCF black liquor carries 12.5% more inorganic compounds, which reduces black liquor heating value. As a result, the production of steam from black liquor is similar for both cases (TCF = 5.23 metric tons steam/a.d. metric ton of pulp; ECF = 5.27 metric tons steam/a.d. metric ton of pulp).

Because of washing filtrate recirculation and lower bleaching temperature profile, the consumption of steam in TCF bleaching stages (0.28 metric ton steam/a.d. metric ton of pulp) is lower than in ECF stages (0.38 metric ton steam/a.d. metric ton of pulp). As a result, total steam consumption is 4.66 metric tons steam/a.d. metric ton pulp for the ECF case and 4.52 metric tons steam/a.d. metric ton of pulp for the TCF case.

Power production for the TCF case (750 kW•h/a.d. metric ton pulp) is higher than the ECF case (742 kW•h/a.d. metric ton of pulp) because of lower process steam consumption. However, the TCF scenario consumes more electricity (627 kW•h/a.d. metric ton of pulp), which is due to ozone production (10 kW•h/kg ozone), ozone off-gas recompression (0.3 kW•h/kg O_2), higher oxygen production (0.40 kW•h/kg O_2), and ozone mixers (8 kW•h/a.d. metric ton of pulp). On the other hand, total electricity consumption for the ECF scenario is 552 kW•h/a.d. metric ton of pulp, which is due to lower power consumption with chlorine dioxide production (0.30 kW•h/kg ClO_2) and chlorine dioxide mixers (2 kW•h/a.d. metric ton of pulp), and lower consumption of oxygen. As a result, the TCF case produces 123 kW•h/a.d. metric ton of pulp as surplus power, whereas the ECF case produces 190 kW•h/a.d. metric ton of pulp.

Process Area	Capital Investment, millions US$	
	ECF Bleached Pulp Mill	TCF Bleached Pulp Mill
Bleach plant	79	90
Chlorine dioxide plant	18	—
Ozone plant	—	21
Oxygen plant	6	10
Other areas	1,378	1,380
Total	1,482	1,502

III. Capital investment, 1,000,000 a.d. metric tons/year (values in million US$).

Capital investment

An early stage capital investment was estimated for all pulp mill areas, including infrastructure (i.e., land, roads, offices, water, and effluent treatment), wood and chip system, fiberline, oxygen delignification, bleaching, pulp dryer, evaporators and concentrators, recausticizing, lime kiln, recovery boiler, hog fuel boiler, power plant, chlorine dioxide plant (R8 process [ECF]), ozone production and destruction (TCF), ozone off-gas recompression (TCF), and oxygen plant. The estimated capital investment for ECF (US$1.482 million) and TCF mill (US$1.502 million) are similar (**Table III**). The TCF mill consumes more oxygen, resulting in higher capital for the oxygen plant. The bleaching area is more expensive for the TCF mill because of longer residence time for bleaching, which results in higher capital for bleaching towers, and

Material/Cost	Elemental Chlorine Free (ECF)	Totally Chlorine Free (TCF) 1*	Totally Chlorine Free (TCF) 2**	Totally Chlorine Free (TCF) 3***
	Direct Costs, US$/a.d. metric ton of pulp			
Eucalyptus	164.14	164.16	164.16	164.16
Magnesium sulfate	3.23	5.24	5.24	5.24
Sulfuric acid	1.40	1.15	1.15	1.15
Sodium hydroxide	15.96	16.49	17.58	19.07
Hydrogen peroxide	3.89	4.27	4.27	4.27
Sodium sulfate	-0.57	0.38	0.73	1.08
Lime	4.05	4.13	4.09	4.06
Sodium chlorate	7.70	–	–	–
Methanol	0.74	–	–	–
Natural gas	11.25	11.47	11.38	11.29
Electricity	-14.86	-9.62	-9.67	-9.63
Finishing materials	3.31	3.31	3.31	3.31
Freight	33.07	33.07	33.07	33.07
Total Direct Costs	**233.31**	**234.05**	**235.29**	**237.09**
	Indirect Costs, US$/a.d. metric ton of pulp			
Labor	8.25	8.25	8.25	8.25
Operating materials	12.86	12.86	12.86	12.86
Maintenance	32.93	33.37	33.45	33.45
Depreciation	109.75	111.24	111.51	111.50
Other fixed cost + Overhead	68.22	68.22	68.22	68.22
Total Indirect Costs	**232.00**	**233.93**	**234.28**	**234.28**
Total Costs	**465.31**	**467.99**	**469.57**	**471.37**
Internal Rate of Return, %	**16.51**	**16.47**	**16.37**	**16.28**

* TCF 1 = 100% bleaching filtrate recycled from first ZEO stage to oxygen stages.
** TCF 2 = 75% bleaching filtrate recycled from first ZEO stage to oxygen stages.
*** TCF 3 = 50% bleaching filtrate recycled from first ZEO stage to oxygen stages.

IV. Operating costs and internal rate of return.

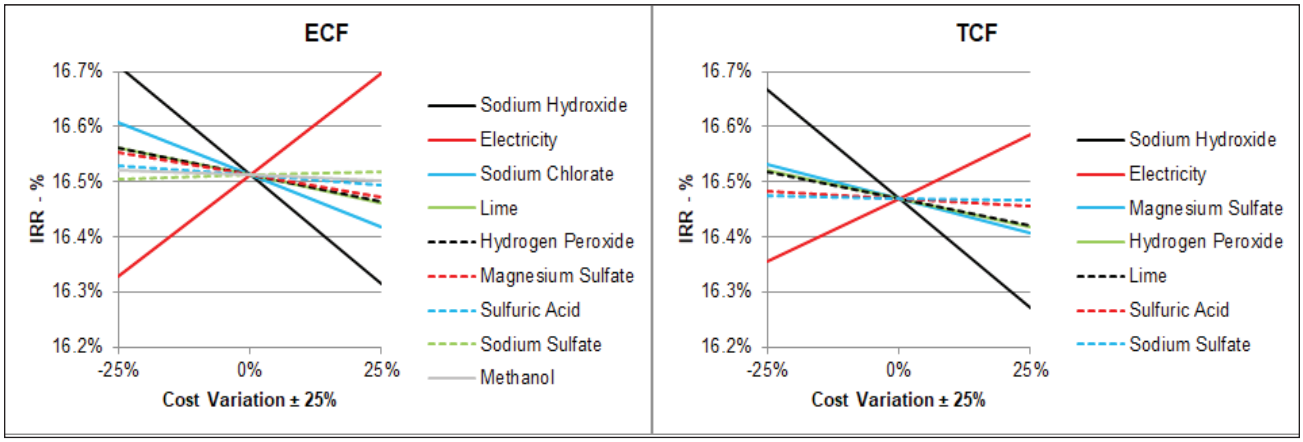
more expensive ozone mixers when compared with chlorine dioxide mixers. Mass and energy balances performed for the other process areas did not show significant differences (< 2%) between the ECF and TCF cases that could justify differences in capital investment. Although the partial closure of TCF bleaching is capable of reducing effluent emissions, no differences in capital or operating costs for effluent treatment were considered in this analysis.

Operating costs and IRR

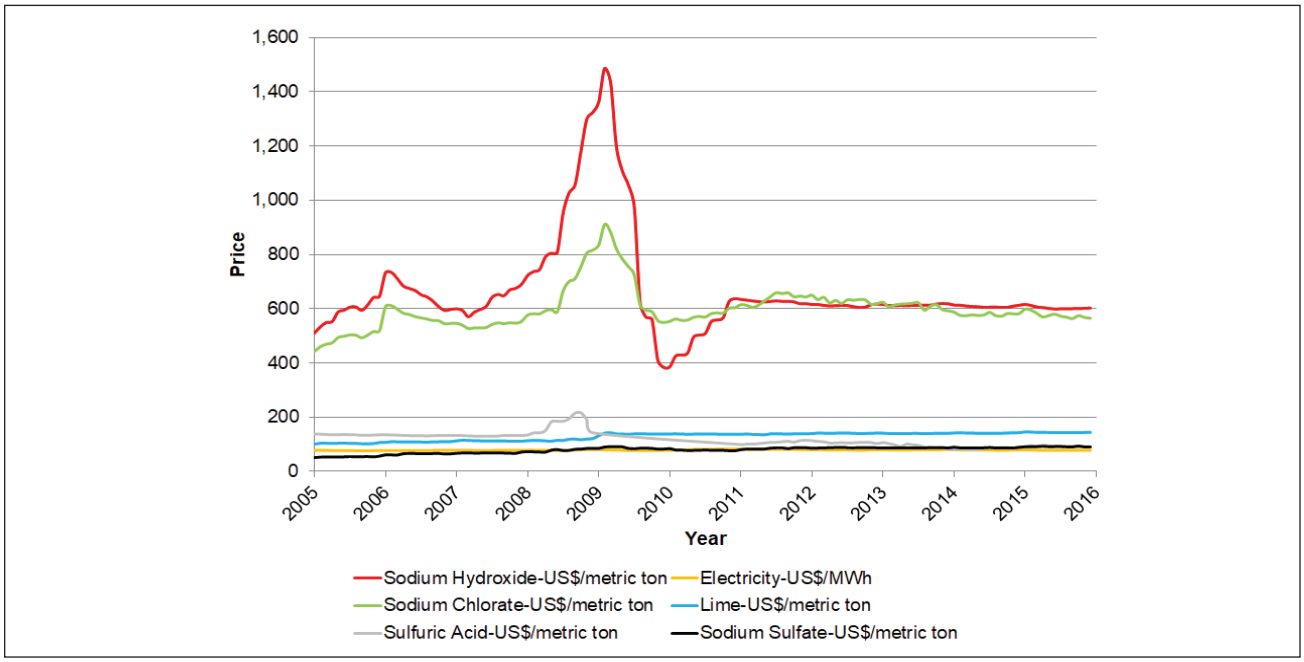
Despite the savings with methanol and sodium chlorate, and the lower consumption of steam, the TCF plant consumes more power, consumes more magnesium sulfate, and sells less surplus electrical power to the grid. Consequently, direct costs for both cases are similar (**Table IV**). Although a more rigorous and detailed capital investment estimation for bleaching areas, chlorine dioxide plant, ozone plant, and effluent treatment could result in a more precise comparison between both cases, the results presented here, based on early stage techno-economic analysis, show that the economic performance of both alternatives are similar.

Impact of bleaching filtrate purge on TCF scenarios

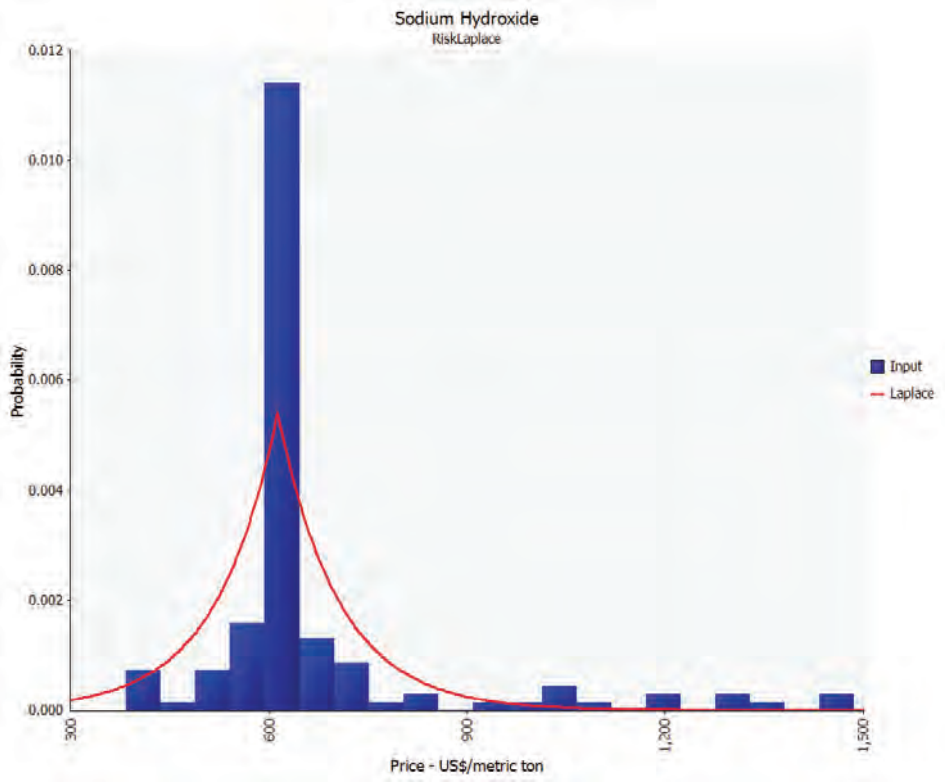
The impact of filtrate purge on TCF scenarios is presented in Table IV. As expected, the increase of filtrate purge (TCF 1, TCF 2, and TCF 3) decreases the recovery of sodium and sulfur, which results in higher consumption of sodium hydroxide and sodium sulfate to replace chemical losses. In a similar trend, the lower recovery of chemicals slightly reduces the calcium oxide makeup and the consumption of natural gas in the lime kiln. Steam and power balances do not change significantly. Hence, the operating costs increase around US$3.00/a.d. metric ton of pulp when up to 50% of the washing filtrate is purged for the TCF cases.

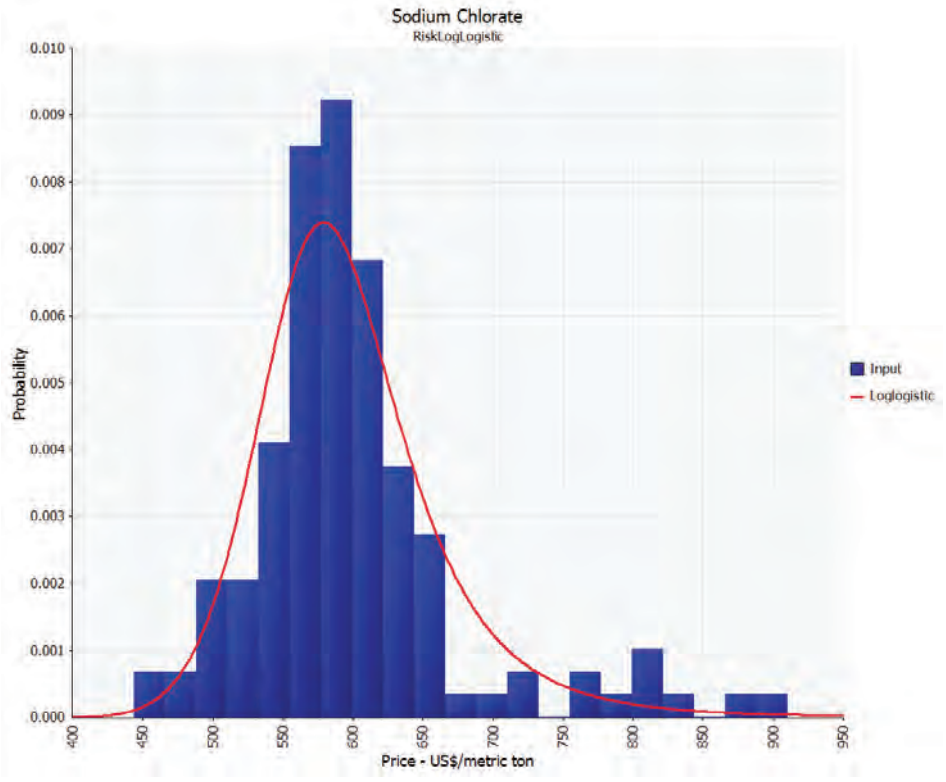


4. Sensitivity analysis spider plot.

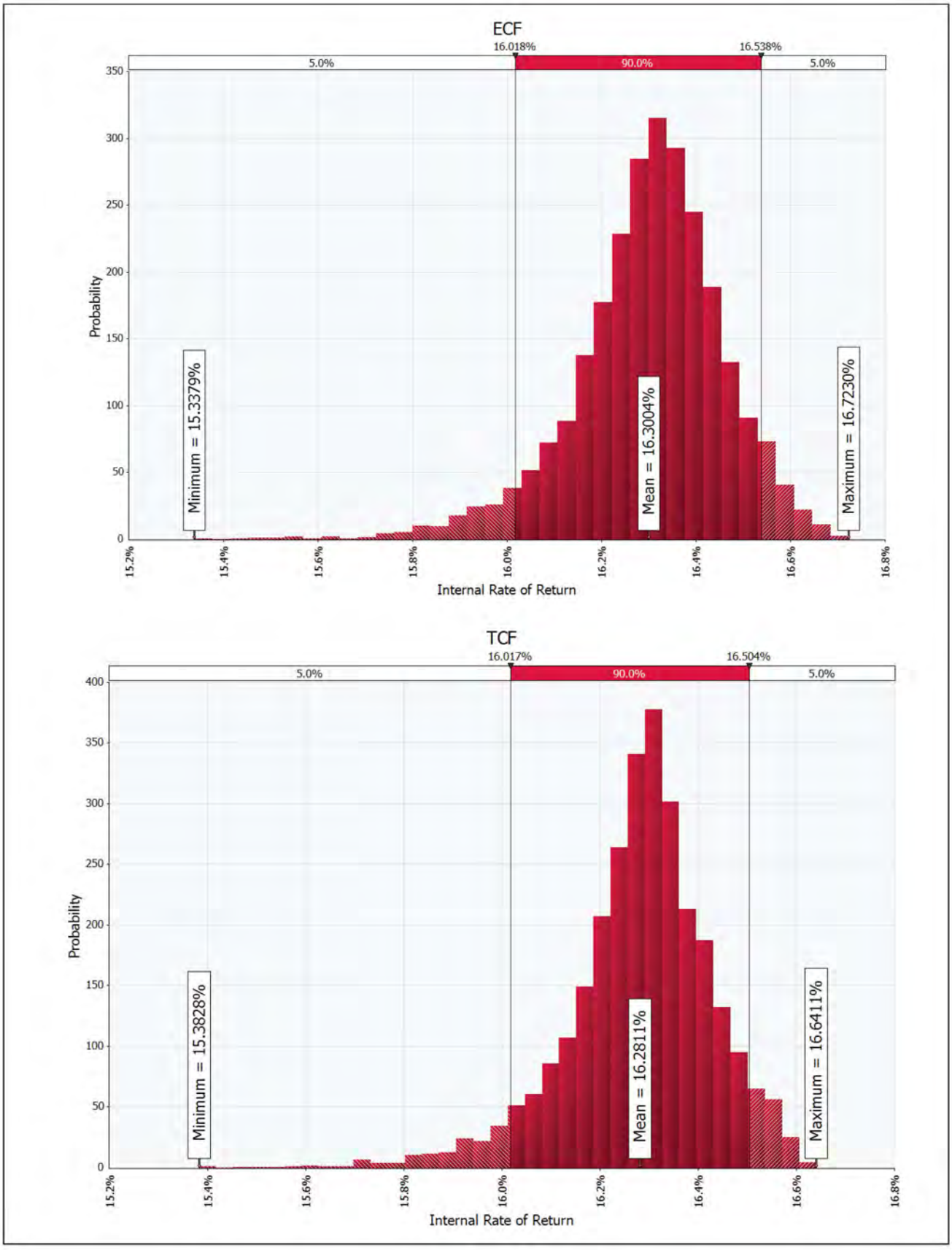


5. Real value of chemical and electricity prices in 2015 (US$).

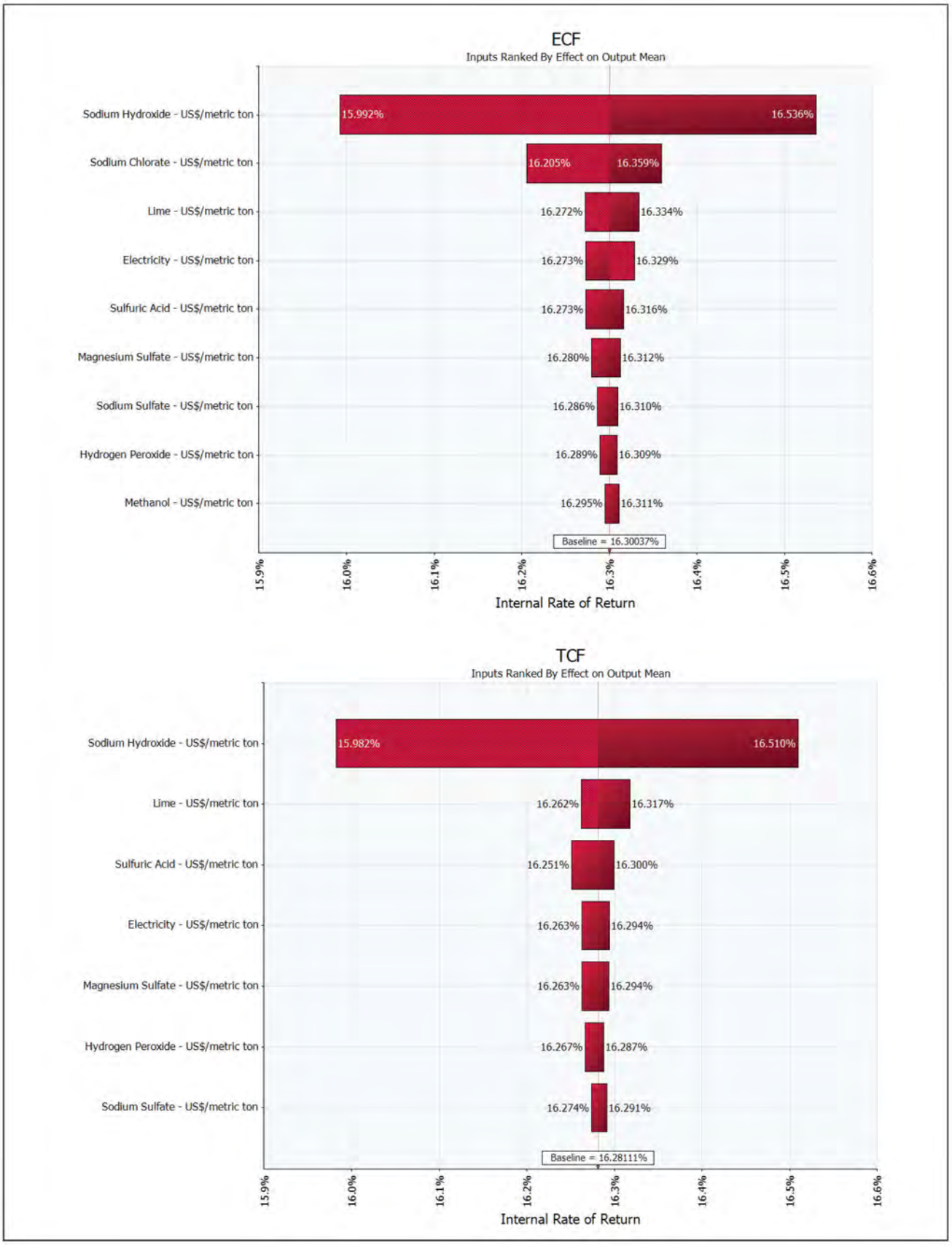




6. Probability density functions for sodium hydroxide and sodium chlorate. Blue bars represent real data. Red curve represents a best fit for the real data.



7. Probability distribution for internal rate of return.



8. Sensitivity analysis tornado plot showing the effect of inputs volatility on internal rate of return.

Sensitivity and probabilistic analyses

Sensitivity analyses were performed for ECF and TCF scenarios where cost and revenue drivers were arbitrarily varied by ± 25% (**Fig. 4**). IRR is more sensitive to variations in the costs and prices of sodium hydroxide, electricity, and sodium chlorate. Variations of other chemicals have a lower impact on IRR.

The previous results have compared both cases via techno-economic assessment on the basis of deterministic analysis, where actual or average values for the inputs (e.g., price of wood, chemicals, electricity, and pulp) are introduced in the financial model, resulting in a single value for the output (e.g., IRR). However, the volatility of economic inputs (**Fig. 5**) and its impact on the economics cannot be assessed by deterministic analysis. In this context, the @Risk software program is capable of performing probabilistic analyses by transforming the historical data presented in Fig. 5 into probability density functions (**Fig. 6**). At each iteration, the financial software program samples the probability density functions and records the financial output (IRR) to build a probability distribution (**Fig. 7**). Figure 7 shows that the volatility of chemical and electricity prices results in an IRR variation of 1.5% for both cases. Moreover, sensitivity analyses presented in **Fig. 8** show that the volatility of sodium hydroxide and sodium chlorate prices have the highest impact on the probability distribution of IRR for the ECF case. On the other hand, TCF does not use any chlorine-containing oxidants and is not affected by sodium chlorate volatility, which minimizes the risks associated with this chemical agent. The volatility of the electrical price did not show a significant impact on the probability distribution of IRR for both ECF and TCF cases (Fig. 8), which is related to the relatively stable electricity price (Fig. 5) for the period considered in the analyses. Although the sensitivity analyses performed under a deterministic approach (Fig. 4) showed that IRR is sensitive to variations in the sequence and evaluate the impact of filtrate recycle on process performance (i.e., chemical consumption, pulp properties, and deposits).

ABOUT THE AUTHORS


de Assis


Jameel


Gonzalez


Phillips


Kirkman


Perrin


Lachenal

The objective of this work was to compare techno-economic performance between a traditional elemental chlorine free (ECF) bleaching sequence and a new totally chlorine free (TCF) bleaching sequence. Literature from the 1990s shows that ECF pulp has better properties and economics. However, as TCF technology, chemistry, and pulp properties have improved through the years, it was of interest to reevaluate the economic performance of ECF and TCF processes.

Techno-economic analysis for the TCF sequence was performed using data obtained from laboratory experiments where clean water is used to wash the pulp. Therefore, we cannot anticipate how the processed TCF sequence would perform in an industrial scale considering partial closure of the bleach plant as we propose in the paper. To address this, we evaluated scenarios where a fraction of the recycled filtrate is replaced by clean water.

This type of research teaches a lot about how a kraft process is a sensitive and integrated process. Any changes in any part of the recovery loop has be to evaluated carefully because those changes may or may not have an impact on other process areas and pulp properties.

Techno-economic analysis shows that the processed TCF sequence has the potential to produce pulp with similar costs and properties as ECF bleaching. Mills might consider the proposed TCF sequence as an alternative for bleached pulp manufacturing.

The next step would be to perform more experimental work (laboratory and pilot scale) to optimize

de Assis is a doctoral student, Jameel and Gonzalez are professors, Phillips is professor emeritus, and Kirkman is academic dean in the College of Natural Resources, Department of Forest Biomaterials, North Carolina State University, Raleigh, NC, USA. Perrin is a postdoctoral student at Aalto University Department of Forest Products Technology, Aalto, Finland. Lachenal is a professor at Grenoble INP-Pagora, Laboratory of Pulp and Paper Science and Graphic Arts, Saint-Martin d'Hères, France. Email Jameel at jameel@ncsu.edu.

electricity price, the small volatility of electricity prices (Fig. 5) does not contribute significantly to the probability distribution of the IRR (Fig. 8).

CONCLUSIONS

Techno-economic analyses showed that the new TCF sequence studied by Perrin et al. [10], capable of producing bleached pulp with similar properties as ECF pulp, presented similar IRR when compared with a traditional ECF bleaching sequence (ECF IRR = 16.5%; TCF IRR = 16.4%). Despite the savings with methanol and sodium chlorate, and lower consumption of steam, the TCF plant consumes more power, consumes more magnesium sulfate, and sells less surplus electrical power to the grid. As a result, operating costs for both cases are very similar (ECF = US$465/a.d. metric ton; TCF = US$468/a.d. metric ton). The partial recycle of TCF bleaching filtrates considerably decreased the liquid effluent emission when compared with the ECF case.

Sensitivity analyses showed that IRR is more sensitive to sodium hydroxide, electricity, and sodium chlorate prices among all cost and revenue drivers evaluated (chemical costs and electrical price). Moreover, the volatility of bleaching chemicals was assessed by probabilistic analyses, which showed that sodium hydroxide and sodium chlorate have a significant impact on the probability distribution of IRR for the ECF case. However, TCF bleaching does not rely on any chlorine source, which minimizes the risk associated with sodium chlorate.

Despite the promising results, the competitiveness presented by the TCF sequence has to be interpreted with caution. The presented work is based on early stage techno-economic analyses and additional detailed analyses are necessary to confirm the results. The TCF sequence was only tested in laboratory scale and further scaleup has to be performed to prove the technology, stable operation, and product specification. However, the early stage techno-economic analyses showed that the new TCF sequence has promising potential, which deserves additional research and investigation as a viable alternative bleaching process. **TJ**

ACKNOWLEDGMENTS

Financial support for this work was provided by the Brazil Scientific Mobility Program (CAPES Scholarship: process number 88888.075726/2013-00). This work was a joint project by the Department of Forest Biomaterials at North Carolina State University in Raleigh, NC, USA, and the Laboratory of Pulp and Paper Science and Graphic Arts at Grenoble INP-Pagora in Saint-Martin d'Hères, France.

LITERATURE CITED

1. Lancaster, L.M., Renard, J.J., Yin, C., et al., "The effects of alternative pulping and bleaching processes on product performance—economic and environmental concerns," *Proceedings: International Symposium on Pollution Prevention in the Manufacture of Pulp and Paper—Opportunities & Barriers*, U.S. Environmental Protection Agency, Washington, DC, 1992, pp. 194-205.
2. Homer, G. and Govers, T., "Ozone-based ECF and TCF bleaching: mill experience, laboratory data, and cost considerations," *Pulping Conf.*, TAPPI Press, Atlanta, 1994.
3. Brooks, T.R., Edwards, L.L., Nepote, J.C., et al., *TAPPI J.* 77(11): 83(1994).
4. Parthasarathy, V.R., "Is extended cooking necessary for the closure of bleach plant?—a strategic shift in pulping and bleaching," *Pulping Conf.*, TAPPI Press, Atlanta, 1997.
5. Albert, R.J., *Pulp Pap.* 68(7): 83(1994).
6. Brunner, F.L. and Pulliam, T.L., *Tappi J.* 76(7): 65(1993).
7. Alliance for Environmental Technology, "TCF and ECF: separating fact from fiction—is retrofitting to TCF manufacture cost-effective?" Alliance for Environmental Technology (AET), Orangeville, ON, Canada. Available [Online] http://www.aet.org/reports/technical/fact2.html <06Oct2017>.
8. Suhr, M., Klein, G., Kourti, I., et al., in *Best Available Techniques (BAT) Reference Document for the Production of Pulp, Paper and Board*, Joint Research Centre–Institute for Prospective Technological Studies (JRC-IPTS), European Commission, Seville, Spain, 2015, pp. 195-368.
9. Maples, G.E., Ambady, R., Caron, J.R., et al., *TAPPI J.* 77(11): 71(1994).
10. Perrin, J., Pouyet, F., and Lachenal, D., "Totally chlorine-free bleaching sequences for paper and dissolving eucalypt pulps," *7th International Colloquium on Eucalyptus Pulp*, ABTCP, Sao Paulo, SP, Brazil, 2015.
11. Metais, A., Germer, E., and Hostachy, J.C., "Achievements in industrial ozone bleaching," *Int. Pulp Bleaching Conf.*, TAPPI Press, Atlanta, 2011.
12. Germer, E., Métais, A., and van Wyk, B., "Standard bleaching sequences with modern ozone technology," *PEERS Conf.*, TAPPI Press, Atlanta, 2016.
13. Ragnar, M., Eriksson, T., and Reitberger, T., *Holzforschung* 53(3): 292(1999).
14. Pouyet, F., Chirat, C., and Lachenal, D., *BioResources* 8(4): 5289(2013).
15. Bryntesson, H., Dahllof, H., Petterson, E.A., et al., "New compact technology for washing of chemical pulp," *African Pulp and Paper Week Conf. Proc.*, Technical Association of Pulp and Paper Industry of South Africa (TAPPSA), Durban, 2002. Available [Online] http://www.tappsa.co.za/archive/APPW2002/Title/New_compact_technology_for_was/new_compact_technology_for_was.html <24Oct2017>.
16. Homer, G., Epiney, M., Johnson, S., et al., "High yield cooking, oxygen delignification and ozone for high yield bleached pulp," *Pulping Conf.*, TAPPI Press, Atlanta, 1997.
17. ICIS, "Indicative Chemical Prices A-Z," *Chemical Market Reporter*, 28 August 2006. Available [Online] https://www.icis.com/chemicals/channel-info-chemicals-a-z/ <24Oct2017>.
18. Bureau of Labor Statistics, Producer price index, U.S. Department of Labor, Washington, DC, 2017. Available [Online] https://data.bls.gov/timeseries/WPU06130213?include_graphs=false&output_type=column&years_option=all_years <24Oct2017>.

Formation mechanisms of "jellyroll" smelt in kraft recovery boilers

HONGHI TRAN AND ANDREW K. JONES

ABSTRACT: Molten smelt normally flows smoothly down the smelt spout of a recovery boiler like water, but at times it suddenly becomes sluggish and forms a viscous blob on the spout trough that partially or completely blocks the smelt flow. This form of smelt is commonly referred to as "*jellyroll*" smelt. How such smelt forms has been a puzzle to boiler operators and mill personnel for years. Numerous mill observations and the results of a recent study performed on both smoothly flowing smelt and jellyroll smelt collected from a recovery boiler suggest that that jellyroll smelt can form through three main mechanisms: i) the freezing of the molten smelt, ii) the melting of fallen deposits, and iii) the inclusion of a large amount of unburned char in the molten smelt. These mechanisms are consistent with mill experience that jellyroll smelt tends to form in older recovery boilers burning liquor with low solids and low sulfidity.

Application: This paper discusses three mechanisms through which jellyroll smelt forms and provides operating strategies for minimizing jellyroll smelt formation.

In recovery boiler operation, maintaining a steady flow of molten smelt from smelt spouts is critically important for ensuring a safe operation of the dissolving tank and a steady flow of green liquor. Smelt spout openings need to be periodically cleaned, as they are often clogged by unburned char and frozen smelt if left unattended. Some boilers experience smelt clogging more often than others for no apparent reasons. In some cases, smoothly flowing smelt suddenly becomes sluggish and forms a viscous blob on the spout trough, partially or completely blocking the smelt flow (**Fig. 1**).

This type of smelt is commonly referred to as "*jellyroll*" smelt. The name arises presumably from the appearance of the smelt since it resembles the jelly in a jelly roll cake. Jellyroll smelt is lumpy and viscous and may block the spout openings. Spout blockage often allows a large pool of molten smelt to accumulate behind it, making spout cleaning a dangerous task for boiler operators. As the molten smelt pool becomes larger, deeper, and heavier, it can push the clogged smelt away, resulting in a massive amount of molten smelt pouring into the dissolving tank. Such heavy smelt run-offs have been known to cause violent smelt-water explosions, damages to the dissolving tank, and in severe cases, operator fatality [1-3].

How jellyroll smelt forms is not well understood. Poor combustion, low furnace temperature, low liquor sulfidity, and deposits fallen from waterwalls/upper furnace tubes have often been claimed to play a role in jellyroll smelt formation, but no good explanations have been offered to support the claims. The creeping motion of jellyroll smelt on spout troughs suggests that jellyroll smelt is much more viscous than fluid smelt and cannot be shattered readily into pieces by a steam jet. Whatever the mechanism by which jellyroll smelt is formed, it must explain what makes a smoothly flowing molten smelt suddenly become sluggish and stop flowing.

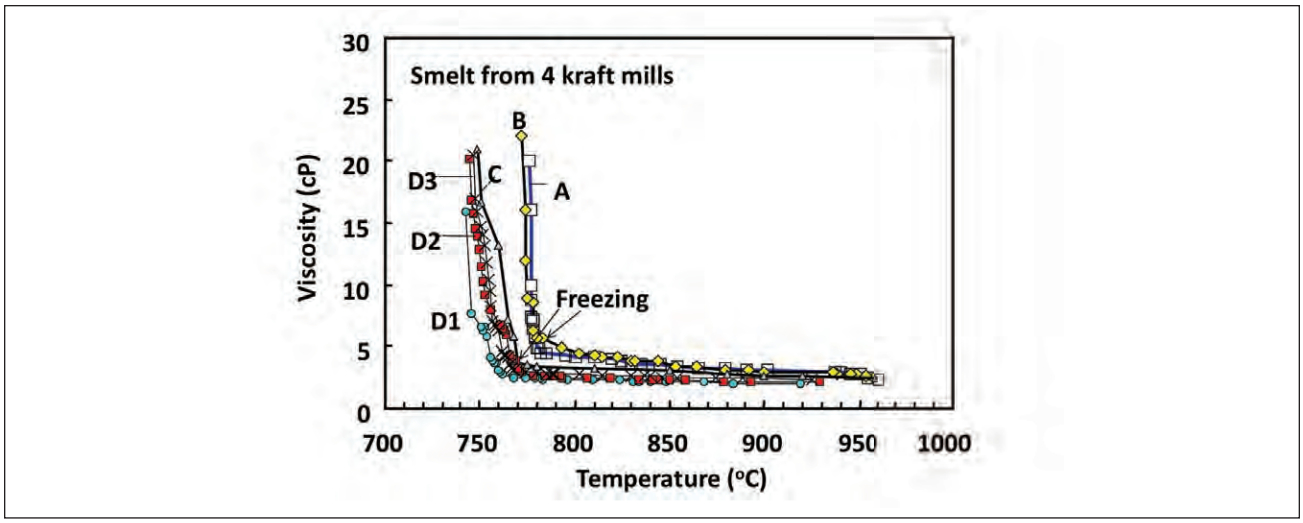


1. A jellyroll smelt blob "sitting" on a spout trough.

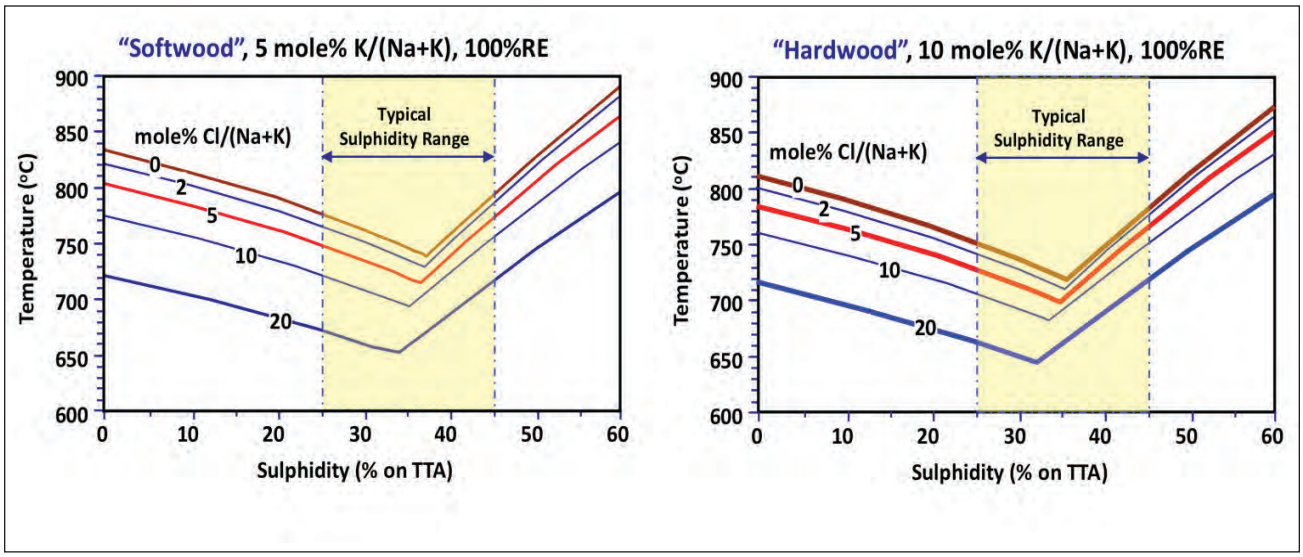
In this paper, we will first examine the key factors that make fluid smelt less fluid, and how the smelt fluidity is affected by smelt composition and lower furnace conditions. We will then propose possible mechanisms for jellyroll smelt to form and practical strategies for minimizing the problem.

FLUIDITY OF MOLTEN SMELT

Smelt consists of 60–70 wt% sodium carbonate (Na_2CO_3), 20–30 wt% sodium sulfide (Na_2S), and small amounts of sodium sulfate (Na_2SO_4), sodium chloride (NaCl), potassium



2. Effect of smelt freezing temperature on viscosity [4].



3. Effects of liquor sulfidity and chloride content on smelt freezing temperatures of softwood smelt (upper) and hardwood smelt (lower).

salts, and char, and it has a freezing temperature between 740°C and 780°C. At its typical operating temperature of 820°C to 830°C in the boiler, the smelt must be completely molten.

Figure 2 shows the change in viscosity of 5 smelt samples as they cooled slowly from 960°C (1760°F) in a laboratory setting [4]. In all cases, the viscosity increased only a few centipoises (cP) as the smelt temperature decreased to about 770°C to 780°C (1420°F to 1440°F), and then increased drastically as the temperature decreased further. The abrupt increase in viscosity of each smelt occurred at its freezing temperature. This implies that as long as it is still completely molten, molten smelt has a low viscosity between 2 and 5 cP, which is roughly the same as that of milk (3 cP) at room temperature, but it can become very viscous as it starts to freeze.

The fluidity of a liquid is the ability of that liquid to flow. It is inversely related to the viscosity of the liquid, which in turn, is a function of the liquid composition and temperature. The fluidity drastically decreases when the liquid also contains fine solid particles. Coal-water slurry fuel, clay slip, concrete mix, ice flurry, etc., are all good examples of such solid/liquid mixtures. The higher the solids content, the higher the mixture viscosity is and the poorer the fluidity becomes.

Molten smelt is made of alkali salts. As it cools and reaches its freezing point, one of the salt components precipitates, forming fine solid particles of that component in the melt. As the temperature decreases further, more and more components precipitate, forming a solid mass that continues to grow. As the temperature is below the first melting temperature of the salt mixture, the whole mass becomes solid. The abrupt increase in molten smelt viscosity shown in Fig. 2 is likely caused by the sudden appearance of the solid phase in the melt as it cools below its freezing temperature.

SMELT FREEZING TEMPERATURE

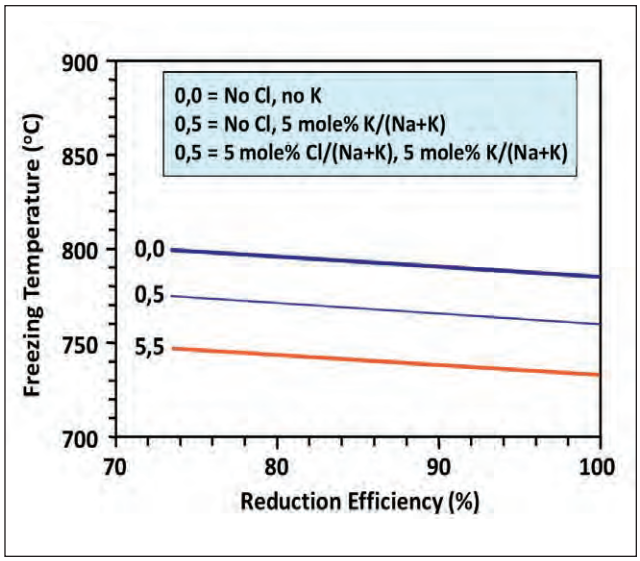
Since freezing plays the key role in the sudden decrease in molten smelt fluidity, it is important to examine how the freezing temperature of molten smelt may be affected by smelt composition. **Figure 3** shows the freezing temperature of molten smelt as a function of smelt sulfidity and chloride content for two levels of potassium (K) content: 5 mole% K/(Na+K) for a typical softwood smelt and 10 mole% K/(Na+K) for a typical hardwood smelt. The freezing temperature data was calculated using FactSage (Thermfact/CRCT Montreal, Canada; GTT-Technologies, Aachen, Germany), a commercially available thermodynamic program. In both cases, the freezing temperature decreases as the sulfidity increases up to 32% to 36% on total active alkali (TTA). Beyond this point, it increases with an increase in sulfidity. At the same sulfidity and chloride content, hardwood smelt has a lower freezing temperature than softwood smelt due to its higher potassium content.

Chloride also has a small effect on smelt freezing temperature. At a given liquor sulfidity and potassium content, a decrease in chloride content from 2 to 5 mole% Cl/(Na+K) in smelt, or from 0.6 to 1.5 wt% in black liquor dry solids, would increase the smelt freezing temperature by 18°C.

A decrease in smelt reduction efficiency is expected to increase the freezing temperature as shown in **Fig. 4**. However, the effect is small. The freezing temperature of a typical softwood smelt with 5 mole% Cl/(Na+K) and 5 mole% K/(Na+K), for example, increases only 12°C as the reduction efficiency decreases from 100% to 75%, or about 0.5°C per every 1% decrease in reduction efficiency. Since the smelt reduction efficiency typically varies between 90% to 94% under normal operating conditions, the difference in freezing temperature may be only 2°C.

JELLYROLL SMELT ANALYSIS

Figure 5 shows a series of images extracted from a video footage of a jellyroll smelt formation episode that occurred during normal recovery boiler operation at Mill A. Prior to the episode, the smelt was fluid, flowing freely down on the spout trough into the dissolving tank beneath. At 00:00 (minutes:seconds), a piece of jellyroll smelt suddenly appeared and occupied the first 20% of the trough length, greatly restricting the smelt flow. As the jellyroll smelt blob edged slowly downward, it grew thicker and longer, occupying 60% of the trough length at 00:10. The remaining 40% of the trough length was still filled with fluid smelt. At 00:20 and 00:25, the jellyroll smelt blob covered the entire trough length, but continued to pour slowly down into the dissolving tank. Bright spots of char burning were clearly visible on the surface of the dark-pink jellyroll smelt. At 00:28, fluid smelt emerged from the furnace, pushing the jellyroll smelt off the trough into the dissolving tank. At 00:30, almost all of the remaining jellyroll smelt was expunged from the trough. At 00:40, the entire trough was covered with fluid smelt and the smelt flow returned to normal. The entire episode occurred in less than 40 s.



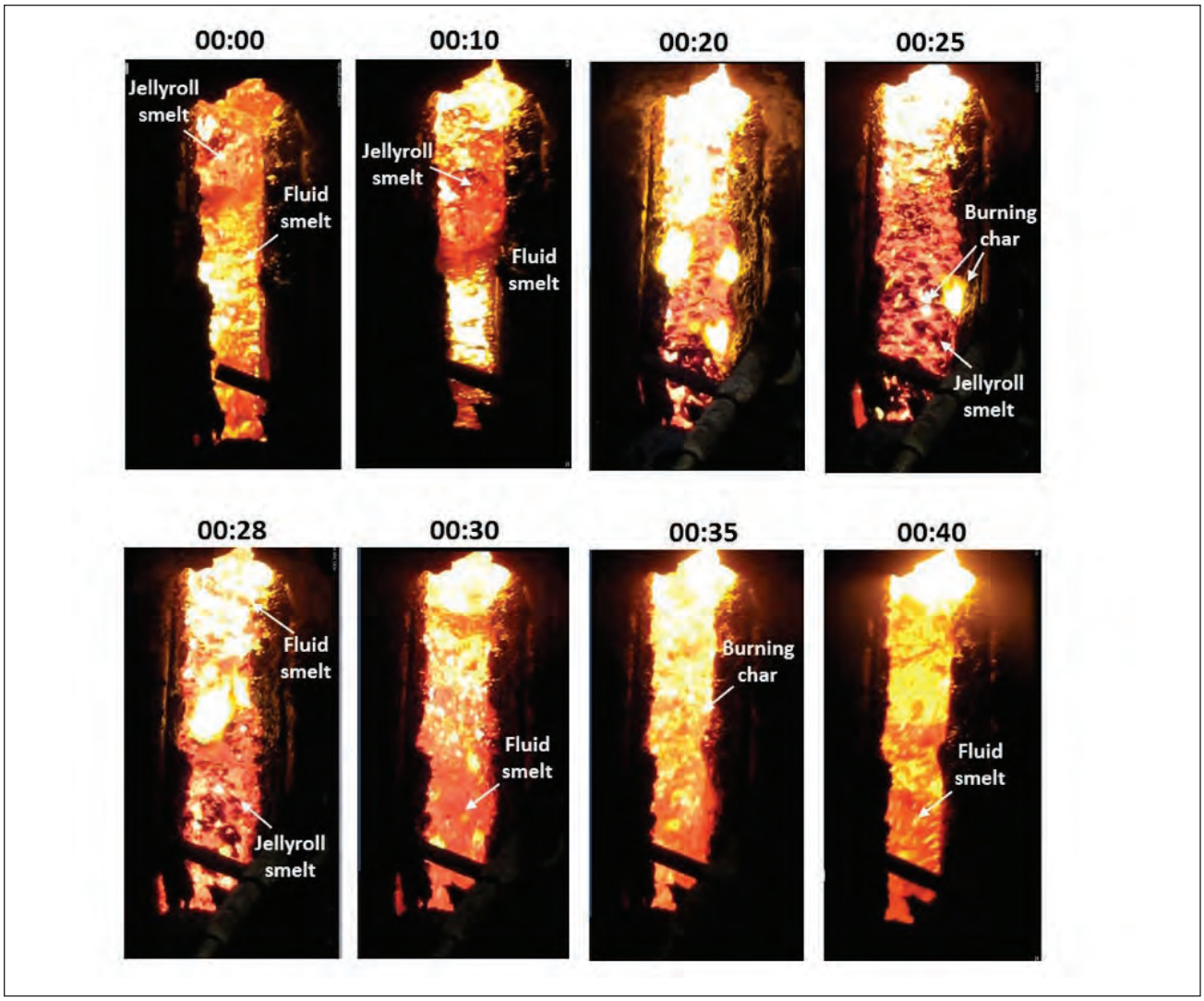
4. Effect of smelt reduction efficiency on the freezing temperature of smelts with different combinations of chloride (Cl) and potassium (K) contents.

Numerous episodes of jellyroll smelt formation occurred on that day. Some were short and over in less than a minute as described previously. Others, however, were much longer. The jellyroll smelt blobs were large and viscous and could not be pushed away by the fluid smelt. The boiler operators were busy that day watching and cleaning smelt spout openings and troughs to ensure safe and stable operation of the dissolving tank.

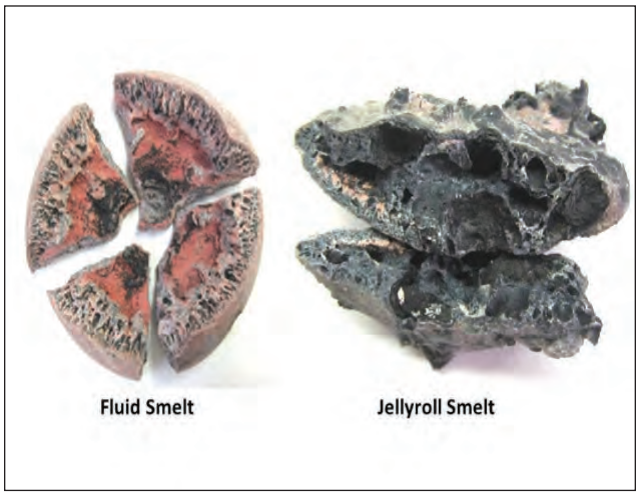
Two smelt samples (one fluid smelt and the other jellyroll smelt) from two adjacent smelt spouts were collected at the same time that day and cooled in two separate galvanized steel buckets. **Figure 6** shows photos of these samples after they were cooled and taken out of the buckets. The fluid smelt was pink, porous, and contained some black char, while the jellyroll smelt was black, porous, and contains pink dots. The pink color was the typical color of smelt, while the black color was that of unburned char. The large pores in the samples were likely formed as a result of gas release during the char burning stage of black liquor combustion.

Chemical and physical analyses

Each smelt sample was dissolved in hot water and the resulting solution was filtered. The filtrate (the water-soluble part of the smelt) was analyzed for Na, K, sulfur (S), sulfate (SO_4), carbonate (CO_3), and chlorine (Cl), which were then used to calculate the reduction efficiency and sulfidity of the smelt. The residue on the filter paper was dried at 105°C for 24 h. The dried residue (the water-insoluble part of the smelt) was essentially a mixture of unburned char and insoluble impurities. It was burned at 80°C to remove the char (carbon). The weight difference of the residue before and after burning was considered to be the char content of the smelt. The bulk density of the residue was also calculated from its weight and volume. The dried residue of the fluid smelt was a brownish



5. A jellyroll smelt formation incident in the recovery boiler at Mill A. Numbers are times in minutes:seconds.

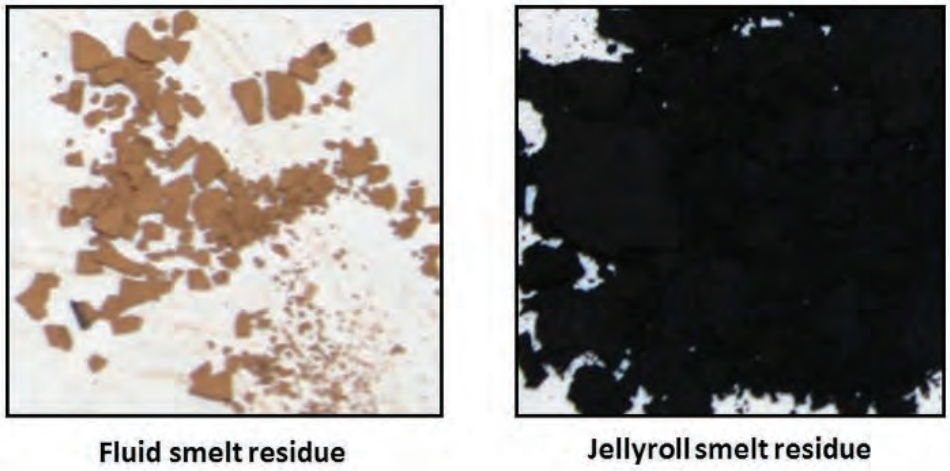


6. Appearance of fluid and jellyroll smelt samples (pink parts are smelt; black parts are char) after being cooled down to room temperature.

fine powder, whereas that of the jellyroll smelt was a black powder, resembling black carbon printer toner (**Fig. 7**).

Table I summarizes the analysis results. Both fluid smelt and jellyroll smelt had almost the same composition, reduction efficiency, and sulfidity. The main difference was that the jellyroll smelt contained roughly 2 wt% residue, nearly 6 times more than the fluid smelt, and 1.4 wt% char, compared to almost no char in the fluid smelt. The bulk density of the char from the jellyroll smelt was low, about 0.06 g/cm^3, suggesting that char was light and highly porous. The bulk density of the char from fluid smelt char could not be determined since the sample obtained was too small to analyze.

Since there is no significant difference in composition (particularly sulfidity and reduction efficiency) between fluid smelt and jellyroll smelt, this jellyroll smelt formation incident cannot be attributed to either sudden smelt freezing or fallen deposits. The key difference between these two smelts is the char content. The jellyroll smelt contained 1.4 wt% char whereas the fluid smelt had very little or no char. It is therefore



7. Appearance of dried residues left on filter papers of fluid smelt and jellyroll smelt solutions.

Color	Fluid Smelt	Jellyroll Smelt
	Pink with black char	Black with pink smelt
Composition		
Na, wt%	43.44	42.49
K, wt%	3.28	3.29
CO_3, wt%	46.11	44.70
S, wt%	6.19	6.07
SO_4, wt%	0.83	1.02
Cl, wt%	0.80	0.83
Total	101.0	100.4
Reduction, %	95.7	94.7
Sulfidity, % on TTA	20.1	20.3
Dried residue color	Light brown	Black
Dried residue, wt%	0.35	1.98
Combustion ash residue, wt%	0.34	0.60
Char content, wt%	0.01	1.38
Char density, g/cm^2	*	0.06

Na = sodium, K = potassium, CO_3 = carbonate, S = sulfur, SO_4 = sulfate, Cl = chlorine.
*Amount too small to measure

I. Analysis summary.

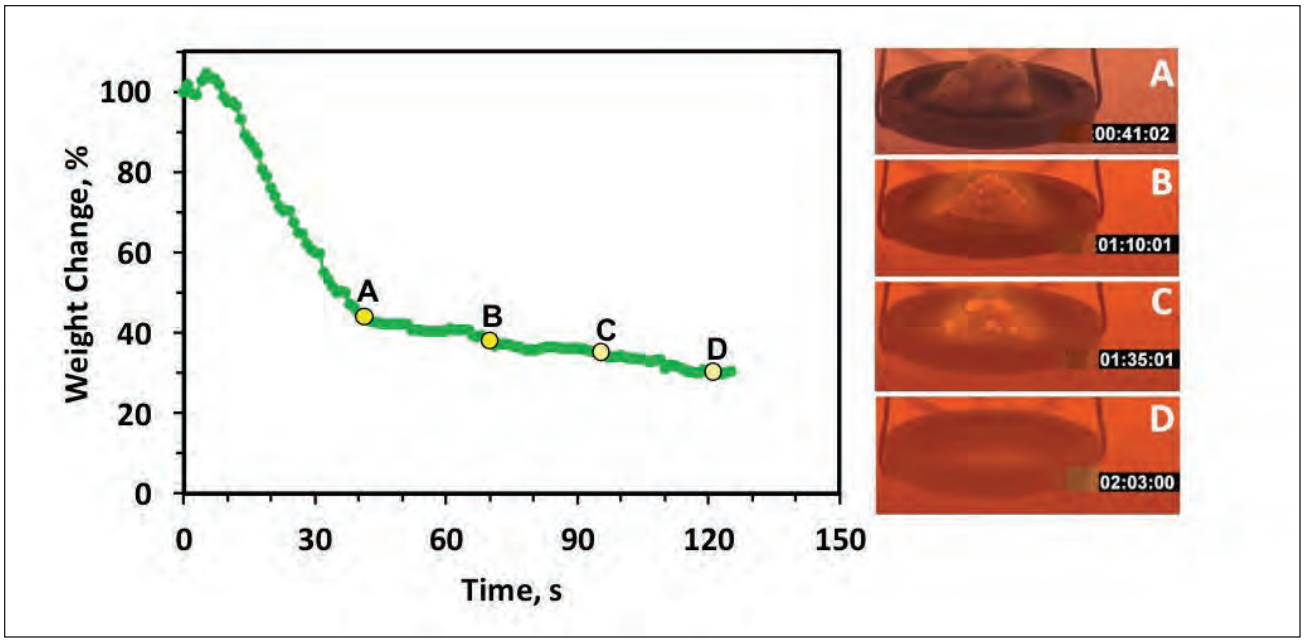
important to examine the property of the black liquor char from Mill A in order to understand how such a small amount of char can possibly turn a fluid smelt into a jellyroll smelt.

CHAR PROPERTY

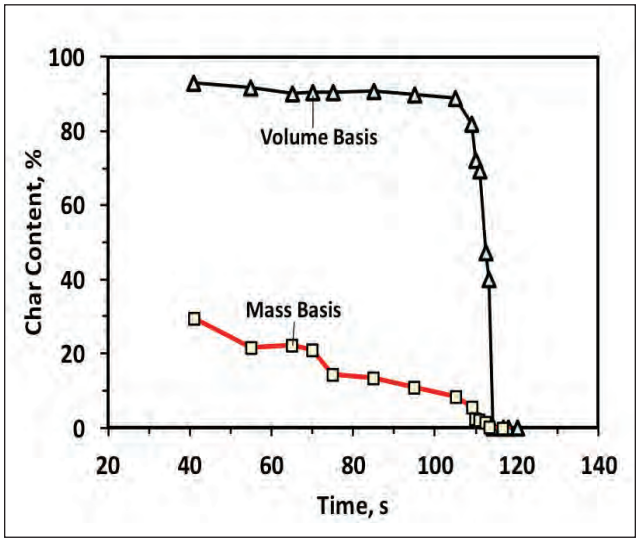
Figure 8 shows the thermogravimetric (TG) profile for a black liquor sample from Mill A collected at the time when the liquor burnability was poor. The test was performed on a 0.3 g black liquor sample with a dry solids content of 70 wt%, while the combustion process was recorded using a video camera. Details of this test method have been described elsewhere [5,6]. Snapshots of the sample during the test at times corresponding to A, B, C and D on the TG curve are also shown. The change in slope of the TG curve and the absence of yellow flame around the sample suggest that the sample started its char burning stage at time A.

The volume of the combustion residue (char and smelt) at any given time can be estimated from the video image at that time. This volume value and the corresponding sample weight obtained from the TG profile enables the calculation of the approximate char content in the combustion residue, on both a volume basis and a mass basis, as shown in **Fig. 9**. On a mass basis, the char content steadily decreased as the char burning proceeded, whereas on a volume basis, the char continued to occupy almost 90% of the total volume of combustion residue until the very end when it almost completely burned off. At time between 110 and 115 s, for example, the char content in the combustion residue was about 1% to 3% on mass, but was much higher, 10% to 70%, on volume.

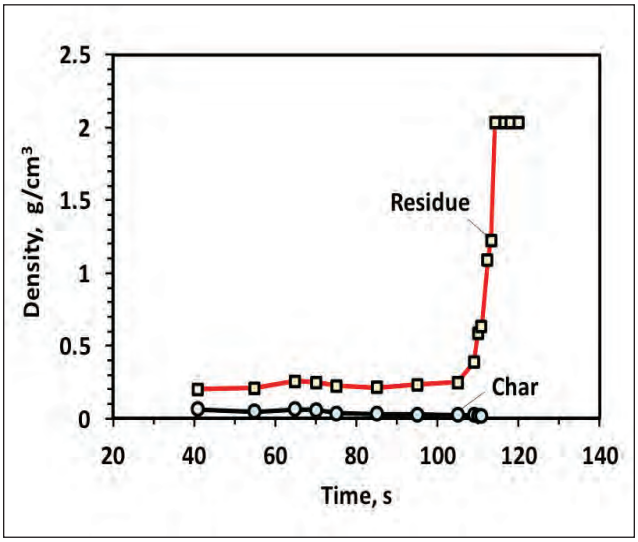
The volume and weight data also enable the calculation of the density of the combustion residue (char and smelt) as well as the density of the char only at a specific time. The results are shown in **Fig. 10**. The char density varied from 0.02 to 0.11 g/cm^3, with an average of about 0.05 g/cm^3,



8. Weight change and appearance of black liquor from Mill A during a combustion test. A: beginning of char burning; B and C: smelt formation during char burning; and D: completion of char burning with only molten smelt remaining on the test tray.



9. Char content of the combustion residue of Mill A black liquor during char burning.



10. Densities of combustion residue and char of Mill A black liquor during char burning.

which is comparable to the actual measurement result shown in Table I. The density of the combustion residue was also fairly constant at 0.3 g/cm³ due to the presence of char, but increased to 2 g/cm³ when all char burned off, leaving behind only molten smelt. This density value is about the same as the density of a typical molten smelt.

JELLY SMELT FORMATION MECHANISMS

Mill experience and the evidence presented suggest that jellyroll smelt can form through three main mechanisms: i) the freezing of molten smelt, ii) the melting of fallen deposits, and iii) the inclusion of a large amount of unburned char in the molten smelt. All these mechanisms can well explain why smoothly flowing molten smelt suddenly becomes sluggish and stops flowing.

Freezing of molten smelt

This mechanism prevails when the smelt temperature (T_{SM}) drops locally below the smelt freezing temperature (T_{FZ}). The difference between these two temperatures (i.e., $\Delta T = T_{SM} - T_{FZ}$) in a recovery boiler is the key parameter that determines the likelihood of jellyroll smelt formation in that boiler.

The smaller the ΔT at which the boiler is operated, the more likely the jellyroll smelt will form.

T_{FZ} is an intrinsic property of molten smelt. As discussed earlier, T_{FZ} is affected mainly by the liquor sulfidity (the sulfide content of the smelt or the sulfur content of the black liquor), and to a much lesser extent, by the chloride and potassium contents and the reduction efficiency of smelt. For a given mill, the liquor sulfidity is often well controlled, and hence, T_{FZ} does not usually change much, except during the first few days of boiler startup after a long mill-wide outage when the sulfidity can be 5% to 10% lower than target. In such a case, T_{FZ} can be 15°C to 30°C higher than normal, resulting in a smaller ΔT and making it easier for jellyroll smelt to form.

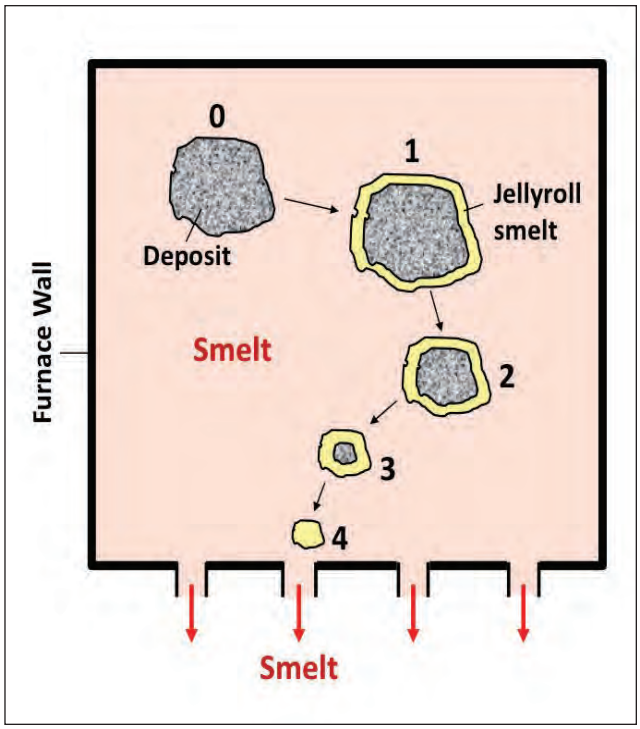
The smelt temperature T_{SM}, on the other hand, is strongly related to boiler operation, especially the combustion condition in the lower furnace. Higher thermal load to the boiler (high firing load, high liquor solids content, high liquor heating value, etc.) and better combustion conditions (optimum air flow, better air distribution and temperature, good swelling liquor, etc.) are key to ensuring high T_{SM}. As long as T_{SM} can be kept well above T_{FZ}, there will be little chance for the molten smelt to freeze or for the jellyroll smelt to form by this freezing mechanism.

Low sulfidity mills must therefore operate their boilers at a hotter bed than high sulfidity mills in order to avoid jellyroll smelt formation problems. This can be attained by increasing the heat input to the boiler, and/or ensuring good combustion near the smelt spouts, and/or installing small hearth burners. If it is impractical to raise the smelt temperature by these means, the only course of action would be to increase the smelt sulfidity to lower its freezing temperature so that the boiler can operate at a larger ΔT. One commonly used method for increasing the smelt sulfidity is to add emulsified sulfur to the as-fired black liquor in the saltcake mix tank. The addition of emulsified sulfur, however, must be done carefully, as it can lead to accelerated corrosion in the lower furnace and to near drum corrosion associated with acidic sulfates. A practical guideline is to discontinue emulsified sulfur addition when the pH of a 1% precipitator ash solution drops below 10.5.

Melting of fallen deposits

Deposits in the superheater region typically consist of 60 wt% Na_2SO_4, 35 wt% Na_2CO_3, and small amounts of Na_2S, NaCl, potassium salts, and char, and have a complete melting temperature between 780°C and 840°C. The gas temperature in this region varies between 600°C and 850°C while the tube surface temperature varies between 300°C and 500°C. Thus, the deposit temperature can be between 500°C and 700°C, which is much lower than the molten smelt temperature.

After being knocked off from tube surfaces by sootblowers, deposits fall on to the char bed where they interact with molten smelt. **Figure 11** schematically shows the fate of a piece of deposit after it has fallen from the upper furnace into the molten smelt pool (0). The deposit is immediately heated up by the molten smelt, and in the process, it lowers the temperature of the surrounding molten smelt. The heat transfer

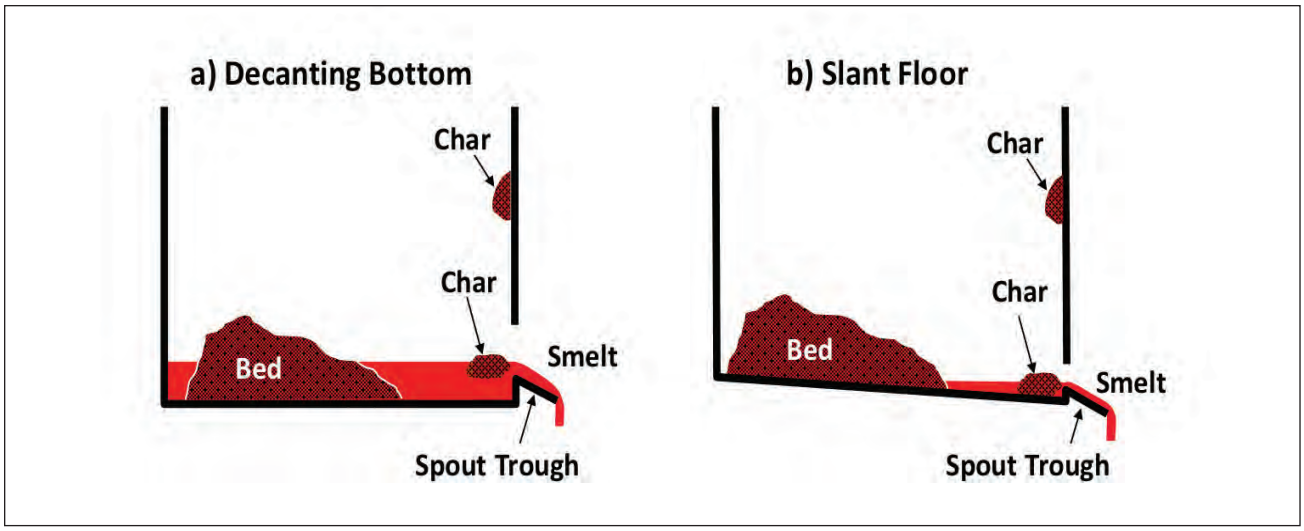


11. Transition from fallen deposit to jellyroll smelt.

between the deposit and the molten smelt allows a partially molten smelt layer to form at the deposit-smelt interface, which temporally increases the deposit mass and size (1). As the deposit temperature rises, the deposit continues to melt and become smaller and smaller with time (2 and 3). Eventually, it becomes a viscous mass or jellyroll smelt (4) that floats and moves along with the molten smelt. If such viscous deposit/smelt mass does not completely melt by the time it reaches smelt spouts, it may block the spout opening or move slowly on the spout trough, restricting the smelt flow.

Whether or not a piece of fallen deposit can completely melt by the time it reaches the smelt spout depends on its size, temperature, composition and residence time in the boiler, as well as the temperature, composition, and the movement of the molten smelt. Small pieces of deposit can "disappear" and become part of the molten smelt, while large pieces cannot. For boilers that burn low sulfidity black liquor, the smelt freezing temperature is high, making it easier for the molten smelt to be frozen by fallen deposits, and at the same time, more difficult for the molten smelt and deposits to mix.

Many more deposits and larger pieces of deposits fall during thermal shedding events than during normal boiler operation, particularly during the time when the boiler is heated up after the event [7]. The formation of jellyroll smelt by this deposit melting mechanism is consistent with mill experience that the problem is much more severe during thermal shedding. Since deposits contain very little or no char, one way to verify if fallen deposits are the root cause of the problem is to check if the jellyroll smelt contains char "sparklers" as it emerges from the boiler.



12. Floating char block near smelt spout opening: a) decanting bottom unit and b) slant floor unit.

Inclusion of char

The physical appearance and chemical composition of fluid smelt and jellyroll smelt at Mill A (Fig. 5) suggest that this jellyroll smelt formation incident was likely caused by char inclusion, not by smelt freezing or fallen deposits. With a density of 0.05 g/cm^3, char is very porous. Like a sponge, it can absorb a large volume of molten smelt and turn it into a viscous jellyroll smelt blob.

Char bed formation in recovery boilers is a dynamic process with constant changes in bed size, height, and position. If not controlled by boiler operators, char bed will keep building up to a point when it spontaneously collapses and rebuilds. Char blocks may break away from the main bed pile when it collapses or is struck by fallen deposits from above. Char blocks can also be partially burned black liquor residues fallen off from the waterwalls. Since they are light, they float and drift along with the molten smelt toward smelt spouts, where they become jellyroll smelt blobs and block the smelt spout openings (**Fig. 12**). Small jellyroll smelt blobs can flow with fluid molten smelt into the dissolving tank. Large jellyroll smelt blobs can float freely inside the boiler where the molten smelt level is deep, but once they are on the spout trough, they can no longer float due to the shallow molten smelt level on the trough. As a result, large jellyroll smelt blobs will "sit" on the trough and only move slowly as they are pushed from behind by the fluid smelt or are removed by the operators.

It is important to note that while the char content in the jellyroll smelt examined in this study was only 1.4% on a mass basis, it is about 50% on a volume basis. This means that the char can occupy as much as half of the molten smelt volume, and it can serve as a supporting frame that keeps molten smelt in place.

These formation mechanisms are consistent with mill experience that older recovery boilers burning black liquor with low solids and low sulfidity tend to be susceptible to jellyroll smelt formation. The mechanisms also suggest that recovery boilers with a decanting bottom are probably less susceptible to jellyroll smelt formation than those with a slant floor. This is because the deeper molten smelt level in decanting bottom boilers not only allows the fluid smelt to flow around or under the jellyroll smelt to reach the smelt spout (Fig. 12a), but also prevents the jellyroll smelt blob to "jump" over and sit on the smelt spout trough. In older and smaller decanting bottom boilers, however, conditions for jellyroll smelt to form still prevail since char can fall and accumulate on top of existing jellyroll smelt blobs near smelt spouts. In slant floor boilers, the smelt spout is typically at a level slightly higher than the floor, making it easier for the jellyroll smelt blob to roll or slide over onto the spout trough (Fig. 12b).

PREVENTION STRATEGIES

While the previously described mechanisms for jellyroll smelt formation appear to be different, they share one common requirement: the molten smelt must contain a large amount of particles to make jellyroll smelt. Particles can be the precipitated salts in the molten smelt as it freezes, or the solids in the partially molten deposit as it continues to melt, or the partially burned black liquor char in the case of char inclusion. Therefore, minimizing the presence of such particles in the molten smelt is key to the prevention of jellyroll smelt formation. The strategies may include:

- Increasing the molten smelt temperature by adopting "hot bed" operation (i.e., high solids black liquor, high heating value black liquor, optimal air flow rate and distribution, high air temperatures, good fuel/air mixing, etc.).
- Lowering the smelt freezing temperature by increasing the liquor sulfidity (this can be effective only up to 35% on TTA). For mills that already operate at a high liquor sulfidity, the smelt freezing temperature can be lowered by decreasing the liquor sulfidity instead.

- Optimizing sootblowing strategies to minimize deposit buildup in the superheater region during normal boiler operation.
- Optimizing sootblowing strategy to minimize massive deposit falling at once during thermal shedding events.
- Avoiding operation with large and/or steeply sloping char beds to minimize blackouts and bed collapsing that can generate a large amount of char (a carbon monoxide monitoring system can help identify poor bed conditions).
- Using bed cameras with local bed temperature monitoring systems to identify problem areas that may require air flow and temperature adjustments, or that may show where a large char lump has fallen or a local black out is taking place.
- Avoiding liquor burning on the furnace walls that forms large lumps of char near smelt spout openings.
- Keeping char away from spouts by increasing primary air flow, pressure, and temperature.

SUMMARY

Jellyroll smelt is commonly referred to as a type of molten smelt that suddenly becomes sluggish and forms a viscous blob on the spout trough, restricting the smelt flow. Mill experience and the results of a recent study performed on smoothly flowing smelt and jellyroll smelt collected at the same time from a recovery boiler suggest that that jellyroll smelt can form through three main mechanisms: i) the freezing of the molten smelt, ii) the melting of fallen deposits, and iii) the inclusion of a large amount of unburned char in the molten smelt. These mechanisms are consistent with mill experience that older recovery boilers burning black liquor with low solids and low sulfidity tend to be susceptible to jellyroll smelt formation and that deposits fallen from the upper furnace can be a contributing factor.

The common requirement for these three mechanisms to prevail is the presence of a large amount of solid phase in the molten smelt. Smelt freezing and fallen deposit melting are related to a net balance between the lower furnace temperature and smelt/deposit thermal properties, while char inclusion is related to black liquor burning behavior and the combustion environment around spout openings. To prevent jellyroll smelt from forming, it is ideally important to keep smelt completely molten and free of char particles. This may be attained by: i) operating the boiler at hot bed operation; ii) increasing the liquor sulfidity; iii) minimizing the falling of large pieces of deposits; iv) keeping char away from spouts by increasing primary air flow, pressure and temperature; and v) minimizing wall spraying above spouts. **TJ**

ACKNOWLEDGEMENTS

This work was conducted as part of the research program on "Increasing Energy and Chemical Recovery Efficiency in the Kraft Process - III", jointly supported by the Natural Sciences and Engineering Research Council of Canada (NSERC) and a consortium of the following companies: Andritz, AV Nackawic, Babcock & Wilcox, Boise, Canadian Kraft Paper, Carter Holt Harvey, Celulose Nipo-Brasileira, Clyde-Bergemann, DMI Peace River Pulp, Eldorado, ERCO Worldwide, Fibria, FPInnovations, International Paper, Irving Pulp & Paper, Kiln Flame Systems, Klabin, Stora Enso, Suzano, Tembec, Valmet and WestRock.

ABOUT THE AUTHORS

We chose to study this topic because jellyroll smelt formation has been a persistent safety problem in recovery boiler operation. We wanted to see if we could logically explain the phenomenon so that engineers and boiler operators can identify the root cause of the problem at their mills and devise viable solutions to them. This research compliments previous work on black liquor combustion and deposit formation in recovery boilers by our research group and others. The difference is that, in this work, we used the knowledge obtained from previous research to explain how jellyroll smelt may form.

The most difficult part of this research was to be able to see what jellyroll smelt looks like as it flows out of the boiler, and to obtain samples of jellyroll smelt and normal smelt at the same time so that meaningful comparison can be made. We were lucky to be in a recovery boiler control room when a jellyroll smelt incident occurred. Our most interesting finding was that while there are several mechanisms by which jellyroll smelt can form, they all share one common cause: the presence of solid particles in the molten smelt.

This study yielded logical explanations for how jellyroll smelt may form, and mills may use this information to identify the main cause of their jellyroll smelt problem and devise a viable solution to the problem.



Tran



Jones

Tran is Frank Dottori Professor of Pulp & Paper Engineering, Department of Chemical Engineering & Applied Chemistry, at the University of Toronto, Toronto, ON, Canada. Jones is senior engineering fellow at International Paper, Loveland, OH, USA. Email Tran at honghi.tran@utoronto.ca.

LITERATURE CITED

1. Tran, H.N., Jones, A.K., and Grace, T.M., *TAPPI J.* 14(1): 41(2015).
2. Lien, S. and DeMartini, N., "Dissolving Tank Explosions – a review of incidents between 1993 and 2005," Report to AF&PA Recovery Boiler Committee, AF&PA, Washington, DC, 6 February 2008.
3. Grace, T.M. "Dissolving Tank Explosions – A Review of Incidents Reported to BLRBAC," Report to AF&PA Recovery Boiler Committee, AF&PA, Washington, DC, 26 November 2013.
4. Tran, H.N., Sunil, A., and Jones, A.K., *J. Pulp Pap. Sci.* 32(3): 182(2006).
5. Zhao, L. and Tran, H.N., *J. Sci. Technol. For. Prod. Processes* 4(6): 50(2015).
6. Zhao, L., Tran, H.N., and Maki, K., *TAPPI J.* 14(7): 451(2015).
7. Tran, H.N., Martinez, M., Reeve, D.W., et al., *Pulp Pap. Can.* 94(11): 49(1993).

TAPPI JOURNAL
WWW.TAPPI.ORG
THE PAPER AND PACKAGING INDUSTRIES' TECHNICAL RESOURCE **NOVEMBER 2017** | VOL. 16 NO. 11



Progress in Paper Recycling

COMMENTARY **619**
The Chinese ban on recovered paper imports: An international disruption
Carl Houtman

MACROCONTAMINANTS **623**
New automated method for macrocontaminant analysis: Industrial applications
Sylvie Ossard, Patrick Huber, Pascal Borel, Davy Soysouvanh, and Thierry Delagoutte

PAPER PROPERTIES **633**
Innovative technology for making improved paper from the poorest fibers
Marion Sterner and Mikael Magnusson

STICKIES **639**
Improved deinking and stickies removal
Cesar Basilio

DEINKING **645**
Deinking process water flotation: An innovative solution to improve deinking and papermaking processes efficiency
Thierry Delagoutte, Bruno Carré, and Elisa Zeno

November 2017

TABLE OF CONTENTS VOL. 16 NO. 11

Featuring Exclusive Content from
Progress in Paper Recycling

615 EDITORIAL
Celebrating Wayne Carr: A true recycling visionary
Mahendra Doshi and Carl Houtman

619 COMMENTARY
The Chinese ban on recovered paper imports: An international disruption
Carl Houtman

623 MACROCONTAMINANTS
New automated method for macrocontaminant analysis: Industrial applications
Sylvie Ossard, Patrick Huber, Pascal Borel, Davy Soysouvanh, and Thierry Delagoutte

633 PAPER PROPERTIES
Innovative technology for making improved paper from the poorest fibers
Marion Sterner and Mikael Magnusson

639 STICKIES
Improved deinking and stickies removal
Cesar Basilio

645 DEINKING
Deinking process water flotation: An innovative solution to improve deinking and papermaking processes efficiency
Thierry Delagoutte, Bruno Carré, and Elisa Zeno

»COVER CREDIT: Researchers Ossard, Huber, Borel, et al., of the Centre Technique du Papier (CTP) in Grenoble, France, have created a 3D-Stick device for measuring macrocontaminants that lets mills analyze and control stickies removal throughout the recycling process (p. 623). The cover shows results of 3D-Stick measurement on filter paper at Asian mills, both after pulping (top two filters) and at the end of the process (bottom filter). This research won the Wayne Carr Best Paper Award for recycling (p. 615).

TAPPI JOURNAL
WWW.TAPPI.ORG

Editor-in-Chief
Scott Rosencrance scott.rosencrance@kemira.com
+1 770 429-2753

Associate Editor
Brian N. Brogdon brian.brogdon@gmail.com
+1 678 581-9114

Editorial Director
Monica Shaw mshaw@tappi.org
+1 770 367-9534

PRESS Manager
Jana Jensen jjensen@tappi.org
+1 770 209-7242

Webmaster
Trina Heath theath@tappi.org
+1 770 209-7416

***TJ* EDITORIAL BOARD**

Brian N. Brogdon, FutureBridge Consulting & Training LLC
brian.brogdon@gmail.com, +1 678 581-9114

David A. Carlson, Carlson Consulting
dacarlson39@aol.com, +1 847 323-2685

Jere W. Crouse, JWC Consulting
cj522@inwave.com, +1 608 362-4485

Mahendra Doshi, Doshi and Associates
mahen@aol.com, +1 920 832-9101

Marc Foulger, GL&V USA Inc.
Marc.foulger@glv.com +1 315 767-2920

Peter W. Hart, WestRock
peter.hart@westrock.com, +1 409 276-3465

Carl J. Houtman, USDA Forest Products Laboratory
choutman@fs.fed.us, + 1 608 231-9445

John A. Neun, John A. Neun LLC
john.neun@gmail.com, +1 518 275-8139

Jim Niemiec, Verso Corporation
jim.niemiec@versoco.com, +1 715 422-7404

Steven P. Ottone, Omya
steven.ottone@omya.com, +1 919 641-7854

Gaurav Pranami, Imbed Biosciences
gpranami@imbedbio.com, +1 515 230-7005

Arthur Ragauskas, Oak Ridge National Laboratory
aragausk@utk.edu

Gerard J.F. Ring, University of Wisconsin—Stevens Point
gerrryring@wi-net.com, +1 715 592-3732

Scott Rosencrance, Kemira Chemicals
scott.rosencrance@kemira.com, +1 770 429-2753

Paul Wiegand, NCASI
pwiegand@ncasi.org, +1 919 941-6417

Junyong Zhu, USDA Forest Products Laboratory
jzhu@fs.fed.us, +1 608 231-9520

Join TAPPI *today!*

TAPPI JOURNAL is a free benefit of TAPPI membership, and is only available to members. To join TAPPI, to renew your TAPPI Membership, or to learn about other valuable benefits, visit www.tappi.org.

TAPPI, 15 Technology Parkway S., Suite 115, Peachtree Corners, GA 30092, publishes *TAPPI JOURNAL* monthly.

ATTENTION PROSPECTIVE AUTHORS: All papers published are subject to *TAPPI JOURNAL's* peer-review process. Not all papers accepted for review will be published. Before submitting, check complete author guidelines at http://www.tappi.org/s_tappi/doc.asp?CID=100&DID=552877.

Statements of fact and opinions expressed are those of individual authors. TAPPI assumes no responsibility for such statements and opinions. TAPPI does not intend such statements and opinions or construe them as a solicitation of or suggestion for any agreed-upon course of conduct or concerted action of any sort.

Copyright 2017 by TAPPI, all rights reserved. For copyright permission to photocopy pages from this publication for internal or personal use, contact Copyright Clearance Center, Inc. (CCC) via their website: www.copyright.com. If you have questions about the copyright permission request process, please contact CCC by phone at +1 978 750-8400. To obtain copyright permission to use excerpts from this publication in another published work, send your specific request in writing to Editor, TAPPI JOURNAL, 15 Technology Parkway S., Suite 115, Peachtree Corners, GA 30092, USA; or by fax to +1 770 446-6947. Send address changes to TAPPI, 15 Technology Parkway S., Suite 115, Peachtree Corners, GA 30092, USA; Telephone +1 770 446-1400, or FAX +1 770 446-6947. www.tappi.org

Editorial



MAHENDRA DOSHI, PH. D.
TAPPI Journal
Editoral Board Member



CARL HOUTMAN, PH.D.
TAPPI Journal
Editoral Board Member

Celebrating Wayne Carr: A true recycling visionary

Editor's Note: *In this issue,* TAPPI Journal *(*TJ*) once again welcomes the inclusion of exclusive content from* Progress in Paper Recycling *(*PPR*). TAPPI thanks Mahendra Doshi and Carl Houtman of the* TJ *Editorial Board for organizing this content.*

– Monica Shaw, Editorial Director



Wayne Carr (1935–1995)

In the late 1970s, Wayne Carr began his journey to becoming a great visionary and a persistent proponent for recycling. Even though recycled paper was not a dominant product in the 1970s and 1980s, he worked diligently to keep TAPPI's Recycling Committee looking forward. After his passing in 1995, the Wayne Carr Best Paper Award for recycling was established to honor his many years of meritorious service to TAPPI and his advocacy for the field.

As a reminder of Carr's influence on the recycling industry in its early days, below are excerpts of what some of the TAPPI members thought of his contributions to the recycling profession, as published in the February 1996 issue of *Progress in Paper Recycling*:

- "Wayne was pioneer in fiber recycling. His vision will continue to inspire scientists around the world to strive for excellence, as he always did." – Michel Dubreuil.
- "The pulp and paper industry and, in particular, TAPPI, owes a lot to Wayne. I think back to those days when the Secondary Fiber Pulping Committee was struggling to put together a session(s) for the pulping conference. Wayne was always there to keep the committee focused and moving ahead." – Lee Bingham.
- "From the first time I met Wayne, in 1970, he was supportive and encouraged me to become active in committee activities. Wayne was a fountainhead of knowledge in his beloved field of recycling. The industry has lost a champion. I have lost a mentor and a friend." – Dick Spangenberg.
- "In a technical sense, Wayne was world-class with first hand responsibility in numerous deinking advancements." – Jim Catlin
- "Wayne was a 1957 graduate of the Paper Science and Engineering Department at Western Michigan University and a member of the Paper Technology Foundation. His foresight and expertise in secondary fibers will be greatly missed." – Bill Forester



Progress in Paper Recycling

Wayne Carr Award winners continue his legacy

In the years since the Wayne Carr Best Paper Award was established, there have been 19 winners who perpetuate Carr's legacy of excellence in the field of recycling. These authors have grappled with topics such as deinking, screening, stickies, environmental factors, equipment advances, and more.

The winning papers, which are listed in the table on the next page, were assessed by the Recycling Committee using the following criteria:

- Technical and scientific excellence
- Practical and economic utility
- Clarity of oral presentation and written manuscript

In this special recycling issue of *TAPPI Journal*, we are pleased to include the latest winner of the Wayne Carr Best Paper Award (p. 623) by authors Ossard, et al., of the Centre Technique du Papier (CTP) in Grenoble, France.

AUTHORS	YEAR	RECYCLING TOPIC
Shawn Berg, D.A. Johnson, and E.V. Thompson	1996[a]	"Toner detachment during repulping of laser printed office copy paper."
Helga K. Zollner and L.R. Schroeder	1997[a]	"Enzymatic deinking of non-impact printed white office paper with alpha-amylasa."
R. Daniel Haynes	1999[a]	"The impact of the summer effect on ink detachment and removal."
Bruno Carre, L. Magnin, G. Galland, et al.	1999[a]	"Deinking difficulties related to ink formulation, printing process and type of paper."
Bradley Lucas, R. Venditti, and H.J. Chang	2002[b]	"Factors in the passage of pressure sensitive adhesive particles through a slot."
Benjamin Fabry and B. Carre	2002[b]	"Comparison between different types of pulpers devoted to deinking processes."
Tiina Sarja, P. Kourunen, and M. Zabihian	2003[b]	"Control of potential secondary stickies in deinked pulp."
Shisei Goto and T. Miyanishi	2004[c]	"Effects of structures and properties of surfactants on office waste deinking."
Yuxia Ben, G. Dorris, and N. Pagé	2004[c]	"Application of column flotation in waste paper recycling."
William K. Sacia and J. Simmons	2005[d]	"The impact of changing ONP quality on a newsprint mill."
Hanna Jokinen, A. Ämmälä, J.A. Virtanen, et al.	2006[d]	"Pressure screen capacity - current findings on the role of wire width and height."
J. A. Olson, C. Pflueger, S. Delfel, et al.	2007[c]	"High performance foil rotor improves deink pulp screening."
R. Daniel Haynes, J. Malloch, J. Tecklenborg, et al.	2008[d]	"Ask the Mill Gals" Panel
Mika Körkkö, O. Laitinen, A. Haapala, et al.	2009[d]	"The influence of PCC filler on near-infrared scattering, absorption and residual ink measurement error."
Michelle Ricard, G. Dorris, S. Gendron, et al.	2010[d]	"A new online image analyzer for macrocontaminants in recycled pulps."
Danny Haynes	2012[e]	"Colloidal organic content and tackiness of coated broke and recycled fiber."
Shisei Goto, H. Tsuji, I. Onodera, et al.	2013[c,e]	"Pilot-scale development of cavitation jet deinking."
Fernando Luiz Neves, E.M. Merendino, M. Piva, et al.	2015[e]	"Aseptic carton packages: Recycling review."
Sylvie Ossard, P. Huber, P. Borel, et al.	2016[c,e]	"New automated method for macrocontaminants analysis: Industrial applications."

[a] TAPPI Recycling Symposium
[b] TAPPI Fall Technical Conference
[c] Research Forum on Recycling: 7th – 2004; 8th – 2007; 9th – 2010; 10th – 2013; 11th – 2016
[d] TAPPI EPE Conference
[e] TAPPI PEERS Conference

Mahendra Doshi, Ph.D., is a member of the TAPPI Journal *Editorial Board, founder of Progress in Paper Recycling, and president of Doshi & Associates Inc., in Appleton, WI, USA. Email Doshi at mahen@aol.com.*

Carl Houtman, Ph.D., is a member of the TAPPI Journal *Editorial Board and a research chemical engineer with the U.S. Department of Agriculture's Forest Products Laboratory in Madison, WI, USA. Email Houtman at choutman@fs.fed.us.*

The Chinese ban on recovered paper imports: An international disruption

CARL HOUTMAN

Mountains of paper grow on the docks of Hong Kong, waiting to enter China. Elderly paper collectors in Hong Kong lose income because they cannot find buyers for their baskets full of used boxes. A German shipper no longer accepts paper shipments bound for China. Old corrugated cardboard (OCC) prices in Arkansas drop by $50/ton. From New Zealand to Great Britain, and everywhere in between, the disruption of fiber flow into China continues to shake the world of recovered paper.

In a document sent to the World Trade Organization (WTO), China indicated a desire to reduce the trash entering their country. In addition, China delayed issuing the required import licenses and caused everyone in the recovered paper business to adapt. Material transfer facilities around the world are looking for new buyers for their material. Outside of China, recycle plants are filling their warehouses with cheaper recovered paper and considering ways to store more paper. Chinese recycle mills are searching for fiber, and companies in China are struggling to find packaging and shipping materials.

CHINESE DEMAND SHIFTS GLOBAL CAPACITY

Over the last decade, China's hunger for fiber has driven large shifts in recycling capacity around the world. Sometimes called the "Chinese price support", the country's strong demand makes it difficult for mills outside the country to negotiate more favorable pricing. Recycle mills have to live on a thin margin between high recovered paper costs and low prices for their products. Many companies have responded by looking for fiber in "mixed waste" or closing mills.

Why has China taken these steps? In his address to the Chinese Communist Party Congress, President Xi placed particular emphasis on creating an "ecological civilization." It is possible that Chinese officials in charge of import licenses are waiting to see what new policies the President will favor as he starts his new term. Even without presidential mandates, China is facing a trash disposal problem. Domestic production of residential waste has steadily increased over the last few years. This trend compounds the problems faced by the country's recycling mills in disposing the trash that comes with imported recovered paper.

Bill Moore of Moore & Associates, an Atlanta-based paper recycling consultant, thinks that beyond this environmental push, there may be Chinese officials that don't understand the difference between raw materials and trash, or that large Chinese mills are trying to put pressure on their smaller competitors.



The disruption of fiber flow into China continues to shake the world of recovered paper.

A FUTURE IN LIMBO—FOR NOW

So, what is the future of the recovered paper business? China needs fiber and does not have sufficient domestic supply. Imports to China will start again, but when and under what conditions? In fact, there have been recent moves by China to relax the proposed recovered paper contaminant limit.

In the meantime, the temporary price reduction in recovered fiber elsewhere will help recycle mills fill their storage lots or warehouses. Perhaps these same mills will start looking at idled equipment and consider bringing recycling capacity back online. Finally, material transfer facilities will continue to look for other buyers by cultivating contacts in developing countries. They also will be reviewing their processes to look for ways to meet tighter restrictions on contamination.

This event has shown us, once again, that we live in an interconnected world and paper recycling plays an important role in the global economy. **TJ**

Carl Houtman, Ph.D., is a member of the TAPPI Journal *Editorial Board and a research chemical engineer with the U.S. Department of Agriculture's Forest Products Laboratory in Madison, WI, USA. Email Houtman at choutman@fs.fed.us.*

New automated method for macrocontaminant analysis: Industrial applications

SYLVIE OSSARD, PATRICK HUBER, PASCAL BOREL, DAVY SOYSOUVANH, AND THIERRY DELAGOUTTE

ABSTRACT: In recycled paper processes, stickies are the origin of many production disturbances. In this paper, we present how the recently developed method for macrocontaminant analysis was used with industrial samples for process analysis. The new automated stickies measurement method allows (i) determination of the three-dimensional (3D) morphology of screened particles (without any deformation) and (ii) classification of the particles as stickies among contaminants. This is achieved by a combination of laser triangulation and local near-infrared spectroscopy (NIR).

Measurement of macrocontaminants in pulp samples and their classification allow meaningful evaluation of their specific removal. Chemical nature and amount of the macrocontaminants coming from different raw materials were studied and were shown to be very different in two different mills. In an Asian mill, a low removal of pressure-sensitive adhesives (PSAs) in the process (46%) was found in comparison with high removal of other stickies (99%). Applications of this device are shown, while the new on-line sensor for macrocontaminant analysis is being developed.

Application: This study demonstrates how mills can analyze stickies removal throughout the recycling process. As a consequence, they could control the process depending on the chemical nature of incoming stickies contamination.

In recycled paper processes, stickies are at the origin of many production disturbances, such as machine breaks, defects in paper, and converting problems. Monitoring of macrocontaminants is an essential task for most recycling mills. Currently, mills use tedious and laborious measurement methods. Macrocontaminants are generally separated from the pulp by screening, followed by various inspection and classification methods.

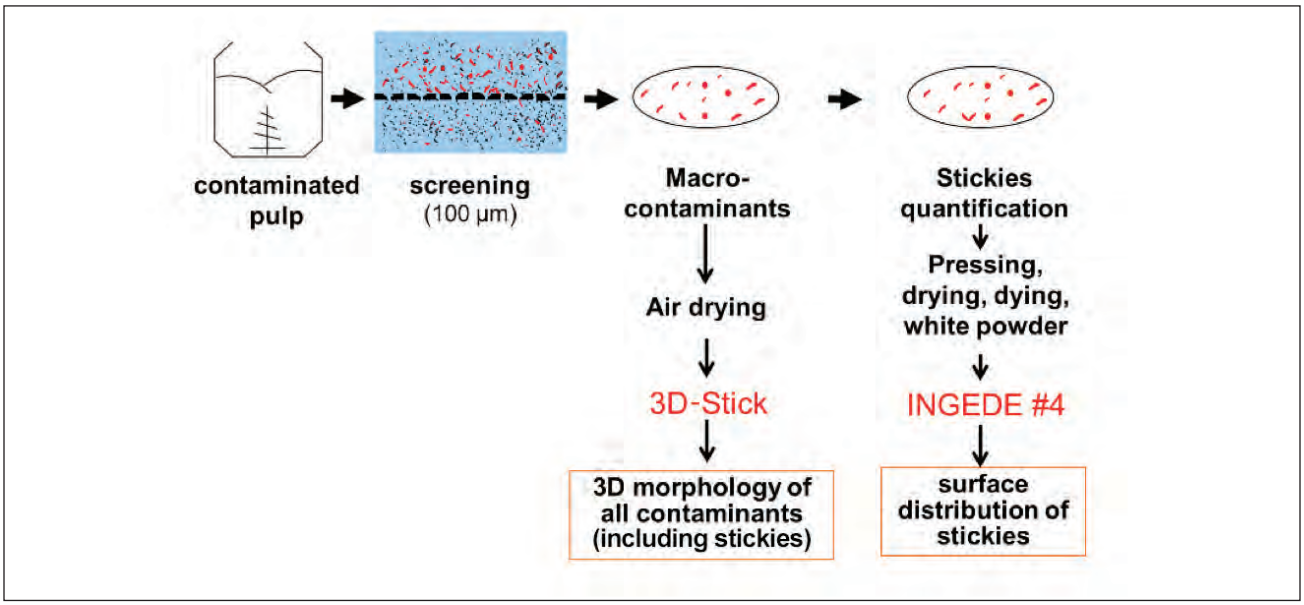
The most recognized methods in Europe are INGEDE #4 [1] and TAPPI Standard Test Method T 277 pm-99 "Macro stickies content in pulp: The 'pick-up' method." They give useful information about stickies particles count and size. Tacky particles (stickies) are specifically colored and quantified by image analysis.

The chemical nature of stickies makes them suitable for analysis by near infrared spectroscopy (NIRS). The technique is rapidly gaining acceptance in the industry, with applications in paper recycling such as sorting a recovered paper stream [2-4], raw material quality assessment [5-7], or quantification of stickies embedded in handsheets [8,9]. According to Doshi, a stickies measurement method should give access to quality of the furnish, efficiency removal processes, deposit control on paper machines, and performance improvement of recycled paper products [10]. In this context, the objective of this work is to describe the use of this new measurement method for stickies studies in recycled pulps in industrial applications for process analysis. The proposed 3D-Stick automated method for macrocontaminant analysis allows (i) determination of the 3-dimensional (3D) morphology of those screened particles (without any deformation) and (ii) classification of the particles as stickies among contaminants, meaning a tool to have both quantitative information (mm^2, or better yet mm^3, of stickies per kilogram of pulp, for example) and qualitative information such as the chemical nature of the stickies.

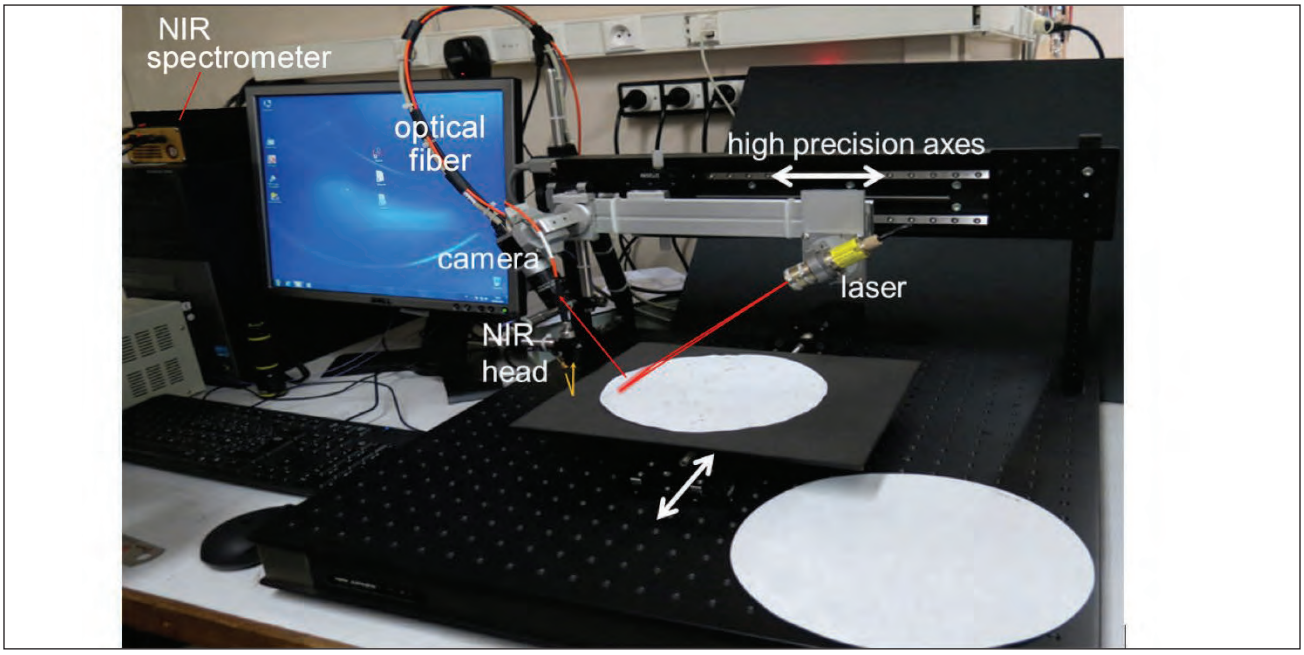
MATERIALS AND METHODS

Conventional characterization of stickies with INGEDE #4 and TAPPI T 277

Contaminants were previously separated from the fibers on a screening device with a 100 µm slots plate. The principles of the INGEDE #4 and the TAPPI T 277 methods are compared with the new proposed 3D-Stick method (**Fig. 1**). The INGEDE #4 and TAPPI T 277 methods are similar in principle, with only a difference in the dying step. The filter with the contaminants particles is covered with non-stick silicone paper and then dried on a Rapid-Köthen device (10 min, 94°C, pressure of 95 kPa). This step causes the sticky particles to strongly adhere to the filter paper. They are also subsequently pressed and deformed. The silicone paper is then released, and non-tacky contaminants are removed



1. Sample preparation for 3D-Stick analysis and for INGEDE #4 method.

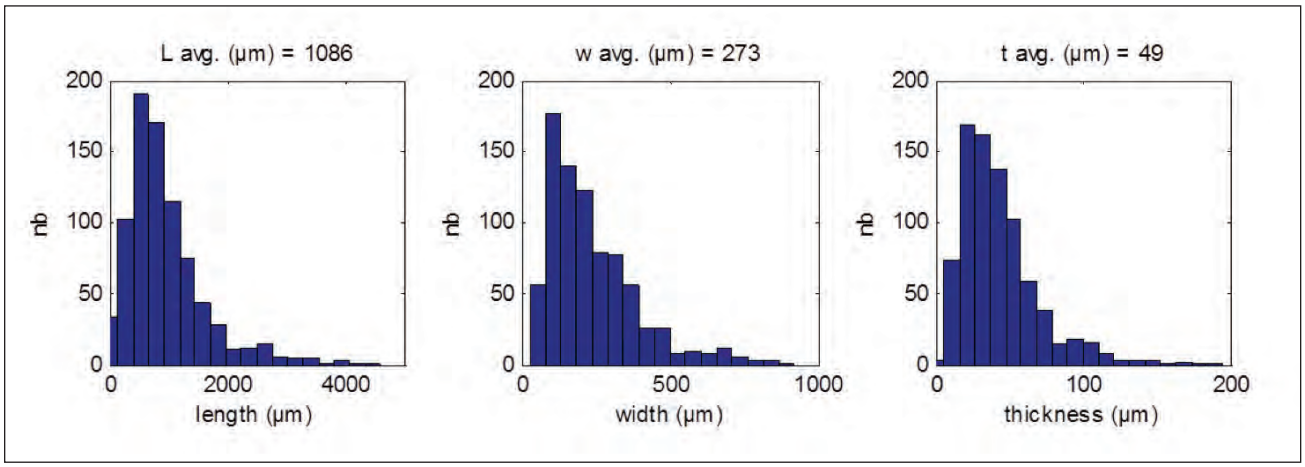


2. Three-dimensional (3D) stick device: A laser line and a camera perform the mapping by laser triangulation, and a near infrared (NIR) head analyzes chemical composition of contaminants.

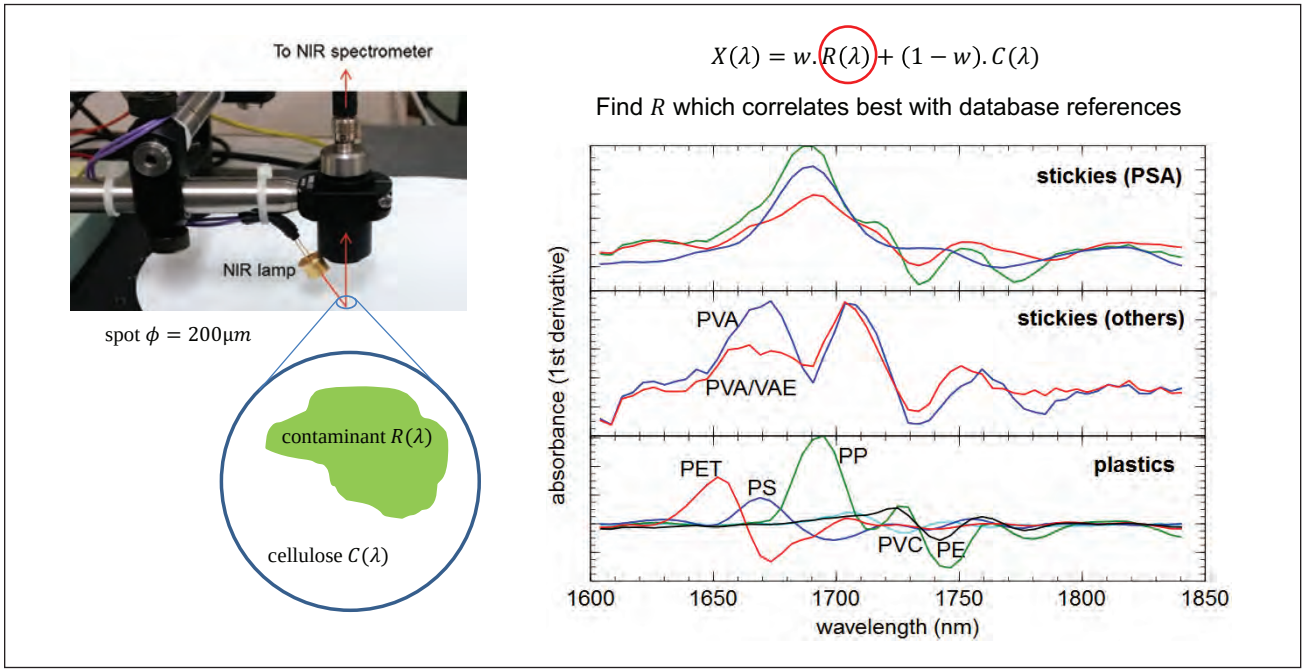
from the surface with a soft brush. The filter is then completely dyed through immersion in a water-soluble black ink bath. The dyed filter is dried on a Rapid Köthen device between 2 silicone papers under the same conditions described previously. Then, the stickies particles are revealed with a white alumina powder (INGEDE) or white coated paper (TAPPI) after pressing and drying again. This leaves only white stickies particles on a black background. Stickies are then counted and characterized on a desktop scanner through image analysis.

3D-Stick measurement

The principle of the 3D-Stick measurement has been previously described [11]. This method is briefly described as follows. The 3D-Stick analysis is achieved by a combination of laser triangulation and local NIRS (**Fig. 2**). First, the contaminants deposited on a filter paper are scanned by a moving laser line. The reconstruction of the altitude profiles gives access to the length, width, and thickness distributions of the macrocontaminants, with a resolution of 20 µm x 20 µmx 3 µm. An example of stickies size distribution



3. Example of industrial stickies size distribution (based on the analysis of 819 stickies).



4. NIR recognition of chemical nature of contaminants.

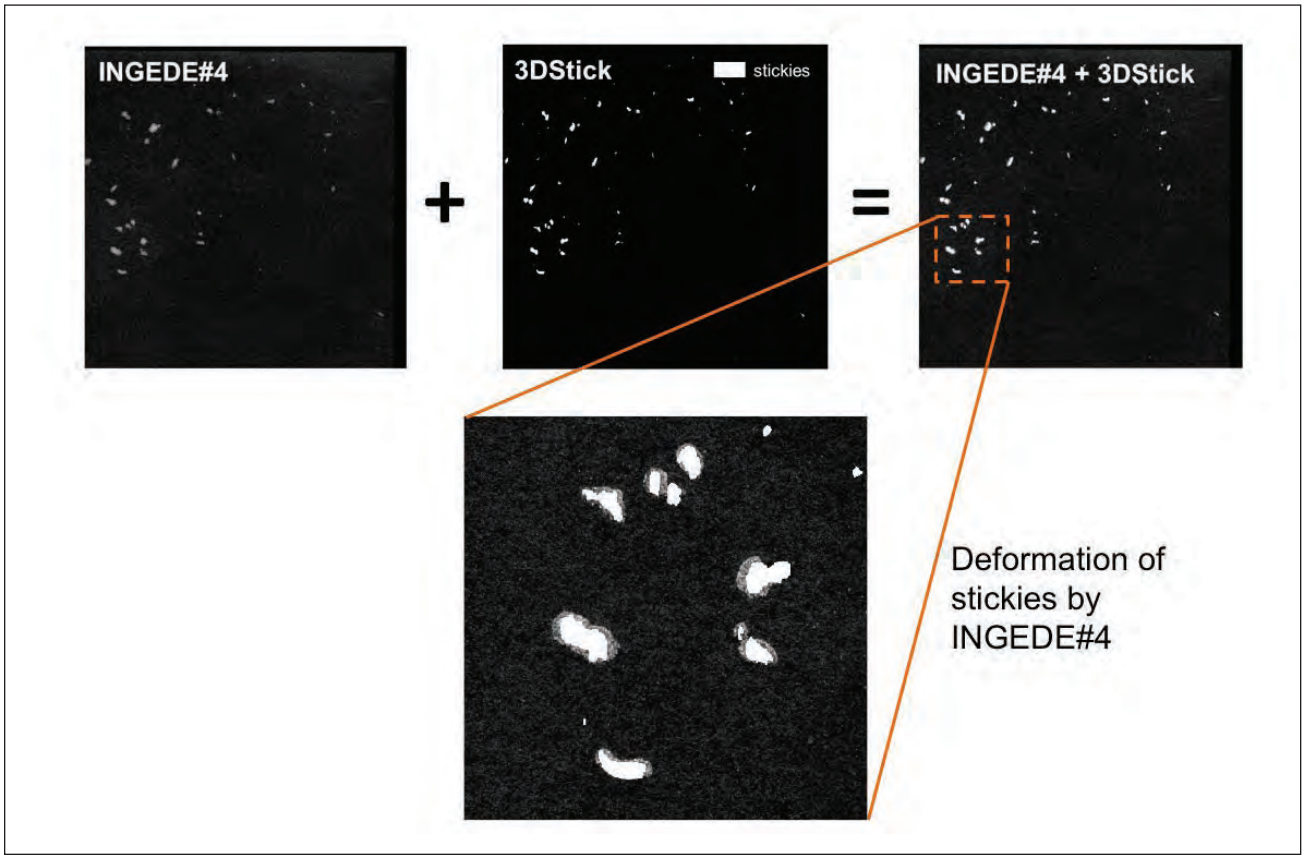
is illustrated in **Fig. 3**, where the average size is 1100 µm x 250 µm x 50 µm. Then, the chemical nature of the contaminants is assessed by NIRS. A database of expected compounds was built with model glues present on the market (**Fig. 4**). Several classes of contaminants were defined for classification according to previous mill experiences: stickies (pressure sensitive adhesives [PSAs]), stickies (others), and plastics. For the "stickies PSA" class, several acrylic model samples from glue suppliers were analyzed and added to the database. For the "stickies (others)" class, several model glues were included: among them several polyvinyl acetate (PVA)-based compounds (PVA homopolymers) and several mixtures of PVA and vinyl acetate ethylene (VAE) copolymer glues. Several glue formulations based on ethylene vinyl acetate (EVA) have been used as model hot melt stickies.

RESULTS AND DISCUSSION

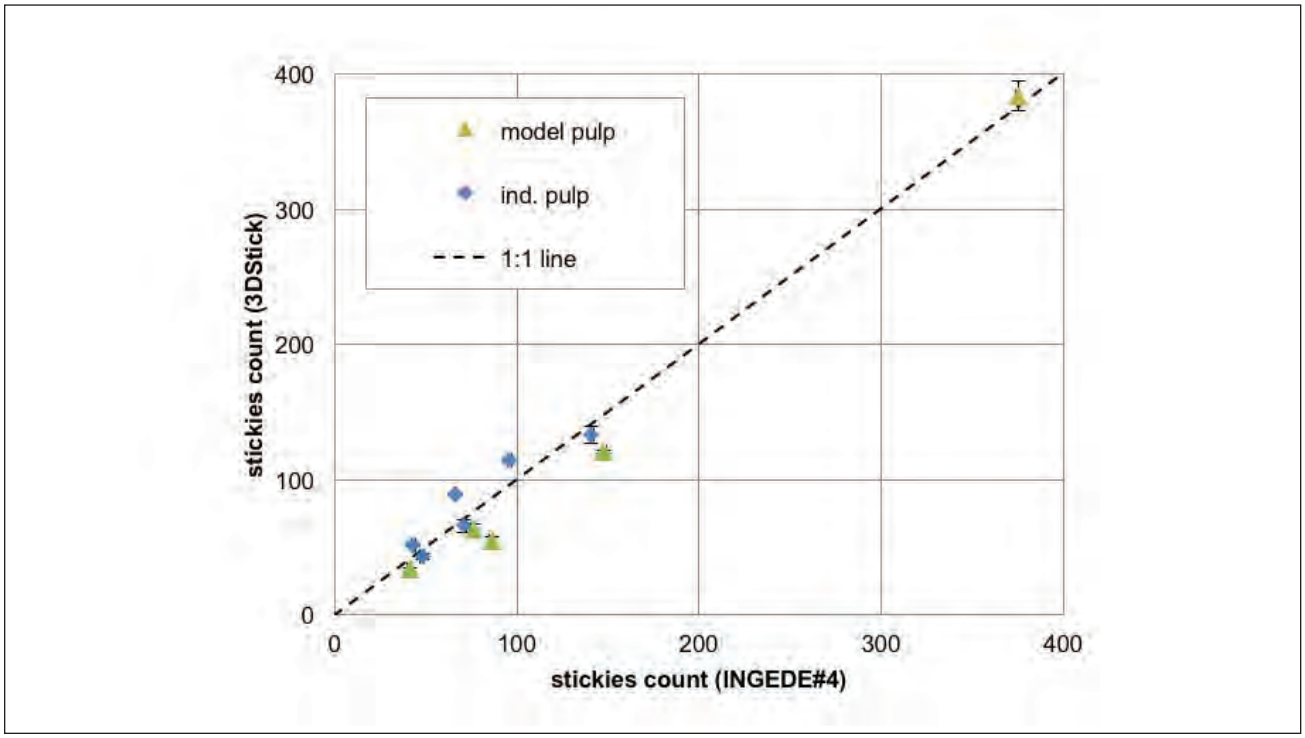
Method comparison

The comparison between the INGEDE #4 method and the 3D-Stick measurement has previously been published [11]. It was shown that contaminant morphologies are modified through pressing and heating steps in the INGEDE #4 method, as illustrated in **Fig. 5**. They are measured in their initial state in the proposed 3D-Stick method, avoiding this deformation. Also, the comparison of stickies count in number between the two methods was well correlated, as shown in **Fig. 6**.

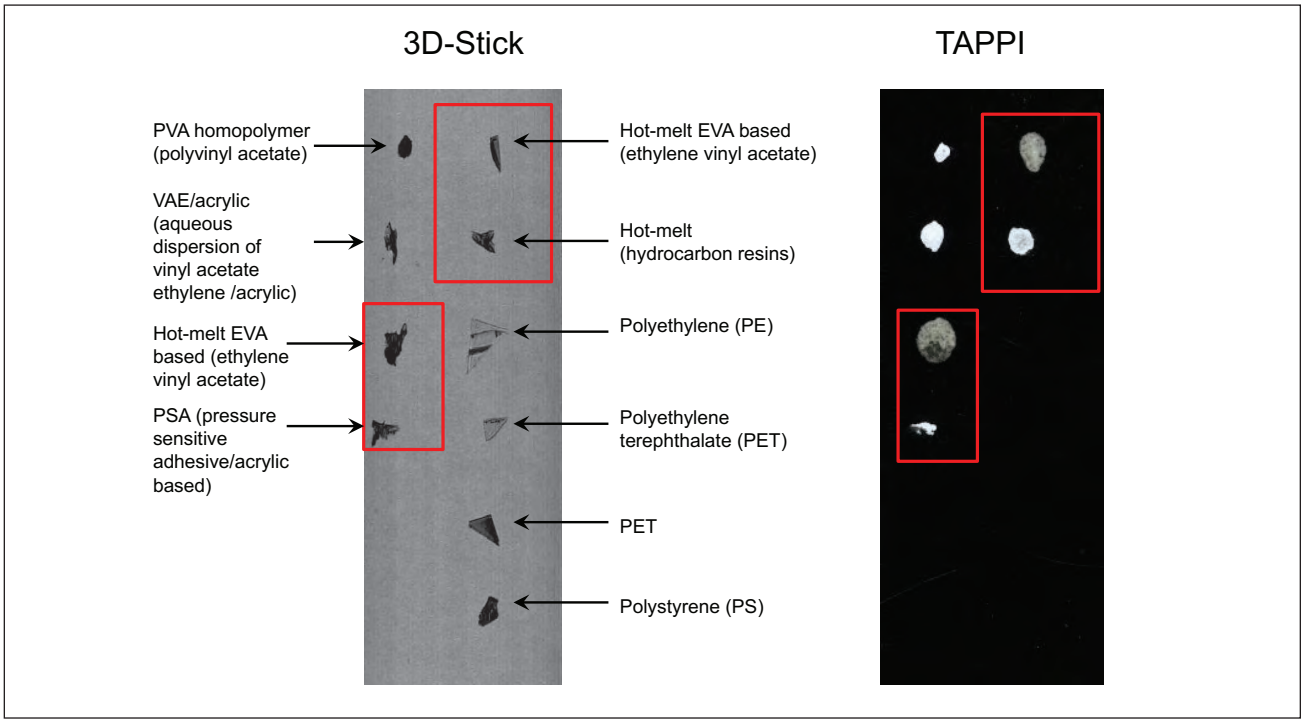
Besides those results, it was found that comparisons between 3D-stick measurements and the TAPPI T 277 method were not correlating in a specific industrial mill. This was not expected, as previous results indicate that INGEDE #4 and the TAPPI T 277 method were similar, with the main difference



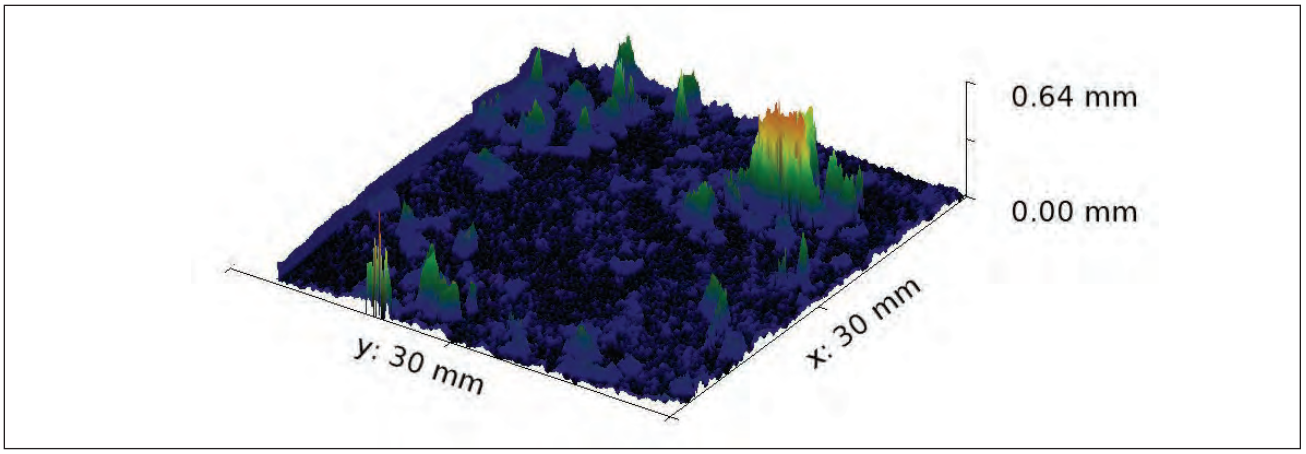
5. Illustration of deformation of the stickies due to pressing and heating.



6. Stickies count in number with 3D-Stick and INGEDE #4 methods.



7. Model contaminants deposited on a filter paper and identified with 3D-Stick (left) and with TAPPI Standard Test Method T 277 pm-99 (right).



8. A 3D image of part of sample 1 for illustration.

being that alumina powder is used to whiten sticky contaminant in the first, and coated paper in the second. The principles of the methods are similar.

The comparisons of the results on model contaminants analyzed with both methods are shown in **Fig. 7**. EVA-based hot melt, hydrocarbon hot melt, and PSA appear grey with the TAPPI T 277 method. They are not counted with the mill protocol and optical device. In this method, tacky particles are colored in white when they are pressed and heated in contact with a white coated paper. The grey color indicates that the coating has not been well detached and transferred to the stickies particles. On the other hand, the 3D-Stick perfectly identified the particles as EVA contaminants. These differences may be at the core of the differences between mill and 3D-Stick measurements and of the poor correlation between paper machine issues and stickies measurement performed in this mill. Those results indicate that 3D-Stick measurement gives more information than the mill method, with breakdown in contaminant classes (hot melt, total PSA and plastic contamination).

Process studies

The objectives of the process studies were to (i) evaluate contamination between two Asian mills, called production A and



9. Filter paper where stickies were deposited.

	Production A After Pulping	Production B After Pulping	Production B End of Process
Stickies (PSA)	3556	135	72
Stickies (others)	15227	7151	62
Plastic	101	49	9
Total stickies	18783	7286	134
PSA = pressure sensitive adhesive.			

I. Contamination in mm²/kg of the pulp in productions A and B (from 3D-Stick measurement).

	Process Removal Efficiency (in % surface area)
PSA	46%
Other stickies	99%
PSA = pressure sensitive adhesive.	

II. Process removal efficiency, in percent surface area, for grade B, according to nature of stickies.

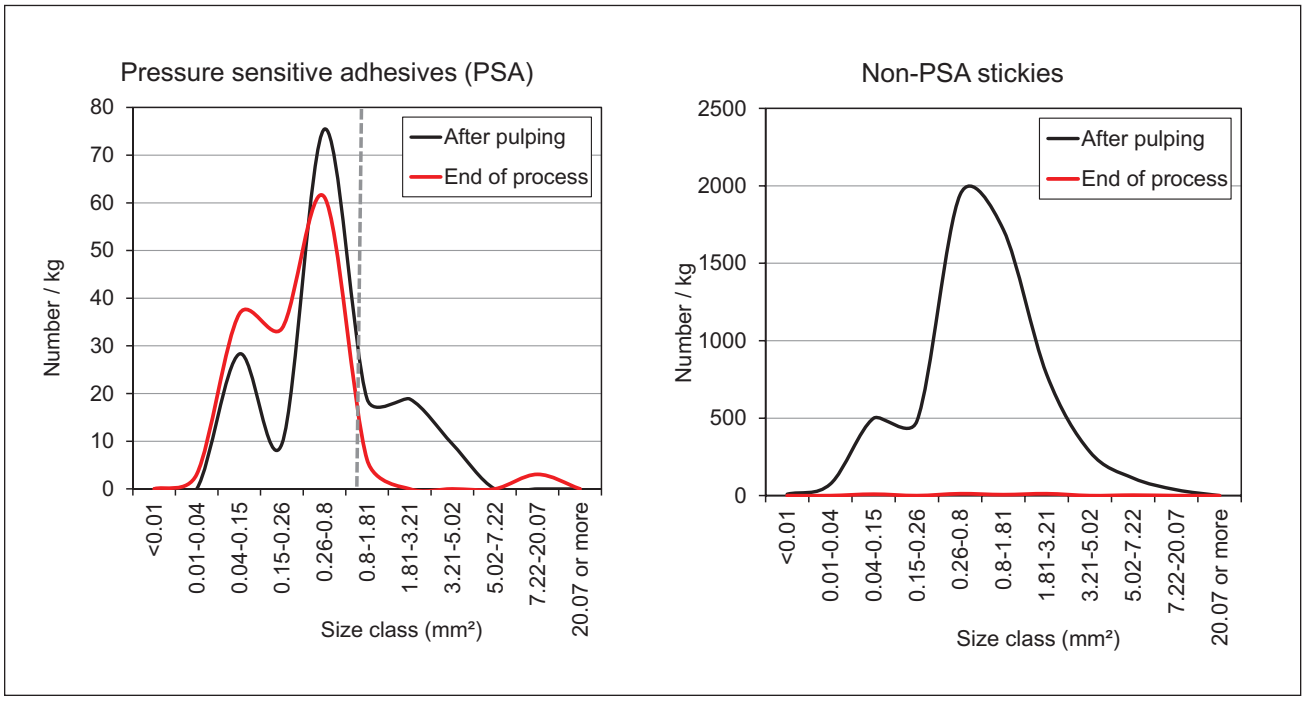
production B, and (ii) evaluate contaminant removal in production B. A reconstructed 3D map is shown in **Fig. 8**, for example. Results of 3D-Stick measurements on the filter paper (**Fig. 9**) are shown in **Table I**.

The macrostickies contamination of production A after pulping is very high and much higher than that in production B (18800 versus 7300 mm²/kg). The raw materials are very different in the two mills, explaining those results. PSA stickies are found to represent about 19% of total stickies contamination in production A and 2% in production B. Those ratios are much lower than in European mills, where PSAs represent about 60% to 80% of the stickies contamination at the process inlet [12]. Those results indicate that the classification of stickies could be different in Asian mills (and probably in U.S. mills, which have not been tested up to now) than in European mills. In Europe, a differentiation of PSA and non-PSA stickies is adequate for process analysis; another stickies classification may be proposed with 3D-Stick analysis, and may be more adequate in the future for mills on other continents. However, PSAs represent 53% of the final pulp contamination in production B, indicating that their removal is lower than for other stickies, as found in Europe [13].

As presented in **Table II**, the process of removal is very different for PSA and non-PSA stickies. Overall, the removal of non-PSA stickies is very good and exceeds 99% as shown. On the contrary, PSA removal is lower, calculated as 46%. A similar result was already shown in a previous study through INGEDE #4 measurements [14] and a derived method for specific PSA count [13]. The proposed 3D-Stick method gives access to those results with a fast (20 min) and easy method (fully automated once the screen rejects have been deposited on a filter paper).

The morphological characteristics of stickies can be studied and their removal according to their size range evaluated. The frequencies by size classes of the stickies for production B samples are shown in **Fig. 10**. The decontamination of the stickies through the process is very good for non-PSA stickies for all the size ranges. This is consistent with the 99% removal of this stickies category.

On the contrary, for PSA particles, the size has a clear impact in their removal. The larger stickies with a size above 0.8 mm² (equivalent diameter of 1009 µm) are efficiently removed by the process. The PSAs smaller than 0.8 mm² are not effectively removed in the process. Those small stickies have been called mini-stickies in previous publications and



10. Stickies distribution according to size classes at the production B (i) inlet pulp and (ii) the end of the process.

have been shown to pass through the screening steps of most mills [12,14]. Hence, our results are consistent with previously shown PSA behaviors. It is noticeable that the size range of those mini-stickies seems to switch to smaller particles from the beginning to the end of process. This may be due either to:

(i) Fragmentation of PSA particles.

(ii) Better removal of stickies in the size range of 0.26–0.8 mm² and no or nearly no removal of smaller PSA particles. Hence, the smaller stickies are following the pulp flow. Some pulp and solids in suspension are removed from the process through flotation and screening steps, inducing weight losses. As a consequence, a small PSA number expressed per kilogram of pulp will be higher at the end of the process, and apparent contamination increases through the process.

Remarks

Please note that the results in this report are expressed in number/kg and in mm²/kg to be comparable with most methods used for stickies analysis (microscopic count, TAPPI, INGEDE methods), but the data obtained with the 3D-Stick will in the future be presented in mm³/kg to take into account the three dimensions of the stickies.

In the case of this Asian mill, the number of unidentified objects was quite high (up to 10% on the total objects, fibers, and contaminants) compared to amounts normally less than 5% in European mills. The update procedure of the database is straightforward (only one reference spectrum must be added), and this has already been performed in other mill cases.

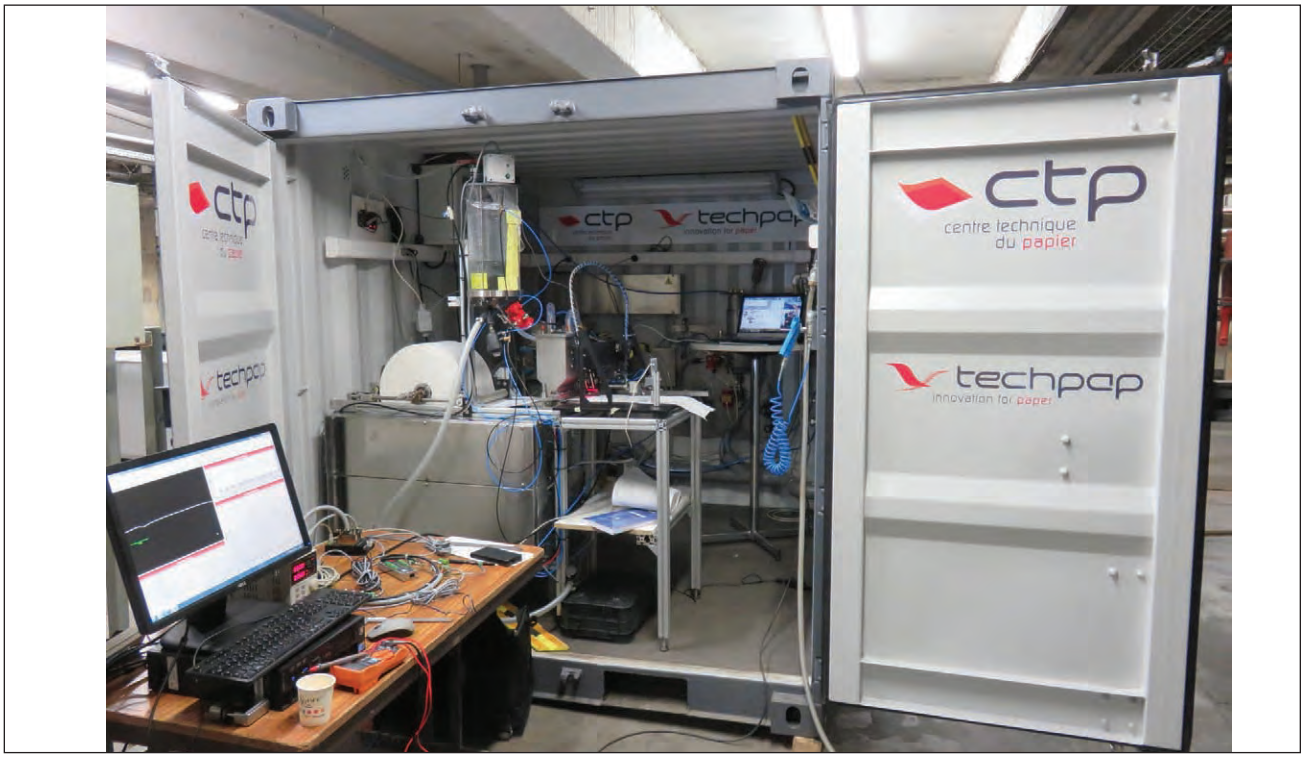
3D-Stick Class	Chemical Base
PSA	Acrylic-based PSA
PSA (hot melt)	SBR and styrene acrylic
Hot melt (non-PSA)	EVA-based hot melt and others
PVAE	PVA-VAE based
PVA	PVA based
Plastics	PE, PET, PP, PVC, PS
Stickies (other)	Non-classical glues as latex

PSA = pressure sensitive adhesive; SBR = styrene butadiene; EVA = ethylene vinyl acetate; PVA = polyvinyl acetate; VAE = vinyl acetate ethylene; PE = polyethylene; PET = polyethylene terephthalate; PP = polypropylene; PVC = polyvinyl chloride; PS = polystyrene.

III. Stickies classification performed by the 3D-Stick.

PERSPECTIVES

As described in the previous "3D-Stick measurement" section, many different model glues have been used to differentiate the stickies according to their chemical nature. Overall, a total of 45 different contaminants have been included into the database, and the main categories are presented in **Table III**. Those classes can be used for more precise analysis, depending



11. Photo of the first prototype of the PI-Stick for on-line macrocontaminant analysis.

on specific mill needs or issues. As previously cited in this research paper, PSAs and other stickies behave very differently in the process. Also, one can easily anticipate that PVA aqueous dispersion will behave very differently in the process compared to the hard hot melt glues. Those different behaviors within the process can now be tracked with the 3D-Stick.

Moreover, the interest around the results obtained with this new tool led the Centre Technique du Papier (CTP; Grenoble, France) and TechPap (Grenoble, France) to further develop an on-line measurement. A first prototype of such on-line sensor for stickies measurement has been built (**Fig. 11**), and initial industrial trials have been performed. This promising PI-Stick device allows following of macrocontaminant concentration and removal along the process for different stickies types.

CONCLUSION

The 3D-Stick is a new analytical tool for stickies characterization that will allow mills to:

1. Have quantitative, qualitative (nature), and morphological characterization of the macrocontaminant in pulp samples without any deformation.
2. Evaluate contamination modifications due to raw material changes.
3. Assess macrocontaminant removal efficiencies of each process step, per type of contaminant (PSA, hot melt, PVA, plastics, etc.).

The main advantages of this analytical tool are quantitative and qualitative measurements; fully automated, fast measurements (20 min for 300 objects); and a non-contact method (stickies not pressed).

As a perspective, CTP works closely with TechPap on an on-line measurement based on this 3D-Stick principle. This new, on-line fully-automated sensor would help mills follow up on stickies contamination at several points in their process, as well as address stickies removal. The final target is to perform a control-command of specific removal steps (screening rejects, flotation rejects) based on initial stickies contamination and final target. **TJ**

ACKNOWLEDGEMENTS

The authors wish to thanks Dallal Hadjseyd for efficient laboratory work. We also offer warm thanks to workers from the studied mills for preparation of samples and for discussions of results.

LITERATURE CITED

1. Ackermann, C., Putz, H.-J., and Göttsching, L., *Prog. Pap. Recycl.* 7(2): 22(1998).
2. Rahman, M.O., Hussain, A., and Basri, H., *Int. J. Environ. Sci. Technol.* 11(2): 551(2014).
3. Vidal, M., Gowen, A., and Amigo Rubio, J.M., *NIR News* 23(1): 13(2012).

4. Tatzer, P., Wolf, M., and Panner, T., *Real-Time Imaging* 11(2): 99(2005).
5. Riba Ruiz, J.-R., Canals, T., and Cantero Gomez, R., *IEEE Trans. Instrum. Meas.* 61(4): 1029(2012).
6. Borel, P., Cochaux, A., and Eymin Petot Tourtollet, G., "NIR spectroscopy for recovered raw material quality control," *CTP/PTS Int. Symp. Packaging Design Recycl., 6th*, CTP, Grenoble, France, 2010,
7. Pigorsch, E., *J. Near Infrared Spectrosc.* 18(1): 225(2010).
8. Pigorsch, E., Petzold, M., and Gärtner, G., *Int. Papwirtsch.* 1: 44(2012).
9. Pigorsch, E. and Behnsen, P., *Rev. ATIP* 64(4): 19(2010).
10. Doshi, M.R., *Prog. Pap. Recycl.* 18(3): 20(2009).
11. Huber, P., Borel, P., Soysouvanh, D., et al., *Nord. Pulp Pap. Res. J.* 30(2): 234(2015).
12. Fabry, B., Delagoutte, T., Kumar, S., et al., "From industrial macrostickies mapping to the identification of mini-stickies," *Int. Symp. Pap. Recycl. Res. Technol.*, ABTCP/RIADICYP, São Paulo, Brazil, 2009.
13. Delagoutte, T., Fabry, B., Guyard, A., et al., "Benchmarking of macrostickies contamination along several deinking lines," *PTS-CTP Deinking Symp.*, PTS, Munich, Germany, 2010.
14. Fabry, B., Delagoutte, T., Kumar, S., et al., "Identification of mini-stickies from industrial mapping: an interesting tool to determine the efficiency of your process," *Fall Conf. Korea Tech. Assoc. Pulp Pap. Ind.*, KTAPPI, Seoul, 2013.

ABOUT THE AUTHORS

Stickies have been an issue in the paper recycling process for decades, yet they remain a hot topic. However, until now, no clear differentiation between stickies by their chemical nature has been performed as part of the process. NIR analysis offers a very powerful tool for differentiating contaminants with close chemical composition, such as some stickies and plastics.

In this study, statistical analysis of the spectra was challenging, and gathering a team with the right competencies was critical to solving the issue. One interesting thing we discovered was that while the chemistry of glues seems similar all over the world, the breakdown of stickies from different countries can be drastically different, especially over different continents.

This study demonstrates how mills can analyze stickies removal throughout the recycling process and also control the process according to the chemical nature of incoming stickies contamination. Our next step is to develop on-line stickies measurements.

Ossard, Huber, Borel, and Delagoutte are project engineers and Soysouvanh is team leader at the Centre Technique du Papier (CTP), Grenoble, France. Email Huber at Patrick.Huber@webCTP.com.


Ossard


Huber


Borel


Delagoutte


Soysouvanh

Innovative technology for making improved paper from the poorest fibers

MARION STERNER AND MIKAEL MAGNUSSON

ABSTRACT: The trademarked Papermorphosis technology, consisting of two novel units for separately increasing cross direction (CD) and machine direction (MD) elongation over purely mechanical processes, has been successfully tested on recycling fiber, reaching high elongation values in each direction of over 15% in CD or 20% in MD. Increase of elongation has also had a positive influence on the relative tensile energy absorption (TEA) values in CD and MD. It is well known that mechanical properties in paper basically depend on fiber choice, headbox properties, and refining. With the novel system, elongations in cross direction (CD) and machine direction (MD) can be individually customized, even in paper grades with lower strength deriving from recycled fiber. Customizing elongations also has the effect of improving or better balancing TEA values in both directions. The aim is to improve existing recycling papers and to broaden the use of recycling fiber with respect to the past.

Application: For mills, using this technology on recycled papers or recycled fibers as blends might lower costs for raw materials and refining.

Technologies for reaching machine-direction (MD) elongation are available on the market as so-called extensible units. They do increase only MD elongation by about 15%. Potential cross-direction (CD) elongation derives from pure virgin pulp and costly high refining and does not usually exceed 8%, limiting such existing technologies to a total symmetric performance of 8% in each direction. The trademarked Mould Paper technology, owned and patented by the company of the first author and licensed to Billerudkorsnas where the product is on the market under the trade name FiberForm, can reach 16% of elongation in CD and 20% in MD, but the performance is not symmetric and the values in either direction cannot be separately tuned.

The first need was to develop a device for the customization of CD elongation only. Such a unit could then be combined with traditional, as well as new, devices for the customization of MD elongation. Our development consisted of such a CD unit, which can today treat fibrous webs from standard values up to around 15% on top of the paper's existing elongation. We also developed a novel MD unit, improving existing devices with an adjustable nip size/paper contact area, flexibility for intensity of treatment according to the desired outcome, and uniformity of treatment over the whole width, with no need for lubrication.

CUSTOMIZING/IMPROVING PAPERS

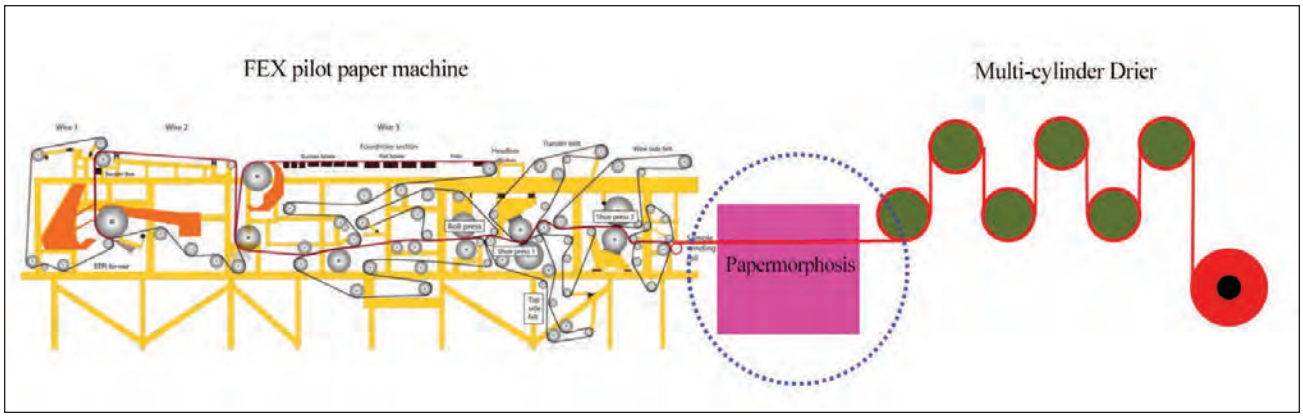
Today, both the CD and MD units are installed on the FEX paper pilot line at the paper science and research institute Innventia AB (now known as Rise Bioeconomy) in Stockholm, Sweden, where we have successfully processed all sorts of furnishes. All evaluations on elongations and tensile energy absorption (TEA) values have been carried out at the institute according to standard measurements for tensile testing. The CD unit is operated at a dry content of 50% or less, the MD unit is operated at a dry content of about 65%, and both are placed after the press section on a paper machine. **Figure 1** shows the schematic of installation on the paper pilot line.

The system has been successfully tested in applications where high stretch and high TEA in high quality and specialty papers are needed, using, i.e., a pulp of long virgin fiber with a refining of 30°SR. The treatment was carried out with both the CD and the MD units, as **Fig. 2** shows.

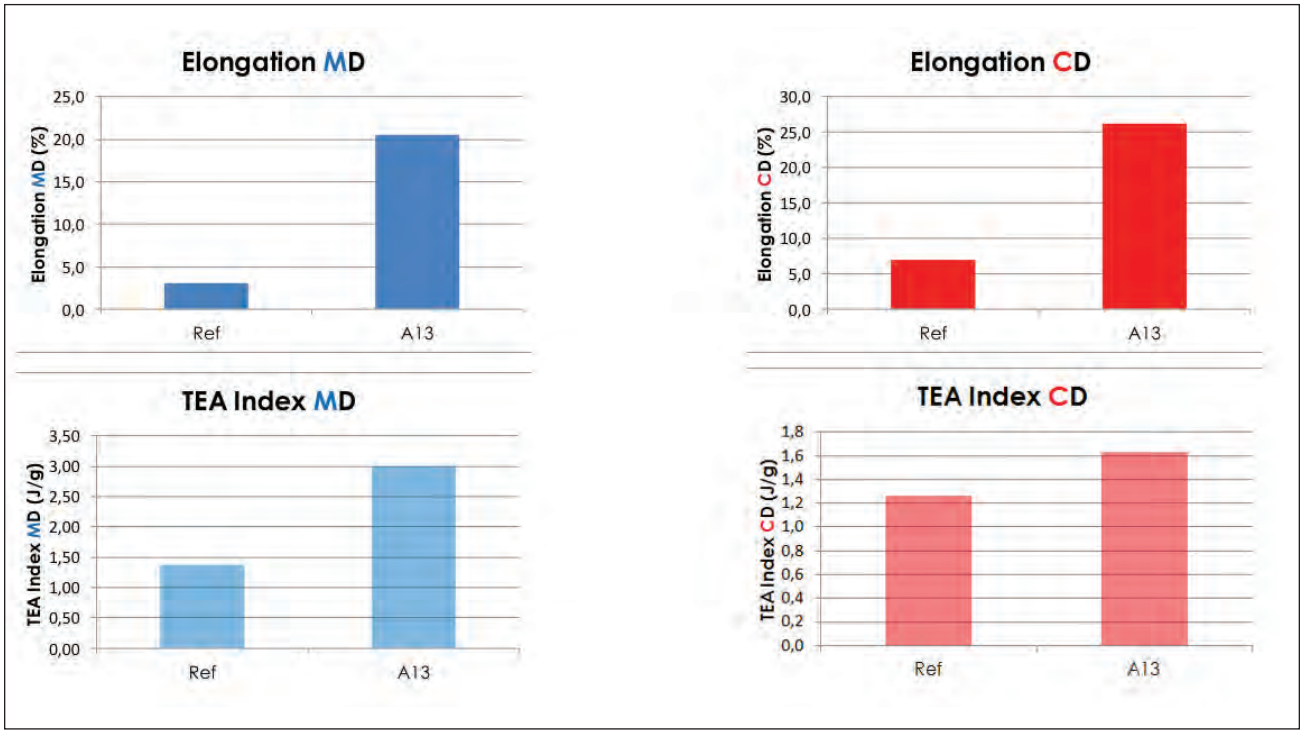
The CD and the MD treatment can be used in combination or separately according to specific needs, arriving from absolute increases of just a few percentage points in elongation up to very high values, together with the relatively increased TEA in either direction. The system forms an integrated, on-demand system within a paper machine that can be excluded if not needed for a particular paper's production.

From many focused customer trials, we found that this system is flexible enough to meet or to get very close to the targets for the most specific of needs:

- High symmetric stretch in both CD and MD (i.e., for three-dimensional [3D] packaging)
- Improved TEA values
- Focused joints of stretch/TEA where needed
- Reproduction of standard qualities, with less refining or raw material costs



1. Schematic of the system's installation on the paper pilot line.



2. On the left top in blue, elongations in MD of reference and MD-treated sample A13, with the increase of TEA index in MD below it. On the right top in red, elongations in the CD using the same reference and CD-treated sample, with the increase of TEA index in CD below it.

After the proof of concept, we have investigated the focused and tailor-made use of both units for making an improved paper out of the poorest of recycling fibers. Our base pulp for all trials was repulped paper containing 30% unbleached kraft and 70% OCC, with a final 28°SR.

Target 1

Target 1 was to achieve high symmetric elongation by the use of both the CD and MD unit. As **Fig. 3** shows, the result was symmetric elongation of around 15% in each direction and increased TEA values for recycling paper.

Target 2

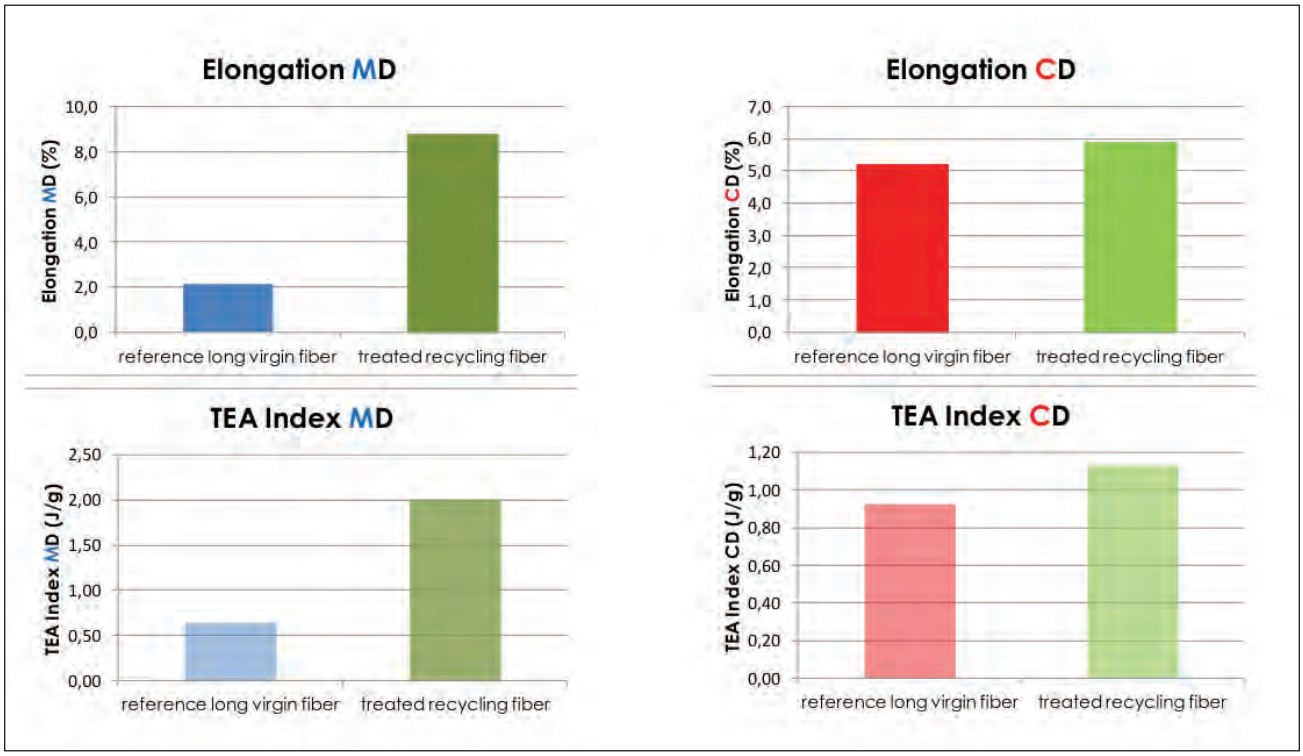
Target 2 was a simulation of paper from long virgin fiber with high refining (30°SR). **Figure 4** shows that for the recycling base paper, even treatment with slight intensity provided, apart from increased elongation, an appreciable increase of TEA in CD and MD that was better than the untreated reference in pure long virgin fiber with high refining.

Target 3

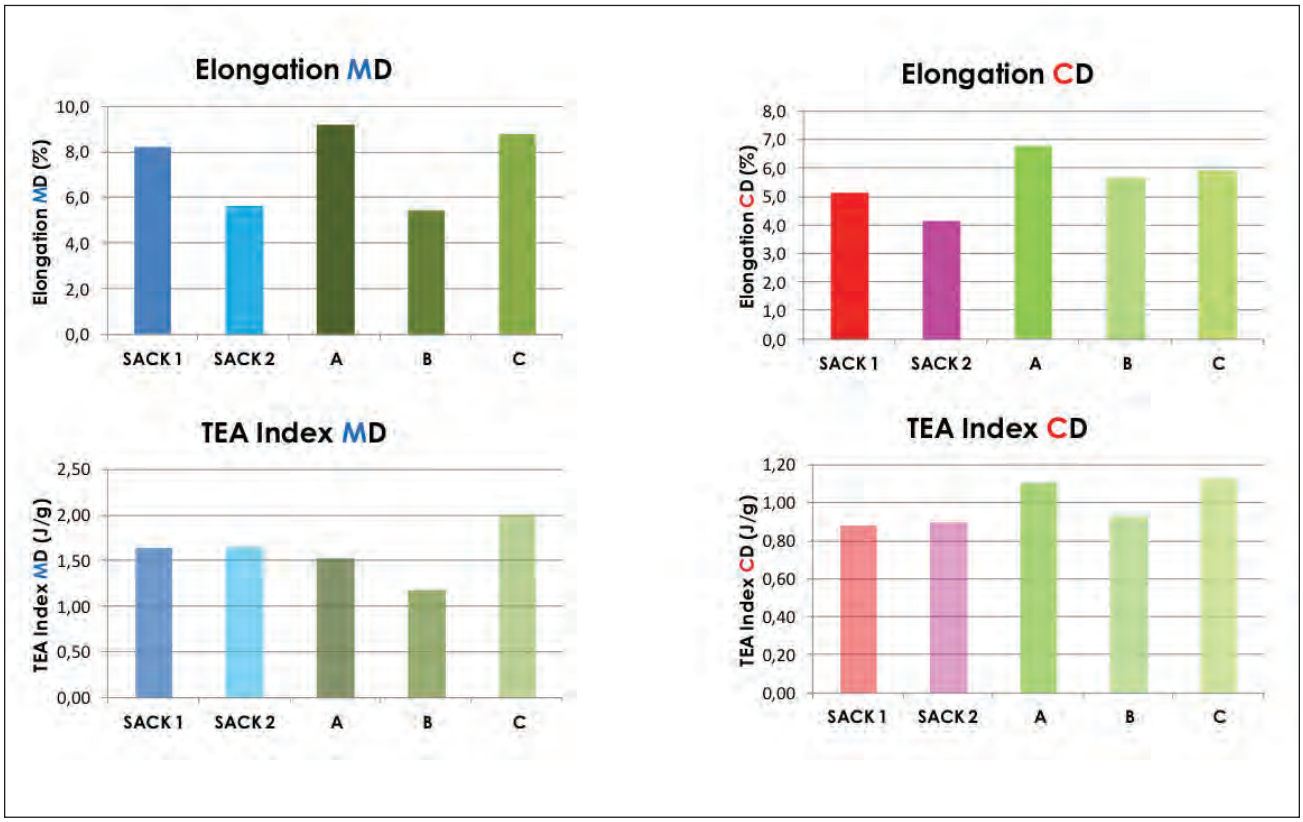
Target 3 was a simulation of standard sack kraft paper. The results, shown in **Fig. 5**, demonstrated that elongations could



3. On the left top, MD elongation of reference and MD-treated sample C6, with improved TEA index in MD below it. On the right top, CD elongation of reference and CD-treated sample C6, with improved TEA index in CD below it.



4. On the left top, MD elongation (virgin fiber reference [blue] compared with recycling fiber [green]), with improved TEA index in MD below it. On the right top, CD elongation (virgin fiber reference [red] compared with recycling fiber [green]), with improved TEA index in CD below it.



5. On the left, MD elongation and TEA index in MD (comparison between two industrial standard sack materials [blues] and recycling fibers [greens A, B, and C]) with different intensities of treatment. On the right, CD elongation and TEA index in CD (comparison between the same two industrial standard sack materials [reds] and recycling fibers [greens A, B, and C]).

be reproduced or increased. In almost all cases, TEA was also remarkably improved.

CONCLUSIONS

Papermorphosis is a trademarked, flexible system that allows many process parameters to be fine-tuned according to desired performance of the final material. Even though the only thing that cannot be added by the system is strength, the results of our trials showed that the system can benefit recycling paper, in the same way it does for specialty and high-performance papers, by adding customized elongation and TEA in CD and MD to the final material and by providing the flexibility to decide how far to extend this performance. The field of recycling pulp and its mixtures within a furnish is huge, ranging from pre-consumer to post-consumer, and it is combined from the highest to the lowest level with other fibers. The aim was to provide a tool for adding performance, broadening applications, and exploring new fields and markets for the world of recycling paper as a cost saving and sustainable alternative to traditional materials. **TJ**

ABOUT THE AUTHORS

We saw that by improving elongations in a customized way, other paper properties, such as TEA values, could be improved. We wanted to study the application of our technology for a separate increase of cross direction and/or machine direction elongation, not only for papers made of virgin fibers for 3D packaging applications, but also for recycling papers, in order to improve them and broaden their field of application. Overall, we wanted to investigate improving existing paper grades, such as recycling papers, even when such improvements are not even visible to a final customer yet are important to the papermaker in terms of cost.

Applying this technology on recycled fiber was not difficult; it was more of a confirmation—and also our goal from the very beginning—that it works on any paper, even that made of the poorest fibers.

Though not documented in this manuscript, we managed to produce a novel longitudinal corrugate with our technology, also out of recycling grades. This novel discovery produces a stable wave in the machine direction (without the need of fixing it with a liner) and does not shrink the web width.

For mills, using this technology on recycled papers or recycled fibers as blends might lower costs for raw materials and refining. We have started discussions with papermakers and machine manufacturers, and the first industrial applications will hopefully be on the market within the near future.



Sterner



Magnusson

Sterner is head of Research & Development for Gruppo X di X Gruppo srl, Venice, Italy. Magnusson is senior research associate, RISE Bioeconomy (Invenntia AB), Stockholm, Sweden. Email Sterner at marion.sterner@gruppox.it.

Improved deinking and stickies removal

CESAR BASILIO

ABSTRACT: Previous work had shown that a novel flotation deinking reagent using modified kaolin was able to more efficiently separate and remove ink and dirt particles from recovered paper. The mechanism for this reagent is based on the ability of the modified kaolin to act as a collector for the fine ink, dirt, and contaminant particles. Deinking mills using this reagent experienced deinked pulp with an increase in brightness and lower dirt count values. Further work has been carried out to determine whether this mechanism can be used to improve the removal of stickies in recovered pulp. Test results showed that use of this modified kaolin together with a reagent capable of effectively separating the sticky contaminants from the fiber improved the removal of stickies. The synergy of this reagent with the modified kaolin further improved ink and dirt removal.

Application: Mills can take advantage of this technology to help handle their stickies issues.

The deinked pulp (DIP) from recovered paper and paperboard, such as old newspaper (ONP), old magazine (OMG), mixed office waste (MOW), sorted white ledger (SWL), and sorted office paper (SOP), has become a principal source of raw material for making paper in the United States and Europe, with significant growth in China and other Asian countries [1]. In India, the share of recovered paper used as raw material for the paper industry is about 47% [2]. Although the production of recycled newsprint and printing paper has been significantly reduced in the United States and Europe, those of recycled tissue, brown, and paperboard grades have continued to grow.

One of the current concerns in paper recycling is the quality of the recovered paper. With single stream recycling becoming more common, the quality of the recovered paper and paperboard has been getting poorer. It has also resulted in stickies being more prevalent in paper recycling operations. Stickies are now a global problem that affects recycling all grades of paper. Stickies not only affect the operational side of recycling but the quality of the product itself. Operational problems associated with stickies typically involve excessive downtimes as a result of increases in maintenance, cleaning, equipment replacement, and breaks. On the product side, stickies can cause holes, sheet defects, high dirt count, and problems in converting that all cause an increase in breakages and rejects. Both problems reduce process efficiency and increase production costs and contribute to decreased machine productivity. Thus, there is a strong need to solve the stickies problem.

Stickies control by its very nature just cures the symptoms. This approach focuses on minimizing the effect of the stickies on the paper machine and in the final product. Current stickies control methods include passivation, dispersion, fixation, and detackification [3]. In passivation, the stickies are stabilized through the use of an additive such as talc, bentonite, smectite, and other minerals [4]. Stickies control by dispersion is achieved through the use of anionic or nonionic dispersants [5]. Stickies control through fixation into the fibers is typically carried out using cationic polymers [6]. For stickies control via detackification, various chemical compounds such as enzymes are generally used [7]. However, there is a need to remove the stickies instead.

Previously, it has been shown that a modified kaolin-based deinking reagent developed for use in the flotation deinking of recovered paper can improve the removal of ink, dirt, and other contaminants [8]. Unlike the previous deinking technology based on untreated hydrous kaolin clay, this kaolin-based deinking reagent uses surface modified kaolin particles. The modified kaolin is blended with a deinking surfactant to produce the deinking kaolin (DK) reagent that provides a more efficient separation and removal of the ink, dirt, and contaminant particles from the recovered paper fibers. Further work has been carried out here to determine whether this mechanism can be used to improve the removal of stickies in recovered paper. In this work, the deinking kaolin reagent is modified with the addition of various reagents to produce this DK reagent that can further improve the removal of stickies. The results of this work are presented here.

EXPERIMENTAL

Various recovered papers such as ONP, SOP, SWL, MOW, and coated book stock, as well as unprinted office copy paper, were used in these studies. The feed furnish was shredded and mixed with hot tap water (45°C) to 15% consistency. The required amount of chemicals for pulping and deinking reagent (control: nonionic surfactant) was added and then pulped for 10 min. After pulping, the sample was diluted to 1% consistency with tap water and floated in a Denver flotation cell for 5 min. After flotation, the accepts containing the deinked fiber from each of the flotation tests were collected. Three different flotation tests were conducted for each condition and the results were averaged. Brightness measurement

Reagent (0.5 kg/ton)	Feed Total Stickies Count	Product Total Stickies Count	% Stickies Reduction
DK stickies removal reagent A	404	288	29
DK stickies removal reagent B	404	299	26
DK stickies removal reagent C	**404**	**172**	**58**
DK stickies removal reagent D	404	290	28
DK stickies removal reagent E	404	318	22
DK stickies removal reagent F	404	322	21

I. Laboratory flotation test—unprinted office paper with adhesive label (DK = deinking kaolin).

Reagent (2.5 kg/ton)	Average Brightness			Average ERIC		
	Feed	Product	Delta	Feed	Product	% Reduction
Control: Surfactant	33.4	44.5	+11.1	1862	503	73
DK reagent	33.5	47.2	+13.7	1843	487	74
DK stickies removal reagent C	**34.0**	**48.3**	**+14.3**	**1990**	**449**	**77**

II. Laboratory flotation test—old newspaper (DK = deinking kaolin).

was conducted by forming the deinked pulp (DIP) into a pad, drying it in an oven, and measuring the GE brightness using TAPPI Standard Test Method T-218 "Forming handsheets with reflectance testing of pulp (Büchner funnel procedure)" with a Brightimeter Model Micro S-5 (Technidyne; New Brighton, IN, USA). In addition, the effective residual ink concentration (ERIC) was also measured using a Technidyne Technibrite ERIC 950. For the macrostickies measurement, the stickies were collected using a Pulmac Masterscreen with 0.006-in. slots (Pulmac Systems; Williston, VT, USA) and then quantified using the transparency film lamination method. The Pulmac Sticky Scan 200 was used for the image analysis.

To produce this DK reagent, the kaolin is first treated to modify the hydrophobicity of its surface and is then concentrated. This surface treated kaolin concentrate is then blended with a deinking surfactant that has been identified in previous work to optimize the deinking capability of this reagent. The DK stickies removal reagent is treated with other proprietary reagents to enhance its capability to separate the stickies and other contaminants from the fiber. Both DK reagents are a complete replacement for the deinking surfactant used in any flotation deinking applications.

RESULTS AND DISCUSSIONS

Initial tests were conducted on unprinted copier paper that was spiked with stickies through the addition of pressure sensitive adhesives. This was done to ensure that the feed furnish was consistent and had a relatively constant amount of stickies present. Tests were conducted on various DK stickies removal reagents (i.e., reagents A–F) to determine the best reagent. Each reagent contained various types of reagents or a combination of reagents. The results of the laboratory flotation tests are shown in **Table I**. As shown, DK stickies removal reagent C showed the best stickies removal of the various reagents tested; DK stickies removal reagent C was then used in further tests. Although not presented in the table, the average flotation yield values for each reagent were similar in all the tests (i.e., 90% ±1). This applies to all the flotation tests reported here.

The flotation deinking performance of a nonionic surfactant, the DK reagent, and the DK stickies removal reagent C was tested on a 100% ONP blend using the standard alkaline flotation chemistry (i.e., 1.8% sodium silicate, 0.6% sodium hydroxide, 0.7% hydrogen peroxide, 0.05% calcium chloride, and 2.5 kg/ton deinking reagent). The results of the laboratory flotation deinking tests are shown in **Table II**. As shown, using a nonionic surfactant typically used in ONP deinking, flotation was able to achieve a brightness gain of +11.1 with an ERIC reduction of about 73%. Using the DK reagent, instead of the deinking surfactant, the brightness gain after flotation increased to +13.7 while the ERIC reduction was slightly higher at 74%. However, when the DK stickies removal reagent was used, it surprisingly yielded an even higher brightness gain of +14.3 and an ERIC reduction of 77%. It appears that the modification of the DK reagent to produce the DK stickies removal reagent resulted in some synergy with the additional proprietary chemicals to give improved ink removal. No significant difference was observed in the

Reagent (2.5 kg/ton)	Feed Total Stickies Count	Product Total Stickies Count	% Stickies Reduction
Control: Surfactant	67	58	13
DK reagent	67	51	24
DK stickies removal reagent C	**67**	**39**	**42**

III. Laboratory flotation test—old newspaper (DK = deinking kaolin).

Reagent (0.4 kg/ton)	Average Brightness			Average ERIC		
	Feed	Product	Delta	Feed	Product	% Reduction
Control: Surfactant	72.3	76.8	+4.5	178	86	52
DK reagent	72.8	78.2	+5.4	178	75	58
DK stickies removal reagent C	**72.8**	**78.0**	**+5.2**	**178**	**68**	**62**

IV. Laboratory flotation deinking test—recycled printing paper (DK = deinking kaolin).

Reagent (0.4 kg/ton)	Feed Total Stickies Count	Product Total Stickies Count	% Stickies Reduction
Control: Surfactant	180	152	16
DK reagent	180	123	32
DK stickies removal reagent C	**180**	**78**	**57**

V. Laboratory flotation deinking test—recycled printing paper (DK = deinking kaolin).

average flotation yield for the various reagents.

The stickies removal performance of the DK stickies removal reagent compared with the surfactant and DK reagent was then determined. The stickies measurements used here were aimed at looking at the macrostickies only. Results of the laboratory flotation tests are presented in **Table III**. As shown, the DK reagent achieved a stickies reduction of about 24% while the surfactant only yielded a stickies removal of 13%. In the case of the DK stickies removal reagent, the stickies removal increased further to 42%. This shows that the modified deinking kaolin-based reagent is capable of the significant improvement in stickies removal.

The next set of tests was carried out on a typical furnish for recycled printing paper. The furnish consisted of SOP, SWL, MOW, and coated book stock. The control surfactant used is a nonionic surfactant typically used for this type of deinking with an alkaline chemistry used in the pulper (i.e., sodium hydroxide and sodium silicate). This was then compared with the DK reagent and the DK stickies removal reagent C. Laboratory flotation deinking tests results are presented in **Table IV**. Although not presented in the table, the average flotation yield values for each reagent were not much different from each other (i.e., ±1.6). The flotation deinking test results show improved ERIC reduction and higher brightness gain with the use of DK reagent vs. the control surfactant. Stickies measurements were then carried out to determine the difference in stickies removal between the DK reagent and the control deinking surfactant. **Table V** shows that improved stickies removal is obtained with the use of DK reagent. The amount of stickies removed by the DK reagent was double that obtained by the control surfactant.

Tests were then carried out to compare the DK stickies removal reagent with the DK reagent and control surfactant. As shown in Table IV, the use of the DK stickies removal reagent further improved the ERIC reduction but with no significant change in brightness gain. With regard to stickies removal, the DK stickies removal reagent showed a higher percentage of stickies reduction compared with the DK reagent (Table V). Overall, it appears that the DK reagent and the DK stickies removal reagent C both can achieve better stickies and ERIC reduction than the control surfactant. The DK stickies removal reagent C achieves even further improvements in stickies and ERIC reduction than the DK reagent.

SUMMARY AND CONCLUSIONS

The kaolin-based deinking reagent developed previously for flotation deinking was modified with the addition of proprietary reagents to help improve the separation of stickies from the fiber. This DK stickies removal reagent was found to be capable of further improving the removal of stickies by this deinking technology. The proposed mechanism for this improved stickies removal is the deinking kaolin's ability to collect the stickies and separate them from the fiber during flotation. Laboratory tests showed that it was capable of increasing stickies removal in different types of furnishes as compared with a nonionic deinking surfactant.

Interestingly, the modified DK reagent also improved the removal of inks from ONP and recycled printer paper furnish. Brightness gain and ERIC reduction were both higher with the use of this DK stickies removal reagent compared with the DK reagent and the nonionic deinking surfactant. This DK stickies removal reagent is a complete replacement for the deinking surfactant used in any flotation deinking applications. **TJ**

LITERATURE CITED

1. Grossman, H., "The limits of paper recycling – an European approach to identify and extend the limits of paper recycling," *Proceedings of Innovations in Recycling*, TAPPI Press, Atlanta, GA, USA, 2007.
2. Agarwal, A., "Paper through time," Indian Paper Manufacturers Association, New Delhi, India, 2010.
3. Doshi, M., *Recent Advances in Paper Recycling—Stickies*, TAPPI Press, Atlanta, GA, USA, 2002.
4. Yordan, J.L. and Williams, G.R., in *Paper Recycling Challenge, Vol. 1: Stickies* (M.R. Doshi and J.M. Dyer, Eds.), TAPPI Press, Atlanta, 1997, pp. 76-80.
5. Dykstra, G.M. and May, O.W., "Controlling stickies with water soluble polymers," *Pulping Conf.*, TAPPI Press, Atlanta, 1998.
6. Woodward, T., "Controlling contaminants in the production and use of deinked pulp," *Proc. WastePaper VII*, Miller Freeman, San Francisco, CA, USA, 1996.
7. Klungness, J.H., Sykes, M.S., Jeffries, T.W., et al. in *Paper Recycling Challenge, Vol. 20: Deinking & Bleaching* (M.R. Doshi and J.M. Dyer, Eds.), TAPPI Press, Atlanta, 1997, pp. 155-160.
8. Basilio, C.I., "Development of a deinking reagent based on modified kaolin," *PTS-Deinking-Symp.: Altpapieraufbereit. Druckpapierherstell* (E. Hanecker and B. Carre, Eds.), Paper Technology Specialists and Centre Technique du Papier, Munich, 2010.

ABOUT THE AUTHORS

I chose this topic to research because the stickies problem has become a global issue that affects recycling of all paper grades. Previous work showed that using the kaolin-based technology improved the removal of inks and dirt. This research further improves this technology and its ability to remove stickies.

Finding the optimum chemistry to allow the current technology to also be able to significantly remove stickies was difficult. After a literature search was conducted to fully understand the required chemistry for removing stickies, the screening tests were successful. When conducting this research, I was able to discover the required chemistries to modify this kaolin-based technology to achieve improved stickies removal.

Interestingly, certain chemistries that appear to be promising theoretically don't work as well as expected. The current kaolin-based technology had good synergy with the reagent. Mills can use this technology to help handle their stickies problem.



Basillo

Although the current technology helps in instances where flotation deinking is used, it doesn't work for other recovered paper that is washed, like old corrugated containers (OCC). Future work will focus on applying the new kaolin-based technology to OCC and brown paper recycling.

Basilio is group leader at Thiele Kaolin Company, Sandersville, GA, USA. Email Basilio at cesar.basilio@thielekaolin.com.

Deinking process water flotation: An innovative solution to improve deinking and papermaking processes efficiency

THIERRY DELAGOUTTE, BRUNO CARRÉ, AND ELISA ZENO

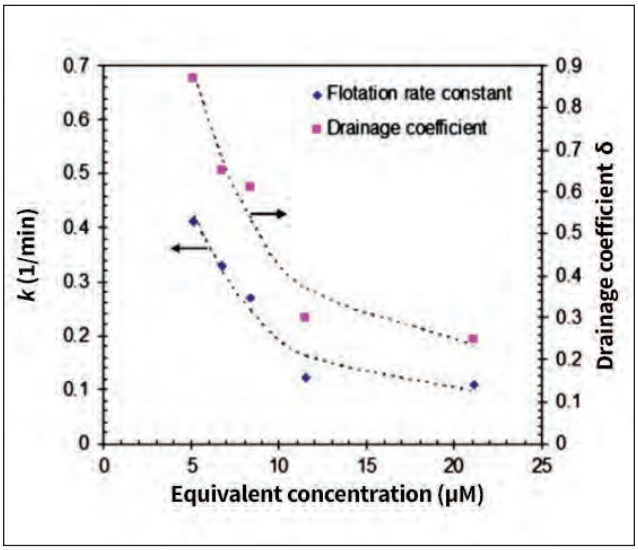
ABSTRACT: High and uncontrolled surface active substances (SAS) concentrations in deinking line process waters strongly disturb flotation deinking. Indeed, their adsorption at air/water and ink/water interfaces stabilizes air bubbles and ink particles, reducing ink collection during flotation. In addition, foam stabilization promoted by SAS reduces froth drainage and consequently enhances suspended solids losses. All in all, selectivity of flotation is negatively affected by excessive SAS concentrations. Floating process water with adapted technology, a patented solution, is an efficient way to decrease SAS concentration and thereby recover flotation deinking selectivity. This concept was tested at industrial scale with success. First loop clear filtrates of a deinked pulp line (for newsprint production) were floated. At steady state, this treatment allows a 20% reduction of the SAS concentration in first loop process water. Evaluation of ink removal selectivity at pre-flotation and post-flotation showed a significant improvement in comparison with reference values. During the trial, the mill could either produce pulp with lower ink content and consequently higher brightness (50 ppm effective residual ink concentration [ERIC] less, corresponding to a 1 brightness point increase) for similar losses, or similar pulp quality with 1% to 2% yield improvement, representing a huge cost reduction. In addition, beneficial side effects were reported, such as reduced deinking chemicals consumption (soda, silicate, and bleaching agents) and better paper machine runnability, especially in terms of stickies breaks.

Application: Mills might be able to increase brightness or yield in their deinking line using the process described here.

In a deinking line, concentrations of surface active substances (SAS) are usually high. These SAS come from many sources. Some are voluntarily added in the pulp and paper manufacture processes, such as deinking chemicals, dispersants (in coating colors, sizing, glues, etc.), and defoamers. Some, such as fatty and resin acids, are released by the fibers themselves. The amounts of SAS released from recovered paper or mechanical pulp can be very significant. For recovered papers, their release depends on the grades of recovered papers, but also on the alkaline treatments used during the recycling process [1].

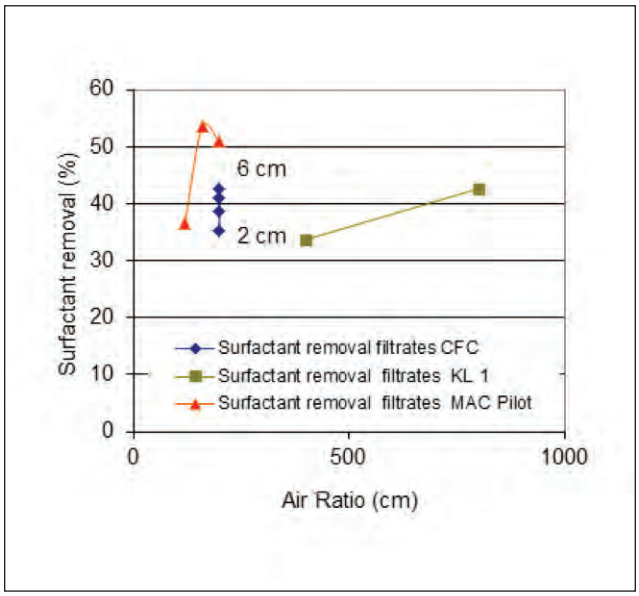
The presence of SAS in process water is reported to impair flotation deinking by decreasing ink removal and fiber yield [2-5]. **Figure 1** shows the influence of increasing surfactant concentrations on the reduction of ink removal efficiency by flotation [6]. Similarly, the foam drainage coefficient is also decreased when surfactant concentration increases, meaning that more stable foam is generated, resulting in an increase of flotation losses.

The detrimental action is explained by the surfactant adsorption onto the hydrophobic surfaces, mainly ink particles and air bubbles, thus reducing their adhesion energy [7] and by the froth stabilizing action that reduces the drainage of the fibers back to the suspension [8].



1. Influence of surface active substances (SAS) concentration on ink flotation removal constant and foam drainage coefficient [6].

Process water flotation by concentrating SAS in foam that is rejected has a great potential to decrease SAS concentrations in process water and to improve flotation deinking efficiency and selectivity. SAS removal achieved by process



2. Surfactant removal achieved during deinking process water flotation. Comparison of various flotation cells (laboratory batch, laboratory continuous, and pilot continuous) [9].

water flotation can vary from 35% to 70%, depending on the flotation technology used [9,10] (**Fig. 2**). The influence of this process water treatment on flotation deinking efficiency was also evaluated at laboratory scale showing improvement of ink removal, and flotation losses were significantly reduced (**Fig. 3**) [9]. Gendron et al., Ben et al., and Ricard et al. [11-13] reported the results of long-term mill trials of column flotation implemented in a thermomechanical pulp (TMP) newsprint mill. The treatment is claimed to be efficient on resinous materials (most having structures similar to surfactants) contained in the treated filtrate. Removal efficiency achieved by the flotation column is in the range of 30%-45%.

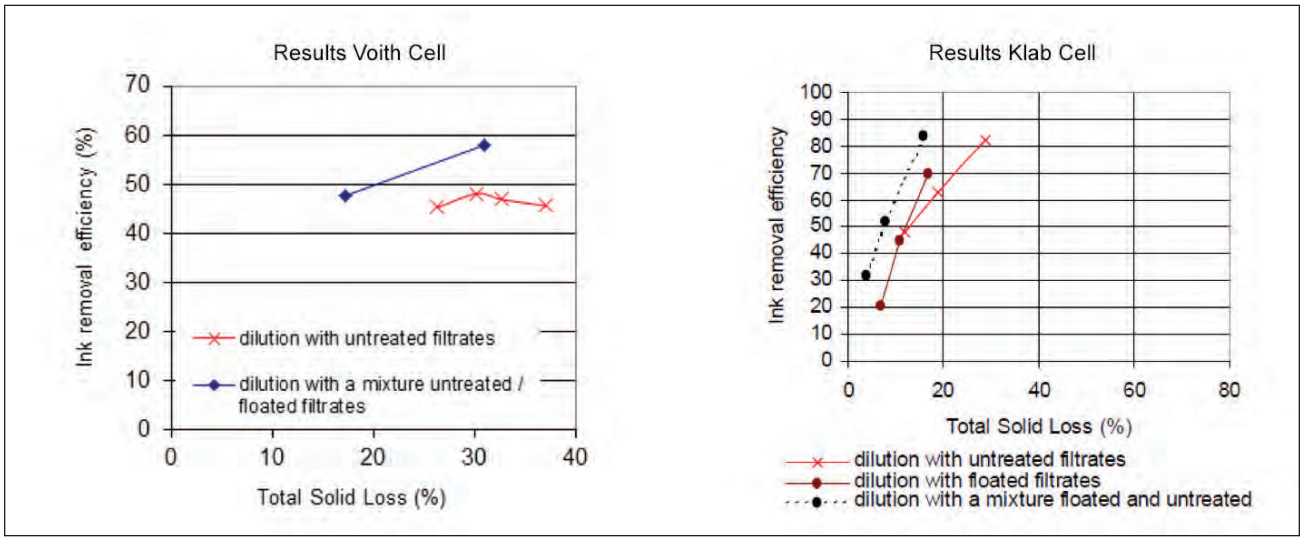
All in all, previous works at the Centre Technique du Papier (CTP) in Grenoble, France, have emphasized the importance of released surface active substances on ink flotation selectivity. This led CTP to apply for a patent [14] aiming at removing these substances from the process waters by an adapted flotation process. If the major effects have been identified at laboratory and then pilot scale, the real impact of this treatment on the runnability of an industrial process was not quantified yet. Since that time, CTP was able to evaluate such a treatment at mill scale. This paper reports the main outcomes of these trials, focusing on reduction of SAS concentration in process water, improvement of deinking selectivity, and some additional beneficial effects regarding chemicals consumption and pulp runnability on the paper machine side.

MATERIALS AND METHODS

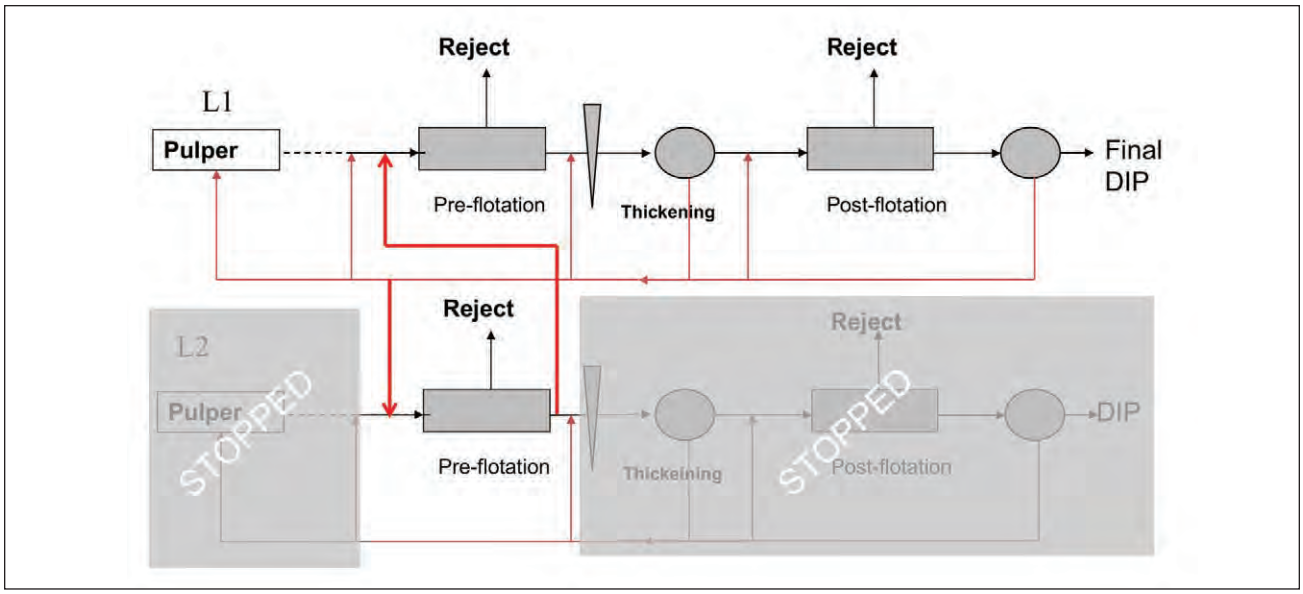
Description of the trial

A trial was conducted in a deinking mill producing newsprint based on deinked pulp (DIP) and TMP. The mill owns two deinking lines organized according to a conventional two loops process. The presence of these two parallel lines made the trial possible. One of the two lines was stopped and its pre-flotation was used to treat a part of the first loop water from the other line, which was still running. **Figure 4** describes the structure of the trial.

The first loop filtrate flow treated represents 610 m³/h, corresponding to 25% of the water available in the first loop. The foam that is generated is rejected from the mill through the effluent treatment plant. The rejected foam flow is estimated at 12% of the entering flow, representing 2.9 m³ additional rejected water per metric ton of DIP produced. Total suspended materials concentration of the treated water is 1.2 g/L.



3. Ink removal efficiency versus total solid losses achieved during deinking flotation. Influence of process water nature (unfloated versus floated waters) [9]. Results obtained with two types of laboratory flotation cells (left: Voith cells; right: Klab cell from Kadant).



4. Schematic of the mill trial, with only pulper flotation and thickening represented.

Water flotation process characterization

Surface tension measurement is done using a maximum bubble pressure technique based on the Laplace Law. A SITA apparatus (SITA Messtechnik GmbH; Dresden, Germany) is used, with average bubble time life set at 15 s. In all cases, surface tension is given for a water temperature of 25°C. This measurement is used to assess the SAS concentration in the water.

The SAS rejection rate was determined by measurement of surface tension. Serial dilutions of water flotation rejects (highly concentrated in SAS) are produced and their surface tension (dynamic measurement) is measured. This enables us to draw a dilution curve reporting the evolution of surface tension versus dilution rate of the foam. Then, determining the surface tension in the inlet and flotation accepts enables us to estimate SAS concentration relative to the flotation reject SAS concentration. SAS rejection rate was determined using relative SAS concentrations at inlet, outlet, reject, and flotation flows balance. The method is fully described elsewhere [3].

Total suspended solids (TSS) losses are determined through ash measurements in the inlet, accepts, and rejects of the cell treating the filtrate. The calculations were made according to the following equation:

$$TSS\ losses = \frac{(ash\ in - ash\ acc)}{(ash\ rej - ash\ acc)}$$

where:
ash in = ash percentage at the flotation inlet
ash acc = ash percentage at flotation accept
ash rej = ash percentage at flotation reject

Flotation deinking characterization

Pre-flotation and post-flotation were investigated before the trial to set the baseline and then during the trial at 3 h, 16 h, 20 h, and 24 h. Ink removal efficiency and TSS losses were evaluated.

The ink removal rate was followed through the effective residual ink concentration (ERIC), and brightness measurements were performed on pulp pads produced during the trial. The ink balance was calculated using the ERIC value and TSS mass flow. Ink mass flow rate is approached in multiplying ink concentration (ERIC) by pulp mass flow rate.

TSS losses were determined using ashes measurement as already described in the case of the water flotation (yield calculation method).

Apart from these laboratory measurements, online mill records were collected over the trial period (before and after) regarding ERIC and brightness at different positions in the process.

RESULTS AND DISCUSSION

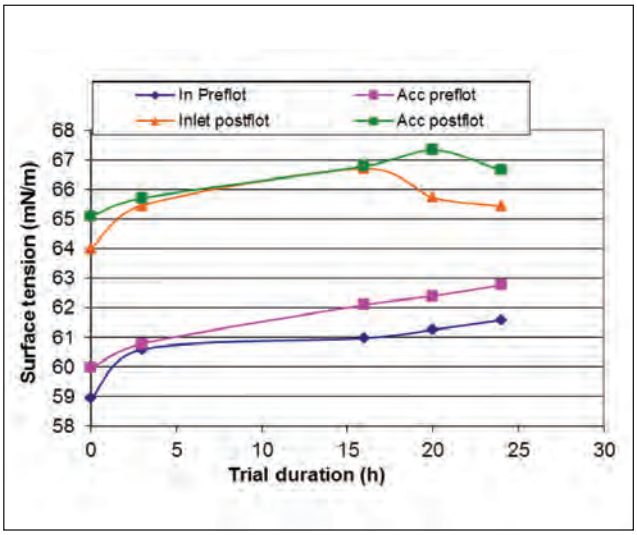
Water flotation efficiency

Water flotation efficiency was determined primarily in terms of SAS removal. Calculations were based on the dilution curve obtained from flotation rejects, surface tension measurements at the inlet, and rejects for the different times of the trial (3 h, 16 h, 20 h, and 24 h). Reject water flow was estimated at 12% for all measurements.

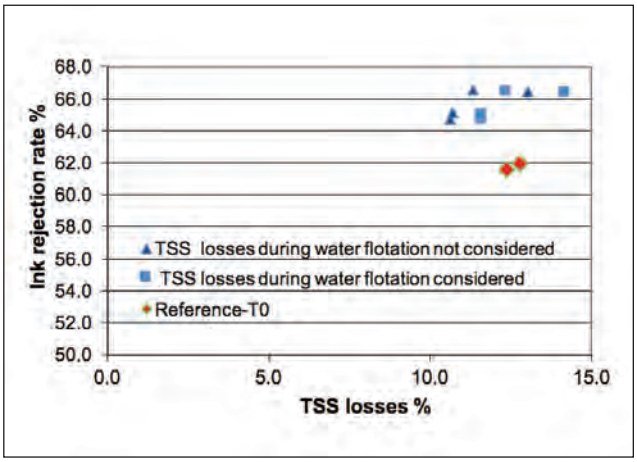
Table I shows the SAS rejection rates. Water flotation treats only 25% of the total available water in the first loop. Considering that, the configuration of the process (internal loop treatment with treated flow sent backwards), and pulp consistency at the end of the first loop, we can estimate, by a simple simulation that a reduction of 20% of the SAS amount entering the pre-flotation is achieved when compared with reference values.

Time	Inlet Surface Tension, mN/m	Reject Surface Tension, mN/m	Concentration Factor	SAS Reject Rate, %
3 h	60.9	54.9	1.9	23.2
16 h	61.9	55.1	2.2	25.9
20 h	61.5	55.0	2.1	24.8
24 h	62.6	54.8	2.3	27.9
			Average SAS Reject Rate, %	**25.4**

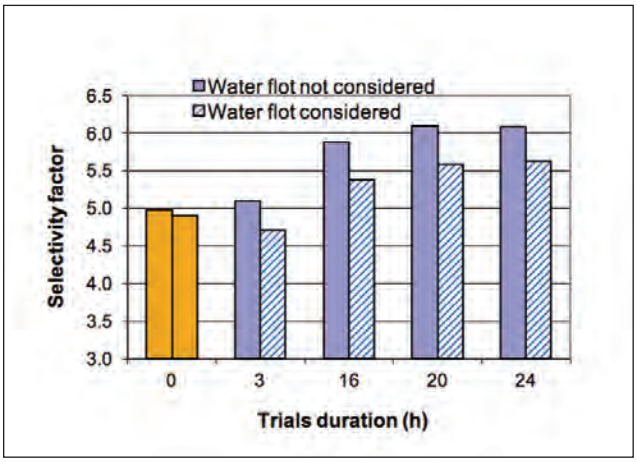
I. Surface active substances (SAS) rejection rates determined during flotation trials.



5. Evolution of surface tension at pre-floation and post-flotation during water flotation trials.



6. Evolution of ink removal rate versus total suspended solids (TSS) losses during water flotation trials.



7. Evolution of pre-flotation selectivity factor (ink rejection rate/ TSS rejection rate) during water flotation trials.

This estimated reduction is confirmed by the evolution of the surface tension measured at different positions during the trial period. **Figure 5** shows the results. It clearly appears from these measurements that surface tension increases in all process parts (first loop as well as second loop) as soon as water flotation is started, which indicates a reduction of the SAS concentration.

Influence on deinking efficiency

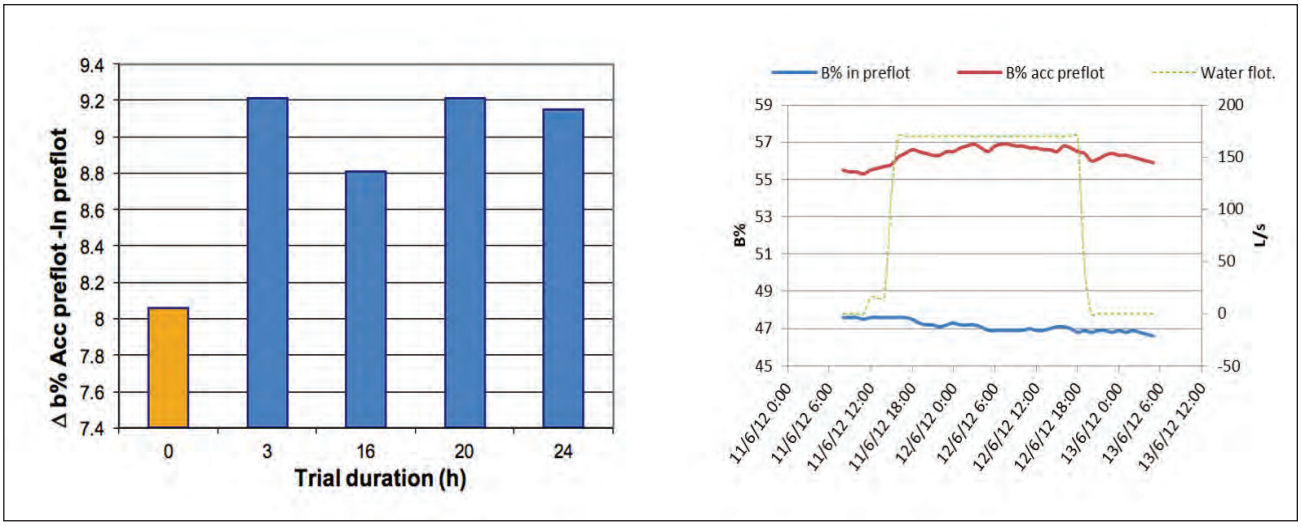
Reduction of SAS concentration should result in an improved flotation efficiency and selectivity. In order to check this aspect, ink and TSS balances were performed during the trials in both pre and post-flotation.

Influence on pre-flotation

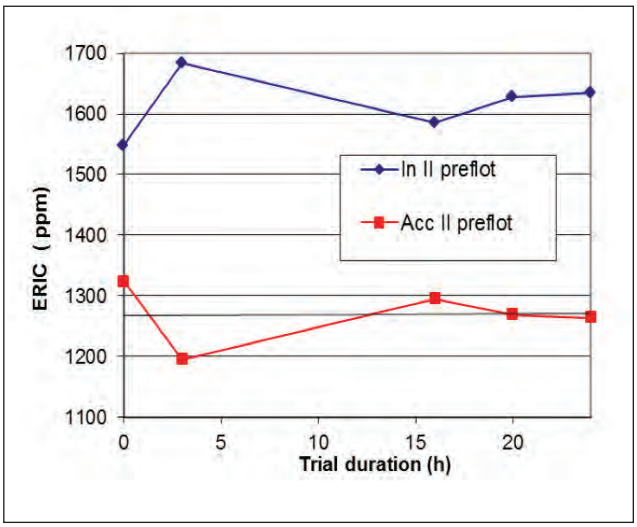
Ink removal rates and TSS losses were determined during the trial and compared with those of the reference period (T0). The results **(Fig. 6)** show two positive aspects achieved by the water treatment implemented:

1. For all trial durations, the ink removal rate was higher than what is commonly achieved in usual conditions (without water flotation): 65%–66% versus 62%.
2. This additional ink removal rate is obtained for similar or lower suspended solids losses (except at one point, corresponding to the shorter trial duration).

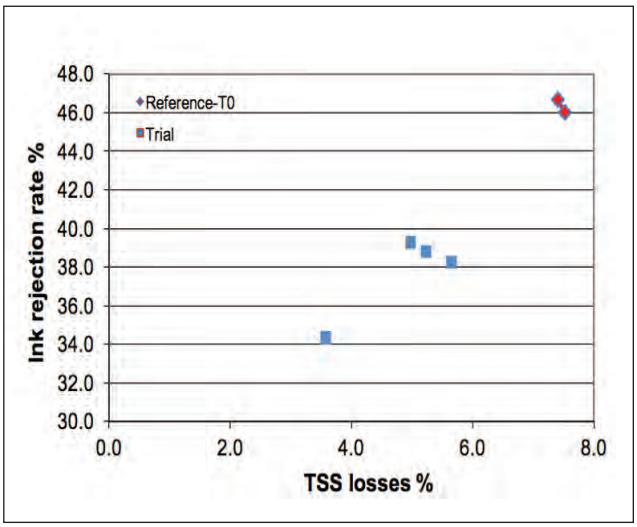
Furthermore, this is always true when suspended material losses generated by water flotation are counted with pre-flotation losses.



8. Evolution of brightness in pre-flotation. Left hand side: off-line measurements performed on pads. Brightness gain between inlet and accept reported. Right hand side: brightness value measured through mill sensor at the end of first loop.



9. Evolution of effective residual ink concentration (ERIC) at secondary stage inlet and accept.



10. Evolution of ink removal rate versus TSS losses during water flotation trial.

Thus, the ink rejection rate and the selectivity of the pre-flotation step were improved. **Figure 7** shows the evolution of the selectivity factor (representing ink quantity rejected achieved on average when 1% of TSS are lost). The selectivity factor increases from 5 to 6 in pre-flotation, or from 5 to 5.5 if we also consider the losses generated by the water flotation step.

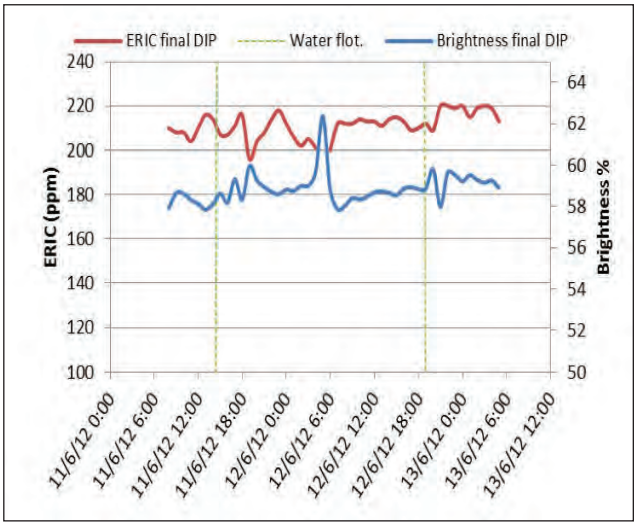
In the framework of this trial, the treated first loop process water contained high concentrations of suspended solids (1.2 g/L). Nevertheless, it is recommended, as the treatment is mostly intended to remove SAS, to treat a water flow having a lower suspended solids concentration (clear filtrate should be more suitable).

As a consequence, deinked pulp after pre-flotation has improved optical properties compared with the reference situation; residual ink content is reduced (from 290 ppm to 255 ppm, on average) and brightness is increased. **Figure 8** shows the evolution of brightness determined on pulp samples collected during the trial and by an on-line mill sensor at the end of first flotation. An increase of 1 to 2 points is reported.

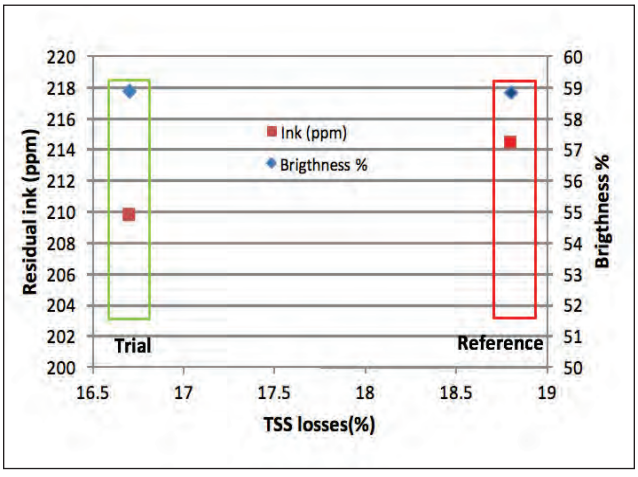
A better functioning of the secondary stage of the pre-flotation probably explained the improvement observed at pre-flotation. **Figure 9** shows the evolution of ink content at the secondary stage inlet and outlet during the trial. An increase of ink concentration at the inlet is in accordance with a better ink removal rate and selectivity at the primary stage. Moreover, in spite of this ink concentration increase at the inlet, accepts show a reduced ink concentration, which indicates better ink removal and selectivity at the secondary stage. As SAS are concentrated in the secondary stage, it makes this stage particularly sensitive to any variations of SAS concentration.

Influence on post-flotation

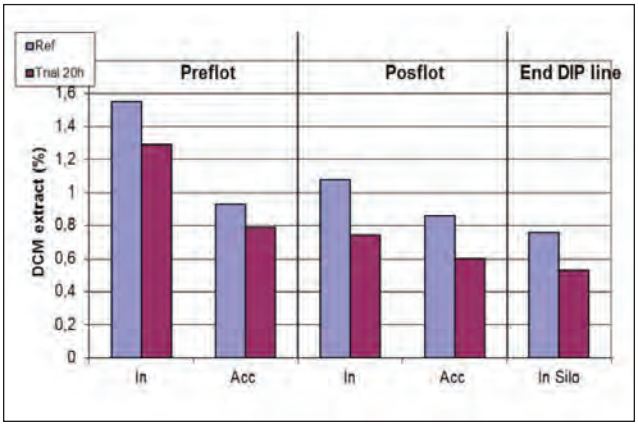
As in pre-flotation, the ink removal rate and TSS losses were determined during the trial and compared with the reference period. **Figure 10** shows the results obtained. Contrary to pre-flotation, the ink removal rate was slightly reduced when water flotation is applied. This might be the consequence of reduced foam stability, which favors the drainage of ink particles back to the suspension. However, in parallel, a decrease of TSS losses is observed. All in all, a slightly better selectivity of the post-flotation is observed (selectivity factor from 6.5 to 7 during trial versus 6.1 to 6.3 in reference). This reduced ink removal in post-flotation is compensated for by the lower residual ink level achieved at the end of the first loop, resulting in a final pulp having optical quality close to that measured in the reference period (**Fig. 11**). This same quality is achieved for improved yield, due to lower losses generated in pre- and post-flotations. As shown in **Fig. 12**, a roughly 2% yield improvement is observed for a pulp production of similar optical characteristics.



11. Evolution of final deinked pulp brightness and ERIC during the trial.



12. Final pulp quality (brightness and ink content) versus total deinked pulp process losses.



13. Influence of water flotation on dichloromethane extract content of the pulp at different locations in the deinking line.

Additional effects

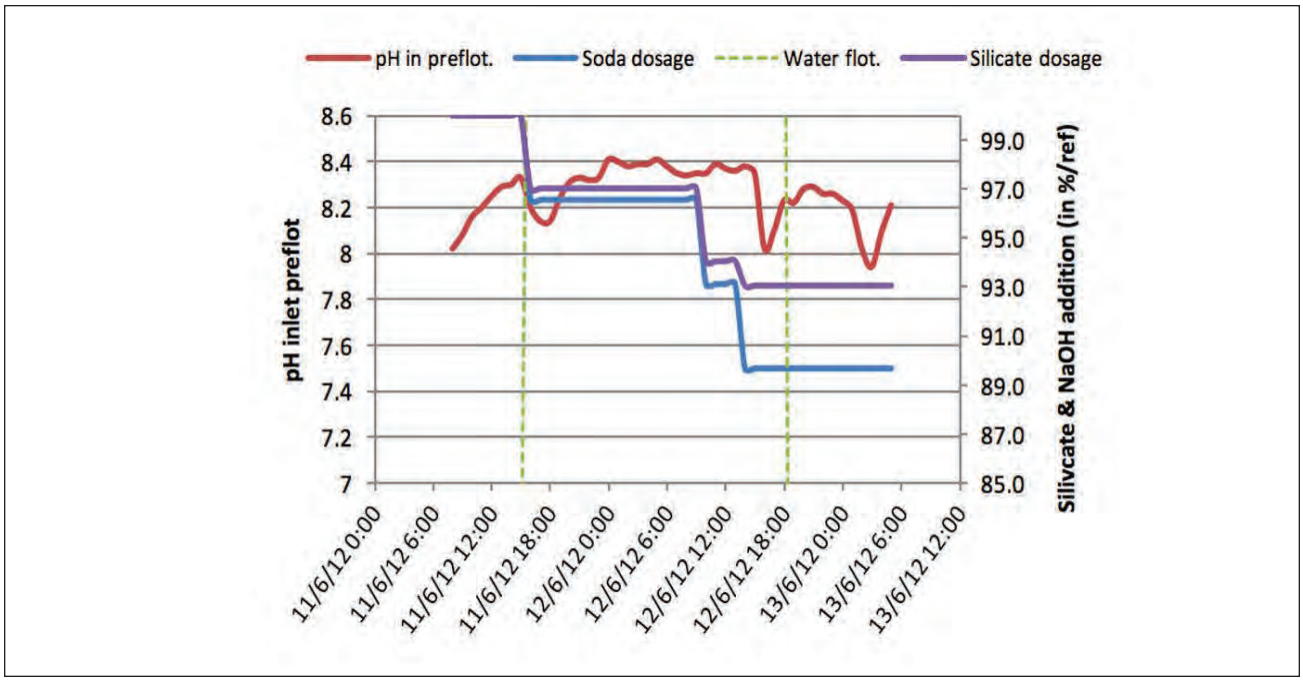
Apart from the improvement of deinking, water flotation has some additional beneficial effects, including a reduction of stickies-related material contained in the pulp. Dichloromethane extract of the pulp was measured during the reference period and during the trial. Results show a significant decrease of the extract rate contained in the pulp in all samples tested: pre-flotation (in and accept), post-flotation (in and accept), and inlet of DIP storage (**Fig. 13**). This improvement results from removal of microstickies contained in process water. As in this trial, treated filtrate was rather rich in fine suspended solids (1.2 g/L – mainly fillers). The good runnability of the paper machine during the trials and immediately after was probably partly explained by this pulp quality improvement.

An increase of pH in pulping was observed during the trial. As a consequence, the mill has had to reduce the alkaline sources added in the pulper (soda and silicate) to maintain pH in the same range (**Fig. 14**). This probably originates from the aeration of the water, which acts on different parameters, stripping CO_2 and volatile fatty acids and reducing anaerobic conditions that reduce the production of volatile fatty acids by the bacteria. Another consequence of these modified conditions is the presence of residual peroxide at the pulper outlet, which is rarely observed in usual conditions and which is also reported as a positive effect.

CONCLUSION

Innovative, patented, concept to control SAS in deinking lines

Floating process water with adapted technology is an efficient way to decrease SAS concentration in the deinking line. This concept was tested at industrial scale with success; first loop clear filtrates of a deinked pulp line (for newsprint production) were floated. At steady state, treating 25% of the water



14. Evolution of pH, soda, and silicate dosages during the flotation trial.

available in first loop allows for a 20% reduction of SAS concentration, with extremely limited solid losses.

Positive effect on the deinking line

Floating process water has two major effects on the deinking line:

1. It improves deinking selectivity, corresponding to a brightness improvement of 1 to 2 points, and yield remains constant; or the reverse, yield improves 1 to 2 points, and brightness remains at the same level.
2. It significantly reduces consumption of deinking and bleaching chemicals: soda = -30%, silicate = -35%, and bleaching agent = -80%.

Attractive economical balance

Economic calculations were made taking into account all aspects of DIP production: raw material costs, energy and chemical consumption, reject management, and yield. Depending on the strategy of the mill, two situations must be considered:

1. The mill wants to improve the brightness, while keeping yield at the same level. In this condition, the gain is estimated at 1.2 €/metric ton when water flotation is applied.
2. The mill wants to improve yield and keep brightness at the same level. In this case, the gain is estimated at 3 €/metric ton.

The second option seems to be more attractive, but the drastic reduction of bleaching in the first option might have a very positive effect on paper machine runnability, which is not counted in this estimation. **TJ**

LITERATURE CITED

1. Beneventi, D., Carré, B., and Gandini, A., "Surfactant release and removal during flotation," *CTP Recycled Fibres Forum*, Centre Technique du Papier, Grenoble, France, 2001.
2. Williams, J.A. and Springer, A.M., *Prog. Pap. Recycl.* 7(1): 19(1997).
3. Zeno, E., Angelier, M.C., Beneventi, D., et al., "Surfactant mass balance in industrial deinking plants: a tool for flotation control," *PTS-CTP Deinking Symp.*, Centre Technique du Papier, Grenoble, 2008.
4. Beneventi, D., Leroy, L., and DeLuca, P., *Prog. Pap. Recycl.* 14(1): 14(2004).
5. Carré, B., Vernac, Y., and Beneventi, D., *Pulp Pap. Can.* 102(7): T189(2001).
6. Beneventi, D., Alix, J., Zéno, E., et al., *Int. J. Miner. Process.* 87(3-4): 134(2008).
7. Beneventi, D., Belgacem, M.N., and Carré, B., *Nord. Pulp Pap. Res. J.* 21(5): 25(2006).
8. Carré, B., Zéno, E., and Huber, P., "Detrimental effect of DIP process water on flotation mechanisms: possible solution," *PTS-CTP Deinking Symp.*, Centre Technique du Papier, Grenoble, France, 2012.
9. Carré, B. and Zéno, E., "Effect of process water contamination on flotation mechanisms," *Technical Conference on Deinking of Digital Prints*, Centre Technique du Papier, Grenoble, 2011.
10. Carré, B., Vernac, Y., and Beneventi, D., "New insights in the reduction of flotation losses: input of dynamic interfacial tension measurements," *Res. Forum Recycl., 5th*, PAPTAC, Montreal, 1999.
11. Gendron, S., Ricard, M., Ben, Y., et al., "Impacts of white water flotation on the operation of a line producing newsprint from TMP," *TAPPI Peers Conf.*, TAPPI Press, Atlanta, GA, USA, 2012.
12. Ben, Y., Ricard, M., Gendron, S., et al., "Startup of a large industrial flotation column for white water cleaning," *TAPPI Peers Conf.*, TAPPI Press, Atlanta, 2012.
13. Ricard, M., Dorris, G., Ben, Y., et al., *J. Sci. Technol. For. Prod. Processes* 2(3): 23(2012).
14. Carré, B., European pat. EP1881105(B1) (March 4, 2009).

ABOUT THE AUTHORS

We conducted this study to help deinking mills solve deinking difficulties resulting from increased water contamination by surfactants. The mill trials reported in this paper are the complement of years of laboratory and pilot studies performed in our laboratory and which had led to a patented technology.

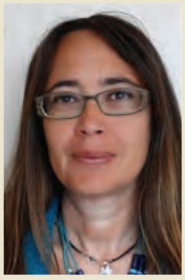
The most difficult part of this research was to move from laboratory and pilot research to industrial trials. In these studies, we discovered the influence of surfactants (positive and negative) in many aspects of the deinking.

The most interesting findings concerned the additional effects of the treatment that were not anticipated from the previous laboratory and pilot studies. These additional effects strongly enhance the interest of the technology.

Mills can benefit from this study by implementing the technology in their production lines.



Delagoutte



Zeno



Carré

Our next step will be implementation of the technology in deinking mills.

Delagoutte and Zeno are research engineers and Carré is team manager at the Centre Technique du Papier (CTP), Grenoble, France. Email Delagoutte at Thierry.Delagoutte@webctp.com.